# ADVANCEMENTS IN THE INTERPRETATION OF SEISMIC PIEZOCONE TESTS IN CLAYS AND OTHER GEOMATERIALS

A Dissertation
Presented to
The Academic Faculty

by

Shehab Sherif Wissa Agaiby

In Partial Fulfillment
of the Requirements for the Degree
Doctor of Philosophy in the
School of Civil and Enironmental Engineering

Georgia Institute of Technology
[May 2018]

# ADVANCEMENTS IN THE INTERPRETATION OF SEISMIC PIEZOCONE TESTS IN CLAYS AND OTHER GEOMATERIALS

Approved by:


Dr. Paul W. Mayne, Advisor
School of Civil and Environmental Engineering
*Georgia Institute of Technology*

Dr. J. David Frost
School of Civil and Environmental Engineering
*Georgia Institute of Technology*

Dr. Susan E. Burns
School of Civil and Environmental Engineering
*Georgia Institute of Technology*

Dr. Sheng Dai
School of Civil and Environmental Engineering
*Georgia Institute of Technology*

Dr. Emanuele Di Lorenzo
School of Earth and Atmospheric Sciences
*Georgia Institute of Technology*


Date Approved: [Dec. 07, 2017]

To the most loving and caring parents,
*Sherif W. Agaiby* and *Amani R. Nashed*
To my beloved sister,
*Shireen W. Agaiby*

Thank you for giving me the tools to be successful in life
and the motivation to use them.

# ACKNOWLEDGEMENTS

I am deeply indebted to my mentor, thesis supervisor, research advisor, and my friend; Prof. Paul W. Mayne. Grateful acknowledgment is due for his endless sincere support, valuable guidance, motivation, continuous hard work, fruitful discussions, and comments throughout the course of this study. Dr. Mayne spared no effort to help me become a better researcher, writer, speaker, and presenter. Dr. Mayne pushed my boundaries to explore new potential and capabilities on both the professional and personal levels. I am grateful for the opportunities Dr. Mayne gave me throughout my journey at Georgia Tech from teaching to interacting with the industry and working with GDOT to attending and presenting at international conferences. Working closely with Dr. Mayne is a rewarding experience that has enriched me both professionally and personally.

I would also like to express my gratitude and appreciation to my guidance committee members: Dr. James D. Frost, Dr. Susan E. Burns, Dr. Sheng Dai, and Dr. Emanuele Di Lorenzo for their constructive feedback and valuable advice that enhanced the quality and the value of the presented research. I would also like to thank the faculty members at the Geosystems group for providing me with the needed knowledge through interesting challenging courses that helped me better understand and appreciate the merits of geotechnical engineering.

I would also like to thank the staff at the CEE Department who have helped me a lot and made the journey easier; Robert Simon, Daniela Estrada, Ellen Cormack, Jenny Eaton, and Mike Anderson. I would like to particularly thank Andrew Udell for his effort in

restoring the Georgia Tech cone truck and the anchorage system and his help in designing and manufacturing the rod rack.

I also wish to acknowledge the support and cooperation of my colleagues, office mates, and classmates during my study at Georgia Tech. The Geosociety was a much-needed outlet to balance the graduate student life and to encourage interdisciplinary research collaborations and discussions and to explore the culture and heritage of different international students. I would like to particularly thank my office mate Zhongkun Ouyang or as I call him Frankie for his amazing friendship, encouraging energetic spirit, cheerful personality, optimism and for being my true companion at Georgia Tech.

I also like to express my gratitude to my sponsors throughout the years I spent at Georgia Tech: ConeTec Investigations of Richmond, BC and Design House Consultancy of Dubai and the Georgia Department of Transportation. I would also like to express my thanks to the department of civil and environmental engineering, college of engineering, the in-situ testing research group and the Anne Robinson Clough fund for graciously providing me with travel grants and sufficient funds to cover my expenses for the international conferences I have participated in.

In addition, I can't forget the support and belief from my best friends: Hazem H. EL Anwar, Ali F. Helwa, Ahmed Khashila, Fatma Tarek and Albalyra Vargas who supported me as they always have despite the thousands of miles that were between us.

I would also like to thank my family in North America and Canada for their constant love, encouragement, and support. The Ishacs were always by my side from day one as I started my graduate studies in 2011 in MIT and shared every single step with me and the Megallys opened their hearts and houses providing the warmth and care of the family that

supported me through thin and thick. I would also like to thank aunt Karen and Shannon Mayne for always considering me a part of their family and for always including me in their celebrations and for being my second family away from home.

I would also like to thank Aunt Samar, Uncle Sherif, Noor and Farah for their endless encouragement and support. As for my loving grandparents, Geddo Makram, Teita Faiza, and Teita Lola: thanks for your endless love, continuous prayers, deep faith in me and for your moral support. I hope that with this achievement I can make you proud of me. Special thanks to my late grandfather Rafik who passed away before I finish my studies but who I am sure is watching me from heaven with a happy proud smile.

Finally, special appreciation and sincere deep gratitude are due to my parents Sherif W. Agaiby and Amani R. Nashed, and my sister Shireen W. Agaiby for their patience, encouragement, extraordinary contribution, and their continuous love and support throughout the course of this work.

Dad, you have given me the tools, the genes, the knowledge, and the strength to be the man I am right now. Thank you for believing in me. Mum, I cannot find the right words to express my gratitude and appreciation. I owe you everything, thank you for always being by my side empowering, inspiring, guiding my way and sharing my dream. Nina, you are my rock, true mirror and supporting back. Thank you for adding depth to my life. Thank you for bringing the best out of me. Thank you for joining me on this journey. Mum, Dad, and Nina; I owe this achievement to you.

## TABLE OF CONTENTS

## LIST OF TABLES

## LIST OF FIGURES

# SUMMARY

Seismic piezocone testing (SCPTu) offers an economic and expedient means for the modern collection of geotechnical data during site investigation of soils. It is actually a hybrid test that has all the advantages and the merits of classic cone penetration testing (CPT) where it obtains three continuous readings with the depth: cone tip resistance ($q_t$), sleeve friction ($f_s$), and porewater pressure ($u_2$); plus, geophysical component involving downhole testing, where shear wave velocity ($V_s$) measurements are recorded at 1-m depth intervals. The conducted study aims at making full usage of the four main readings obtained from the seismic piezocone test: cone tip resistance, cone sleeve friction, porewater pressure and downhole shear wave velocity.

New links between undrained shear strength and shear wave velocity are investigated and previous relationships between stress history and shear wave velocity are revisited and improved. A unified approach for estimating stress history of wide variety of geomaterials using net cone tip resistance is presented. Predictive equations for detecting sensitive clays from seismic shear wave velocity are introduced with a focus on sensitive and structured clays within North America. Modification of a hybrid spherical cavity expansion theory- critical state soil mechanics solution is introduced addressing the stress history of sensitive and structured clays. A new analytical approach allows the direct assessment of undrained rigidity index from CPTu data which finds value in assessing undrained shear strength, yield stress, and coefficient of consolidation, the latter from piezodissipation tests. The special nature and difficulties of organic clays are discussed and an indirect means of detecting their existence using piezocone testing is presented. Finally, an effort is undertaken to calibrate an analytical model for evaluating the undrained shear strength and stress history of clays using two large databases

# Chapter 1. INTRODUCTION

## 1.1 Motivations and Research Objectives

Seismic piezocone testing (SCPTu) offers an economic and expedient means for the modern collection of geotechnical data during site investigation of soils. It is actually a hybrid test that has all the advantages and merits of classic cone penetration testing (CPT) where it obtains three continuous readings with depth: cone tip resistance ($q_t$), sleeve friction ($f_s$), and porewater pressure ($u_2$); plus a geophysical component involving downhole testing (DHT), where shear wave velocity ($V_s$) measurements are recorded at 1-m depth intervals. A diagram illustrating the seismic piezocone penetration testing is presented in **Figure 1.1**. If desired, the additional monitoring of porewater pressure dissipations with time provides a fifth reading ($t_{50}$), thus designated SCPTù.

The test was introduced some three decades ago (Campanella et al. 1986) and is finally gaining acceptance as a reliable and valuable tool in the arsenal of in-situ geotechnical testing methods. Accordingly, SCPTù is an optimal means of collecting information about the subsurface stratigraphy and quantification of many geoparameters, including unit weight, stress history, strength, stiffness, geostatic stress state, and permeability. To illustrate the measurements obtained by SCPTu, **Figure 1.2** presents the results of a deep seismic piezocone sounding with readings of $q_t$, $f_s$, $u_2$ and $V_s$ with depth. The sounding extending to a depth of 130 m was conducted by ConeTec at a test site in Vancouver, Canada.

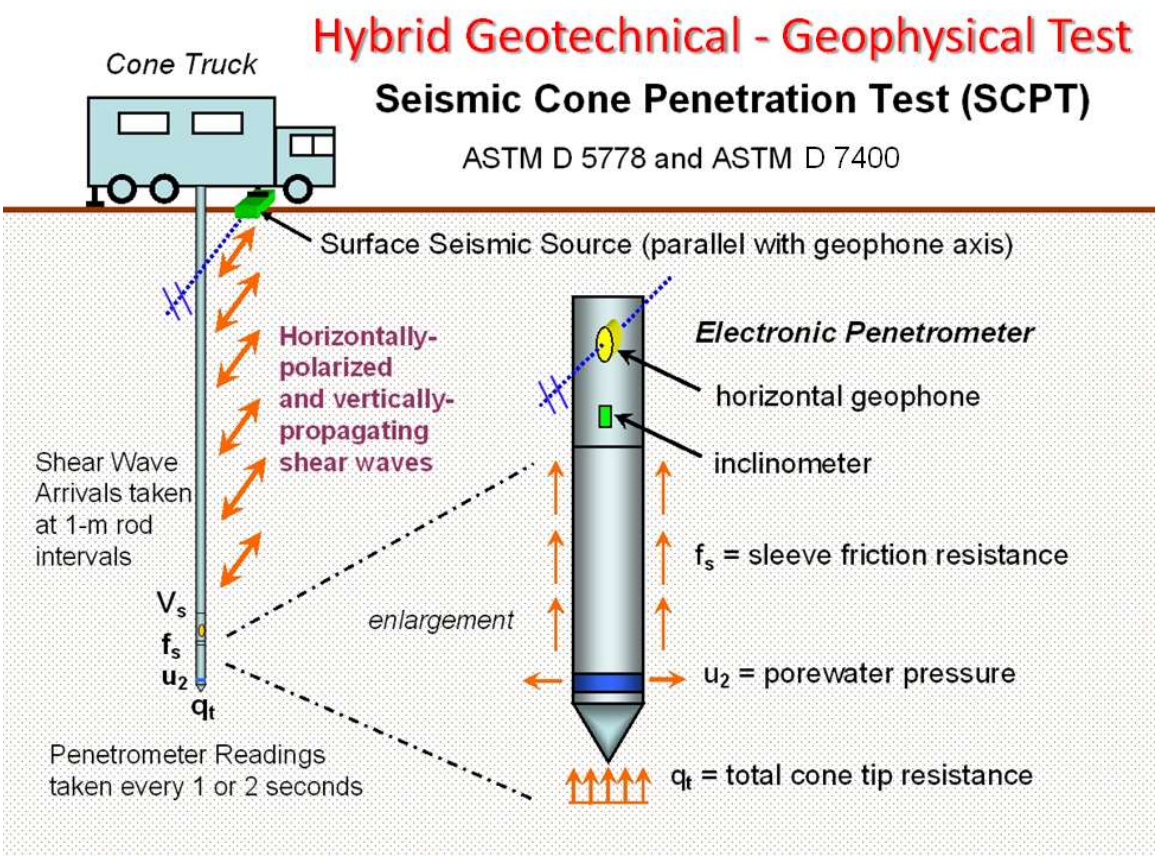


Figure 1.1. Illustration of the seismic cone penetration test (SCPT)

This research program offers improvements to the interpretation of CPTu and SCPTu data obtained during geotechnical site characterization, with the main focus on the undrained behavior of clays and clayey geomaterials, including shear strength, stress history, and rigidity index. Where possible, evaluations have been made within an effective stress framework, specifically utilizing concepts from critical state soil mechanics. In addition to addressing results obtained in well-behaved normal clays that are inorganic and have low to medium sensitivity, special attention has also been given towards application of CPTu and/or SCPTu in organic clays, sensitive clays, and structured clays. With regard

to yield stress evaluations, a simplified approach to CPT interpretations for all types of soils has been developed, including clays, silts, sands, and mixed geomaterials.

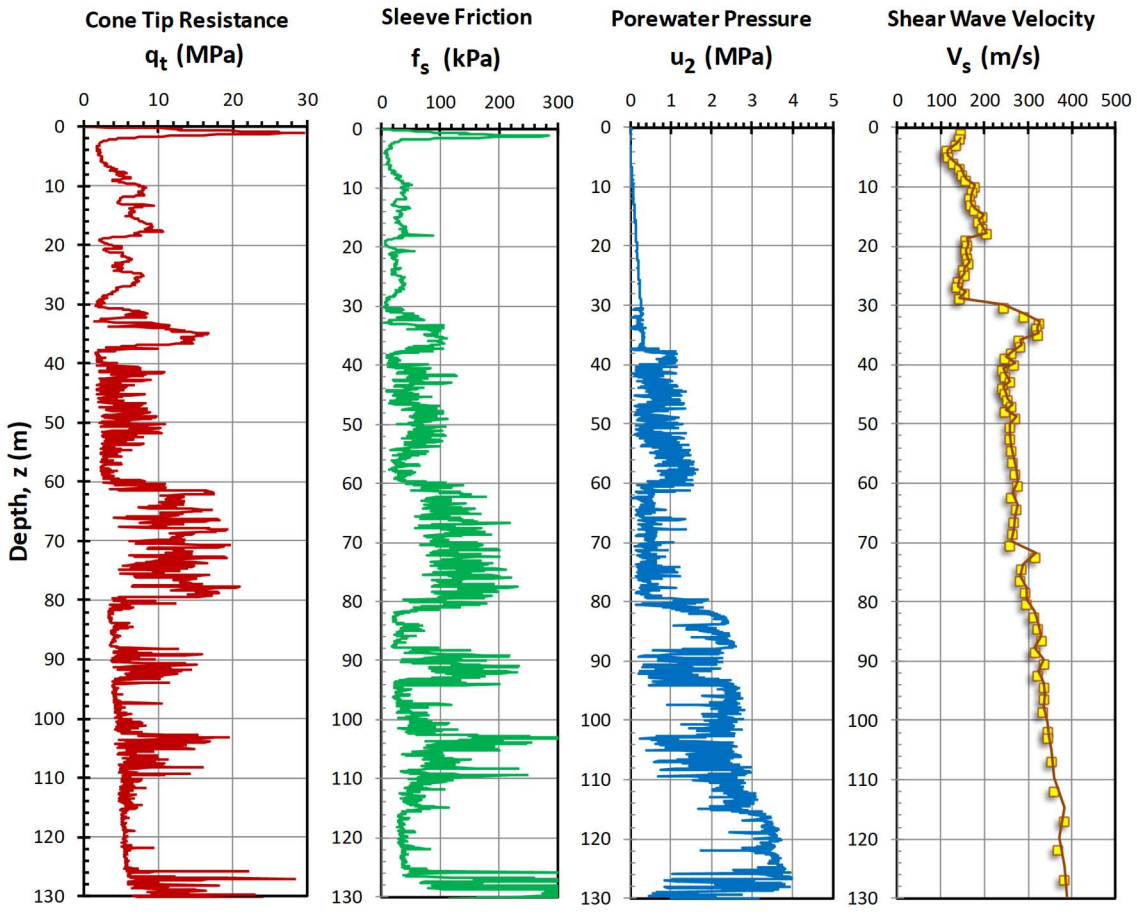


Figure 1.2. Example of deep seismic piezocone soundings conducted in Vancouver by ConeTec showing: (a) cone tip resistance, $q_t$, (b) sleeve friction, $f_s$, (c) penetration porewater pressure, $u_2$, and (d) shear wave velocity, $V_s$

The conducted study aims at making full usage of the four main readings obtained from the seismic piezocone test: cone tip resistance, cone sleeve friction, porewater pressure and downhole shear wave velocity. New links between undrained shear strength and shear wave velocity are investigated and previous relationships between stress history and shear wave velocity are revisited and improved. A unified approach for estimating

stress history of different geomaterials using net cone tip resistance and CPT material index is presented. Predictive equations for detecting sensitive clays from seismic shear wave velocity are introduced with a focus on sensitive clays within North America.

Modification of a hybrid spherical cavity expansion theory-critical state soil mechanics solution is introduced addressing the profiling of stress history of sensitive and structured clays. A new analytical approach allows the direct assessment of undrained rigidity index from CPTu data which finds value in assessing undrained shear strength, yield stress, and coefficient of consolidation, as well as applications involving foundation bearing capacity. The special nature and difficulties of organic clays are discussed and an indirect means of detecting their existence using piezocone testing is presented. Finally, an effort is undertaken to calibrate a more versatile analytical model for evaluating the undrained shear strength and stress history of clays using two large databases. **Figure 1.3** presents a summary diagram highlighting the main studies conducted in the dissertation.

## 1.2 Research Outline and Thesis Structure

The dissertation is divided into nine more chapters, as listed below:

- *Chapter 2 - Field Testing at Georgia Tech W-21 Experimental Site,* this chapter presents a summary of field testing conducted at testing site W-21 located at the Georgia Institute of Technology campus near the intersection of Hemphill Street and Ferst Drive in Atlanta, Georgia, USA. The site is underlain by native residual soils of the Piedmont geologic province. These are mainly silty soils, ranging from micaceous fine sandy silts to silty fine sands that grade with depth to saprolites and partially-weathered rocks (PWR), eventually reaching bedrock refusal. The performed field geotechnical site

investigations included: seismic cone penetration tests (SCPTu), flat plate dilatometer tests (DMT), continuous-interval seismic piezocone testing (CiSCPTu), non-invasive Rayleigh waves measurements for shear wave velocity using multi-channel analyses of surface waves (MASW), and helical probe tests (HPT). This chapter was partially published in Agaiby et al. (2016) in the Proceedings of the 5th International Conference on Geotechnical & Geophysical Site Characterization (ISC-5), Gold Coast, Australia. The helical probe testing section was submitted and approved for publication in Agaiby et al. (2017) in *Geomechanics and Geoengineering: An international Journal*.

- Chapter 3 - *Interpretation of Geotechnical Parameters using In-Situ Data for The Bolivian Experimental Site for Testing (B.E.S.T.),* the engineering properties of the Bolivian Experimental Site for Testing (B.E.S.T.) are examined in detail based on the field results of the geotechnical site investigation. The performed investigation includes four main in-situ tests: Standard Penetration Tests (SPT), Cone Penetration Tests (CPTu), Flat Plate Dilatometer Tests (DMT), and Downhole Shear Wave Velocity ($V_{sVH}$). The in-situ testing program was comprised of 8 SPTs, 15 CPTus, 6 DMTs, and 3 $V_{sVH}$ measurements. Complementary laboratory tests included: grain size distribution, water content, plastic and liquid limits tests. Practical methods from the literature for estimating the geotechnical properties of the site from in-situ tests are discussed with a presented comparison between the interpreted values from the different in-situ methods. The investigated design parameters include soil type, unit weight ($\gamma_t$), effective friction angle ($\phi$'), stress history (OCR), and elastic shear modulus (E). This chapter was published in Agaiby & Mayne (2017) in the proceedings of the 3rd Bolivian Conference on Deep Foundations, 2017 at Universite Privada de Santa Cruz de la Sierra.

- Chapter 4 - *Stress History Evaluation of Soils from Piezocone.* Here, a generalized methodology is presented for evaluating the stress history of a wide variety of soils from piezocone data, where stress history is represented in terms of a yield stress or effective preconsolidation stress ($\sigma_p'$), as commonly interpreted from laboratory one-dimensional consolidation tests. A well-established analytical model developed as a hybrid of spherical cavity expansion theory combined with critical state soils mechanics (SCE-CSSM) is used as a basis for defining stress history in intact well-behaved clays from net cone tip resistance ($q_{net} = q_t - \sigma_{vo}$). For clean quartz-silica sands, CPT results from 26 series of calibration chamber testing defined a statistical stress history relationship from net cone tip resistance. A resemblance between the two simplified expressions for intact clays and clean sands guided the formulation of a generalized expression for evaluating yield stress from net cone resistance for a wide variety of soil types. A comprehensive database of 78 worldwide sites covering many types of geomaterials ranging from clays to silts to sands and mixed soil types was compiled and a unified relationship was formulated in terms of a power law function.

The algorithm expresses yield stress in terms of net cone tip resistance having an exponent designated m' which increases with fines content (FC) and decreases with particle size ($D_{50}$). Moreover, direct relationships for m' with several pre-defined CPT material indices ($I_{cR\&W}$, $I_{cJ\&B}$, $I_{SBT}$, $I_B$) are investigated and their reliability is discussed for uncemented and inorganic soils of low-medium sensitivity. Several case studies are presented showing the agreement between the CPT-estimated stress history profile using the interpreted exponent value and the laboratory measured values from consolidation tests. Special considerations must be undertaken when applying the methodology to sensitive

fine-grained soils, organic clays, and fissured geomaterials. Results from this chapter are prepared to be published in Agaiby & Mayne (2018) – *In preparation*.

- Chapter 5 - *Evaluating Undrained Rigidity Index of Clays from Piezocone Data.* This chapter presents a review on the evaluation of undrained rigidity index of clays ($I_R = G/s_u$), including laboratory testing, empirical correlations, and analytical methodologies that are on record. Using the hybrid spherical cavity expansion – critical state framework, an expression is derived for obtaining the operational rigidity index ($I_R$) directly from post-processing of CPTu data, specifically using the cone tip resistance and porewater pressure readings, or their normalized quantities. The evaluated rigidity indices are in reasonable agreement with reference laboratory-based and seismic-based in-situ approaches.

Using data from 12 well-documented clay sites, the derived values of $I_R$ values are used to evaluate the yield stress profiles using three expressions obtained from the SCE-CSSM framework, based on: (a) net cone resistance: $q_{net} = q_t - \sigma_{vo}$; (b) excess porewater pressure: $\Delta u = u_2 - u_o$; and effective cone resistance: $q_E = q_t - u_2$. The acquired value of $I_R$ is also input into the cone bearing factor ($N_{kt}$) to obtain the undrained shear strength, where $s_u = q_{net}/N_{kt}$. For the case studies, it is shown that the three separate CPTu profiles of $\sigma_p'$ generally agree with lab reference values from consolidation tests and the corresponding CPTu profiles of undrained shear strength values match well with laboratory results, usually obtained from the triaxial compression mode (CAUC or $CK_0UC$).

- Chapter 6 - *SCPTu identification of sensitive clays in North America.* A review is made of the various CPT soil classification schemes that are available, along with

their corresponding soil behavioral type (SBT) charts and post-processing schemes. The shortcomings of the available SBT methods in correctly and adequately identifying sensitive fine-grained geomaterials by CPTu are discussed. It is shown that the shear wave velocity ($V_s$) measured during seismic piezocone (SCPTu) testing can be utilized as an independent means of identifying sensitive clays, specifically in North America. Commonly-used correlations of estimating shear wave velocity from CPTu data were examined and generally found unsatisfactory for use in sensitive clays. Hence, by comparing measured $V_s$ with estimated $V_s$ profiles using standard correlative trends helps identify when sensitive clays may exist within a soil profile. A special database developed from 20 sensitive clays from Canada and the northern USA was compiled and two recent correlations (NGI: L'Heureux & Long 2016) and KIGAM: Sun et al. 2013) were modified for estimating shear wave velocity from CPTu data in sensitive clays. Results from this chapter are under preparation to be published in Agaiby & Mayne (2018) – *In preparation*.

- Chapter 7 - *Modified Cavity Expansion - Critical State Solution for Evaluating Stress History and Piezodissipation from CPTu in Sensitive or Structured Clays.* In this section, an established CPTu analytical solution based on spherical cavity expansion and critical state soil mechanics (SCE-CSSM) is employed for assessing the effective yield stress ($\sigma_p'$), undrained shear strength ($s_u$), and flow rate parameter ($c_v$) in sensitive and/or structured clays. Examining the results of CAUC and CIUC triaxial tests on structured sensitive to quick clays, it is evident that there is strain incompatibility between the deviator stress and excess porewater pressures that peak at different levels of strain. A modified-CSSM approach is devised that utilizes the mobilized effective stress friction angle ($\phi'$) defined at two points: (a) maximum deviatoric stress ($\phi'_{qmax}$), corresponding to the cone tip

resistance ($q_t$); and (b) maximum obliquity ($\phi'_{MO}$), relating to the measured CPTu porewater pressure ($u_2$).

A direct CPTu means of assessing the undrained rigidity index for sensitive and structured clays in a reliable manner is also developed. This is shown to provide good agreement with profiles of undrained shear strength ($s_{uTC}$) obtained from triaxial compression tests (CIUC, CAUC, and/or $CK_0UC$). The modified solution is implemented on data from three sites: (1) sensitive Leda clay at Gloucester, Ontario; (2) sensitive-quick clay at Tiller, Norway, and (3) structured varved clay at Amherst, Massachusetts. The OCR and $s_{uTC}$ profiles interpreted from CPTu soundings agree well with results from laboratory consolidation and triaxial testing, respectively, for all three sites.

For dissipation testing in sensitive and/or structured clays, the original SCE-CSSM solution (Burns 1998) is utilized without alternation to assess the coefficient of consolidation ($c_{vh}$), yet specifically using $\phi'_{MO}$ as the input value for excess porewater pressure calculations. While the solution requires a trial-and-error iteration for rigorous assessments involving monotonic and/or dilatory porewater pressure behavior, a simplified solution for monotonic curves is presented. For the sensitive Gloucester clay, interpreted profiles of $c_{vh}$ and hydraulic conductivity (k) with depth from piezodissipations are shown comparable with independent values obtained from benchmark laboratory and field tests. For the special case where $\phi'_{qmax} = \phi'_{MO}$, then the modified SCE-CSSM solution collapses to the original model that is applicable to CPTus in inorganic "well-behaved" clays and clayey silts of low to medium sensitivity. Results from this chapter were published in McQueen et al. (2016)- *Canadian Geotechnical J.* and in Agaiby and Mayne (2018) – *In preparation*.

- Chapter 8 - *Organic Clay Detection Using CPTu*. The special nature of organic soils, which are highly compressible and exhibit very low undrained shear strengths is noted, thus highlighting their problematic issues and unfavorable engineering properties. During CPTu, soil sampling is not normally performed and thus the identification of organic versus inorganic soil becomes important. There are no direct CPT methods for detecting the organic matter, hence soil behavior type charts can be used as a preliminary screening means for soil type. A database derived from 23 organic soils subjected to piezocone testing was used to develop a more reliable approach for (a) identification of organic clays, and (b) assessing yield stress profiles in such deposits. It is shown that the CPTu excess porewater pressure readings ($\Delta u_2$) can be used to help indicate the presence of organic clays if compared to the net cone tip resistance ($q_{net}$). This study used three predictions from the hybrid SCE-CSSM framework for estimating the yield stress in defining a hierarchical behavior where the porewater pressure-based prediction was found the smallest followed by the net cone tip resistance then the effective cone tip resistance. The mismatch in the three predictions indicates the absence of well-behaved inorganic insensitive clays and suggests the presence of organic soils. It is noted that the order of this hierarchical behavior is opposite to what is observed in sensitive and structured clays.

- Chapter 9 - *Calibrating an advanced analytical CPTu model for undrained shear strength and yield stress in clays.* Here, an advanced analytical model for representing undrained shear strength and stress history of clays is explored using a more versatile cone bearing factor expression based on finite element results which consider rigidity index ($I_R$), soil-cone interface roughness ($\alpha_c$), and initial stress state ($K_0$). Two

comprehensive databases were carefully collected for both undrained shear strength under triaxial compression shearing and stress history covering various clay types from well-documented worldwide geotechnical sites. An anisotropic simple plastic model was utilized in developing the link between the stress history and undrained shear strength with a rotated yield surface about the $K_0$-line. The failure mode around the cone tip was addressed to provide five different definitions for the shear-induced excess pore water pressure around the cone. Based on the predictions of both the undrained shear strength and stress history models, it was observed that the simple shear mode provided better agreement with the trends observed from the collected databases.

- Chapter 10 – *Conclusions and Future Work*.

At the end of the dissertation, 10 appendices are compiled presenting the raw data and carried out analyses covered in different chapters as follows:

- Appendix A – Intact clays: Piezocone Soundings with Shear Wave Velocity, Undrained Shear Strength and Stress History Data.
- Appendix B – Silts: Piezocone Soundings with Shear Wave Velocity, Undrained Shear Strength and Stress History Data.
- Appendix C – Sands: Piezocone Piezocone Soundings with Stress History Data.
- Appendix D – Organic clays: Piezocone Soundings with Stress History and Undrained Shear Strength Data.
- Appendix E – Sensitive clays: Piezocone Soundings with Shear Wave Velocity, Undrained Shear Strength and Stress History Data.
- Appendix F – Fissured and highly overconsolidated clays: Piezocone Soundings with Shear Wave Velocity, Undrained Shear Strength and Stress History Data.

- Appendix G- Seismic Piezocone Soundings with Soil Behavioral Type Classifications and Shear Wave Velocity Predictions for Sensitive Clays in North America.
- Appendix H - Additional Plots for Calibration of Analytical Model for Estimating Undrained Shear Strength in Clays.
- Appendix I - Derivation of OCR Expressions for Calibration of Analytical Model for Estimating Stress History in Clays.

Additional studies covering the relationships between downhole shear wave velocity ($V_{sVH}$) and undrained shear strength ($s_u$) and stress history ($\sigma_p'$) of clays are presented in the following appendices:

- Appendix J - Relationship between Undrained Shear Strength and Shear Wave Velocity for Clays, by Agaiby and Mayne (2015) published in the 6th International Symposium on Deformation Characteristics of Geomaterials, Vol. 6, Buenos Aires, Argentina.
- Appendix K - Use of Shear Wave Velocity to Estimate Stress History and Undrained Shear Strength of Clays, by Agaiby and Mayne (2016) published in the 5th International Conference on Geotechnical & Geophysical Site Characterization, ISC-5, Jupiters Gold Coast, Australia.
- Appendix L - Evaluation of undrained shear strength and stress history in intact clays using seismic piezocone tests, by Agaiby et al. (2016) published in the 69th Canadian Geotechnical Conference: GeoVancouver 2016, Vancouver, Canada.

In addition, the findings of an implementation study conducted for the Georgia Department of Transportation (GDOT) are presented. This provides a methodology for the sizing of spread footing foundations for GDOT bridge structures and retaining walls which address AASHTO design recommendations in computing bearing stresses and corresponding settlements by changing from Allowable Stress Design (ASD) to Load Resistance Factor Design (LRFD):

- Appendix M - Geotechnical LRFD Calculations of Settlement and Bearing Capacity of GDOT Shallow Bridge Foundations and Retaining Walls.

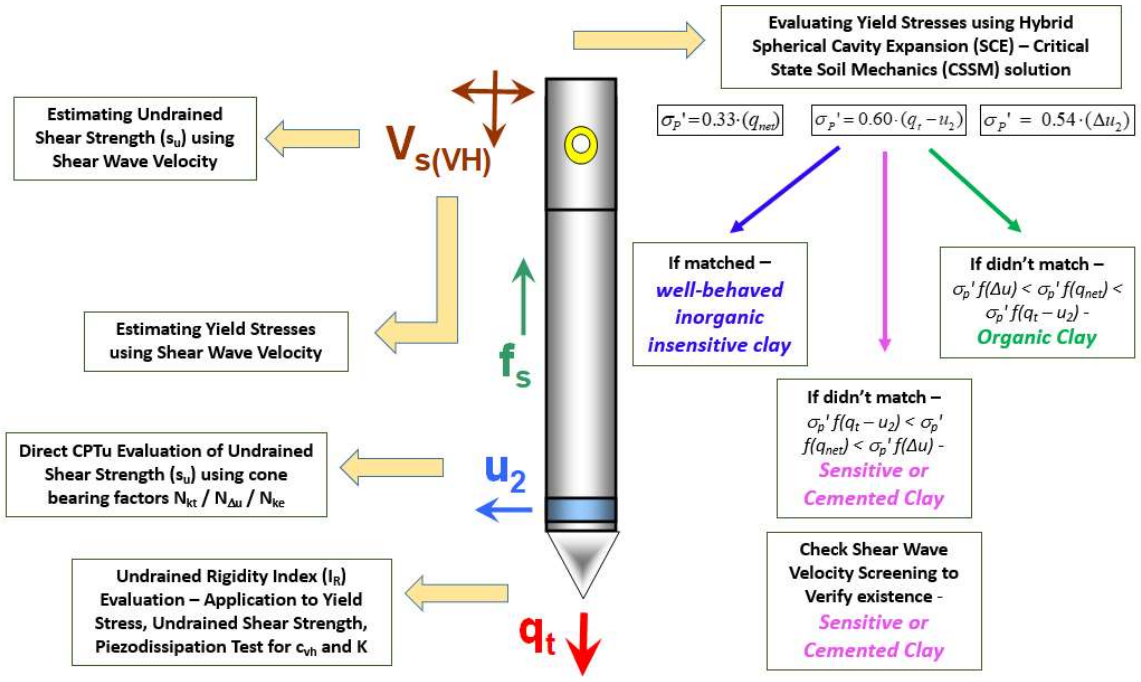


Figure 1.3. Diagram highlighting the main studies conducted in the dissertation making usage of the readings of the seismic piezocone test

# Chapter 2. Field Testing at Georgia Tech W-21 Experimental Site

## 2.1 Introduction

A variety of in-situ tests were performed at the GT campus during 2012-2017. This chapter presents a summary of these field testing conducted at testing site W-21 which is a parking lot located northwest of the CEE Mason Building in Atlanta. The site is underlain by native residual soils of the Piedmont geologic province. These are mainly silty soils, ranging from micaceous fine sandy silts to silty fine sands that grade with depth to saprolites and partially-weathered rocks (PWR), eventually reaching bedrock refusal. At this site, PWR is encountered at about 12.8 m (42 feet) with groundwater variable but often found at depth of 12 m (40 feet). The performed field geotechnical site investigations included: seismic cone penetration tests (SCPTu), flat plate dilatometer tests (DMT), continuous-interval seismic piezocone testing (CiSCPTu), non-invasive Rayleigh waves measurements for shear wave velocity using multi-channel analyses of surface waves (MASW and ReMi), and helical probe tests (HPT).

## 2.2 Geology of the state of Georgia

The state of Georgia is composed of four separate geologic areas, as illustrated by **Figure 2.1**: Piedmont; Blue Ridge, Coastal Plain, and Valley & Ridge/Plateau. As such, the natural soils and rocks, as well as compacted fills made from native geomaterials in these regions, can behave somewhat differently from each other. We can group the Appalachian Piedmont and Blue Ridge together due to their similarity. At one time, a range of mountains over 12 km in height dominated the region but have since essentially vanished

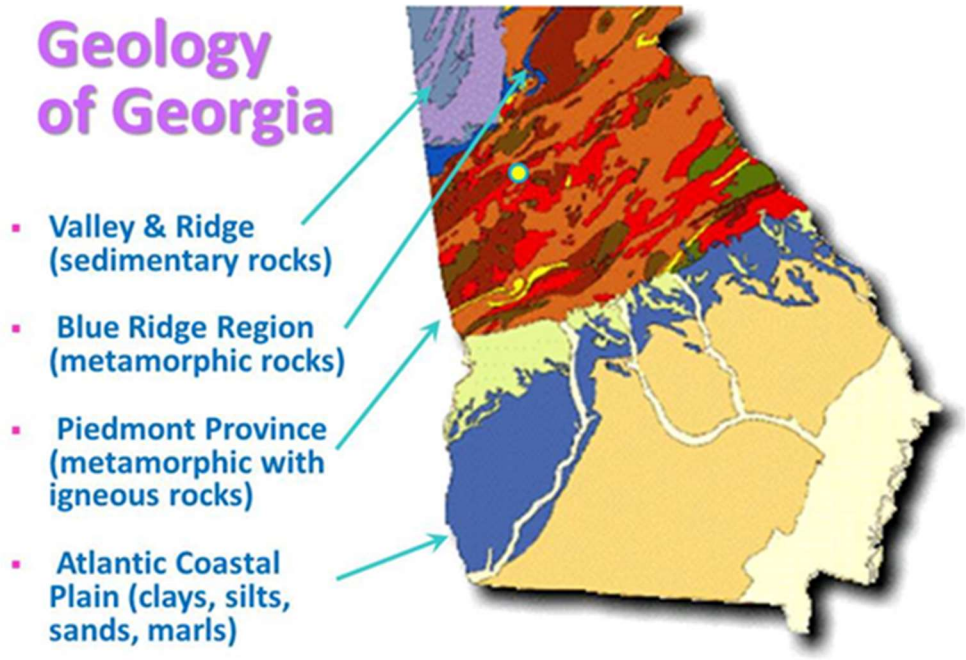


Figure 2.1. Geology of the State of Georgia

due to extensive erosion, weathering, decomposition, and exposure to the elements over many millennia (Chew 1993). Parent bedrock is comprised primarily of gneiss and schist of Pre-Cambrian Z-age, with lesser amounts of igneous intrusives (granites) that appeared in Paleozoic times. The ground is underlain by residuum derived by the in-place weathering of metamorphic and igneous bedrock. The residual soils are often found to be silty, ranging from micaceous fine sandy silts to silty fine sands, that transition with depth to saprolites, partially-weathered rocks, and bedrock refusal. Locally, the layman's term for the upper few centimeters of native soils is called "Georgia red clay" due to the red-orange-tan colors due to iron oxides. **Figure 2.2** illustrates a subsurface profile of the Appalachian Piedmont. In contrast, the Coastal Plain consists of various marine sediments that were deposited in various times ranging from very old Cretaceous to Miocene to recent Holocene ages, including complex interbedding of clays, silts, sands, and gravels. Finally, the Valley &

Ridge/Plateau include sedimentary type bedrocks (shales, limestones, sandstones) that have also produced a clayey to sandy type residuum cover, as well as karstic terrain, sinkholes, and caves (Weary, 2005).

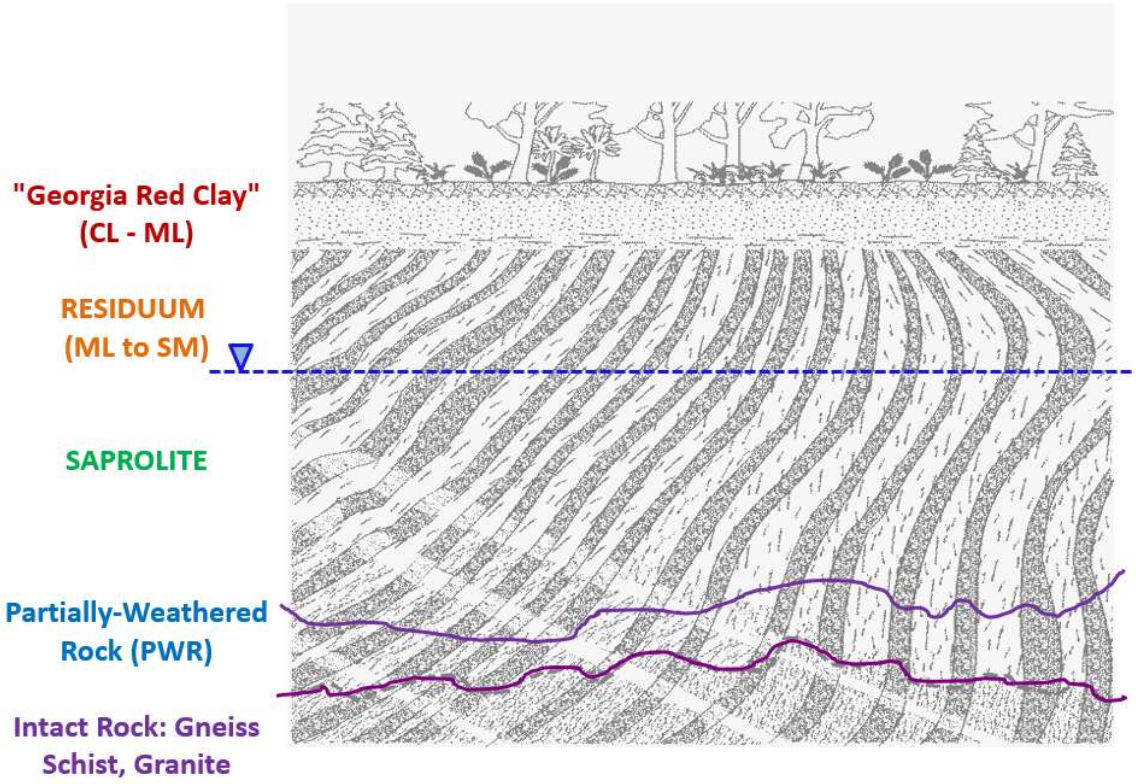


Figure 2.2. Piedmont subsurface profile

## 2.3 Seismic Cone Penetration Testing (SCPTu)

The cone penetration test (CPT) involves the hydraulic pushing of an instrumented steel probe at a constant rate to obtain continuous vertical profiles of stress, friction, and pressure with depth. Cone penetration testing can be conducted for measurement of tip and sleeve resistances (i.e., CPT) or the additional readings of penetration porewater pressures using a piezocone (i.e., CPTu). Some equipment includes the ability to measure shear wave

velocities, called a seismic piezocone test and designated SCPTu. The data presentation from an SCPTu sounding includes cone resistance ($q_t$), sleeve friction ($f_s$), porewater pressures ($u_2$), and downhole shear wave velocity ($V_{sVH}$) plotted with depth in side-by-side graphs.

A standard cone penetrometer is a 35.7-mm diameter cylindrical probe with a 60° apex at the tip, 10-$cm^2$ cross-sectional area, and a 150-$cm_2$ sleeve surface area. More robust penetrometers are available with a 44-mm diameter body, a 15-$cm^2$ projected tip area, and 200- to 225-$cm^2$ sleeve surface area. For a piezocone penetration test (CPTu), the penetration porewater pressures are monitored using a transducer and porous filter element. Porewater readings can be taken at the apex or mid-face (designated $u_1$), shoulder (just above the cone tip, or $u_2$), or behind the sleeve ($u_3$). The standard required position per ASTM D 5778 is the shoulder position (type 2) because the $u_2$ value is required for the correction of tip resistance. Filter elements consist of high-density polypropylene, ceramic, or sintered metal. Fluids for saturation include water, glycerine, or silicone. For the seismic piezocone test, a geophone is located approximately 500 mm uphole from the cone tip. The geophone detects shear waves generated at the ground surface at depth intervals of approximately 1-meter, corresponding to successive rod additions (Agaiby & Mayne, 2016).

Over the past few years, the testing site at W-21 has been used for class demonstration and geotechnical field characterization. A large 25-tonne cone truck was used by ConeTec for performing the invasive downhole test (DHT) via ASTM D 7400 using seismic piezocone testing. Four standard seismic piezocone soundings (SCPTu) conducted in 2014; 2015; and 2016 with pseudo-interval arrays at 1-m depth intervals

where paired sets of left and right strikes were accomplished using a sledgehammer and beam arrangement. **Figure 2.3** presents an example of filtered 1-m interval paired left and right strike raw shear wave signals from SCPTu-A that are used in evaluating the shear wave velocity profile.

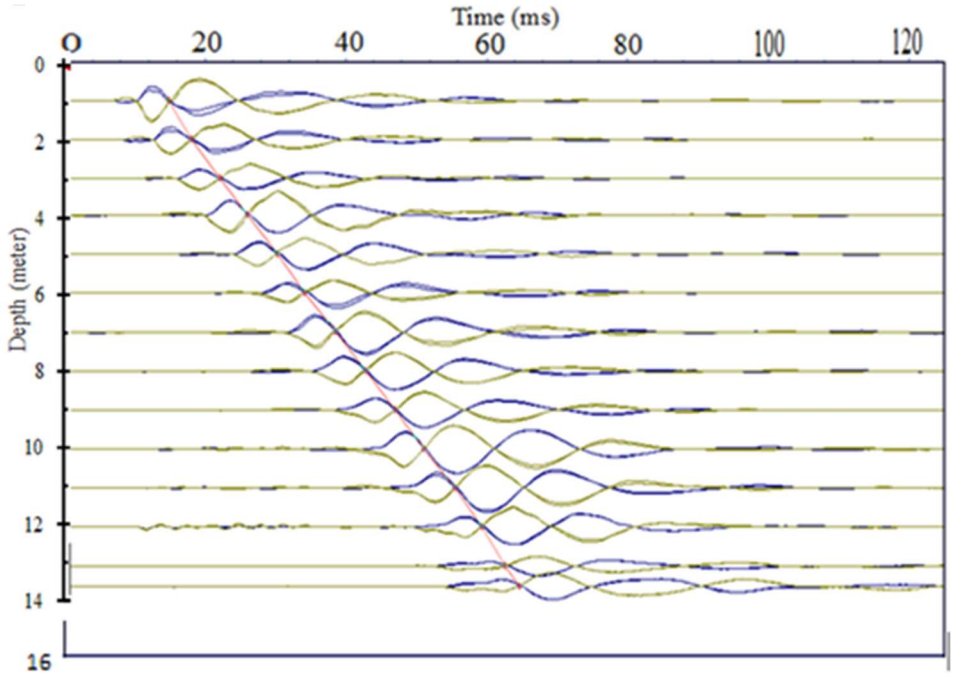


Figure 2.3. Filtered 1-m interval paired (left and right strike) shear wave signals from SCPTu-A at the Georgia Tech W21 test site

**Figure 2.4** summarizes the four seismic piezocone soundings conducted at W-21 test site over 3 years with soundings A and B conducted in 2014, sounding C in 2015 and sounding D in 2016.

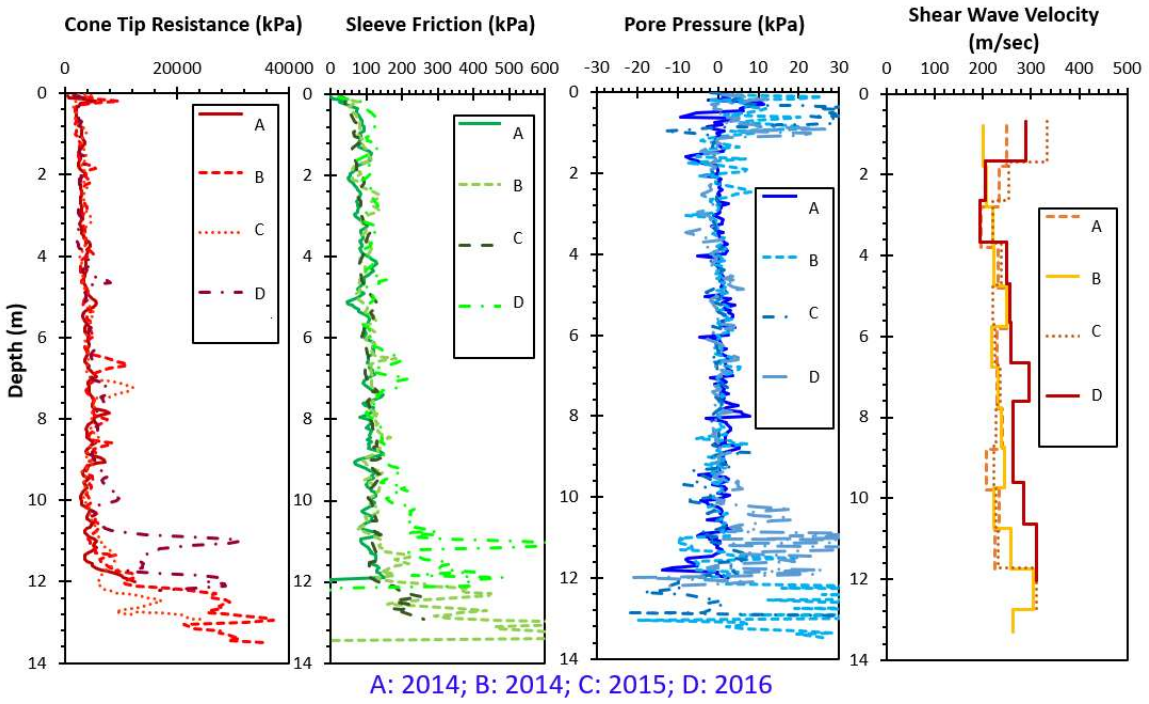


Figure 2.4. Seismic piezocone soundings conducted at Georgia Tech campus by ConeTec showing: (a) cone tip resistance, $q_t$, (b) sleeve friction, $f_s$, (c) penetration porewater pressure, $u_2$, and (d) shear wave velocity, $V_{sVH}$

By comparing the four $V_s$ profiles over the 3 years, a clear increase in the magnitude of velocity is observed within the crust top 4 meters that may be attributed to the possibility of capillarity, desaturation, or effective stress changes in the vadose zone (soil above water table which was found to be at a depth of 12.5 meters) where soils in unsaturated states may have an increase in the Vs at shallow depths (Cho & Santamarina, 2001).

## 2.4 Continuous-interval Seismic Cone Penetration Testing (CiSCPTu)

### *2.4.1 Introducing the Rotoautoseis*

The conventional geophysical techniques carried out in boreholes such as crosshole and downhole tests are relatively slow and sometimes inconvenient as they require a

number of procedures including rotary drilling, installation of plastic casing, grouting, slope inclinometer, and positioning of geophones for seismic readings. Many of these obstacles are overcome using direct-push technologies such as seismic cone penetration test (SCPT) or seismic dilatometer test (SDMT) where the vertically-propagating horizontally-polarized shear wave velocity, or $V_{sVH}$ mode, is measured at regular intervals of 1m without the need for drilled-cased-grouted boreholes. However, direct-push techniques usually generate the $V_s$ profile at 1-m intervals as the advancing probe stops at the rod breaks which can affect the resolution and the quality of the measured shear wavelets. To obtain a more detailed clear successive continuous shear wave velocity profile with a higher resolution and expedited shorter field testing time, a portable automated triggering system named "rotoautoseis" has been developed and introduced by Mayne and McGillivray (2008) as pictured in **Figure 2.5**. Together with an enhanced data acquisition system, the automatic seismic surface source can generate consistent repeatable strikes via an electromechanical gear system per every 1 to 10 seconds. Additional details with basic schematic and diagrams of the rotoautoseis are presented by McGillivray and Mayne (2008).

The automated impulse source system can be used with conventional piezocone testing to generate continuous shear waves during the standard penetration rate of 20 mm/sec. Thus, all readings ($q_t$, $f_s$, $u_2$, $V_s$) are collected during non-stopping cone pushing and the test is called continuous-interval seismic piezo-cone test (CiSCPTu).

Figure 2.5. Georgia Tech electromechanical rotoautoseises

Since a significantly larger number of shear wavelets are generated and measured, a consequence is that more sophisticated and elaborate techniques are needed for interpreting the signals and evaluating the shear wave velocity profile data. Careful post-processing analyses are required to handle errors from noisy signals, overlapping refracted and reflected wavelets, and readings taken over very short distance intervals. A brief description of the post-processing procedure for continuous shear wave profiling is presented herein with fuller details presented elsewhere (Ku & Mayne 2012; Ku et al., 2013a, 2013b).

In 2015, a CiSCPTu sounding was carried out at the W-21 test site, a series of successive shear wave measurements were obtained using a rotoautoseis, a 15 $cm^2$ cone with a biaxial geophone positioned 0.2 m above the cone tip, and an equipped cone truck. The automated triggering system provided uni-directional strikes for the series of

continuous shear waves where it was situated at ground level with a horizontal offset of about 1m from the CPT rod string axis. **Figure 2.6** presents successive raw shear wave signals recorded from special continuous-push where with the continuous pushing and advancement of the piezocone, shear wavelets are generated at the ground surface every 5 seconds.

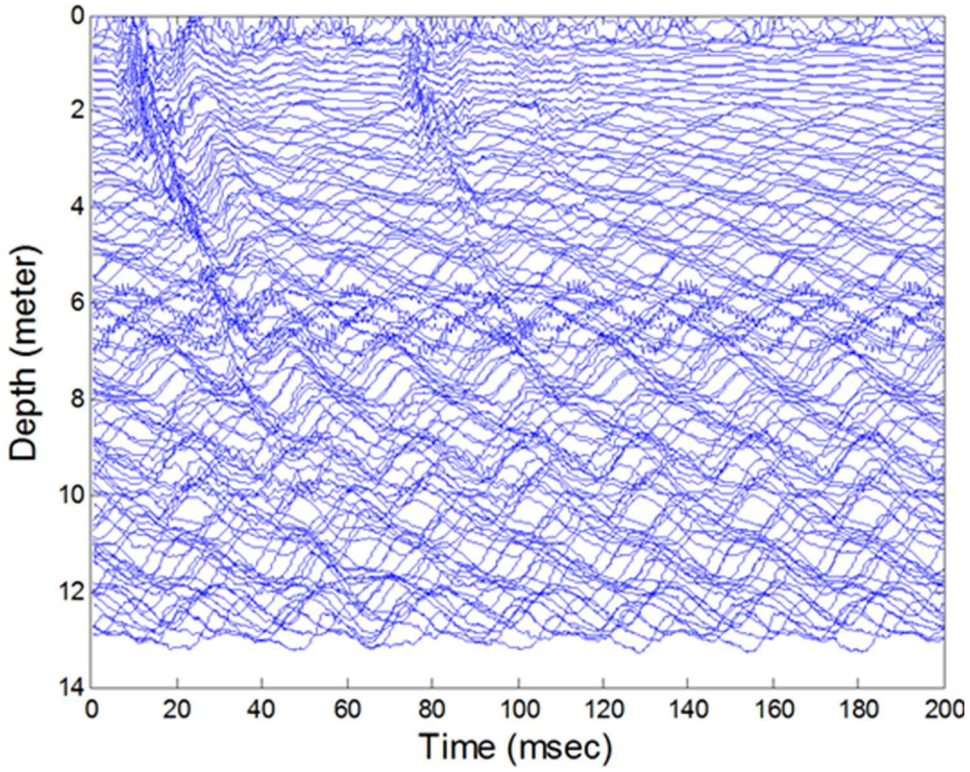


Figure 2.6. Successive raw continuous shear wave data from automatic seismic source at the Georgia Tech W21 test site (Agaiby et al., 2016)

### *2.4.2 Signal Processing*

Shear wave time series signals should first be detrended and then filtered in order to eliminate any noise or interference in the measured wavelets. Detrending is a statistical operation for removing ab-normal unexpected trends or any signal distortion such that the

detrended raw data signals approach a baseline value. Filtering should be carefully conducted at the lowest possible level in both time and frequency domains to reduce the noise level (Santamarina & Fratta 1998, Ku et al. 2013a). In the current study, noise levels were mitigated using a band-pass filter to capture the desired frequency range of interest as presented in **Figure 2.7** where a low- and high-cutoff frequency filter ranging from 150Hz to 350Hz was applied on the basis of visual examinations of fluctuations in signals.

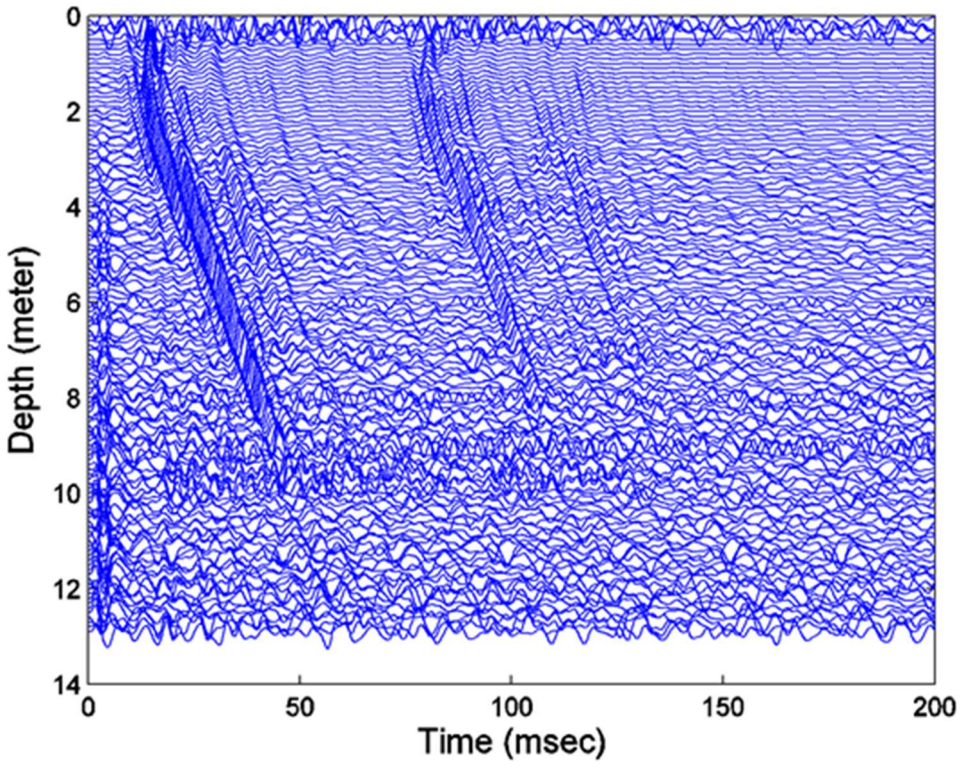


Figure 2.7. Successive continuous shear wave data after applying a band filter ranging from 150Hz to 350Hz (Agaiby et al., 2016)

After applying a band-pass filter to the raw wavelets, windowing was used to minimize the effect of spectral leakage of the data (Santamarina & Fratta 1998) and to provide better Vs evaluations for the cross-correlation method (Liao & Mayne 2006). **Figure 2.8** shows the filtered successive continuous shear wavelets after windowing where

only the zone of interest for the expected main shear wave remains. Typically, a combined window using both a rectangular window for the majority of the signal and a hamming window for the tailing areas is applied.

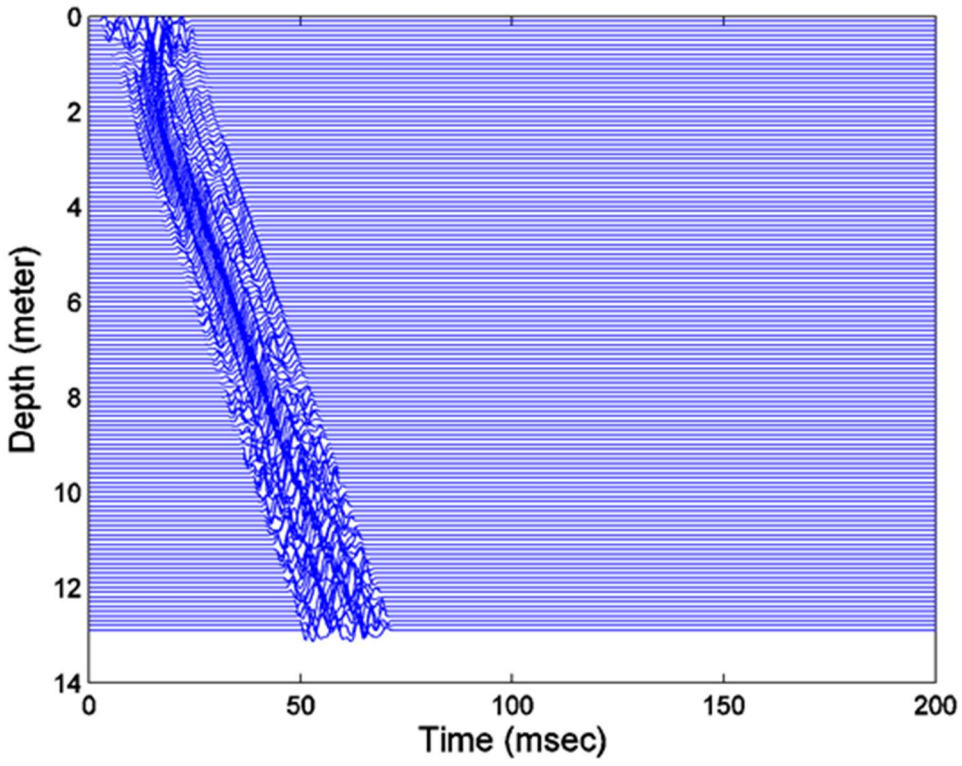


Figure 2.8. Successive continuous filtered shear wave data with window (Agaiby et al., 2016)

After detrending, filtering, and windowing are completed, the cascaded continuous shear waves are evident and can be used for evaluating the shear wave velocity profile with depth. The simplest method in signal post-processing and evaluation involve manually choosing the first arrival, first peak, and/or first crossover point. However, these manual methods are time-consuming in the field work where paired opposite strikes are needed for the crossover and also time-consuming in the evaluation process where the points are visually picked. Accordingly, cross-correlation in the time domain and cross-spectral

analysis in the frequency domain can be adopted using coded software packages such as MATLAB which is convenient in handling large amounts of data and can provide finer higher quality results.

### *2.4.3 Cross-Correlation Analysis in the Time Domain*

This technique is usually recommended when successive wavelets have the same nature and characteristics, such as those that are generated with the rotoautoseis. The cross-correlation function is used to evaluate the time shift between two independent wavelets by finding the lag time corresponding to the maximum covariance or maximum cross-correlation in the time domain. The function reaches a maximum value when two consecutive signals that have similar shapes either overlap or coincide (Ku et al., 2013b).

### *2.4.4 Cross-Spectral Analysis in the Frequency Domain*

The cross-spectral analysis is a technique used to identify the correlation between two-time series at given frequencies (e.g., peak frequency). The analysis provides a phase spectrum in the frequency domain allowing the calculation of time shifts and phase velocities between two different wavelets. More details on the analysis technique can be found in Ku et al. (2013a, 2013b).

### *2.4.5 Obtaining Final Corrected Continuous $V_s$ Profile*

After applying both the cross-correlation and cross-spectral analyses on the filtered successive continuous shear wavelets, the results were somewhat sensitive and scattered. This can be attributed to different factors and issues that arise during the in-situ testing procedure, or also in the post-processing analyses such as the extremely short time lapse,

cone penetration test rate variants, unfiltered noise, and the possibility of refracted and reflected signals. Hence, to obtain a representative corrected $V_s$ profile with depth, a running-mean filter coefficient vector for the time interval ($\Delta t$) is applied for the $V_s$ profiles obtained from both analyzing techniques. A special zero-phase forward and reverse digital filtering technique is used following the recommendations of Trauth (2010). By increasing the order of the running-mean filter ($10^{th}$ in the presented study), a more accurate and a less scattered $V_s$ profile with depth is obtained. **Figure 2.9** presents the post-processed $V_s$ profiles using cross-correlation and cross-spectral techniques after applying $10^{th}$ order running mean filter.

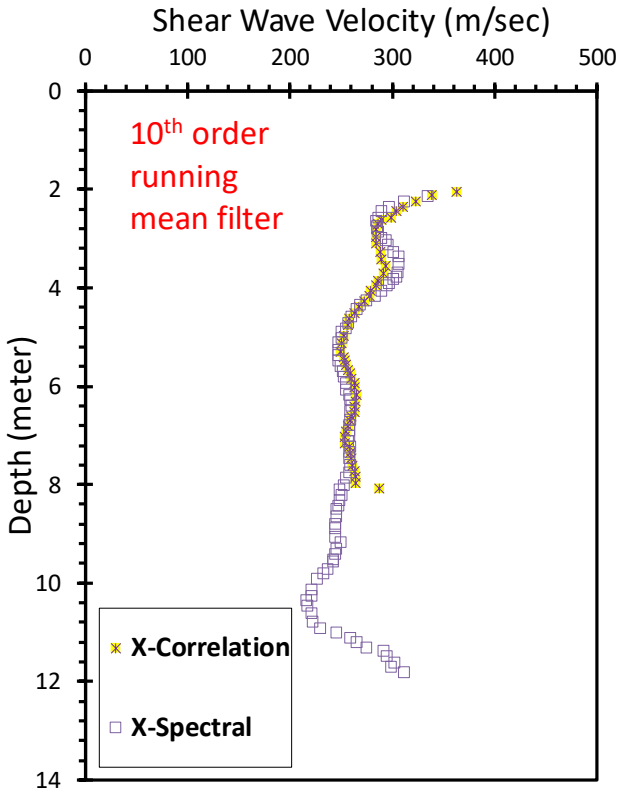


Figure 2.9. Post-processed $V_s$ profiles using cross-correlation and cross-spectral techniques after applying $10^{th}$ order running mean filter

## 2.5 Multi-channel Analyses of Surface Waves (MASW) Testing

In-situ methods for the measurement of shear wave velocity can be classified into two main categories: invasive and non-invasive methods (Wightman et al. 2003). Invasive methods include cased borehole methods such as: crosshole test (CHT), downhole test (DHT), uphole test (UHT), and P-S suspension logger, as well as direct push methods: seismic cone penetration test (SCPT) and seismic flat dilatometer test (SDMT) that are efficient versions of the DHT mode, in addition to continuous-interval seismic piezocone testing (CiSCPTu). Non-invasive methods include refraction survey, reflection survey, and surface wave methods that use either active sources to measure Rayleigh waves, including: spectral analyses of surface waves (SASW), multi-channel analyses of surface waves (MASW), and continuous surface wave method (CSW), or passive source techniques, such as passive surface waves (PSW)/microtremor array measurements (MAM) or reflection microseis (ReMi). **Figure 2.10** presents a schematic diagram of both invasive and non-invasive shear wave velocity measurements techniques conducted at the W-21 test site.

For the non-invasive MASW carried out in 2014, a spectrum analyzer provided with 24 geophones were used in conducting the test by Shane Hickman of EGSci. The geophones were equidistant at the ground surface and a sledgehammer was used to produce the surface wave and in seconds the wavelets were sensed using the geophones and recorded onto an on-site computer with values generally increasing from 200 m/s to about 300 m/s in the interval from the ground surface to about 13 meters as presented in **Figure 2.11a.** In 2016, a reflection microseis (ReMi) test was conducted by Fikret Atalay of GT as another non-invasive measurement technique, as presented in **Figure 2.11b**.

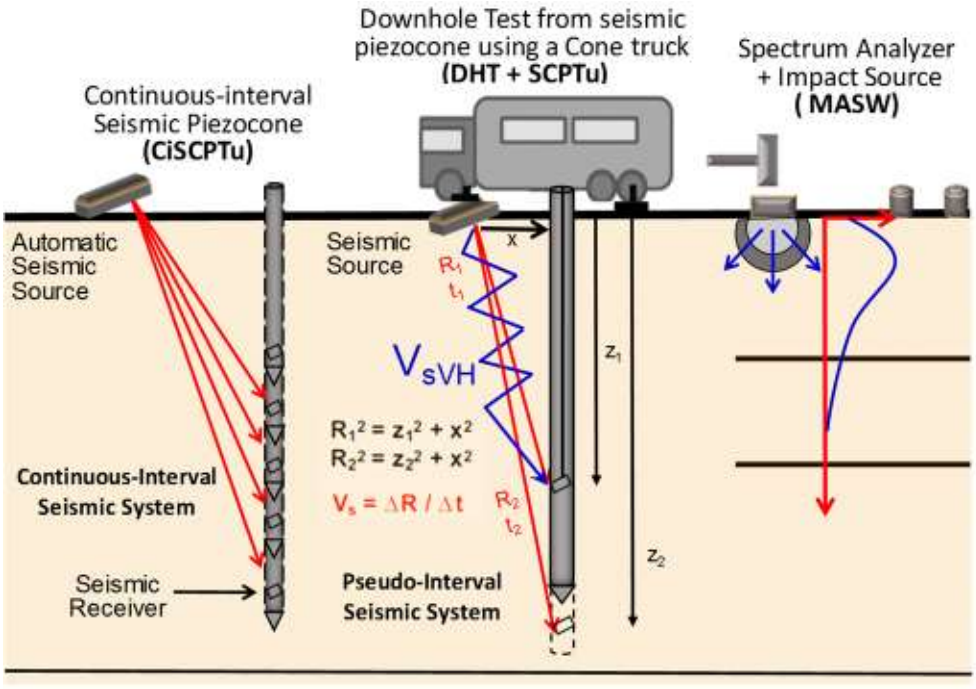


Figure 2.10. Schematic of different geophysical methods measuring $V_s$: Continuous-interval seismic piezocone test, Pseudo-interval seismic piezocone test, and non-invasive multi-channel analyses of surface waves test

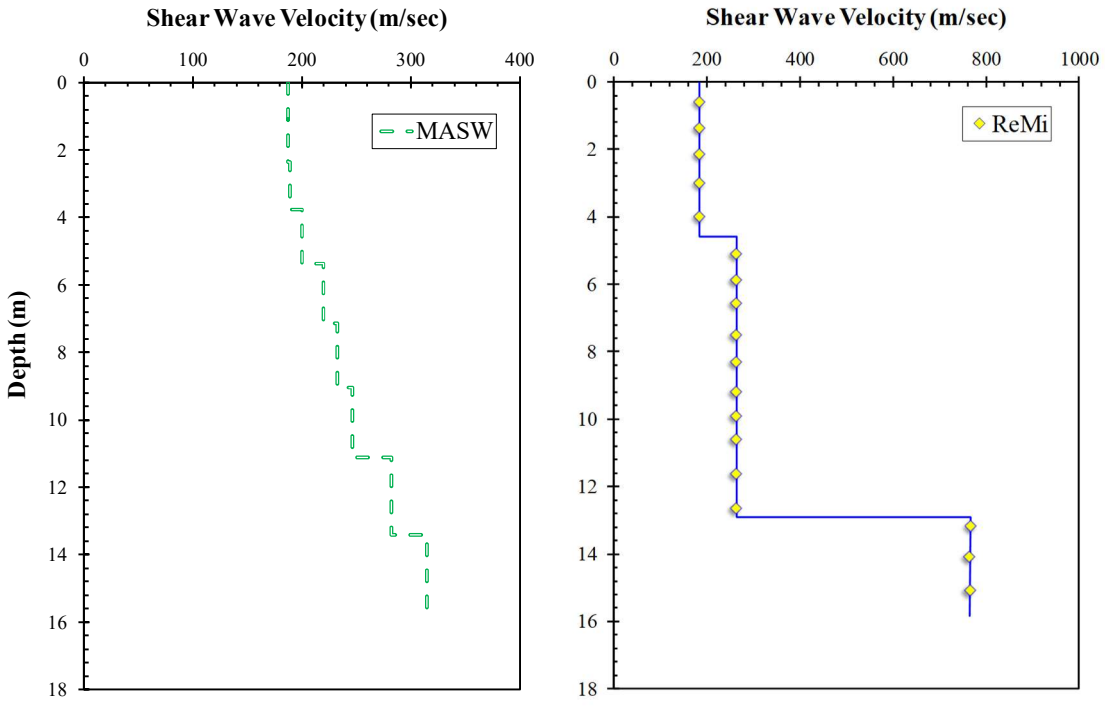


Figure 2.11. Shear wave velocity profiles measured using non-invasive techniques: (a) multi-channel analyses of surface waves test (MASW); (b) reflection microseis tests (ReMi) conducted at W-21 test site

**Figure 2.12** shows the evaluated $V_s$ profiles with depth for the different testing techniques carried out at the Georgia Tech W-21 test site. Both of the derived continuous $V_s$ profiles using cross-correlation and spectral analysis seem to match well with the reference downhole test using the SCPTu and the MASW and ReMi test data when adopting the $10^{th}$ order running mean filter. The different methods show differences in the shear wave velocity profiles, mostly due to changes in the degree of saturation and capillarity in the seasons and times of the year, since the residual silty soils are partially saturated and the testing was done within the vadose zone. Also, water level fluctuations and wetting/drying can cause changes in the shear wave velocity magnitude over time (Cho & Santamarina 2001). Despite the deviations, all six profiles show reasonable agreement in the $V_s$ profiles with values between 200 and 300 m/s.

## 2.6 Flat Plate Dilatometer Testing (DMT)

The flat plate dilatometer test (DMT) is an in-situ method that involves pushing an instrumented flat steel blade into soils and recording two horizontal pressures at each test depth. The specific pressure measurements are utilized to obtain stratigraphy and estimates of geoparameters, including unit weight, at-rest lateral stresses, elastic modulus, stress history, and shear strength.

The flat dilatometer test is simple, robust, repeatable, quick, economic, and operator-independent. The field of applications of the DMT is diverse, ranging from extremely soft soils to dense sands. However, the DMT is difficult to push in very dense and hard materials and not applicable to gravels. The DMT analyses primarily rely on correlative relationships and require calculations for local geologies.

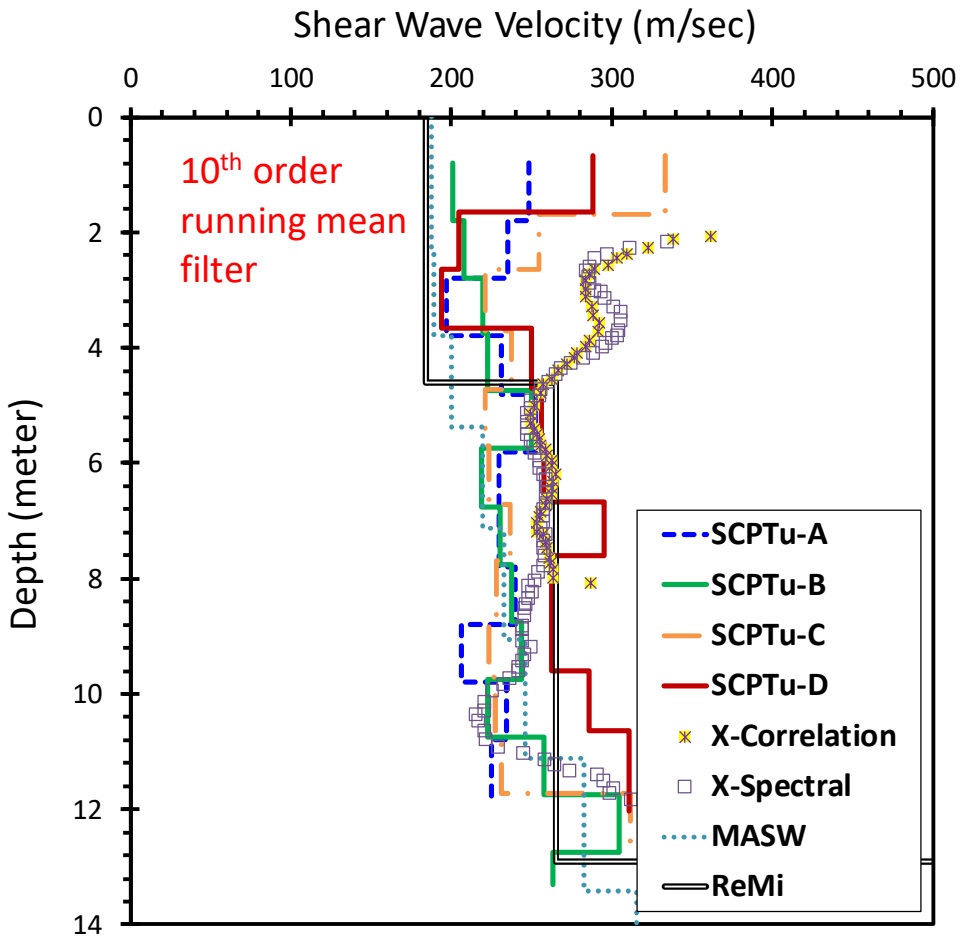


Figure 2.12. Downhole results showing a comparison of various shear wave velocity measuring techniques: MASW, ReMi, SCPTu, and CiSCPTu using x-correlation and x-spectral methods at the W-21 test site.

Procedures for the test are given by ASTM D 6635 and Schmertmann (1986). **Figure 2.13** provides an overview of the DMT test and its setup. Two calibration readings are taken for membrane stiffness: $\Delta A$ = pressure required in the air to move the flexible membrane inward a distance 0.05 mm; $\Delta B$ = pressure required in the air to move membrane outward a distance 1.1 mm. Each of the pressure readings A and B are then converted into $p_0$ (contact pressure) and $p_1$ (expansion pressure), respectively per **Figure 2.13**.

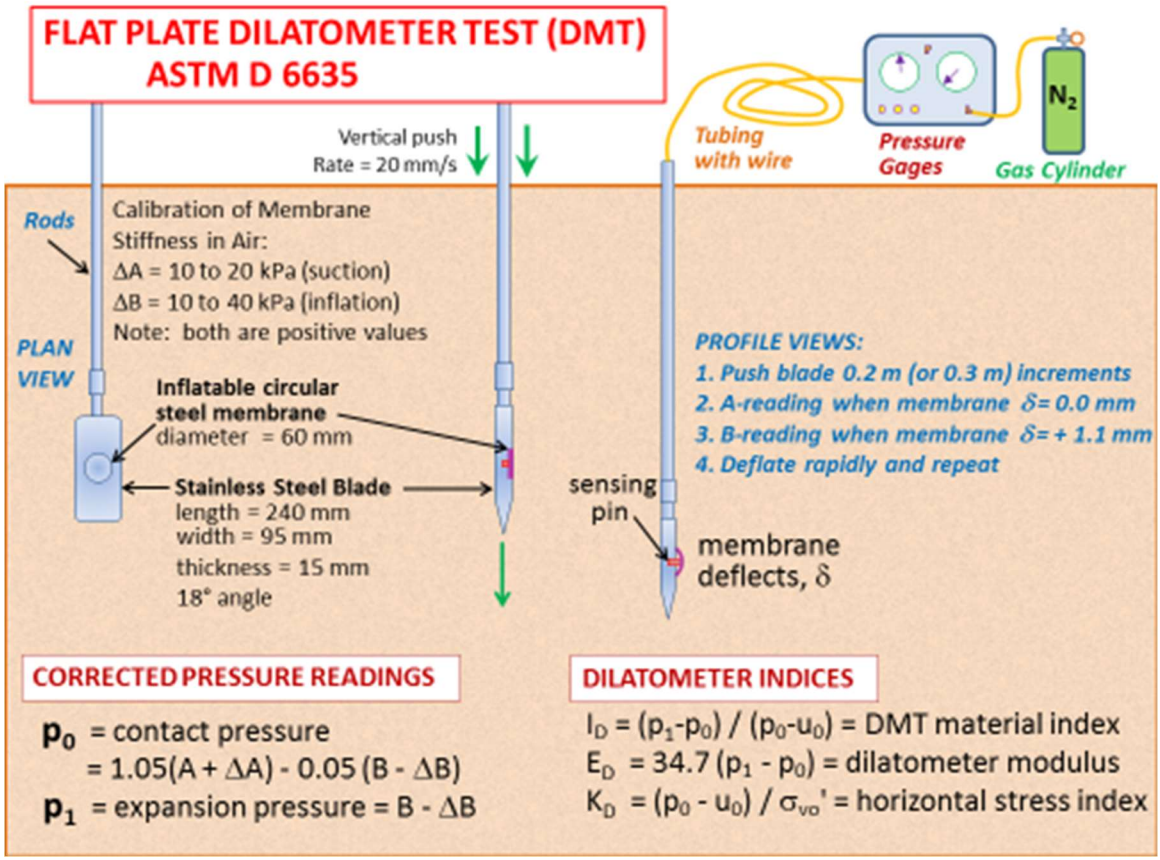


Figure 2.13. Illustration of Setup and Procedure for the Flat Dilatometer Test (DMT)

The two dilatometer pressures, $p_0$ and $p_1$, are combined with the hydrostatic water pressure, $u_o$, to provide three index parameters: (a) material index $I_D$, (b) horizontal stress index $K_D$, and (c) dilatometer modulus $E_D$. These were developed by Marchetti (1980) to provide information on the stratigraphy, soil types, and the evaluation of soil parameters. Hydrostatic water pressure ($u_0$) can be evaluated based on available groundwater table information. The material index, $I_D$, is related to the soil classification and is presented as:

$$I_D = (p_1 - p_0)/(p_0 - u_0) \quad [2.1]$$

The above definition of $I_D$ was introduced having observed that the $p_0$ and $p_1$ profiles are systematically "close" to each other in clay and "distant" in sand. According to Marchetti (1980), the soil type can be identified: clay: $0.1 < I_D < 0.6$, silt: $0.6 < I_D < 1.8$, and sand: $1.8 < I_D < 10$. In general, $I_D$ provides an expressive profile of soil type, and for normal soils, a reasonable soil description.

The horizontal stress index, $K_D$, is related to the in-situ horizontal stress-state of the soil. The index $K_D$ will always be greater than $K_0$ due to disturbance caused during insertion of the blade. This parameter is presented as:

$$K_D = (p_0 - u_0)/\sigma'_{v0} \quad [2.2]$$

$K_D$ provides the basis for several soil parameter correlations and is a key result of the dilatometer test. The horizontal stress index $K_D$ can be regarded as $K_0$ amplified by the penetration (Marchetti et al., 2001). In NC clays; with no aging, structure, cementation; the value of $K_D \approx 2$. The $K_D$ profile is similar in shape to the OCR profile with depth, hence can be used to better understand the soil deposit and its stress history (Marchetti 1980, Jamiolkowski et al. 1988).

The dilatometer modulus $E_D$ is obtained from $p_0$ and $p_1$ from the theory of elasticity (Gravesen 1960). For the 60 mm membrane diameter and required 1.1 mm displacement, it is found (Marchetti 1980):

$$E_D = 34.7\,(p_1 - p_0) \quad [2.3]$$

**Figure 2.14** presents the results of flat plate dilatometer sounding conducted at the W-21 test site with corrected $p_0$ and $p_1$ readings along with the interpreted material index

($I_D$), horizontal stress index ($K_D$), and dilatometer modulus ($E_D$) profiles with depth. As illustrated by the material index profile, the soils at the W-21 site are mostly silt to sandy silt, with some silty sands, as anticipated from the Piedmont geology.

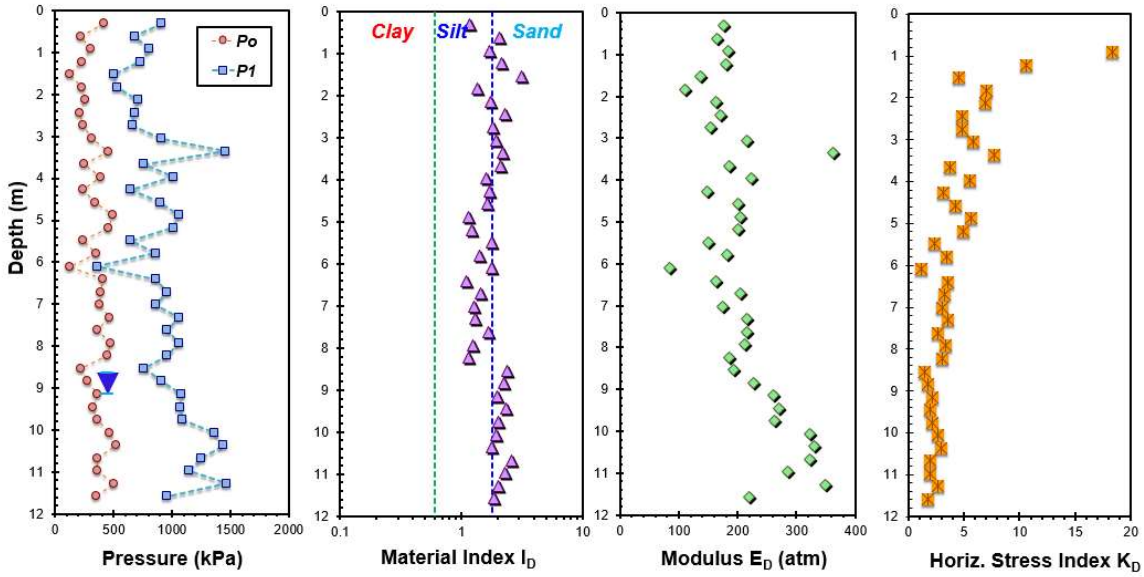


Figure 2.14. Flat plate dilatometer sounding at the W-21 test site: (a) $p_0$ and $p_1$ readings, (b) material index ($I_D$), (c) dilatometer modulus ($E_D$); (d) horizontal stress index ($K_D$)

## 2.7 Helical Probe Testing (HPT)

Helical probe tests (HPT) are a quick and economical means for manual field testing of soils to depths of 1.5 m with readings taken at 0.15-m intervals in only 10 minutes. HPT is a simple and inexpensive device which can provide quick and dependable means for evaluating geostratigraphic profiles and soil properties at relatively shallow depths. It is advantageous for small geotechnical projects because it is lightweight, portable, and can be performed by one person very quickly. Small cuttings are also available from the auger to confirm soil type. The idea of applying a measured torque to the top of a steel rod to advance a small auger was first used by Robinson and Taylor

(1969). The torque required to turn the probe is used as an index measure of the natural soil's in-place strength or stiffness, or in the case of controlled fills, a measure of the degree of compaction. Preliminary ASTM reporting (Yokel and Mayne 1988) has determined that the HPT method correlates well to standard penetration testing (SPT: ASTM D 1586), cone penetration testing (CPT: ASTM D 5778), and flat plate dilatometer tests (DMT: ASTM D 6635).

Typical HPT soil probes are about 1.5 m (60 inches) long and manufactured using precision machined helical bits with a 19 mm (0.75 in) auger diameter welded at the rod bottom. A hex coupler fits at the top of alloy steel shaft head to permit contact with the torquemeter. The entire system weighs approximately 2.2 kg (4.8 lb) so that the device is easily carried to the field for deployment by a single individual. Components of the HPT are shown in **Figure 2.15**.

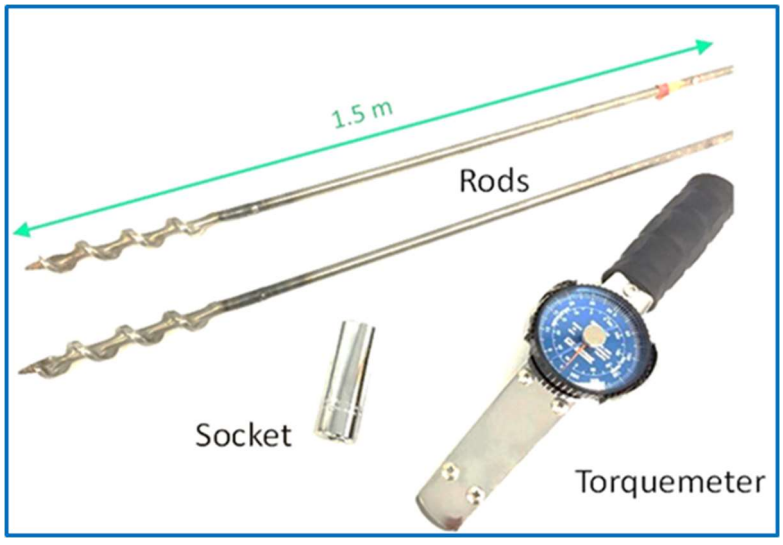


Figure 2.15. Helical probe testing (HPT) equipment including steel rod with augers, rods, socket, and torquemeter

The HPT can be used for exploration of natural soils and/or compacted fills (Yokel and Mayne 1986, 1988). A moment is applied at the top of the rod and the torque is measured at 150 mm (6 in) intervals during the auger penetration. For the operation of the helical probe, a beam style torque wrench is fitted to the hex coupler using a socket. The rods are then rotated by hand using the wrench at about 90°/s while the peak torque is noted. The value of torque is used as a measure, usually in either unit of inch-pounds (in-lb) or Newton-meters (N-m).

### *2.7.1 HPT Calibration in the Piedmont*

While the HPT is useful in a wide range of soils, including sands, silts, clays, and mixed soils, some initial applications focused mainly on residual silts and sands of the Appalachian Piedmont and natural sands of the Atlantic Coastal Plain geology (Yokel and Mayne 1988). This required HPT calibrations in side-by-side field testing that utilized data from adjacent borings and soundings from SPT, CPT, and DMT, as well as field density measurements (Yokel and Mayne 1986).

Helical torque readings were compiled from 58 tests from 18 project sites within the Washington, DC - Virginia - Maryland area where the data are grouped from two main geologic regions: (a) Appalachian Piedmont Region and (b) Atlantic Coastal Plain. For the Piedmont region, the ground is underlain by residuum derived by the in-place weathering of metamorphic and igneous bedrock. The residual soils are often found to be silty, ranging from micaceous fine sandy silts to silty fine sands, that transition with depth to saprolites, partially-weathered rocks, and bedrock refusal. In contrast, the Atlantic Coastal Plain consists of various marine sediments that were deposited in various times ranging from

very old Cretaceous to Miocene to recent Holocene ages, including complex interbedding of clays, silts, sands, and gravels. **Figure 2.16** presents a list of the individual test sites and their corresponding symbols. Sites located within the Piedmont region were assigned green symbols, Atlantic Coastal Plain sands were assigned yellow/ orange symbols, and finally, a sole site in the Atlantic Coastal Plain clays was assigned a blue symbol.

The helical probe tests were performed alongside different conventional in-situ tests (SPT, CPT, DMT). The results were used to develop correlations with the torque readings within the shallow depths where HPTs were performed. These relationships can be used for estimating the soil SPT N value, cone tip resistance ($q_t$), or the dilatometer modulus ($E_D$).

### *2.7.2 Correlation between SPT and HPT*

For the data set reviewed, standard penetration tests were performed as per ASTM D1586 with an average energy rating of 60 %. The main advantages of the SPT are obtaining both a sample and a number, the test is simple, rugged, and suitable for many soil types except for soft clays and coarse gravels. The SPT is usually performed using a conventional geotechnical drill rig and can provide a rough index of the relative strength and compressibility of the soil. Measured SPT resistances record the numbers of blows from a drop hammer to drive an open split-barrel sampler a vertical distance of 0.305 m (1 foot) into the ground. An energy correction to 60% efficiency is required for any reasonable use of the test (ASTM D 4633). The energy-corrected N-value is termed $N_{60}$. Helical probe tests were performed along ongoing SPTs or near prior-conducted borings.


Figure 2.16. List of sites and their symbols for the compiled database for HPT calibration

**Figure 2.17** presents the relation between the helical probe torque readings ($t_{HPT}$) and the energy-corrected SPT N value ($N_{60}$). The torque values reported represent an average torque readings for the cases where more than a single HPT was performed. A unique correlation was found regardless the type of the soil under study, the correlation between $N_{60}$ and $t_{HPT}$ can be expressed (Yokel and Mayne 1986, 1988):

$$N_{60} \approx 0.2 \cdot t_{HPT}(in-lb) \qquad [2.4]$$

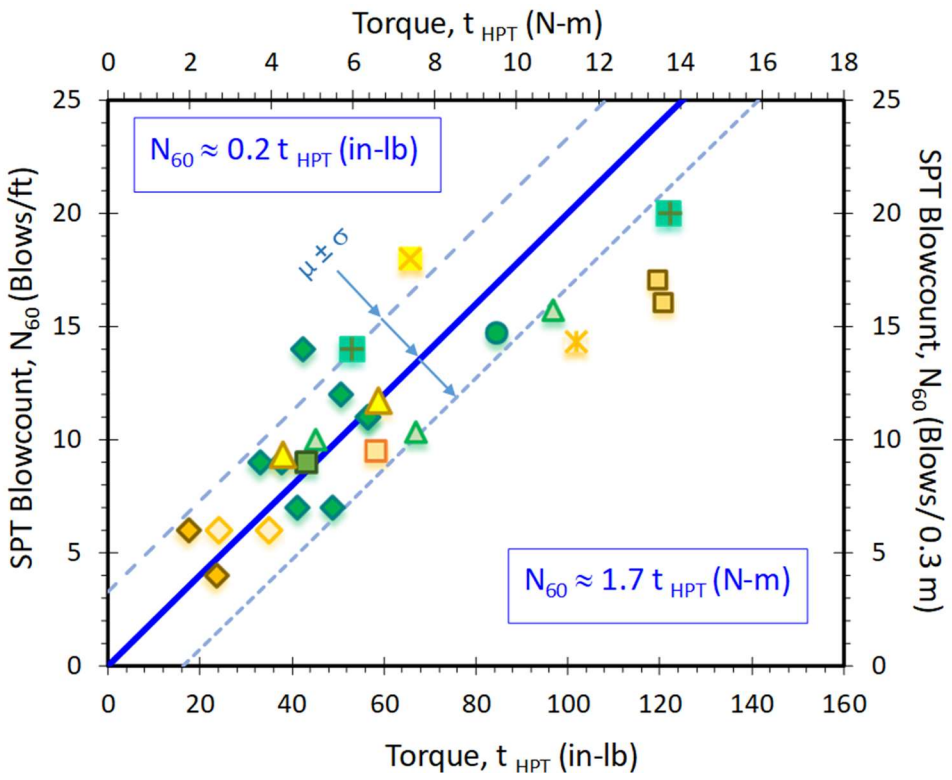


Figure 2.17. Correlation between SPT blow counts ($N_{60}$) and helical torque reading ($t_{HPT}$)

### *2.7.3 Correlation between CPT and HPT*

Cone penetration tests (CPT) in the dataset included both mechanical type (ASTM D 3441) and electric type soundings (D 5778). The CPT is an excellent tool for profiling strata changes, delineating the interfaces between soil layers, soil consistency, and detecting small lenses, inclusions, and stringers within the ground. The measured data include cone resistance, sleeve friction, and porewater pressure readings with depth. The results can be post-processed to interpret a number of geotechnical engineering parameters: unit weight, relative density, soil strength, stiffness, stress state, and permeability (Mayne 2007).

By investigating the trends between the cone tip resistance ($q_c$) and the helical torque reading ($t_{HPT}$), it was found that that the relation is soil type dependent, specifically related to the mean soil grain size ($D_{50}$). For sands, **Figure 2.18** presents the trend for cone tip resistance ($q_c$) and torque readings ($t_{HPT}$) which can be expressed as:

$$q_{cSANDS}(bar) \approx 0.8 \cdot t_{HPT}(in-lb) \quad [2.5]$$

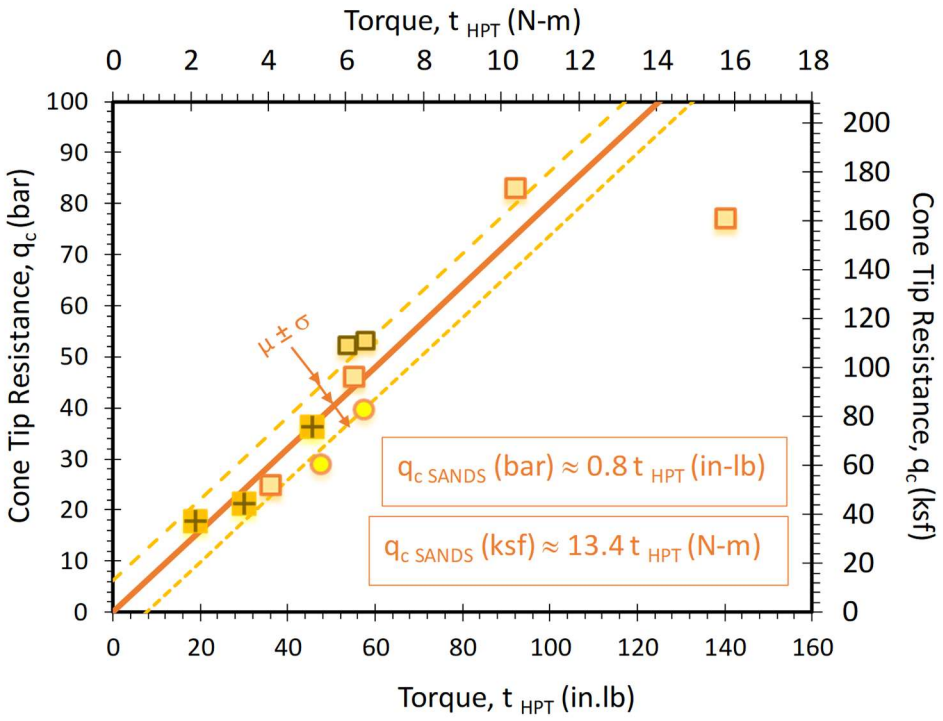


Figure 2.18. Correlation between cone tip resistance ($q_c$) and helical torque reading ($t_{HPT}$) for sands

For Piedmont sandy silts and silty sands (and one clay), **Figure 2.19** presents the trend between the cone tip resistance and helical torque reading for clays which can be expressed (Yokel and Mayne 1986):

$$q_{cCLAYS}(bar) \approx 0.4 \cdot t_{HPT}(in-lb) \quad [2.6]$$

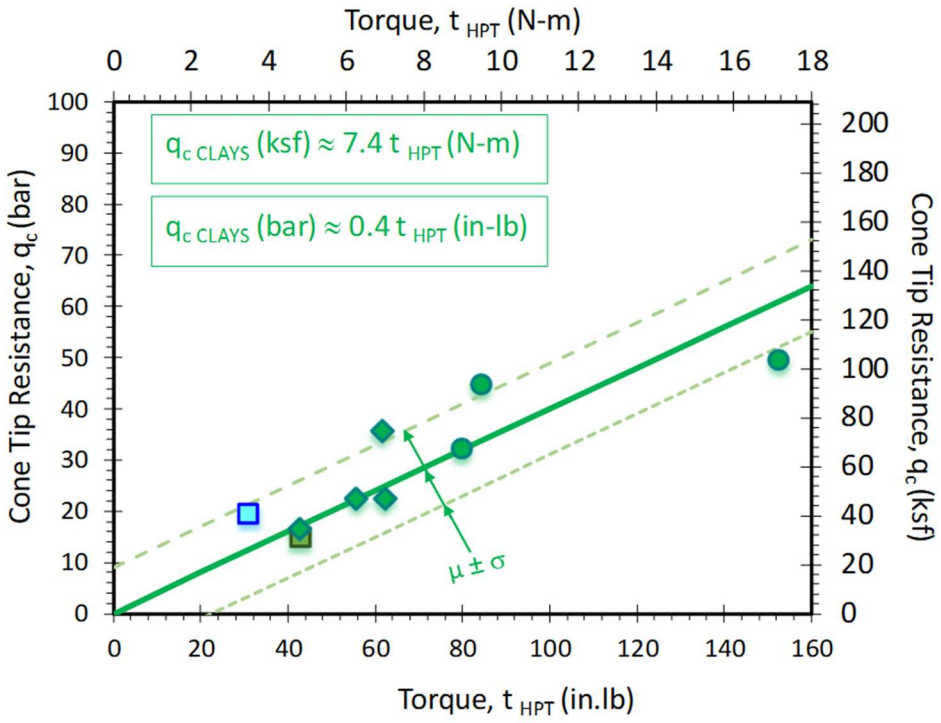


Figure 2.19. Correlation between cone tip resistance ($q_c$) and helical torque reading ($t_{HPT}$) for Piedmont residual soils

### *2.7.4 Correlation between DMT and HPT*

At a few sites, flat dilatometer tests (DMT) were performed as per ASTM D 6635. The DMT involves pushing an instrumented flat steel blade into the soil and recording two horizontal pressures at each test depth. The specific pressure measurements are utilized to obtain stratigraphy and estimates of geoparameters, including unit weight, at-rest lateral stresses, elastic modulus, stress history, and shear strength (Marchetti 1980*)*. The flat dilatometer test is simple, robust, repeatable, quick, economic, and operator-independent. The field of application of the DMT is very wide, ranging from extremely soft soils to dense sands. However, the DMT is difficult to push in very dense and hard materials and not applicable to gravels. The DMT analyses primarily rely on correlative relationships and require calculations for local geologies. No borehole cuttings or spoil are generally

produced by this test, although it is possible to advance a conventional soil boring and then perform the DMT downhole within the borehole.

**Figure 2.20** presents the relation between the dilatometer modulus ($E_D$); obtained from the two pressure readings ($p_0$ and $p_1$) of the flat dilatometer; and the helical probe torque reading ($t_{HPT}$) which can be expressed as:

$$E_D(MPa) \approx 0.2 \cdot t_{HPT}(in-lb) \qquad [2.7]$$

It is worth noting that for Piedmont residual soils, there is a direct relationship between the elastic modulus ($E_D$) obtained from flat dilatometer tests (DMT) and cone tip resistance ($q_t$) from CPT (Mayne and Liao 2004) that can be expressed as $E_D = 5\ q_t$ and presented in **Figure 2.21**.

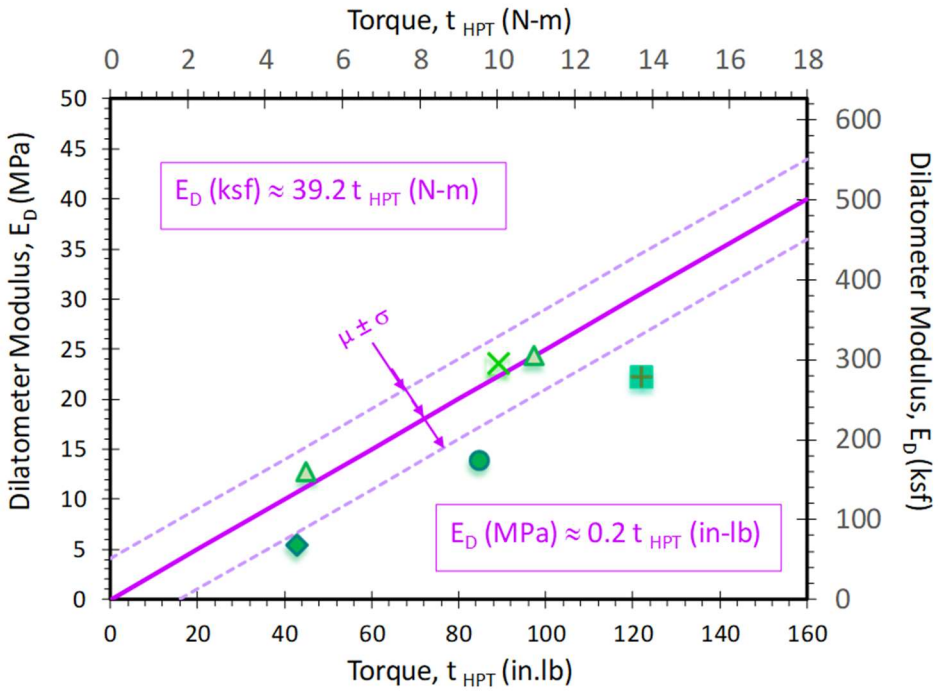


Figure 2.20. Relationship between dilatometer modulus ($E_D$) and helical torque reading ($t_{HPT}$)

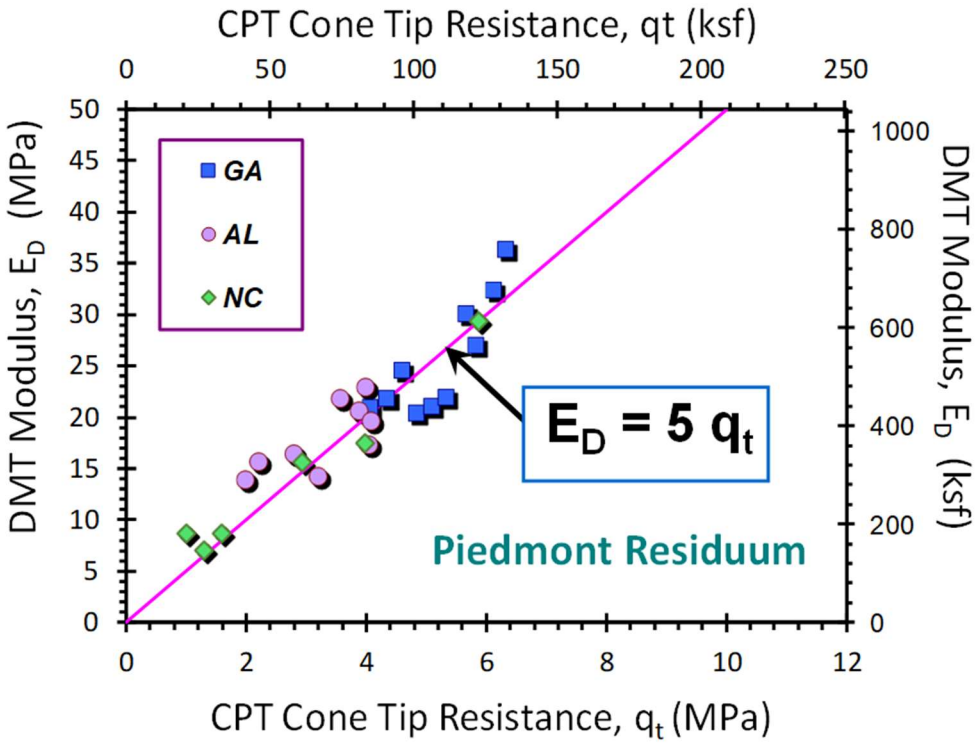


Figure 2.21. Relationship between dilatometer modulus ($E_D$) and cone penetration resistance ($q_t$), as reported by Mayne & Liao (2004)

### *2.7.5 Testing at Georgia Tech W21 Test Site*

A number of helical probe tests were recently performed at the site that has been used for class demonstrations on campus over the past several years. The results of 4 helical probe tests advanced to depths of 1.1 meters are presented in **Figure 2.22**. The mean torque ($t_{HPT}$) from these series is also shown.

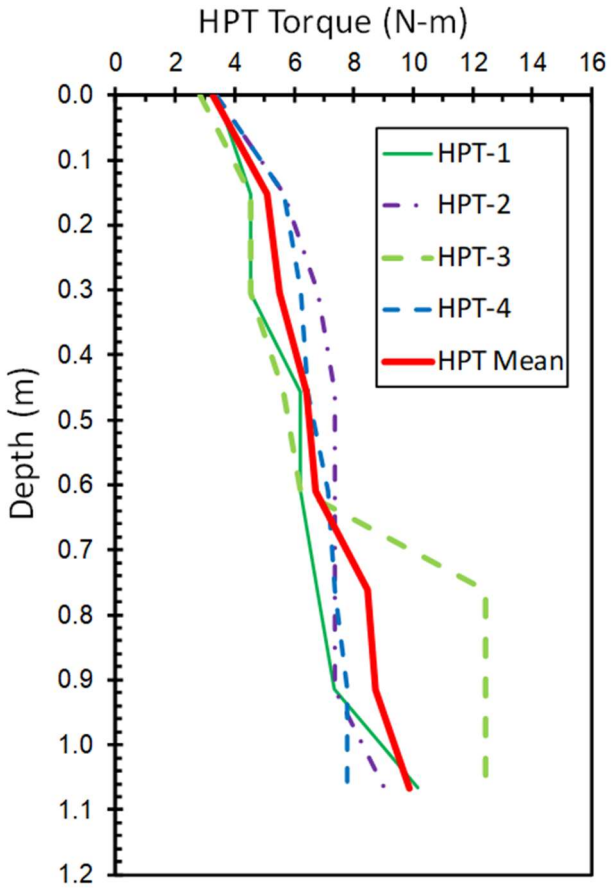


Figure 2.22. Results from four helical probe soundings at the Georgia Tech W21 test site with mean trend

For each of the past 3 years, a series of seismic piezocone soundings measuring cone tip resistance, sleeve friction, porewater pressure and shear wave velocity has been performed in the spring term season. The measured cone tip readings from those soundings are presented in **Figure 2.23** over a shallow depth range of 1.2 meters and. Also shown is the estimated cone tip resistance obtained from the mean helical probe torque readings using Equation [2.6]. A rather good agreement is observed indicating the general applicability of using the HPT to estimate the cone tip resistances at shallow depths. For other geologic settings, a localized calibration between CPT and HPT would be warranted

in order to verify the trends and confirm the relationships for general use in geotechnical engineering practice.

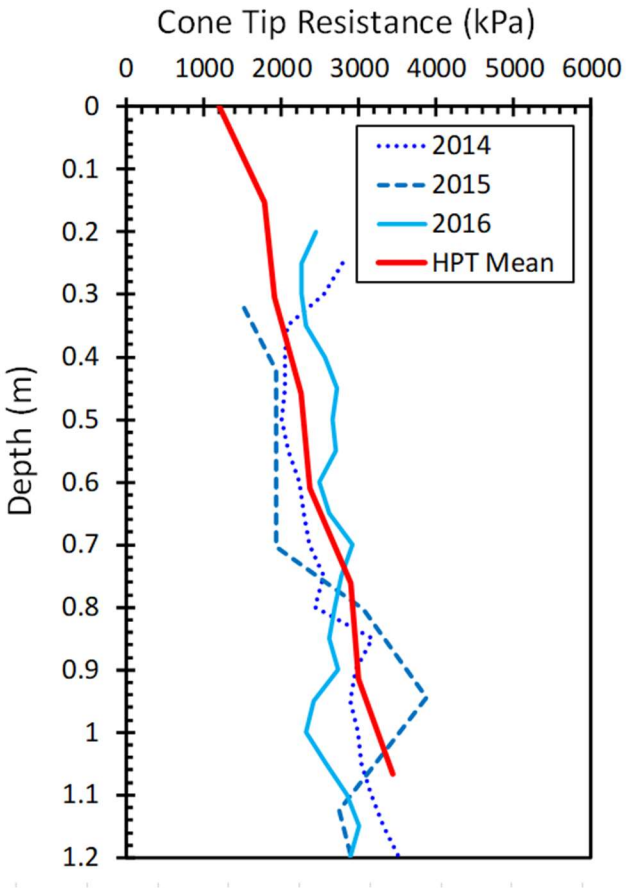


Figure 2.23. Estimated cone tip resistance ($q_t$) from mean helical probe readings compared to in-situ measured values at Georgia Tech W21 test site

A DMT sounding was also conducted at the W21 test site and the pressure readings ($p_0$ and $p_1$) were used to evaluate the dilatometer modulus ($E_D$). The resulting $E_D$ profile is presented in **Figure 2.24**. Also shown are the estimated moduli using Equation [2.7] and the helical torque readings. From the presented results, a fair to good agreement is evident, indicating the possibility of using HPT in estimating dilatometer moduli at shallow depths.

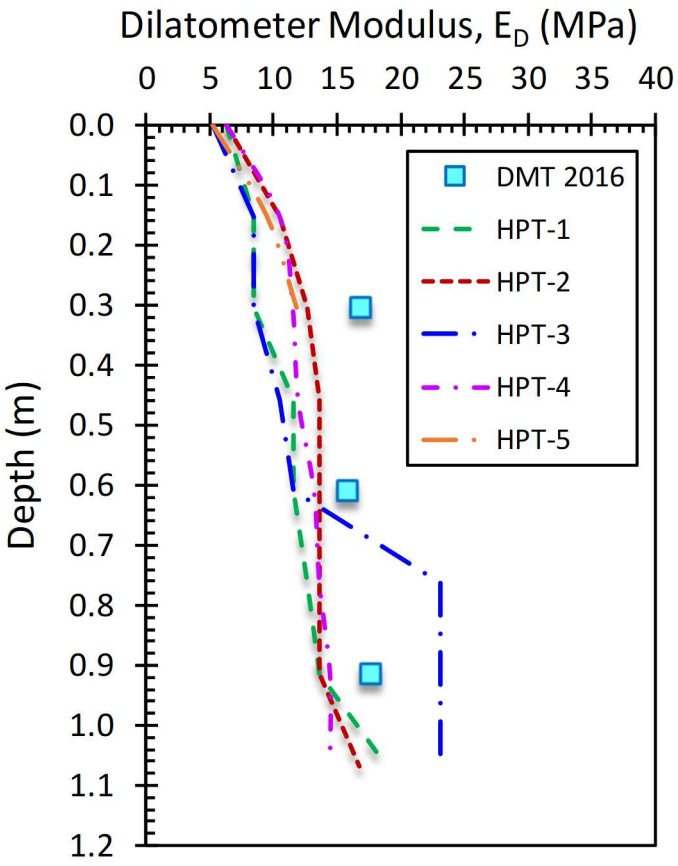


Figure 2.24. Measured dilatometer modulus ($E_D$) and estimated profiles from individual helical probe readings at Georgia Tech W21 site

# Chapter 3. Interpretation of Geotechnical Parameters using In-Situ Data for The Bolivian Experimental Site for Testing (B.E.S.T.)

## 3.1 Introduction

The engineering properties of the Bolivian Experimental Site for Testing (B.E.S.T.) are examined in detail based on the field results of the geotechnical site investigation. The performed investigation includes four main in-situ tests: Standard Penetration Tests (SPT), Cone Penetration Tests (CPTu), Flat Plate Dilatometer Tests (DMT), and Downhole Shear Wave Velocity ($V_{sVH}$). The in-situ testing program was comprised of 8 SPTs, 15 CPTus, 6 DMTs, and 3 $V_{sVH}$ measurements. Complementary laboratory tests included: grain size distribution, water content, plastic and liquid limits tests. Practical methods from the literature for estimating the geotechnical properties of the site from in-situ tests are discussed with a presented comparison between the interpreted values from the different in-situ methods. The investigated design parameters include soil type, unit weight ($\gamma_t$), effective friction angle ($\phi$'), stress history (OCR), and elastic shear modulus (E).

## 3.2 Standard Penetration Tests (SPT)

### *3.2.1 Overview*

The standard penetration test (SPT) is performed during the advancement of a soil boring to obtain an approximate measure of the dynamic soil resistance, as well as a disturbed drive sample (split barrel type). The test was introduced by the Raymond Pile Company in 1902 and remains today as one of the most common in-situ test worldwide

following ASTM D 1586 standards. The main advantages of the SPT are obtaining both a sample and a number. The test is simple, rugged, and suitable for many soil types except for soft clays and coarse gravels.

### *3.2.2 Corrections to the SPT N-value*

Numerous correction factors to the measured N-value are necessary because of energy inefficiencies and procedural variation in practice. The most important correction factor is the energy efficiency which is obtained by a onetime calibration using the procedures outlined in ASTM D 4633.

The efficiency of the system can be obtained by comparing the kinetic energy ($KE=½mv^2$), with the potential energy of the system (PE=mgh), where m = mass, v = impact velocity, g = 9.8 $m/s^2$ = gravitational constant, and h = drop height. The energy ratio (ER) is defined as KE/PE. Over the years, the standard of practice has varied from about 30% to 95% with different hammer systems. As of 1985 when the inefficiencies were realized (e.g. Skempton 1986), the N values corresponding to a mean ER = 60 % are the corrected values and termed $N_{60,}$ as given by:

$$N_{60} = (ER/60) \cdot N_{measured} \quad [3.1]$$

A total of eight boreholes were drilled at B.E.S.T. with SPT split-spoon samplers with varying depths ranging from 9.5 m to 25 m. The 8 SPTs were carried out with an average measured energy rating (ER) of 44 % covering the site location. **Figures 3.1a** and **3.1b** present the raw measured SPT – N values with depth in addition to the energy-corrected $N_{60}$ values with depth. The obtained samples from the drilled boreholes were

used to identify the soil type at the site using laboratory grain size distribution. **Figure 3.1c** presents the profiles of percentage of fines (passing sieve #200) for the eight borehole locations; where "Sands" indicate a percentage of fines less than 50% while "Clays and Silts" indicate a percentage of fines greater than 50%. The average trend presented in **Figure 3.1c** indicates that the majority of the soil profile at B.E.S.T. can be identified as sands with an exception to a 1-m thick clay/silt layer at a depth of 3 m and at a depth greater than 11m.

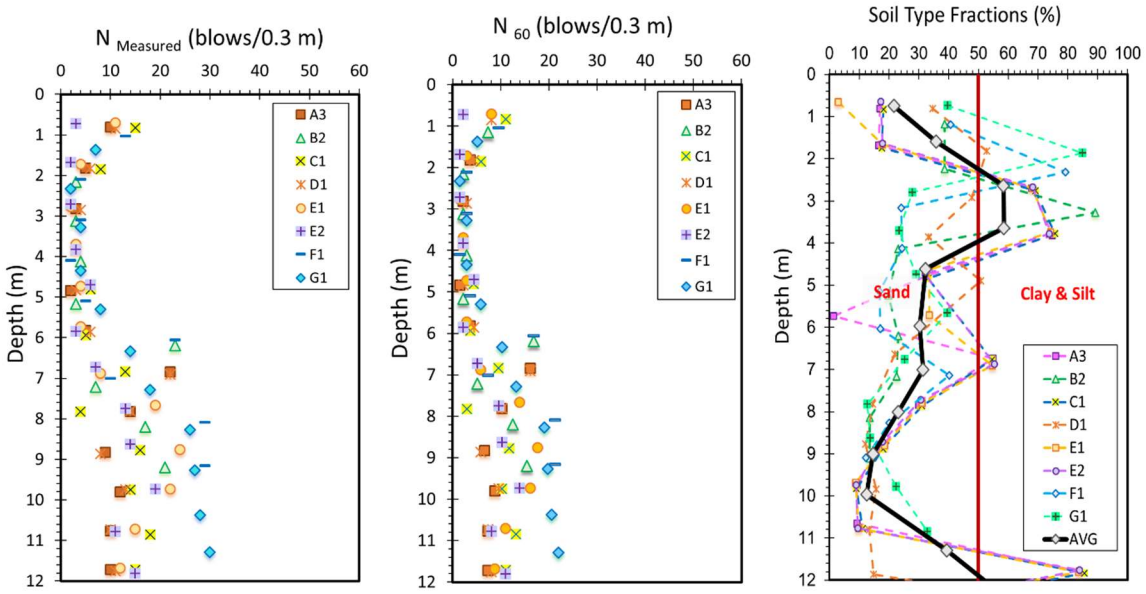


Figure 3.1. B.E.S.T. SPT- N values with depth: (a) Uncorrected; (b) Corrected to 60% efficiency; and (c) grain size distribution

Since SPT N-values in the same geomaterial will increase with increasing effective overburden stress, the energy-corrected blow count ($N_{60}$) is often stress-normalized to an equivalent effective overburden stress of 1 atmosphere ≈ 100 kPa known as overburden correction. The stress-normalized and energy-corrected blow count is referred to as $(N_1)_{60}$, and is equal to:

$$(N_1)_{60} = C_N \cdot N_{60} \quad [3.2]$$

$$C_N = (\sigma_{atm}/\sigma_{vo}')^{n'} \quad [3.3]$$

where $C_N$ is the stress normalization parameter, $\sigma_{atm}$ is atmospheric pressure in the same units as $\sigma_{vo}'$ (i.e., 1 atm ≈ 1 bar ≈ 100 kPa), and n' is a stress exponent equal to 0.5 in clean sands (Liao & Whitman, 1986; Kulhawy & Mayne 1990) and increases to 1 in clays (Mayne & Kemper, 1988).

### *3.2.3 Soil Unit Weight from SPT*

When undisturbed samples or natural water contents are not available, the unit weight can be estimated from the shear wave velocity ($V_s$ in m/s) and depth (z in meters) as investigated by Mayne (2001):

$$\gamma_t \, (\mathrm{kN/m^3}) = 8.31 \log(V_s) - 1.61 \log(z) \quad [3.4]$$

The relationship applies to particulate geomaterials that are not cemented or bonded, thus would not be applicable to saprolites, rocks, cemented or structured diatomaceous or calcareous or carbonate soils. By using the measured in-situ SPT resistance (N value), one can estimate the corresponding shear wave velocity ($V_s$) value to be used in estimating in the unit weight of the soil following Eq. [3.4]. **Figure 3.2a** shows the interpreted soil unit weight values from the 8 SPT soundings ranging from 16.3 to 19.4 $\mathrm{kN/m^3}$ with an average trend with depth.

Imai and Tonouchi (1982) compiled a database of a variety of ground conditions through Japan where they collected data points from over 400 boreholes covering different soil types ranging from alluvial clays to diluvial clays, gravels, peats, and sands, in addition

to special soils such as loam, fill, and sirasu. The database included 1654 measured SPT resistance N values with an average energy rating of 78 % with corresponding shear wave velocity (S-wave) measured mainly using a suspension logging method. The direct relationship between the measured shear wave velocity ($V_s$) and the SPT (N-value) can be expressed as:

$$V_S \left(\frac{m}{s}\right) = 97.0\ N^{0.314} \qquad [3.5]$$

### *3.2.4 Effective Friction Angle from SPT*

For sands, a developed correlation between the effective stress friction angle (ϕ') and stress-normalized and energy-corrected SPT resistance, $(N_1)_{60}$, was derived by Hatanaka and Uchida (1996) where high-quality undisturbed samples of natural sands were obtained by special freezing method. Once mounted in the triaxial cell and allowed to thaw, specimens permitted direct measurements of ϕ' in triaxial compression tests. Corresponding field SPT data were obtained at the same elevations as the undisturbed samples using a Japanese automatic trip hammer system where energy efficiency is reported as 78 percent. For a reference 60% efficiency in the U.S., the expression for peak ϕ' is given as:

$$\emptyset^{\circ} = \sqrt{15.4\ (N_1)_{60}} + 20^{\circ} \qquad [3.6]$$

In the case of clays, there is no direct relationship between the SPT resistance and the effective stress friction angle, hence, a mean value of ϕ' = 30 degrees is assigned (Mayne 2013). **Figure 3.2b** presents the interpreted effective friction angle values from the 8 SPT soundings ranging from 27.7 to 44.5 degrees with an average trend with depth.

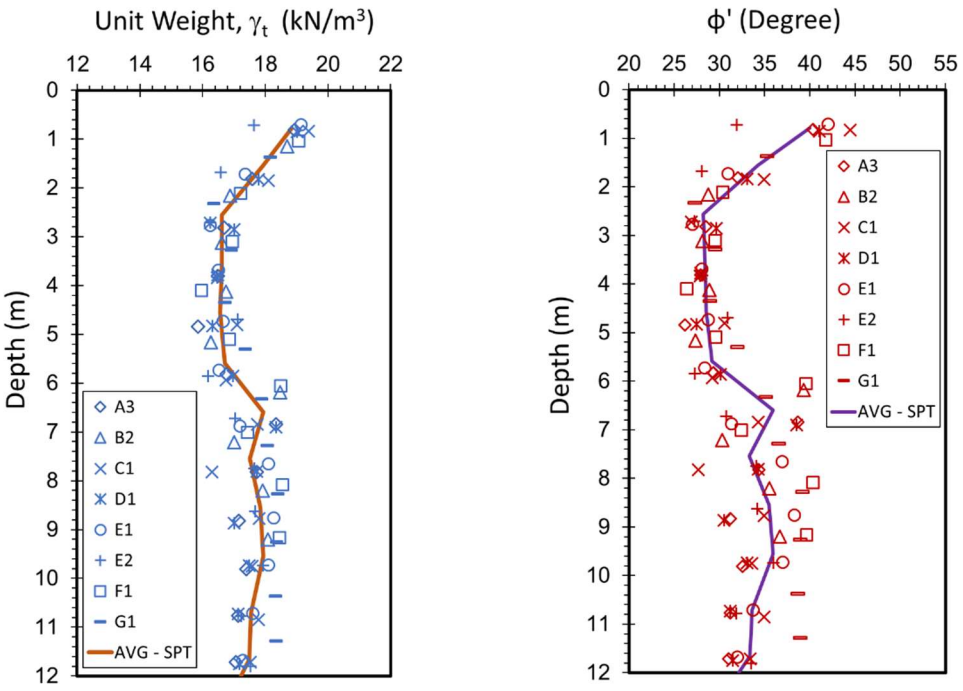


Figure 3.2. B.E.S.T. profiles from SPT data: (a) soil unit weight ($\gamma_t$) and (b) effective stress friction angle ($\phi$')

### *3.2.5 Stress History from SPT*

The preconsolidation stress ($\sigma_p$') is defined as the maximum effective overburden stress experienced by the soil during its stress history. The overconsolidation ratio (OCR) is a normalized and dimensionless parameter based on $\sigma_p$' and effective vertical stress ($\sigma_{v0}$'), such that:

$$OCR = \sigma_p' / \sigma_{v0}' \quad [3.7]$$

To overcome issues associated with laboratory methods, $\sigma_p$' can be evaluated using direct correlations with in-situ test measurements such as standard penetration, cone penetration, flat dilatometer, and/or vane shear tests that are faster, more economical, and productive than laboratory tests. Kulhawy and Mayne (1990) investigated the relationship

between the SPT resistance (N) and the effective preconsolidation stress ($\sigma_p'$) for 51 fine-grained soils. These were mainly firm to stiff to hard clays which were neither sensitive nor structured, resulting in the following expression:

$$\sigma_p' \approx 0.47 \cdot \sigma_{atm} \cdot \mathrm{N} \qquad [3.8]$$

The SPT data were obtained primarily using safety hammers for which the average ER ≈ 60%. Later, a more detailed study investigated the relationship between energy-corrected standard penetration resistance ($N_{60}$) and the preconsolidation stress for different soil types as expressed:

$$\sigma_p' \approx 0.47 \cdot \sigma_{atm} \cdot (\mathrm{N}_{60})^{\mathrm{m}} \qquad [3.9]$$

where m is an exponent that depends on the soil type: m = 0.6 for clean quartzitic sands and gravels, m = 0.7 for silty to clayey sands, m = 0.8 for sandy silts, m = 0.9 for silts to clayey silts, and m = 1.0 for intact clays (Mayne 1992). **Figure 3.3a** presents the interpreted overconsolidation ratios from the 8 SPT soundings ranging from 1.3 to 19 and showing an average trend with depth.

### *3.2.6 Soil Modulus of Elasticity from SPT*

Mayne & Frost (1988) investigated the results for Appalachian Piedmont residual silty to sandy soils compiling over 160 flat dilatometer tests with supplementary routine soil borings and cone penetrometer soundings in the vicinity of Washington DC, Virginia, and Maryland. The DMT elastic moduli were compared with values obtained from laboratory tests and back-calculated moduli from field performance of full-scale foundation measurements. By considering the SPT penetration resistance measured at the

same testing locations which had an average energy rating of 60 % in the late 1980s, a direct relationship between the derived elastic modulus (E') obtained from flat dilatometer tests (DMT) assuming v' = 0.2 and corrected SPT penetration resistance ($N_{60}$) was developed expressed by:

$$E_D \text{ (bars)} = 22 \cdot \sigma_{atm} \cdot (N_{60})^{0.82} \quad [3.10]$$

**Figure 3.3b** presents the interpreted soil modulus of elasticity values from the 8 SPT soundings ranging from 10 to 280 bars and showing an overall average trend with depth.

## 3.3 CONE PENETRATION TESTS (CPT)

### *3.3.1 Overview*

The cone penetration test (CPT) involves the hydraulic pushing of an instrumented electronic steel probe at a constant rate of 20 mm/s to obtain vertical profiles of stress, friction, and pressure with depth. By recording continuous measurements with depth, the CPT is an excellent tool for detailing strata changes, delineating the interfaces between soil layers, measuring soil consistency, and detecting small lenses, inclusions, and layers within the ground. The data presentation from a CPT sounding includes cone resistance ($q_t$), sleeve friction ($f_s$), and porewater pressures ($u_2$) plotted with depth in side-by-side graphs.

Test procedures for the CPT are performed in accordance with ASTM D 5778 using either a standard drill rig or specialized cone truck. The advance of the probe requires the successive addition of rods at approximately 1 m intervals. Cone penetrometer readings are

taken at regular intervals of 1-cm to 5-cm by a field computer and data acquisition system. **Figure 3.4** presents the raw measured 15 CPTu soundings carried out at the testing site.

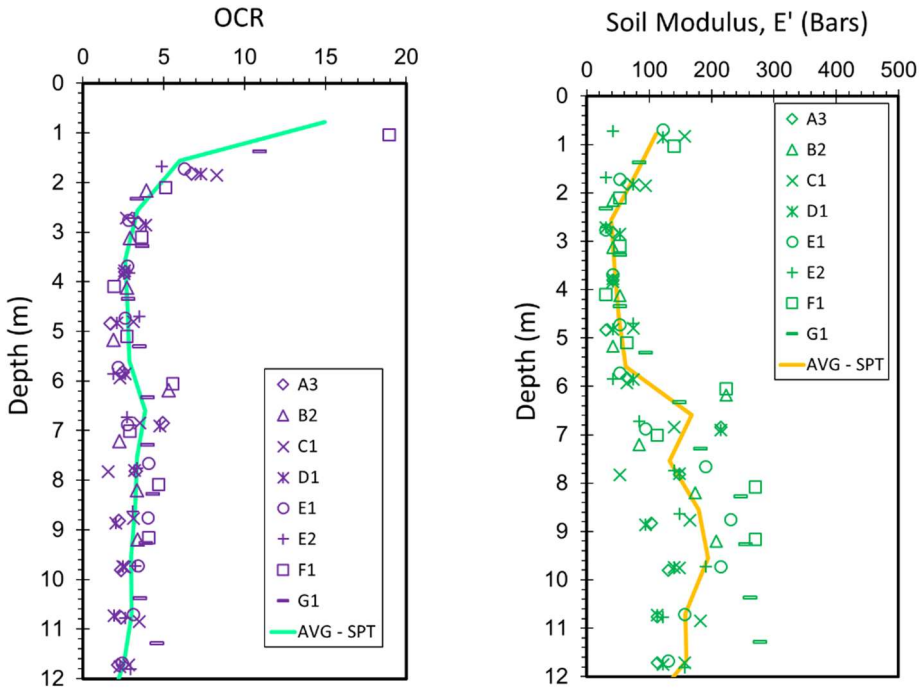


Figure 3.3. Interpreted profiles from SPT data at the B.E.S.T. site: (a) overconsolidation ratio (OCR) and (b) soil modulus of elasticity (E)

### *3.3.2 Soil Identification and Classification from CPT*

For soil type identification, simple "rules of thumb" rely on one or more of the cone readings, where a reference cone resistance value $q_t$ = 5 MPa should be identified. When the measured $q_t$ > 5 MPa, the results imply clean sands; whereas when $q_t$ < 5 MPa the readings suggest clays. For the friction sleeve, it is convenient to plot this in terms of friction ratio, FR = $f_s/q_t$ (%). As such, clean sands are identified by FR < 1%, whereas insensitive clays exhibit FR > 4%.

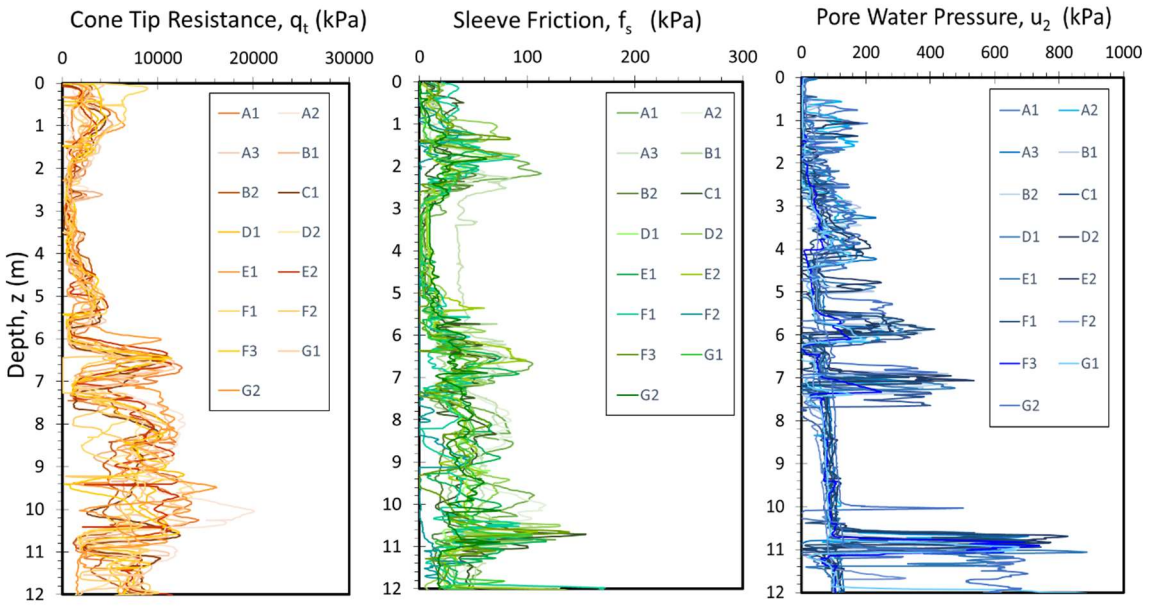


Figure 3.4. B.E.S.T. CPTu measurements with depth: (a) cone tip resistance, $q_t$; (b) sleeve friction, $f_s$; and (c) porewater pressure, $u_2$

In order to account for depth effects on the readings, stress-normalized CPT parameters have been defined by Lunne, et al. (1997) as follows:

$$Q = (q_t - \sigma_{vo}) / \sigma_{vo}' \quad [3.11]$$

$$F = 100 \cdot f_s / (q_t - \sigma_{vo}) \quad [3.12]$$

To better identify the soil type, it is convenient to use the CPT material index, $I_c$ which is defined (Robertson & Wride, 1998):

$$I_c = \sqrt{\{3.47 - \log(Q)\}^2 + \{1.22 + \log(F)\}^2} \quad [3.13]$$

The aforementioned stress normalization for tip resistance (Q) directly with effective overburden stress works well in soft clays and silts, however, in sands, the stress

normalization is proportional to the square root of effective stress, probably due to particle grain crushing or breakage effects. In this case, a modified normalized cone tip resistance has been defined as (Robertson, 2004; 2009):

$$Q_{tn} = \frac{(q_t - \sigma_{vo})}{\sigma_{atm}} \cdot \left( \frac{\sigma_{atm}}{\sigma_{vo}'} \right)^n \quad [3.14]$$

where $\sigma_{atm}$ = 1 atmosphere ≈ 1 bar = 100 kPa and the exponent n is varying with soil type, with typical values of 1.0 in the general case of clays ($I_c$ > 2.95), n = 0.75 for silty soils, and n = 0.5 for clean sands ($I_c$ < 2.05). The exponent *n* is a function of the material index $I_c$ which in turn is dependent on the modified normalized cone tip resistance (Q = $Q_{tn}$). Therefore, an iterative approach is needed to find the appropriate exponent *n* to identify the CPT material index using:

$$n = 0.381 \cdot (I_c) + 0.05 \cdot \left(\frac{\sigma_{vo}'}{\sigma_{atm}}\right) - 0.15 \quad [3.15]$$

**Figure 3.5a** presents the profiles for the CPT material index, $I_c$ with depth for the 15 conducted CPTus with an averaged trend indicating that the studied soil at B.E.S.T. can be mainly classified as sand and/ or sand mix except for the crust layer within the top 1 m that can be identified as gravelly sand and an intermediate 1-m thick clay layer at depth of 3 m that exists in some soundings and several thin silty layers at depths of 6, 7, and 11 m.

A different means to classify the soil type is using empirical soil behavioral type (SBT) charts as proposed by Robertson et al. (1986). The original 12-zone SBT system has been updated and modified to a 9-zone classification scheme. The SBT number is determined by plotting the CPTu data in terms of $Q_{tn}$ versus F. According to Robertson (2009), basic clay is found in zone 3 while "hourglass" sands form zone 6, guidelines for

the modified SBTn classifications are identified in **Table 3.1**. **Figure 3.5b** presents the evaluated soil behavioral type number for the 15 conducted CPTus where the soil profile mainly lies within zone 6 (sands) with the crust in the uppermost 1 m in zone 7 (gravelly sands) and some exceptions at 3 m depth lying in zone 3 (clays) which agrees with the previously presented classification by the CPT material index, $I_c$ and the grain size distribution from the samples obtained from the split-spoon samplers along the SPTs.

Table 3.1. Soil Behavioral Type and Zone Number as defined by CPTu Material Index, $I_c$

| Soil Classification | SBT Zone | Range CPT Material Index $I_c$ |
|---|---|---|
| Stiff sands and clays | 8 and 9 | (see note 1) |
| Sands with gravels | 7 | $I_c < 1.31$ |
| Sands: clean to silty | 6 | $1.31 < I_c < 2.05$ |
| Sandy mixtures | 5 | $2.05 < I_c < 2.60$ |
| Silty mixtures | 4 | $2.60 < I_c < 2.95$ |
| Clays | 3 | $2.95 < I_c < 3.60$ |
| Organic soils | 2 | $I_c > 3.60$ |
| Sensitive soils | 1 | (see note 2) |

Notes: 1. Zone 8 ($1.4 < F < 4.5$ %) and Zone 9 ($F > 4.5$ %) and following criterion:

$$Q_{tn} \geq \frac{1}{0.006 \cdot (F - 0.9) - 0.0004 \cdot (F - 0.9)^2 - 0.002}$$

2. Sensitive soils of zone 1 identified when $Q < 12 \exp(-1.4 F)$

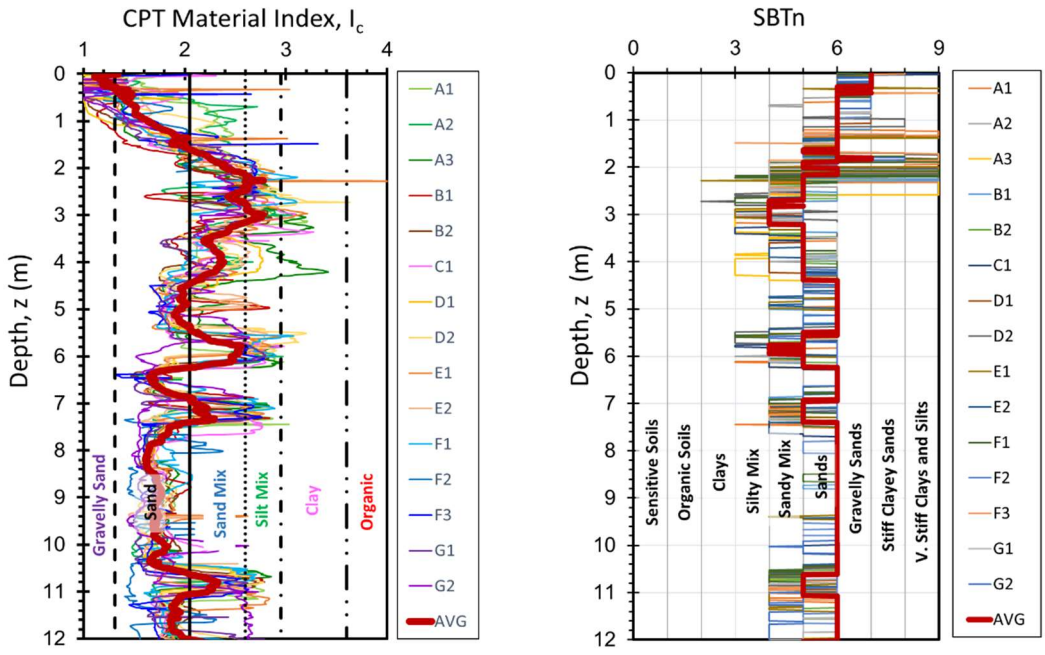


Figure 3.5. Soil Classification from CPT: (a) profiles of CPT material indices ($I_c$) and (b) soil behavioral type number (SBTn) with depth

### *3.3.3 Soil Unit Weight from CPT*

A direct unit weight relationship with the sleeve friction has been investigated by Mayne (2014) on a comprehensive database of sands, silts, and clays and is expressed as:

$$\gamma_t = \gamma_w \cdot [1.22 + 0.15 \cdot \ln(100 \cdot f_s/\sigma_{atm} + 0.01)] \quad [3.16]$$

where $\gamma_w$ = unit weight of water. **Figure 3.6a** shows the interpreted soil unit weight values from the 15 CPT soundings that range from 14 to 20 $kN/m^3$ and showing an average trend with depth.

### *3.3.4 Effective Friction Angle from CPT*

For evaluating the friction angle of sands, an elite database was compiled from special expensive undisturbed samples of clean sands (Mayne 2006). Primarily, these sands were initially frozen in-place using one-dimensional thermal techniques and, after careful mounting of specimens in triaxial apparatuses with membranes and confinement, they were allowed to thaw, then sheared to failure in triaxial compression. The results from undisturbed sands were shown to match well with the expression derived by Kulhawy & Mayne (1990):

$$\phi° = 17.6° + 11.0 \cdot \log\left(\frac{(q_t/\sigma_{atm})}{\sqrt{(\sigma'_{vo}/\sigma_{atm})}}\right) \qquad [3.17]$$

For estimating the effective stress friction angle of clays, a typical value ϕ' = 28° to 30° can be assumed, or alternatively the NTH method can be adopted which involves an effective stress limit plasticity solution for undrained penetration developed by Senneset et al. (1989) at the Norwegian Institute of Technology (NTH). In this method, a cone resistance number ($N_m$) is defined:

$$N_m = \frac{N_q - 1}{1 + N_u \cdot B_q} = \frac{q_t - \sigma_{v0}}{\sigma_{vo}' + a'} \qquad [3.18]$$

where a' = c'· cotϕ' = attraction, $N_q = K_p \cdot \exp[(\pi - 2\beta)\cdot\tan\phi']$ is the end-bearing factor for the cone tip resistance, $K_p = (1+\sin\phi')/(1-\sin\phi')$ is the passive stress coefficient, β = angle of plastification ($-20^o < \beta < +20^o$) which defines the size of the failure zone beneath the tip, $N_u = 6\cdot\tan\phi'\cdot(1+\tan\phi')$ is the porewater pressure bearing factor. The full solution allows for

an interpretation of a paired set of Mohr-Coulomb strength parameters (c' and ϕ') for all soil types.

For soft clays, it can be adopted that c' = 0, thus the term $N_m$ reduces to the well-known normalized cone resistance, $Q = q_{net}/\sigma_{vo}'$. Further simplification is achieved by taking the angle β = 0 (Terzaghi equation) for the case of undrained loading and an approximate deterministic expression for $B_q > 0.1$ is obtained (Mayne 2007):

$$\phi' = 29.5° B_q^{0.121} [0.256 + 0.336 B_q + \log Q] \quad [3.19]$$

**Figure 3.6b** presents the interpreted effective friction angle values from the 15 CPT soundings ranging from 24 to 48 degrees with an average trend with depth.

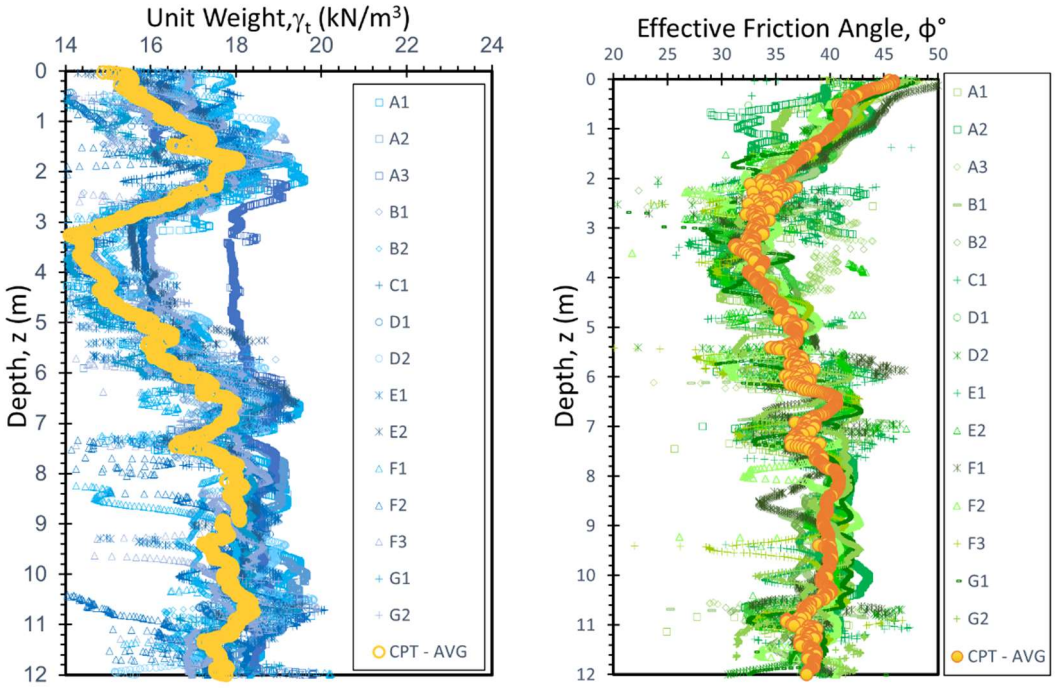


Figure 3.6. Interpreted B.E.S.T. profiles from CPT data: (a) soil unit weight ($\gamma_t$) and (b) effective friction angle (ϕ')

### *3.3.5 Stress History from CPT*

For estimating the effective preconsolidation stress using the cone penetrometer, a general equation for all types of natural soils, including sands, silts, clays, and mixed soil types has been introduced by Mayne et al. (2009) with a generalized expression is expressed as:

$$\sigma_p{}' = 0.33 \cdot (q_t - \sigma_{vo})^{m'} \cdot (\sigma_{atm}/100)^{1-m'} \quad [3.20]$$

where the *exponent m'* is a parameter that increases with fines content and decreases with mean grain size. The approximate value of parameter m' ≈ 0.72 in clean quartz sands, 0.8 in silty sands, up to m' = 1.0 in intact clays of low sensitivity. Using the CPT material index $I_c$ one can identify the magnitude of the parameter m' for general profiling of $\sigma_p$' in homogeneous or heterogeneous deposits, as well as mixed soils. For basic uncemented and non-structured soils, the exponent m' can be estimated as follows:

$$m' = 1 - \frac{0.28}{1 + (I_c / 2.65)^{20}} \quad [3.21]$$

**Figure 3.7a** presents the interpreted overconsolidation ratio values from the 15 CPT soundings that range from 1.5 to 20 along with an overall average trend of OCR with depth.

### *3.3.6 Soil Modulus of Elasticity from CPT*

Elastic theory allows for interrelationships between the equivalent elastic Young's modulus (E), shear modulus (G), and constrained modulus (D) in terms of the Poisson's ratio, such that:

$$E = 2 \cdot G \cdot (1 + \upsilon) \quad [3.22]$$

$$D' = E' \cdot \frac{(1-\nu')}{(1+\nu')(1-2\nu')} \quad [3.23]$$

For a value $\nu' \approx 0.2$ that is characteristic of sands and granular soils, the ratio D'/E' = 1.1 and therefore the constrained modulus and drained Young's modulus are often used somewhat interchangeably. For an approximate evaluation of the constrained modulus (and drained Young's modulus) from CPT results, the common approach is expressed in the form:

$$D' \approx \alpha_D \cdot (q_T - \sigma_{V0}) \quad [3.24]$$

where $\alpha_D$ is an empirical scaling factor that has been shown to depend upon soil type, confining stress level, overconsolidation, and other factors (Kulhawy & Mayne, 1990).

From numerous studies in the literature, $\alpha_D \approx 5$ is an approximate starting place, excepting soft plastic organic clays and cemented geomaterials (Mayne 2007b). **Figure 3.7b** presents the interpreted soil modulus of elasticity values from the 15 CPT soundings, with E' ranging between 5 to 60 MPa. The overall average trend of E' is also shown with depth.

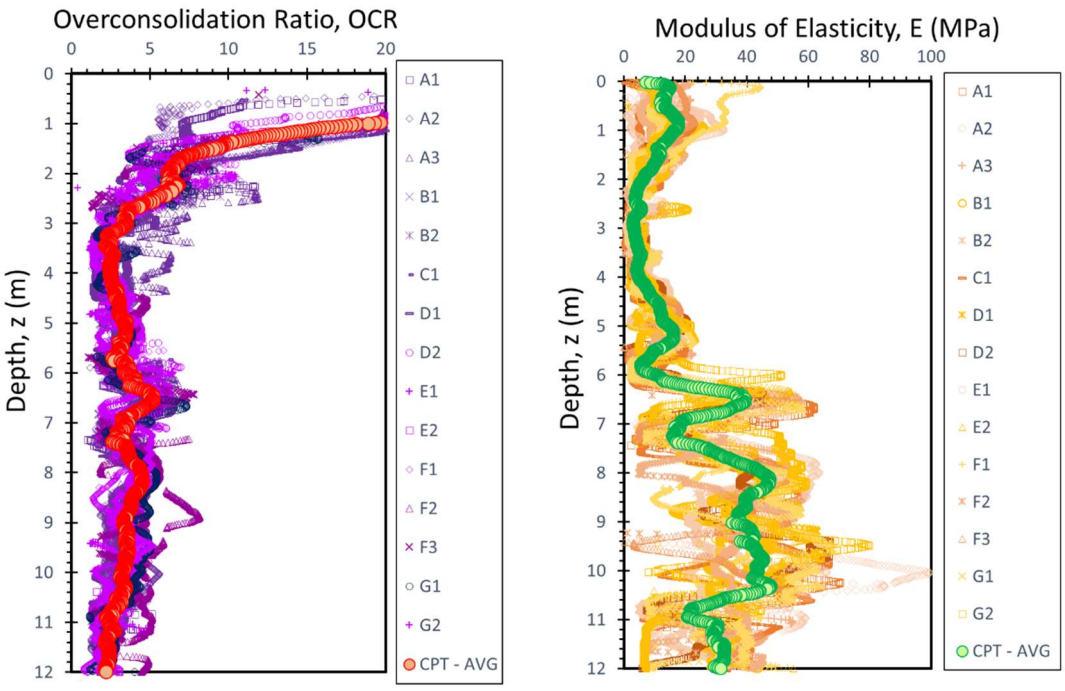


Figure 3.7. Interpreted profiles from B.E.S.T. CPTs: (a) overconsolidation ratio (OCR) and (b) soil modulus of elasticity (E)

## 3.4 FLAT PLATE DILATOMETER TEST (DMT)

### *3.4.1 Overview*

The flat dilatometer test (DMT) is simple, repeatable, economic, and operator-independent. The device consists of a tapered stainless steel blade with 18° wedge tip that is vertically advanced into the ground at either 20-cm or 30-cm interval per ASTM D 6635. Two pressure readings are taken at each test depth (A and B) as a flexible steel membrane is inflated with nitrogen gas. The DMT analyses primarily rely on empirical correlative relationships and may require adjustments for local geologies. No borehole cuttings or spoil are generally produced by this test, although it is possible to advance a conventional soil boring and then perform the DMT downhole within the borehole.

### *3.4.2 DMT Index Parameters*

The field A- and B- readings need to be corrected for membrane stiffness effects to obtain the contact or lift-off pressure, $p_o$, and expansion pressure, $p_1$. Corrections of the readings have been presented by Schmertmann (1986):

$$p_0 = 1.05\,(A + \Delta A - z_m) - 0.05\,(B - \Delta B - z_m) \quad [3.25]$$

$$p_1 = B - \Delta B - z_m \quad [3.26]$$

where $\Delta A$ and $\Delta B$ are reported as positive absolute values for the calibration factors for applied suction and expansion of the membrane in the air, respectively, and $z_m$ is the gage offset zero reading when vented to atmospheric pressure (typically set to zero for a new gage). **Figure 3.8** presents the corrected lift-off and expansion pressure profiles with depth for the 6 DMTs performed at the B.E.S.T. site.

The two dilatometer pressures, $p_0$ and $p_1$, are used together with the hydrostatic water pressure, $u_o$, to provide three index parameters: (a) material index $I_D$, (b) horizontal stress index $K_D$, and (c) dilatometer modulus, $E_D$. These were developed by Marchetti (1980) to provide information on the stratigraphy, soil types, and the evaluation of soil parameters. Hydrostatic water pressure ($u_0$) can be evaluated based on available groundwater table information. The DMT material index, $I_D$, is related to the soil classification and is presented as:

$$I_D = (p_1 - p_0)/(p_0 - u_0) \quad [3.27]$$

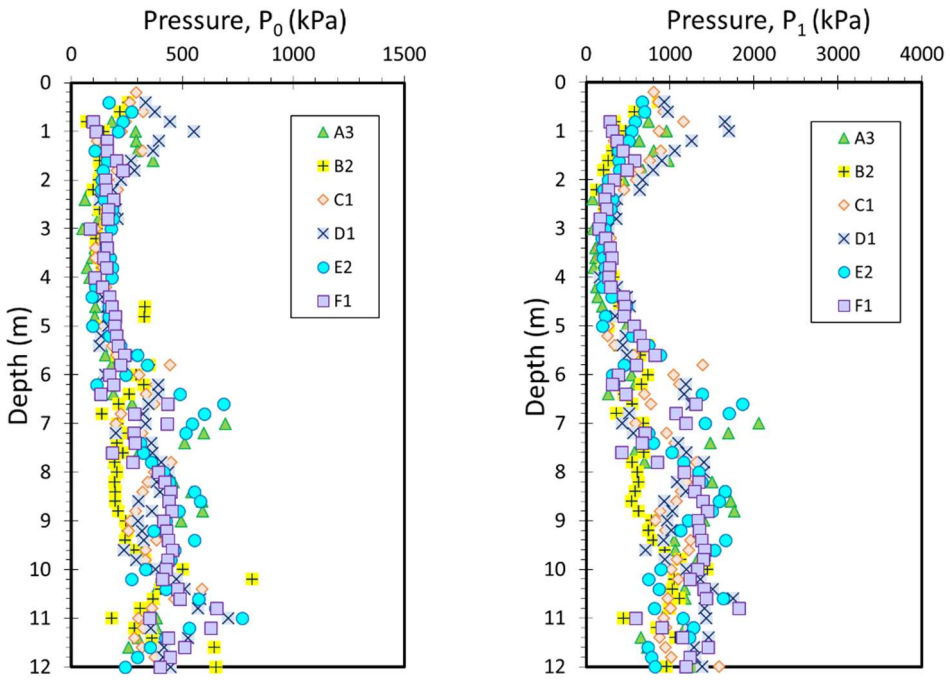


Figure 3.8. B.E.S.T. DMT readings with depth: (a) lift off pressure $p_0$ and (b) expansion pressure $p_1$

According to Marchetti (1980), the soil type can be identified: clay: $0.1 < I_D < 0.6$, silt: $0.6 < I_D < 1.8$, and sand: $1.8 < I_D < 10$. In general, $I_D$ provides an expressive profile of soil type, and for normal soils, a reasonable soil description as illustrated in **Figure 3.9a**, whereby considering the averaged trend with depth it can be determined that most of the soil profile under study can be considered as sand mixed with sand-silt mixture with an exception for a 1-m thick clay layer at about 3 m depth which agrees with the soil classification presented earlier by both SPTs and CPTs.

The horizontal stress index, $K_D$, is related to the in-situ horizontal stress-state of the soil. The index $K_D$ will always be greater than $K_0$ due to disturbance caused during insertion of the blade. This parameter is presented in **Figure 3.9b** and is expressed as:

$$K_D = (p_0 - u_0)/\sigma'_{v0} \qquad [3.28]$$

The dilatometer modulus $E_D$; presented in **Figure 3.9c**; is obtained from $p_0$ and $p_1$ from the theory of elasticity. For the 60-mm membrane diameter and required 1.1 mm displacement, it is found according to Marchetti (1980) that the modulus is evaluated as:

$$E_D = 34.7\,(p_1 - p_0) \qquad [3.29]$$

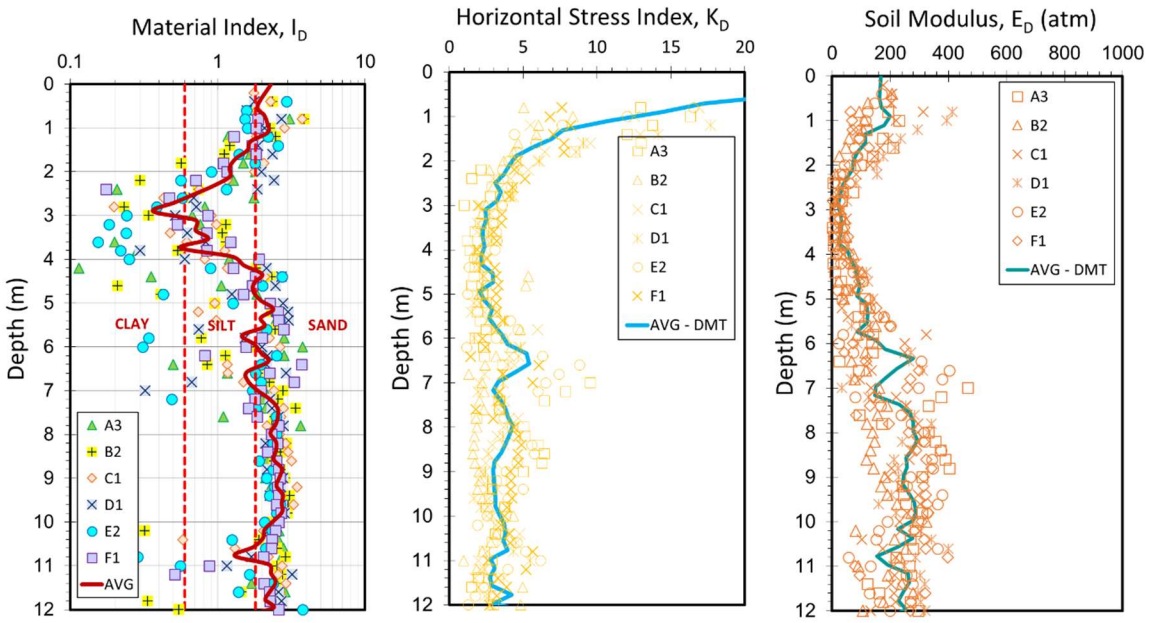


Figure 3.9. B.E.S.T. profiles from DMTs: (a) soil material index ($I_D$), (b) horizontal stress index ($K_D$), and (c) dilatometer modulus ($E_D$)

### *3.4.3 Soil Unit Weight from DMT*

The total soil unit weight ($\gamma_t$) can be evaluated using an approximate expression from the material index and dilatometer modulus as:

$$\gamma_t = 1.12\,\gamma_w (E_D/\sigma_{atm})^{0.1} (I_D)^{-0.05} \qquad [3.30]$$

where $\gamma_w$ = unit weight of water and $\sigma_{atm}$ = atmospheric pressure. For each successive layer, the cumulative total overburden stress ($\sigma_{vo}$) can be calculated, as this is needed for the

determination of the effective vertical overburden stress ($\sigma_{vo}$'= $\sigma_{vo}$ - $u_o$) and the evaluation of the $K_D$ parameter (Mayne et al., 2002). **Figure 3.10a** shows the interpreted soil unit weights from the 6 DMT soundings, ranging from 13.5 to 19.5 $kN/m^3$, and also present an average trend with depth.

### *3.4.4 Effective Friction Angle from DMT*

The peak friction angle in sands can be assessed using the flat plate dilatometer test. A wedge plasticity solution for the CPT was presented by Marchetti (1985) that was later cross-correlated for CPT-DMT relationships by Campanella & Robertson (1991). The wedge solutions relate the DMT lateral stress index ($K_D$) as a function of φ' and lateral stress state including active, at-rest (NC), and passive conditions. The passive case provides a generally conservative evaluation of peak friction angle and gives a good agreement with field data from different sand sites (Mayne, 2001). The expression for the passive case can be approximated by a hyperbola in the form:

$$\phi' = 20° + \frac{1}{0.04 + 0.06/K_D} \quad [3.31]$$

As for clays and silts, Ouyang & Mayne (2016) use the NTH method, as explained earlier with the cone penetration test in Eq. [3.19], with the following DMT equivalent quantities:

$$(u_2 - u_0)_{DMT} = (p_0 - u_0) \quad [3.32]$$

$$(q_t - \sigma_{vo})_{DMT} = 2.93 \cdot p_1 - 1.93 \cdot p_0 - u_0 \quad [3.33]$$

**Figure 3.10b** shows the interpreted effective friction angle values from the 6 DMT soundings using methods for sands and clays ranging from 26 to 45 degrees with an average trend with depth.

### *3.4.5 Stress History from DMT*

Initial studies by Marchetti (1980) investigated the relationship between the overconsolidation ratio (OCR) and the DMT horizontal stress index, $K_D$. The correlation was based on the results of the database from only five clays that were later investigated by Mayne (1995) to include data from 24 clays ranging from intact to calcareous to fissured clays. The correlation is expressed in terms of net contact pressure ($p_0 - u_0$):

$$\sigma_p' \approx 0.5 \cdot (p_0 - u_0) \quad [3.34]$$

**Figure 3.10c** shows the interpreted OCRs from the 6 DMT soundings that range from 1.5 to 18. The overall average trend with depth is also shown and over much of the profile suggests low OCR soils in the range of 1 to 2.

### *3.4.6* Soil Modulus of Elasticity from DMT

The constrained modulus $M_{DMT}$ determined from the flat dilatometer test is the drained tangent modulus at $\sigma'_{v0}$ and is equivalent to the oedometer modulus obtained in the laboratory. $M_{DMT}$ is evaluated using correction factor $R_M$ to dilatometer modulus $E_D$ using adjustment factor $R_M$:

$$M_{DMT} = R_M . E_D \quad [3.35]$$

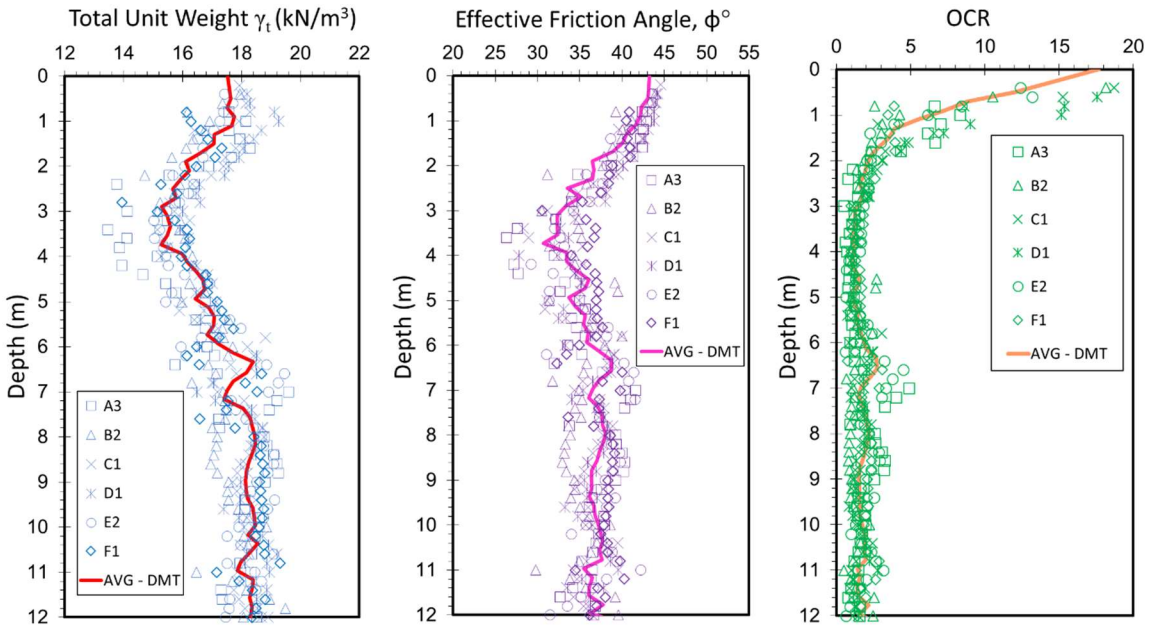


Figure 3.10. B.E.S.T. profiles from DMT soundings: (a) soil unit weight ($\gamma_t$), (b) effective stress friction angle ($\phi$'), and (c) overconsolidation ratio (OCR)

The equations defining $R_M$ as a function of both $I_D$ and $K_D$ are described by (Marchetti 1980) and are given in **Table 3.2**.

Table 3.2. Equations defining modifier term $R_M = M_{DMT}/E_D$

| Condition | $R_M$ Definition |
|---|---|
| For $I_D < 0.6$ | $R_M = 0.14 + 2.36 \log K_D$ |
| For $I_D > 3$ | $R_M = 0.5 + 2 \log K_D$ |
| For $0.6 < I_D < 3$ | $R_M = 0.05 + 0.15 \cdot I_D + (2.45 - 0.15 \cdot I_D) \log K_D$ |
| For $K_D > 10$ | $R_M = 0.32 + 2.18 \log K_D$ |
| If $R_M < 0.85$ | Set $R_M = 0.85$ |

The Young's modulus E' of the soil skeleton can be derived from $M_{DMT}$ using the theory of elasticity equation:

$$E' = \frac{(1+\upsilon')(1-2\upsilon')}{(1-\upsilon')} M_{DMT} \qquad [3.36]$$

In sands, using a representative value for Poisson's ratio $\nu' = 0.2$, then $E' = 0.9\ M_{DMT}$.

## 3.5 DOWNHOLE SHEAR WAVE VELOCITY TESTS ($V_{sVH}$)

### *3.5.1 Overview*

A fundamental parameter of the ground is the shear wave velocity ($V_s$) which can be determined either using field geophysics or laboratory tests on small specimens. Shear waves can be measured on all geomaterials ranging from clays and silts to sands and gravels as well as in mixed soil types, fractured to intact rocks, and artificial ground. Thus, it serves as an excellent reference benchmark in comparing stiffness and stress state in almost all applications.

The profile of $V_s$ is a necessary input for static and dynamic geotechnical analyses since it directly provides the small-strain shear modulus (initial shear modulus):

$$G_{\max} = G_0 = \rho_t \cdot V_s^2 \qquad [3.37]$$

$\rho_t$ = total mass density = $\gamma_{sat} / g_a$ [3.38]

where $g_a$ is acceleration due to gravity = 9.81 m/s$^2$.

In-situ methods for the measurement of shear wave velocity are many and can be classified into two main categories: non-invasive and invasive methods. Non-invasive methods include refraction survey, reflection survey, and surface wave methods, or Rayleigh waves. Invasive methods include cased borehole methods such as: crosshole test (CHT), downhole test (DHT), uphole test (UHT), and P-S suspension logger, as well as direct push methods: seismic cone penetration test (SCPT) and seismic flat dilatometer test (SDMT) which are efficient versions of the DHT mode.

For in-situ geotechnical testing, the most common shear wave mode is obtained by DHT (ASTM D 7400) that measures a vertically-propagating horizontally-polarized shear wave velocity, or $V_{sVH}$ mode. This can be carried out using a horizontal wave generating surface source and downhole horizontally-oriented geophones positioned in either drilled-cased-grouted boreholes, or by direct-push SDMT as carried out at B.E.S.T. **Figure 3.11** presents the raw downhole shear wave velocity profiles with depth carried out as a part of the SDMTs, in addition to the corresponding small strain shear modulus profiles evaluated using Eq. [3.37] and [3.38].

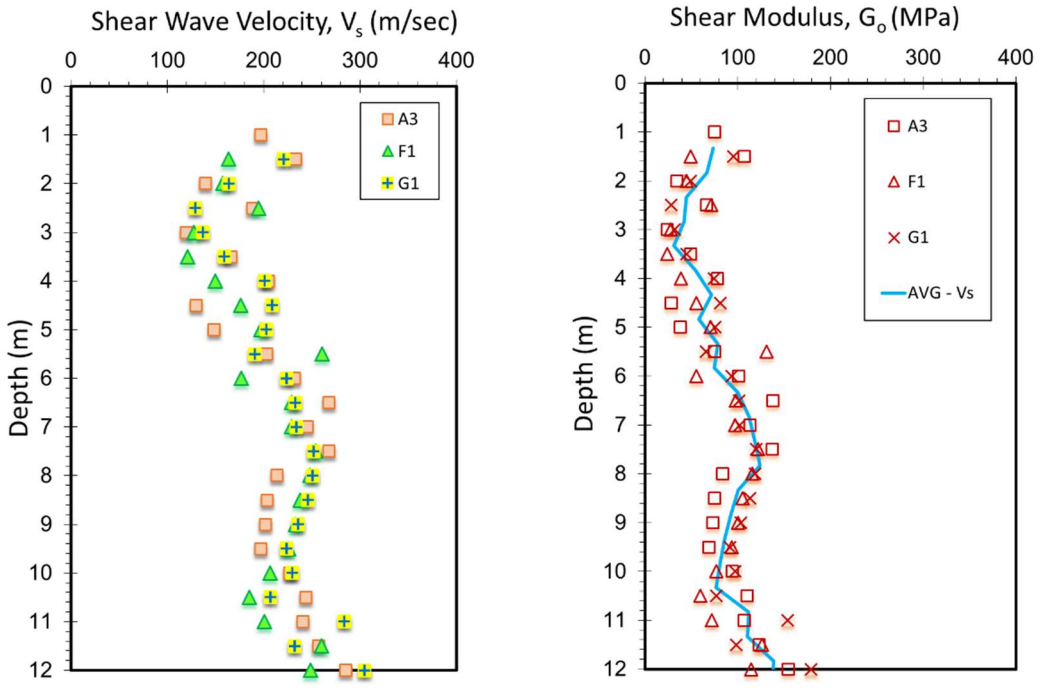


Figure 3.11. Profiles of downhole shear wave velocity ($V_{sVH}$) with depth and corresponding small strain shear modulus ($G_o$)

### *3.5.2 Soil Unit Weight from Shear Wave Velocity*

The soil unit weight can be directly evaluated from the profile of downhole shear wave velocity with depth as previously mentioned in Eq. [3.4]. **Figure 3.12a** shows the interpreted soil unit weight values from the 3 $V_{sVH}$ soundings ranging from 16 to 19 $kN/m^3$ with an average trend also presented with depth.

### *3.5.3 Effective Friction Angle from Shear Wave Velocity*

A direct relation between stress-normalized shear wave velocity and effective friction angle for clean quartz sands has been introduced by Uzielli et al. (2013), where a dataset of a total of 16 sands sampled from 12 sites using special undisturbed freezing techniques has been investigated and expressed as:

$$\phi' = 3.90\ (V_{s1})^{0.44} \qquad [3.39]$$

$$\text{where } V_{s1} = (V_s) / (\sigma_{vo}' / \sigma_{atm})^{0.25} = \text{stress-normalized shear wave velocity (m/s)} \qquad [3.40]$$

As for clays and silts, there is no direct developed relationship with DHT, hence, an assumed friction value of 30 degrees can be assigned. Better yet, the procurement of undisturbed samples for triaxial compression tests is recommended. **Figure 3.12b** shows the interpreted effective friction angle values from the three $V_{sVH}$ profiles shows and interpreted $\phi'$ varying from 35 to 45 degrees along with an overall average trend with depth.

### *3.5.4 Stress History from Shear Wave Velocity*

A compiled database covering different geomaterials has investigated the evaluation of soil stress history in terms of shear wave velocity. The shear wave velocity

is used to evaluate the small-strain shear modulus as per Eqns. [3.37] and [3.38], and by knowing the shear wave velocity profile with depth, the unit weight can be evaluated using Eq. [3.4] which is used to evaluate the effective vertical overburden pressure. Accordingly, the effective preconsolidation stress can be evaluated using (Mayne 2005):

$$\sigma_p' = 0.101\,(\sigma_{atm})^{0.102}(G_0)^{0.478}(\sigma_{vo}')^{0.42} \qquad [3.41]$$

where $\sigma_{atm}$ is atmospheric pressure = 1 bar = 100 kPa = 1 kg/cm$^2$. **Figure 3.12c** shows the interpreted overconsolidation ratio values from the three $V_{sVH}$ profiles. Corresponding OCRs range from 1.5 to 6.2 with an average profile of interpreted OCR shown with depth.

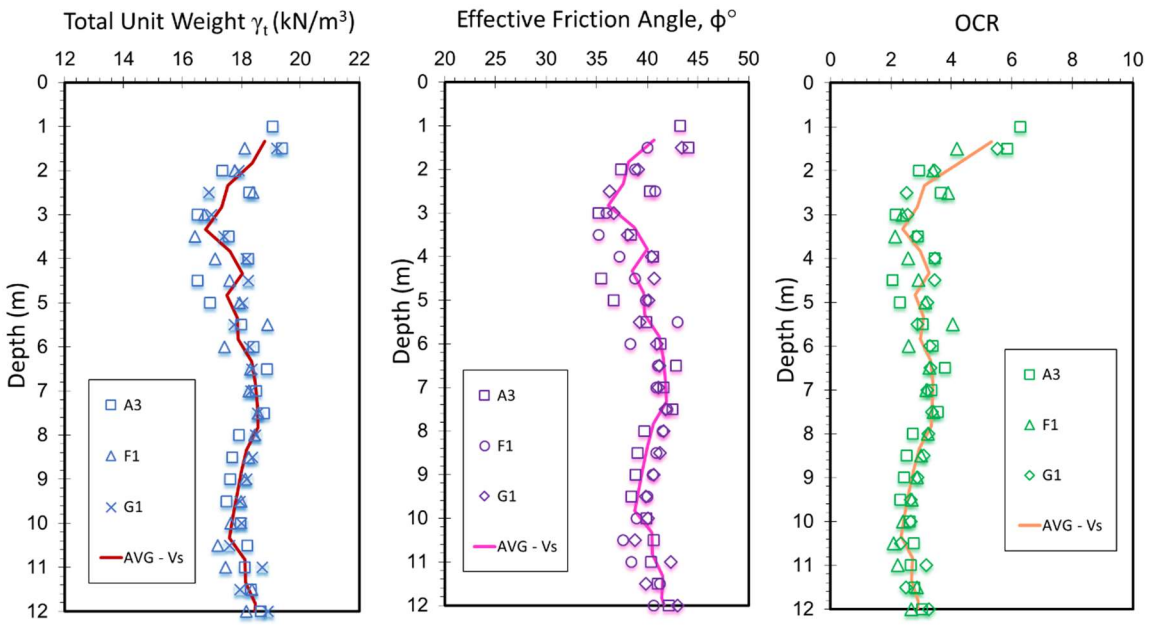


Figure 3.12. B.E.S.T. profiles from $V_{sVH}$ data: (a) interpreted soil unit weight ($\gamma_t$), (b) effective friction angle ($\phi$'), and (c) overconsolidation ratio (OCR)

## 3.6 COMPARISON AND CONCLUSIONS

By considering the presented field measurements and the interpreted geotechnical parameters using different in-situ measuring techniques, it can be concluded that there is a relatively good agreement and consistency amongst the various tests. By considering the soil classification and stratigraphy, we find that the grain size distribution results obtained from the SPT split-spoon samplers agree with the classification methods by CPT; whether using the material index, $I_c$ or the soil behavioral type number (SBTn); that also agree with the results obtained using DMT material index, $I_D$ indicating the overall general sandy nature of the soil profile with the existence of a one-m clay layer at about 3m depth and silty layers around 0.5 m thick at depths of 6, 7, and 11 m.

A comparison of the interpreted mean trends with depth for the different geotechnical parameters using SPT, CPT, DMT, and $V_s$ is presented in **Figure 3.13** for soil unit weight, $\gamma_t$ and effective friction angle, $\phi'$ and in **Figure 3.14** for OCR and soil modulus. Overall, it can be observed that there is reasonable agreement from the different methods within an acceptable deviation of ± 10 %. Perhaps, an observed exception is the SPT interpreted friction angle data which may be attributed to the low energy rating (ER) assigned to this equipment.

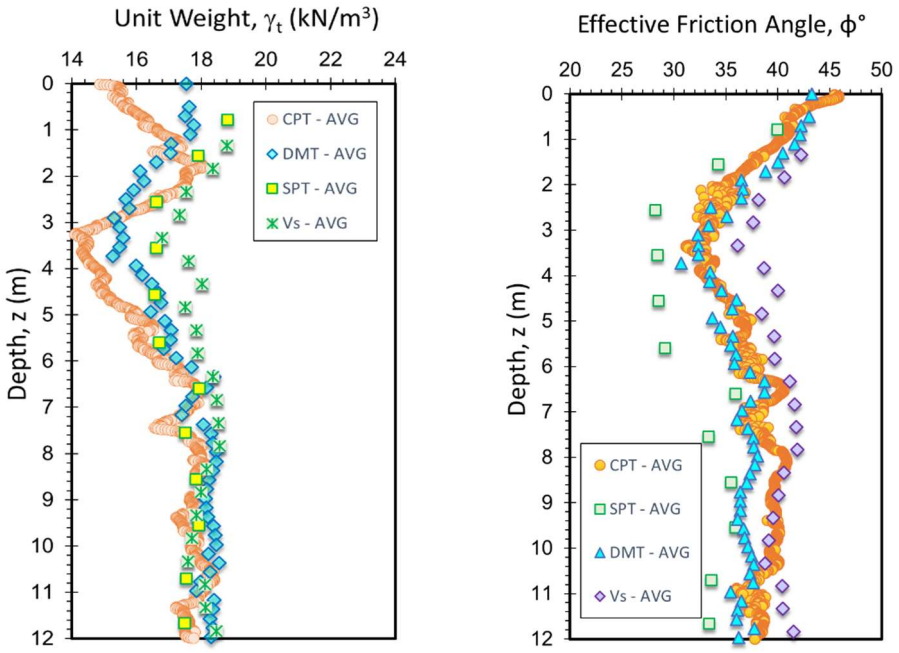


Figure 3.13. Comparison between averaged interpreted soil unit weight ($\gamma_t$) and effective friction angle ($\phi$') values from CPT, SPT, DMT, and $V_{sVH}$ data

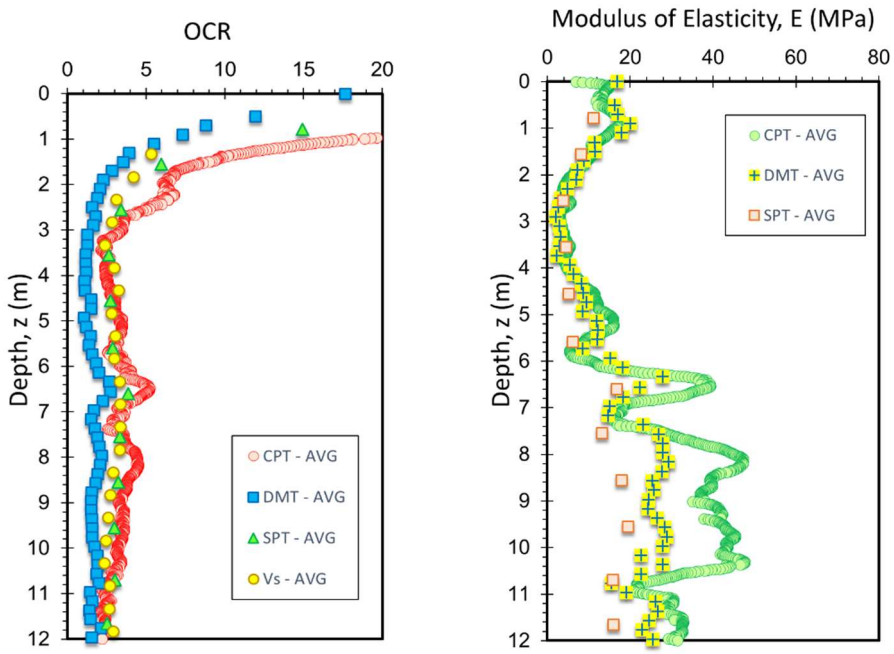


Figure 3.14. Comparison between averaged interpreted overconsolidation ratio (OCR) and soil modulus of elasticity (E) values from CPT, SPT, DMT, and $V_{sVH}$ data

# Chapter 4. Stress History Evaluation of Soils from Piezocone

## 4.1 Abstract:

This chapter presents a generalized methodology for evaluating the stress history of different soils and geomaterials using piezocone data, where stress history is represented in terms of a preconsolidation stress or effective yield stress, commonly interpreted from results obtained on laboratory one-dimensional consolidation tests. A well-established analytical model developed as a hybrid of spherical cavity expansion theory and critical state soils mechanics (SCE-CSSM) is used as a basis for defining stress history expressions in intact clays from net cone tip resistance ($q_{net} = q_t - \sigma_{vo}$). Results from calibration chamber testing defined the stress history relationship for clean quartz-silica sands from net cone tip resistance. A resemblance between the two expressions of intact clays and clean sands guided the formulation of a generalized expression for evaluating stress history from net cone resistance for different soil types.

A comprehensive database of 78 worldwide sites covering a variety of geomaterials ranging from clays to silts to sands and mixed soil types was compiled and a unified relationship was formulated in terms of a power law function for expressing yield stress in terms of net cone tip resistance having an exponent designated m'. The exponent m' varies with fines content (FC) and mean grain size ($D_{50}$). Moreover, direct relationships for m' with several defined CPT material indices are investigated and appear reliable for uncemented and inorganic soils of low sensitivity. Several case studies are presented

showing the agreement between the estimated stress history profile using the interpreted exponent value and the laboratory measured values.

## 4.2 Stress History in Soils

The loading memory and geological processes that a soil has experienced since its formation, collectively termed stress history, largely determines the soil strength, stiffness, flow, and compressibility characteristics as well as the geostatic stress state of the formation. Stress history is often represented by the preconsolidation stress ($\sigma_p'$) that is defined as the maximum effective overburden stress ever felt by the soil since its formation. The preconsolidation, or yield, stress, separates regions of normally consolidated (NC) and overconsolidated states (OC) of the soil behavioral response (Holtz et al. 2011).

The overconsolidation ratio (OCR) is a normalized parameter based on $\sigma_p'$ and the current effective vertical stress ($\sigma_{vo}'$) such that:

$$OCR = \sigma_p' / \sigma_{vo}' \quad [4.1]$$

Yield stress ($\sigma_{vy}'$) and yield stress ratio ($YSR = \sigma_{vy}'/\sigma_{vo}'$) are used more recently to express additional effects (in addition to mechanical overconsolidation) such as diagenesis, bonding, and ageing (Jardine et al. 2004). Overconsolidation difference (OCD) is an alternative quantity representing the stress history of the soil where $OCD = (\sigma_p' - \sigma_{vo}')$ as discussed by Locat et al. (2003). OCD may be used to represent the stress history profile of soils that are preconsolidated due to effects of erosion, glaciation, or excavation. The value of OCD is constant with depth, unlike the typical OCR profile which varies with depth; OCD and OCR are related as follows:

$$OCD = \sigma_{vo}' (OCR - 1) \quad [4.2]$$

Stress history is typically evaluated from the results of series of one-dimensional laboratory consolidation tests carried out on undisturbed specimens using either an oedometer or a consolidometer (ASTM D2435), where specimens are subjected to constrained compressive stresses in a mechanical oedometer, pneumatic or hydraulic consolidometer, or automated constant rate of strain (CRS) device. There are at least 28 different plotting and curve fitting methods that have been proposed to evaluate the preconsolidation stress from consolidation tests (Ku and Mayne, 2013), yet the most commonly used method is the first developed by Casagrande (1936).

## 4.3 Stress History Evaluation

Laboratory testing using an oedometer or consolidometer or CRS device is associated with several issues, the most significant is disturbance which can be attributed to the sampling process, specimen handling, and stress relief due to bringing the sample from some depth to the ground surface with possible swelling and expansion. To overcome issues associated with the laboratory methods, $\sigma_p'$ can be estimated using empirical correlations or analytical solutions with in-situ test measurements that avert the issues of sample disturbance. Moreover, these in-situ are also faster and more economical than laboratory tests, with digital data available to the geoengineer as soon as the sounding is completed. Therefore, it has become more demanding and of great value to investigate and develop CPT-based methods to evaluate stress history profiles of soils.

## 4.4 Estimating Stress History Using CPTu Measurements

Over the past few decades, a number of correlative methods were introduced towards the evaluation of soils stress history from field tests. For the CPT, some methods relied on the measurement of undrained shear strength ($s_u$) in clay soils, as suggested by Schmertmann (1978). Alternatively, other approaches were developed based on a direct linkage to the different piezocone readings or parameters. For instance, Wroth (1984) related the overconsolidation ratio (OCR) to the normalized porewater pressure parameter: $B_q = \Delta u_2/(q_t - \sigma_{v0})$. Kulhawy and Mayne (1990) developed correlations between OCR and the normalized cone tip resistance: $Q = (q_t - \sigma_{v0})/\sigma'_{v0}$. Houlsby (1988) linked OCR to the normalized effective cone tip resistance: $Q_u = (q_t - u_2)/\sigma'_{v0}$. Mayne and Holtz (1988) associated the effective preconsolidation stress to the change in porewater pressure measurements from CPTu soundings ($\Delta u_1$ and $\Delta u_2$). Tavenas and Leroueil (1990) correlated $\sigma_p'$ to net cone tip resistance ($q_{net} = q_t - \sigma_{v0}$). Konrad and Law (1987) developed an analytical model that tied $\sigma_p'$ to the effective cone tip resistance ($q_{eff} = q_t - u_2$).

While these approaches could be developed on the basis of calibrating laboratory consolidation test results from undisturbed samples of clay with field piezocone readings, a similar approach was not as easily done or possible with other geomaterials, such as silts, sandy silts, silty sands, sands, and granular soils where undisturbed samples are most difficult and expensive in order to procure (i.e., special freezing methods, injection of gels and/or gum resins, etc.). Hence, a methodology based on a sound analytical framework and then applied to a comprehensive global database was considered crucial and therefore investigated in the following sections.

## 4.5 Analytical SCE-CSSM Model for CPTu in Clays

A hybrid analytical model for piezocone penetration in clays was developed from Spherical Cavity Expansion theory and Critical State Soil Mechanics (SCE-CSSM), as detailed by Mayne (1991) and Chen & Mayne (1994). The hybrid formulation expresses the measured cone tip resistance and porewater pressure in closed-form solutions:

$$q_t = \sigma_{vo} + [(4/3)\cdot(\ln I_R + 1) + \pi/2 + 1]\cdot(M/2)\cdot(OCR/2)^{\Lambda}\cdot\sigma_{vo}' \qquad [4.3]$$

$$u_2 = u_o + [(2/3)\cdot(\ln I_R)\cdot(M)\cdot(OCR/2)^{\Lambda}\cdot\sigma_{vo}'] + [1-(OCR/2)^{\Lambda}]\cdot\sigma_{vo}' \qquad [4.4]$$

where $M = 6\cdot\sin\phi'/(3-\sin\phi')$, $I_R = G/s_u$ = undrained rigidity index, G = shear modulus, $s_u$ = undrained shear strength, and $\Lambda = 1 - C_s/C_c$ = plastic volumetric strain potential, with $C_s$ = recompression or swelling index, and $C_c$ = virgin compression index. The value of $\Lambda \approx 0.8$ to 0.9 for most clays (Kulhawy & Mayne 1990).

The developed equations can be rearranged to express the OCR in terms of normalized net cone resistance, $Q = (q_t - \sigma_{vo}) / \sigma_{vo}'$ and normalized excess porewater pressure, $U^* = \Delta u / \sigma_{vo}'$, where:

$$OCR = 2\cdot\left[\frac{(q_t - \sigma_{vo})/\sigma_{vo}'}{(2/3)\cdot M\cdot(\ln I_R + 1) + \pi/2 + 1}\right]^{(1/\Lambda)} \qquad [4.5]$$

$$OCR = 2\cdot\left[\frac{(\Delta u/\sigma_{vo}') - 1}{(2/3)\cdot M\cdot\ln(I_R) - 1}\right]^{(1/\Lambda)} \qquad [4.6]$$

$$OCR = 2 \cdot \left[ \frac{(\Delta u / \sigma_{vo}') - 1}{(2/3) \cdot M \cdot \ln(I_R) - 1} \right]^{(1/\Lambda)} \quad [4.6]$$

For soft to firm clays, the shear-component of porewater pressures is small ( < 20%) of the total measured porewater pressures. At low OCRs < 3, that portion can essentially be neglected which reduces equation [4.6] to:

$$OCR = 2 \cdot \left[ \frac{(\Delta u / \sigma_{vo}')}{(2/3) \cdot M \cdot \ln(I_R)} \right]^{(1/\Lambda)} \quad [4.7]$$

Finally, by combining the expressions for Q and $\Delta u/\sigma_{vo}'$, a third expression for OCR can be derived in terms of the normalized effective cone resistance, $Q_u = (q_t - u_2)/\sigma_{vo}'$. In this case, there is no need to rely on the input value of rigidity index which reduces the number of unknown input parameters:

$$OCR = 2 \cdot \left[ \frac{1}{1.95 \cdot M + 1} \left( \frac{q_t - u_2}{\sigma_{vo}'} \right) \right]^{(1/\Lambda)} \quad [4.8]$$

The solutions require only three input parameters (M, $I_R$, and $\Lambda$) for each clay soil.

In a first step to simplify the presented power law equations into simpler linear expressions for use in low OCR soils, a value of $\Lambda = 1$ is adopted converting the equations into:

$$\sigma_p' = \frac{(q_t - \sigma_{vo})}{M \cdot (1 + \tfrac{1}{3} \cdot \ln I_R)} \quad [4.9]$$

$$\sigma_p' = \frac{(u_2 - u_0)}{\frac{1}{3} \cdot M \cdot \ln I_R} \quad [4.10]$$

$$\sigma_p' = \frac{(q_t - u_2)}{0.975 \cdot M + 0.5} \quad [4.11]$$

## 4.6 Evaluating Stress History from CPTu in Intact Clays

In the case of uncemented and inorganic clays with low sensitivity, further simplification can be applied for stress history equations by adopting characteristics values for the effective stress friction angle $\phi' = 30^\circ$ (i.e., M = 1.2) and rigidity index $I_R = 100$ (Mayne, 2005) as follows:

$$\sigma_p' = 0.33 (q_t - \sigma_{vo}) \quad [4.12]$$

$$\sigma_p' = 0.54 (u_2 - u_o) \quad [4.13]$$

$$\sigma_p' = 0.60 (q_t - u_2) \quad [4.14]$$

The simplified expressions agree with the findings of an extensive statistical study carried out by Chen and Mayne (1996) on some 206 clays relating the measured yield stress to $q_{net}$, $\Delta u_2$ and $q_{eff}$. The above coefficients (0.33, 0.54, and 0.60) were more or less confirmed by an independent study using new data from 22 Canadian clay sites investigated by Demers and Leroueil (2002). Furthermore, the coefficients can be modified and adjusted to fit with local geologies with site-specific behavior that do not fit with the above coefficients.

The general trend relating the effective yield stress to the net cone tip resistance from equation [4.12] along with the clay sites compiled by Chen and Mayne (1996) is presented in **Figure 4.1**. From the plotted data, the clay sites can be subdivided into two distinct main groups: intact and fissured clays. The data from fissured clays do not fit the general trend of the intact clays and generally lie above it in a distinct separate cluster.

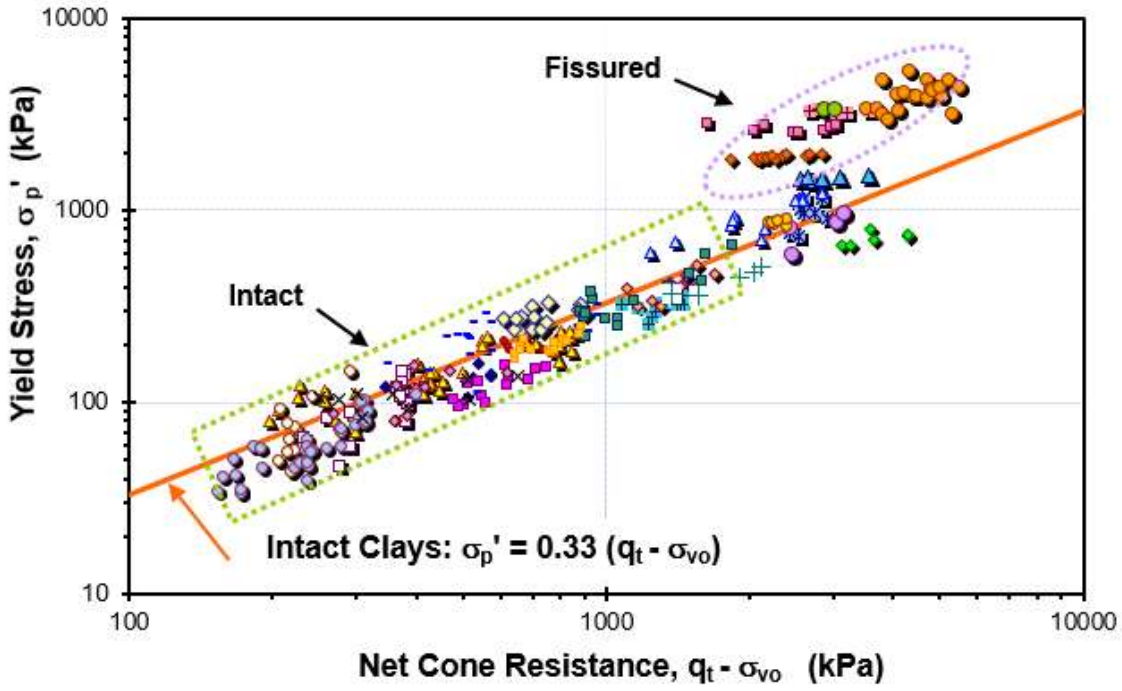


Figure 4.1. Relating effective yield stress to net cone resistance in intact and fissured clays (after Mayne et al., 2009)

## 4.7 Evaluating Stress History of Overconsolidated Sands

Mayne (2007) has carried out extensive statistical analyses on 626 CPT calibration chamber tests performed on 26 silica and quartz sands. The main aim of the conducted statistical review was to develop a link between the induced overconsolidation ratio (OCR), the coefficient of geostatic lateral stress ($K_0 = \sigma_{hc}'/\sigma_{vc}'$), effective vertical stresses and

measured cone tip resistance ($q_t$) in clean sands. The final results were expressed in terms of normalized cone tip resistance (Q), OCR, $q_t$, $\sigma_{vc}'$, and $K_0$, as presented in **Figure 4.2.** Here, the sands can be grouped upon the corresponding OCR range.

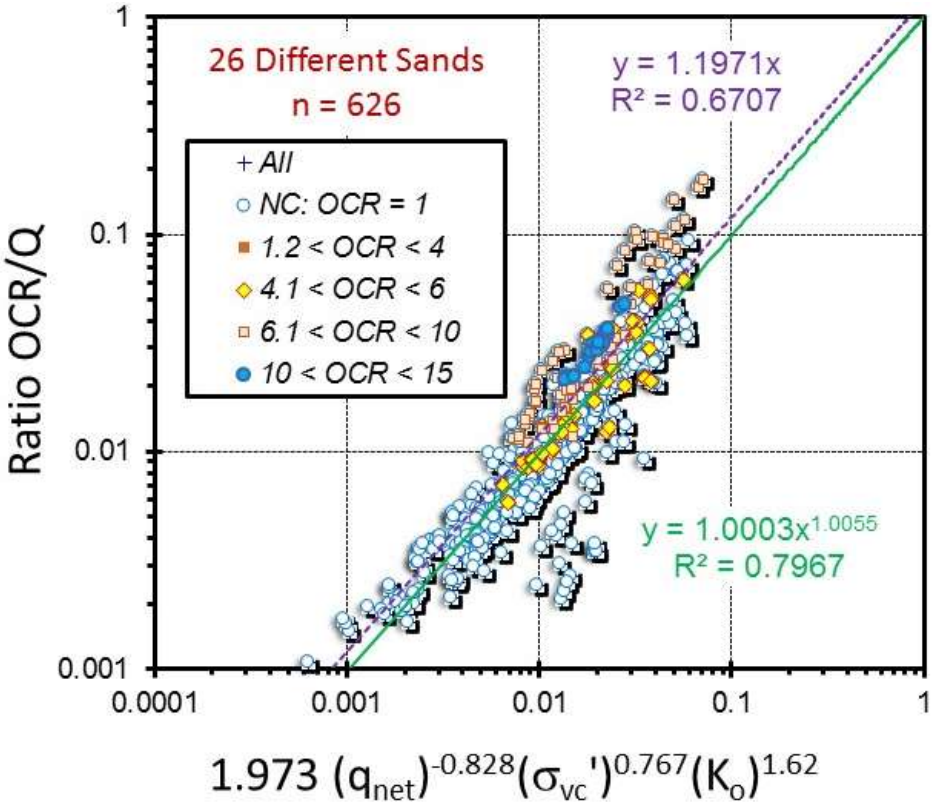


Figure 4.2. Statistical trends from post-processing of CPT resistances in sand calibration chamber tests (Mayne, 2017). Note cone resistance and stresses in bars.

Given that the CPT tests were conducted in large flexible-walled calibration chambers with specific limited sizes (D), the measured tip resistances were corrected to account for boundary effects for specific the relative density and relative size of the calibration chamber to the cone diameter (D/d). The direct correlation between YSR and net cone resistance for clean sands from calibration chamber testing is expressed as:

$$YSR \quad = \quad \left[ \frac{0.192 \cdot (q_{net} / \sigma_{atm})^{0.22}}{(1 - \sin\phi') \cdot (\sigma_{vo}' / \sigma_{atm})^{0.31}} \right]^{\frac{1}{\sin\phi' - 0.27}} \qquad [4.15]$$

where $\sigma_{atm}$ = atmospheric pressure (1 atm ≈ 1 bar = 100 kPa).

The above expression can be simplified to a simpler linear equation by adopting a characteristic value of friction angle $\phi' = 35°$ for clean sands:

$$YSR \quad \approx \quad \left[ \frac{(q_{net} / \sigma_{atm})^{0.72}}{13.8 \cdot (\sigma_{vo}' / \sigma_{atm})^{1.02}} \right] \qquad [4.16]$$

and since $YSR = \sigma_p'/\sigma_{vo}'$, the above can be reduced to simply:

$$\sigma_y' \quad \approx \quad \left[ \frac{(q_{net})^{0.72} \cdot (\sigma_{atm})^{0.3}}{13.8} \right] \qquad [4.17]$$

Furthermore, by expressing the effective preconsolidation stress in terms of net cone resistance for the case where units are specifically SI, that is: $1\ \sigma_{atm} = 100$ kPa:

$$\sigma_y' \quad \approx \quad 0.32 \cdot (q_{net})^{0.72} \qquad \text{(expressed in SI units of kPa)} \qquad [4.18]$$

The simplified power law expression in equation [4.18] is compared to the actual more complex solution from calibration chamber testing given using equation [4.15] as presented in **Figure 4.3-a.** Here, several values of effective friction angles ($\phi'$) are plugged into the equation ranging from 32° to 45° which is the general range observed for clean quartz and silica sands. Moreover, the influence of effective vertical stresses is investigated in **Figure 4.3-b** where stresses ranging from 25 to 300 kPa are input into the expressions.

From both figures, it can be observed that there is a reasonable agreement between the two algorithms (with an exception for the uncommon case of very high friction angle of $\phi' = 45°$ where the simplified approach provides a conservative evaluation). Thus, the parametric study indicates the general applicability for employing the simplified power law expressions in estimating stress history of clean silica-quartz sands from CPT data.

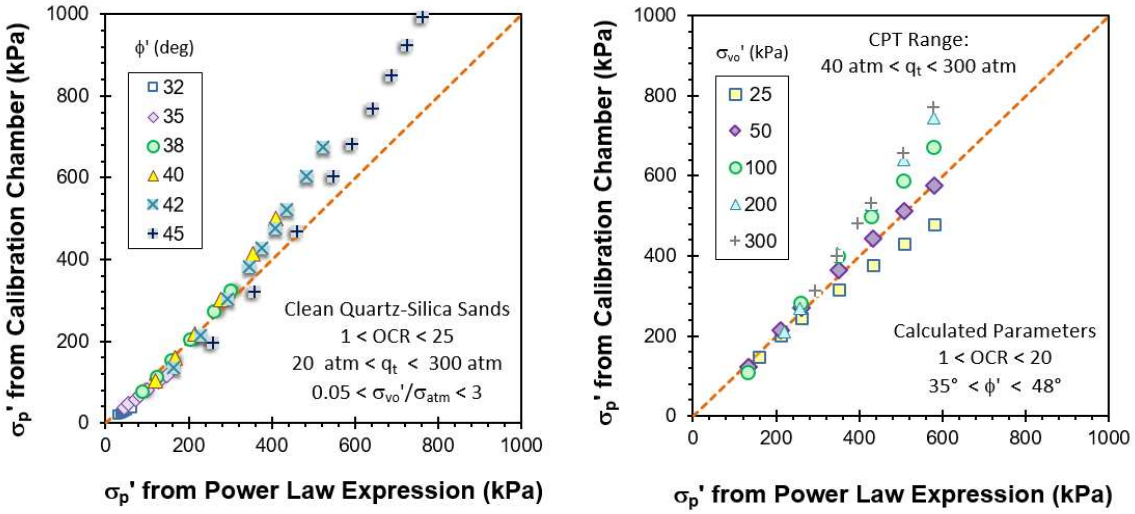


Figure 4.3. Comparison of CPT calibration chamber solution with simplified power law expression for clean quartz-silica sands over a range of (a) effective friction angles; (b) effective stress levels

## 4.8 Generalized Expression for Stress History Evaluation

Comparing the simplified equation [4.12] for evaluating the preconsolidation stress in intact clays to the simplified power law in equation [4.18] for estimation in clean sands, it is evident that both expressions have the same structure and format of a common coefficient of 0.33 associated to the net cone tip resistance raised to a certain exponent value m' where the value m' = 1.0 for clay and 0.72 for sands (Mayne 2014). This

resemblance can be used to formulate a universal expression that can address a wide variety of different soils and geomaterials.

To investigate the relationships between the effective preconsolidation stress and the net cone tip resistance for a diversity of soil types, a comprehensive database was prepared from a total of 78 well-documented worldwide geotechnical test sites covering a wide variety of soils as summarized in **Table 4.1.** For each reported site, electric or electronic cone penetration tests (CPT) or piezocone (CPTu) soundings following the general ASTM D5778 procedures were collected with at least the 3 main piezocone readings ($q_t$, $f_s$, and $u_2$) with depth. In addition, each site provided results from high-end laboratory tests for stress history profiles measured using standard 1-D consolidation tests by incremental type loading oedometers following ASTM D2435, pneumatic or hydraulic consolidometers, computerized electric load frames, and/or constant rate of strain (CRS) tests following ASTM D4186. Details of the compiled in-situ and laboratory tests are presented in subsequent appendices.

The compiled database can be divided into 6 main categories: (a) 31 intact soft to firm normally consolidated clays which are presented in **Appendix A**; (b) 15 silts presented in **Appendix B**; (c) 8 sands in **Appendix C**; (d) 8 organic clays in **Appendix D**; (e) 8 sensitive clays in **Appendix E**; and finally, (f) 8 stiff to hard highly overconsolidated clays and fissured fine-grained soils in **Appendix F**.

**Figure 4.4** presents the overall dataset with a summary graph showing effective yield stress versus net cone tip resistance for all investigated soil sites. The compiled database is presented where yellow dots indicate sands, green indicates silts, blue indicates

intact clays, gray indicates organic clays, purple indicates sensitive clays and black indicates highly overconsolidated and fissured clays. From the plotted results for the 6 soil type groups and using the resemblance in equations [4.12] and [4.18], a general format can be adopted:

$$\sigma_p' = 0.33 \cdot (q_t - \sigma_{vo})^{m'} (\sigma_{atm}/100)^{1-m'} \quad [4.19a]$$

where the exponent m' ranges from 0.7 to 1.1+. The exponent m' increases with fines content moving from sands to clays and decreases with mean grain size ($D_{50}$) moving from clays to sands (Mayne et al. 2009; Mayne 2013). The exponent m' value is obtained based on the values of the effective preconsolidation stress and its relation to one-third of the net cone tip resistance for each site. For the dataset, the site-specific interpreted exponent values are summarized in **Table 4.1**.

Based on the clustering of data for different soil types, general m' values can be assigned: m' ≈ 0.72 in clean quartz sands, 0.8 in silty sands, 0.85 in silts, 0.9 in organic clays, and 1.0 in intact clays of low sensitivity. For sensitive clays, a preliminary value of 0.9 to 1.0 can be assigned for 1$^{st}$ order approximation, however, stress history in sensitive clays is investigated in further detail later, as discussed in Chapter 7. For fissured and highly overconsolidated clays the exponent value can exceed 1.1. Likely, the degree of fissuring and spacing of discontinuities in these geomaterials affects their behavior and the relationship shown here (Powell & Quarterman 1988). Corresponding lines for each general m' value are presented in **Figure 4.4** with the associated soil/geomaterial type. When using SI units (specifically, 1 $\sigma_{atm}$ = 100 kPa) for the atmospheric pressure, the generalized stress history expression becomes simply:

$$\sigma_p' = 0.33 \cdot (q_t - \sigma_{vo})^{m'} \quad \text{(SI units of kPa)} \quad [4.19b]$$

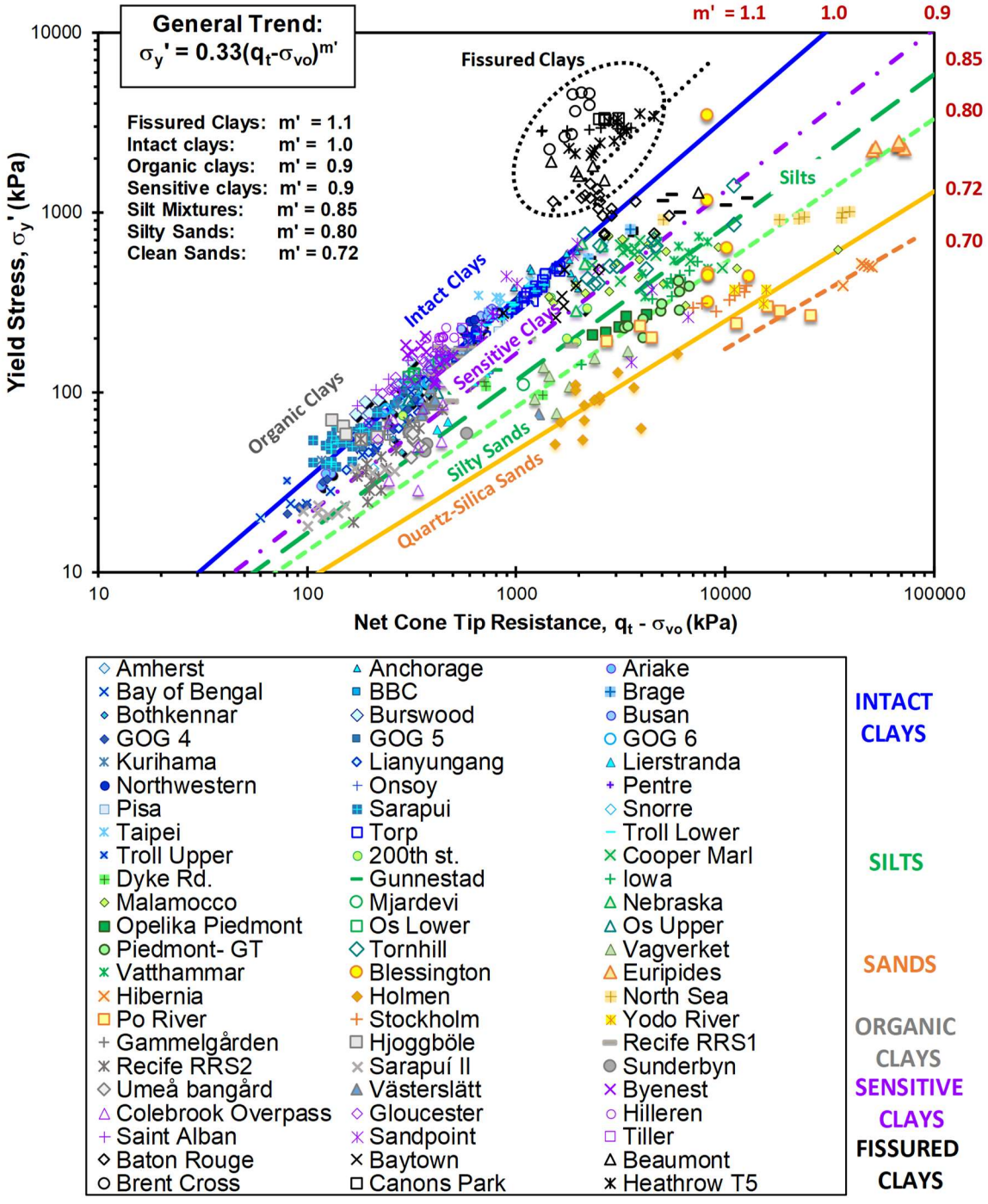


Figure 4.4. General relationship for yield stress in soils from CPT net cone resistance. (modified after Mayne, 2013)

Table 4.1. Compiled Database Listing for Piezocone -Yield Stress Relationship with Interpreted m' Exponent Values and Sources of Information

| Site | Location | Soil Type | Exponent m' | References |
|---|---|---|---|---|
| Amherst | MA, USA | Soft Varved Silt-Clay | 1 | Hegazy (1998); DeGroot & Lutenegger (2003) |
| Anchorage | AK, USA | Stiff Lean OC Clay | 1 | Zapata-Medina (2012); Mayne & Pearce (2005) |
| Ariake | Japan | Soft Marine Clay | 0.99 | Tanaka et al. (2001); Lunne et al. (2006) |
| Ballina | Australia | Soft Estuarine Clay | 1 | Pineda et al. (2014; 2016) |
| Bay of Bengal | India | Offshore Soft Clay | 0.98 | Mayne et al. (2015) |
| Belfast | Ireland | Soft Clay "Sleech" | 0.98 | Crooks (1981); Lehane (2003) |
| BBC (Boston Blue Clay) | MA, USA | NC-OC Clay | 0.99 | Whittle et al. (2001) |
| Bothkennar | Scotland, UK | Silty Estuarine Clay | 1 | Hight et al. (2003); Powell & Lunne (2005) |
| Brage | North Sea | Offshore Silty Clay | 0.96 | Rad & Lunne (1989) |
| Burswood | Perth, Australia | Soft Clay | 1 | Chung (2005); Landon (2007); Low et al. (2011) |
| Busan | Korea | Soft Clay | 1.01 | Chung et al. (2011, 2012) |
| Cooper Marl | SC, USA | OC Calcareous Clay | 0.93 | Singha (1998); Camp (2004) |
| GOG 2b | Gulf of Guinea, West Africa | Offshore Clay | 0.89 | Mayne et al. (2015) |
| GOG 4 | | Offshore Clay | 0.97 | Lunne et al. (2006) |
| GOG 5 | | Offshore Clay | 1 | Lunne et al. (2006) |
| GOG 6 | | Offshore Clay | 0.98 | Lunne et al. (2006) |

| Site | Location | Soil Type | Exponent m' | References |
|---|---|---|---|---|
| Hachirogata | Japan | Soft Plastic Clay | 1 | Tanaka (2007) |
| Hamilton AFB | CA, USA | Soft Bay Mud | 1.04 | Robertson (2010); Sabbagh & Koutsoftas (2011) |
| Kurihama | Japan | Soft Alluvial Clay | 0.98 | Tanaka (1995); Shibuya & Tanaka (1996) |
| Lianyungang | China | Soft Clay | 0.98 | Liu et al. (2008); Cai et l. (2014) |
| Lierstranda | Norway | Soft Drammen Clay | 1 | Lunne & Lacasse (1999) |
| Newbury | MA, USA | Soft LOC Silty Clay | 1 | Landon (2007) |
| Nong Ngu Hao | Thailand | Soft Bangkok Clay | 1 | Shibuya & Tamrakar (2003) |
| Northwestern University, NGES | Evanston, IL, USA | Soft Glacial Clay Till | 1 | Finno et al. (2000); McGillivray (2007) |
| Onsøy | Norway | Soft Marine Clay | 0.99 | Lunne et al. (2003; 2006) |
| Pentre | UK | Silty Clay Deposit | 1 | Lambson et al. (1993); Powell & Lunne (2005) |
| Perniö | Finland | Soft Clay | 1.02 | Lehtonen (2015); Di Buò et al. (2016) |
| Pisa | Italy | Firm Pancone Clay | 0.98 | Lo Presti et al. (2003) |
| Sarapuí | Brazil | Very Soft Clay | 0.99 | Ortigao et al (1983); Almeida - Marques (2003) |
| Snorre | The North Sea | Firm Offshore Clay | 1 | Lunne et al. (2006) |
| Taipei | Taiwan | Soft Alluvial Lacustrine Clay | 1 | Chin et al. (2007) |
| Torp | Sweden | Soft Clay | 1 | Larsson & Åhnberg (2003) |
| Troll Lower | Norway | Firm Lean NC Clay | 1 | Amundsen et al. (1985); |

| Site | Location | Soil Type | Exponent m' | References |
|---|---|---|---|---|
| Troll Upper | | Soft plastic NC Clay | 1 | Lunne et al. (2007) |
| 200th st. | BC, Canada | Soft Clayey Silt | 1.02 | Cruz (2009) |
| Dyke Rd. | Richmond, BC, Canada | Clayey Silt | 0.9 | Cruz (200) |
| Gunnestad | Norway | Silt | 0.93 | Habtegiorghis (2012) |
| Iowa- Sioux | IA, USA | Silt / Loess | 0.82 | Saye et al. (2013) |
| Malamocco | Venice, Italy | Silt Mixtures | 0.85 | Simonini (2004) |
| Mjardevi | Sweden | Silt | 0.8 | Larsson (1997) |
| Nebraska-Omaha | NE, USA | Aeolian Silt | 0.96 | Saye et al. (2013) |
| Opelika Piedmont – NGES | AL, USA | Residual fine sandy Silt | 0.83 | Mayne & Brown (2003) |
| Os Lower | Norway | Soft Clayey Silt | 1 | Long et al. (2010) |
| Os Upper | | Soft Silt Deposit | 0.95 | |
| Piedmont- GT | GA, USA | Residual Silty Fine Sand | 0.8 | Harris & Mayne (1994) |
| Tornhill | Sweden | Glacial Till / Silt | 0.95 | Larsson (2001) |
| Vagverket | Sweden | Silt | 0.75 | Larsson (1997) |
| Vatthammar | Sweden | Silt | 0.78 | Larsson (1997) |
| Blessington | Ireland | OC Dense Fine Sand | 0.72 | Doherty et al. (2012) |
| Euripides | Netherlands | OC Dense Sand | 0.78 | Baaijens & Kolk (2004) |
| Hibernia | Newfoundland, Canada | Offshore Sand | 0.7 | Thompson & Long (1989) |
| Holmen | Drammen, Norway | Loose Alluvial Sand | 0.73 | Lunne et al. (2003) |
| North Sea - Ekofisk | The North Sea | Dense OC Sand | 0.74 | Mitchell & Lunne (1978) |
| Po River | Italy | Loose NC Sand | 0.72 | Bruzzi & Battaglio (1987) |
| Stockholm | Sweden | OC Glacial Sand | 0.717 | Norconsult AB (2016) |
| Yodo River | Osaka, Japan | Alluvial Sand | 0.72 | Mimura (2003) |
| Gammelgården | Sweden | Organic Sulfide Clay | 0.92 | Larsson et al. (2007); Westerberg et al. (2015) |
| Hjoggböle | | | 0.98 | |

| Site | Location | Soil Type | Exponent m' | References |
|---|---|---|---|---|
| Recife RRS1 | Brazil | Soft Organic Clay | 0.95 | Coutinho (2007) |
| Recife RRS2 | Brazil | Soft Organic Clay | 0.90 | Coutinho (2007) |
| Sarapuí II | Brazil | Very Soft Organic Clay | 0.9 | Jannuzzi et al. (2015) |
| Sunderbyn | Sweden | Organic Sulfide Clay | 0.91 | Larsson et al. (2007); Westerberg et al. (2015) |
| Umeå bangård | | | 0.87 | |
| Västerslätt | | | 0.94 | |
| Byenest | Esp, Norway | Sensitive Clay | 1.03 | Montafia (2013) |
| Colebrook Overpass | Surrey, BC, Canada | Marine Sensitive Silty Clay | 0.97 | Crawford and Campanella (1991); Weech (2002) |
| Gloucester | Ottawa, ON, Canada | Sensitive Leda Clay | 1.025 | McRostie & Crawford (2001); Styler & Mayne (2013) |
| Hilleren | Norway | Sensitive to Quick Clay | 1.06 | Long et al. (2009) |
| Saint Alban | Québec, Canada | Sensitive Champlain Sea Clay | 1.04 | LaRochelle et al. (197); Lefebvre et al. (1994); Leroueil et al. (1995) |
| St. Monique de Nicolet | Quebec, Canada | Sensitive Soft Clay | 0.93 | Locat (2012) |
| Sandpoint | ID, USA | NC Sensitive Silty Clay | 1 | Altaee & Fellenius (2002) |
| Tiller | Norway | Sensitive to Quick Clay | 1.01 | Gylland et al. (2013; 2014); L'Heureux & Long (2016) |
| Baton Rouge | LA, USA | OC Fissured Clay | 1.05 | Chen & Mayne (1994) |
| Baytown | TX, USA | OC Fissured Clay | 0.94 | Stuedlein (2008) |
| Beaumont | Houston, TX, USA | Stiff Fissured Clay | 1.12 | Mahar & O'neill (1983); Yoon & O'neill (1995) |

| Site | Location | Soil Type | Exponent m' | References |
|---|---|---|---|---|
| Brent Cross | Hendon, UK | Fissured HOC Clay | 1.16 | Hight et al. (2003) |
| Canons Park | London, UK | Fissured London Clay | 1.164 | Hight et al. (2003); Powell & Lunne (2005) |
| Heathrow T5 | London, UK | Fissured London Clay | 1.13 | Hight et al. (2003) |
| Madingley | Cambridge, UK | Fissured Gault Clay | 1.147 | Lunne et al. (1986); Jardine et al. (2015) |
| Montgomery | Houston, TX, USA | Stiff Fissured Formation below Beaumont Clay | 0.95 | Mahar & O'Neill (1983); Yoon & O'neill (1995) |

## 4.9 Case Study Applications for assigned m' exponent values

To confirm the applicability of the assigned m' exponent values for different soil types, case study applications for each soil type are presented. **Figure 4.5** presents the cone tip resistance of a piezocone sounding conducted in Bothkennar clay site in Scotland by Hight et al. (2003) and the results of the laboratory measured preconsolidation stresses and corresponding yield stress ratio. By assigning an exponent m' = 1.0 for intact clays, an excellent agreement can be seen between the reference laboratory consolidation tests and the estimated profiled using exponent m' of 1.0.

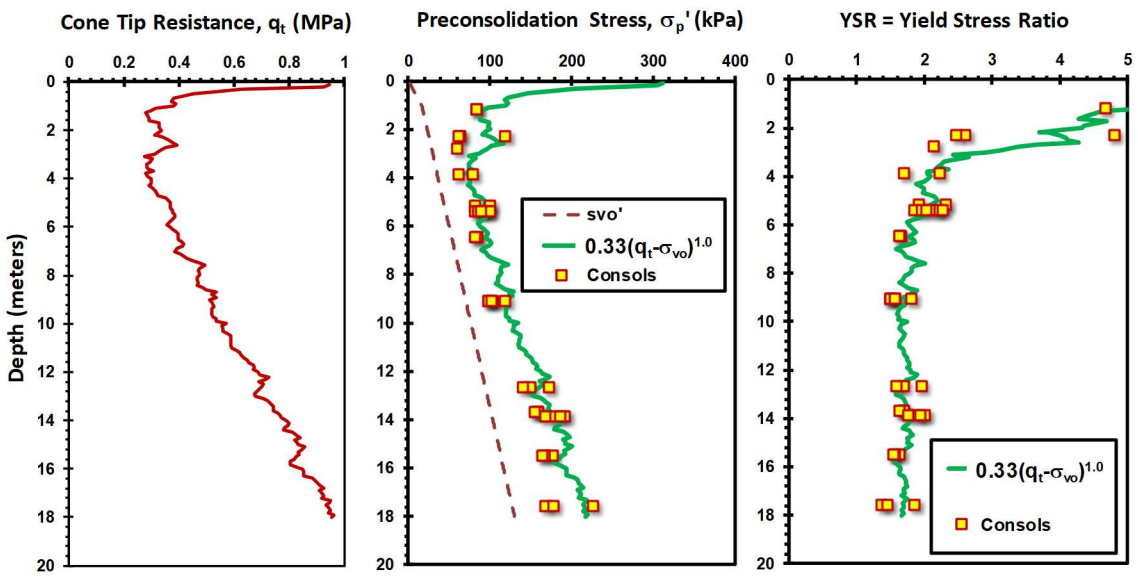


Figure 4.5. Profile in intact clay of Bothkennar: (a) cone resistance; (b) preconsolidation stress; (c) yield stress ratio. Data from Hight et al. (2003); Powell & Lunne (2005)

**Figure 4.6** presents the cone tip resistance of a piezocone sounding conducted in the very soft organic site of Sarapuí II in Brazil along with the results of the laboratory measured preconsolidation stresses and corresponding yield stress ratio as reported by Jannuzzi et al. (2015). By assigning an exponent m' = 0.9 for organic clays, a very good match can be seen between the reference laboratory consolidation tests and the CPT profile.

**Figure 4.7** presents the cone tip resistance of a piezocone sounding conducted in Malamocco silt site in Venice, Italy as reported by Simonini (2004). The figure also presents the results of the laboratory measured preconsolidation stresses and corresponding yield stress ratio. By assigning an exponent m' = 0.85 for silts, a reasonable match is evident between the reference laboratory tests and the CPT developed profiles.

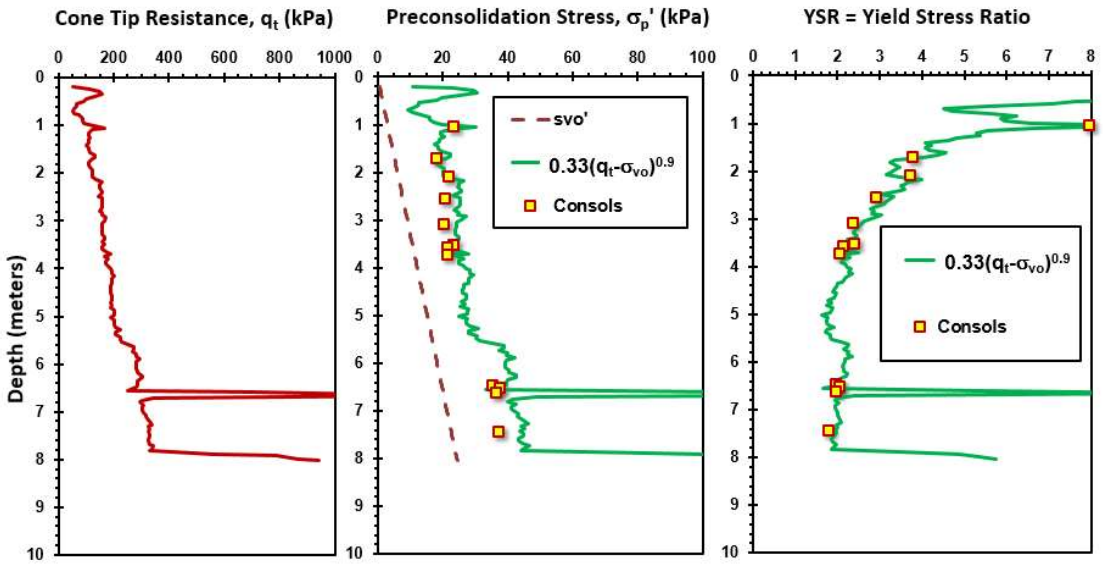


Figure 4.6. Profile in very soft organic Sarapui II, Brazil: (a) cone resistance; (b) preconsolidation stress; (c) yield stress ratio. Data from Jannuzzi et al. (2015)

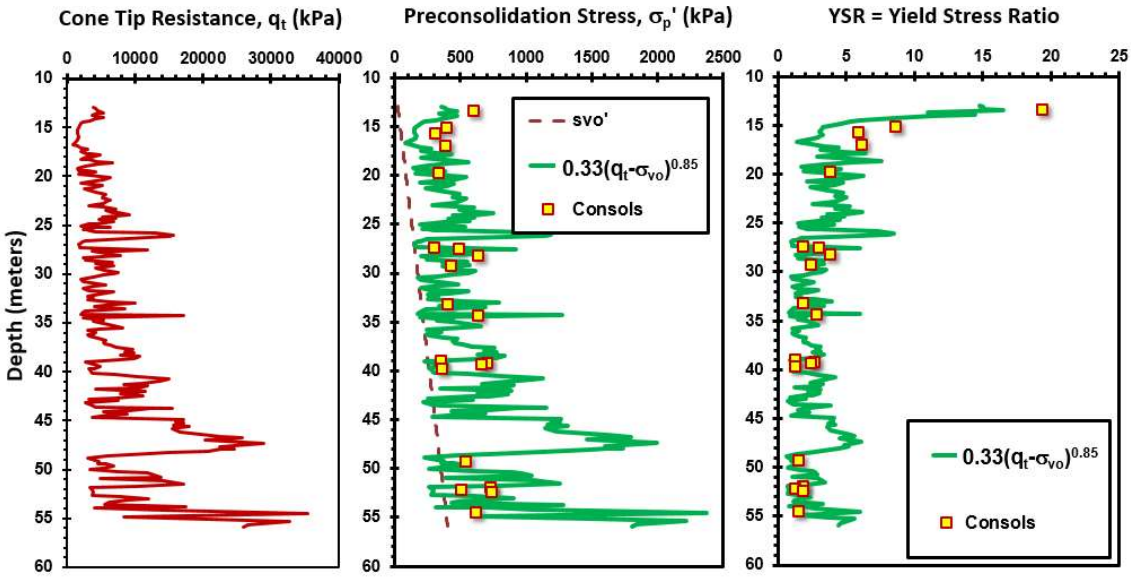


Figure 4.7. Profile in silts at Malamocco, Italy: (a) cone resistance; (b) preconsolidation stress; (c) yield stress ratio. Data from Simonini (2004)

**Figure 4.8** presents the cone tip resistance of a piezocone sounding conducted in Blessington dense sand site in Ireland as reported by Doherty et al. (2012). The results of laboratory measured yield stresses and corresponding yield stress ratio are also shown.

Assigning an exponent m' = 0.72 for sands, compatible results are observed between the reference lab tests and the CPT profile.

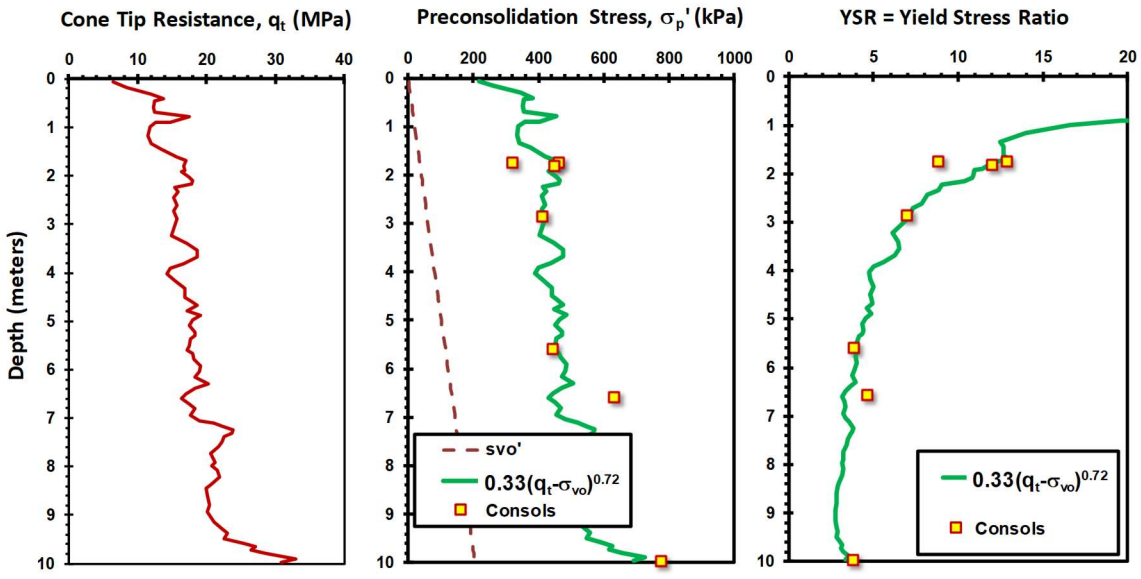


Figure 4.8. Profile in dense sands at Blessington, Ireland: (a) cone resistance; (b) preconsolidation stress; (c) yield stress ratio. Data from Doherty et al. (2012)

## 4.10 Yield Stress Exponent Evaluation from Grain Size Distribution

The exponent m' inversely tracks with the particle size of the soil, where fine-grained soils have higher exponent values and coarse-grained soils have lower values. Soil particle size is usually obtained from grain size distributions (also called "mechanical analyses"), following ASTM D 2487 using sieves to separate out different size particles. Two key parameters resulting from these tests include: (1) mean grain size ($D_{50}$); and (2) percentage of fines content (FC). To fully investigate the trend of particle size on the value of the yield stress exponent, a subset database of 56 soils covering different geomaterials,

where their corresponding $D_{50}$ and FC were available, was created, as summarized in **Table 4.2**.

The relationship between the yield stress exponent and the mean grain size ($D_{50}$) is presented in **Figure 4.9** where the exponent value (ranging from 0.72 to 1.1) is seen to be inversely proportional to the representative $D_{50}$ (mm) that ranges from 0.001 to 1 mm. The trend of the relationship can be expressed:

$$m' = 0.72 + \frac{0.28}{1 + (16 \cdot D_{50})^5} \quad [4.20]$$

Based on grain size distribution results, the amount of fines can be determined for any soil mixture, as summarized in Table 4.2 for the compiled database. Typically, the range of fines content for sands is less than 10% and for clays is greater than 90% while silts are intermediate ranging from 40 to 60%. The relationship between the yield stress exponent m' and the average fines content (FC) is explored as presented in **Figure 4.10** and is expressed as:

$$m' = 1 - \frac{0.28}{1 + (FC / 55)^{20}} \quad [4.21]$$

Table 4.2. Summary of mean grain size ($D_{50}$) and fines content for the compiled database

| Site | Soil Type | Exponent m' | $D_{50}$ (mm) | Fines Content (%) |
|---|---|---|---|---|
| Amherst | Varved Silty Clay | 1.00 | 0.001 | 100 |
| Anchorage | Stiff Clay | 1.00 | 0.0035 | 97 |
| Ariake | Soft Marine Clay | 0.99 | 0.020 | 95 |
| Ballina | Soft Estuarine Clay | 1.00 | - | 96 |
| BBC | NC-OC Clay | 0.99 | 0.002 | 88 |
| Bothkennar | Silty Estuarine Clay | 1.00 | 0.014 | 92 |
| Brage | Silty Clay | 0.96 | 0.0035 | 100 |
| Burswood | Soft Clay | 1.00 | 0.010 | 95 |
| Busan | Soft Clay | 1.01 | 0.006 | 90 |
| Cooper Marl | Calcareous Clay | 0.93 | 0.02 | 80 |
| GOG | Offshore Clay | 0.97 | 0.004 | 94 |
| Hachirogata | Soft Clay | 1.00 | 0.002 | 99 |
| Hamilton AFB | Soft Bay Mud | 1.04 | 0.013 | 100 |
| Kurihama | Alluvial Clay | 0.98 | - | 97 |
| Lianyungang | Soft Clay | 0.98 | 0.003 | 99 |
| Lierstranda | Soft Drammen Clay | 1.00 | - | 100 |
| Newbury | Soft Silty Clay | 1.00 | - | 98 |
| Nong Ngu Hao | Soft Bangkok Clay | 1.00 | 0.002 | 96 |
| Northwestern Uni., NGES | Glacial Till | 1.00 | 0.0027 | 84 |
| Onsøy | Soft Marine Clay | 0.99 | 0.002 | 100 |
| Pentre | Silty Clay Deposit | 1.00 | 0.004 | 95 |
| Perniö | Soft Clay | 1.02 | 0.002 | 97 |
| Pisa | Pancone Clay | 0.98 | - | 97 |
| Sarapuí | Very Soft Clay | 0.99 | - | 90 |
| Taipei | Soft Clay | 1.00 | - | 93 |
| Troll Lower | Firm Lean NC Clay | 1.00 | 0.0085 | 70 |
| Troll Upper | Soft plastic NC Clay | 1.00 | 0.005 | 95 |
| Dyke Rd. | Silt | 0.90 | - | 55 |

| Site | Soil Type | Exponent m' | $D_{50}$ (mm) | Fines Content (%) |
|---|---|---|---|---|
| Iowa- Sioux | Silt / Loess | 0.82 | 0.07 | 50 |
| Malamocco | Silt | 0.85 | 0.062 | 58 |
| Nebraska – Omaha | Silt | 0.96 | 0.045 | 60 |
| Opelika Piedmont – NGES | Silt | 0.83 | 0.07 | 55 |
| Os Lower | Clayey Silt | 1.00 | 0.026 | 93 |
| Piedmont- GT | Silt | 0.80 | 0.140 | 33 |
| Tornhill | Glacial Till / Silt | 0.95 | 0.054 | 60 |
| Vagverket | Silt | 0.75 | 0.10 | - |
| Blessington | Sand | 0.72 | 0.15 | 11 |
| Euripides | Sand | 0.78 | 0.33 | 5 |
| Hibernia | Sand | 0.70 | 0.39 | 4 |
| Holmen | Sand | 0.73 | 0.58 | 12 |
| North Sea - Ekofisk | Sand | 0.74 | 0.20 | 8 |
| Po River | Sand | 0.72 | 0.30 | 8 |
| Stockholm | Sand | 0.717 | 0.79 | 1 |
| Yodo River | Sand | 0.72 | 0.59 | 9 |
| Colebrook Overpass | Marine Sensitive Silty Clay | 0.97 | 0.035 | 82 |
| Gloucester | Sensitive Leda Clay | 1.025 | 0.001 | 100 |
| Sandpoint | Sensitive Clay | 1.00 | - | 100 |
| Tiller | Sensitive Clay | 1.01 | 0.004 | 100 |
| Baton Rouge | OC Fissured Clay | 1.05 | 0.002 | 98 |
| Baytown | OC Fissured Clay | 0.94 | 0.002 | 97 |
| Beaumont | Stiff Fissured Clay | 1.12 | - | 94 |
| Brent Cross | Fissured HOC Clay | 1.16 | 0.002 | 100 |
| Canons Park | Fissured Clay | 1.164 | 0.001 | 100 |
| Madingley | Fissured Gault Clay | 1.147 | 0.001 | - |
| Montgomery | Stiff Fissured Formation | 0.95 | - | 78 |

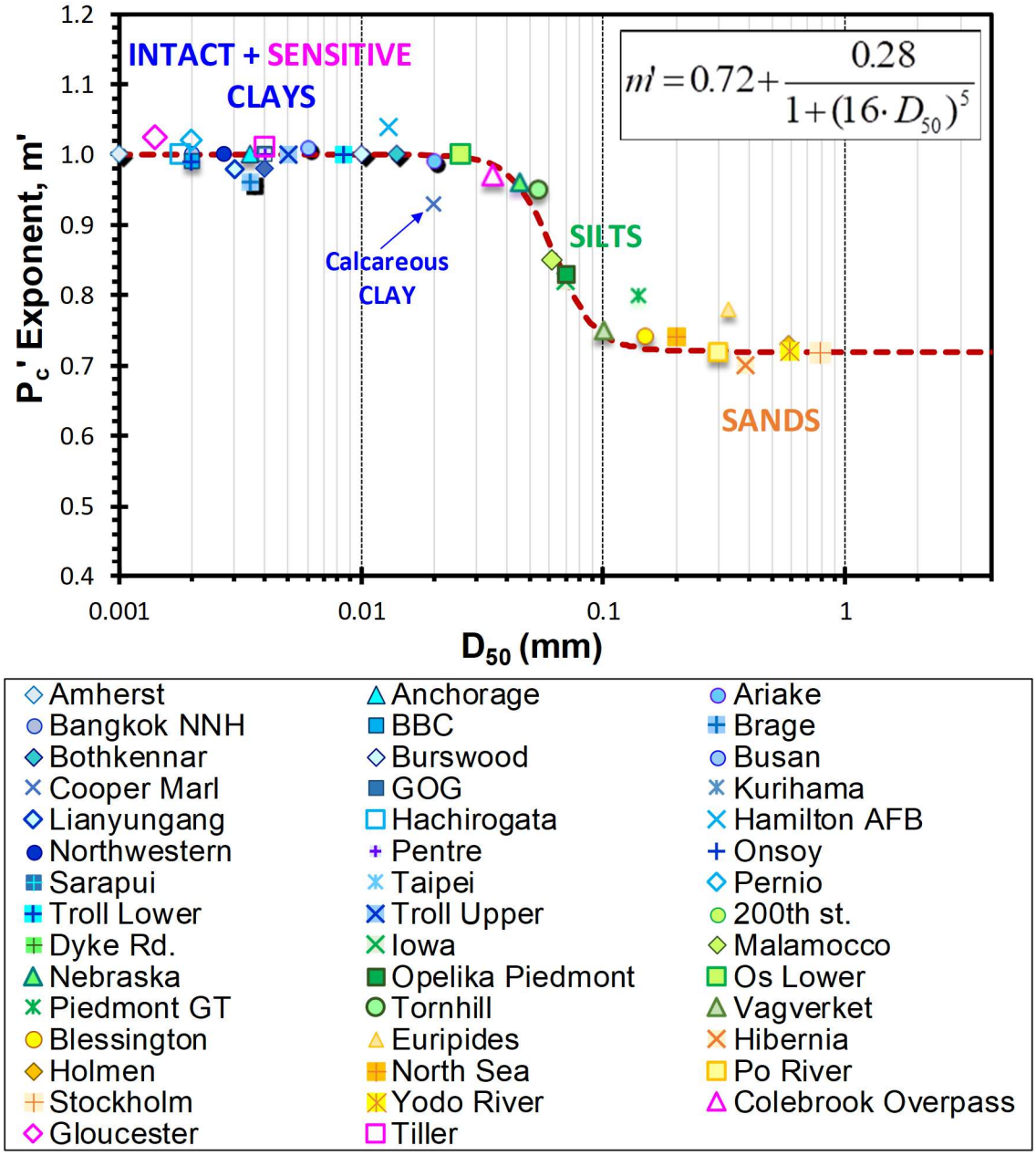


Figure 4.9. Trend for yield stress exponent (m') with the mean effective grain size ($D_{50}$)

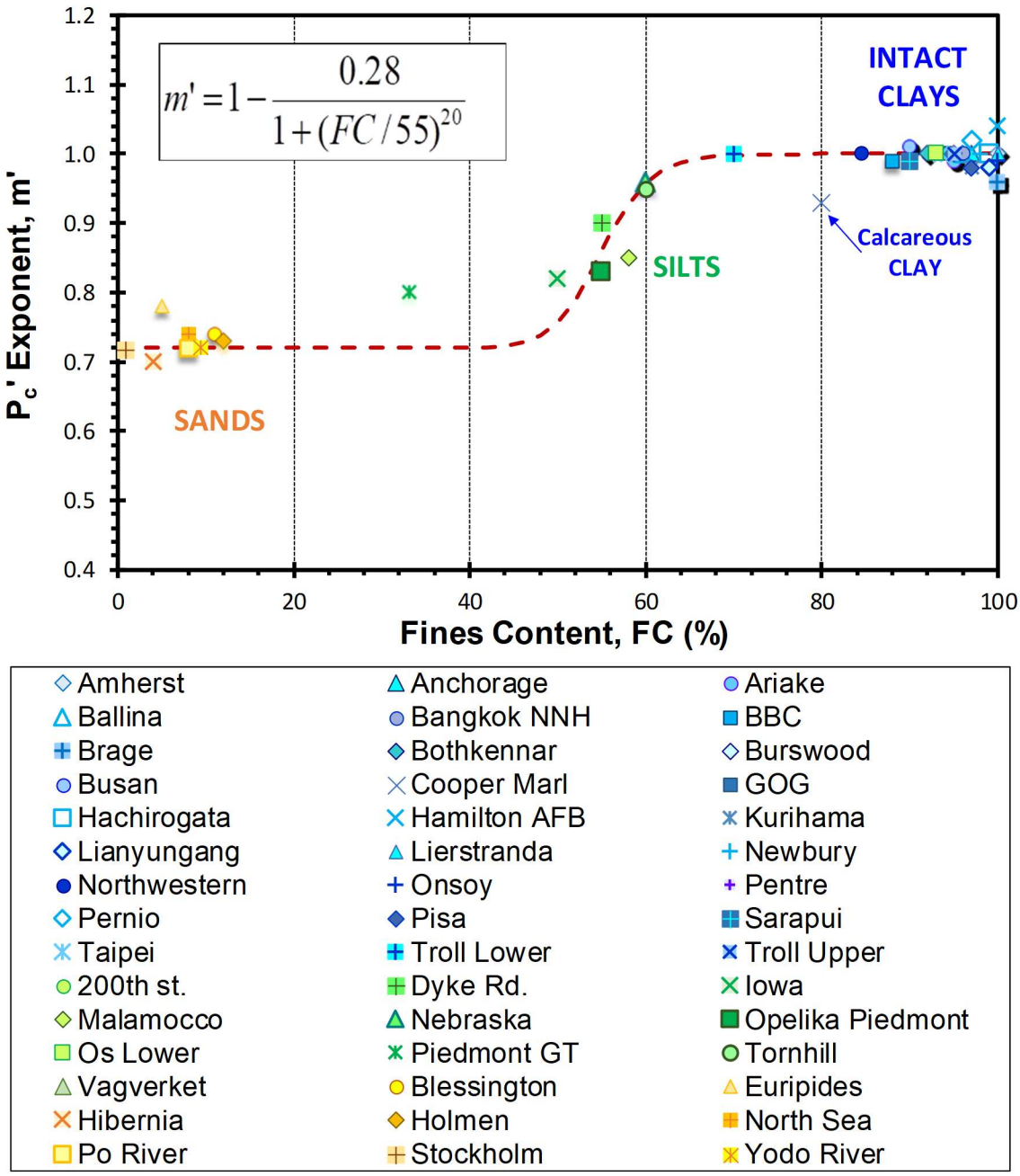


Figure 4.10. Trend for yield stress exponent (m') with amount of fines content (FC)

## 4.11 Yield Stress Exponent Evaluation from CPT Material Index

The CPT material index $I_c$ is a convenient means used to classify the soil type according to a particular soil behavior type (SBT) chart (Robertson 2009; Jefferies & Been 2016). Therefore, it is logical to explore a direct link between the yield stress exponent m' and $I_c$. In this section, different SBT systems with their corresponding definitions for CPT material index will be reviewed and the trends between m' will be established.

In one of the more popular CPT classification systems, normalized cone parameters are used in the SBT charts to account for the depth effects on the measured readings as follows:

$$Q = (q_t - \sigma_{vo})/\sigma_{vo}' \quad [4.22]$$

$$F = 100 \cdot f_s/(q_t - \sigma_{vo}) \quad [4.23]$$

For this system, the CPT material index follows the definition introduced by Robertson and Wride (1998):

$$I_{cRW} = \sqrt{\{3.47 - \log(Q)\}^2 + \{1.22 + \log(F)\}^2} \quad [4.24]$$

While the definition for normalized Q originally established by Wroth (1984) works well in soft clays, the format needs a modification for sands and granular soils (e.g. Olsen & Malone 1988; Olsen & Mitchell 1995; Moss et al. 2006; Idriss & Boulanger 2006).

The definition has subsequently been upgraded to work better in sands and coarse-grained materials, using a modified Q parameter given by Robertson (2009) and designated $Q_{tn}$:

$$Q_{tn} = \frac{(q_t - \sigma_{vo})}{\sigma_{atm}} \cdot \left( \frac{\sigma_{atm}}{\sigma_{vo}'} \right)^n \quad [4.25]$$

where the exponent n varies with soil type: n = 1.0 in the general case of inorganic and insensitive clays ($I_c > 2.95$), n = 0.75 for silty soils, and n = 0.5 for clean sands ($I_c < 2.05$). The exponent n specifically depends on the value of the material index and stress level, as defined by:

$$n = 0.381 \cdot (I_c) + 0.05 \cdot \left(\frac{\sigma_{vo}'}{\sigma_{atm}}\right) - 0.15 \quad [4.26]$$

This requires a couple of iterations to find $Q_{tn}$, $I_c$, and exponent n for each row of CPT data.

Plotting the normalized cone tip resistance $Q_{tn}$ versus F while using the modified Robertson & Wride CPT material index, a modified 9-zone SBT system has been developed (Robertson, 2009), as presented in **Figure 4.11**.

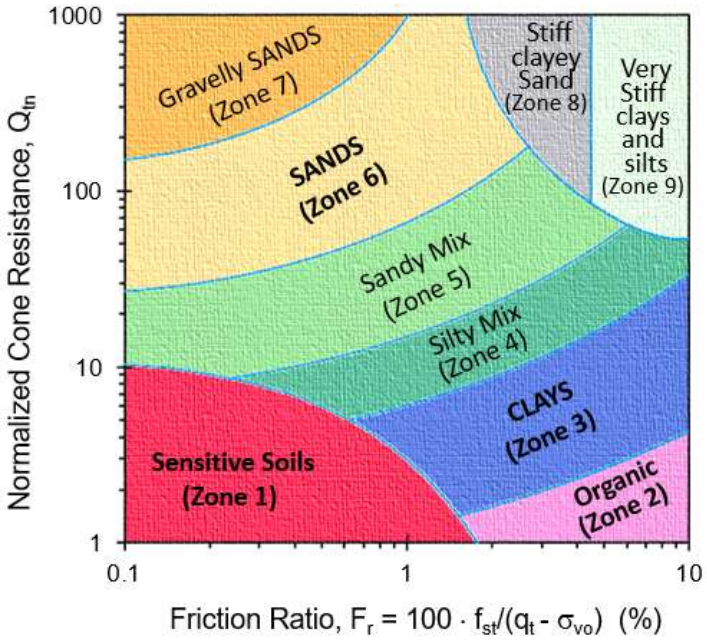


Figure 4.11. Colorized 9-Zone Soil Behavioral Type (SBTn) Chart for normalized CPT readings (after Robertson 2009)

A representative and average CPT material index for each of the different soils in the compiled database was evaluated following the modified Robertson & Wride (1998) definition (Robertson 2009). This representative $I_c$ was plotted against the yield stress exponent m' for intact clays, silts, and sands, as presented in **Figure 4.12.** The relation takes a hyperbolic form clearly showing distinct zone for sands at $I_c < 2.05$ and for clays at $I_c > 2.95$, with silts occupying an intermediate region. For the basic grouping of uncemented quartz-silica sands and inorganic fine-grained soils, the developed correlative trend can be expressed:

$$m' = 1 - \frac{0.28}{1+(I_{cRW}/2.64)^{25}} \qquad [4.27]$$

For the remaining special soil groups showing exceptions from the generic developed trend as presented in **Figure 4.13**, the organic clays are clustered together below the developed trend, the sensitive clays are scattered having m′ values greater than the intact clays group while the fissured clays do not follow the developed equation.

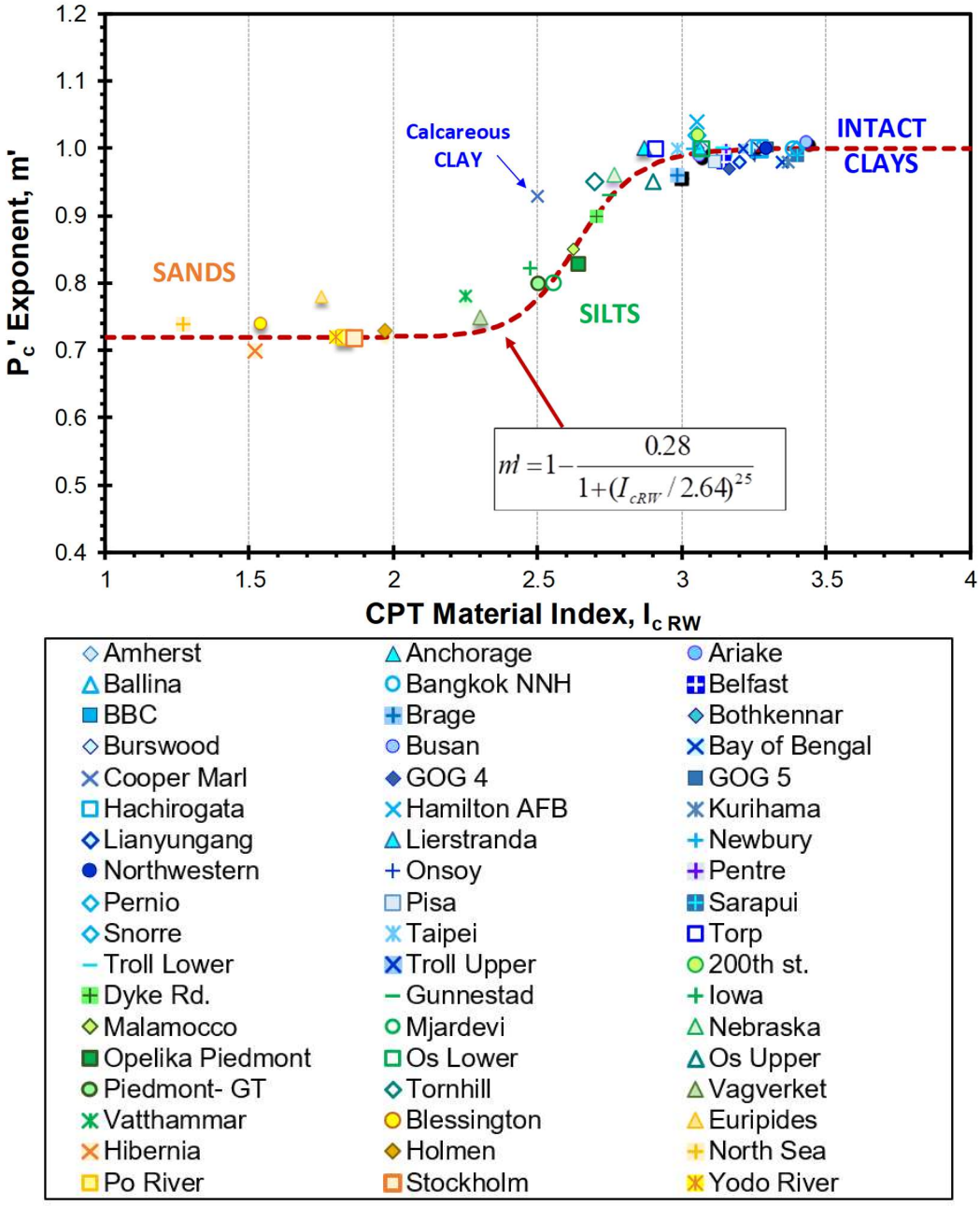


Figure 4.12. Trend for yield stress exponent (m') with CPT material index ($I_c$) for uncemented quartz-silica sands and intact inorganic silts-clays.

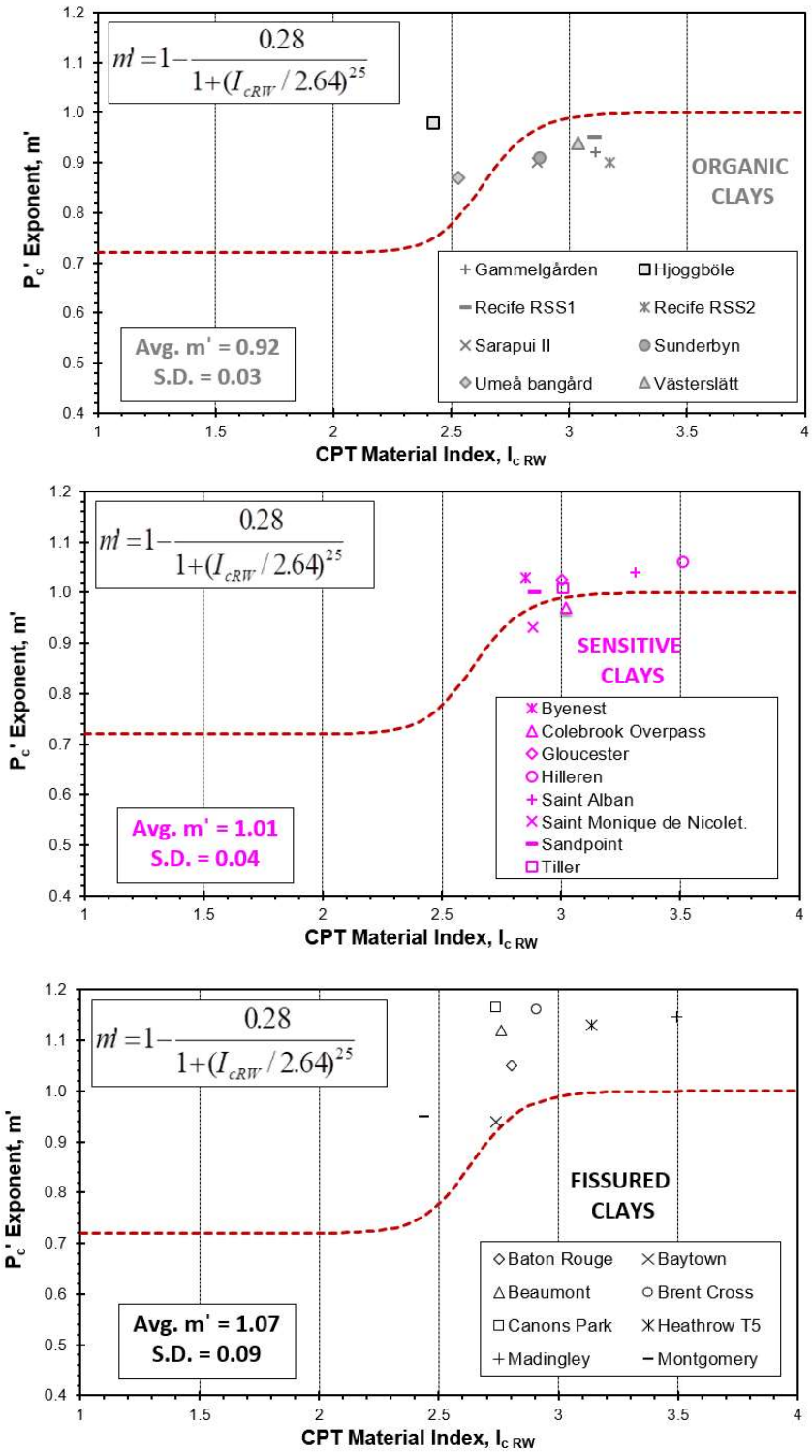


Figure 4.13. Behavior of yield stress exponent (m') with CPT material index ($I_c$) for (a) organic clays; (b) sensitive clays; and (c) fissured clays.

An earlier version of SBT chart based on non-normalized parameters developed by UBC (Robertson et al. 1986; Lunne et al. 1997) still finds use in practice. The chart uses $q_t$ vs FR, as presented in **Figure 4.14**, and also has a second chart of $q_t$ vs. $B_q$ (not shown here). The chart can be represented using a non-normalized soil behavior type index ($I_{SBT}$) value which only uses basic piezocone measurements (cone tip resistance and sleeve friction) and is evaluated from (Robertson 2010):

$$I_{SBT} = \sqrt{\left(3.47 - log\ \left(\frac{q_t}{P_a}\right)\right)^2 + \left(1.22 + log\ 100 \cdot \left(\frac{f_s}{q_t}\right)\right)^2} \quad [4.28]$$

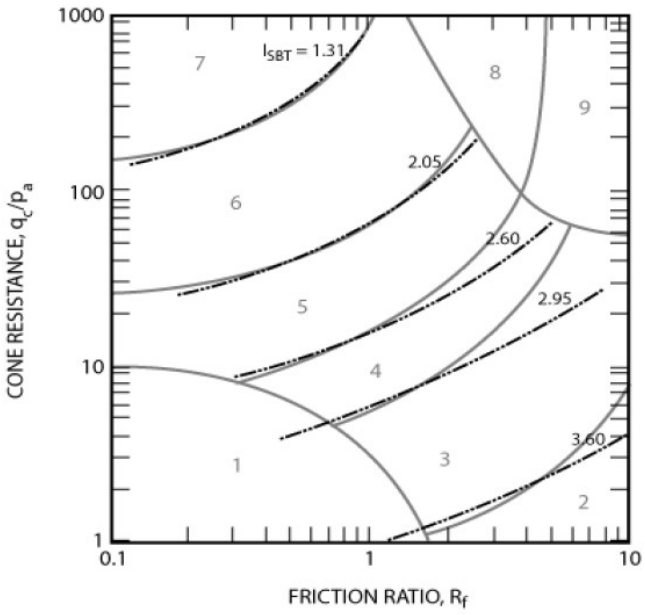


| Zone | Soil Behaviour Type (SBT) |
|---|---|
| 1 | *Sensitive fine-grained* |
| 2 | *Clay - organic soil* |
| 3 | *Clays: clay to silty clay* |
| 4 | *Silt mixtures: clayey silt & silty clay* |
| 5 | *Sand mixtures: silty sand to sandy silt* |
| 6 | *Sands: clean sands to silty sands* |
| 7 | *Dense sand to gravelly sand* |
| 8 | *Stiff sand to clayey sand** |
| 9 | *Stiff fine-grained** |

** Overconsolidated or cemented*

Figure 4.14. Non-normalized SBT chart based on dimensionless cone resistance, ($q_c/p_a$) and friction ratio, $R_f$ (after Robertson, 2010)

An averaged value $I_{SBT}$ was calculated for each site and plotted against the yield stress exponent with a focus on uncemented quartz-silica sands and intact inorganic silts-clays as presented in **Figure 4.15.** From the plotted figure, sands exist at $I_{SBT} < 2.01$ which agrees with SBT non-normalized classification chart. Clays mostly exist at $2.95 < I_{SBT} < 3.6$. The silts agree mostly with zone 5 of silty sand to sandy silt with $2.05 < I_{SBT} < 2.6$. The relation between the non-normalized soil behavior type index and the yield stress exponent is expressed as:

$$m' = 1 - \frac{0.28}{1+(I_{SBT}/2.4)^{20}} \quad [4.29]$$

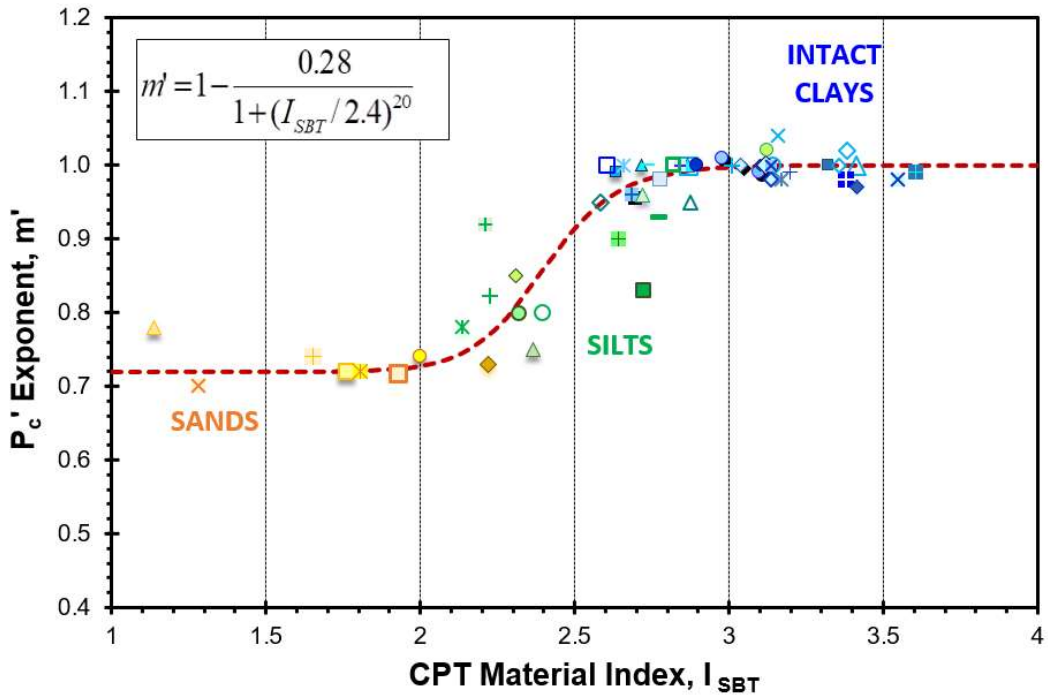


Figure 4.15. Trend for yield stress exponent (m') with CPT non-normalized soil behavior type index ($I_{SBT}$) according to Robertson (2010) for uncemented quartz-silica sands and intact inorganic silts-clays

Jefferies and Been (2016) have modified the soil behavior type index that was originally introduced by Jefferies and Davies (1991), where they added a new dimensionless term "Q (1 – $B_q$) +1" in their classification chart as presented in **Figure 4.16**. The modified chart consists of 6 main soil zone which can be approximated into circles with a radius value obtained from the material behavior type index, $I_{c\,JB}$ where:

$$I_{c\,JB} = \sqrt{[3 - \log\{Q\,(1 - B_q) + 1\}]^2 + [1.5 + 1.3\log(F)]^2} \qquad [4.30]$$

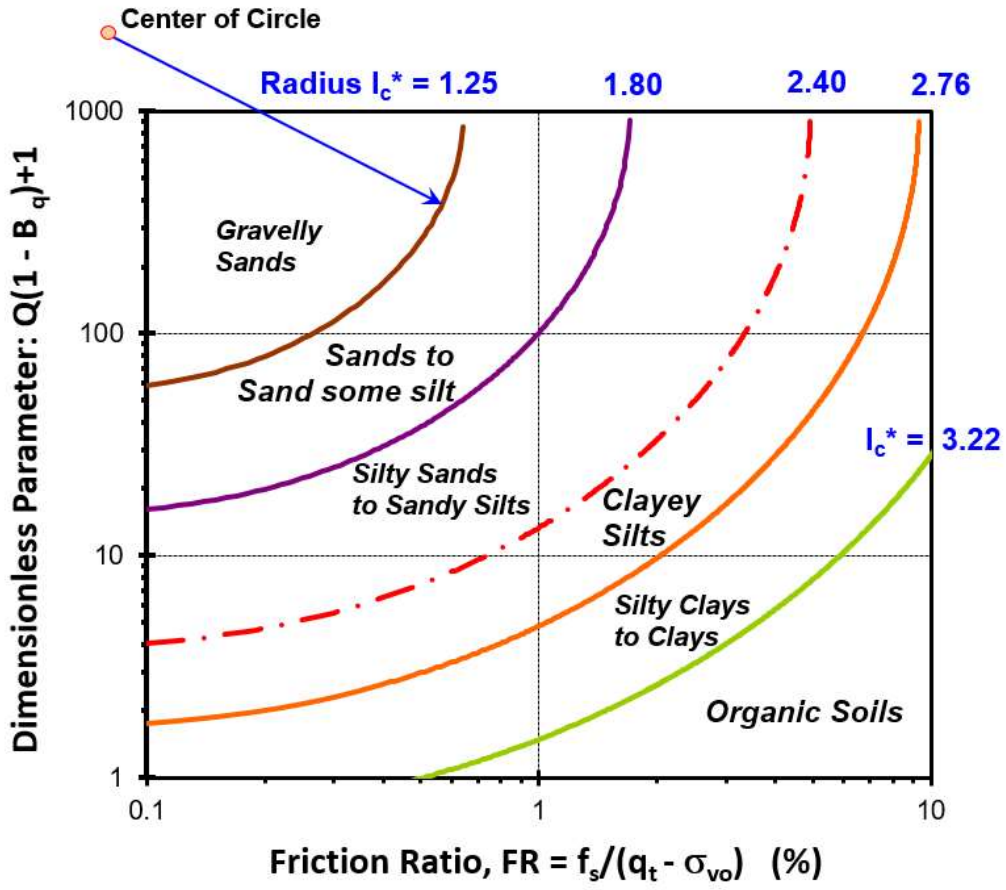


Figure 4.16. Modified Jefferies and Been Soil Profiling Chart (Jefferies and Been, 2016)

Similarly, the CPT material index was evaluated based on the Jefferies and Been (2016) definition and was plotted against the yield stress exponent as shown in **Figure 4.17**. From the plot, it can be seen that at $I_{CJB} < 1.8$, there are mainly sands in addition to sands with some silts which agree with their profiling chart. At $I_{CJB} > 2.76$ there are clays and silts at $2.4 < I_{CJB} < 2.76$. The equation relating the two quantities for uncemented quartz-silica sands and intact inorganic silts-clays can be expressed as:

$$m' = 1 - \frac{0.28}{1+(I_{cJB}/2.7)^{30}} \quad [4.31]$$

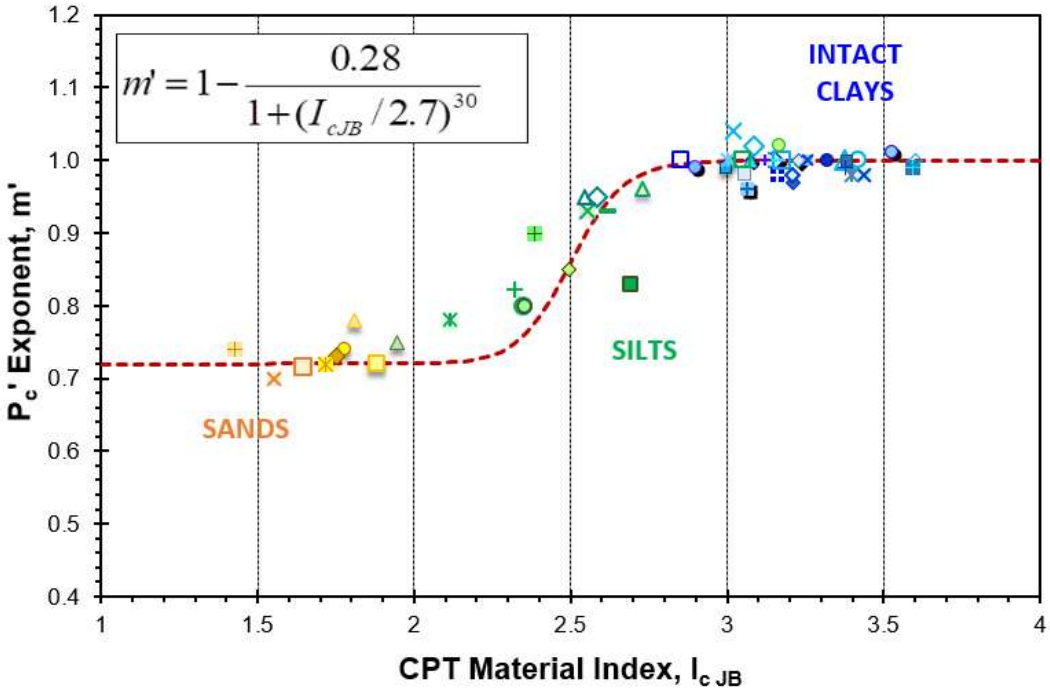


Figure 4.17. Trend for yield stress exponent (m') with CPT material index ($I_{cJB}$) according to Jefferies and Been (2016) for uncemented quartz-silica sands and intact inorganic silts-clays

Most recently, Robertson (2016) introduced an update to his classic 9-zone SBT and his non-normalized SBT chart, where the chart was modified to identify if the soil has

a significant microstructure and to capture the transition between the contractive and dilative behavior of different geomaterials to be eventually used in liquefaction-assessment applications. According to Robertson (2009), overconsolidated soils with OCR > 4 are most likely dilative with $Q_{tn}$ > 12, hence a boundary between contractive and dilative geomaterials was developed when plotted in $Q_{tn}$-$F_r$ chart; as presented in **Figure 4.18**; mark as (CD = 70) and is evaluated from:

$$CD = (Q_{tn} - 1) \cdot (1 + 0.06 \cdot F_r)^{17} \quad [4.32]$$

Also presented in **Figure 4.18**, modified boundaries for SBTn chart based on hyperbolic shape expressed using a modified soil behavior type ($I_B$). The lower boundary defined by $I_B$ = 32 represents sandlike materials (coarse-grained) while an upper boundary defined by $I_B$ = 22 represents claylike materials (fine-grained) with the zone defined by 22 < $I_B$ < 32 defines transitional soils which lie in between sandlike and clay-like materials which are typically silts. The modified material index ($I_B$) is defined as:

$$I_B = 100 \cdot \frac{(Q_{tn}+10)}{(70+Q_{tn} \cdot F_r)} \quad [4.33]$$

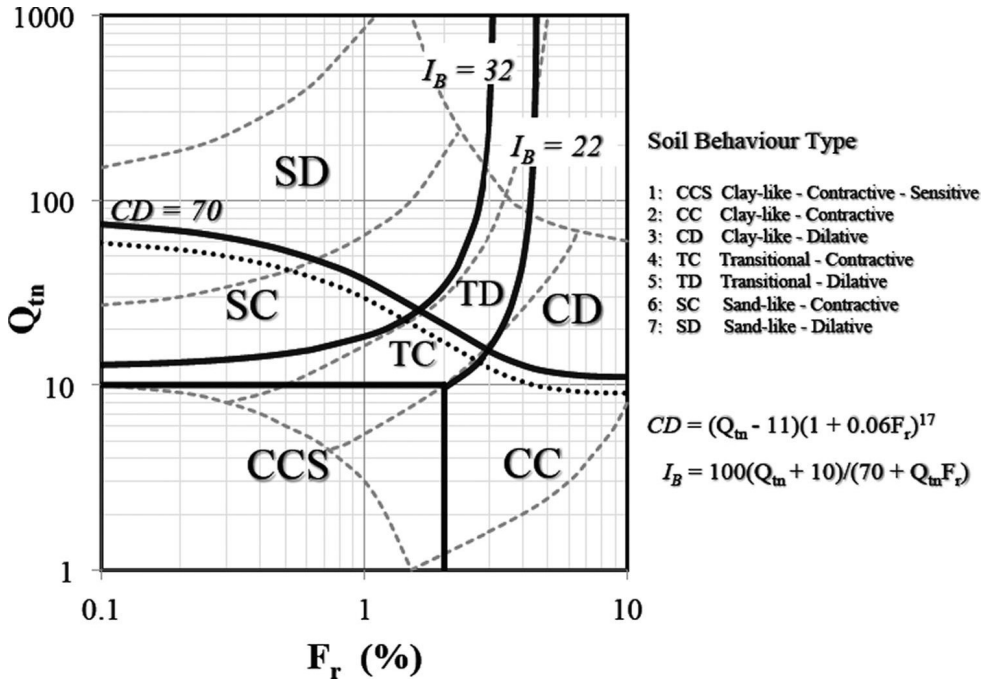


Figure 4.18. Updated SBTn chart showing contractive and dilative transition (after Robertson, 2016)

The modified soil behavior type index ($I_B$) as per Robertson (2016) was computed for all the soils in the compiled database and were plotted against the corresponding yield stress exponent as presented in **Figure 4.19**, from the plotted results it can be observed that sands with an exponent value of 0.72 exist at $I_B$ values > 32 and intact clays are clustered at exponent value of 1.0 at $I_B$ values < 22 while all silts (defined as transitional soils) exist at $22 < I_B < 32$ as defined in **Figure 4.18** with exponent values of 0.8 – 0.85. The developed correlation between the modified soil behavior type index ($I_B$) and the yield stress exponent can be expressed as:

$$m' = 0.72 + \frac{0.28}{1+(I_B/32)^8} \quad [4.34]$$

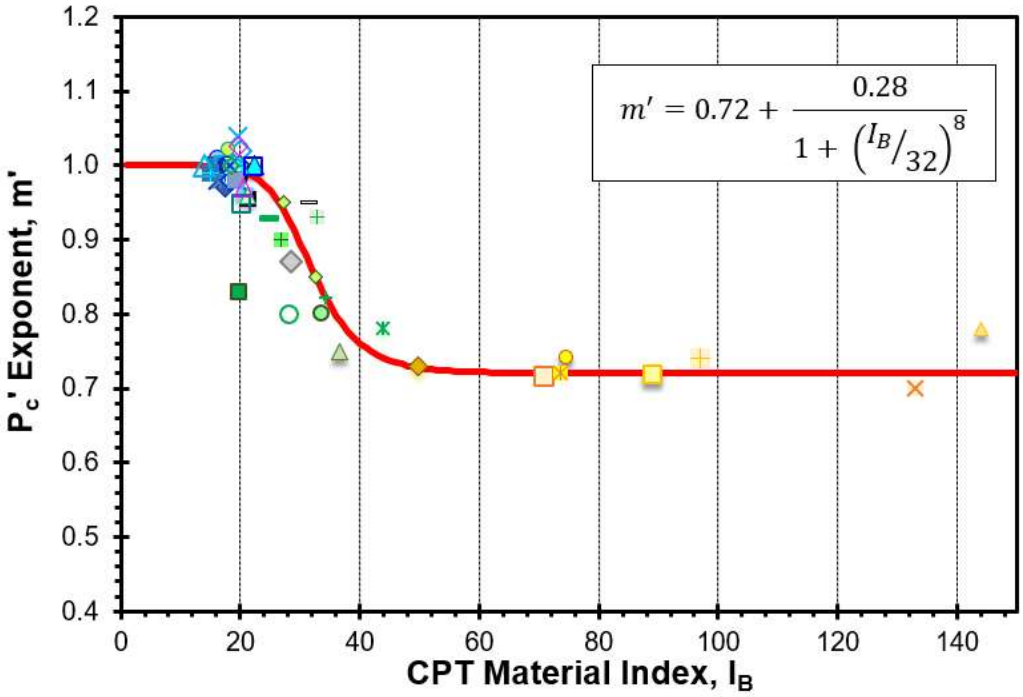


Figure 4.19. Trend for yield stress exponent (m') with CPT material index ($I_B$) according to Robertson (2016)

## 4.12 Conclusions

The relationship between effective yield stresses of different soils and the net cone tip resistance is explored as a power law expression where the exponent (m') is a variable that tracks with grain size. A generalized solution is developed by merging of two independent methods: (1) analytical hybrid spherical cavity expansion and critical state soil mechanics (SCE-CSSM) solution for intact clays; (2) algorithms derived from CPT calibration chamber test data on clean silica and quartz sands. A commonality in the simplified expressions of the two methods has been used to define a more global power law formulation with a yield stress exponent (m') that is extended to cover a variety of different geomaterials such as clays, silts, mixed soils, and sands. A look at data from

fissured OC clays and organic clays was also quantified. For that purpose, a large database of 78 worldwide well-documented geotechnical sites has been compiled where both CPT data and the results of one-dimensional consolidation tests and/or engineering geologic information were available.

A number of case studies are presented to verify the applicability of the unified approach using a yield stress exponent for sands, silts, mixtures, and intact clays. Special considerations are needed for organic soils and fissured clays. The yield stress exponent was found inversely proportional to the soil grain size where it increases with fines content moving from sands to clays and decreases with mean grain size moving from clays to sands. Direct relationships between the yield stress exponent and the mean grain size ($D_{50}$) and average fines content (FC) were developed based on a subset database of 56 sites covering different particle sizes.

To better quantify the value of the variable exponent, it was further linked to the CPT material index ($I_c$). Four different definitions for the material index have been investigated covering the classic definition by Robertson & Wride (1998) and Robertson (2009), non-normalized SBT material index (Robertson 2010), updated Jefferies and Been (2015) definition, and finally a new definition based on contractive-dilative behavior separation (Robertson 2016). Utilization of the CPT material index provided a convenient quick means of identifying and assigning the exponent value for different geomaterials. **Table 4.3** summarizes the developed correlations between the yield stress exponent $m'$ and the different CPT material indices in addition to grain size distribution measurements.

Table 4.3. Summary of yield stress exponent (m') correlations with CPT material indices and grain size distribution measurements

| | | | |
|---|---|---|---|
| | **Generalized Expression** | $\sigma_p' = 0.33 \cdot (q_t - \sigma_{vo})^{m'}$ | Fissured Clays: m'=1.1<br>Intact Clays: m'=1.0<br>Organic Clays: m'=0.90<br>Sensitive Clays: m'=0.90<br>Silt Mixtures: m'=0.85<br>Silty Sands: m'=0.80<br>Clean Sands: m'=0.72 |
| **CPT Material Index - Based** | Robertson & Wride (1998) | $m' = 1 - \frac{0.28}{1+(I_{cRW}/2.64)^{25}}$ | |
| | Robertson (2010) | $m' = 1 - \frac{0.28}{1+(I_{SBT}/2.4)^{20}}$ | |
| | Jefferies and Been (2015) | $m' = 1 - \frac{0.28}{1+(I_{cJB}/2.7)^{30}}$ | |
| | Robertson (2016) | $m' = 0.72 + \frac{0.28}{1+(I_B/32)^{8}}$ | |
| **Grain Size Distribution - Based** | Fines Content (%) | $m' = 1 - \frac{0.28}{1+(FC/55)^{20}}$ | |
| | Mean Grain Size (mm) | $m' = 0.72 + \frac{0.28}{1+(16 \cdot D_{50})^{5}}$ | |

# Chapter 5. Evaluating Undrained Rigidity Index of Clays from Piezocone Data

## 5.1 Introduction

The rigidity index ($I_R$) is an important input parameter for geotechnical applications involving bearing capacity, pile driving, porewater pressure generation, and piezodissipations. The value of soil rigidity index is incorporated in various theories and analytical solutions involving cavity expansion, strain path method, and finite element analyses. For piezocone penetration into clays, the magnitude of undrained rigidity index is needed in the interpretation of coefficient of consolidation ($c_{vh}$) and its associated hydraulic conductivity (k).

The rigidity index is defined as the ratio of shear modulus to shear strength, $I_R = G/\tau_{max}$. The value of rigidity index depends on the conditions of loading, and for undrained conditions at constant volume, the modulus and undrained shear strength can both be determined from laboratory tests such as direct simple shear or triaxial compression tests. For undrained loading, the rigidity index is given by:

$$I_R = \frac{G}{s_u} = \frac{E_u}{3 \cdot s_u} \qquad [5.1]$$

Direct evaluation of rigidity index from its definition as the ratio of shear modulus to shear strength ($I_R = G/s_u$) is quite elusive and difficult (Vardanega & Bolton 2013; Krage et al. 2014). For one, the shear modulus of any given clay can be evaluated over a wide range of mobilized strengths and levels of strain. The value of G varies and can be taken as the initial tangent shear modulus at small strains ($G_0 = G_{max}$), or as either a tangent modulus

($G_{tan} = d\tau/d\gamma_s$) or as a secant value ($G_{sec} = \tau/\gamma_s$), as well as the value at the failure strain, $G_f = \tau_{max}/\gamma_f$. This is so in part because of the highly nonlinear stress-strain-strength behavior of soil, and a corresponding range of stiffness that is represented in terms of modulus reduction curves, ($G/G_{max}$), as discussed by Mayne (2005).

**Figure 5.1** expresses the relationship between shear stress and shear strain with a definition of the rigidity index taken at $G_f$ or $G_{min}$. For penetration tests, as in the case of CPT, the appropriate value of the shear modulus is likely close to the minimum shear modulus, as defined at peak shear stress: $G_{min} = \tau_{max}/\gamma_f$, where $\gamma_f$ = strain at failure (Mayne 2007a). As presented in Figure 5.1, the corresponding value for $I_R$ can be taken as the reciprocal of the strain at failure, $I_R = 1/\gamma_{REF}$.

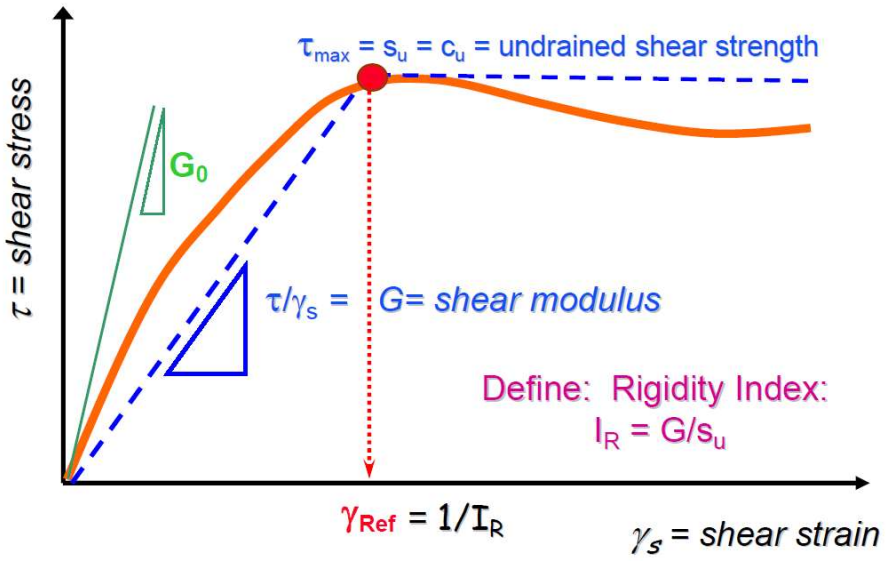


Figure 5.1. Schematic diagram illustrating shear stress vs. shear strain for clay soils and definitions of $\tau_{max}$, G, $\gamma_f$, and $I_R$. (Mayne, 2007a)

## 5.2 Intermediate Stiffnesses of the Soil

Given the high non-linearity in the stress-strain-strength behavior of different geomaterials, it is difficult to assign a single set value of the appropriate shear modulus. As presented in **Figure 5.1** the shear modulus definition depends on the corresponding shear strain level, since decreasing magnitudes of shear moduli are obtained at increasing shear strains. The range of the measured shear strains depends on the testing tool or technique employed, geophysical tests cover very small shear strain levels < $10^{-6}$ while in-situ tests such as flat dilatometers (DMT) detect a higher range of about $10^{-3}$ while penetration tests such as the CPT captures much higher shear strain levels on the order of 1% to 100%. **Figure 5.2** presents a schematic of the shear modulus reduction with the variation in the measured shear strain level with the appropriate measuring tool for each stage.

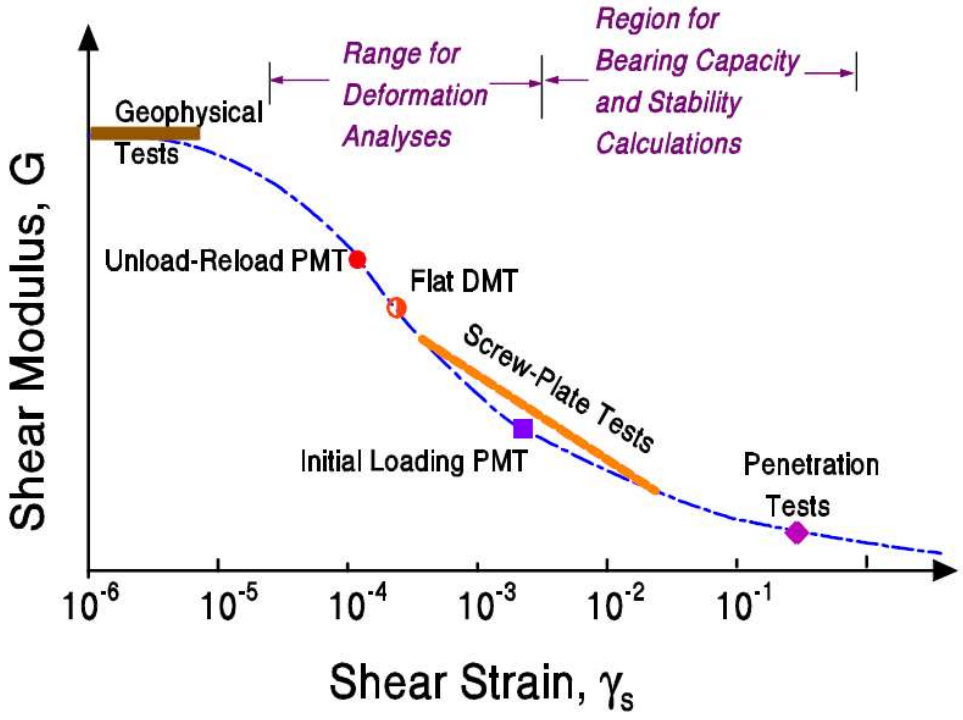


Figure 5.2. Reduction of shear modulus with shear strain level (Mayne, 2001)

## 5.3 Undrained Rigidity Index Definition

When a cone penetrometer is pushed into the ground, a bulb of soil around the cone is deformed plastically. According to spherical cavity expansion theory, the size of the zone of the soil that goes plastic (diameter D) is related to the size of the intruding body (diameter d) and that ratio depends upon the rigidity index (Vesić 1977):

$$D/d = (I_R)^{0.33} \quad [5.2]$$

Therefore, the rigidity index can be considered as a measure of the volume of clay affected by the advancing penetrometer and thus an operational value should be considered.

The main quantities defining the magnitude of the rigidity index are the shear modulus and undrained shear strength. The selection of the appropriate means to measure each quantity is challenging and requires careful evaluation. By simulating the piezocone advancement into the ground, it is difficult to decide which predominant failure mode exists around the cone. Hence, the selection of the correct shearing mode and testing technique is not easy. Broussard (2012) summarized the recommendations made by different researchers and the reasoning behind the selection for both $s_u$ and G values. As per Broussard (2012), for the selection of undrained shear strength, Keaveny (1985) and Schnaid et al. (1997) recommended the usage of $CK_0UC$ triaxial compression test, while Konrad and Law (1987) promoted the pressuremeter test. Also, Teh and Houlsby (1991) Yu and Mitchell (1998), and Yu et al. (2000) deemed the triaxial compression mode as the most appropriate.

A more difficult issue lies in the selection of the correct shear modulus as its magnitude depends on the level of shear strain. The initial shear modulus ($G_{max}$) represents the tangent modulus at very low strain levels, but this is restricted to nondestructive strains. The secant

modulus represents higher strain levels with G reducing with strains (Mayne, 2007). As a compromise, Konrad & Law (1987) and Schnaid et al. (1997) chose to use a shear modulus at 50% mobilized strength ($G_{50}$) to give an average response.

It is evident that there are difficulties in properly selecting strength mode and mobilization level of shear modulus values using laboratory-based techniques. These also are affected by issues related to sample disturbance, stress relief and high costs of obtaining and testing quality samples. Therefore, it is of great interest and benefit to develop methods of obtaining the rigidity index based on direct CPT measurements.

## 5.4 Existing Methods for Estimating Undrained Rigidity Index

Keaveny and Mitchell (1986) proposed an empirical approach relating the rigidity index to the overconsolidation ratio (OCR) and clay plasticity index (PI), as presented in **Figure 5.3.** The developed approach was based on triaxial CAUC test data where the $I_R$ was defined using $G_{50} = E_{50}/3$. The developed correlation can be expressed from the approximation:

$$I_{R50} \approx \frac{\exp\left(\frac{137 - PI}{23}\right)}{1 + \ln[1 + \frac{(OCR - 1)^{3.2}}{26}]^{0.8}} \qquad [5.3]$$

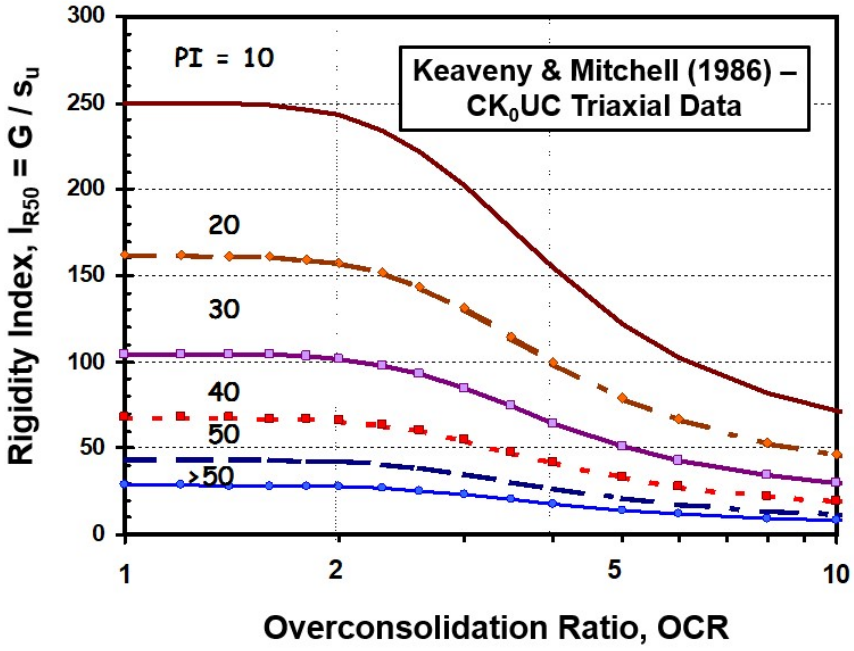


Figure 5.3. Undrained rigidity index estimate from clay plasticity index and overconsolidation ratio (Keaveny & Mitchell, 1986)

Another means to estimate the rigidity index is via a Cam-clay derivation which was obtained by Kulhawy and Mayne (1990) based on routine soil parameters. The initial modulus was evaluated by differentiation as the strain approaches zero, then using this modulus value in a normalized form to evaluate undrained rigidity index, as presented in **Figure 5.4** and given by the following expression:

$$I_R = \left(\frac{2}{3}\right) \cdot M \left(\frac{1+e_0}{C_c}\right) \cdot \ln(10) \frac{[1+\ln(OCR)]\exp(\Lambda)}{\Lambda(1-\Lambda)OCR^{\Lambda}} \qquad [5.4]$$

Where $M = 6 \cdot \sin\phi'/(3-\sin\phi')$, $\Lambda = (1 - C_s / C_c)$ = plastic volumetric strain potential, $C_s$ = swelling index, $C_c$ = virgin compression index, and $e_0$ is the initial void ratio.

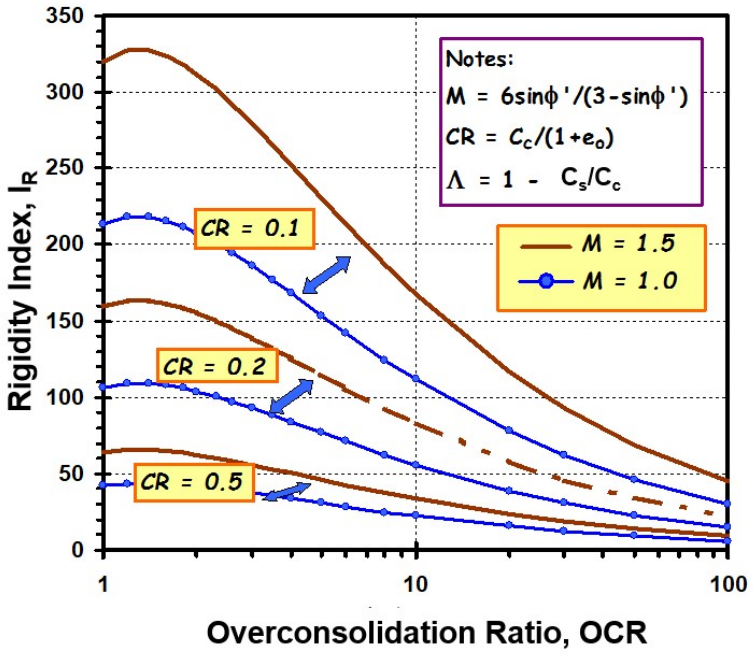


Figure 5.4. Rigidity index derivation from Cam-clay model as a function of overconsolidation ratio (Kulhawy and Mayne, 1990)

According to equation [5.1], the undrained modulus ratio ($E_u/s_u$) is a measure of the undrained rigidity index, since $E_u/s_u = 3 \cdot I_R$. Hence, several researchers have investigated the relationship between ($E_u/s_u$) and the overconsolidation ratio for clays of varying plasticity characteristics, as seen in **Figure 5.5 (**Duncan & Buchignani 1976). This normalized quantity ($E_u/s_u$) was also investigated by Ladd et al. (1977) for various OCR values and several stress levels in defining guidance charts that can be used indirectly to determine the undrained rigidity index, as presented in **Figure 5.6.**

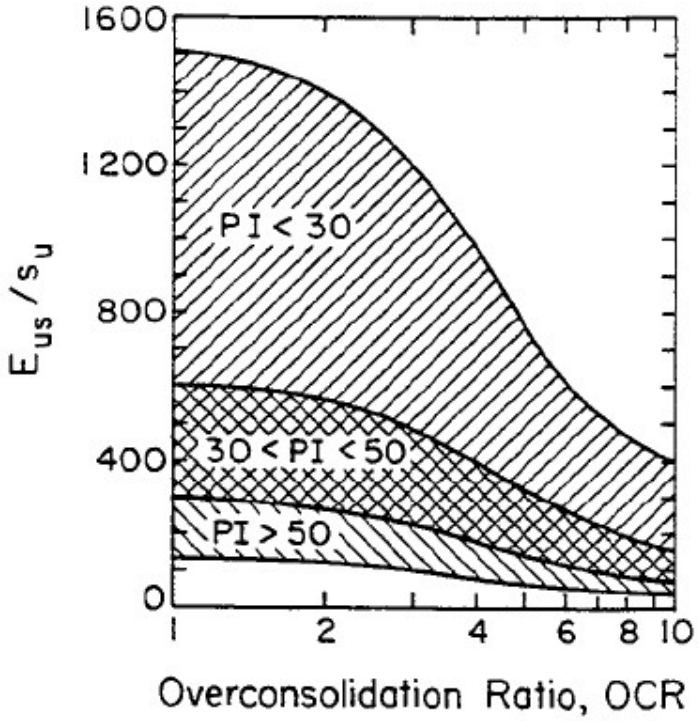


Figure 5.5. Undrained modulus of elasticity ratio ($E_u/s_u$) versus overconsolidation ratio and plasticity index (Duncan and Buchignani, 1976)

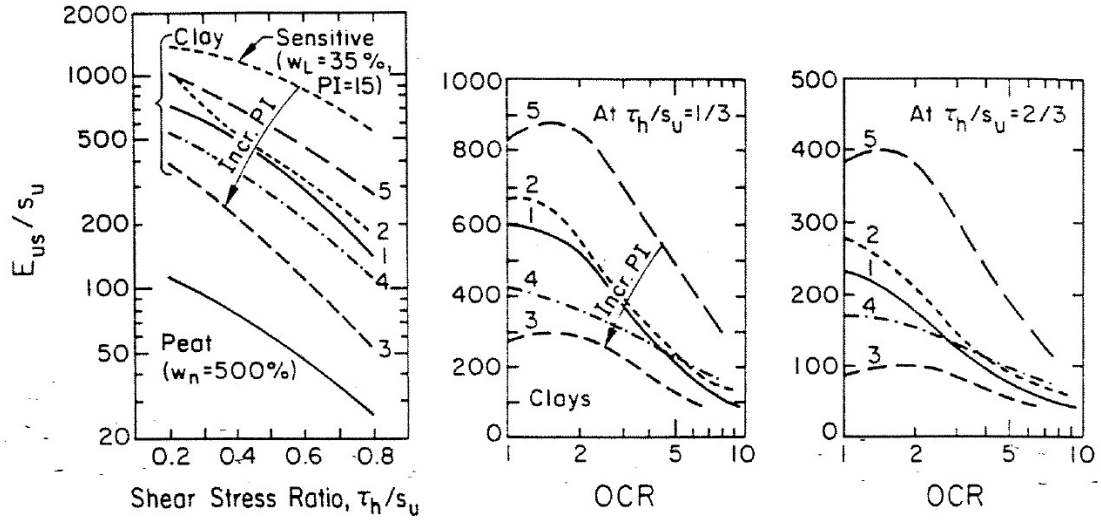


Figure 5.6. Undrained modulus of elasticity ratio ($E_u/s_u$) versus overconsolidation ratio and stress level (Ladd et al., 1977)

Mayne (2001) developed an expression for estimating the rigidity index based on CPTu data in clays from the hybrid spherical cavity expansion - critical state framework (SCE-CSSM). The $I_R$ expression was given by:

$$I_R = \exp \cdot \left[ \frac{(q_t - \sigma_{vo})}{(q_t - u_2)} \cdot \left( \frac{1.5}{M} + 2.925 \right) - 2.925 \right] \quad [5.5]$$

where M = (6 sinϕ')/(3 - sinϕ'). However, as the values of net cone resistance and effective cone resistance are close, a line-by-line evaluation of data showed that the assessed $I_R$ profile was highly variable with depth.

A recent empirical approach introduced by Krage et al. (2014) using the shear wave velocity profile and net cone tip resistance from SCPTu has been developed to evaluate $I_R$ at 50% level. This can be investigated here where $I_R$ can be determined from:

$$(I_R)_{50} = \left[ \frac{1.81 \cdot G_0}{(q_{net})^{0.75} (\sigma'_{vo})^{0.25}} \right] \quad [5.6]$$

and consistent units used for $G_0$, $q_{net}$, and $\sigma_{vo}'$ terms.

Finally, Mayne (2016) developed an expression for estimating rigidity index based on the normalized pore water pressure parameter ($B_q$) from the CPTu data using spherical cavity expansion theory. The $I_R$ expression is given by:

$$I_R = \exp \cdot \left[ \frac{2.93 \cdot (B_q)}{(1 - B_q)} \right] \quad [5.7]$$

where $B_q = (u_2 - u_0) / (q_t - \sigma_{vo})$.

## 5.5 Direct CPTu Solution for Evaluating Undrained Rigidity Index

### 5.5.1 Original SCE-CSSM Solution

A hybrid formulation of spherical cavity expansion and critical state soil mechanics (SCE-CSSM) expresses the cone tip resistance ($q_t$) and porewater pressure ($u_2$) using closed-form equations as follows (Mayne 1992; Chen & Mayne 1994; Mayne 2007a):

$$q_t = \sigma_{vo} + [(4/3)\cdot(\ln I_R + 1) + \pi/2 + 1]\cdot(M/2)\cdot(OCR/2)^{\Lambda}\cdot\sigma_{vo}' \quad [5.8]$$

$$u_2 = u_o + [(2/3)\cdot(\ln I_R)\cdot(M)\cdot(OCR/2)^{\Lambda}\cdot\sigma_{vo}'] + [1-(OCR/2)^{\Lambda}]\cdot\sigma_{vo}' \quad [5.9]$$

where M = (6 sinϕ')/(3-sinϕ') = slope of the frictional envelope for triaxial compression in q-p' space, $\Lambda = (1 - C_s / C_c)$ = plastic volumetric strain potential, $C_s$ = swelling index, $C_c$ = virgin compression index, $I_R$ = rigidity index = $G/s_u$, and OCR = $\sigma_p'/\sigma_{vo}'$. Typically, the value of $\Lambda \approx 0.8$ to 0.9 for most clays.

The hybrid SCE-CSSM model can be rearranged to determine the overconsolidation ratio (OCR) of the clay in three separate formulations using net cone resistance ($q_{net} = q_t - \sigma_{vo}$), excess porewater pressure ($\Delta u = u_2 - u_0$), and effective cone resistance ($q_{eff} = q_t - u_2$):

$$OCR = 2\cdot\left[\frac{(2/M)\cdot(q_t-\sigma_{vo})/\sigma_{vo}'}{(4/3)\cdot(\ln I_R + 1) + \pi/2 + 1}\right]^{(1/\Lambda)} \quad [5.10]$$

$$OCR = 2\cdot\left[\frac{(\Delta u/\sigma_{vo}') - 1}{(2/3)\cdot M\cdot\ln(I_R) - 1}\right]^{(1/\Lambda)} \quad [5.11]$$

$$OCR = \quad 2 \cdot \left[ \frac{1}{1.95 \cdot M + 1} \left( \frac{q_t - u_2}{\sigma_{vo}'} \right) \right]^{(1/\Lambda)} \qquad [5.12]$$

where Q = normalized tip resistance = $(q_t - \sigma_{vo})/\sigma_{vo}'$.

By combining equations [5.10] and [5.11] from the original hybrid SCE-CSSM framework, the value of the rigidity index, $I_R$ can be obtained in terms of piezocone normalized measurements and the effective friction angle as:

$$I_R = \exp \cdot \left[ \frac{1.5 \cdot Q + 2.925M \cdot \left( U^* - 1 \right)}{Q \cdot M - M \cdot \left( U^* - 1 \right)} \right] \qquad [5.13a]$$

$$I_R = \exp \cdot \left[ \frac{1.5 + 2.925M \cdot \left( \frac{U^* - 1}{Q} \right)}{M - M \cdot \left( \frac{U^* - 1}{Q} \right)} \right] \qquad [5.13b]$$

where Q = normalized tip resistance = $(q_t - \sigma_{vo}) /\sigma_{vo}'$; U* = normalized porewater pressure = $(u_2 - u_o)/\sigma_{vo}'$; and M = $(q/p')_f$ is the friction parameter from Cambridge q-p space.

Since the expression for $I_R$ is an exponential form, however, the use of [5.13] in a line-by-line post-processing of CPTu results in highly variable and skittish profiles with depth, therefore a moving average (over say 10 to 20 readings) is necessary for any practical use.

A stable representation for [5.13] is obtained in the following format:

$$I_R = \exp \cdot \left( \frac{1.5 + 2.925 \cdot M \cdot a_q}{M \cdot (1 - a_q)} \right) \qquad [5.14]$$

where $a_q = (U^* - 1)/Q = (u_2 - \sigma_{vo})/(q_t - \sigma_{vo})$. Hence, $a_q$ can be determined as a single value for any clay deposit by taking the slope of a plot of the parameter (U*-1) versus Q, or alternatively as the slope of $(u_2 - \sigma_{vo})$ versus $(q_t - \sigma_{vo})$. Using regression analyses, slightly different slope values for $a_q$ are obtained.

As a simplification, the shear-induced excess pore water pressure can be relatively neglected in the final expression for evaluating the rigidity index at it represents less than 20% of the excess porewater pressure. The rigidity index in such case can be evaluated using the following simplified expression:

$$I_R = \exp\cdot\left[\frac{1.5\cdot Q + 2.925M\cdot\left(U^*\right)}{Q\cdot M - M\cdot\left(U^*\right)}\right] \qquad [5.13c]$$

Another expression for evaluating the rigidity index can be obtained by combining equations [5.11] and [5.12] from the original hybrid model as a function of the effective cone tip resistance and the quantity $(u_2 - \sigma_{v0})$ as expressed:

$$I_R = \exp\left[\left(\frac{u_2 - \sigma_{vo}}{q_t - u_2}\right)\cdot\left(\frac{1.5}{M} + 2.925\right) + \frac{1.5}{M}\right] \qquad [5.15]$$

### 5.5.2 Effective Friction Angle Evaluation

The derived expression for rigidity index depends on the value of the effective friction angle ($\phi'$). In the event that laboratory-measured values from triaxial tests are not available, the effective friction angle can be evaluated using the NTH method (now NTNU). This is an effective stress limit plasticity solution for undrained penetration developed by Senneset et al. (1989) at the Norwegian Institute of Technology (NTH), presented in **Figure 5.7**. In this method, a cone resistance number ($N_m$) is defined:

$$N_m = \frac{N_q - 1}{1 + N_u \cdot B_q} = \frac{q_t - \sigma_{v0}}{\sigma_{vo}' + a'} \quad [5.16]$$

where $a' = c' \cdot \cot\phi'$ = attraction, $N_q = K_p \cdot \exp[(\pi - 2\beta) \cdot \tan\phi']$ is the end-bearing factor for the cone tip resistance, $K_p = (1+\sin\phi')/(1-\sin\phi')$ is the passive stress coefficient, $\beta$ = angle of plastification ($-20^o < \beta < +20^o$) which defines the size of the failure zone beneath the tip, $N_u = 6 \cdot \tan\phi' \cdot (1+\tan\phi')$ is the porewater pressure bearing factor. The full solution allows for an interpretation of a paired set of Mohr-Coulomb strength parameters (c' and $\phi'$) for all soil types.

For soft to firm clays, it can be adopted that $c' = 0$, thus the term $N_m$ reduces to the well-known normalized cone resistance, $Q = q_{net}/\sigma_{vo}'$. Further simplification is achieved by taking the angle $\beta = 0$ (Terzaghi equation) for the case of undrained loading and an approximate deterministic expression is obtained (Mayne 2007b):

$$\phi' = 29.5^\circ \cdot B_q^{\,0.121} [0.256 + 0.336 \cdot B_q + \log Q] \quad [5.17]$$

which is valid for the following parameter ranges: $20^\circ \leq \phi' \leq 45^\circ$ and $0.1 \leq B_q \leq 1.0$.

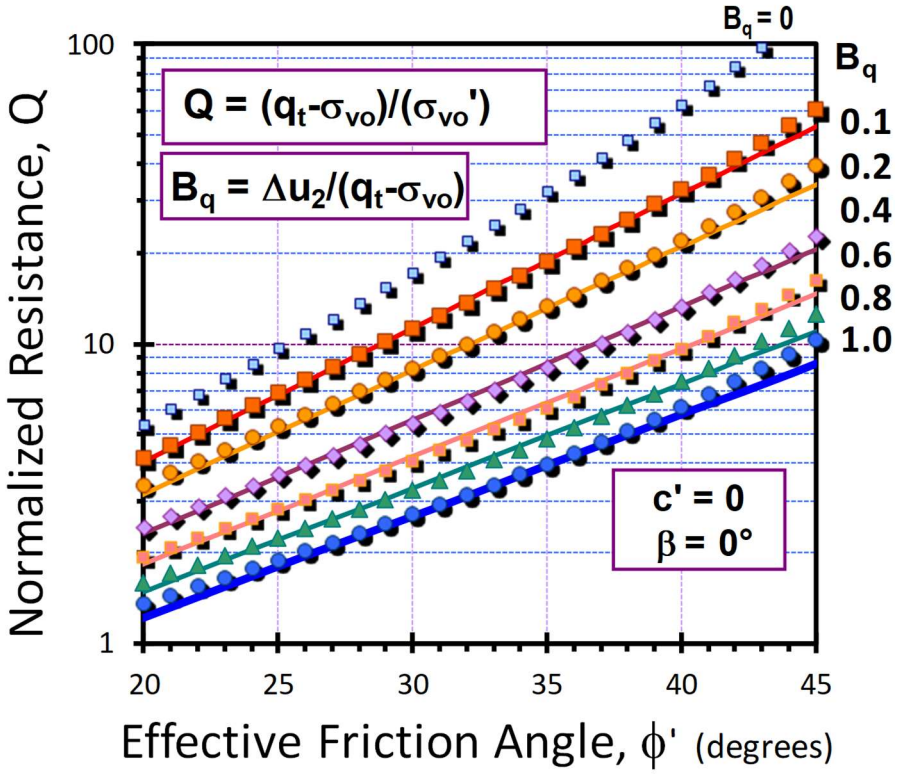


Figure 5.7. NTH Method for evaluating ϕ' from CPTu in clays: theory is shown as dots (Senneset et al., 1989); approximation by lines (Mayne, 2007)

### 5.5.3 Undrained Shear Strength Evaluation

After obtaining an operational value for the rigidity index using the derived solution, $I_R$ can be directly used to evaluate the undrained shear strength of the clay under study using a cone bearing factor ($N_{kt}$) with the net cone tip resistance, where undrained shear strength is obtained from:

$$s_{uc} = \frac{q_{net}}{N_{kt}} \qquad [5.18]$$

From spherical cavity expansion theory, the cone bearing factor ($N_{kt}$) is expressed solely in terms of the rigidity index (Vesić 1977):

$$N_{kt} = [(4/3) \cdot (\ln I_R + 1) + \pi/2 + 1] \quad [5.19]$$

Accordingly, the cone factor is evaluated from the post-processed value of $I_R$. Using the net cone tip resistance, one can evaluate a profile of undrained shear strength with depth.

Moreover, the same input parameters (M and $I_R$) can be used in [5.10], [5.11], and [5.12] to obtain 3 independent profiles of OCR in the clay deposit.

## 5.6 Flow Properties from Piezodissipation Tests

The results of piezocone dissipation tests can be used to evaluate the permeability and the coefficient of consolidation of fine-grained soils (Jamiolkowski et al. 1985). As the piezocone penetrates the ground, transient excess porewater pressures are generated around the probe. When the penetration is halted, the measured $u_2$ readings decay over time until eventually reaching the hydrostatic porewater pressure value ($u_0$) which is the equilibrium condition. The coefficient of consolidation, $c_{vh}$ controls the rate of dissipation over time and is computed as:

$$c_{vh} = \frac{k \cdot D'}{\gamma_w} \quad [5.20]$$

where k = coefficient of permeability, D' = soil constrained modulus, and $\gamma_w$ = unit weight of water.

While several procedures are available (e.g., Robertson et al. 1992; Chai et al. 2012), the original SCE-CSSM approach is detailed by Burns & Mayne (1998a, 1998b) can be used here without alterations since the solution depends solely on the porewater pressures and input parameters. The generated excess porewater pressures that are measured are the sum of octahedral plus shear-induced components, which are computed:

$$\Delta u_{2\,i} = (\Delta u_{oct})_i + (\Delta u_{shear})_i \quad [5.21]$$

where the octahedral component is represented by spherical cavity expansion that extends the plastic zone out into the surrounding ground and the shear-induced part occurs at the soil-structure interface as the steel of the penetrometer rubs against the clay soil (thin shear zone) and represented by CSSM. The initial values are determined from:

$$(\Delta u_{oct})_i = (2 \cdot M/3)\,(OCR/2)^{\Lambda} \cdot \ln(I_R) \cdot \sigma_{vo}' \quad [5.22]$$

$$(\Delta u_{shear})_i = [1 - (OCR/2)^{\Lambda}] \cdot \sigma_{vo}' \quad [5.23]$$

These two components dissipate at different rates because they are separate phenomena. Coupled flow is unwarranted and not applicable here. Hence, porewater pressure can be evaluated at any time (t) using the following algorithm (Mayne 2001):

$$(\Delta u_2)_t = \frac{(\Delta u_{oct})_i}{1 + 50 \cdot T'} + \frac{(\Delta u_{shear})_i}{1 + 5000 \cdot T'} \quad [5.24]$$

where the modified time factor (T') is given by:

$$T' = \frac{c_{vh} \cdot t}{a_c \cdot I_R^{0.75}} \quad [5.25]$$

where t = elapsed time after stopping penetration and $a_c$ = piezocone radius.

The value of $c_{vh}$ is found by trial-and-error fitting of the theoretical curves to the measured dissipation data, where assigned values of T' are used to obtain the corresponding time for a given rigidity index and cone radius.

## 5.7 Case Studies Validating the $I_R$ Evaluation

### *5.7.1 Sandpoint, Idaho*

The test site is a part of a realignment project for US95 to include a bridge over the north shore of Lake Pend Oreille in the town of Sandpoint, North Idaho. The soils at the site consist of post-glacial alluvial deposits which are soft silty clay with high compressibility to depths exceeding 80 m (Altaee and Fellenius, 2002). The clay at Sandpoint has the following characteristics and index values: LL = 45.2 ± 6.3 %, PI = 19.9 ± 4.7 %, and $w_n$ = 45.2 ± 6.4 %.

**Figure 5.8** presents a deep seismic piezocone sounding (SCPTu) extending to depths of 80m where the downhole shear wave velocity extends to 60 m (Mayne 2005). An average effective friction angle ϕ' = 32° is evaluated using the NTH method that compares well with CIUC triaxial tests (ϕ' = 33°) made on undisturbed samples (Mayne 2014).

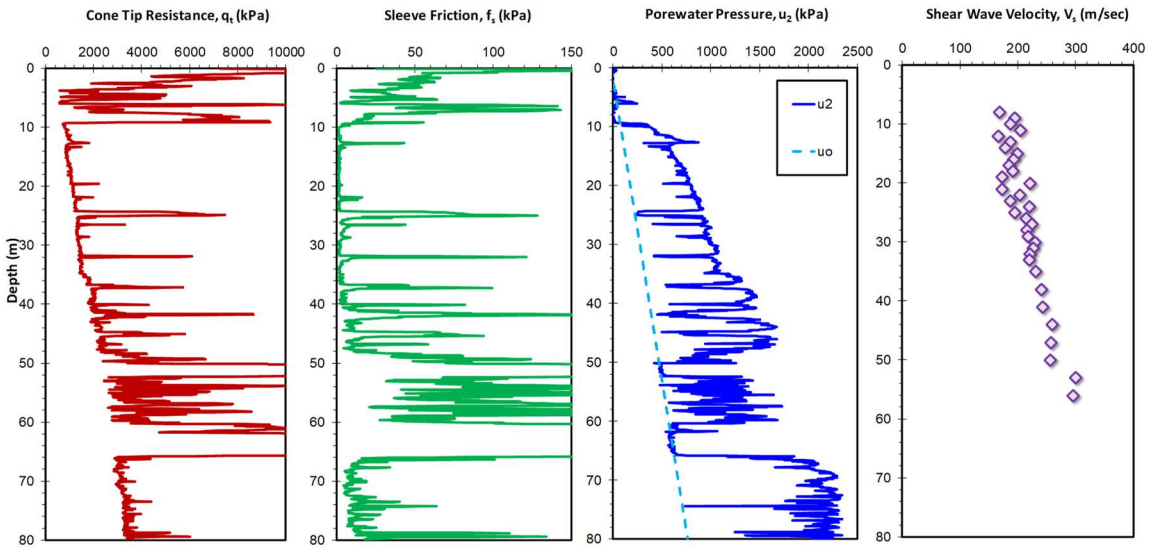


Figure 5.8. Seismic piezocone sounding at Sandpoint, Idaho (a) cone tip resistance, $q_t$; (b) sleeve friction, $f_s$; (c) porewater pressure, $u_2$; and (d) shear wave velocity, $V_s$

According to the stress history data reported by (Altaee and Fellenius, 2002), the silty clay has a representative overconsolidation ratio (OCR) = 1.5 and plasticity index (PI) value of

20%. These values are applied to the empirical equation [5.3] given by Keaveny and Mitchell (1986) to give an average $I_R$ = 170. The same input values are applied into equation [5.4] by Kulhawy and Mayne (1990) in addition to $C_c$ value of 0.60 and initial void ratio of 1.12 to give an average $I_R$ = 120.2 with a lambda value of 0.95.

The profile of the shear wave velocity is used to evaluate the small strain shear modulus ($G_0$) which is used in Krage et al (2014) seismic procedure presented in equation [5.6] along with the cone tip readings to give an average rigidity index value of $I_R$ = 244.

**Figure 5.9** shows the evaluation of the slope parameter used in the new $I_R$ solution where ($u_2$-$\sigma_{vo}$) is plotted versus net cone tip resistance ($q_{net}$), giving a slope value of $a_q$ = 0.5074. This slope value is used with the friction parameter M to give an operational rigidity index value ($I_R$) of 217 at Sandpoint.

Similarly, **Figure 5.10** shows the evaluation of the slope parameter used in the alternative proposed $I_R$ solution where normalized porewater pressure parameter (U*-1) is plotted versus normalized net cone tip resistance (Q), giving a slope value of 0.5428. The slope value is used with effective friction angle to give an operational rigidity index value ($I_R$) of 412.

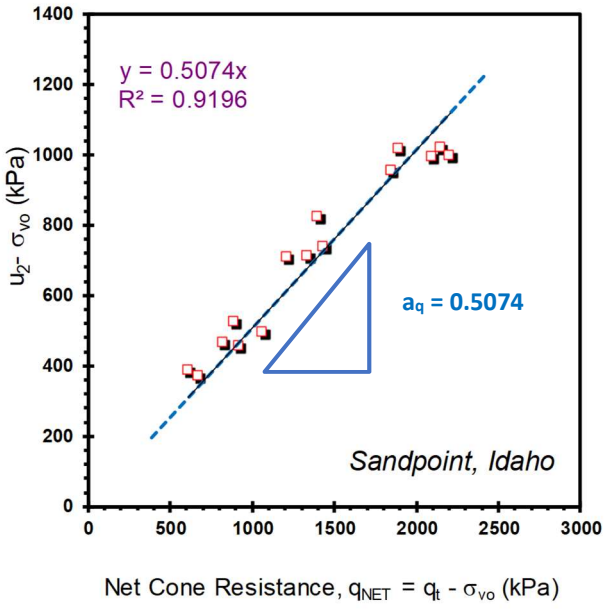


Figure 5.9. Evaluation of slope parameter, $a_q$ for proposed $I_R$ solution using CPTu data from Sandpoint, Idaho

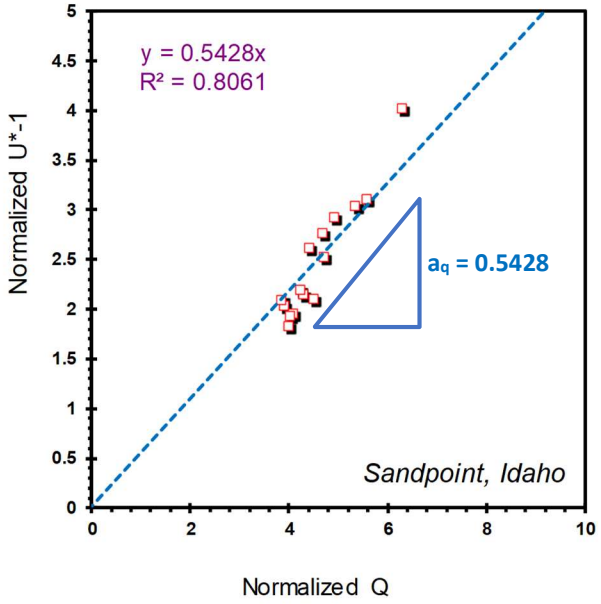


Figure 5.10. Alternative evaluation of slope parameter for using (U*-1) versus Q using CPTu data from Sandpoint, Idaho

**Figure 5.11a** presents a comparison between the values of rigidity index obtained using five different expressions: three methods from the literature in addition to two derived

expressions based on hybrid SCE-CSSM framework. For the Sandpoint clay site, the Keaveny and Mitchell approach gave the lowest $I_R$ value while the proposed alternative solution – function (U*-1, Q) gave the highest $I_R$ value. It is clear that the two proposed new expressions give rigidity index values that are reasonable, comparable and within the same order of magnitude of other expressions from the literature.

The new solution which is expressed as a red line in **Figure 5.11** will be used in evaluating the undrained shear strength ($s_u$) and stress history profiles for Sandpoint (and 11 other subsequent case studies). The evaluated profiles will be compared to laboratory-measured reference values to investigate the suitability and correctness of the proposed expression in estimating the undrained rigidity index.

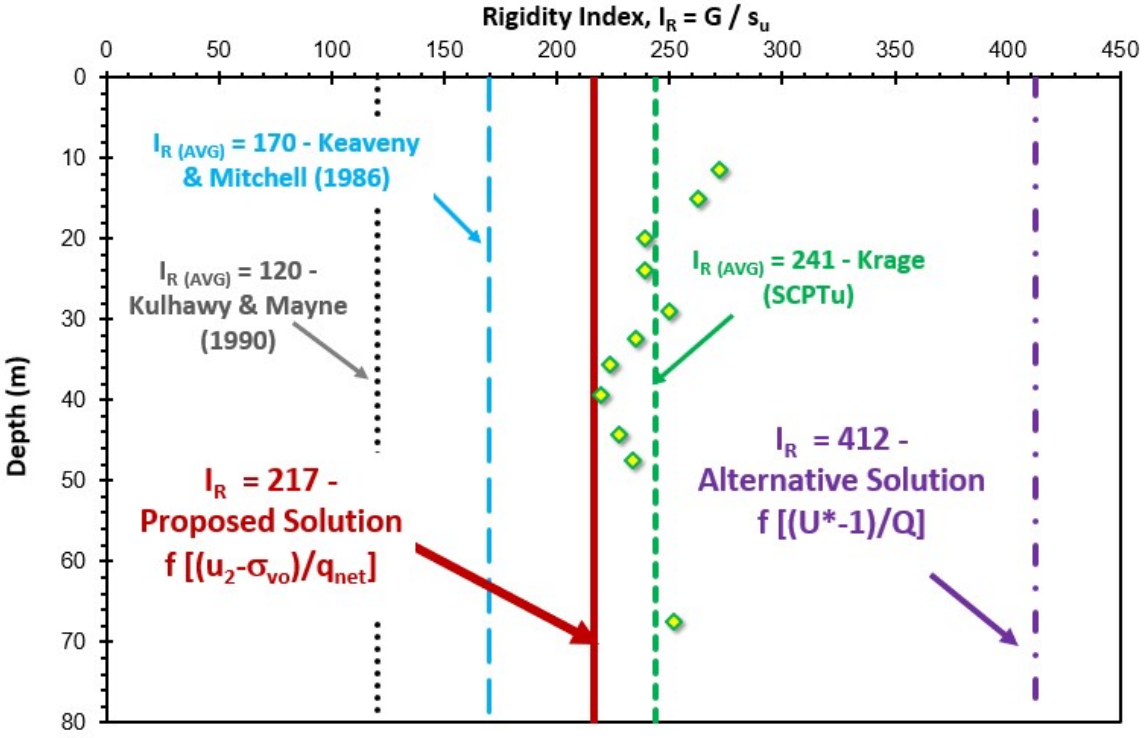


Figure 5.11. Comparison between different approaches for estimating rigidity index value for Sandpoint, Idaho test site

The obtained $I_R$ value is used to calculate the cone bearing factor ($N_{kt}$) as per equation [5.19] for evaluating the undrained shear strength ($s_u$). Using the $I_R$ = 217, the corresponding $N_{kt}$ = 11.08 provides an excellent agreement with the laboratory measured triaxial compression $s_u$ reference values reported by Altaee and Fellenius (2002), as presented in **Figure 5.12.**

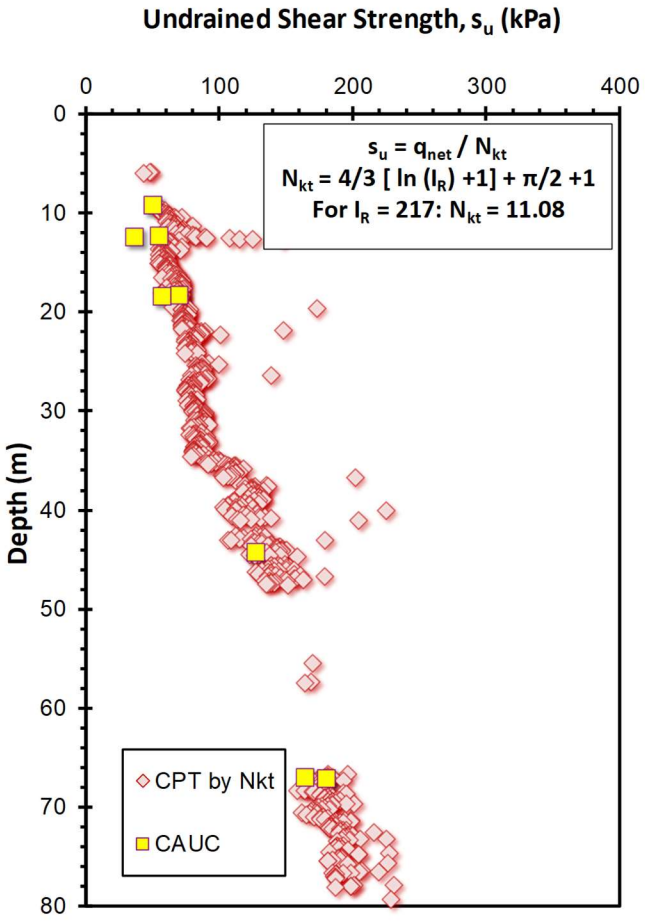


Figure 5.12. Undrained shear strength profile for Sandpoint, Idaho using the proposed SCE-CSSM operational rigidity index value and cone bearing factor $N_{kt}$
(Note: triaxial data from Altaee and Fellenius, 2002)

By applying equations [5.10], [5.11], and [5.12] of the hybrid SCE-CSSM to the results of piezocone sounding from **Figure 5.8** with an operational rigidity index value of $I_R$ = 217

from the proposed expression and effective friction angle value ($\phi' = 32°$), the three stress history predictions coincide and match with each other as presented in **Figure 5.13**. Overall, excellent agreement is observed when compared with laboratory measured $\sigma_p'$ and OCR profiles reported by Altaee and Fellenius, 2002.

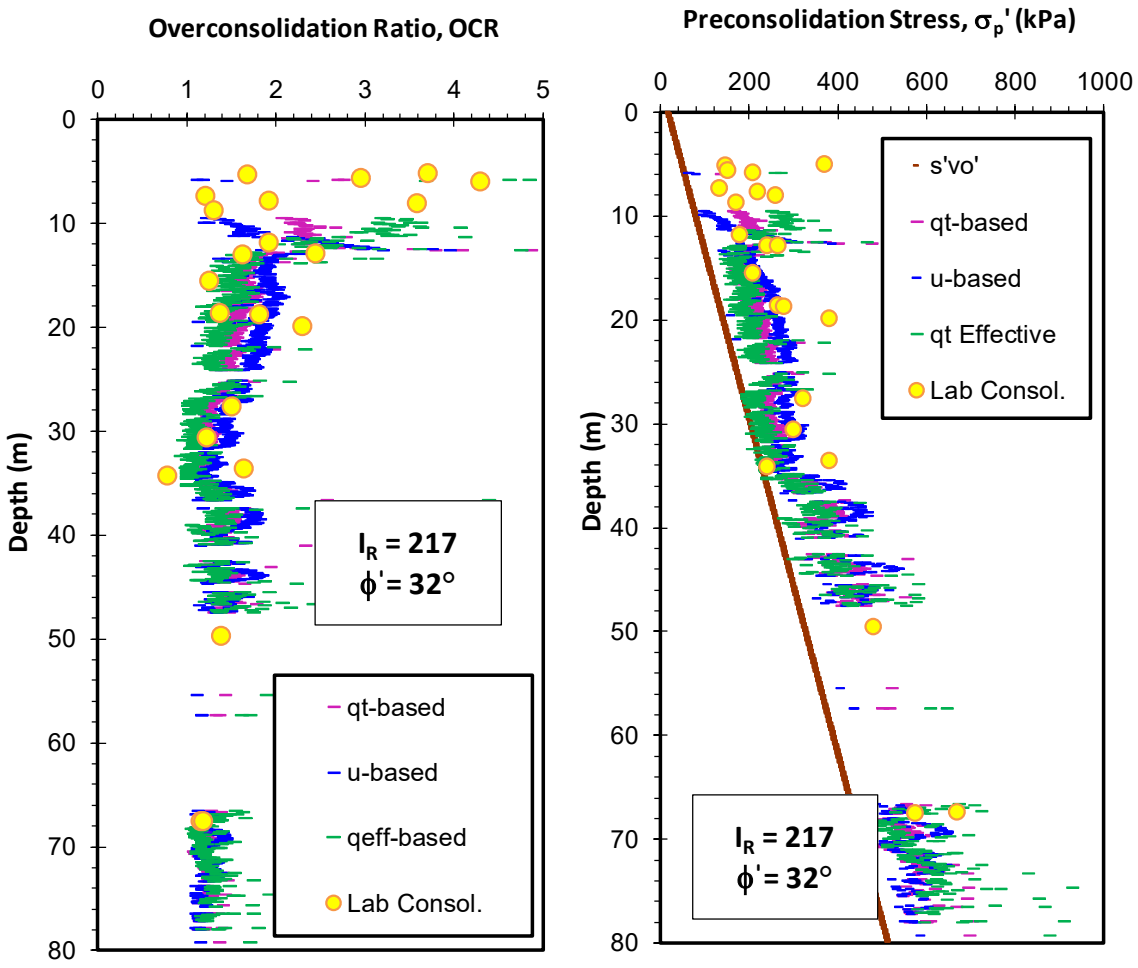


Figure 5.13. OCR and preconsolidation stress prediction using original hybrid SCE-CSSM framework with new $I_R$ expression for Sandpoint, Idaho
(Note consolidation data from Altaee and Fellenius, 2002)

### 5.7.2 Ariake, Japan

Ariake is a normally consolidated soft marine deposit located in Hizen-Kashima, Saga Prefecture in Kyushu Island in Japan with OCR values ranging from 1.24 to 1.55 (Tanaka,

2000). Ariake is classified as highly plastic clay with average plasticity index ranging from 65 to 70%, water content between 100 – 150% and liquid limit between 110 – 120%. **Figure 5.14** presents a representative piezocone sounding conducted by Tanaka et al. (2001). Based on the piezocone data, an effective friction angle was evaluated using the NTH method and the site has a characteristic effective friction angle $\phi' = 32.2°$.

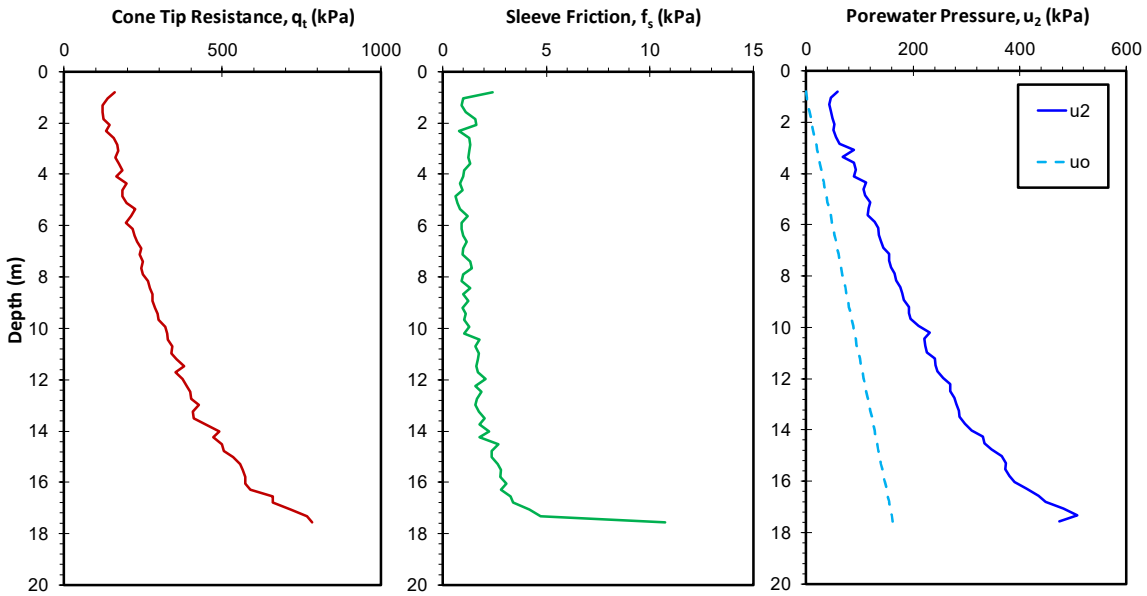


Figure 5.14. Piezocone sounding Ariake, Japan: (a) cone tip resistance, $q_t$; (b) sleeve friction, $f_s$; (c) porewater pressure, $u_2$. (after Tanaka et al., 2001)

**Figure 5.15** shows the evaluation of the slope parameter $a_q$ used in the proposed $I_R$ solution where $(u_2-\sigma_{vo})$ is plotted versus net cone tip resistance ($q_{net}$), giving a slope value of $a_q$ = 0.455. The slope value is used with the effective friction angle to give an operational rigidity index value $I_R = 97$.

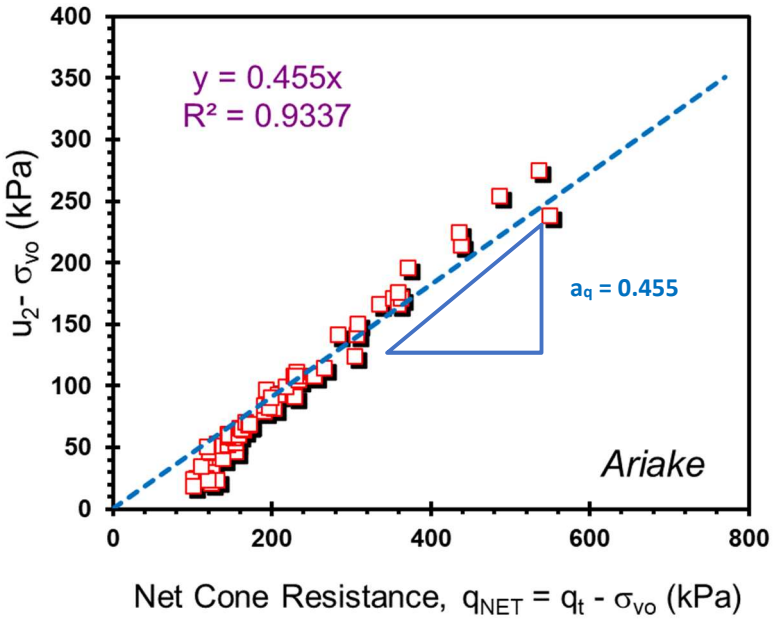


Figure 5.15. Evaluation of slope parameter for proposed $I_R$ solution f [ $(u_2-\sigma_{vo}) / q_{net}$] using CPTu data from Ariake, Japan

The obtained $I_R$ value is used to obtain cone bearing factor ($N_{kt}$) as per equation [5.19] for evaluating the undrained shear strength ($s_u$). Using an $I_R = 97$, the corresponding $N_{kt} = 10$ which provides an excellent agreement with the CAUC undrained shear strength data reported by Lunne et al. (2006) for Ariake, as presented in **Figure 5.16.**

Applying equations [5.10], [5.11], and [5.12] of the hybrid SCE-CSSM to the results of piezocone sounding from **Figure 5.14** with an operational rigidity index value of $I_R = 97$ and $\phi' = 32.2°$, the three separate equations for stress history give predictions that coincide and match with each other, as seen in **Figure 5.17**. Overall, excellent agreement is observed when compared with laboratory measured $\sigma_p'$ and OCR profiles reported by Tanaka et al. (2001) and Lunne et al. (2006) for this site.

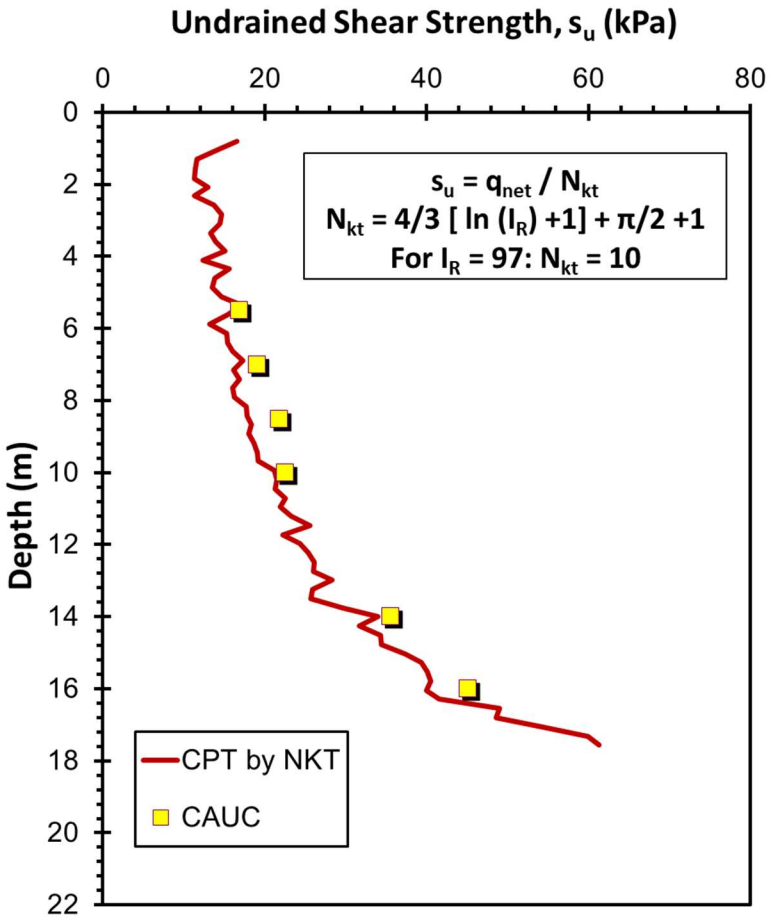


Figure 5.16. Undrained shear strength profile for Ariake, Japan using the proposed SCE-CSSM operational rigidity index value and cone bearing factor $N_{kt}$ (Note: triaxial data from Lunne et al., 2006)

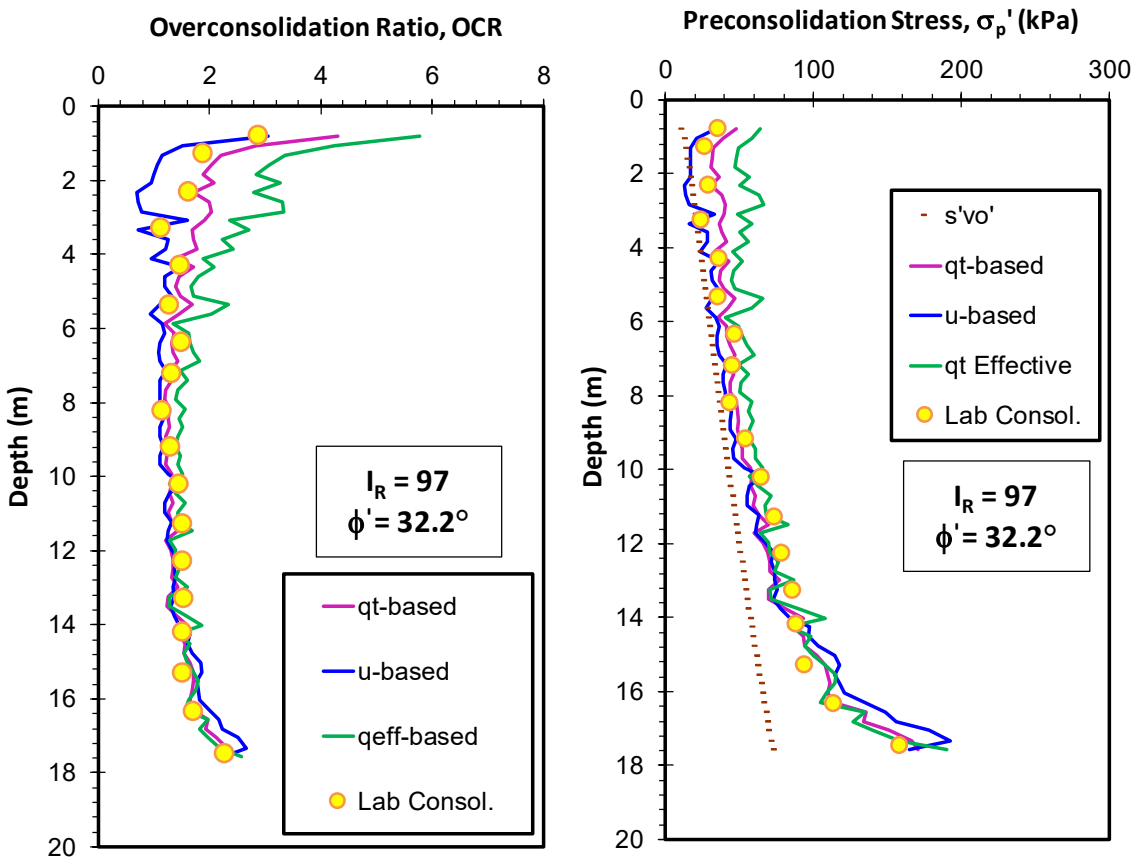


Figure 5.17. OCR and preconsolidation stress prediction using original hybrid SCE-CSSM framework with new $I_R$ expression for Ariake, Japan (consolidation data from Tanaka et al. 2001; Lunne et al. 2006)

### 5.7.3 Ballina, Australia

Ballina is a soft estuarine clay located in northern New South Wales in Australia. The clay has high plasticity with plasticity index value ranging 80% and liquid limit value ranging 130% (Pineda et al. 2016). The clay has an average organic content of 6%. The clay is characterized by its high compressibility and low undrained shear strength as measured in triaxial compression tests. Preconsolidation stresses were measured using constant rate of strain tests and incremental loading oedometer tests. **Figure 5.18** presents the readings of

a piezocone sounding conducted by Pineda et al. (2014). A characteristic effective friction angle $\phi' = 33.7°$ is evaluated using the piezocone data following the NTH method.

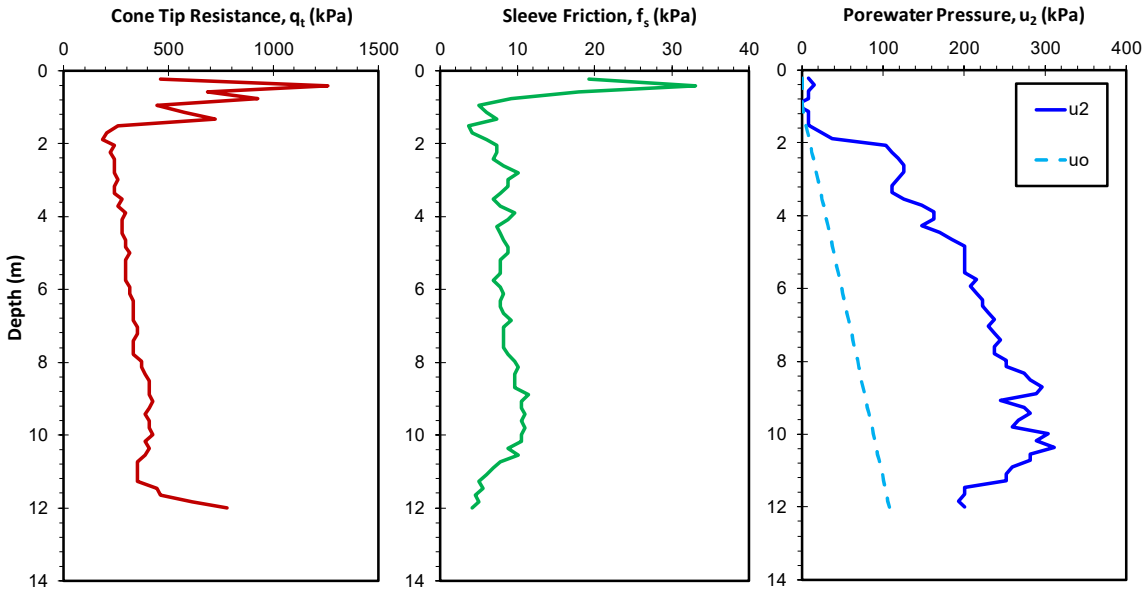


Figure 5.18. Piezocone sounding in Ballina, Australia: (a) cone tip resistance, $q_t$; (b) sleeve friction, $f_s$; (c) porewater pressure, $u_2$ (Pineda et al. 2014)

**Figure 5.19** shows the evaluation of the slope parameter used in the proposed $I_R$ solution where $(u_2-\sigma_{vo})$ is plotted versus net cone tip resistance ($q_{net}$), giving a slope value of $a_q$ = 0.5. This slope value is used with the effective friction angle to give an operational rigidity index value $I_R$ =168.

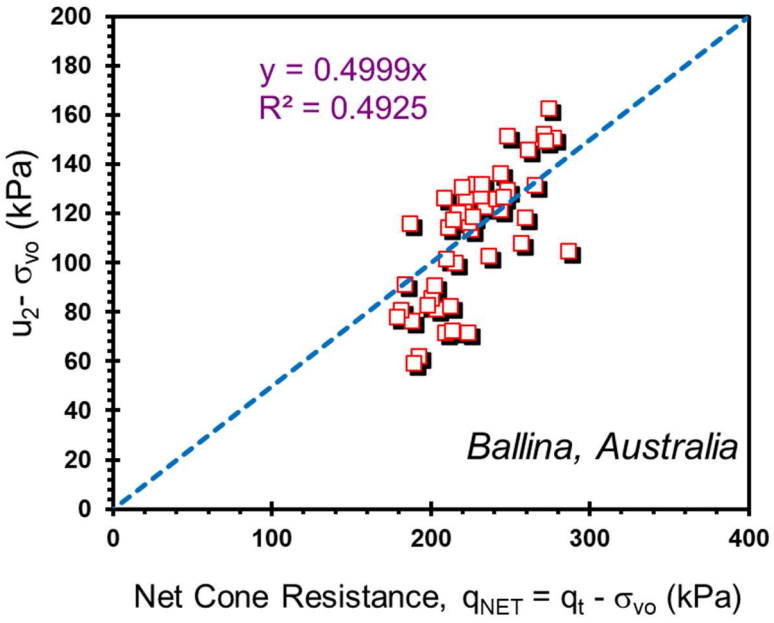


Figure 5.19. Evaluation of slope parameter $a_q$ for obtaining $I_R$ from CPTu data at soft clay site, Ballina, Australia

The obtained $I_R$ value is used to obtain cone bearing factor ($N_{kt}$) as per equation [5.19] for evaluating the undrained shear strength ($s_u$). Using an $I_R$ =168, the corresponding $N_{kt}$ = 10.74 that provides a nice agreement with the CAUC laboratory-measured $s_u$ reference values and field vane $s_u$ measurements, as evident in **Figure 5.20.**

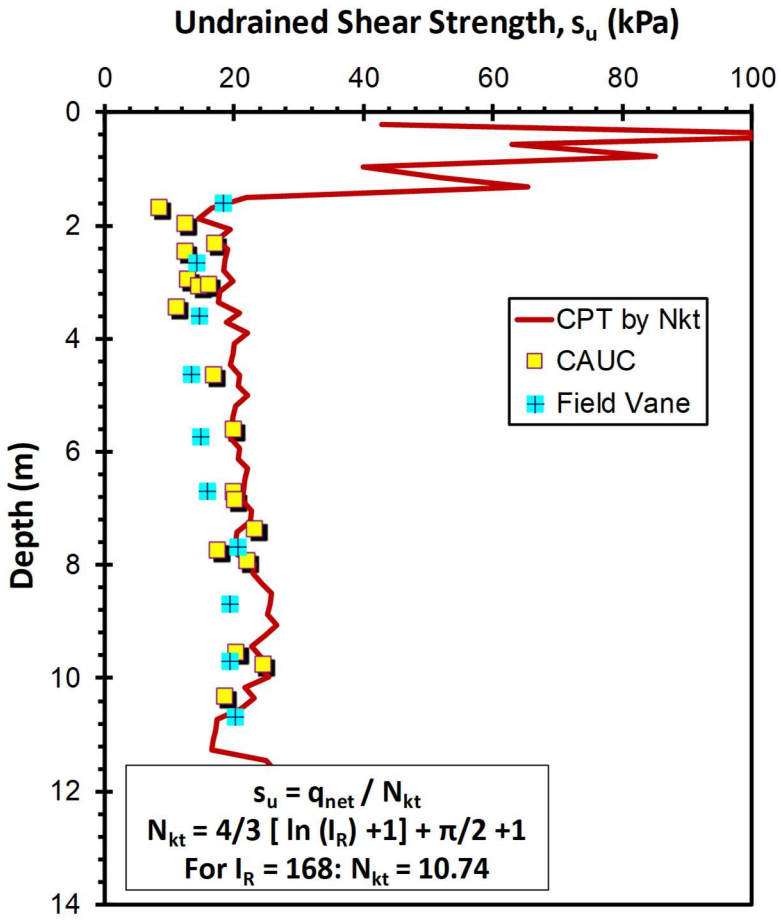


Figure 5.20. Undrained shear strength profile for Ballina, Australia using the proposed SCE-CSSM operational rigidity index value and cone bearing factor $N_{kt}$ (Note: triaxial data from Pineda et al. 2016)

By applying equations [5.10], [5.11], and [5.12] of the hybrid SCE-CSSM to the results of piezocone sounding from **Figure 5.18** with an operational rigidity index value of $I_R = 168$ and $\phi' = 33.7°$, the three expressions give stress history predictions which match well with each other, as presented in **Figure 5.21**. Overall, very good agreement is observed when compared with laboratory-measured $\sigma_p'$ and corresponding OCR profiles reported by Pineda et al. 2016.

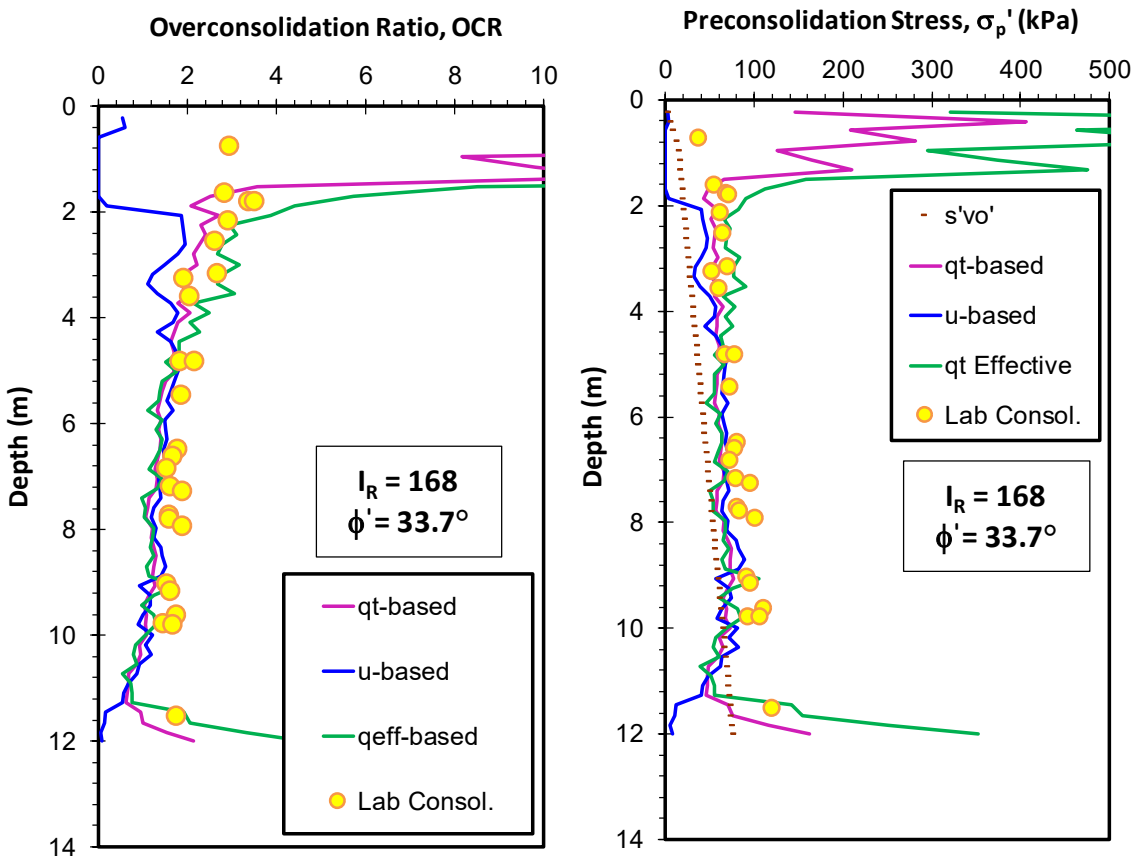


Figure 5.21. OCR and preconsolidation stress prediction using hybrid SCE-CSSM framework with new $I_R$ expression for Ballina soft clay, Australia (Note: consolidometer data from Pineda et al. 2016)

### 5.7.4 *Bothkennar, Scotland*

Bothkennar is a soft silty estuarine clay that is located on the south side of the River Forth, between Edinburgh and Glasgow in Scotland (Hight et al., 2003). The clay has the following average index parameters and soil properties: $e_0$ = 1.69, $w_n$ = 61%, LL = 72.63%, PI = 41.88%, clay fraction of 30%, $G_s$ = 2.65, and bulk density ($\rho_t$) = 1.607 Mg/m$^3$. The soil deposit consists of a thin overconsolidated clayey silt crust underlain by a thick layer of soft silty clay. The profile of preconsolidation stresses from one-dimensional consolidation tests gives an average OCR = 1.54 with depth. Laboratory $CK_0UC$ tests on

undisturbed samples using Laval and Sherbrooke samplers are reported by (Hight et al., 2003). **Figure 5.22** presents the piezocone reading for a sounding conducted at Bothkennar by Hight et al. (2003).

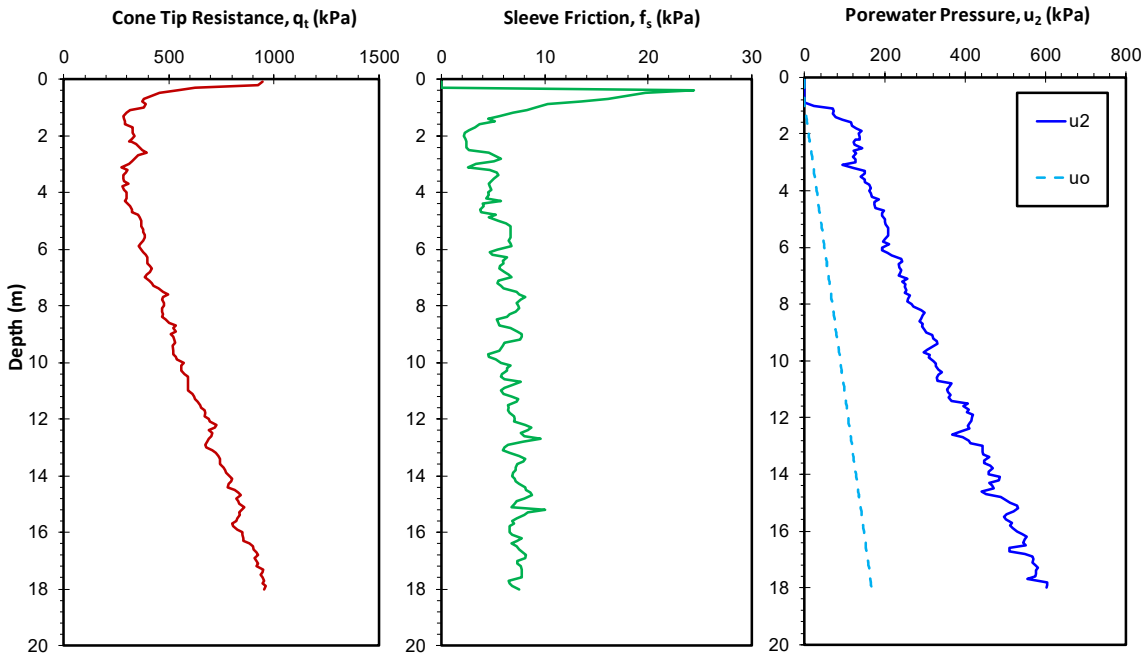


Figure 5.22. Piezocone sounding at Bothkennar, Scotland: (a) cone tip resistance, $q_t$; (b) sleeve friction, $f_s$; (c) porewater pressure, $u_2$ (Hight et al. 2003)

**Figure 5.23** shows the evaluation of the slope parameter $a_q$ used in the proposed $I_R$ solution, where ($u_2$-$\sigma_{vo}$) is plotted versus net cone tip resistance ($q_{net}$), giving a slope value of $a_q$ = 0.42. The slope value is used with the effective friction angle to give an operational rigidity index value $I_R$ = 55.

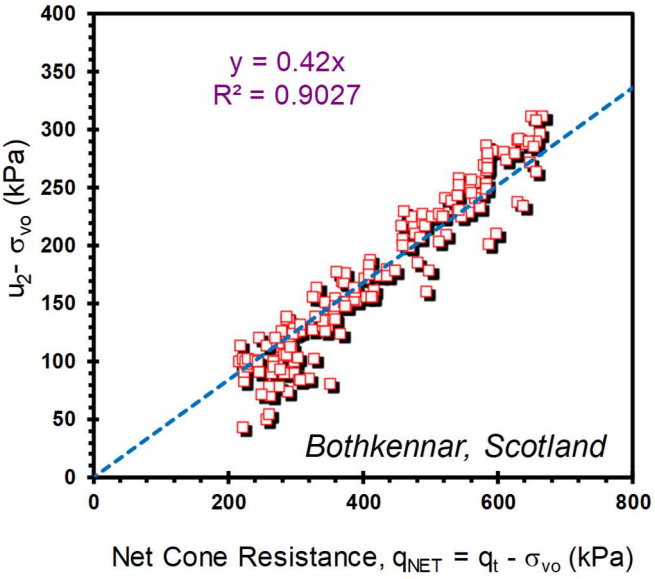


Figure 5.23. Evaluation of slope parameter for the $I_R$ determination using CPTu data from Bothkennar, Scotland (data from Hight et al. 2003)

A representative effective friction angle $\phi' = 34°$ is evaluated using the NTH method which agrees with laboratory measured values using triaxial compression tests reported by Hight et al. (2003).

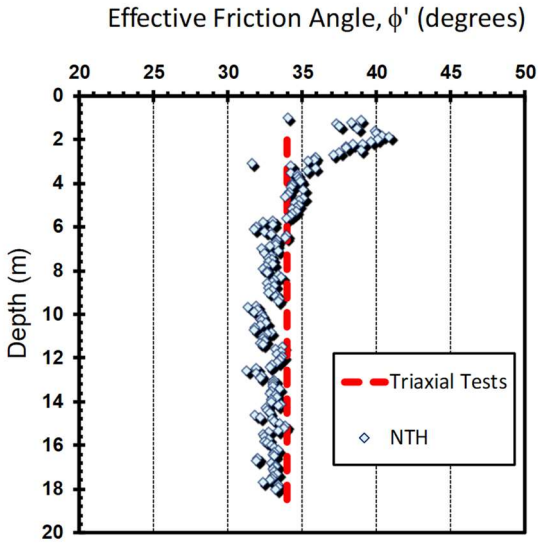


Figure 5.24. Profiles of laboratory measured effective friction angle ($\phi'$) after Hight et al. 2003 and CPTu-evaluated values using the NTH method for Bothkennar clay

The obtained $I_R$ value is used to obtain cone bearing factor ($N_{kt}$) as per equation [5.19] for evaluating the undrained shear strength ($s_u$). Using an $I_R = 55$, the corresponding $N_{kt}$ value is 9.24 that provides a good profile in comparison with field vane strengths and also a reasonable agreement with reference CAUC values, as seen in **Figure 5.25.**

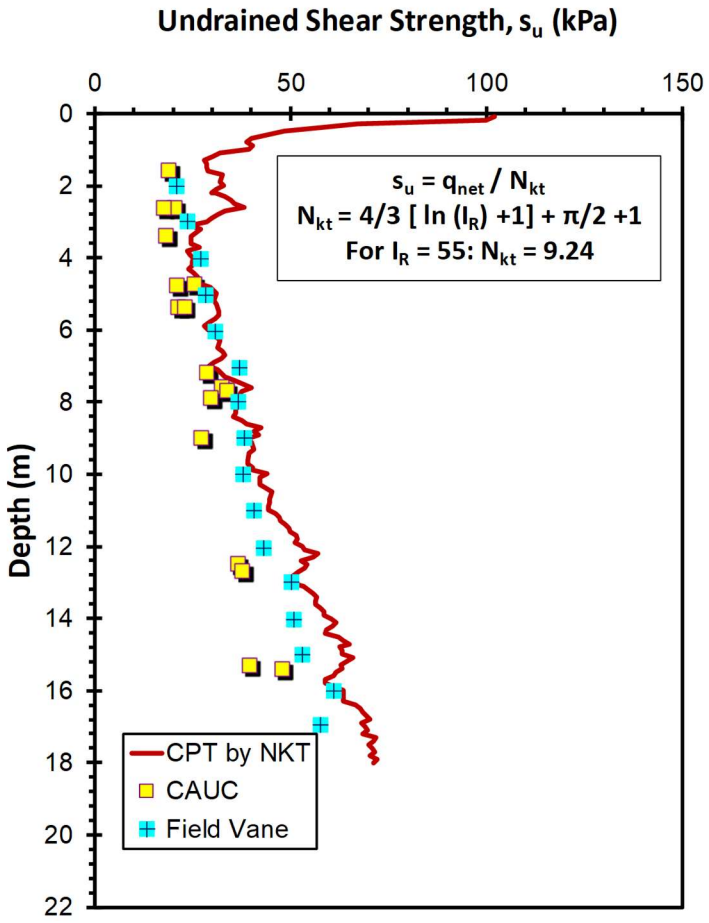


Figure 5.25. Undrained shear strength profiles for soft clay at Bothkennar, Scotland using the operational rigidity index value and cone bearing factor $N_{kt}$ (Note: CPTu and triaxial data from Hight et al. 2003)

By applying equations [5.10], [5.11], and [5.12] of the hybrid SCE-CSSM to the results of piezocone sounding from **Figure 5.22** with an operational rigidity index value of $I_R = 55$ from the derived expression and effective friction angle value ($\phi' = 34°$), the three CPTu

equations are consistent with each other, as evident in **Figure 5.26**. Excellent agreement is observed when compared with laboratory measured $\sigma_p'$ and OCR profiles reported by Hight et al. 2003.

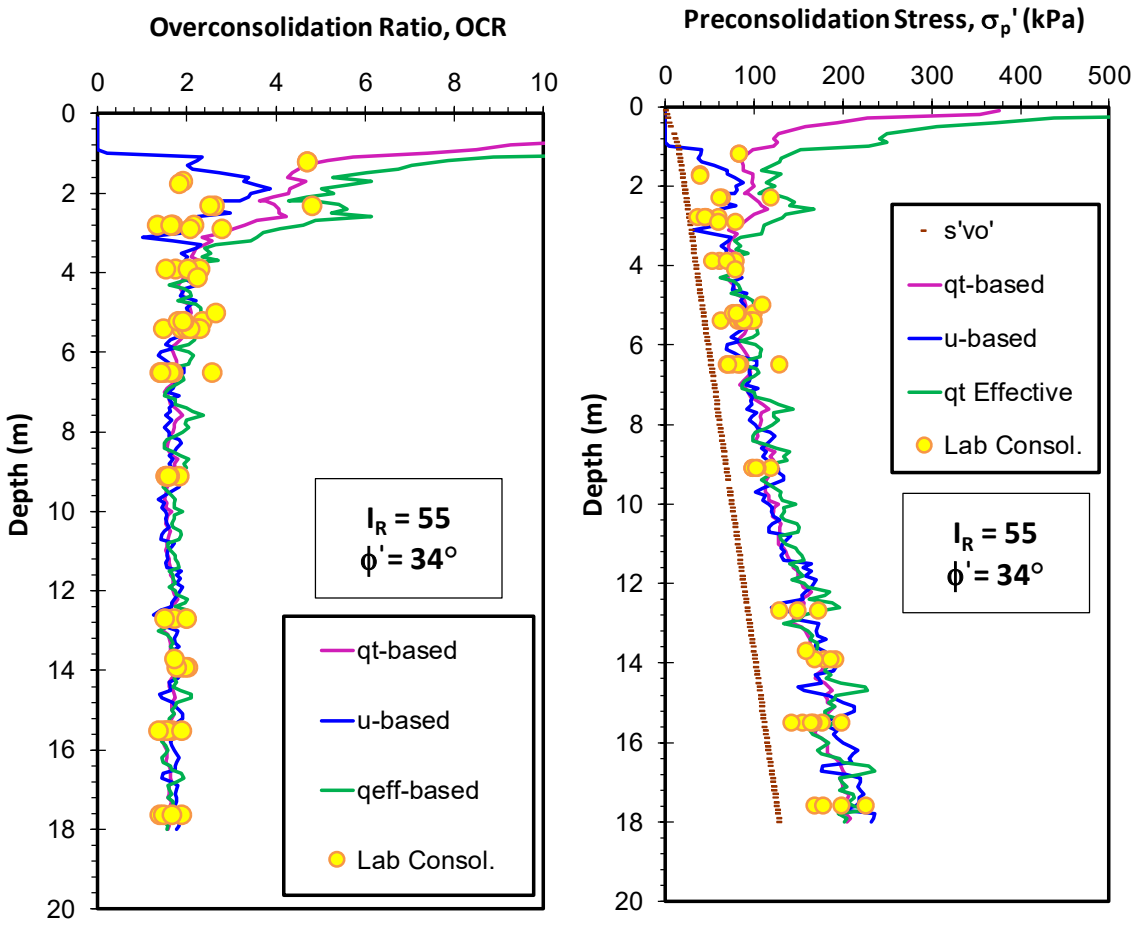


Figure 5.26. OCR and preconsolidation stress evaluations using hybrid SCE-CSSM framework with new $I_R$ expression at Bothkennar, UK (CPTu and consolidometer data from Hight et al. 2003)

By using the same evaluated rigidity index value of 55 along with an effective friction angle value (ϕ' = 34°), the original Burns & Mayne solution is applied to investigate flow properties from piezodissipation tests at Bothkennar. **Figure 5.26 b** presents the measured disputation tests conducted at depth: 12 m. Using the evaluated rigidity index value and friction angle, the predicted solution using SCE-CSSM is calculated and presented using

red line showing a good agreement with the in-situ measured porewater pressure. The corresponding coefficient of consolidation value is calculated: 0.14 $mm^2$/sec which is in an agreement with the laboratory reference values as reported by Nash et al. (1992) where $c_{vh}$ = 0.08 ~ 0.32 $mm^2$/sec.

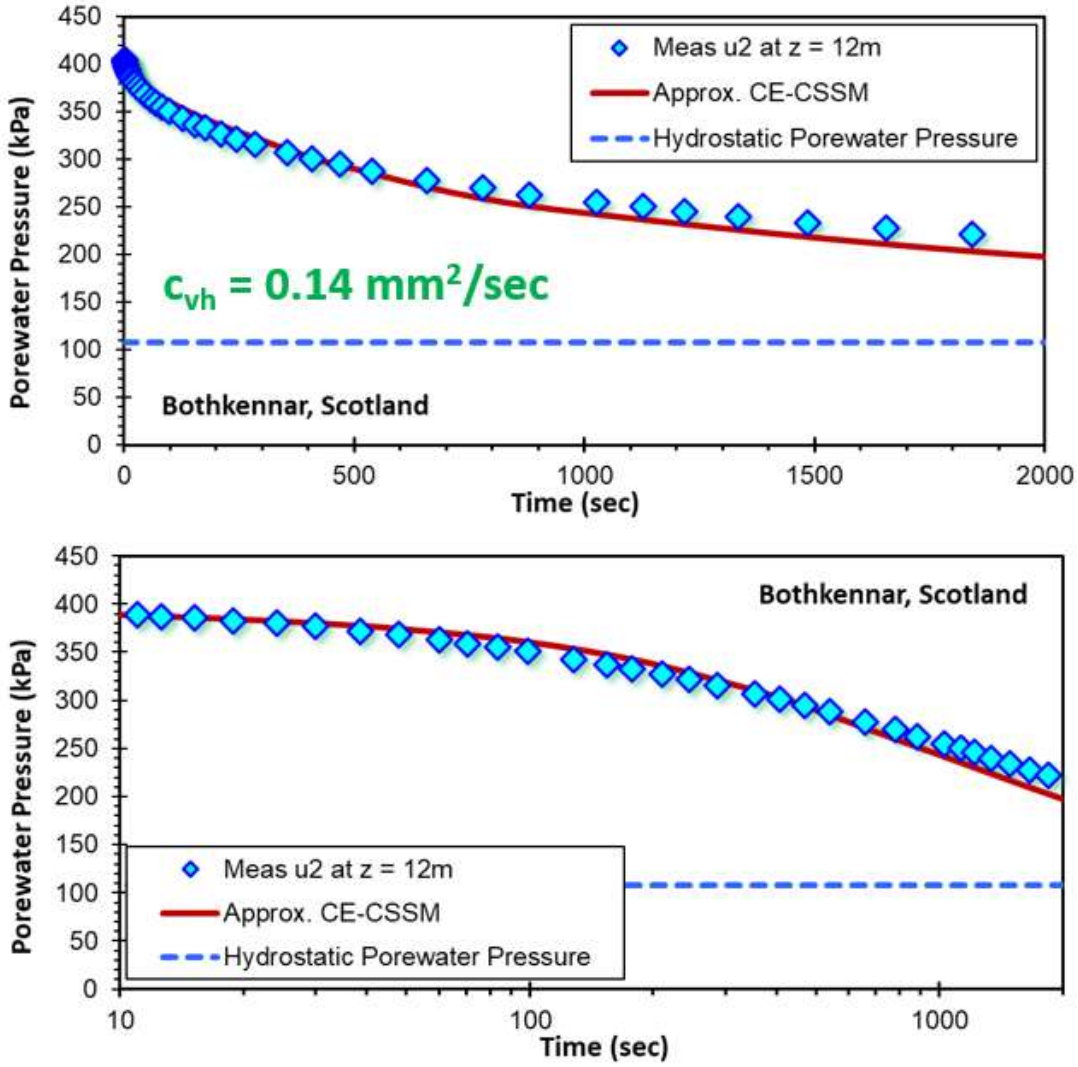


Figure 5.26b. Measured piezodissipation record for Bothkennar clay in Scotland at depth of 12 meters with prediction using hybrid SCE-CSSM framework

### 5.7.5 *Burswood, Australia*

Burswood is a soft estuarine clay deposit located in Perth, Australia. The site has high plasticity silt with the following index properties: liquid limit (LL) ranging from 71 to 99% and plasticity index (PI) ranging from 32 to 54%. The organic content ranges from 3.2 to 6%, the soil has low to high sensitivity value ranging from 3 to 14 (Lunne et al., 2006). The soil profile consists of a thin overconsolidated crust followed by a thick aged normally consolidated silty clay layer (Landon, 2007). A series of CAUC triaxial tests was conducted on high-quality Sherbrooke samples (Landon 2007; Low et al. 2001). The OCR profile in the thick soft clay at the site ranges from 1.2 to 1.9. **Figure 5.27** presents the main readings of piezocone sounding as reported by Low et al. (2011). An effective friction angle $\phi' = 28.4$ degrees is evaluated using the NTH method.

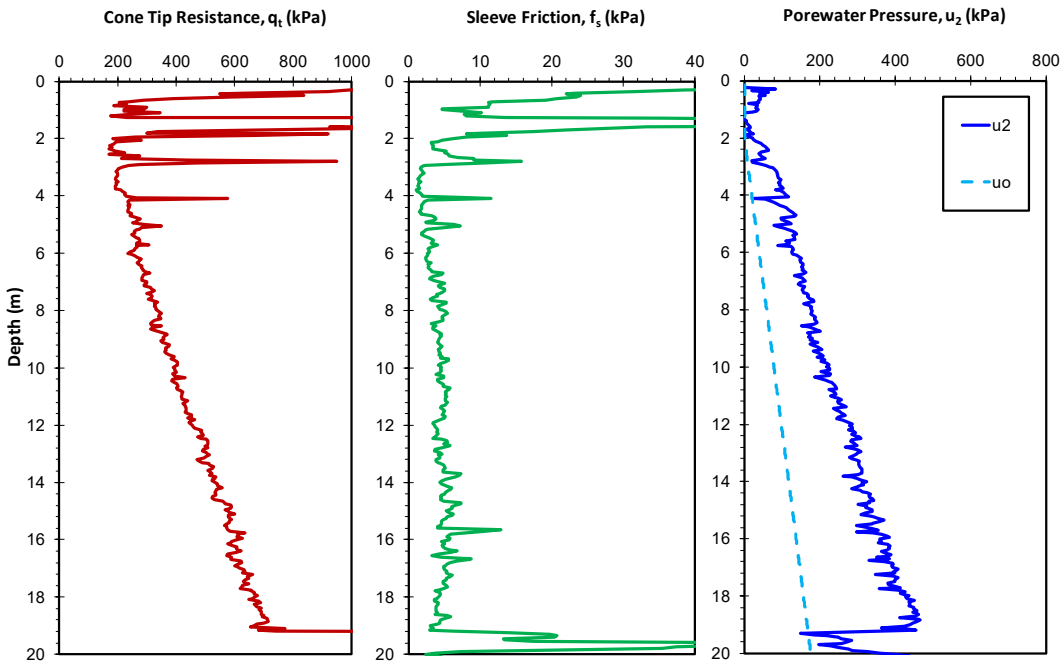


Figure 5.27. Piezocone sounding in Burswood, Australia: (a) cone tip resistance, $q_t$; (b) sleeve friction, $f_s$; (c) porewater pressure, $u_2$. (Low et al., 2011)

**Figure 5.28** shows the evaluation of the slope parameter used in the proposed $I_R$ solution where ($u_2$-$\sigma_{vo}$) is plotted versus net cone tip resistance ($q_{net}$), giving a slope value of $a_q$ = 0.3078. The slope value is used with the effective friction angle to give a rather low value of operational rigidity index ($I_R$) of 25.

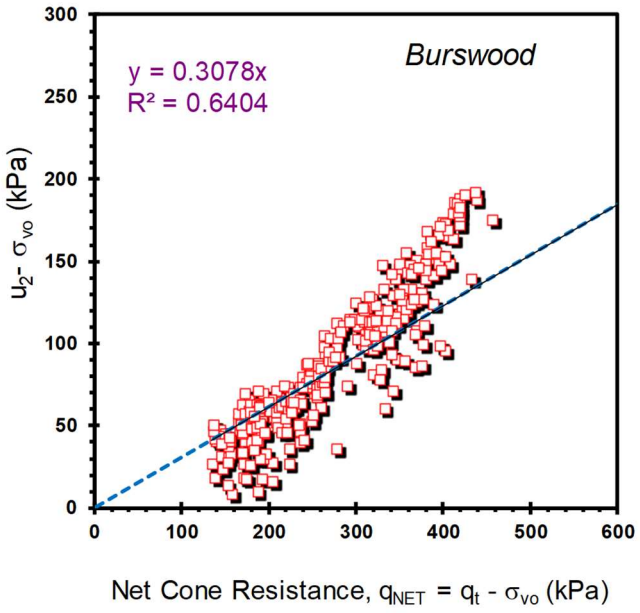


Figure 5.28. Evaluation of slope parameter for assessing $I_R$ using CPTu data in soft clay at Burswood, Australia

The obtained $I_R$ value is used to obtain the cone bearing factor ($N_{kt}$) as per equation [5.19] for evaluating the undrained shear strength ($s_u$). By using an $I_R$ value of 25, the corresponding $N_{kt}$ value is 8.2 which overestimates the strength in relation to the reference CAUC and DSS $s_u$ values at the site, as presented in **Figure 5.29.** From this particular case study, it seems that the classic Vesic cone bearing factor ($N_{kt}$) definition from spherical cavity expansion that solely depends on rigidity index is not sufficient. Other factors should

be taken into consideration such as the roughness of the interface between the cone and the soil in addition to the initial stress state condition which will be addressed subsequently in Chapter 9.

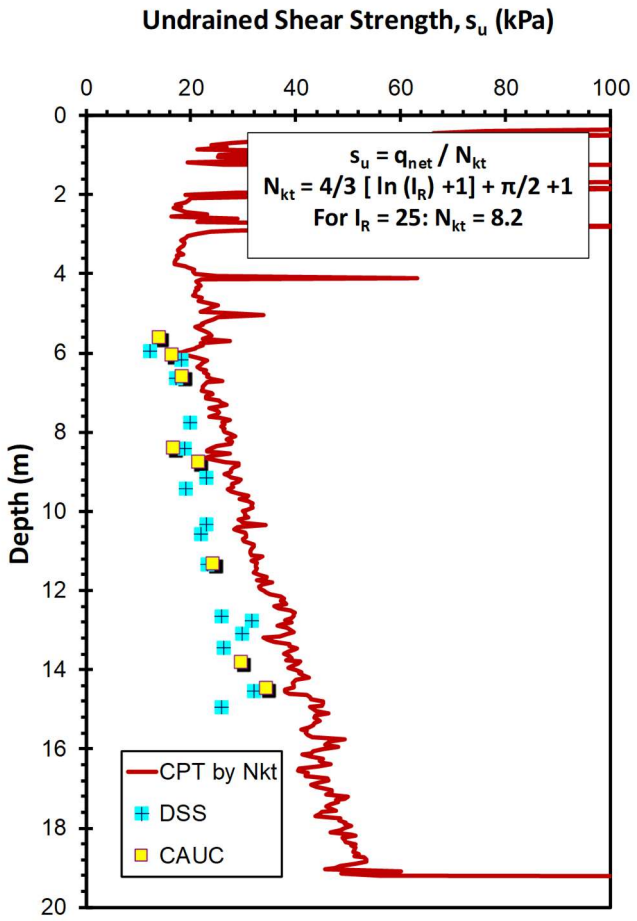


Figure 5.29. Undrained shear strength profile for Burswood, Australia using the proposed SCE-CSSM operational rigidity index value and cone bearing factor $N_{kt}$ (Note: triaxial data from Landon 2007; Low et al., 2011)

Applying equations [5.10], [5.11], and [5.12] of the hybrid SCE-CSSM to the results of piezocone sounding from **Figure 5.27** with $I_R = 25$ and $\phi' = 28.4°$, the three expressions given good and consistent evaluations of stress history, as seen in **Figure 5.30**. Overall,

good agreement is observed in comparison with laboratory measured $\sigma_p'$ and OCR profiles reported by Low et al. (2011).

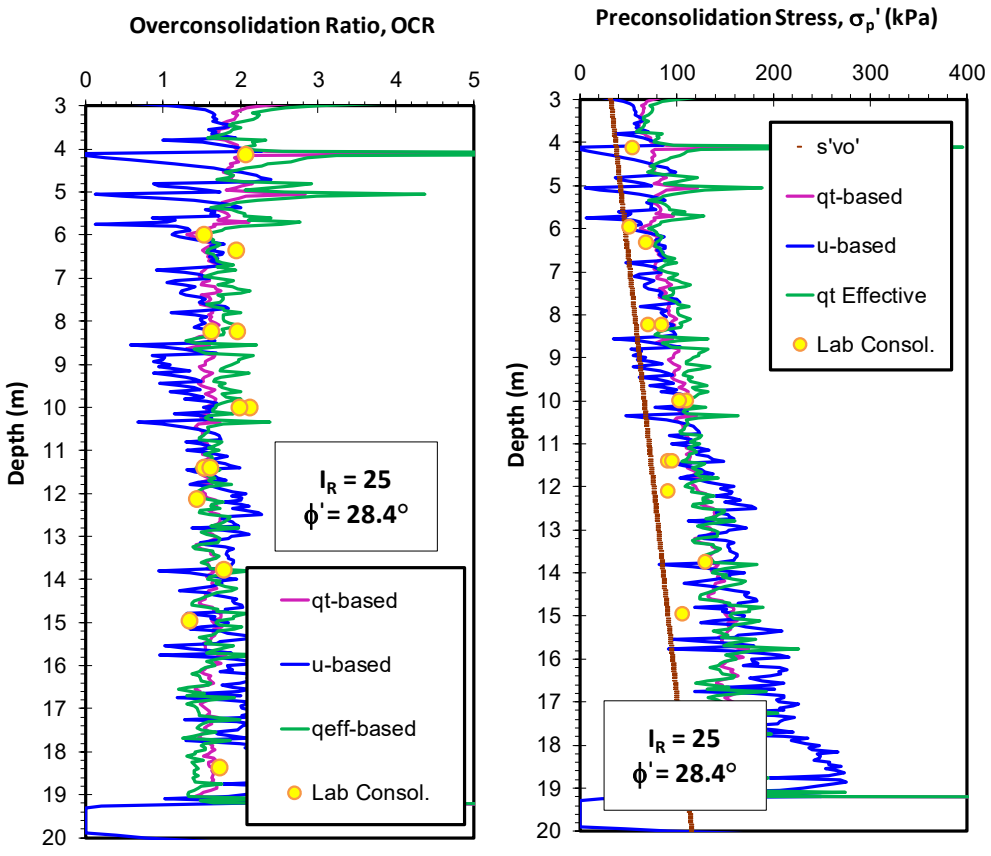


Figure 5.30. OCR and preconsolidation stress evaluations at Burswood soft clay, Australia using hybrid SCE-CSSM solutions with new $I_R$ expression (Note: consolidometer data from Low et al., 2011)

### 5.7.6 *Busan, South Korea*

Busan is a soft clay that covers the Nakdong River delta in South Korea (Hong et al. 2010). The clay has the following average index parameters and soil properties: $e_0$ = 1.59, $w_n$ = 58.4%, LL = 61.5 %, PI = 27.2%, clay fraction of 27%, $G_s$ = 2.71, and bulk density ($\rho_t$) = 1.60 Mg/m$^3$ (Chung et al., 2011). The profile of preconsolidation stresses from one-dimensional consolidation tests gives an average OCR = 1.26. **Figure 5.31** presents the

readings of piezocone sounding reported by Chung et al. (2012). A value of effective friction angle ($\phi'$) of 30.2 degrees is evaluated using the NTH method using the presented piezocone data.

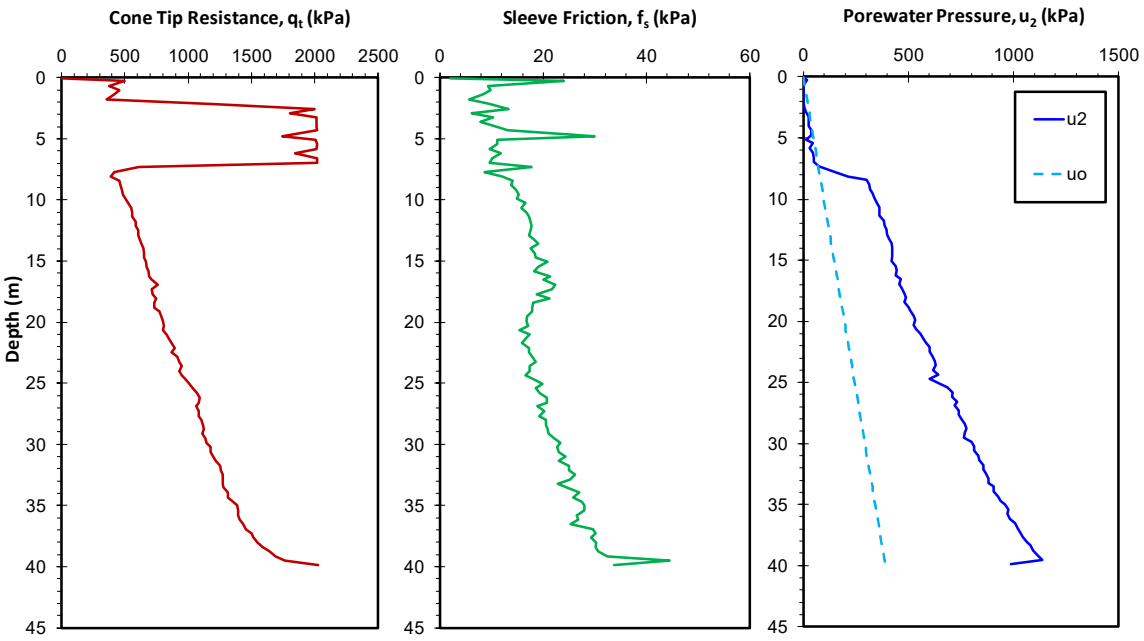


Figure 5.31. Piezocone sounding in Busan clay in South Korea: (a) cone tip resistance, $q_t$; (b) sleeve friction, $f_s$; (c) porewater pressure, $u_2$. (Chung et al., 2012)

**Figure 5.32** shows the evaluation of the slope parameter used in the proposed $I_R$ solution where ($u_2$-$\sigma_{vo}$) is plotted versus net cone tip resistance ($q_{net}$), giving a slope value of 0.4673. The slope value is used with the effective friction angle to give an operational rigidity index value ($I_R$) of 134.

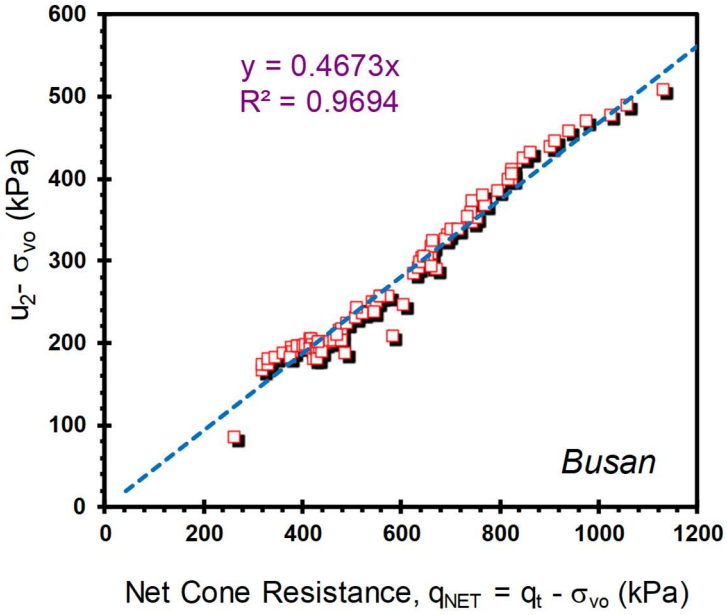


Figure 5.32. Evaluation of slope parameter for proposed $I_R$ solution f [ $(u_2-\sigma_{vo}) / q_{net}$] using CPTu data from Busan, South Korea

The obtained $I_R$ value is used to obtain cone bearing factor ($N_{kt}$) as per equation [5.19] for evaluating the undrained shear strength ($s_u$). An $I_R$ = 134 is obtained and the corresponding $N_{kt}$ = 10.43. This gives a good agreement with the reference CAUC triaxial data reported by Chung et al. 2011 as presented in **Figure 5.33.**

Applying equations [5.10], [5.11], and [5.12] of the hybrid SCE-CSSM to the results of piezocone sounding from **Figure 5.31** with $I_R$ = 134 and $\phi'$ = 30.2°, the three CPTu formulations are used to profile OCR and yield stress history in this soft clay deposit, as presented in **Figure 5.34**. When compared with reference values from laboratory-measured $\sigma_p'$ and OCR values reported by Chung et al. 2012, the CPTu soundings give reasonable evaluations with depth.

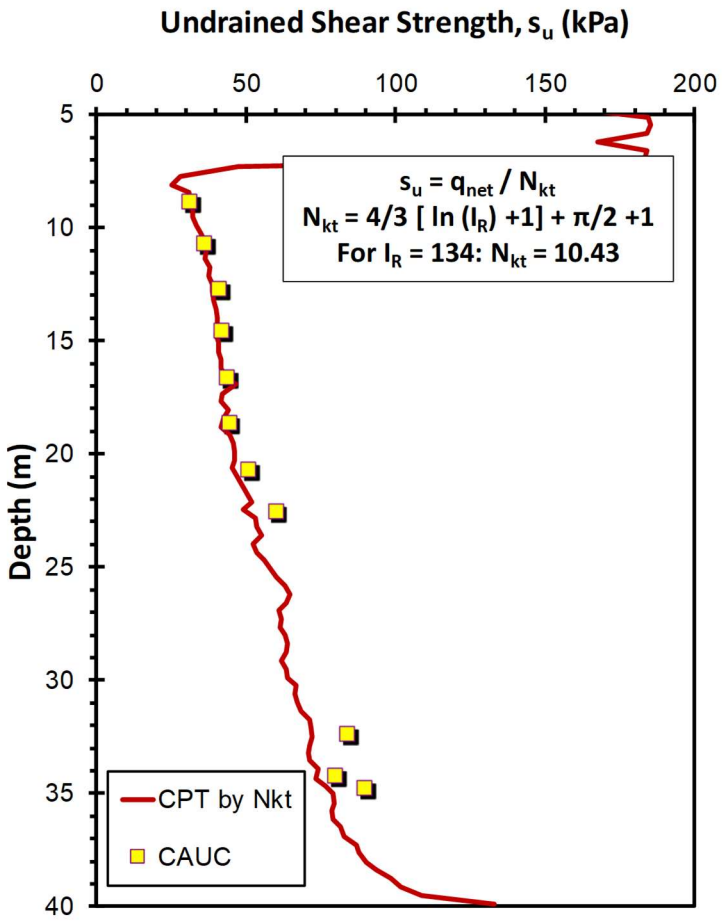


Figure 5.33. Undrained shear strength profile for Busan, South Korea using the proposed SCE-CSSM operational rigidity index value and cone bearing factor $N_{kt}$ (Note: CPTu and CAUC data from Chung et al., 2011)

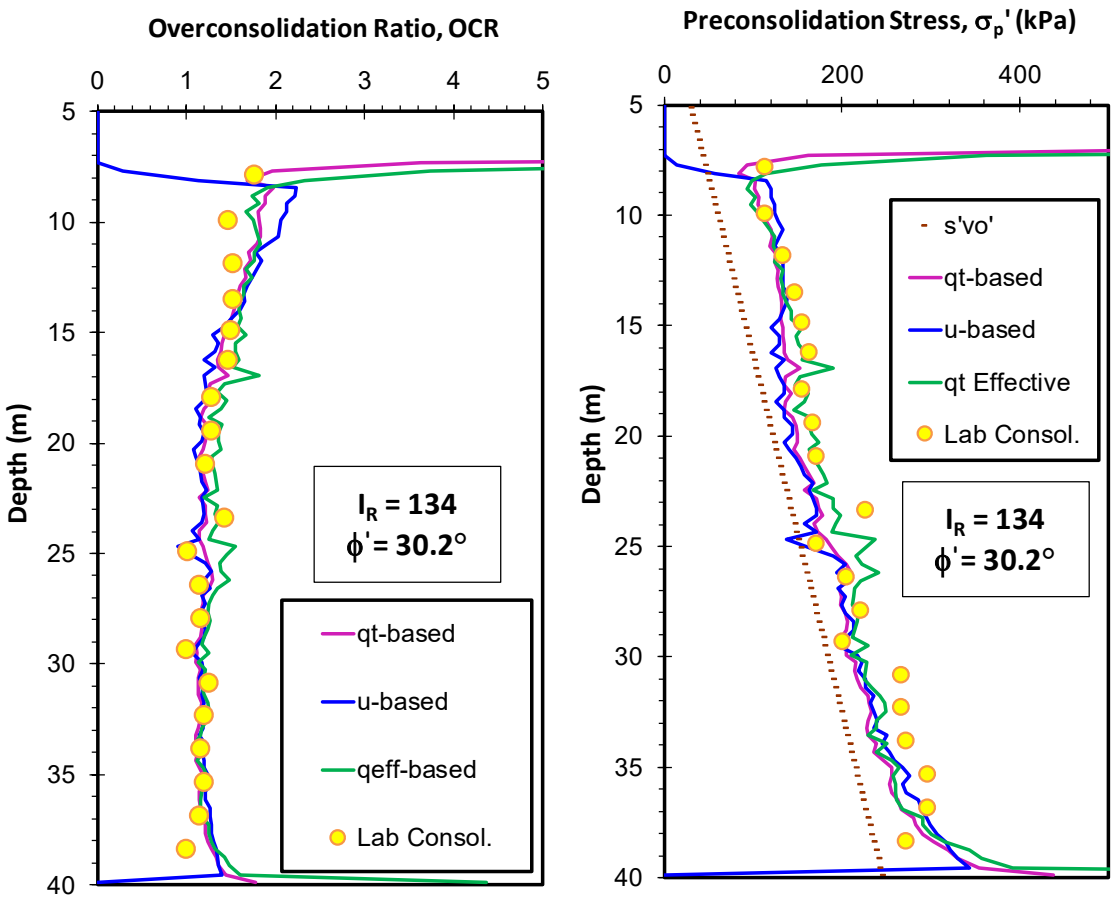


Figure 5.34. OCR and preconsolidation stress evaluations using hybrid SCE-CSSM framework with new $I_R$ expression at Busan, South Korea (consolidometer data from Chung et al., 2012)

### 5.7.7 Newbury, MA

Newbury is glacial marine deposit consisting mainly of soft silty Boston Blue Clay, the soil profile can be divided into an overconsolidated clay crust followed by a thicker layer of lightly overconsolidated clay layer (Landon, 2007). The clay at Newbury has the following index values: plasticity index (PI) ranging from 19 to 21 %, liquid limit (LL) ranging from 45 to 49% and natural water content ranging from 40 to 54%, plastic limit (PL) ranging from 24 to 30%. The clay can be classified as inorganic with low sensitivity value from 2 to 4 for the shallow layers. **Figure 5.35** presents the readings of a

representative piezocone sounding reported by Landon (2007). CAUC triaxial tests were conducted at the test site giving an effective friction angle of about 36 degrees which agrees with the average value obtained using the NTH method.

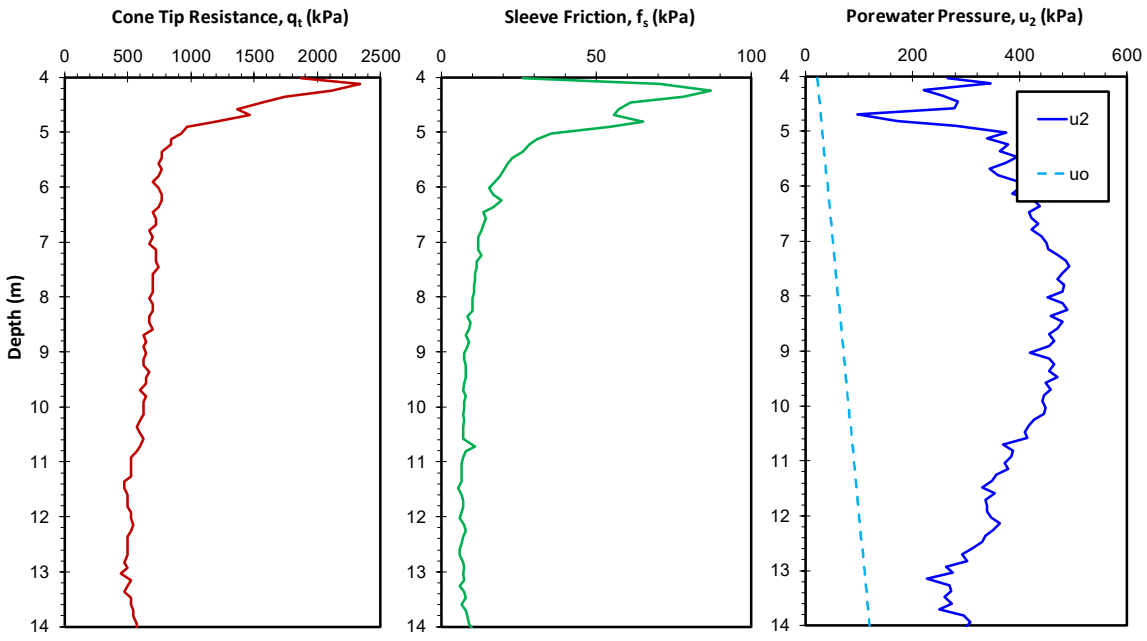


Figure 5.35. Piezocone sounding at Newbury, MA: (a) cone tip resistance, $q_t$; (b) sleeve friction, $f_s$; (c) porewater pressure, $u_2$. (Landon 2007)

**Figure 5.36** shows the evaluation of the slope parameter used in the proposed alternative $I_R$ solution where modified porewater parameter (U*-1) is plotted versus normalized cone tip resistance (Q), giving a slope value of $a_q$ = 0.5509. The slope value is used with the effective friction angle to give an operational rigidity index value ($I_R$) of 343.

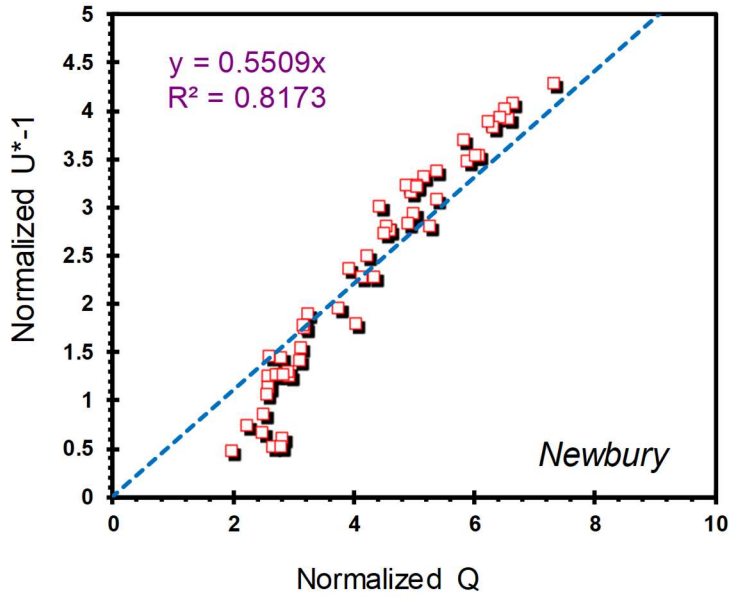


Figure 5.36. Evaluation of slope parameter for alternative $I_R$ solution f [ (U*-1) / Q] using CPTu data from Newbury, MA

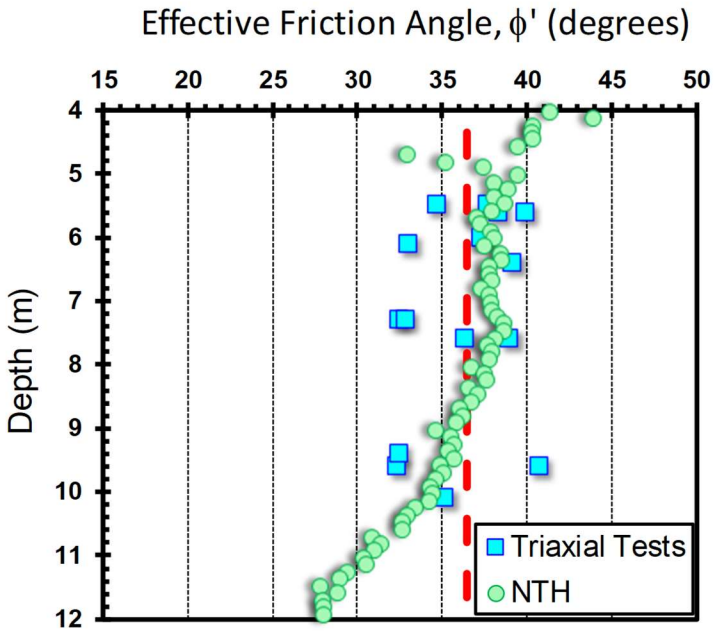


Figure 5.37. Profile of laboratory measured effective friction angle (ϕ') from Landon 2007 and evaluated values using the NTH method for Newbury, MA

The obtained $I_R$ value is used to obtain cone bearing factor ($N_{kt}$) as per equation [5.19] for evaluating the undrained shear strength ($s_u$). By using an $I_R$ value of 343 the corresponding $N_{kt}$ = 11.7. This provides a good agreement with the reference CAUC triaxial data, as presented in **Figure 5.38.**

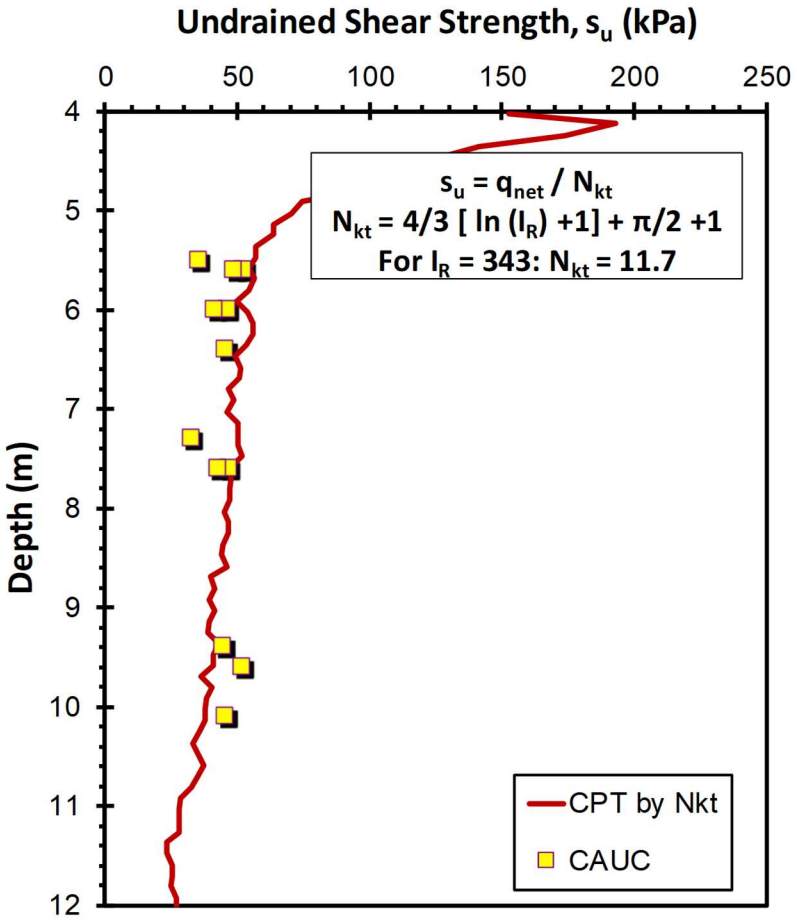


Figure 5.38. Undrained shear strength profile for Newbury, MA using the SCE-CSSM operational rigidity index value and cone bearing factor $N_{kt}$ (Note: CPTu and CAUC data from Landon 2007)

By applying equations [5.10], [5.11], and [5.12] of the hybrid SCE-CSSM to the results of piezocone sounding from **Figure 5.35** with an operational rigidity index value of $I_R$ = 343

from the new expression and effective friction angle value ($\phi'$ = 36.5°), the three stress history predictions from the CPTu are seen to match well with each other, as seen in **Figure 5.39**. Overall, a good agreement is observed when compared with laboratory measured $\sigma_p'$ and OCR profiles reported by Landon (2007).

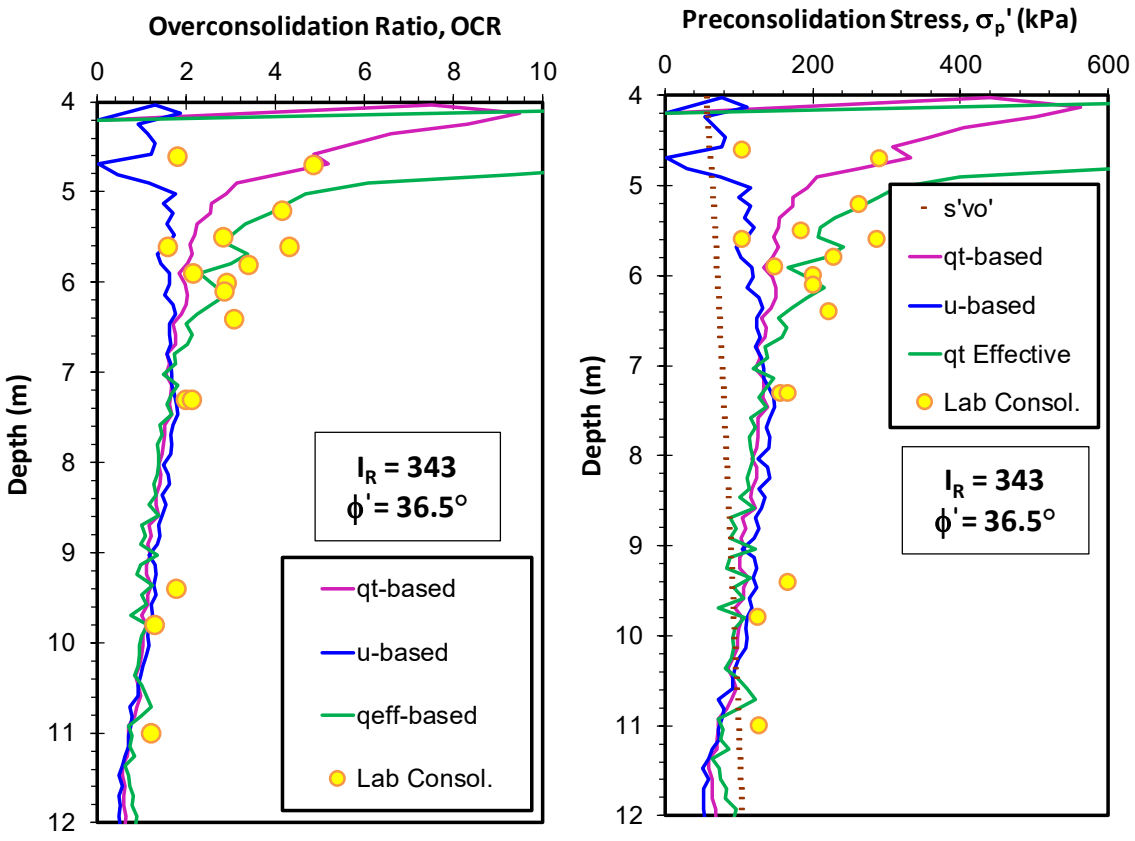


Figure 5.39. OCR and preconsolidation stress prediction using original hybrid SCE-CSSM framework with new $I_R$ expression for Newbury, MA (data from Landon 2007)

### 5.7.8 NGES at Northwestern University, Evanston, Illinois

The national geotechnical experimentation site (NGES) at Northwestern University is in Evanston, Illinois on the northeast corner of the university campus and adjacent to Lake

Michigan. The subsurface stratigraphy consists of 9-m clean sand over soft lacustrine clays extending to 22 m (Finno, 2000).

**Figure 5.40** shows the results of the piezocone sounding conducted by McGillivray (2007) using the GT cone penetrometer system. The piezocone readings were used to evaluate effective friction angle using NTH method giving a value of 28.3 degrees that agrees with the friction angle from $CK_0UC$ triaxial tests conducted by Chung and Finno (1992).

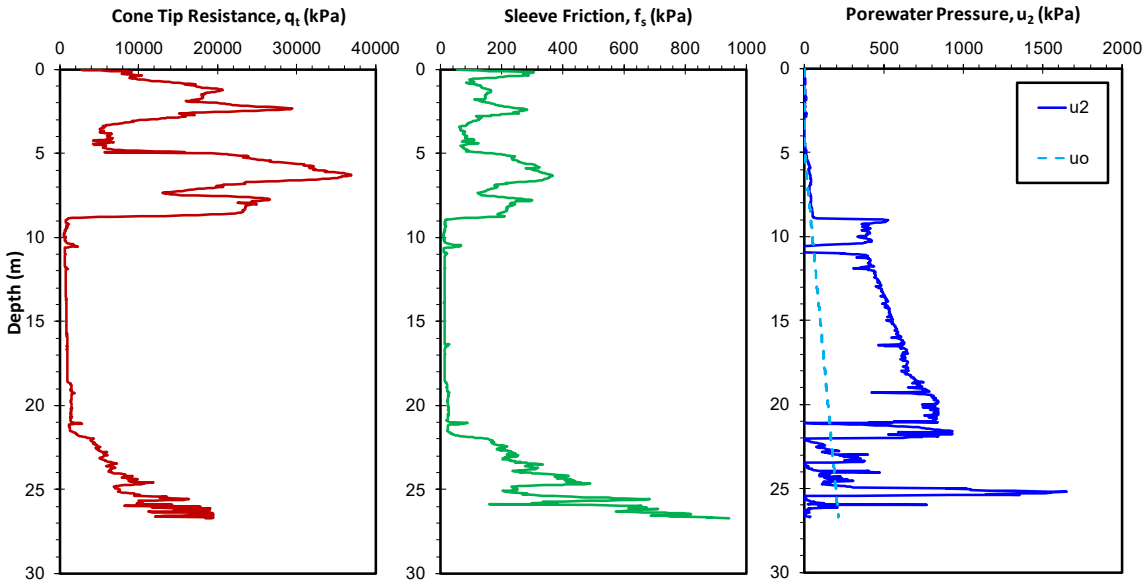


Figure 5.40. Piezocone sounding at NGES in Northwestern University, USA: (a) cone tip resistance, $q_t$; (b) sleeve friction, $f_s$; (c) porewater pressure, $u_2$. (McGillivray, 2007)

**Figure 5.41** shows the evaluation of the slope parameter used in the proposed $I_R$ solution where ($u_2$-$\sigma_{vo}$) is plotted versus net cone tip resistance ($q_{net}$), giving a slope value of $a_q$ = 0.467. The slope value is used with the effective friction angle to give an operational rigidity index $I_R$ = 143.

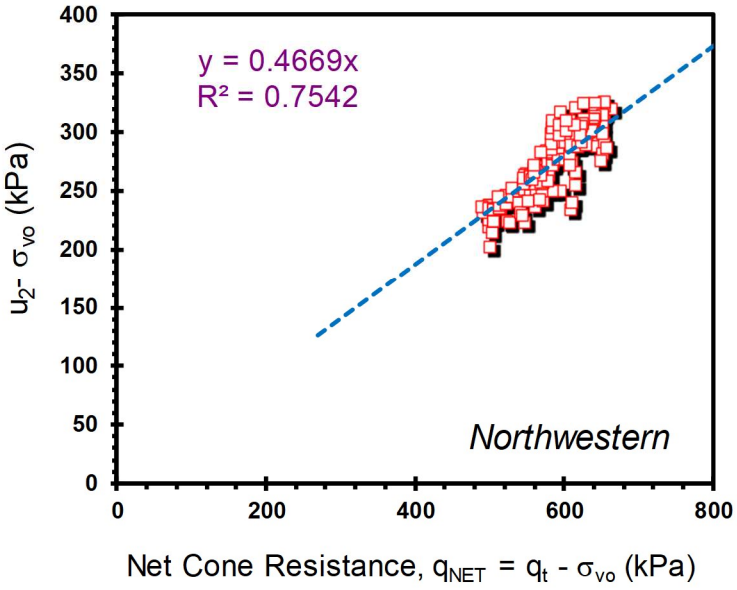


Figure 5.41. Evaluation of slope parameter for proposed $I_R$ solution f [ $(u_2-\sigma_{vo}) / q_{net}$] using CPTu data from NGES at Northwestern, IL

The obtained $I_R$ value is used to obtain cone bearing factor ($N_{kt}$) as per equation [5.19] for evaluating the undrained shear strength ($s_u$). Using $I_R$ = 143 the corresponding $N_{kt}$ = 10.52 which provides very good agreement with reference CAUC triaxial data for this site, reported by Finno and Chung (1992), as evident by **Figure 5.42.**

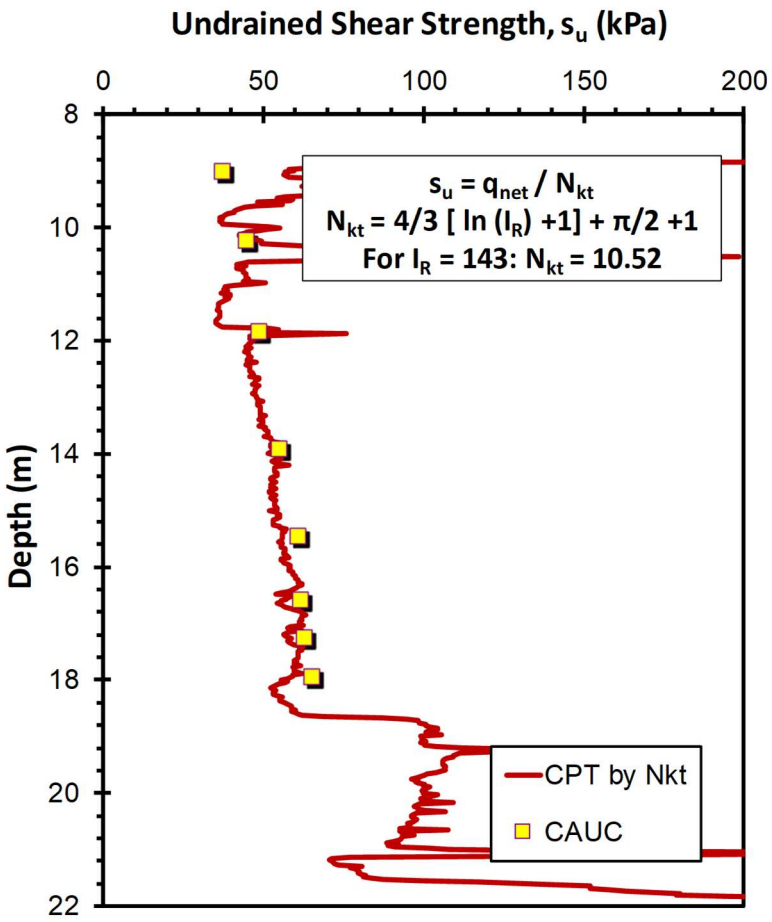


Figure 5.42. Undrained shear strength profile for soft clay at NGES - Northwestern University using the SCE-CSSM operational $I_R$ and cone bearing factor $N_{kt}$ (Note: triaxial data from Finno and Chung, 1992)

Applying the three OCR equations from the hybrid SCE-CSSM solution to the results of piezocone sounding from **Figure 5.40** with $I_R$ = 143 and $\phi'$ = 28.3° within the Deerfield soft clay layer, the separate profiles are seen to be consistent, as shown by **Figure 5.43**. When compared with laboratory- measured $\sigma_p'$ and OCR profiles reported by Chung and Finno 1992, the CPTu soundings give a good match.

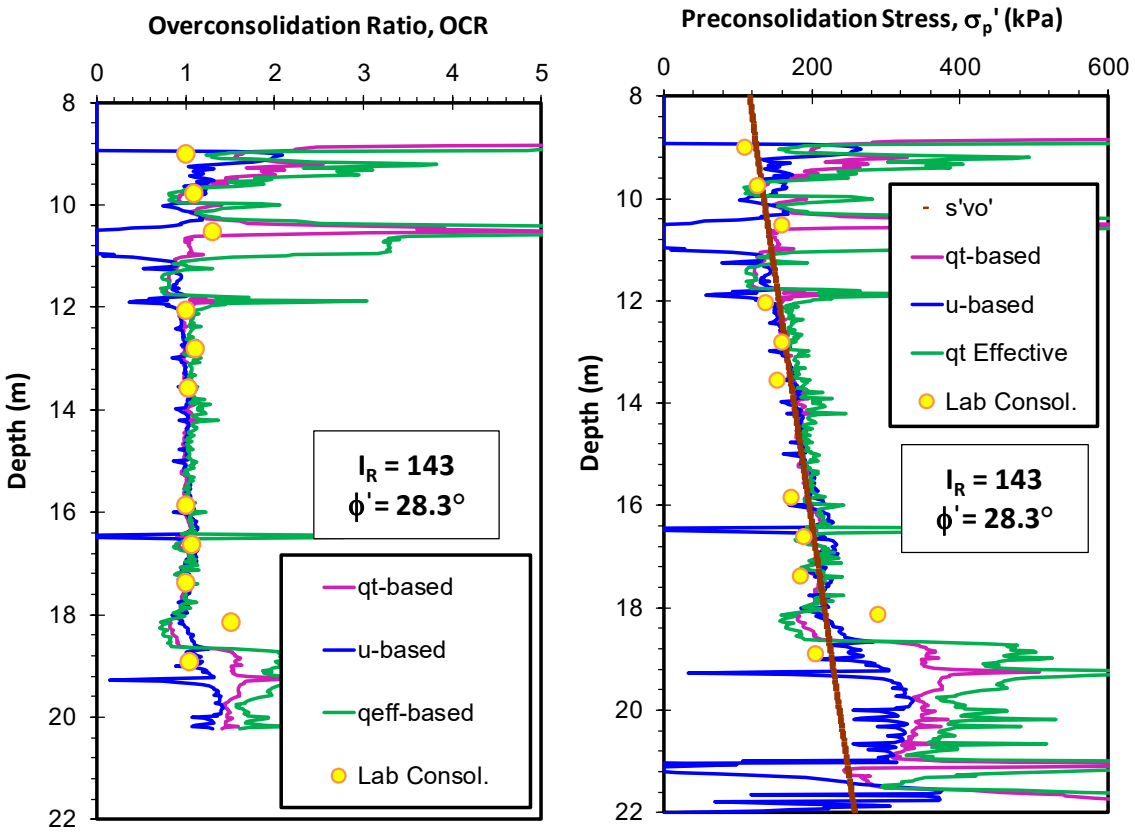


Figure 5.43. OCR and preconsolidation stress prediction using original hybrid SCE-CSSM framework with new $I_R$ expression for NGES at Northwestern (consolidometer data from Chung and Finno, 1992)

### 5.7.9 Onsøy, Norway

Onsøy consists of a soft marine clay that is located in Norway, southeast of Oslo (Lunne et al. 2003). The soil profile at Onsøy is comprised of a one-meter thick weathered crust followed by an 8-m thick soft clay layer underlain by a soft medium plastic clay layer over the remaining thickness of 36 m over bedrock (Lunne et al., 2003). The clay has the following average index parameters and soil properties: clay fraction of 53 %, $e_0$ = 1.75, $w_n$= 64%, LL= 68%, PI= 35%, $G_s$= 2.71, and bulk density ($\rho_t$) = 1.587 Mg/m$^3$. The profile of preconsolidation stresses from one-dimensional consolidation tests gives an average

OCR = 1.69. The profiles of the cone tip resistance, sleeve friction and porewater pressure are presented in **Figure 5.44**. These data are used to provide an estimate for the effective friction angle using the NTH method, where an average effective friction angle ($\phi'$) of 32.2 degrees is evaluated. Laboratory $s_u$ from $CK_0UC$ tests have been obtained and reported by Lunne et al. (2003).

**Figure 5.45** shows the evaluation of the slope parameter used in the proposed $I_R$ solution where ($u_2$-$\sigma_{vo}$) is plotted versus net cone tip resistance ($q_{net}$), giving a slope value of 0.516. The slope value is used with the effective friction angle to give an operational rigidity index value ($I_R$) of 251.

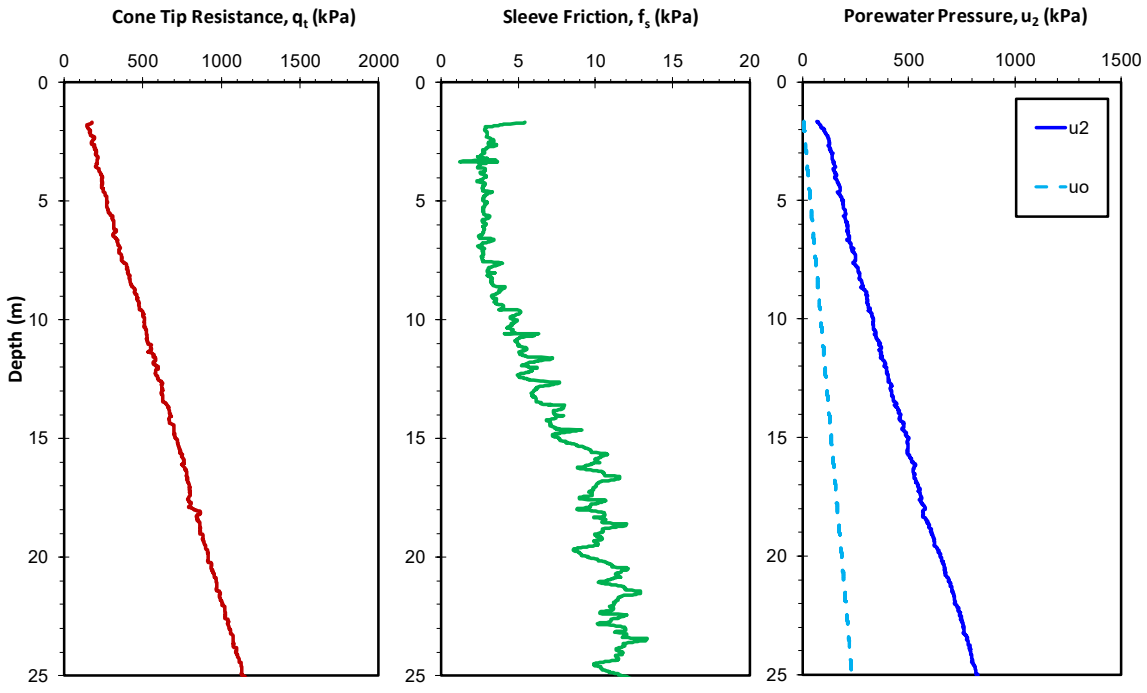


Figure 5.44. Piezocone sounding at Onsøy site in Norway: (a) cone tip resistance, $q_t$; (b) sleeve friction, $f_s$; (c) porewater pressure, $u_2$. (Lunne et al., 2003)

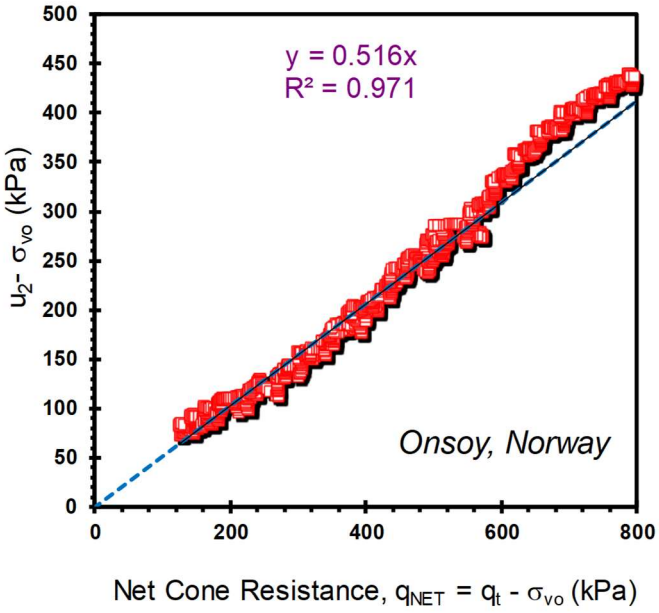


Figure 5.45. Evaluation of slope parameter for assessing $I_R$ from CPTu data in soft clay at Onsøy, Norway

The obtained $I_R$ value is used to obtain cone bearing factor ($N_{kt}$) as per equation [5.19] for evaluating the undrained shear strength ($s_u$). With $I_R = 251$, the corresponding $N_{kt}$ value is 11.27. This provides a good match with the reference triaxial data as presented in **Figure 5.46.**

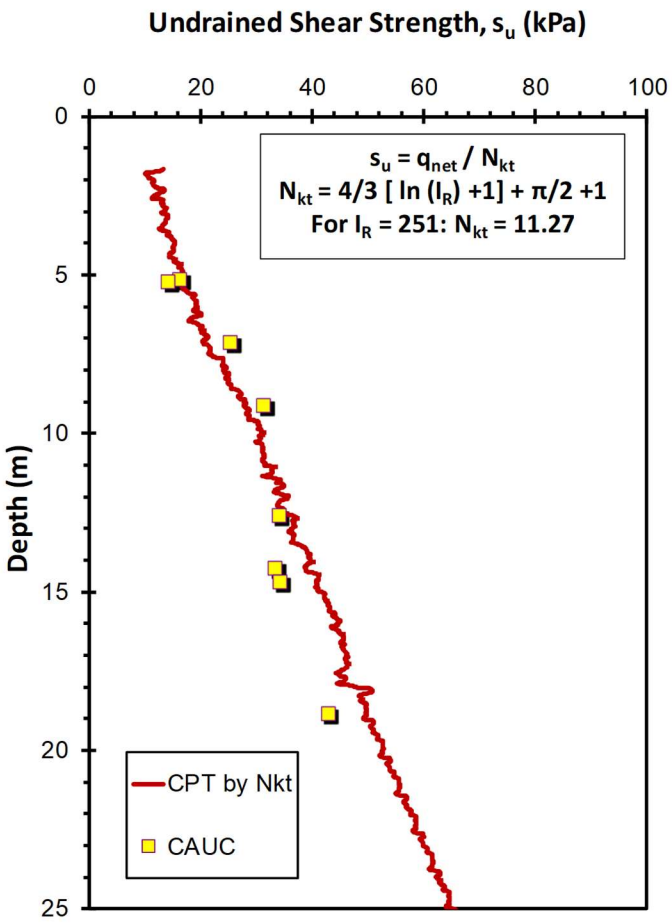


Figure 5.46. Undrained shear strength profile for Onsøy, Norway using the proposed SCE-CSSM operational rigidity index value and cone bearing factor $N_{kt}$ (Note: triaxial data from Lunne et al., 2003)

The hybrid SCE-CSSM is applied to the results of the piezocone sounding from **Figure 5.44** with $I_R = 251$ and $\phi' = 32.2°$. The three separate estimates of stress history predictions agree with each other, as presented in **Figure 5.47**. Very good agreement is observed when compared with laboratory measured $\sigma_p'$ and OCR profiles reported by Lunne et al., 2003.

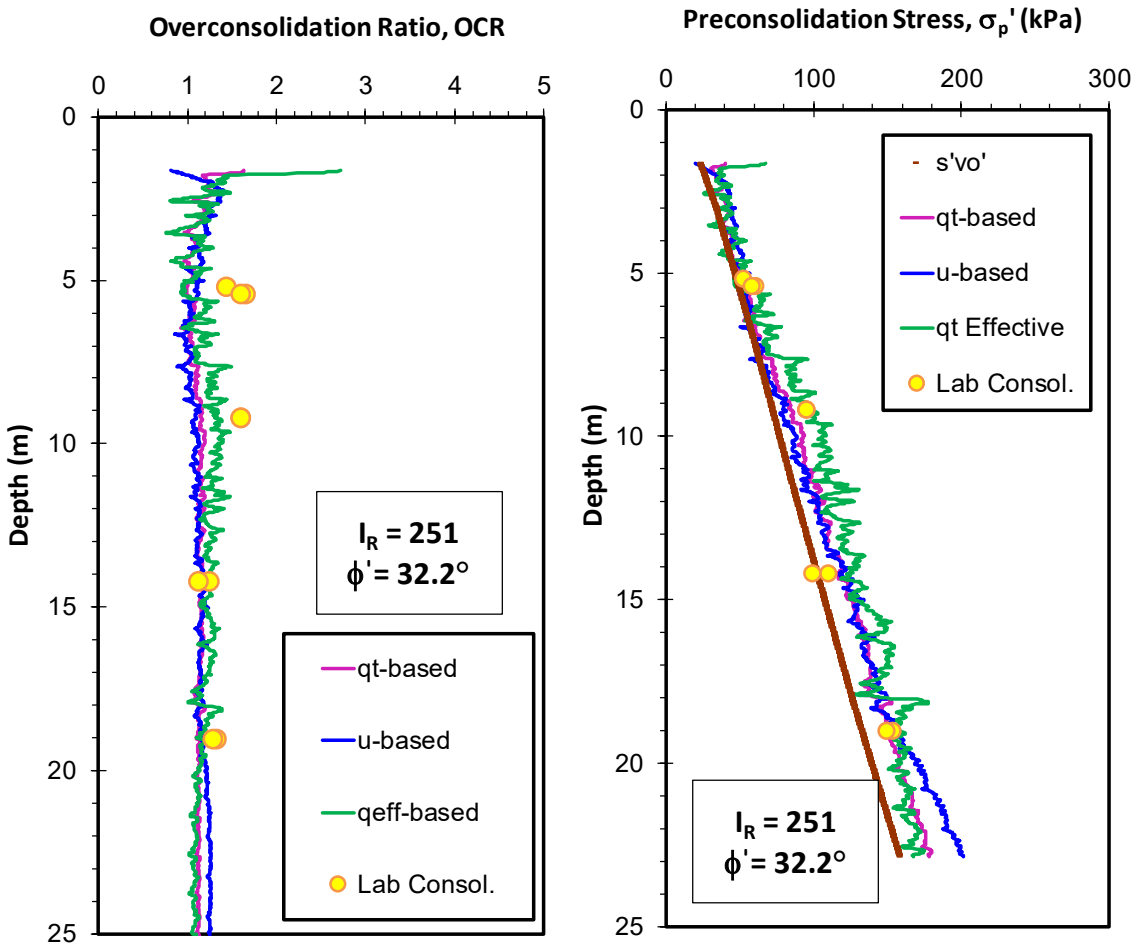


Figure 5.47. OCR and preconsolidation stress prediction using original hybrid SCE-CSSM framework with new $I_R$ expression for Onsøy, Norway (consolidometer data from Lunne et al., 2003)

By using the same evaluated rigidity index value of 251 along with an effective friction angle value ($\phi' = 32.2°$), the original hybrid SCE-CSSM Burns & Mayne solution is applied to investigate flow properties from piezodissipation tests at Onsøy. **Figure 5.47 b** presents the measured disputation tests conducted at two depths: 18.5 and 20.3 m. Using the evaluated rigidity index value and friction angle, the predicted solution using SCE-CSSM is calculated and presented using red dashed lines showing a good agreement with the in-situ measured porewater pressure at the two depths. The corresponding coefficient of consolidation values are calculated: 0.1 $mm^2$/sec at depth of 18.5 m and 0.085 $mm^2$/sec at

depth of 20.3 m which is in an agreement with the laboratory reference values as reported by Robertson et al. (1992) where $c_{vh}$ = 0.1 ~ 0.22 mm$^2$/sec.

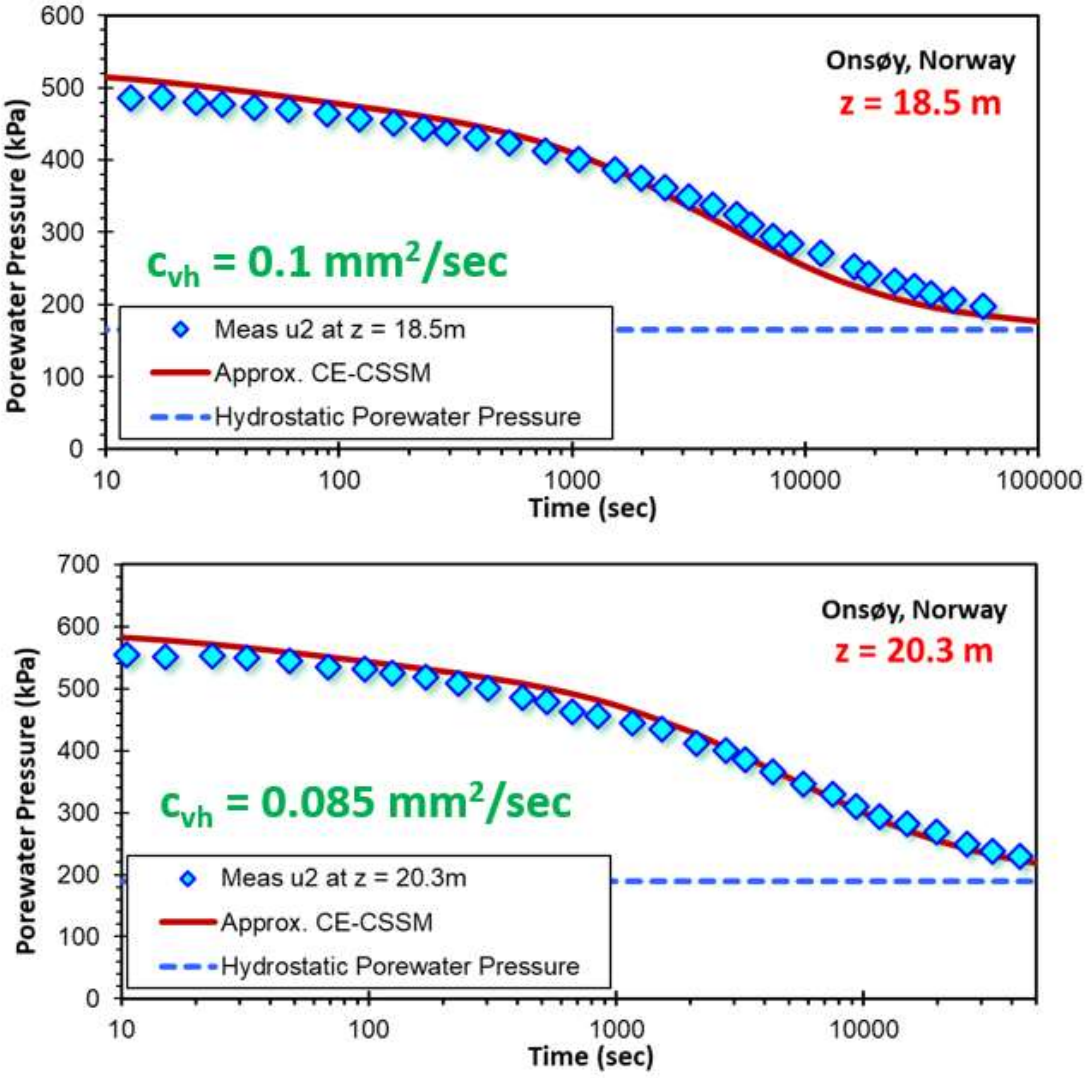


Figure 5.47b. Measured piezodissipation record for Onsøy clay in Norway at depths of 18.5 and 20.3 meters with prediction using hybrid SCE-CSSM framework

### 5.7.10 Perniö, Finland

Perniö is a testing site situated on the south-west coast of Finland. The site was primarily used for a full-scale embankment failure load test in 2009 whereby in-situ data and monitored load-displacement measurements were collected in order to evaluate new soil model parameters in numerical FEM studies (Lehtonen et al., 2015).

The soil profile at Perniö consists of 1.5-m thick weathered clay crust, underlain by 9-m thick soft clay layer, underlain by silty stiff sand layer. The soft clay layer has the following characteristic properties: water content values ranging from 60 - 120%, unit weight ranging from 14 -15 kN/m$^3$, and sensitivity ($S_t$) ranging from 20 to 60 (Di Buò et al., 2016).

Undisturbed samples were obtained using tube and piston samplers, and the stress history of the clay was measured in the laboratory using constant rate-of-strain (CRS) tests as reported by Di Buò et al. (2016). **Figure 5.48** presents the results of piezocone sounding reported by Lehtonen (2015). An effective friction angle ($\phi'$) of 34.7 degrees is evaluated using the NTH method.

**Figure 5.49** shows the evaluation of the slope parameter used in the proposed $I_R$ solution where ($u_2$-$\sigma_{vo}$) is plotted versus net cone tip resistance ($q_{net}$), giving a slope value of 0.5063. The slope value is used with the effective friction angle to give an operational rigidity index value ($I_R$) of 163.

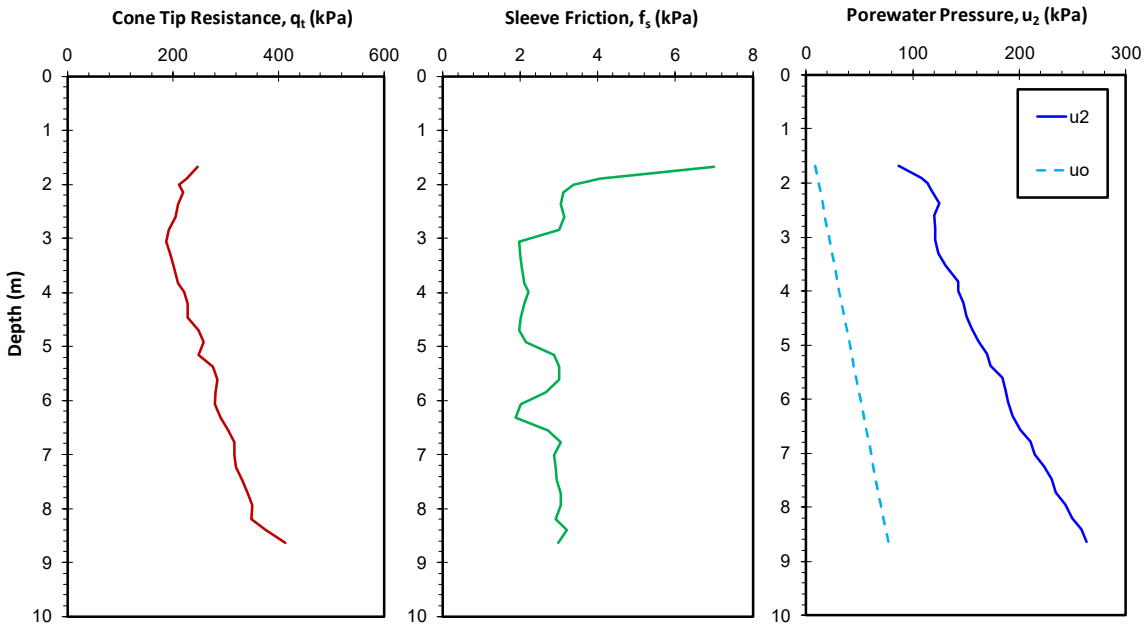


Figure 5.48. Piezocone sounding at Perniö site in Finland: (a) cone tip resistance, $q_t$; (b) sleeve friction, $f_s$; (c) porewater pressure, $u_2$. (Lehtonen, 2015)

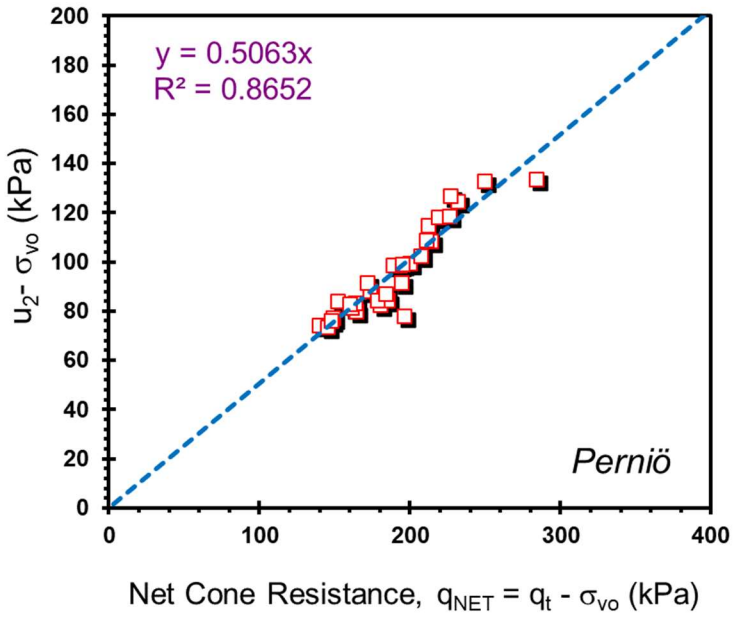


Figure 5.49. Evaluation of slope parameter for proposed $I_R$ solution f [ $(u_2-\sigma_{vo}) / q_{net}$] using CPTu data from Perniö, Finland

The obtained $I_R$ value is used to obtain cone bearing factor ($N_{kt}$) as per equation [5.19] for evaluating the undrained shear strength ($s_u$). By using an $I_R$ value of 163, the corresponding $N_{kt}$ value is 10.7 which provides a reasonable agreement with the reference CAUC, CIUC, and DSS undrained shear strength data reported by Lehtonen (2015); Di Buò et al. (2016); and D'Ignazio et al. (2017) as presented in **Figure 5.50.**

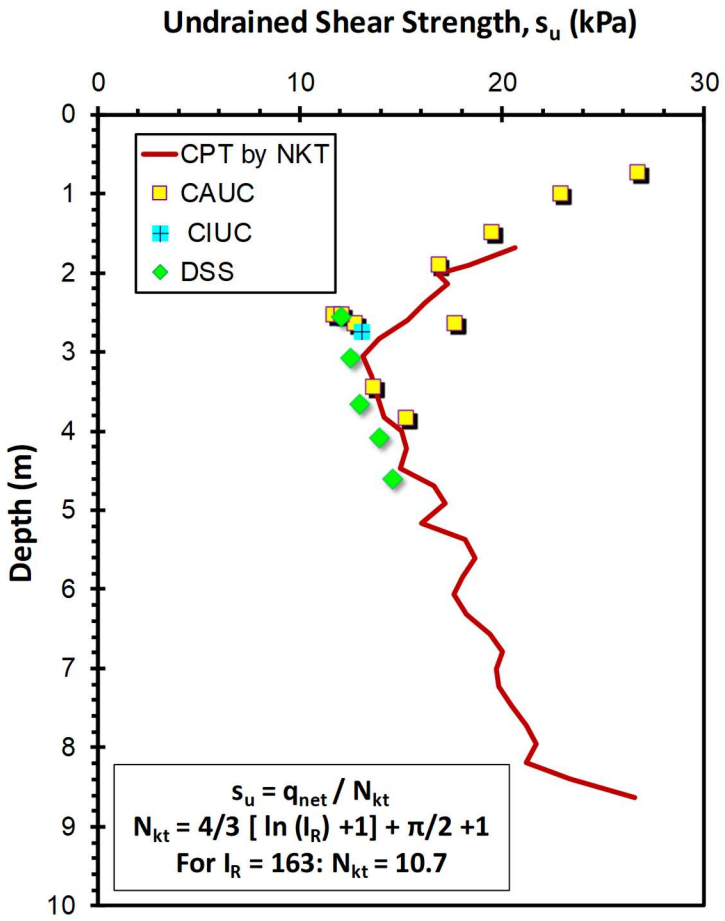


Figure 5.50. Undrained shear strength profile for Perniö, Finland using the proposed SCE-CSSM operational rigidity index value and cone bearing factor $N_{kt}$ (Note: $s_u$ data from Lehtonen 2015; Di Buò et al. 2016; D'Ignazio et al. 2017)

By applying equations [5.10], [5.11], and [5.12] of the hybrid SCE-CSSM to the results of piezocone sounding from **Figure 5.48** with an operational rigidity index value of $I_R$ = 163

from the proposed expression and effective friction angle value ($\phi'$ = 34.7°), the three stress history predictions coincide and match with each other as presented in **Figure 5.51**. Overall, excellent agreement is observed when compared with laboratory measured $\sigma_p'$ and OCR profiles reported by Di Buò et al. (2016).

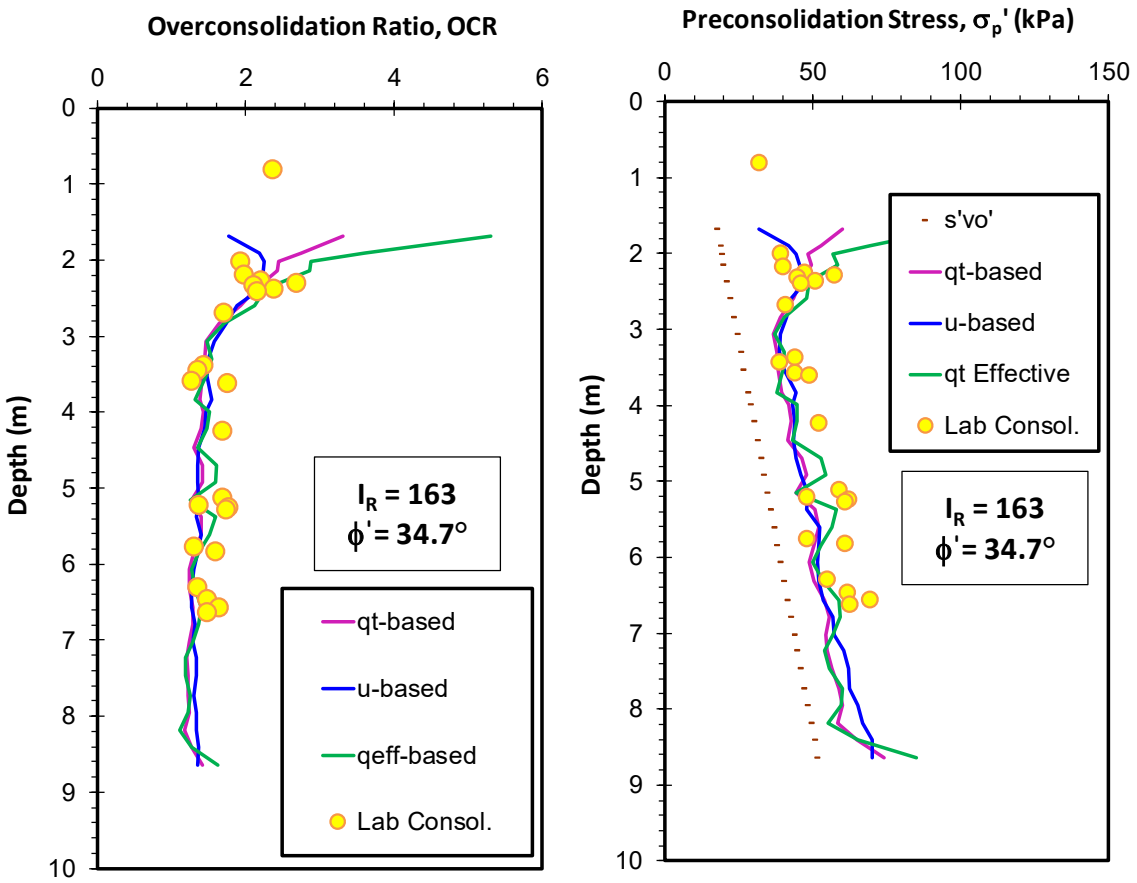


Figure 5.51. OCR and preconsolidation stress prediction using original hybrid SCE-CSSM framework with new $I_R$ expression for Perniö, Finland (consolidometer data from Di Buò et al. 2016)

### 5.7.11 Sarapuí, Brazil

Sarapuí is a very soft Brazilian clay located near Guanabara Bay in Rio de Janeiro city in Brazil. The main composition of the soft soil is 69% clay, 18% silt, and 13% sand. The

clay has very high natural water content and Atterberg limits, reaching a liquid limit value of 120% and water content value of 140% (Almeida & Marques, 2003). The clay has a sensitivity value measured using vane tests of about 4.4, the specific gravity ranges from 2.40 to 2.69 gm/cm$^3$, and the bulk unit weight lies between 12.4 and 14.5 kN/m$^3$.

The stress history of the clay was investigated using restricted flow consolidation tests, constant rate of strain (CRS) in addition to conventional incremental loading oedometer tests. The undrained shear strength was investigated using unconsolidated undrained tests (UU) in addition to consolidated anisotropic triaxial compression CAUC (using SHANSEP approach) and consolidated isotropic triaxial compression (CIUC) tests as carried by Gerscovich (1983). From the triaxial tests, an effective friction angle value of 25° was measured and used in the current calculations. **Figure 5.52** presents the readings of a piezocone sounding carried at Sarapui and reported by Almeida & Marques, 2003.

**Figure 5.53** shows the evaluation of the slope parameter used in the proposed $I_R$ solution where ($u_2$-$\sigma_{vo}$) is plotted versus net cone tip resistance ($q_{net}$), giving a slope value of 0.5147. The slope value is used with the effective friction angle to give an operational rigidity index value ($I_R$) of 515.

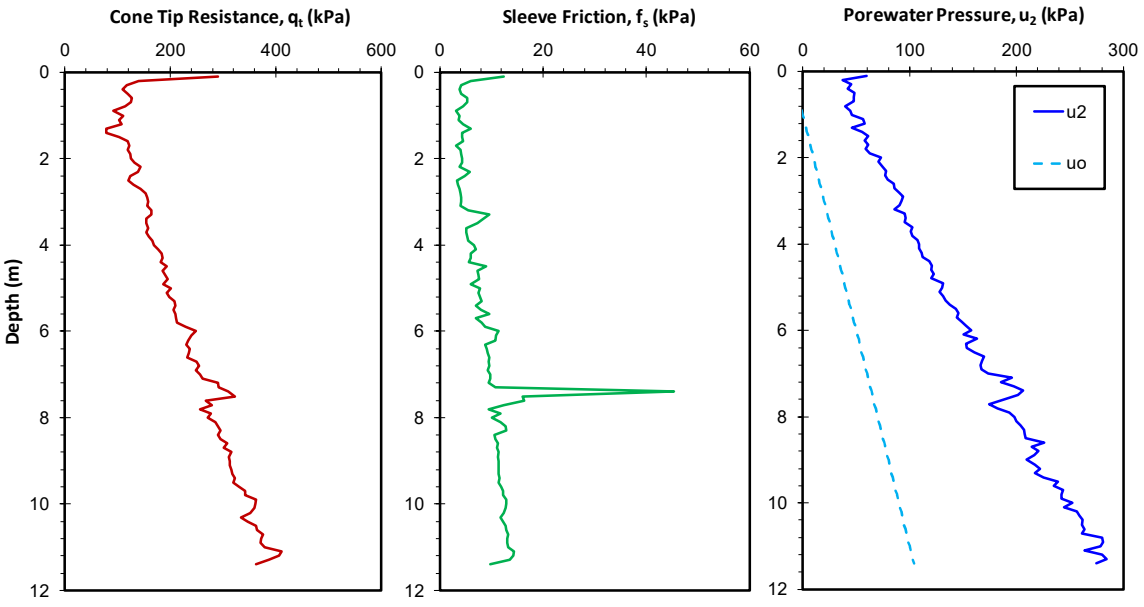


Figure 5.52. Piezocone sounding at Sarapuí site in Brazil: (a) cone tip resistance, $q_t$; (b) sleeve friction, $f_s$; (c) porewater pressure, $u_2$ (Almeida & Marques, 2003)

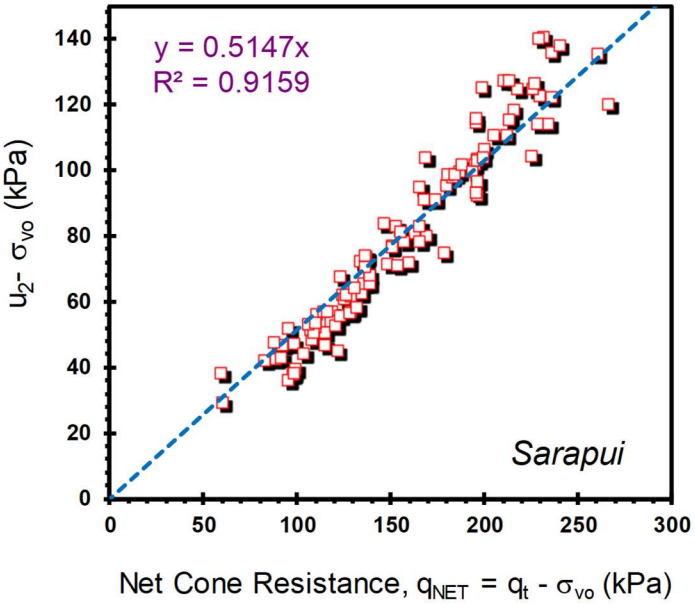


Figure 5.53. Evaluation of slope parameter for proposed $I_R$ solution f [ ($u_2$-$\sigma_{vo}$) / $q_{net}$] using CPTu data from Sarapuí, Brazil

The obtained $I_R$ value is used to obtain cone bearing factor ($N_{kt}$) as per equation [5.19] for evaluating the undrained shear strength ($s_u$). Using an $I_R$ = 515, the corresponding $N_{kt}$

= 12.2 that provides a fair match with the reference CAUC triaxial tests and field vane data, as seen in **Figure 5.54.** The mismatch in this case study may be attributed to the very soft nature of the clay under study as it is organic. Also, the CAUC data were obtained using SHANSEP approach where destruction to the natural clay structure is induced. In SHANSEP, the clay samples are loaded until reaching normally consolidated state then unloaded to a specific OCR value then loaded again in undrained compression. The entire loading process can possibly affect the clay structure and affect its stress history resulting in lower undrained shear strength values.

By applying equations [5.10], [5.11], and [5.12] of the hybrid SCE-CSSM to the results of piezocone sounding from **Figure 5.53** with an operational rigidity index value of $I_R = 515$ from the new expression and effective friction angle value ($\phi' = 25°$), the three stress history predictions coincide and match with each other as presented in **Figure 5.55**. Overall, excellent agreement is observed when compared with laboratory measured $\sigma_p'$ and OCR profiles reported by Almeida & Marques, 2003.

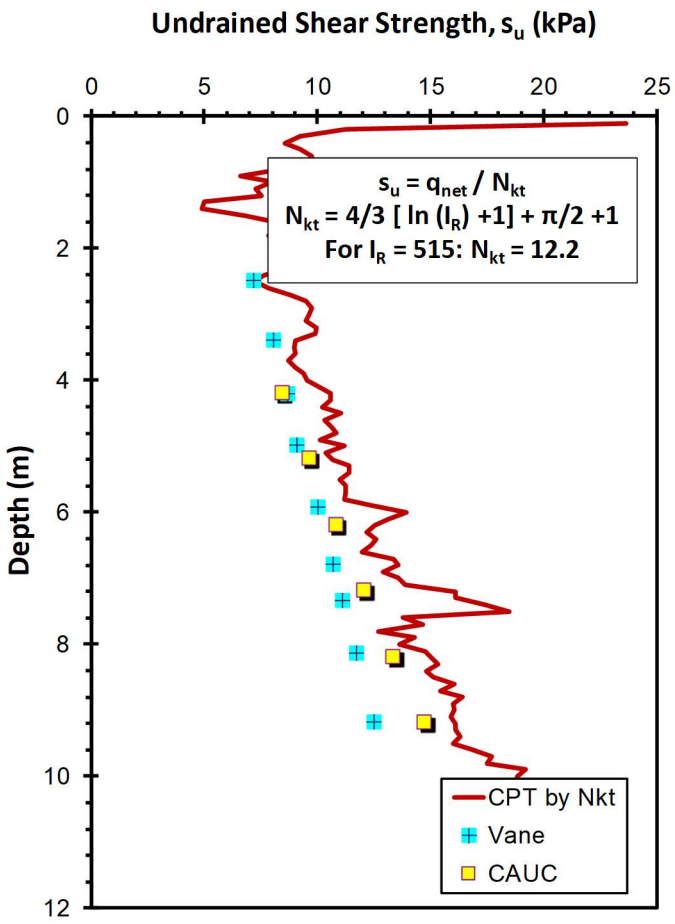


Figure 5.54. Undrained shear strength profile for Sarapuí, Brazil using the proposed SCE-CSSM operational rigidity index value and cone bearing factor $N_{kt}$ (Note: triaxial data from Almeida & Marques, 2003)

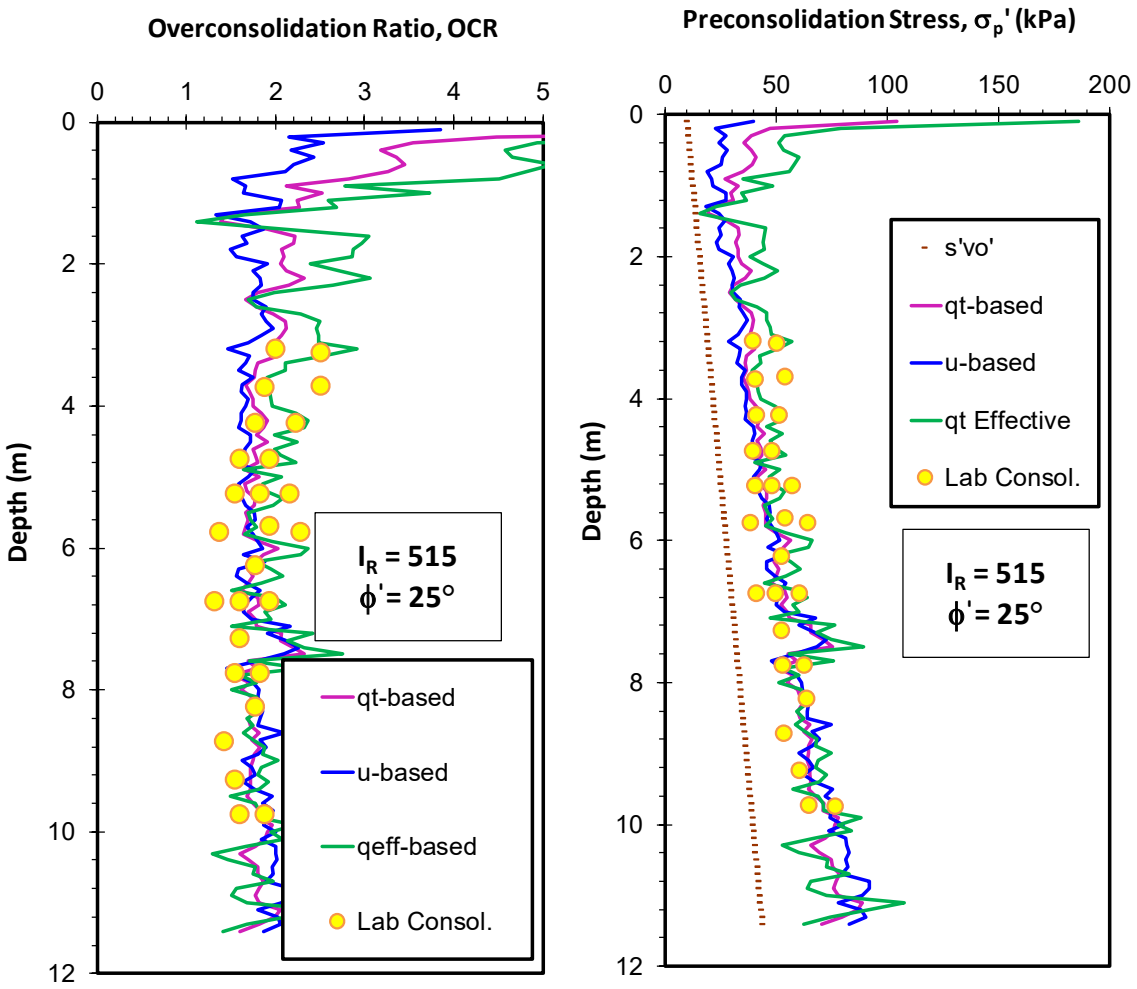


Figure 5.55. OCR and preconsolidation stress prediction using original hybrid SCE-CSSM framework with new $I_R$ expression for Sarapuí, Brazil (consolidometer data from Almeida & Marques, 2003)

### *5.7.12 Torp, Sweden*

The test site is located in the Örekilsälven river valley, north of the river mouth in the Saltkällefjorden fjord in the northern part of the province of Bohuslän in Sweden (Larsson & Åhnberg, 2003). The preconsolidation stresses ($\sigma_p$') were obtained from 27 constant rate of strain oedometer tests as presented in **Figure 5.59.** Undrained triaxial compression and extension tests have been conducted in addition to drained triaxial tests.

**Figure 5.56** presents the cone tip, sleeve and pore water profiles with depth for location S9. The results from the deep piezocone sounding extending to 58 m were used to evaluate the effective friction angle using the NTH method where an average effective friction angle ($\phi'$) of 32 degrees was obtained.

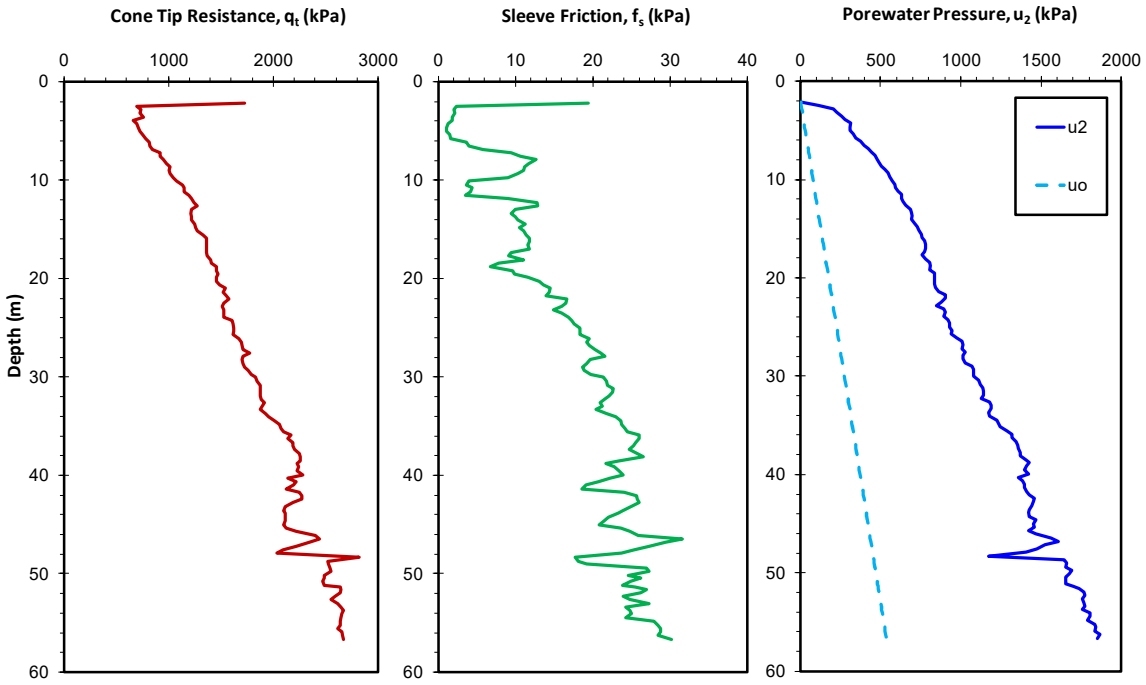


Figure 5.56. Piezocone sounding at Torp site in Sweden: (a) cone tip resistance, $q_t$; (b) sleeve friction, $f_s$; (c) porewater pressure, $u_2$. (data from Larsson & Åhnberg, 2003)

**Figure 5.57** shows the evaluation of the slope parameter used in the proposed $I_R$ solution where ($u_2$-$\sigma_{vo}$) is plotted versus net cone tip resistance ($q_{net}$), giving a slope value of 0.465. The slope value is used with the effective friction angle to give an operational rigidity index value ($I_R$) of 112.

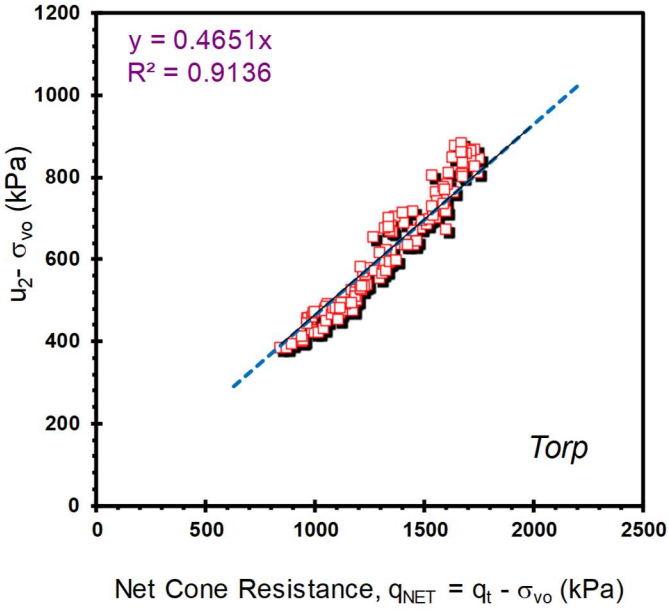


Figure 5.57. Evaluation of slope parameter for proposed $I_R$ solution f [ $(u_2-\sigma_{vo}) / q_{net}$] using CPTu data from Torp, Sweden

The obtained $I_R$ =112 is used to obtain cone bearing factor ($N_{kt}$) as per equation [5.19], giving $N_{kt}$ = 10.2. This provides a fair agreement with an overestimation when seen next to the measured CAUC data reported at the site, as presented in **Figure 5.58.**

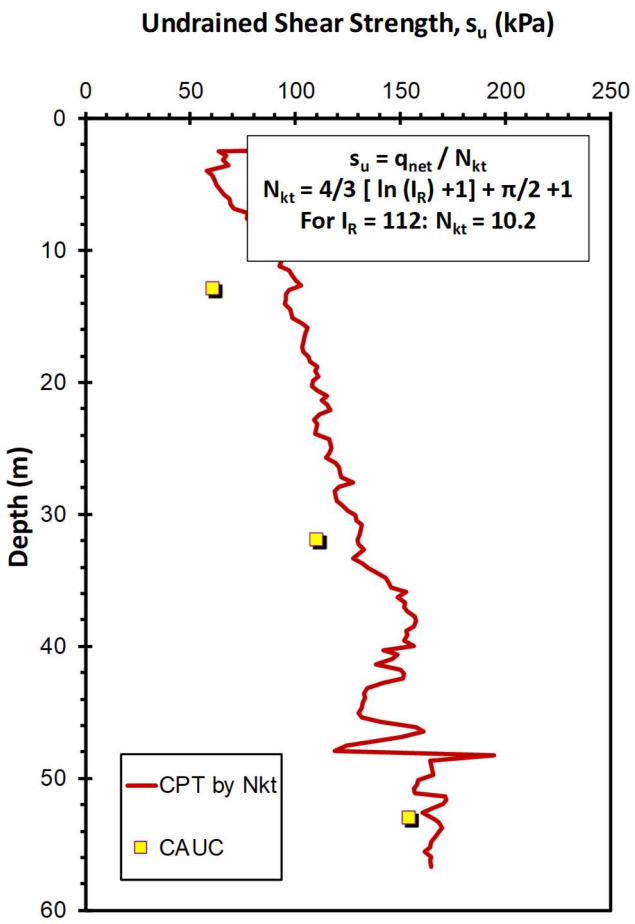


Figure 5.58. Undrained shear strength profile for Torp, Sweden using the proposed SCE-CSSM operational rigidity index value and cone bearing factor $N_{kt}$ (Note: triaxial data from Larsson & Åhnberg, 2003)

By applying equations [5.10], [5.11], and [5.12] of the hybrid SCE-CSSM to the results of piezocone sounding from **Figure 5.56** with an operational rigidity index value of $I_R = 112$ from the proposed expression and effective friction angle value ($\phi' = 32°$), the three stress history predictions coincide and match with each other as presented in **Figure 5.59**. Overall, excellent agreement is observed when compared with laboratory measured $\sigma_p'$ and OCR profiles reported by Larsson & Åhnberg, 2003.

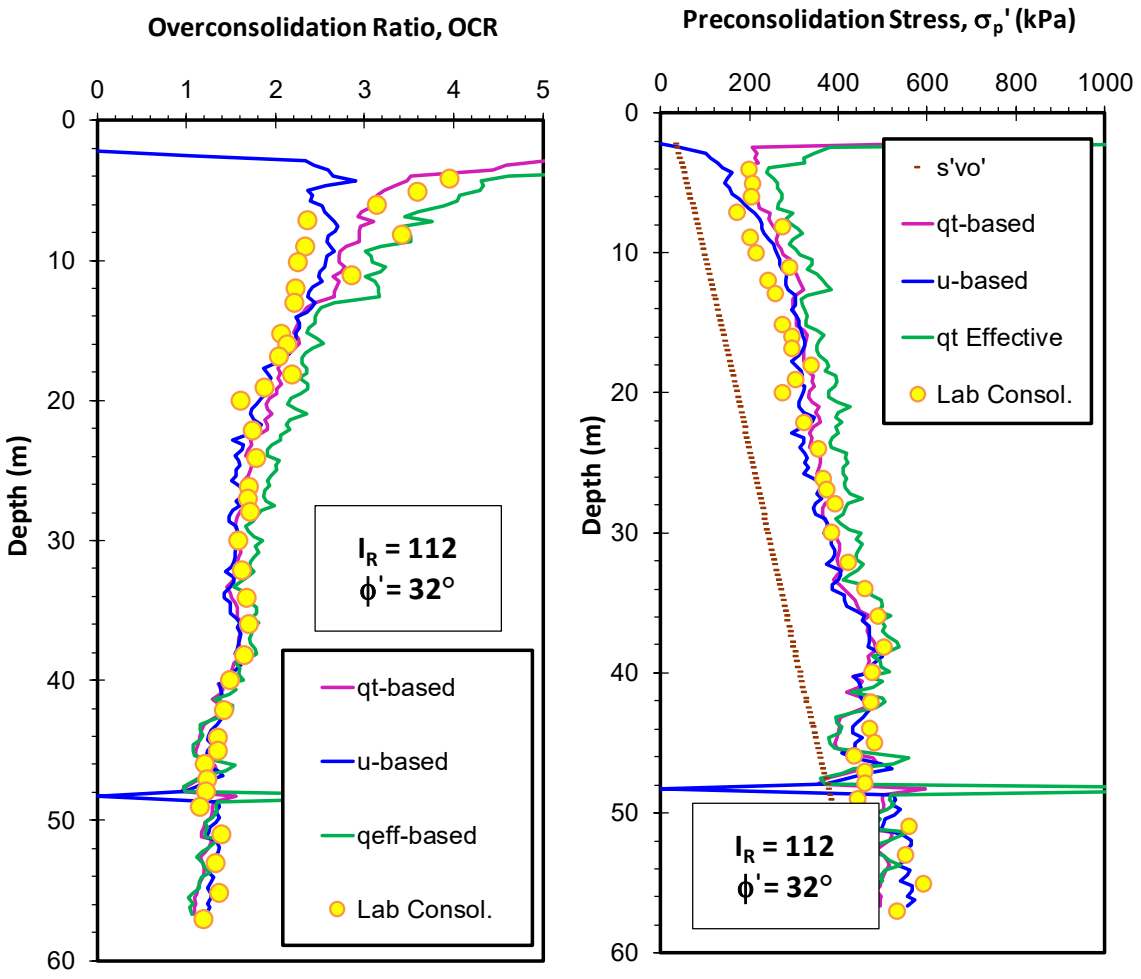


Figure 5.59. OCR and preconsolidation stress prediction using original hybrid SCE-CSSM framework with new $I_R$ expression for Torp, Sweden (consolidometer data from Larsson & Åhnberg, 2003)

## 5.7 Conclusions

The chapter discusses means of evaluating the rigidity index of clays, including empirical methodologies that have been reported elsewhere. Using the hybrid spherical cavity expansion – critical state framework, two expressions are proposed for obtaining operational rigidity index ($I_R$) based on cone tip resistance and pore water pressure readings, or their normalized quantities.

**Figure 5.60** presents a design chart with contour lines for different effective friction angles ($\phi'$), relating the slope parameter ($a_q$) with the evaluated rigidity index value ($I_R$). From the piezocone sounding, the slope $a_q$ is determined as a single value for any clay deposit by taking the slope of a plot of the parameter (U*-1) versus Q, or alternatively as the slope of ($u_2$ - $\sigma_{vo}$) versus ($q_t$ - $\sigma_{vo}$). The effective friction angle can be determined either from laboratory measurements or evaluated from a method like NTH. By knowing the slope value and the effective friction angle, one can evaluate an operational value for the rigidity index.

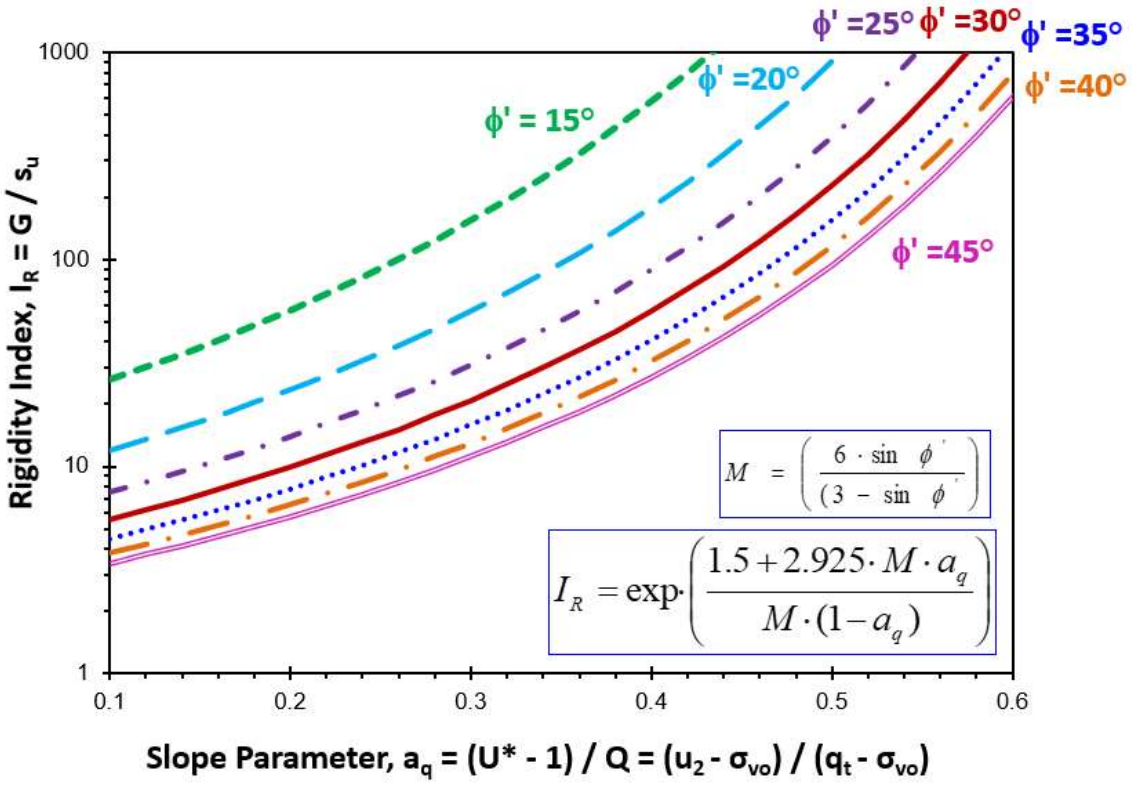


Figure 5.60. Contour lines for different effective friction angles ($\phi'$) for rigidity index ($I_R$) evaluation from the slope parameter ($a_q$)

**Figure 5.61** presents the contour lines from the design chart of **Figure 5.60** with the values of the 12 presented case studies superimposed on the contour lines. In the figure, a zoom-in to the practical range of $a_q$ and $I_R$ is presented based on the presented 12 case studies.

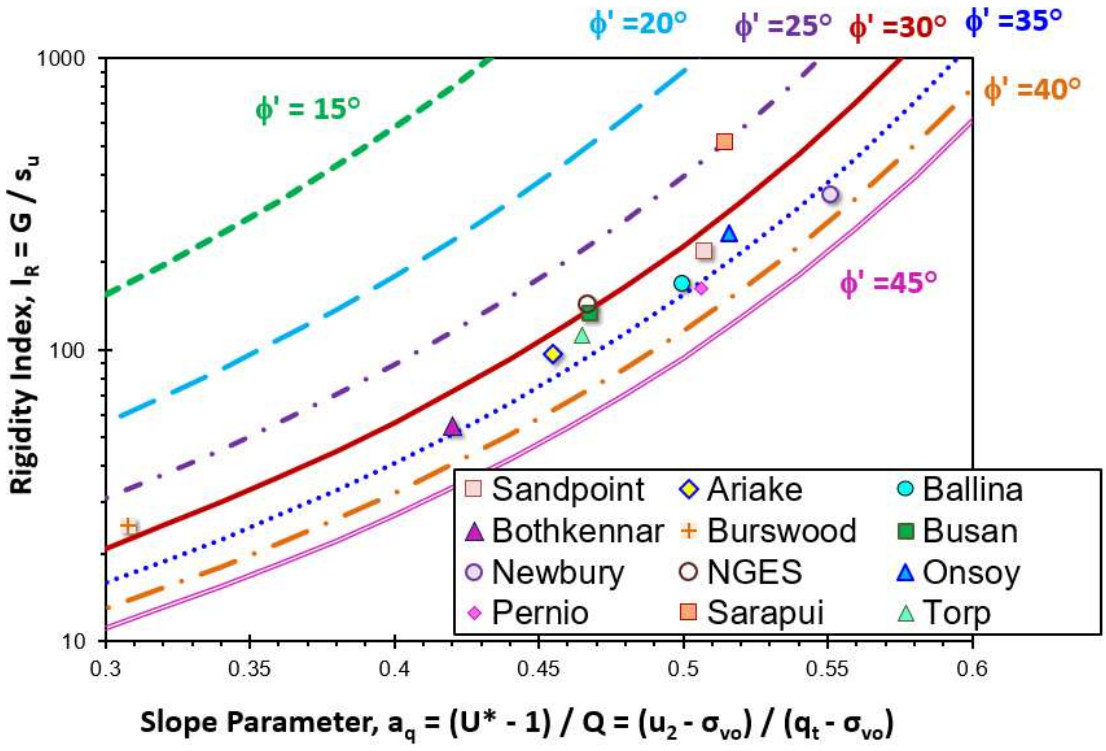


Figure 5.61. Zoomed in contour lines for different (ϕ') for rigidity index ($I_R$) evaluation from the slope parameter ($a_q$) with superimposed 12 case studies

The evaluated rigidity index values are in reasonable agreement with reference laboratory-based and seismic-based in-situ approaches. The evaluated $I_R$ values are tested in estimating the stress history profiles using three definitions from SCE-CSSM framework, the three predictions fully agree and match with lab reference values. The proposed method gives a very good agreement with lab-measured undrained shear strength values using corresponding cone bearing factors. Twelve case studies covering well-behaved clays with

different geologies from several countries were used to demonstrate the effectiveness of the proposed methodology for obtaining $I_R$.

# Chapter 6. SCPTu identification of sensitive clays in North America

**6.1 Abstract:** The identification of sensitive clays is very important during geotechnical site investigations because these geomaterials are prone to collapse, instability during excavation, and associated with landslide events. It is shown that the shear wave velocity ($V_s$) measured during seismic piezocone (SCPTu) testing can be utilized as a new means of identifying sensitive clays, specifically in North America. Common correlations of estimating shear wave velocity from CPTu data were examined and generally found unsatisfactory for use in sensitive clays. Hence, by comparing measured $V_s$ with estimated $V_s$ profiles using standard correlative trends helps identify when sensitive clays may exist within a soil profile.

This chapter presents a summary of the different soil classification schemes for cone penetration testing (CPT) that are available, along with their corresponding soil behavioral type (SBT) charts and post-processing schemes. The shortcomings of the available SBT methods in correctly and adequately identifying sensitive fine-grained materials by CPTu are reviewed. Hence, a special database developed from 20 sensitive clays from Canada and the northern USA was compiled and two recent correlations (NGI: L'Heureux & Long 2016) and KIGAM: Sun et al. 2013)* were modified for evaluating shear wave velocity from CPTu data in sensitive clays.

*Note: NGI = Norwegian Geotechnical Institute and KIGAM = Korean Institute of Geosciences and Minerals.

## 6.2 Soil Identification and Classification from CPT

Given the lack of routine soil sampling during cone penetration testing, different approaches can be used for processing CPT data to identify soil type and classify the different strata beneath the ground surface: (a) relating CPT readings to the logs of adjacent boreholes and recovered samples; (b) relying on rules-of-thumb; (c) using empirical soil behavioral type (SBT) charts; (d) adopting probabilistic methods.

### 6.2.1 Simple Rules of Thumb

The simple rules of thumb depend on one or more of the cone penetration readings. For instance, a guideline reference cone tip resistance $q_t$ = 5 MPa (≈ 50 atm) can be identified, whereby any measured $q_t$ value > 5 MPa implies clean "hourglass" sands and $q_t$ < 5 MPa suggests "vanilla" clays. Here, we are referring to "well-behaved" geomaterials, including quartz and silica sands of common occurrence, as well as inorganic kaolinitic and illitic clays of low to medium sensitivity. For the friction sleeve reading, it is convenient to plot this in terms of friction ratio, FR = $100 \cdot f_s/q_t$ (%). Accordingly, clean sands are identified by FR < 1%, whereas fine-grained soils (silts and clays) of low to medium sensitivity often exhibit FR > 3%.

The measured porewater pressure can be compared with the hydrostatic porewater pressure ($u_0$). Specifically, in clean uncemented "hourglass" sands, the measured porewater pressures are often close to hydrostatic ($u_2 \approx u_0$). However, if the sands are very dense, dilatancy effects may result in $u_2$ readings below $u_0$. Below the groundwater table, intact clays can be found by examining where $u_2 > u_0$. Specifically, in soft clays ($u_2 \approx 2 \cdot u_0$), firm clays ($u_2 \approx 4 \cdot u_0$), stiff clays ($u_2 \approx 6 \cdot u_0$), and hard clays ($u_2 > 10 \cdot u_0$). However, in fissured

clays, it is found that $u_2 < u_0$ and more commonly: $u_2 < 0$ because of dilative behavior and/or the presence of discontinuities. Also, note that for onshore deposits: $u_2 > -100$ kPa.

### 6.2.2 Probabilistic Methods

A CPT soil classification scheme based on fuzzy logic was introduced by Zhang and Tumay (1999). The results of soil identification are displayed in the form of percentages of probability of the soil constituency of clay-silt-sand components, thus analogous to the US Department of Agriculture textural soil classification system. Additional details are given in Tumay et al. (2008, 2011) and a free software program (P-Class) is available for providing the automated post-processing of the CPT for the output (www.usucger.org).

### 6.2.3 Soil Behavioral Type Charts

The most popular method of soil classification uses empirical soil behavioral type (SBT) charts which have been developed by various researchers. Begemann (1965) can be considered one of the first researchers to consider soil profiling using CPT data by relying on two readings: cone tip resistance ($q_c$) and sleeve friction ($f_s$), where he performed tests using a mechanical cone penetrometer in Dutch soils, and organized similar soil types in a chart format based on their paired readings. By grouping available data, zones in the form of fanned-out lines for the main soil types can be defined ranging from coarse sands with gravel to silts to clays, as presented in **Figure 6.1**.

Schmertmann (1978) introduced a revised soil profiling chart based on the cone tip resistance and the friction ratio, $FR = 100 \cdot f_s/q_t$ (%), that relied on mechanical cone data

primarily from Florida, as presented in **Figure 6.2**. Schmertmann's chart introduced specific boundaries for loose and dense sands, soft to medium to stiff insensitive and non-fissured inorganic clays, in addition to defining zones for other soil types including a new zone for limerocks, organic clays, and mixed soils.

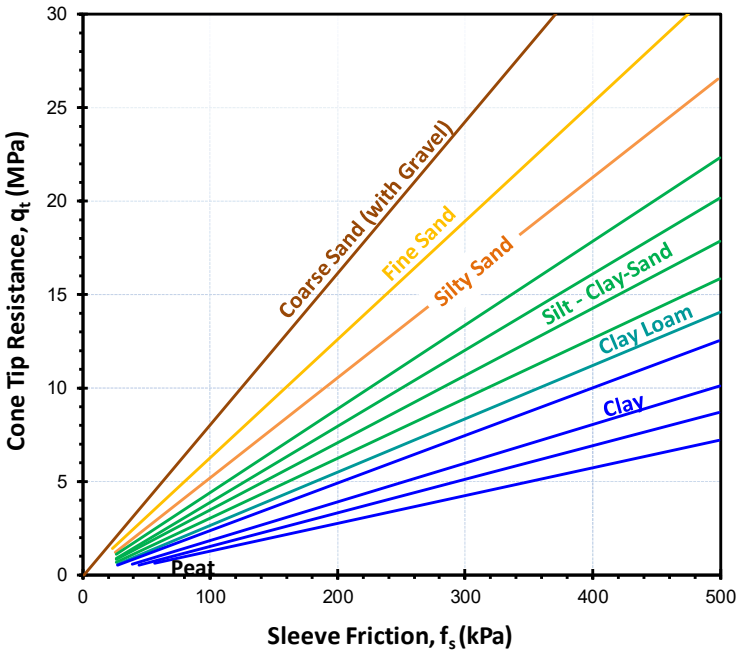


Figure 6.1. Early Soil Profiling Chart from CPT Readings (after Begemann, 1965)

Douglas and Olsen (1981) defined a more detailed soil classification chart, also based on cone tip resistance and friction ratio, but continuous readings were available from electrical cone penetrometer data. **Figure 6.3** illustrates their classification chart which was intentionally linked to the terminology of the Unified Soil Classification System (USCS) defining sands, silts, and clays with different plasticity levels. The chart divides fine-grained soil materials into 4 main regions from non-cohesive to cohesive. Moreover, the chart also introduced new zones for metastable sands and sensitive clays which were not identified in the earlier classification schemes.

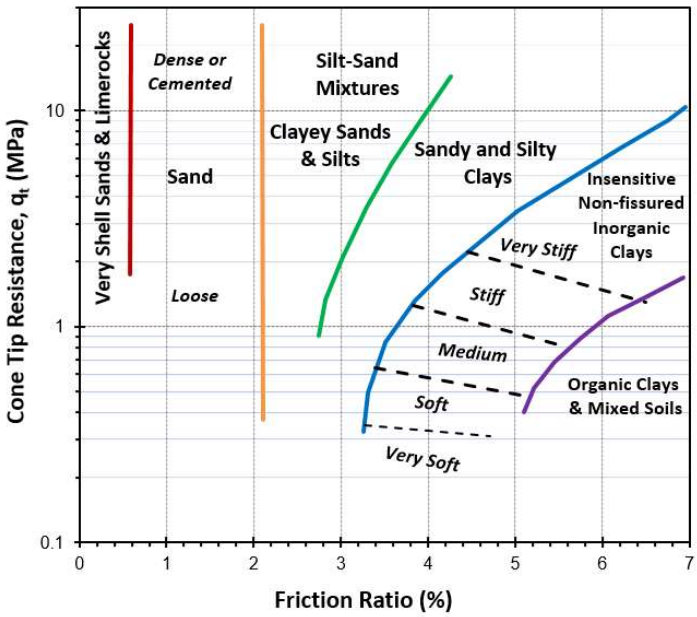


Figure 6.2. Modified Soil Profiling Chart from Mechanical CPT Readings (after Schmertmann, 1978)

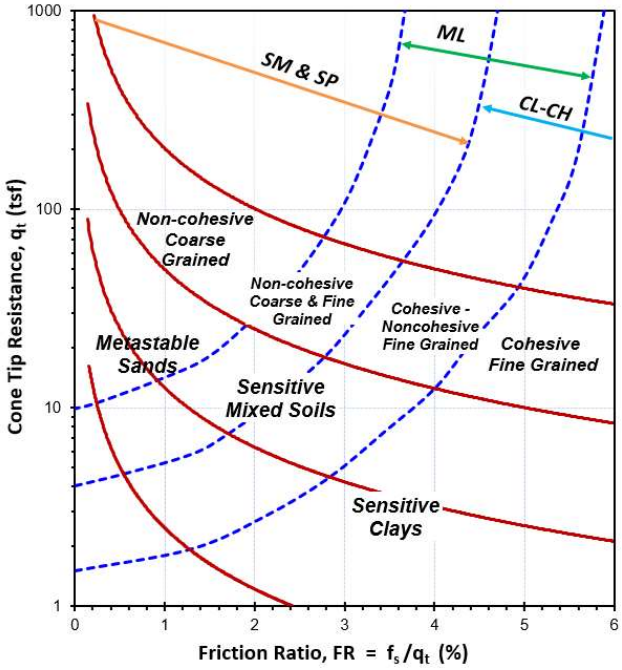


Figure 6.3. Soil Profiling Chart for Electric CPT (after Douglas and Olsen, 1981)

Robertson, et al. (1986) presented a 12-zone SBT system that uses a three-axis plot of total cone tip resistance ($q_t$), friction ratio (FR), and normalized porewater pressure ($B_q$),

where $B_q = (u_2 - u_0) / (q_t - \sigma_{vo})$. Due to the complexity of working with 3-d graphs directly, the system is usually presented in two paired graphs: (a) $q_t$ vs. FR (%); presented in **Figure 6.4**; and (b) $q_t$ vs $B_q$. The chart introduced transitional zones for silts and clays, in addition to noting new zones for sensitive fine-grained clays, very stiff fine-grained soils, and overconsolidated to cemented sands.

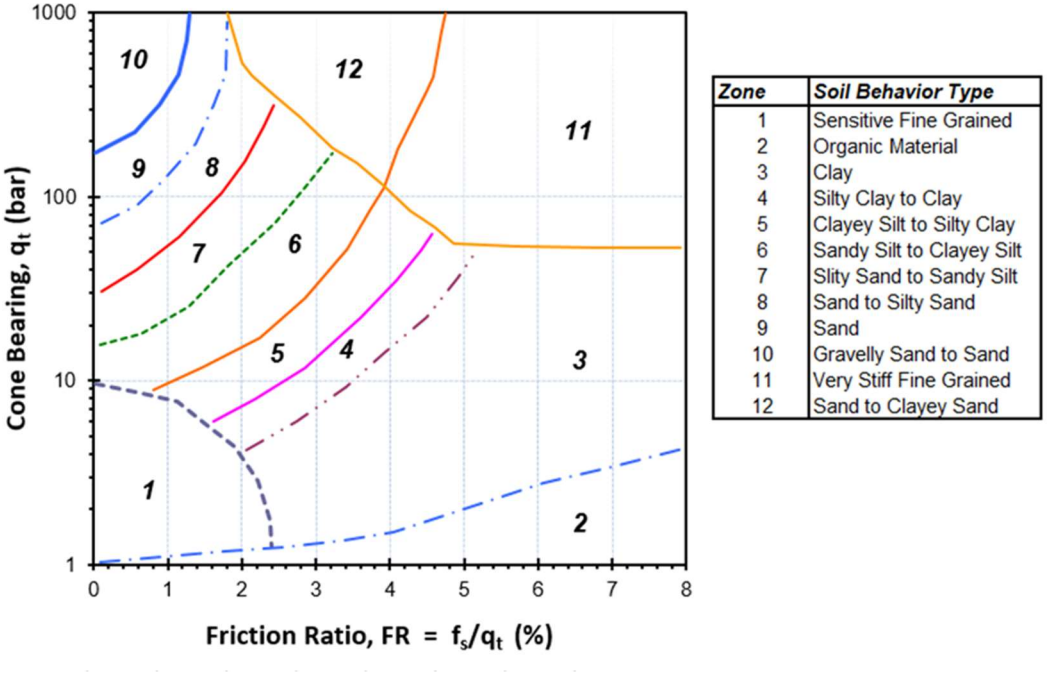


| Zone | Soil Behavior Type |
|---|---|
| 1 | Sensitive Fine Grained |
| 2 | Organic Material |
| 3 | Clay |
| 4 | Silty Clay to Clay |
| 5 | Clayey Silt to Silty Clay |
| 6 | Sandy Silt to Clayey Silt |
| 7 | Slity Sand to Sandy Silt |
| 8 | Sand to Silty Sand |
| 9 | Sand |
| 10 | Gravelly Sand to Sand |
| 11 | Very Stiff Fine Grained |
| 12 | Sand to Clayey Sand |

Figure 6.4. 12-Zone Soil Behavioral Type Chart by Univ. British Columbia (after Robertson et al., 1986)

Senneset et al., (1989) at NTNU followed a similar procedure by developing a soil classification chart based on total cone tip resistance ($q_t$) and porewater pressure ratio ($B_q$), as presented in **Figure 6.5**. The classification chart defines 7 main zones for common soil types ranging from very soft clay to silts to loose sands to hard stiff soils. The chart did not note the additional zones identified by UBC and is limited to maximum cone resistances of 16 MPa.

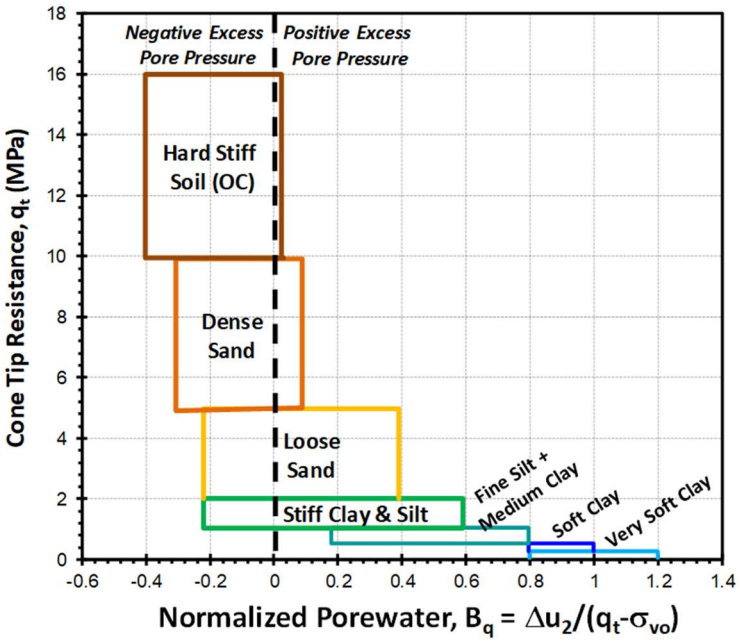


Figure 6.5. Soil Profiling Chart by Norwegian University of Science & Technology, NTNU (after Senneset et al. 1986)

Eslami and Fellenius (1997) developed a classification chart based on piezocone test data that was used for piling foundation design. Their chart is classified into five main soil types including (1) sensitive - collapsive soils, (2) soft clays and silts, (3) stiff silts and clays, (4) sandy silts and silty sands, and (5) sands and gravels, as illustrated in **Figure 6.6**. The novelty in their approach is in the use of all three CPTU readings in a single chart; namely: effective cone resistance ($q_E = q_t - u_2$) along with the sleeve friction ($f_s$) in defining the different chart zones. The use of effective cone resistance is significant in fine-grained soils where the clays or silts can generate high excess pore water pressures when advancing the penetrometer into the soil, in contrast to coarse-grained geomaterials where $q_E \approx q_t$.

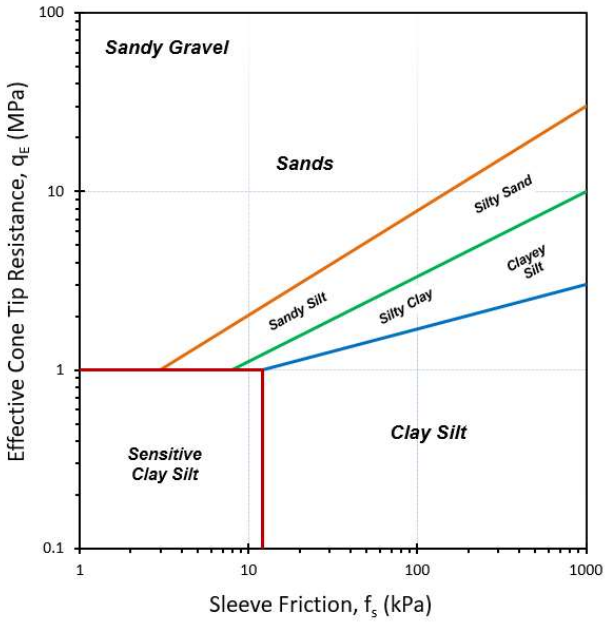


Figure 6.6. Unicone Soil Profiling Chart (after Fellenius and Eslami, 2000)

Robertson (1990; 2009) introduced an improved version of his earlier 12-zone soil classification system relying on stress-normalized parameters (Q, F, and $B_q$) to account for depth effects where:

$$Q = (q_t - \sigma_{vo})/\sigma_{vo}' \quad [6.1]$$

$$F\ (\%) = 100 \cdot f_s/(q_t - \sigma_{vo}) \quad [6.2]$$

By plotting the data in terms of Q versus F and Q versus $B_q$, a nine-zone SBT system was developed, as shown in **Figure 6.7**. In this system, basic "vanilla" clay is found in zone 3 while "hourglass" sands form zone 6. The classification system also included zones for sensitive fine-grained materials, organic soils, and very stiff fine-grained overconsolidated soils. The nine-zone SBTn classifications can be identified as per Robertson (2009) following **Table 6.1** using the values of the CPT material index ($I_{cRW}$) which is defined (Robertson & Wride, 1998), an updated version of normalized cone tip resistance ($Q_{tn}$) is presented in Chapter 4:

$$I_{cRW} = \sqrt{\{3.47 - \log(Q)\}^2 + \{1.22 + \log(F)\}^2} \qquad [6.3]$$

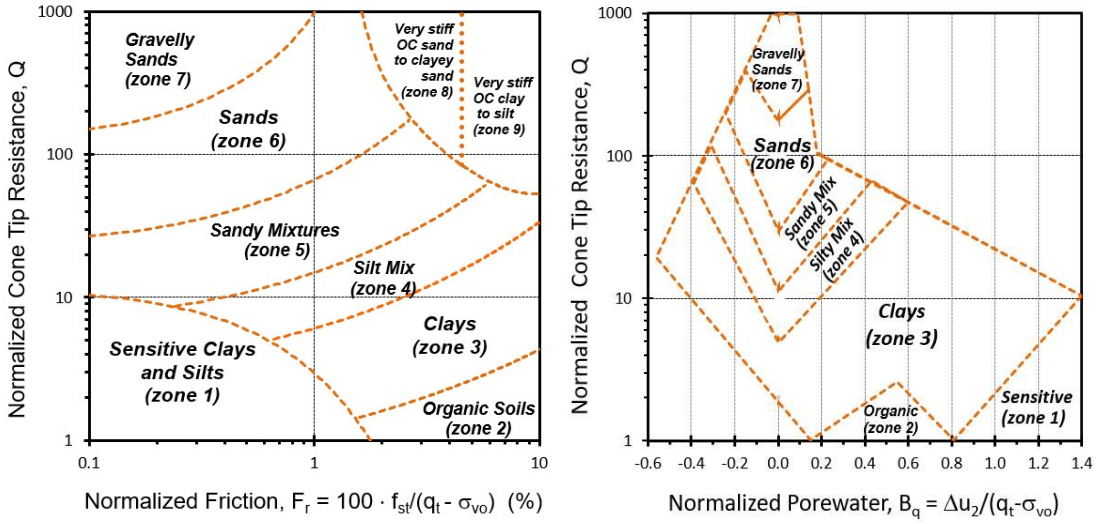


Figure 6.7. CPT Soil Classification Zones Using Nine-Part Soil Behavioral Type (after Robertson, 2009)

*Table 6.1.* Soil Behavioral Type and Zone Number as defined by CPTu Material Index, $I_c$

| Soil Classification | SBT Zone | Range CPT Material Index $I_{cRW}$ |
|---|---|---|
| Stiff clayey sand | 9 | F > 4.5 % (see note 1) |
| Stiff sandy clay | 8 | 1.4 < F < 4.5 % (see note 1) |
| Sands with gravels | 7 | $I_{cRW}$ < 1.31 |
| Sands: clean to silty | 6 | 1.31 < $I_{cRW}$ < 2.05 |
| Sandy mixtures | 5 | 2.05 < $I_{cRW}$ < 2.60 |
| Silty mixtures | 4 | 2.60<$I_{cRW}$ <2.95 |
| Clays | 3 | 2.95<$I_{cRW}$ <3.60 |
| Organic soils | 2 | $I_{cRW}$ >3.60 |
| Sensitive soils | 1 | (see note 2) |

Notes: 1. Zone 8 and Zone 9 are found by the following criterion:

$$Q \geq \frac{1}{0.006 \cdot (F - 0.9) - 0.0004 \cdot (F - 0.9)^2 - 0.002}$$

2. Sensitive soils of zone 1 are identified when Q < 12 exp (-1.4 F)

Schneider et al. (2008), proposed a new CPT classification chart distinguishing between drained and undrained soil conditions with an emphasis on the variations in the

degrees of consolidation and drainage for different soil types during cone penetration that can be attributed to changes in yield stress ratio. The proposed classification chart; presented in **Figure 6.8**; relies on normalized cone tip resistance, Q and penetration porewater pressure expressed in the form of normalized porewater pressure, $U^* = \Delta u_2 / \sigma'_{v0}$. The chart is divided into 5 main zones: sensitive undrained clays (Zone 1c); undrained clays (Zone 1b); partially drained silts and undrained clays with low rigidity index, $I_R$ (Zone 1a); transitional soils which can be drained, undrained, or partially consolidated (Zone 3); and finally, drained sands (Zone 2).

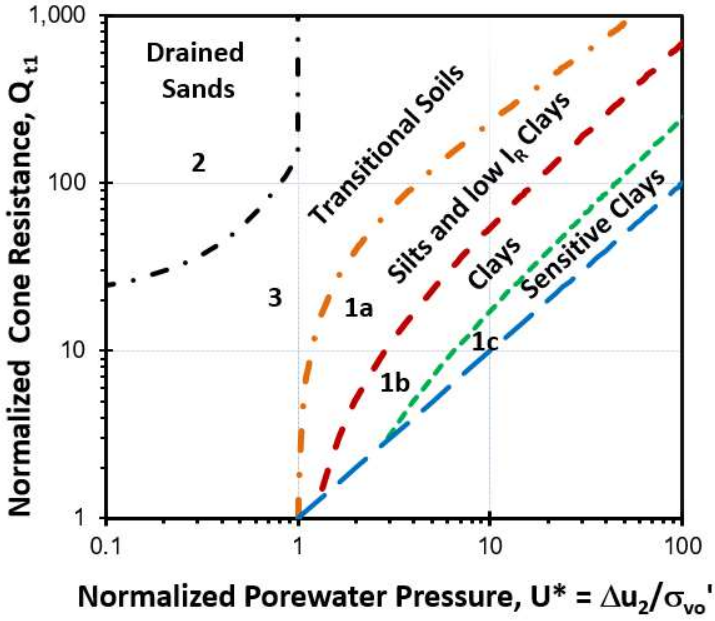


Figure 6.8. Soil Profiling Chart Using Normalized Porewater Pressure, U* (after Schneider et al., 2008)

Schneider et al. (2012) extended their framework for soil classification to include the friction ratio, F. An extended field database was used to investigate the proposed soil zones with different degrees of consolidation and drainage which led to an overlap between zone 3 (of transitional soils) and zone 1a (silts and clays with low $I_R$) where silts should be

grouped with transitional soils having intermediate drainage conditions. The conventional Q-F diagram; which is mainly used when lacking high-quality porewater pressure measurements; was modified to reflect the 5 main zones that were proposed in Q-U* diagram as presented in **Figure 6.9**. Both charts should be used in a parallel complementing manner for better soil identification especially with soils that exhibit sensitivity, cementation or special structure.

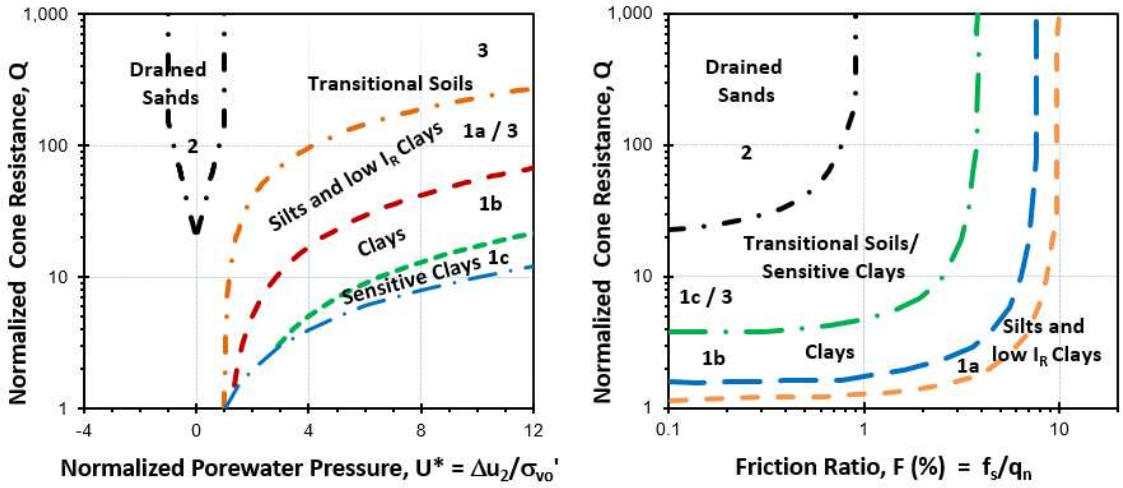


Figure 6.9. Comparison of Q–F and Q–$\Delta u_2/\sigma'_{v0}$ CPTU soil classification charts (after Schneider et al., 2012)

Serratrice (2013) has introduced an identification method where the procedure advances in two stages: 1st stage is soil classification based on triaxial data using drained and undrained strength parameters from soil samples then the 2nd stage is the identification of sensitive soils based on piezocone measurements from the same sampling location. The method is illustrated in **Figure 6.10** where 1st the triaxial test data are plotted in a conventional q-p space identifying 3 main geomaterials: sands, silts, and clays based on total stress measurements. From the q-p diagram, $q_c$ is the deviator stress ½ ($\sigma_1$-$\sigma_3$) and $p_c$ is the mean total stress ½ ($\sigma_1$+$\sigma_3$). Then the piezocone readings (effective cone tip

resistance, $q_E$ and sleeve friction, $f_s$) are used to identify 4 main zones to detect sensitive soils. This method is relatively more complicated as it requires both in-situ and laboratory measurements with intact undisturbed samples for triaxial sampling which is both inconvenient and impractical.

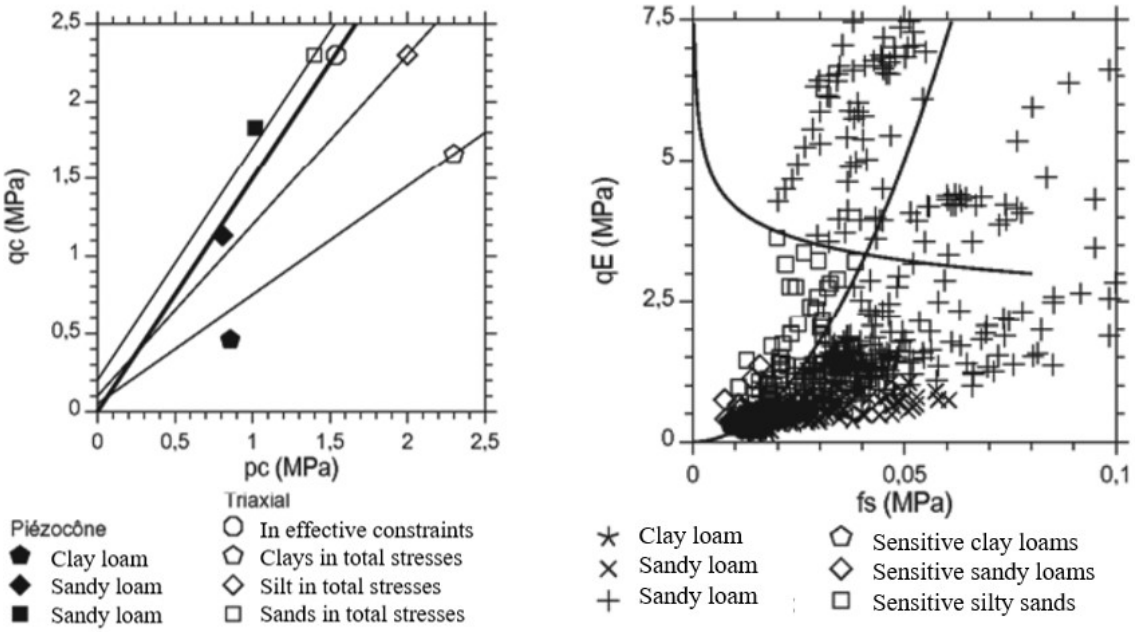


Figure 6.10. Two-step soil profiling chart (after Serratrice, 2013)

Specifically, towards the discovery of sensitive and quick clays that provide a hazardous situation, Sandven et al. (2015) have proposed a new NIFS soil identification technique, where NIFS = natural hazards, infrastructure, flooding, and slides. The technique is based on the usage of a cone resistance number, $N_{mc}$, which considers the effective preconsolidation stress effect, in addition to a revised porewater pressure ratio, $B_{q1}$ where $u_1$ porewater pressures are measured on the tip of the cone. The proposed charts are helpful to identify zones of brittle materials (S-I) and quick clays (S-II), as presented in **Figure 6.11**. The chart has two forms based on the position of the porewater pressure

transducer either measuring $u_1$ or $u_2$ hence, defining $B_{q1}$ or $B_{q2}$. The boundary of the zones is defined based on the corrected cone resistance number, $N_{mc}$ which is defined as:

$$N_{mc} = q_{net} / (\sigma_A' + a) \quad [6.4]$$

where: $q_{net}$ = net cone tip resistance = $q_{net} - \sigma_{vo}$

$\sigma_A'$ = reference stress taken as $\sigma_c'^{(m)}$. $\sigma_{vo}'^{(1-m)}$, with $\sigma_c'$: preconsolidation stress, $\sigma_{vo}'$: effective overburden stress and m: stress exponent to account for swelling (0.7 - 0.8).

a = attraction value to account for the depth effect, with small influence for z > 5 m

The revised pore pressure ratio, $B_{q1}$ is used to account for the effects of yield stress ratio and dilatancy properties. Since the shoulder $u_2$ reading is more common because of the cone tip resistance correction, the equivalent ratio can be computed from either $u_1$ or $u_2$ readings using:

$$B_{q1} = (u_1 - u_0) / q_{net} = [k_{clay} * (u_2 - u_0)] / q_{net} \quad [6.5]$$

where $k_{clay}$ = correction factor expressing the ratio between $\Delta u_1$ and $\Delta u_2$; specifically, for soft NC clay: k = 1.25, for medium soft clay: k = 1.50, and for dense OC clay: k = 1.90.

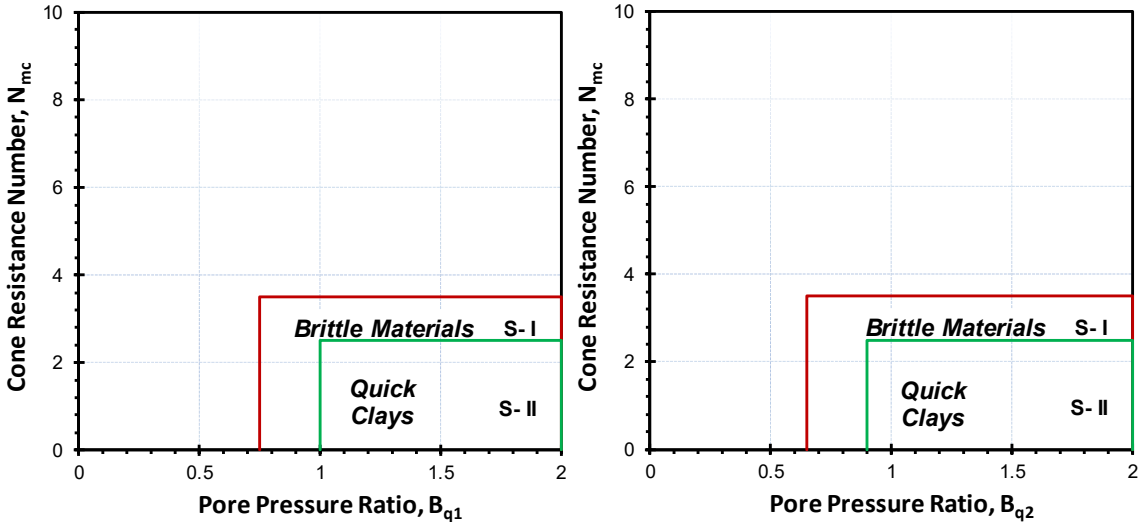


Figure 6.11. Identification Charts for Brittle & Sensitive Materials by Sandven el al. (NIFS, 2015)

Jefferies and Been (2016) modified the soil behavior type index that was originally introduced by Jefferies and Davies (1991), where they relied on a new dimensionless term $[Q\cdot(1 - B_q) + 1]$ in their classification chart and claimed that it captured soil behavior better than the conventional normalized cone tip resistance, Q, and their alternate parameter $[Q\cdot(1\text{-}B_q)]$, especially with silts, when plotted versus friction ratio as presented in **Figure 6.12**. The modified chart consists of 6 main soil zone which can be approximated into circles with a radius value obtained from the material behavior type index, $I_{c\,JB}$ where:

$$I_{c\,JB} = \sqrt{\left(3 - \log[Q\,(1 - B_q) + 1]\right)^2 + [1.5 + 1.3\log(F)]^2} \qquad [6.6]$$

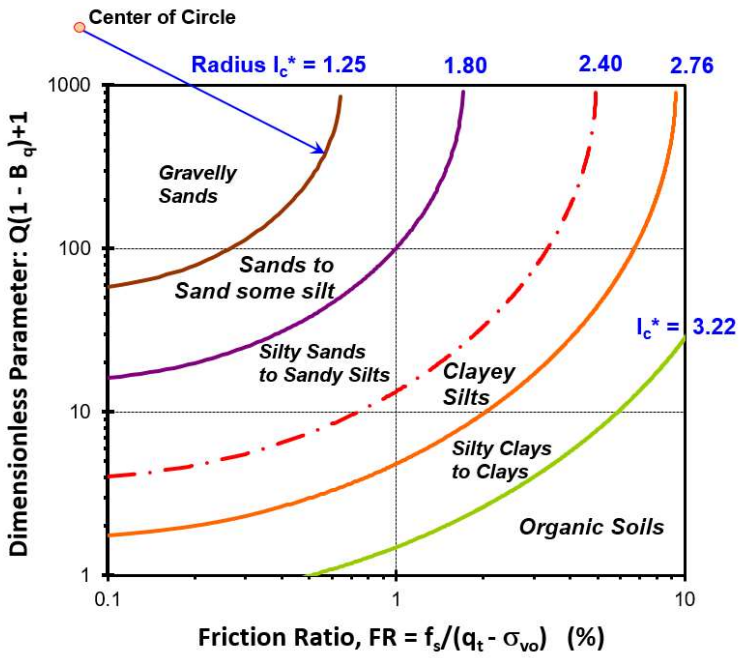


Figure 6.12. Modified soil profiling chart using $[Q\cdot(1 - B_q) + 1]$ vs. $F_r$
(after Jefferies and Been, 2016)

Valsson (2016), proposed a new 3-D model utilizing the 3 main readings from the piezocone simultaneously where better results were obtained by plotting on three axes rather than the conventional two axes diagrams. The proposed model plotted the variables:

normalized pore pressure ratio, $B_q$ (on a linear scale), sleeve friction, $f_s$ (on a logarithmic scale), and net cone tip resistance, $q_{tn}$ (on a logarithmic scale) as presented in **Figure 6.13**. The proposed model can be defined as a convex hull from the remaining points using an automated meshing algorithm (Valsson, 2016). The employed database contains results mainly from Norwegian clays and is not sufficient to accurately define a 3-D model for sensitive clays detection.

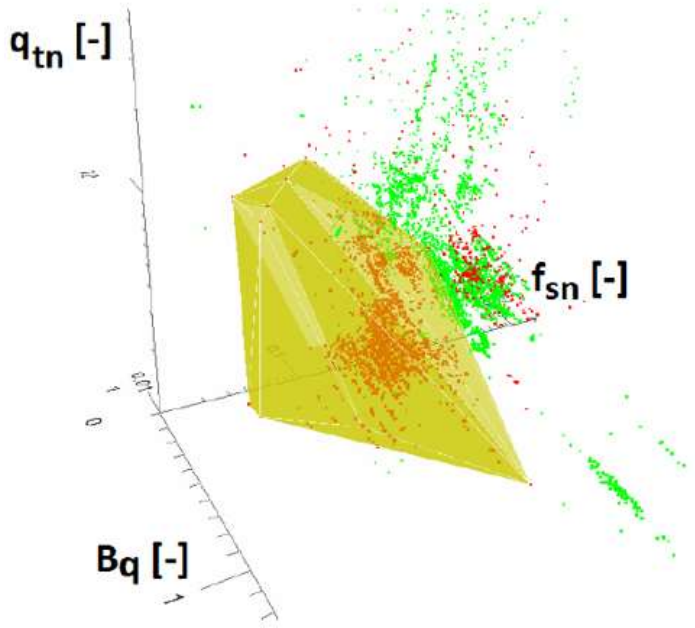


Figure 6.13. Proposed 3-D Quick Clay Detection Model by Valsson (2016)

Saye et al. (2017) proposed a new soil classification chart where the normalized cone tip resistance, Q is plotted against the sleeve friction normalized by effective vertical stress, $f_s/\sigma'_{vo}$ as presented in **Figure 6.14**. Plotting the data in Q vs. $f_s/\sigma'_{vo}$ space for a given soil gives a linear relationship with a slope designated $\Delta_Q$. By compiling the linear relationships from different soils with different stress history ranges and different origins, they converge to a common origin offsetting from zero which defines the starting point for

the 5 main soil types in the classification chart ranging from sands to silts to clays to organics and peat which are grouped based on typical Unified Soil Classification System (USCS) and $\Delta_Q$ values which can be related to soil index properties such as fines content, organic content, and Atterberg limits.

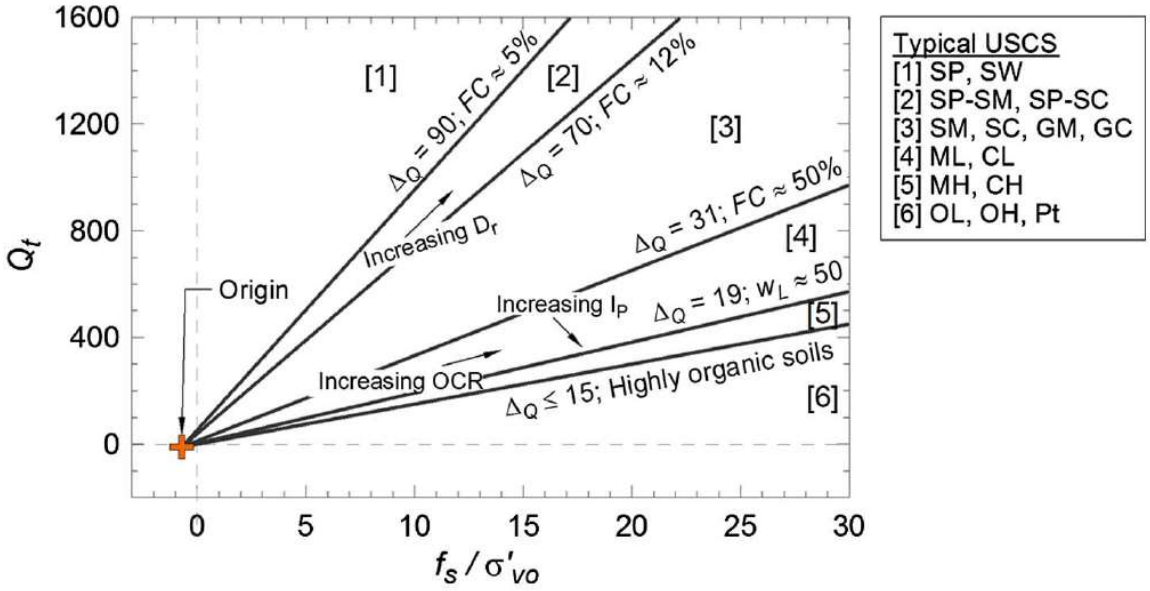


Figure 6.14. Design chart for soil classification using ΔQ index by Saye et al. (2017)

Finally, Eslami et al. (2017) suggested the usage of the three cone measurements ($q_t$, $f_s$, and $u_2$) simultaneously by introducing a new triangular-format chart resembling the USDA soil classification chart. The triangular chart presented in **Figure 6.15**, consists of 7 main soil zones ranging from sensitive soils to clays to silts to very dense sands by defining expected ranges for each of the 3 cone readings. This method is relatively new and has been applied to 54 case studies of deltaic soils.

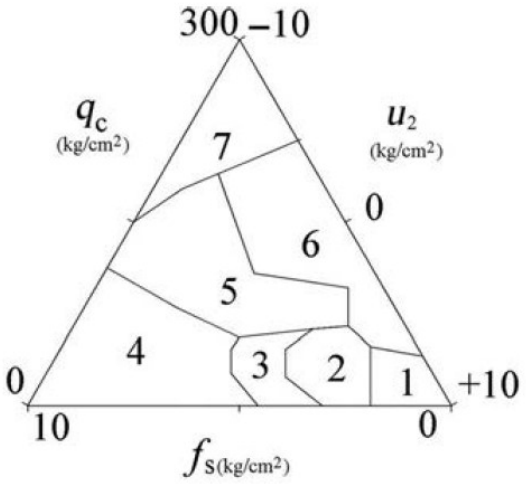


| 1 | 2 | 3 | 4 | 5 | 6 | 7 |
|---|---|---|---|---|---|---|
| Sensitive soils | Clays | Silts | Over consolidated clay | Mixed soils (clayey silt to sandy silt) | Sands | Very dense sand |

Figure 6.15. CPT Triangular Soil Classification Chart by Eslami et al. (2017)

## 6.3 Definition of Sensitive Clays

By considering the various soil classification schemes using CPT and CPTu data, it can be clearly noticed that not all soil behavior charts attempt to detect and identify soils having a special nature as sensitive fine-grained geomaterials (silts and/ or clays). Unstable slopes are abundant in Sweden, Norway, and Canada where many landslides with significant consequences are designated to occur in clays known to be quick or highly sensitive clay (Lundstrom et al., 2009). Sensitive clays have also been reported in Labrador (L'Heureux et al., 2014) and New England (Lutenegger, 2015). The designation of sensitive fine-grained soils applies to deposits that were originally sedimented in marine environments but later were leached by exposure to freshwater aquifers. This caused the clay particles to be edge versus face oriented not the conventional parallel orientation which explains the high-water content values with collapsible grain nature upon remodeling due to disturbance causing complete loss of shear strength (Valsson, 2016).

The sensitivity of any fine-grained soil is defined as:

$$S_t = \frac{s_u}{s_{ur}} \quad [6.7]$$

where $s_u$ is the peak undisturbed undrained shear strength and $s_{ur}$ is the remolded undrained shear strength value, both at the same water content.

The nature and abundance of sensitive and quick clays differ from one location to another. In Sweden, for instance, it is common to detect very sensitive clays, while in North America highly sensitive clays (with $S_t > 80$) are rare. Quick clays in Norway and Sweden are defined based on the value of their remolded undrained shear strength, where any clay with $s_{ur} < 0.5$ kPa is considered quick and can be considered in fluid state, while sensitive clays are defined based on both their sensitivity value; $S_t > 15$ and their remolded shear strength $s_{ur} < 2.0$ kPa (Lundstrom et al., 2009). In Canada and Northern USA, the boundaries are slightly different where sensitive clays are defined as clays with $s_{ur} < 1$ kPa having a liquidity index of more than 1.2 (Robitaille et al., 2002).

The main difference between quick and non-quick clays is the relation between water content, Atterberg limits, and clay activity where two clays may share the exact same mineralogy yet have completely different sensitivity values. Typically, for quick and sensitive clays, the natural water content value is higher than the liquid limit and the soil has relatively low plasticity indices. Hence, sensitivity is not associated with particle size distribution or mineralogy, it is dependent on the microstructure of the clay with all the physical, chemical and biological processes within the clay pore water (Talme et al., 1966).

Mitchell and Soga (2005) summarized the main causes/ mechanisms of sensitivity in soils with approximate upper limit of sensitivity values as follows: "*Sensitivity can be caused due to metastable fabric mechanism with approximate $S_t$ values ranging from 8 –*

*16, if cementation is the main cause of sensitivity then the expected range appears within extra quick soils with $S_t > 64$. In case that weathering is the main cause then the expected sensitivity range is low between 2 -4. In case of thixotropic hardening the clay is considered very sensitive. For leaching or ion exchange taking place in glacial or postglacial marine clays, the expected sensitivity for extra quick clays is very high > 64. Finally, in case of formation or addition of dispersing agents affecting inorganic clays, the expected sensitivity is very high for extra quick clays >64."*

### 6.4 Tests to Measure Clay Sensitivity

Different testing techniques are available for evaluating the sensitivity of fine-grained soils either in- situ or in the laboratory. Unconfined compression test is considered one of the oldest and simplest testing techniques for measuring the undrained shear strength. The test follows ASTM D-2166 where a cylindrical undisturbed intact specimen with height to diameter ratio of around 2.5 is subjected to unconfined axial loading with maximum stress value defining the unconfined undrained undisturbed shear strength. The same procedure is followed on the same specimen after remolding at the same moisture content to obtain the remolded shear strength, hence, the sensitivity is calculated as:

$$S_t = \frac{s_{u-UC}(undisturbe\ d)}{s_{u-UC}(remolded)} \quad [6.8]$$

This method is not applicable for highly sensitive clays having a liquidity index approaching one as it will be difficult to remold the specimens. Moreover, even though simple, the UC is only a basic index test. Its use in measuring $S_t$ should be avoided.

Another commonly used technique is the field vane test (FVT), where a four-bladed vane is pushed into the ground and a torque is applied for measuring undrained shear

strength following ASTM D-2573. The geometry (height H, width D, and thickness t) and the shape of the blade (top taper, bottom taper, rectangular) can affect the expression for quantifying the undrained shear strength. For instance, in the case of a rectangular vane (H/D = 2) subjected to uniform shear stresses:

$$S_{u-FV} = \frac{6 \cdot T_{\max}}{7 \cdot \pi \cdot D^3} \quad [6.9]$$

where $T_{max}$ is the maximum applied torque value and D is the diameter of the used vane. After determining the maximum applied torque for the peak undisturbed shear strength, the remolded undrained shear strength value is determined by measuring the torque value after ten revolutions. Hence, sensitivity can be evaluated as:

$$S_t = \frac{s_{u-FV}(undisturbe\,d)}{s_{u-FV}(remolded)} \quad [6.10]$$

A similar testing procedure can be conducted in laboratories using a mini-laboratory vane test (LVT) following ASTM D-4648. A miniature four-bladed vane is pushed into an intact soil specimen cut from a soil tube and then an applied torque is recorded to measure the undrained shear strength value. The test is repeated after the soil specimen is remolded.

Another frequently-used testing device for sensitivity measurements is the fall cone (FC), where a cone of well-known geometry, mass, and height is released to fall freely and penetrate the surface of the tested soil specimen. The penetration depth is recorded and converted to undrained shear strength following Hansbo (1957):

$$S_u = \frac{k \cdot Q}{H^2} \quad [6.11]$$

where Q is the cone weight, H is the measured penetration depth, and k is a cone constant dependent on the geometry ($\alpha$ = 30°, 60°, etc). The same procedure can be applied to both undisturbed and remolded specimens to measure the respective undrained shear strengths.

Abuhajar et al. (2010) considered the variety of $S_t$ measurement techniques and compared their relative assessment by plotting the trends of sensitivity value versus the corresponding liquidity index (LI) for different datasets, as presented in **Figure 6.16.** It is evident that the various testing techniques measure different undrained shear strengths and hence their sensitivity ranges. For instance, for a clay with liquidity index value of 1.6, the sensitivity can be any value ranging from 10 to 100 depending on the testing method. In general, the fall cone method provides the upper and lower bounds for all testing methods. For comparison, the trends obtained from 5 different testing techniques are compared to an empirical correlation proposed by Bjerrum (1954) relating $S_t$ to LI:

$$S_t = \exp(\alpha \cdot LI) \quad [6.12]$$

where $\alpha \approx 2$ and this value is related to the mineralogy and the stress history of the soil under study.

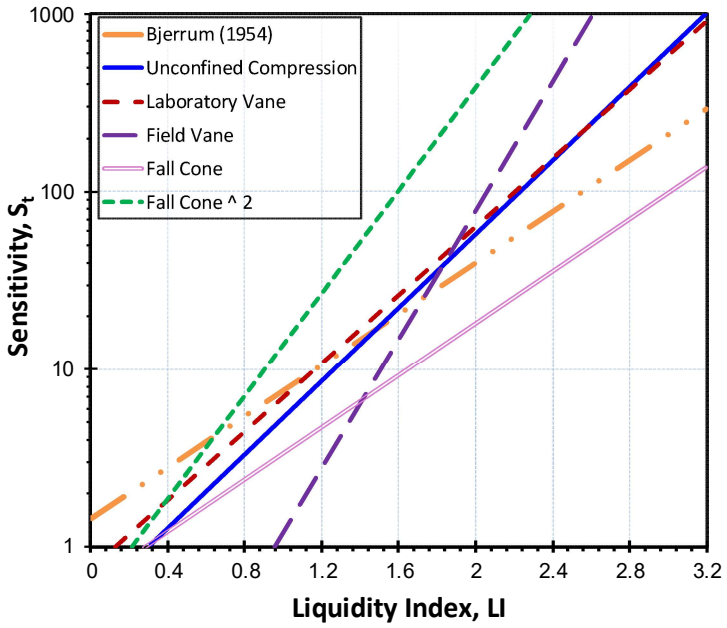


Figure 6.16. Trends between measured sensitivity ($S_t$) and liquidity index (LI) using 6 test methods (modified after Abuhajar et al., 2010)

Given the difficulty of obtaining undisturbed samples and then subsequently testing them carefully in the lab, it has been thought to determine the sensitivity values of clays using in.situ measurements such as performing rotary pressure soundings followed by field vane testing (Sandven et al. 2015).

Alternatively, it has been suggested that cone penetration testing can be used where the measured sleeve friction can be used to give guidance for remolded shear strength value, where $f_s \approx s_{ur}$, however, this requires cones with high accuracy in the sleeve friction measurements which is not always feasible. As the cone tip resistance provides the peak strength evaluation, the sensitivity is found from the friction ratio ($R_f$):

$$S_t = \frac{N_s}{R_f(\%)} \qquad [6.13]$$

where Lunne et al. (1997) recommend using $N_s$ value of 7.5. More recently, Robertson & Cabal (2016) suggested estimating the sensitivity value using the normalized friction ratio ($F_R$) and an adopted cone bearing factor ($N_{kt}$ =15) as follows:

$$S_t = \frac{s_u}{s_{ur}} = \frac{q_t - \sigma_{vo}}{N_{kt}} \left( \frac{1}{f_s} \right) = \frac{7}{F_R} \quad [6.14]$$

Full flow penetrometers, such as the ball and T-bar penetrometer, have been developed for the in-situ determination of undrained shear strength in very soft soils and hence can be used to evaluate the sensitivity (Yafrate and DeJong 2006). Using full flow penetrometers can be more reliable in very soft clays for three reasons: (a) no need for net reading with overburden stress; (b) magnitudes of porewater pressure corrections for tip resistance are much less than CPT and CPTu; and (c) electronic load cells are better utilized in their operable ranges of accuracy. The ball and T-bar tests depend on measured penetration resistance for evaluating undrained shear strength:

$$s_u = \frac{q}{N} \quad [6.15]$$

where q is the in-situ measured penetration resistance and N is a bearing factor for shear strength that is established from theoretical solutions and calibrated using either laboratory tests or field vane tests (Randolph 2004).

Remolded shear strength can also be computed using a similar expression but by measuring the remolded penetration resistance ($q_{rem}$) which is obtained after repeated loading the full flow penetrometer for 10 cycles to achieve adequate remolding. It is worth noting that the bearing factor for intact specimens (N) was experimentally found different from the values for remolded ones ($N_{rem}$). Hence, the sensitivity from full flow penetrometers is calculated as:

$$S_t = \frac{(q / N)}{(q_{rem} / N_{rem})} \quad [6.16]$$

In summary, based on current practices, the most reliable laboratory means of assigning $S_t$ to a given clay appears to be the fall cone test and the most reliable field test is the ball penetrometer (DeJong et al. 2011).

## 6.5 Use of SBT Charts for Identifying Sensitive Clays

Sensitive and quick clays require special attention and are not easily and always successfully detected using CPT data with SBT charts. Some CPT classification schemes do not even include any category of sensitive geomaterial zones, while schemes that include a sensitive soil zone often fail in carefully identifying the sensitive or quick clay layer, as well as show conflicting results amongst each other (e.g., Tilahun 2013; Shahri et al. 2015; Valsson 2016).

To illustrate the shortcomings of the common and popular SBT charts, data from the sensitive clay at Quyon, Québec will be used (Wang et al. 2015a). Quyon is the site of a large landslide located within the Champlain Sea clay deposits which are characterized as very sensitive Leda clay. **Figure 6.17** presents a representative CPTu sounding that is used in testing the various SBT charts (Wang et al. 2015b). The raw CPTu readings ($q_t$, $f_s$, $u_2$), post-processed values (FR and $q_E$), along with their normalized parameters (Q, F, and $B_q$) are evaluated and plotted into five different soil classification schemes that presumably identified sensitive fine-grained soils, as presented in **Figure 6.18**.

From the plotted CPTu data, it can be clearly seen that common SBT charts do not capture and identify these sensitive clays. For Quyon, the 12-zone and 9-zone SBT charts classify the soils as "clay/silt mix" and fail to lie within zone 1 associated with sensitive clays and silts. As for the Douglas and Olsen (1981) chart, the soil is classified to lie mostly

with "meta-stable sands" with a few data points falling in "sensitive mixed soils" zones. For the Unicone chart (Eslami and Fellenius 1997), the soils from Quyon identify as mostly as "soft clay - soft silt", with a few dots falling in the "sensitive" soils region. Schneider et al. (2012) chart classified it between zones 1b and 1c between clays and sensitive clays.

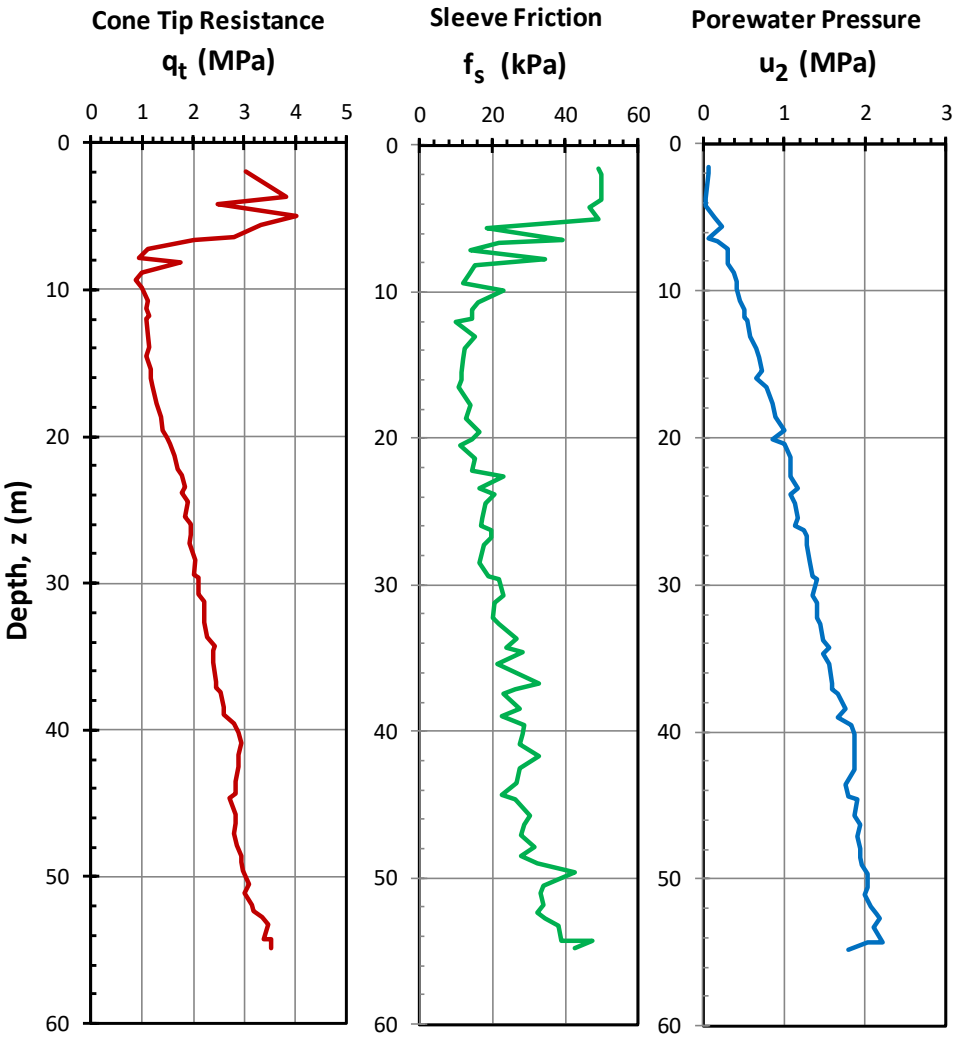


Figure 6.17. CPTu Sounding at Quyon, Québec (Wang et al., 2015a)

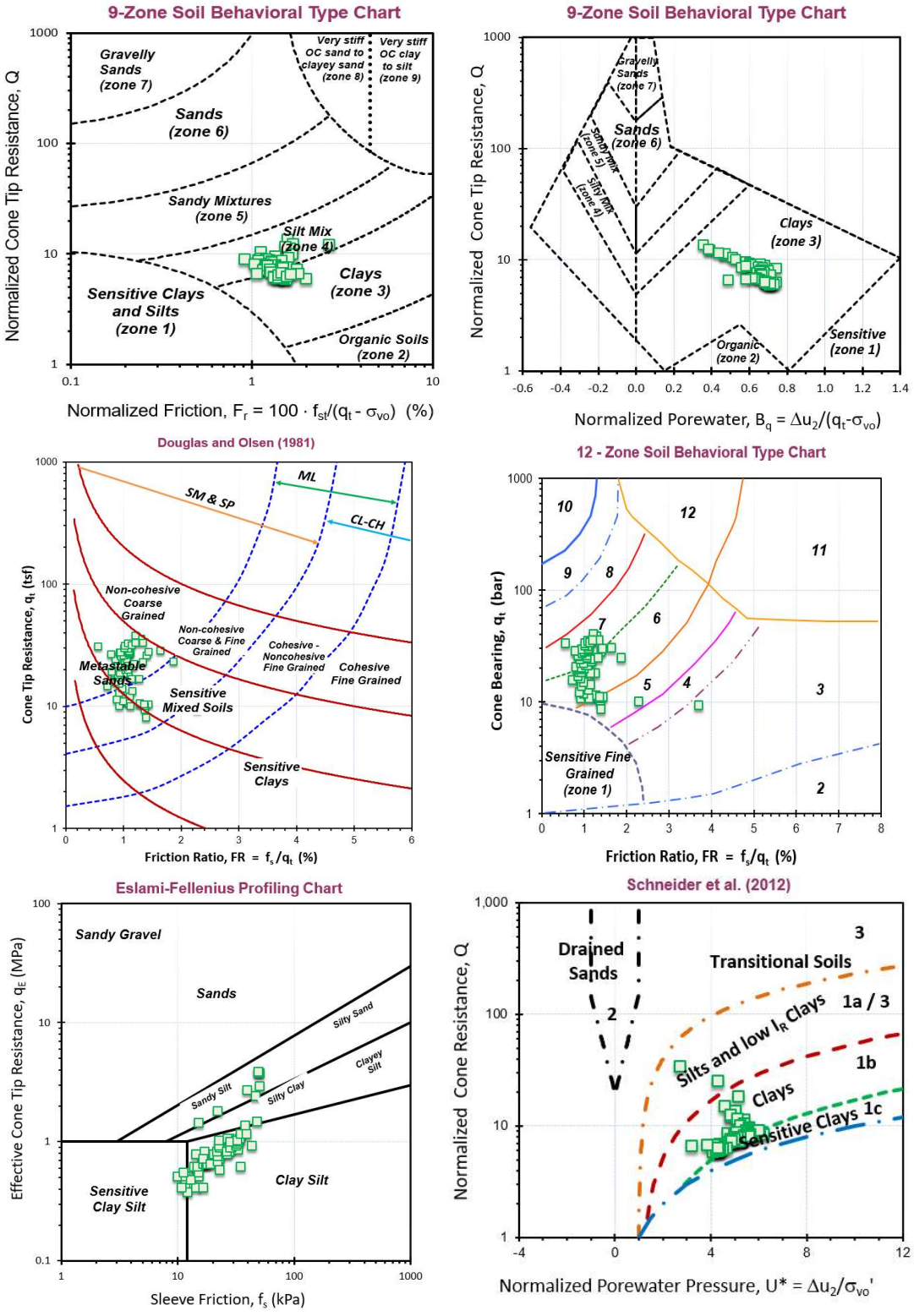


Figure 6.18. Quyon sensitive clay classification from CPTu data using various SBT Charts

To overcome major shortcomings in the detection and identification of sensitive clays, one should rely on additional measurements. The seismic piezocone (SCPTu) can be a versatile tool in this regard as it collects the three penetrometer readings ($q_t$, $f_s$, and $u_2$) as well as a fourth profile of downhole shear wave velocity ($V_{sVH}$) with depth.

## 6.6 Estimating Shear Wave Velocity from CPTu Readings

The relationship between shear wave velocity ($V_s$) and piezocone data has been extensively investigated by researchers over the past few decades. **Table 6.2** presents a brief selection of available correlations relating shear wave velocity to the CPT readings. From the presented correlations, it can be observed that some correlations are soil type dependent (i.e., applicable to either sands or clays), some correlations are local and are based on specific geologies and site conditions, hence not applicable globally, and finally, none of the correlations is solely addressing sensitive and quick clays in North America.

To check the suitability of the available correlations for estimating shear wave velocity in sensitive clays from North America, two sensitive clays with SCPTu measurements were selected: (a) Quyon site that consists of sensitive Champlain Sea (Leda) clay from Québec; and (b) Massey Tunnel Site which contains a sensitive silty clay layer in British Columbia. The Massey site includes a very deep SCPTu sounding of 168 m. Measured readings from the two seismic piezocone soundings ($q_t$, $f_s$, $u_2$ and $V_s$) are presented in detail in **Appendix G**.

Several correlative methods from **Table 6.2** were selected to estimate the $V_s$ profile that were then compared to the measured values, as presented in **Figure 6.19** for Quyon and in **Figure 6.20** for Massey Tunnel. Also shown in these figures is the soil classification plot with depth based on CPT material index ($I_c$) to indicate the sand and clay layers. For

both sites, it can be clearly observed that the conventional correlations are not applicable in these sensitive Canadian clays and that the available correlative trends provide a wide range of estimated shear wave velocity. For instance, for Quyon clay at depth of 40 m, the estimated shear wave velocities from various correlative algorithms range from 145 to 365 m/s which is nearly a factor of 2.5. The true measured $V_s$ at 40 m is about 275 m/s.

A similar situation applies for the sensitive clay layer at the Massey Tunnel site in **Figure 6.20**, where at depth of 100 m, the predicted shear wave from various methodologies ranges from about 140 m/s to around 600 m/s, which is a factor of 4.25. The actual measured value by SCPTu at 100 m was in fact $V_s$ = 330 m/s. Hence, special correlations for sensitive clays in North America are needed.

## 6.7 Use of SCPTu in Identification of Sensitive Clays

To be able to detect the presence of sensitive or quick clay at the site under study, one should first try using several of the conventional global correlations, such as those presented in **Table 6.2**. In a study funded by the Pacific Earthquake Engineering Research (PEER) Center, Wair et al. (2012) reviewed various $V_s$-CPT relationships, and subsequently recommended using an average $V_s$ profile in Quaternary soils based on the following expressions: (a) Mayne (2006); (b) Andrus et al. (2007); and (c) Robertson (2009). This procedure can be recommended herein, or alternatively, the use of all 3 methods above can be implemented.

In the second step, compare the estimated shear wave velocity profiles with the actual in-situ measured $V_s$. If the profiles agree, then the clay under study is more likely to be a "normal" or "well-behaved" clay of low to medium sensitivity value. However, if

the estimated values differ more than 25% from the measured ones, then the clay is most likely anomalous, perhaps quick or sensitive. A follow-up study using borings to obtain samples and a series of field vanes, ball penetrometer tests, and/or lab fall cone tests would be warranted to confirm or repudiate the findings.

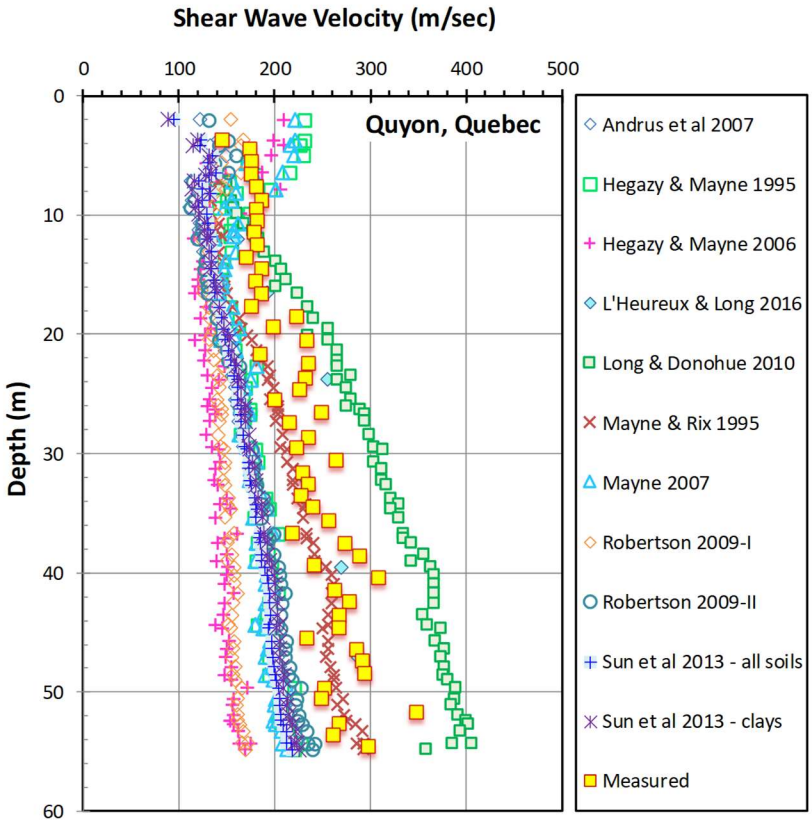


Figure 6.19. Measured and predicted shear wave velocity profiles using different correlative methods at Quyon, Québec

Table 6.2. Selected Relationships for Estimating Shear Wave Velocity from CPTu Data

| **Reference** | **$V_s$ – CPTu Relationship** | **Comments** |
|---|---|---|
| Jaime & Romo (1988) | $V_s(m/s) \approx 0.1\ q_c(kPa)$ | Mexico City Clays only |
| Hegazy & Mayne (1995) | $V_s = (10.1 \log q_c - 11.4)^{1.67} \cdot \left(\frac{f_s}{q_c} \cdot 100\right)^{0.3}$ where $V_s$ in m/s and $q_c$ and $f_s$ in kPa | 30 worldwide sites for all soil types (Most CPT data have $q_t$, but only $q_c$ were available at a few sites) |
| Mayne & Rix (1995) | $V_s(m/s) = 1.75 \cdot (q_t)^{0.627}$ where $q_t$ in kPa | 31 worldwide clays - intact & fissured |
| Piratheepan (2002) | $V_s = 11.9 \cdot (q_c)^{0.269} \cdot (f_s)^{0.108} \cdot D^{0.127}$ where $V_s$ in m/s, D (depth) m, $q_c$ &$f_s$ kPa | All soil types - USA, Canada & Japan |
| Hegazy & Mayne (2006) | $V_s = 0.083 \cdot q_{c1N} \cdot \left(\frac{\sigma'_v}{P_a}\right)^{0.25} \cdot e^{1.786 \cdot I_c}$ where $V_s$ in m/s, $q_{c1N}$ = Q (normalized tip resistance) and $P_a$: atmospheric pressure | 73 worldwide sites covering all soil types |
| Andrus et al. (2007) | $V_s = 2.27 \cdot (q_t)^{0.412} \cdot (I_c)^{0.99} \cdot D^{0.033} \cdot ASF$ where $V_s$ in m/s, D (depth) in m, ASF: age scaling factor (0.92 – 1.12) | Soils from California, South Carolina, Japan |
| Mayne (2007a) | $V_s = 56.1 \cdot \ln(f_s) + 18.5$ where $V_s$ in m/s and $f_s$ in kPa | Global database (731 data points) sands, silts, clays |
| Robertson (2009) | $V_s = (\alpha_{vs} \cdot Q)^{0.5} \cdot \left(\frac{\sigma'_v}{P_a}\right)^{0.25}$<br>$V_s = \sqrt{\alpha_{vs} \cdot (q_t - \sigma_v)/P_a}$<br>where $V_s$ in m/s, $\alpha_{vs} = 10^{0.55 \cdot I_c + 1.68}$ | Uncemented Soils mainly from California |
| Long & Donohue (2010) | $V_s = 1.961 \cdot (q_t)^{0.579} \cdot (1 + B_q)^{1.202}$ where $V_s$ in m/s and $q_t$ in kPa | 10 Norwegian soft clays |
| Sun et al. (2013) | $V_s = \frac{14.716 \cdot (q_t)^{0.168} \cdot (\sigma'_v)^{0.246}}{(f_s)^{0.108} \cdot (1 + B_q)^{0.126}}$ | Korean - clays |
| | $V_s = \frac{24.215 \cdot (q_t)^{0.091} \cdot (f_s)^{0.037} \cdot (\sigma'_v)^{0.232}}{(1 + B_q)^{0.181}}$ where $V_s$ in m/s and $q_t$ $f_s$ and $\sigma'_v$ in kPa | Korean - all soil deposits |
| Cai et al. (2014) | $V_s = 4.541 \cdot (q_t)^{0.487} \cdot (1 + B_q)^{0.337}$ where $V_s$ in m/s and $q_t$ in kPa | Soft Chinese clays |

| Reference | $V_s$ – CPTu Relationship | Comments |
|---|---|---|
| L'Heureux & Long (2016) | $V_s = 71.7\ (q_{net})^{0.09} \cdot \left(\frac{\sigma'_v}{w}\right)^{0.33}$ where $V_s$ in m/s, w (water content) and $q_{net}$ in kPa | 29 Norwegian soft clays |
| Shahri & Naderi (2016) | $V_s = 3.839 \cdot (q_t)^{0.5151} \cdot (1 + B_q)^{0.174}$ where $V_s$ in m/s and $q_t$ in kPa | Clays – Southwest Sweden |

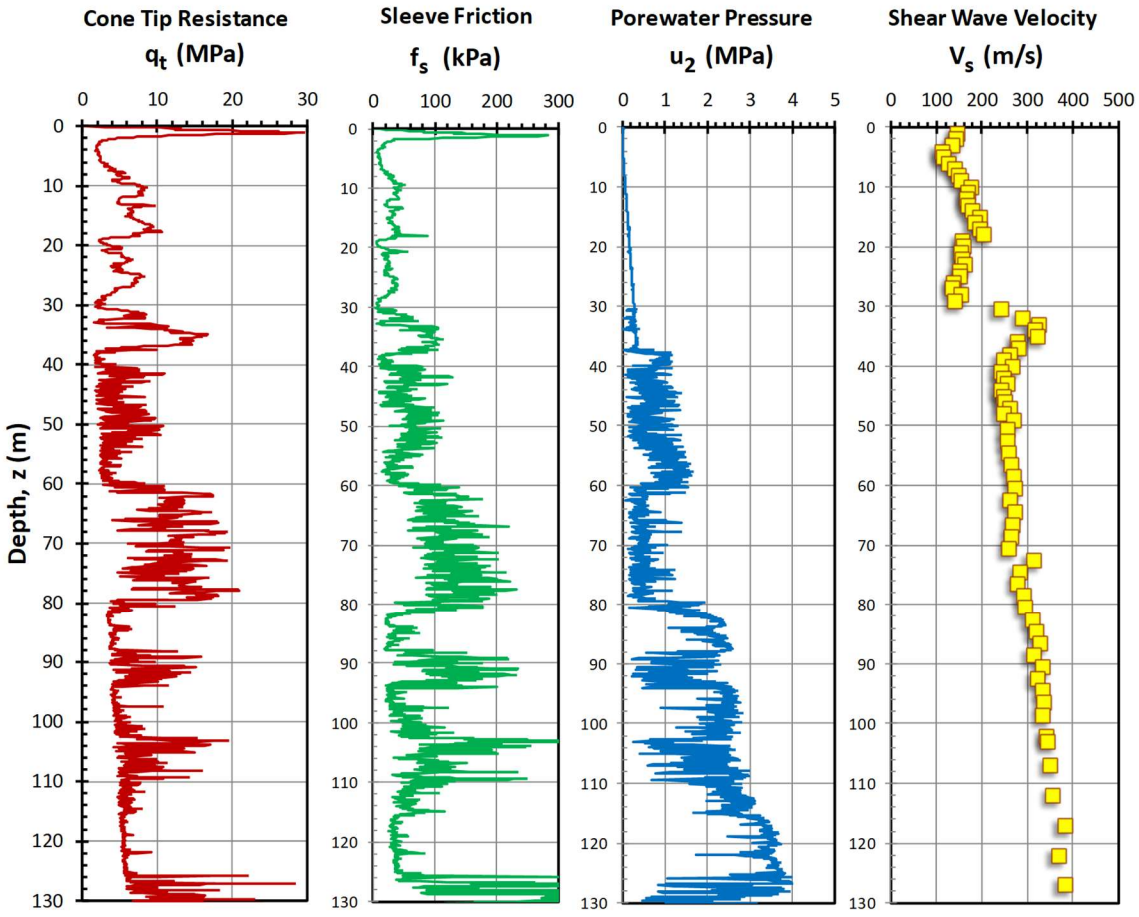


Figure 6.20 a. Seismic piezocone sounding at Massey Tunnel site, BC: (a) cone tip resistance, (b) sleeve friction, (c) porewater pressure, (d) shear wave velocity

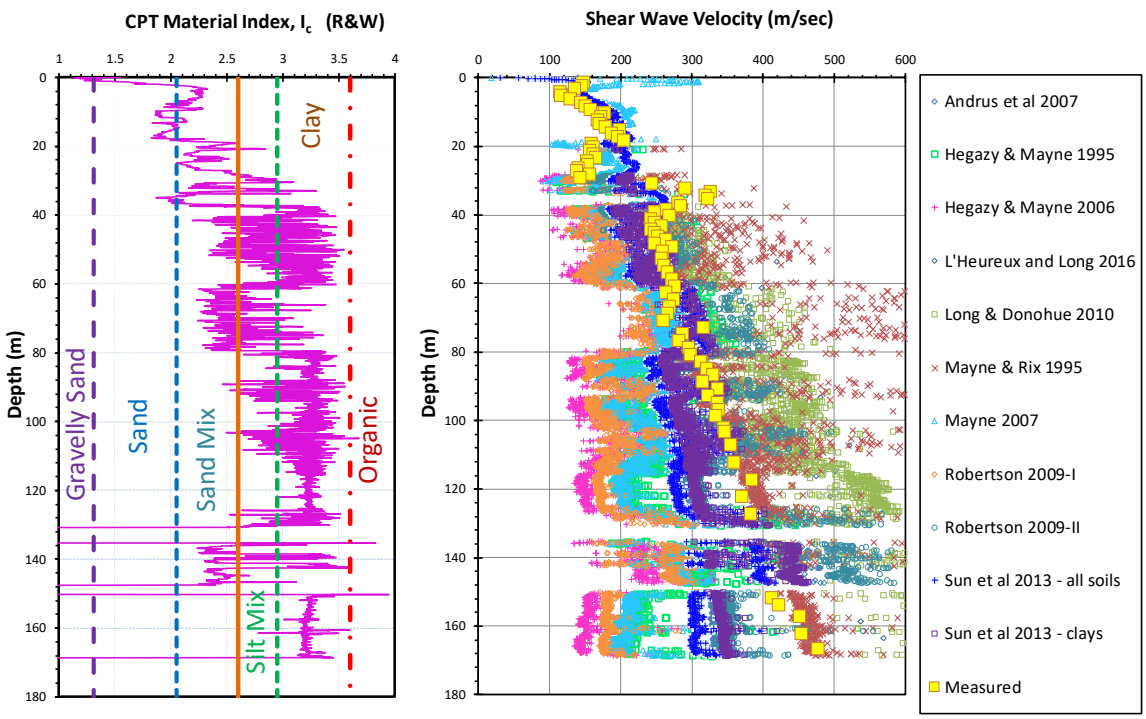


Figure 6.20 b. Profiles at Massey Tunnel site, BC: (a) soil classification based on CPT material index ($I_c$) and (b) measured and predicted $V_s$ profiles using different correlations

## 6.8 Estimating Shear Wave Velocity for Sensitive Clays

To validate the methodology, a special database of 20 sensitive clays with SCPTu soundings have been collected from North American clay sites, as presented in **Table 6.3**. The sensitive clay sites under study are mainly from the vicinity of British Columbia and Québec, with a few sites from Illinois, Maine, Massachusetts, and Idaho. The individual SCPTu soundings along with lab water content measurements for the compiled database are presented in **Appendix G.**

To test the suitability of the earlier proposed correlations with the compiled sensitive database, four well-established correlations were picked and applied to estimate shear wave velocity. **Figure 6.21** presents the measured versus predicted plots using the

correlations by Hegazy & Mayne (1995); Andrus et al. (2007); Robertson (2009); and Long & Donohue (2010). It can be clearly observed that the conventional methods are not working well for the special collected database, since the measured versus predicted plots trends have low coefficients of determination ($r^2$) and high values for the SEY (standard error of the y-estimator). It is evident that the expression of Long & Donohue (2010) generally overestimates the $V_s$, while in contrast, the algorithm of Hegazy & Mayne (1995) underestimates the values. Hence, new correlations addressing the special nature of sensitive clays are desired.

Further detailed predictions for each of the 20 sensitive clays using 12 different correlations from those listed in Table 6.2 are plotted in **Appendix G**, showing the overall general unsuitability of the conventional correlations in estimating $V_s$ within the sensitive clays deposits.

Table 6.3. Special SCPTu Database of Sensitive Clays in North America

| **Sensitive Clay** | **Location** | **Description** | **Water Content (%)** | **Sensitivity ($S_t$)** | **References** |
|---|---|---|---|---|---|
| Amherst | Connecticut Valley, Massachusetts | Varved clay and silt | 28 – 66 | 5 – 25 | Hegazy (1998) DeGroot & Lutenegger (2003) |
| Colebrook Overpass | Surrey, British Columbia | Marine clayey silt-silty clay | 38 – 49 | 10 –70 | Crawford and Campanella (1991); Weech (2002) |
| Dyke Road | Richmond, BC | Silt, clayey silt | 36 – 41 | 5 – 25 | Cruz (2009) |
| Ford Design Center | Evanston, Illinois | Glacial Till | 13 – 48 | 2 – 5 | Mayne (2007 b) |
| Gloucester | Southeast Ottawa, Ontario | Leda clay | 21 – 98 | 20 – 100 | Styler & Mayne (2013) |
| Golden Ears Bridge | Langley, BC | Stiff silty clay | 36 – 76 | 6 – 36 ‡ | Amini et al. (2008) |
| Haney | British Columbia | Soft clay | 41 – 44 | 3 – 13 | Vaid (1971); Woeller (2004) |

| Sensitive Clay | Location | Description | Water Content (%) | Sensitivity ($S_t$) | References |
|---|---|---|---|---|---|
| Louiseville | Québec | Firm highly plastic clay | 67 – 81 | 20 – 22 | Yafrate & DeJong (2006) |
| Martin's PointBridge | Maine | Presumpscot Clay | 24 – 42 | 2.1 – 19.6 | Hardison (2015) |
| Massey Tunnel | Delta, BC | Silty clay - clayey silt | 24 – 51 | 2 – 14 [X] | Kong (2015) |
| McDonald's Farm | Vancouver | Sand - soft clayey silt | 23 – 40 | 2 – 7 | Campanella et al. (1986) |
| Newbury | Massachusetts | Boston Blue Clay | 40 – 60 | 2 – 32 | Landon (2007) |
| Pier Park | Richmond, BC | Soft - firm silt & clay | 30 – 40 | 3 – 26 | Christian et al. (1998) |
| Quyon | Québec | Champlain Sea clay | 25 – 48 | 3 – 9 | Wang et al. (2015) |
| Route 197 Bridge | Maine | Presumpscot Clay | 33 – 47 | 7.5 – 45 | Hardison (2015) |
| Route 26 /100 | Maine | Presumpscot Clay | 25 – 42 | 9 – 268 | Hardison (2015) |
| Sandpoint | Idaho | Post-glacial alluvial deposit | 31 – 55 | 5 – 8 | Altaee & Fellenius (2002) |
| St. Alban* | Québec | Soft silty marine clay | 44–100 | 8 – 22 | LaRochelle et al. (1974); Lefebvre et al. (1994); Leroueil et al. (1995) |
| Vancouver | British Columbia | Sand - soft silty clay | NA | 2 – 12 [X] | Mayne & Woeller (2015) |

Notes: ‡ Remolded undrained shear strength values are obtained from liquidity index, LI as per Leroueil & Hight (2003): $s_{ur}$ (kPa)= 1 / (LI – 0.21)$^2$

[X] Sensitivity values are evaluated based on normalized friction ratio, $F_R$ as per Robertson & Cabal (2016): $S_t = 7 / F_R$.

* $V_s$ is measured using spectral analyses of surface waves (SASW) and sleeve friction, $f_s$ is measured using Laval piezocone with $f_s \approx 0.1(q_t – \sigma_{v0})$ as per Leroueil et al. (1995).

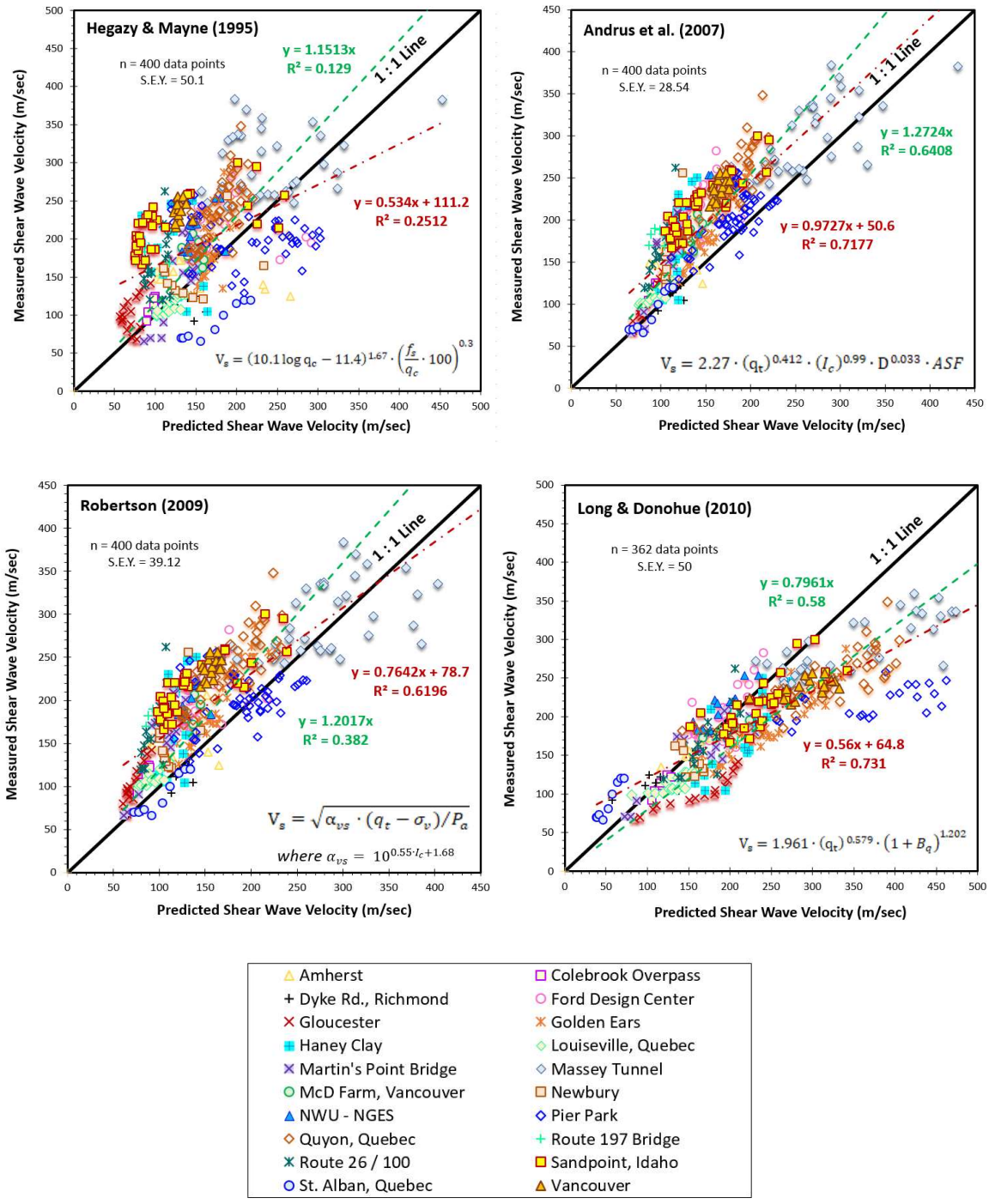


Figure 6.21. Measured versus predicted shear wave velocity profiles for compiled database using: a) Hegazy & Mayne (1995); b) Andrus et al. (2007); c) Robertson (2009); and d) Long & Donohue (2010)

By careful examination of the individual predictions for each clay presented in **Appendix G**, it was observed that two recent correlations provided better estimates for most of the clay sites. This involves the correlation by Sun et al. (2013) mainly addressing Korean clays and utilizing the 3 main readings of the piezocone in terms of $q_t$, $f_s$, and $B_q$:

$$V_s = 14.716 \cdot \frac{(q_t)^{0.168} \cdot (\sigma'_v)^{0.246}}{(f_s)^{0.108} \cdot (1+B_q)^{0.126}} \quad [6.17]$$

With cone tip resistance, sleeve friction and effective vertical stress in kPa. Also, the correlation introduced by L'Heureux & Long (2016) addressing Norwegian quick clays, in addition to other non-quick soft clays, provided reasonable estimates utilizing net cone tip resistance and the corresponding measured water content value which can be more challenging and inconvenient to obtain in case of absence of laboratory tested specimens.

$$V_s = 71.7 \cdot (q_{net})^{0.09} \cdot \left(\frac{\sigma'_v}{w_n}\right)^{0.33} \quad [6.18]$$

With net cone tip resistance and effective vertical stress in kPa.

**Figure 6.22** presents the measured versus predicted plots using the correlations by Sun et al. (2013) and L'Heureux & Long (2016) for the compiled database, where a noticeable improvement in the predictions is presented with higher coefficients of determination and lower values in S.E.Y. However, further, improvement may be possible. From a practical viewpoint, the NGI correlation will not normally be pragmatic since water contents are not available from CPTu data. However, use of a dielectric piezocone or resistivity piezocone may be able to provide information about volumetric water content, which is easily converted to gravimetric water content for saturated soils below the groundwater table.

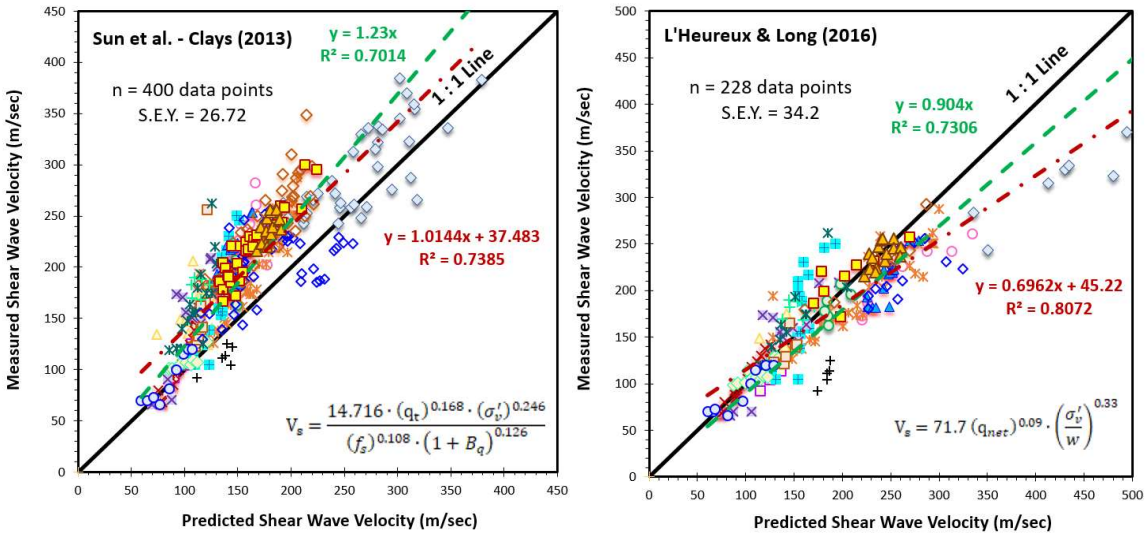


Figure 6.22. Measured versus predicted shear wave velocity profiles for compiled database using: a) KIGAM equation (Sun et al. 2013); b) NGI expression (L'Heureux & Long 2016)

Following the same equation formats as the ones proposed by Sun et al. (2013) and L'Heureux & Long (2016), two modified correlations were introduced by altering the coefficients and the exponents in the original equations to specially predict shear wave velocity for sensitive clays in Northern USA and Canada. The two modified proposed correlations are given by:

$$V_s = 16 \cdot \frac{(q_t)^{0.16}}{(f_s)^{0.015}} \cdot \frac{(\sigma'_{vo})^{0.255}}{(1+B_q)^{0.02}} \quad [6.19]$$

$$V_s = 75 \cdot (q_{net})^{0.1} \cdot \left(\frac{\sigma'_{vo}}{W_n}\right)^{0.2} \quad [6.20]$$

with net cone tip resistance ($q_{net}$) in kPa, effective vertical stress ($\sigma'_{vo}$) in kPa.

**Equation 6.19** depends on the 3 main readings of CPTu while **Equation 6.20** can be used if samples are available for laboratory water content measurement. The two proposed modified equations were applied to the Golden Ears Bridge location at Langley, British Columbia. The raw SCPTu data and water content measurements are presented in

Appendix G. The predicted shear wave velocity profiles using the two equations were compared to the downhole measured profile as presented in **Figure 6.23** showing an excellent agreement between the measured and predicted values.

**Figure 6.24** presents the measured versus predicted values for the entire compiled database using the two new proposed correlations. For both expressions, very good statistical agreement can be observed for the sites under study with much narrower scatter, higher coefficients of determination values, and lower S.E.Y values, when compared to the relationships by Sun et al. (2013); and L'Heureux and Long (2016).

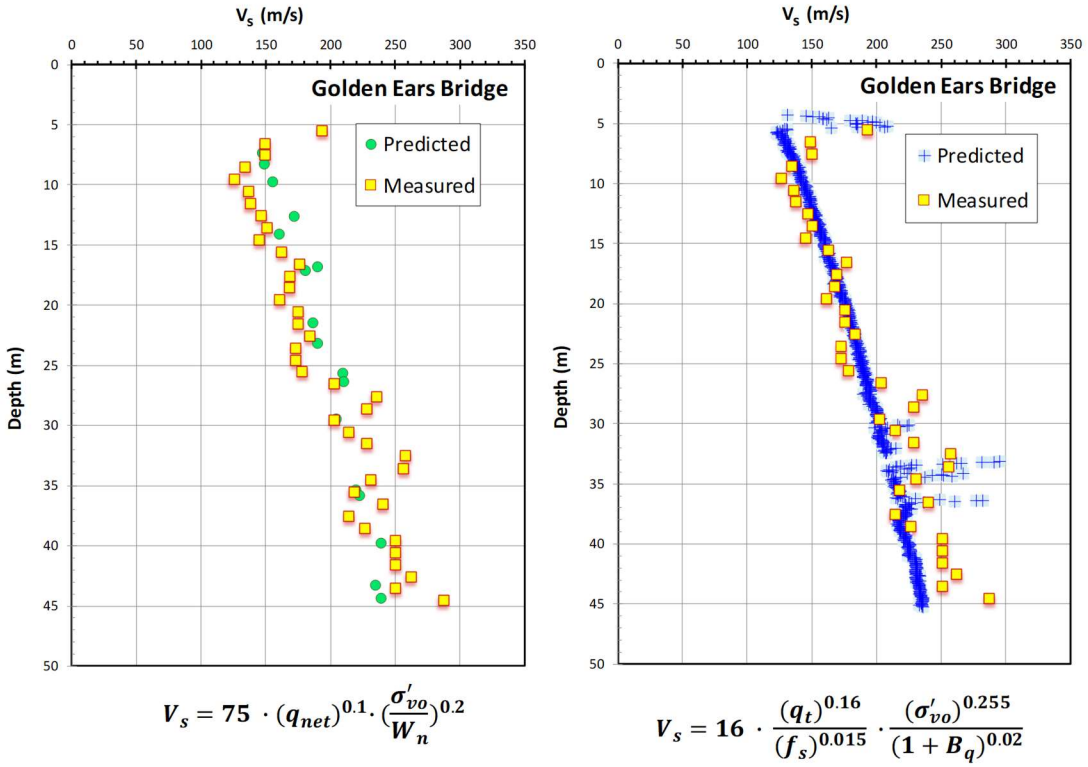


Figure 6.23. Measured and predicted shear wave velocity profiles using the two proposed modified correlations for Golden Ears Bridge, Langley, BC

## 6.9 Conclusions

Conventional soil behavioral type (SBT) classification systems using CPTu data often perform unreliably in detecting sensitive and quick clays during routine site exploration. Hence, a new SCPTu means for identifying sensitive clays is investigated by relying on shear wave velocity values estimated from the piezocone measurements which are in turn compared with the actual measured $V_s$ profiles. If the two profiles appreciably differ, then there is cause to require further site testing and confirm or deny the presence and occurrence of sensitive soils.

Previously published correlations are not suitable for the sensitive clays under study, hence, a special database of sensitive clays from Northern USA and Canada has been collected and used to develop two modified correlations for estimating shear wave velocity in sensitive clays are introduced.

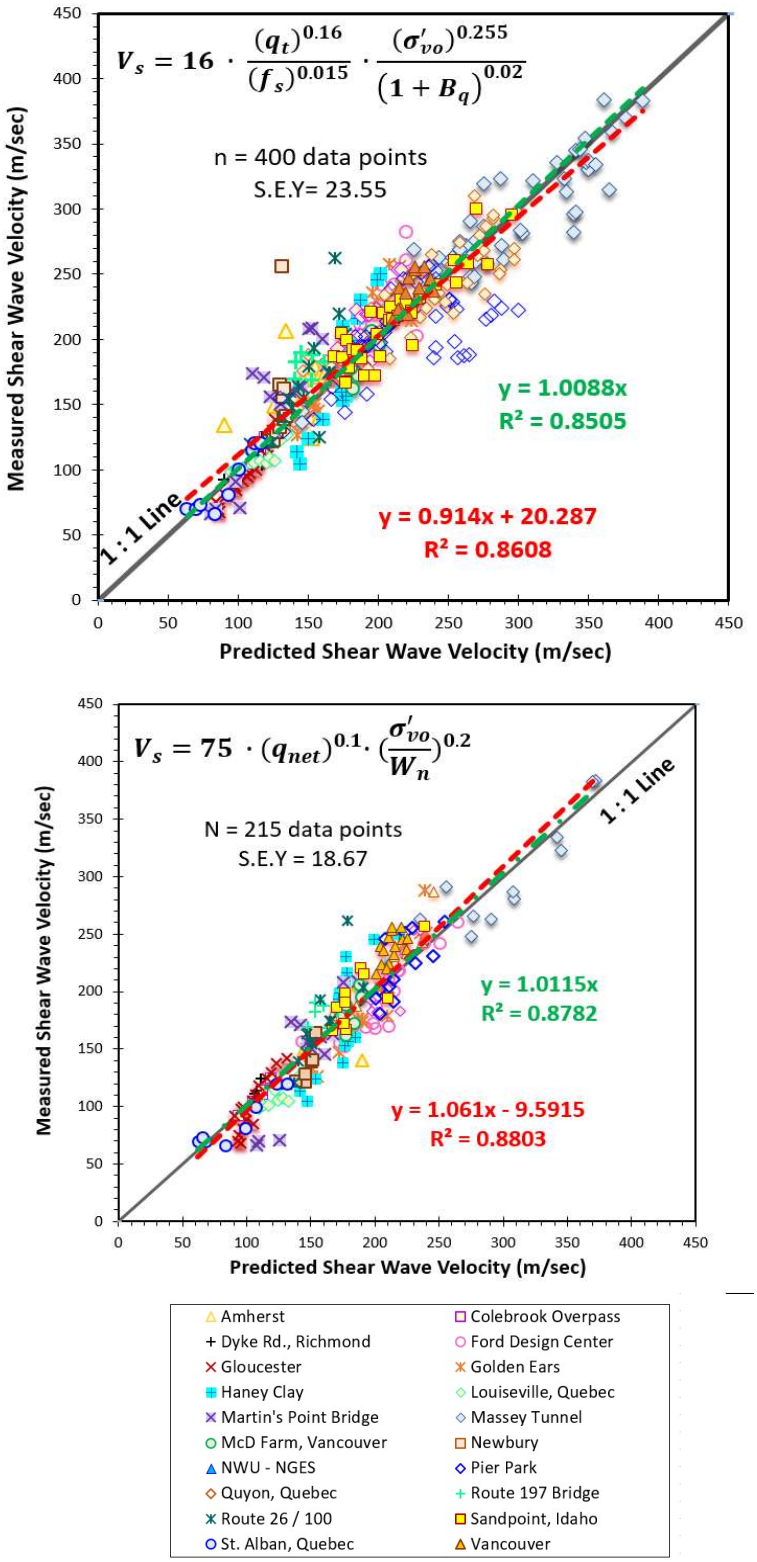


Figure 6.24. Measured versus predicted shear wave velocity profiles for the compiled database using the two proposed modified correlations

# Chapter 7. Modified Cavity Expansion - Critical State Solution for Evaluating Stress History and Piezodissipation from CPTu in Sensitive or Structured Clays

## 7.1 Abstract:

An established CPTu analytical solution based on spherical cavity expansion and critical state soil mechanics (SCE-CSSM) is employed for assessing the stress history and flow rate parameters of sensitive or structured clays. Examining the results of CAUC and CIUC triaxial tests on structured sensitive to quick clays, it is evident that there is strain incompatibility between the deviator stress ($q = \sigma_1 - \sigma_3$) which reaches a peak strength at low strain levels ($\varepsilon \approx 1\%$) and excess porewater pressures that are maximized later at higher strains of around 15% or more. To minimize the impact to the original model, a slightly modified-CSSM approach is devised that utilizes the mobilized effective stress friction angle ($\phi'$) defined at two levels of strain: (a) one at maximum deviatoric stress ($\phi'_{qmax}$), corresponding to the cone tip resistance ($q_t$); and (b) another at maximum obliquity ($\phi'_{MO}$), relating to the measured porewater pressure ($u_2$). Input parameters for assessing the overconsolidation ratio ($OCR = \sigma_p'/\sigma_{vo}'$) from CPTu results include: undrained rigidity index ($I_R = G/s_u$), plastic volumetric strain potential ($\Lambda = 1\text{-}C_s/C_c$), $\phi'_{qmax}$, and $\phi'_{MO}$. A direct CPTu means of assessing the undrained rigidity index in a reliable manner is also developed and used to obtain the CPT bearing factor, $N_{kT}$ is shown to provide good agreement with profiles of undrained shear strength ($s_{uTC}$) obtained from triaxial compression tests (CIUC, CAUC, and/or $CK_0UC$).

The modified solution is implemented on data from 3 different sites: sensitive Leda clay at Gloucester, Ontario; sensitive-quick clay at Tiller, Norway, and structured varved clay at Amherst, Massachusetts. The OCR and $s_{uTC}$ profiles interpreted from CPTu soundings agree well with results from laboratory consolidation and triaxial testing, respectively, for all three sites.

For dissipation testing, the original SCE-CSSM solution (Burns 1998) is utilized without alternation to assess the coefficient of consolidation ($c_{vh}$), specifically using $\phi'_{MO}$ as the input value for excess porewater pressure calculations. While the rigorous solution requires a trial-and-error iteration for assessments involving monotonic and/or dilatory porewater pressure behavior, a simplified solution for monotonic curves is provided. For the sensitive Gloucester clay, interpreted profiles of $c_{vh}$ and hydraulic conductivity (k) with depth from piezodissipations are shown comparable with independent values obtained from laboratory and field tests.

For the case where $\phi'_{qmax} = \phi'_{MO}$, then the modified SCE-CSSM solution collapses to the original model that is applicable to CPTUs in inorganic "well-behaved" clays and clayey silts of low to medium sensitivity.

## 7.2 Introduction

Sensitive and structured clays are characterized by their special mechanical and physical engineering properties, where upon remolding, significant disturbance can result in a severe loss of shear strength and collapse. They also may exhibit chemo-hydro-mechanical aspects as well. Hence, more detailed analyses are needed in the understanding of the stress-strain-strength behavior of such clays and in quantifying their stress history.

For marine deposits, sensitive clays consist of fine-grained geomaterials that were originally sedimented in salt-water environments but later leached by exposure to freshwater aquifers. They commonly exist in Canada, Norway, Sweden, and Labrador (L'Heureux et al., 2014), as well as in the New England area of the USA (Lutenegger 2015). Other types of structured clay deposits can occur due to environments that contain chemical constituents in groundwater regimes that result in soil characteristics which render them unstable or collapsible (Locat et al., 2003).

The sensitive Leda clay (also known as Champlain Sea clay) at South Gloucester, Ontario is used to examine and understand the behavior of these clays given their high sensitivity values ($20 < S_t < 100$). The findings from Gloucester are used to set the stage for other sensitive and structured clays in Norway and Northern America, as will be discussed in later sections of the chapter.

### 7.3 Gloucester Test Site

A recent series of piezocone penetration tests (CPTu) have been conducted at Canadian Test Site No. 1 in Gloucester, Ontario (McQueen et al. 2016). **Figure 7.1** presents the summary profiles from three CPTu soundings performed in 2012, including cone resistance ($q_t$), sleeve friction ($f_s$), and penetration porewater pressure ($u_2$) with depth. One of these soundings (CT-2) was used to provide baseline readings with depth at the standard rate of 20 mm/s. Another sounding (CT-1) focused on the collection of 23 piezodissipation readings, as evidenced by the drops in porewater pressures at regular one-meter interval depths. Also shown is a third recent sounding (2012) which was provided from an independent site investigation at the site by the Geological Survey of Canada (GSC:

courtesy of Dr. Didier Perret, personal communication). All tests were conducted using type 2 penetrometers where the porewater pressures are measured with filters at the shoulder location, in accordance with ASTM D 5778 procedures. The CPTu profiles clearly show very comparable and repeatable measurements with depth.

The site is underlain by soft very sensitive clays known as Leda clays and designated as Canadian Test Site No. 1, the only official national experimentation geotechnical research property (McRostie & Crawford 2001). The clays are complex marine deposits that are subject to destructuring and loss of strength (Leroueil et al. 1983).

The property originally served as a military installation following World War II. An extensive geotechnical study for a large instrumented test embankment was completed with soil borings, field vanes, and laboratory triaxial, consolidation, and index testing (Bozozuk 1972; Bozozuk & Leonards 1972). Over the past five decades, a large variety of additional laboratory, in-situ, geophysical, and full-scale load tests of footings, embankments, and pilings have been implemented at the Gloucester site (McQueen et al. 2016).

**Figure 7.2** shows the interpreted soil behavioral types (SBT) per the 9-part soil classification charts for sounding (CT-1) based on normalized piezocone parameters (Q, F, and $B_q$), as detailed by Robertson (1990, 2009). Below variable shallow soils at depths of 2 m, these sediments classify primarily as SBT zone 1 (sensitive fine-grained soils), with various layers of zone 2 (organic soils) and zone 3 (clays to silty clays) interspersed in the profile.

Based on the laboratory testing at Gloucester, the mean index readings in the clay layers include: natural water content, $w_n$ = 64%, liquid limit, LL = 52%, plasticity index, PI = 26%, and unit weight, $\gamma_t$ = 15.83 kN/m$^3$ (Bozozuk and Leonards 1972), thus classified as highly-plastic clay (CH) per the Unified Soils Classification System (ASTM D 2487). **Figure 7.3** presents a profile of selected index properties including natural water content, Atterberg limits, and unit weight (data taken from Bozozuk and Leonards 1972).

### 7.4 Clay Stress History

The stress history of clays is commonly represented by a preconsolidation stress ($\sigma_p'$), or effective vertical yield stress ($\sigma_{vy}'$), that can be defined as the maximum effective overburden stress experienced by the soil during its stress history. The overconsolidation ratio (OCR = $\sigma_p'/\sigma_{vo}'$) is the normalized and dimensionless form, where $\sigma_{vo}'$ is the current effective vertical stress. More recently, the term yield stress ratio (YSR= $\sigma_{vy}'/\sigma_{vo}'$) has been recommended (e.g., Leroueil & Hight 2003) since other factors and mechanisms can result in a quasi-preconsolidation state, including ageing, desiccation, groundwater changes, repeated cycles of wetting-drying, geochemical environments, sequences of freezing-thawing, and diagenesis. The term OCR will be retained herein because of its commonplace recognition.

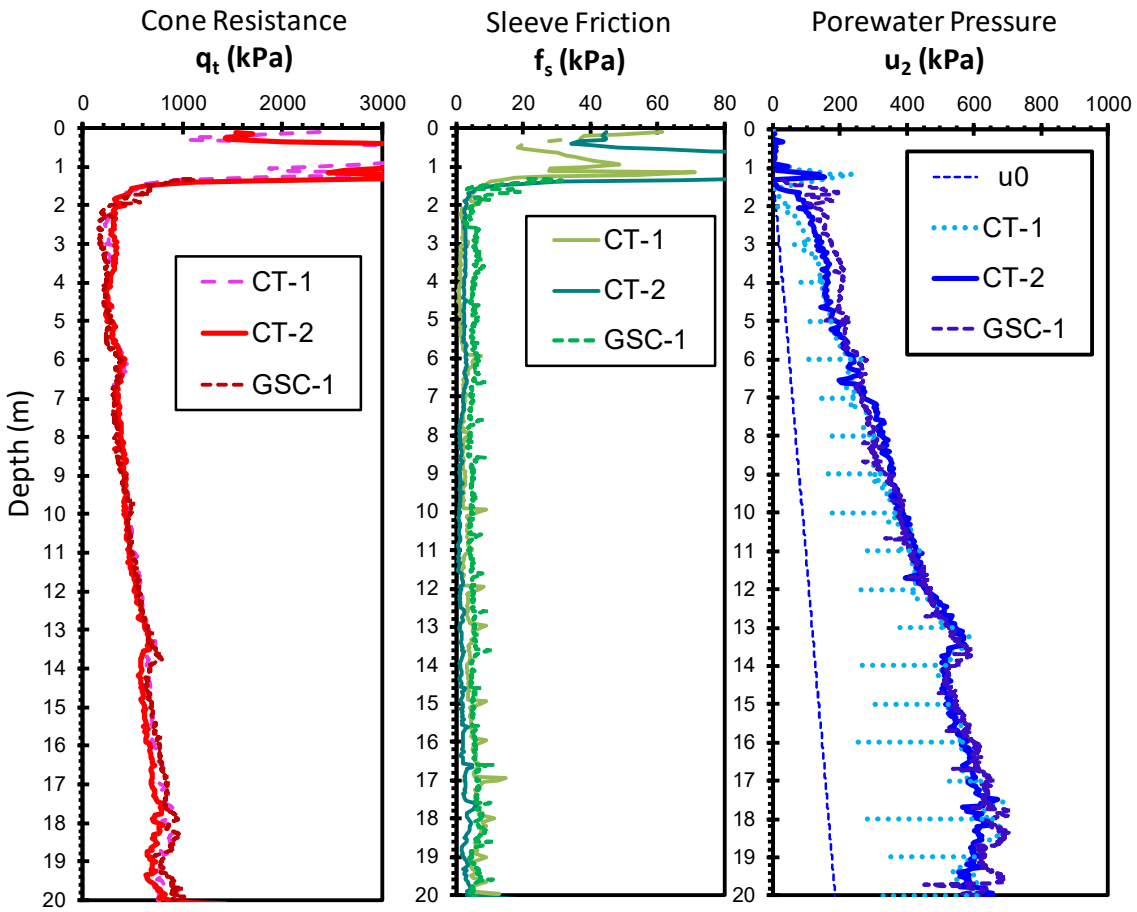


Figure 7.1. Results from independent piezocone soundings in sensitive clay at Gloucester test site: (a) total cone tip resistance, $q_t$; (b) sleeve friction, $f_s$; (c) porewater pressure, $u_2$. Data courtesy of Will McQueen and Bruce Miller (CT = ConeTec) and Didier Perret (GSC = Geological Survey of Canada).

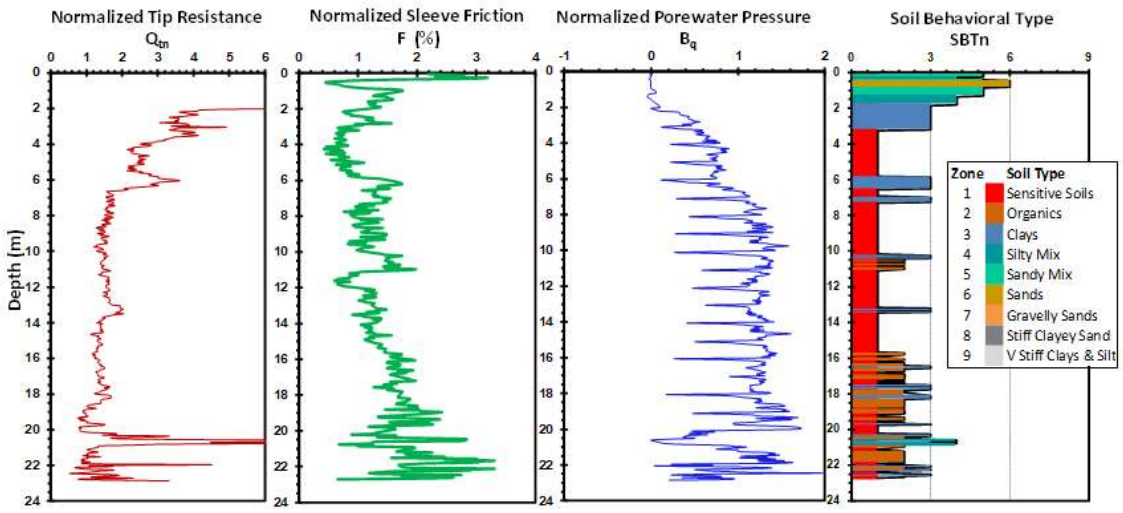


Figure 7.2. Normalized piezocone profiles at Gloucester site: (a) cone resistance, $Q_{tn}$; (b) sleeve friction, F (c); porewater pressure ratio, $B_q$; and (d) soil behavioral type (SBTn) (after McQueen et al., 2016)

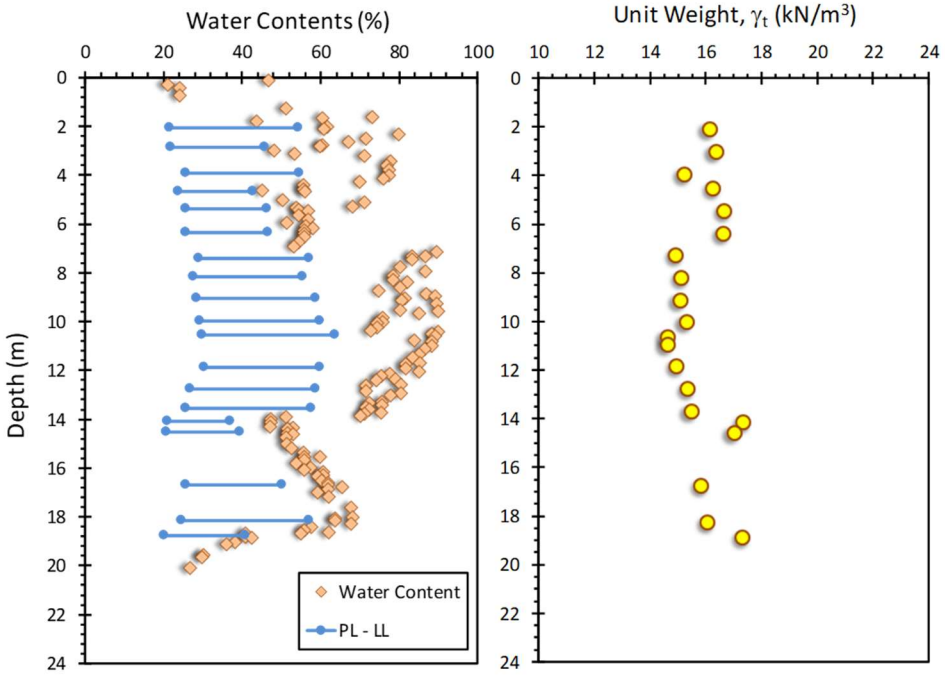


Figure 7.3. Index Properties at Gloucester test site: Atterberg limits, water content, and unit weight (data after Bozozuk and Leonards, 1972)

The most basic and conventional means to determine the preconsolidation stress is from the results of laboratory one-dimensional consolidation testing performed on undisturbed samples using an oedometer or consolidometer (ASTM D 2435). A trimmed specimen is subjected to constrained compression in either a mechanical oedometer, pneumatic or hydraulic consolidometer, or automated constant rate of strain (CRS) device (ASTM D 4186). Laboratory-based techniques are associated with many issues such as sampling disturbance and handling, stress relief with possible swelling, change in effective stress, specimen trimming method, load application duration, secondary consolidation consideration, temperature, salt concentration in pore fluid, lack of proper saturation, specimen slenderness, and capacity of loading frame (Germaine and Germaine, 2009). To help unmask the interpreted value of $\sigma_p'$ from consolidation test results, at least 28 different graphical procedures have been recommended (Ku and Mayne, 2013).

The independent evaluation of $\sigma_p'$ from field test data can assist in corroborating lab interpretations, as well as fill in the information between sampling depths. Also, the results from in-situ tests are immediately available for evaluation, whereas lab consolidation tests can take 2 days to 2 weeks for completion. As such, the use of cone penetration tests (CPT) and piezocone tests (CPTu) for assessing profiles of $\sigma_p'$ in various clay deposits has been promoted by Konrad & Law (1987), Mayne (1991), Chen & Mayne (1994; 1996), Demers & Leroueil (2002), Larsson & Åhnberg (2005), Robertson (2009), and others.

Specifically of interest herein is the analytical solution developed by Mayne (1991) that relates OCR to CPTu parameters using a set of algorithms developed from spherical

cavity expansion (SCE) and critical state soil mechanics (CSSM) since that same approach was extended to allow interpretations of flow parameters ($c_{vh}$ and k) from piezodissipation tests (Burns & Mayne 1998). While these solutions are applicable to clays, silty clays, and clayey silts of low sensitivity, it became evident that the structured clays at Gloucester required special attention. As such, a slightly modified SCE-CSSM hybrid model is introduced to address the evaluation of stress history of very sensitive to quick clays, as well as piezocone dissipation test results.

## 7.5 Original SCE-CSSM Solution

Chen and Mayne (1994) detail the derivation of a hybrid formulation of spherical cavity expansion and critical state soil mechanics (SCE-CSSM) to express the cone tip resistance ($q_t$) and porewater pressure ($u_2$) using closed-form equations as follows:

$$q_t = \sigma_{vo} + [(4/3)\cdot(\ln I_R + 1) + \pi/2 + 1]\cdot(M/2)\cdot(OCR/2)^{\Lambda}\cdot\sigma_{vo}' \quad [7.1]$$

$$u_2 = u_o + [(2/3)\cdot(\ln I_R)\cdot(M)\cdot(OCR/2)^{\Lambda}\cdot\sigma_{vo}'] + [1-(OCR/2)^{\Lambda}]\cdot\sigma_{vo}' \quad [7.2]$$

where M = (6 sinϕ')/(3-sinϕ') = slope of the frictional envelope for triaxial compression in q-p' space, $\Lambda = (1 - C_s / C_c)$ = plastic volumetric strain potential, $C_s$ = swelling index, $C_c$ = virgin compression index, $I_R$ = rigidity index = $G/s_u$, and OCR = $\sigma_p'/\sigma_{vo}'$. Typically, the value of $\Lambda \approx 0.8$ to 0.9 for most clays.

The hybrid SCE-CSSM model can be rearranged to determine the overconsolidation ratio (OCR) of the clay in three separate formulations using net cone

resistance ($q_{net} = q_t - \sigma_{vo}$), excess porewater pressure ($\Delta u = u_2 - u_0$), and effective cone resistance ($q_{eff} = q_t - u_2$):

$$OCR = 2 \cdot \left[ \frac{(2/M) \cdot (q_t - \sigma_{vo}) / \sigma_{vo}'}{(4/3) \cdot (\ln I_R + 1) + \pi / 2 + 1} \right]^{(1/\Lambda)} \quad [7.3]$$

$$OCR = 2 \cdot \left[ \frac{(\Delta u / \sigma_{vo}') - 1}{(2/3) \cdot M \cdot \ln(I_R) - 1} \right]^{(1/\Lambda)} \quad [7.4a]$$

$$OCR = 2 \cdot \left[ \frac{1}{1.95 \cdot M + 1} \left( \frac{q_t - u_2}{\sigma_{vo}'} \right) \right]^{(1/\Lambda)} \quad [7.5]$$

Measured excess porewater pressures on the penetrometer have two components: octahedral and shear-induced. For soft to firm clays with OCRs < 2, the shear-induced component of measured porewater pressures is small (< 20%) of the total $u_2$ reading (Baligh 1986; Mayne 1991; Burns & Mayne 1998). Thus, it can be neglected for all practical purposes to give a slightly simpler form:

$$OCR = 2 \cdot \left[ \frac{(\Delta u / \sigma_{vo}')}{(2/3) \cdot M \cdot \ln(I_R)} \right]^{(1/\Lambda)} \quad [7.4b]$$

A set of stepped down versions of the equations can be developed to determine the stress history ($\sigma_p'$) by assuming $\Lambda = 1$ so that the power law formats become linear equations for yield stress:

$$\sigma_p' = \left[ \frac{(q_t - \sigma_{vo})}{M \cdot [1 + \frac{1}{3}(\ln I_R)]} \right] \quad [7.6]$$

$$\sigma_p' = \left[ \frac{(u_2 - u_o)}{\frac{M}{3}(\ln I_R)} \right] \quad [7.7]$$

$$\sigma_p' = \left[ \frac{2 \cdot (q_t - u_2)}{1.95 \cdot M + 1} \right] \quad [7.8]$$

Further simplified approximations for stress history can be can be obtained for convenience and practical use in normal inorganic clays of low sensitivity by adopting characteristics values for the effective stress friction angle $\phi' = 30°$ and rigidity index $I_R = 100$ (Mayne, 2005) as follows:

$$\sigma_p' \approx 0.33 \cdot (q_t - \sigma_{vo}) \quad [7.9]$$

$$\sigma_p' \approx 0.54 \cdot (u_2 - u_o) \quad [7.10]$$

$$\sigma_p' \approx 0.60 \cdot (q_t - u_2) \quad [7.11]$$

### 7.6 Application to Clay at Torp, Sweden

The SCE-CSSM solutions have found use in profiling OCR from CPTu results in a variety of clays with low to medium sensitivity (e.g., Lunne et al. 1997; Niazi et al. 2011; Ozkul et al. 2013). As an example, **Figure 7.4** presents a representative piezocone sounding

(location S9) from Torp, Sweden reported by Larsson and Åhnberg (2003). Profiles of cone tip resistance ($q_t$) and porewater pressure ($u_2$) with depth are presented in **Figure 7.4a** and **Figure 7.4b**, respectively. The preconsolidation stresses ($\sigma_p'$) from 27 laboratory consolidation tests are available from this location. Application of equations [7.3], [7.4], and [7.5] with input values of effective stress friction angle $\phi' = 32°$, $\Lambda = 0.8$, and rigidity index value of $I_R = 100$, one can get three evaluations for the OCR as a function of: $q_{net} = (q_t - \sigma_{v0})$, $\Delta u = (u_2 - u_0)$ and $q_{eff} = (q_t - u_2)$, as illustrated in **Figure 7.4c**. For this site, a rather good agreement between the lab $\sigma_p'$ values and CPTu-evaluated profiles is evident.

### 7.7 Yield Stresses of Sensitive Clay at Gloucester, Canada

Using the SCE-CSSM solution, site-specific values for the input parameters are needed which include the effective friction angle ($\phi$'), rigidity index ($I_R$), and plastic potential ($\Lambda$), along with the main measurements of the piezocone ($q_t$ and $u_2$). As noted before, $\Lambda$ is often between 0.8 to 0.9, but at low OCRs, a value of $\Lambda = 1$ suffices. Using the results from anisotropically consolidated triaxial compression (CAUC) tests reported by Bozozuk (1972), a summary of the effective stress paths in q-p' space indicates an operational value of effective friction angle $\phi' = 39°$ can be assigned to this Champlain Sea clay deposit, as presented in **Figure 7.5**.

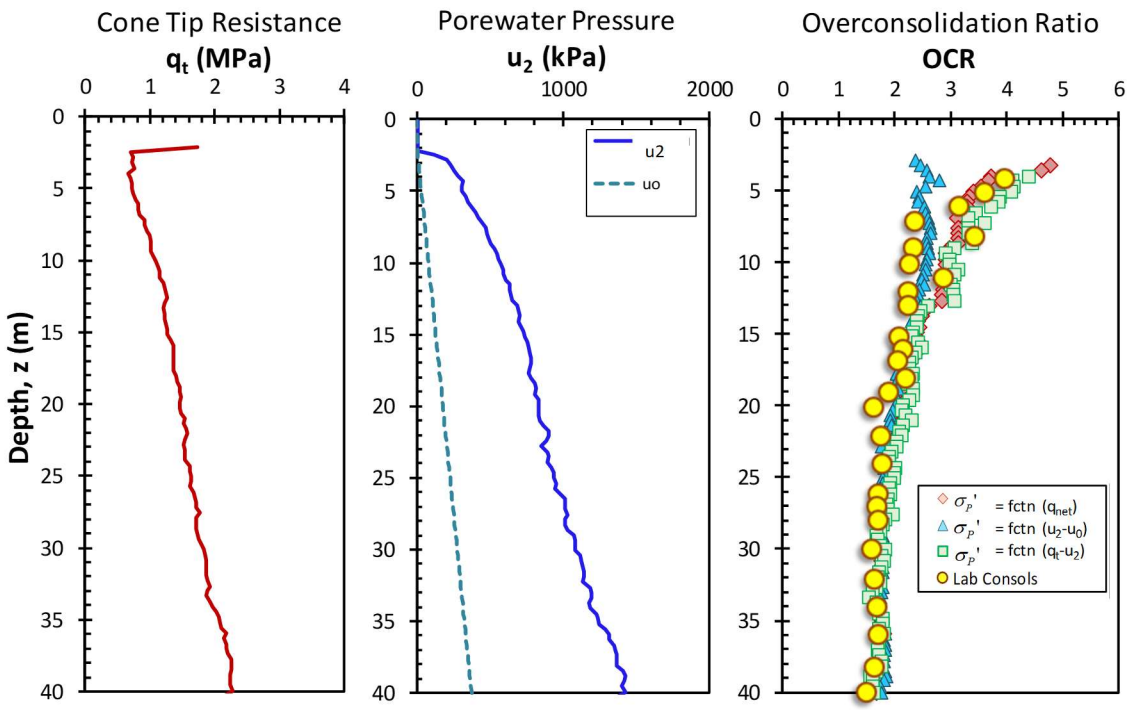


Figure 7.4. Results from piezocone sounding S9 in clay at Torp, Sweden: (a) total cone tip resistance, $q_t$; (b) porewater pressure, $u_2$; (c) OCR evaluation using three expressions from the original hybrid SCE-CSSM framework (data from Larsson & Åhnberg, 2003)

As for the operational value of rigidity index, it was obtained directly using undrained shear strength ($s_u$) and cone bearing factor ($N_{kt}$), where undrained shear strength is obtained from:

$$s_{uc} = \frac{q_{net}}{N_{kt}} \qquad [7.12]$$

From spherical cavity expansion theory, the cone bearing factor ($N_{kt}$) is expressed solely in terms of the rigidity index (Vesić 1977):

$$N_{kt} = [(4/3)\cdot(\ln I_R + 1) + \pi/2 + 1] \qquad [7.13]$$

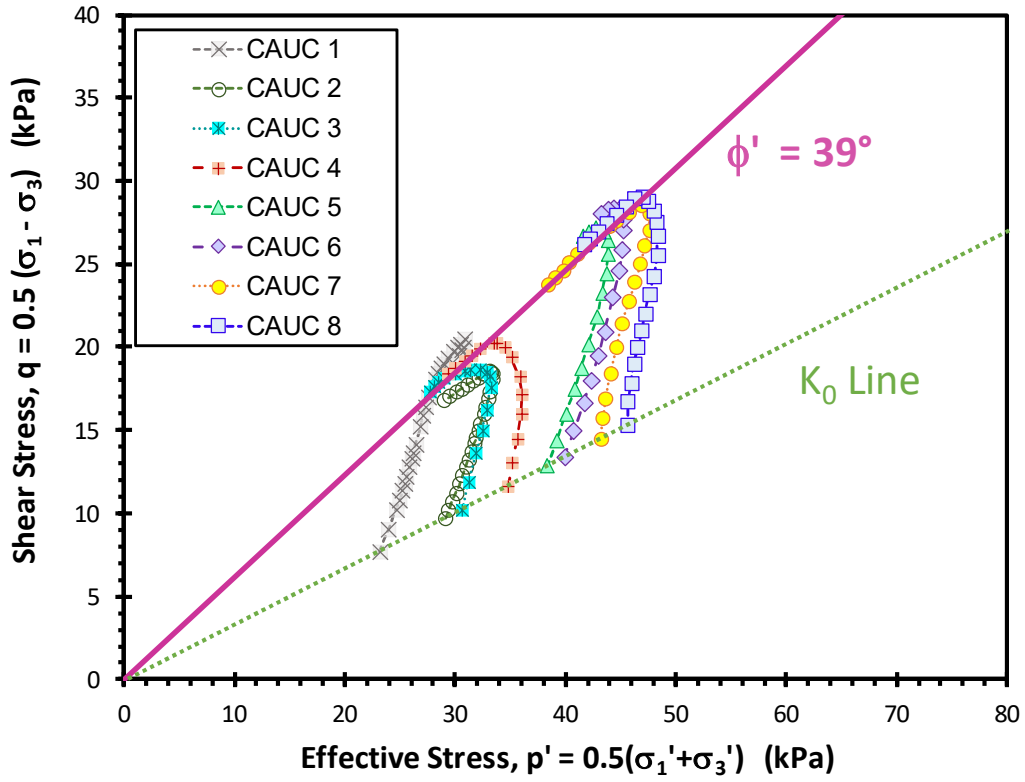


Figure 7.5. CAUC stress paths for Gloucester site indicating one effective friction angle (data from Bozozuk, 1972)

As a preliminary approach, one can assign a fitted value for cone bearing factor ($N_{kt}$) with the field measured net cone tip resistance ($q_{net}$) by varying the values for $I_R$ to match the laboratory and/ or field measured undrained shear strength values. **Figure 7.6** presents a compilation of undrained shear strengths from different investigations at Gloucester, including: CAUC triaxials (Bozozuk, 1972; Landon, 2007), CIUC triaxials (Bozozuk), and field vane (Leroueil et al., 1983; CT 2012; Nader et al., 2015; GSC, 2016). It was found that by assigning a rigidity index ($I_R$) value of 60 for Gloucester test site, a calculated $N_{kt}$ value of 9.34 used with net cone tip resistance gave a good match, as evident in **Figure 7.6**.

Note that the direct evaluation of rigidity index from its definition as the ratio of shear modulus to shear strength ($I_R = G/s_u$) is quite elusive and difficult (Vardanega & Bolton 2013; Krage et al. 2014). This is so in part because the shear modulus of soil covers a wide range as related to its highly nonlinear stress-strain-strength behavior, starting with the fundamental initial tangent shear modulus ($G_{max}$) at small-strains corresponding to nondestructive range through to moderate stiffnesses at intermediate strains (G), onto lower values at failure strains when reaching peak strength.

In SCE theory, the size of the zone of the soil that goes plastic (diameter D) is related to the size of the intruding body (diameter d) and the ratio depends upon the rigidity index (Vesić 1977):

$$D/d = (I_R)^{0.33} \quad [7.14]$$

Therefore, the rigidity index can be considered as a measure of the volume of clay affected by the advancing penetrometer and thus an operational value should be considered.

Applying the assigned values of geoparameters: $\phi' = 39°$, $I_R = 60$, and $\Lambda = 1$ for the Gloucester test site, **Figure 7.7** shows that the three CPTu expressions for $\sigma_p'$ and OCR give rather poor agreement for the sensitive Leda clay deposit. Parametric studies by altering the aforementioned values over reasonable ranges ($20° < \phi' < 45°$; $20 < I_R < 1000$; $0.5 < \Lambda < 1$) produced similarly incompatible and inconsistent results.

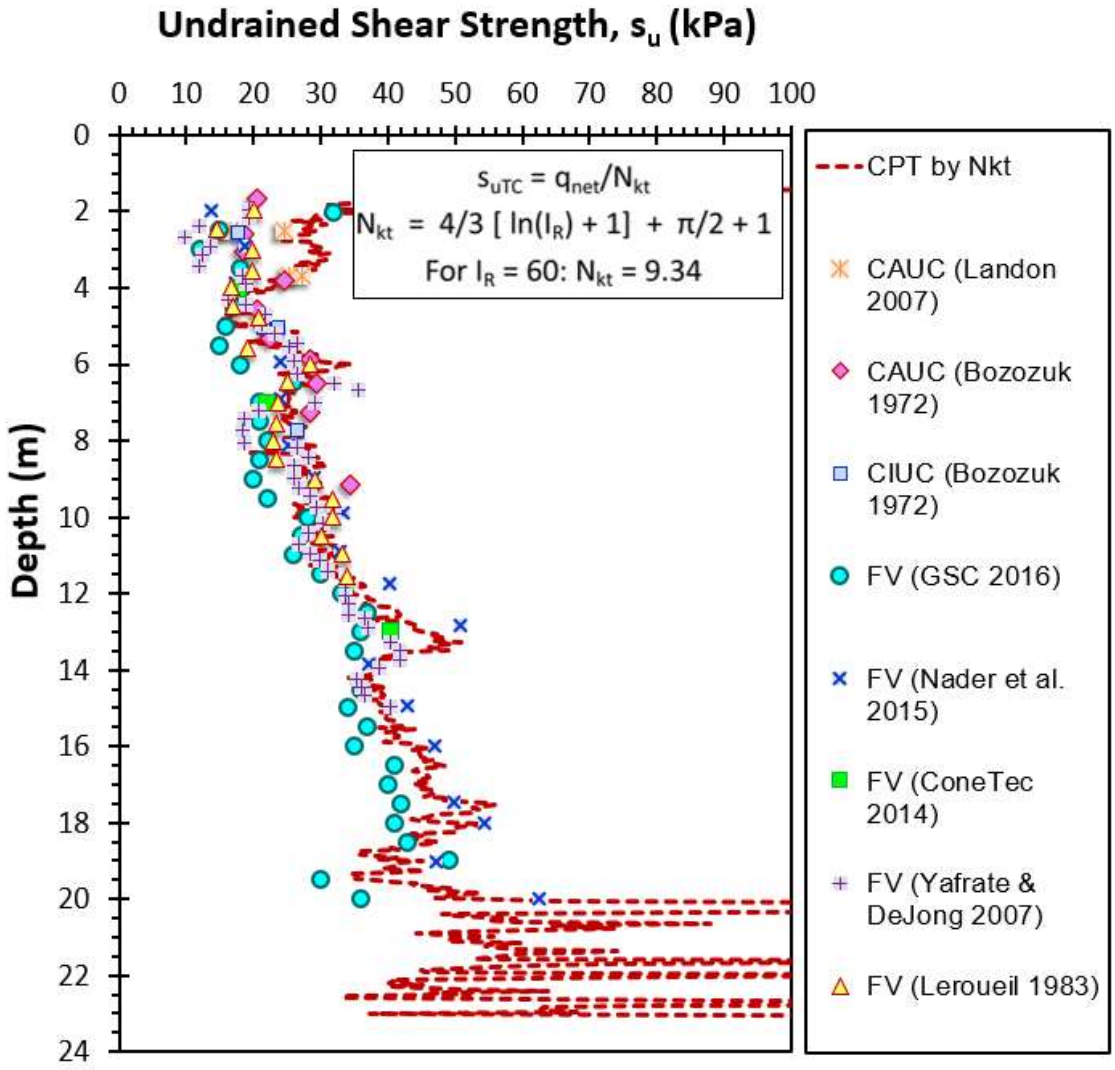


Figure 7.6. Undrained shear strength profile for Gloucester test site with evaluation using cone bearing factor ($N_{kt}$) for the determining operational value of rigidity index

### 7.8 Triaxial Stress-Strain and Porewater Response

Representative behavior of the sensitive Leda clay at Gloucester under triaxial compression testing (CAUC) is presented in **Figure 7.8** (data from Landon 2007). From the stress-strain and porewater pressure behavior, it can be clearly observed that there is a strain incompatibility issue whereby the deviator stress ($\sigma_1 - \sigma_3$) reaches a peak strength at a strain level of about 1 % while the pore-water pressure is still developing. The maximum

porewater pressures occur much later at strain levels of about 11 %, or more. Similar results are observed in the CIUC and CAUC data presented by Bozuzuk (1972).

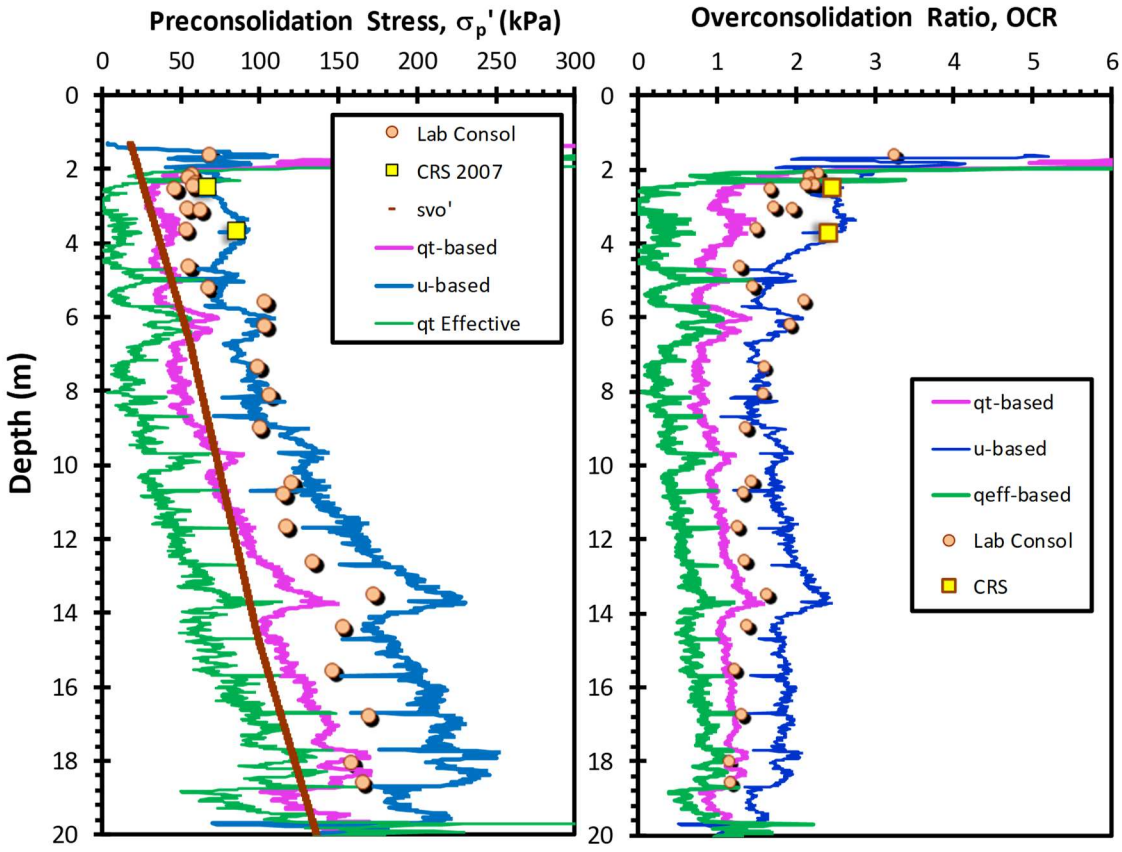


Figure 7.7. Profiles of effective preconsolidation stress and OCR evaluated using the original hybrid SCE-CSSM framework for Gloucester test site
(Note: oedometer data from Bozozuk, 1972)

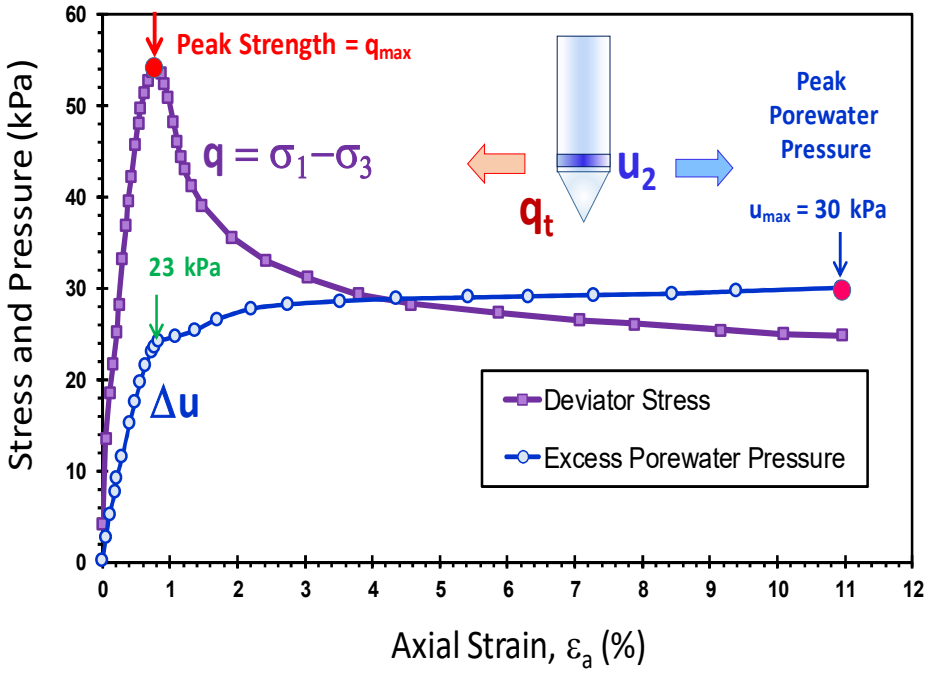


Figure 7.8. Strain incompatibility between $q_{max}$ and $\Delta u_{max}$ for Gloucester test site (CAUC triaxial data from Landon, 2007)

Consequently, **Figure 7.9** shows that the mobilized effective stress friction angle at two definitions are applicable: (a) value at peak stress ($q_{max}$) and (b) value at maximum obliquity $(\sigma_1'/\sigma_3')_{max}$. It is, in fact, common to report effective friction angles mobilized at both maximum stress and maximum obliquity for triaxial conditions (e.g., Koutsoftas & Ladd, 1985; Berre 2014). In an analogous concept for the piezocone, the measured cone resistance ($q_t$) corresponds to the peak friction angle mobilized at $\phi'_{qmax}$ while the measured porewater pressure ($u_2$) relate to the value taken at larger strains, corresponding to maximum obliquity, or $\phi'_{max\ q/p'}$. For Gloucester, the corresponding values are $\phi'_{qmax} = 28°$ and $\phi'$ (max. obliquity) = 39°. These are in excellent agreement with series of $CK_0UC$ triaxial results reported by Landon (2007) giving: $\phi'$ ($q_{max}$) = 29° and $\phi'$ (max. obliquity) = 41°.

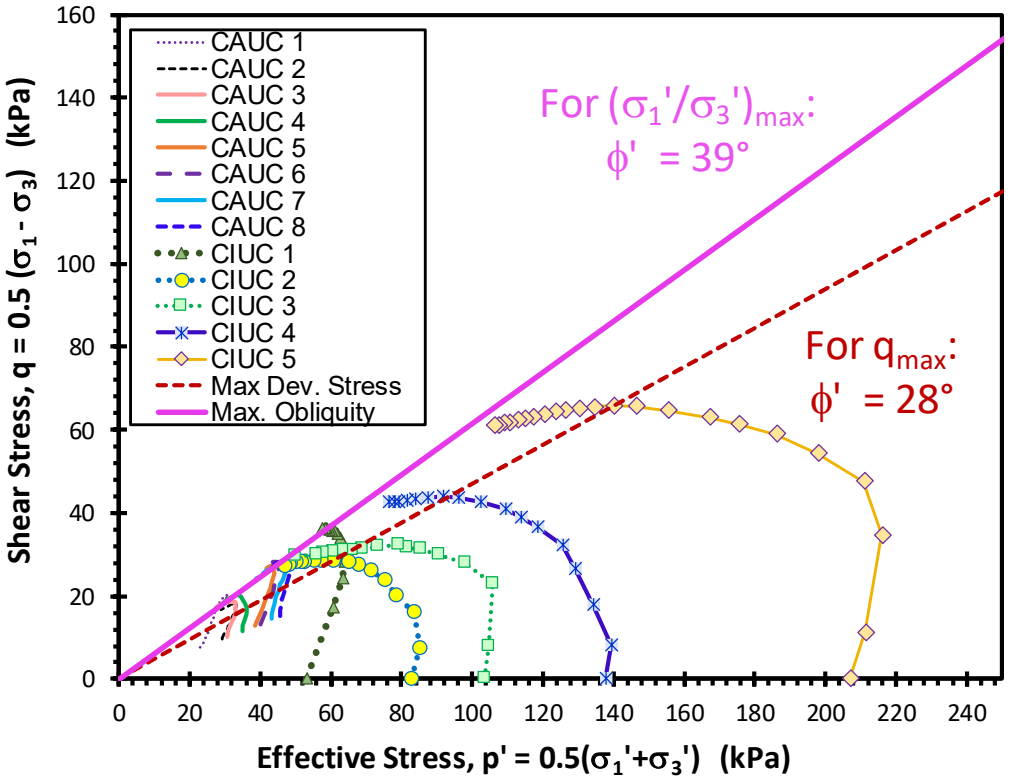


Figure 7.9. Triaxial stress paths for Gloucester clay indicating mobilized friction angles: (1) $\phi_1'$ at $q_{max}$ and (b) $\phi_2'$ at maximum obliquity
(CIUC data from Law, 1975; CAUC data from Bozozuk, 1972)

### 7.9 Modified SCE-CSSM Solution

To overcome the issues with highly sensitive clays in the application of the SCE-CSSM expressions, alternative possible solutions can be posed:

1. Empirically modify porewater pressure equations using an adjustment factor for strain compatibility where the ratio of maximum porewater pressures exceeds the value that is recorded at peak stress. Based on the data shown in **Figure 7.8**, the ratio is about 1.35, giving $x_u \approx 35\%$ that can be used in the following:

$$u_2 - u_o = (1+x_u)\cdot\{[(2/3)\cdot(\ln I_R)\cdot(M)\cdot(OCR/2)^{\Lambda}\cdot\sigma_{vo}']+[1-(OCR/2)^{\Lambda}]\cdot\sigma_{vo}'\} \quad [7.15]$$

2. Use two values of mobilized friction angles; one at maximum deviator stress (corresponding to cone resistance, $q_t$) and a second defined at maximum obliquity (related to measured CPT $u_2$):

$$q_t = \sigma_{vo} + [(4/3)\cdot(\ln I_R + 1) + \pi/2 + 1]\cdot(M_{c1}/2)\cdot(OCR/2)^{\Lambda}\cdot\sigma_{vo}' \quad [7.16]$$

$$u_2 = u_o + [(2/3)\cdot(\ln I_R)\cdot(M_{c2})\cdot(OCR/2)^{\Lambda}\cdot\sigma_{vo}'] + [1-(OCR/2)^{\Lambda}]\cdot\sigma_{vo}' \quad [7.17]$$

3. Represent the effective stress envelope using both an effective friction angle with an effective cohesion intercept, c'.

To minimize the alterations to the original formulation, the second solution was adopted in the current study. The modified SCE-CSSM equations were developed reflecting the two effective friction angles at different failure criteria as follows:

$$OCR = 2\cdot\left[\frac{(q_t - \sigma_{vo})/\sigma_{vo}'}{M_{c1}\{\frac{2}{3}(\ln I_R + 1) + \frac{\pi}{4} + \frac{1}{2}\}}\right]^{(1/\Lambda)} \quad [7.18]$$

$$OCR = 2\cdot\left[\frac{(\Delta u/\sigma_{vo}') - 1}{\frac{2}{3}M_{c2}\cdot\ln(I_R) - 1}\right]^{(1/\Lambda)} \quad [7.19]$$

$$OCR = 2\cdot\left[\frac{Q - (M_{c1}/M_{c2})[(\Delta u/\sigma_{vo}') - 1]}{1.95M_{c1} + (M_{c1}/M_{c2})}\right]^{(1/\Lambda)} \quad [7.20]$$

where Q = normalized tip resistance = $(q_t - \sigma_{vo})/\sigma_{vo}'$; $M_{c1} = (6\cdot\sin\phi_1')/(3-\sin\phi_1')$ is taken at maximum stress (peak strength); and $M_{c2} = (6\cdot\sin\phi_2')/(3-\sin\phi_2')$ occurs at maximum obliquity corresponding to a peak porewater pressure. In terms of effective stress strength

envelopes, the onset of the mobilized friction angle at $q_{max}$ could alternatively be called a *phase angle* ($\phi_1'$), and that at the later stage termed the *effective stress friction angle* ($\phi_2'$).

Of course, a more involved and versatile modification that included an effective cohesion intercept term (c'), plus two friction angles ($\phi_1'$ and $\phi_2'$), two rigidity indices ($I_{R1}$ and $I_{R2}$), and two plastic strain terms ($\Lambda_1$ and $\Lambda_2$) could also be implemented, however, at the higher cost of complexity.

By combining equations [7.18] and [7.19] from the modified hybrid SCE-CSSM framework, the value of the rigidity index, $I_R$ can be obtained in terms of the two effective friction angles as:

$$I_R = \exp\cdot\left[\frac{1.5\cdot Q + 2.925 M_{c1}\cdot\left(U^* - 1\right)}{Q\cdot M_{c2} - M_{c1}\cdot\left(U^* - 1\right)}\right] \qquad [7.21a]$$

$$I_R = \exp\cdot\left[\frac{1.5 + 2.925\, M_{c1}\cdot\left(\frac{U^* - 1}{Q}\right)}{M_{c2} - M_{c1}\cdot\left(\frac{U^* - 1}{Q}\right)}\right] \qquad [7.21b]$$

$$I_R = \exp\cdot\left[\frac{1.5 + 2.925\, M_{c1}\cdot a_q}{M_{c2} - M_{c1}\cdot a_q}\right] \qquad [7.21c]$$

where Q = normalized tip resistance = $(q_t - \sigma_{vo}) / \sigma_{vo}'$; U* = normalized porewater pressure = $(u_2 - u_o) / \sigma_{vo}'$; $M_{c1}$ is the frictional parameter taken at peak strength; and $M_{c2}$ defined at maximum obliquity. And $a_q$ is the slope between (U*-1) and q. Since the expression for $I_R$ is an exponential form, however, the direct use of [7.21] results in highly variable and skittish profiles with depth, therefore a moving average (over say 10 to 20 readings) is necessary for any practical use or an assigned slope value expressing the quantity (U* - 1

/ Q) can be directly implemented in equation [7.21b] with the corresponding frictional parameters $M_{c1}$ and $M_{c2}$. To illustrate for Gloucester test site, **Figure 7.10** presents a plot of normalized (U*-1) plotted versus normalized Q with a corresponding slope value of 0.78. Using the slope value with the values of mobilized effective friction angle at $q_{max}$: $\phi_1' = 28°$ and at $(\sigma_1'/\sigma_3')_{max}$ : $\phi_2' = 39°$ and applying equation [7.21b], the corresponding rigidity index value ($I_R$) is 94.

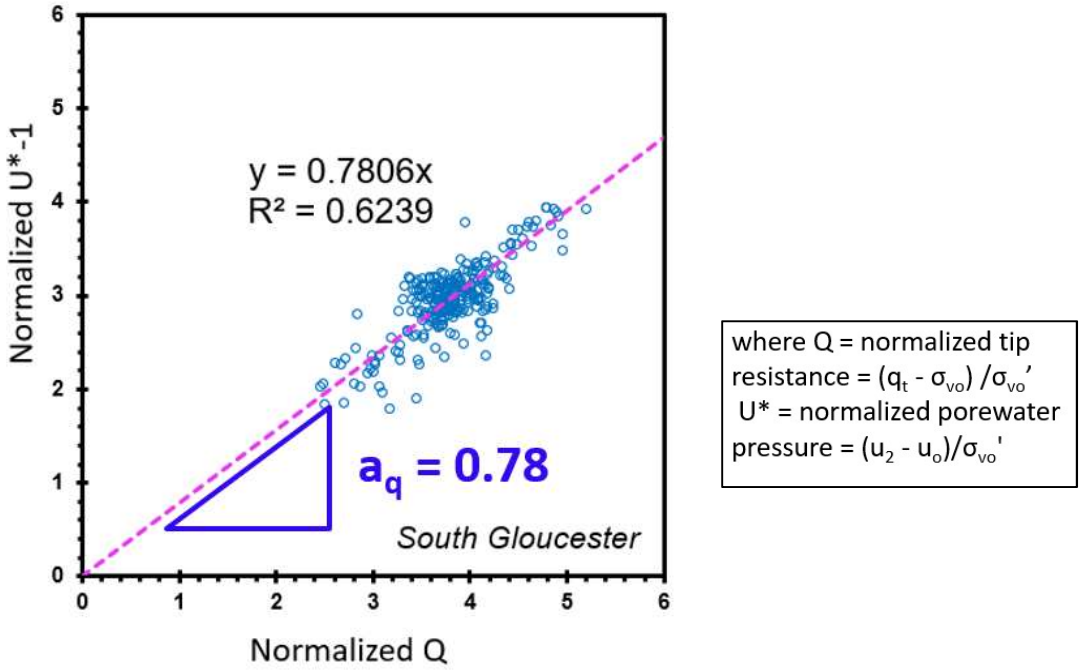


Figure 7.10. Normalized porewater pressure ratio (U*-1) versus normalized cone tip resistance (Q) for Gloucester test site

The evaluated value based on modified SCE-CSSM approach is compared to values obtained from other methods for reference. From the stress-strain plots at the different depths, the axial strain (ε axial) at failure was determined as reported by Bozozuk (1972) in **Figure 7.11**.

After defining the axial strain at failure (ε axial), the shear strain at failure (γ shear) is determined from the relation between the modulus of elasticity (E) and the shear modulus (G) by assigning a Poisson's ratio (ν) of 0.50:

$$E = 2G \cdot (1+ \nu) \quad [7.22a]$$

$$\varepsilon_{axial} = \gamma_{shear} / (1+ \nu) \quad [7.22b]$$

The values of shear strain at failure ($\gamma_{shear}$) are used to evaluate the corresponding rigidity index where:

$$I_R = 1 / \gamma_{shear} \quad [7.23]$$

The evaluated values of the rigidity index based on the shear strain are presented in **Figure 7.13** using purple dots with a lower average $I_R$ boundary value of 65.

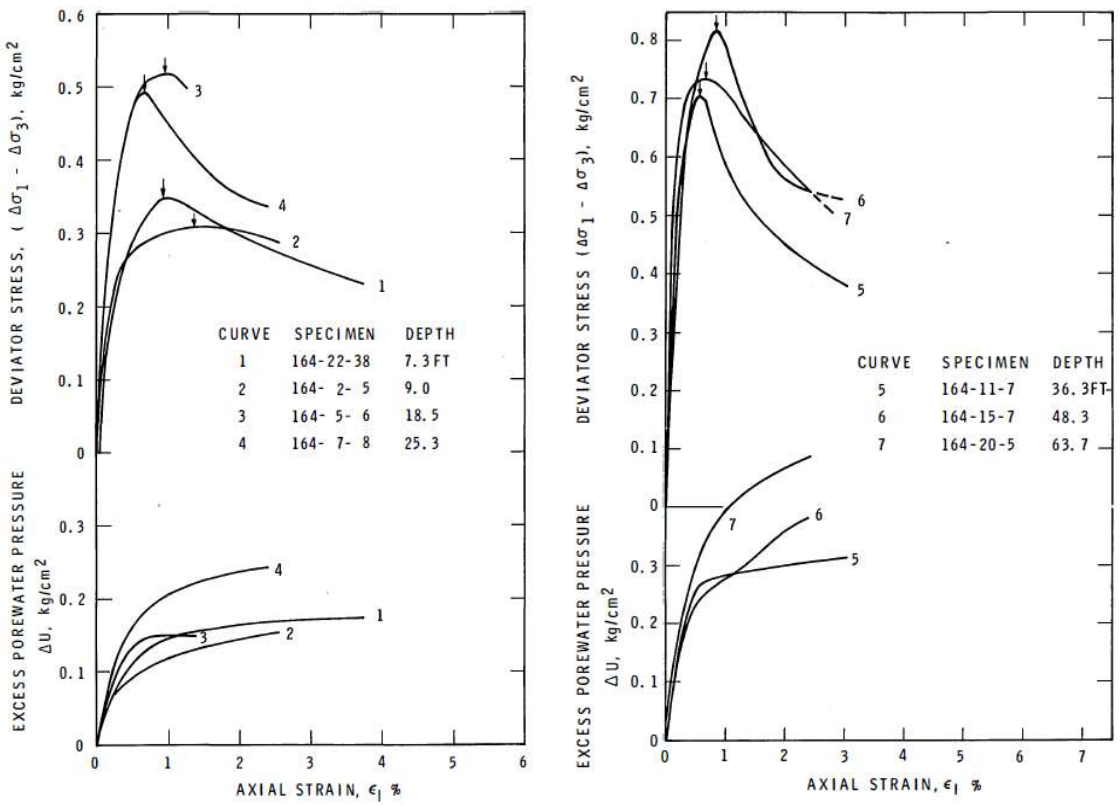


Figure 7.11. Results of CAUC triaxial tests showing deviator stress and excess porewater pressure versus axial strain and the axial strain at failure (ε axial) marked by arrows as determined by Bozozuk (1972)

A recent approach introduced by Krage et al. (2014) using the shear wave velocity profile and net cone tip resistance ($q_{net}$) from SCPTu has been developed to evaluate $I_R$ value at 50% strain level. This can be investigated here where $I_R$ can be determined from:

$$(I_R)_{50} = \left[ \frac{1.81 \cdot G_0}{(q_{net})^{0.75} (\sigma'_{vo})^{0.25}} \right] \quad [7.24]$$

The above formula is applied to a recent seismic piezocone sounding conducted at Gloucester test site as reported by Styler and Mayne (2013) with shear wave velocity and

shear moduli profiles presented in **Figure 7.12.** Using the shear modulus profile with the net cone tip resistance, a continuous profile of $I_R$ with depth is evaluated as shown in **Figure 7.13** using blue dots. The seismic approach by Krage et al. (2014) gave an average rigidity index value of 165 which is an intermediate value that is slightly higher than the value obtained from the modified SCE-CSSM approach. From **Figure 7.13**, it is evident that the rigidity index value obtained from modified SCE-CSSM is reasonable and comparable to other assessments and methods.

The obtained $I_R$ value is used to obtain cone bearing factor ($N_{kt}$) as per equation [7.13] for evaluating the undrained shear strength ($s_u$). By using an $I_R$ value of 94 the corresponding $N_{kt}$ value is 9.96 which provides an excellent agreement with the different laboratory measured $s_u$ reference values as presented in **Figure 7.14.**

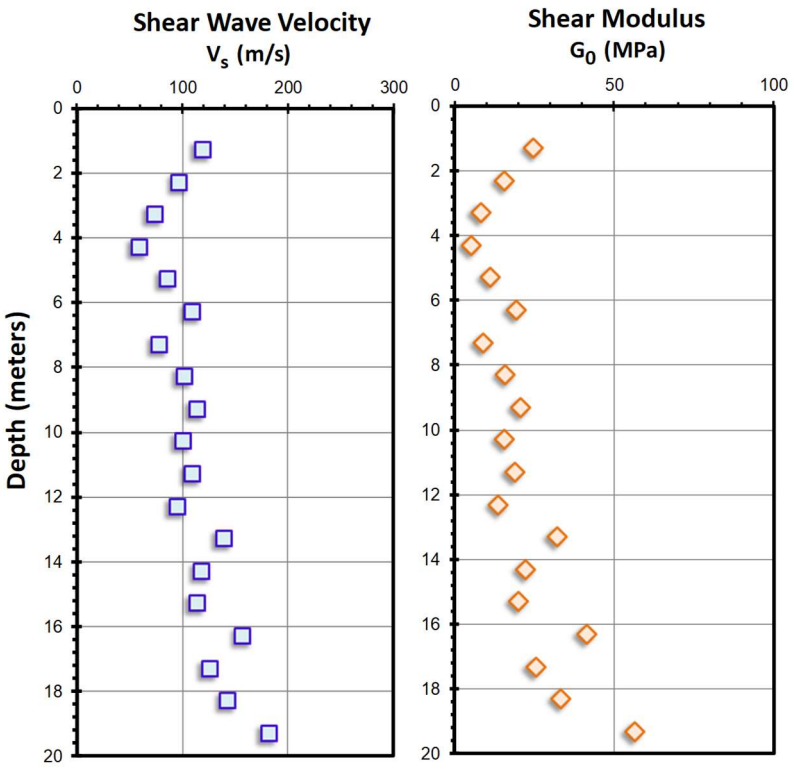


Figure 7.12. Shear wave velocity profile and corresponding shear modulus for Gloucester test site (after Styler & Mayne, 2013)

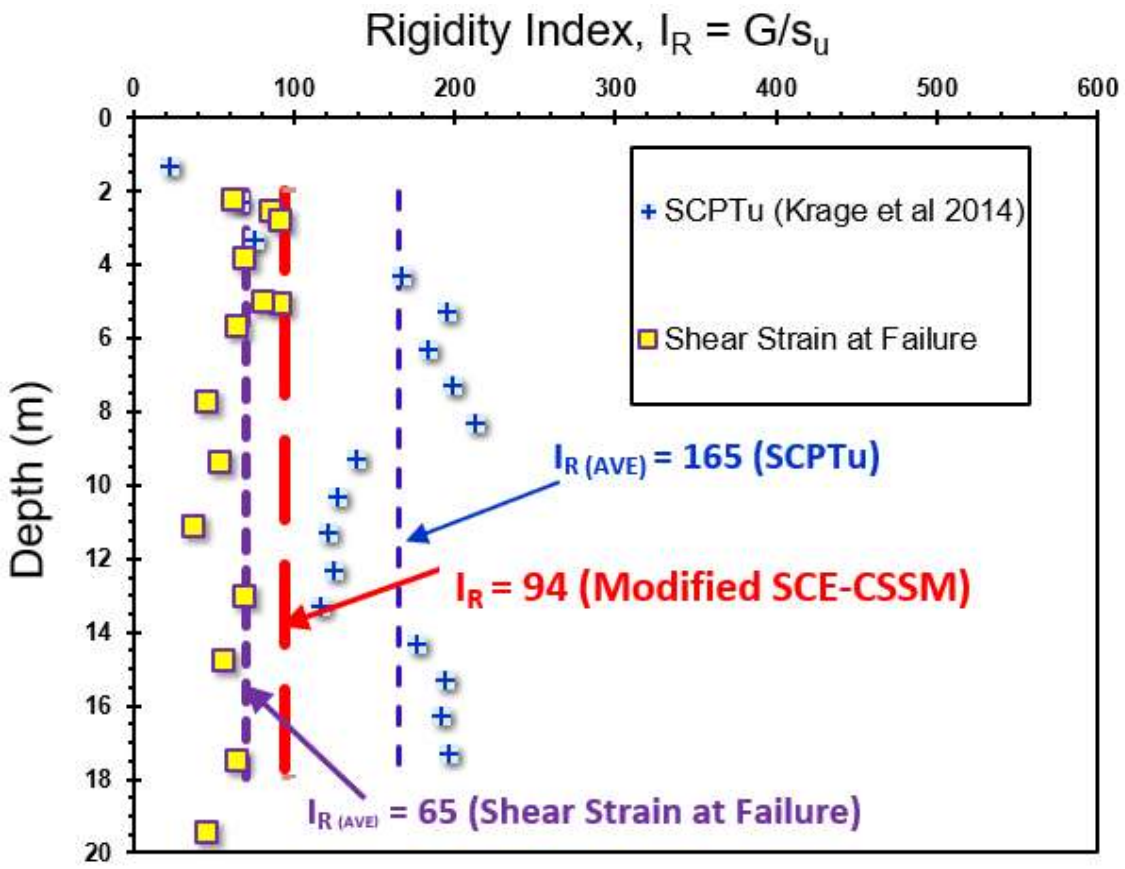


Figure 7.13. Comparison between different approached for estimating rigidity index value for Gloucester test site

By applying equations [7.18], [7.19], and [7.20] to the results of piezocone sounding CT-2 with an operational rigidity index value of $I_R = 94$ and mobilized effective friction angle values at $q_{max}$ ($\phi_1' = 28°$) and at $(\sigma_1'/\sigma_3')_{max}$ ($\phi_2' = 39°$), an improved stress history evaluation is obtained as presented in **Figure 7.15**. Overall, for the highly sensitive middle clay layer from 7 m to 20 m, excellent agreement is observed when compared with laboratory measured $\sigma_p'$ and OCR profiles reported by Bozozuk (1972) and Landon (2007).

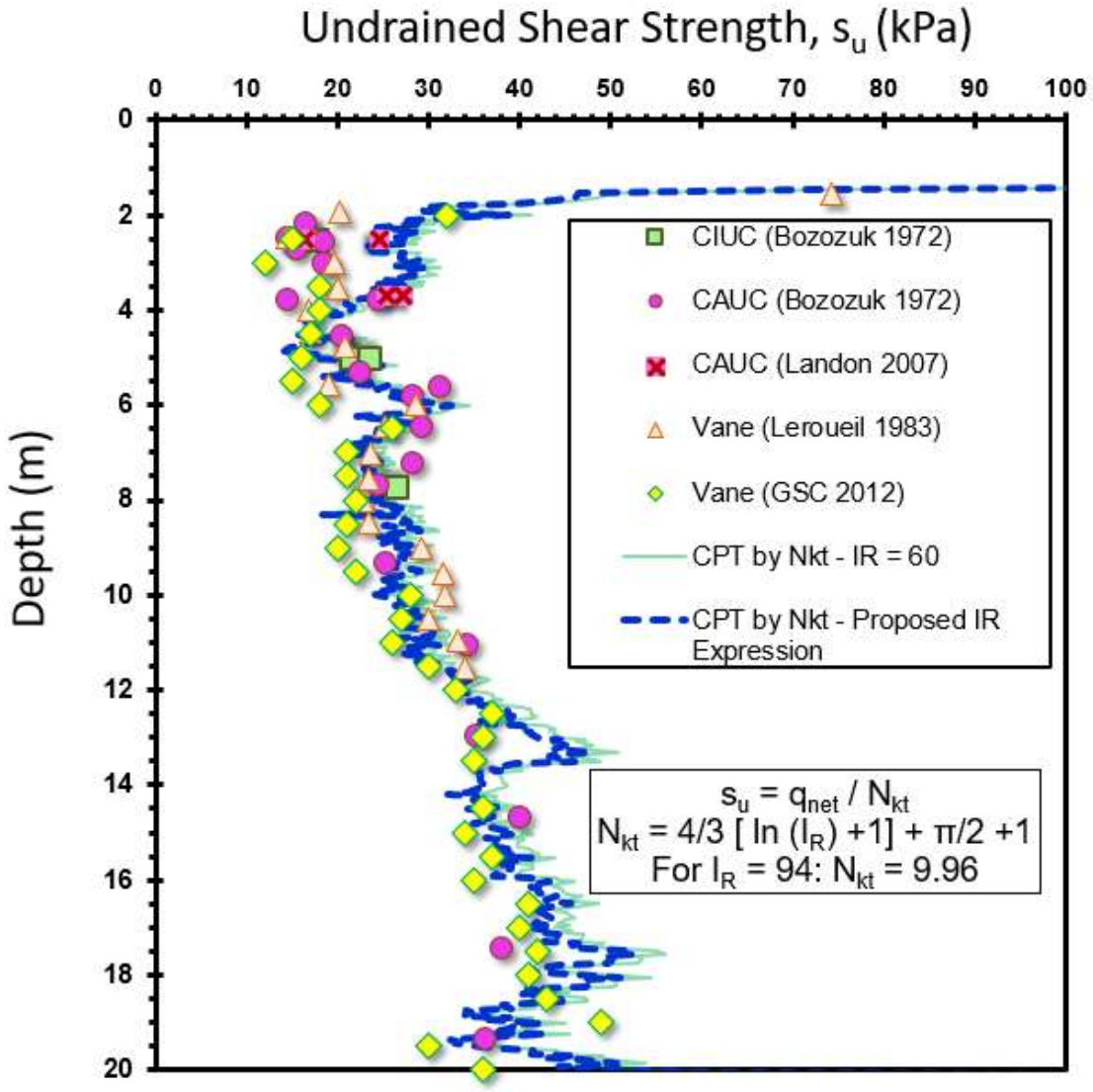


Figure 7.14. Undrained shear strength profile for Gloucester test site using the proposed modified SCE-CSSM operational rigidity index value and the corresponding cone bearing factor ($N_{kt}$)

For the depth range of 2 to 14 m which includes the upper clay and most of the middle clay layer, an equally satisfying agreement is observed when applying the same equations with the same values for the operational rigidity index and mobilized effective friction angles to piezocone sounding GSC-1 as presented in **Figure 7.16**. Below 14 m,

less agreement is seen between the three predictive profiles, however, they are closer than the original unmodified SCE-CSSM solution.

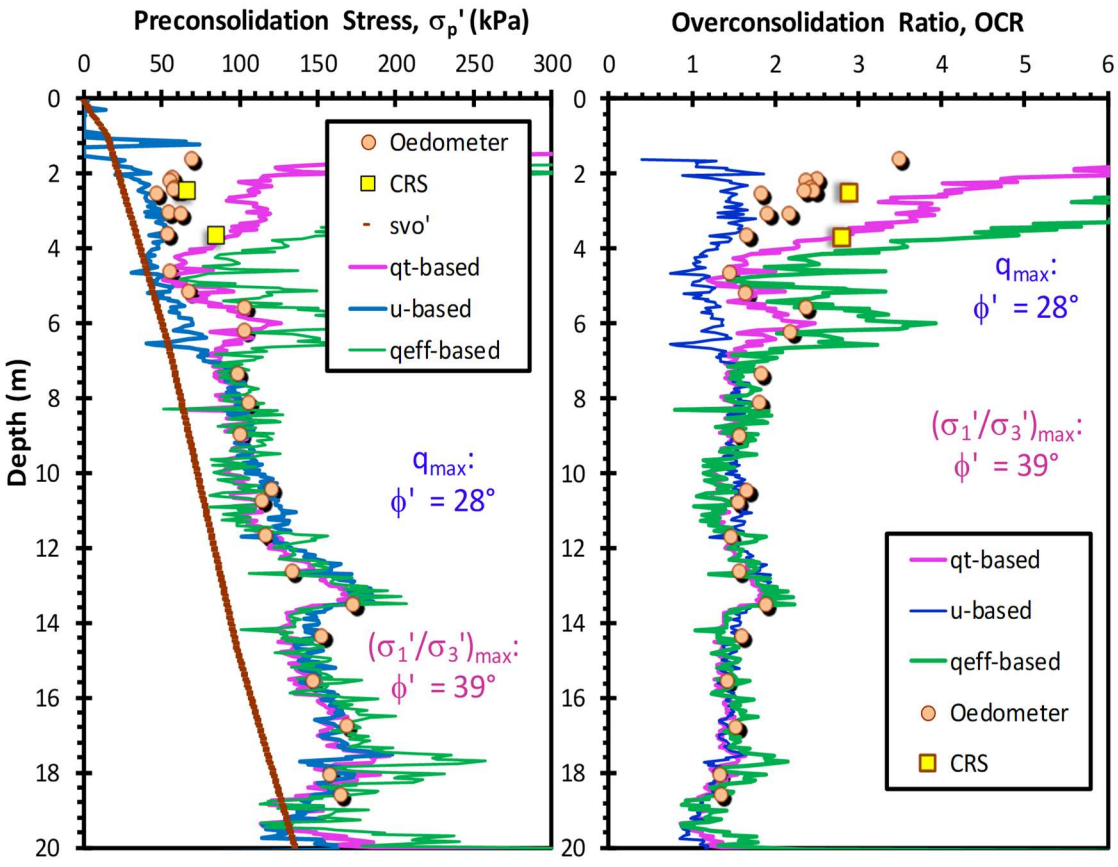


Figure 7.15. Profiles from modified SCE-CSSM solution and laboratory consolidation tests at Gloucester using CT-2 sounding: (a) effective preconsolidation stress, and (b) OCR (Note: oedometer data from Bozozuk, 1972; CRS data from Landon, 2007)

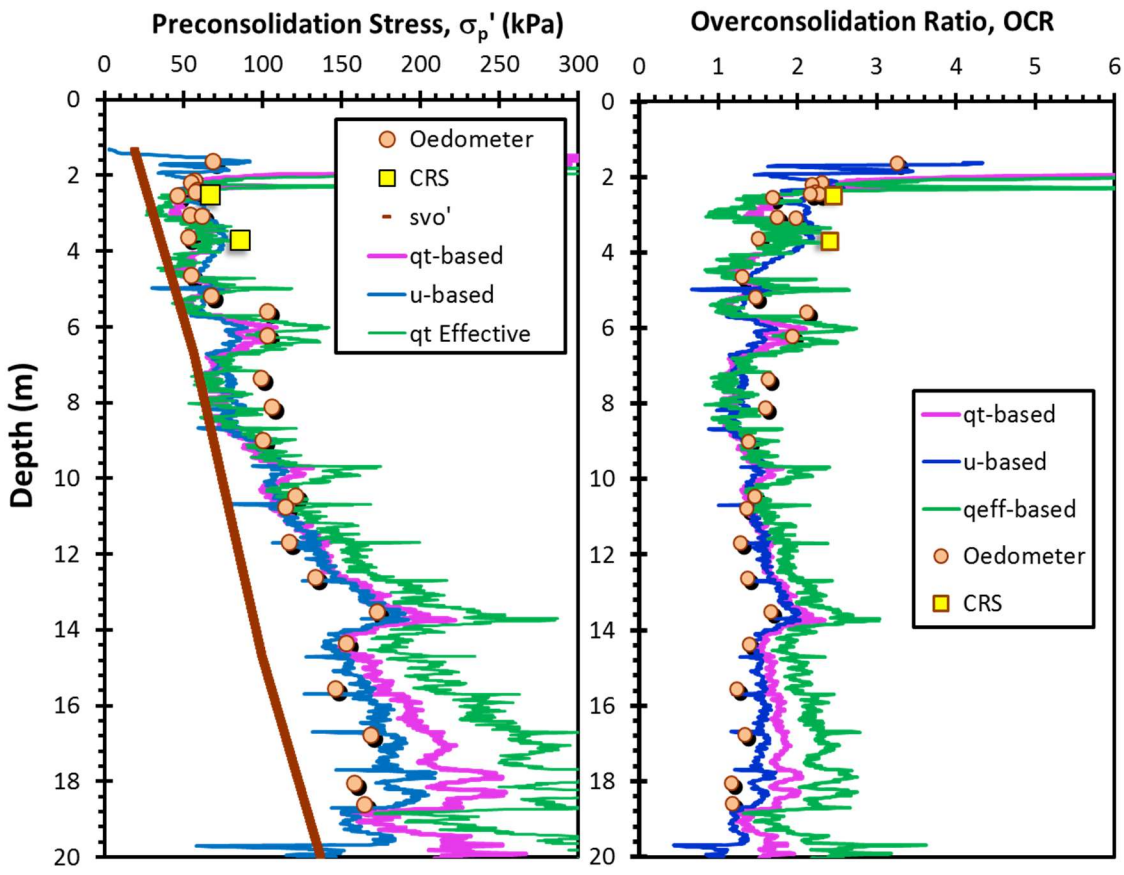


Figure 7.16. Profiles from modified SCE-CSSM solution & lab consolidation tests at Gloucester using GSC-1 sounding: (a) effective preconsolidation stress, and (b) OCR

## 7.10 Yield Stresses of Sensitive Clay at Tiller, Norway

Addition validation and suitability of the modified hybrid SCE-CSSM solution using results from other sensitive clays should be investigated. The Tiller site is underlain by a sensitive to quick Scandinavian clay and located at the Norwegian University of Science and Technology (NTNU) campus in Trondheim, Norway. The site is characterized by high degree of structure and high sensitivity values ($S_t > 30$), average water content (w) of about 40% and low plasticity index (PI) of about 5%. The clay has peak undrained shear strength values on the order of 50 kPa and can be considered within the lightly to the moderately overconsolidated range with OCRs < 5 (Gylland et al., 2013). **Figure 7.17**

presents the readings of a piezocone sounding conducted at the site which will be implemented in the modified hybrid solution.

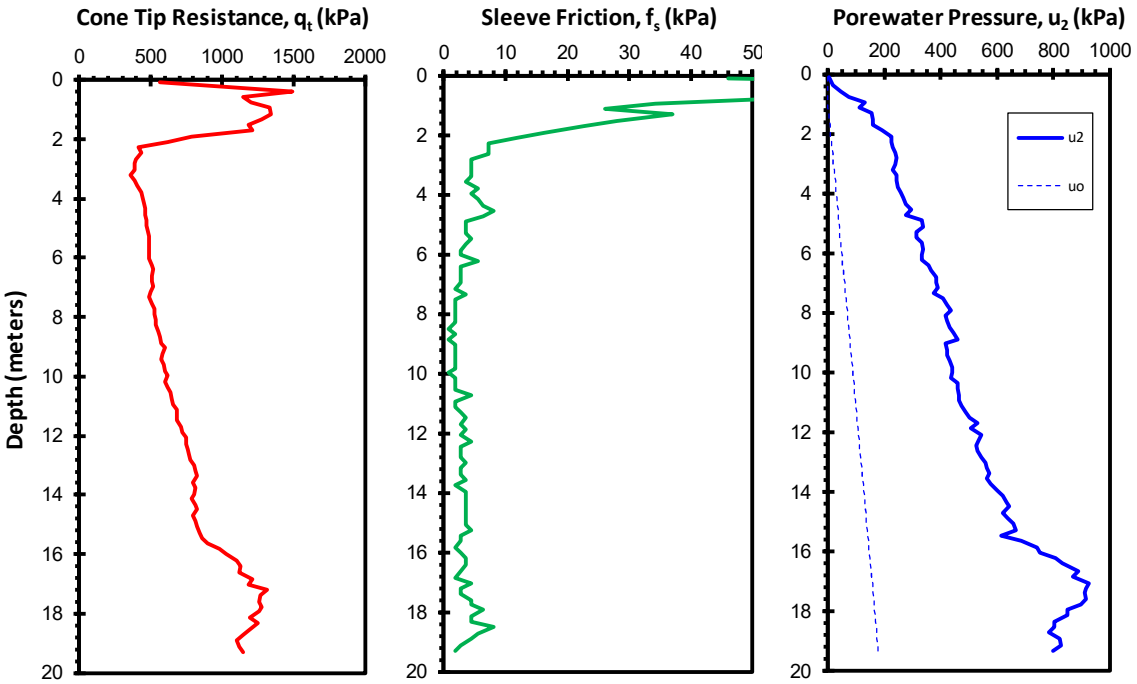


Figure 7.17. Piezocone sounding in sensitive clay at Tiller site in Norway: (a) cone tip resistance, $q_t$; (b) sleeve friction, $f_s$; (c) porewater pressure, $u_2$. (after Gylland et al., 2013)

Several site-specific input parameters are needed for the hybrid model along with piezocone readings ($q_t$ and $u_2$), such as the mobilized effective friction angles ($\phi_1'$ and $\phi_2'$), rigidity index ($I_R = G/s_u$), and plastic volumetric strain potential ($\Lambda = 1 - C_s/C_c$).

Gylland et al. (2013) conducted several CIUC tests on thin-walled steel fixed piston samples and block samples taken from different depths. The representative behavior of the sensitive clay at Tiller under triaxial compression testing at a depth of 9.65 m is presented in **Figure 7.18**. Similar to the behavior at Gloucester, the stress-strain, and porewater pressure behavior indicates that there is strain incompatibility, whereby the deviator stress ($\sigma_1 - \sigma_3$) reaches a peak strength at a strain level of about 2 % while the excess porewater

pressure is still developing. The maximum porewater pressures occur much later at strain levels of about 11 %.

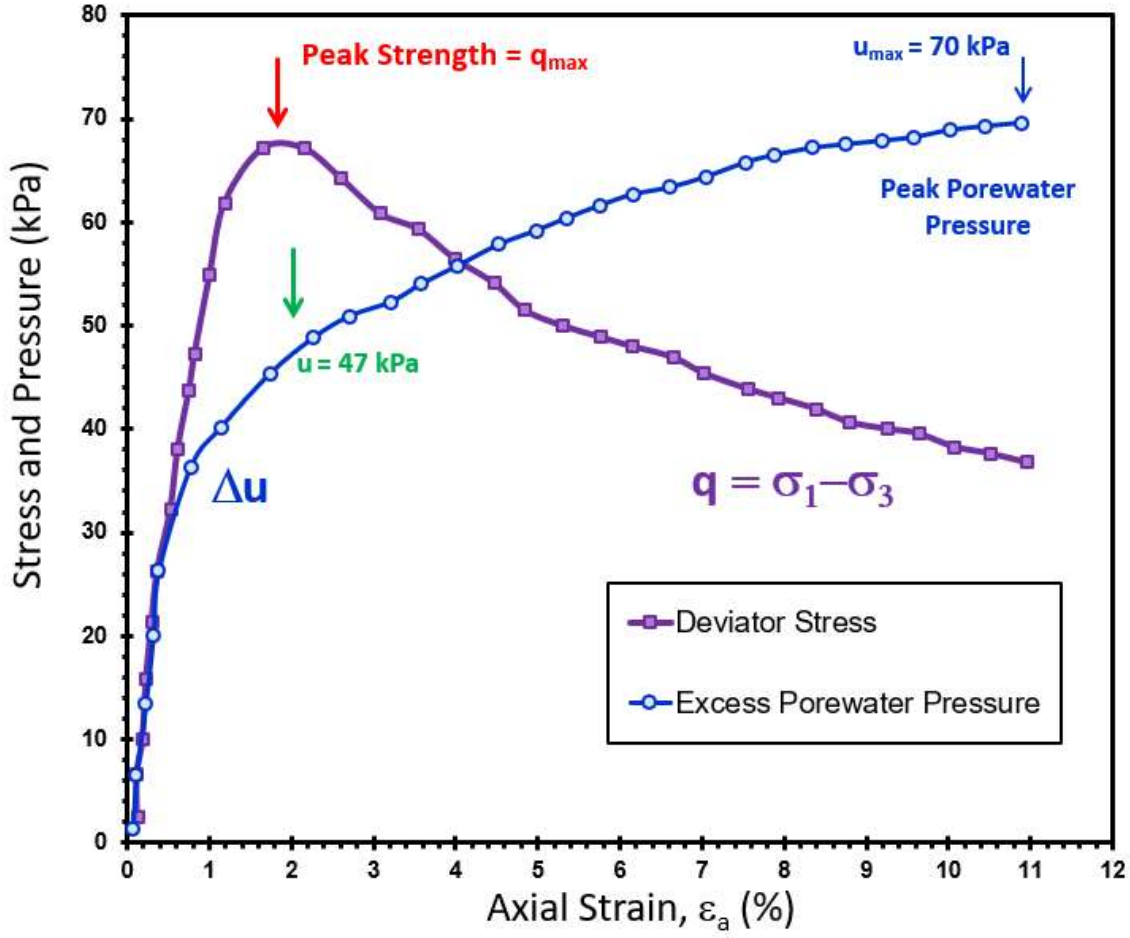


Figure 7.18. Strain incompatibility between $q_{max}$ and $\Delta u_{max}$ for Tiller site (CIUC triaxial data from Gylland et al., 2013)

Consequently, **Figure 7.19** shows that the mobilization of effective stress friction angle can be defined at: (a) peak stress ($q_{max}$) and (b) maximum obliquity $(\sigma_1'/\sigma_3')_{max}$. For Tiller, using five CIUC stress paths reported by Gylland et al. (2013) yields the corresponding values: $\phi'$ ($q_{max}$) = 31° and $\phi'$ (max. obliquity) = 36°. These values will be implemented in the modified hybrid solution.

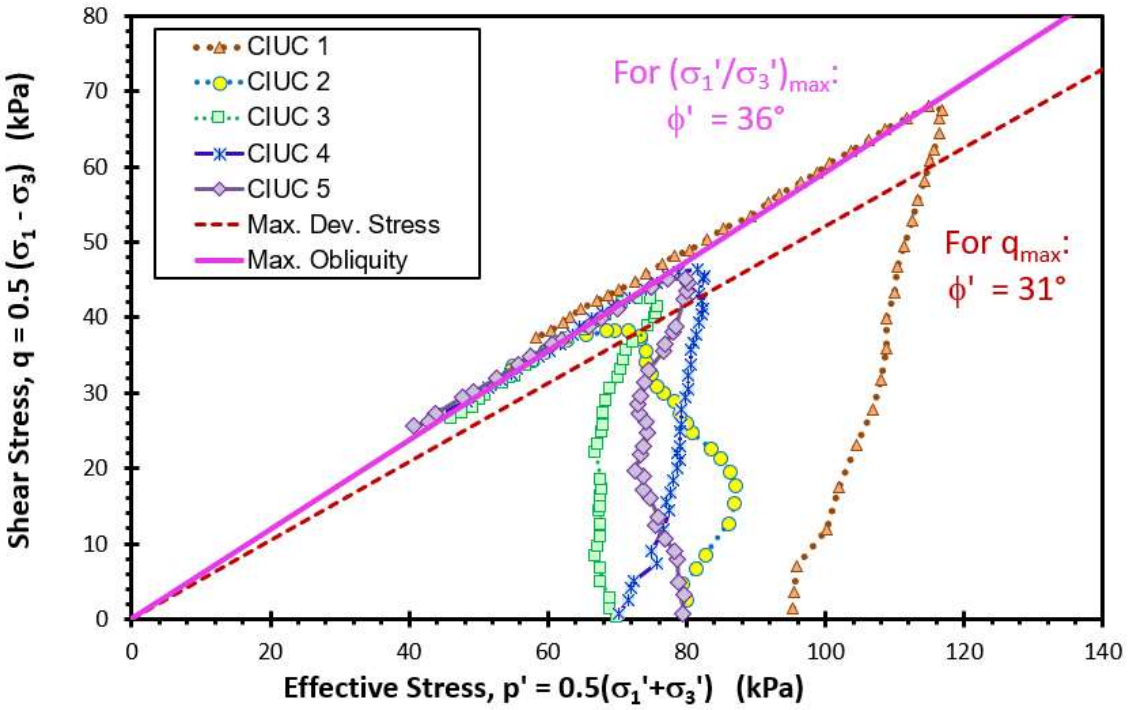


Figure 7.19. CIUC stress paths for Tiller site indicating two effective friction angles: at maximum triaxial stress $q_{max}$ and at $u_{max}$ corresponding to maximum obliquity (data after Gylland et al., 2013)

The operational value of rigidity index was obtained following the modified SCE-CSSM approach expressed in equation [7.21]. **Figure 7.20** presents the normalized porewater pressure term (U*-1) plotted versus the normalized cone tip resistance (Q) with a slope value of 0.60. Using equation [7.21b] with $\phi'_{qmax} = 31°$ and $\phi'_{MO} = 36°$, the evaluated operational rigidity index value is $I_R = 172$.

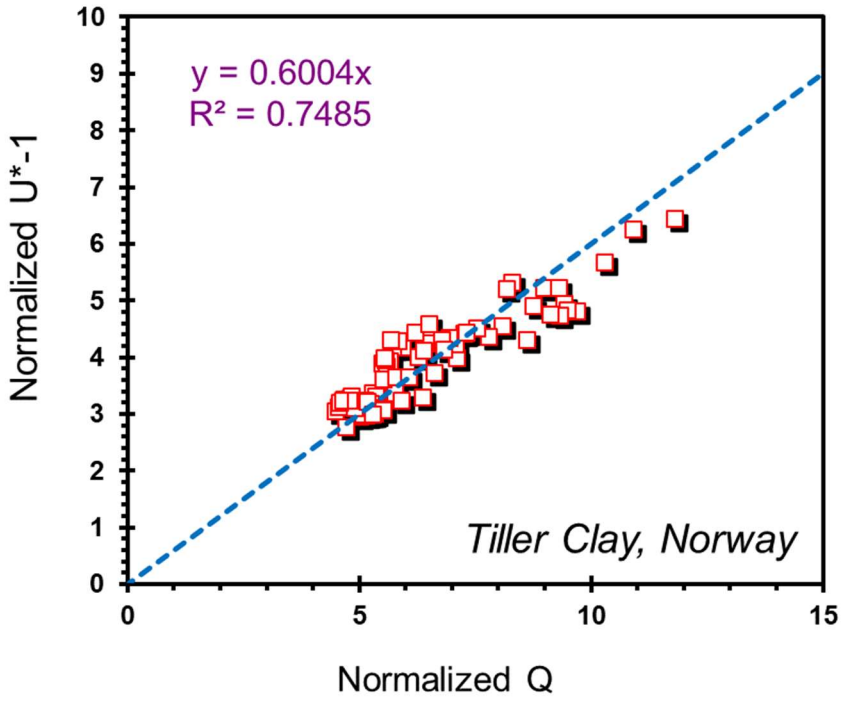


Figure 7.20. Normalized porewater pressure ratio (U*-1) versus normalized cone tip resistance (Q) for Tiller clay in Norway

**Figure 7.21** presents a compilation of CAUC and CIUC undrained shear strengths with depth reported by Gylland et al. (2013). Using the operational rigidity index $I_R = 172$ for the Tiller site, a calculated $N_{kt}$ value of 10.77 is obtained. This together with net cone tip resistance provides the calculated profile of $s_{uTC} = q_{net}/N_{kt}$ to give a reasonable match, as evident in **Figure 7.21**.

The assigned values of the geoparameters are input into the original hybrid SCE-CSSM model using a single effective friction angle value $\phi' = 31°$ along with an operational $I_R$ value of 100 and $\Lambda = 1$. **Figure 7.22** shows that the three CPTu expressions for $\sigma_p'$ and OCR give rather poor agreement for the sensitive Norwegian clay with wide scatter and

variability in the estimated parameters, thus indicating the inadequacy of the original hybrid model in capturing the stress history behavior of Tiller clay.

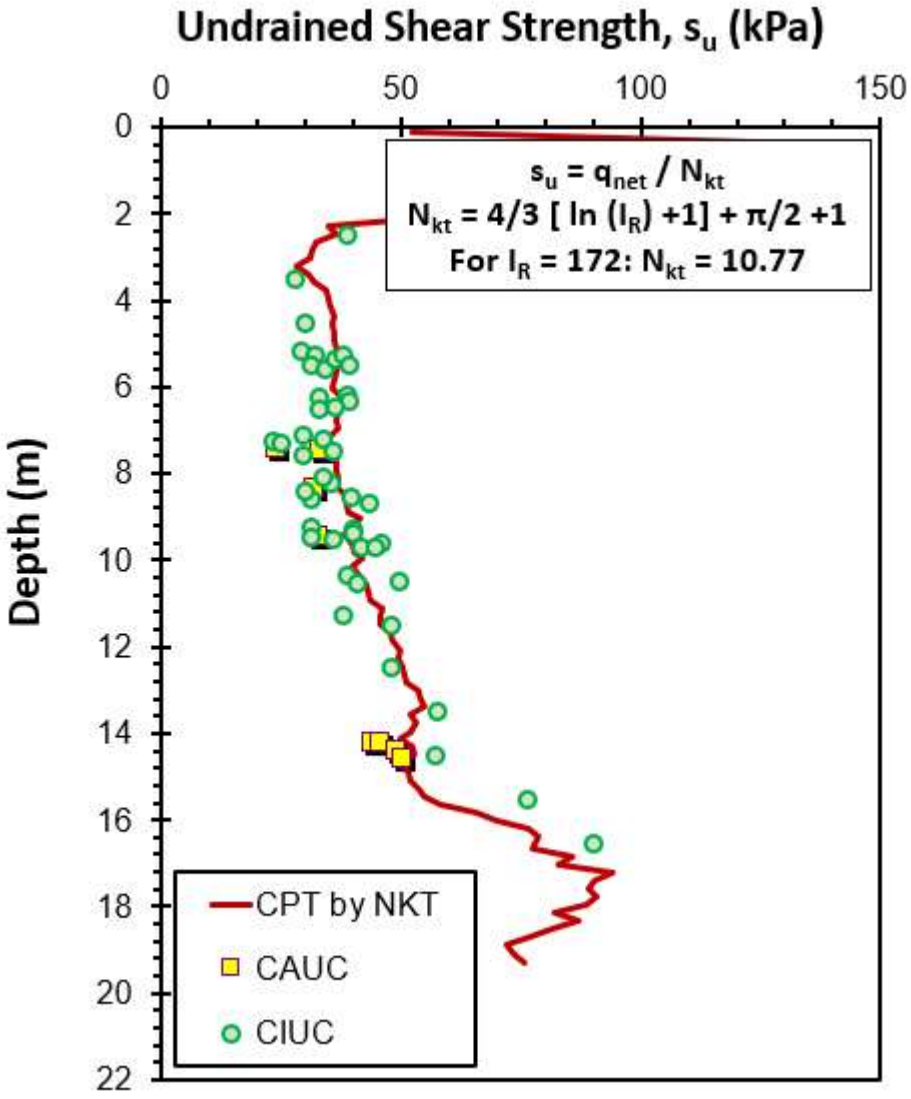


Figure 7.21. Undrained shear strength profile for Tiller clay using the proposed modified SCE-CSSM operational rigidity index value and the corresponding cone factor $N_{kt}$ (Note: data from Gylland et al. 2013)

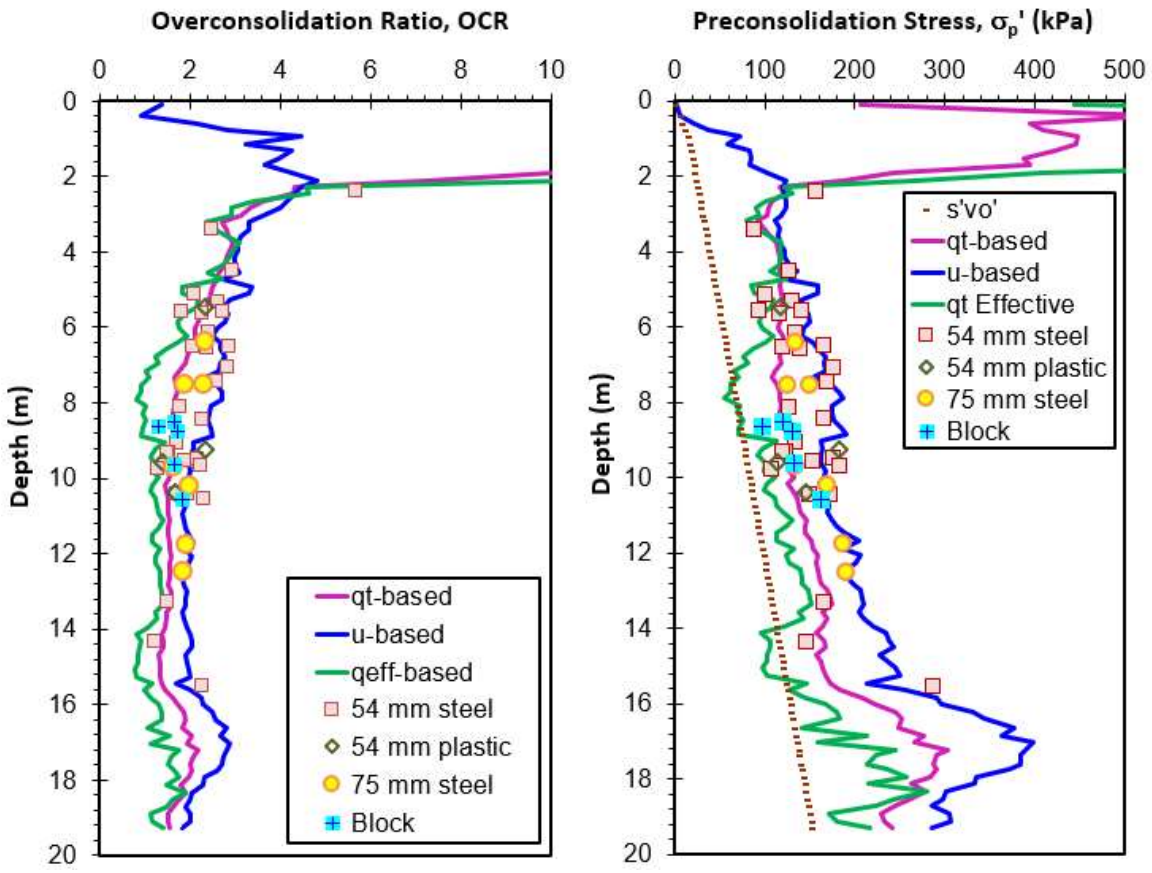


Figure 7.22. OCR and preconsolidation stress prediction using original hybrid SCE-CSSM framework for Tiller, Norway (consolidometer data from Gylland et al., 2013)

Alternatively, by applying equations [7.18], [7.19], and [7.20] to the results of the same piezocone sounding with an operational rigidity index value from modified SCE-CSSM approach of $I_R = 172$, $\Lambda = 1$, and mobilized effective friction angles values ($\phi_1' = 31°$ and $\phi_2' = 36°$), a much-improved and consistent stress history evaluation is obtained with relatively good agreement evident between the laboratory measured $\sigma_p'$ and OCR results, as presented in **Figure 7.23**. Accordingly, the modified hybrid SCE-CSSM solution appears to work in evaluating the stress history profile for Tiller clay and can be extended to sensitive and quick clays.

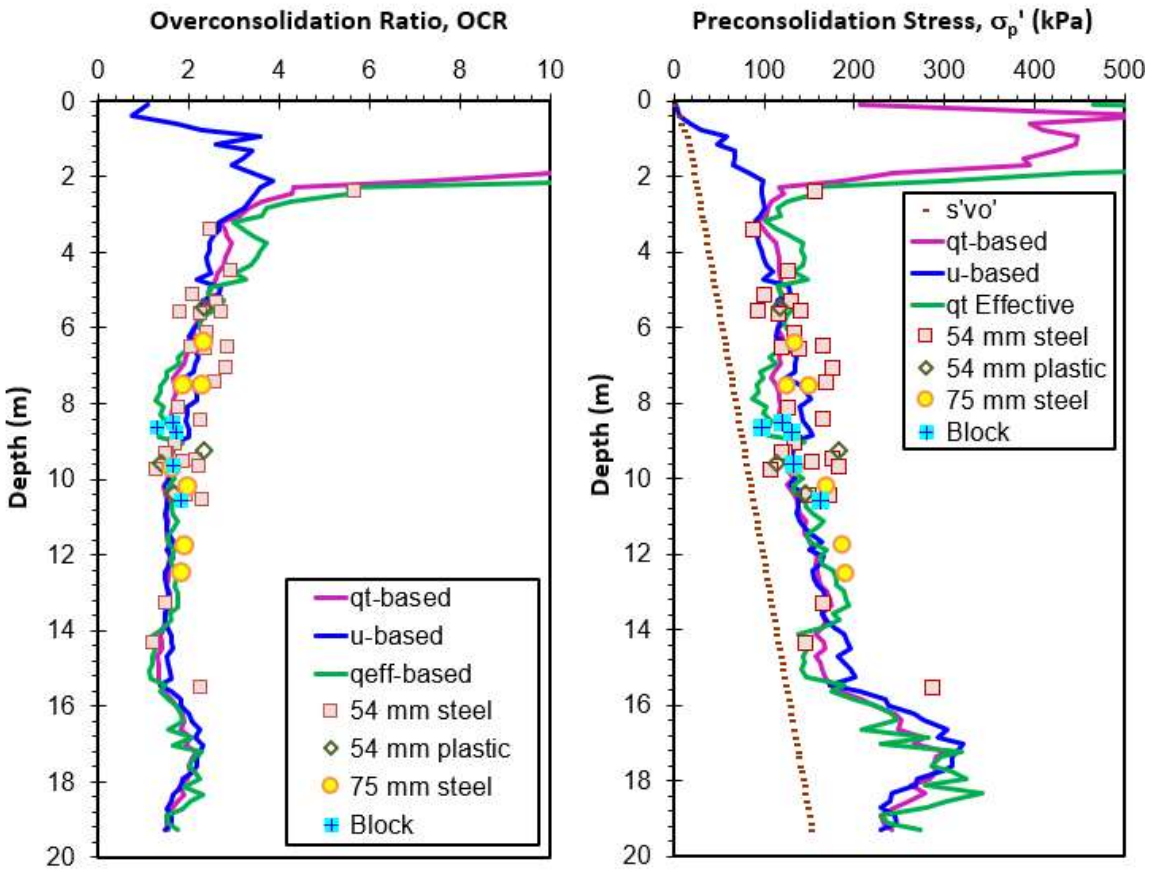


Figure 7.23. Profiles from modified SCE-CSSM solution and laboratory consolidation tests at Tiller, Norway: (a) OCR, and (b) effective preconsolidation stress

## 7.11 Yield Stresses of Structured Lacustrine Varved Clay at Amherst, MA, USA

The national geotechnical experimentation site (NGES) at the University of Amherst, Massachusetts, USA is underlain by Connecticut Valley Varved Clay (CVVC) which is a lacustrine soil deposit characterized by its varved nature with altering layers of silts and clays (Hegazy 1998; Lutenegger 2000). Given the complex stratification at this clay site, the undrained shear strength and hydraulic conductivity are anisotropic. The soil profile is composed of a shallow clay fill layer for the upper 1-2 m followed by 2-3 m of desiccated crust over a thick soft clay-silt deposit exceeding 20 to 30 m. The thick soft

varved clay layer has an average water content of 62%, average liquid limit of 51%, average plasticity index of 20% and average density of 1.66 $Mg/m^3$ (DeGroot & Lutenegger, 2003). The clay-silt deposit is characterized by high field vane sensitivity values ranging from 5 to 25 which makes it suitable for investigation of the modified SCE-CSSM model. While the clay is lacustrine in origin, it does not actually qualify as a sensitive clay since it was not originally a marine deposit. Instead, it appears to have developed bonding and cementation by other geoenvironmental processes and therefore found to be a structured soft clay deposit (DeGroot & Lutenegger 2003).

Given the nature of the site, extensive field and laboratory testing programs have been carried out to characterize the soils at this national experimentation site. For instance, Hegazy (1998) performed 15 seismic piezocone soundings (SCPTu) on the property. **Figure 7.24** presents the results of a representative piezocone sounding that will be implemented in the modified hybrid solution. As for the input geoparameters, the effective friction angle ($\phi$') was investigated by considering the results of anisotropically consolidated triaxial compression (CAUC) tests conducted by Sambhandharaksa (1977). The representative stress-strain and porewater pressure behavior of Amherst varved clay is presented in **Figure 7.25**. As before, strain incompatibility is noted whereby the deviator stress ($\sigma_1 - \sigma_3$) reaches a peak strength at a strain level of about 1 % while porewater pressures reach a maximum much later at strain levels > 16 %.

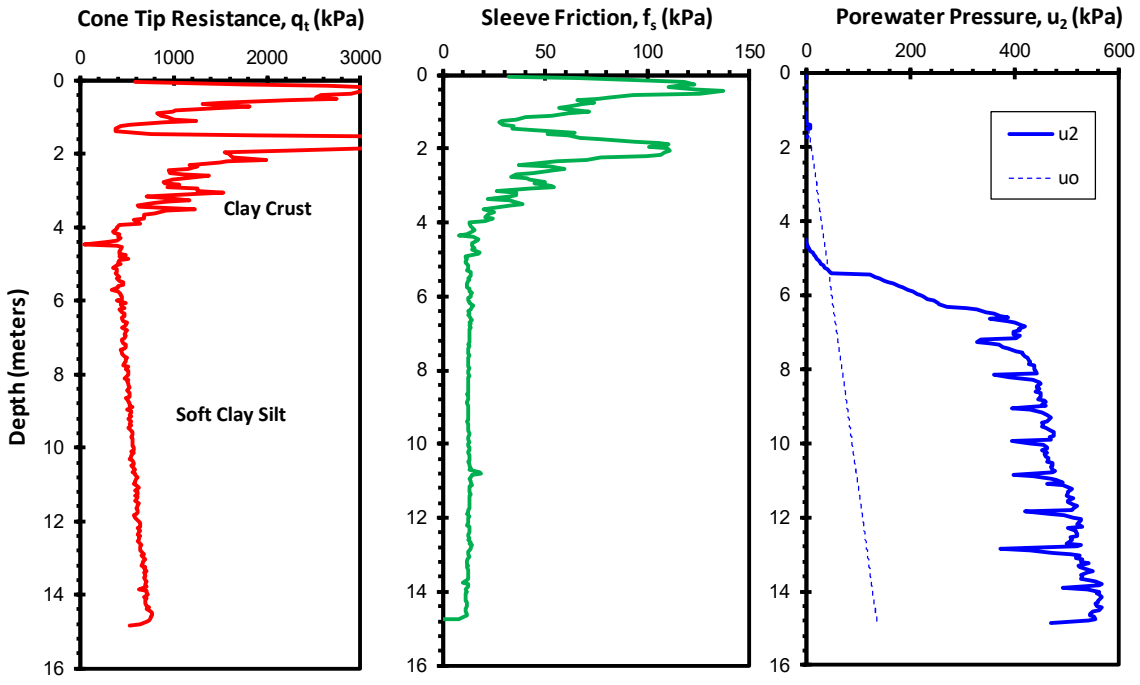


Figure 7.24. Results from a representative piezocone sounding in structured clay at Amherst, MA: (a) total cone tip resistance, $q_t$; (b) sleeve friction, $f_s$; (c) porewater pressure, $u_2$ (data from Hegazy, 1998)

Consequently, **Figure 7.26** shows that mobilized effective stress friction angles at maximum deviator stress and maximum obliquity. Using three CAUC tests reported by Sambhandharaksa (1977) which were conducted at OCR values of 1, 2, and 4 yields the corresponding values: $\phi'_{qmax} = 22°$ and $\phi'_{MO} = 30°$.

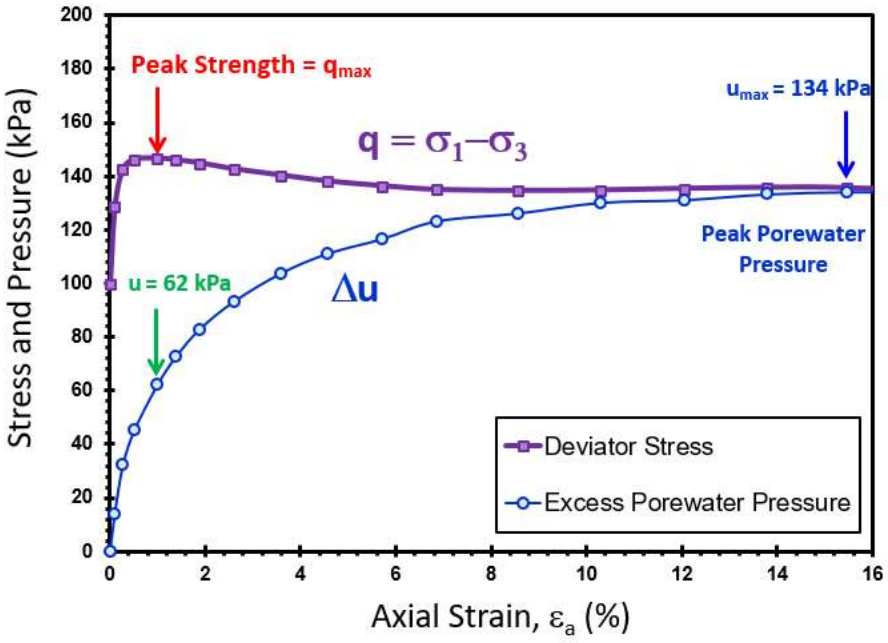


Figure 7.25. Stress vs. strain and Δu versus strain for structured varved clay at Amherst, Massachusetts (CAUC triaxial data from Sambhandharaksa, 1977)

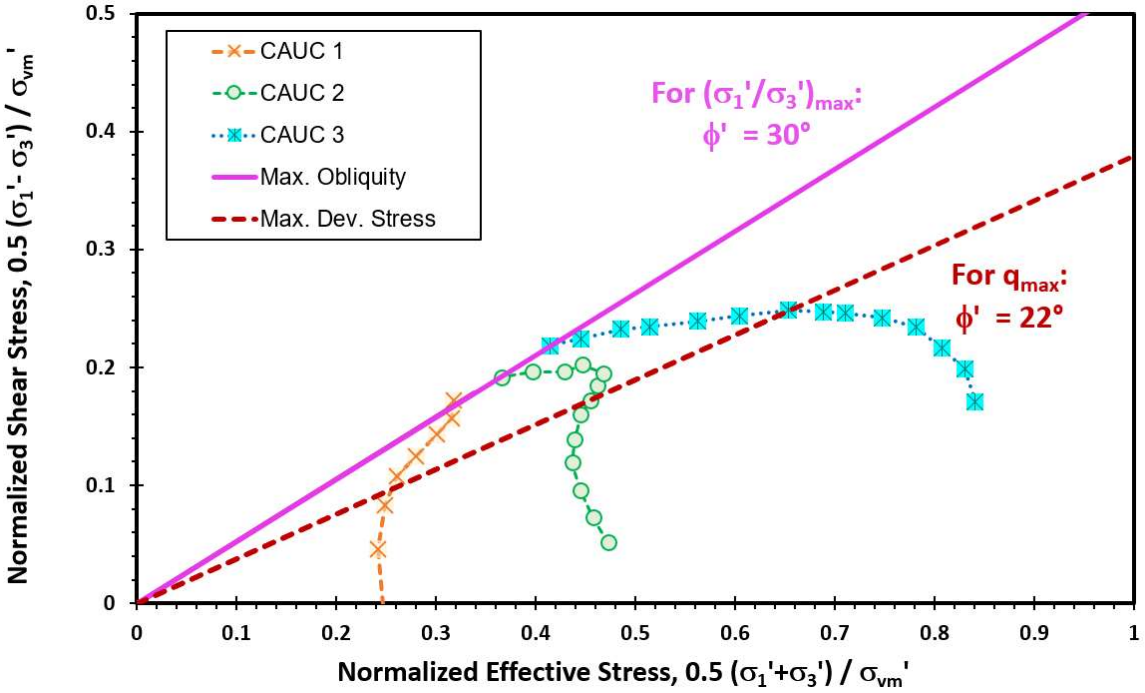


Figure 7.26. CAUC stress paths for Amherst, MA indicating mobilized effective friction angles: (1) $\phi_1'$ at $q_{max}$ and (2) $\phi_2'$ at $u_{max}$ (data from Sambhandharaksa, 1977)

As for the rigidity index, the approach from modified SCE-CSSM was adopted where normalized porewater pressure term (U*-1) is plotted against the normalized cone resistance (Q) as shown in **Figure 7.27.** This gives a corresponding slope of 0.737 for the ratio: (U*-1)/Q. Using the slope value with $\phi_1' = 22°$ and $\phi_2' = 30°$, $\Lambda = 0.95$, the evaluated operational rigidity index value from equation [7.21b] is $I_R = 356$.

**Figure 7.28** presents profiles of CAUC and CIUC undrained shear strengths reported by DeGroot & Lutenegger (2003) for thick soft varved clay-silt deposit at depths > 5 m. Assigning rigidity index of $I_R = 356$ for the Amherst CVVC site, a calculated $N_{kt}$ value of 11.74 is obtained. This together with net cone tip resistance gave a reasonable match to the triaxial results, as evident in **Figure 7.28**.

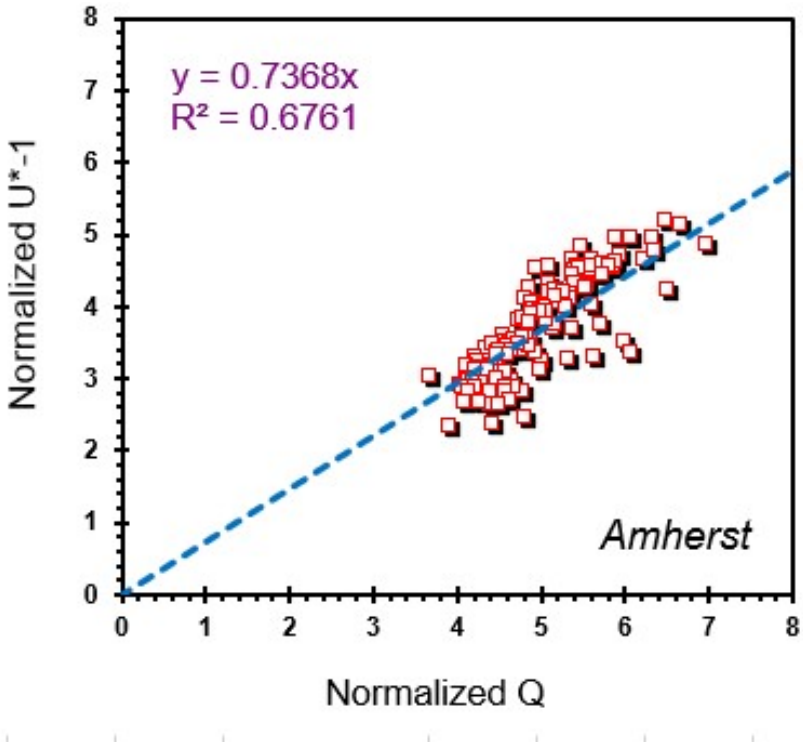


Figure 7.27. Normalized porewater pressure ratio (U*-1) versus normalized cone tip resistance (Q) for Amherst clay

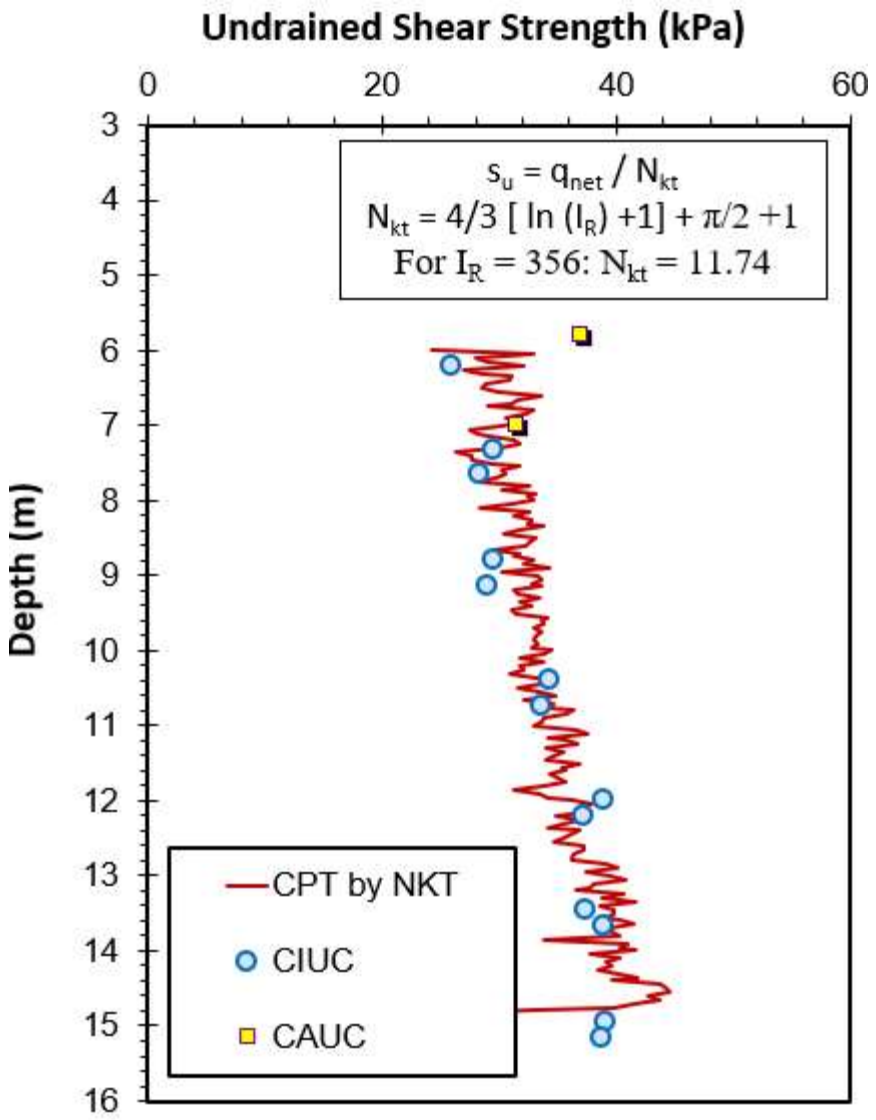


Figure 7.28. Undrained shear strength profile for Amherst, MA using the proposed modified SCE-CSSM operational rigidity index value and cone bearing factor $N_{kt}$ (Note: triaxial data from DeGroot & Lutenegger, 2003)

The assigned geoparameter values ($\phi_1' = \phi_2' = 30°$ and $\Lambda = 0.85$) are applied to the original SCE-CSSM model with an operational rigidity index value of 200 is first investigated. **Figure 7.29** shows that the three CPTu expressions for $\sigma_p'$ and OCR give rather poor agreement with wide scatter and variability in the estimated evaluations. This

shows the unsuitability of the original formulae in capturing the stress history in Amherst varved clay.

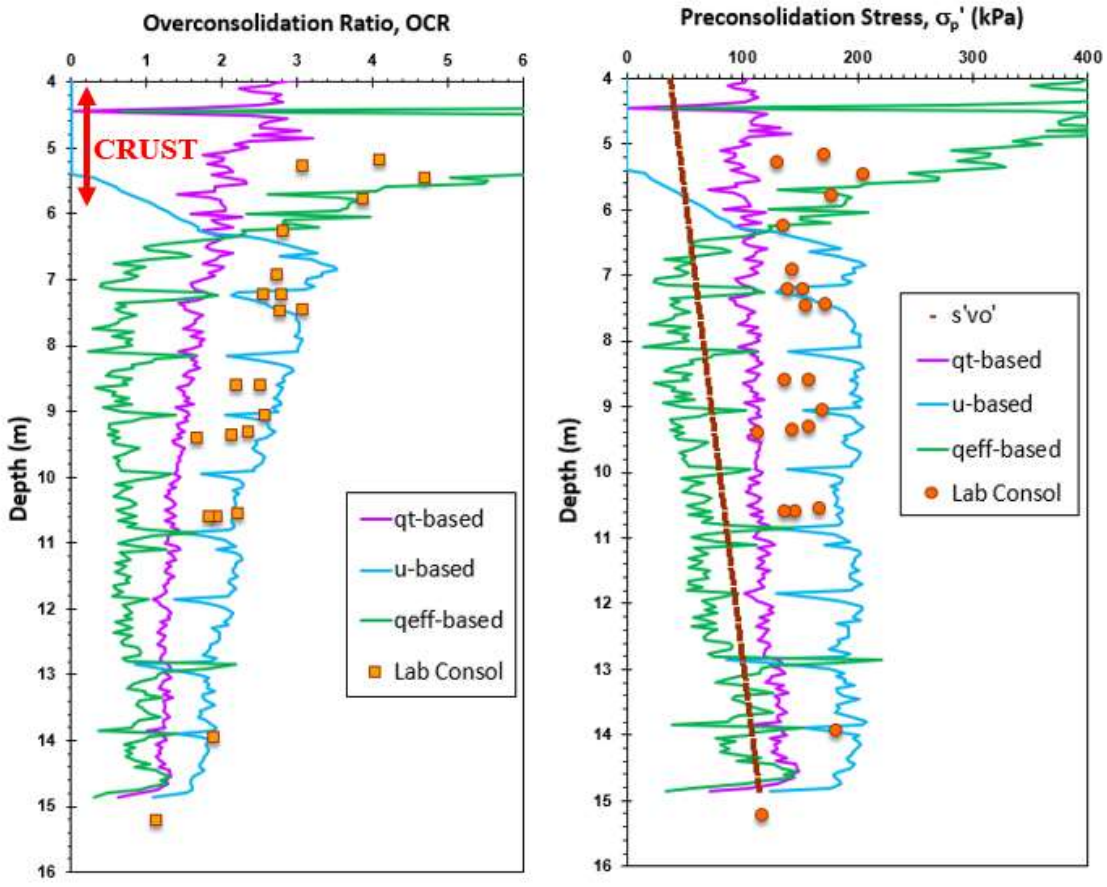


Figure 7.29. Profiles of OCR and effective preconsolidation stress using the original SCE-CSSM framework in structured varved clay at Amherst, MA
(Note: lab consolidometer data from DeGroot & Lutenegger, 2003)

By employing the modified solution given by equations [7.18], [7.19], and [7.20] to the results of the same piezocone sounding with input value of $I_R = 356$, $\Lambda = 0.85$, and mobilized effective friction angle values ($\phi_1' = 22°$ and $\phi_2' = 30°$), an improved stress history evaluation is obtained. The relatively good agreement between the laboratory measured $\sigma_p'$ and OCR results with CPTU-evaluations are presented in **Figure 7.30**.

Accordingly, the modified hybrid SCE-CSSM solution works in estimating the stress history profile for Amherst varved clay.

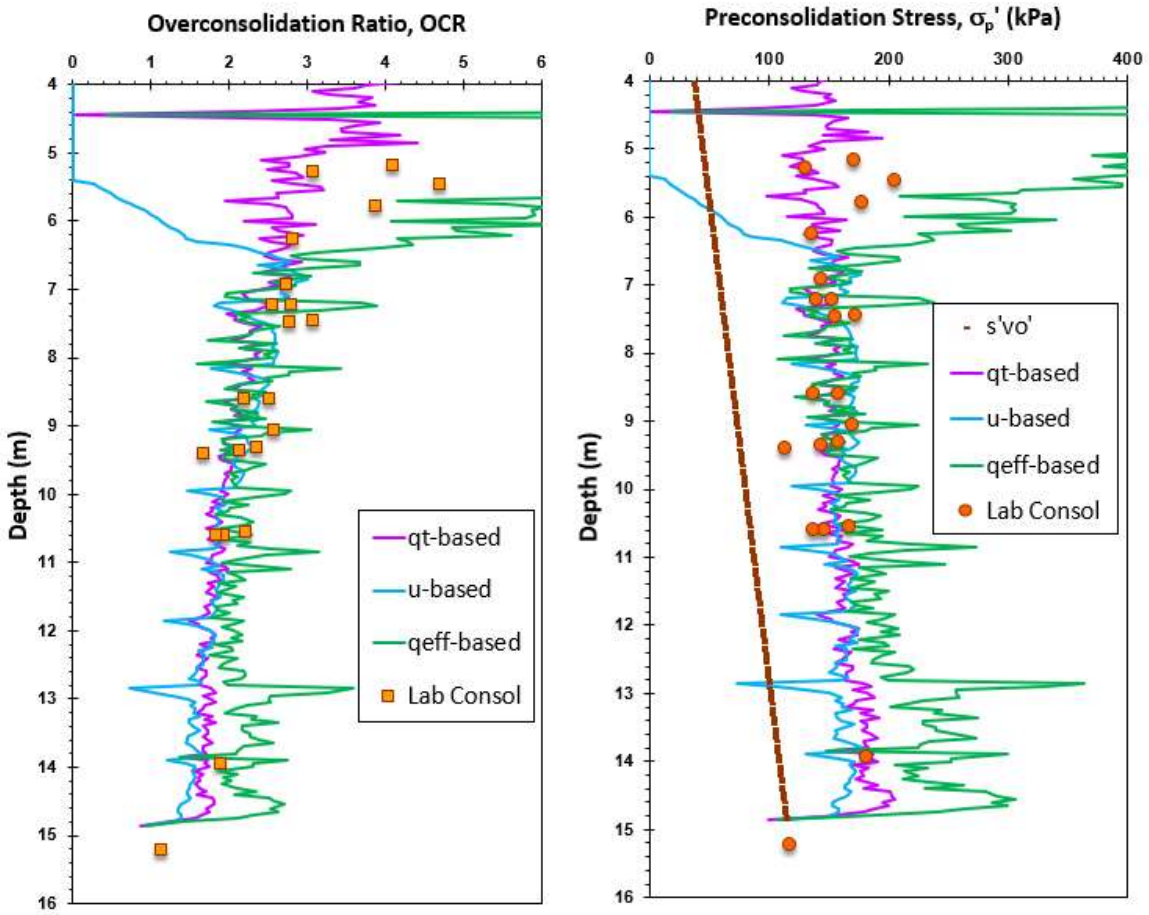


Figure 7.30. Profiles from modified SCE-CSSM solution and laboratory consolidation tests at Amherst, MA: (a) OCR and (b) effective preconsolidation stress

### 7.12 Flow Properties from Piezodissipation Tests

The results of piezocone dissipation tests can be used to evaluate the permeability and the coefficient of consolidation of fine-grained soils (Jamiolkowski et al. 1985). As the piezocone penetrates the ground, transient excess porewater pressures are generated around the probe. When the penetration is halted, the measured $u_2$ readings decay over time until eventually reaching the hydrostatic porewater pressure value ($u_0$) which is the equilibrium

condition. The coefficient of consolidation, $c_{vh}$ controls the rate of dissipation over time and is computed as:

$$c_{vh} = \frac{k \cdot D'}{\gamma_w} \quad [7.25]$$

where k = coefficient of permeability, D' = soil constrained modulus, and $\gamma_w$ = unit weight of water.

The nomenclature for the coefficient of consolidation from consolidation tests is designated $c_v$ to indicate the flow of water in the vertical direction. Often, for piezocone dissipation tests, the nomenclature $c_h$ has been used to indicate flow predominant in the horizontal direction, such as applied to piezocones, driven piling foundations, and wick drains. Herein, the parameter is designated $c_{vh}$ to indicate essentially flow occurs in both vertical and horizontal directions. Careful laboratory studies have clearly shown that most natural marine, deltaic, and glaciomarine clays have, in fact, nearly isotropic permeability characteristics (Tavenas et al. 1982; Leroueil et al. 1990; Leroueil & Jamiolkowski 1991; Leroueil and Hight, 2003; Kelly 2006; Mayne 2007).

Results of the piezodissipation tests at Gloucester are analyzed to evaluate the coefficient of consolidation ($c_{vh}$) and hydraulic conductivity (k), also termed the coefficient of permeability. While several procedures are available (e.g., Robertson et al. 1992; Chai et al. 2012), the original SCE-CSSM approach is detailed by Burns & Mayne (1998a, 1998b) and can be used here without alterations since the solution depends solely on the porewater pressures and input parameters. In this case, simply the higher mobilized $\phi_2'$ value is used for evaluating the excess porewater pressure responses.

The generated excess porewater pressures that are measured are the sum of octahedral plus shear-induced components, which can be computed as:

$$\Delta u_{2\,i} = (\Delta u_{oct})_i + (\Delta u_{shear})_i \quad [7.26]$$

where the octahedral component is represented by spherical cavity expansion that extends the plastic zone out into the surrounding ground (i.e., D/d ratio) and the shear-induced part occurs at the soil-structure interface as the steel of the penetrometer rubs against the clay soil (thin shear zone) and represented by CSSM. The initial values are determined from:

$$(\Delta u_{oct})_i = (2 \cdot M_{c2}/3)\,(OCR/2)^{\Lambda} \cdot \ln(I_R) \cdot \sigma_{vo}' \quad [7.27]$$

$$(\Delta u_{shear})_i = [1 - (OCR/2)^{\Lambda}] \cdot \sigma_{vo}' \quad [7.28]$$

These two components dissipate at different rates because they are separate phenomena. Coupled flow is unwarranted and not applicable here. Hence, porewater pressure can be evaluated at any time (t) using the following algorithm (Mayne 2001):

$$(\Delta u_2)_t = \frac{(\Delta u_{oct})_i}{1 + 50 \cdot T'} + \frac{(\Delta u_{shear})_i}{1 + 5000 \cdot T'} \quad [7.29]$$

where the modified time factor (T') is given by:

$$T' = \frac{c_{vh} \cdot t}{a_c \cdot I_R^{\,0.75}} \quad [7.30]$$

where t = elapsed time after stopping penetration and $a_c$ = piezocone radius.

The value of $c_{vh}$ is found by trial-and-error fitting of the theoretical curves to the measured dissipation data, where assigned values of T' are used to obtain the corresponding time for a given rigidity index and cone radius. According to Burns and Mayne (1998), the actual size of the thin sheared zone is uncertain and depends on several factors, including

verticality of the sounding, penetrometer roughness, soil type, plasticity, and residual shear strength. The fitted values of $c_{vh}$ are not affected by the actual size of the thin shearing zone as the excess porewater pressure around this region should have fully dissipated by the time the peak value is reached, therefore a thin shear zone on the order of 2 mm was adopted by Burns and Mayne (2002) for pragmatic considerations.

### 7.13 Flow Parameters at Gloucester

While the Gloucester site has previously been subjected to piezocone testing (e.g., Konrad & Law 1987; Yafrate & DeJong 2006; Nader et al. 2015), the piezodissipation series reported by McQueen et al. (2016) are the first of their kind. It is therefore of interest to analyze these data and evaluate the flow parameters of the clays, specifically the coefficient of consolidation ($c_{vh}$) and hydraulic conductivity (k).

The recent piezocone sounding CT-1 accumulated a total 23 dissipation tests at Gloucester, as presented in **Figure 7.31** in terms of measured $u_2$ versus square root of time (McQueen et al. 2016). The data can be expressed alternatively in terms of normalized excess porewater pressures versus the logarithm of time, as seen in **Figure 7.32** where the $\Delta u_2 = (u_2-u_0)$ at each depth and time are divided by the initial $\Delta u_{2i}$ obtained during the CPTu. Beneath a 3-m thick crustal clay layer, a review of the dissipation responses at each one-meter depth shows that the clay soil profile at Gloucester can be classified into three distinct groupings: (a) an upper clay layer at depths from 4 to 7 m; (b) middle clay layer from depths of 8 to 18 m; and (c) lower clay at depths of 19 to 21 m.

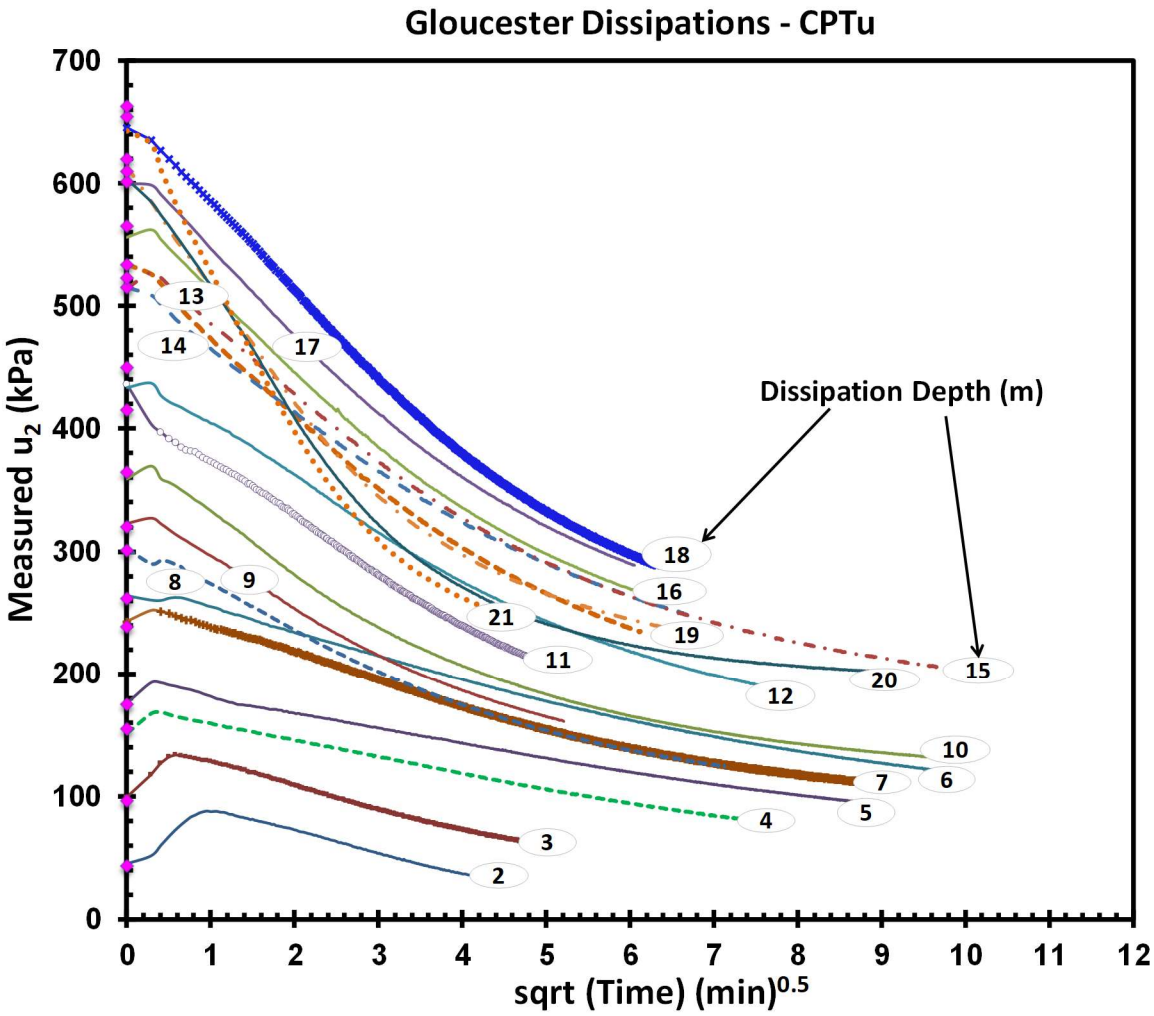


Figure 7.31. Individual dissipation records at Gloucester at one-meter depth intervals showing measured porewater pressure versus square root of time (after McQueen et al., 2016)

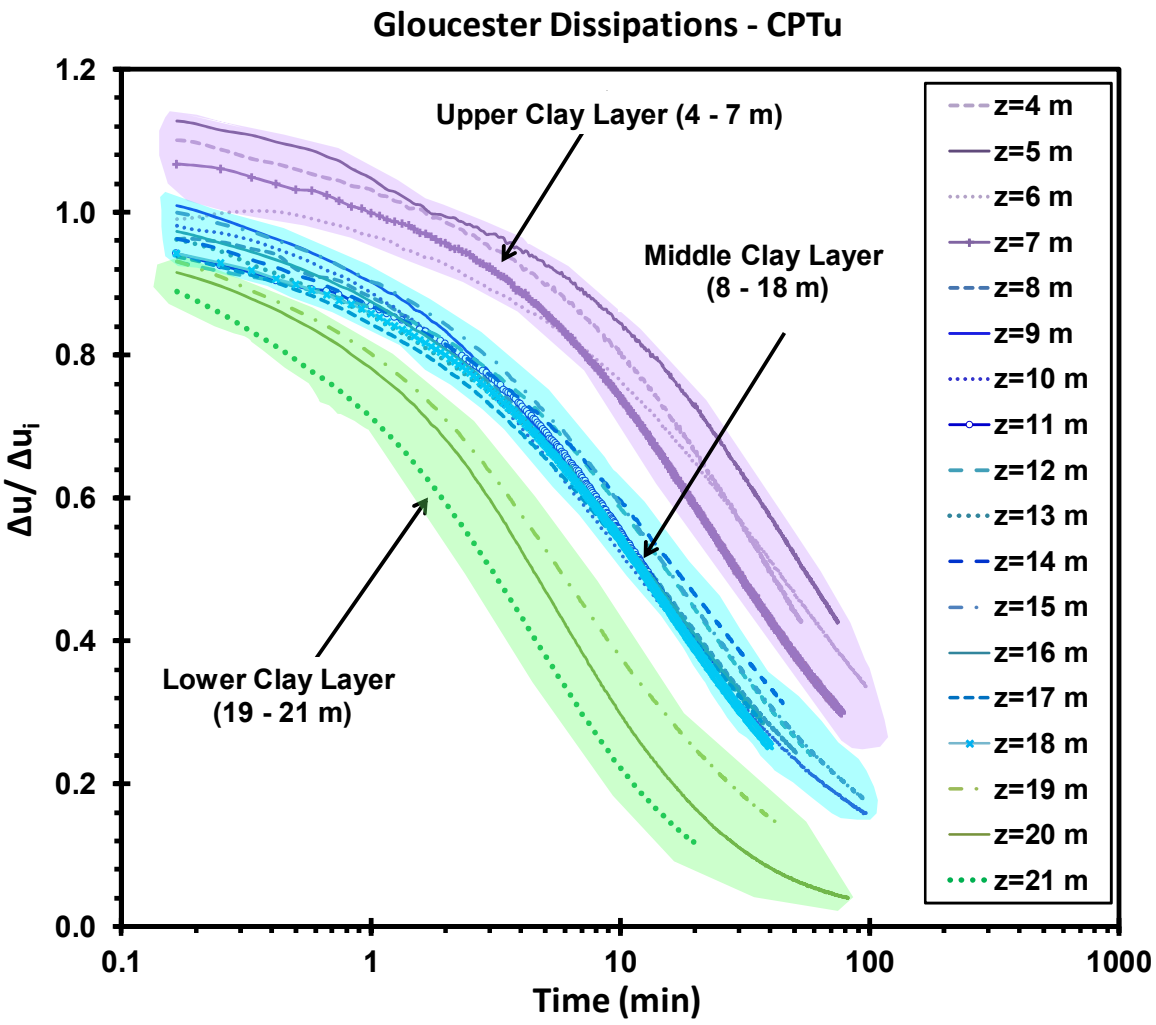


Figure 7.32. Normalized excess porewater pressures versus logarithm of time at Gloucester test site (after McQueen et al., 2016)

Results using the hybrid cavity expansion-critical state soil mechanics (SCE-CSSM) analytical method are presented in Figures **7.33**, **7.34**, **7.35, and 7.36** for respective depths of 6m, 9m, 12 m, and 19 m, with corresponding values of $c_{vh}$ found using trial-and-error fitting of the theoretical curves with the measured dissipation data. **Figure 7.33** illustrates a dissipation test for the upper clay layer at depth of 6 meters where the back figured value of $c_{vh}$ is 0.065 $mm^2$/sec. **Figures 7.34 and 7.35** illustrate two piezodissipation test for the middle clay layer at depth of 9 and 12 meters where the back figured value of

$c_{vh}$ is 0.28 and 0.20 mm$^2$/sec. **Figure 7.36** illustrates a dissipation test for the lower clay layer at depth of 19 meters where the back figured value of $c_{vh}$ is 0.7 mm$^2$/sec.

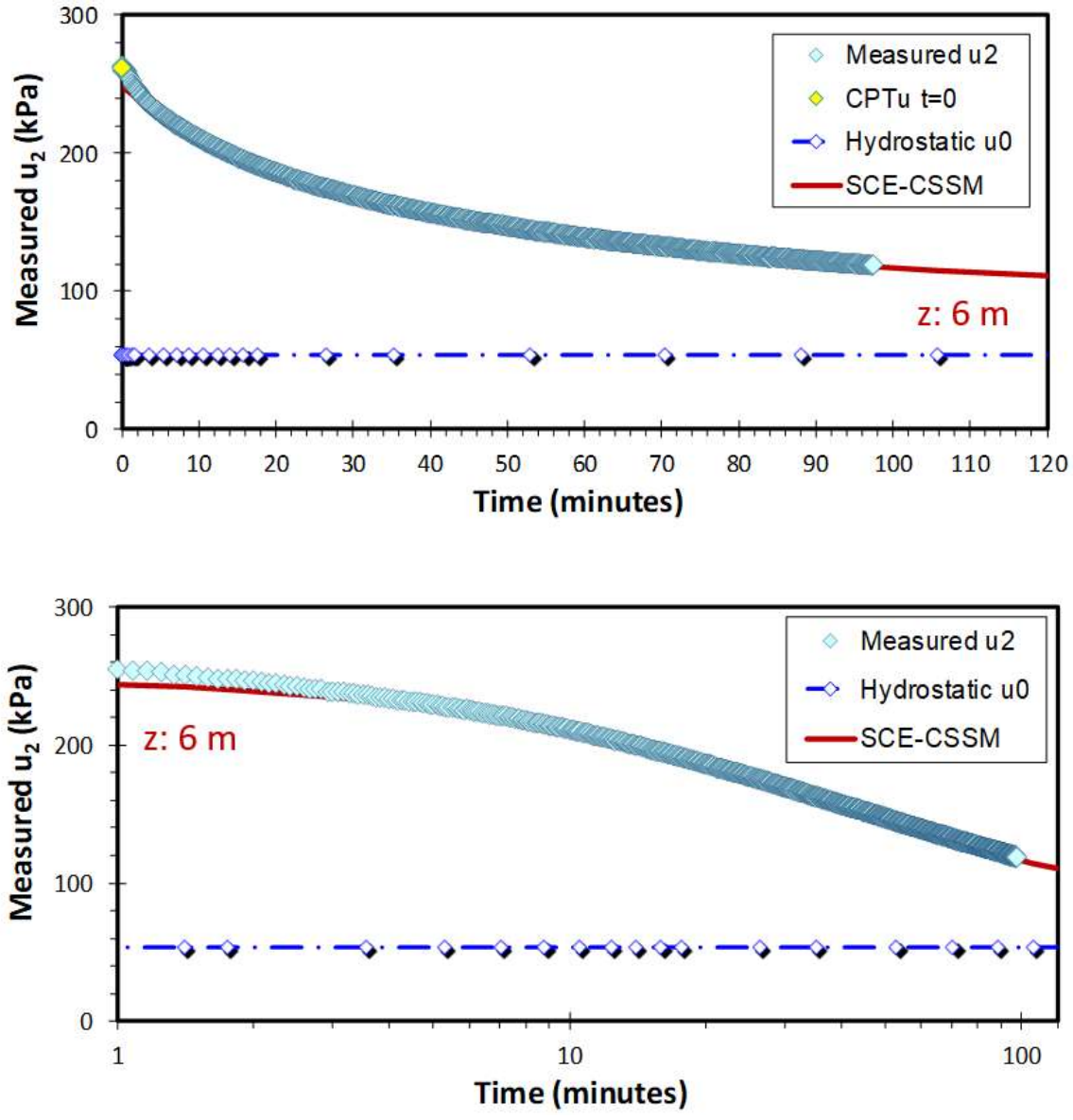


Figure 7.33. Measured piezodissipation record for upper clay layer at Gloucester test site at depth of 6 meters with prediction using hybrid SCE-CSSM framework

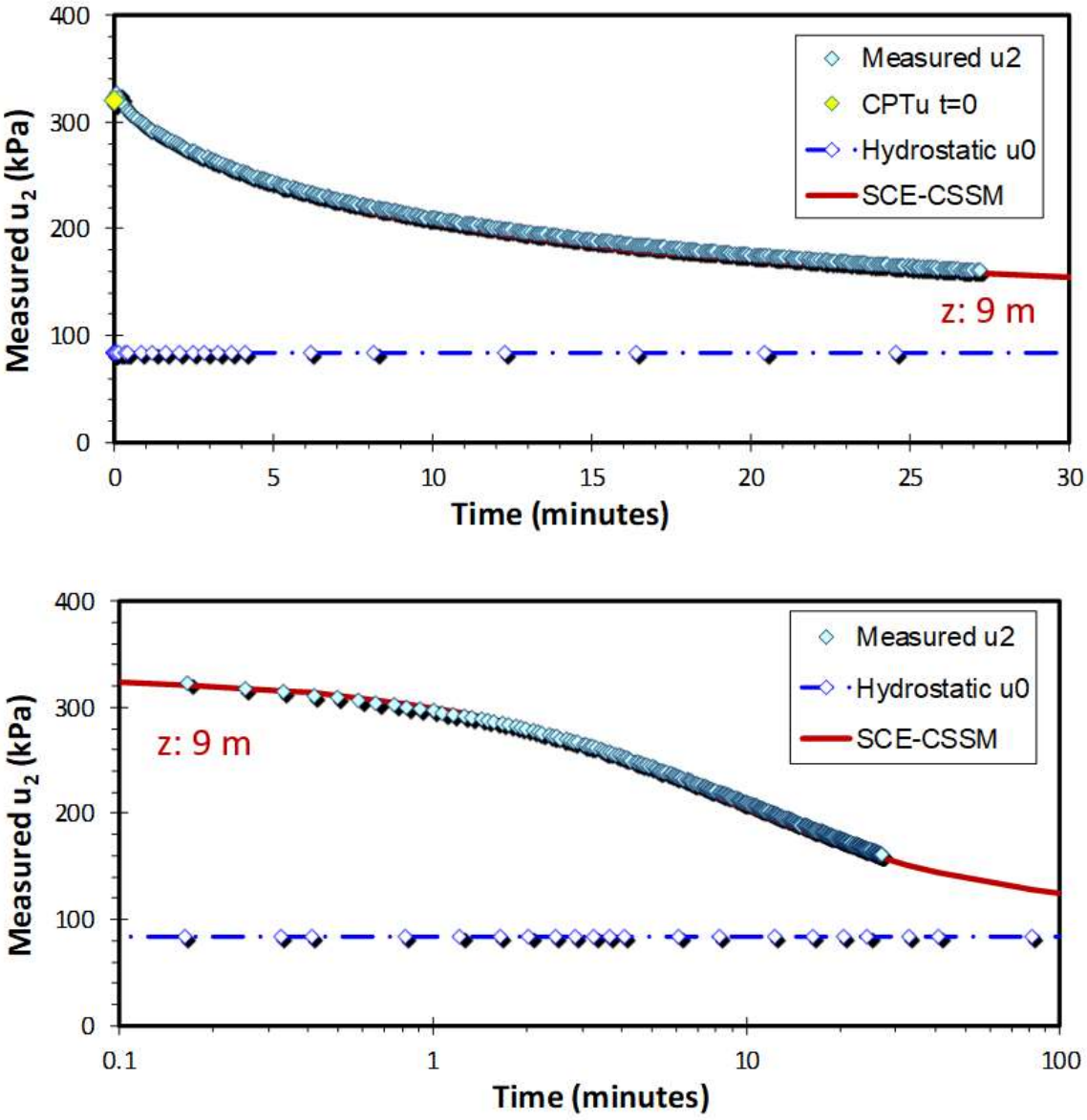


Figure 7.34. Measured piezodissipation record for middle clay layer at Gloucester test site at depth of 9 meters with prediction using hybrid SCE-CSSM framework

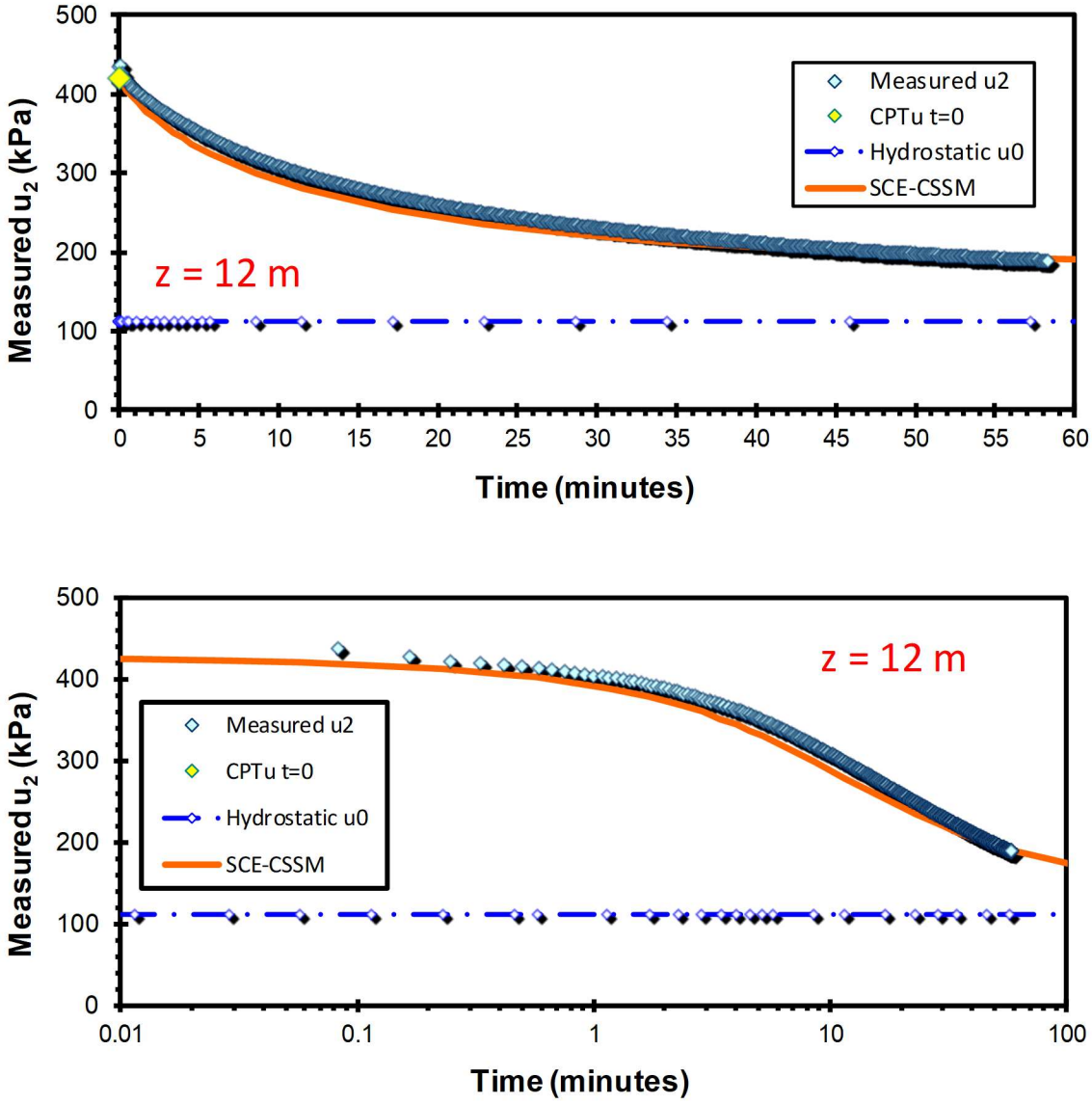


Figure 7.35. Measured piezodissipation record for middle clay layer at Gloucester test site at depth of 12 meters with prediction using hybrid SCE-CSSM framework

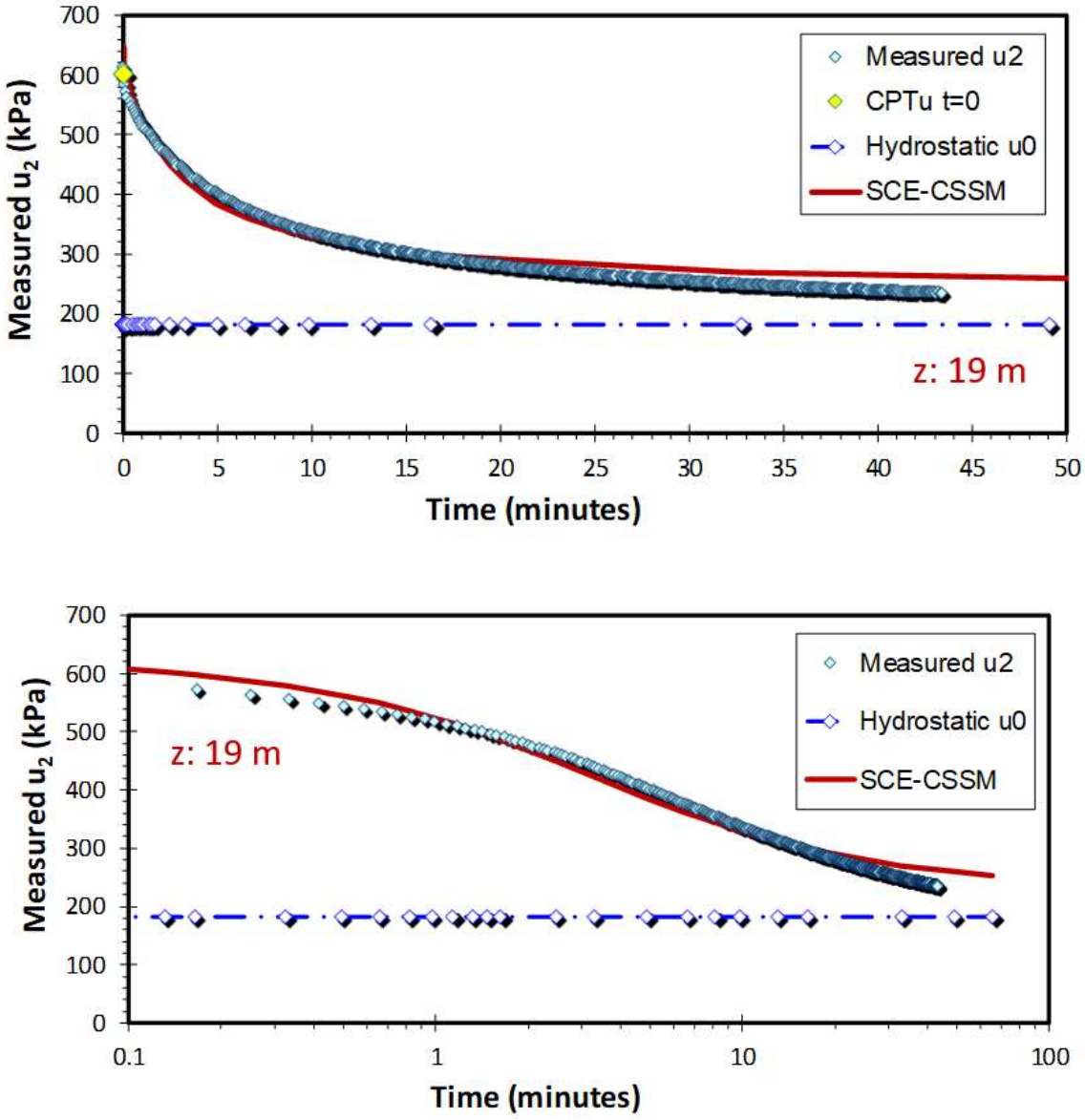


Figure 7.36. Measured piezodissipation record for lower clay layer at Gloucester test site at depth of 19 meters with prediction using hybrid SCE-CSSM framework

A summary of all interpreted $c_{vh}$ values with depth is given in **Figure 7.37** for 21 dissipation tests. Also shown are reference benchmark values for the coefficient of consolidation obtained from laboratory tests (Bozozuk 1972; Lo et al. 1976) and field piezometer data (Bozozuk 1972). Good agreement is seen between the reference tests and piezo-dissipation interpretations.

## 7.14 Simplified Approach for Monotonic Dissipations

For normally-consolidated (NC) to lightly overconsolidated (LOC) clays with monotonic dissipations and OCRs < 3, a simplified solution for the evaluation of $c_{vh}$ can be expressed as:

$$c_{vh} = \frac{T'_{50} \cdot (a_c)^2 \cdot (I_R)^{0.75}}{t_{50}} \quad [7.31]$$

where $T'_{50}$ is the time factor for 50% consolidation and is equal to 0.030, $a_c$ is the radius of the piezocone and $I_R$ = undrained rigidity index. This solution is obtained for the special analytical case when shear-induced porewater pressures are zero (i.e., OCR = 2).

To apply the simplified approach to the Gloucester site, $t_{50}$ values are presented in **Table 7.1**. A piezocone radius of $a_c$ = 1.78 cm for the 10 $cm^2$ cone and operational rigidity index value of $I_R$ = 60 are utilized in [7.28]. **Figure 7.38** presents the results of the simplified approach in obtaining $c_{vh}$, where there is an excellent agreement with the back-figured values using SCE-CSSM and independent supporting lab and field data.

Both analyses can also be compared with a well-established solution from Oxford University; specifically, the Strain Path Method (SPM) developed by Houlsby and Teh (1988) for which the value of $c_{vh}$ is calculated from:

$$c_{vh} = \frac{T^*_{50} \cdot (a_c)^2 \cdot \sqrt{I_R}}{t_{50}} \quad [7.32]$$

where $T^*_{50}$ is the time factor for 50% consolidation, $a_c$ is the radius of the piezocone, and $I_R$ = rigidity index. The time factor $T^*_{50}$ is equal to 0.118 for type 1- midface filter element piezocones and is equal to 0.245 for and type 2-shoulder filter element piezocone. Teh and Houlsby (1991) provide further information for different degrees of consolidation and corresponding time factors T*. As for the undrained rigidity index, the value can be estimated following the empirical relationships that depend on plasticity index (PI) and overconsolidation ratio (OCR), as detailed by Keaveny and Mitchell (1986), or alternate approaches discussed by Mayne et al. (2002) and Krage et al. (2014).

In applying the SPM solution to the Gloucester dissipations, the $t_{50}$ values are obtained from **Table 7.1** with $a_c$ = 1.78 cm for the 10 $cm^2$ cone, $T_{50}$* value of 0.245 for type 2 element, and an operational rigidity index of $I_R$ = 130 assigned on the basis of the average PI = 25 % and OCR = 1.5 for the clay. The results from the SPM solution are also presented in **Figure 7.37** showing slightly higher values when compared to the benchmark laboratory and field reference measurements. **Table 7.1** presents a summary of the coefficient of consolidation values as determined by SCE-CSSM and strain path method (SPM).

Table 7.1. Summary of measured piezocone porewater dissipation records at Gloucester site with interpreted coefficient of consolidation ($c_{vh}$)values as per SCE-CSSM and SPM

| | | | | | | | SCE-CSSM | SPM |
|---|---|---|---|---|---|---|---|---|
| **Depth** | **Layer *** | **Initial $u_2$** | **Final $u_2$** | **Estimated $u_o$** | **Length of Dissipation** | **$t_{50}$** | **$c_{vh}$** | **$c_{vh}$** |
| (m) | | (kPa) | (kPa) | (kPa) | (sec) | (sec) | ($mm^2/s$) | ($mm^2/s$) |
| 2.00 | B | 45.03 | 36.00 | 7.85 | 1000.00 | 1308.00 | 0.35 | 0.23 |
| 3.00 | C | 98.69 | 63.27 | 17.66 | 1325.00 | 1439.00 | 0.20 | 0.21 |
| 4.00 | C | 151.07 | 82.11 | 27.47 | 3200.00 | 2527.00 | 0.08 | 0.12 |
| 5.00 | C | 175.50 | 95.84 | 37.28 | 4500.00 | 3252.00 | 0.07 | 0.09 |
| 6.00 | D | 263.99 | 82.11 | 47.09 | 3200.00 | 2500.00 | 0.07 | 0.12 |
| 7.00 | D | 242.99 | 111.44 | 56.90 | 4650.00 | 1660.00 | 0.17 | 0.18 |
| 8.00 | E | 302.34 | 123.90 | 66.71 | 3050.00 | 772.00 | 0.26 | 0.39 |
| 9.00 | E | 322.85 | 160.79 | 76.52 | 1630.00 | 735.00 | 0.28 | 0.41 |
| 10.00 | E | 359.05 | 103.50 | 86.33 | 33750.00 | 715.00 | 0.28 | 0.42 |
| 11.00 | E | 436.64 | 212.78 | 96.14 | 1400.00 | 660.00 | 0.21 | 0.45 |
| 12.00 | E | 433.60 | 189.14 | 105.95 | 3500.00 | 1040.00 | 0.20 | 0.29 |
| 13.00 | E | 534.45 | 234.66 | 115.76 | 2250.00 | 740.00 | 0.18 | 0.40 |
| 14.00 | E | 515.42 | 247.80 | 125.57 | 2700.00 | 1000.00 | 0.17 | 0.30 |
| 15.00 | F | 514.63 | 204.73 | 135.38 | 5700.00 | 985.00 | 0.25 | 0.30 |
| 16.00 | F | 556.13 | 268.11 | 145.19 | 2200.00 | 805.00 | 0.24 | 0.37 |
| 17.00 | F | 599.98 | 288.71 | 155.00 | 2200.00 | 795.00 | 0.21 | 0.38 |
| 18.00 | F | 645.30 | 288.51 | 164.81 | 2400.00 | 760.00 | 0.25 | 0.39 |
| 19.00 | G | 614.01 | 235.83 | 174.62 | 2600.00 | 320.00 | 0.70 | 0.93 |
| 20.00 | H | 603.81 | 190.71 | 184.43 | 21500.00 | 275.00 | 1.00 | 1.08 |
| 21.00 | NA | 643.14 | 249.37 | 194.24 | 1200.00 | 200.00 | 1.20 | 1.49 |
| 22.00 | NA | 486.87 | 243.29 | 204.05 | 300.00 | NA | NA | NA |
| 23.00 | NA | 280.86 | 214.45 | 213.86 | 700.00 | NA | NA | NA |
| 23.65 | NA | 231.12 | 223.08 | 220.23 | 300.00 | NA | NA | NA |

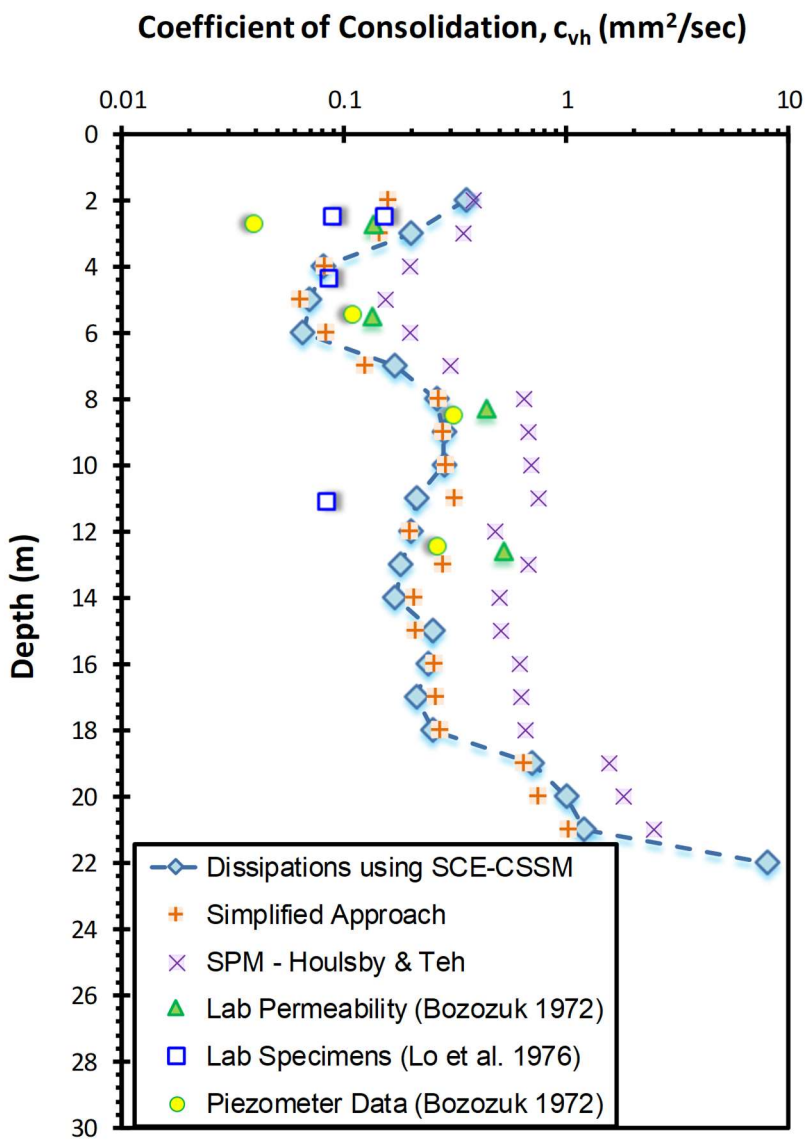


Figure 7.37. Laboratory and field measured profiles of coefficient of consolidation with depth at Gloucester test site compared with dissipation results using SCE-CSSM solution, simplified approach, and strain path method (SPM)

### 7.15 Evaluation of the Soil Permeability, k

The assessment of the permeability (k) at Gloucester can be made from the interpreted values of coefficient of consolidation ($c_{vh}$) using:

$$k = \frac{c_{vh} \cdot \gamma_w}{D'} \quad [7.33]$$

where $\gamma_w$ = unit weight of water and D' = constrained modulus that can directly be obtained from oedometer tests ($D' = \Delta\sigma_v'/\Delta\varepsilon$) or indirectly estimated using CPT data. For an approximate evaluation of the constrained modulus from CPT results, the common approach is expressed in the form:

$$D' \approx \alpha_D \cdot (q_T - \sigma_{V0}) \quad [7.34]$$

where $\alpha_D$ is an empirical scaling factor that has been shown to depend upon soil type, confining stress level, overconsolidation, and other factors (Kulhawy & Mayne, 1990). Based on a comprehensive study on a wide range of geomaterials (excepting soft plastic organic clays and cemented geomaterials), a value of $\alpha_D \approx 5$ is an approximate starting point for insensitive clays, silts, and quartz-silica sands (Mayne 2007). More detailed approaches for estimating D' from CPT results in soils are discussed by Robertson (2009).

**Figure 7.38** presents a summary of the interpreted profile of hydraulic conductivity (k) values with depth using $c_{vh}$ values from dissipation tests and equation [7.31]. The k values are seen comparable to benchmark reference laboratory results reported by Bozozuk (1972) and Hinchberger and Rowe (1998) and field piezometer tests by Bozozuk (1972).

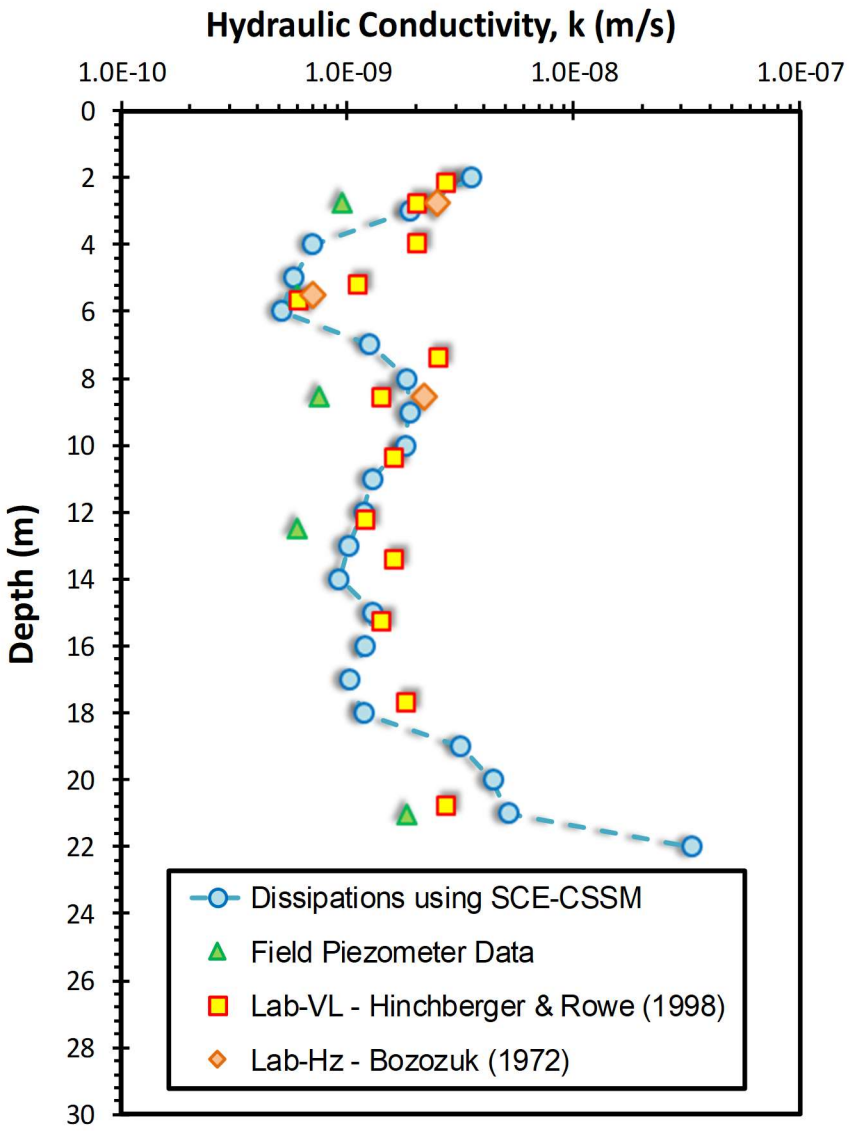


Figure 7.38. Laboratory- and field- measured hydraulic conductivity profiles for Gloucester test site with results from dissipation tests using SCE-CSSM solution

## 7.16 Conclusions

For sensitive and structured clays, an acknowledged strain incompatibility occurs during triaxial compression, such that the deviator stress ($\sigma_1 - \sigma_3$) reaches a peak strength at low strains ($\varepsilon \approx 1\%$) whereas excess porewater pressures are maximized later at much

higher strains ($\varepsilon > 15\%$). Thus, the effective strengths at these points can be implemented to represent these phenomena. This stress-strain and porewater pressure behavior is witnessed within different sensitive and/or structured clays under study: Leda clay at Gloucester, Ontario; quick Tiller clay in Norway, and Amherst varved clay in Massachusetts.

A slightly modified SCE-CSSM solution is presented that incorporates the following definitions of mobilized effective stress friction angles ($\phi'$): (1) maximum deviatoric stress ($\phi'_{qmax}$) and (2) maximum obliquity ($\phi'_{MO}$). In concert with field CPTU soundings, these correspond to the measured cone tip resistances ($q_t$) and penetration porewater pressures ($u_2$), respectively. The derivation provides three formulations for clay stress history for evaluating OCR from CPTu in terms of (a) net resistance ($q_t - \sigma_{vo}$), (b) excess porewater pressures ($u_2 - u_0$), and (c) effective cone resistance ($q_t - u_2$), all of which agree well with the benchmark laboratory consolidation testing and corresponding profiles of preconsolidation stress at the three selected sensitive clay sites. The modified approach provides a methodology to obtain operational rigidity index ($I_R$) which is in reasonable agreement with reference laboratory based and seismic-based in-situ approaches. The proposed method gives a very good agreement with lab-measured undrained shear strength values using corresponding cone bearing factors.

In addition, the hybrid SCE-CSSM framework is used to interpret flow parameters from piezodissipation tests taken in the sensitive Champlain Sea clays at the Gloucester test site, specifically to directly evaluate the profiles of coefficient of consolidation ($c_{vh}$) and permeability (k) by matching theoretical curves with field measured dissipation data

that agree well with independent laboratory and field measured reference values. This solution can handle both monotonic and dilatory porewater pressure behavior. A simplified approach is also presented for soils exhibiting a monotonic porewater pressure response.

# Chapter 8. Organic Clay Detection Using CPT

## 8.1 Introduction

Organic soils are very compressible and exhibit very low undrained shear strength with high strain rate, secondary consolidation, and creep characteristics, thus making them problematic with unfavorable engineering properties. Their identification and recognition during geotechnical site characterization is therefore paramount in order to avert problems during construction and long-term structural performance.

The term *organic* usually refers to any material containing carbon derived from the incomplete decomposition of plant remains in wet areas when there is lack of oxygen, however, for geomaterials a more precise quantitative definition is needed to identify an organic soil. In geotechnical engineering practice, organic soils are typically encountered as a part of a wetland system where the groundwater table is near or above the ground surface. Organic deposits exist as dark brown or black, very soft unconsolidated wet deposits with a distinctive fragrant odor. In some situations, organic deposits exist buried underneath inorganic alluvial soils making it more difficult to detect which can cause significant differential settlements for shallow foundations, as well as instabilities during excavations, embankment construction, or wall placement (Huat et al., 2014). In common geotechnical practice, it has been frequently advised to avoid dealing or constructing on any organic soil, with recommendations to remove or displace the soil whenever possible.

During CPT, soil sampling is not normally performed and thus the identification of organic versus inorganic becomes important. There are no direct CPT methods for detecting the organic matter, hence soil behavior type charts can be used as a preliminary

means to detect the soil type. The usage of optical vision penetrometers (i.e., vision cones) aids in determining the shape and color of the encountered soil particles which can give an insight towards the soil type (Hryciw et al. 2014).

Herein, a database derived from 23 organic soils tested by piezocones was used to develop a reliable approach for (a) identification of organic clays; and (b) assessing yield stress profiles in such deposits. It is shown that the excess porewater pressure readings from the CPT ($\Delta u_2$) can be used to help indicate the presence of organic clays if compared to the net cone tip resistance ($q_{net}$). This study found that the normalized porewater pressure parameter ($B_q$) can highlight the existence of organic clays, where it is observed that $B_q$ values for organic clays are smaller than $B_q$ values of well-behaved clays.

## 8.2 Classification of Organic Soils

The amount of organic matter within any soil mixture defines the nature of the organic soil encountered, however, there is not a global cut-off value for the percentage of organic matter to define a specific soil deposit as organic as this margin is variable from one location to another, depending on the local geology and the purpose of the soil classification system (engineering or agricultural or scientific). For instance, Laboratoire de Physique Corpusculaire (LPC) in France defines any soil as organic (O) if it has greater than 10% organic matter, and if ranging from 3 to 10% as slightly organic soil (fO); between 10 and 30% as medium organic (mO) and if greater than 30% as highly organic (tO) as presented in **Figure 8.1**.

According to the unified soil classification system (USCS) covered in ASTM D 2487 and D 2488, organics are treated as fine-grained soils. For fine-grained soils, the

percentage of fines passing sieve # 200 (particle sizes < 0.075 mm) is greater than 50%. Hence, organics can either be organic silts or organic clays which are determined based on the liquid limit and plasticity index value of the organic deposit. The ratio of liquid limit subjected to oven drying is compared to that of air drying and in the case where this ratio is less than LL(oven)/LL(air) < 0.75, then the soil is considered organic. Moreover, ASTM D4427 defines the organic content ranges as for clay or silt or sand with organic matter content ranging from 2 to 20% to be described as slightly organic, while organic soils are defined if the organic matter content ranges from 25 to 75% and peat is any soil with organic matter content greater than 75%.

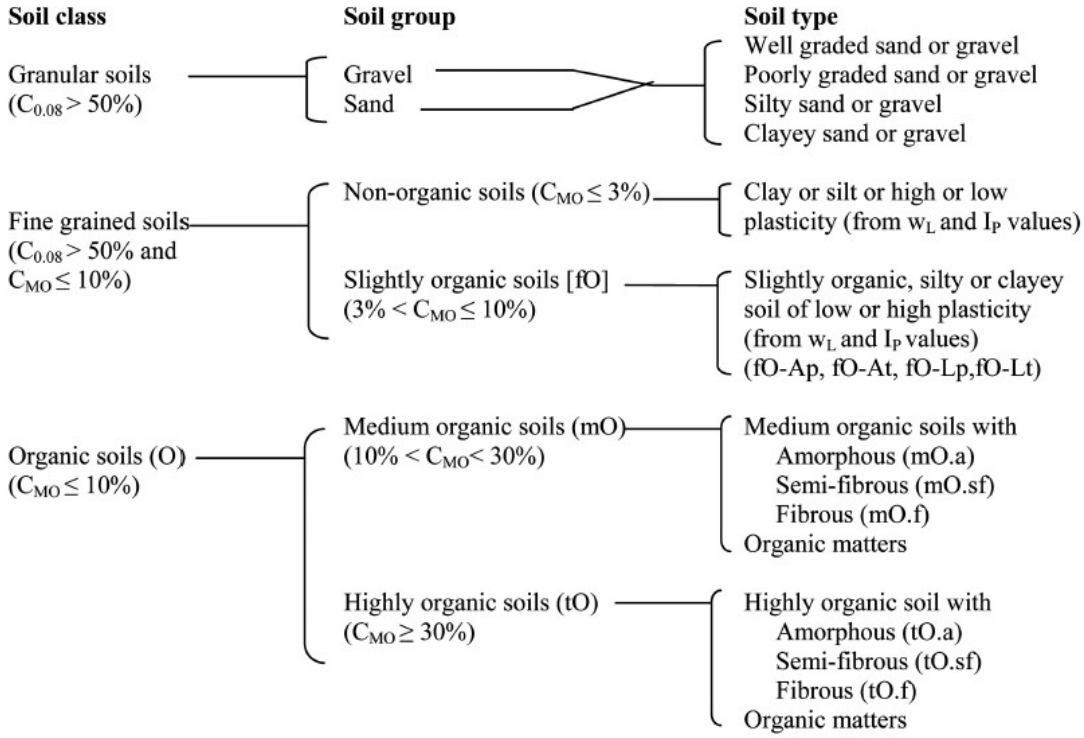


Symbols:
$C_{MO}$ : organic content
$C_{0.08}$ : content of particles finer than 0.08 µm
A : clay
L : silt

Figure 8.1. Laboratoire de Physique Corpusculaire (LPC) classification scheme for organic soils (Magnan, 1994)

According to the soil classification system by American Association of State Highway and Transportation Officials (AASHTO) covered by ASTM Standard D3282, soil category Group A-8 has been assigned to indicate highly organic soil as based on visual inspection. As quoted, these materials are described as "*Highly organic soils (peat or muck) may be classified in Group A-8. Classification of these materials is based on visual inspection and is not dependent on the percentage passing the No. 200 (75-µm) sieve, liquid limit, or plasticity index. The material is composed primarily of partially decayed organic matter, generally has a fibrous texture, a dark brown or black color, and an odor of decay. These organic materials are unsuitable for use in embankments and subgrades. They are highly compressible and have low strength*".

Both peat and organic soils can be defined based on fiber content, amount of organic matter and the degree of decomposition. **Figure 8.2**, presents a summary prepared by Andrejko et al. (1983) comparing different classification systems for peat and organic soils based on their ash and organic contents.

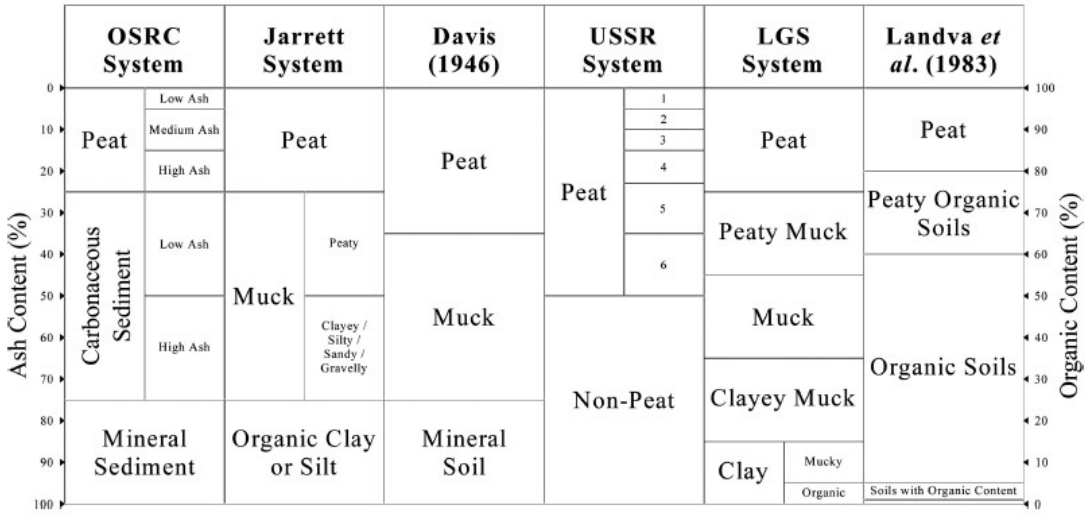


Figure 8.2. Different classification systems for peats and organic soils based on ash and organic content values (Andrejko et al. 1983)

An FHWA classification system has been introduced by Huang et al. (2009) for the Indiana Department of Transportation as illustrated in **Figure 8.3**. The proposed soil classification is based on results of experimental work and critical evaluation of other methods in the geotechnical literature. The approach depends solely on the value of the organic matter content (O.M.C.); expressed in percentage; dividing the soils into 4 main categories: (a) mineral soils with O.M.C. < 3%; (b) mineral soils with 3% < O.M.C. < 15%; (c) organic soils with 15% < O.M.C. < 30%; and (d) highly organic soils (peat) with O.M.C. > 30%.

The proposed system uses dual symbols as defined by AASHTO and USCS for convenience. Recommendations and guidelines are also provided regarding the optimum method for quantifying the organic matter and the expected ranges for the loss on ignition (LOI) for different organic soil groups as illustrated in **Figure 8.4**.

## 8.3 Methods for Quantifying Organic Matter in Soils

Organic content in soils is directly measured in the laboratory following ASTM D2974, where the organic matter is determined based on the amount of the organic matter removed based on different laboratory-based tests. The percentage of the lost dry weight represents the organic content within the soil. The most common laboratory-based technique for measuring the organic content is the loss on ignition (LOI) methods.

The loss on ignition method depends on the degradation and thermal decomposition of the organic matter within the soil matrix. Based on test method *C*, an oven dried specimen is placed in a special furnace with well-temperature control. The weight of the soil specimen is recorded twice: once after oven-drying to a temperature of 105ºC for 24

hours, denoted as $Weight_{105}$ and then the soil specimen is weighted after ignition at 440ºC for a period until the specimen is completely ashed, denoted as $Weight_{440}$ (no change of mass occurs after at least 1-hour period of heating). A loss in the weight of the specimen will be recorded which is due to the oxidation of the organic matter, the lost weight is defined as loss on ignition (LOI) which is the same as the soil organic matter content (SOM) and is calculated from:

$$SOM\ (\%) = LOI\ (\%) = \frac{Weight_{105} - Weight_{440}}{Weight_{105}} \times 100 \qquad [8.1]$$

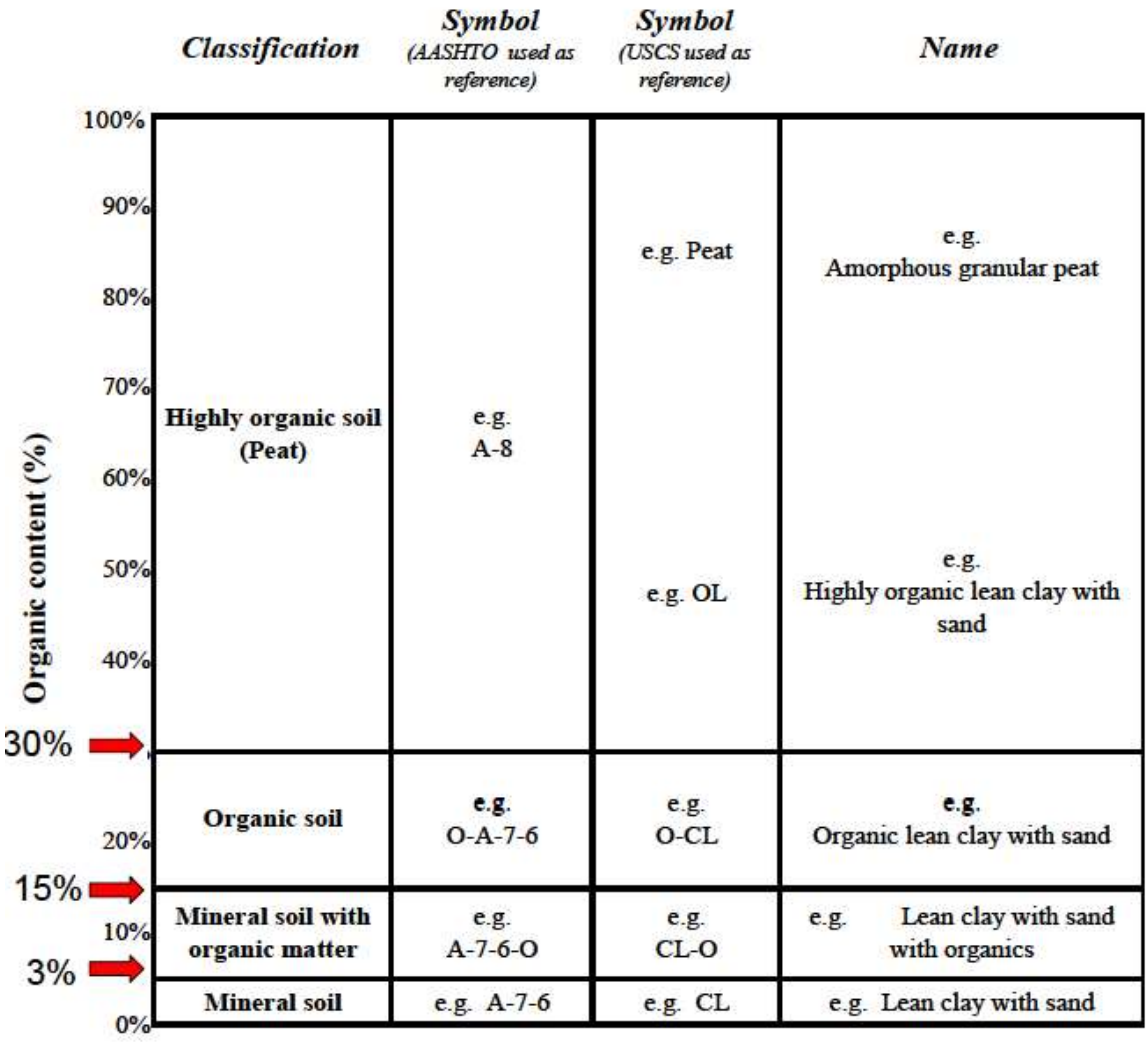


Figure 8.3. Summary of FHWA Organic Soil Classification System (Huang et al. 2009)

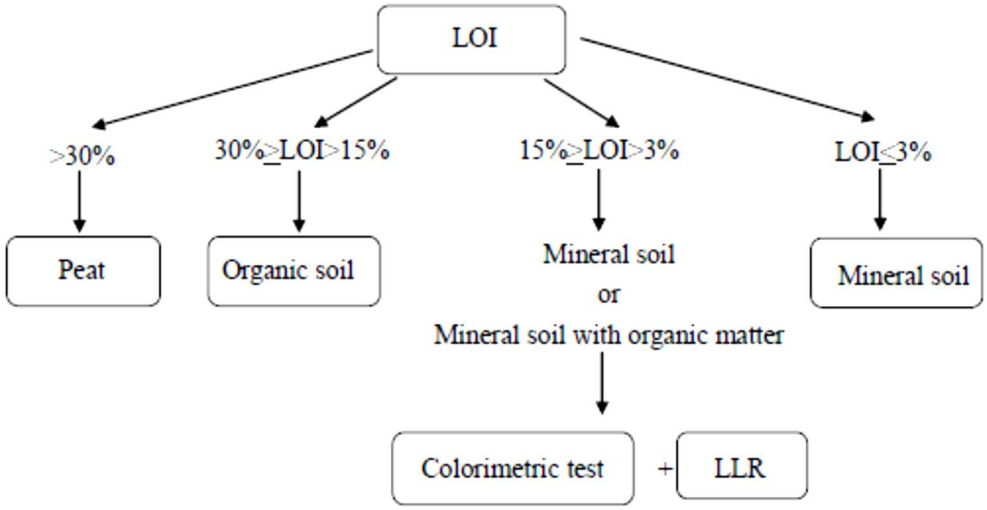


Figure 8.4. Flow Chart for Organic Soil Classification based on Loss on Ignition, LOI (Huang et al., 2009)

Another laboratory-based technique for measuring the organic content is the hydrogen peroxide ($H_2O_2$) method. The test depends on the usage of an alkaline solution to digest the organic matter within the soil specimen. Typically, 10 ml of a 30% or 50% hydrogen peroxide ($H_2O_2$) solution at a temperature < 110ºC is used with the soil specimen to cause the oxidation of the organic matter. The hydrogen peroxide solution is added gradually to the specimen until no more bubbling takes place, indicating the completion of the organic matter digestion. The soil specimen is taken to a furnace and oven-dried to a temperature of 105ºC and the new weight of the specimen after oven drying is recorded and compared to the original weight of the specimen. The soil organic matter content (SOM) is determined based on the loss of the specimen weight from:

$$SOM\ (\%) = \frac{Weig_{\text{Loss}}}{Weight_{\text{Original}}} \times 100 \qquad [8.2]$$

There are other indirect methods that can be used to estimate the organic content of the soil, such methods rely on measuring the concentration of the total organic carbon (TOC) within the soil then using a reduction factor to determine the organic matter content. Total organic carbon can be measured in the laboratory using either dry combustion or wet combustion or dichromate oxidation method (Huang et al., 2009). Such methods are more sophisticated as they may require treatment for the soil specimen if it contains any inorganic carbon in the form of calcite or dolomite.

## 8.4 Characterization of Organic Soils

Mechanical and physical properties of the organic soils are greatly influenced by the amount of the organic matter and by the depositional environment, the amount of degradation and decomposition is affected by the water table, amount of oxygen for oxidation and time when chemical and biological changes can occur. Hence, organic soils should not be treated as the conventional fine-grained clays and silts as the properties and behavior of the organic matter are dynamic and variable.

### 8.4.1 Grain Size Distribution

Huat et al. (2014) described the grain size distribution of organic soils as "*Aggregation and dispersion are two different mechanisms affecting grain size distribution. And given that organic matter is absorbed on the clay surface then it affects the aggregation of the soil grains in multiple forms: organic matter can act as a glueing agent that binds the clay particles together visa hydrogen bonding which neutralized the negatively charged clay plates and reduces the repulsion between the particles; a different role can be achieved via increasing the cementation between the particles which densifies the soil packing and holds the grains together, and finally the soil grains can be attached*

*through fungal hyphen or the microscopic plant roots where the organic matter originally is formed*"

### 8.4.2 Specific gravity

According to Kazemian et al. (2009), for organic soils, the relationship between the specific gravity and organic content is inversely proportional as presented in **Figure 8.5**. The expected range for $G_s$ can vary from 1.4 to 1.8 where peats, having higher organic content, have lower $G_s$ values.

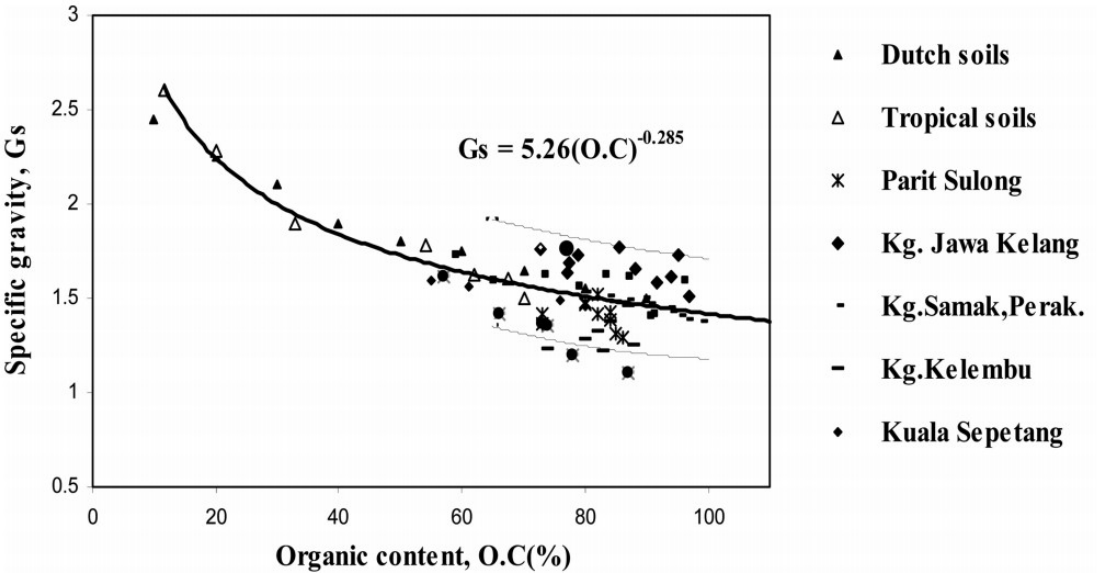


Figure 8.5. Relationship between the specific gravity and organic content (Kazemian et al., 2009)

### 8.4.3 Moisture content

Natural moisture (water) content typically exceeds 100% in organic soil with low organic content and can reach up to 800% for some fibrous peats where the organic content exceeds 75%. The relationship between the water content and the organic content expressed in terms of loss of ignition value (LOI) has been studied by O'Loughlin and Lehane (2003) as presented in **Figure 8.6** where they compiled values for different organic

soils and peats from numerous investigators in the geotechnical literature. The relation increases linearly between the two variables until it reaches a nearly constant plateau of LOI > 85% corresponding to water content values > 600%.

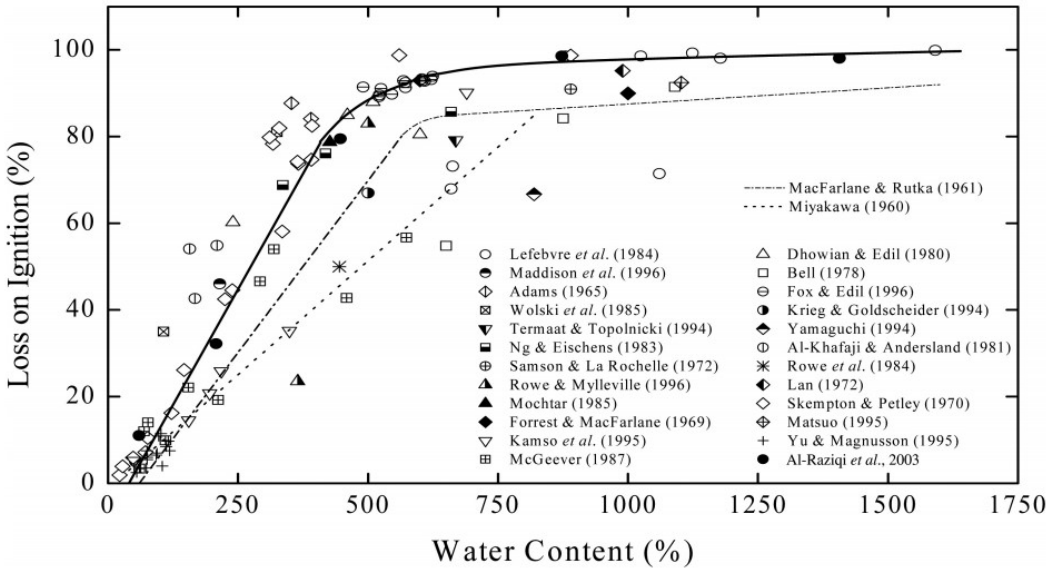


Figure 8.6. Relationship between loss on ignition value and the natural water content of different organic soils (after O'Loughlin and Lehane, 2003)

### 8.4.4 Bulk Density

Given the lower values of specific gravity ($G_s$) and higher values of water content for organic soils and peats when compared to inorganic soils, the values of the bulk density for organic soils are expected to be less than inorganic ones. Al-Raziqi et al. (2003) compared the bulk density and corresponding loss on ignition values for different organic soils and peats as presented in **Figure 8.7**, where the range of bulk density for organic soils was reported between 0.8–1.2 Mg/m$^3$ which is smaller than the common range of 1.80–2.00 Mg/m$^3$ of inorganic soils. Based on the compiled data points in **Figure 8.7**, the value of bulk density decreases as the loss on ignition value increases (i.e. more organic content).

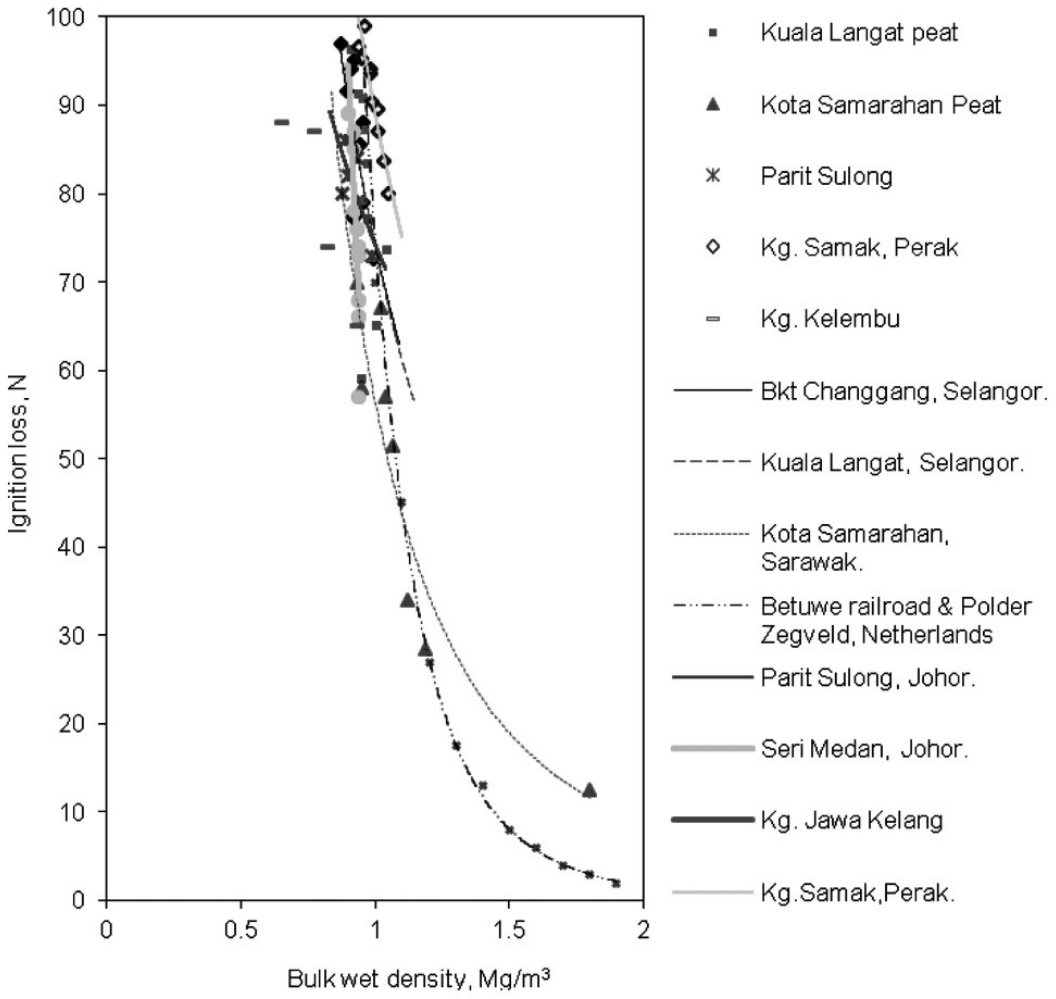


Figure 8.7. Relationship between loss on ignition value and the bulk density (Al-Raziqi et al., 2003)

## 8.5 Engineering Properties of Organic Soils

### *8.5.1 Shear Strength Parameters*

The value of the shear strength within any organic soil depends on the amount of the organic matter relative to the amount of the soil mineral itself. As the mineral content increases, the shear strength increases. Other factors affecting the shear strength of any organic soil include the high moisture content value which may reduce the shear strength; the degree of decomposition of the organic matter and the presence of fibers which can

enhance the shear strength of the organic soil deposit (Arman, 1969). As in the hydraulic conductivity, the shear strength of organic soils and peats is anisotropic (Hanzawa et al., 1994).

Organic soils with high fiber content which are characterized by their spatial orientation can be treated as frictional non-cohesive geomaterial with high effective friction angle values if compared to inorganic soils (Huat et al., 2014). **Figure 8.8** presents the different effective friction angle values as a function of the organic content as collected by Edil (2003), it is evident from the figure that as the organic matter increases the effective friction angle increases as in the case of fibrous peats. Based on the compiled data by Edil (2003), the average effective friction for organic soils (with organic content < 30%) is about 41 degrees while the average friction angle for peats (with organic content > 30%) can reach up to 53 degrees.

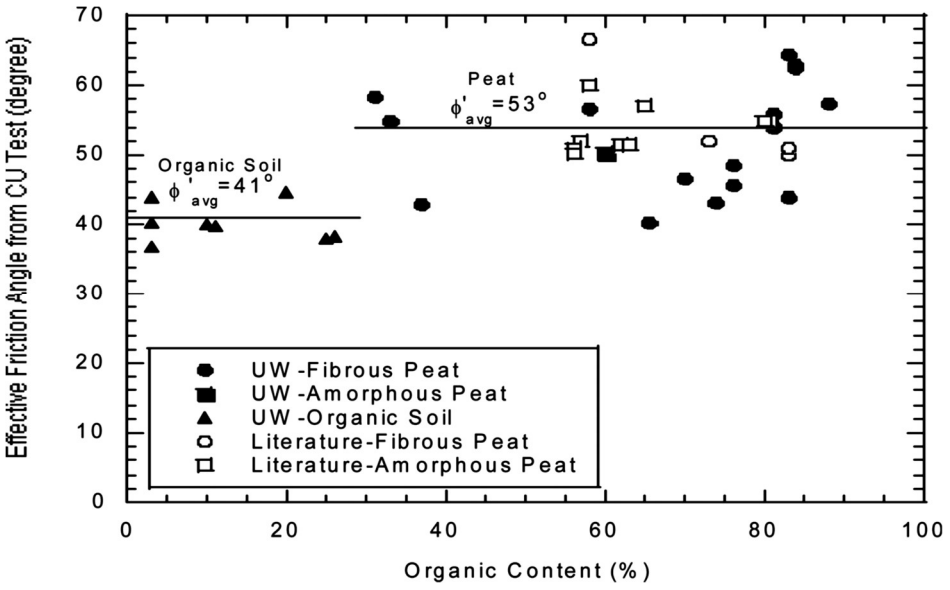


Figure 8.8. Effective friction angle versus organic content for organic soils and peats (Edil, 2003)

As for the undrained shear strength evaluation in organic soils, it is as challenging as in inorganic soils where obtaining undisturbed soil samples is problematic. Besides the sampling issues and the special nature of organics especially in case of fibrous ones, investigators have used numerous in-situ measuring techniques to evaluate undrained shear strength in the field such as cone penetration, dilatometer, vane shear, pressure-meter, plate load, and screw plate load tests (Edil, 2001).

Edil and Wang (2000) compiled the undrained shear strength ratio values ($s_u$ / $\sigma'_{vo}$) for several organic soils and peats as presented in **Figure 8.9**. It is evident from the plotted values that an average ratio of 0.59 can be reported for organic soils and peats which is relatively higher than the conventional value of (0.2 – 0.3) for inorganic soils.

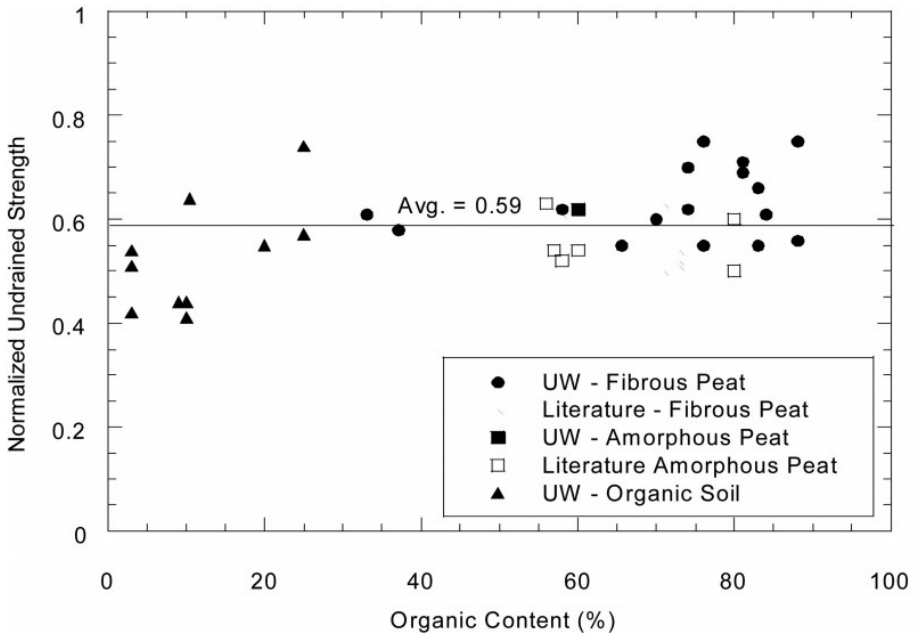


Figure 8.9. Normalized undrained shear strength ratio versus organic content (Edil and Wang, 2000)

## 8.6 Organic Soil Identification from CPT

Given the difficulty in obtaining undisturbed and representative organic soil samples in situations where the organic soil is buried in wetland systems, it is critical to find means to detect the existence of organic soils using in-situ techniques such as cone penetration testing (CPT). As there are not any routine soil sampling procedures carried out during cone penetration, then indirect approaches using CPT data can be used to detect the encountered organic soils. Typically, the CPT data can be interpreted based on one of the following methods: (a) relating CPT readings to the logs of adjacent boreholes and recovered samples; (b) relying on rules-of-thumb; (c) using vision cone penetrometers (VisCPT); (d) adopting probabilistic methods; and (e) using empirical soil behavioral type (SBT) charts.

### 8.6.1 Simple Rules of Thumb

As pointed in an earlier chapter, the main readings of the cone: cone tip resistance ($q_t$), sleeve friction ($f_s$), and porewater pressure ($u_2$) can provide initial guidance to the type of soil encountered. The tip resistance and porewater pressure provide a clear separation between fine-grained and coarse-grained soils. The sleeve friction is used in defining the friction ratio (FR % = $f_s$ /$q_t$ *100), high FR > 8% or 10% is an indication to the presence of organic soils and peats.

### 8.6.2 The Vision Cone Penetrometer (VisCPT)

Given that no soil sampling usually takes place during piezocone advancement into the ground, then no information regarding the color, shape, size, and texture of the encountered soil can be determined with certainty. Hence, optical geo-characterization has

been implemented over the past 20 years using advances in digital camera resolution and image analyses with geotechnical applications giving further insight on the soil visual characterization (Hryciw et al. 2014).

Optical geo-characterization is mainly used for site characterization, particle identification and motion, and deformation. Main applications include sedimaging vision cone penetrometers (ViscCPT), translucent Segregation Table (TST), stereography and in-situ particle tracking techniques. The vision cone penetrometer provides visual inspection for soils without sampling, which can be used in different geotechnical and environmental applications. Given the distinctive black or dark brown color of soils with high organic matter, the usage of vision cone penetrometers can be considered a good preliminary means in detecting the existence of organic soils, especially in wetlands.

The Vision Cone Penetrometer (VisCPT) was first developed at the University of Michigan in 1995. The cone has the ability to visually observe the soil using two video cameras, lenses and lighting systems with individual housing units as illustrated in **Figure 8.10**. The vision cone provides a continuous recording of the soil stratigraphic column at high resolution showing anomalous clay lenses, fissures and sand seams (Hryciw et al. 1998). The two camera records the visual soil record using synthetic sapphire windows as shown in **Figure 8.11**. Imagery is recorded in real time and is digitized for further image-texture analyses for the soil and for inferring the grain size distribution using textural analyses.

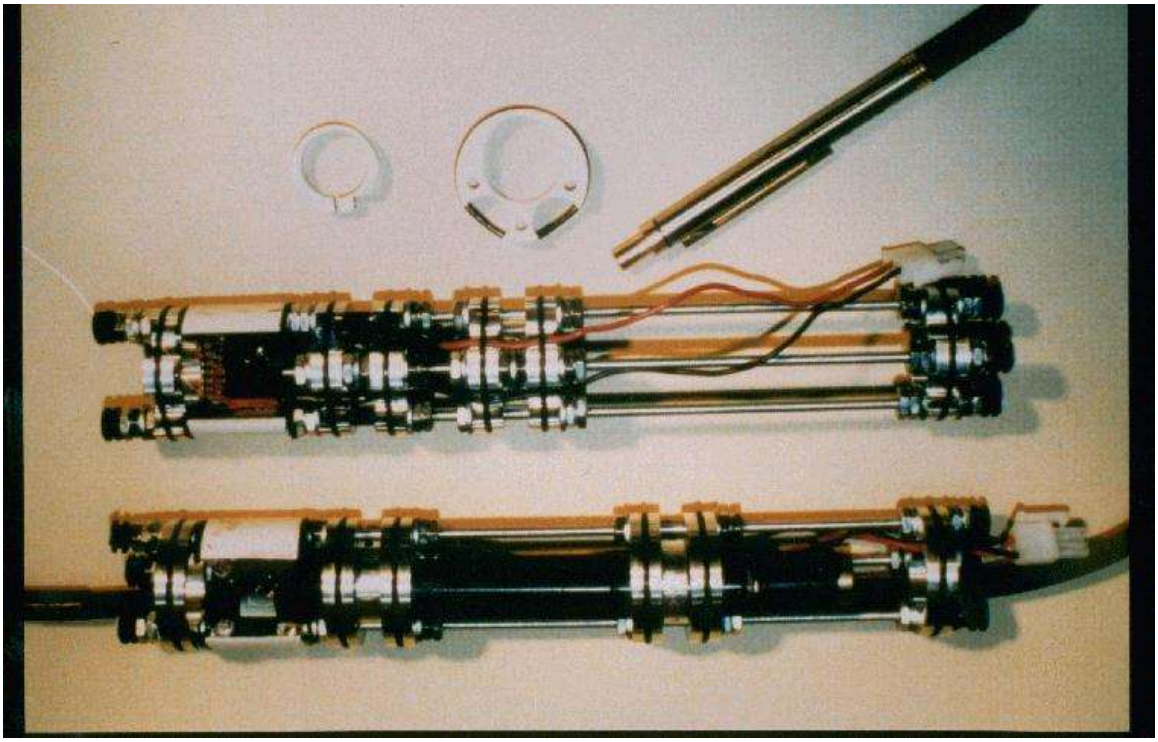

Figure 8.10. Camera assembly for the Vision Cone Penetrometer (VisCPT) (from http://www.personal.umich.edu/~romanh/viscpt/viscpt.htm)

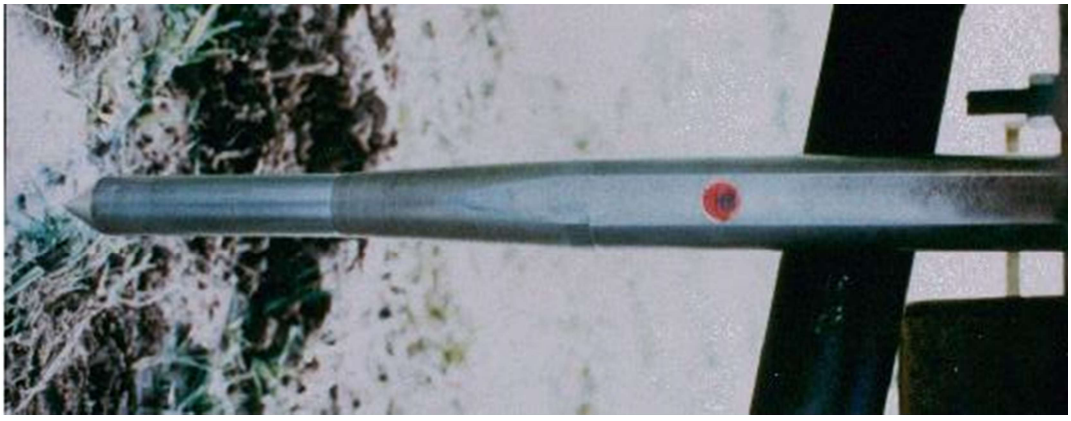

Figure 8.11. Illuminated sapphire window of the Vision Cone Penetrometer (VisCPT) (from http://www.personal.umich.edu/~romanh/viscpt/viscpt.htm)

### 8.6.3 Probabilistic Methods

A CPT soil classification scheme based on fuzzy logic was introduced by Zhang and Tumay (1999). The results of soil identification are displayed in the form of percentages of probability of the soil constituency of clay-silt-sand components, thus analogous to the US Department of Agriculture textural soil classification system. Additional details are given in Tumay et al. (2008, 2011). The method is developed based on mapping of the Douglas & Olsen (1981) soil classification chart, resulting in two quantities: the soil classification index (U) and the in-situ behavior index (V). **Figure 8.12** presents a schematic diagram for the approach relating the U-soil classification index to the probability of occurrence of different soil groups with 3 main curves for sands, silts, and clays. Tumay et al. (2013) introduced an update to their probabilistic soil classification method to include a new quantity (V-U) to detect the presence of organic soils where the (V-U) > 3 indicates significant organic content.

According to Tumay et al. (2013), the organic content indicator (V-U) can be used as a reference to detect any significant changes in profiling the organic content with depth within any given soil composition. The newly proposed methodology is interesting to explore yet it lacks the ability to quantify the organic matter within any soil composition, it just detects the existence of organic matter. No clear definition for the organic soils was provided, which organic content value is considered marginal to separate between organic and inorganic soils, in addition, no rational bases were provided to explain the cut-off value of (V-U) greater than 3, is it based on local experience or personal judgment. The proposed method needs to be calibrated and tested against several different organic soil compositions from other countries with different characteristics and properties.

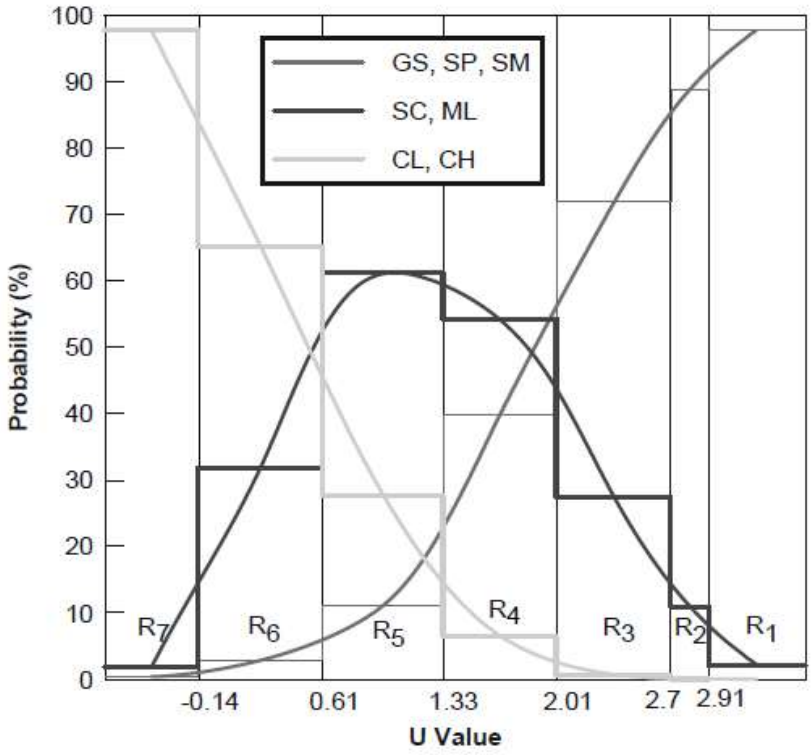


Figure 8.12. Regional boundaries and corresponding probabilities for different soil groups according to the probabilistic soil classification method (Tumay et al. 2013)

### 8.6.4 Soil Behavioral Type Charts

Soil behavioral type (SBT) charts are the most popular method of soil classification for CPT data. The main focus of most charts is to assign readings to simple soil types, such as sands, silts, and clays, specifically uncemented quartz-silica sands and intact inorganic silts-clays.

There are some exceptions that included a zone or definition for organic soils such as Schmertmann (1978) who introduced a revised soil profiling chart based on the cone tip resistance and the friction ratio, FR = $f_s/q_t$ (%) as illustrated in **Figure 8.13**.

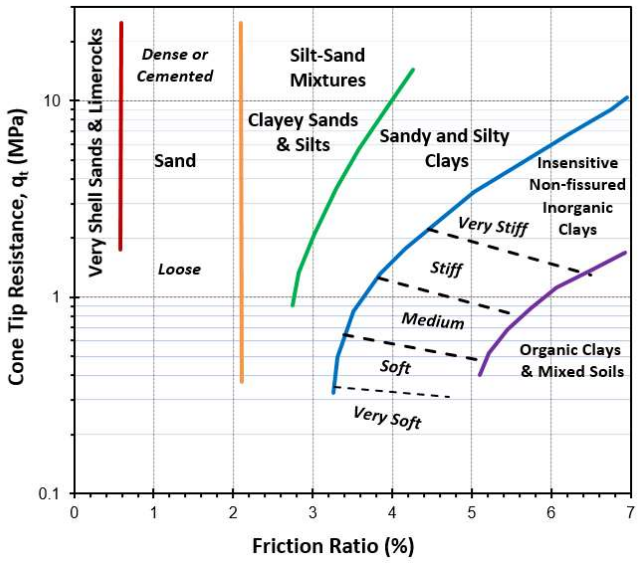


Figure 8.13. Soil behavior classification chart (Schmertmann, 1978)

Robertson, et al. (1986) presented a zone for organic soils in his 12-zone SBT system that used a three-axis plot of total cone tip resistance ($q_t$), friction ratio (FR), and normalized porewater pressure ($B_q$), where $B_q = (u_2 - u_0) / (q_t - \sigma_{vo})$. **Figure 8.14** shows zone 2 which is assigned for organic clays on cone bearing – friction ratio diagram.

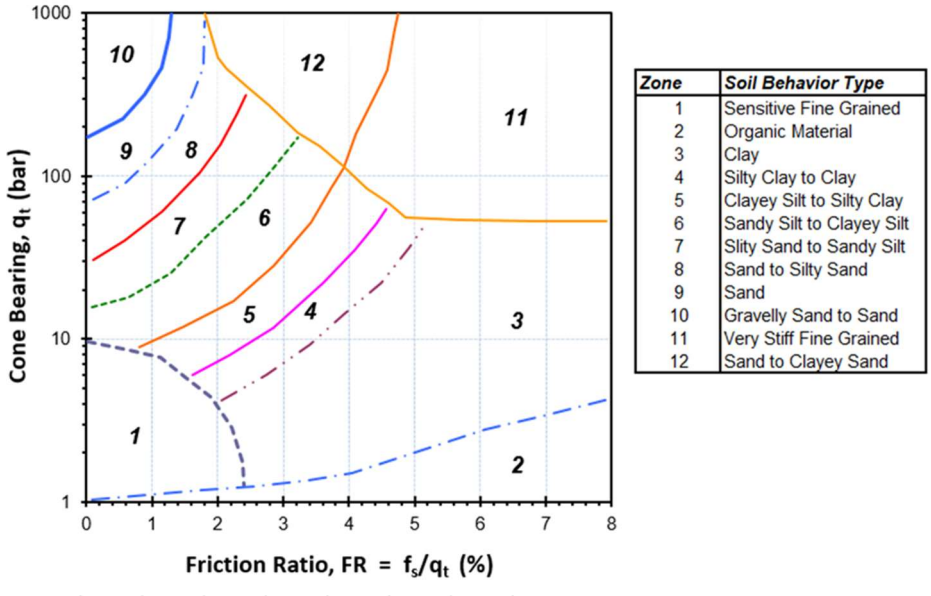


| Zone | Soil Behavior Type |
|---|---|
| 1 | Sensitive Fine Grained |
| 2 | Organic Material |
| 3 | Clay |
| 4 | Silty Clay to Clay |
| 5 | Clayey Silt to Silty Clay |
| 6 | Sandy Silt to Clayey Silt |
| 7 | Slity Sand to Sandy Silt |
| 8 | Sand to Silty Sand |
| 9 | Sand |
| 10 | Gravelly Sand to Sand |
| 11 | Very Stiff Fine Grained |
| 12 | Sand to Clayey Sand |

Figure 8.14. Twelve-Zone Soil Behavioral Type Chart by Robertson et al., 1986

Later Robertson (2009) updated his 12-zone classification chart to an adjusted version relying on stress-normalized parameters (Q, F, and $B_q$) to account for depth effects where:

$$Q = (q_t - \sigma_{vo})/\sigma_{vo}' \quad [8.3]$$

$$F\,(\%) = 100 \cdot f_s/(q_t - \sigma_{vo}) \quad [8.4]$$

By plotting the data in terms of Q versus F and Q versus $B_q$, a nine-zone SBT system was developed, as shown in **Figure 8.15** where organic clays are assigned zone 2 with a CPT material index value > 3.60 as illustrated in **Table 8.1** which identifies the boundaries of the 9 zones using the values of the CPT material index ($I_{cRW}$) which was earlier defined by Robertson & Wride, 1998, an updated CPT material index is currently used as defined by Robertson (2009):

$$I_c = \sqrt{\{3.47 - \log(Q_{tn})\}^2 + \{1.22 + \log(F)\}^2} \quad [8.5]$$

where $Q_{tn} = [(q_t - \sigma_{vo})/\sigma_{atm}] / [(\sigma_{vo}' / \sigma_{atm})^{n}]$ is the normalized cone tip resistance, $\sigma_{atm}$ is atmospheric pressure. The exponent "n" varies from 1 in intact clays to 0.5 in sands, as given by (Robertson, 2009):

$$n = 0.381 \cdot I_c + 0.05 \cdot (\sigma_{vo}'/\sigma_{atm}) - 0.05 \leq 1.0. \quad [8.6]$$

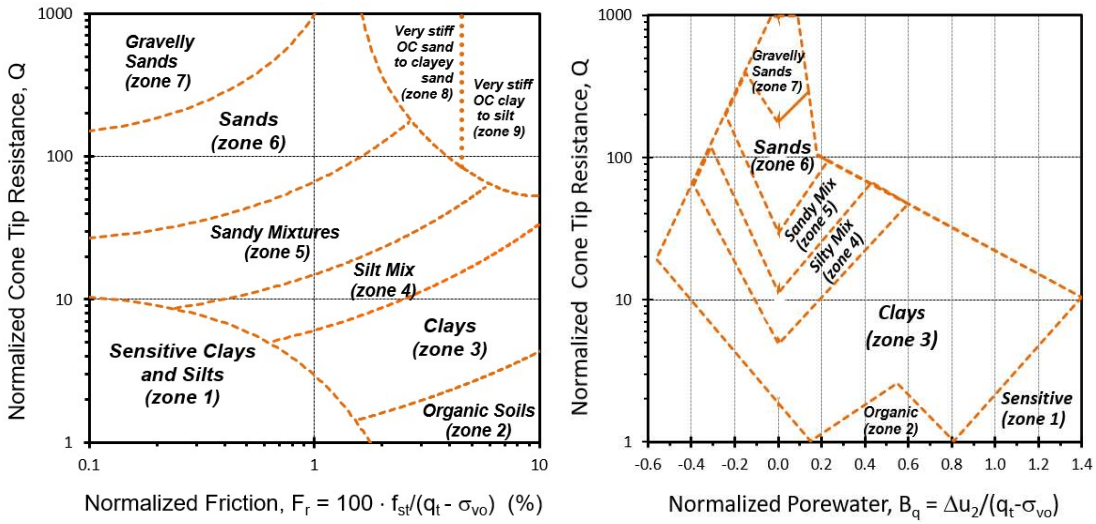


Figure 8.15. CPT Soil Classification Zones Using Nine-Part Soil Behavioral Type (after Robertson, 2009)

*Table 8.1* Soil Behavioral Type and Zone Number as defined by CPTu Material Index, $I_c$

| Soil Classification | SBT Zone | Range CPT Material Index $I_c$ |
|---|---|---|
| Stiff clayey sand | 9 | F > 4.5 % (see note 1) |
| Stiff sandy clay | 8 | 1.4 < F < 4.5 % (see note 1) |
| Sands with gravels | 7 | $I_c < 1.31$ |
| Sands: clean to silty | 6 | $1.31 < I_c < 2.05$ |
| Sandy mixtures | 5 | $2.05 < I_c < 2.60$ |
| Silty mixtures | 4 | $2.60 < I_{cR} < 2.95$ |
| Clays | 3 | $2.95 < I_c < 3.60$ |
| Organic soils | 2 | $I_c > 3.60$ |
| Sensitive soils | 1 | (see note 2) |

Notes: 1. Zone 8 and Zone 9 are found from the following criterion:

$$Q_{tn} \geq \frac{1}{0.006 \cdot (F - 0.9) - 0.0004 \cdot (F - 0.9)^2 - 0.002}$$

2. Sensitive soils of zone 1 are identified when $Q_{tn} < 12 \exp(-1.4\ F$

Jefferies and Been (2016) modified their soil behavior type index that was introduced by Jefferies and Davies (1991) using the dimensionless term $[Q \cdot (1 - B_q) + 1]$ in their classification chart versus friction ratio [FR % = $100 \cdot f_s/(q_{net})$], as presented in **Figure 8.16**. The modified chart consists of 6 main soil zones which included organic soils

at CPT material index values greater than 3.22. The updated CPT material index ($I_{c\,JB}$) can be defined as:

$$I_{c\,JB} = \sqrt{[3 - \log\{Q\,(1 - B_q) + 1\}]^2 + [1.5 + 1.3\log(F)]^2} \qquad [8.7]$$

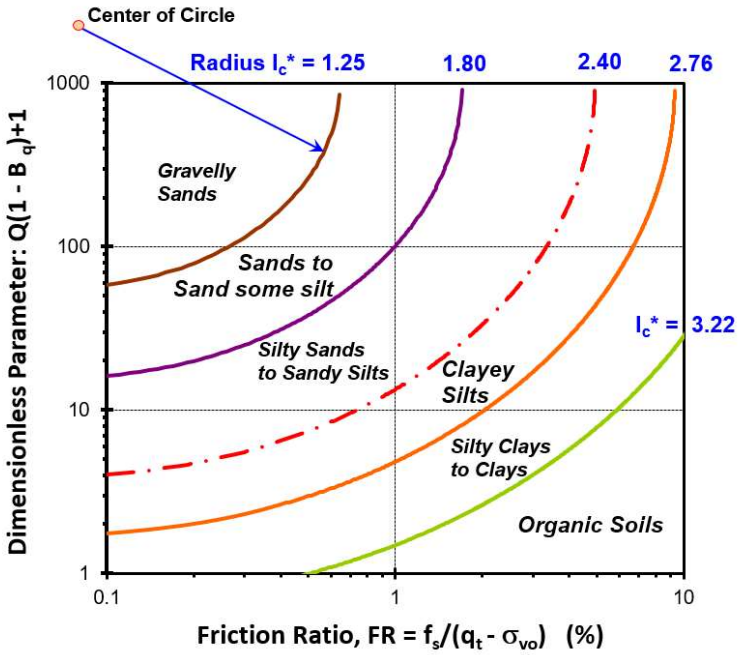


Figure 8.16. CPT Soil Profiling Chart Developed by Jefferies and Been (2016)

## 8.7 Use of SBT Charts for Identifying Organic Clays

As pointed out in the previous section, very few SBT charts have defined a zone or region for organic soils. To investigate the available SBT charts with organic soil zones, a special database of 23 worldwide and well-documented organic soil sites was compiled as summarized in **Table 8.2**. The database covers organic soils from several countries including Brazil, Mexico City, Poland, Holland, China, and the USA. The organic content of the reported sites ranges from as low as 3% to > 35%. For each organic soil, the organic content data were collected based on loss on ignition (LOI) tests and an average value of

organic matter content (O.M.C.) is summarized in the table. Additional information regarding the unit weight and natural water content for each site was also collected.

For each organic soil, a representative CPT sounding was selected to investigate the various SBT charts and to develop links between the organic content and the piezocone readings. Additional normalized cone parameters: normalized cone tip resistance (Q); normalized friction (F); and normalized porewater pressure parameter ($B_q$) were evaluated for each organic soil and an average representative value for each site was summarized in **Table 8.3.** In addition, a representative CPT material index ($I_c$) was assigned, which will eventually be used in helping to estimate the organic content from the piezocone readings.

By plotting the compiled database on Schmertmann's (1978) soil classification chart using cone tip resistance ($q_t$) in MPa and friction ratio ($f_s/q_t$) as presented in **Figure 8.17**, it is evident that most organic clays do not fall within the assigned organic clay zone with the exception of 3 organic soils that partially lie within the correct zone. Overall, the SBT chart by Schmertmann does not correctly identify the organic soils regardless of their origin or their organic content value.

Normalized cone parameters are evaluated for the various organic soils in the compiled database to plot them on Robertson's (2009) 9-zone soil behavior classification chart, as presented in **Figure 8.18**. It is clear that most organic soils fall within the incorrect zone of clays (zone 3) instead of the predefined zone 2 for organics. Some data points even fall within zone 4 for silt mixtures or zone 5 for sandy mixtures. The main exception is Mexico City clay and soft Ballina clay from Australia which fall within zone 2 of organic clays with the correct ranges for Q, F, and $B_q$**.**

A similar analysis was carried out using the modified Jefferies and Been (2016) chart, as presented in **Figure 8.19**. The chart shows a relatively improved identification if compared to other SBT charts, where more of the organic soil sites lie within the correct assigned zone at $I_c > 3.22$. This suggests the possibility of using a modified version of Jefferies and Been SBT chart in detecting the presence of organic clays. However, it should be pointed that some organic soils regardless their organic content value do not fall within the correct zone, hence, the organic soil detection from the chart is preliminary and approximate.

Table 8.2. Special compiled database of different world-wide organic soils

| Organic Clay | Location | Unit Weight ($kN/m^3$) | Organic Matter Content (%) | References |
|---|---|---|---|---|
| Ballina soft clay | Australia | 14.6 | 6 | Colreavy et al. (2015) |
| Barra da Tijuca - CM1 | Brazil | 12.4 | 26 | de Almeida et al. (2010) |
| Barra da Tijuca - Gleba | | 11.6 | 17 | |
| Gammelgården | Sweden | 14.2 | 6 | Larsson et al. (2007); Westerberg et al. (2015) |
| Hjoggböle | | 15.8 | 3 | |
| Huaiyan | China | 17.6 | 4 | Cai et al. (2016) |
| Markermeer peat | Holland | 11.7 | 17 | Zwanenburg & Jardine (2015) |
| Jefferson Parish B-7, LA | USA | 15.1 | 7 | Tümay et al. (2013) |
| Jefferson Parish B28, LA | USA | 15.4 | 8 | |
| Mexico City Clay | Mexico | 12.8 | 6 | Cruz & Mayne (2006) |
| MN – TH 241 | Minnesota USA | 18.7 | 10 | Dehler & Labouz (2007) |
| MN – TH 23 | | 18.9 | 8 | |
| MN – TH 19 | | 18.9 | 16 | |
| Recife RRS1 | Brazil | 15.6 | 6 | Coutinho (2007) |
| Recife RRS2 | | 13.9 | 8 | |
| Raszynka River valley | Poland | 14.2 | 10 | Kowalczyk et al. (2017) |
| Sarapuí II | Brazil | 13.3 | 8 | Jannuzzi et al. (2015) |
| Stargard Szczeciński | Poland | 11.3 | 14 | Młynarek et al. (2014) |
| Suape subarea A | Brazil | 11.8 | 39 | Coutinho & Bello (2014) |
| Sunderbyn | Sweden | 15.0 | 4 | Larsson et al. (2007); Westerberg et al. (2015) |
| Suisun Bay, CA | USA | 10.7 | 24 | Merani et al. (2016) |
| Umeå bangård | Sweden | 16.0 | 3 | Larsson et al. (2007); Westerberg et al. (2015) |
| Västerslätt | | 16.0 | 3 | |

Table 8.3. Summary of normalized CPT parameters and material index values for compiled organic soils database

| Organic Clay | Location | Q | F | $B_q$ | $I_c$ | References |
|---|---|---|---|---|---|---|
| Ballina soft clay | Australia | 3.9 | 2.5 | 0.58 | 3.31 | Colreavy et al. (2015) |
| Barra da Tijuca - CM1 | Brazil | 2.1 | 5.9 | 0.56 | 3.71 | de Almeida et al. (2010) |
| Barra da Tijuca - Gleba | | 4.7 | 4.8 | 0.49 | 3.43 | |
| Gammelgården | Sweden | 11.3 | 3.6 | 0.32 | 3.11 | Larsson et al. (2007); Westerberg et al. (2015) |
| Hjoggböle | | 23.5 | 1.5 | 0.11 | 2.58 | |
| Huaiyan | China | 32.8 | 3.8 | 0.21 | 2.91 | Cai et al. (2016) |
| Markermeer peat | Holland | 13.2 | 7.8 | 0.02 | 3.15 | Zwanenburg & Jardine (2015) |
| Jefferson Parish B-7, LA* | USA | 8.1 | 5.8 | - | 3.29 | Tümay et al. (2013) |
| Jefferson Parish B28, LA* | USA | 8.4 | 2.3 | - | 3.00 | |
| Mexico City Clay | Mexico | 2.3 | 5.9 | 0.38 | 3.71 | Cruz & Mayne (2006) |
| MN – TH241 | USA | 4.5 | 15.5 | 0.50 | 3.30 | Dehler & Labouz (2007) |
| MN – TH23 | | 15.9 | 3.4 | 0.19 | 2.93 | |
| MN – TH19 | | 5.6 | 5.8 | 0.31 | 3.44 | |
| Recife RRS1 | Brazil | 6.6 | 2.1 | 0.52 | 3.11 | Coutinho (2007) |
| Recife RRS2 | | 4.10 | 1.0 | 0.61 | 3.17 | |
| Raszynka River valley | Poland | 39.7 | 2.7 | 0.02 | 2.52 | Kowalczyk et al. (2017) |
| Sarapuí II | Brazil | 16.8 | 3.2 | 0.42 | 2.90 | Jannuzzi et al. (2015) |
| Stargard Szczeciński | Poland | 14.2 | 4.7 | 0.35 | 3.41 | Młynarek et al. (2014) |
| Suape subarea A** | Brazil | 4.9 | - | - | - | Coutinho & Bello (2014) |
| Sunderbyn | Sweden | 19.05 | 2.4 | 0.23 | 2.86 | Larsson et al. (2007); Westerberg et al. (2015) |
| Suisun Bay, CA | USA | 6.8 | 4.4 | 0.24 | 3.28 | Merani et al. (2016) |
| Umeå bangård | Sweden | 24.3 | 1.1 | 0.18 | 2.58 | Larsson et al. (2007); Westerberg et al. (2015) |
| Västerslätt | | 9.4 | 2.9 | 0.30 | 3.15 | |

NOTES:

* no porewater pressure measurements were recorded

** only cone tip resistance was reported

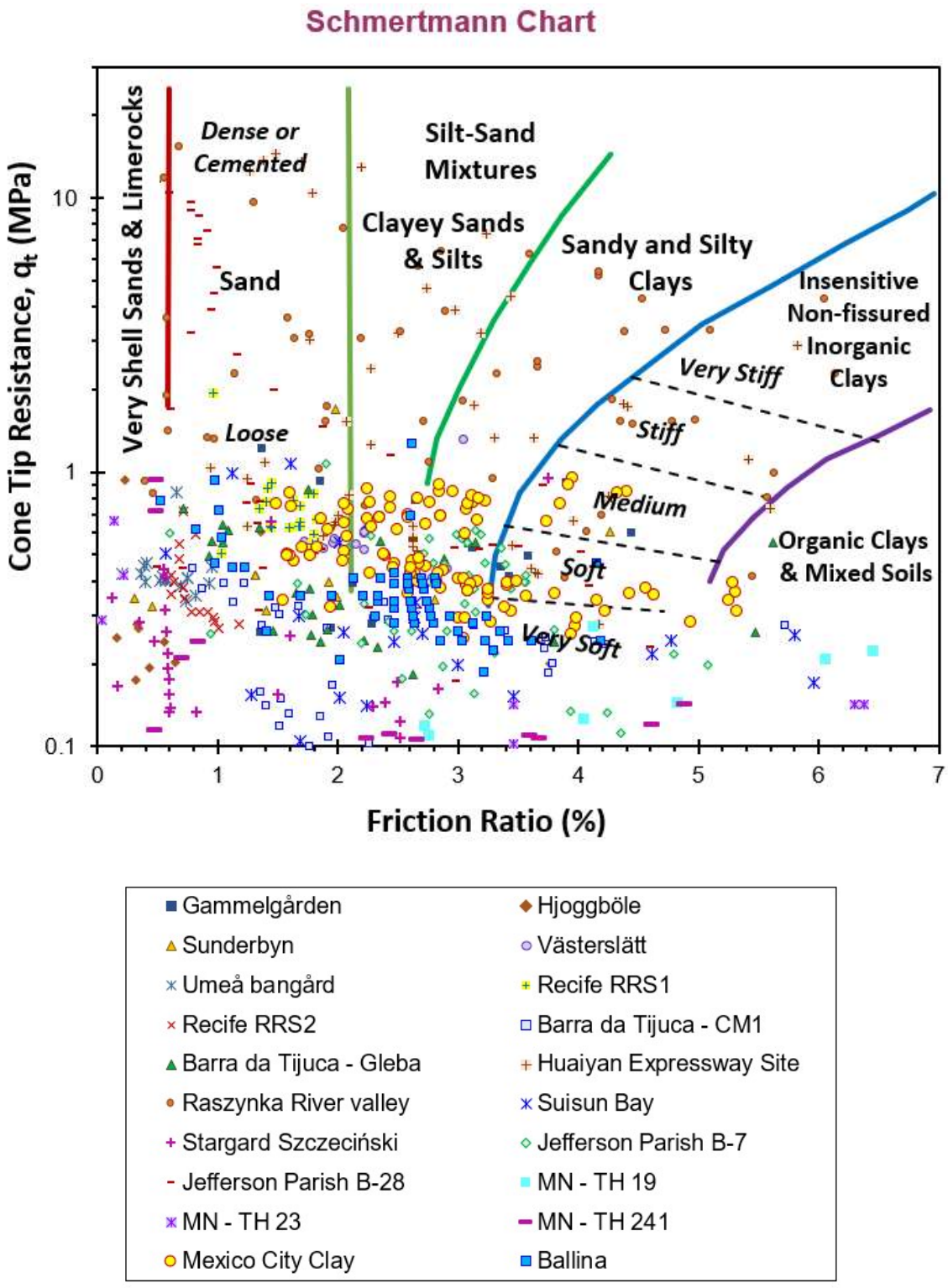


Figure 8.17. Compiled database of organic soils on Schmertmann (1978) SBT chart

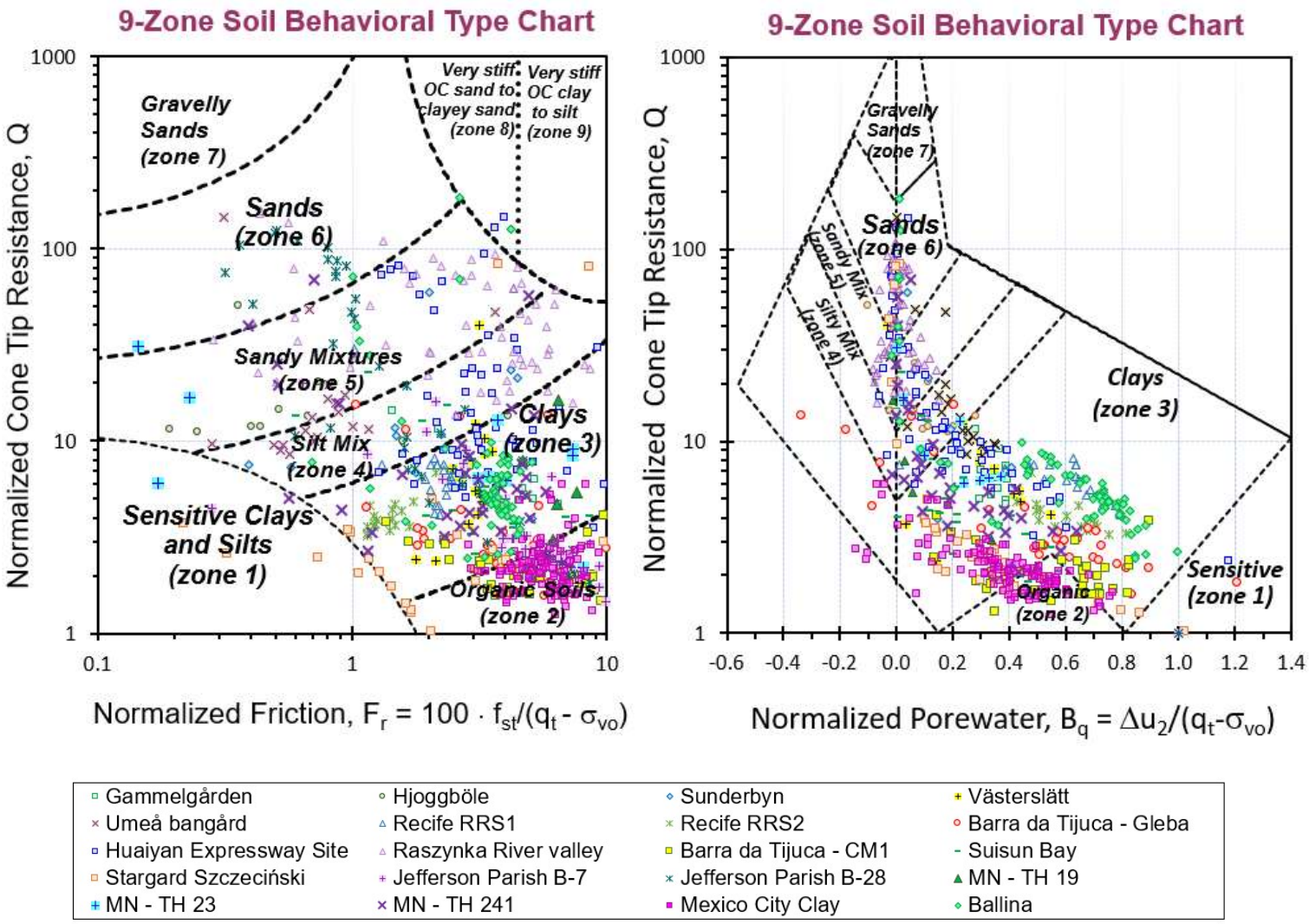


Figure 8.18. Compiled database of organic soils assigned on Robertson (2009) 9-zone SBT chart

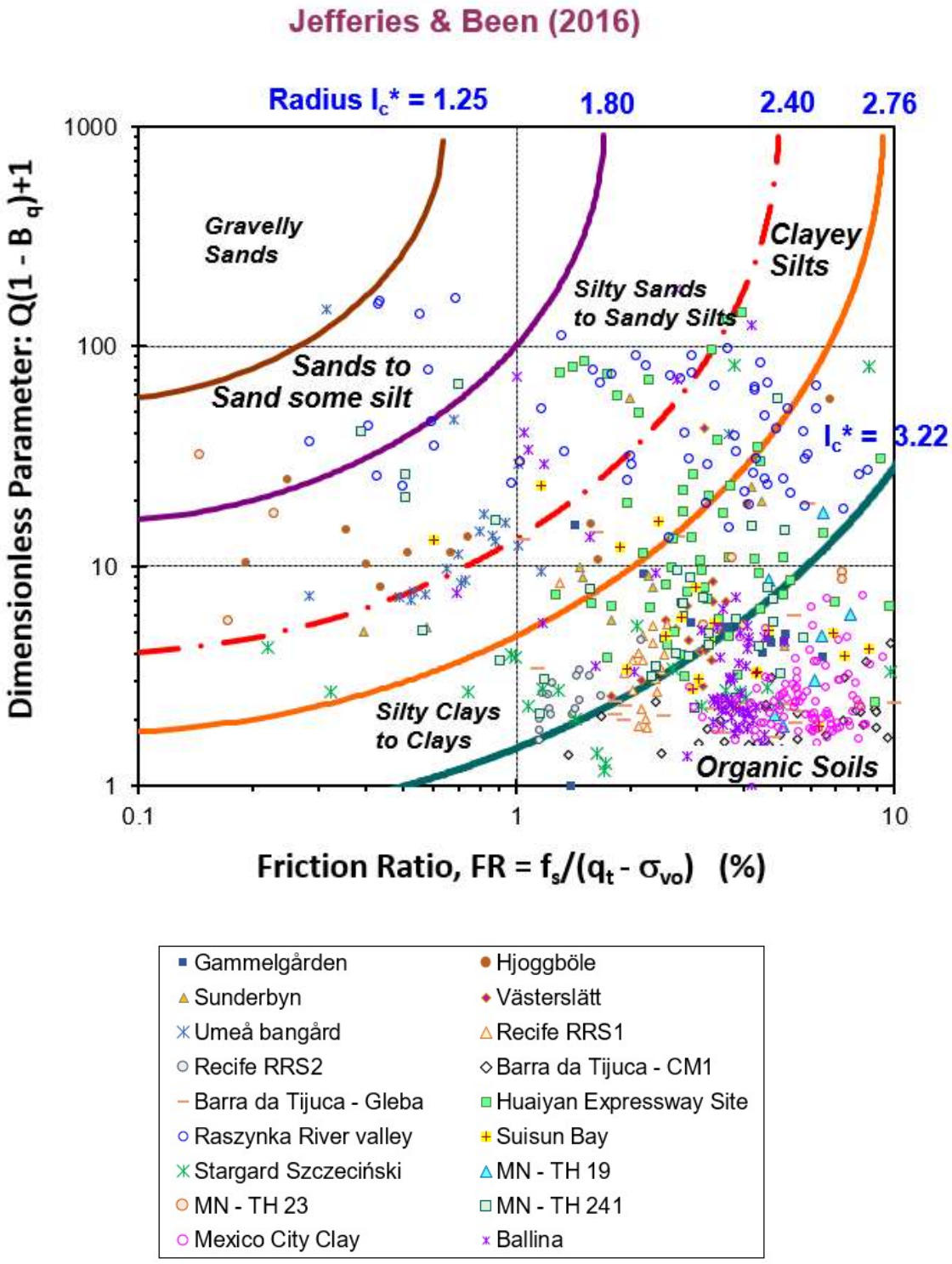


Figure 8.19. Compiled database of organic soils on Jefferies & Been (2016) SBT chart

## 8.8 Use of Pore Water Pressure Readings for Identifying Organic Clays

Given that the different CPTu soil behavior type charts did not identify the correct zone for all 23 organic clay sites, further investigation for the CPT readings was required. The cone tip resistance ($q_t$) and the porewater pressure ($u_2$) readings from the representative piezocone soundings were used to evaluate the corresponding normalized porewater pressure parameter ($B_q = \Delta u_2 / q_t - \sigma_{vo}$) and normalized cone tip resistance (Q), as presented in **Figure 8.20**. Three groups of clays are presented: (a) well-behaved insensitive and inorganic clays (reported in Chapter 4) which are given blue symbols; (b) sensitive and structured clays (listed in Chapter 6) represented by pink symbols; and (c) organic clays (listed in Tables 8.2 and 8.3), plotted with green symbols. A reference mean value of $B_q = 0.6 \pm 0.1$ can be taken as characteristic of the normal inorganic and insensitive clay group. From the plotted results, it can be observed that $B_q$ (organic clays) < $B_q$ (vanilla clays) < $B_q$ (sensitive clays). Using the benchmark $B_q$ value of 0.60, a range of $0.5 < B_q < 0.7$ can be assigned to the normal clays. When $B_q < 0.5$, the expected clay is organic, while $B_q > 0.7$ suggests that the encountered clay is sensitive or structured.

For further assessment, the three clay groups are superimposed onto the Robertson 2009 nine-zone soil behavioral chart, where it evidently only captures the correct soil zone for all of the inorganic and insensitive intact clays. The chart only identifies one data point of the organic clay sites and only a single value of the sensitive clays.

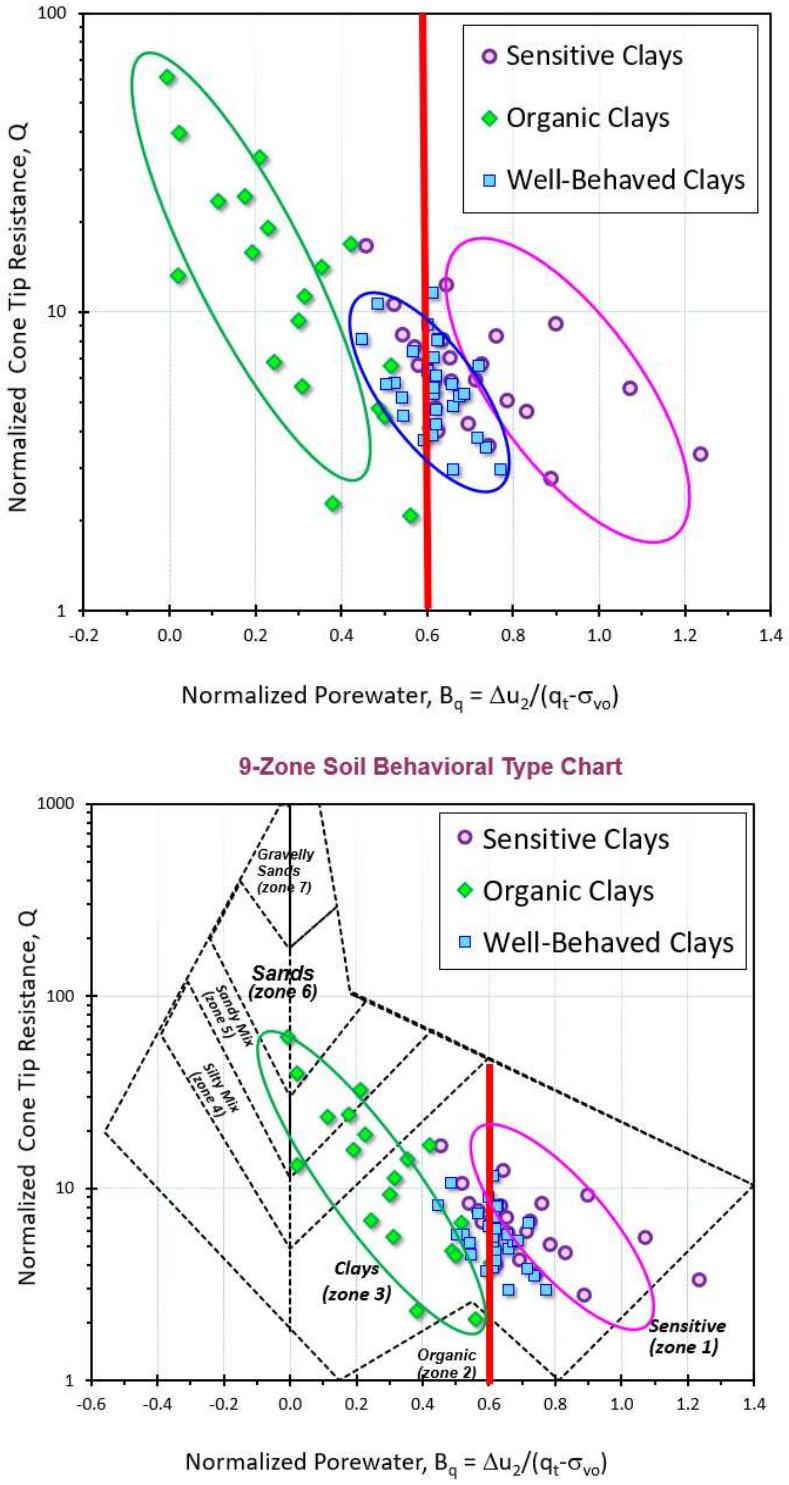


Figure 8.20. (a) Q versus $B_q$ plot showing data from organic clays compared to well-behaved and sensitive clays; (b) data superimposed on Robertson's soil behavior type chart

The normalized sleeve friction ratio [Fr % = $100 \cdot f_s/(q_{net})$] of organic soils is also investigated and plotted against $B_q$ as presented in **Figure 8.21**, also plotted the compiled sensitive and well-behaved clays, from the plot is evident that a sort of grouping separating the three different clay types can be achieved. The $B_q$ benchmark value of $0.6 \pm 0.1$ is clear for the well-behaved insensitive inorganic clays. As for the normalized friction, it is noticed that organic clays tend to have relatively higher Fr values if compared to the well-behaved clays followed by the sensitive clays with the lowest Fr values.

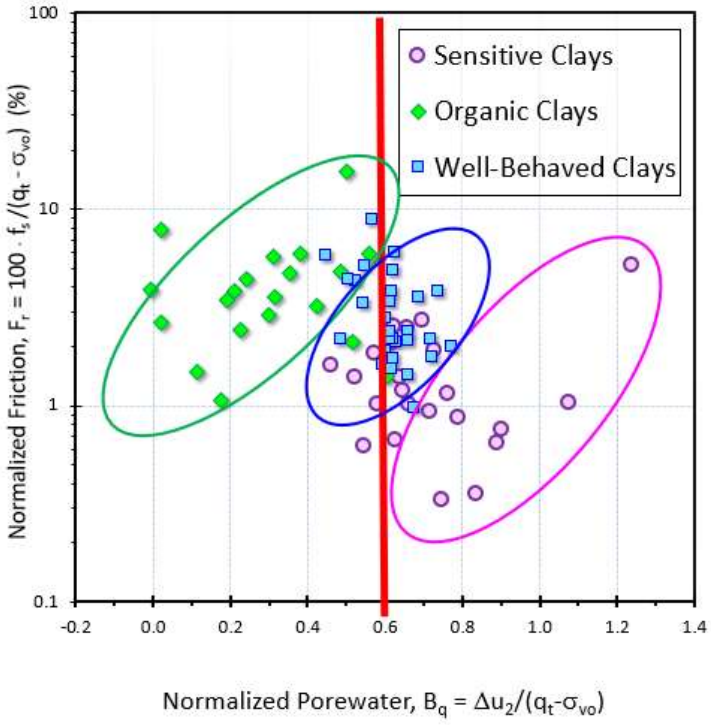


Figure 8.21. $F_r$ versus $B_q$ plot showing data from organic clays compared to well-behaved and sensitive clays

The $Q_{tn}$-$F_r$ plot as per Robertson (2009) were also investigated as presented in **Figure 8.22** where no clear separation between the different clay groups can be assigned based on the combination of $Q_{tn}$-$F_r$ paired readings. **Figure 8.22b** presents the same data points but superimposed on Robertson's 9-zone soil behavior type chart where it is evident

that the Q-Fr chart is relatively better than the Q-Bq chart in correctly detecting and identifying the correct clay group. The well-behaved insensitive inorganic clays are mostly assigned zone 3, as for the organic clays only 2 sites are correctly identified as zone 2, and for the sensitive clays, only 4 sites fall correctly within zone 1 of sensitive clays and silts. Overall the 9-zone SBT chart misses the correct identification of both organic and sensitive clays as evident from **Figures 8.20** and **8.22b**.

## 8.9 Behavior of Organic Clays in CPTU Stress History Profiling

### 8.9.1 Simplied Preconsolidation Profiling by CPTu

The CPTu-OCR solution from the hybrid SCE-CSSM derivation is used to investigate the behavior of organic clays in profiling soil stress history. Chen and Mayne (1994) combined spherical cavity expansion theory and critical state soil mechanics (SCE-CSSM) to express the cone tip resistance ($q_t$) and porewater pressure ($u_2$) in three closed-form equations to determine the overconsolidation ratio (OCR). For normal well-behaved clays, an approximate set of stepped-down versions of the developed expressions is obtained by assigning default values for the plastic volumetric strain potential ($\Lambda$ =1), effective stress friction angle ($\phi'$ = 30°), and rigidity index ($I_R$ = 100). The simplified expressions are:

$$\sigma_p' \approx 0.33 \cdot (q_t - \sigma_{vo}) \quad [8.8]$$

$$\sigma_p' \approx 0.54 \cdot (u_2 - u_o) \quad [8.9]$$

$$\sigma_p' \approx 0.60 \cdot (q_t - u_2) \quad [8.10]$$

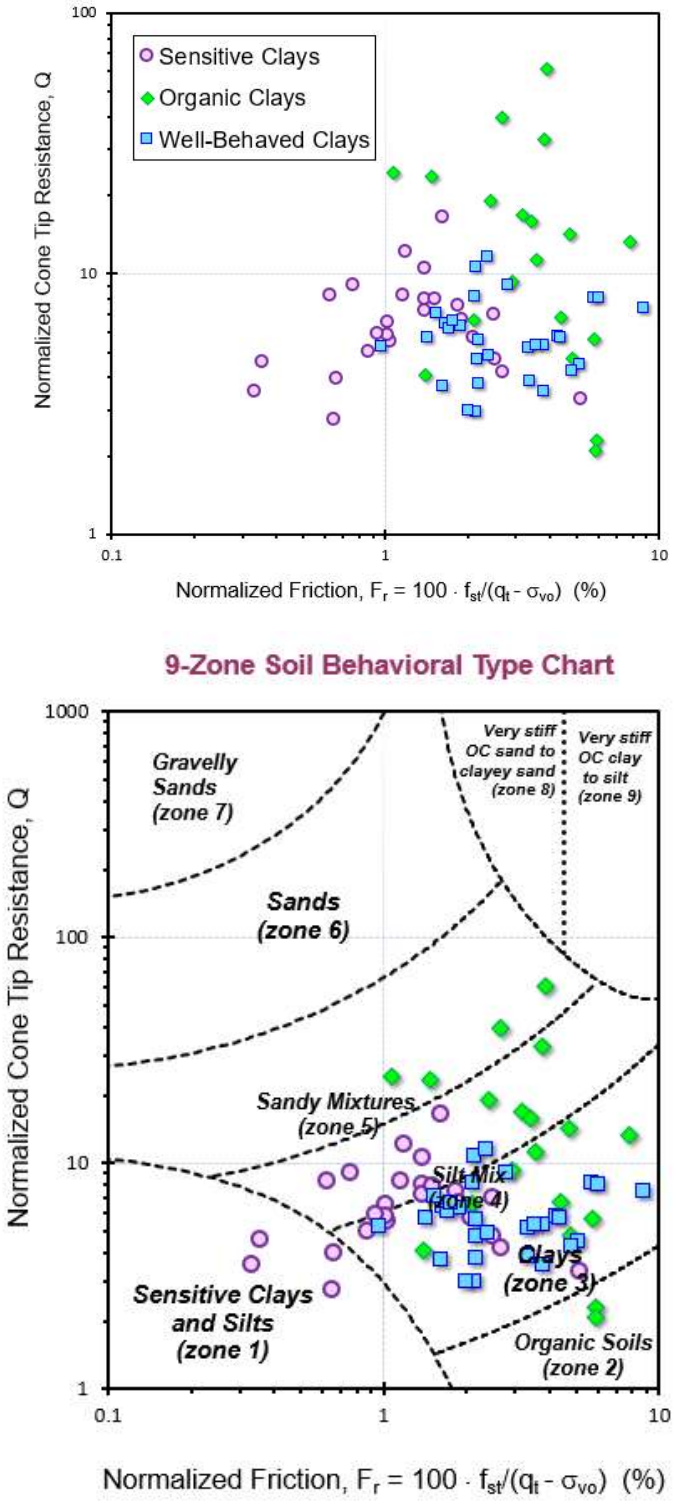


Figure 8.22. (a) Q versus $F_r$ plot showing data from organic clays compared to well-behaved and sensitive clays; (b) data superimposed on Robertson's soil behavior type chart

While these approximations should apply reasonably well for insensitive and inorganic clays, it will be shown that significant deviations will occur in organic clays (as well as sensitive and structured clays), thus provide a warning sign that additional testing, drilling, and sampling may be warranted to fully identify the problematic soils.

### 8.9.2 Application to Bothkennar Clay, Scotland

For illustration, the simplified expressions from original SCE-CSSM solutions are applied to a well-behaved intact estuarine clay from Bothkennar, Scotland, as presented in **Figure 8.23**. Using two series of independent piezocone soundings (one from Hight et al. 2003 and another from Powell and Lunne 2005), the measured profiles of cone tip resistance ($q_t$) and porewater pressure ($u_2$) with depth are presented in **Figure 8.23a** and **Figure 8.23b**, respectively. The preconsolidation stresses ($\sigma_p'$) from three different types of laboratory consolidation tests are available from this location. These include constant rate-of-strain (CRS) type, incremental load (IL) oedometer, and restricted flow (RF) type consolidation tests. Application of equations [8.8], [8.9], and [810] provides three evaluations for the effective preconsolidation stress as functions of: $q_{net} = (q_t - \sigma_{v0})$, $\Delta u = (u_2 - u_0)$ and $q_{eff} = (q_t - u_2)$, as illustrated in **Figure 8.23c**. The three CPTu predictions are similar, indicating low degrees of overconsolidation in the soft clay ($1.5 < OCR < 2.5$) and providing rather good agreement with the lab $\sigma_p'$ values.

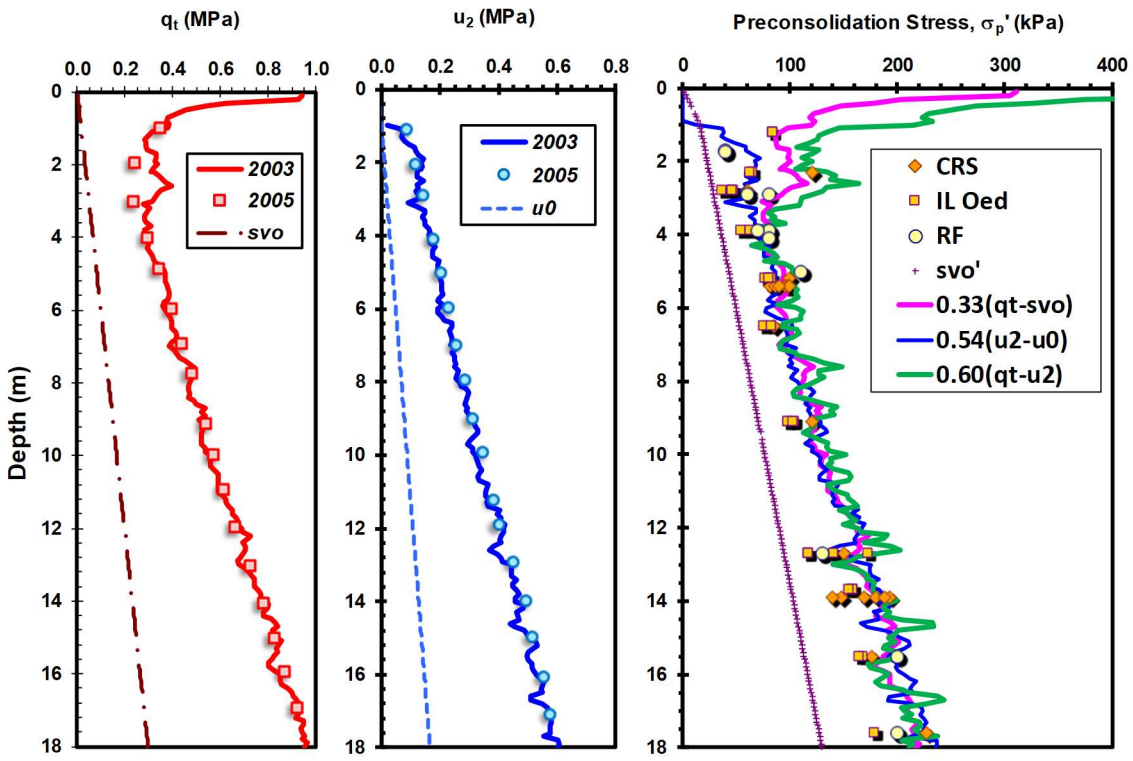


Figure 8.23. Results from two series of piezocone soundings in soft Bothkennar clay: (a) total cone tip resistance, $q_t$; (b) porewater pressure, $u_2$; (c) preconsolidation stress evaluation using three expressions from the hybrid SCE-CSSM framework (data from Hight et al, 2003; Powell and Lunne, 2005)

### 8.9.3 Application of Simplified SCE-CSSM Expressions to Organic Clays

The simplified expressions based on original SCE-CSSM solutions are applied to a number of the organic soils from the compiled database where complementary stress history data are available. As organic clays are not considered "well-behaved" or normal, the intent is that the three separate expressions from the simplified yield stress approach will not agree, thus providing a "red flag" on the results and warning the geoengineer to proceed cautiously.

**Figure 8.24** presents the results of a representative piezocone sounding in Mexico City clay as reported by Cruz and Mayne (2006). The Mexico City clay is considered an extreme geomaterial and characterized by high compressibility, high water contents ($300 < w_n < 1000\%$), high plasticity characteristics ($300 < LL < 600\%$; $200 < PI < 450\%$), high friction angles ($30° < \phi' < 43°$) and unusual and complex mineralogy (Diaz-Rodriguez et al. 1992). Moreover, Mexico City clay has been described as a "very organic montmorillontic thixotropic" clay and also as "an organic silty clay composed of ... fossils... and diatoms" (Mesri et al. 1975). The organic content varies and was shown by Leonards & Girault (1961) to be around 8 to 10%, while Mesri et al. (1975) gave values of 5 to 10%.

By examining the three predictive stress history profiles in Mexico City clay based on $q_{net}$, $\Delta u$, and $q_E$, it is evident that they do not agree. This is a first sign that the soil encountered is not a well-behaved clay. Upon closer inspection, the hierarchy of the stress history predictions is as follows: $\sigma_p' f(\Delta u) < \sigma_p' f(q_{net}) < \sigma_p' f(q_E)$. Note that the observed hierarchy is surprisingly the complete opposite that was found for sensitive and structured clays (Chapter 7) where: $\sigma_p' f(q_E) < \sigma_p' f(q_{net}) < \sigma_p' f(\Delta u)$.

This observation was further investigated using piezocone and stress history data from other organic clays as presented in **Figure 8.25** for Sarapui II clay, **Figure 8.26** for Huaiyan clay in China, **Figure 8.27** for Markermeer peat in Holland, and **Figure 8.28** for three organic sulphide clays from Sweden: Gammelgården, Västerslätt and Umeå bangård.

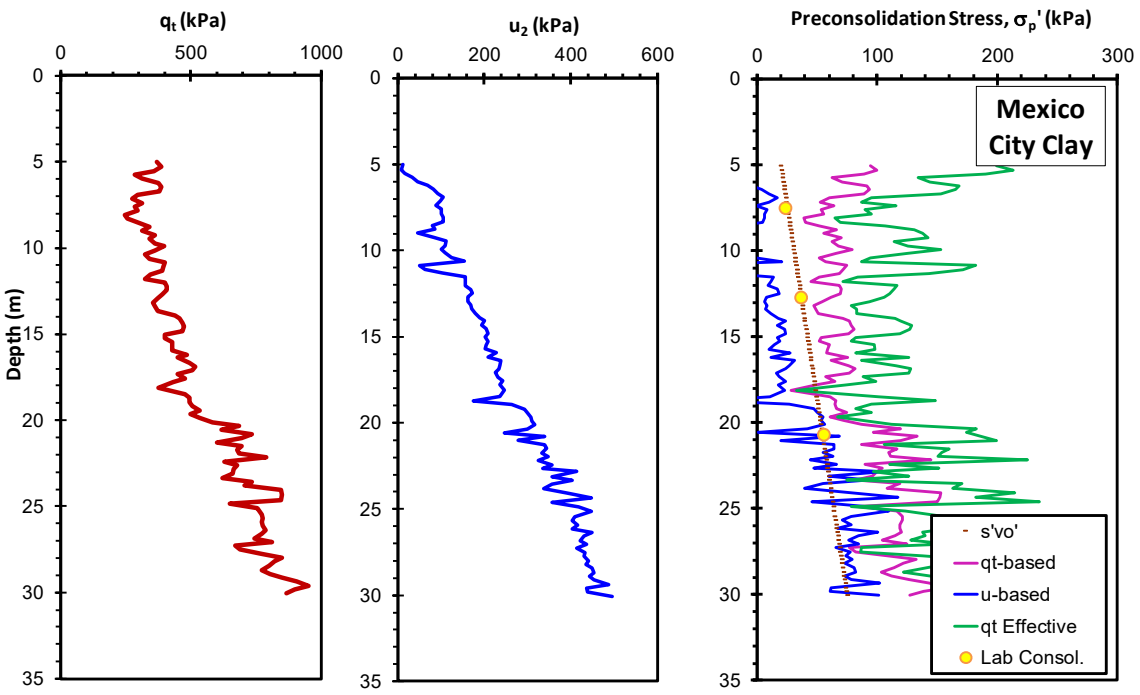


Figure 8.24. Results from a piezocone sounding at site L-2 in Mexico City Clay: (a) cone tip resistance, $q_t$; (b) porewater pressure, $u_2$; (c) yield stress evaluation using three expressions from the hybrid SCE-CSSM framework (data from Cruz & Mayne, 2006)

By examination of the CPTu-estimated $\sigma_p'$ profiles for the organic clays, it is evident that they all share the same hierarchical behavior where: $\Delta u$ – based prediction < $q_{net}$ – based prediction < $q_E$ – based prediction. The mismatch between these separate evaluations of $\sigma_p'$ from CPTu data can be used as a first sign that the clay is not a well-behaved insensitive inorganic clay. The observed hierarchy of having the porewater pressure prediction as the lowest value and the effective cone tip resistance as the highest can be used as a possible indicator in detecting organic soils.

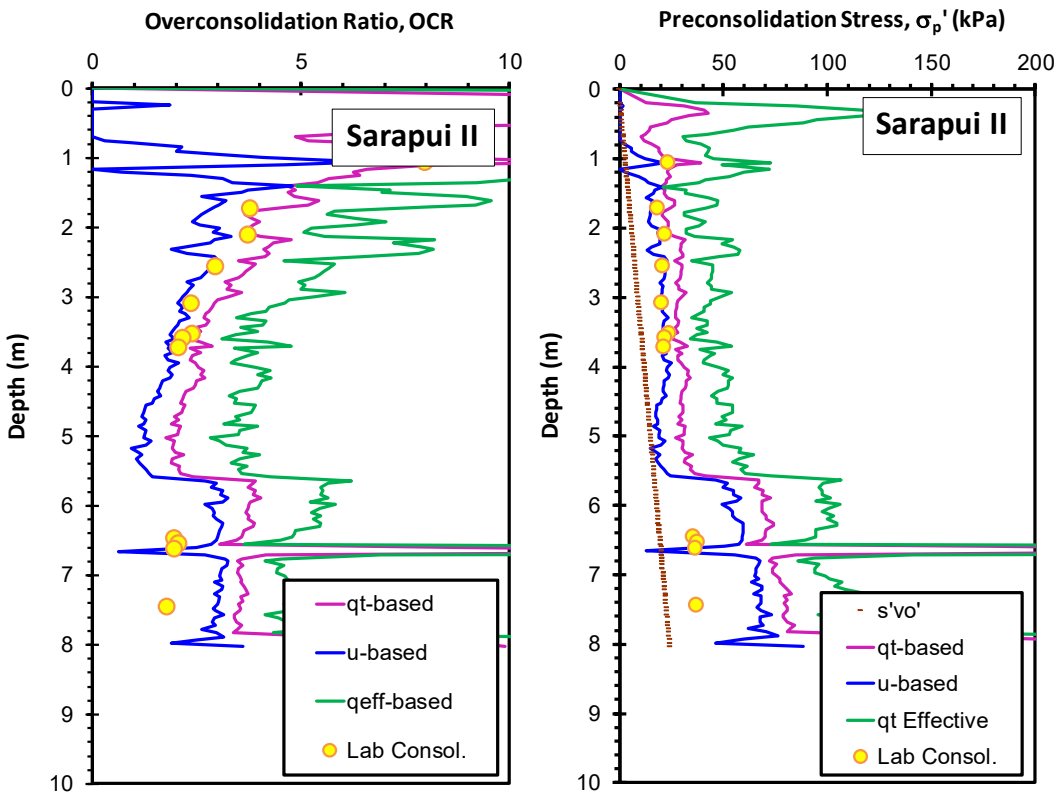


Figure 8.25. OCR and preconsolidation stress evaluations in Sarapui II using three expressions from the SCE-CSSM framework (data from Jannuzzi et al., 2015)

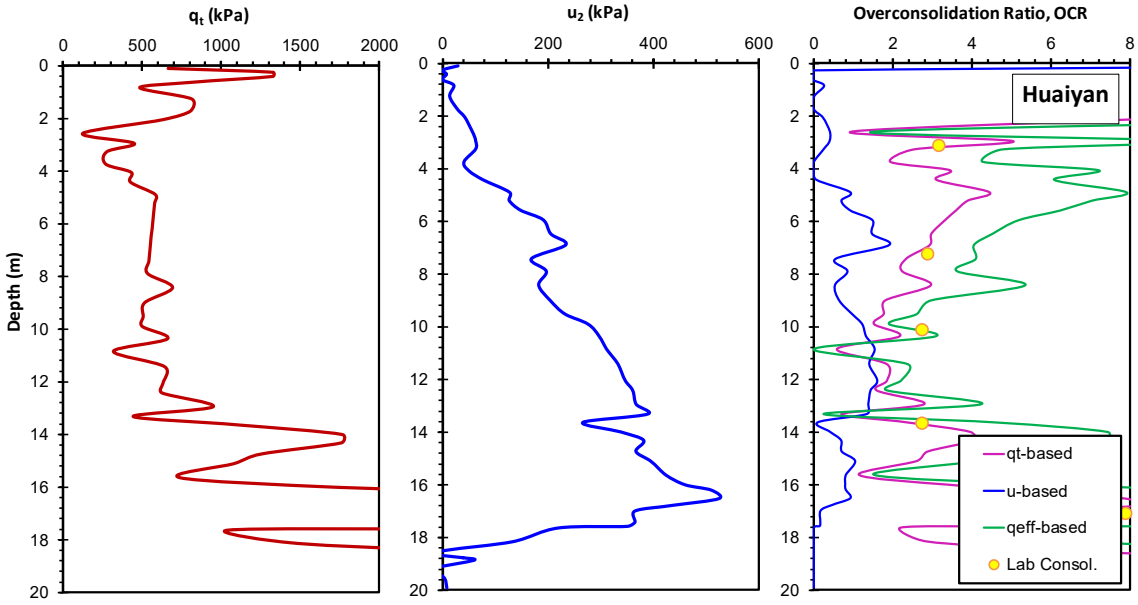


Figure 8.26. Results from piezocone sounding in Huaiyan Clay: (a) cone resistance, $q_t$; (b) porewater pressure, $u_2$; (c) OCR evaluations using three expressions from the hybrid SCE-CSSM framework (data from Cai et al., 2016)

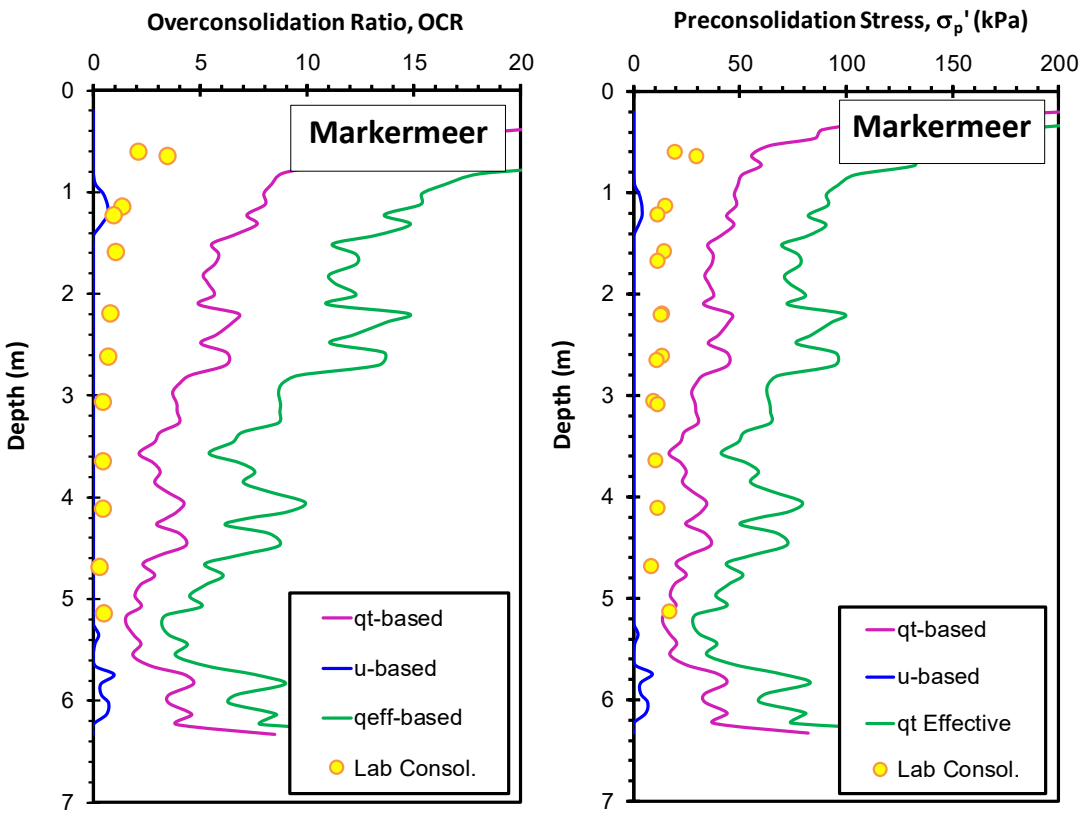


Figure 8.27. OCR and preconsolidation stress evaluations in Markermeer peat using three expressions from SCE-CSSM framework (data from Zwanenburg & Jardine, 2015)

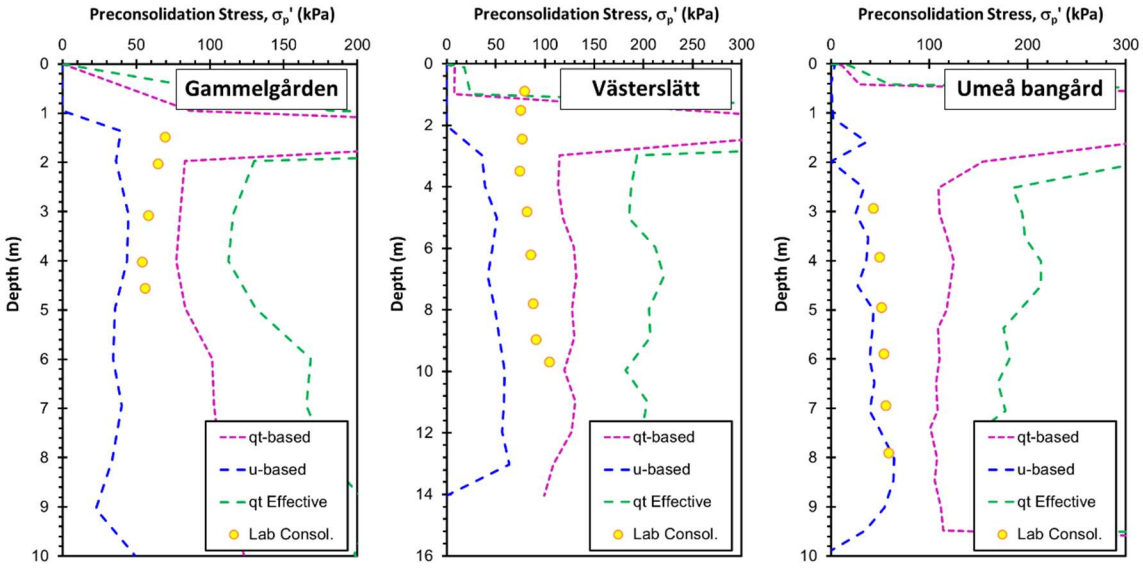


Figure 8.28. Preconsolidation stress evaluations using three expressions from the hybrid SCE-CSSM framework (a) Gammelgården; (b) Västerslätt; and (c) Umeå bangård, Sweden (data from Larsson et al. 2007; Westerberg et al. 2015)

## 8.10 Assessing Yield Stress from CPTu in Organic Clays

Once the soils have been identified as organic, a correct stress history prediction for organic clays can be handled using the generalized stress history power law expression with an exponent (m') detailed in Chapter 4:

$$\sigma_p' = 0.33 \cdot (q_t - \sigma_{vo})^{m'} \qquad \text{(SI units of kPa)} \qquad [8.11]$$

For organic clays, an assigned m' value of 0.9 is appropriate and this value should be cross-validated with companion consolidation testing. **Figure 8.29** presents an example for organic clay from the Mexico City Clay site where an exponent m' of 0.90 was assigned giving good agreement with the laboratory measured values.

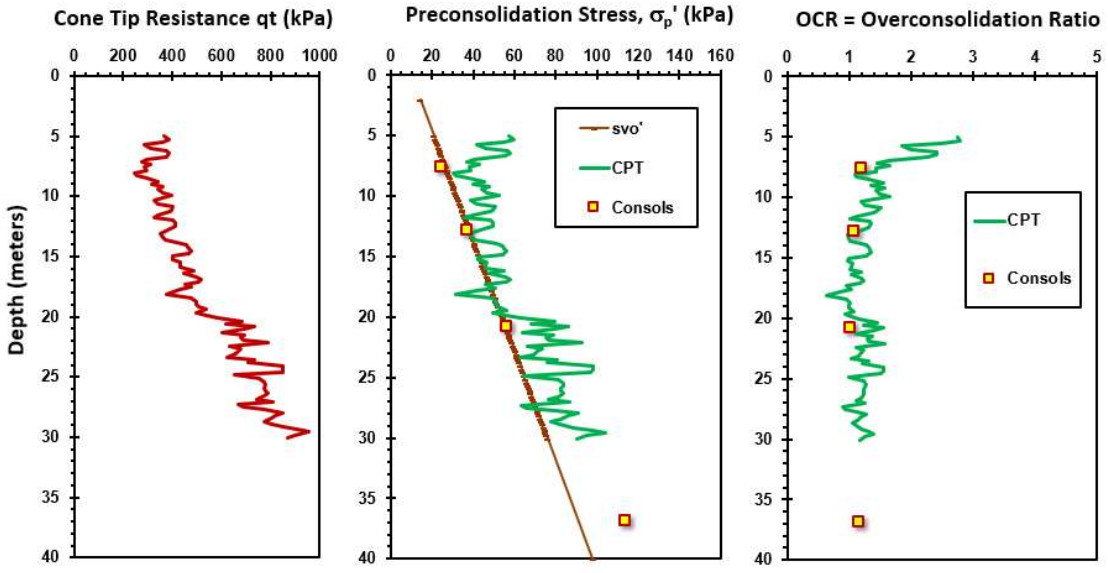


Figure 8.29. Profiles in soft organic Mexico City clay at site L-2: (a) cone resistance; (b) preconsolidation stress; (c) overconsolidation ratio. (data from Cruz & Mayne, 2006)

**Figure 8.30** presents the cone tip resistance of a piezocone sounding conducted in the very soft organic site of Sarapuí II in Brazil along with the results of the laboratory measured preconsolidation stresses and corresponding yield stress ratio as reported by Jannuzzi et al. (2015). By assigning an exponent m' = 0.9 for organic clays, a very good match can be seen between the reference laboratory consolidation tests and the CPT profile.

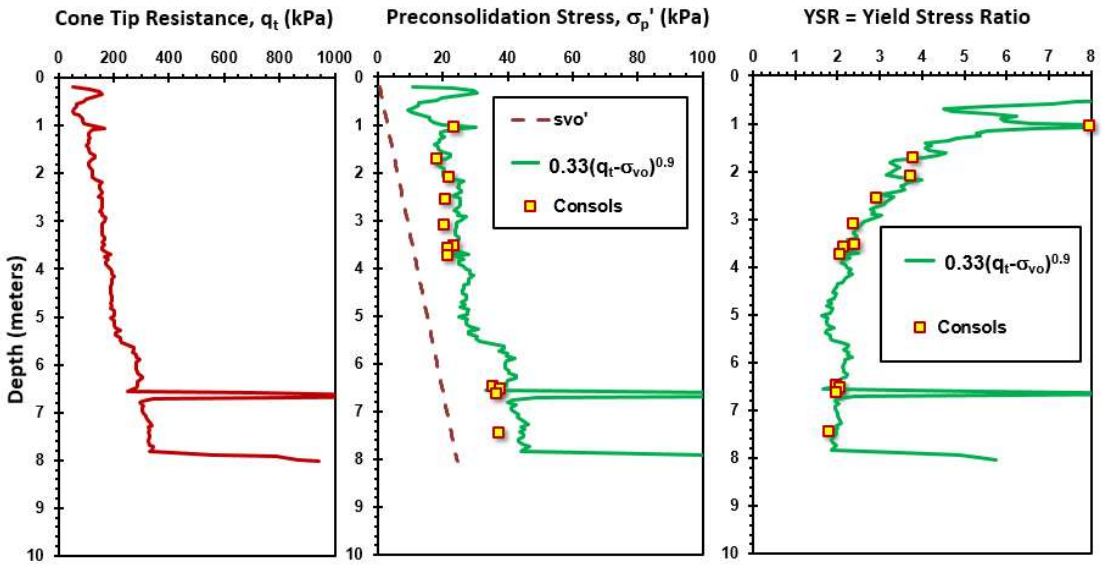


Figure 8.30. Profile in very soft organic Sarapui II, Brazil: (a) cone resistance; (b) preconsolidation stress; (c) yield stress ratio. Data from Jannuzzi et al. (2015)

**Figure 8.31** presents the cone tip resistance of a piezocone sounding conducted in the soft organic clay of Recife RSS1 in Brazil. The results of the laboratory measured preconsolidation stresses and corresponding overconsolidation stress ratio as reported by Coutinho (2007). By assigning an exponent m' = 0.92 for organic clays, a very good match can be seen between the reference laboratory consolidation tests and the CPT profile.

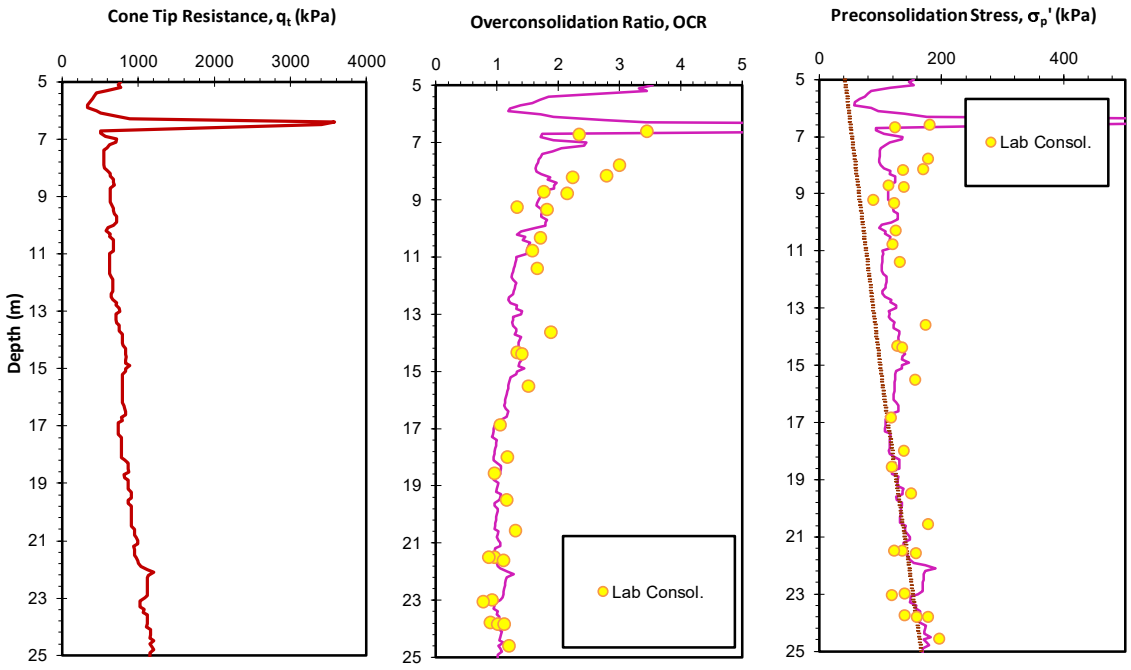


Figure 8.31. Profile in soft organic Recife RSS1 site (a) cone resistance; (b) overconsolidation ratio; (c) preconsolidation stress. Data from Coutinho (2007)

## 8.11 Conclusions

A summary of the different classification methods governing the definition of organic soils is presented where it is evident that there is not a clear cut off organic content value that separated organic soils from inorganic ones. Laboratory-based techniques are reviewed that are used to quantify the amount of organic content within any soil composition. A summary of the various index properties and their relationship to the organic content value is discussed. Engineering properties of organic soils covering its shear strength parameters and effective friction with their relation to the amount of organics are presented.

Indirect means of detecting organic soils by in-situ piezocone penetration tests (CPTu) were detailed, including the well-known soil behavior type (SBT) charts. A database of 23 organic clay sites all tested using CPTu was compiled for calibration and verification purposes. For SBT charts having predefined organic soil zones (Robertson et al. 1986, Robertson 1990; Jefferies & Been 2015), the zone boundaries, in general, do not adequately detect the correct soil type for organic soils. Specifically, organic clay sites have a broader range of CPT material index ranging from 2.8 to 3.7 and not stricted to the proposed $I_c > 3.6$ as in the well-known 9-zone SBT charts of Robertson (1990, 2009).

It is observed that several SBT charts are not "successful" in identifying organic soil zones. This may be attributed to the inherent, and special, nature of organic soils as they can range from fibrous to amorphous and may have experienced different degrees of degradation and decomposition of the organic component that could well affect the chemical and engineering properties of the organic deposit over time. Other factors that could also affect the ability of the piezocone to identify and characterize organic soils include the depositional environments, with its great variability, and the nature of the piezocone itself and the type of metal the cone is made of. In light of this, organic soils should be handled more carefully when tested using piezocones, and conventional standard practices for identifying and characterizing inorganic soils should be carefully used with high levels of cross-calibration and inspection.

This chapter investigates the porewater pressure readings of piezocone soundings carried out in organic soils relevant to readings measured for other well-behaved clays and sensitive/ structured clays. It is shown that organic clays have lower normalized porewater pressure parameters when compared to other clay groups.

Furthermore, the behavior of organic clays in profiling stress history is investigated using the original hybrid SCE-CSSM solution where the predictive profiles mismatch indicating the presence of abnormal soil. Upon closer inspection, it is observed that organic clays tend to have a hierarchical behavior where stress history predictions based on excess porewater pressure are the lowest followed by the net cone tip resistance then the effective cone tip resistance; this is opposite to the hierarchical trend observed in sensitive clays.

# Chapter 9. An advanced analytical CPTu model for undrained shear strength and yield stress in clays

## 9.1 Introduction

A hybrid analytical cavity expansion-critical state model for evaluating the stress history (OCR) from CPTu data in well-behaved inorganic clays of low to medium sensitivity was rather successful since its implementation (Mayne 1991; Chen & Mayne 1994; Burns & Mayne 2002). Data from many clays were originally calibrated using a large compiled database collected from samples where preconsolidation stress (yield stress) was obtained from one-dimensional consolidation tests and corresponding readings ($q_t$ and $u_2$) taken from piezocone tests at the same elevation. The formulations allowed OCR to be related to normalized piezocone results (Q, U*, and $Q_u$*) in terms of geomaterial parameters: frictional parameter $M = 6 \cdot \sin\phi'/(3-\sin\phi')$, plastic volumetric strain potential $\Lambda = 1-C_s/C_c$, and rigidity index $I_R = G/s_u$. A slightly modified version has also been successfully implemented for sensitive and structured clays by introducing definitions of the effective friction angle mobilized at both maximum deviator stress (i.e., $M_{qmax}$) and at maximum obliquity ($M_{MO}$).

Later, it was realized that the associated evaluation of undrained shear strength ($s_u$) was limited when compared to a recent GTRC-Fugro study that assembled 451 CAUC triaxial compression tests from 62 clay sites (Mayne & Peuchen 2018). This limitation was due to the earlier choice of a simple 1977 Vesić solution for relating the $s_{uc}$ to the net cone resistance via spherical cavity expansion theory, thus relying solely on rigidity index. As newer formulations based on numerical strain path method (SPM), finite element modelling (FEM), and finite difference (FD) have become available, it was decided to

modify the original solution using a more robust cone bearing $N_{kt}$ factor that was dependent upon rigidity index ($I_R$), initial stress state ($K_0$), and soil-penetrometer roughness ($\alpha_c$).

Subsequently, the new analytical model was calibrated using two large previously-compiled databases: (a) OCR-CPTu in 150 clays (updated after Mayne 2007); and (b) $s_{uc}$-CPTu in 62 clays (Mayne & Peuchen 2018).

## 9.2 Undrained Shear Strength

Undrained shear strength ($s_u$) is considered an important parameter in geotechnical engineering as it controls the bearing capacity of both shallow and deep foundations in clay. It is also required in short-term analyses of slope stability, excavations, sheet pile retaining walls, and embankment calculations involving clays.

Significant ranges and variations can be observed when comparing undrained shear strength profiles with depth using different testing techniques from in-situ and laboratory devices. This highlights the non-uniqueness of undrained shear strength and its dependence on the specific testing method and shearing mode (Ladd 1991). Undrained shear strength is also affected by several factors such as initial stress state (isotropic vs. $K_0$ consolidation), strength anisotropy, loading direction (compression vs. extension), and boundary conditions (plane strain vs. triaxial). Other influencing effects include strain rate, sensitivity, ageing, inherent fabric anisotropy, strain compatibility, thixotropy, and specimen quality associated with sampling disturbance (Ladd & DeGroot, 2003).

The high-end types of laboratory strength tests require a recompression stage before the shearing phase which is applied in certain devices, including isotropically-consolidated,

anisotropically-consolidated triaxial, and direct simple shear types, as well as plane strain. Those tests intend to re-establish the geostatic stress regime prior to undrained shear and simulate the initial effective stresses and the stress history of the tested specimen (Mayne, 2008). Thus, other various basic lab techniques such as unconfined compression (UC), unconsolidated undrained (UU), pocket penetrometer, and torvane can be considered only as index tests and not true measurements of $s_u$ (Ladd, 1991).

When comparing in-situ and laboratory-based values for $s_u$, the observed ranges become even more widespread where $s_u$ generally increases with depth and takes on the hierarchy of $s_u$ (compression) > $s_u$ (simple shear) > $s_u$ (extension). **Figure 9.1** illustrates the wide range of the various undrained shear strength profiles with depth for the Onsøy soft clay site in Norway measured using different shearing modes and methods. The figure presents the profiles of laboratory anisotropically consolidated triaxial tests in compression ($CK_0UC$), extension ($CK_0UE$), and direct simple shear (DSS), in addition to two in-situ based measuring techniques: field vane and self-boring pressuremeter (SBP) tests. For instance, the range of the measured $s_u$ values at a depth of 25 m reaches 3.5 times which highlights the significance of the testing technique and the shearing mode in correctly quantifying the undrained shear strength.

## 9.3 Direct CPTu evaluation of undrained shear strength in clays

The cone penetration test has been widely employed for evaluating the undrained shear strength of clays. As such, different theories have been adopted to develop links between the cone readings and $s_u$, as summarized by Lunne et al. (1997). These include bearing capacity theory (Terzaghi, 1943); cavity expansion theory (Skempton, 1951; Vesić

1975); strain path theory (Teh, 1987), stress paths (Konrad & Law, 1987), and FEM (Lu et al. 2004).

Two of the main readings from a piezocone sounding with depth include the cone tip resistance ($q_t$) and porewater pressure ($u_2$). Along with the total vertical overburden pressure ($\sigma_{vo}$) and hydrostatic pore water pressure ($u_0$), the CPTu results can be used to evaluate undrained shear strength using expressions of net cone resistance ($q_{net} = q_t - \sigma_{vo}$), excess pore pressure ($\Delta u = u_2 - u_0$), and effective cone resistance ($q_{eff} = q_t - u_2$) with corresponding and respective cone bearing factors $N_{kt}$, $N_{\Delta u}$, and $N_{ke}$. Following an inverted bearing capacity form, the methods include:

$$s_u = \frac{q_{net}}{N_{kt}} = \frac{q_t - \sigma_{vo}}{N_{kt}} \quad [9.1]$$

$$s_u = \frac{\Delta u}{N_{\Delta u}} = \frac{u_2 - u_o}{N_{\Delta u}} \quad [9.2]$$

$$s_u = \frac{q_{eff}}{N_{ke}} = \frac{q_t - u_2}{N_{ke}} \quad [9.3]$$

Notably, the third piezocone reading (sleeve friction, $f_s$) is often taken as the remolded undrained shear strength ($f_s \approx s_{u\text{-remolded}}$), as discussed by Robertson & Cabal (2015).

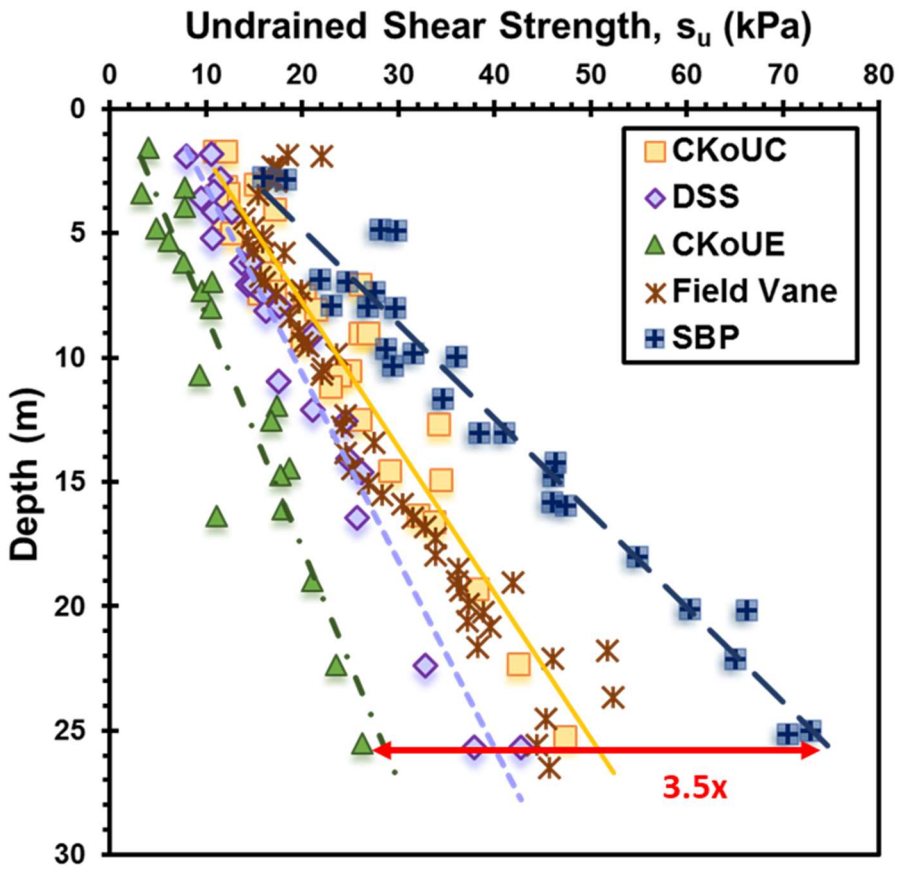


Figure 9.1. Undrained shear strength profiles in soft clay at Onsøy, Norway using five types of testing with different shearing modes (data from Lunne et al., 2003)

The magnitudes of the cone bearing factors have been reported in many studies and show a wide range depending upon the geological soil conditions. For instance, $N_{kt}$ values for triaxial compression mode were reported by Aas et al. (1986) ranging from 8 to 16; Karlsrud et al. (1996) suggested a range from 6 to 15; Hong et al (201) reported values from 7 to 20; Low et al. (2010) showed a range from 8.6 to 15.3 for twelve soft offshore clays and recommended an average value of 12 which agreed with a recent study by Mayne et al. (2015). Agaiby et al. (2016) reviewed data on 34 worldwide clays and found an average $N_{kt}$ value of 11.3 for the CAUC mode.

Similar ranges are reported for the other bearing factors with $N_{\Delta u}$ ranging from 4 to 9 as reported by Hong et al. (2010) and an average value of 6 reported by Lunne (2010). Low et al. (2010) indicated an average value of $N_{\Delta u}$ = 5.88, while the study by Mayne, Peuchen, & Baltoukas (2015) found a representative $N_{\Delta u}$ = 6.5. As for the bearing factor $N_{ke,}$ a range from 3 to 18 was reported by Hong et al. (2010) for triaxial compression mode while Mayne et al. (2015) reported an average $N_{ke}$ value of 8. From data on 17 Norwegian clays, Karlsrud et al. (2005) found that $N_{ke}$ decreased from 8 to 2 as the porewater parameter decreased from 0.5 to 1.0.

A reliable analytical model is needed for post-processing of CPTu readings for $s_u$ and OCR, rather than an assigned averaged value. To achieve such goals and calibrate the cone bearing factors, an elite database has been vetted by GTRC and Fugro which has been recently made available (Mayne 2014; Mayne & Peuchen 2018).

## 9.4 CAUC-CPTu Database

The compiled database relied on high-quality laboratory and field data obtained from the open literature and private unpublished technical reports, many of the latter from high-quality offshore site investigations. The focus of the database was on the triaxial compression mode where the undrained shear strength data were obtained from high-end anisotropically-consolidated triaxial tests (CAUC or $CK_0UC$). Additional simple index parameters were also collected covering natural water content ($w_n$), Atterberg limits (LL and PI), and unit weight ($\gamma_t$). Information regarding the stress history, expressed in terms of preconsolidation stress ($\sigma_p'$) and the overconsolidation ratio (OCR = $\sigma_p'/\sigma_{vo}'$) were also documented.

The database included 62 sites divided into five main groups (Mayne, 2014): (a) 17 normally-consolidated (NC) to lightly overconsolidated (LOC) offshore clays expressed using blue symbols; (b) 28 NC-LOC onshore clays shown as green symbols, (c) 7 sensitive clays that are NC-LOC and represented as pink symbols, (d) 5 overconsolidated (OC) intact clays expressed using purple dots with yellow infilling, and (e) 5 OC fissured clays shown using brown symbols infilled with orange, as shown in **Figure 9.2.** A complete listing of each site, its location, type of soil, and source of data is summarized in **Table 9.1**.


Figure 9.2. List of clays and their symbols for the undrained shear strength-piezocone compiled database (after Mayne, 2014)

Table 9.1. Compiled Database Listing for Piezocone -Undrained Shear Strength Data (modified after Mayne, 2014)

| Site | Location | Soil Description | References |
|---|---|---|---|
| Amherst | MA, USA | Onshore NC-LOC Varved | Hegazy (1998); DeGroot & Lutenegger (2003) |
| Ariake | Japan | Onshore NC-LOC Soft Marine | Tanaka et al. (2001); Lunne et al. (2006) |
| Ballina | Australia | Onshore NC-LOC Soft Estuarine | Pineda et al. (2014; 2016) |
| Belfast | Ireland | Onshore NC-LOC Soft | Crooks (1981); Lehane (2003) |
| BBC (Boston Blue Clay) | MA, USA | Onshore NC-LOC | Whittle et al. (2001) |
| Bothkennar | Scotland, UK | Onshore NC-LOC Silty Estuarine | Hight et al. (2003); Powell & Lunne (2005) |
| Busan | Korea | Onshore NC-LOC Soft Clay | Chung et al. (2011, 2012) |
| Goteborg | Sweden | Onshore Soft NC Clay | Kullingsjö (2007) |
| Hamilton AFB | CA, USA | Onshore NC-LOC Soft Bay Mud | Robertson (2010); Sabbagh & Koutsoftas (2011) |
| Kurihama | Japan | Onshore NC-LOC Alluvial Clay | Tanaka (1995); Shibuya & Tanaka (1996) |
| Lake Bonneville | UT, USA | Onshore NC-LOC Soft Lacustrine | Garner (2007) |
| Lianyungang | China | Onshore NC-LOC Soft Clay | Liu et al. (2008); Cai et al. (2014) |
| Lierstranda | Norway | Onshore NC-LOC Soft Drammen Clay | Lunne & Lacasse (1999) |
| Lilla Mellösa | Sweden | Onshore NC-LOC | Larsson & Mulabdić (1991a) |
| Newbury | MA, USA | Onshore NC-LOC Soft Silty Clay | Landon (2007) |
| Nile River Delta | Egypt | Onshore NC-LOC | Hamza et al. (2005) |
| Nong Ngu Hao | Thailand | Onshore NC-LOC Soft Bangkok Clay | Shibuya & Tamrakar (2003) |
| Northwestern University, NGES | Evanston, IL, USA | Onshore NC-LOC Glacial Till | Finno et al. (2000); McGillivray (2007) |

| Site | Location | Soil Description | References |
|---|---|---|---|
| Onsøy | Norway | Onshore NC-LOC Soft Marine | Lunne et al. (2003; 2006) |
| Pisa | Italy | Onshore NC-LOC Firm Pancone Clay | LoPresti et al. (2003) |
| Porto Tolle | Italy | Onshore NC-LOC | Jamiolkowski et al. (1982); Pane et al. (1995) |
| Recife | Brazil | Soft Organic Onshore Clay | Coutinho (2007) |
| San Francisco Bay | CA, USA | Onshore NC-LOC Bay Mud | Pestana et al. (2002) |
| Sarapuí | Brazil | Onshore NC-LOC Very Soft Clay | Ortigao et al (1983); Almeida & Marques (2003) |
| Saro Road 6/900 | Sweden | Onshore NC-LOC | Larsson & Mulabdić (1991a) |
| Singapore | Singapore | Onshore NC-LOC | Watabe (1999); Tanaka et al. (2001) |
| Taipei | Taiwan | Onshore NC-LOC Soft Alluvial Lacustrine | Chin et al. (2007) |
| Torp | Sweden | Onshore NC-LOC Soft Clay | Larsson & Åhnberg (2003) |
| Bay of Bengal | India | Offshore Soft Clay | Mayne et al. (2015) |
| Brage | The North Sea | Offshore NC-LOC Silty Clay | Rad & Lunne (1989) |
| China | China | Offshore NC-LOC | Lunne et al. (2006) |
| Chinguetti | Mauritania | Offshore NC-LOC | Low et al. (2010) |
| Gullfaks C | The North Sea | Offshore NC-LOC | Lunne et al. (1985) |
| GOG 1 | Gulf of Guinea, West Africa | Offshore NC-LOC | Low et al. (2010) |
| GOG 2b | Gulf of Guinea, West Africa | Offshore NC-LOC | Mayne et al. (2015) |
| GOG 3 | Gulf of Guinea, West Africa | Offshore NC-LOC | Low et al. (2010) |
| GOG 4 | Gulf of Guinea, West Africa | Offshore NC-LOC | Low et al. (2010) |
| GOG 5 | Gulf of Guinea, West Africa | Offshore NC-LOC | Low et al. (2010) |
| GOG 6 | Gulf of Guinea, West Africa | Offshore NC-LOC | Low et al. (2010) |

| Site | Location | Soil Description | References |
|---|---|---|---|
| Laminaria | Timor Sea, Australia | Offshore NC-LOC | Low et al. (2010) |
| Norwegian Sea | Norway | Offshore NC-LOC | Low et al. (2010) |
| Osaka Bay | Japan | Offshore NC-LOC | Tanaka et al. (2003); Watabe et al. (2002; 2007) |
| Snorre | Norway | Offshore NC-LOC | Lunne et al. (2006) |
| Troll Lower | Norway | Offshore NC-LOC Firm Lean | Amundsen et al. (1985); Lunne et al. (2007) |
| Troll Upper | | Soft plastic Clay | |
| Hilleren | Norway | Sensitive to Quick | Long et al. (2009) |
| Louiseville | Québec, Canada | Soft Sensitive NC | Leroueil & Hamouche (2003) |
| South Gloucester (Upper) | Ontario, Canada | Sensitive Leda Clay | McRostie & Crawford (2001); Styler & Mayne (2013) |
| South Gloucester (Lower) | Ontario, Canada | Sensitive Leda Clay | McRostie & Crawford (2001); Styler & Mayne (2013) |
| Tiller | Norway | Sensitive to Quick Clay | Gylland et al. (2014); L'Heureux & Long (2016) |
| Os (Lower) | Norway | Sensitive Clayey Silt | Long et al. (2010) |
| Os (Upper) | Norway | Sensitive Clay | Long et al. (2010) |
| Anchorage | AK, USA | Stiff Lean OC Intact Clay | Zapata-Medina (2012); Mayne & Pearce (2005) |
| Cooper Marl | SC, USA | OC Calcareous Intact Clay | Singha (1998); Camp (2004); Mayne (2005) |
| Haltenbanken | Norway | OC Intact | Rad & Lunne (1988) |
| Haga | Norway | OC Intact | Andersen & Stenhamar (1982); Lacasse & D'orazio (1990) |
| Taranto | Italy | OC Intact | Jamiolkowski et al. (1982) |
| Baton Rouge | LA, USA | OC Stiff Fissured Clay | Chen & Mayne (1994) |
| Baytown | TX, USA | OC Fissured Beaumont Clay | Stuedlein (2008) |
| Beaufort Sea | Canada | OC Stiff Fissured Clay | Jefferies et al. (1985) |
| Brent Cross | Hendon, UK | Fissured HOC London Clay | Hight et al. (2003) |
| Dublin Boulder | Ireland | Hard OC Clay Till | Long & Menkiti (2007) |

Previous studies on the cone bearing factors found trends that showed $N_{kt}$ and $N_{ke}$ decreased with porewater parameter $B_q$, while the factor $N_{\Delta u}$ increased with $B_q$ (Lunne et al. 1985; Karlsrud et al. 1996; Lunne et al. 1997; Hong et al. 2010; Mayne et al. 2015). Studies by Karlsrud et al. (2005) also sought trends with PI, OCR, and sensitivity, albeit clear and definitive relationships were not found, and considerable scatter was observed. The above studies, however, were also restricted in that they considered a limited database, either considered a local geology or data derived from < 17 sites.

To explore the ranges of the cone bearing factors within the large 62 clay database, they were plotted against normalized porewater pressure parameter: $B_q = (u_2-u_o)/(q_t-\sigma_{vo})$ as presented in **Figure 9.3, 9.4 and 9.5** where a wide bandwidth can be observed as indicated earlier and as reported in the literature.

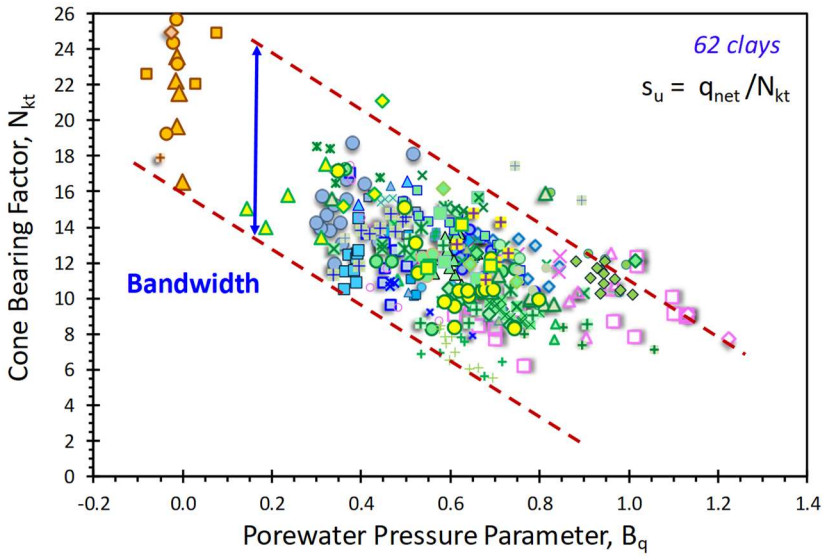


Figure 9.3. Cone factor $N_{kt}$ versus porewater parameter $B_q$ for all clay deposits

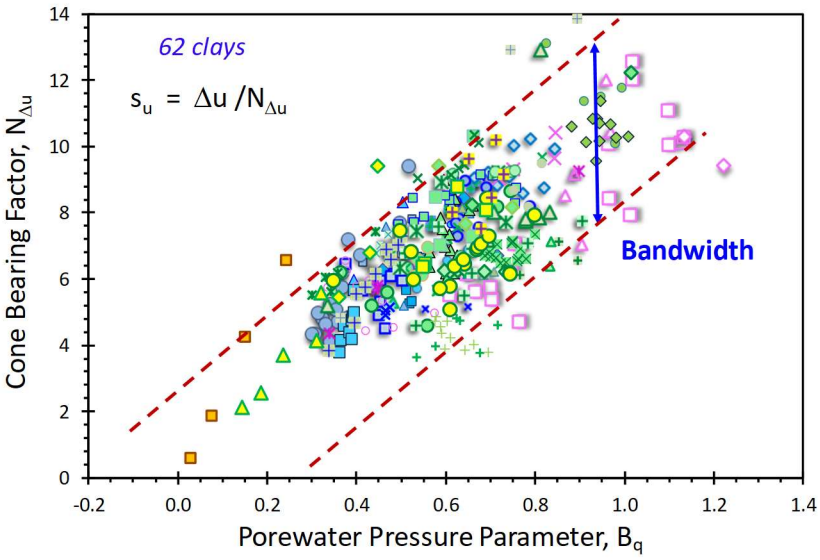


Figure 9.4. Cone factor $N_{\Delta u}$ versus porewater parameter $B_q$ for all clay deposits

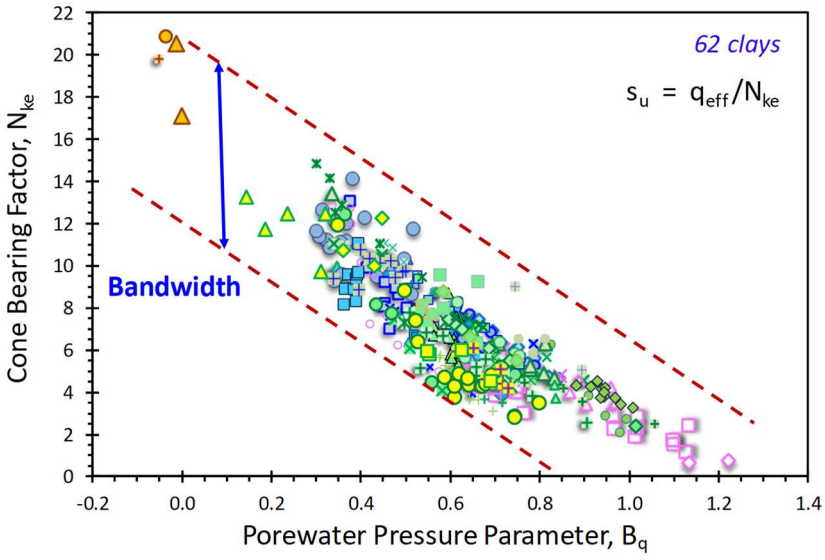


Figure 9.5. Cone factor $N_{ke}$ versus porewater parameter $B_q$ for all clay deposits

By exploring the trends between the cone bearing factors and the corresponding porewater pressure parameter ($B_q$), it can be seen that there is an inversely proportional

link between $N_{kt}$ and $N_{ke}$ with $B_q$ and a directly proportional link between $N_{\Delta u}$ with $B_q$. In an attempt to obtain a first-order approximation for the cone bearing factors from the porewater pressure parameter, an averaged value was assigned to each site using a single unique symbol, as presented in **Figures 9.6, 9.7** and **9.8**, respectively, where the cone bearing factors can be approximately expressed:

$$N_{kt} = 10.5 - 4.6 \cdot \ln (B_q + 0.1) \quad [9.4]$$

$$N_{\Delta u} = 7.9 + 6.5 \cdot \ln (B_q + 0.3) \quad [9.5]$$

$$N_{ke} = 4.5 - 10.66 \cdot \ln (B_q + 0.2) \quad [9.6]$$

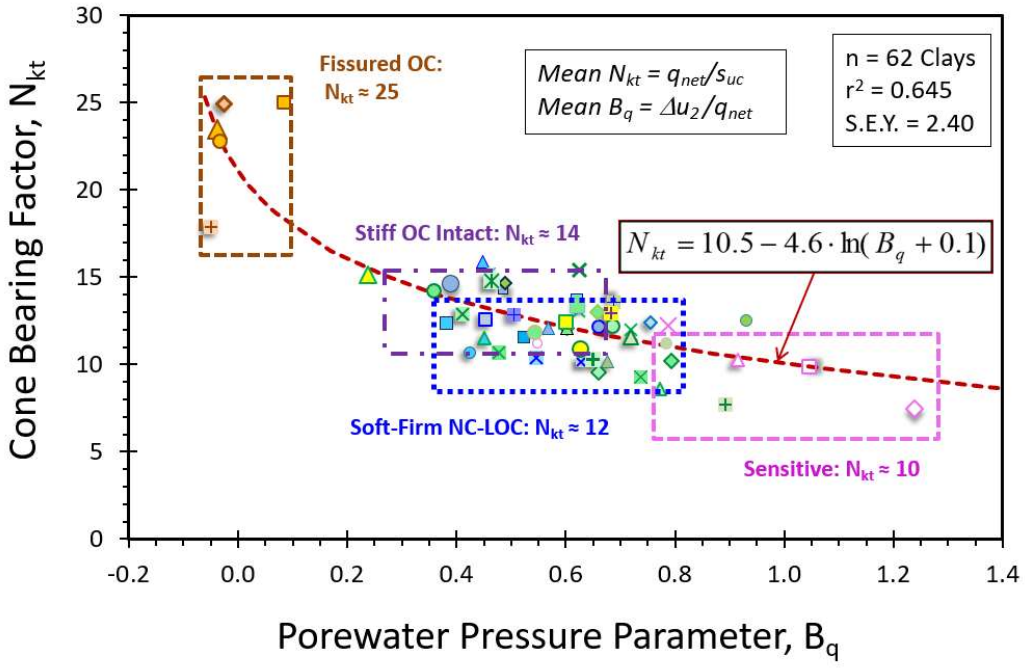


Figure 9.6. Mean cone factor $N_{kt}$ versus mean porewater parameter $B_q$ for five main clay subgroups (modified after Mayne, 2014)

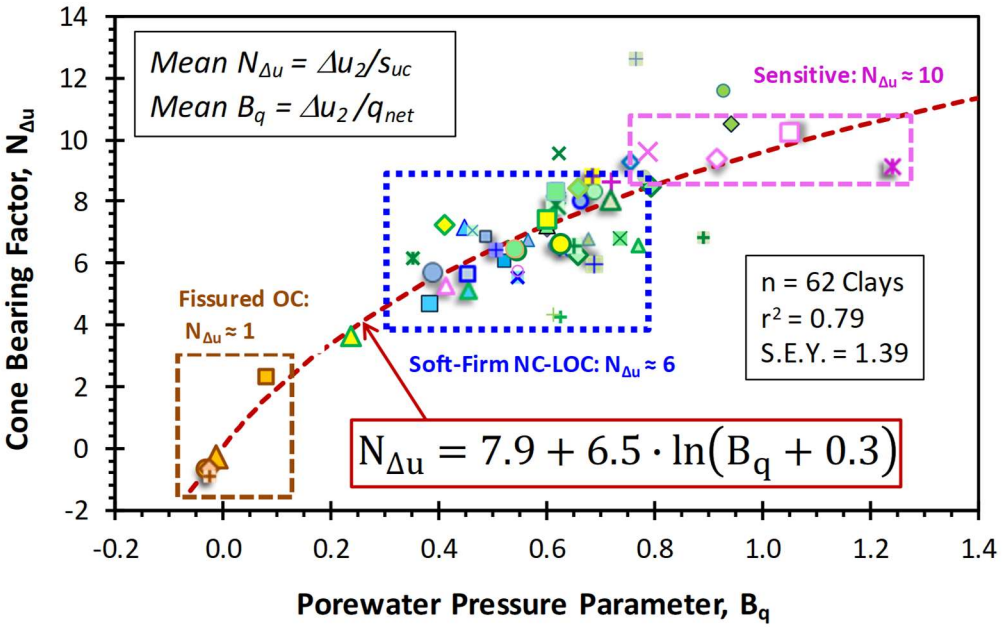


Figure 9.7. Mean cone factor $N_{\Delta u}$ versus mean porewater parameter $B_q > 0.1$ for five main clay subgroups

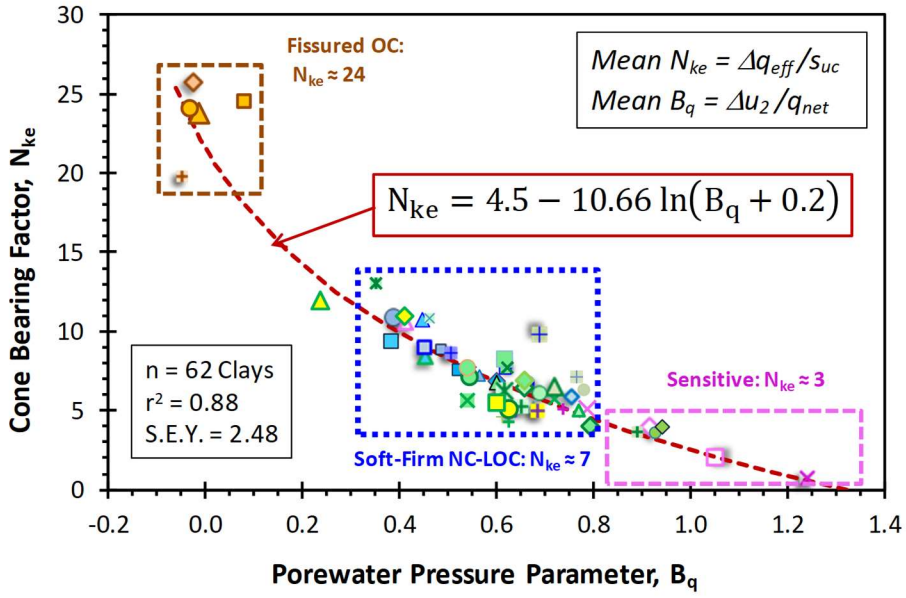


Figure 9.8. Mean cone factor $N_{ke}$ versus mean porewater pressure parameter $B_q$ for five main clay subgroups

## 9.5 Spherical Cavity Expansion Model for Piezocone Parameters

For the past four decades, the spherical cavity expansion (SCE) solutions formulated by Vesić (1972, 1977) have been used to evaluate undrained shear strength using cone bearing factors as a function of both $q_{net}$ and excess porewater pressures ($\Delta u$). Under isotropic states of stress, SCE along with considerations of energy laws, expresses the cone tip resistance as:

$$q_t = p_o + s_u [(4/3) (\ln I_R + 1) + \pi/2 + 1] \quad [9.7]$$

where $p_o$ is the total overburden stress and $I_R = G/s_u$ is rigidity index of the soil, and G is the shear modulus. Hence, the bearing factor is:

$$N_{kt} = [(4/3) (\ln I_R + 1) + \pi/2 + 1] \quad [9.8]$$

According to Vesić (1972), the excess pore water pressure generated due to pushing of the cone into the soil is a result of changes in octahedral normal stress around the cone which is also expresses using spherical cavity expansion as:

$$\Delta u_{oct} = (4/3) (\ln I_R) s_u \quad [9.9]$$

$$\text{Hence, } N_{\Delta u} = (4/3) (\ln I_R) \quad [9.10]$$

For soft to firm clays of low OCRs, the above two representations have shown rather good agreement in assessing undrained shear strengths in nonstructured clays that are inorganic and low sensitivity (Mayne 2016).

For clays with a range in degrees of overconsolidation, Chen and Mayne (1994) derived a hybrid corporation of spherical cavity expansion by Vesić with critical state soil mechanics (SCE-CSSM) to express the cone tip resistance and pore water pressure using closed-form equations as follows:

$$q_t = \sigma_{vo} + [(4/3)\,(\ln I_R + 1) + \pi/2 + 1] \cdot (M/2)\,(OCR/2)^{\Lambda}\,\sigma_{vo}' \qquad [9.11]$$

$$u_2 = u_0 + (4/3)\,(\ln I_R) \cdot (M/2)\,(OCR/2)^{\Lambda}\,\sigma_{vo}' + [(1 - (OCR/2))^{\Lambda}] \cdot \sigma_{vo}' \qquad [9.12]$$

where $M = 6\sin\phi'/(3-\sin\phi')$, $\Lambda = (1 - C_s/C_c)$ = plastic volumetric strain potential (≈ 0.8 to 0.9), $C_s$ = swelling index, $C_c$ = virgin compression index, and $OCR = \sigma_p'/\sigma_{vo}'$.

Using the classic Vesić cone bearing factor $N_{kt}$ expression and varying the values of rigidity index ($I_R$) between 10 and 1000 along with equations [9.11] and [9.12] for cone tip resistance and porewater pressure, one can evaluate the normalized porewater parameter ($B_q$) and investigate the $N_{kt}$ versus $B_q$ relation, as presented in **Figure 9.9** and expressed using a red dashed line. The figure also shows the superimposed values of back-figured $N_{kt} = q_{net}/s_{uc}$ and $B_q$ from the database. It is evident that the SCE solution only captures the bandwidth in one direction for the soft-firm offshore and onshore clays ($1 < OCRs < 2$), and cannot include other groups, including sensitive clays, overconsolidated soils, or fissured clays. This suggests that the SCE expression by itself is insufficient for a robust solution and that additional parameters besides the rigidity index alone need to be investigated.

In a similar manner, using equation [9.10] to backfigure the cone bearing factor $N_{\Delta u}$ based on CAUC lab $s_u$ and CPTu excess porewater pressure, **Figure 9.10** shows the trend

with $B_q$. In the case of cone bearing factor $N_{\Delta u,}$ the correct direction of the trend is achieved yet the prediction does not cover and span most of the data points. Based on **Figure 9.10**, the definition introduced by SCE for octahedral ($\Delta u_{oct}$) induced excess porewater pressure is valid, yet an additional component for the shear-induced excess porewater pressure appears to be missing in order to satisfy all data points.

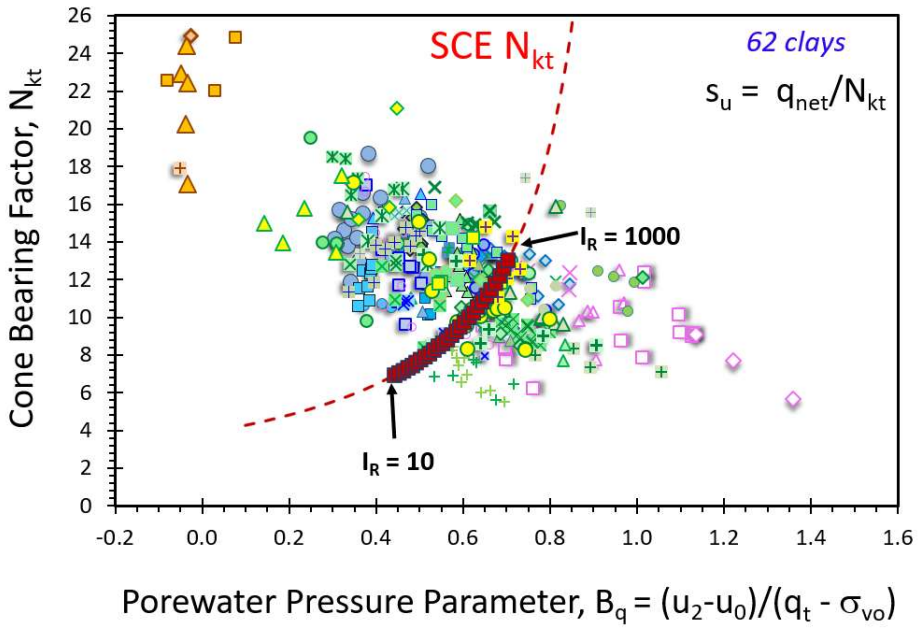


Figure 9.9. Cone bearing factor ($N_{kt}$) as function of porewater parameter $B_q$ from Vesic SCE solution and back-figured values from CAUC-CPTu database

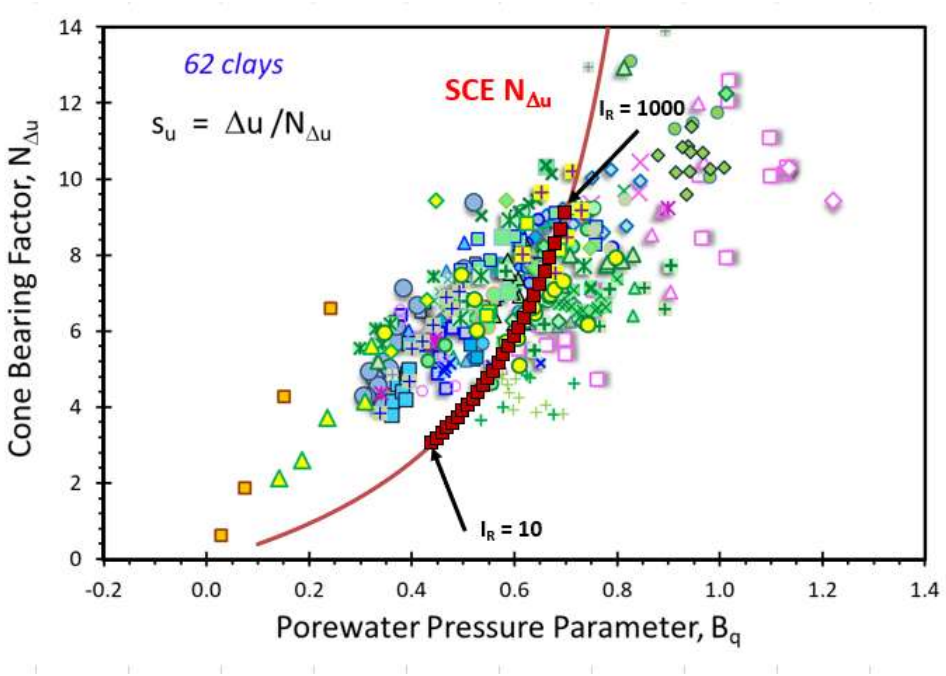


Figure 9.10. Cone bearing factor ($N_{\Delta u}$) as function of porewater parameter $B_q$ from Vesic SCE solution and back-figured values from CAUC-CPTu database

### 9.6 Alternative CPTu $N_{kt}$ bearing factors

In addition to rigidity index, more recent studies have shown considerations of the roughness of the soil-cone interface, initial stress state conditions, and/or stress history of the soil. The bearing factor $N_{kt}$ depends upon the analytical theory, assumed failure mechanism, and methodology behind it, such as limit plasticity, cavity expansion, stress path, or numerical simulation method (strain path method, finite elements, finite differences), as discussed in part by Konrad and Law (1987). **Table 9.2** presents a summary of alternative expressions for cone bearing factor ($N_{kt}$) based on various theories, constitutive models, and schemes.

Finite element modelling (FEM) has been used in simulating the penetration of the piezocone into the ground with interpretations for either the cone tip resistance and the

generated porewater pressure, or both, considering different boundary conditions, frictional characteristics of the soil-cone interface, initial geostatic stress state, strength anisotropy, and penetration into multi-soil layers. FEM relies on either small and/or large strain formulations to capture the stresses and the deformations around the cone tip and sleeve (e.g., Abu-Farsakh et al., 2003). To avoid the distortion in the finite element mesh associated with large strain formulation, two approaches can be adopted: (a) Eulerian-based formulation, where the material is allowed to move freely through a fixed finite element mesh (van den Berg, 1994); or (b) using the re-meshing and interpolation technique along with small strain formulation (RITSS), for instance, as was used by Lu et al. (2004); Ma et al. (2016; 2017); and others.

Table 9.2. Selected expressions for the cone bearing factor, $N_{kt} = q_{net}/s_u$
(updated after Konrad & Law 1987; Lunne et al. 1997; Low, 2009)

| **Reference** | **Expression for Bearing Factor, $N_{kt}$** | **Comments** |
|---|---|---|
| Terzaghi (1943) | $N_{kt} = 7.41$ | Bearing Capacity Theory |
| Gibson (1950) | $N_{kt} = (4/3)[\ln\left(\frac{E_{50}}{3 \cdot s_u}\right) + 1] + \cot\theta$ | Spherical Cavity Expansion |
| Meyerhof (1951) | $N_{kt} = 9.34$ | Bearing Capacity Theory with smooth interface |
| Skempton (1951) | $N_{kt} = (4/3)[\ln\left(\frac{E_{50}}{s_u}\right) + 1] + 1$ | Spherical Cavity Expansion |
| Meyerhof (1951) | $N_{kt} = (4/3)[\ln\left(\frac{E_t}{s_u}\right) + 1] + 1$ | Spherical Cavity Expansion |
| Caquot and Kerisel (1956) | $N_{kt} = 7.0$ | Bearing Capacity Theory |
| Ladanyi (1967) | $\left(\frac{s_a}{s_u}\right) + (4/3)\left(\frac{s_r}{s_u}\right)[\ln\left(\frac{E_r}{3s_{ur}}\right)] + (4/3)[\frac{\left(\frac{E_u}{s_u}\right) - \left(\frac{E_r}{s_{ur}}\right)\left(\frac{s_{ur}}{s_u}\right)}{\left(\frac{E_u}{s_u}\right) - \left(\frac{E_r}{s_{ur}}\right)}]\ln\left(\frac{E_u}{s_u}\right)\left(\frac{s_{ur}}{E_r}\right)$ | Spherical Cavity Expansion Theory + Trilinear stress-strain relationship |
| Vesić (1972) | $N_{kt} = (4/3)[\ln I_R + 1]$ | Spherical Cavity Expansion Theory |
| Ladanyi and Johnson (1974) | $N_{kt} = (4/3)[\ln I_R + 1] + \sqrt{3} \cdot \alpha_c$ | Spherical Cavity Limit Pressure |
| Baligh (1975) * | $N_{kt} = 11 + [\ln I_R + 1]$ | Cylindrical Cavity Expansion Theory |

| Reference | Expression for Bearing Factor, $N_{kt}$ | Comments |
|---|---|---|
| de Beer (1977) | $N_{kt} = 9.74$ | Bearing Capacity Theory with rough interface |
| Vesić (1977) + | $N_{kt} = (4/3)[\ln I_R + 1] + \pi/2 + 1$ | Spherical Cavity Expansion Theory + energy conservation |
| Whittle (1992) | $N_{kt} = 1.51 + 2 \cdot \ln I_R$ | Bilinear and Hyperbolic soil model using strain path method |
| Teh and Houlsby (1991) | $N_{kt} = 1.25 + 1.84 \cdot \ln I_R + 2 \cdot \alpha_c - 2\Delta$ | Elastic-plastic soil model using strain path method and finite element modeling |
| Yu (1993) + | $N_{kt} = 9.4 + 1.55 \cdot \ln(\sqrt{3}/2) \cdot I_R$ - smooth<br>$N_{kt} = 4.18 + 1.55 \cdot \ln(\sqrt{3}/2) \cdot I_R$ - rough | Cylindrical Cavity Expansion Theory |
| Yu et al. (2000) | $N_{kt} = 0.33 + 2 \cdot \ln I_R + 2.37 \cdot (\delta / \phi_{cs}') - 1.83 \cdot \Delta$ | Steady-state finite element model |
| Su and Liao (2002) | $\frac{1+\rho}{\sqrt{1+2\rho}} \cdot \ln I_R + \frac{1-\rho}{3} + R \cdot \left[1 + \frac{1+\rho}{\sqrt{1+2\rho}} + 0.52\rho^{1/8}(1+\rho)\right] - 2 \cdot \Delta$<br>where R is f ($\theta$ and $\alpha_c$) and $\rho$ is anisotropic shear strength between extension and compression modes | Cylindrical Cavity Expansion Theory + anisotropic Von Mises failure criterion |
| Abu-Farsakh et al. (2003) | $N_{kt} = 2.45 + 1.80 \cdot \ln I_R - 2.1 \cdot \Delta$ | Finite element model Lagrangian formulation |

| Reference | Expression for Bearing Factor, $N_{kt}$ | Comments |
|---|---|---|
| Lu et al. (2004) | $N_{kt} \approx 3.4 + 1.6 \cdot \ln I_R - 1.9 \cdot \Delta + 1.3 \cdot \alpha_c$ | Finite element model remeshing and interpolation with small strain (RITSS) |
| Walker & Yu (2006) | $N_{kt} \approx 2.19 \cdot \ln I_R - 1.95 \cdot \Delta + (0.0026 \cdot I_R - 1.19) \cdot \alpha_c$ | Finite element model Lagrangian Eulerian formula |
| Liyanapathirana (2009) | $N_{kt} \approx 1 + 1.825 \cdot \ln I_R - 1.7 \cdot \Delta + (0.33 \cdot \ln I_R + 0.5) \cdot \alpha_c$ | Finite element model Lagrangian Eulerian formula |
| Liyanapathirana (2016) | $N_{kt} = 6.6 + \ln I_R - 1.9 \cdot \Delta + 1.4 \cdot \alpha_c \cdot (I_R)^{-0.14}$ | Finite Element model coupled theory nonlinear porous media with Modified Cam Clay |
| Ma et al. (2017) | $N_{kt} = 3.47 + 1.56 \cdot \ln I_R + 1.3 \cdot \alpha_c$ | large deformation finite-element (LDFE) analyses |

NOTES:

* used horizontal overburden stresses $\sigma_{ho}$

\+ used mean overburden stresses $\sigma_{mean}$

$E_{50}$ = secant Young's modulus at 50% strain

$E_t$ = initial tangent Young's modulus

$E_u$ = undrained Young's modulus

$E_r$ = Young's modulus at remolded strength

$s_a$ = remolded cohesion between cone surface and clay

$\theta$ = cone apex angle

$\alpha_c$ = friction coefficient of the cone-soil interface: the ratio of limiting shear stress on the soil-cone interface to the shear strength, where roughness factor: $0 < \alpha_c < 1$.

$\Delta$ = Initial State Factor = normalized in-situ shear stress = $(\sigma_{vo}' - \sigma_{ho}')/(2s_u)$: $-1 < \Delta < +1$.

$\sigma_{ho}' = K_0 \cdot \sigma_{vo}'$

$\delta$ = angle of friction between soil–shaft and soil–cone interfaces

$\phi'_{cs}$ = critical state friction angle of soil

Reviewing the various expressions for cone bearing factor, it is evident that most equations rely in part on the soil rigidity index. Yet, additional parameters were found influential, including: (a) roughness of the soil-cone interface ($\alpha_c$) defined by the ratio of limiting shear stress on the soil-cone interface to the shear strength, (b) initial state factor ($\Delta$), and (c) the angle of friction between the soil-cone interface.

**Figure 9.12** presents a graphical comparison between the $N_{kt}$ expressions for a wide expected range of rigidity index ($I_R$) ranging from 10 to 1000. Three different scenarios are investigated: a smooth cone with roughness factor $\alpha_c = 0$, an intermediate cone with a roughness factor $\alpha_c$ of 0.5, and a rough cone with roughness factor $\alpha_c$ of 1.0. For the sake of comparison, a normally consolidated clay with OCR = 1.0 will be assumed with an effective friction angle of 30 degrees. As for the expressions having an initial in-situ state factor ($\Delta$), the value can be evaluated from:

$$\Delta = (\sigma_{vo}' - \sigma_{ho}') / (2s_u) \qquad [9.13]$$

$$\text{where } \sigma_{ho}' = K_0 \cdot \sigma_{vo}' \qquad [9.14]$$

For the case of virgin loading-unloading during consolidation, an estimate of the lateral stress coefficient ($K_0$) can be made from (Mayne & Kulhawy 1982, 1990):

$$K_0 = (1-\sin\phi') \, OCR^{\sin\phi} \qquad [9.15]$$

Hence, for a normally consolidated clay with a friction angle of 30°, the coefficient of lateral earth pressure $K_0 = 0.5$. As for the ratio ($\sigma_{vo}'/s_u$ ), it can be obtained from the

reciprocal of the normalized undrained shear strength to the effective overburden stress ratio ($S = s_u/\sigma_{vo}'$). The value of S can be obtained using constitutive soil models, such as the Wroth-Prevost hybrid model presented in **Figure 9.11.** For an effective friction angle $\phi' = 30°$, a value of $S \approx 0.30$ for the CAUC triaxial compression shearing mode. Accordingly, for a normally consolidated clay with 30 degrees friction angle, the value of initial state factor is $\Delta = (1/2)\cdot(1-K_0)\cdot(\sigma_{vo}'/s_u) = 0.83$.

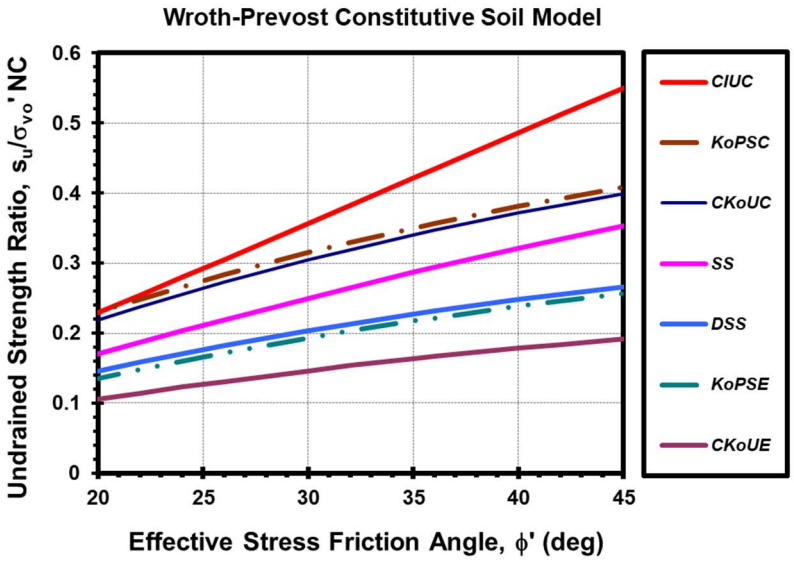


Figure 9.11. Undrained shear strengths ratio (S) from Wroth-Prevost constitutive model (after Mayne, 2008)

For an overconsolidated (OC) clay with the same effective friction angle of $\phi' = 30°$, the ratio $(s_u/\sigma_{vo}')$ can be obtained using critical state soil mechanics (CSSM) where:

$$(s_u / \sigma'_{vo}) = 0.5\cdot \sin\phi'\cdot OCR^{\Lambda} \qquad [9.16]$$

where $\Lambda$ can be taken = 0.8. Assuming an OCR = 5, then $(s_u/\sigma_{vo}') = 0.906$. $K_0 = 1.118$ from equation [9.15]. Hence, the initial state factor $\Delta = (1/2)\cdot(1-K_0)\cdot(\sigma_{vo}'/s_u) = -0.065$. The variation of $N_{kt}$ with $I_R$ for an OC clay is presented in **Figure 9.13**.

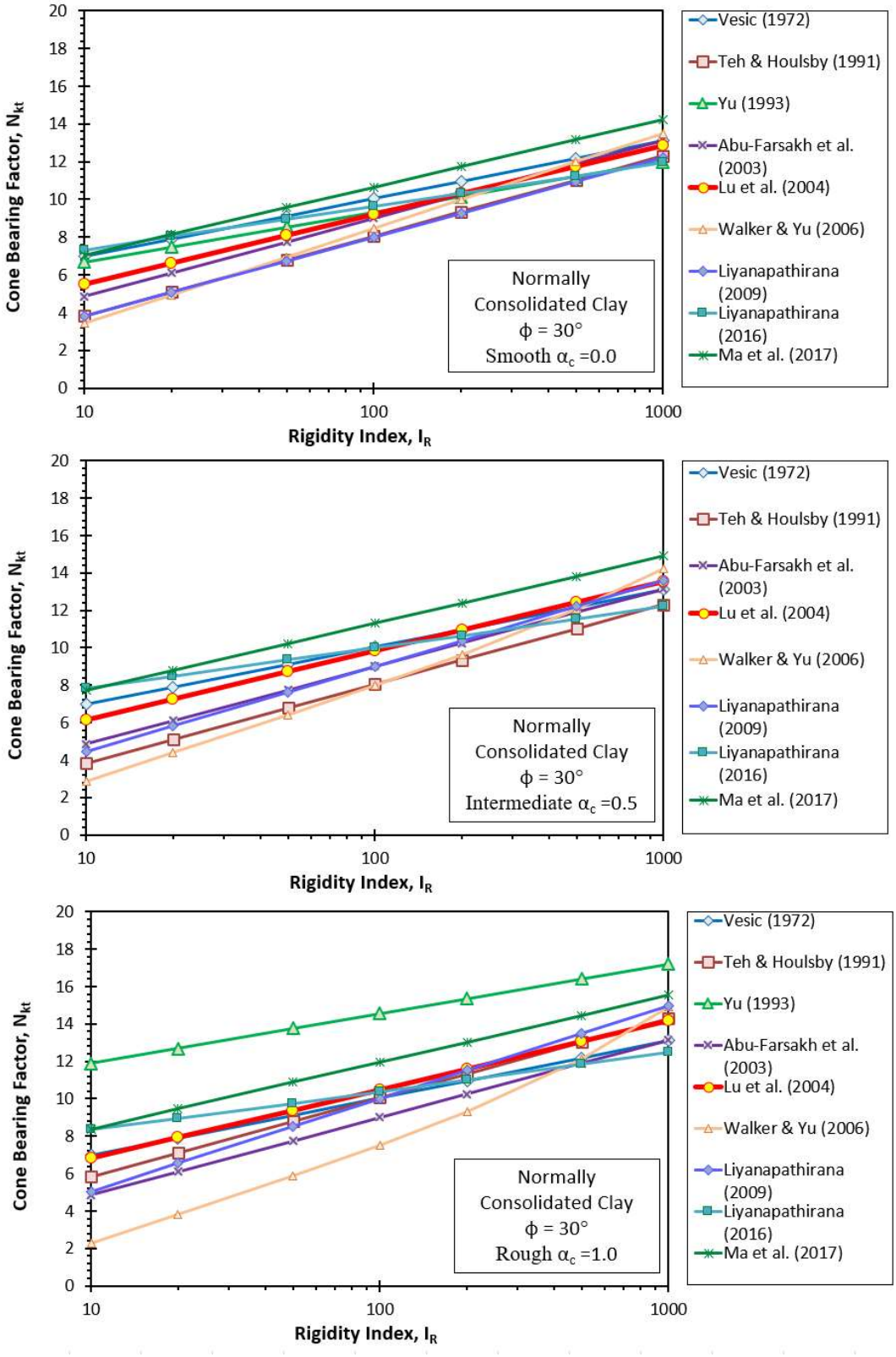


Figure 9.12. Comparison of cone bearing factors versus rigidity index for (a) smooth, (b) intermediate, and (c) rough cone interfaces for normally consolidated clay

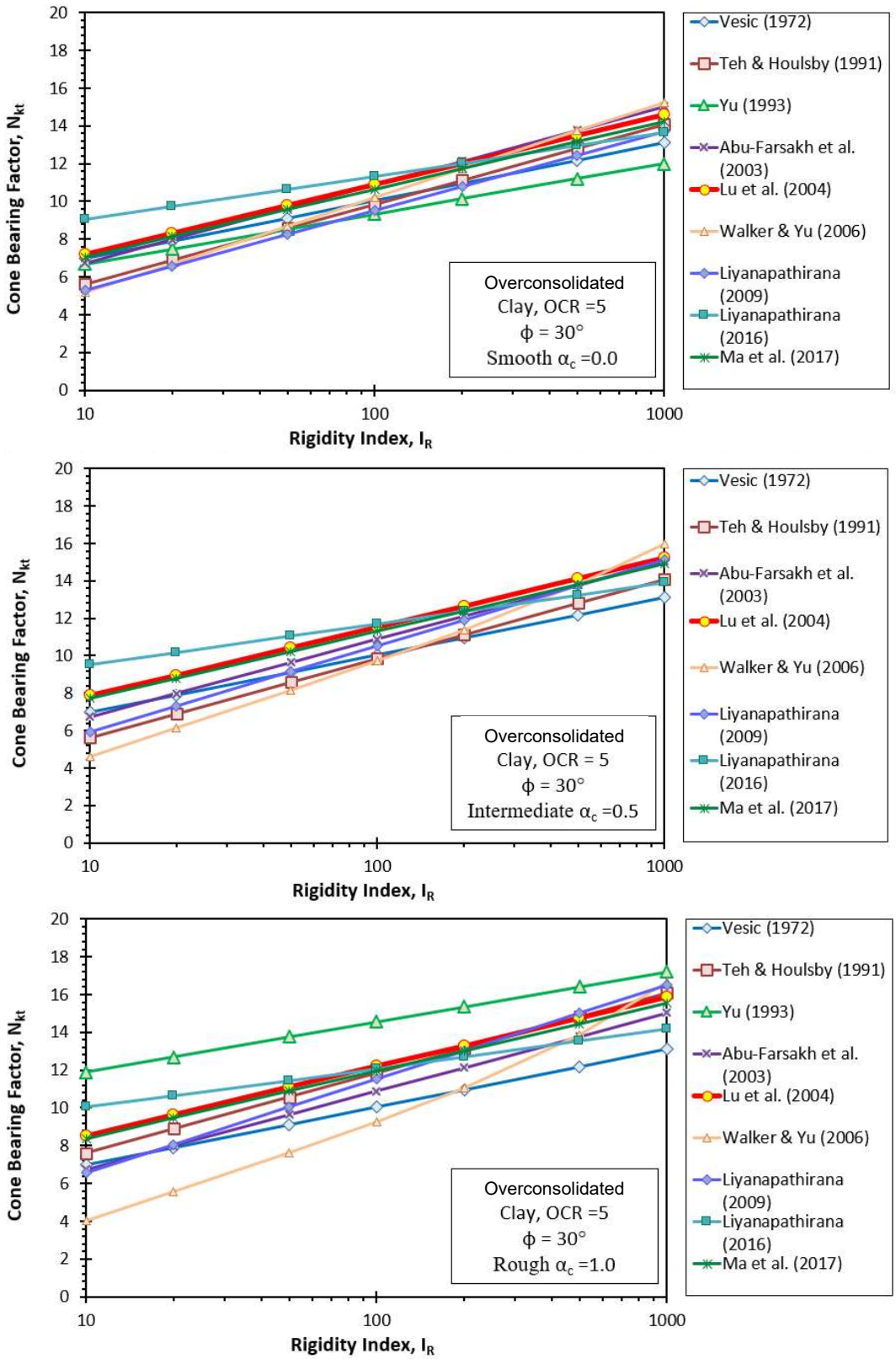


Figure 9.13. Comparison of cone bearing factors versus rigidity index for (a) smooth, (b) intermediate, and (c) rough cone interfaces for an overconsolidated clay

It is clear from both figures that cone bearing factor value is directly proportional to the logarithm of rigidity index value. By comparing the cone bearing factors for three different cases of cone interfaces for both NC and OC clays, it is evident that the calculated $N_{kt}$ value is influenced by the cone interface roughness factor. For all of the expressions, $N_{kt}$ increases with roughness coefficient ($\alpha_c$). By comparing Figures 9.12 and 9.13, OC clays tend to have a higher cone bearing factor values if compared to NC at same $I_R$ value.

A similar trend is observed by Lu et al. (2004) as presented in **Figures 9.14 and 9.15,** showing that as the roughness coefficient ($\alpha_c$) increases (comparing line 1 to line 4), the $N_{kt}$ value increases. And as the rigidity index value ($I_R = G/s_u$) increases, the cone bearing factor increases. Also shown in **Figure 9.15**, as the initial state factor $\Delta$ decreases the cone bearing factor increases which was seen in **Figure 9.13** where $\Delta$ decreases from a value of 0.83 (NC clay) to a value of -0.065 (OC clay) showing an increase in $N_{kt}$ value with OCR.

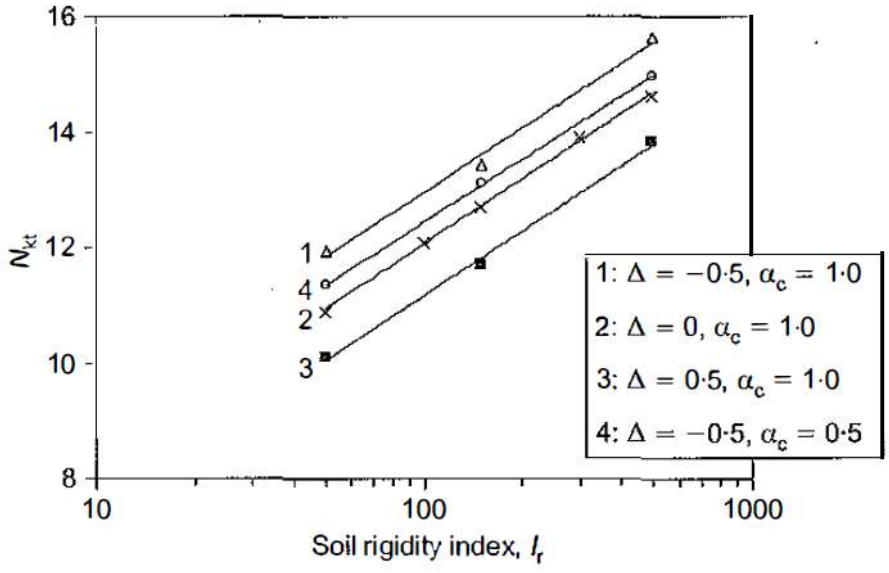


Figure 9.14. Variation of cone bearing factor with rigidity index at different cone interface roughness coefficient for different initial state factors, $\Delta$ (Lu et al., 2004)

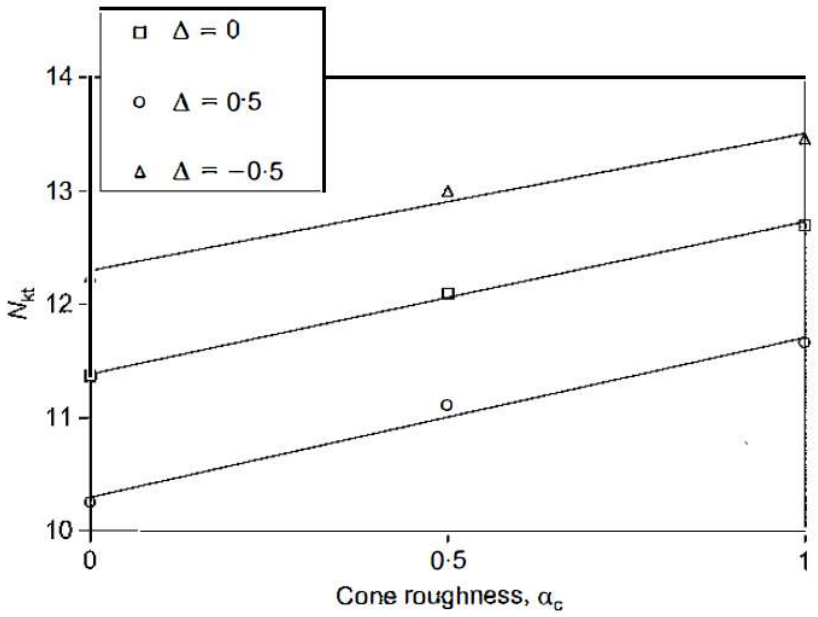


Figure 9.15. Variation of cone bearing factor with cone interface roughness coefficient for different initial state factors, Δ (Lu et al., 2004)

Ceccato et al. (2017) conducted finite element modeling using the Material Point Method (MPM) to investigate the soil-structure interaction and the use of interface elements. Based on their analyses, the computed cone bearing factor ($N_c$) increased from $N_c$ = 10.2 in the case of a cone with a smooth interface to a value of 15.8 in case of the rough interface as presented in **Figure 9.16**. Ma et al. (2016) compared different cone bearing expression for two interface cases: smooth and rough at varying rigidity index values as presented in **Figure 9.17**. From the plotted results, it is evident that as the interface roughness increases, the corresponding $N_{kt}$ value increases.

According to Potyondy (1961), the typical range of roughness factor for steel in contact with clay is 0.25 to 0.5. Lu et al. (2004) indicated that the cone face and the shaft roughness values theoretically range between 0 and 1, but based on their analogy and continuous penetration of piles with measured friction sleeves, the field values for

roughness coefficient ($\alpha_c$) lie in the range between 0.2 and 0.6. DeJong and Randolph (2012) adopted a roughness factor of 0.2 indicating it is the lower bound for clays with typical sensitivities of 3 to 5. Qiu (2014) recommended the usage of a roughness factor of 0.5 while simulating the cone penetration into a clay deposit. According to Ceccato and Simonini (2017), the roughness coefficient depends on the relative dimension of the cone surface and the size of the soil particle in contact. A reasonable value for clays with low plasticity in contact with steel piles should lie between 0.2 and 0.55.

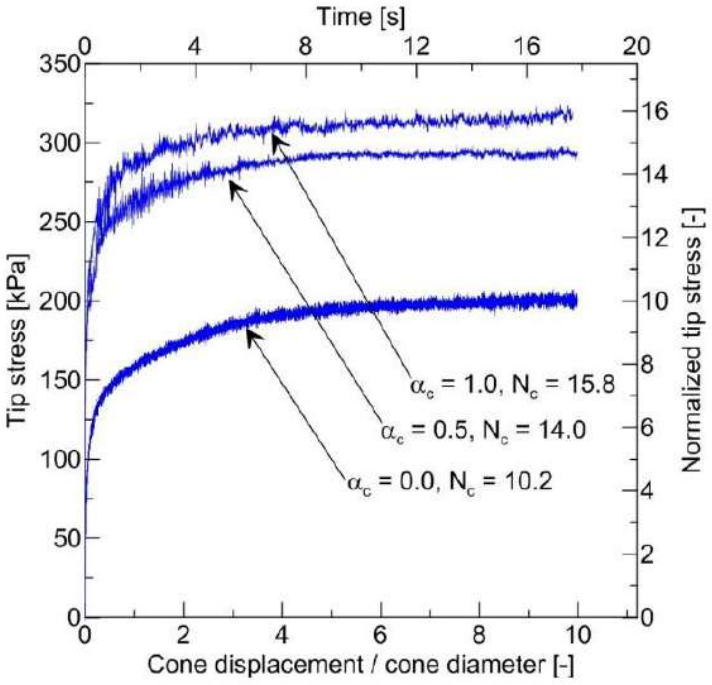


Figure 9.16. Tip stress over normalized displacement reaching equilibrium with rough interface having higher cone bearing factor (Ceccato et al., 2017)

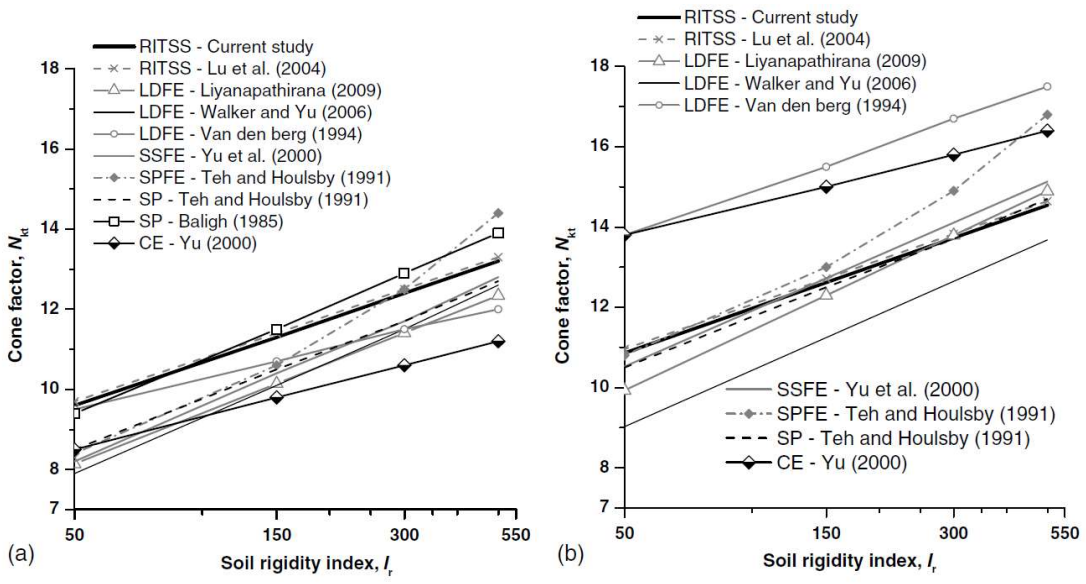


Figure 9.17. Comparison of cone bearing factors versus soil rigidity index for (a) smooth cone; (b) rough cone (Ma et al., 2016)

The influence of the initial stress state factor (Δ) is presented in **Figure 9.18** for the different $N_{kt}$ expressions, adopting three cases of smooth, intermediate and rough interfaces and an assumed rigidity index ($I_R$) value of 200. For most of the expressions (excepting Ma 2014 and Yu 1993), the cone bearing factor decreases as the initial state factor increases from Δ value of -1 resembling passive extension loading to a value of +1 for compression active loading which highlights the significance of the lateral earth pressure coefficient ($K_0$) in correctly quantifying the cone bearing factor. As $K_0$ decreases, the initial state factor (Δ) increases, and the cone bearing factor ($N_{kt}$) decreases. A similar trend is observed in case of a cone with rough interface. It is noticed that for the range of initial stress state factor (Δ) value between 0.5 and 1.0, the corresponding $N_{kt}$ value for a smooth interface is about 10, for intermediate interface $N_{kt}$ is about 11, and for rough interface, $N_{kt}$ is around 12. These values agree with the expected range of most normally consolidated (NC) to lightly overconsolidated (LOC) clays having (Δ) between 0.50 and 1.0.

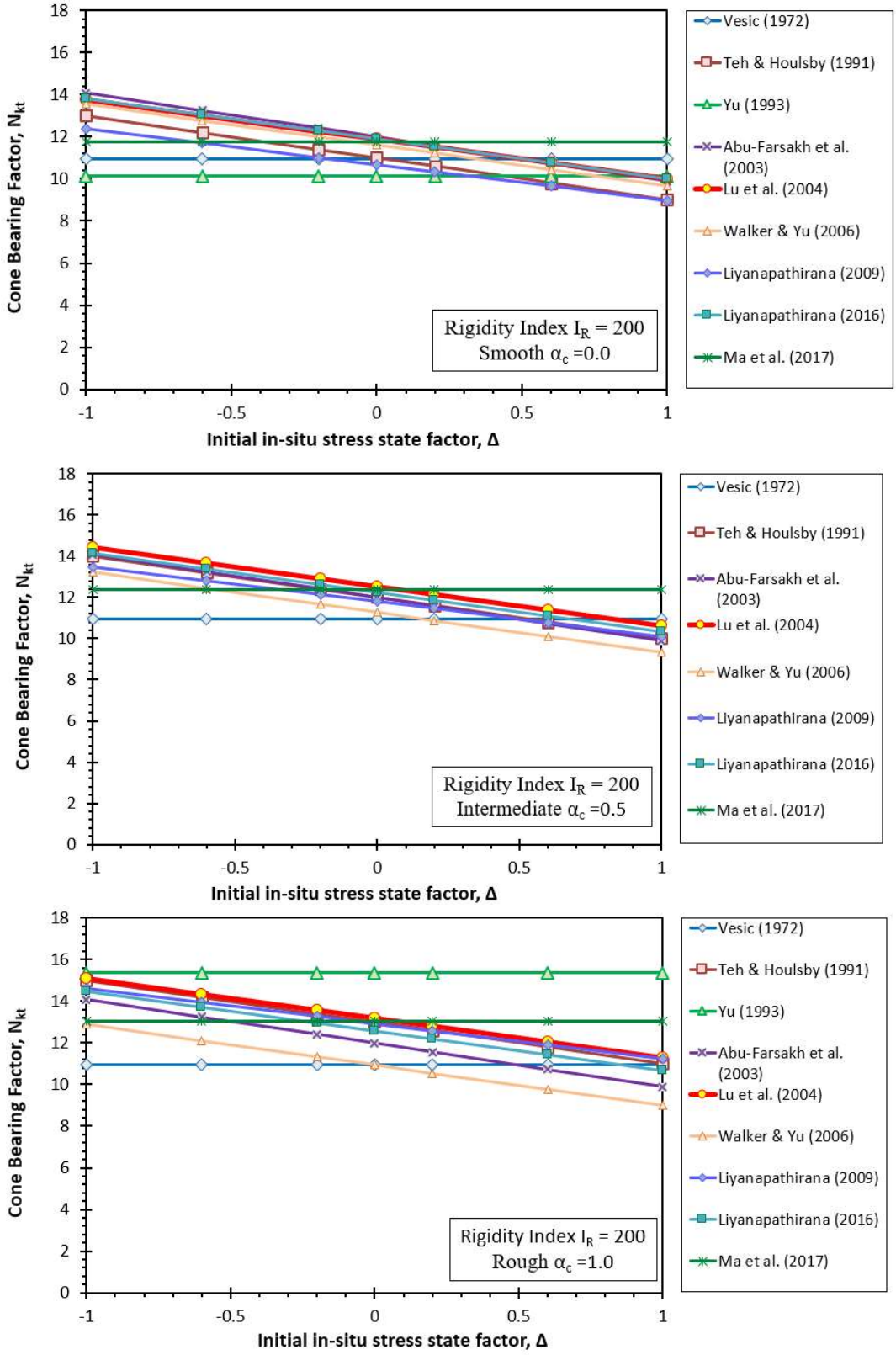


Figure 9.18. Comparison of cone bearing factors versus the initial stress state factor (Δ) for (a) smooth, (b) intermediate, and (c) rough cone interfaces

## 9.7 Analytical Model Development for Evaluating Undrained Shear Strength

Following the basic definition of the cone bearing factor ($N_{kt}$), the cone tip resistance is expressed in terms of undrained shear strength as follows:

$$q_t = q_{net} + \sigma_{vo} = N_{kt} \cdot s_{u\,TC} + \sigma_{vo} \quad [9.17]$$

where $\sigma_{vo}$ is the total vertical overburden stress and $N_{kt}$ is the cone bearing factor for the triaxial compression mode (the focus of the compiled database). Based on the earlier discussion on the appropriate selection of the $N_{kt}$ expression, it is evident that the classic SCE solution by Vesic (1977) can be replaced using a more representative expression that addresses soil rigidity index $I_R$, geostatic stress state $K_0$, and soil-cone interface roughness. After investigating various alternatives, the expression for $N_{kt}$ developed by Lu et al. (2004) based on finite element modeling using the re-meshing and interpolation technique with small strain stiffness (RITSS) is selected herein.

Moreover, this FEM solution for $N_{kt}$ is compatible with the soil behavioral charts developed by Schneider et al. (2008; 2012) distinguishing drained and undrained soil conditions with an emphasis on the variations in the degrees of consolidation and drainage for different soil types during cone penetration that can be attributed to changes in yield stress ratio. The chart uses normalized cone tip resistance (Q) and penetration porewater pressure expressed in the form of a normalized porewater pressure parameter ($U^* = \Delta u_2/\sigma'_{v0} = B_q \cdot Q$) in defining five main soil behavioral type classification zones. In the chart development, the expression by Lu et al. (2004) was used in evaluating the net cone resistance and in defining trends of different soils in the Q vs. U* charts and showing an OCR effect. Also, the same cone bearing definition has been utilized by DeJong and

Randolph (2012) in correctly determining the soil type and interpreting the pore pressure dissipation for soils with partial consolidation during cone penetration. Hence, equation [9.17] can be updated to reflect the chosen cone bearing factor expression:

$$q_t = [3.4 + 1.6 \cdot \ln I_R - 1.9 \cdot \Delta + 1.3 \cdot \alpha_c] \cdot s_{u\,TC} + \sigma_{vo} \quad [9.18]$$

The excess porewater pressures induced during cone penetration are a combination of changes due to octahedral stresses and shear-induced porewater pressures. A similar analogy was developed by Vesic (1972) expressing the porewater pressure for any point in the plastic zone of an expanded spherical cavity, assuming that the initial stress conditions are isotropic compresses and the soil is saturated. Baligh (1984) developed closed-form expressions for the penetration of a piezocone into incompressible homogeneous isotropic material under isotropic state of stress. On the basis of cavity expansion theory, the deformations of the soil around the cone can be determined and four zones of failure modes can be assigned at the cone tip and around the sleeve, as presented in **Figure 9.19.** For zone I which is directly located at the cone tip, the principal major stresses with corresponding deformation act in a vertical direction resembling undrained triaxial compression shearing. For zones II and III, the predominant stresses and strains are in a combination of both direct simple shear and pressuremeter test modes. Finally, for zone IV, the major principal stresses and strains resemble the conditions of a pressuremeter test (Keaveny & Mitchell 1986).

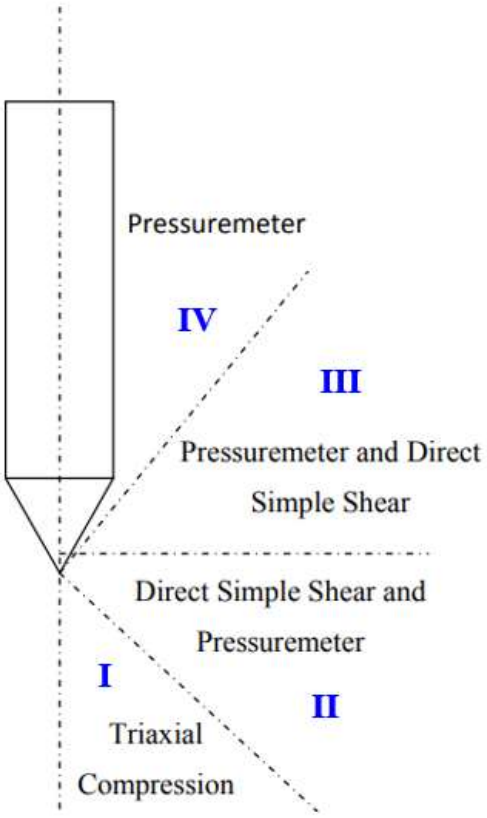


Figure 9.19. Predominant failure modes around an advancing cone penetrometer (after Baligh, 1984)

Based on the aforementioned, the predominant failure mode around the cone tip can be represented using undrained triaxial compression and/or direct simple shear, or a mixture of both. Accordingly, the best choice for representation of the shear-induced excess pore water pressures ($\Delta u_{sh}$) will be defined using different shearing modes: anisotropically consolidated triaxial compression ($CK_0UC$) and direct simple shear ($CK_0U$-DSS), as investigated here.

A stress path in the MIT q-p′ space as presented in **Figure 9.20** is used to illustrate the interpretation of excess porewater pressures in $CK_0UC$ and CAUC tests.

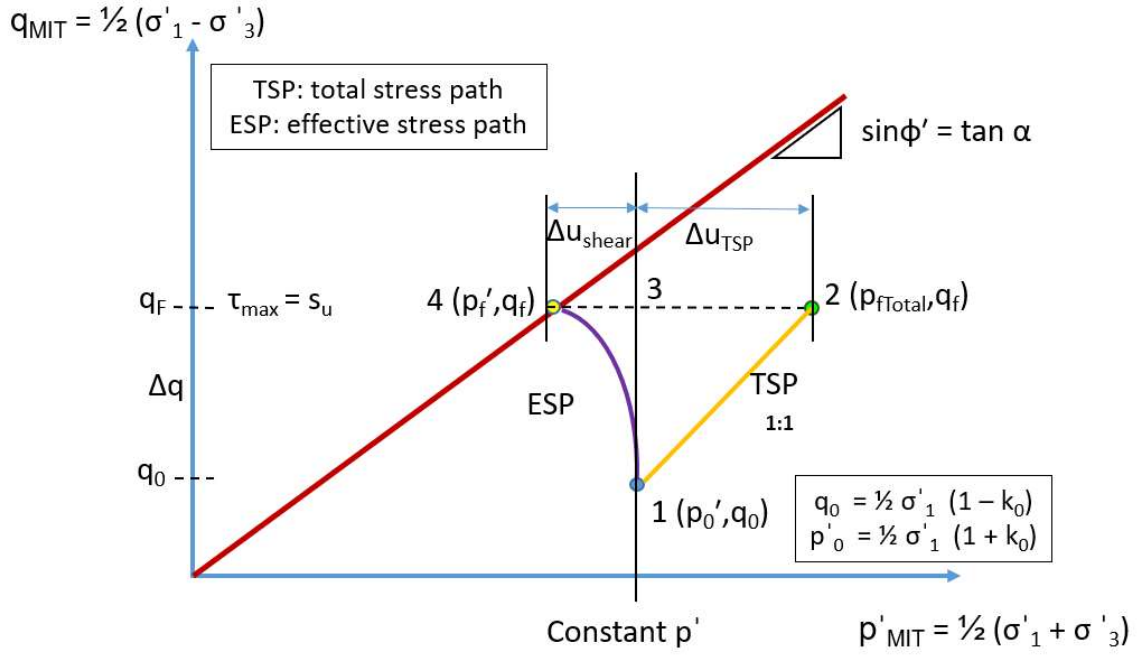


Figure 9.20. Interpretation of excess pore water pressure (Δu) in MIT q-p′ space for $CK_0UC$ and CAUC tests

Two different definitions for the excess porewater pressure can be found in CAUC tests: (a) Δu-shear from a constant p′ test (between points 3 and 4) or (b) full Δu (difference between total stress path (TSP) and effective stress path (ESP) as presented between points 2 and 4). The latter is consistent with Skempton's pore pressure parameter at failure ($A_f$).

$$\Delta u_{sh-const\,p'} = p'_o - p'_f = \frac{\sigma'_{vo}}{2} \cdot (1 + K_0) - \frac{s_u}{\sin\phi'} \quad [9.19]$$

$$\Delta u_{full} = p_{f\,Total} - p'_f = K_0 \cdot \sigma'_{vo} + s_u \cdot (1 - \frac{1}{\sin\phi'}) \quad [9.20]$$

Similarly, for simple shear mode the excess pore water pressure obtained during undrained shearing as presented in **Figure 9.21** can be expressed (Mayne et al. 2017):

$$\Delta u_{DSS-\sigma'_{vo}} = \sigma'_{vo} \cdot (1 - \frac{1}{2}\cos\phi' \cdot OCR^{\Lambda}) \quad [9.21]$$

And for the condition where the shearing is caused by horizontal effective stresses in a rotated simple shear mode rather than the conventional effective vertical stress, the shear-induced excess pore water pressure can be expressed as:

$$\Delta u_{DSS-\sigma'_{ho}} = \sigma'_{ho} \cdot \left(1 - \frac{1}{2}\cos\phi' \cdot OCR^{\Lambda}\right) = K_0 \cdot \sigma'_{ho} \cdot (1 - \frac{1}{2}\cos\phi' \cdot OCR^{\Lambda}) \quad [9.22]$$

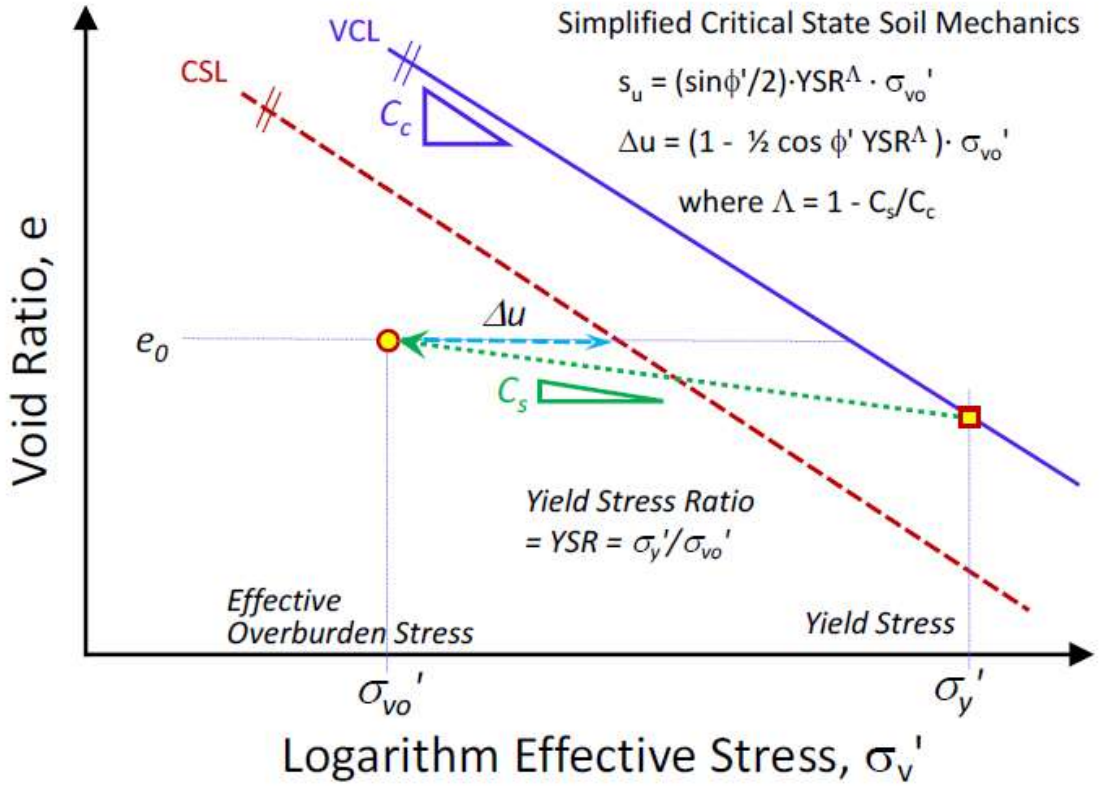


Figure 9.21. Interpretation of excess pore water pressure ($\Delta u_{DSS}$) for undrained simple shear stress path (Mayne, et al. 2017)

A simplified expression for shear-induced porewater pressures in triaxial compression has been introduced by Chen & Mayne (1994) based on critical state soil mechanics and adopted by Schneider et al. (2008) and DeJong and Randolph (2012):

$$\Delta u_{CSSM} \approx \sigma'_{vo} \cdot [1 - \left(\frac{OCR}{2}\right)^{\Lambda}] \quad [9.23]$$

To relate the undrained shear strength to the stress history expressed in terms of OCR, a constitutive model is needed. Given that the focus of the compiled database is on anisotropically-consolidated triaxial compression (CAUC) mode of shearing, then an anisotropic model with a yield surface that can capture the $K_0$-consolidation within the triaxial compression mode of shearing is required. An anisotropic clay plasticity model SANICLAY, which stands for "Simple ANIsotropic CLAY", was developed by Dafalias et al. (2002; 2006) and used herein linking the undrained shear strength to OCR. The model defines the normally-consolidated undrained shear strength ratio ($^{S_u}/_{\sigma_{vo}'}$) which is utilized in computing the initial in-situ state parameter ($\Delta$), overconsolidation ratio, and hence the coefficient of lateral earth pressure ($K_0$). The constitutive model has been developed following the framework of critical state soil mechanics (CSSM) in the triaxial space. This model was derived from energy dissipation balance where coupling between both deviatoric and volumetric strains is taken into account by an anisotropic stress ratio variable leading to a plastic potential function. This can be represented using a rotated and distorted ellipse in triaxial space around the $K_0$-line with measurements of both the rotation and distortion (Dafalias et al., 2002). **Figure 9.22** presents schematic diagram of SANICLAY model surface in the triaxial stress space, showing the rotation of the yield surface around the $K_0$-line where the degree of rotation and distortion is determined by the value of $\alpha$.

The SANICLAY model assumes associative flow rule for a yield surface which captures the behavior of clays during and after anisotropic $K_0$ consolidation. As the model captures rotational anisotropic hardening behavior of clays, it deviates from the uniqueness of the critical state line as promoted in CSSM. The normally consolidated undrained shear strength ratio from the Dafalias model can be expressed as:

$$S = {s_u}/{\sigma_{vo}'} = \frac{M}{2}\,\frac{(1+2K_o)}{3}\left(\frac{\eta_k{}^2 - 2\alpha\,\eta_k + M^2}{2M^2 - 2\alpha M}\right)^{\Lambda} \quad [9.24]$$

$$\eta_k = \frac{3\,(1\,-\,K_o)}{1\,+\,K_o} \quad [9.25]$$

$$\alpha = \frac{(\eta_k{}^2 + 3\Lambda\,\eta_k\,-\,M^2)}{3\,\Lambda} \quad [9.26]$$

where M = 6 sinϕ′/(3-sinϕ′) [9.27]

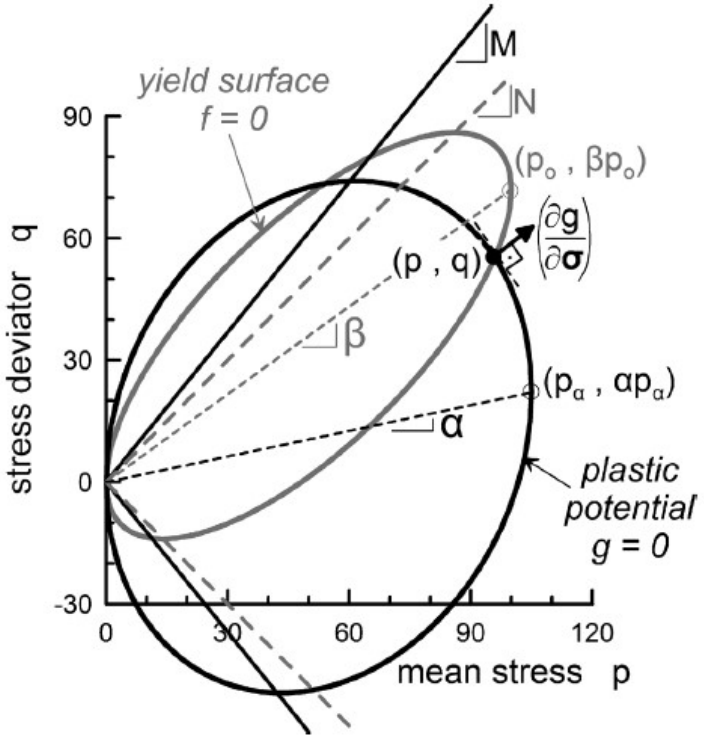


Figure 9.22. SANICLAY model surface in triaxial stress space (Dafalias, 2006)

Given the complexity of the provided equations, the undrained shear strength ratio (S) was plotted versus a wide range of friction angles for different values of Λ to develop a series of approximate expressions (S*) as presented in **Figure 9.23**.

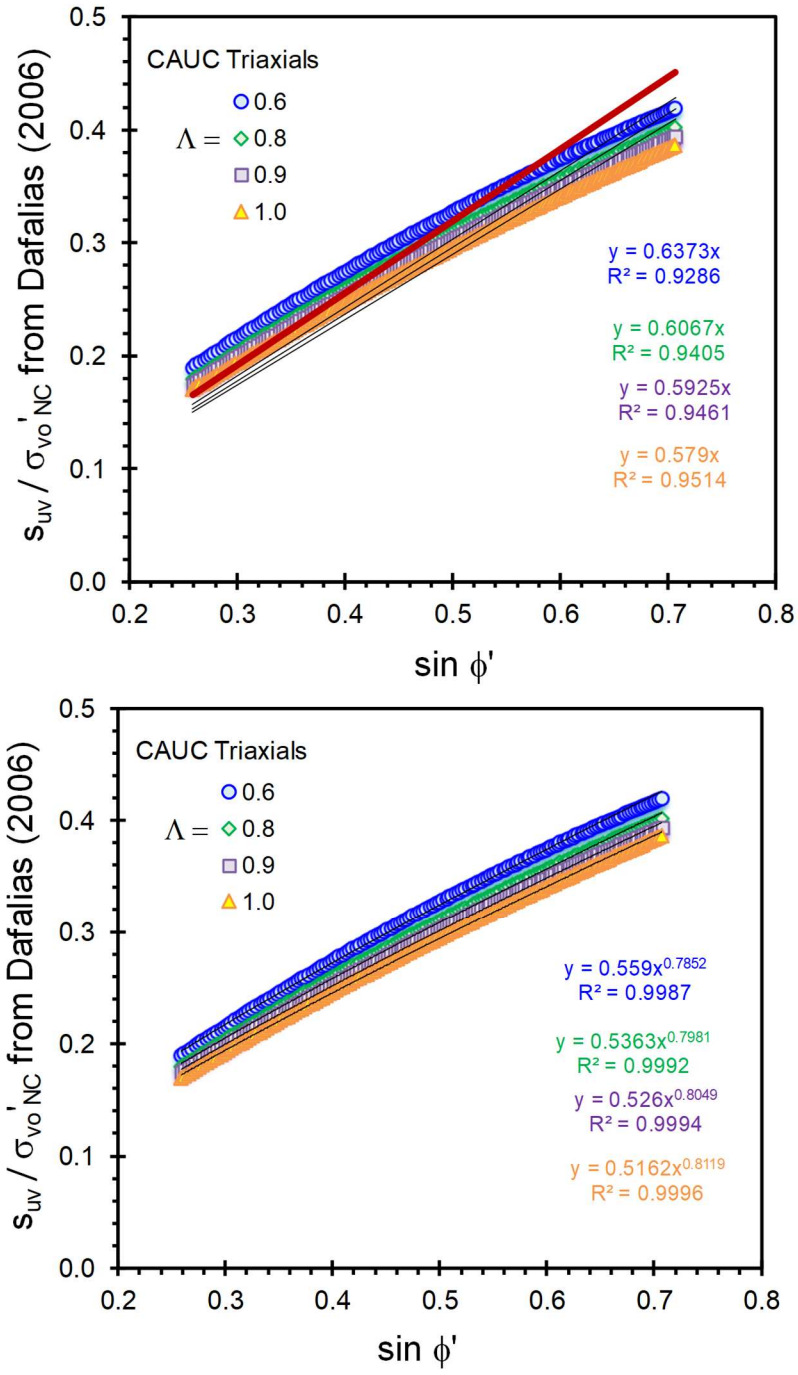


Figure 9.23. Undrained shear strength ratios (S) from SANICLAY model (Dafalais 2006) for different effective friction angles (ϕ') and plastic volumetric strain ratios (Λ)

From the plotted curves at different Λ values, the undrained shear strength ratio (S*) can be approximated as shown in Figure 9.19 and given by:

$$S^* \approx 3/5 \sin \phi' \quad [9.28a]$$

$$\text{or } S^* \approx 0.54 (\sin \phi')^{\Lambda} \quad [9.28b]$$

The undrained shear strength ratio from the Dafalias model for $CK_0UC$ shearing mode is compared to calculated values from other well-established constitutive models in the literature such as the Wroth-Prevost anisotropic modified Cam-clay model and the rotated bullet yield surface model by Ohta et al. (1985) as presented in **Figure 9.24**.

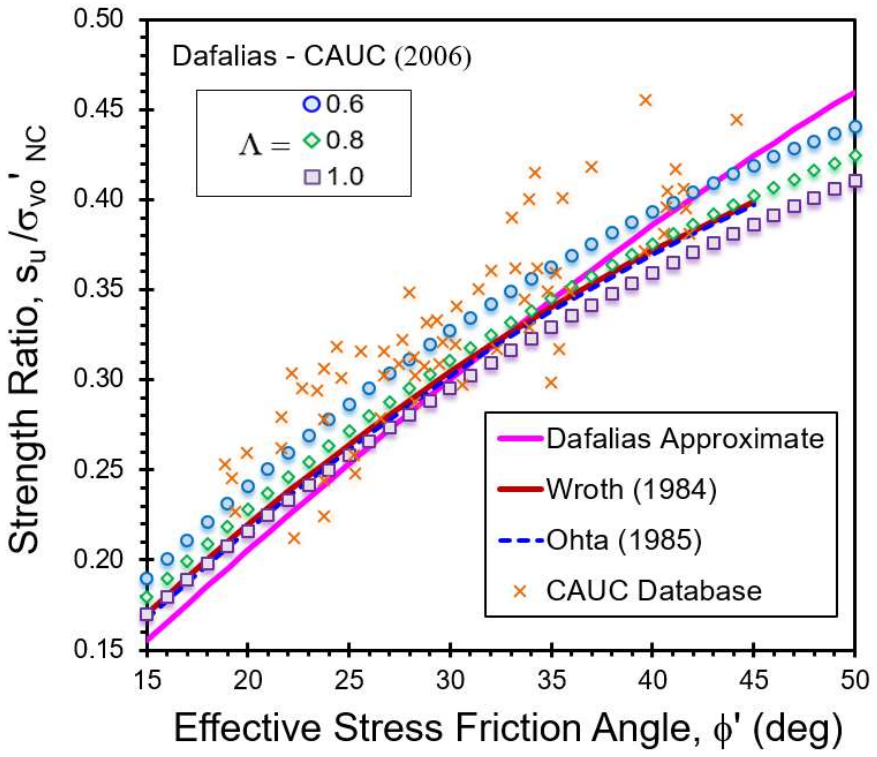


Figure 9.24. Comparison between undrained shear strength ratio (S) from SANICLAY model with two prior constitutive models with superimposed CAUC database

From the plotted contours for the three different constitutive models, it is evident that there is a good match for the range $25° \leq \phi' \leq 35°$, but the approximate solution slightly overestimates the normalized strength ratio ($S = s_u / \sigma'_{vo}$) when $\phi' > 35°$ and slightly underestimated S when $\phi' < 25°$. By superimposing a database of CAUC results for clays with actual S and $\phi'$ values, it is evident that the Dafalias solution provides a reasonable yet conservative evaluation. Also, it is similar to the prior constitutive models (Wroth and Ohta) in evaluating S over most of the expected range: $20° \leq \phi' \leq 40°$. As the yield surface is rotated to a $K_0$ line with respect to the p' axis, it is recommended to use the Dafalais strength ratio (S*) in the analytical model development and calibration with its approximation.

## 9.8 Calibrating Analytical Model for Undrained Shear Strength Evaluation

To calibrate the analytical model for the evaluation of undrained shear strength under triaxial compression shearing mode, the cone bearing factor expression as developed from the FEM analyses of Lu et al. (2004) was used, as given by equation [9.18]. As for the measured CPTu porewater pressures ($u_2$), an expression was developed by summing the three terms: (a) hydrostatic pore water pressure ($u_0$), (b) octahedral porewater pressures ($\Delta u_{oct}$) as expressed by equation [9.9], and (c) shear-induced excess porewater pressures ($\Delta u_{sh}$). The latter were investigated using 5 different definitions covering differing CAUC and DSS modes of failure as expressed by equations [9.19 to 9.23]. These were used in evaluating the corresponding cone bearing factors ($N_{\Delta u}$ and $N_{ke}$) and the corresponding porewater pressure parameter ($B_q$). For the link between undrained shear strength and OCR, the rigorous expressions defining the normalized shear strength ratio (S) from the

SANICLAY model was used as expressed by equation [9.24] – [9.26] and compared to the approximate solution from equation [9.28].

### *9.8.1 Parametric Values*

For the main input parameters used in the analytical model, reasonable parametric values of $\phi'$ must be assigned. Díaz-Rodríguez, Leroueil, & Aleman (1992) reviewed effective stress envelopes and yield surfaces from 50 natural clays. The reported effective friction angles values range from 17.5° for Winnipeg clay in Canada up to 43° for Mexico City Clay (Leroueil & Hight 2003). In more recent publications by Camp (2004), Cooper Marl clay in South Carolina has an effective friction angle of 45°. The soft clay at Burswood Australia reached peak values as high as $\phi' = 53°$ (Low et al. 2011). Accordingly, three effective friction angle values were selected to cover the full range of the reported friction angles in the parametric study: $\phi' = 18°$, 30°, and 45°.

As for the rigidity index ($I_R = G/s_u$), the value depends on the definition of the shear modulus (initial, tangent, secant), level of stress ($q/q_{max}$), and/or appropriate strain level ($\gamma_s$), but expected values typically range from 20 up to 2000. A default value of $I_R = 100$ is commonly adopted for soft-firm inorganic clays of low sensitivity (e.g. Teh 1987). Hence three values were selected for the analytical parametric study, with $I_R = 20$, 100, and 2000.

As for the roughness factor, as presented earlier the cone bearing factor increases with the increase in the roughness coefficient and typical values for steel interface range from 0.25 to 0.5. Accordingly, to cover a case of intermediate roughness between the extreme smooth and rough bounds, a coefficient ($\alpha_c$) of 0.50 was selected in calibrating the model.

As for the plastic volumetric strain parameter ($\Lambda$), its value is typically constant for natural intact uncemented clays with values ranging from 0.75 to 0.85 and in cases of sensitive or structured clays, the value can approach 1.0 (Ladd 1991). In the current study, a representative value of $\Lambda = 0.80$ was adopted in the calibration of the analytical models.

The parametric calibrations using the five separate expressions for the shear-induced porewater pressures were investigated and compared. Complete plots of the different cone bearing factors ($N_{kt}$, $N_{\Delta u}$, and $N_{ke}$) versus normalized porewater pressure ($B_q$) and normalized cone resistance parameters ($Q_u$ and $Q_k$) are presented in **Appendix H,** where $Q_u = q_E/\sigma_{vo}' = (q_t - u_2)/\sigma_{vo}'$ and $Q_k = q_E/q_{net} = (q_t - u_2)/(q_t - \sigma_{vo})$.

**Figures 9.25 to 9.27** present the predicted relationships between the three cone bearing factors ($N_{kt}$, $N_{\Delta u}$ and $N_{ke}$) and porewater pressure parameter ($B_q$) for the parametric range of values of effective friction angle and rigidity index using the conventional DSS mode for shear-induced excess porewater pressures ($\Delta u_{sh}$). By superimposing the compiled database, it can be seen that the Lu et al. (2004) solution captures the correct direction and trend in the CAUC-CPTu data, unlike the classic Vesic solution as pointed out earlier. **Figures 9.28 to 9.30** present the three cone bearing factors versus the normalized quantity $Q_u = (q_t - u_2)/\sigma_{vo}'$ for the conventional DSS test definition for shear-induced excess porewater pressure ($\Delta u_{sh}$), it is evident that the predicted contours capture the correct trend for the compiled database and covers the widespread in the cone bearing factors. Similarly, **Figures 9.31 – 9.33** present the cone bearing factors versus the normalized parameter $Q_k = q_{eff}/q_{net}$ following the standard DSS mode for shear-induced excess porewater pressure ($\Delta u_{sh}$). The predicted contours fit the compiled database and follow the correct trend directions.

A close examination of the alternative definitions of shear-induced excess porewater pressure based on the presented figures in Appendix H, it is evident that all definitions correctly capture the $N_{\Delta u}$ versus $B_q$ trend covering the full range of the compiled data. Yet, the $N_{ke}$ - $B_q$ trends are not properly matched using either the full $\Delta u$ definition from triaxial compression tests (i.e., Skempton's $A_f$ parameter) nor the rotated DSS mode with effective horizontal stress. The triaxial compression test definition with constant p' stress path gives a relatively fair estimate when compared to the simplified CSSM stress path for TC and conventional DSS mode.

Based on the parametric studies, it can be seen that the shear-induced porewater pressures based on conventional DSS mode give the best overall representations for the cone bearing factors when plotted vs normalized parameters: $B_q$, $Q_u$, and $Q_k$. Therefore, the use of triaxial compression mode for $q_t$ and simple shear mode for $u_2$ complies well with the specified stress paths at these locations on an advancing cone penetrometer (Baligh 1984; Keaveny & Mitchell 1986)

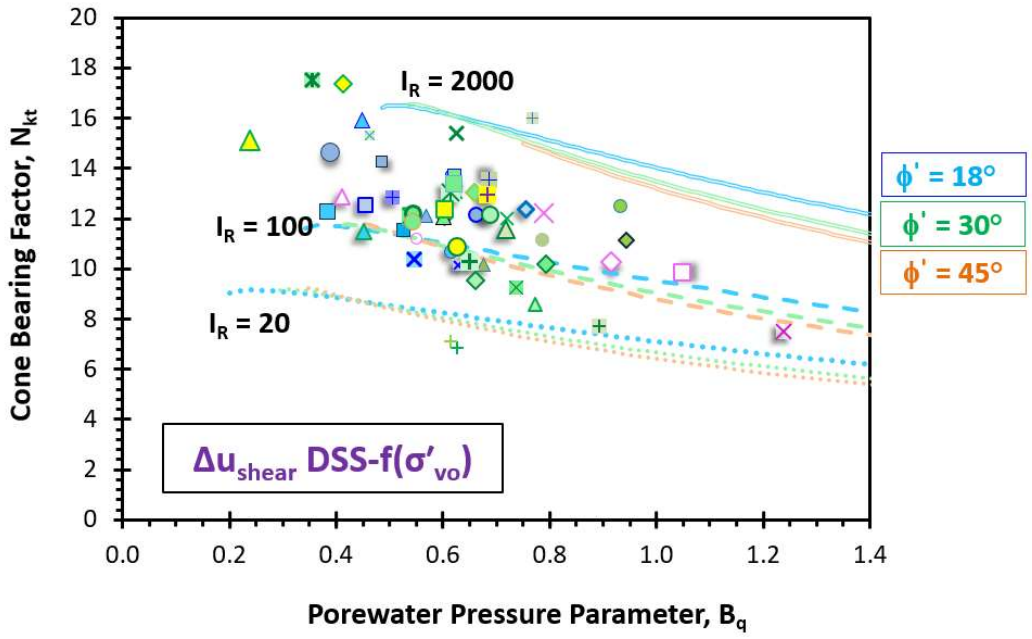


Figure 9.25. Cone bearing factor ($N_{kt}$) versus $B_q$ using shear-induced porewater pressure from DSS and parametric ranges of effective friction angle and rigidity index

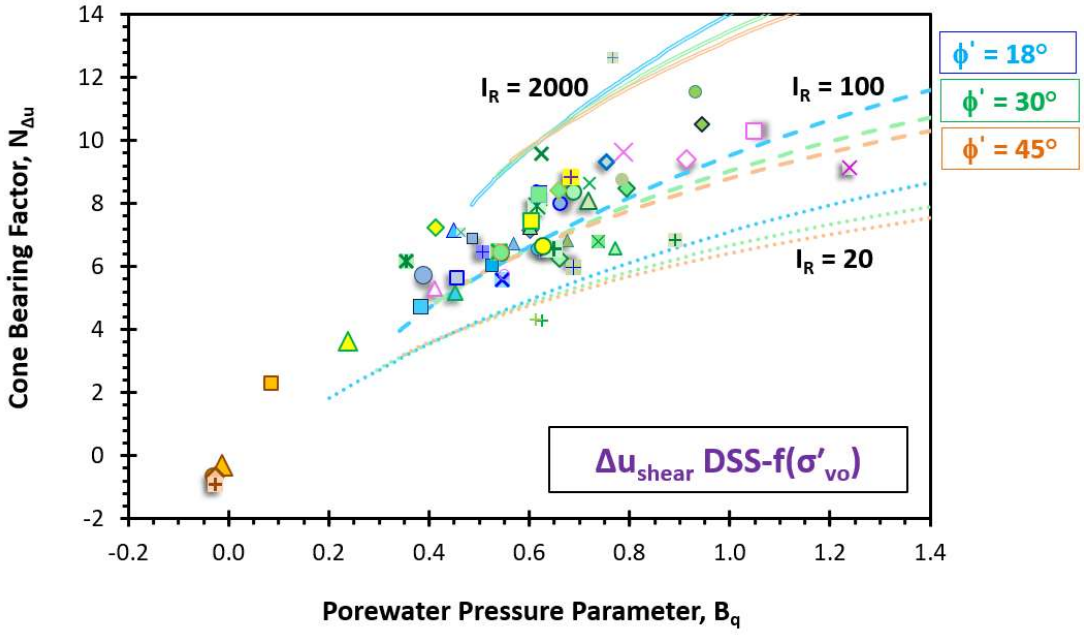


Figure 9.26. Cone bearing factor ($N_{\Delta u}$) versus $B_q$ using shear-induced porewater pressure from standard DSS and parametric ranges of friction angle and rigidity index

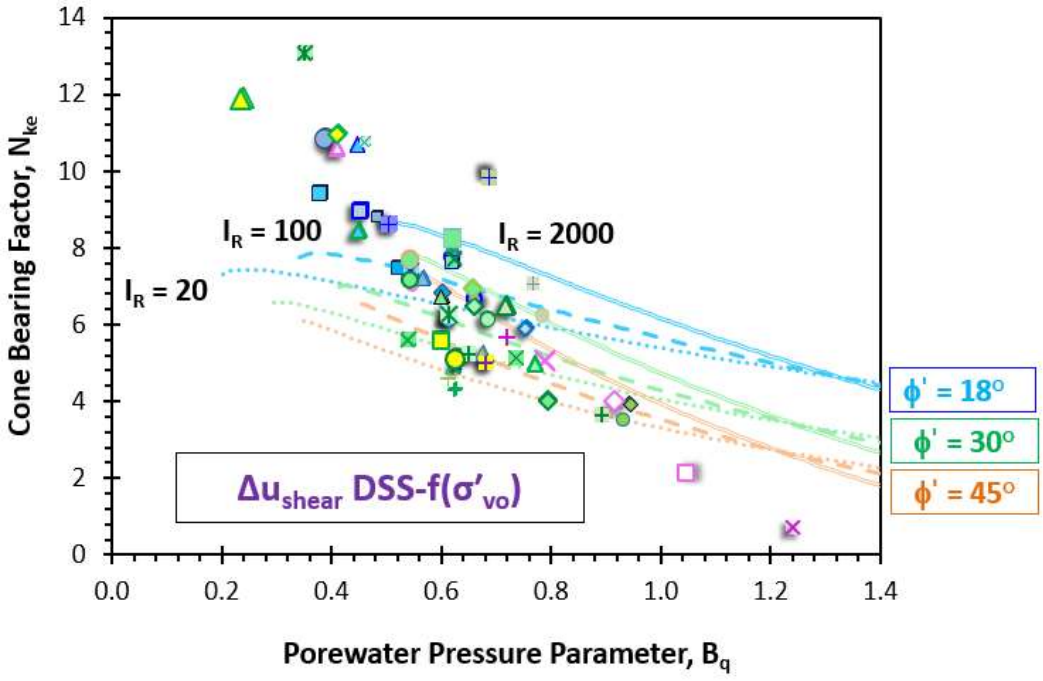


Figure 9.27. Cone bearing factor ($N_{ke}$) versus $B_q$ using shear-induced porewater pressure from DSS and parametric ranges of friction angle and rigidity index

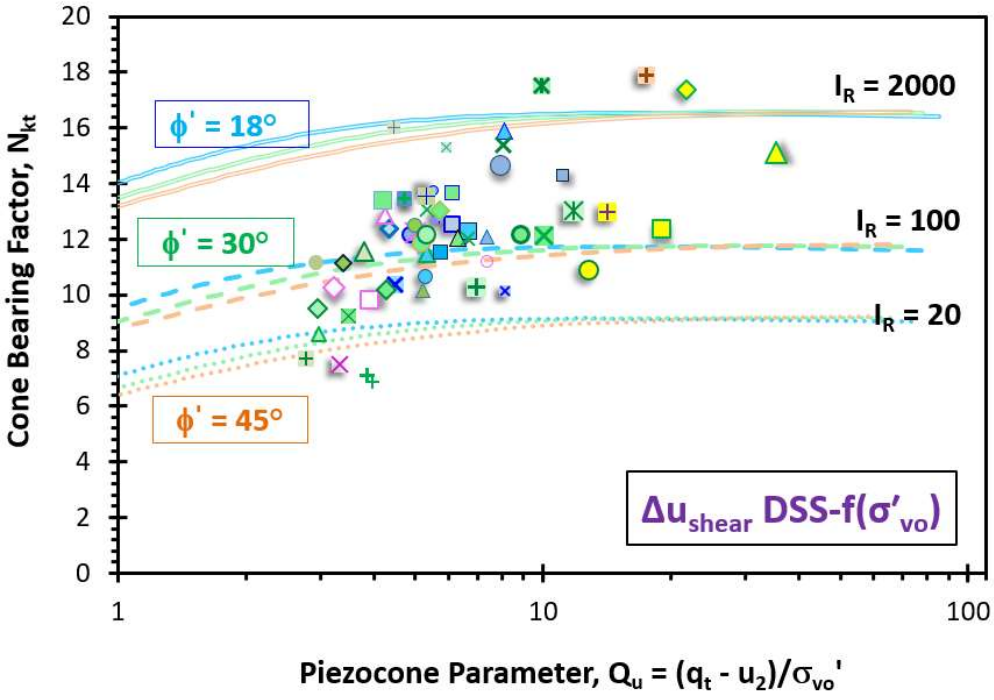


Figure 9.28. Cone bearing factor ($N_{kt}$) versus $Q_u$ using shear-induced porewater pressure from DSS and parametric ranges of effective friction angle and rigidity index

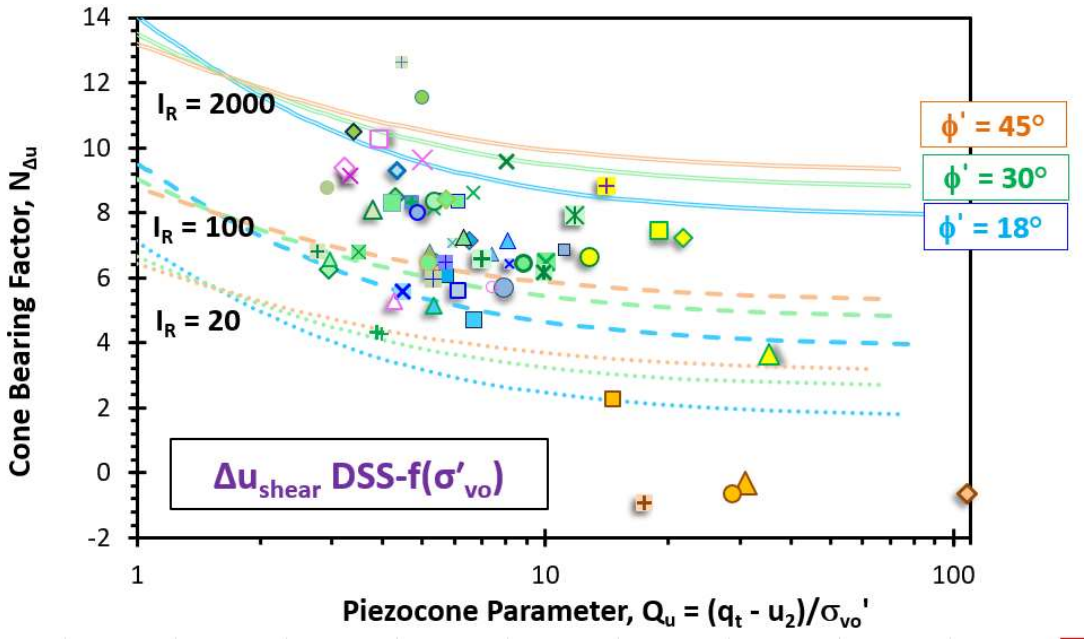


Figure 9.29. Cone bearing factor ($N_{\Delta u}$) versus $Q_u$ using shear-induced porewater pressure from DSS and parametric ranges of effective friction angle and rigidity index

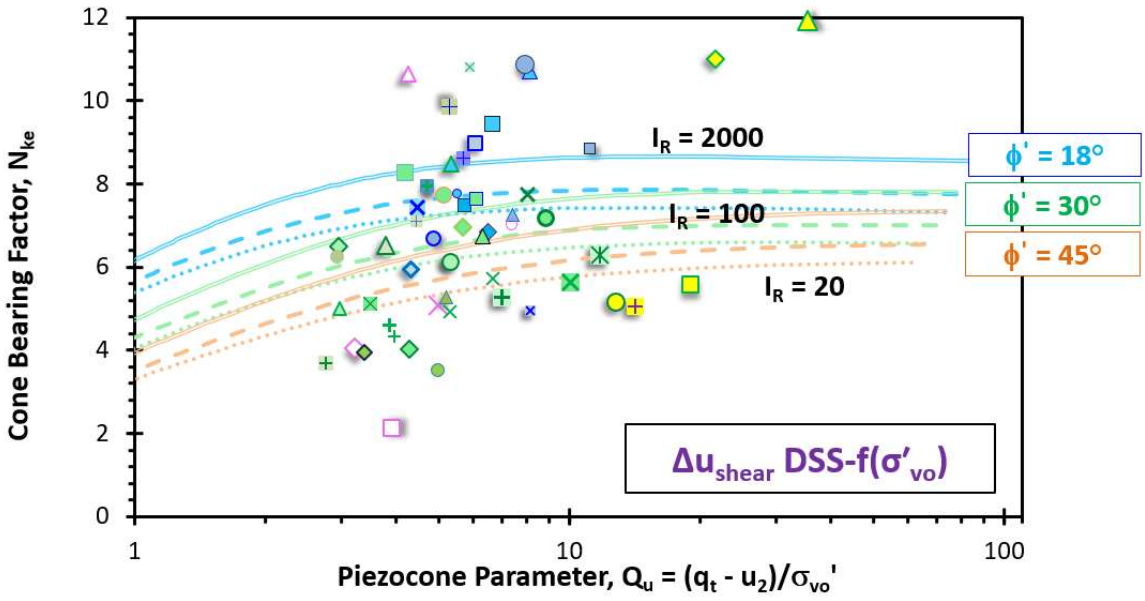


Figure 9.30. Cone bearing factor ($N_{ke}$) versus $Q_u$ using shear-induced porewater pressure from DSS and parametric ranges of effective friction angle and rigidity index

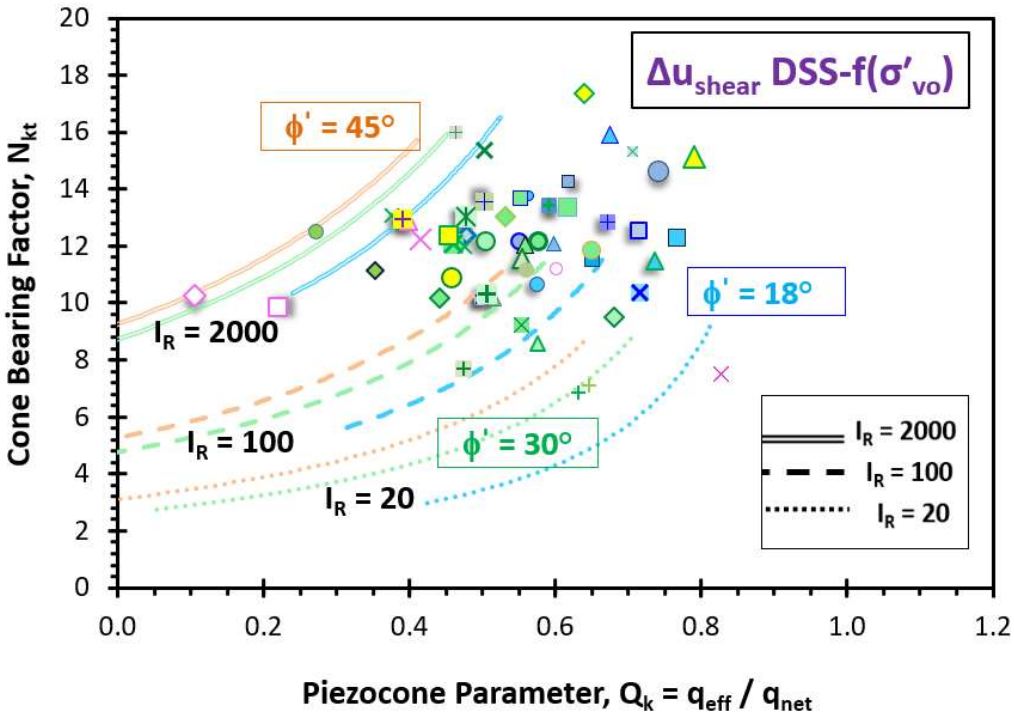


Figure 9.31. Cone bearing factor ($N_{kt}$) versus $Q_k$ using shear-induced porewater pressure from DSS and parametric ranges of effective friction angle and rigidity index

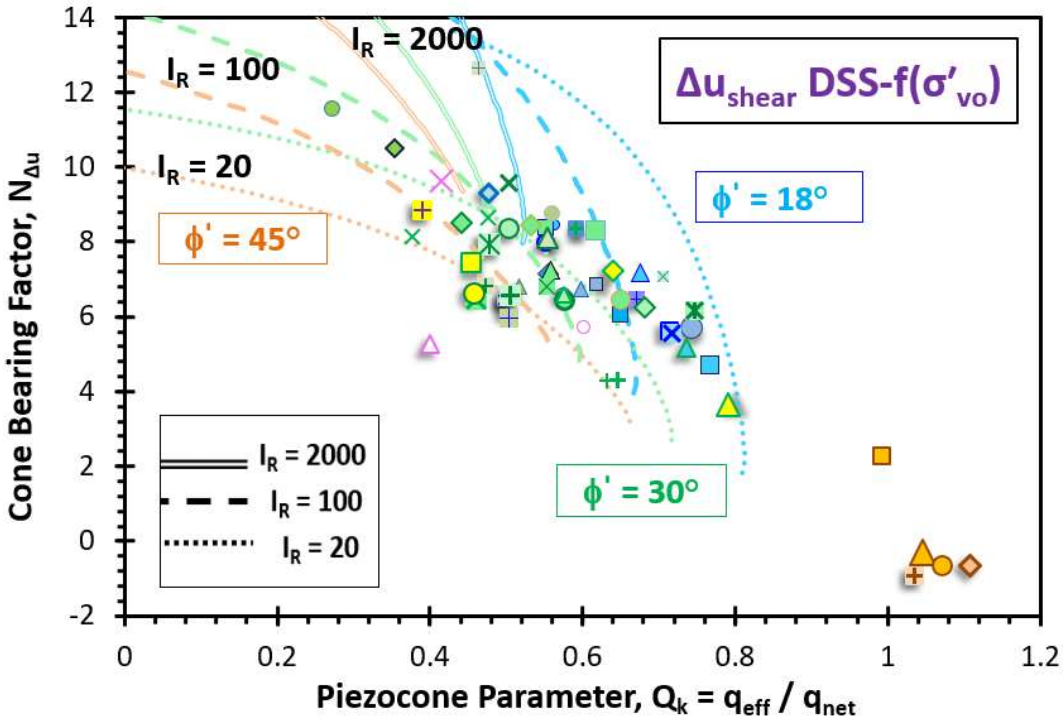


Figure 9.32. Cone bearing factor ($N_{\Delta u}$) versus $Q_k$ using shear-induced porewater pressure from DSS and parametric ranges of effective friction angle and rigidity index

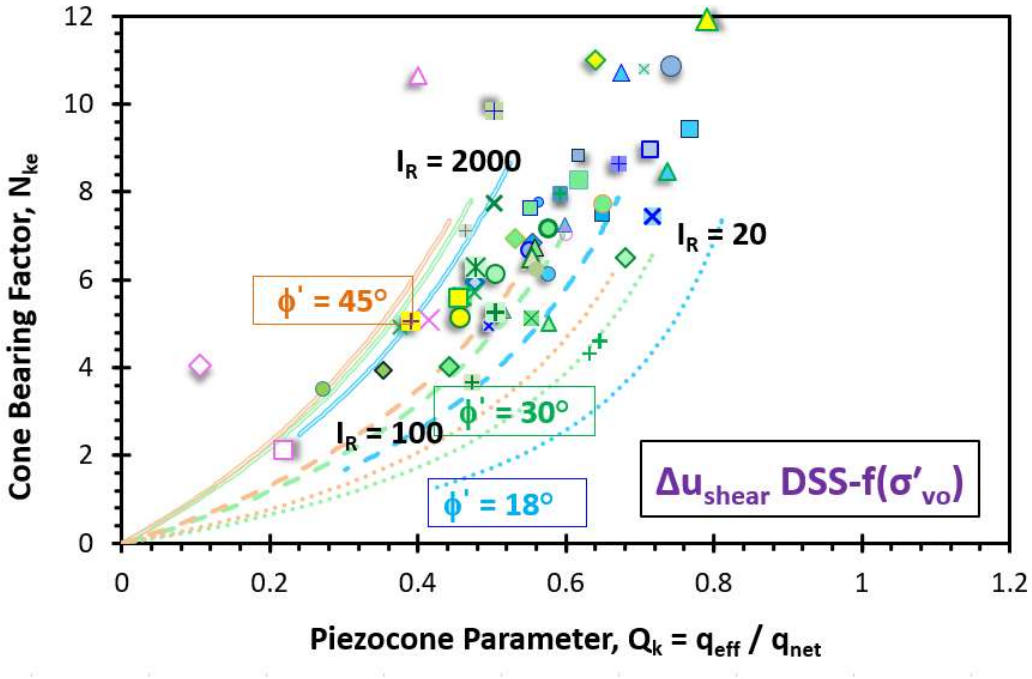


Figure 9.33. Cone bearing factor ($N_{ke}$) versus $Q_k$ using shear-induced porewater pressure from DSS and parametric ranges of effective friction angle and rigidity index

### 9.9 Calibrating an Analytical Model for Stress History Evaluation in clays

The same set of analytical models used in assessing the undrained shear strength under triaxial compression shearing mode from CPTu is now applied to evaluate the stress history in clays. The link between the undrained shear strength and the stress history is defined using normalized shear strength ratio (S) which has been previously defined using the Dafalias (2002) expression, where (Ladd & DeGroot 2003):

$$(s_u/\sigma_{vo}')_{OC} = S \cdot OCR^{\Lambda} \qquad [9.29]$$

The cone bearing factor ($N_{kt}$) from the FEM solution by Lu et al. (2004) was used in defining the cone tip resistance ($q_t$) and the five separate definitions for shear-induced component of excess porewater pressures were investigated for expressing the porewater pressure ($u_2$). The same ranges of input parameters for effective friction angle, rigidity indices, and roughness coefficient, were used as in the undrained shear strength evaluation.

To validate the CPTu expressions for stress history, a more comprehensive global database was prepared from 150 well-documented worldwide clay sites that was collected with a total of n = 1970 data points. The sites primarily include soft to firm normally-consolidated to lightly-overconsolidated young to aged clays, as well as a few sites from stiff to hard overconsolidated clays and fissured fine-grained soils. Only high-quality laboratory tests using incremental-load or constant-rate-of-strain consolidation tests were used for assessing the stress history profiles. The clay database is summarized in **Figure 9.34** that can be subdivided into 3 main groups: (a) 100 intact clays which are given blue symbols and are presented in **Table 9.3**, (b) 40 sensitive clays which are given pink symbols and are presented in **Table 9.4**, and (c) 10 fissured overconsolidated clays given green symbols, as summarized in **Table 9.5**.


Figure 9.34. List of all 150 clays and their symbols for the OCR-CPTu compiled database covering intact NC-LOC clays (blue), sensitive (pink), and fissured OC clays (green)

Table 9.3. Compiled OCR-CPTu database listing of intact NC-LOC-OC clays

| Site | Location | Soil Description | Reference(s) |
|---|---|---|---|
| Amherst | MA, USA | Soft Varved Clay-Silt | DeGroot & Lutenegger (2003) |
| Anchorage | AK, USA | Stiff Lean OC Clay | Mayne & Pearce (2005) |
| Ariake | Japan | Soft Marine Clay | Tanaka et al. (2001) |
| Arnprior | Canada | Soft Marine Clay | Konrad (1986) |
| Askersund | Sweden | Soft Clay | Bergenstahl (1991) |
| Atchafalaya | LA, USA | Soft Backswamp Clay | Baligh et al. (1980) |
| Bäckebol | Sweden | Soft Clay | Larsson & Mulabdić (1991a) |
| Bakklandet | Norway | Intact Clay | Sandven (1990) |
| Ballina | Australia | Soft Estuarine | Pineda et al. (2014; 2016) |
| Bangkok NNH | Thailand | Soft Bangkok | Shibuya & Tamrakar (2003) |
| Belfast | Ireland | Soft Clay (Sleech) | Lehane (2003) |
| BBC (Boston Blue Clay) | MA, USA | Onshore Intact | Whittle et al. (2001) |
| Bothkennar | Scotland, UK | Silty Estuarine Clay | Hight et al. (1992) |
| Brage | The North Sea | Intact Silty Clay | Rad & Lunne (1989) |
| Broadway | CA, USA | Soft Intact | Chameau et al. (1991) |
| Burswood | Australia | Soft Clay | Low et al (2011) |
| Busan | Korea | Soft Intact | Chung et al. (2012) |
| Charles City County | VA, USA | Intact clay | Houlihan & Blodgett (1989) |
| Chek Lap Kok (Lower) | Hong Kong | Alluvium Deposit | Koutsoftas & Foott (1982) |
| Chek Lap Kok (Upper) | Hong Kong | Marine Deposit with Fill Mixture | Koutsoftas & Foott (1982) |
| Chinguetti | Mauritania | Offshore Intact | Lunne et al. (2006) |
| Cooper Marl | SC, USA | OC Calcareous | Camp (2004) |
| Cran | France | Aged Lightly overconsolidated | Juran (1983); Bensaid (1985) |
| Drammen | Norway | Soft Clay | Long & Donohue (2007) |
| Dunkerque | France | Intact clay | Juran & Tumay (1989); Bensaid (1985) |

| Site | Location | Soil Description | Reference(s) |
|---|---|---|---|
| East India- Bay of Bengal | India | Intact Soft Clay | Mayne et al. (2015) |
| Eberg | Norway | Soft Clay | Sandven (1990) |
| Emmerstad | Norway | Soft sensitive LOC Clay | Rad & Lunne (1988); Aas et al. (1986) |
| Empire | LA, USA | Soft Plastic Clay | Azzouz & Lutz (1986) |
| Evanston | IL, USA | Soft low plasticity Clay | Finno et al. (2000) |
| Fort Road | MN, USA | Soft Intact clay | Chen & Mayne (1994) |
| Fucino | Italy | Soft Cemented Clay | Burghignoli et al. (1991) |
| Glava | Norway | Overconsolidated silt | Sandven (1990) |
| Grangemouth | Scotland, UK | Soft Clay | Powell et al. (1988) |
| Gulf of Guinea | Gulf of Guinea, West Africa | Soft Offshore | Lunne et al. (2006) |
| Haga | Norway | OC Intact | Lunne et al. (1986) |
| Halsen | Norway | OC Intact | Sandven (1990) |
| Haltenbanken | Norway | Overconsolidated Intact | Rad & Lunne (1988) |
| Higashi | Japan | Soft Plastic clay | Shibuya et al. (1995) |
| Homestake Mine | SD, USA | Mine Tailing Deposit | East & Ulrich (1989) |
| Inchinnan | Scotland, UK | Soft lightly overconsolidated | Sills et al. (1988) |
| Keelung River | Taiwan | Soft intact | Chern (1992) |
| Kobe | Japan | Soft lightly overconsolidated | Nakase et al. (1988) |
| Kurihama | Japan | Alluvial Clay | Shibuya & Tanaka (1996) |
| Lianyungang | China | Soft Clay | Liu et al. (2008) |
| Lierstranda | Norway | Soft Drammen Clay | Long & Donohue (2007) |
| Lilla Mellösa | Sweden | Soft clay | Larsson & Mulabdić (1991b) |
| Lower 232$^{nd}$ st. | BC, Canada | Silty clay | Sully (1991) |
| Muar | Malaysia | Soft Intact clay | Chen & Mayne (1994) |
| Muni Metro | CA, USA | Intact clay | Koutsoftas (1989) |
| Munkedal | Sweden | Soft clay | Larsson & Mulabdić (1991b) |
| Museumpark | Norway | Drammen Clay | Long & Donohue (2007) |
| Netherlands Z | The Netherlands | Soft normally consolidated | Zuidberg et al. (1982) |
| Newbury | MA, USA | Soft LOC Silty Clay | Landon (2007) |
| Nile River Delta | Egypt | Soft Deltaic Deposit | Hamza et al. (2005) |

| Site | Location | Soil Description | Reference(s) |
|---|---|---|---|
| Norco | LA, USA | Silty Soft Clay | Tumay & Acar (1985), Bensaid (1985) |
| Norfolk Road | Singapore | normally consolidated with low sensitivity | Chen & Mayne (1994) |
| Norrköping | Sweden | Soft clay | Larsson & Mulabdić (1991b) |
| North Sea GC | The North Sea | Stiff lightly Overconsolidated | Lunne et al. (1985) |
| Northwestern University, NGES | Evanston, IL, USA | Soft glacio-lacustrine Clay | Finno et al. (2000); McGillivray (2007) |
| Onsøy | Norway | Soft aged normally consolidated | Lunne et al. (2003) |
| Orinoco | Venezuela | Soft Clay | Azouz et al. (1983) |
| Osaka Bay | Japan | Offshore NC-LOC clay | Tanaka et al. (2003); Watabe et al. (2002) |
| Pisa | Italy | Firm Pancone Clay | LoPresti et al. (2003) |
| Pontida | Italy | Stiff overconsolidated | Jamiolkowski et al. (1985) |
| Port Huron | MI, USA | Lean Glacial Lacustrine Clay | Chen & Mayne (1994) |
| Porto Tolle | Italy | Soft clay with microfabric | Jamiolkowski et al. (1985) |
| Recife | Brazil | Soft Organic Clay | Coutinho (2007) |
| Rio de Janeiro | Brazil | Soft Clay | Rocha-Filho & Alencar (1985) |
| San Francisco Bay Mud | CA, USA | NC-LOC Bay Mud | Pestana et al. (2002) |
| Santa Maria | CA, USA | Highly OC Pleistocene silt | Villet & Darragh (1985); Keaveny & Mitchell (1986) |
| Sarapui | Brazil | Soft organic clay | Almeida & Marques (2003) |
| Saro Rd 6-900 | Sweden | Soft clay | Larsson & Mulabdić (1991b) |
| Saro Rd 7-600 | Sweden | Soft clay | Larsson & Mulabdić (1991b) |
| Sea Island | VN, Canada | Soft NC Fraser River Deposit | Konrad et al. (1985); Masood & Mitchell (1992) |
| Singapore | Singapore | Soft Lightly overconsolidated | Tanaka et al. (2001) |
| Skä Edeby | Sweden | Soft clay | Larsson & Mulabdić (1991b) |

| Site | Location | Soil Description | Reference(s) |
|---|---|---|---|
| Snorre | Norway | Offshore NC-LOC | Lunne et al. (2006) |
| South Africa | South Africa | Soft normally consolidated | Jones & Van Zyl (1981); Jones & Rust (1982) |
| Strong Pit | BC, Canada | Highly overconsolidated clay | Campanella et al. (1988) |
| Surry | VA, USA | Intact Miocene clay | Mayne & Gordon (1987) |
| Taipei | Taiwan | Soft Alluvial Lacustrine Clay | Chin et al. (2007) |
| Tokyo | Japan | Lightly Overconsolidated | Suagawara (1988) |
| Torp | Sweden | NC-LOC Soft Clay | Larsson & Åhnberg (2003) |
| Troll East | The North Sea | Normally consolidated plastic clay | Skomedal & Bayne (1988) |
| Troll Lower | The North Sea | Offshore NC-LOC Firm Lean | Lunne et al. (2007) |
| Troll Upper | The North Sea | Offshore NC-LOC Soft plastic Clay | Lunne et al. (2007) |
| Tuve | Sweden | Soft clay | Larsson & Mulabdić (1991b) |
| Upper 232$^{nd}$ st. | BC, Canada | Soft NC Silty Clay | Sully (1991) |
| Valen | Sweden | Soft Clay | Larsson & Mulabdić (1991b) |
| Valoya | Norway | Soft Intact | Sandven (1990) |
| Vancouver | Canada | Intact Lightly overconsolidated | Rad & Lunne (1988) |
| Washington DC | VA, USA | Potomac river alluvium | Mayne (1987) |
| Yorktown | VA, USA | Stiff OC Marine | Mayne (1989) |

Table 9.4. Compiled OCR-CPTu database listing for sensitive clays

| Site | Location | Soil Description | Reference(s) |
|---|---|---|---|
| Baie Johann-Beetz | Québec, Canada | silt marine deposit + homogeneous gray clay | Demers (2001) |
| Baie Sainte-Catherine | Québec, Canada | Clay of marine origin | Demers (2001) |
| Baleine | Québec, Canada | Quaternary marine deposits | Demers (2001) |
| Batiscan | Québec, Canada | Champlain Sea Clay | Bouchard & Tavenas (1981) |
| Berthierville | Québec, Canada | Silty clay homogenous plastic deposit | LaRochelle et al. (1988); Demers (2001) |
| Bois-des-Filion | Québec, Canada | Embankment of a marine terrace | Delisle & Leroueil (2000) |
| Broadback B6 | Québec, Canada | Clayey plain + thick peat moss | Tavenas & Tremblay (1981); Paré et al. (1983) |
| Colebrook Road | British Columbia, Canada | Marine clayey silt-silty clay | Crawford & Campanella (1991) |
| Grandes-Bergeronnes | Québec, Canada | thick silty-clay sediments | Demers (2001) |
| Havre Saint-Pierre | Québec, Canada | sandy delta + marine clay deposits | Demers (2001) |
| Hilleren | Norway | Sensitive to quick clay | Long et al. (2009) |
| Jonquière | Québec, Canada | Clay + thin peat deposit | Demers (2001) |
| La Baie | Québec, Canada | Silty Clay Deposit | Delisle & Leroueil (2000) |
| Les Cèdres | Québec, Canada | Thick Marine Clay | Demers (2001) |
| Louiseville | Québec, Canada | Marine Clay Deposit | Leroueil & Hamouche (2003) |
| Mascouche | Québec, Canada | Marine Sediment | Demers (2001) |
| Maskinonge | Québec, Canada | finely stratified marine clay deposit | Roy (1990) |
| Massena IDA | NY, USA | Soft lightly overconsolidated | Lutenegger & Kabir (1987; 1988) |
| Massena MHS | NY, USA | Sensitive aged Leda clay | Lutenegger & Kabir (1987; 1988) |
| Massena RRC | NY, USA | Silty lightly overconsolidated | Lutenegger & Kabir (1988) |
| Massena SLS | NY, USA | Aged Leda clay | Lutenegger & Kabir (1988) |
| Massueville | Québec, Canada | Silty Clay | Demers (2001) |

| Site | Location | Soil Description | Reference(s) |
|---|---|---|---|
| Matagami | Québec, Canada | Aged normally consolidated Leda clay | Tavenas et al. (1982) |
| NRCC | Ontario, Canada | Normally consolidated aged Leda clay | Konrad (1987) |
| Ottawa STP | Ontario, Canada | Aged Leda clay | Konrad & Law (1987) |
| Os | Norway | Sensitive Clayey Silt | Long et al. (2010) |
| Port Cartier | Québec, Canada | silty-clay sediments | La flamme & Leroueil (1999) |
| Rimouski | Québec, Canada | Silty clay marine sediments | Demers (2001) |
| Saint Adelphe | Québec, Canada | Champlain Sea Clay | Demers (2001) |
| Saint Alban | Québec, Canada | Champlain Sea Clay | Levesque et al. (2007) |
| Saint Boniface | Québec, Canada | Quaternary Marine sediments | Demers (2001) |
| Saint Esprit | Québec, Canada | Silty Clay Deposit | Bouclin (1990); Grondin et al., (1991) |
| Saint Hilaire | Québec, Canada | Sensitive lightly overconsolidated Leda | Lafleur et al. (1988); Chiasson et al. (1995) |
| Saint Jean Vianney | Québec, Canada | Very sensitive clay | Zebdi (1987); Demers (2001) |
| Saint Marcel | Québec, Canada | Aged Leda clay | Konrad & Law (1987) |
| Saint Polycarpe | Québec, Canada | Clay Loam | Demers (2001) |
| Saint-Thuribe | Québec, Canada | Champlain Sea Clay | Demers (2001) |
| South Gloucester | Ontario, Canada | Leda Clay | Bozozuk (1972) |
| Tiller | Norway | Sensitive to Quick Clay | Gylland et al. (2014); L'Heureux & Long (2016) |
| Varennes | Québec, Canada | Aged Leda clay | Konrad & Law (1987) |
| Warwick | Québec, Canada | Marine clay sediments + deltaic sands + fluvial alluvium | Demers (2001) |

Table 9.5. Compiled OCR-CPTu database listing for intact and fissured OC clays

| Site | Location | Soil Description | Reference(s) |
|---|---|---|---|
| Baton Rouge | LA, USA | Overconsolidated fissured Clay | Chen & Mayne (1994) |
| Brent Cross | UK | Highly Overconsolidated fissured London clay | Hight et al. (2003) |
| Canons Park | UK | HOC fissured London clay | Hight et al. (2003); Powell & Lunne (2005) |
| Cowden | UK | Hard glacial clay till | Hight et al. (2003) |
| Kringalik Plateau | Arctic, Canada | Fissured Beaufort Sea clay | Hughes et al. (1984); Jefferies et al. (1987) |
| Madingley | UK | Fissured Gault clay | Lunne et al. (1986); Jardine et al. (2015) |
| Gullfaks | The North Sea | Stiff fissured clay | Lunne et al. (1985) |
| Surrey | UK | Fissured HOC London Clay | Long & O'Riordan (1988) |
| Taranto | Italy | Cemented Highly Overconsolidated Clay | Battaglio et al. (1986); Jamiolkowski et al. (1988) |
| Tarsuit | Arctic, Canada | Fissured offshore clay | Crooks et al. (1988); Jefferies et al. (1988) |

Using the equations defining the cone tip resistance ($q_t$) and porewater pressure ($u_2$) with alternate shear-induced porewater definitions, cone bearing factor ($N_{kt}$) from Lu et al. (2004), and normalized shear strength ratio (S) from Dafalias (2002), one can obtain expressions relating the overconsolidation ratio (OCR) and normalized piezocone parameters: $Q = (q_t - \sigma_{vo})/\sigma_{vo}'$, $Q_u = (q_t - u_2)/\sigma_{vo}'$, and $U^* = (u_2-u_o)/\sigma_{vo}'$, as presented in the following section. Since the vertical DSS mode was chosen as the appropriate mode for defining the shear-induced excess porewater pressures while calibrating the undrained shear strength model, full derivation for vertical DSS mode for obtaining the OCR expressions is presented herein. The full derivations with accompanying plots for the

remaining four alternative definitions of shear-induced pore water pressure are presented in **Appendix I**.

Derivation of OCR as a function of normalized cone resistance (Q)

$$s_u = S^* OCR^{\Lambda} \sigma'_{vo}$$

$$N_{kt} = \frac{q_{net}}{s_u}$$

$$OCR^{\Lambda} = \frac{q_{net}}{(N_{kt})(S^* \cdot \sigma'_{vo})}$$

$$N_{kt} = 3.4 + 1.6 \ln I_R - 1.9\Delta + 1.3\alpha_c$$

$$\Delta = \frac{\sigma'_{vo} \cdot (1 - K_o)}{2 s_u} = \frac{\sigma'_{vo} \cdot (1 - K_o)}{2 \cdot S^* OCR^{\Lambda} \sigma'_{vo}}$$

$$OCR^{\Lambda} = \frac{(q_{net}/\sigma'_{vo})}{(S^*)[3.4 + 1.6 \ln I_R - \frac{1.9 \cdot (1 - K_o)}{2 \cdot S^* OCR^{\Lambda}} + 1.3\alpha_c]}$$

$$OCR^{\Lambda} = \frac{(q_{net}/\sigma'_{vo})}{(S^*)[3.4 + 1.6 \ln I_R + 1.3\alpha_c] - \frac{0.9\,5 \cdot (1 - K_o)}{OCR^{\Lambda}}}$$

$$OCR^{\Lambda} \{ (S^*)[3.4 + 1.6 \ln I_R + 1.3\alpha_c] - \frac{0.9\,5 \cdot (1 - K_o)}{OCR^{\Lambda}} \} = (q_{net}/\sigma'_{vo})$$

$$OCR^{\Lambda} \{ (S^*)[3.4 + 1.6 \ln I_R + 1.3\alpha_c] \} - 0.9\,5 \cdot (1 - K_o) = (q_{net}/\sigma'_{vo})$$

$$OCR^{\Lambda} \{ (S^*)[3.4 + 1.6 \ln I_R + 1.3\alpha_c] \} = (q_{net}/\sigma'_{vo}) + 0.9\,5 \cdot (1 - K_o)$$

$$OCR^{\Lambda} = \frac{(q_{net}/\sigma'_{vo}) + 0.95\,(1 - K_o)}{(S^*)(3.4 + 1.6 \ln {}_R + 1.3\alpha_C)}$$

$$OCR = \left[\frac{(q_{net}/\sigma'_{vo}) + 0.95\,(1 - K_o)}{(S^*)(3.4 + 1.6 \ln {}_R + 1.3\alpha_C)}\right]^{(1/\Lambda)} \quad [9.30]$$

**Figure 9.35** presents the contours for the OCR versus Q for parametric ranges of effective friction angles and rigidity index values. It is evident that generated predictions cover most of the entire compiled database.

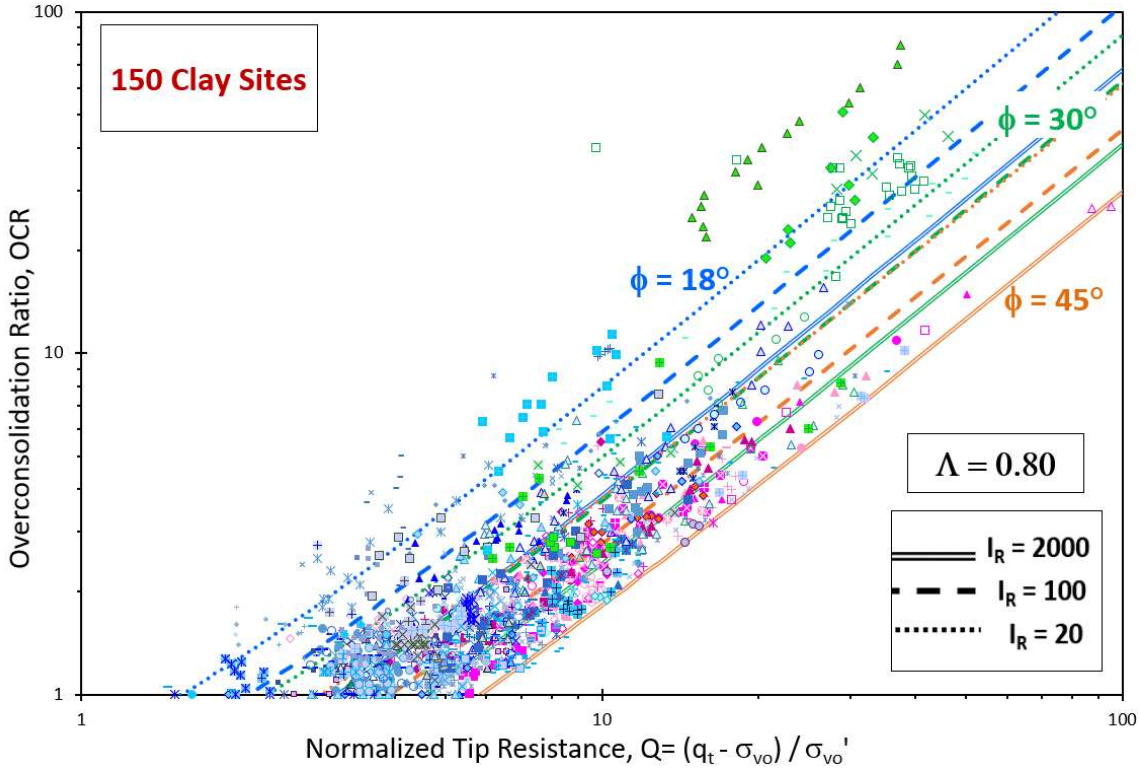


Figure 9.35. Overconsolidation ratio versus normalized cone tip resistance (Q) for parameter ranges of effective friction angle and rigidity index

Derivation of OCR as a function of normalized effective cone resistance ($Q_u$)

$$N_{kt} = \frac{q_{net}}{s_u} = \frac{q_t - \sigma_{vo}}{s_u}$$

$$q_t = \sigma_{vo} + N_{kt} \cdot s_u$$

$$\Delta u = \frac{4}{3} \cdot \ln I_R \cdot s_u + \sigma'_{vo} \cdot (1 - \frac{1}{2}\cos\phi' \cdot OCR^{\Lambda})$$

$$u_2 = u_o + \frac{4}{3} \cdot \ln I_R \cdot s_u + \sigma'_{vo} \cdot (1 - \frac{1}{2}\cos\phi' \cdot OCR^{\Lambda})$$

$$q_t - u_2 = [\sigma_{vo} + N_{kt} \cdot s_u] - u_o - [\frac{4}{3} \cdot \ln I_R \cdot s_u + \ \sigma'_{vo}(1 - \frac{1}{2}\cos\phi' \cdot OCR^{\Lambda})]$$

$$q_t - u_2 = \sigma'_{vo}\left(\frac{1}{2}\cos\phi' \cdot OCR^{\Lambda}\right) + \ s_u\ [\ N_{kt} - \ \frac{4}{3} \cdot \ln I_R]$$

$$\frac{[q_t - u_2]}{\sigma'_{vo}} = \ \left(\frac{1}{2}\cos\phi' \cdot OCR^{\Lambda}\right) + \frac{s_u}{\sigma'_{vo}}\ \left[N_{kt} - \ \frac{4}{3} \cdot \ln I_R\right]$$

$$\frac{[q_t - u_2]}{\sigma'_{vo}} = \ \left(\frac{1}{2}\cos\phi' \cdot OCR^{\Lambda}\right) + S^* OCR^{\Lambda}\left[N_{kt} - \ \frac{4}{3} \cdot \ln I_R\right]$$

$$\frac{[q_t - u_2]}{\sigma'_{vo}} = \ OCR^{\Lambda}\{\left(\frac{1}{2}\cos\phi'\right) + S^*\left[N_{kt} - \ \frac{4}{3} \cdot \ln I_R\right]\}$$

$$OCR^{\Lambda} = \ \frac{(q_t - u_2/\sigma'_{vo})}{(N_{kt} - 1.33\ln\ _R)(S^*) + 0.5\ cos\emptyset}$$

By expanding for $N_{kt}$

$$N_{kt} = 3.4 + 1.6\ \ln I_R - 1.9\Delta + 1.3\alpha_c$$

$$\Delta = \ \frac{\sigma'_{vo} \cdot (\ 1 - K_o)}{2 s_u} = \ \frac{\sigma'_{vo} \cdot (\ 1 - K_o)}{2 \cdot S^* OCR^{\Lambda} \sigma'_{vo}}$$

$$OCR^{\Lambda} = \ \frac{(q_t - u_2/\sigma'_{vo})}{(N_{kt} - 1.33\ln I_R)(S^*) + 0.5\ cos\emptyset}$$

$$OCR^{\Lambda} = \ \frac{(q_t - u_2/\sigma'_{vo})}{\left(3.4 + 0.26\ \ln I_R - \frac{1.9(\ 1 - K_o)}{2 \cdot S^* OCR^{\Lambda}} + 1.3\alpha_c\right)(S^*) + 0.5\ cos\emptyset}$$

$$OCR^{\Lambda} = \ \frac{(q_t - u_2/\sigma'_{vo})}{(3.4 + 0.26\ \ln I_R + 1.3\alpha_c)(S^*) - \frac{0.95(\ 1 - K_o)}{OCR^{\Lambda}} + 0.5\ cos\emptyset}$$

$$OCR^{\Lambda}[(3.4 + 0.26\ \ln I_R + 1.3\alpha_c)(S^*) + 0.5\ cos\emptyset] - 0.95(\ 1 - K_o) = \ (q_t - u_2/\sigma'_{vo})$$

$$OCR^{\Lambda} = \frac{[(q_t - u_2)/\sigma'_{vo}] + 0.95\ (1 - K_o)}{(S^*)(3.4 + 0.26\ \ln\ _R + 1.3\alpha_C) + 0.5\ cos\emptyset}$$

$$OCR = [\frac{[(q_t - u_2)/\sigma'_{vo}] + 0.95\ (1 - K_o)}{(S^*)(3.4 + 0.26\ \ln\ _R + 1.3\alpha_C) + 0.5\ cos\emptyset}]^{(1/\Lambda)} \qquad [9.31]$$

**Figure 9.36** presents the OCR predictions using vertical DSS definition for the shear-induced excess pore water pressure. OCR is plotted against normalized effective cone tip resistance ($Q_u$) for three effective friction angle values and three rigidity index values. Overall, the predictive contours cover most of the intact clays (plotted in blue symbols) with some exceptions for the fissured and sensitive clays where issues maybe encountered with their pore water pressure readings.

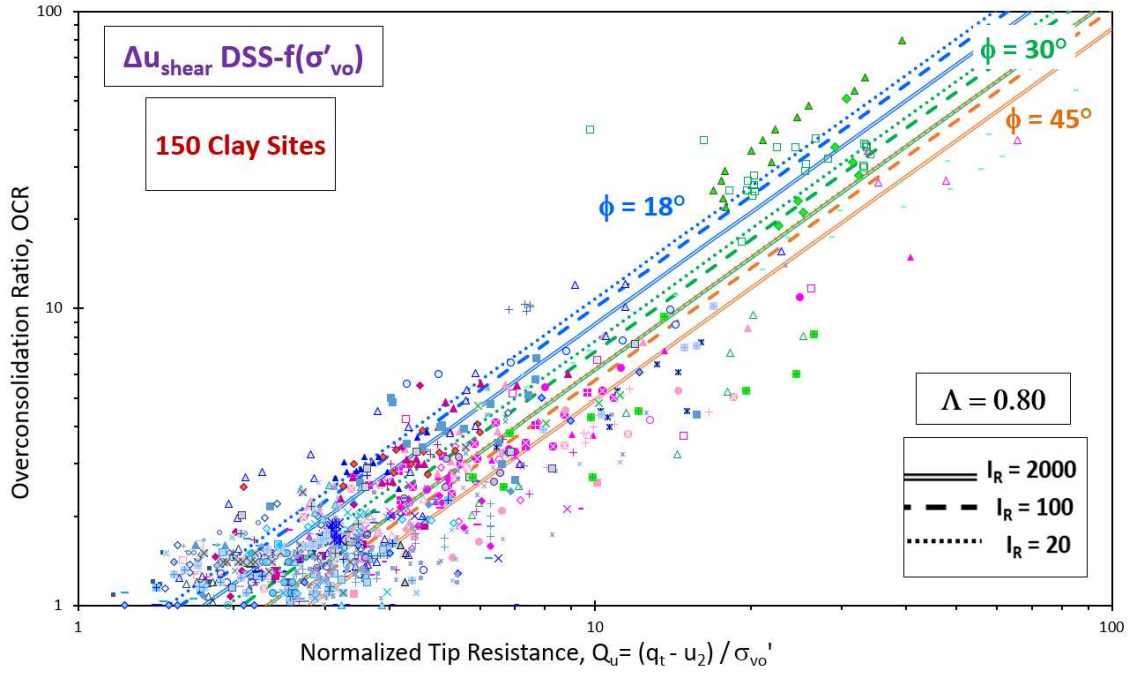


Figure 9.36. Overconsolidation ratio versus normalized effective cone tip resistance ($Q_u$) for shear-induced excess porewater pressure from DSS-f($\sigma'_{vo}$) for different effective friction angle and rigidity index values

## Derivation of OCR as a function of normalized porewater pressure (U*)

$$s_u = S^* OCR^{\Lambda} \sigma'_{vo}$$

$$\Delta u = \Delta u_{oct} + \Delta u_{sh}$$

$$\Delta u_{oct} = \frac{4}{3} \cdot \ln I_R \cdot s_u$$

$$\Delta u_{sh} = \sigma'_{vo} \cdot (1 - \frac{1}{2}\cos\phi' \cdot OCR^{\Lambda})$$

$$\Delta u = \frac{4}{3} \cdot \ln I_R \cdot s_u + \sigma'_{vo} \cdot (1 - \frac{1}{2}\cos\phi' \cdot OCR^{\Lambda})$$

$$\frac{\Delta u}{\sigma'_{vo}} = \frac{s_u}{\sigma'_{vo}}\left[\frac{4}{3} \cdot \ln I_R\right] + (1 - \frac{1}{2}\cos\phi' \cdot OCR^{\Lambda})$$

$$\frac{\Delta u}{\sigma'_{vo}} - 1 = \frac{s_u}{\sigma'_{vo}}\left[\frac{4}{3} \cdot \ln I_R\right] - (\frac{1}{2}\cos\phi' \cdot OCR^{\Lambda})$$

$$\frac{\Delta u}{\sigma'_{vo}} - 1 = S^* OCR^{\Lambda}\left[\frac{4}{3} \cdot \ln I_R\right] - (\frac{1}{2}\cos\phi' \cdot OCR^{\Lambda})$$

$$\frac{\Delta u}{\sigma'_{vo}} - 1 = OCR^{\Lambda} \cdot [S^* \cdot \frac{4}{3} \cdot \ln I_R - \frac{1}{2}\cos\phi']$$

$$OCR^{\Lambda} = \frac{(\Delta u / \sigma'_{vo}) - 1}{(S^*)(1.33\ ln\ _R) - 0.5cos\emptyset}$$

$$OCR = [\frac{(\Delta u / \sigma'_{vo}) - 1}{(S^*)(1.33\ ln\ I_R) - 0.5cos\emptyset}]^{(1/\Lambda)} \quad [9.32]$$

**Figure 9.37** presents the OCR predictions using vertical DSS definition for the shear-induced excess pore water pressure. OCR is plotted against normalized pore water pressure (U*) for different friction angles and different rigidity indices. The generated predictive contours cover the wide spread in the compiled data points and fit the wide range of the measured U* values.

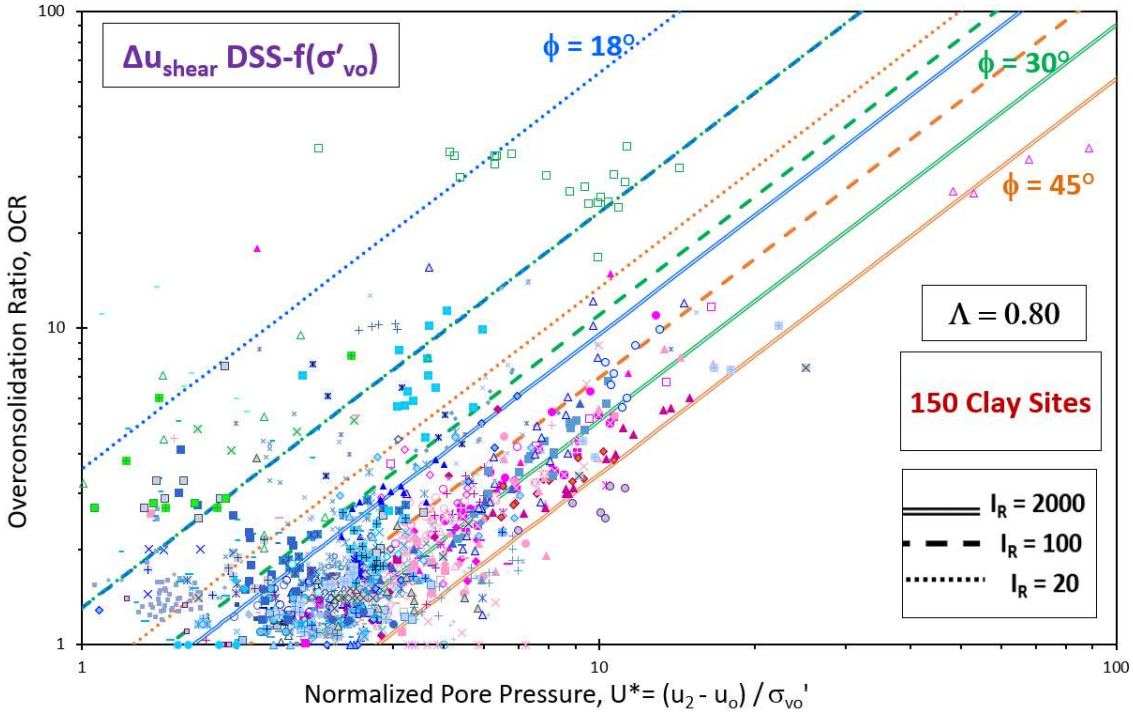


Figure 9.37. Overconsolidation ratio versus normalized porewater pressure (U*) for shear-induced excess porewater pressure from DSS-f($\sigma'_{vo}$) for different effective friction angle and rigidity index values

By considering the different plots relating the overconsolidation ratio to the normalized cone parameters, it is evident that the analytical model gives a good prediction relating OCR to the net cone resistance expressed in terms of Q as presented in Figure 9.34. Overall, the analytical model predicts the trend between OCR and change in porewater pressure ($\Delta u$) expressed in terms of U* for the different shear-induced porewater definitions with a better estimate in case of DSS-f($\sigma'_{vo}$) as observed in the undrained shear strength model. As for the effective cone resistance ($q_{eff}$) expressed in terms of $Q_u$, the model does not capture the bandwidth and the scatter in the superimposed dataset.

By examining the developed equations between OCR and the different cone readings [9.31] – [9.33], the final simplification of most equations contain the term $(1-K_0)$ in the numerator of each fraction which causes issues in dealing with the overall expression as the coefficient of lateral earth pressure ($K_0$) is typically evaluated based on the friction angle and OCR of the soil, where $K_0 = (1-\sin \phi') \cdot OCR^{\sin \phi'}$ which makes the unknown quantity OCR on both sides of the equation which is mathematically impossible to simplify further as a direct equation. It can be solved using iterations or solving by trial and error to reach the correct answer. The solution using iteration is simple and fast using a spreadsheet and the values converge after one or two trails.

**9.10 Simplified Expressions**

To compare the developed equations with the solution from SCE-CSSM framework, an approximation is applied by using input parameters for well-behaved inorganic insensitive clays where the effective friction angle ($\phi'$) = 30°, operational rigidity index ($I_R$) value of 100, smooth interface ($\alpha_c$) = zero, and $\Lambda = 1.0$.

Applying these input parameters into equation [9.30] for net cone tip resistance yields the following expression:

$$OCR = 0.309 \, (q_{net} / \sigma_{vo}') + 0.294 \, (1 - K_0) \qquad [9.33a]$$

For $\phi' = 30°$, the term $(1 - K_0)$ ranges from 0.5 at OCR = 1 to value of -0.58 at OCR = 10.

Hence, the OCR expression becomes:

$$OCR = 0.309 \, (q_{net} / \sigma_{vo}') + 0.147 \approx 0.309 \, (q_{net} / \sigma_{vo}') \text{ ------ } \sigma_p' \approx 0.309 \, (q_{net}) \qquad [9.33b]$$

Or $0.309\ (q_{net} / \sigma_{vo}') - 0.17 \approx 0.309\ (q_{net} / \sigma_{vo}')$ ------ $\sigma_p' \approx 0.309\ (q_{net})$ [9.33c]

Which is essentially the same simplified expression obtained from SCE-CSSM framework.

Considering equation [9.31] for the effective cone tip resistance, using the same input parameters for well-behaved inorganic unsensitive clays, the equation yields to:

$$OCR = 0.595\ [(q_t - u_2) / \sigma_{vo}'] - 0.05\ (1 - K_0) \quad [9.34a]$$

For $\phi' = 30°$, the term $(1 - K_0)$ ranges from 0.5 at OCR = 1 to value of -0.58 at OCR = 10.

Hence, the OCR expression becomes:

$$OCR = 0.595\ [(q_t - u_2)/\sigma_{vo}'] - 0.025 \approx 0.595\ [(q_t - u_2)/\sigma_{vo}']$$ ------ $\sigma_p' \approx 0.595\ (q_{eff})$ [9.34b]

Or $OCR = 0.595[(q_t - u_2)/\sigma_{vo}'] + 0.029 \approx 0.595\ [(q_t - u_2)/\sigma_{vo}']$ --- $\sigma_p' \approx 0.595(q_{eff})$ [9.34c]

Which is exactly the same expression obtained within the SCE-CSSM framework.

As for the change in the porewater pressure expression ($\Delta u$) in equation [9.32], the approximate SCE-CSSM solution assumes that for soft to firm clays with OCRs < 2, the shear-induced component of measured porewater pressures is small (< 20%) of the total $u_2$ reading (Burns & Mayne 1998). Thus, it can be neglected for all practical purposes. By applying the same assumption on equation [9.32] it becomes simpler in the form:

$$OCR^{\Lambda} \approx \frac{(\Delta u / \sigma'_{vo})}{(S^*)(1.33\ \ln\ _R)} \quad [9.35a]$$

By applying the same input parameters of well-behaved clays, the expression becomes:

$$OCR \approx 0.544\ [(\Delta u) / \sigma_{vo}'] \text{ ------ } \sigma_p' \approx 0.544\ (\Delta u) \quad [9.35b]$$

Which is the same expression developed from the SCE-CSSM framework. Hence the obtained equations from the advanced analytical model are compatible with earlier research efforts and previously developed expressions.

## 9.11 Conclusions

The chapter calibrates an analytical model for profiling both the undrained shear strength and OCR of clays by using a cone bearing factor derived from finite element analyses to include the effects of rigidity index, cone interface roughness, and initial stress state. Two comprehensive CPTu databases were carefully collected: (a) undrained shear strength under triaxial compression mode; and (b) stress history, each covering a variety of clay types from well-documented worldwide geotechnical sites. An anisotropic simple plastic model was utilized in developing the link between the stress history and undrained shear strength with a rotated yield surface about the $K_0$-line. The failure mode around the penetrometer tip assigned CAUC triaxial mode to the cone tip resistance ($q_t$). For the shoulder position of penetration porewater pressures ($u_2$), an investigative study was undertaken that looked at five alternative definitions for the shear-induced excess pore water pressure around the cone. These included conventional triaxial compression, constant p' triaxial, simplified triaxial, conventional simple shear, and a rotated simple shear mode. Based on the representations and calibrations of both the undrained shear strength and OCR models, it was observed that the conventional direct simple shear mode provided better estimates and captured the correct trends within the collected databases.

# Chapter 10. CONCLUSIONS AND DIRECTION OF FUTURE RESEARCH STUDIES

## 10.1 Concluding Remarks

- The presented dissertation introduced new enhanced methodologies for better characterization of geomaterials, making full usage of the four readings of the seismic piezocone penetration test (SCPTu): cone tip resistance ($q_t$), sleeve friction ($f_s$), shoulder porewater pressure ($u_2$), and downhole shear wave velocity ($V_{s\ VH}$).
- A unified relationship between effective yield stresses of varied soil types and net cone tip resistance is explored as a power law expression where the exponent (m') is a variable that tracks with grain size. A generalized solution is developed by merging of two independent methods: (1) analytical hybrid spherical cavity expansion and critical state soil mechanics (SCE-CSSM) solution for intact clays; (2) algorithms derived from CPT calibration chamber test data on clean silica and quartz sands. A commonality in the simplified expressions of the two methods has been used to define a more global power law formulation with a yield stress exponent (m') that is extended to cover a variety of geomaterials such as clays, silts, mixed soils, and sands. Trends for fissured OC clays, sensitive soils, and organic clays were also quantified. For that purpose, a large database of 78 worldwide well-documented geotechnical sites has been compiled where both CPT data and the results of one-dimensional consolidation tests and engineering geologic information were available to detail the stress history of each site.
- Direct relationships between the yield stress exponent and the mean grain size ($D_{50}$) and average fines content (FC) were developed based on a subset database of 56 sites

covering different particle sizes. To better quantify the value of the variable exponent, it was further linked to the CPT material index ($I_c$). Four different definitions for the material index have been investigated covering the classic definition by Robertson & Wride (1998) and Robertson (2009), non-normalized SBT material index (Robertson 2010), updated Jefferies and Been (2015) definition, and finally a new definition based on contractive-dilative behavior separation (Robertson 2016). Utilization of the CPT material index provided a convenient quick means of identifying and assigning the exponent value for different geomaterials.

- Means of evaluating the rigidity index of clays are reviewed, including laboratory tests, empirical methodologies, and analytical approaches. Using the hybrid spherical cavity expansion – critical state framework, a direct CPTu expression is derived for obtaining the undrained rigidity index ($I_R$) based on cone tip resistance and porewater pressure readings, or alternate approach using their normalized quantities.
- A design chart with contour lines for parametric values of effective friction angle ($\phi'$) is presented which relates the slope parameter ($a_q$) with the evaluated rigidity index value ($I_R$). From the piezocone sounding, the slope $a_q$ is determined as a single value for any clay deposit by taking the slope of a plot of the parameter (U*-1) versus Q, or alternatively as the slope of ($u_2$ - $\sigma_{vo}$) versus ($q_t$ - $\sigma_{vo}$). The effective friction angle can be determined whether from laboratory measurements or evaluated from the NTH effective stress limit plasticity solution that relies on Q and $B_q$. By knowing the slope value and the effective friction angle, one can evaluate an operational value for the rigidity index.
- The evaluated rigidity indices are in reasonable agreement with reference laboratory-based and seismic-based in-situ approaches. The derived $I_R$ are tested in

evaluating the yield stress profiles from three expressions provided by the SCE-CSSM framework in terms of (1) net cone resistance; (2) excess porewater pressures; and (3) effective cone resistance. Twelve case studies covering well-behaved clays with different geologies from several countries were used to demonstrate the effectiveness of the proposed methodology for obtaining $I_R$. The three expressions give profiles which fully agree and match with lab reference values of $\sigma_p'$ and OCR. The solution also gives a very good agreement with lab-measured undrained shear strengths using the corresponding cone bearing factor ($N_{kt}$).

- Conventional soil behavioral type (SBT) classification systems using CPTu data often perform unreliably in detecting sensitive and quick clays during routine site exploration with an exception for Eslami & Fellenius chart. Hence, a new SCPTu means for identifying sensitive clays is investigated by relying on estimated shear wave velocity profiles using the piezocone penetrometer readings, which are in turn compared with the actual measured $V_s$ profiles. If the two profiles agree, then well-behaved soils are likely. However, if the two profiles appreciably differ, then there is cause to require further site testing and confirm or deny the presence and occurrence of sensitive clays and/or structured soils.
- Previously published correlations are not suitable for the sensitive clays under study, hence, a special database of 20 sensitive clays from Northern USA and Canada has been collected and used to develop two modified correlations for estimating shear wave velocity in sensitive clays are introduced.
- For sensitive and structured clays, an acknowledged strain incompatibility occurs during triaxial compression, such that the deviator stress ($\sigma_1 - \sigma_3$) reaches a peak strength

at low strains ($\varepsilon \approx 1\%$) whereas excess porewater pressures are maximized later at much higher strains ($\varepsilon > 15\%$). Thus, the effective strengths at these points can both be implemented to represent these phenomena. This stress-strain and porewater pressure behavior is witnessed within different sensitive and/or structured clays under study: (1) Leda clay at Gloucester, Ontario; (2) quick Tiller clay in Norway, and (3) structured Amherst varved clay in Massachusetts.

- A slightly modified SCE-CSSM solution is presented that incorporates the following both definitions of mobilized effective stress friction angles ($\phi'$): (1) maximum deviatoric stress ($\phi'_{qmax}$) and (2) maximum obliquity ($\phi'_{MO}$). In concert with field CPTU soundings, these correspond to the measured cone tip resistances ($q_t$) and penetration porewater pressures ($u_2$), respectively. The derivation provides three formulations for clay stress history for evaluating OCR from CPTu in terms of (a) net resistance ($q_t - \sigma_{vo}$), (b) excess porewater pressures ($u_2 - u_0$), and (c) effective cone resistance ($q_t - u_2$), all of which agree well with the benchmark laboratory consolidation testing and corresponding profiles of preconsolidation stress at the three selected sensitive clay sites.
- The modified approach provides a methodology to obtain operational rigidity index ($I_R$) which is in reasonable agreement with reference laboratory based and seismic-based in-situ approaches. The proposed method gives a very good agreement with lab-measured undrained shear strength values using corresponding cone bearing factors.
- The hybrid SCE-CSSM framework is used to interpret flow parameters from piezodissipation tests taken in the sensitive Champlain Sea clays at the Gloucester test site, specifically to directly evaluate the profiles of coefficient of consolidation ($c_{vh}$) and permeability (k) by matching theoretical curves with field measured dissipation data that

agree well with independent laboratory and field measured reference values. This solution can handle both monotonic and dilatory porewater pressure behavior. A simplified approach is also presented for soils exhibiting a monotonic porewater pressure response.

- Indirect means of detecting organic soils by in-situ piezocone penetration tests (CPTu) which are available were detailed, including the well-known soil behavior type (SBT) charts. A database of 23 organic clay sites all tested using CPTu was compiled for calibration and verification purposes. For SBT charts having predefined organic soil zones (Robertson et al. 1986, Robertson 1990; Jefferies & Been 2015), the zone boundaries, in general, do not adequately detect the correct soil type for organic soils. Specifically, organic clay sites have a broader range of CPT material index ranging from 2.8 to 3.7 and not restricted to the proposed $I_c > 3.6$ as in the well-known 9-zone SBT charts of Robertson (1990, 2009).
- The behavior of organic clays in profiling stress history is investigated using the original hybrid SCE-CSSM solution where the predictive profiles mismatch indicating the presence of abnormal soil. Upon closer inspection, it is observed that organic clays tend to have a hierarchical behavior where stress history predictions based on excess pore water pressure are the lowest followed by the net cone tip resistance then the effective cone tip resistance. Note, this order is the complete opposite to the hierarchical trend observed in sensitive clays. The stress history profiling for CPTu in organic clays follows the aforementioned power law format using an exponent $m' = 0.9$.
- An analytical model for profiling both the undrained shear strength and OCR of clays is calibrated by using a cone bearing factor derived from finite element analyses to

include the effects of rigidity index, cone interface roughness, and initial stress state. Two comprehensive CPTu databases were carefully collected: (a) undrained shear strength under triaxial compression mode; and (b) stress history, each covering a variety of clay types from well-documented worldwide geotechnical sites. An anisotropic simple plastic model was utilized in developing the link between the stress history and undrained shear strength with a rotated yield surface about the $K_0$-line.

- The failure mode around the penetrometer tip assigned CAUC triaxial mode to the cone tip resistance ($q_t$). For the shoulder position of penetration porewater pressures ($u_2$), and the investigative study was undertaken that looked at five alternative definitions for the shear-induced excess pore water pressure around the cone. These included conventional triaxial compression, constant p' triaxial, simplified triaxial, conventional simple shear, and a rotated simple shear mode. Based on the representations and calibrations of both the undrained shear strength and OCR models, it was observed that the conventional direct simple shear mode provided better estimates and captured the correct trends within the collected databases.

- In Appendix J, direct relationships between undrained shear strength ($s_u$) and shear wave velocity ($V_s$) were investigated. A global database was developed from well-documented clay sites with field geophysics and laboratory strength measurements was compiled and analyzed that resulted in a general expression for evaluating undrained shear strength ($s_{uTC}$) for the triaxial compression mode (CAUC or $CK_0UC$) from the downhole shear wave velocity ($V_{sVH}$).

- In Appendix K, a global database study was analyzed to produce a general expression relating effective preconsolidation stress ($\sigma_p'$) to shear wave velocity ($V_s$) for

clays. The data were collected from 64 worldwide well-documented natural soils primarily covering primarily NC to LOC clays, as well as some OC to HOC fissured clays.

## 10.2 Recommendations for future work

- Further calibration of the spherical cavity expansion-critical state soil mechanics (SCE-CSSM) solution that provides the direct CPTu value of undrained rigidity index that can be used towards assessing the coefficient of consolidation ($c_v$) and hydraulic conductivity (k) from porewater pressure dissipation tests.
- Cross checking of these advanced methodologies using newly acquired data from the recently initiated national geotechnical experimentation sites in Norway, specifically investigating their stress-strain-strength response, stiffness, stress history, and flow properties.
- Case study comparisons between the UC-Davis empirical approach for estimating the rigidity index ($I_R$) of clays from SCPTu data (Krage et al. 2014) with the new direct CPTu method from SCE-CSSM, as discussed in this study.
- Modifications for adjusting the SCE-CSSM framework to handle organic soils and profile their undrained shear strength, yield stresses, and dissipation response.
- Investigate the time-dependent deformation of organic soils by studying their creep characteristics, such as coefficient of secondary compression ($C_\alpha$), and explore possible links with site-specific aspects, including the soil mineralogy, LOI, OMC, and/or Atterberg limits.
- Check the compatibility of the two new screening methods introduced for identification of sensitive and structured clays: (1) Using measured and estimated

downhole shear wave velocity from seismic piezocone data; and (2) Comparison of yield stress profiles from the three separate CPTu expressions given by the SCE-CSSM framework.

- Explore the interrelationships between the mobilized effective stress friction angles ($\phi'$) for sensitive and structured clays: (a) one at maximum deviatoric stress ($\phi'_{qmax}$), and (b) another at maximum obliquity ($\phi'_{MO}$) from lab testing. Work by Bjerrum and Simons (1960) has provided a nice summary of these for about 19 clays tested in both drained and undrained triaxial compression.
- Further investigation is warranted for screening organic soils and correctly quantifying the organic matter content using piezocone data. New tests involving the texture of the fibrous organic clays on the sleeve of the piezocone should be experimented, in addition to organic clays behavior in dissipation tests of the excess porewater pressure over time.

# APPENDIX A

## Soft Intact Clays:
## Piezocone Soundings,
## with Shear Wave Velocity,
## Undrained Shear Strength, and
## Stress History Data

| Site | CPTu | Shear Wave Velocity, $V_s$ | Undrained Shear Strength, $s_{u\ TC}$ | Stress History |
|---|---|---|---|---|
| Amherst | ✓ | ✓ | ✓ | ✓ |
| Anchorage | ✓ | ✓ | ✓ | ✓ |
| Ariake | ✓ | ✓ | ✓ | ✓ |
| Ballina | ✓ | ✓ | ✓ | ✓ |
| Bay of Bengal | ✓ | | ✓ | ✓ |
| Belfast | ✓ | ✓ | ✓ | ✓ |
| BBC | ✓ | ✓ | ✓ | ✓ |
| Bothkennar | ✓ | ✓ | ✓ | ✓ |
| Burswood | ✓ | ✓ | ✓ | ✓ |
| Busan | ✓ | ✓ | ✓ | ✓ |
| GOG 1 | ✓ | | ✓ | ✓ |
| GOG 2 | ✓ | | ✓ | ✓ |
| GOG 3 | ✓ | | ✓ | ✓ |
| GOG 4 | ✓ | | ✓ | ✓ |
| GOG 5 | ✓ | | ✓ | ✓ |
| GOG 6 | ✓ | | ✓ | ✓ |
| Hachirogata | ✓ | ✓ | | ✓ |
| Hamilton AFB | ✓ | | ✓ | ✓ |
| Kurihama | ✓ | ✓ | ✓ | ✓ |
| Lianyungang | ✓ | ✓ | ✓ | ✓ |
| Lierstranda | ✓ | ✓ | ✓ | ✓ |
| Newbury | ✓ | ✓ | ✓ | ✓ |
| Nong Ngu Hao | ✓ | ✓ | ✓ | ✓ |
| Northwestern University | ✓ | ✓ | ✓ | ✓ |
| Onsoy | ✓ | ✓ | ✓ | ✓ |
| Pentre | ✓ | ✓ | ✓ | ✓ |

| Site | CPTu | Shear Wave Velocity, $V_s$ | Undrained Shear Strength, $s_{u\ TC}$ | Stress History |
|---|---|---|---|---|
| Pernio | ✓ | ✓ | ✓ | ✓ |
| Pisa | ✓ | ✓ | ✓ | ✓ |
| Sarapui | ✓ | ✓ | ✓ | ✓ |
| Snorre | ✓ | | ✓ | ✓ |
| Taipei | ✓ | ✓ | ✓ | ✓ |
| Torp | ✓ | | ✓ | ✓ |
| Troll Lower | ✓ | ✓ | ✓ | ✓ |
| Troll Upper | ✓ | ✓ | ✓ | ✓ |

## Amherst, Connecticut Valley, MA, USA

Data after Hegazy (1998); DeGroot & Lutenegger (2003)

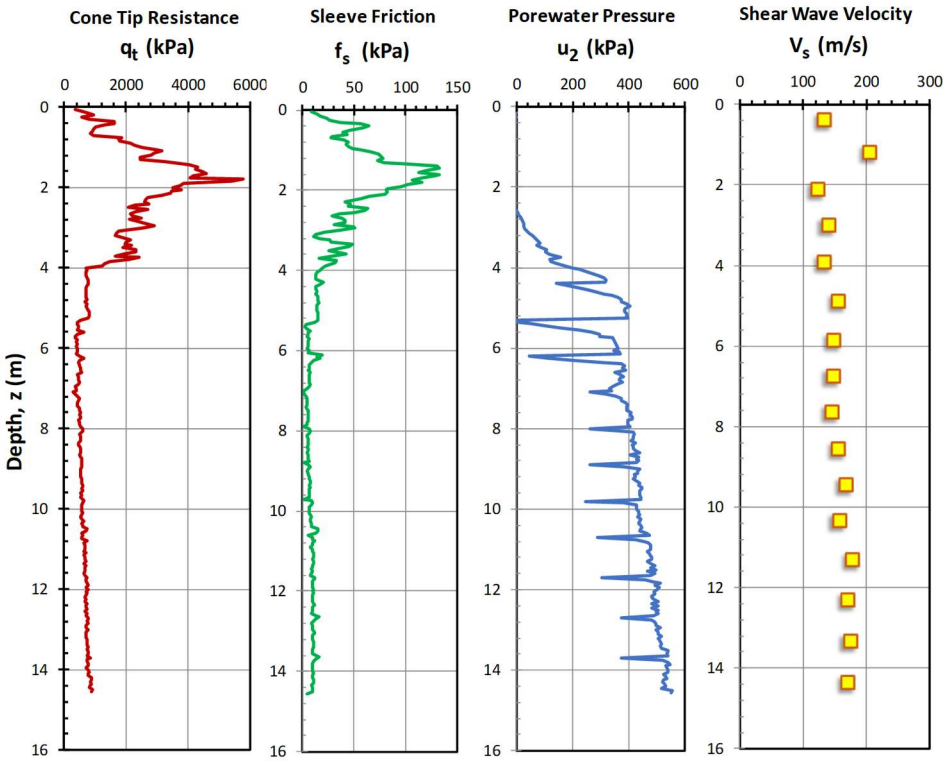


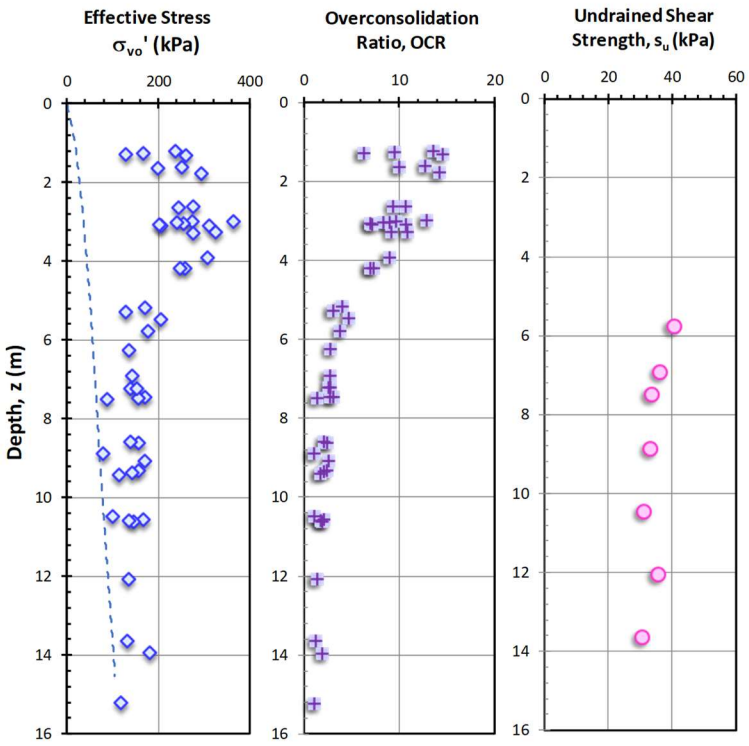

# Anchorage, Bootlegger Cove Formation, AK, USA

Data after Zapata-Medina (2012); Mayne & Pearce (2005)

Nearshore CPTu, the depth is from mean water level. The mudline or seabed starts at around 12 or 15 m.

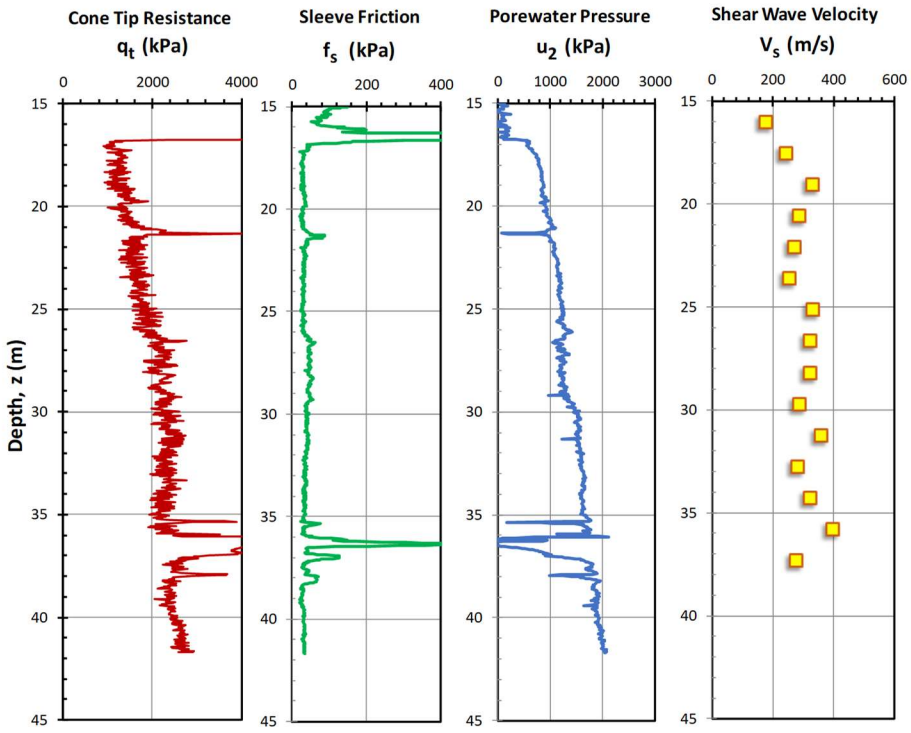


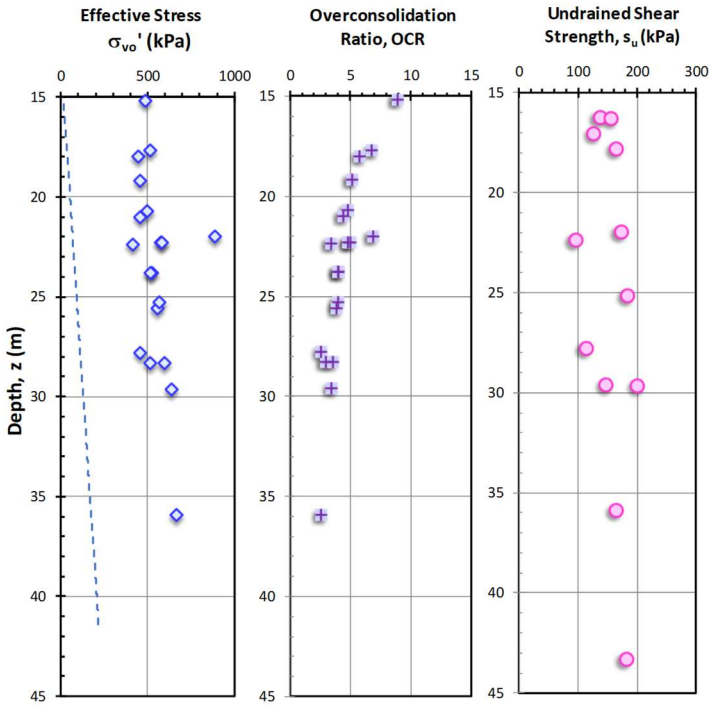

# Ariake, Japan

Data after Tanaka et al. (2001); Lunne et al. (2006)

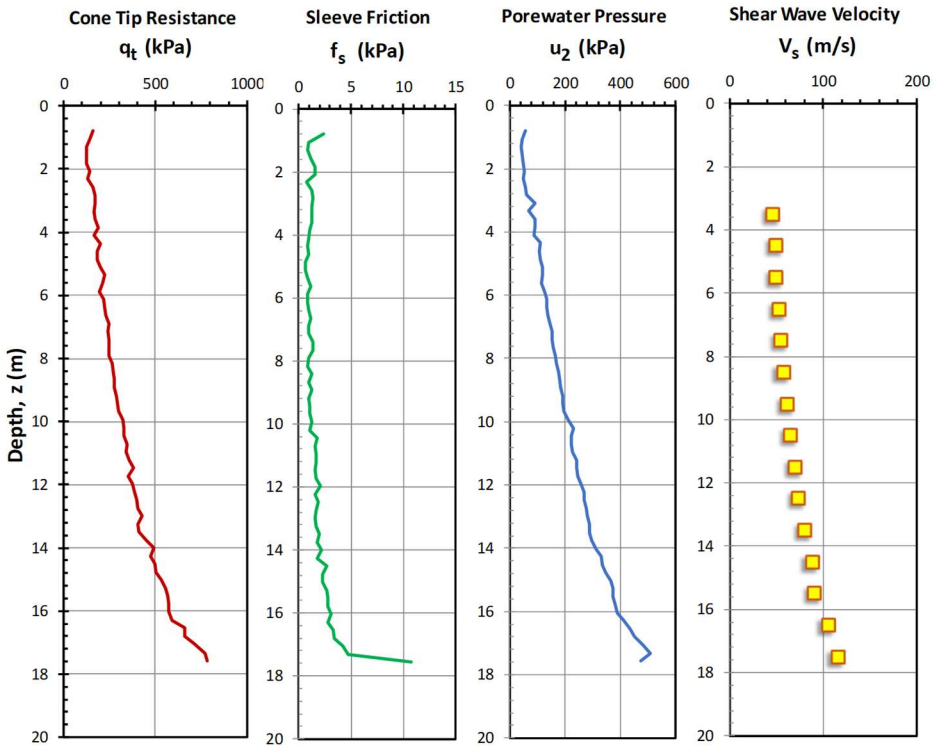


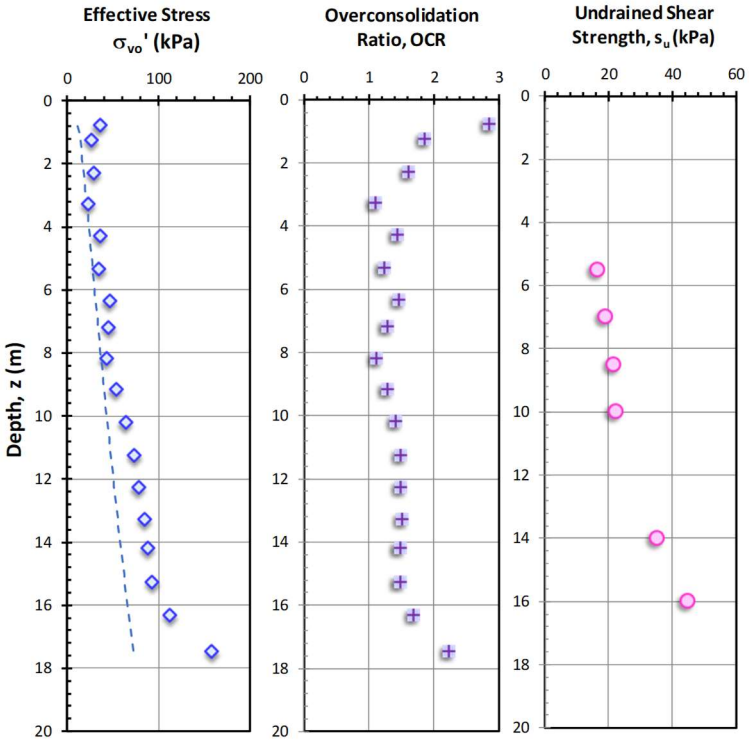

## Ballina, Australia

Data after Pineda et al. (2014)

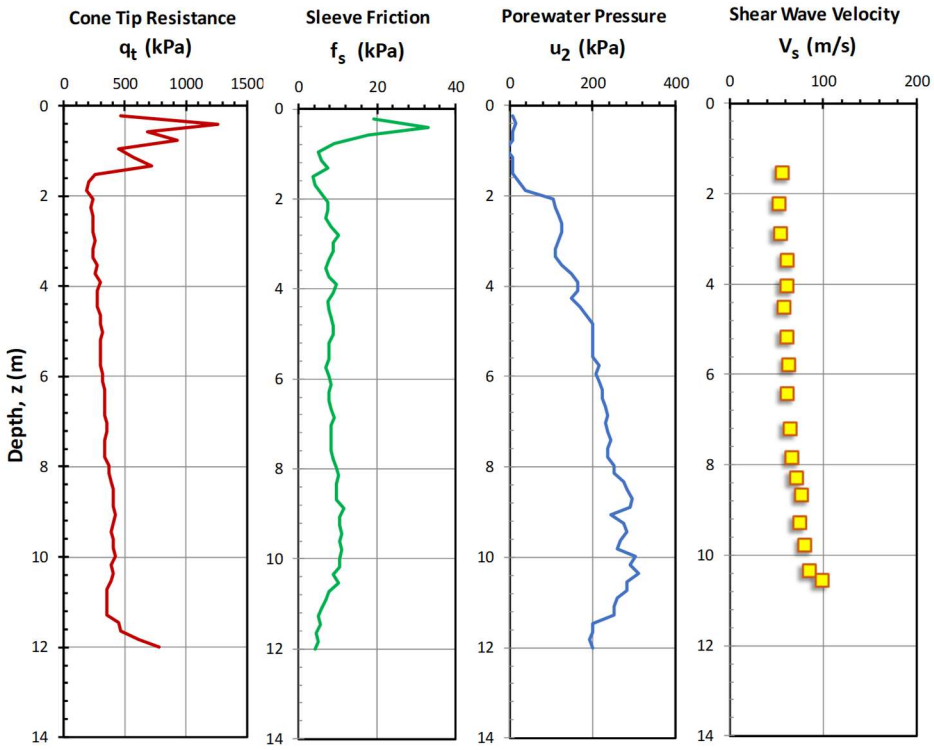


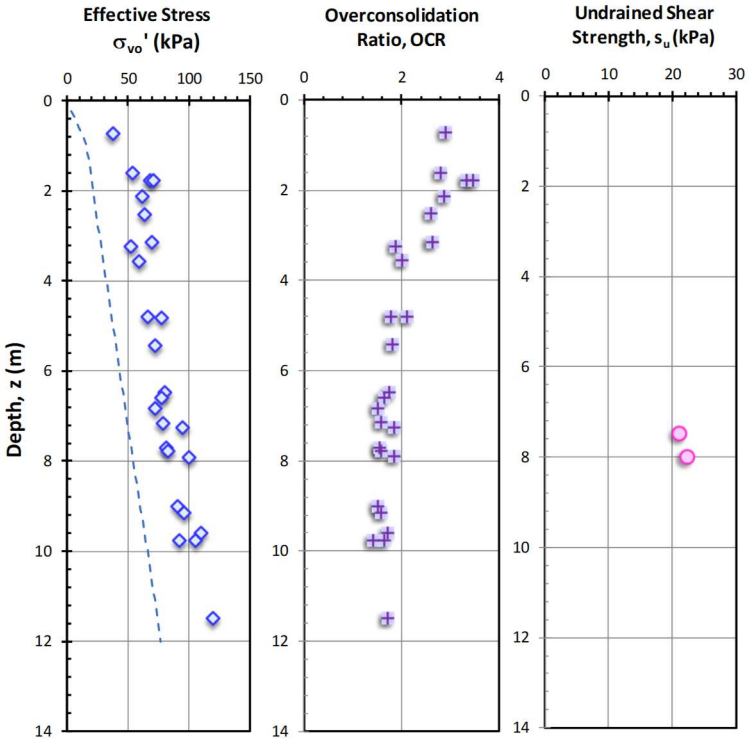

# Bay of Bengal

Data after Mayne et al. (2015)

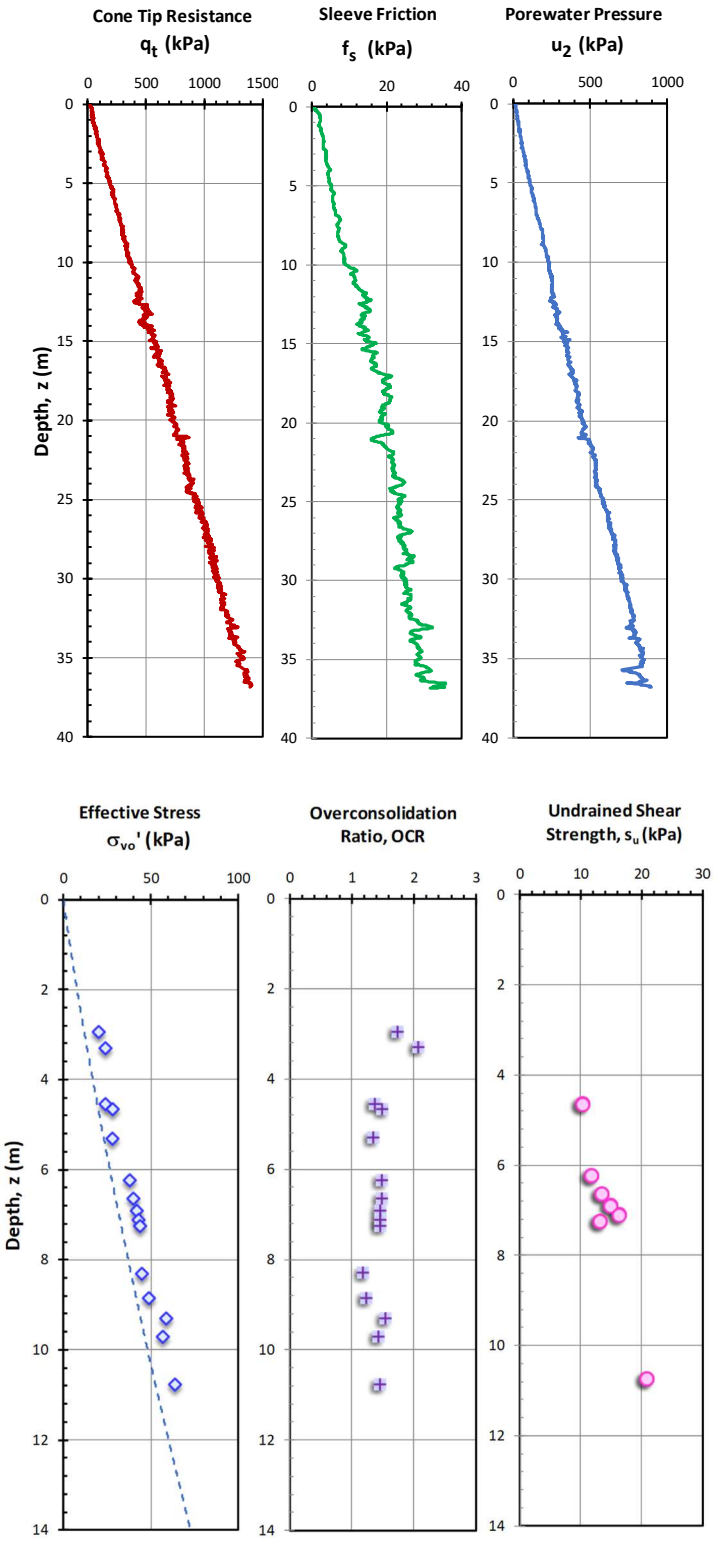

## Belfast, Ireland

Data after Crooks (1981); Lehane (2003)

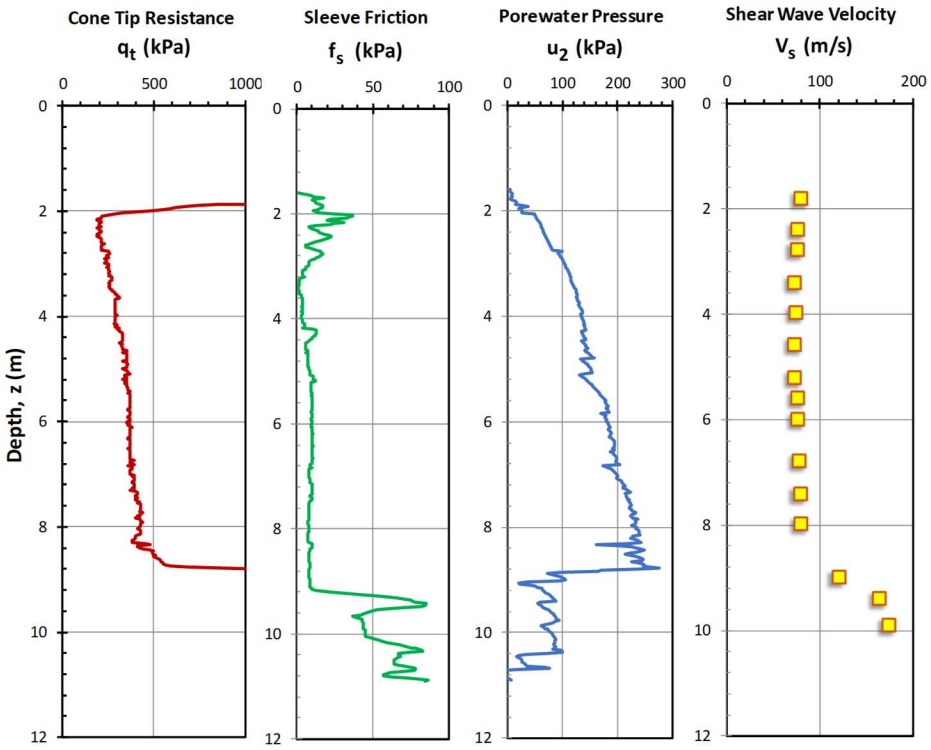


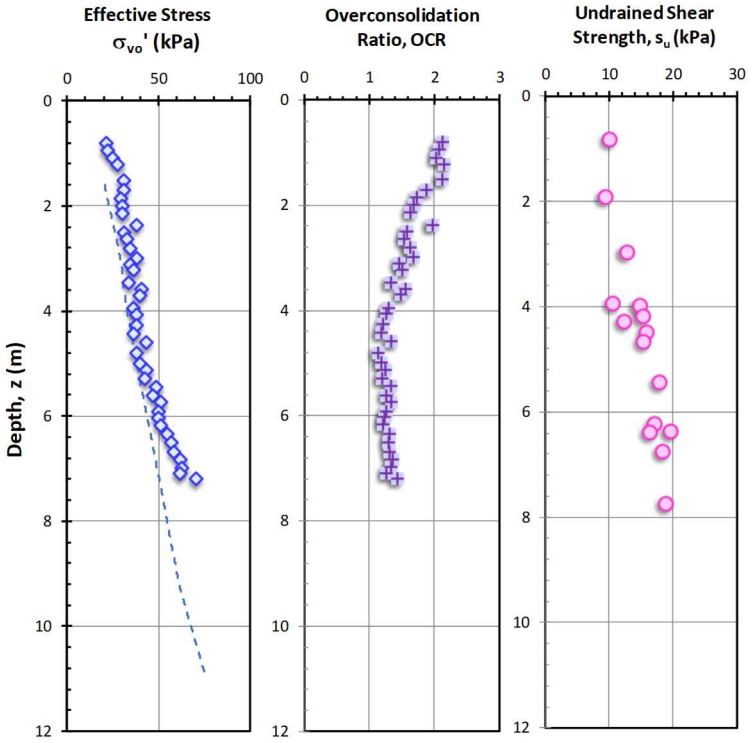

## BBC, MA, USA

Data after Whittle et al. (2001) – Sleeve friction is not reported

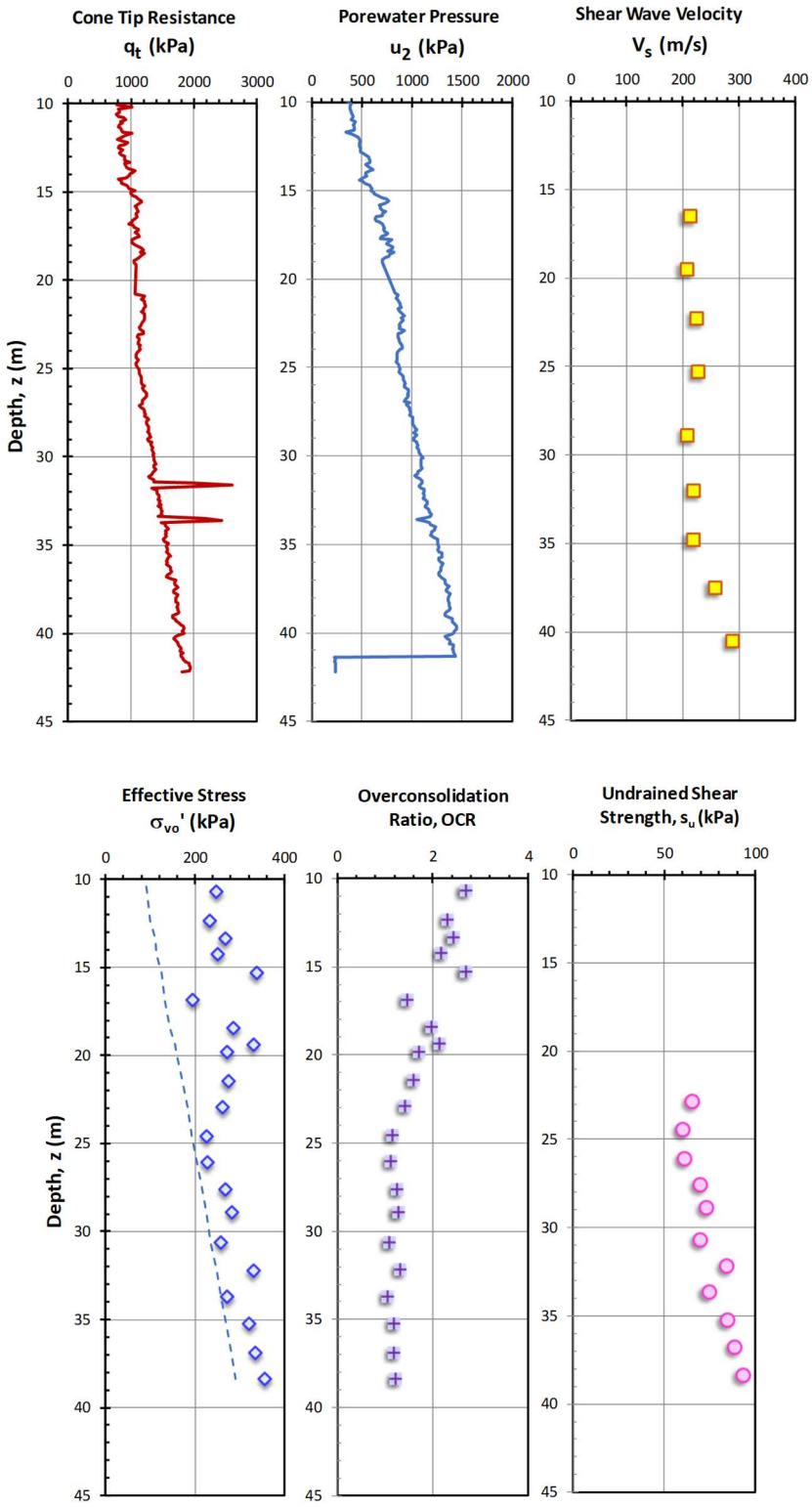

## BBC, MA, USA

Data after Baligh & Azouz (1981) – $u_1$ measurement

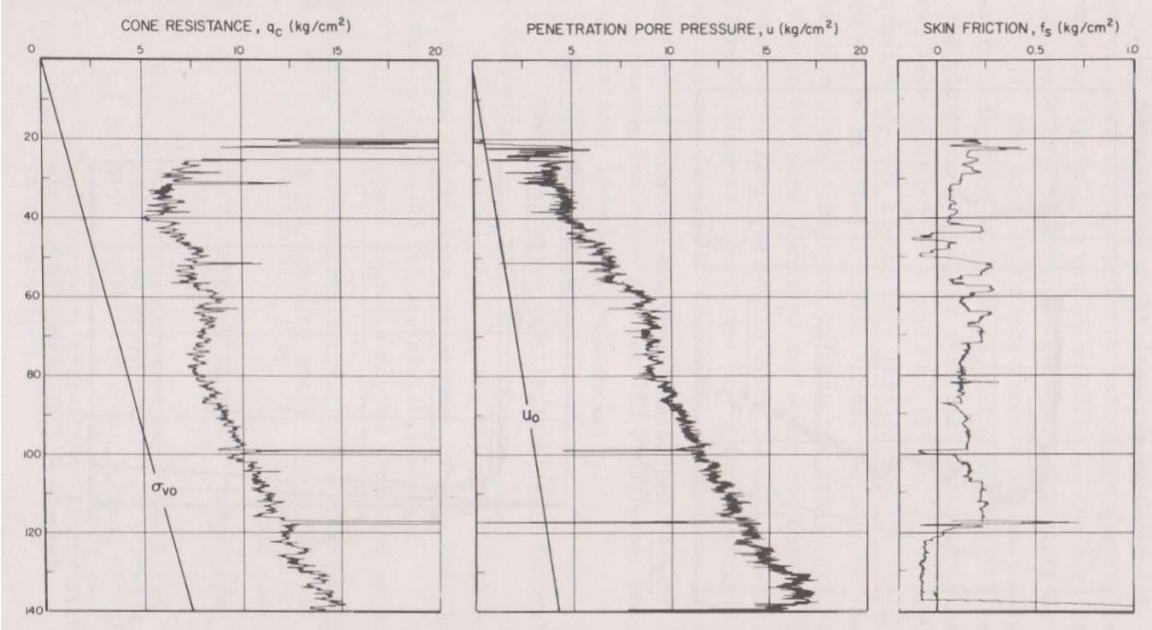

## Bothkennar, Scotland, UK

Data after Hight et al. (2003); Powell & Lunne (2005)

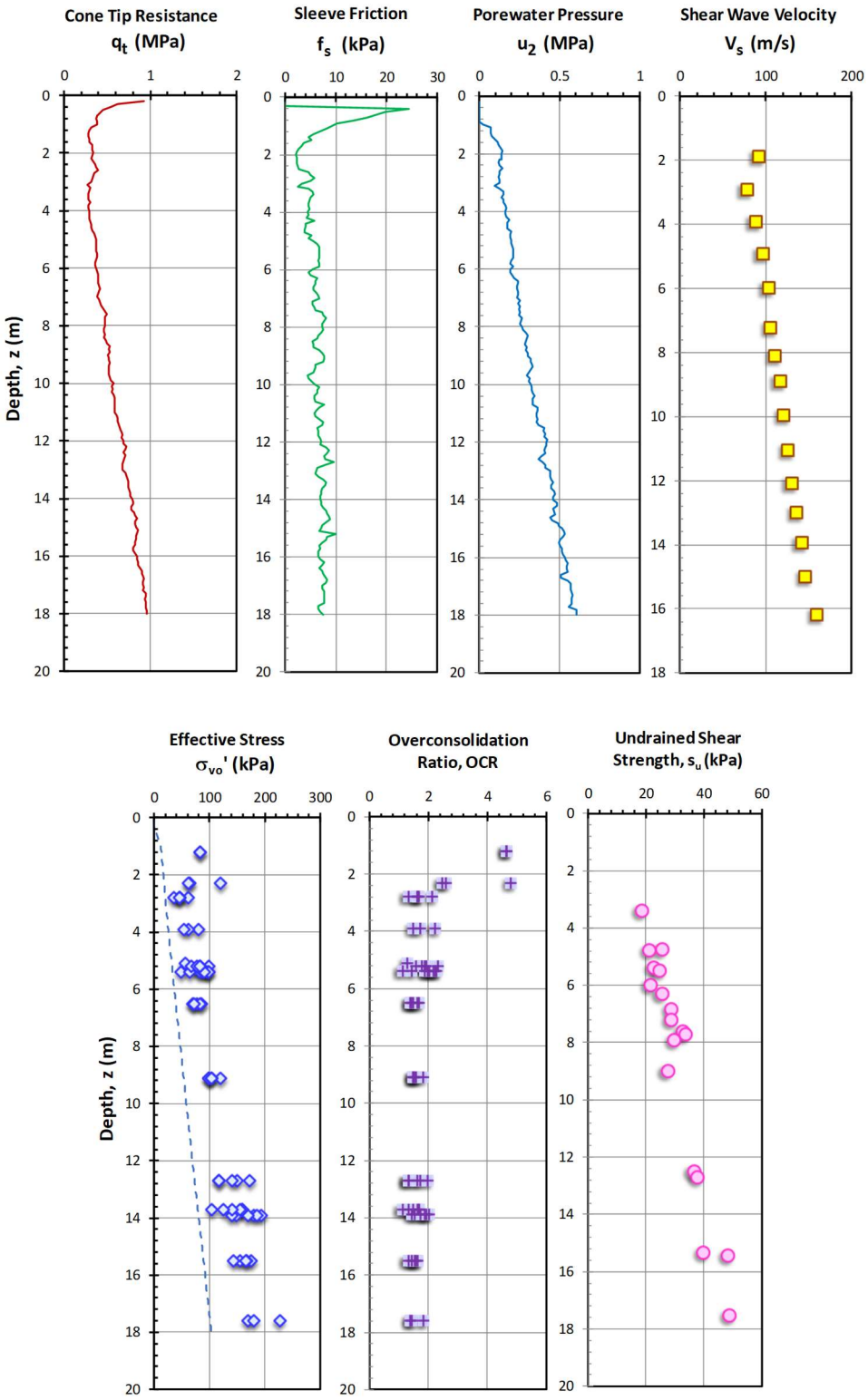

## Burswood, Australia

Data after Chung (2005); Landon (2007); Low et al. (2011)

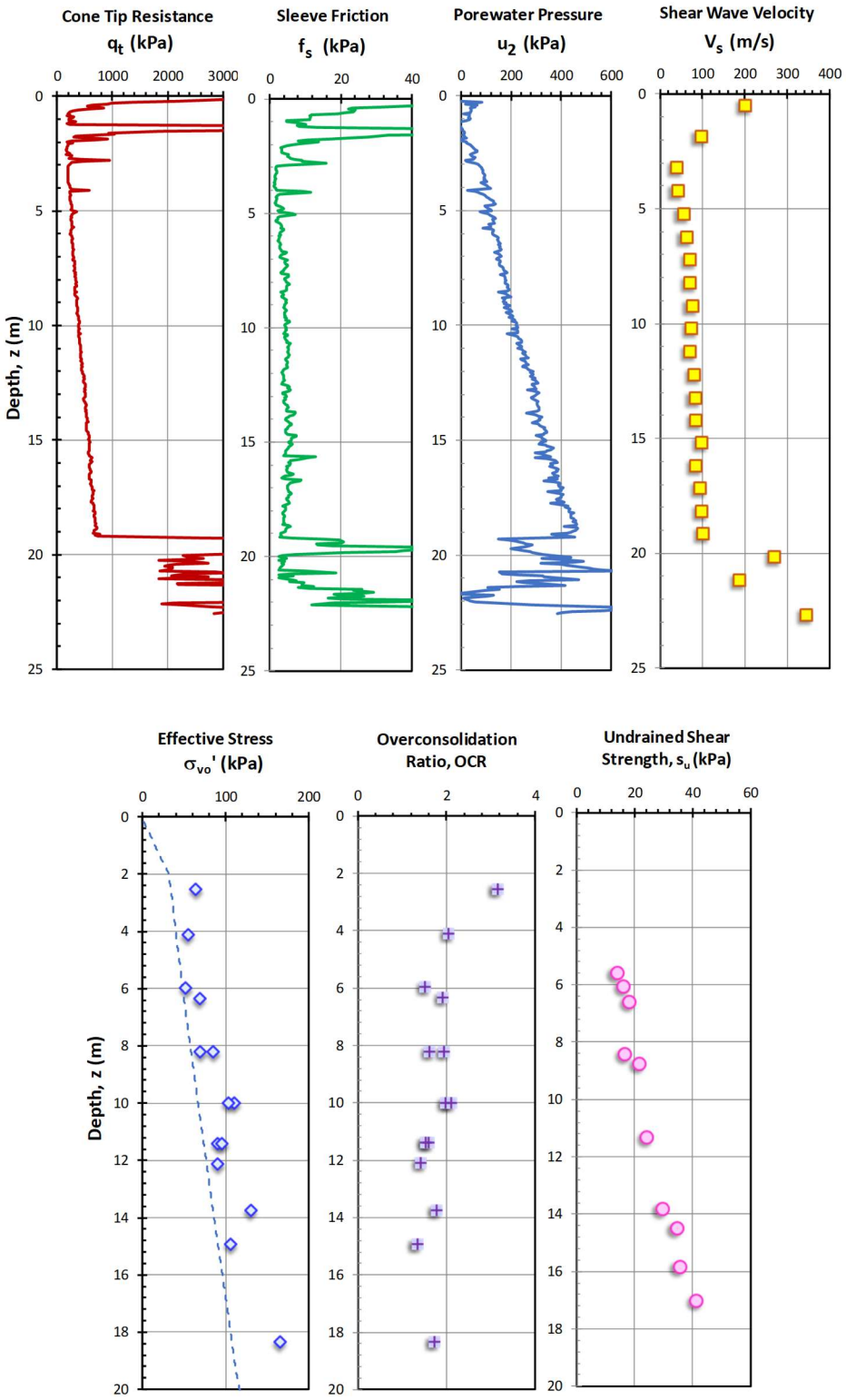

# Busan, Korea

Data after Chung et al. (2011, 2012)

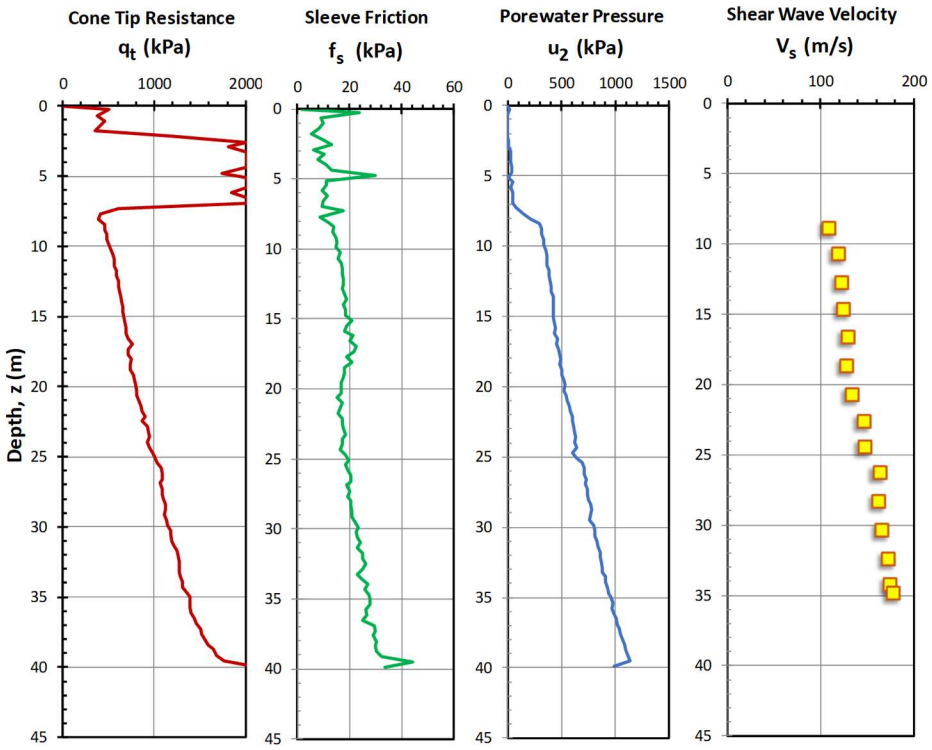


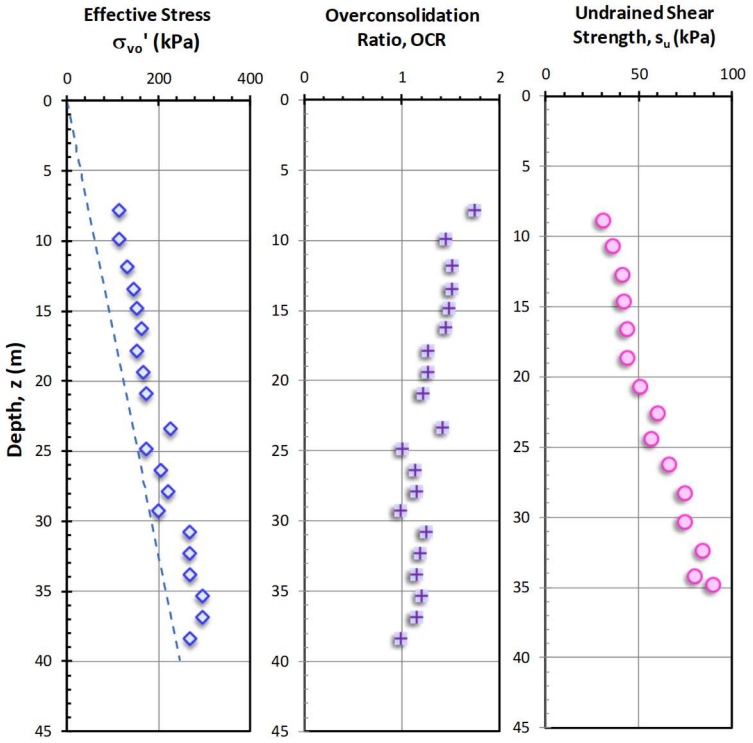

# GOG 1, Gulf of Guinea, West Africa

Data after Lunne at al. (2006)

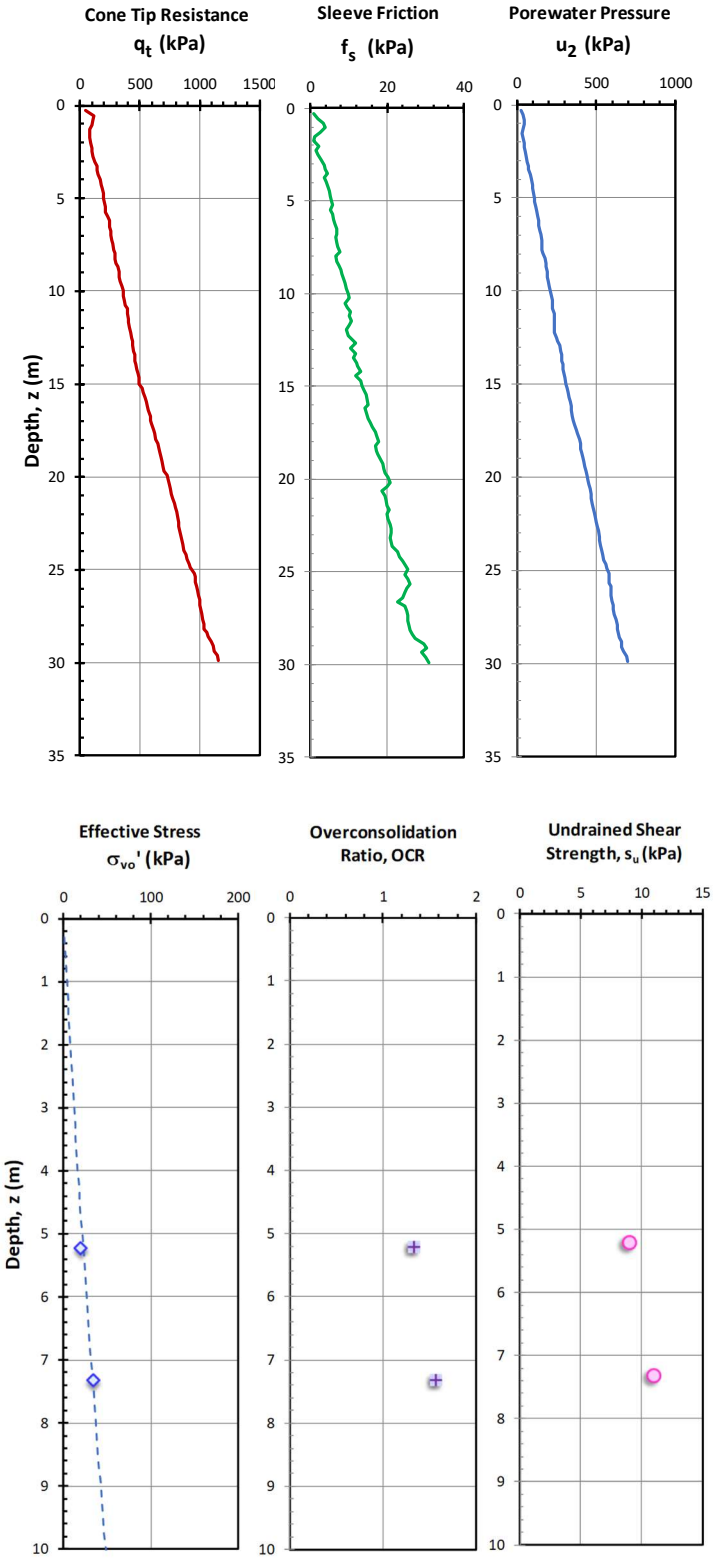

# GOG 2, Gulf of Guinea, West Africa

Data after Mayne et al. (2015)

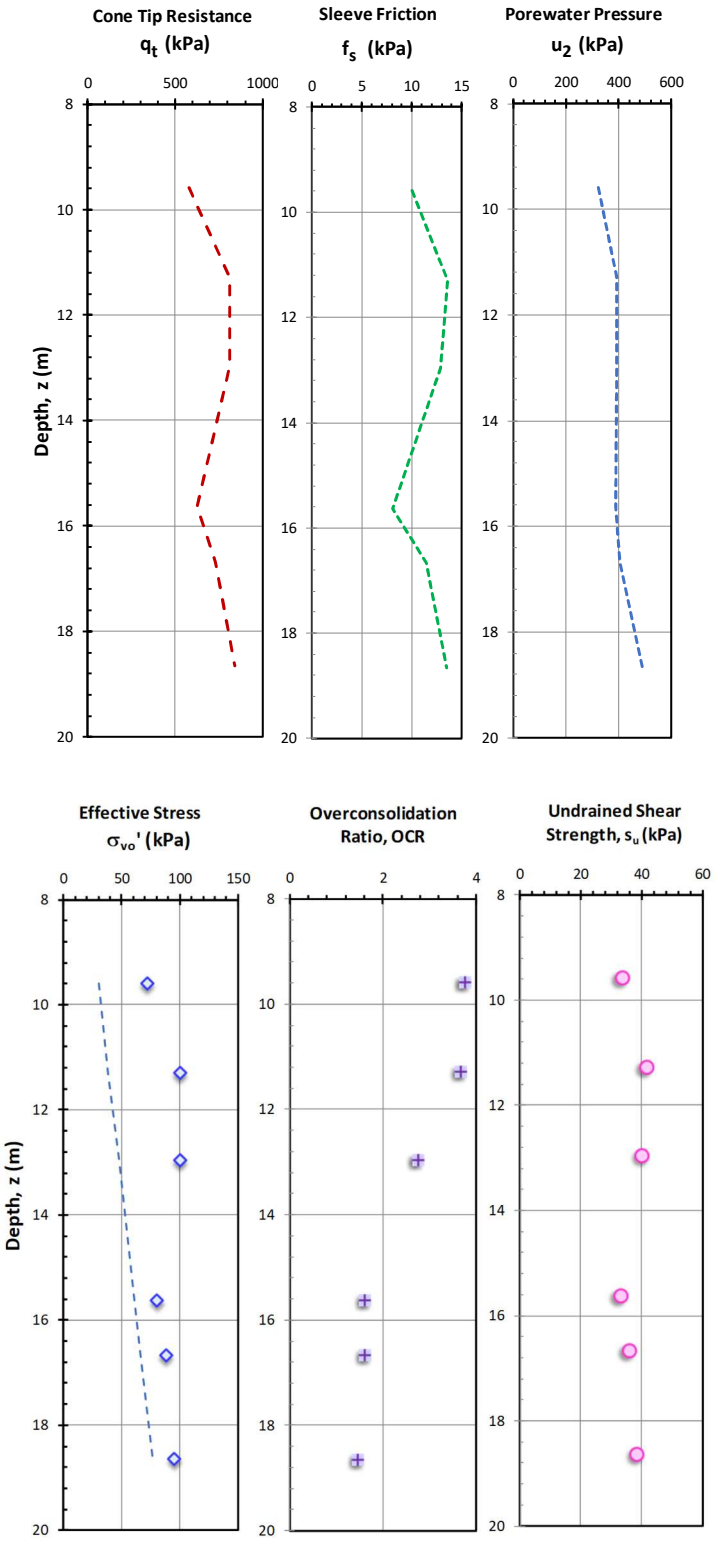

# GOG 3, Gulf of Guinea, West Africa

Data after Lunne at al. (2006)

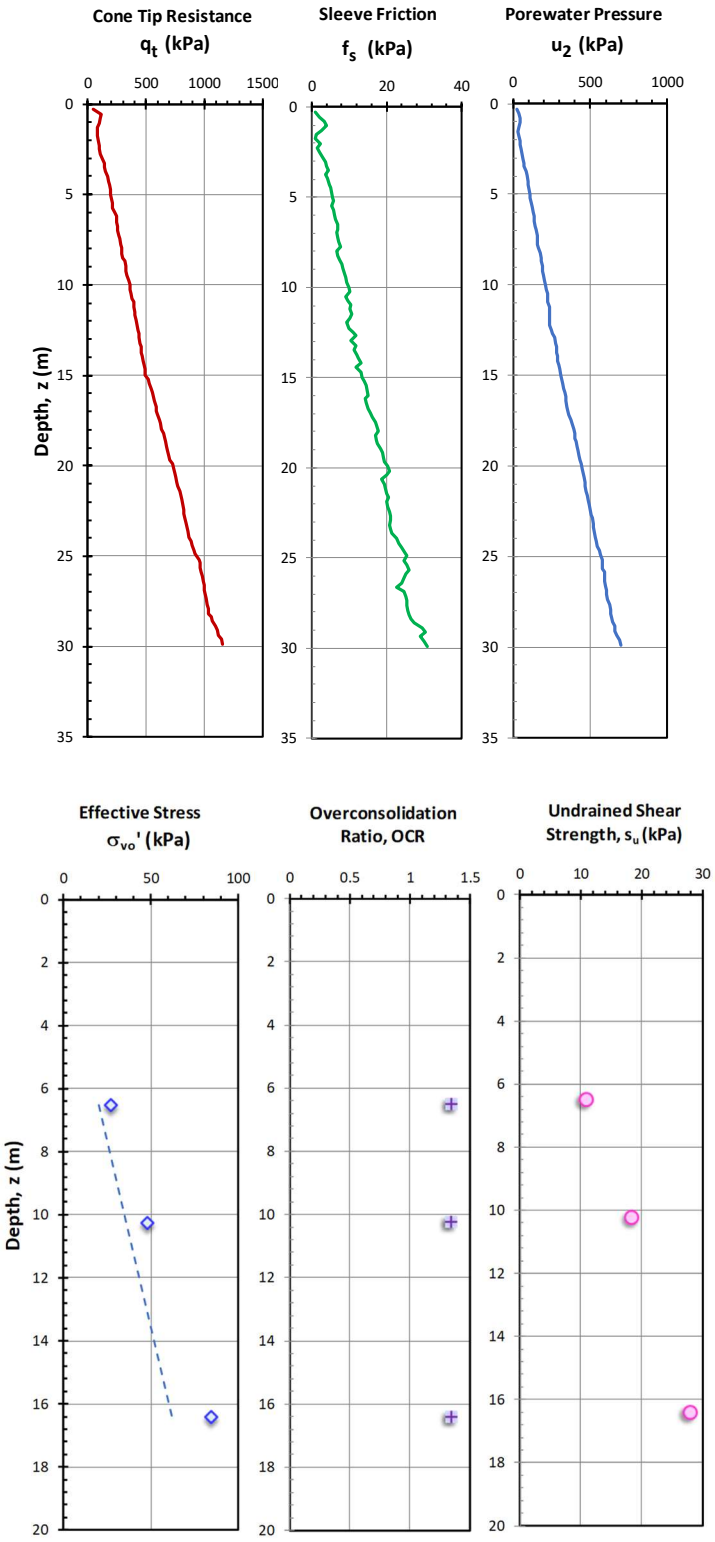

# GOG 4, Gulf of Guinea, West Africa

Data after Lunne at al. (2006)

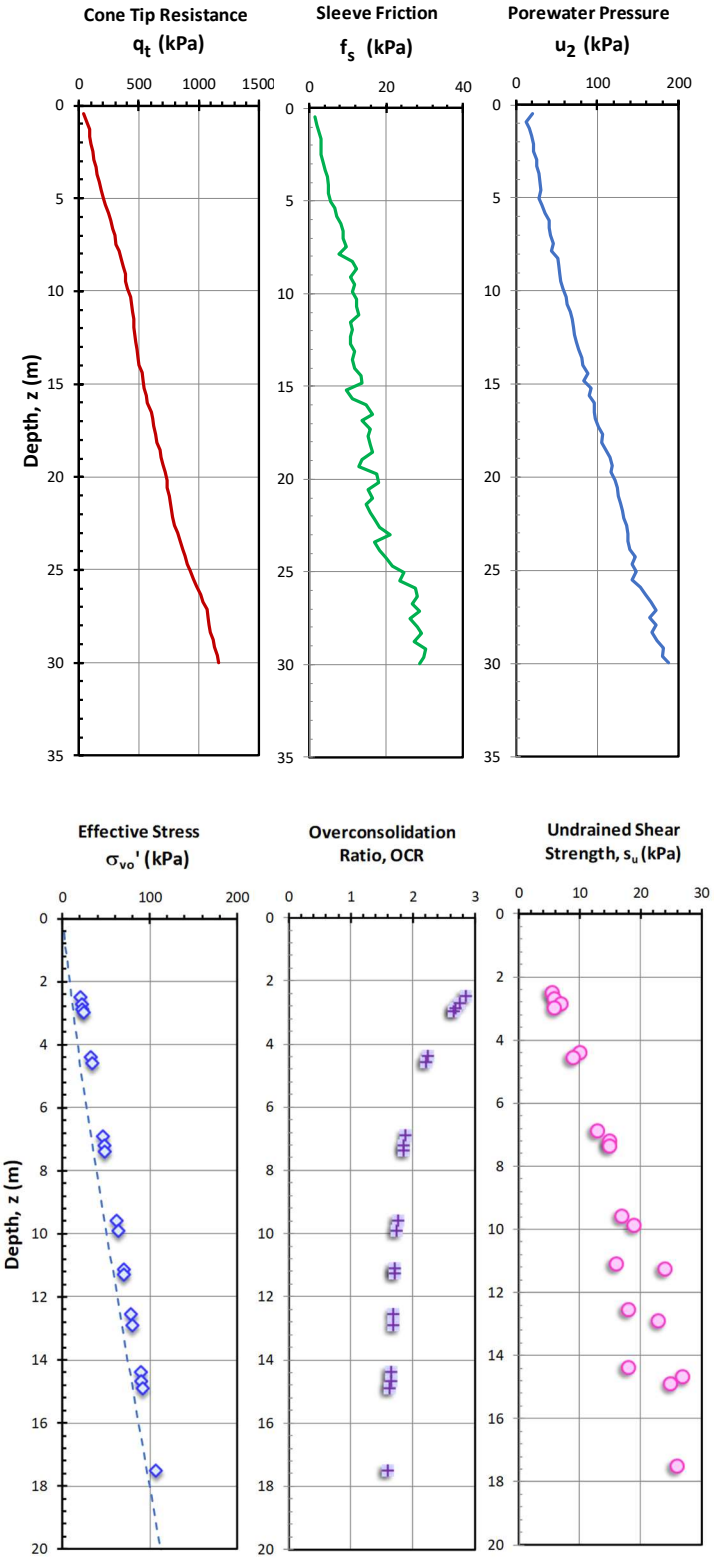

# GOG 5, Gulf of Guinea, West Africa

Data after Lunne at al. (2006)

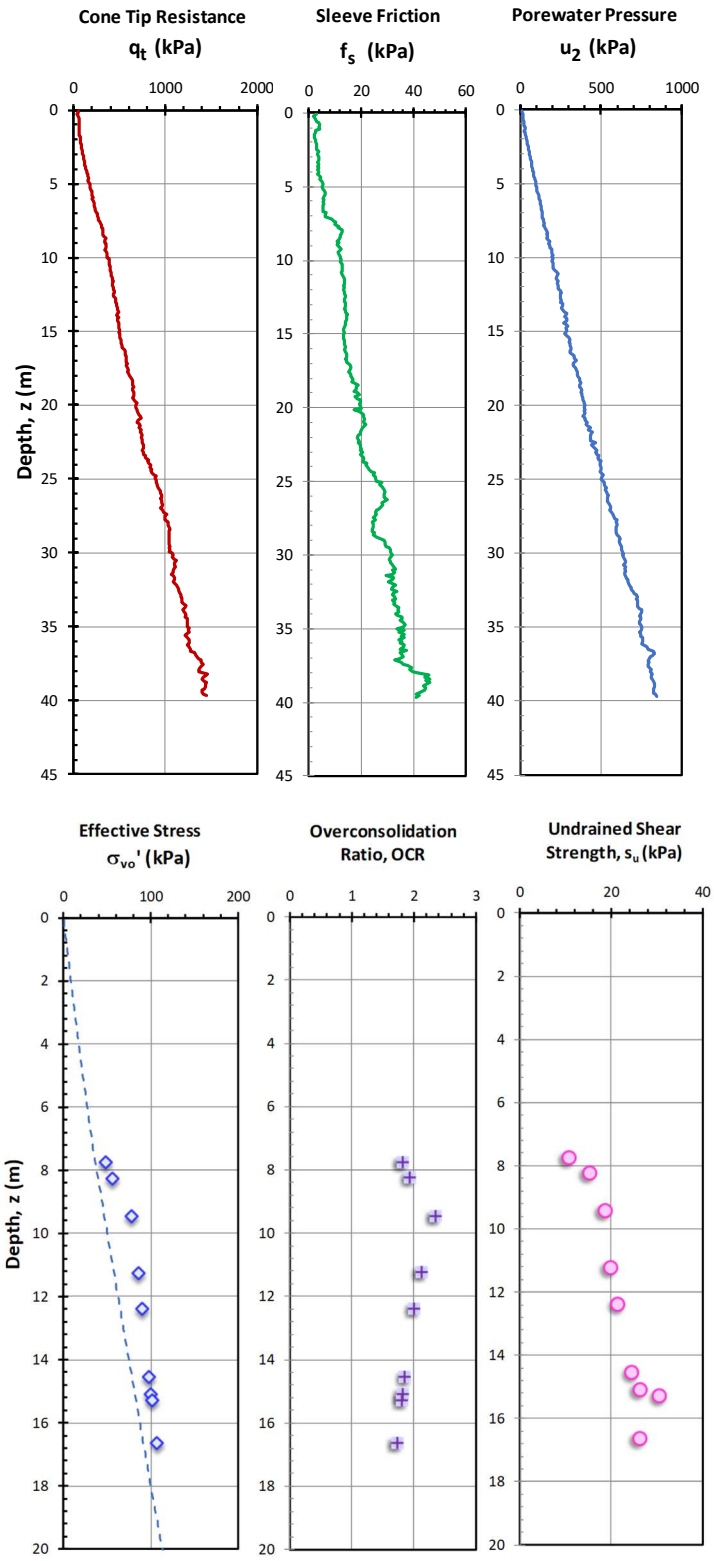

# GOG 6, Gulf of Guinea, West Africa

Data after Lunne at al. (2006)

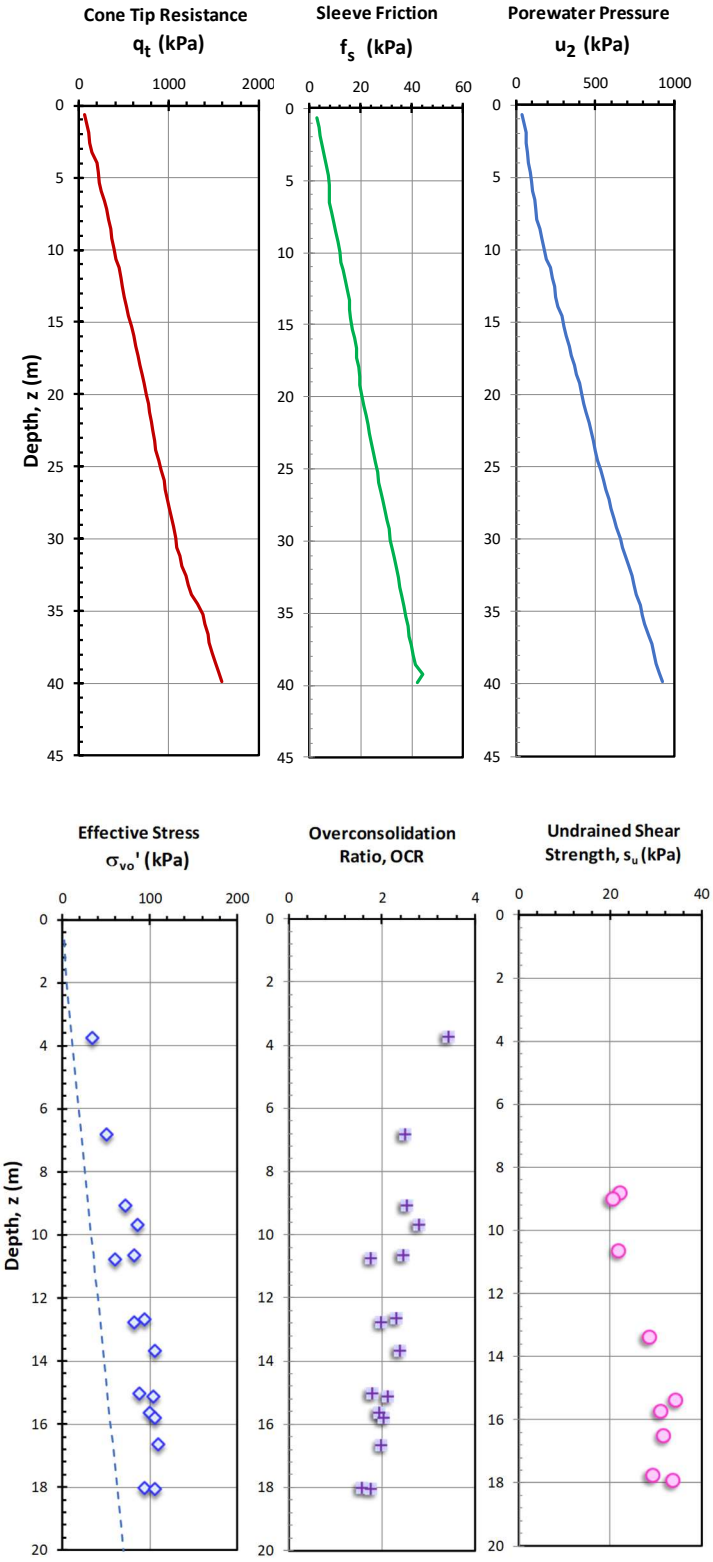

# Hachirogata, Japan

Data after Tanaka (2007)

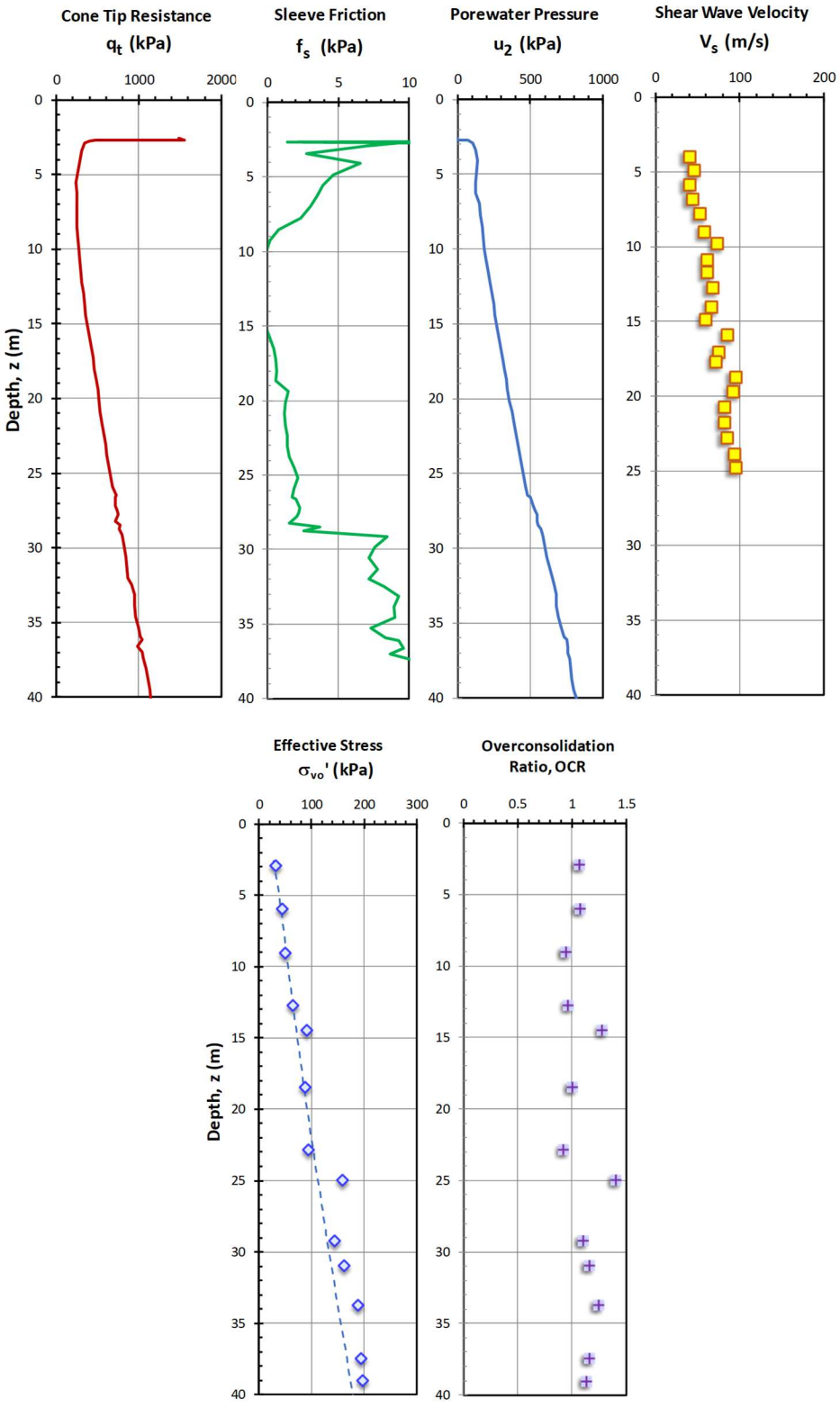

## Hamilton AFB, CA, USA

Data after Robertson (2010); Sabbagh & Koutsoftas (2011)

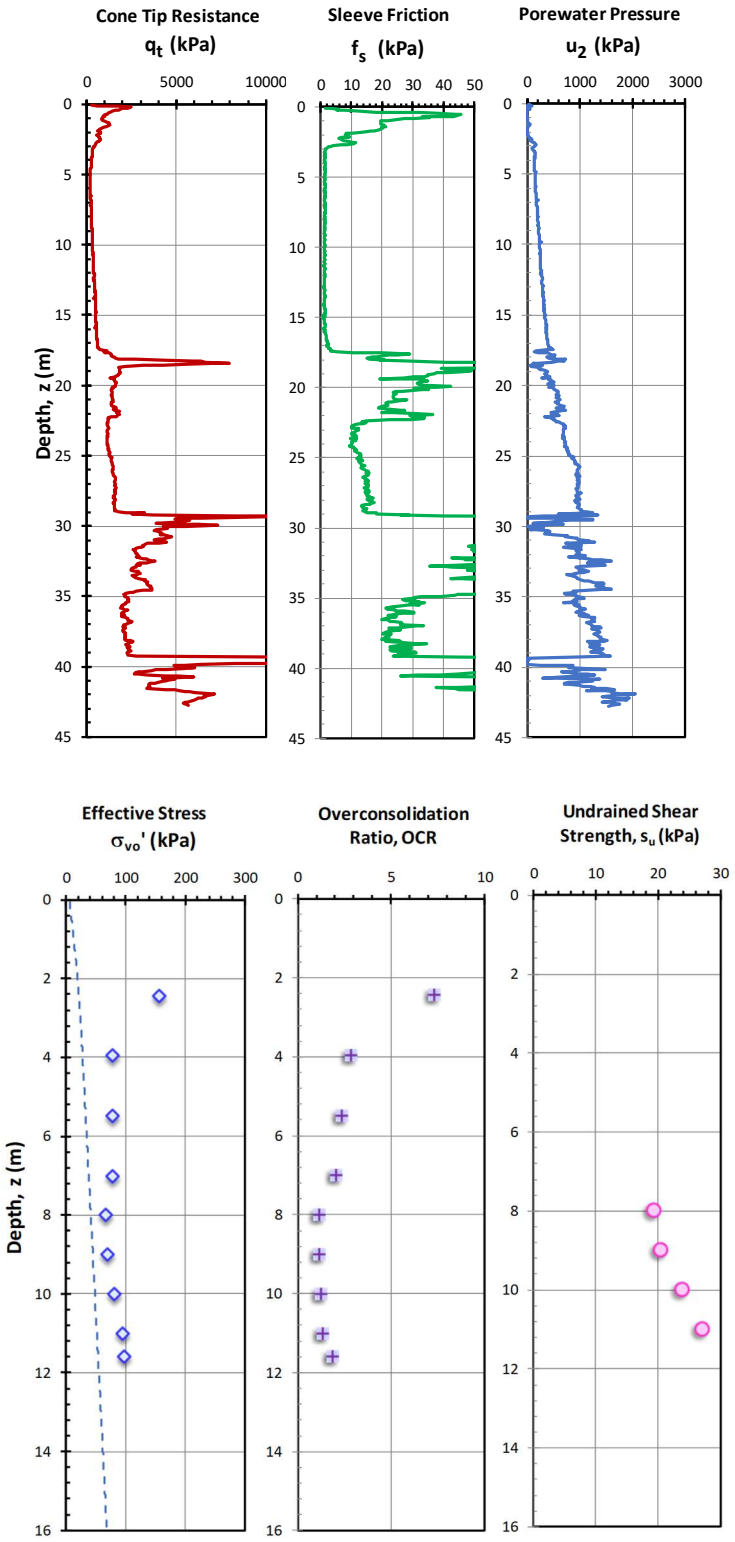

## Kurihama, Japan

Data after Tanaka (1995); Shibuya & Tanaka (1996)

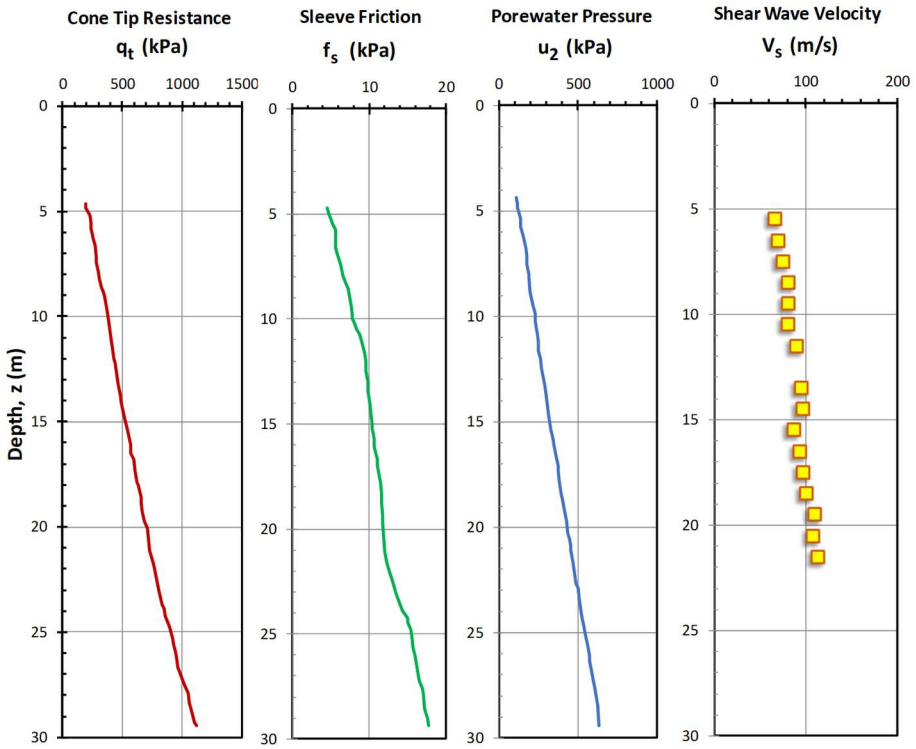


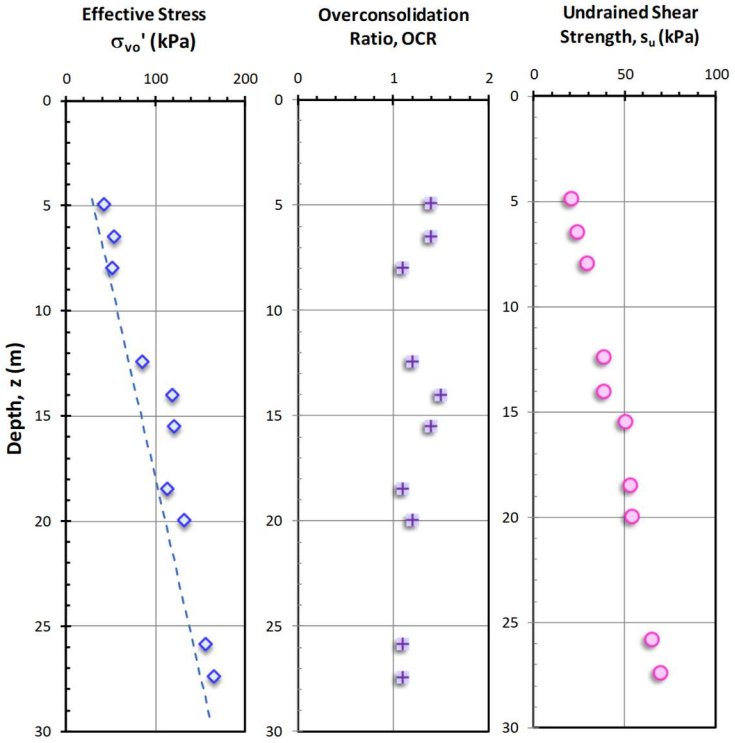

# Lianyungang, China

Data after Liu et al. (2008); Cai et l. (2014)

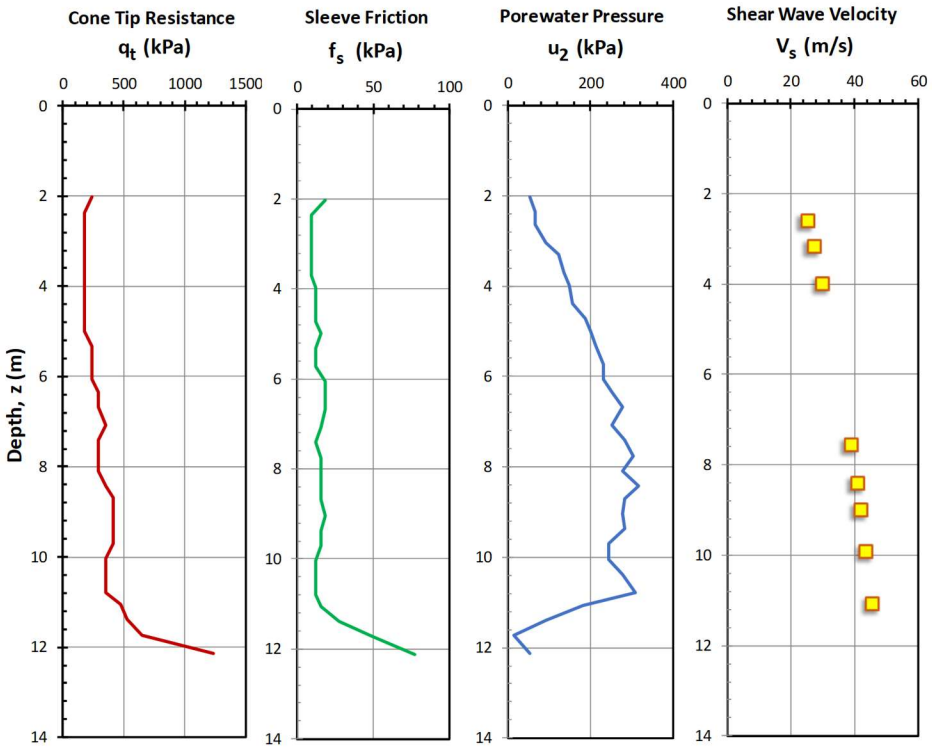


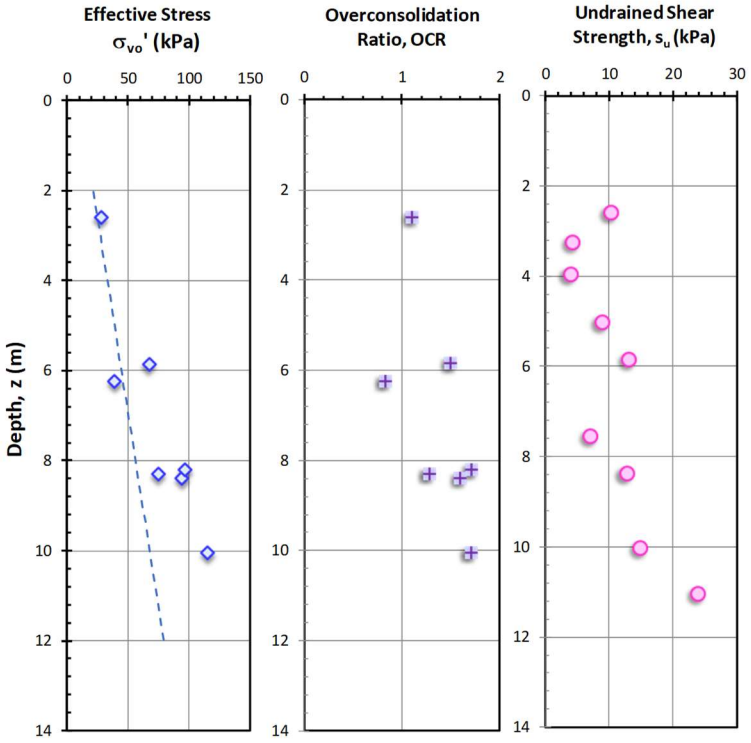

# Lierstranda, Drammen, Norway

Data after Lunne & Lacasse (1999)

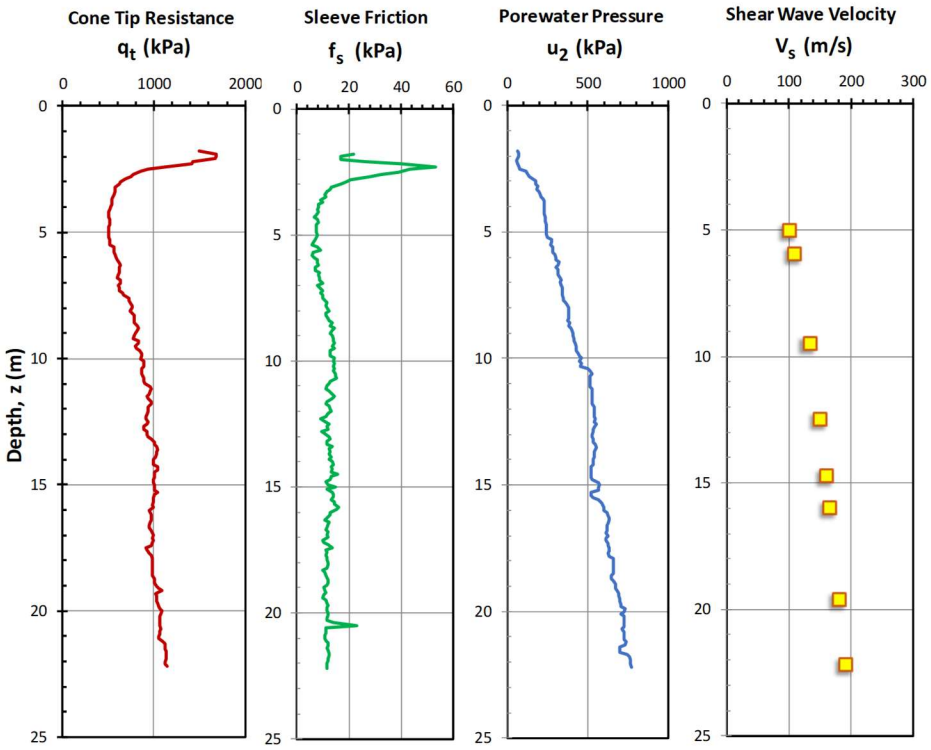


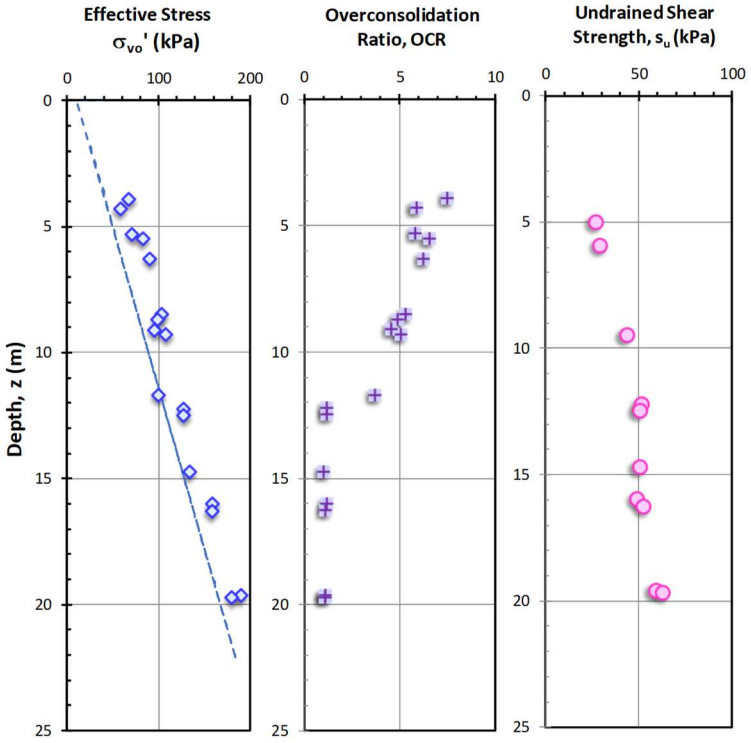

# Newbury, MA, USA

Data after Landon (2007)

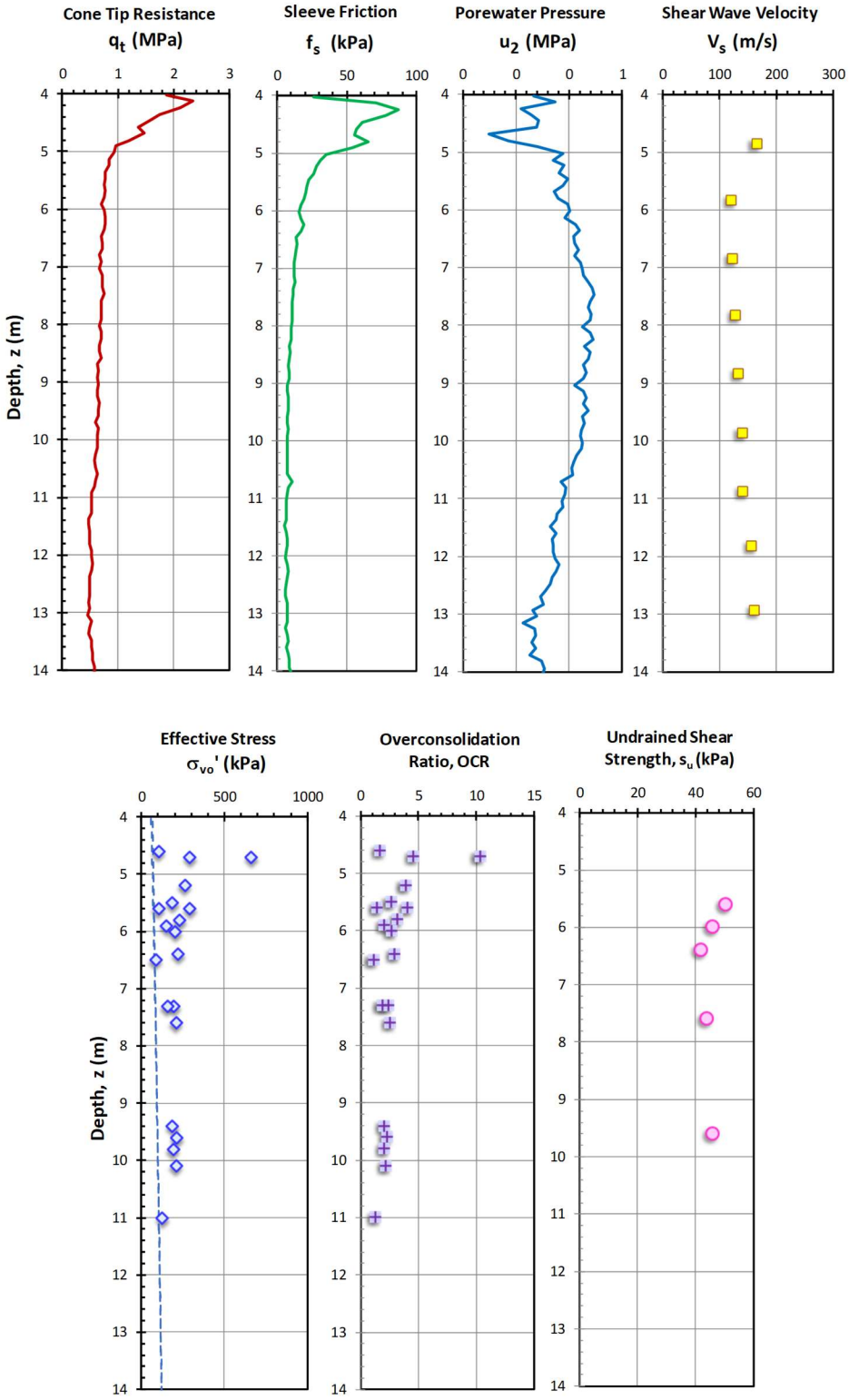

# Nong Ngu Hao, Bangkok, Thailand

Data after Shibuya & Tamrakar (2003)

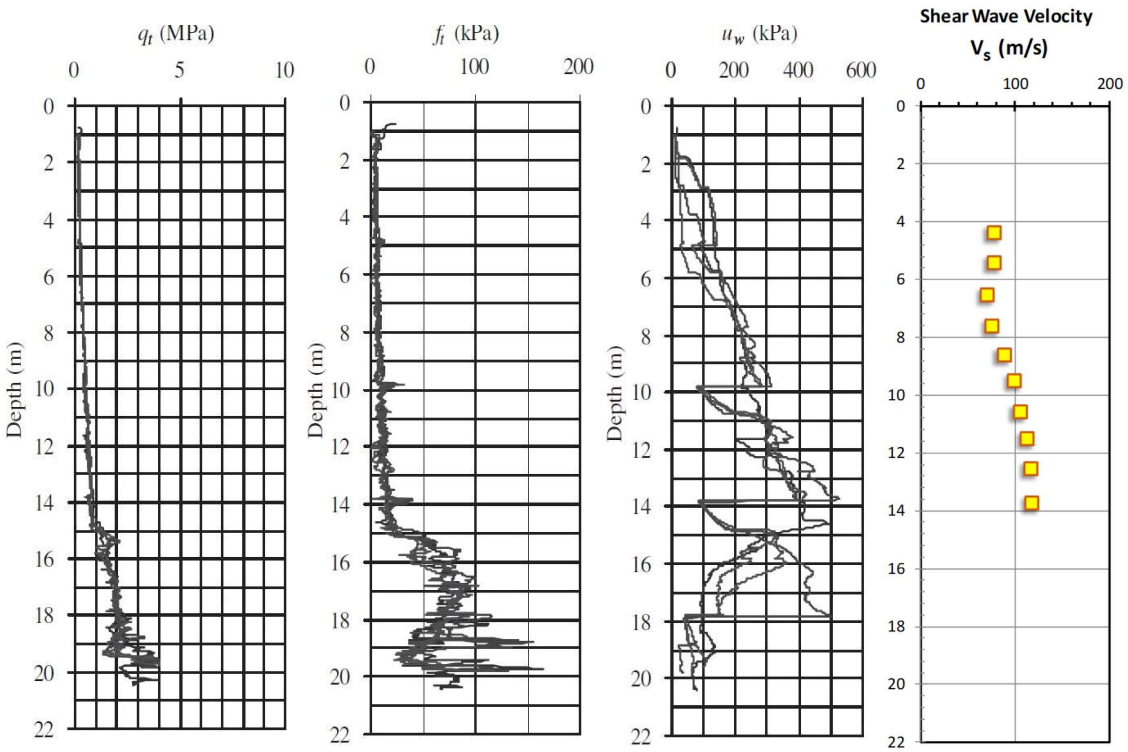


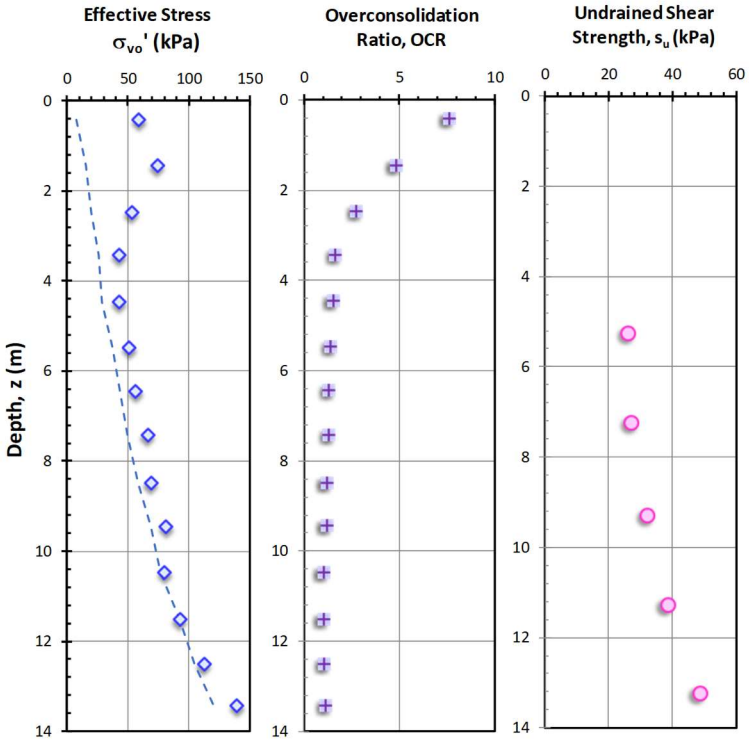

## Northwestern University, IL, USA

Data after Finno et al. (2000); McGillivray (2007)

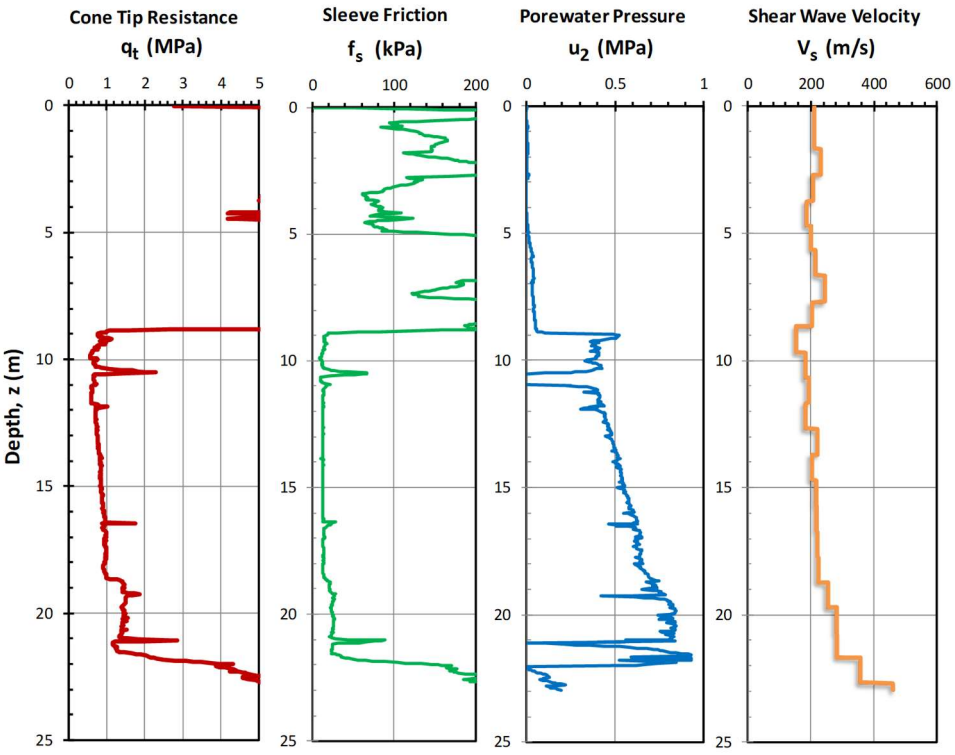


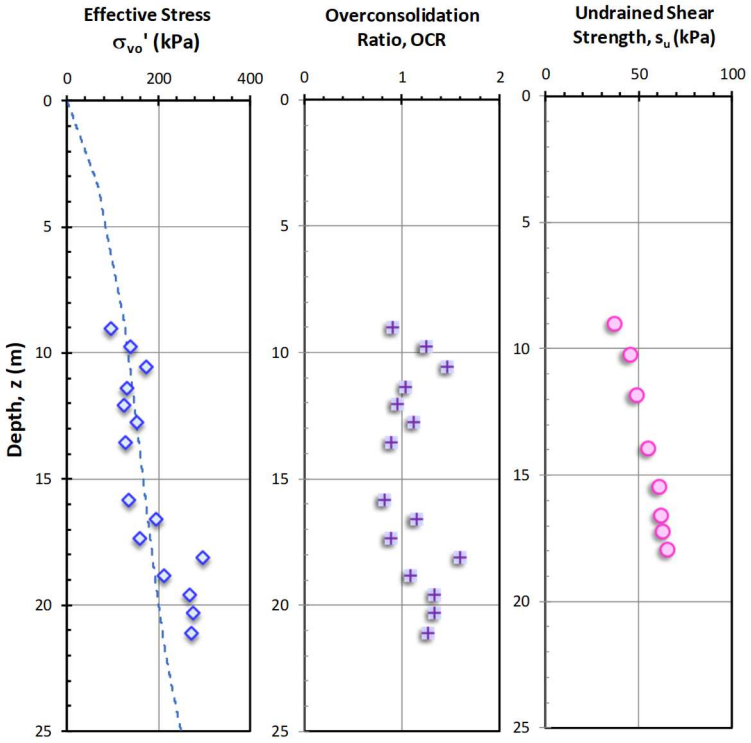

# Onsøy, Norway

Data after Lunne et al. (2003; 2006)

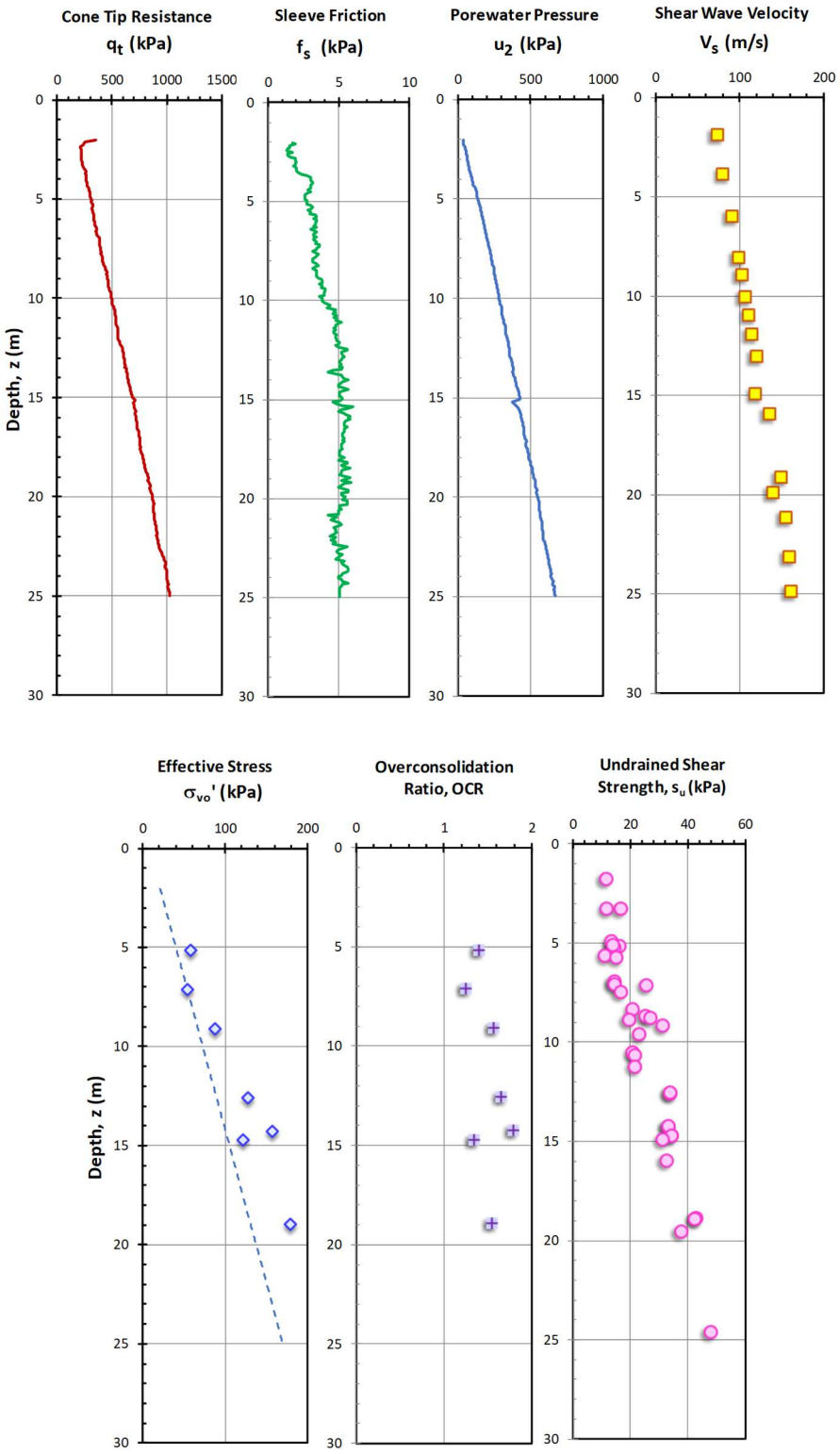

## Pentre, UK

Data after Lambson et al. (1993); Powell & Lunne (2005) – Shear Wave Velocity received from P K Robertson January, 1998.

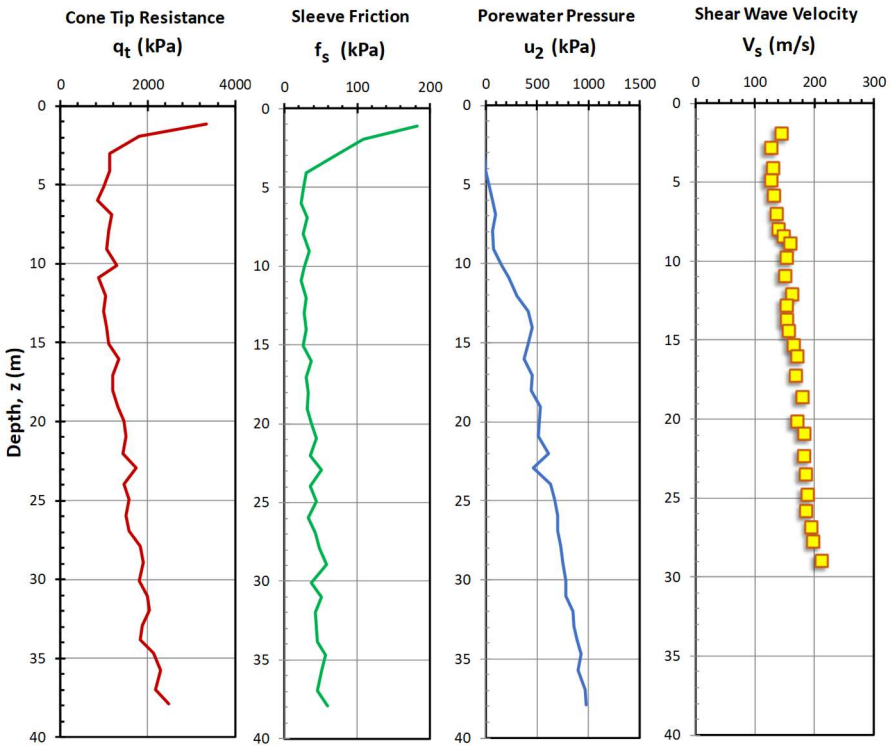


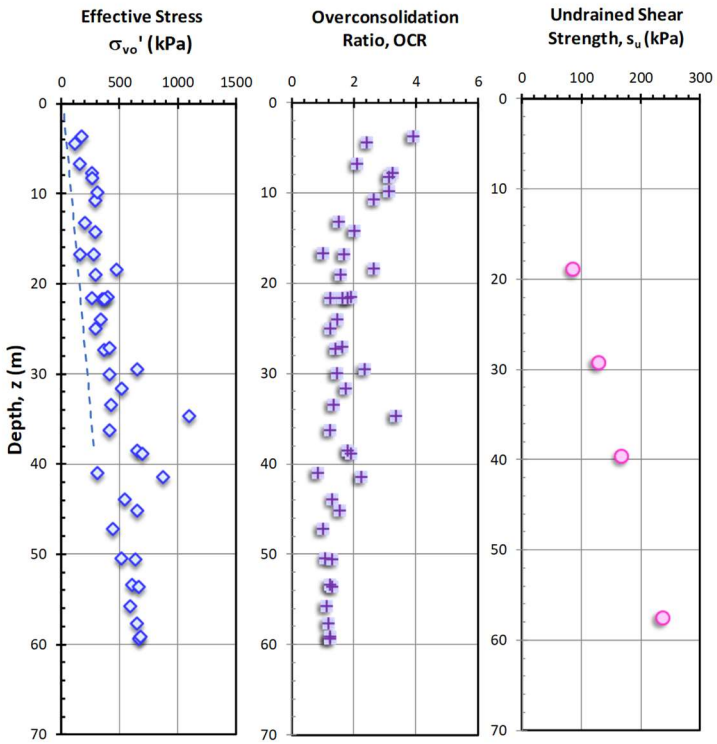

## Perniö, Finland

Data after Lehtonen (2015); Di Buò et al. (2016)

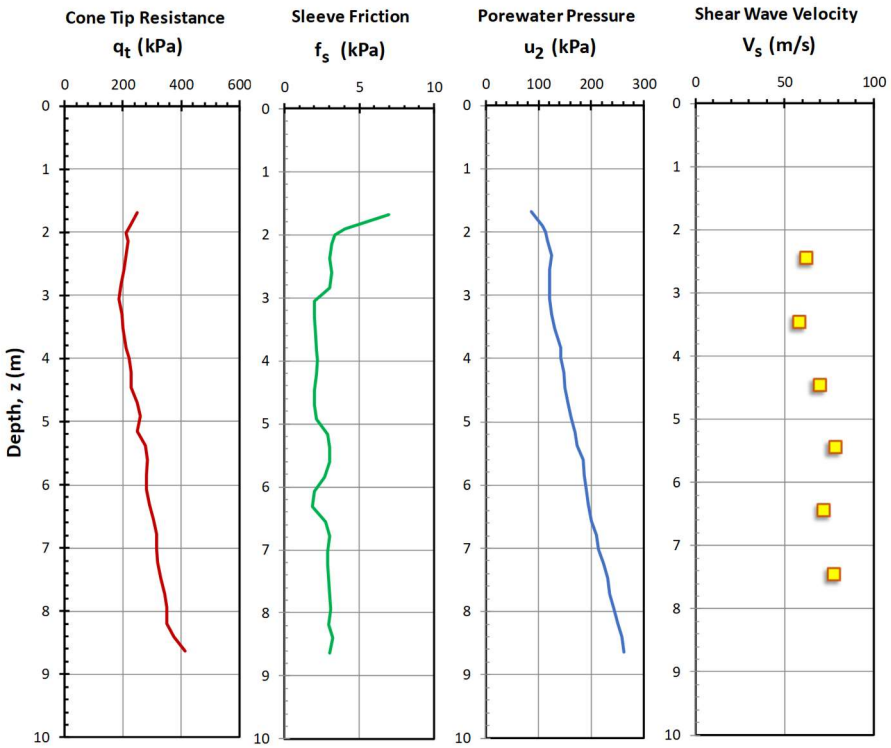


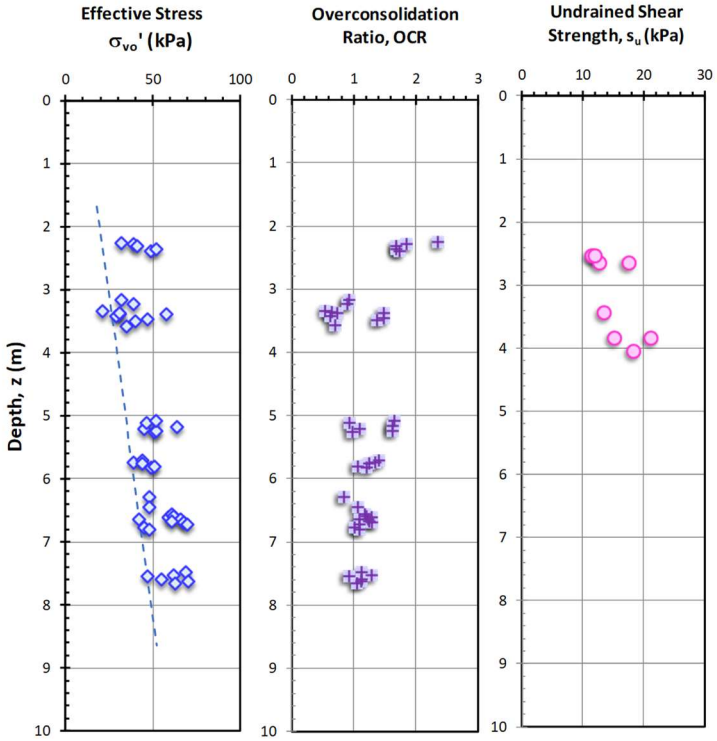

## Pisa, Italy

Data after Lo Presti et al. (2003)

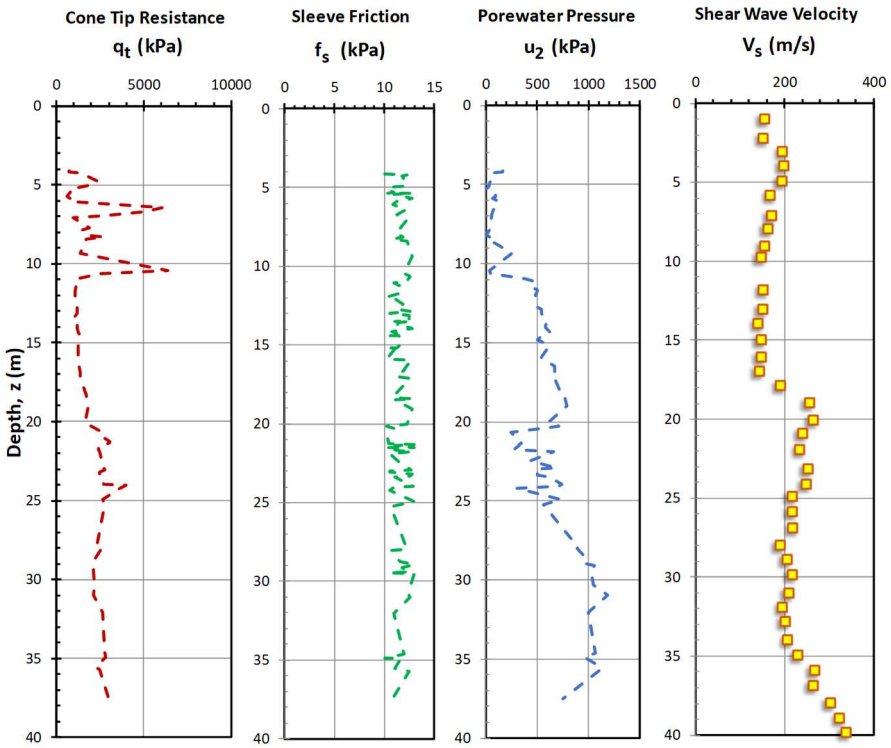


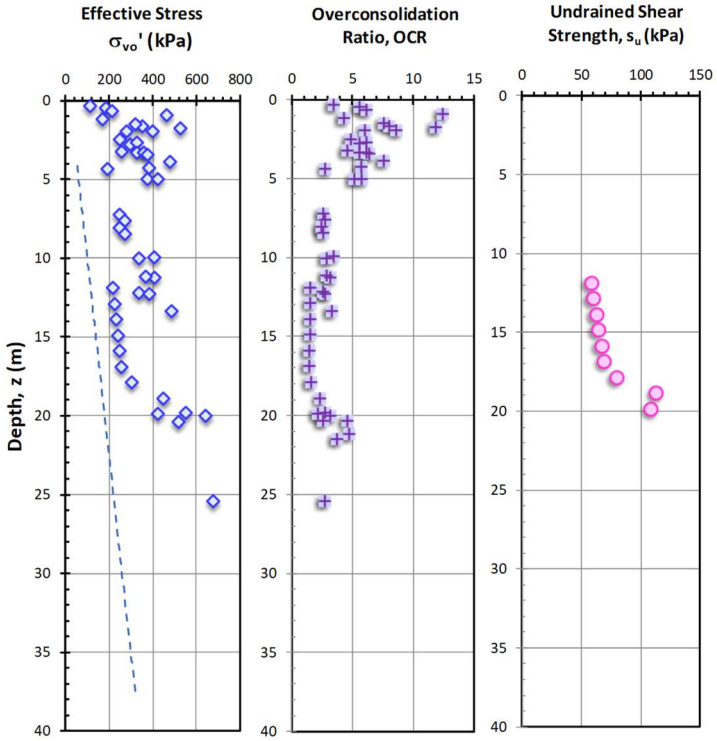

# Sarapuí, Brazil

Data after Ortigao et al. (1983); Almeida & Marques (2003)

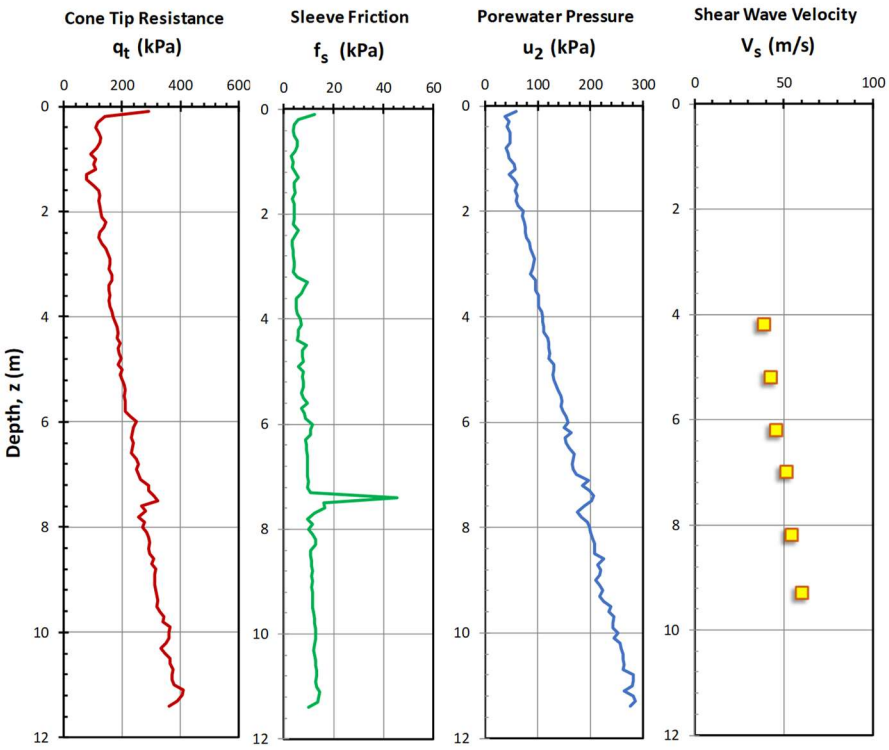


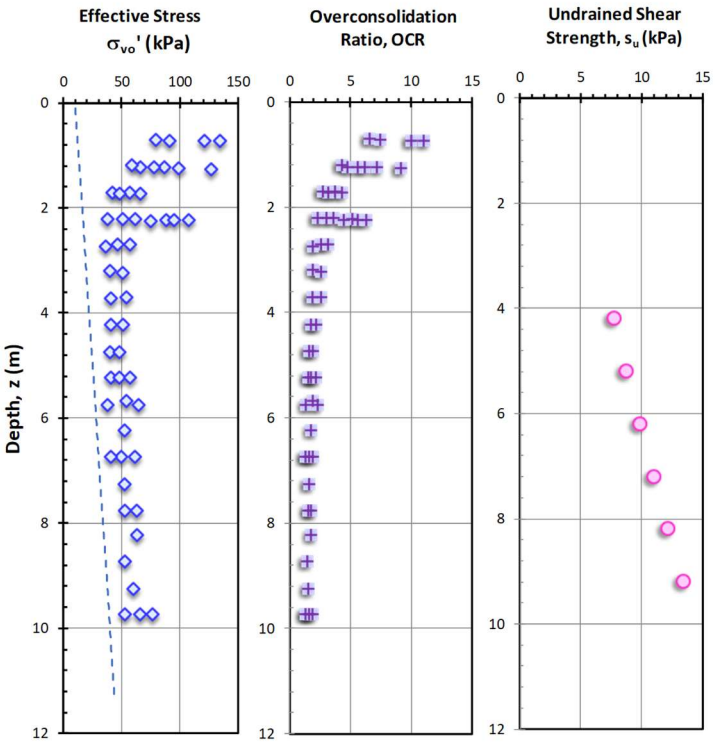

# Snorre, North Sea

Data after NGI REPORT 87260-2

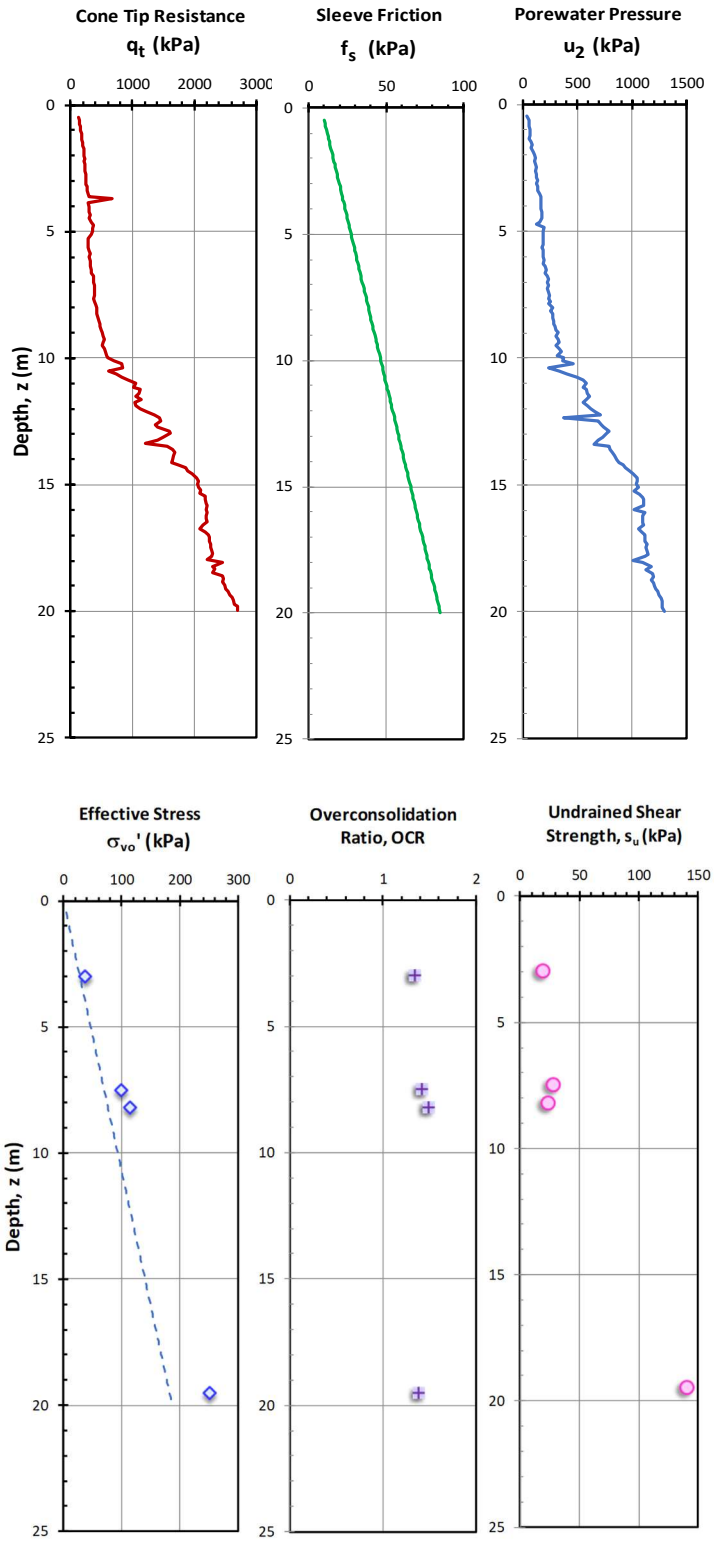

# Taipei, Taiwan

Data after Chin et al. (2007)

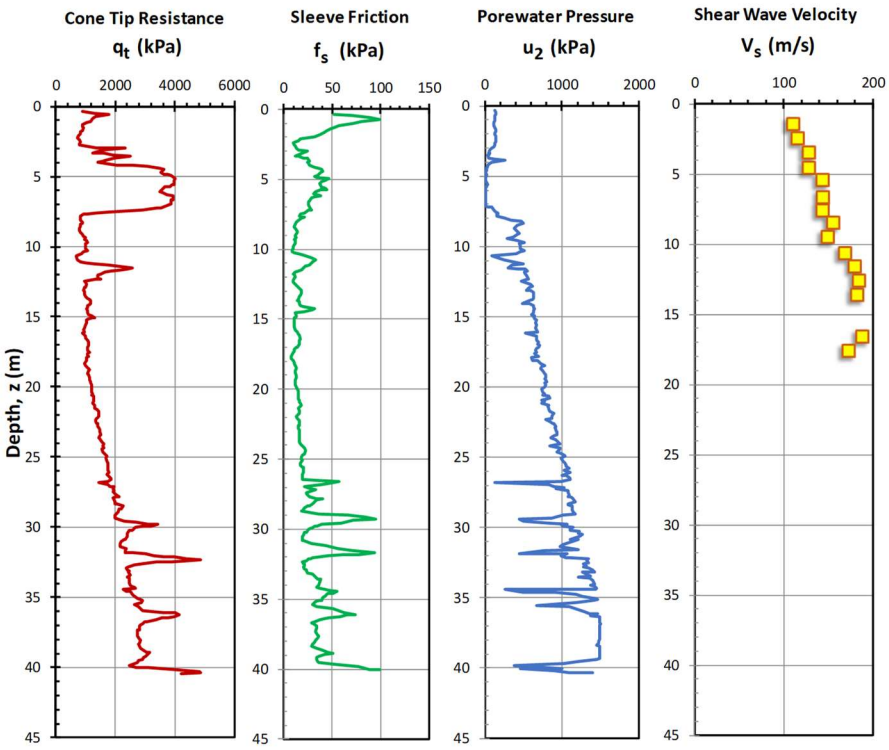


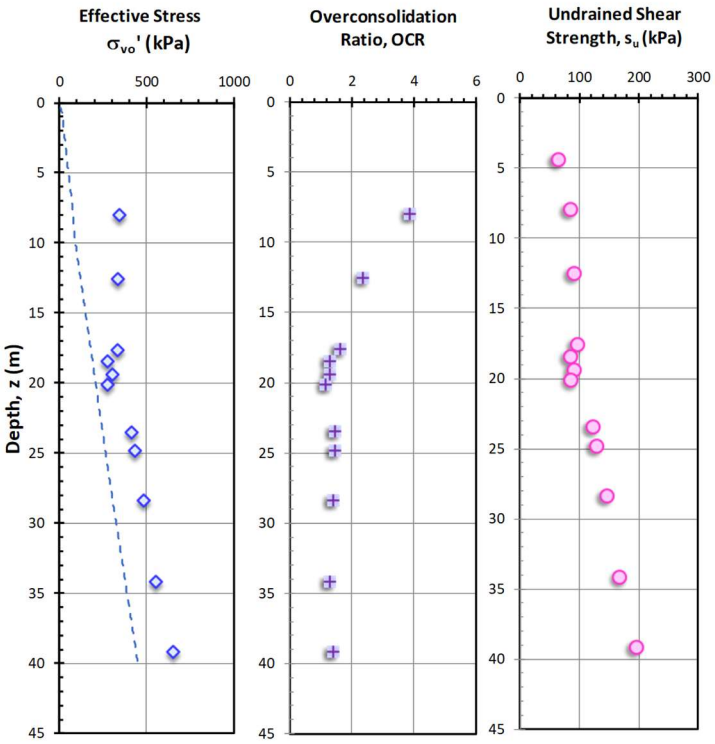

# Torp, Sweden

Data after Larsson & Åhnberg (2003)

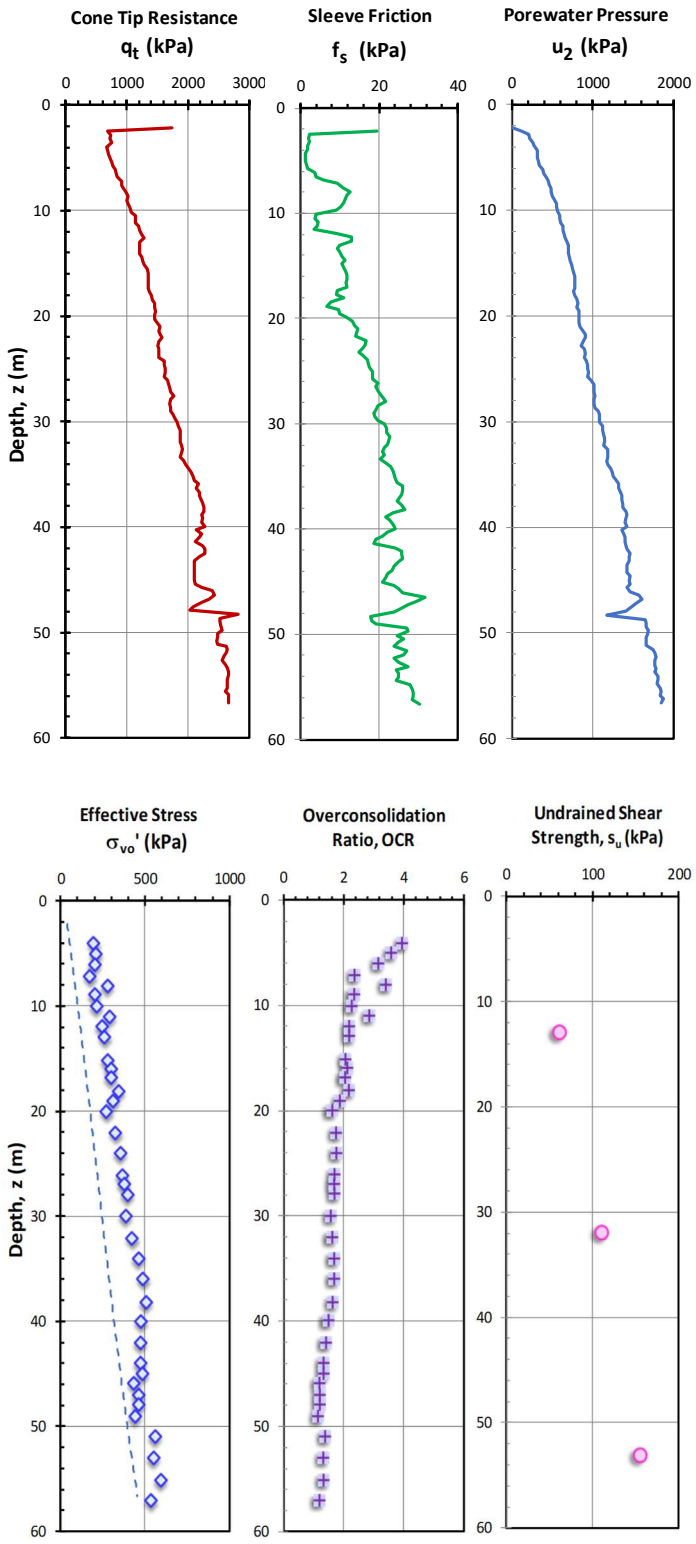

# Troll Upper, North Sea

Data after Amundsen et al. (1985); Lunne et al. (2007)

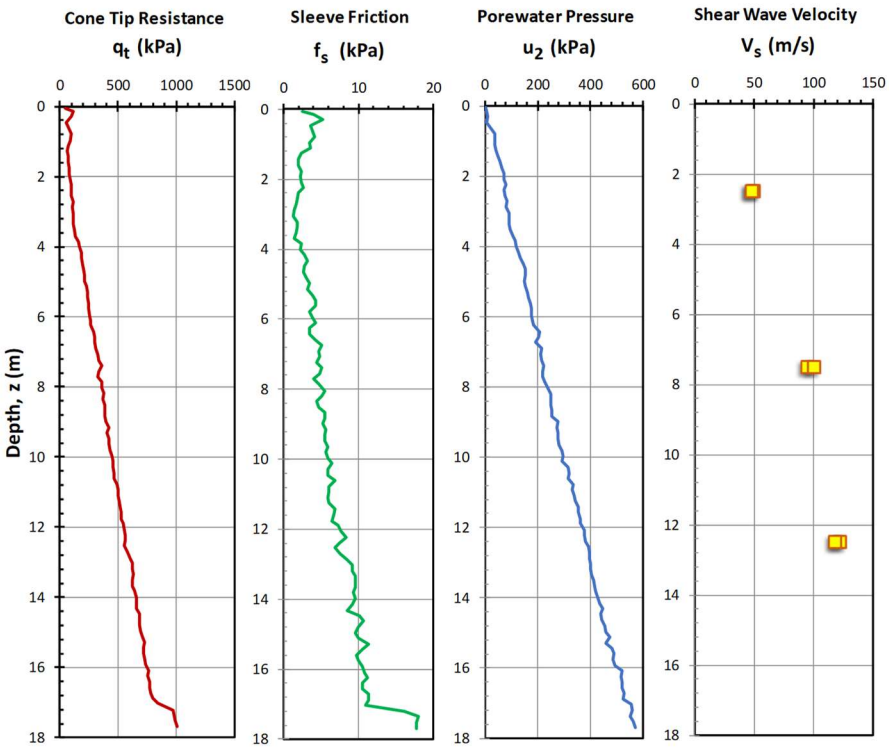


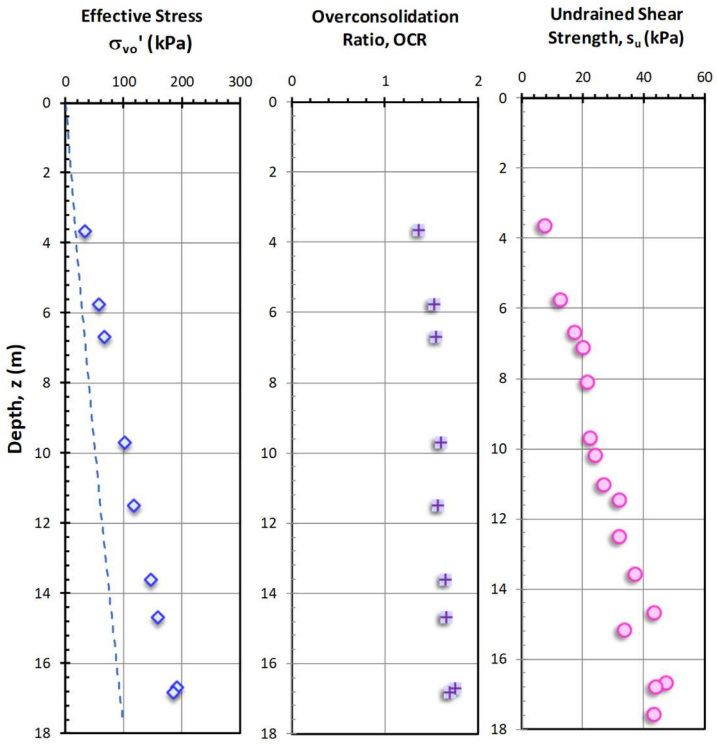

# Troll Lower, North Sea

Data after Amundsen et al. (1985); Lunne et al. (2007)

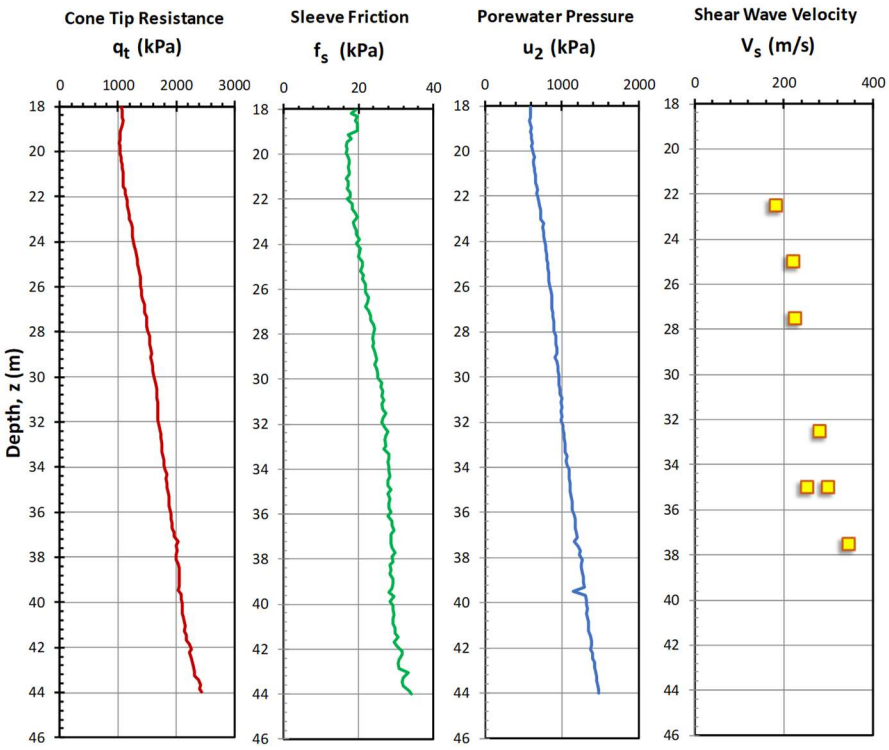


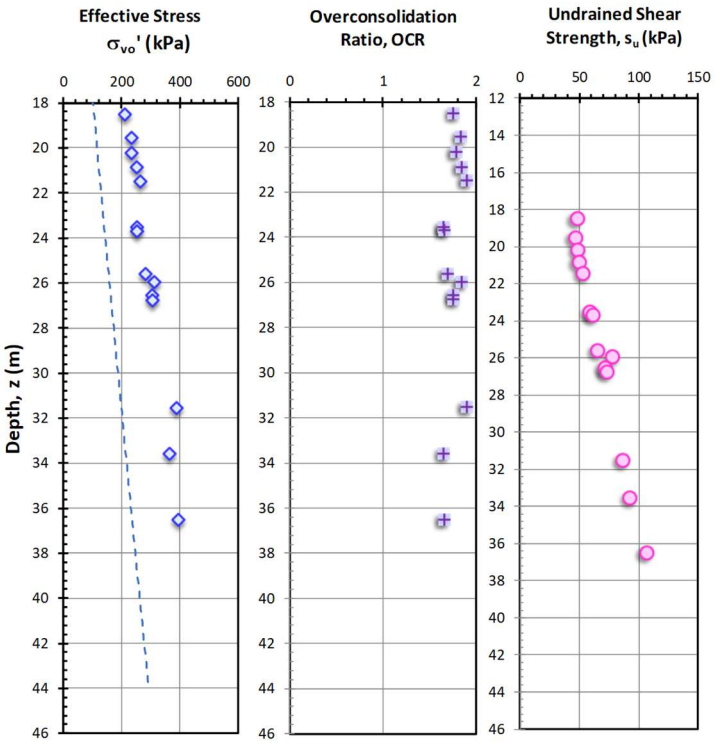

# APPENDIX B

## Silts:
## Piezocone Soundings,
## with Shear Wave Velocity,
## Undrained Shear Strength, and
## Stress History Data

| Site | CPTu | Shear Wave Velocity, $V_s$ | Undrained Shear Strength, $s_{u\ TC}$ | Stress History |
|---|---|---|---|---|
| 200th st. | ✓ | ✓ | ✓ | ✓ |
| Dyke Rd. | ✓ | ✓ | | ✓ |
| Gunnestad | ✓ | | | ✓ |
| Iowa | ✓ | | | ✓ |
| Malamocco | ✓ | ✓ | | ✓ |
| Mjardevi | ✓ | | | ✓ |
| Nebraska | ✓ | | | ✓ |
| Opelika Piedmont | ✓ | | | ✓ |
| Os Lower | ✓ | | ✓ | ✓ |
| Os Upper | ✓ | | ✓ | ✓ |
| Piedmont- GT | ✓ | | | ✓ |
| Tornhill | ✓ | ✓ | | ✓ |
| Vagverket | ✓ | ✓ | | ✓ |
| Vatthammar | ✓ | ✓ | | ✓ |

# 200th St, BC, Canada

Data after Cruz (2009)

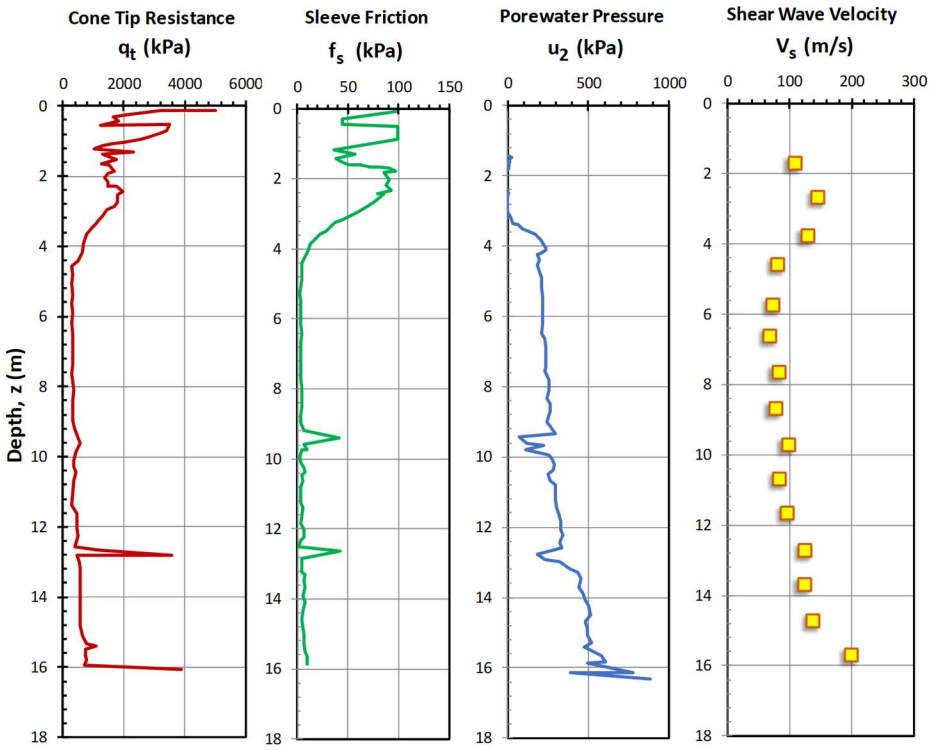


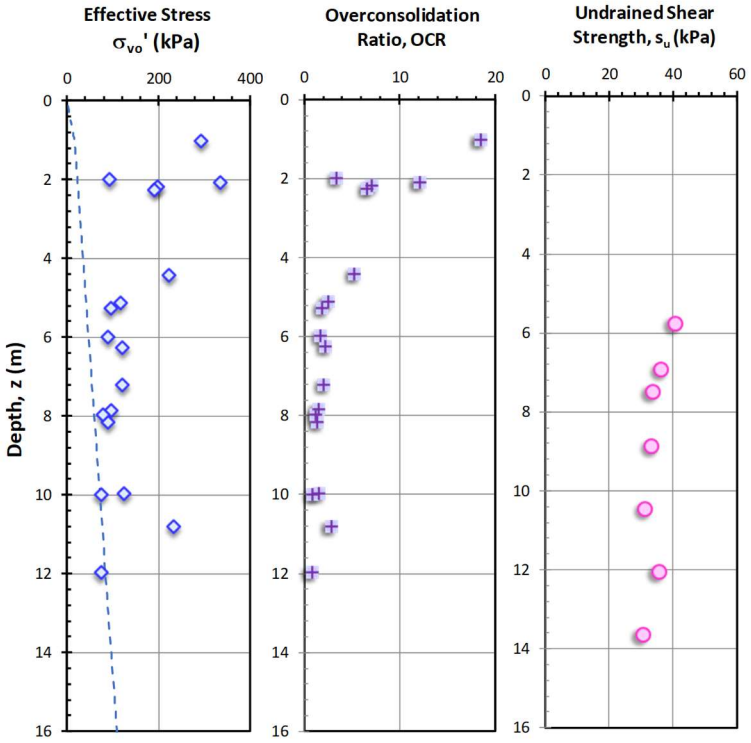

## **Cooper Marl, SC, USA -** Calcareous clay/ silt

Data after Singha (1998); Camp (2004a); and Mayne (2005)

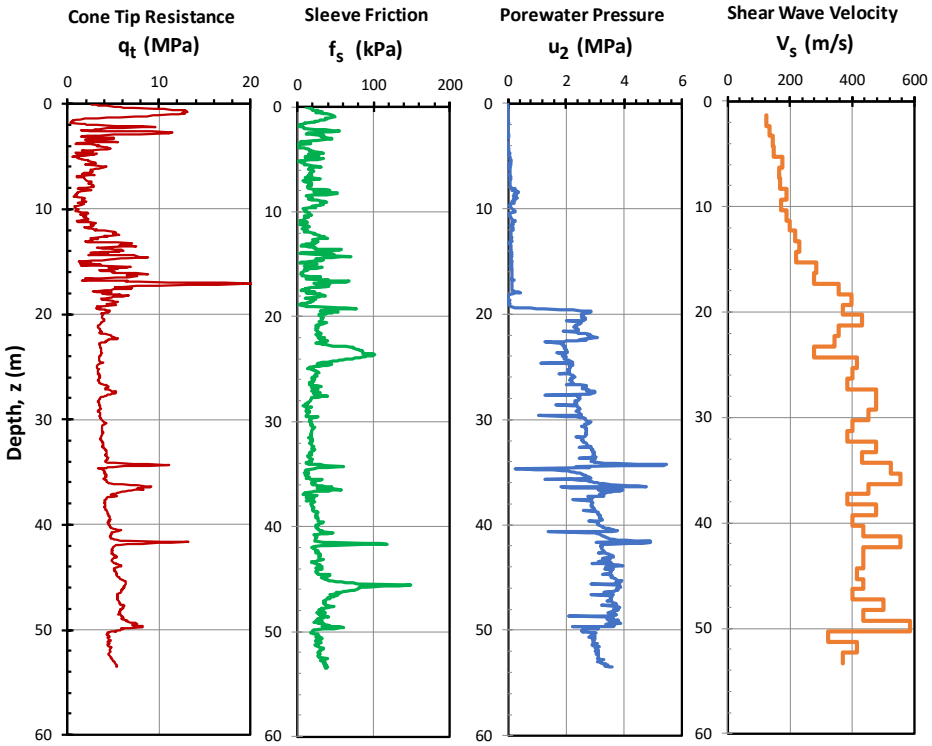


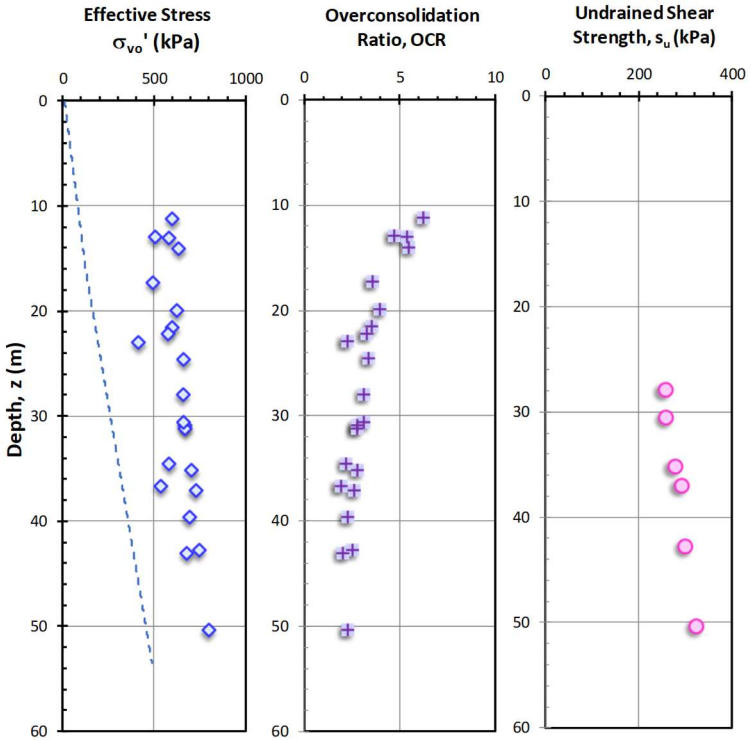

# Dyke Rd, Richmond, BC, Canada

Data after Cruz (2009)

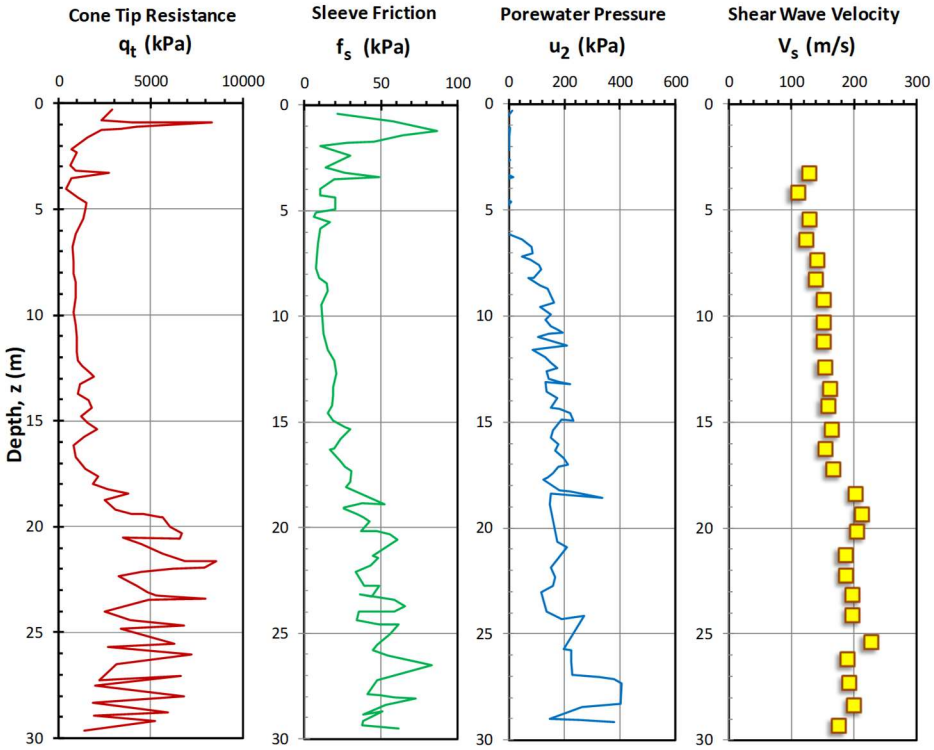


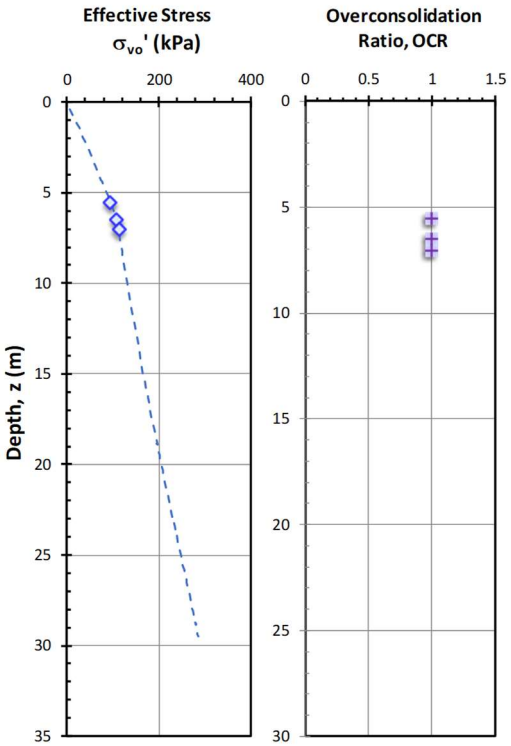

# Guunestad, Norway

Data after Habtegiorghis (2012)

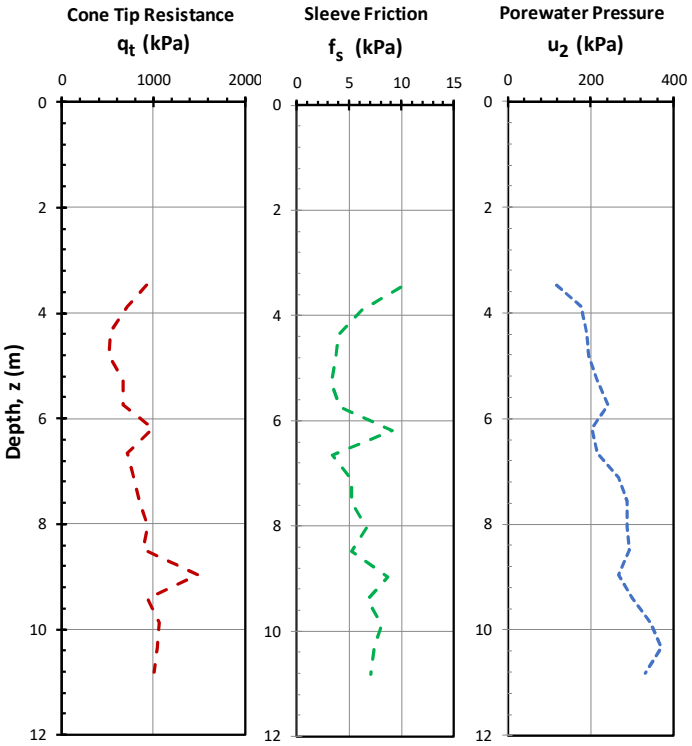


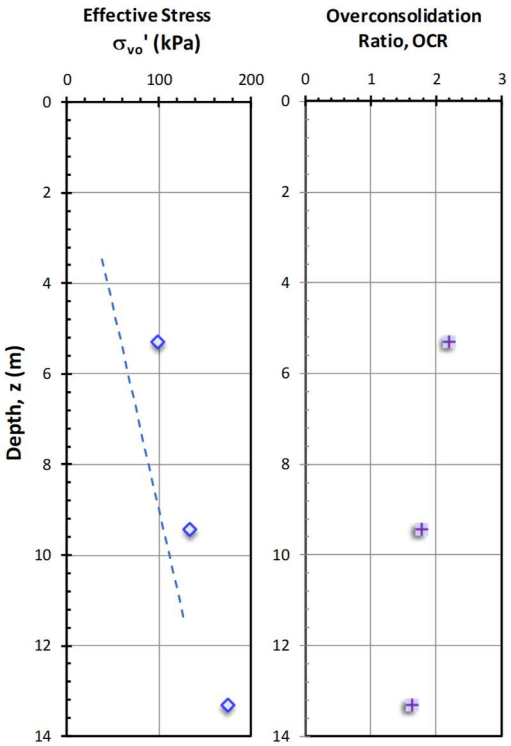

## Iowa / Sioux, USA

Data after Saye et al. (2013) – Pore water pressure measurements not taken

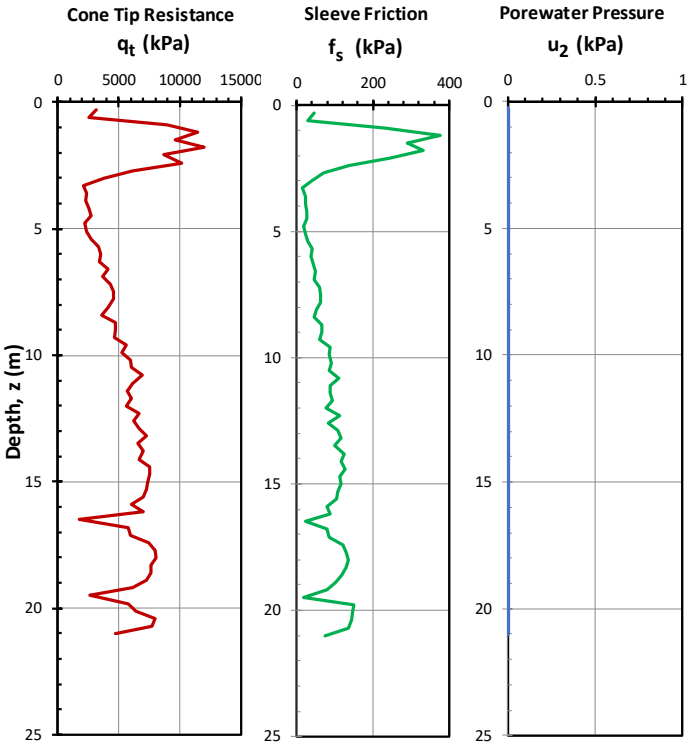


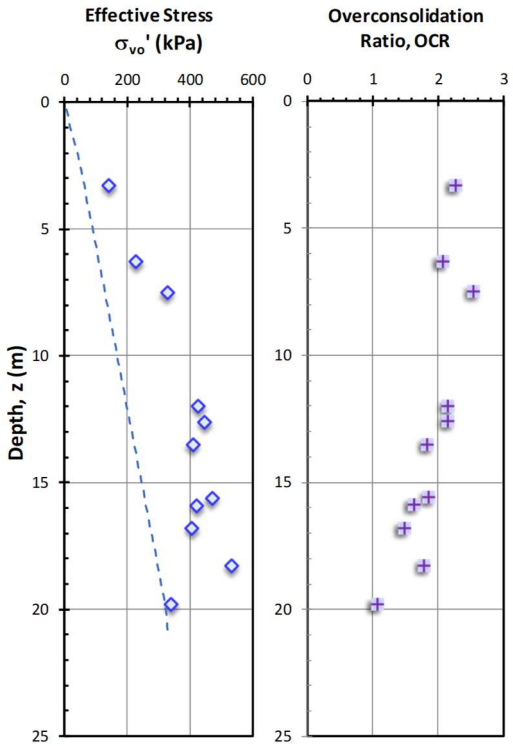

# Malamocco, Venice, Italy

Data after Simonini (2004)

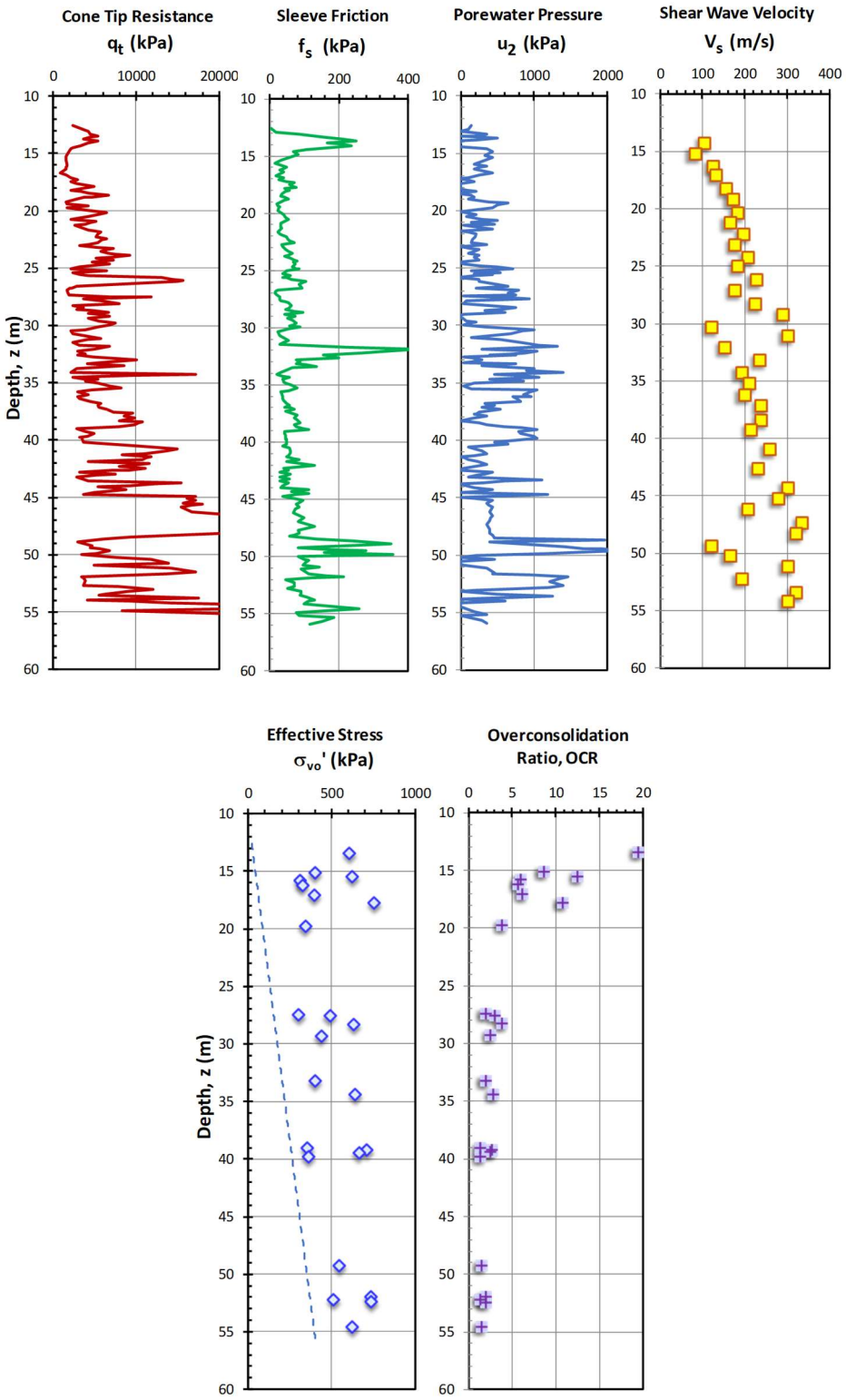

# Mjardevi, Sweden

Data after Larsson (1997)

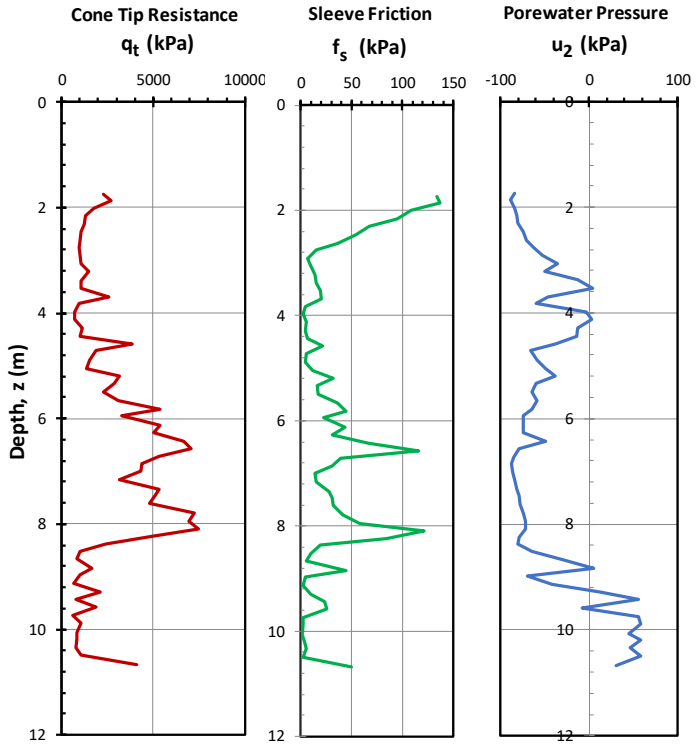


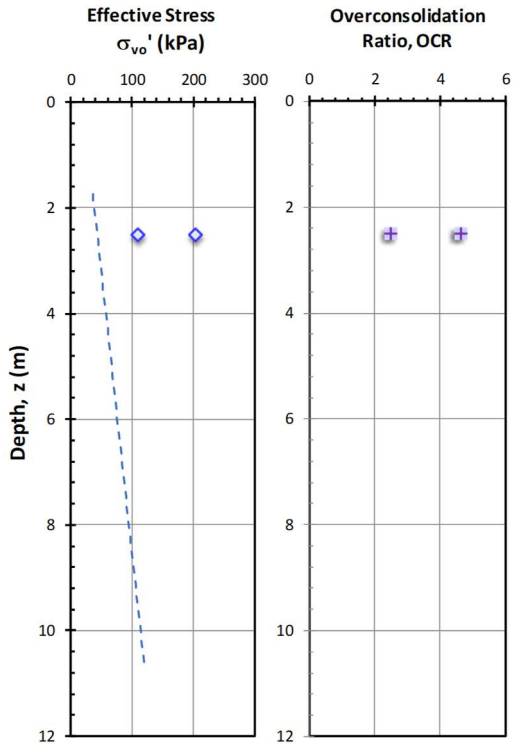

## Nebraska/ Omaha, NE, USA

Data after Saye et al. (2013) – Pore water pressure measurements not taken

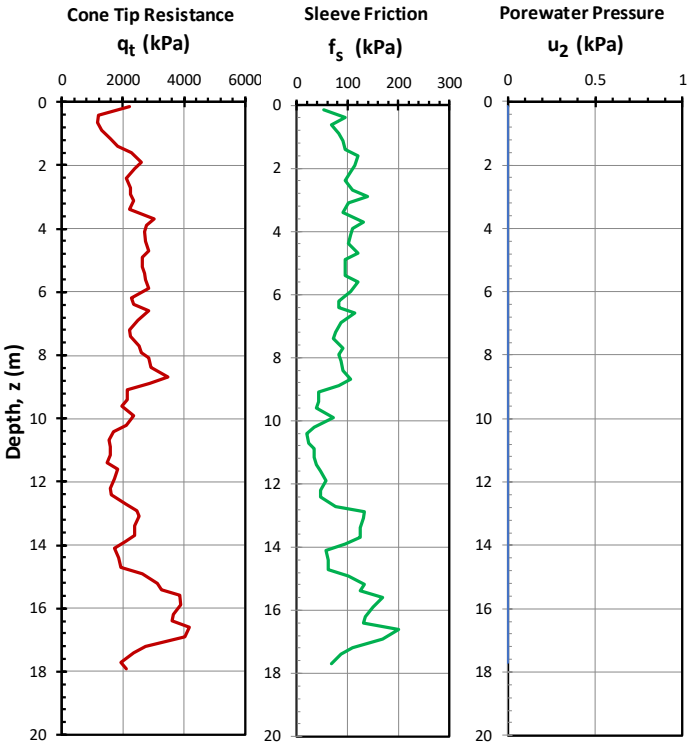


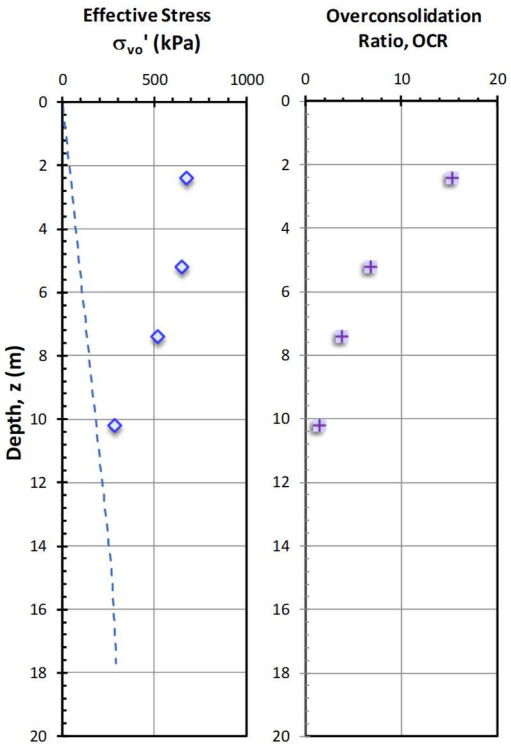

# Opelika Piedmont, AL, USA

Data after Mayne & Brown (2003)

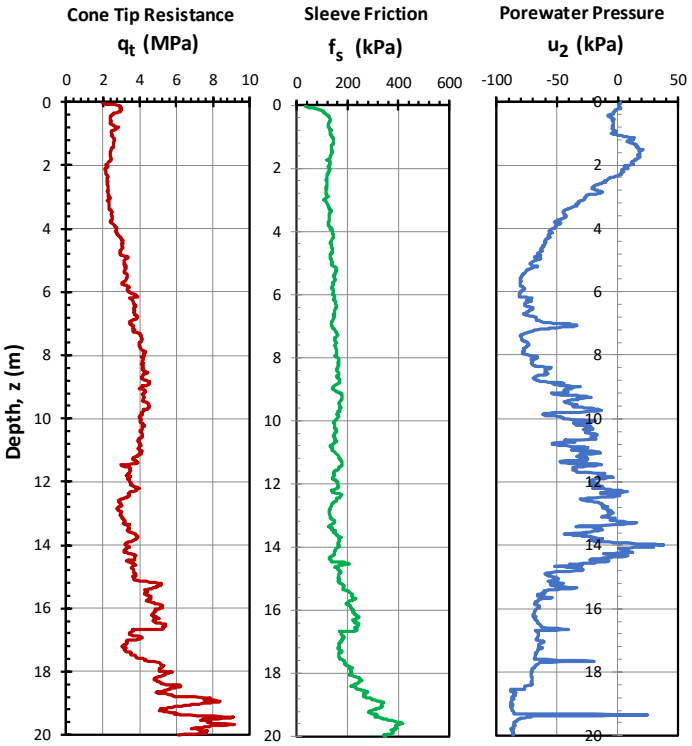


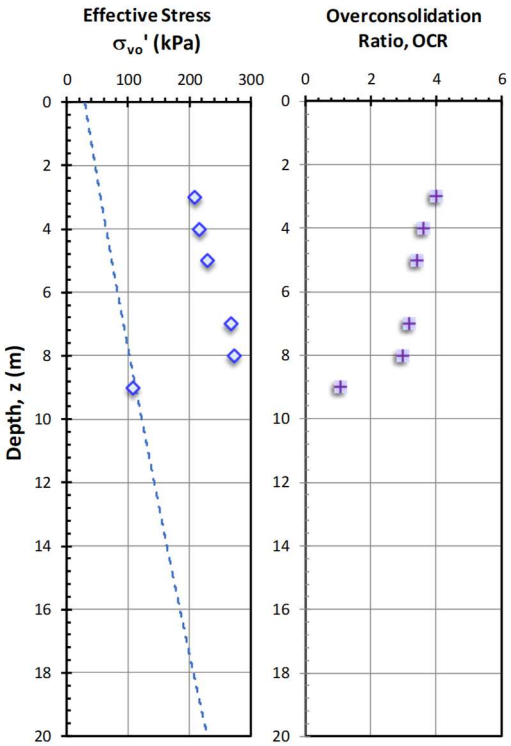

# Os, Norway

Data after Long et al. (2010)

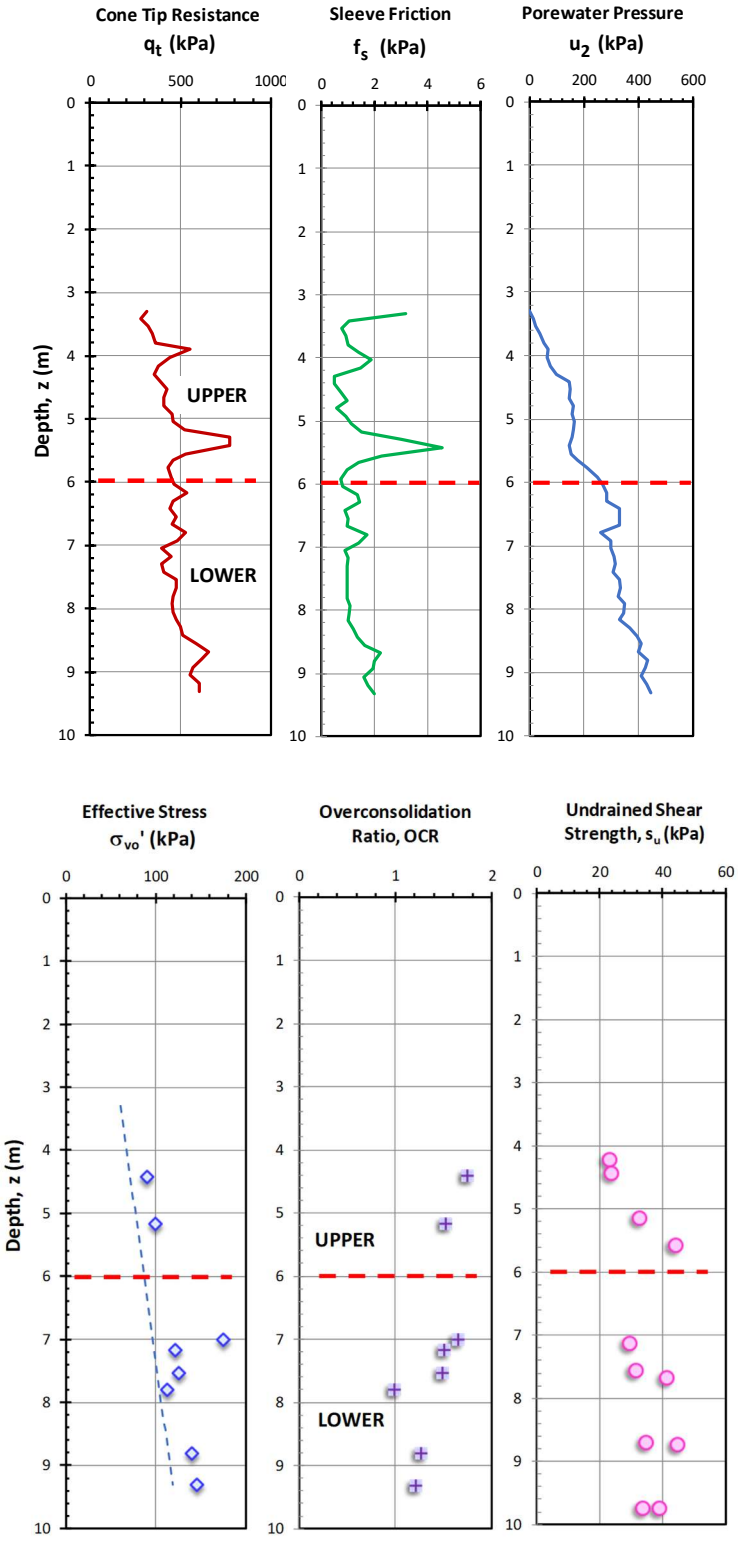

## Piedmont GT, GA, USA

Data after Harris & Mayne (1994) – Pore water pressure measurements not taken

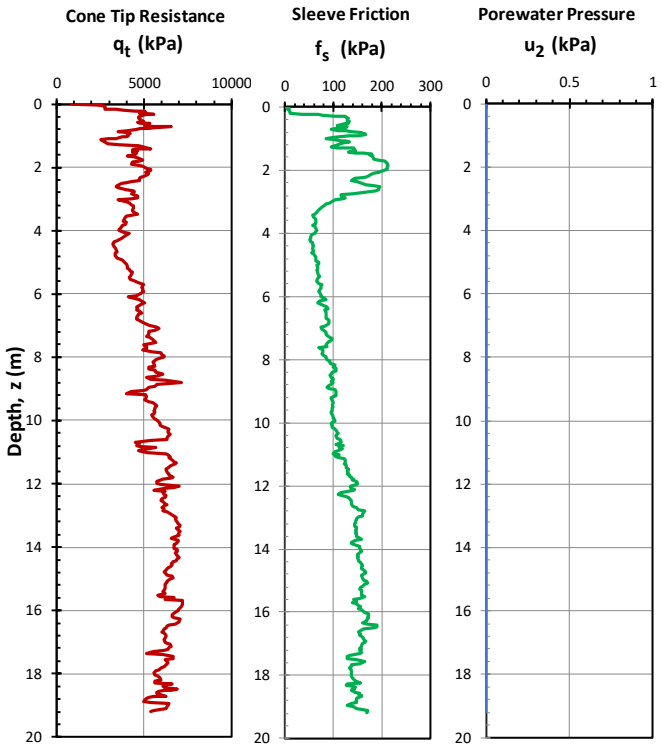


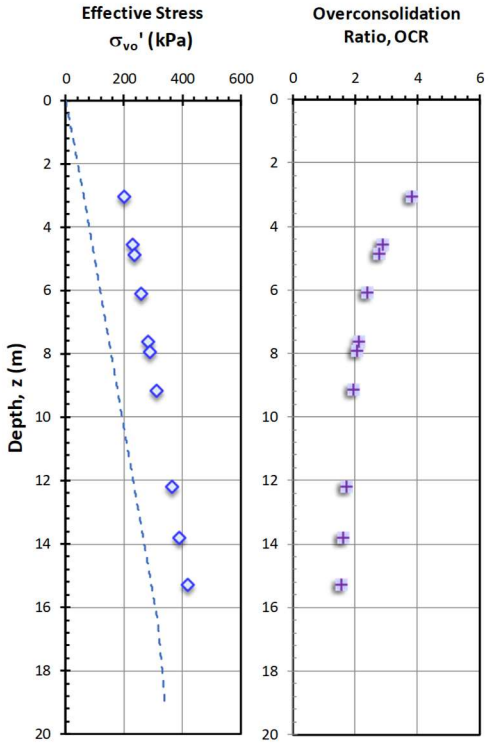

## Tornhill, Sweden

Data after Larsson (2001)

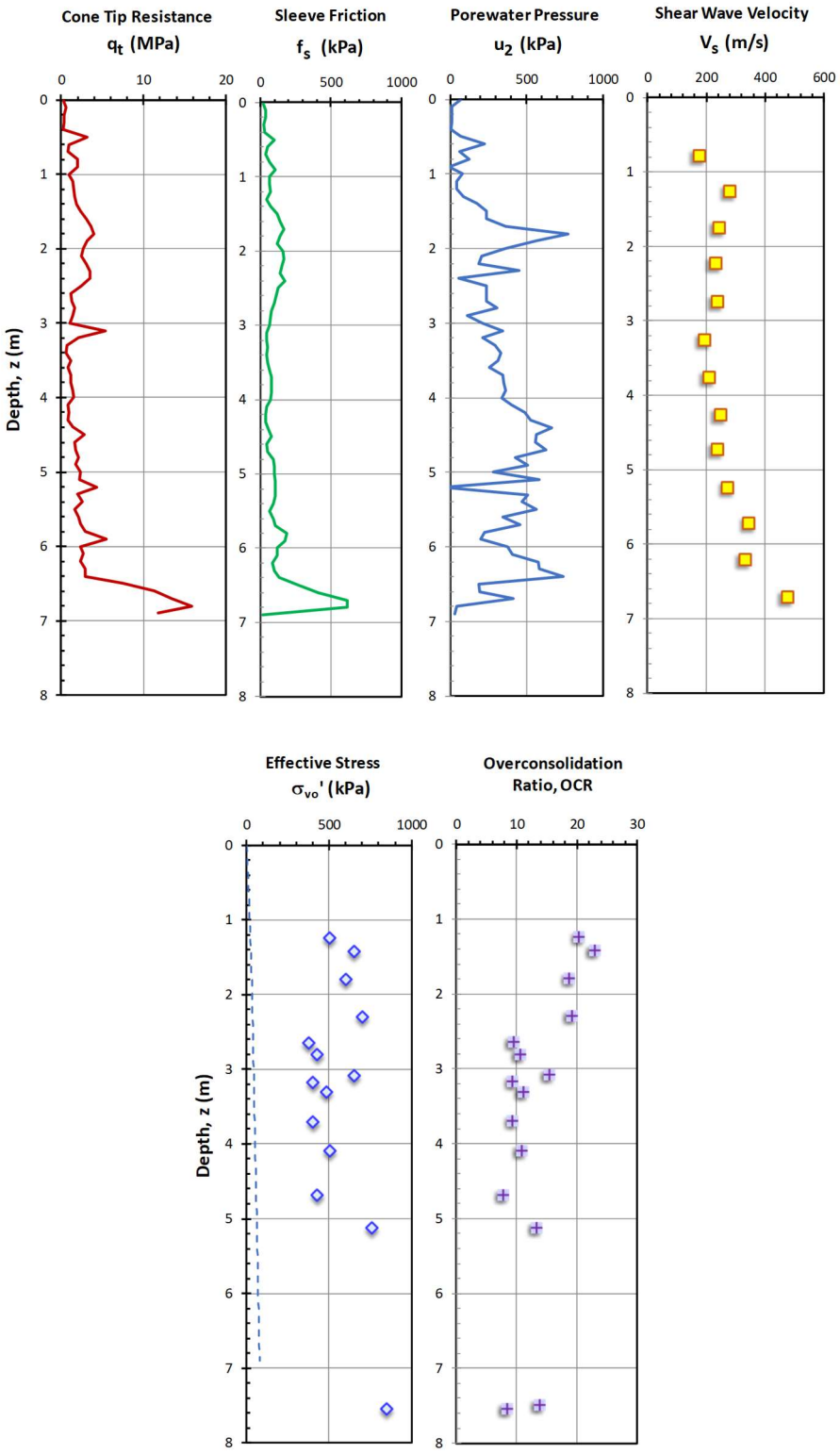

# Vagverket, Sweden

Data after Larsson (1997)

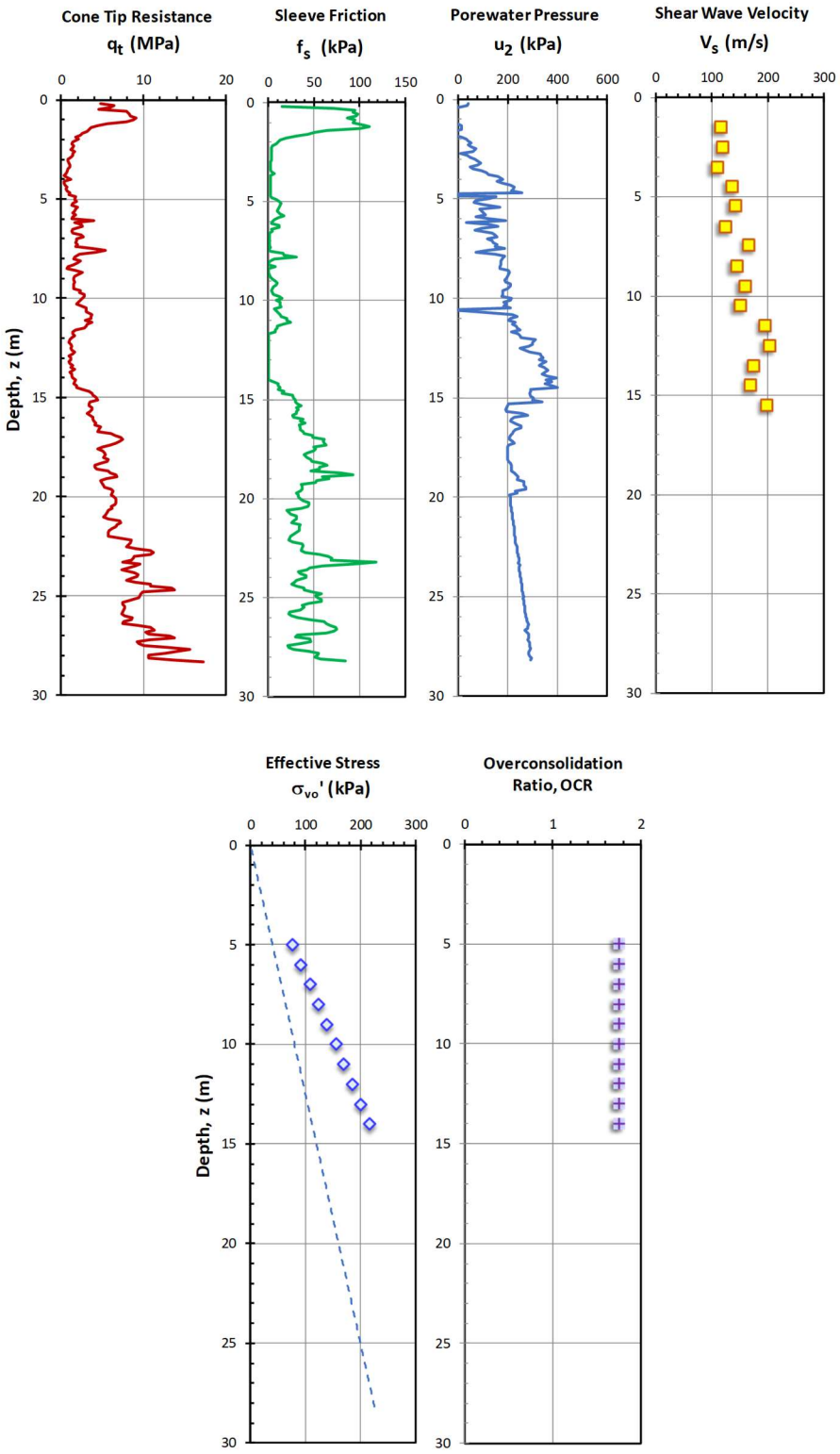

# Vatthammar, Sweden

Data after Larsson (1997)

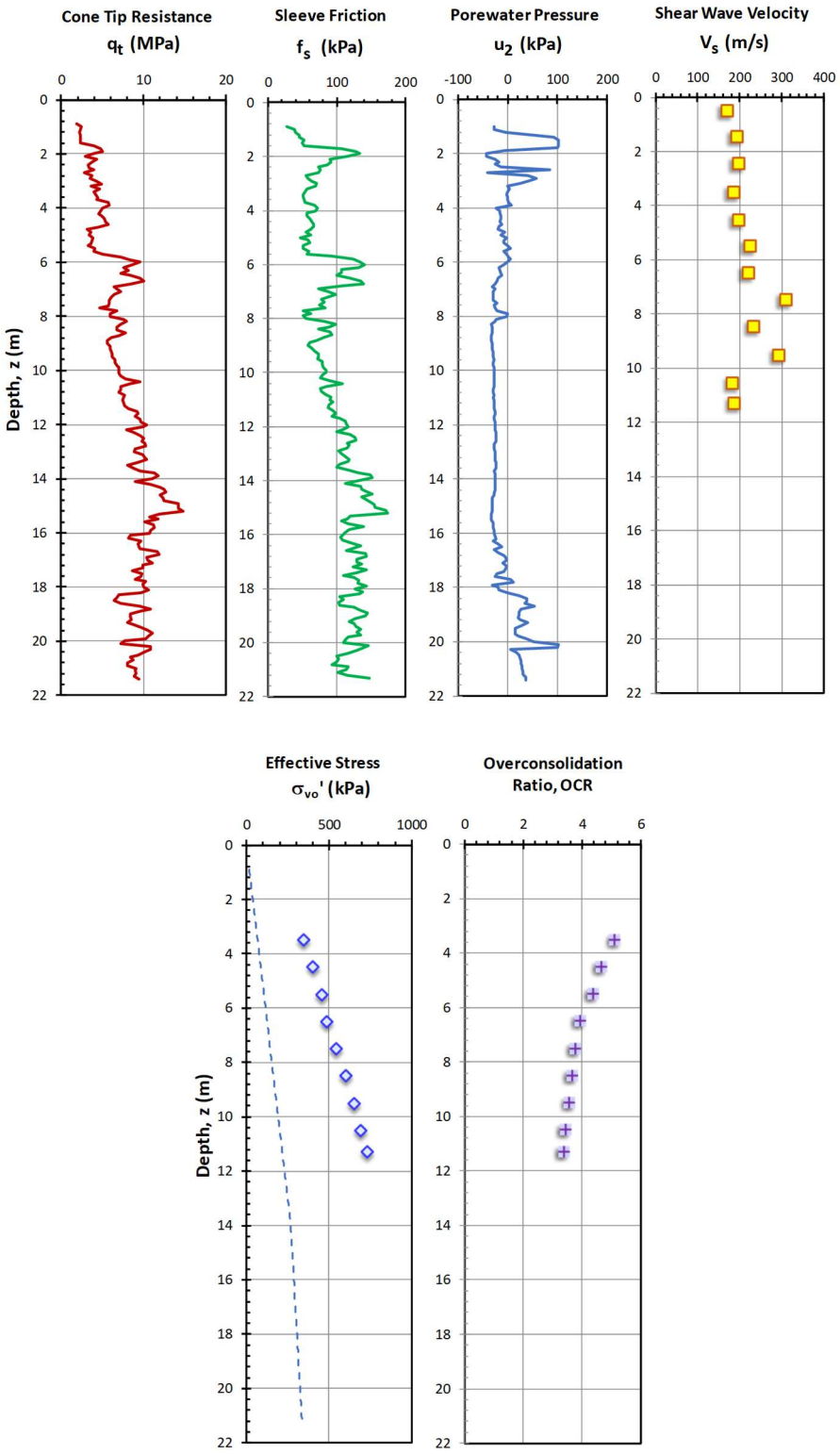

# APPENDIX C

## Sands:
## Piezocone Soundings,
## with Shear Wave Velocity
## and Stress History Data

| Site | CPTu | Shear Wave Velocity, $V_s$ | Stress History |
|---|---|---|---|
| Blessington | ✓ | ✓ | ✓ |
| Euripides | ✓ | ✓ | ✓ |
| Hibernia | ✓ | | ✓ |
| Holmen | ✓ | ✓ | ✓ |
| North Sea | ✓ | | ✓ |
| Po River | ✓ | ✓ | ✓ |
| Stockholm | ✓ | | ✓ |
| Yodo River | ✓ | ✓ | |

## Blessington, Ireland

Data after Doherty et al. (2012) – shear wave velocity from seismic DMT

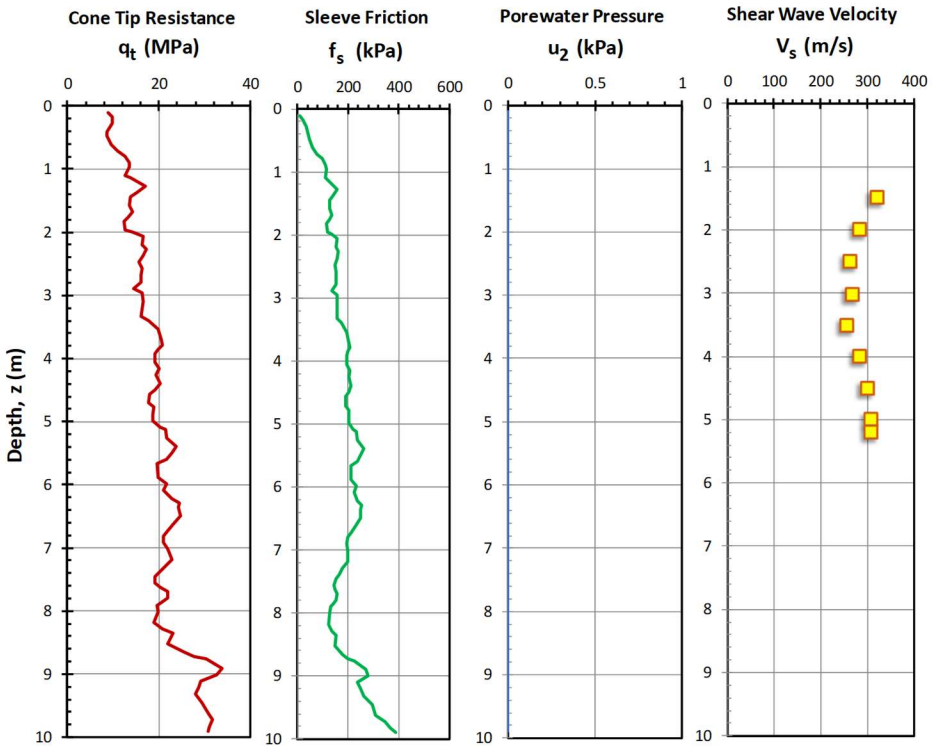


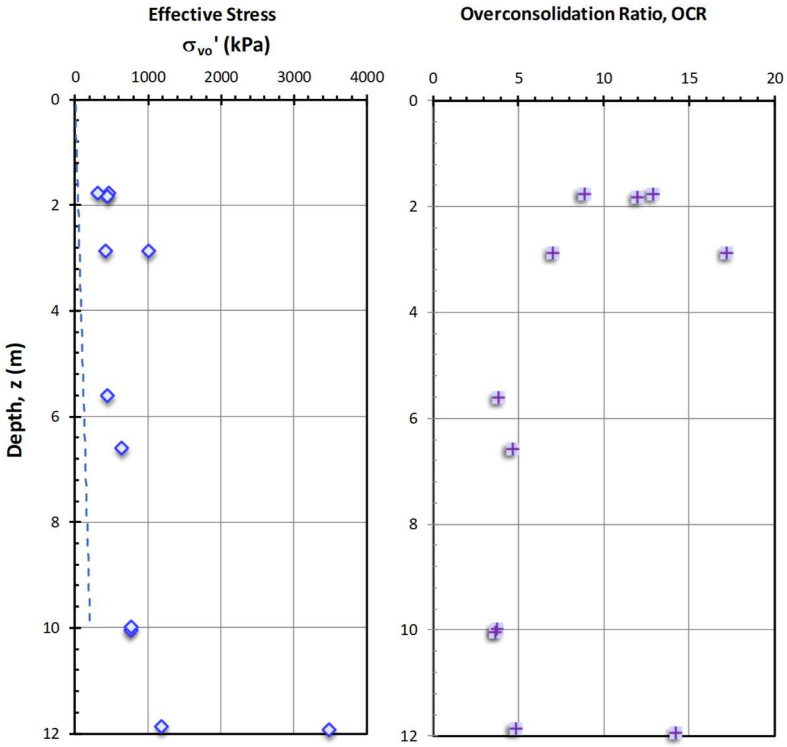

# Euripides, Netherlands

Data after Baaijens & Kolk (2004)

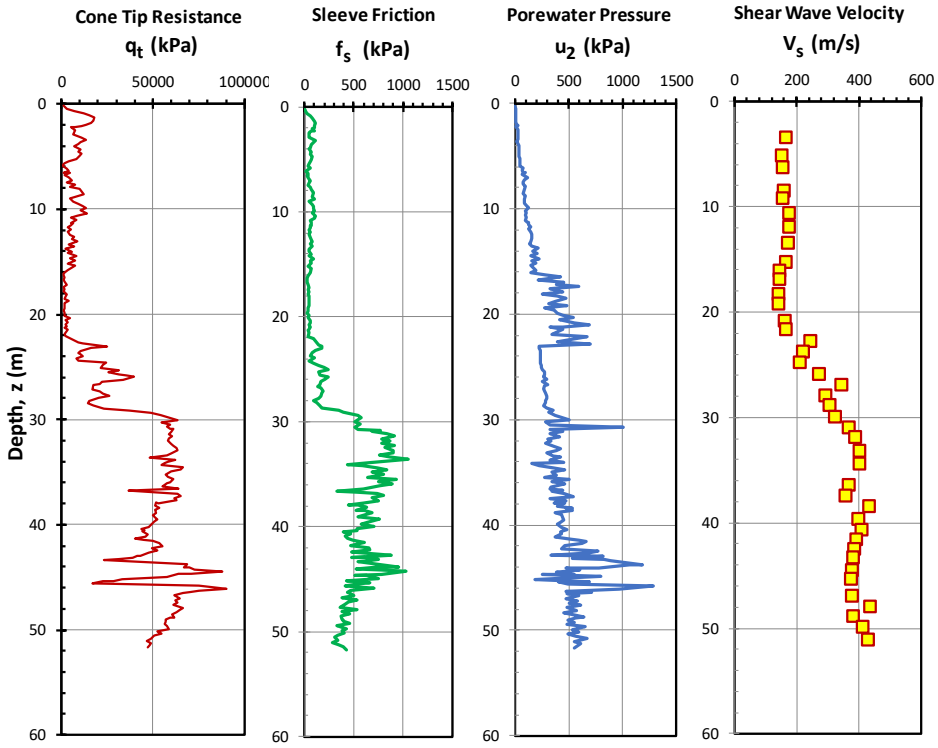


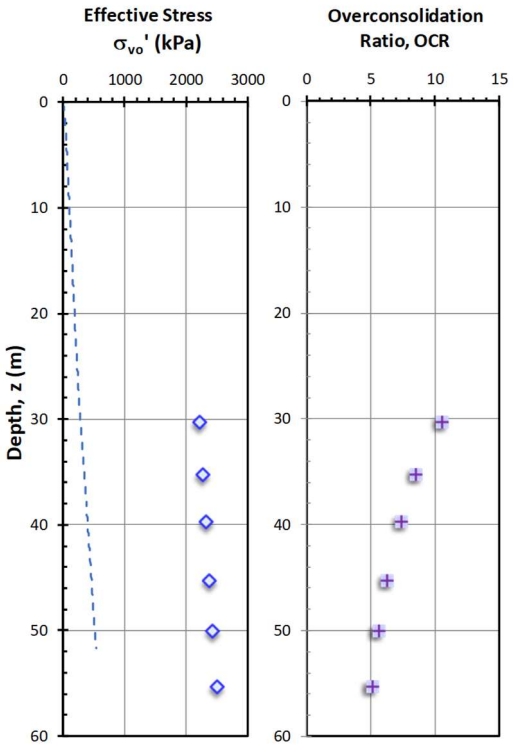

# Hibernia, Newfoundland

Data after Thompson & Long (1989)

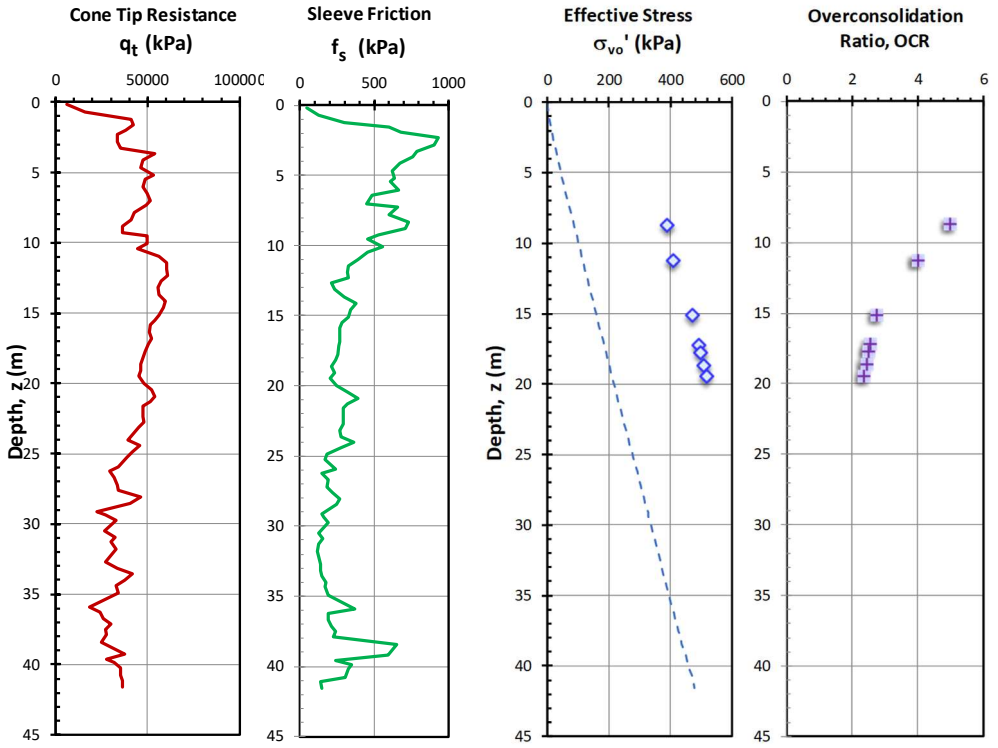


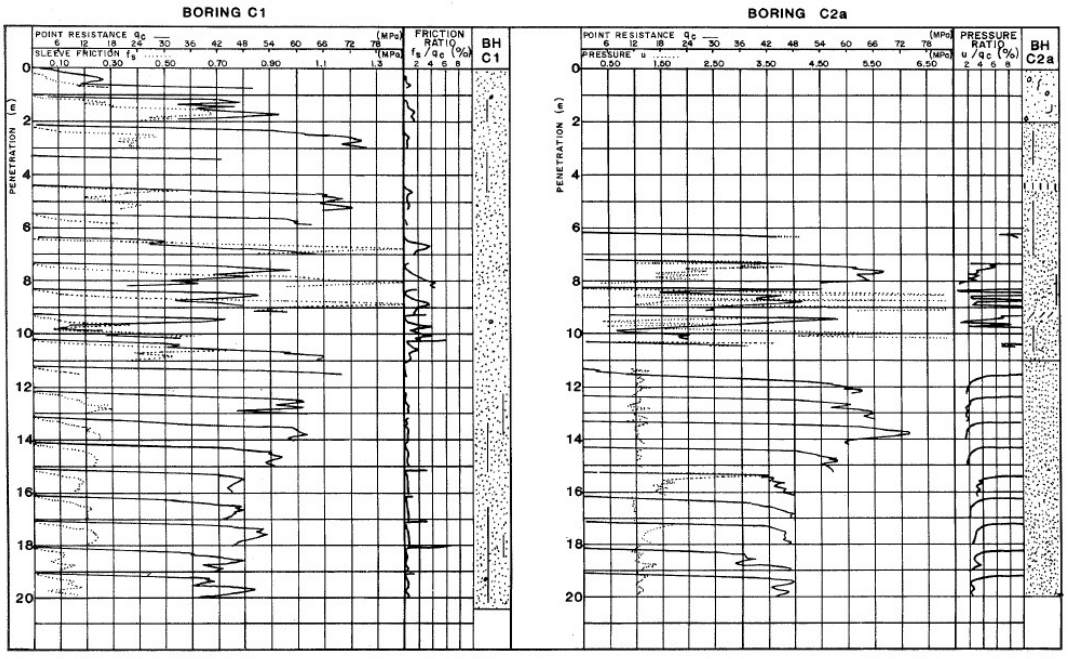


CAN. GEOTECH. J. VOL. 26, 1989

## Holmen, Drammen, Norway

Data after Lunne et al. (2003)

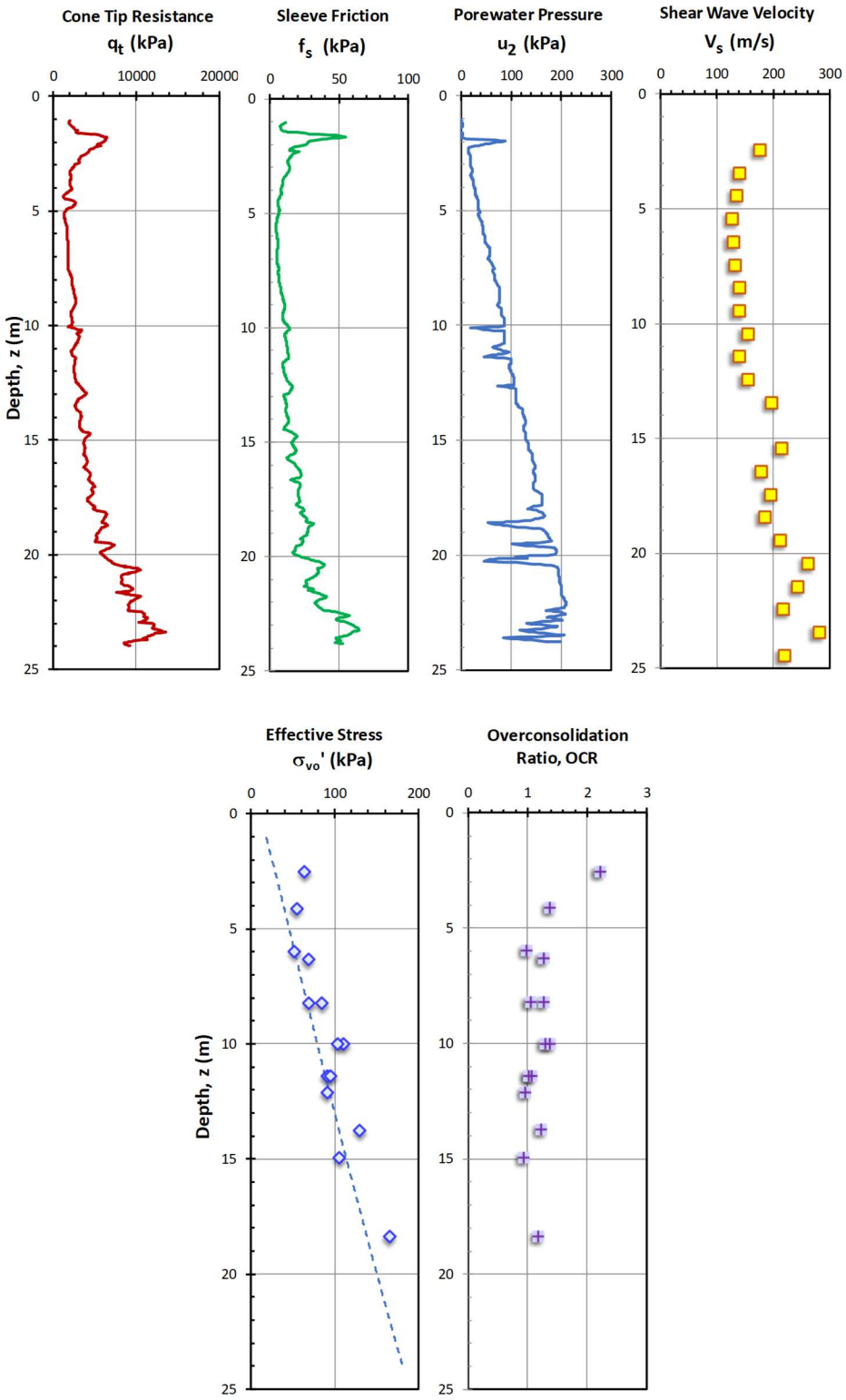

## North Sea - Ekofisk, North Sea

Data after Mitchell & Lunne (1978)

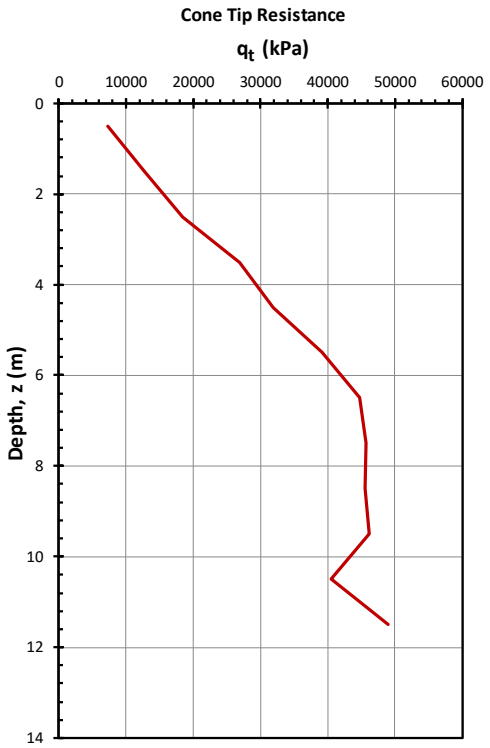


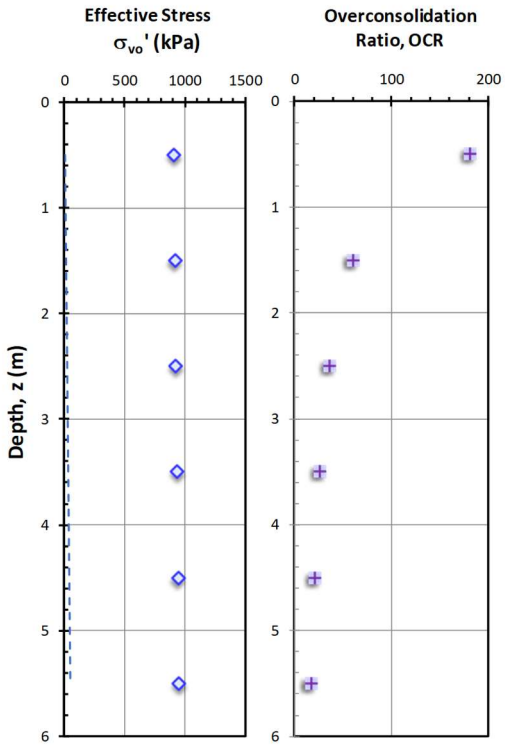

## North Sea

Data after Tom Lunne – Personal Communication

Additional piezocone sounding used to associate sleeve friction ($f_s$) data to evaluate FR%

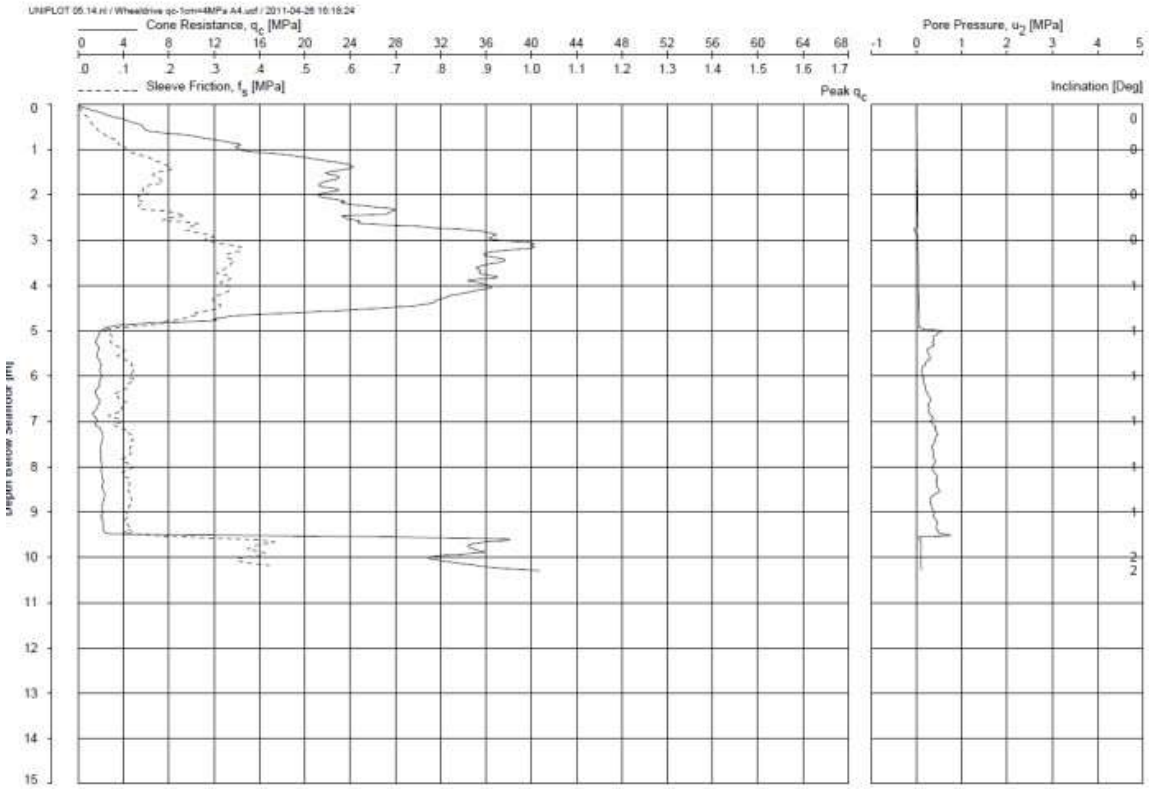

# Po River, Italy

Data after Bruzzi & Battaglio (1987)

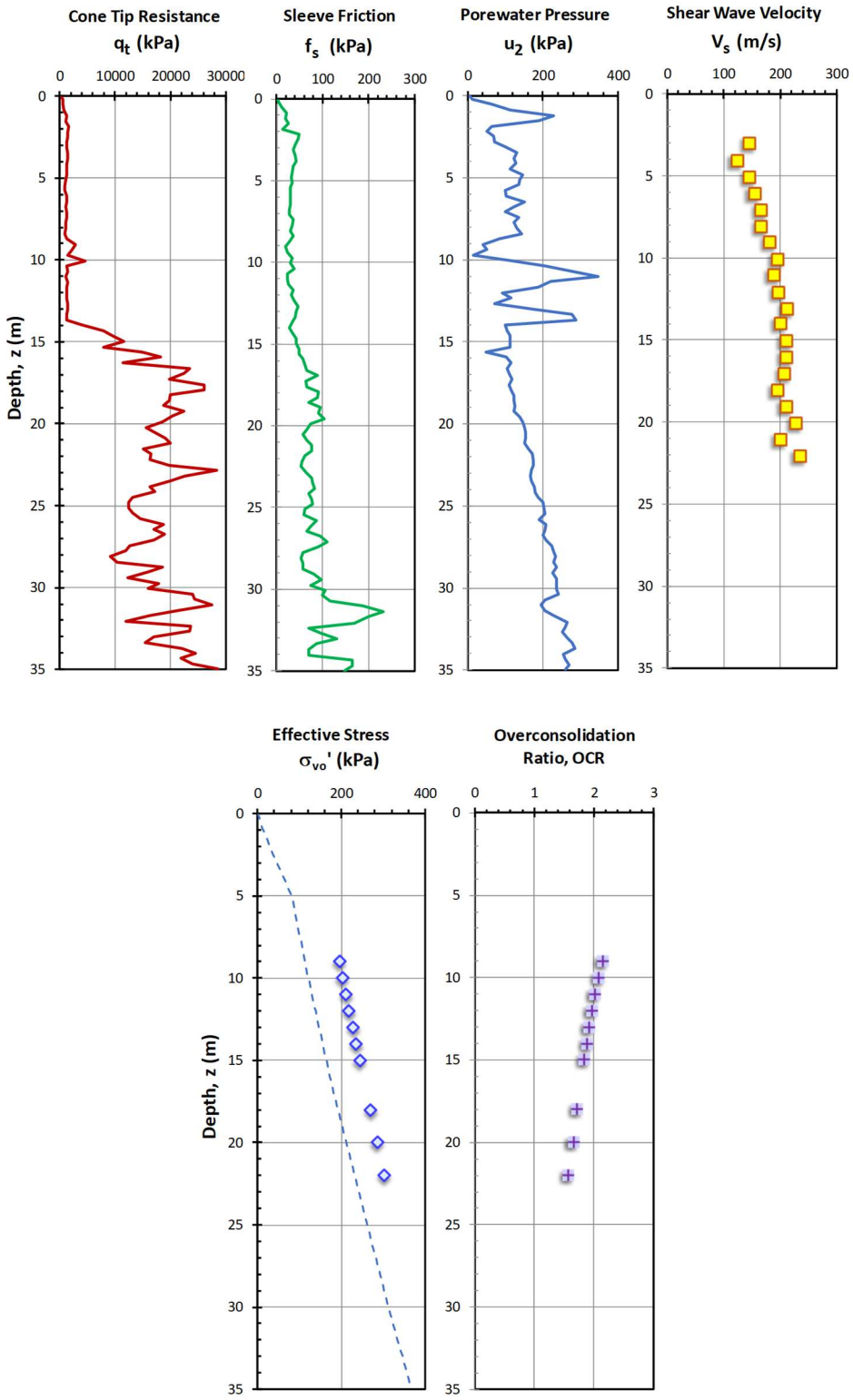

## Stockholm, Sweden *

Data after Dahlberg (1974) - The sand is OC with 4 presented CPT soundings. No sleeve Friction data were measured. A near by sounding by Norconsult AB was used to have an estimate of the sleeve friction value.

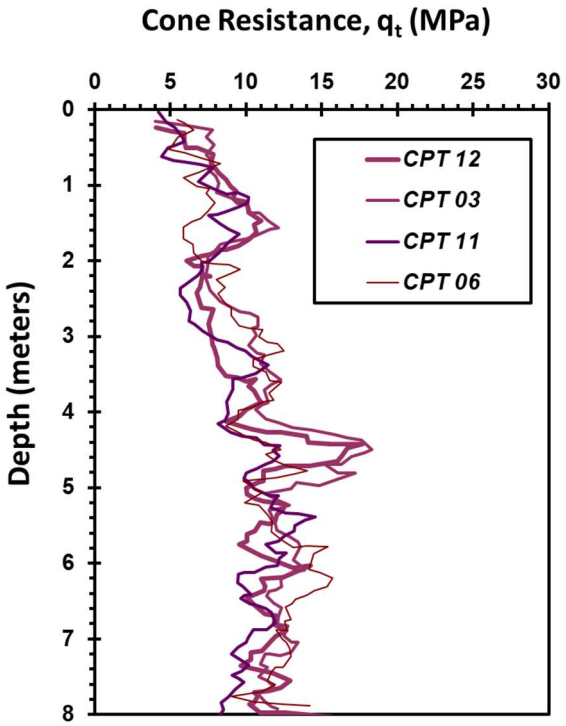


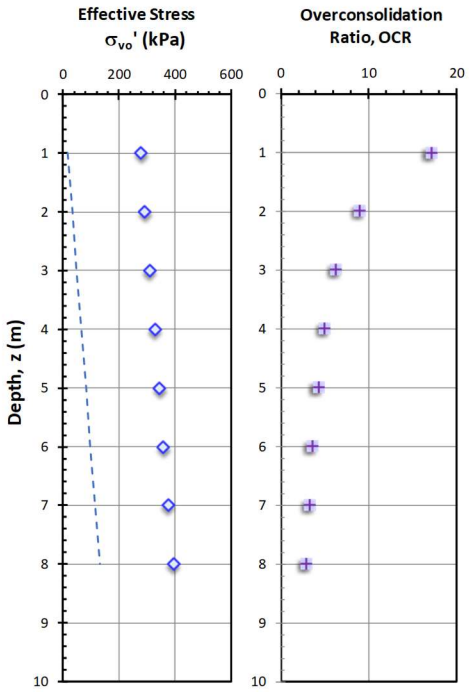

## Stockholm, Sweden *

A near by sounding by Norconsult AB was used to have an estimate of the sleeve friction value. The sands here are located below 9.5 m.

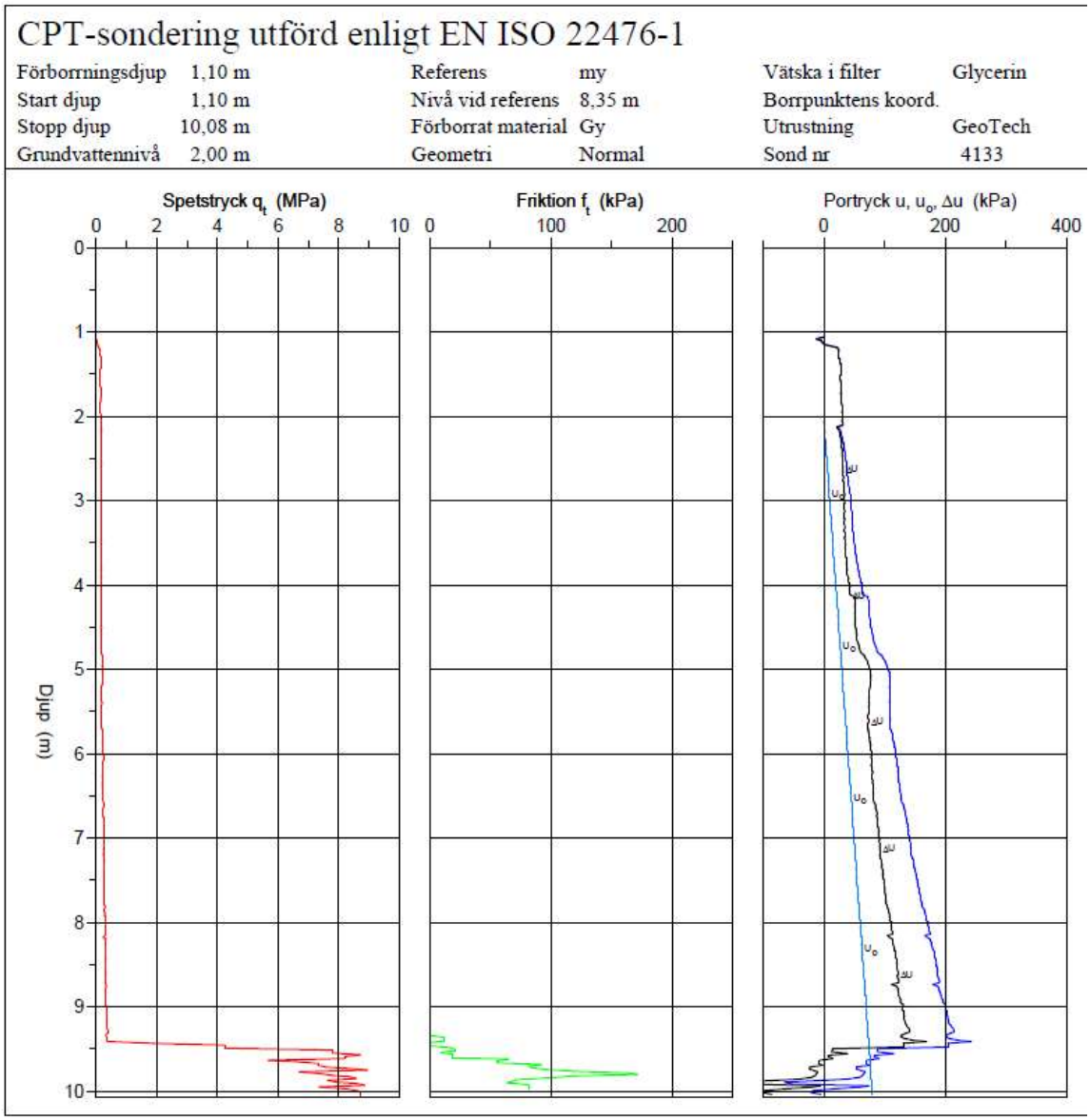

## Yodo River-Yodogawa, Osaka, Japan

Data after Mimura (2003), Yamashita et al. (2003) – $V_s$ from PS Logging

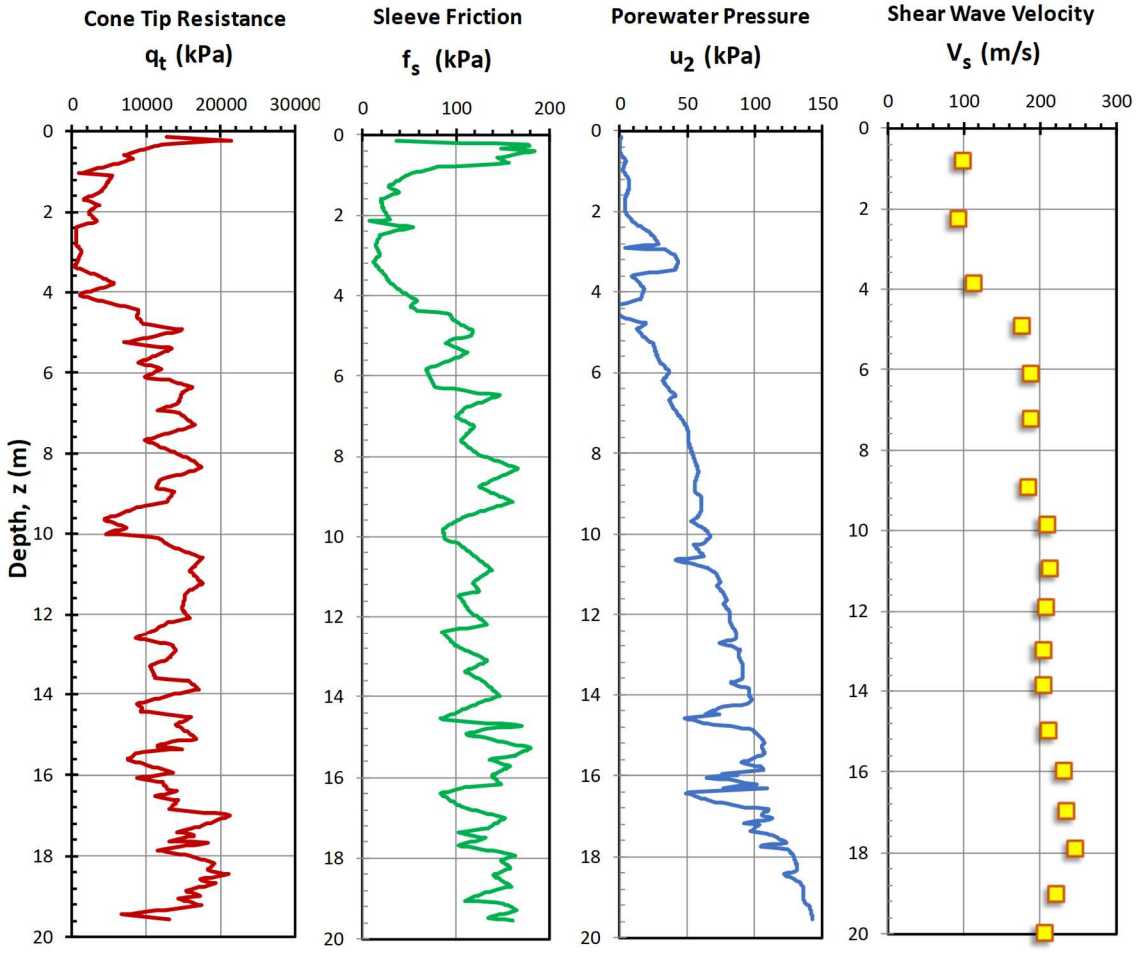

# APPENDIX D

## Organic Clays:
## Piezocone Soundings,
## with Stress History and
## Undrained Shear Strength Data

| Organic Clay | Location | References |
|---|---|---|
| Barra da Tijuca - CM1 | Brazil | de Almeida et al. (2010) |
| Barra da Tijuca - Gleba | | |
| Gammelgården | Sweden | Larsson et al. (2007); Westerberg et al. (2015) |
| Hjoggböle | | |
| Huaiyan | China | Cai et al. (2016) |
| Markermeer peat | Holland | Zwanenburg & Jardine (2015) |
| Jefferson Parish B-7, LA | USA | Tümay et al. (2013) |
| Jefferson Parish B28, LA | USA | |
| Mexico City Clay | Mexico | Cruz & Mayne (2006) |
| Recife RRS1 | Brazil | Coutinho (2007) |
| Recife RRS2 | | |
| Raszynka River valley | Poland | Kowalczyk et al. (2017) |
| Sarapuí II | Brazil | Jannuzzi et al. (2015) |
| Stargard Szczeciński | Poland | Młynarek et al. (2014) |
| Suape subarea A | Brazil | Coutinho & Bello (2014) |
| Suape subarea C | Brazil | Coutinho & Bello (2014) |
| Sunderbyn | Sweden | Larsson et al. (2007); Westerberg et al. (2015) |
| Suisun Bay, CA | USA | Merani et al. (2016) |
| Umeå bangård | Sweden | Larsson et al. (2007); Westerberg et al. (2015) |
| Västerslätt | | |

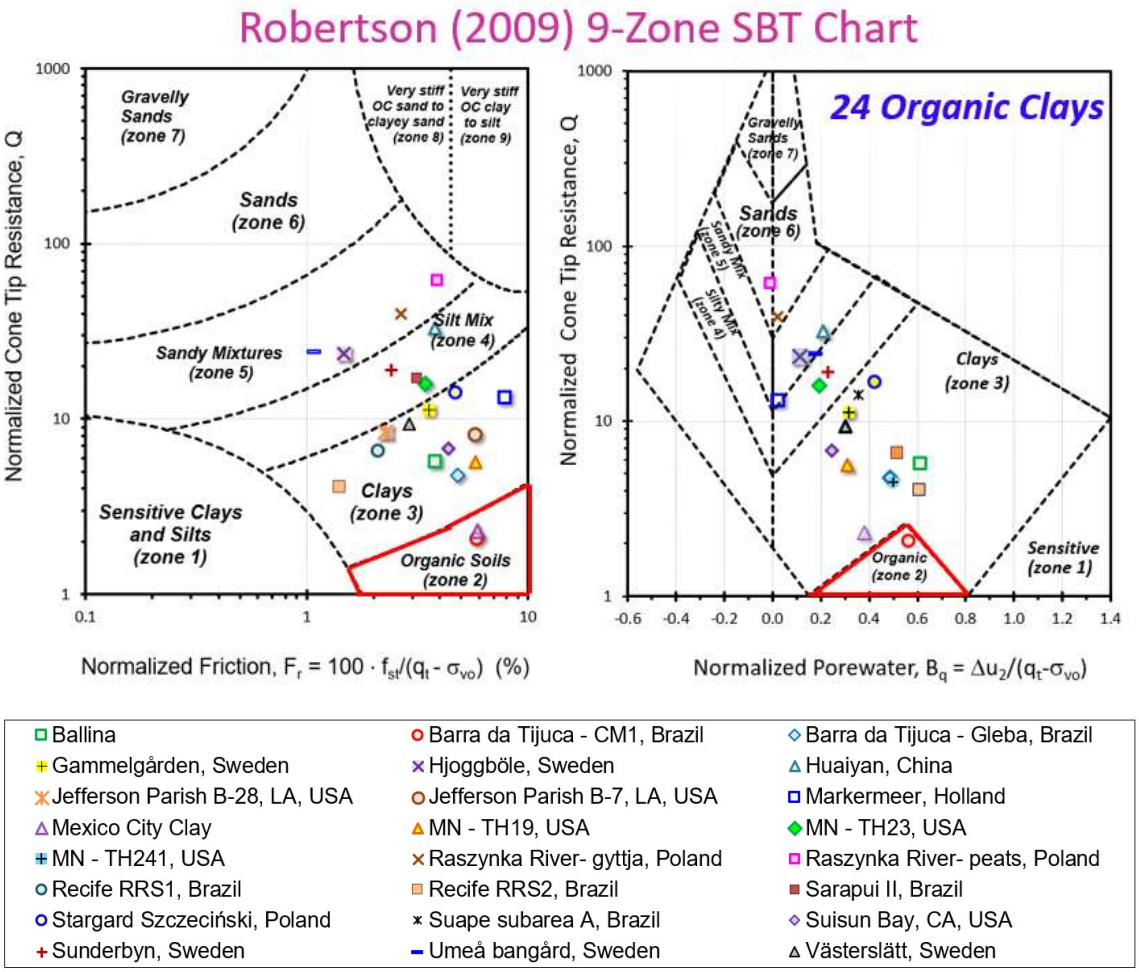


A representation of all compiled organic clays from chapters 4 and 8 on Robertson (2009) 9 – zone chart where clearly most of the organic clays do **NOT** fall within the correct zone (ZONE 2). Indicating the presence of an issue in detecting organic clays using conventional soil classification charts.

## Gammelgården, Sweden

Data after Larsson et al. (2007); Westerberg et al. (2015)

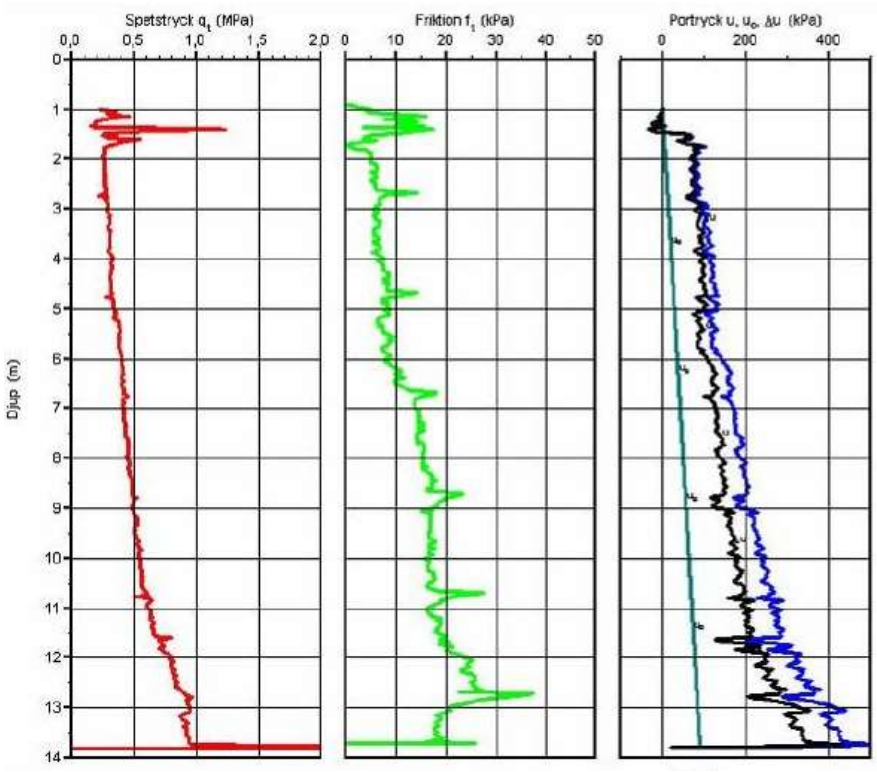


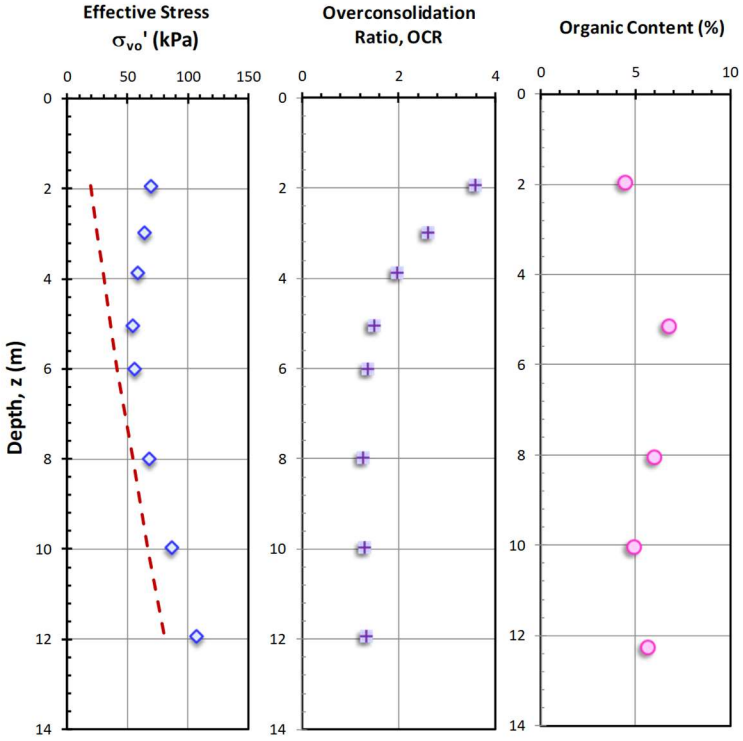

## Hjoggböle, Sweden

Data after Larsson et al. (2007); Westerberg et al. (2015)

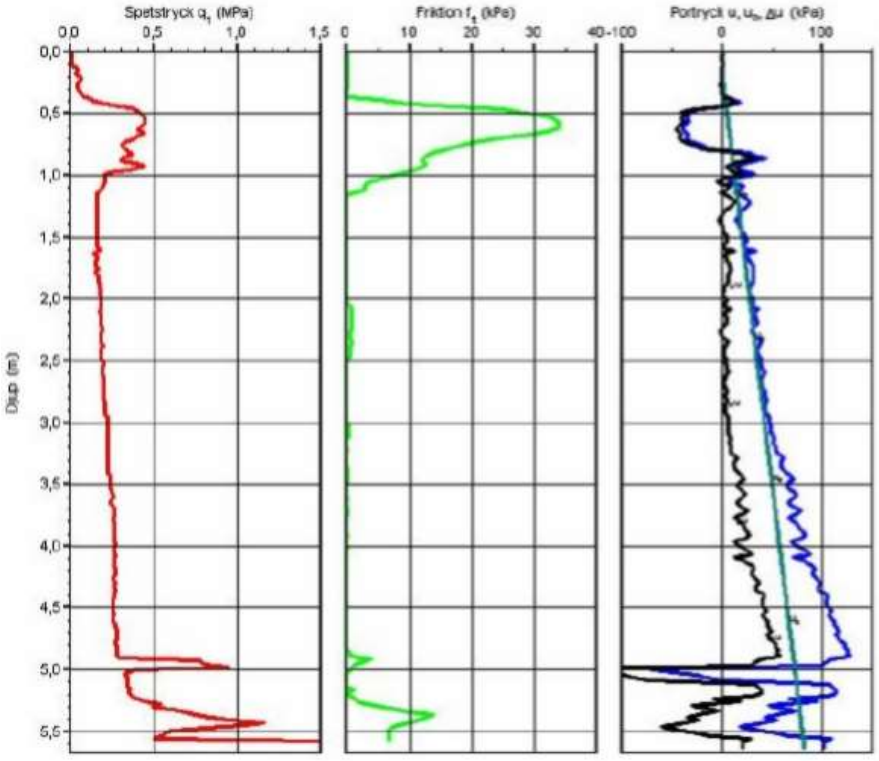


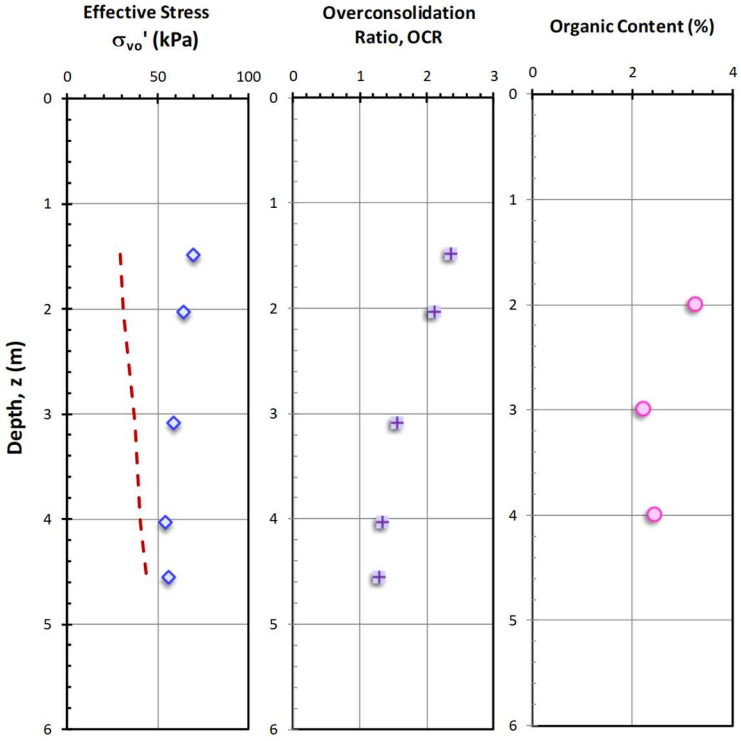

# Recife RRS1, Brazil

Data after Coutinho (2007)

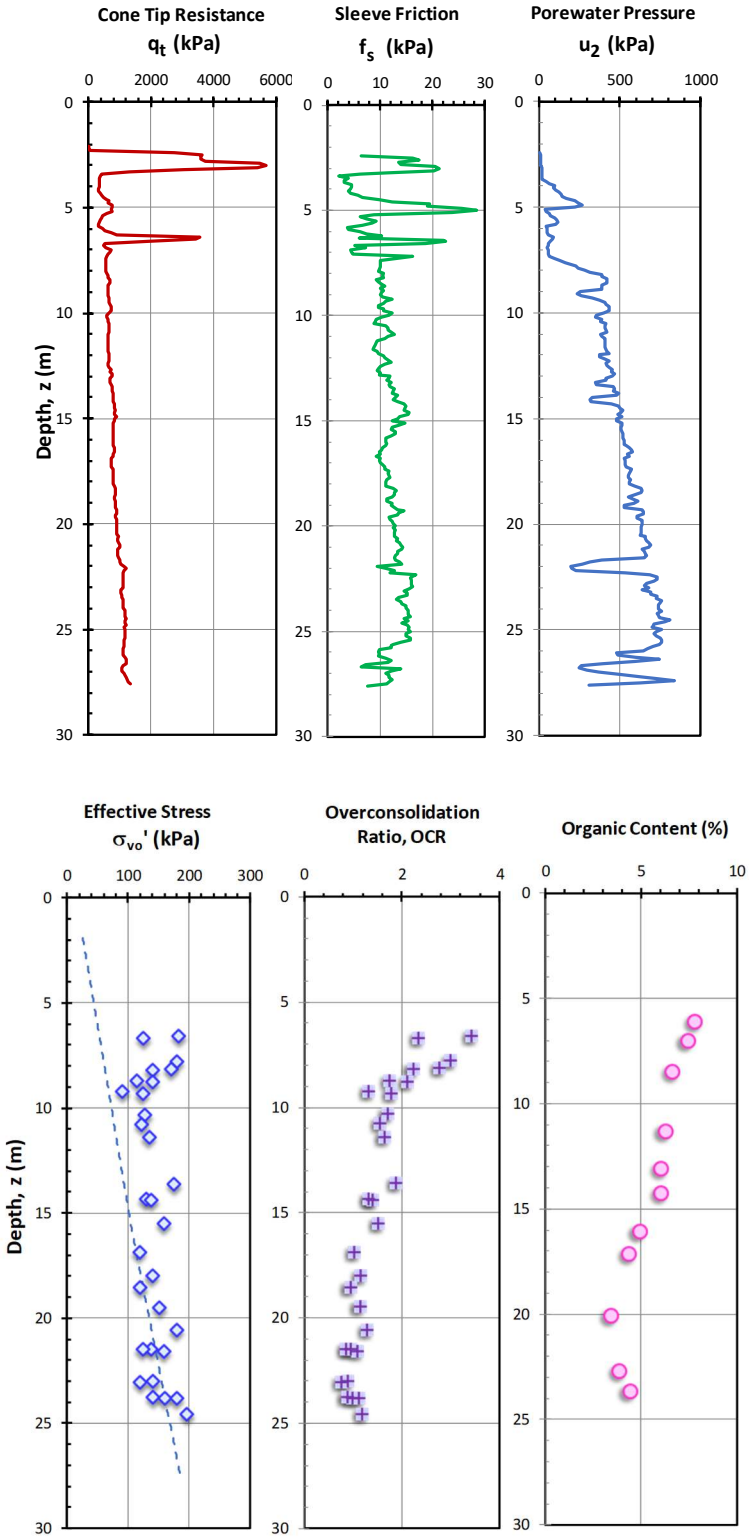

# Recife RRS2, Brazil

Data after Coutinho (2007)

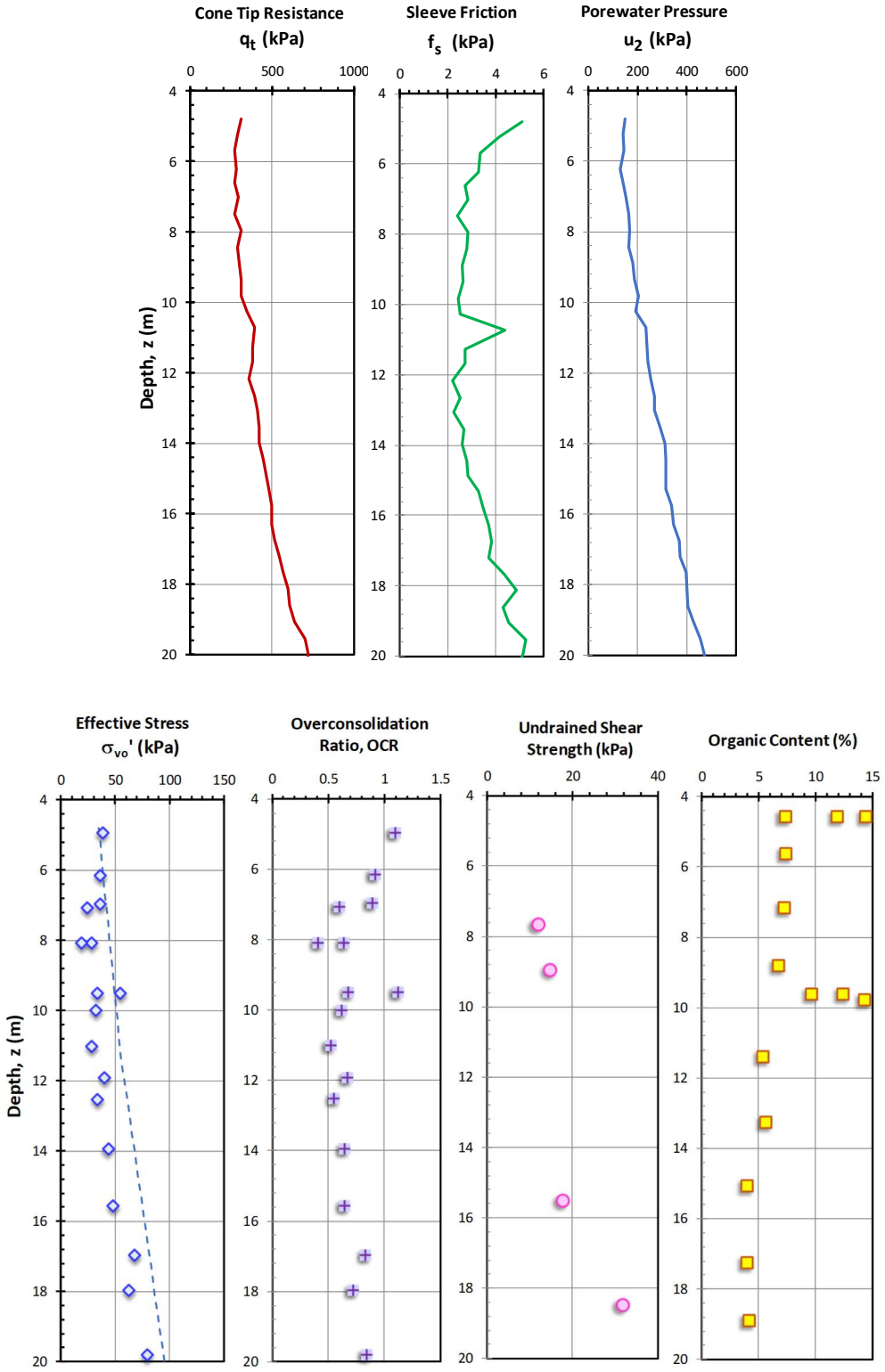

# Sarapuí II, Brazil

Data after Jannuzzi et al. (2015)

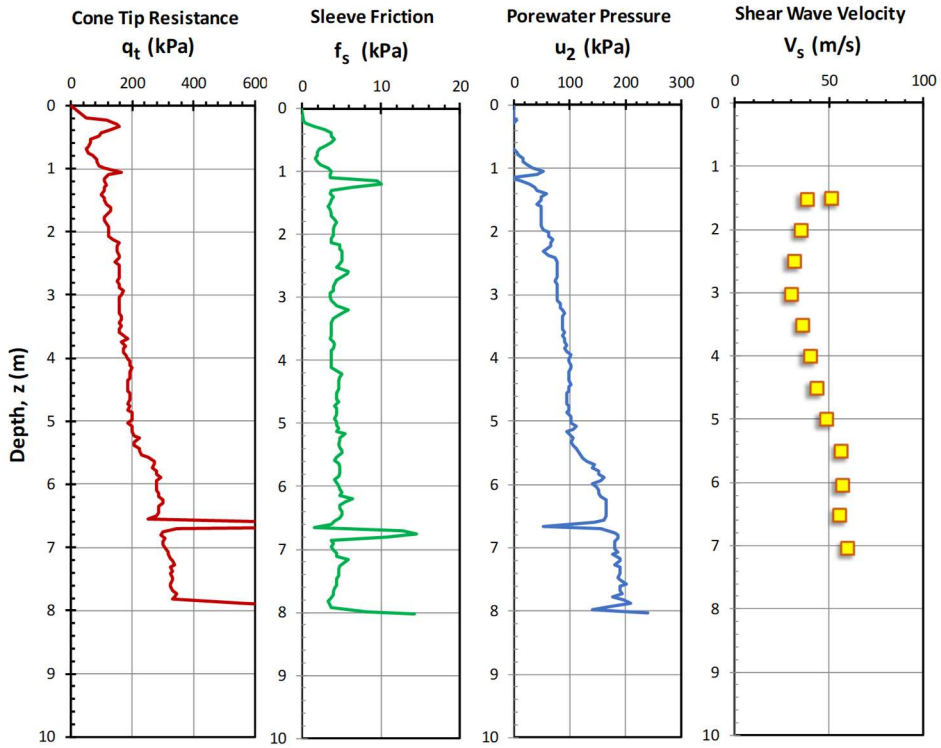


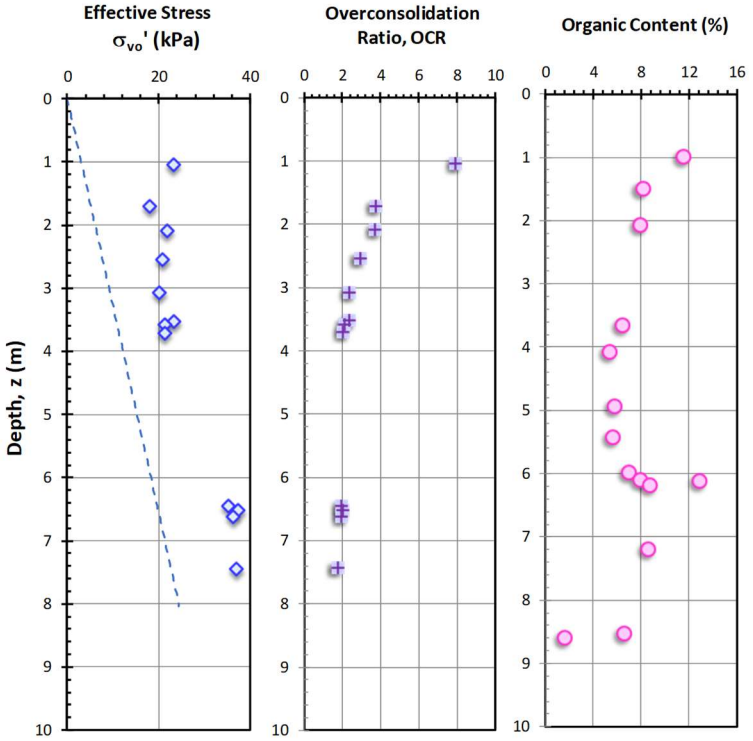

## Sunderbyn, Sweden

Data after Larsson et al. (2007); Westerberg et al. (2015)

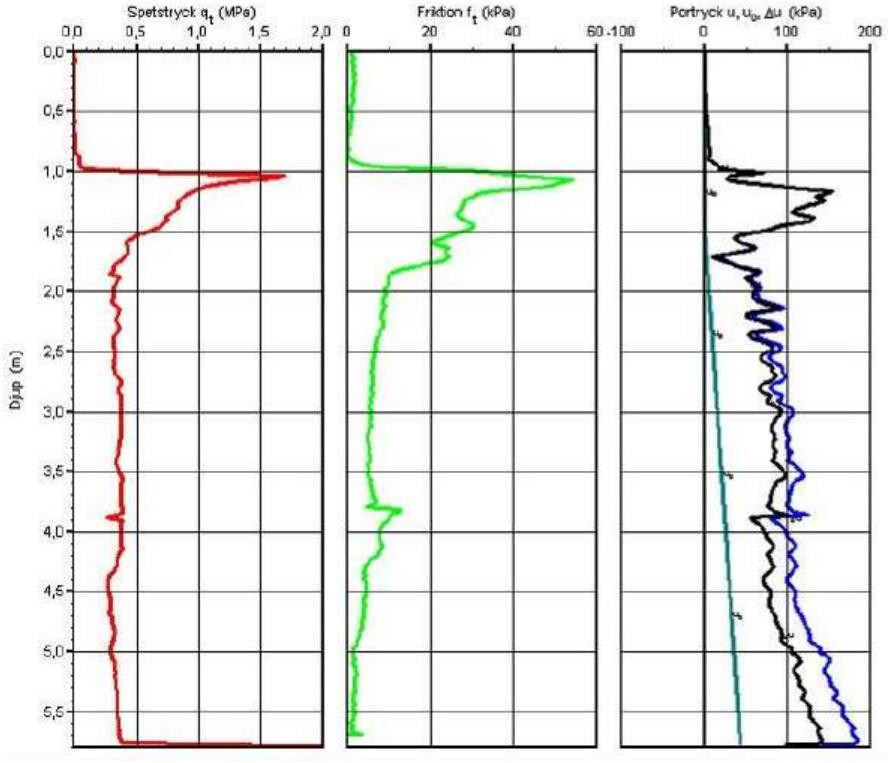


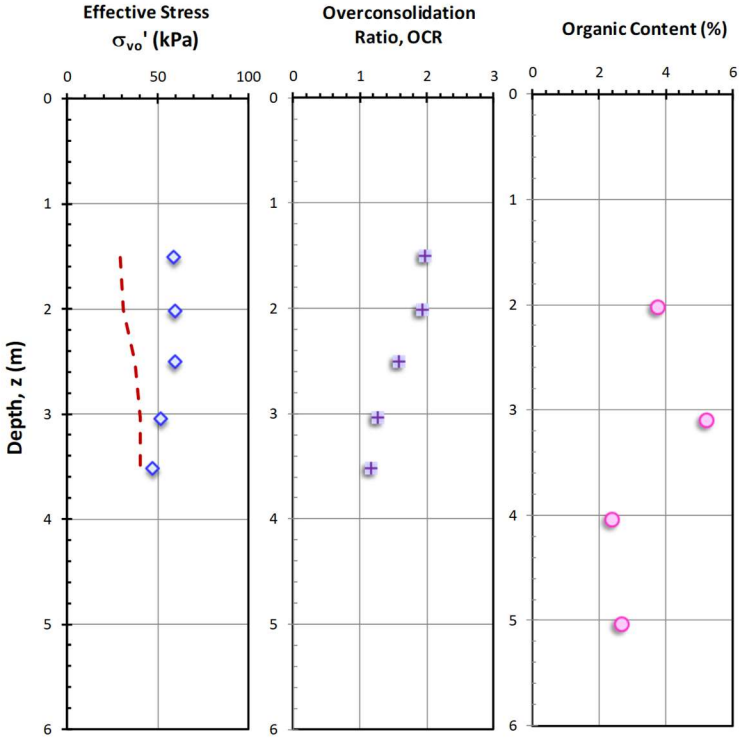

## Umeå bangård, Sweden

Data after Larsson et al. (2007); Westerberg et al. (2015)

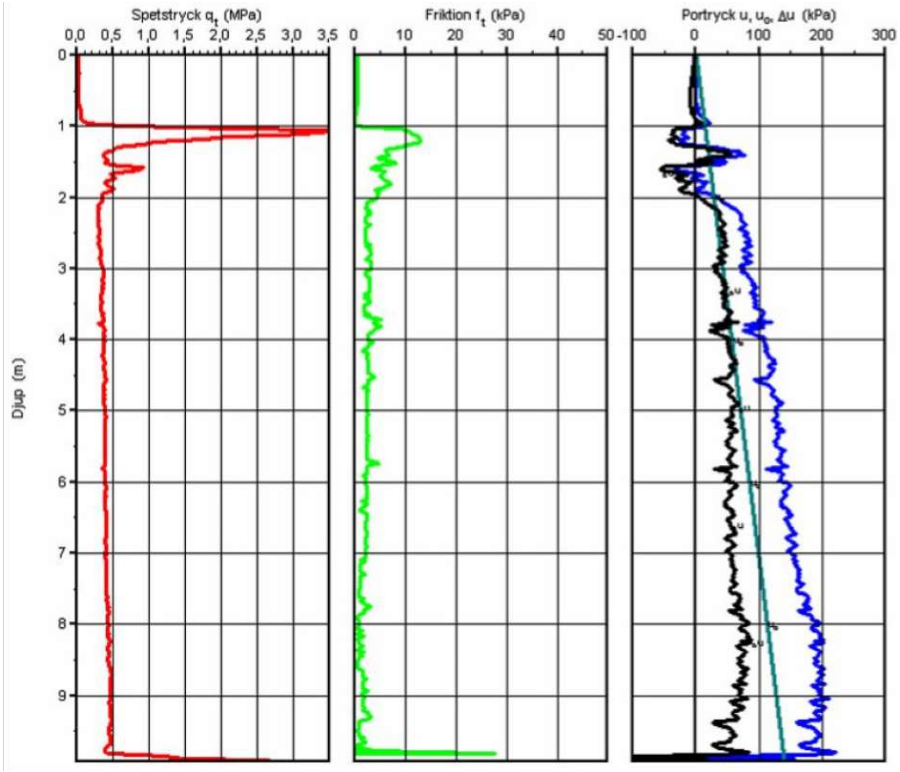


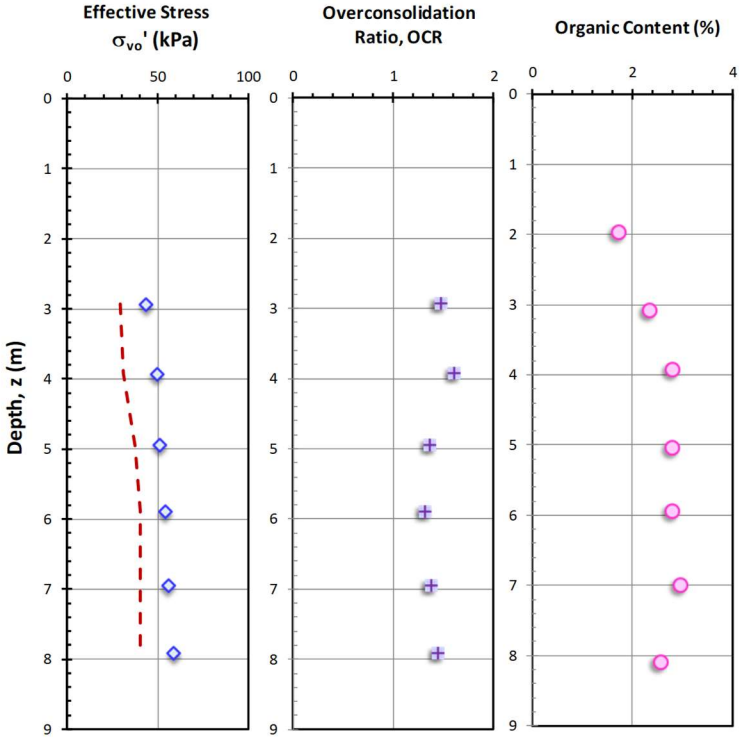

## Västerslätt, Sweden

Data after Larsson et al. (2007); Westerberg et al. (2015)

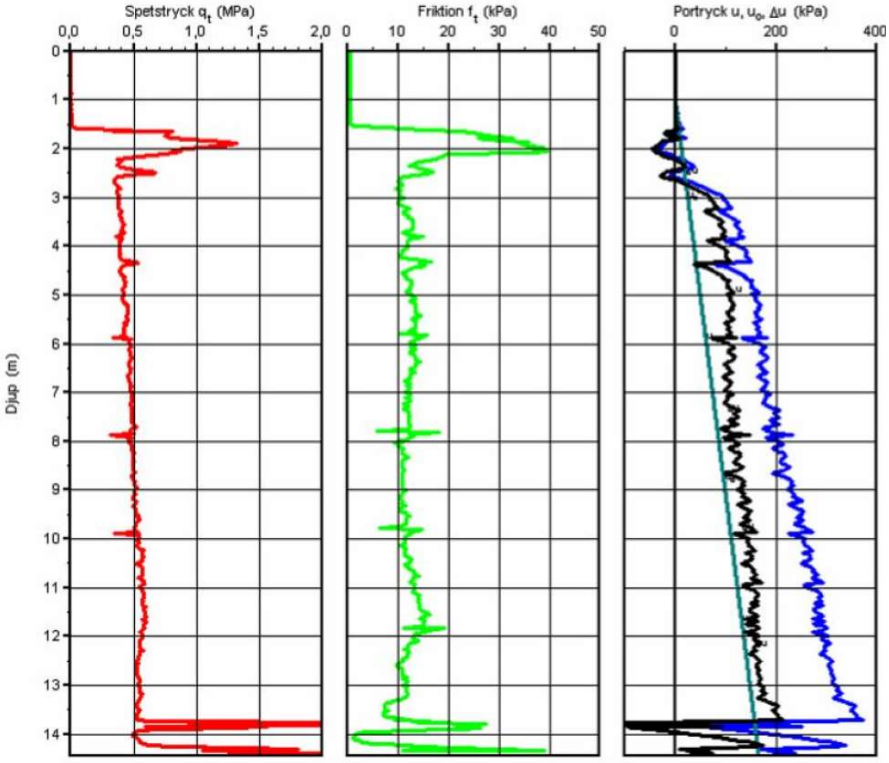


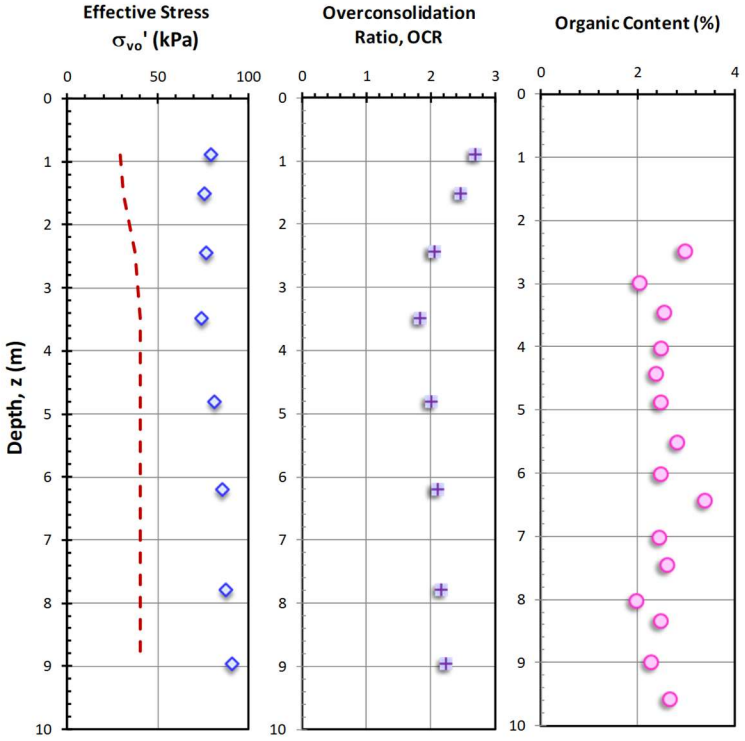

## Markermeer, Holland

Data after Zwanenburg (2015)

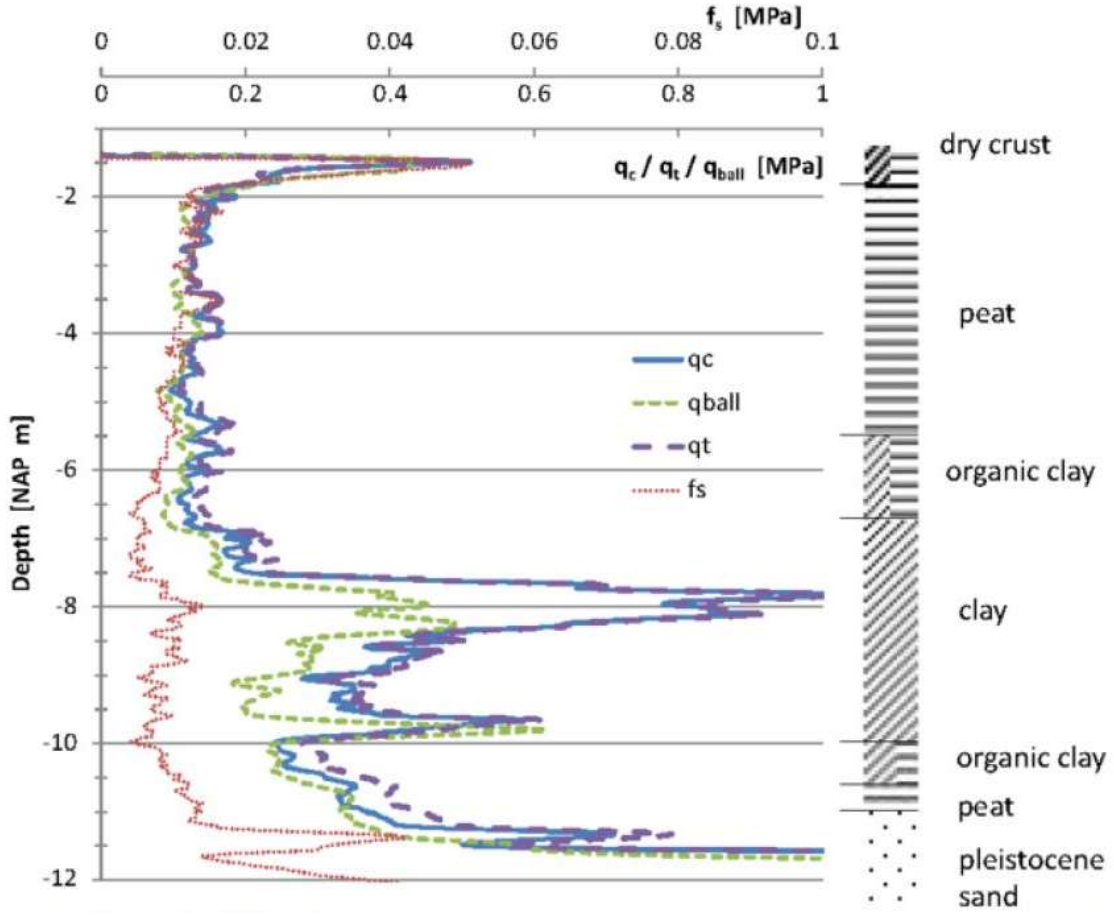

## Huaiyan Expressway Site, China

Data after Cai et al. (2016)

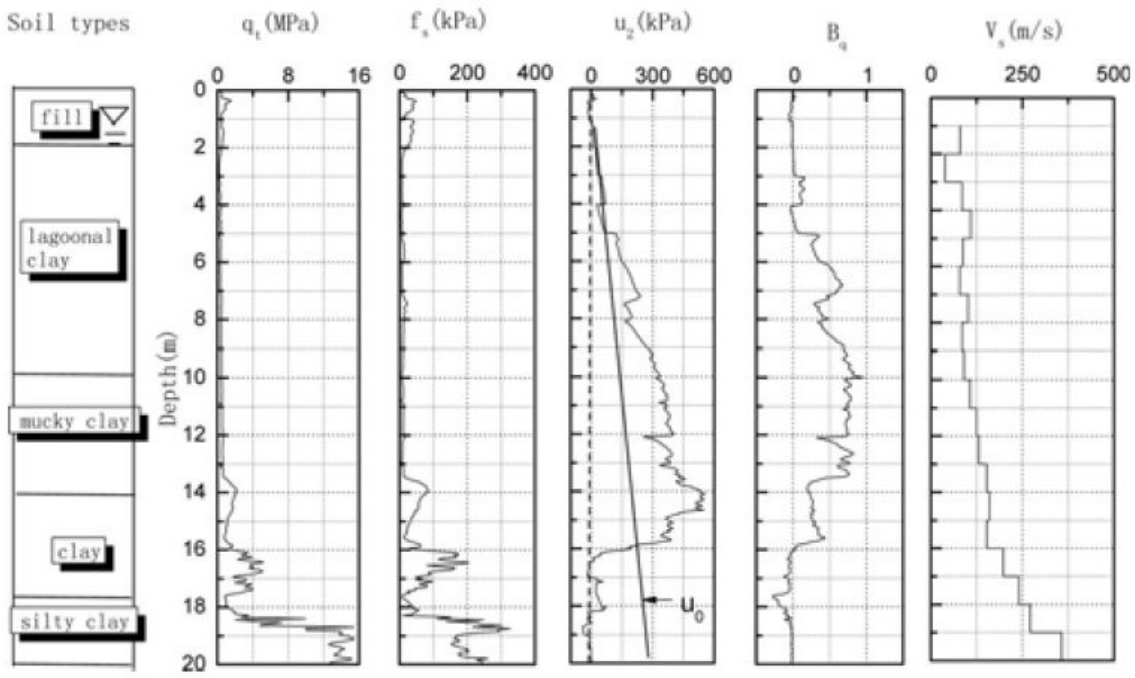

## Jefferson Parish B-28, LA

Data after Tümay et al. (2013)

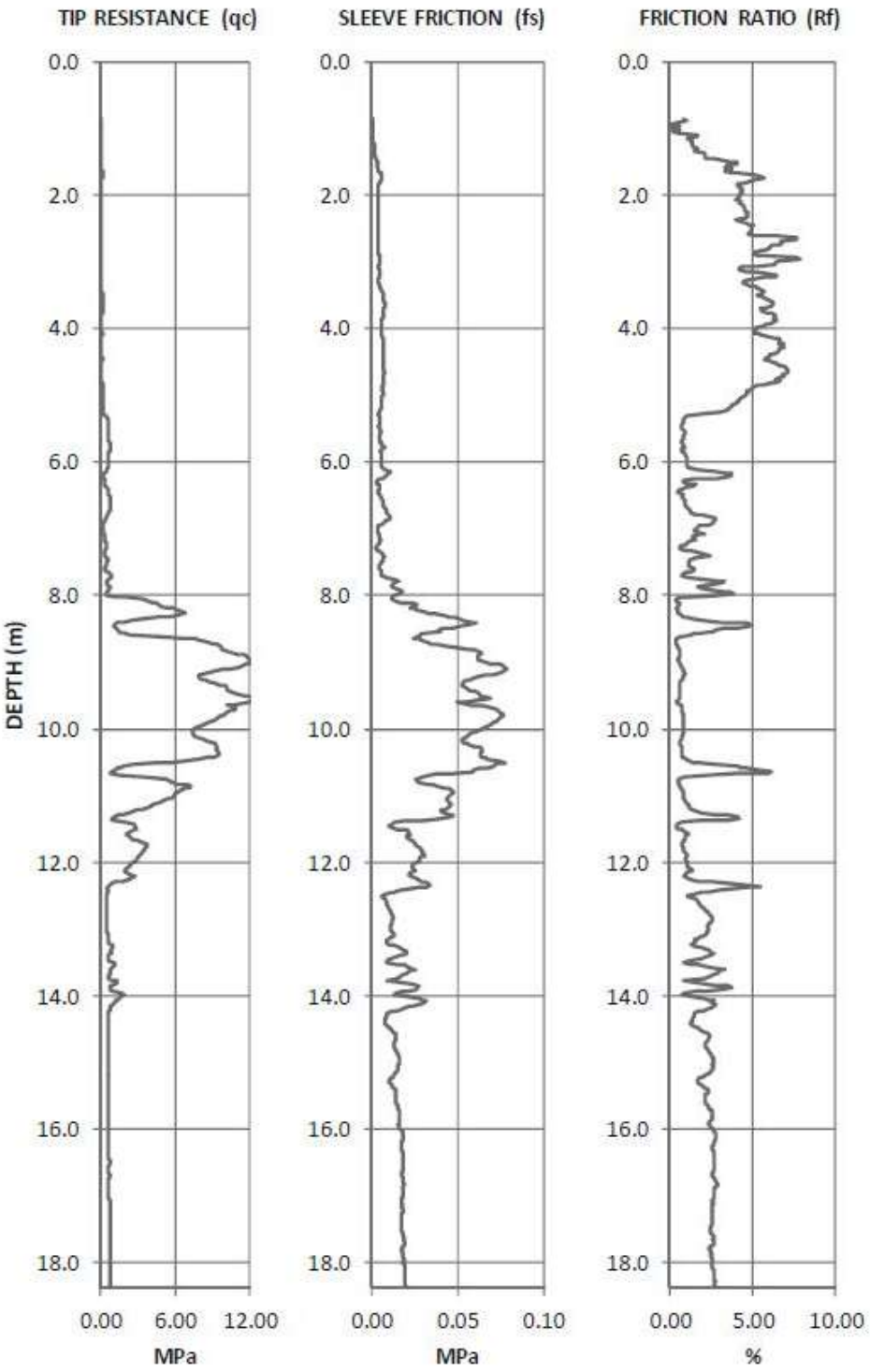

## Jefferson Parish B7, LA

Data after Tümay et al. (2013)

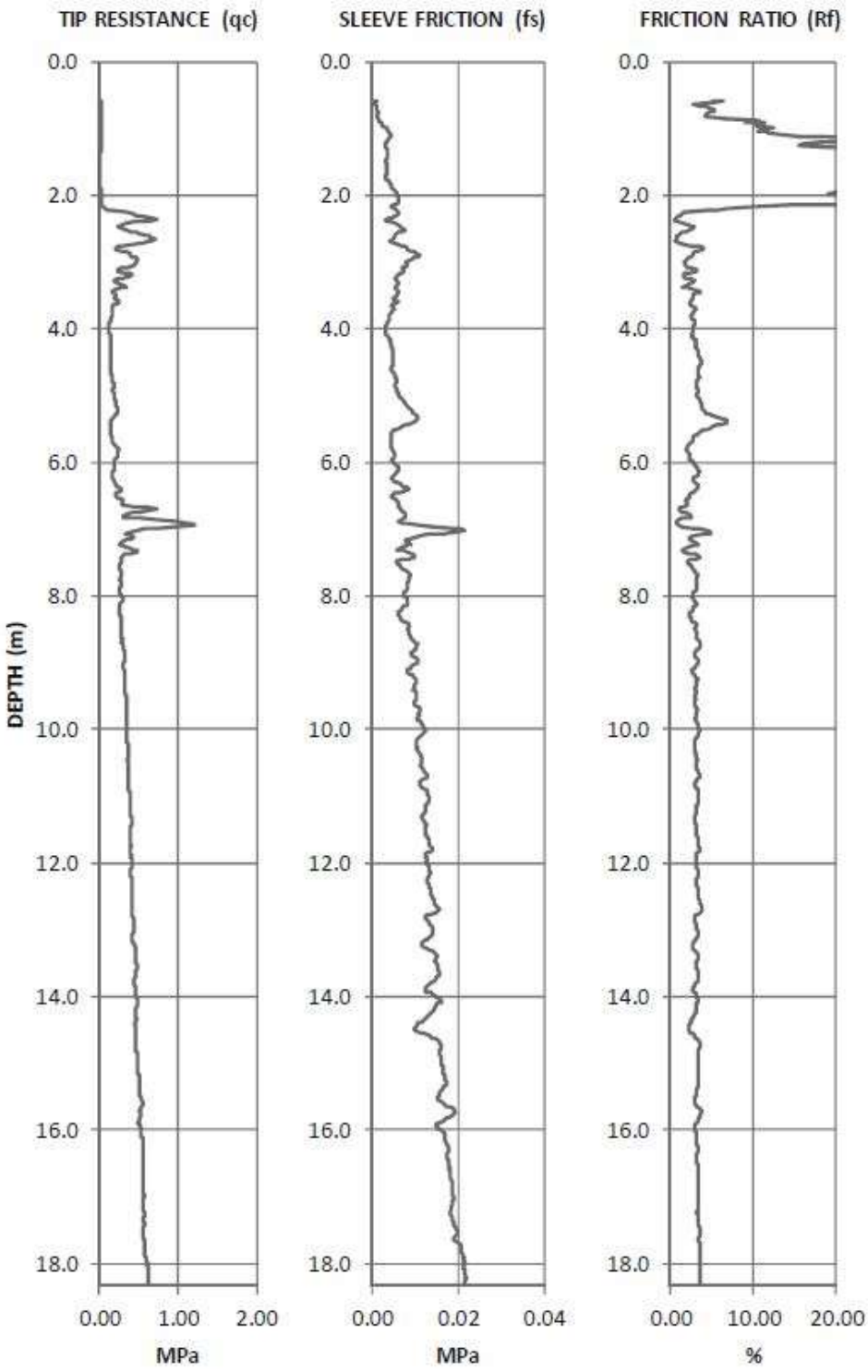

## Stargard Szczeciński, Poland

Data after Młynarek et al. (2014)

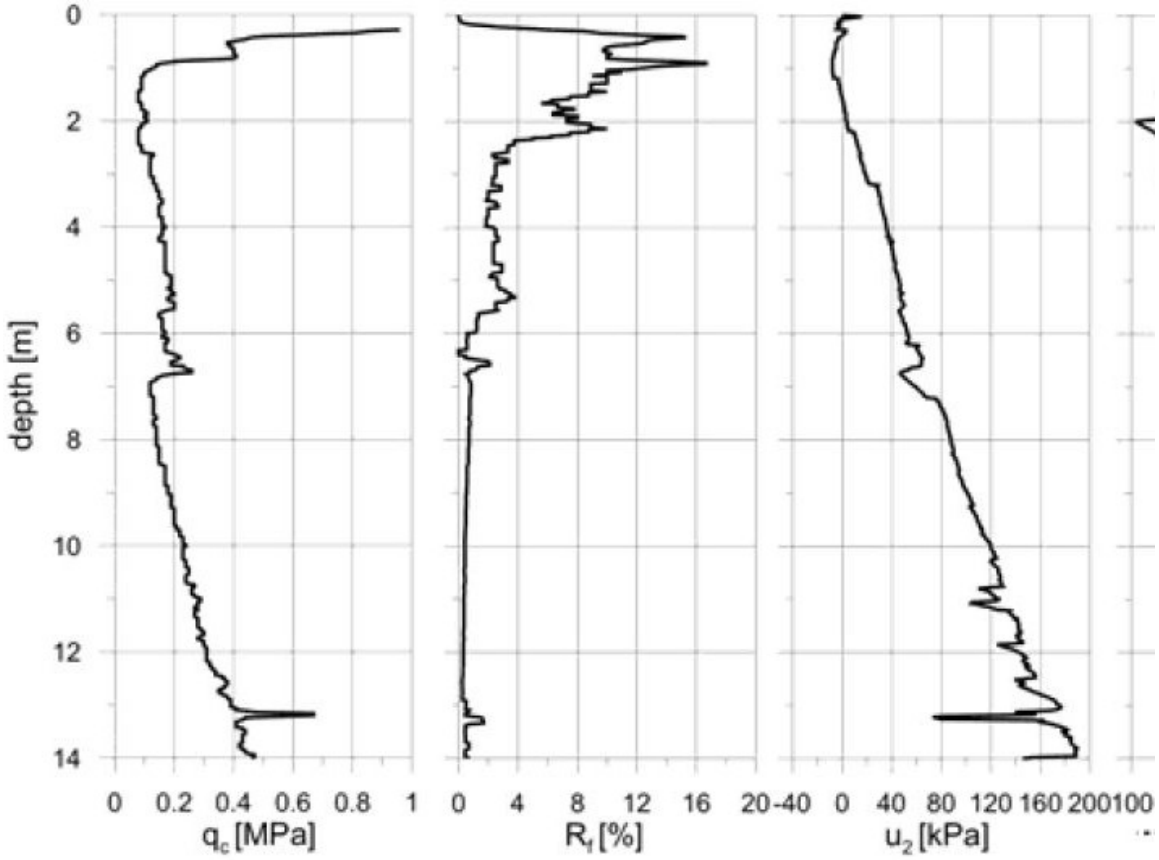

## Suisun Bay, CA

Data after Merani et al. (2016)

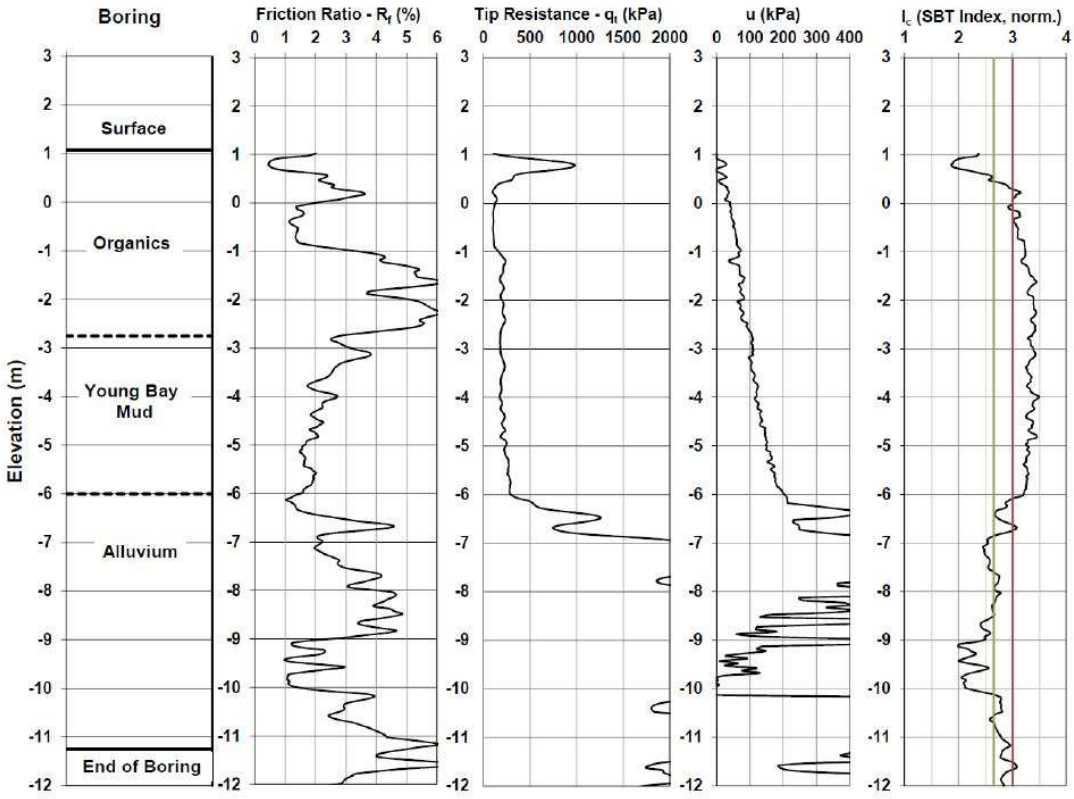

## Raszynka River valley, Poland

Data after Kowalczyk et al. (2017)

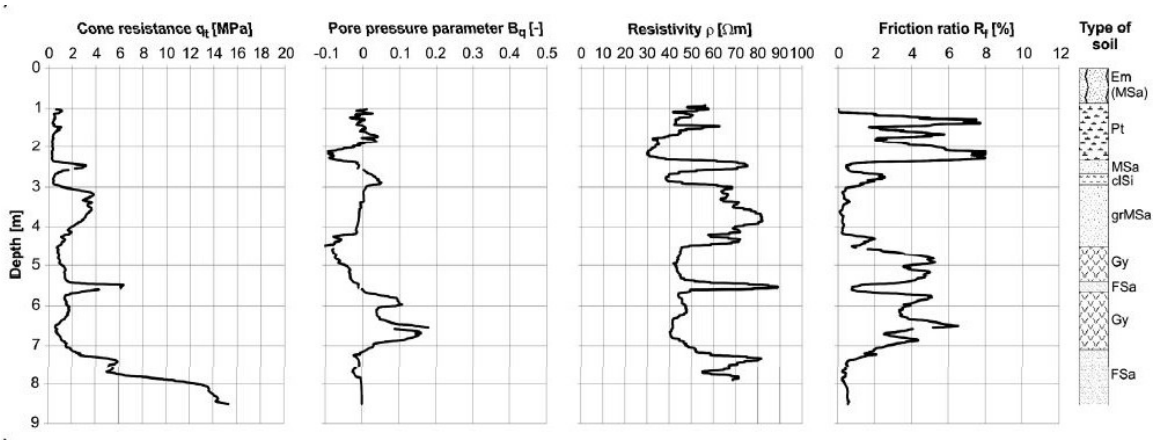

## Barra da Tijuca - CM1, Brazil

Data after de Almeida et al. (2010)

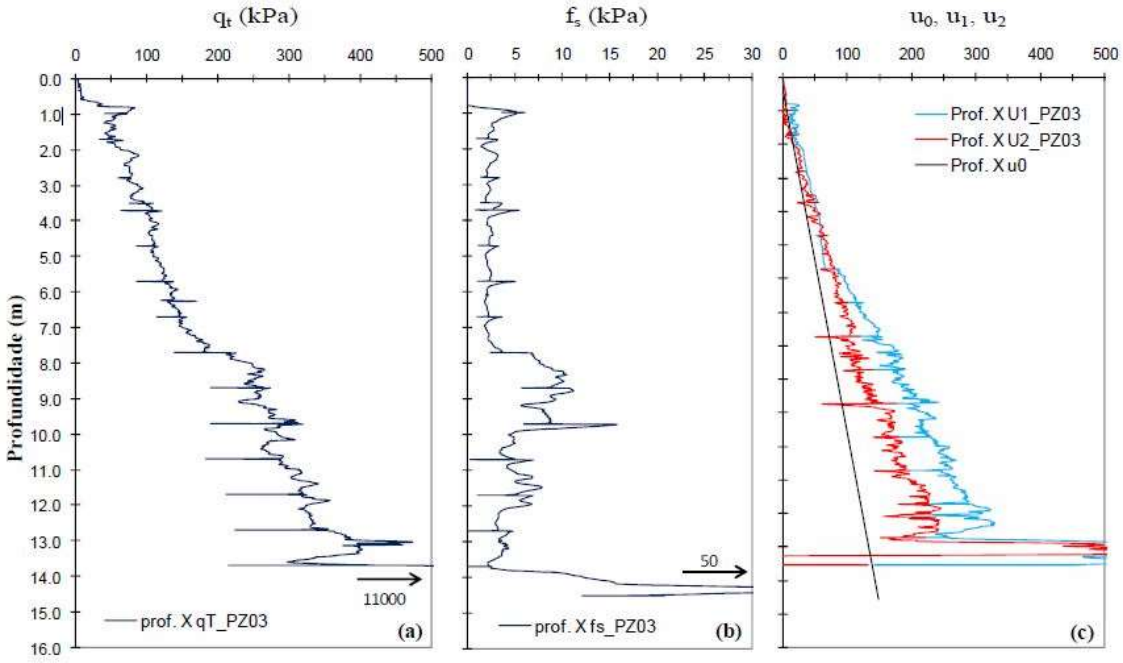

## Barra da Tijuca – Gleba, Brazil

Data after de Almeida et al. (2010)

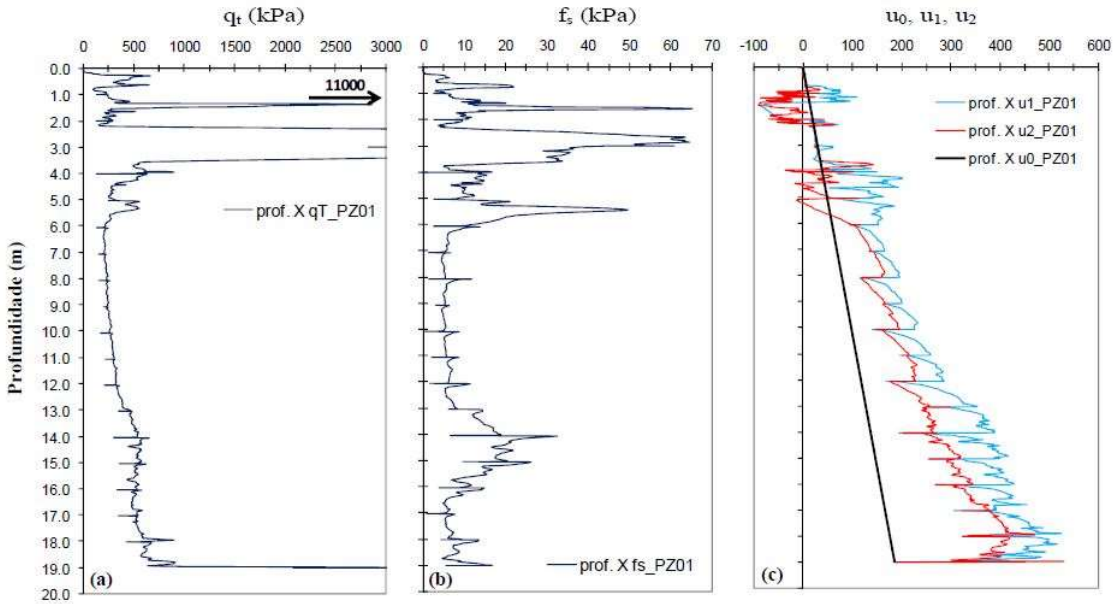

## Mexico City Clay, Mexico

Data after Cruz & Mayne (2006)

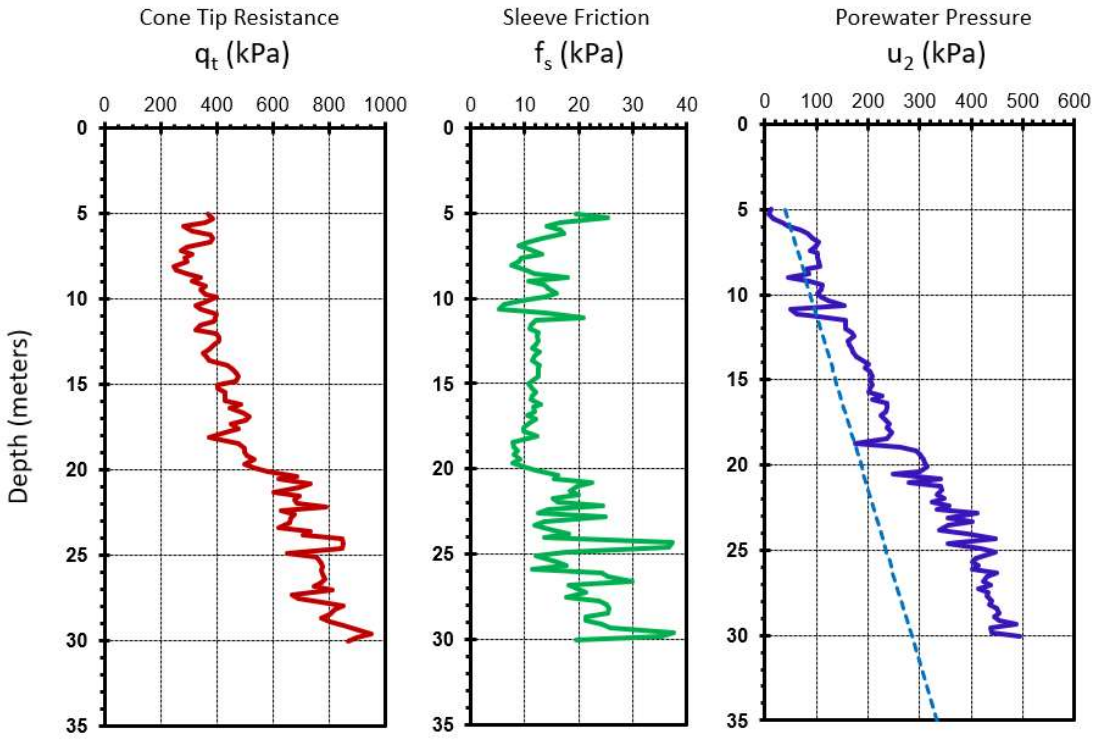

## Suape subarea A, Brazil

Data after Coutinho & Bello (2014)

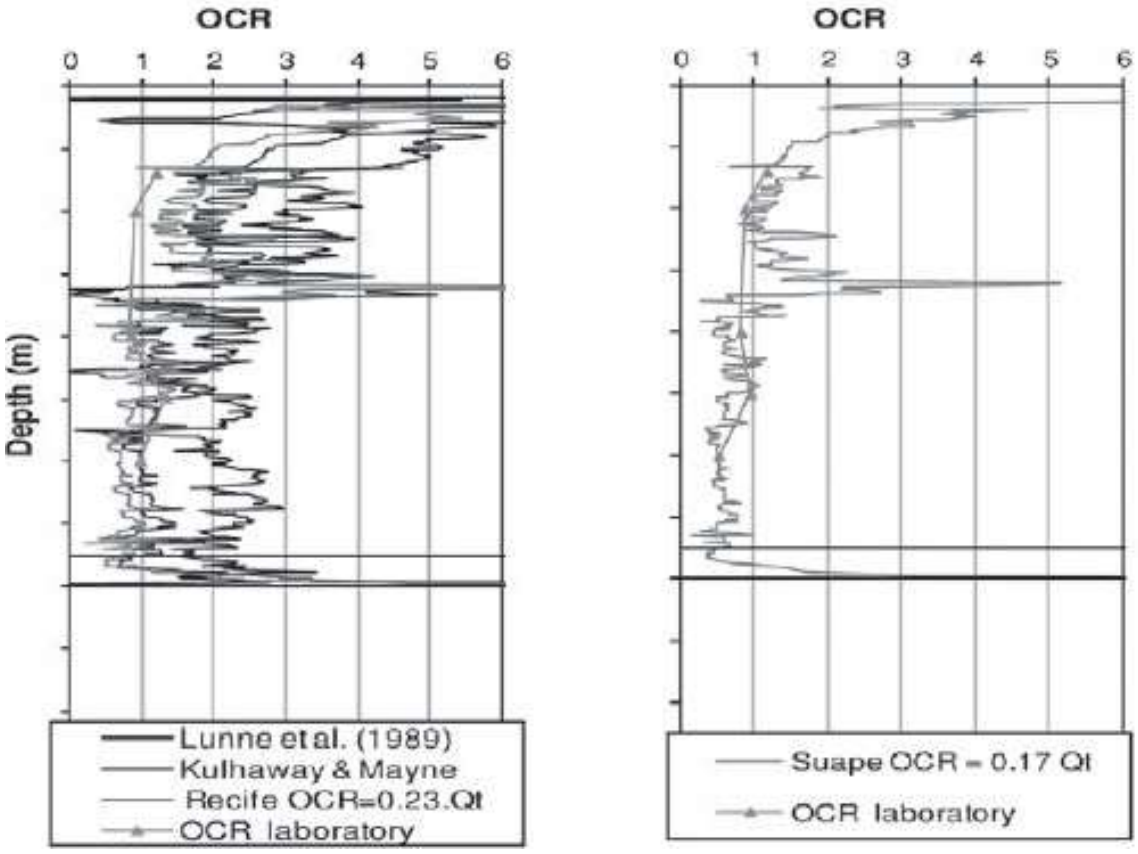


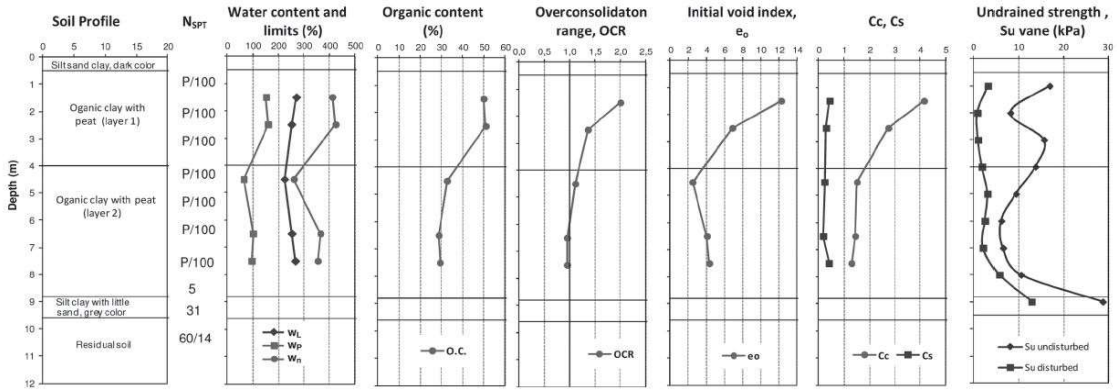

## Suape subarea C, Brazil

Data after Coutinho & Bello (2014)

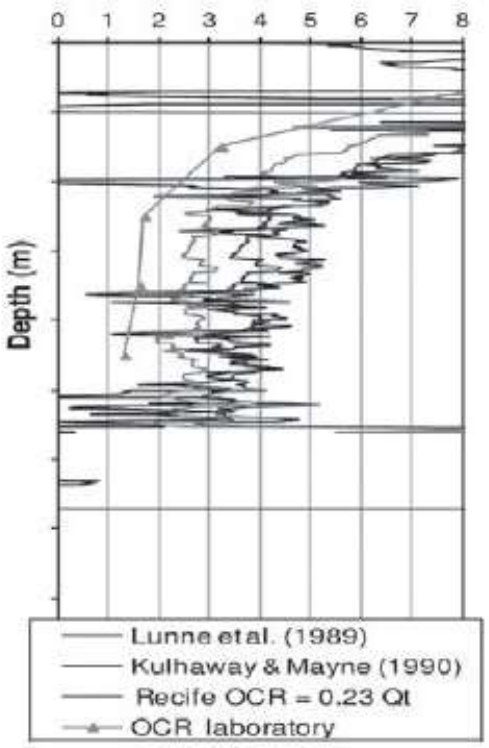


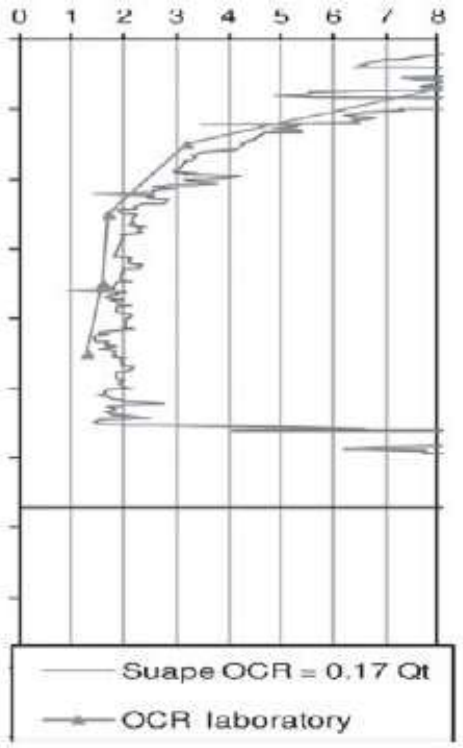


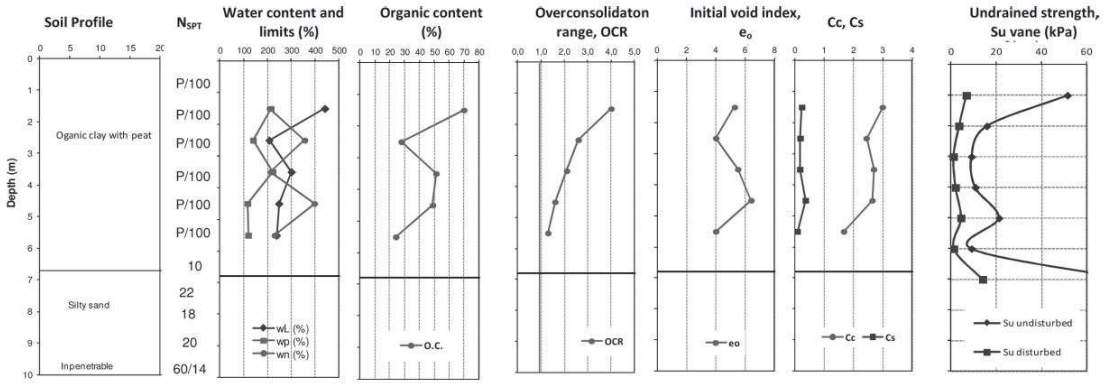

# APPENDIX E

## Sensitive Clays:
## Piezocone Soundings,
## with Shear Wave Velocity,
## Undrained Shear Strength, and
## Stress History Data

| Site | CPTu | Shear Wave Velocity, $V_s$ | Undrained Shear Strength, $s_{u\ TC}$ | Stress History |
|---|---|---|---|---|
| Byenest | ✓ | | | ✓ |
| Colebrook Overpass | ✓ | ✓ | | ✓ |
| Gloucester | ✓ | ✓ | ✓ | ✓ |
| Hilleren | ✓ | | ✓ | ✓ |
| Saint Alban | ✓ | ✓ | ✓ | ✓ |
| Saint Monique de Nicolet | ✓ | | ✓ | ✓ |
| Sandpoint | ✓ | ✓ | | ✓ |
| Tiller | ✓ | ✓ | ✓ | ✓ |

# Byenest, Esp, Norway

Data after Montafia (2013)

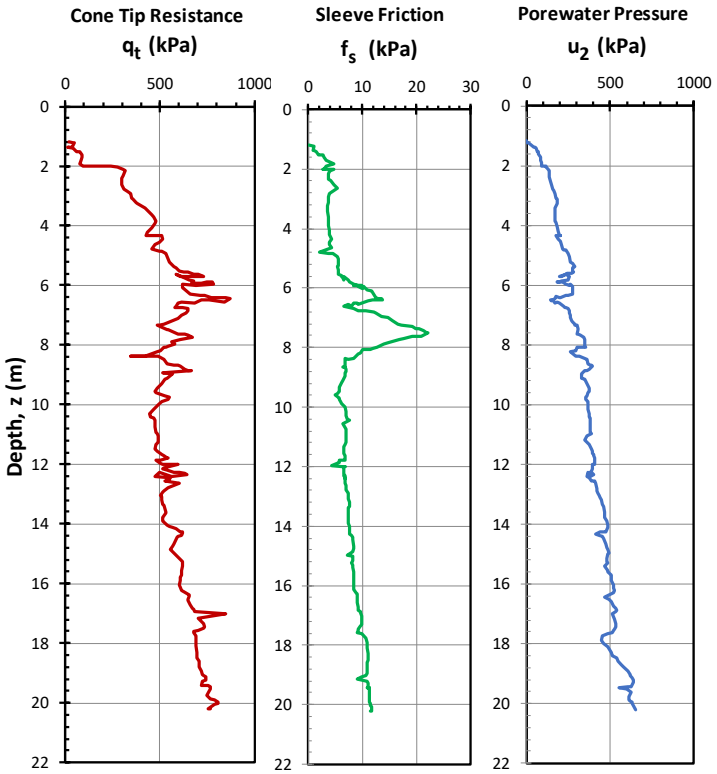


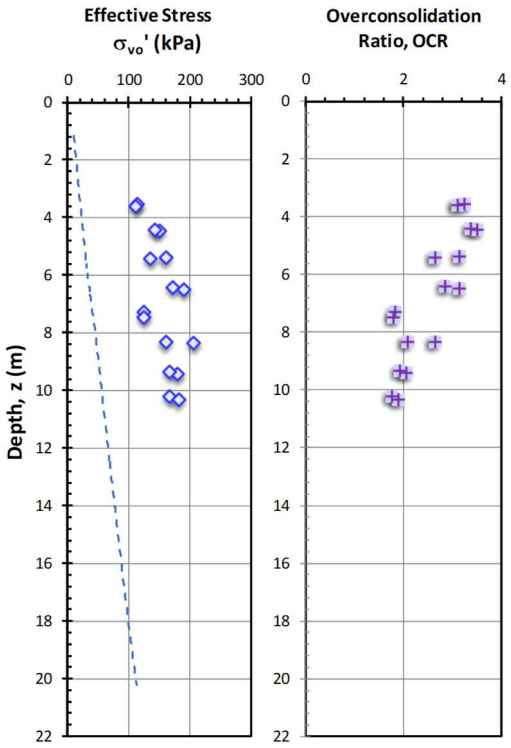

# Colebrook Overpass, Surrey, BC, Canada

Data after Crawford and Campanella (1991); Weech (2002)

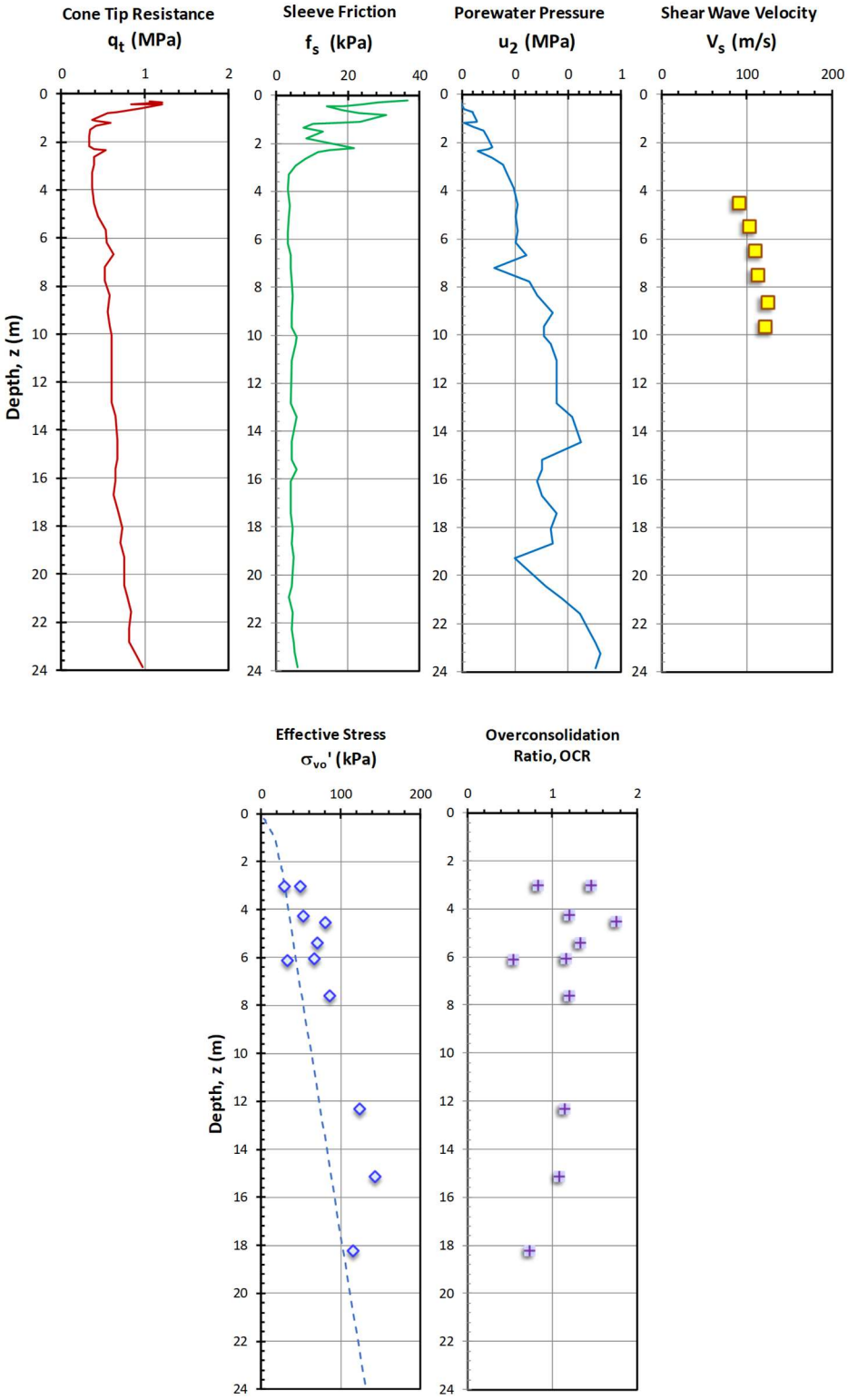

## Gloucester, ON, Canada

Data after McRostie & Crawford (2001); Styler & Mayne (2013)

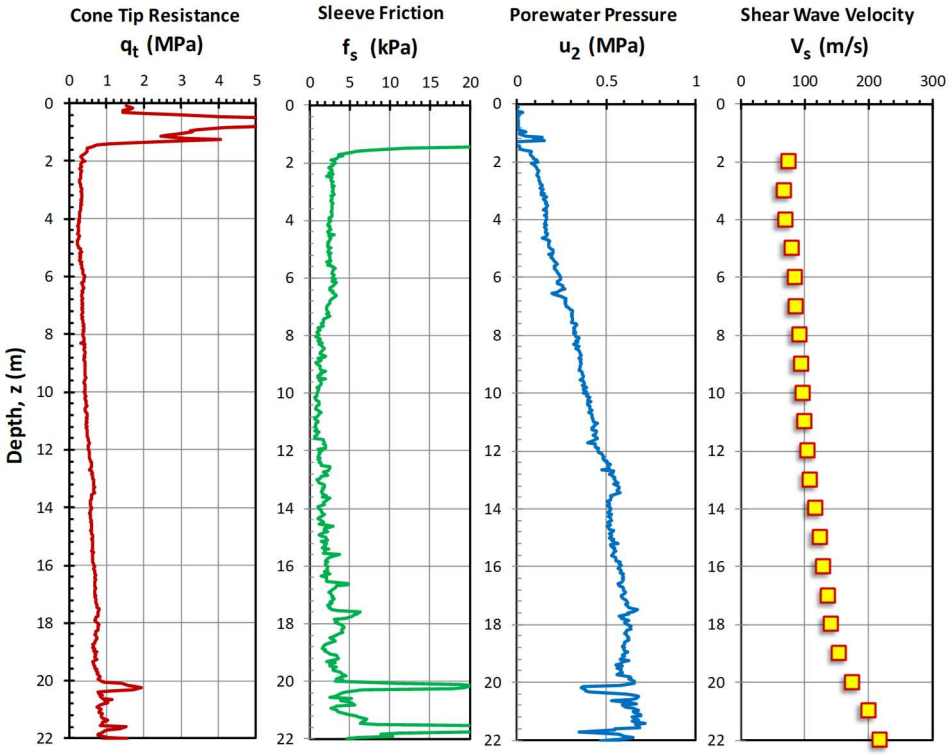


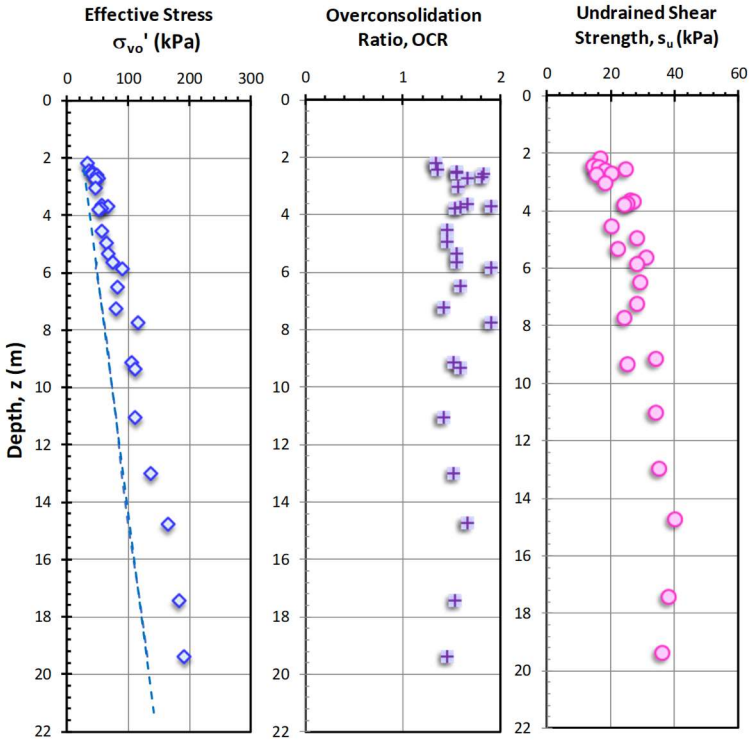

## Hilleren, Norway

Data after Long et al. (2009)

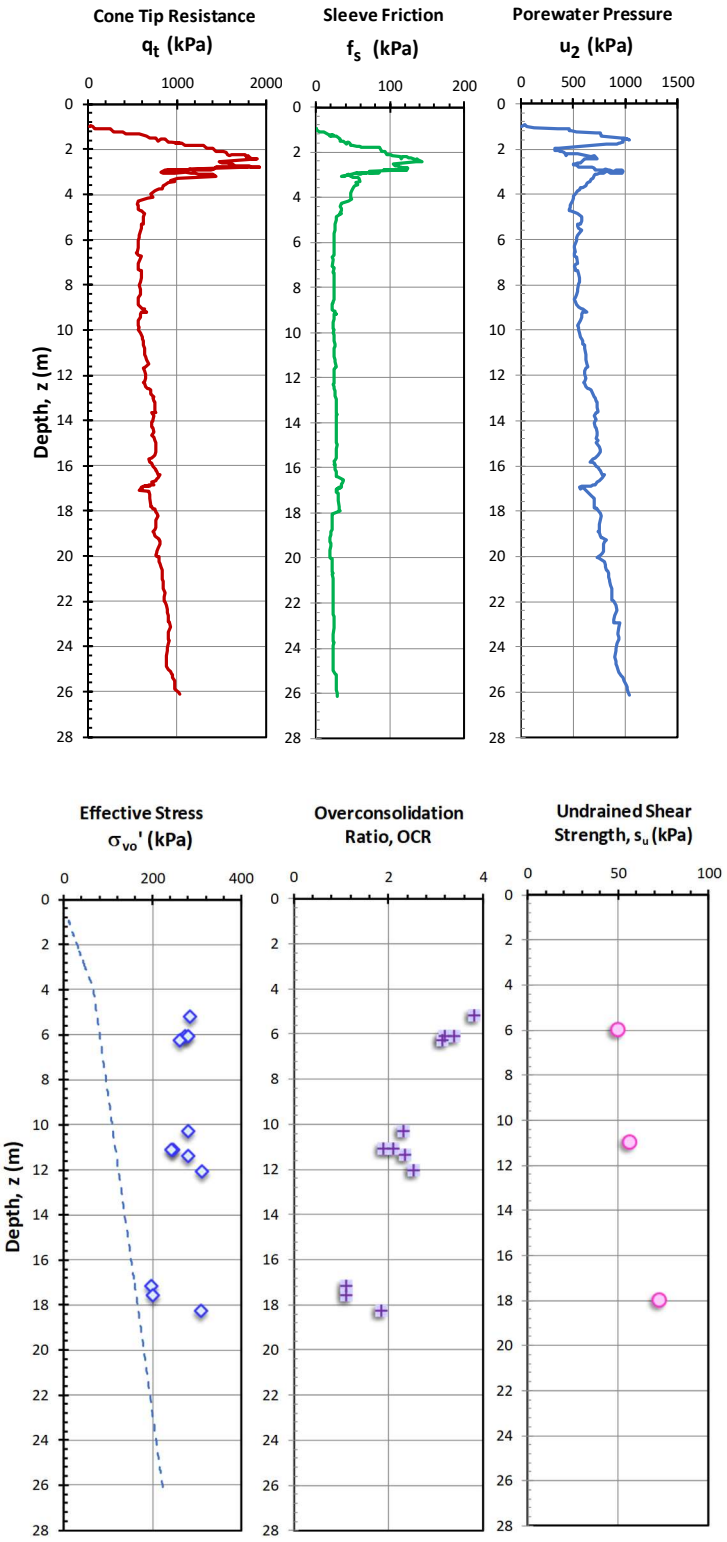

## Saint Alban, Québec, Canada[1]

Data after LaRochelle et al. (1974); Lefebvre et al. (1994); Leroueil et al. (1995)

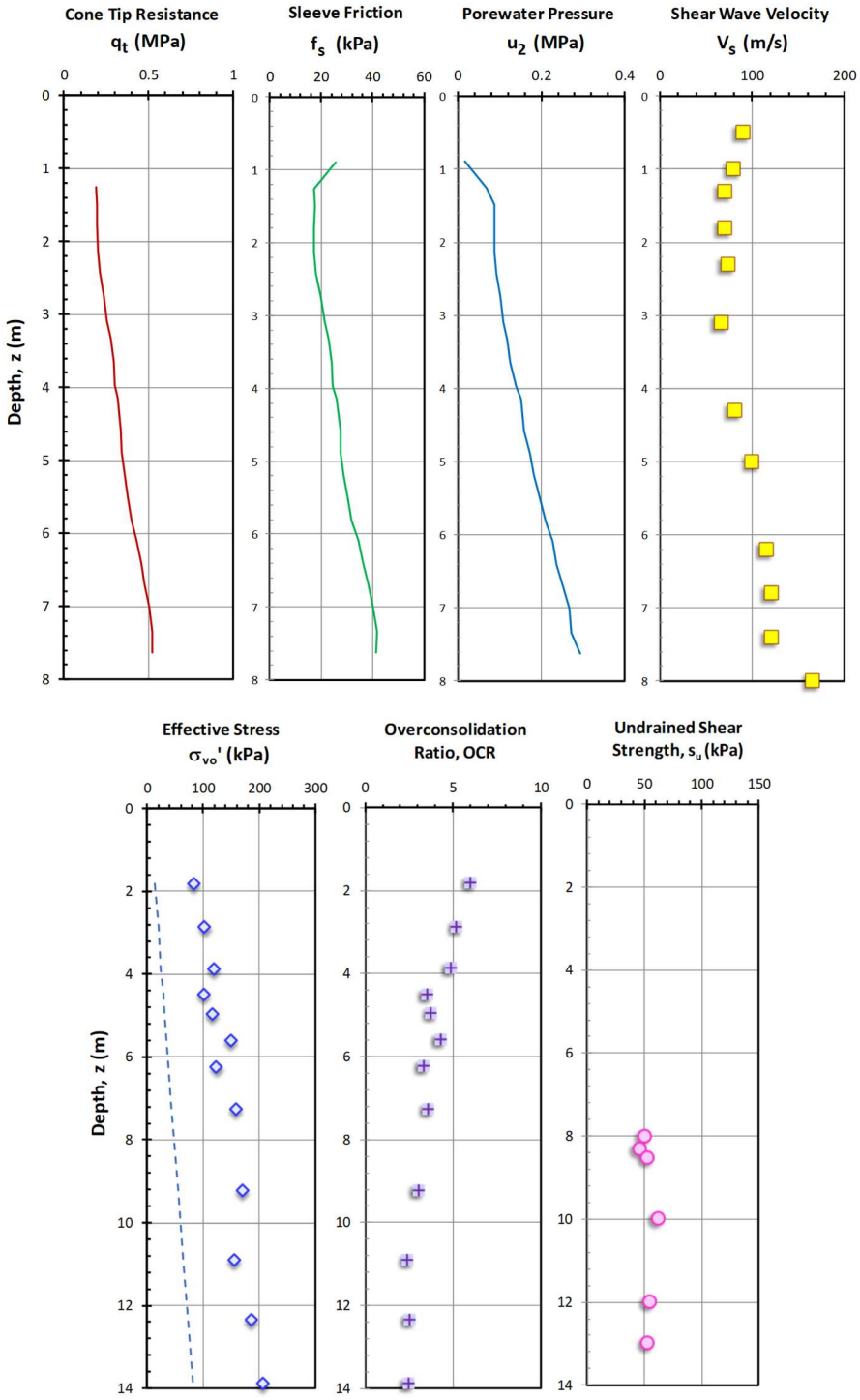


[1] $V_s$ is measured using multi-channel analyses of surface waves (MASW) and sleeve friction, $f_s$ is measured using Laval piezocone with $f_s \approx 0.1(q_t - \sigma_{v0})$ as per Leroueil et al. (1995).

## Saint Monique de Nicole, Canada

Data after Locat (2012) – No sleeve friction data available

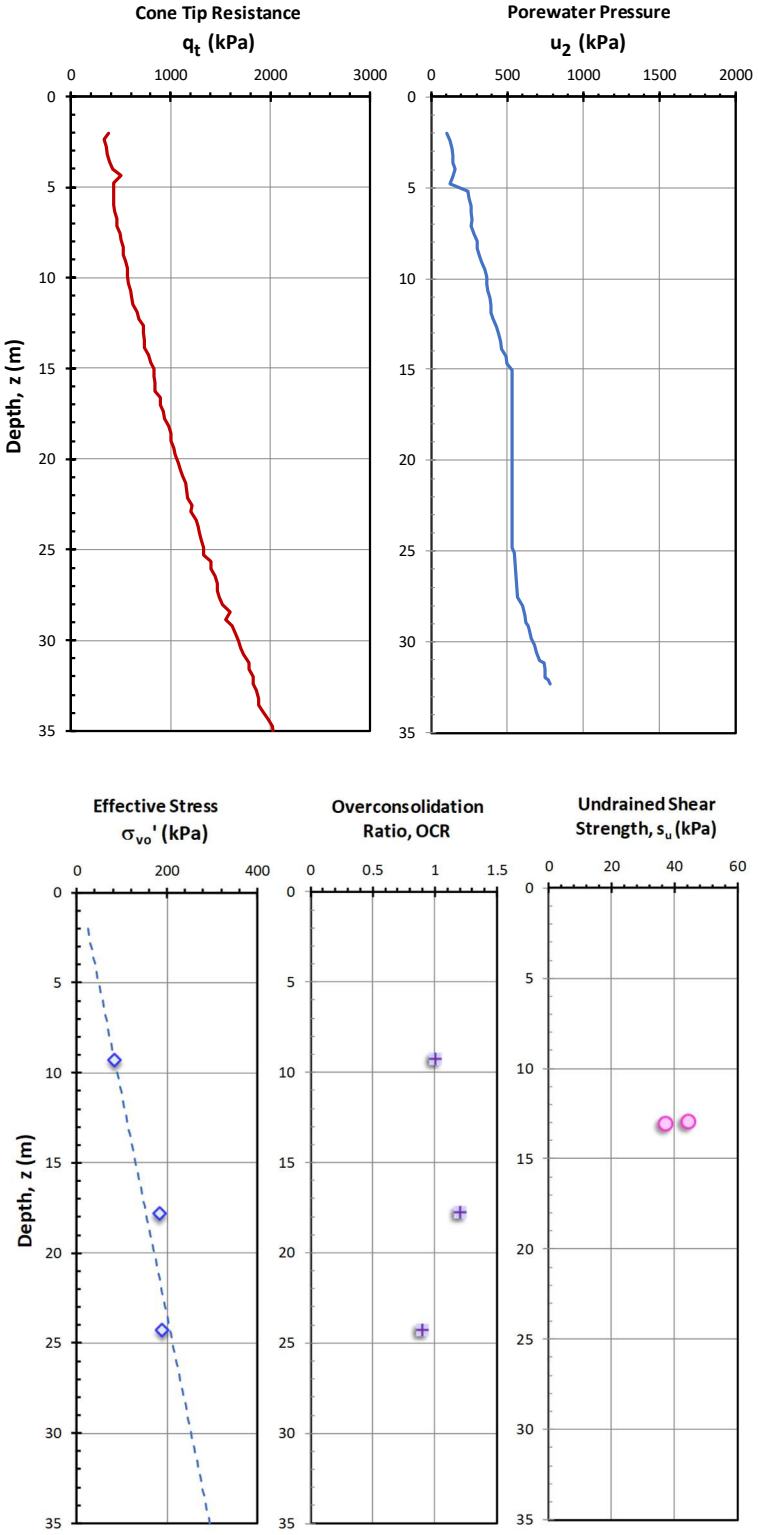

## Sandpoint, ID, USA

Data after Altaee & Fellenius (2002); Mayne (2005)

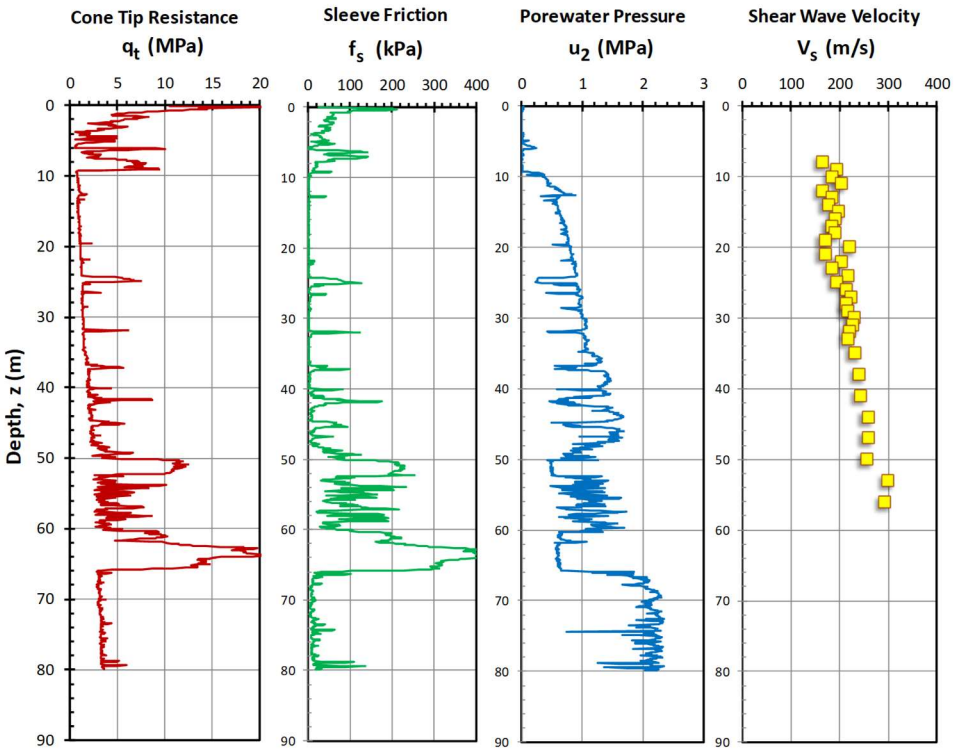


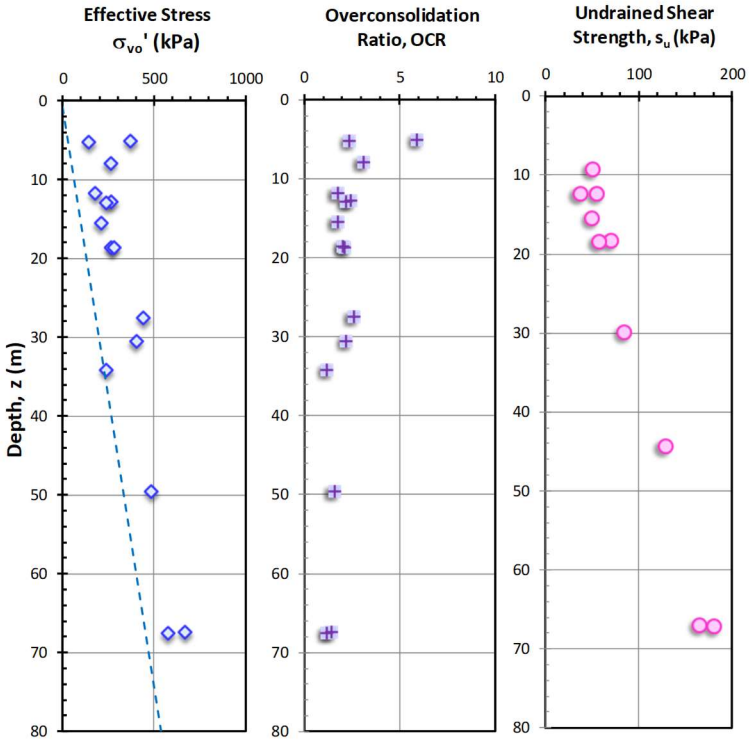

## Tiller, Norway

Data after Gylland et al. (2013; 2014); L'Heureux & Long (2016)

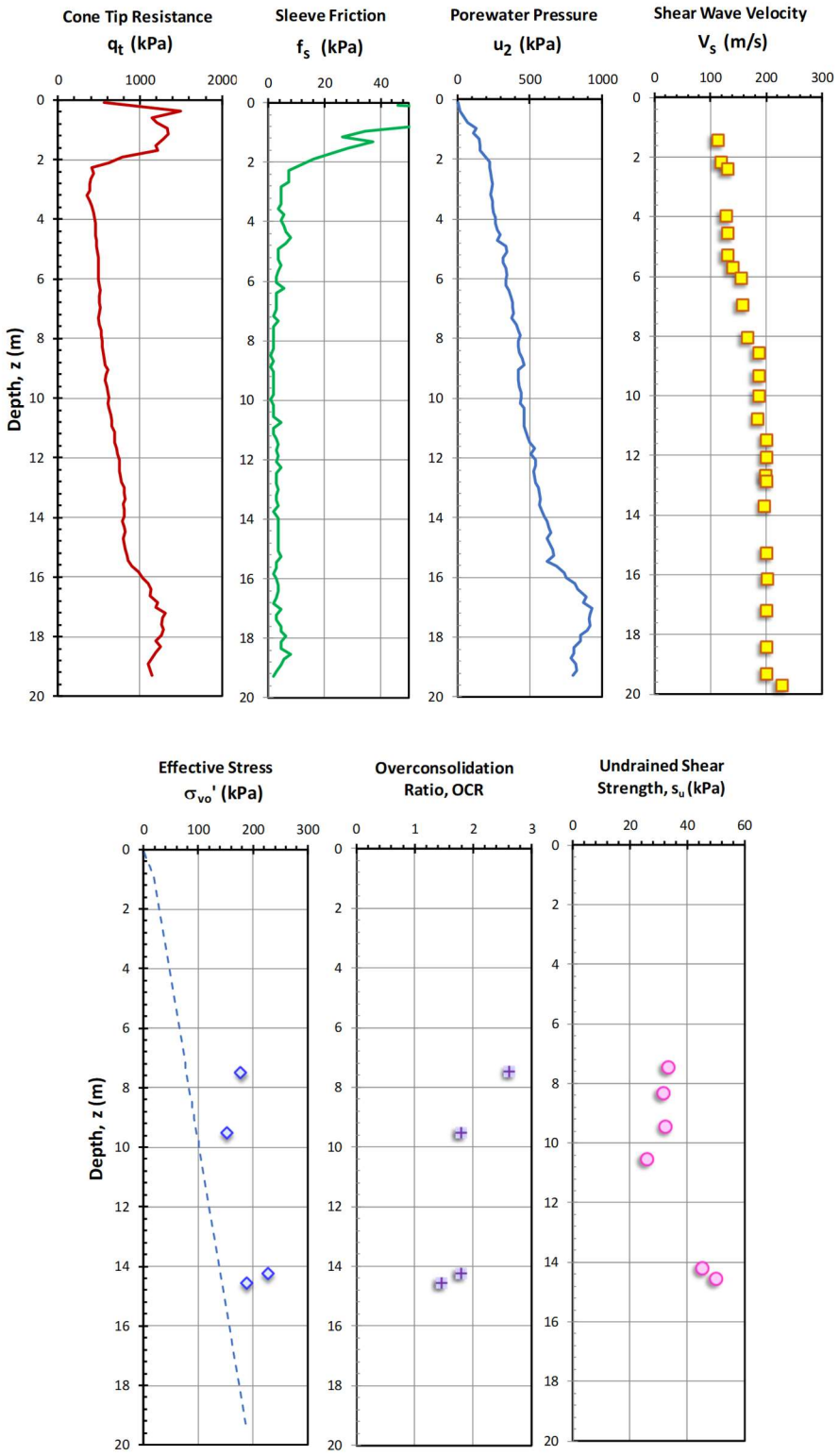

# APPENDIX F

## Fissured and Highly Overconsolidated Clays: Piezocone Soundings, with Shear Wave Velocity, Undrained Shear Strength, and Stress History Data

| Site | CPTu | Shear Wave Velocity, $V_s$ | Undrained Shear Strength, $s_{u\ TC}$ | Stress History |
|---|---|---|---|---|
| Baton Rouge | ✓ | | ✓ | ✓ |
| Baytown | ✓ | | ✓ | ✓ |
| Beaumont | ✓ | ✓ | ✓ | ✓ |
| Brent Cross | ✓ | ✓ | ✓ | ✓ |
| Canons Park | ✓ | ✓ | | ✓ |
| Heathrow T5 | ✓ | ✓ | ✓ | ✓ |
| Madingley | ✓ | ✓ | | ✓ |
| Montgomery | ✓ | ✓ | ✓ | ✓ |

# Baton Rouge, LA, USA

Data after Chen & Mayne (1994)

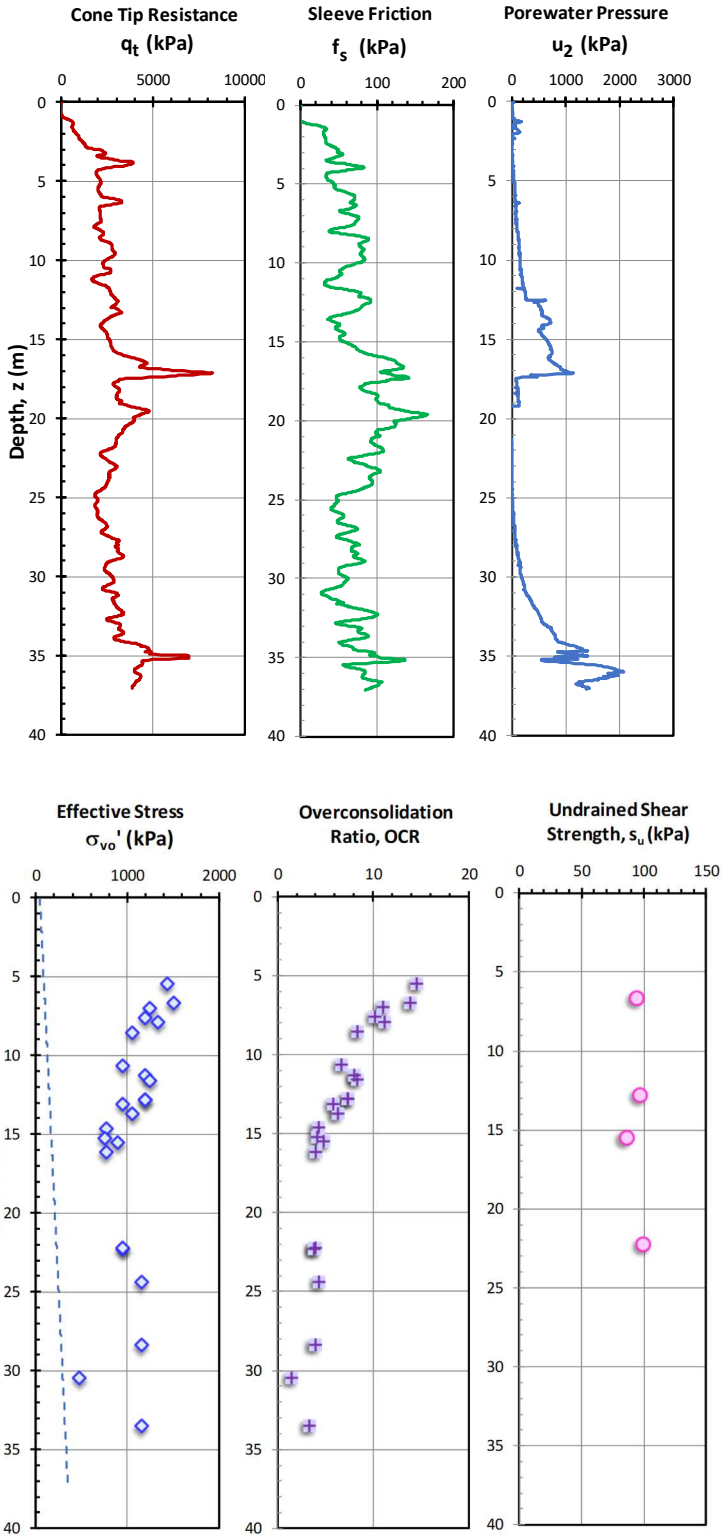

# Baytown, TX, USA

Data after Stuedlein (2008)

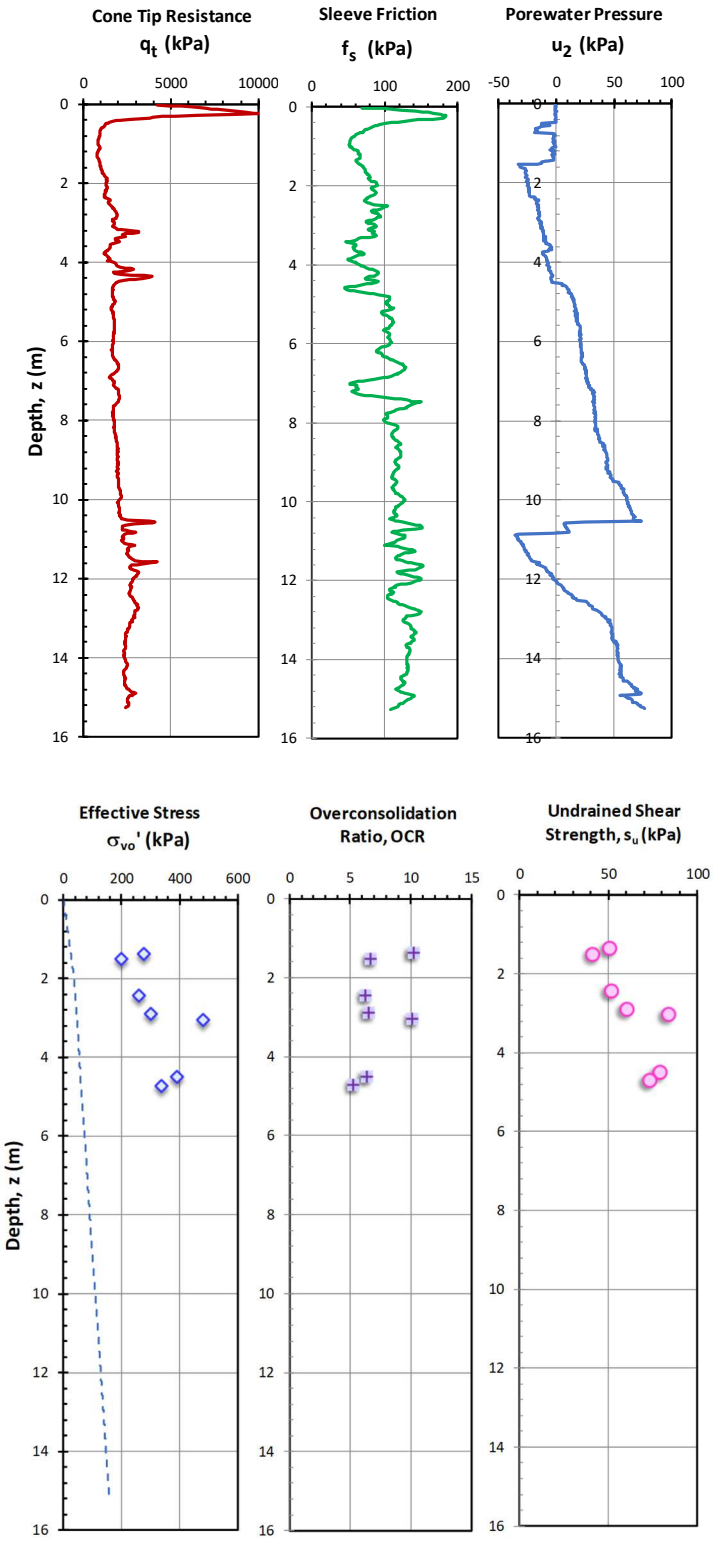

## Beaumont, TX, USA

Data after Mahar & O'Neill (1983); Yoon & O'Neill (1995)

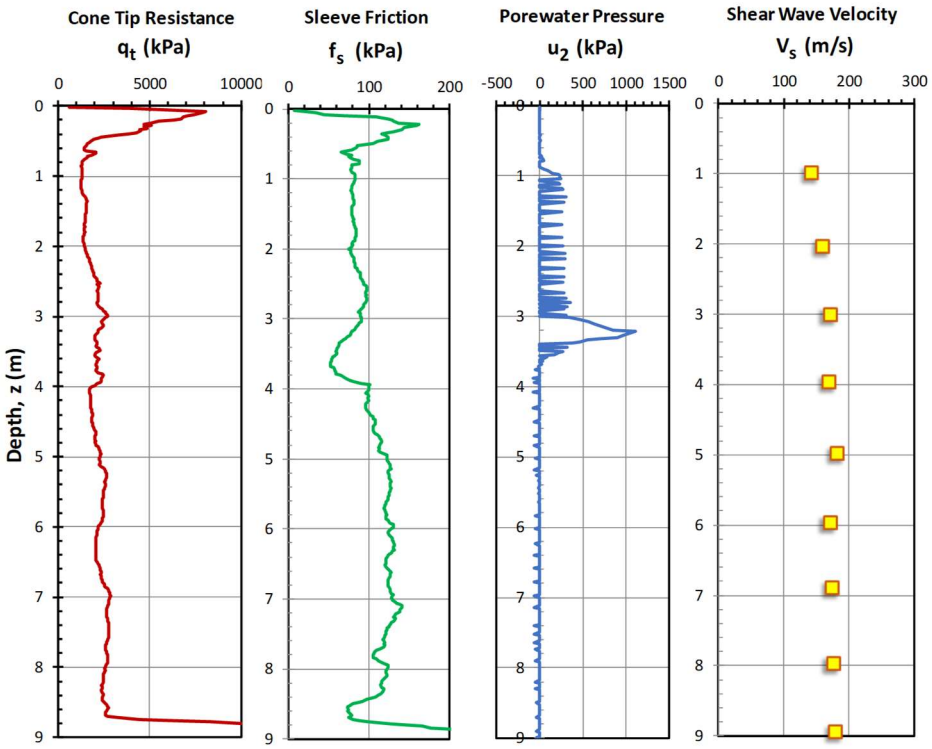


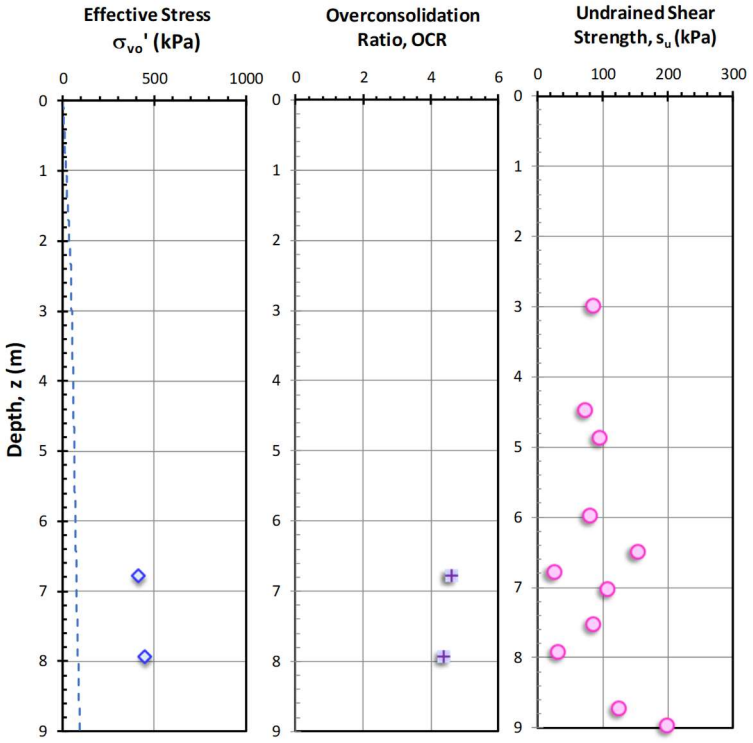

# Brent Cross, UK

Data after Hight et al. (2003)

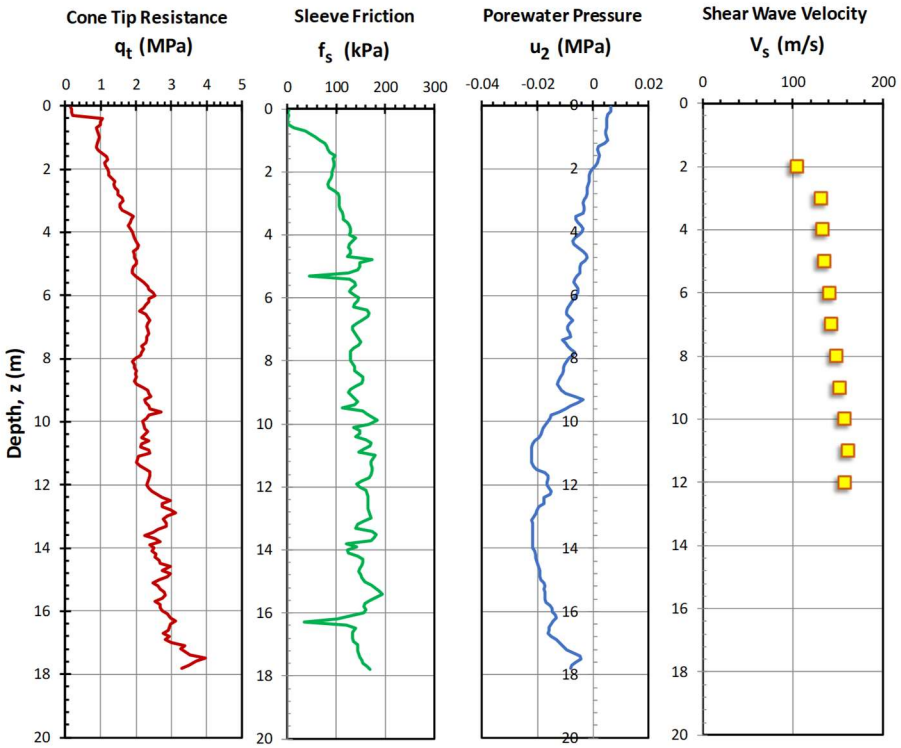


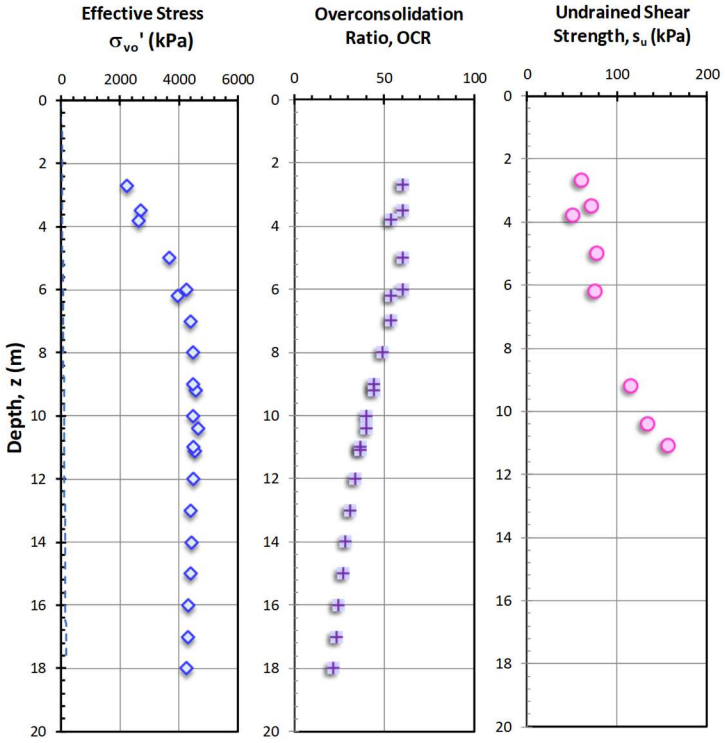

## Canons Park, UK

Data after Hight et al. (2003); Powell & Lunne (2005)

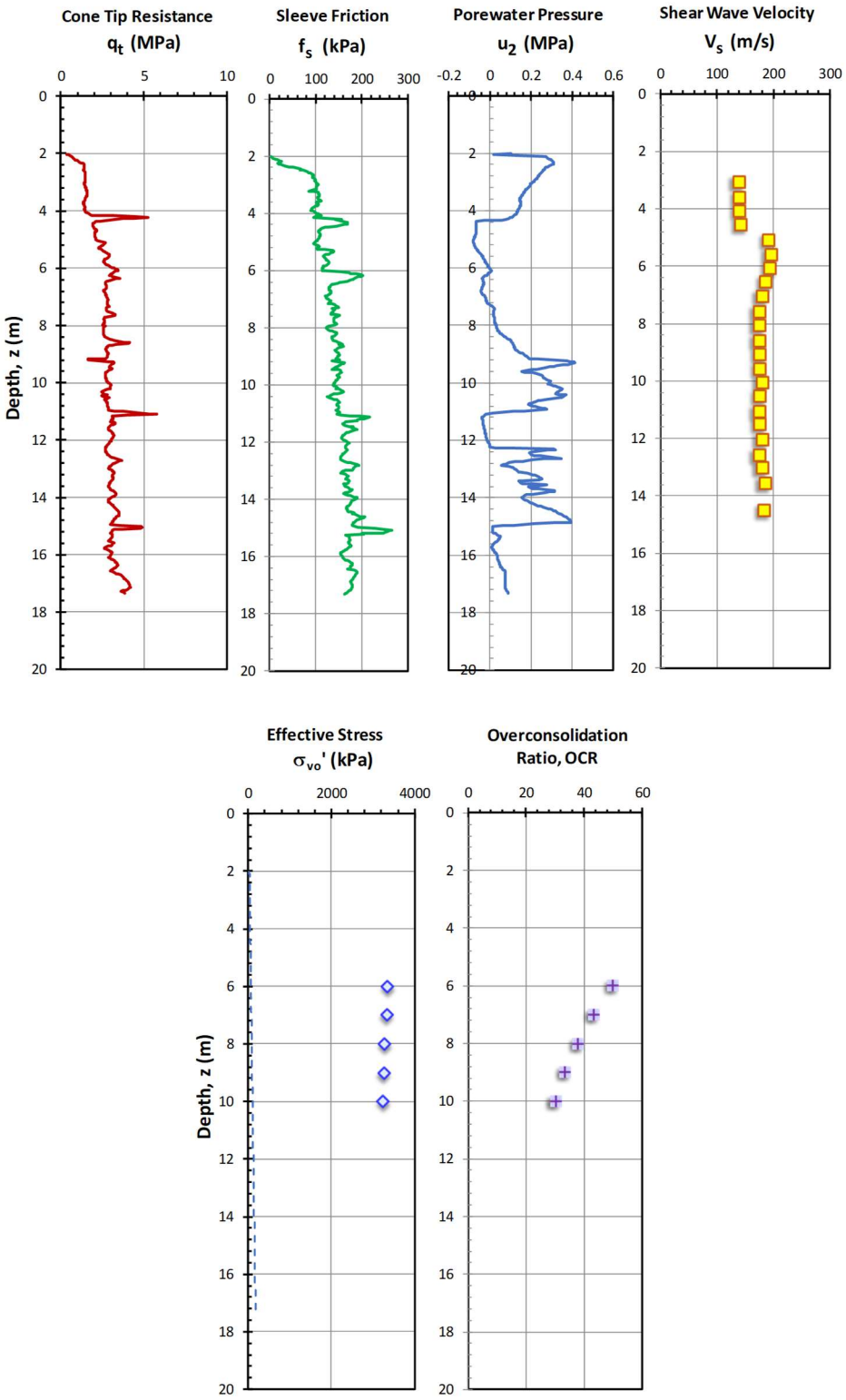

# Heathrow T5, UK

Data after Hight et al. (2003)

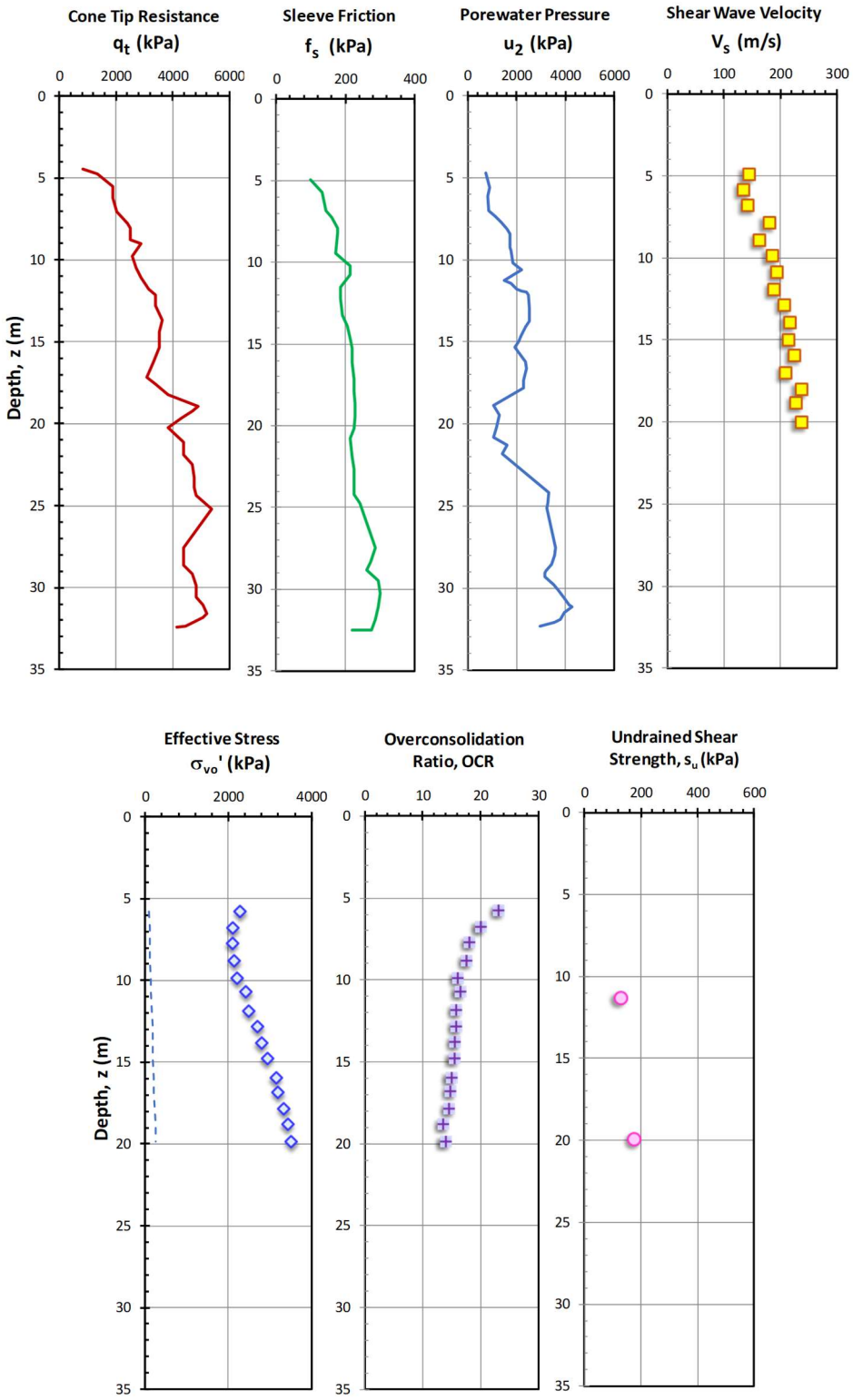

## Madingley, Cambridge, UK

Data after Lunne et al. (1986); Jardine et al. (2015)

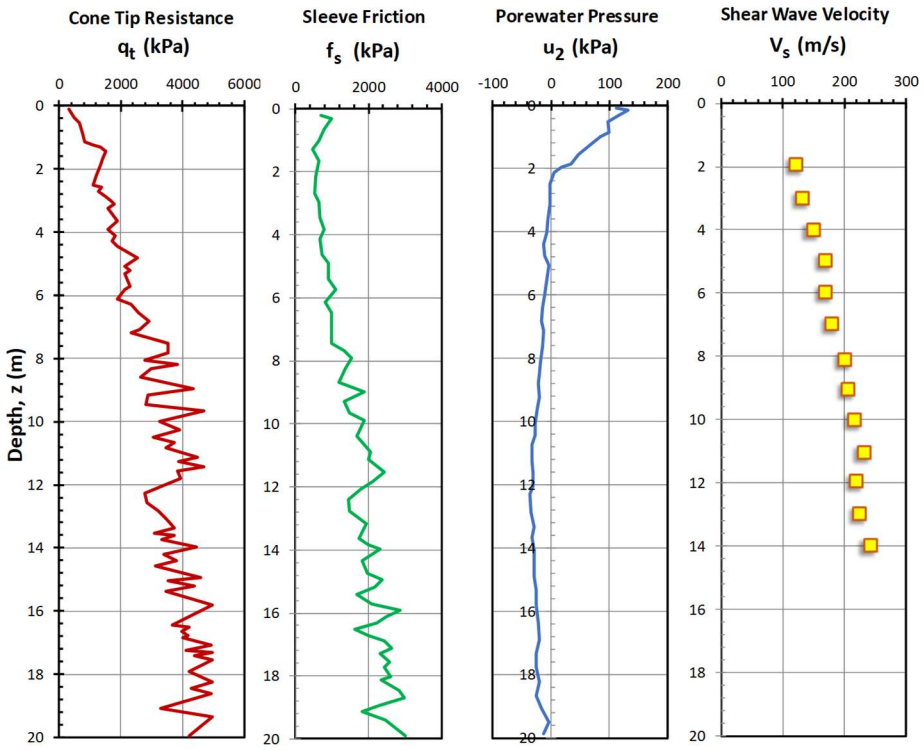


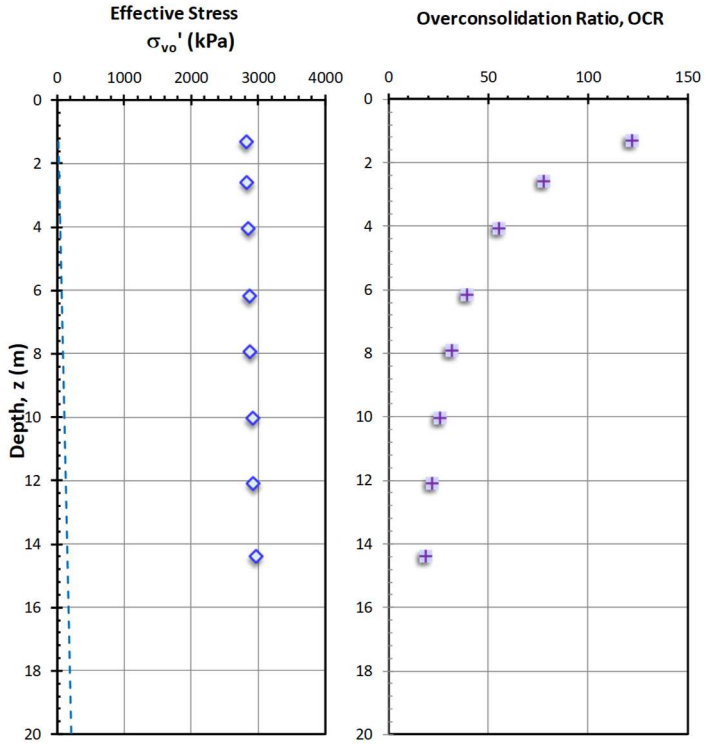

## Montgomery, TX, USA

Data after Mahar & O'Neill (1983); Yoon & O'Neill (1995)

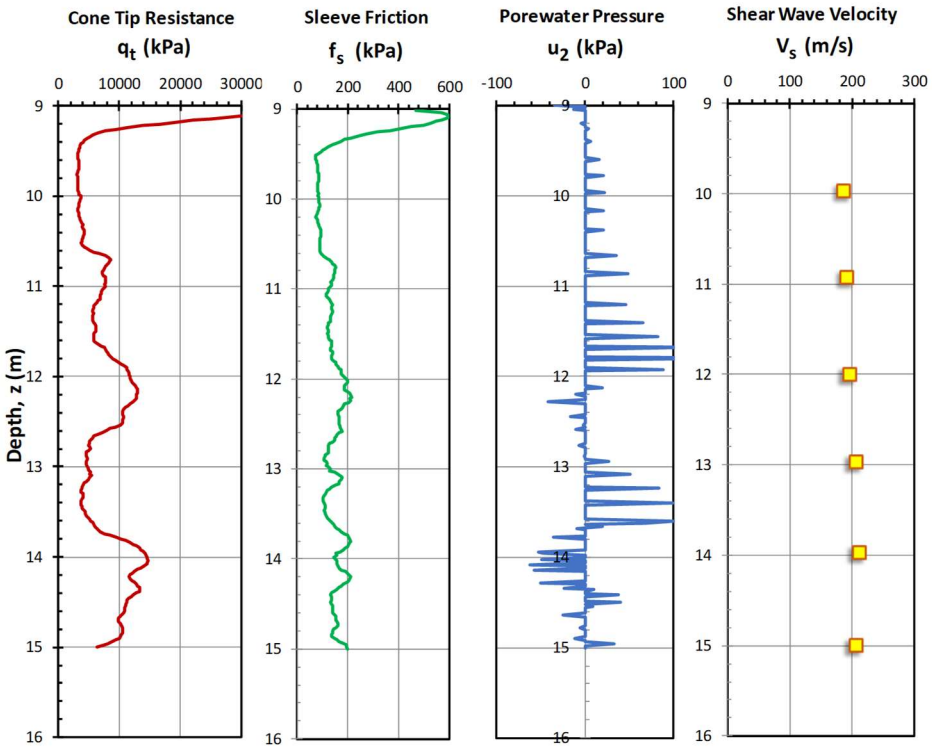


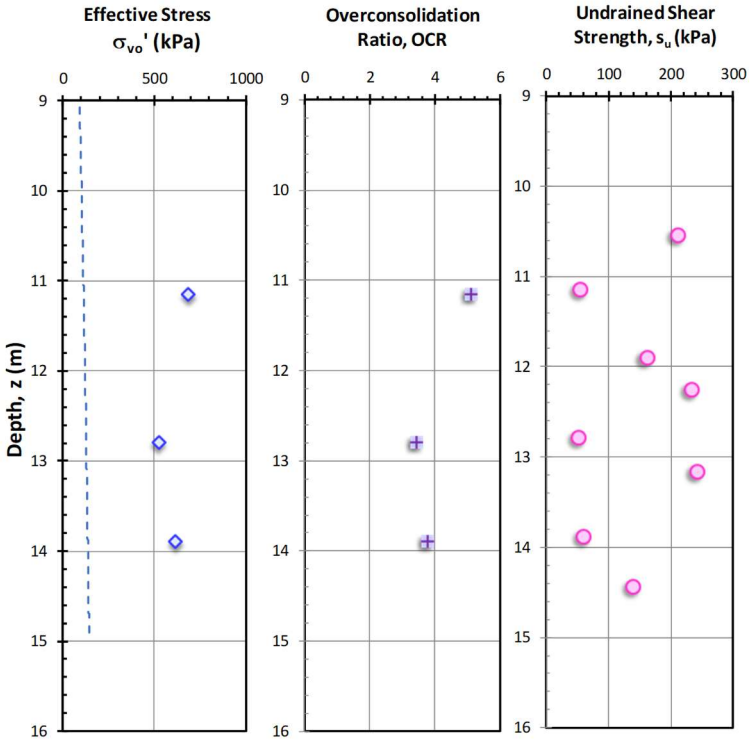

# APPENDIX G

# Seismic Piezocone Soundings with Soil Behavioral Type Classifications and Shear Wave Velocity Predictions for Sensitive Clays in North America

| Sensitive Clay | Location | Description | References |
|---|---|---|---|
| Amherst | Connecticut Valley, Massachusetts | Varved clay and silt | Hegazy (1998) DeGroot & Lutenegger (2003) |
| Colebrook Overpass | Surrey, British Columbia | Marine clayey silt- silty clay | Crawford and Campanella (1991); Weech (2002) |
| Dyke Road | Richmond, BC | Silt, clayey silt | Cruz (2009) |
| Ford Design Center | Evanston, Illinois | Glacial Till | Mayne (2007 b) |
| Gloucester | Southeast Ottawa, Ontario | Leda clay | Styler & Mayne (2013) |
| Golden Ears Bridge | Langley, BC | Stiff silty clay | Amini et al. (2008) |
| Haney | British Columbia | Soft clay | Vaid (1971); Woeller (2004) |
| Louiseville | Québec | Firm highly plastic clay | Yafrate & DeJong (2006) |
| Martin's PointBridge | Maine | Presumpscot Clay | Hardison (2015) |
| Massey Tunnel | Delta, BC | Silty clay - clayey silt | Kong (2015) |
| McDonald's Farm | Vancouver | Sand - soft clayey silt | Campanella et al. (1986) |
| Newbury | Massachusetts | Boston Blue Clay | Landon (2007) |
| Pier Park | Richmond, BC | Soft - firm silt & clay | Christian et al. (1998) |
| Quyon | Québec | Champlain Sea clay | Wang et al. (2015) |
| Route 197 Bridge | Maine | Presumpscot Clay | Hardison (2015) |
| Route 26 /100 | Maine | Presumpscot Clay | Hardison (2015) |
| Sandpoint | Idaho | Post-glacial alluvial deposit | Altaee & Fellenius (2002) |
| St. Alban* | Québec | Soft silty marine clay | LaRochelle et al. (1974); Lefebvre et al. (1994); Leroueil et al. (1995) |
| Vancouver | British Columbia | Sand - soft silty clay | Mayne & Woeller (2015) |

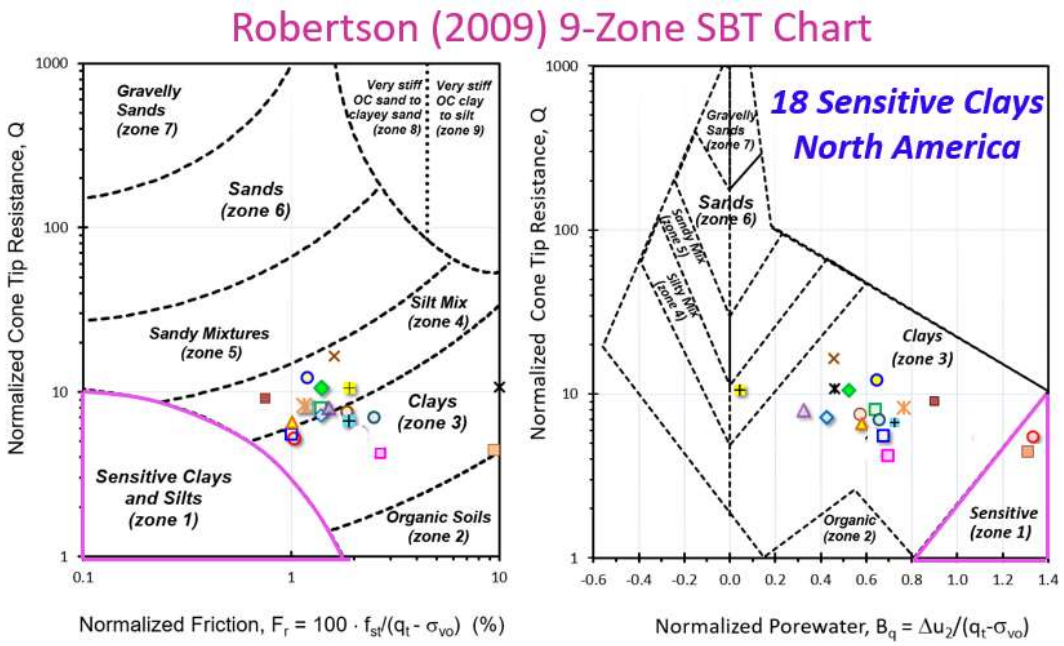


A representation of compiled sensitive and structured clays in North America from chapters 4 and 6 on Robertson (2009) 9 – zone chart where clearly most of the sensitive and structured clays do **NOT** fall within the correct zone (ZONE 1). Indicating the presence of an issue in detecting sensitive and structured clays using conventional soil classification charts.

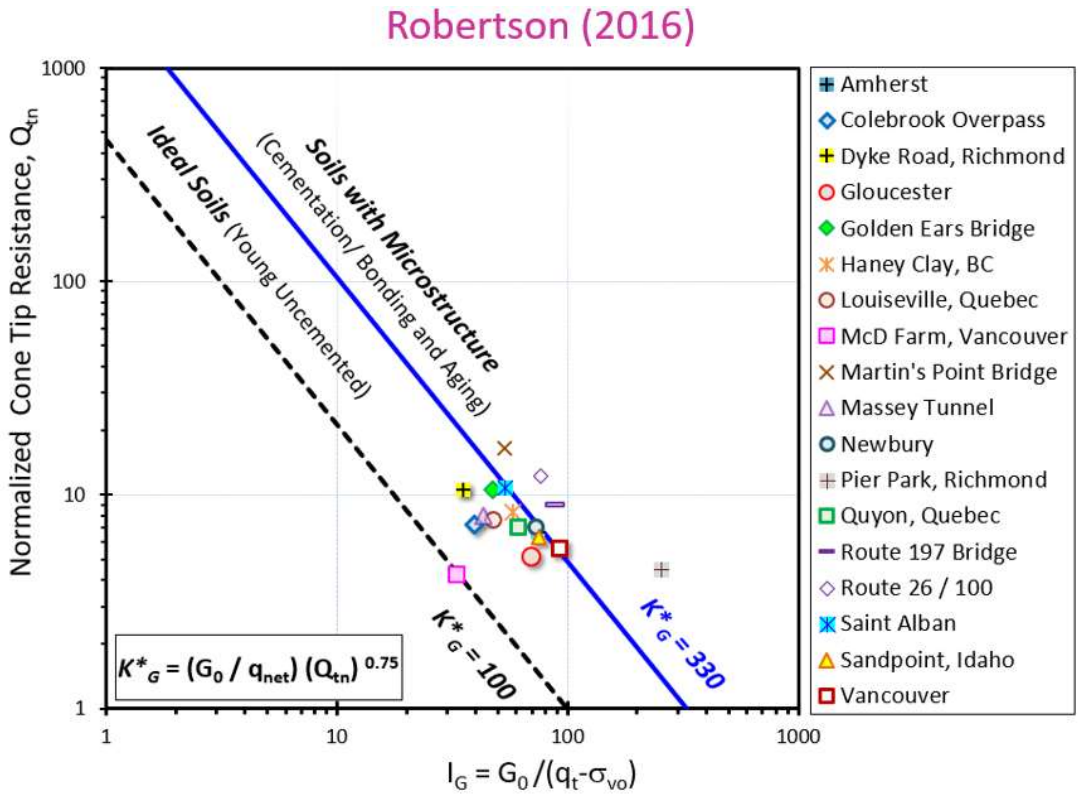


Same issue exists using an updated chart by Robertson (2016) where the sensitive and structured clays should fall above the blue line while in reality most of the sensitive clays fall within the ideal soils zone.

## Amherst, Connecticut Valley, MA

Data after Hegazy (1998)

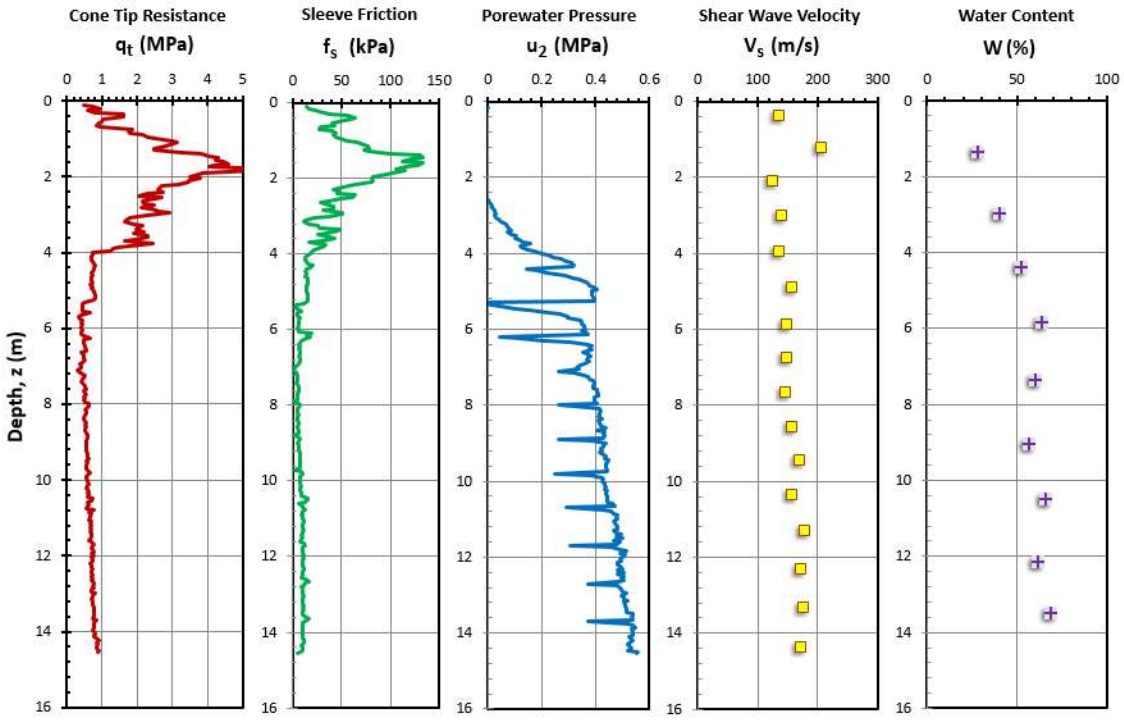

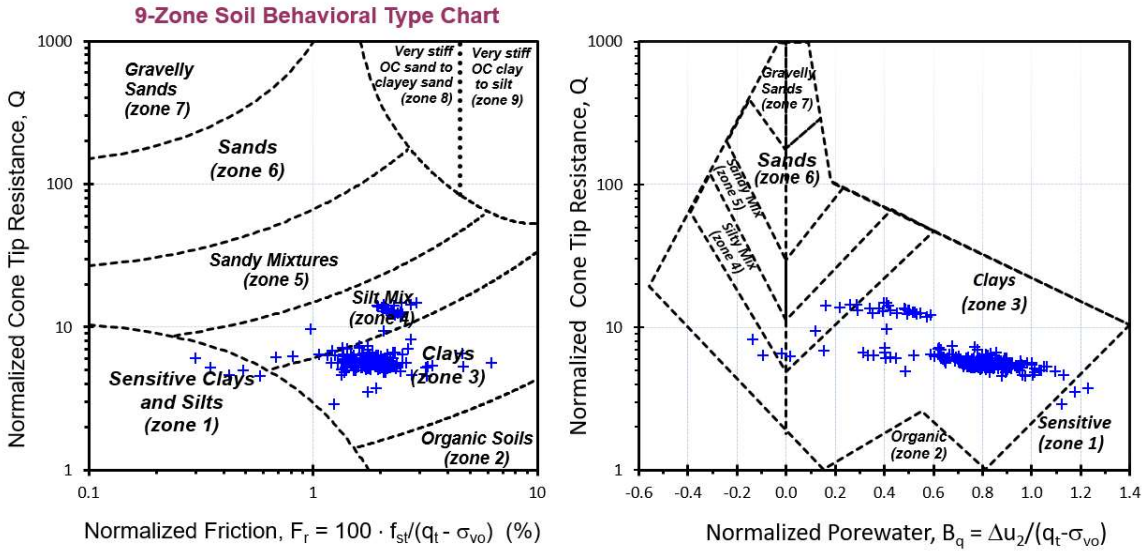


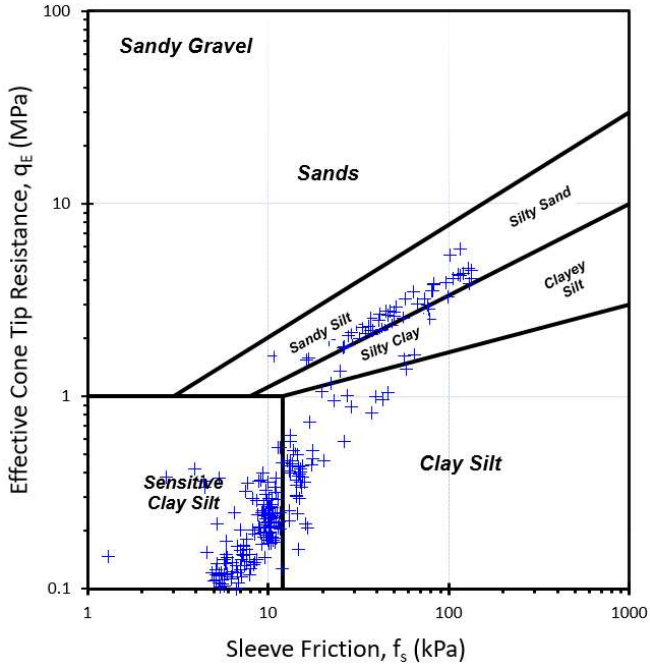


**CPT soil classification using 9-zone Robertson SBT and Fellenius and Eslami soil profiling charts for Amherst, MA**

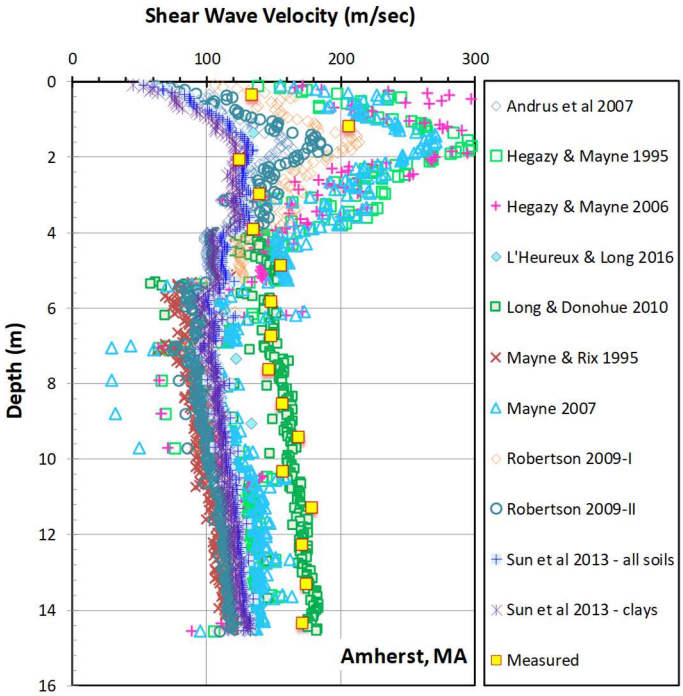


**Measured and predicted shear wave velocity profiles using different correlations for Amherst, Connecticut Valley, MA**

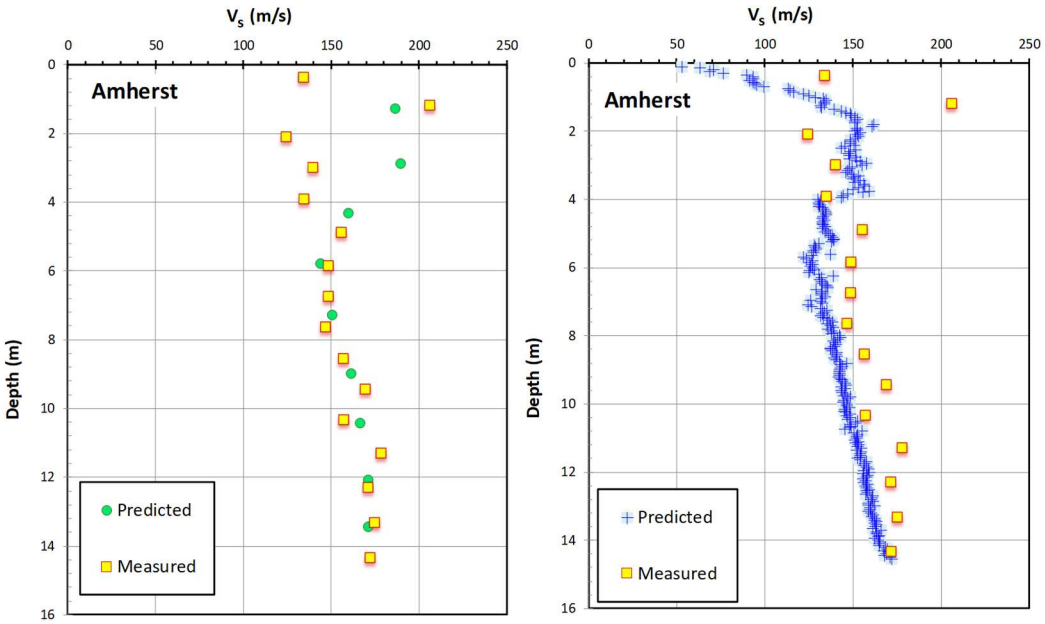


$$V_s = 75 \cdot (q_{net})^{0.1} \cdot \left(\frac{\sigma'_{vo}}{W_n}\right)^{0.2}$$

$$V_s = 16 \cdot \frac{(q_t)^{0.16}}{(f_s)^{0.015}} \cdot \frac{(\sigma'_{vo})^{0.255}}{(1+B_q)^{0.02}}$$

**Measured and predicted shear wave velocity profiles using the two proposed correlations for Amherst, Connecticut Valley, MA**

## Colebrook Overpass, Surrey, BC

Data after Crawford & Campanella, 1991; Weech, 2002)

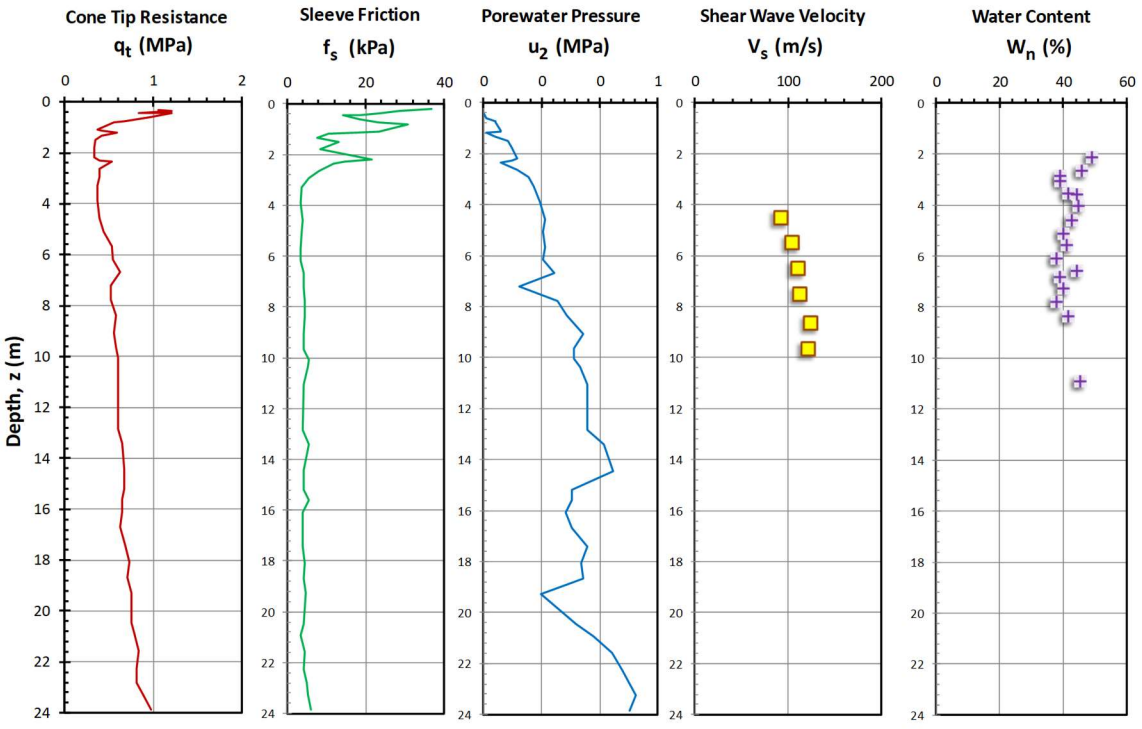

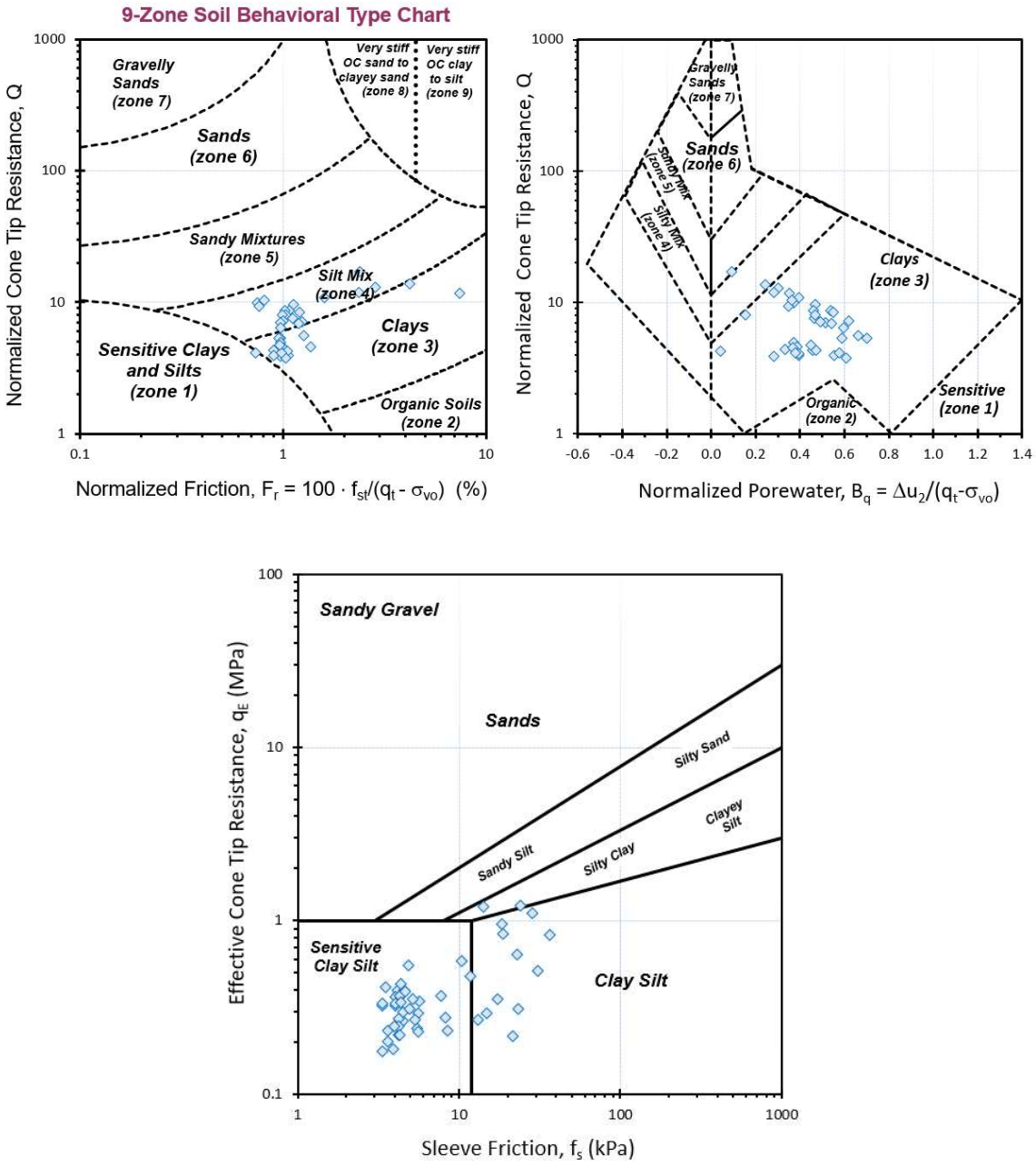


**CPT soil classification using 9-zone Robertson SBT and Fellenius and Eslami soil profiling charts for Colebrook Overpass, Surrey, BC**

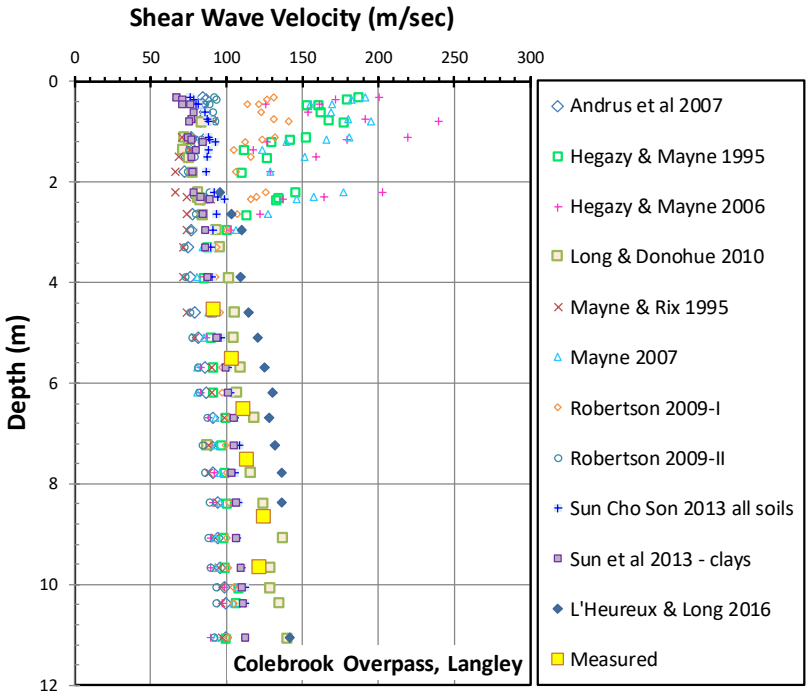


**Measured and predicted shear wave velocity profiles using different correlations for Colebrook Overpass, Surrey, BC**

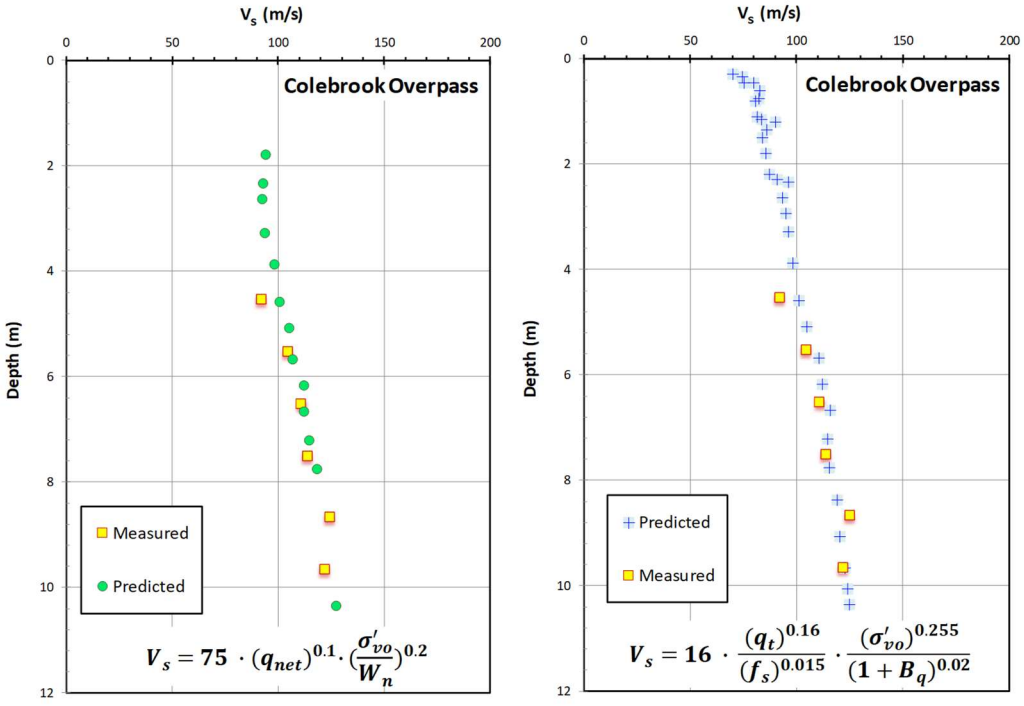


**Measured and predicted shear wave velocity profiles using the two proposed correlations for Colebrook Overpass, Surrey, BC**

## Dyke Road, Richmond, BC

Data after Sanin (2005)

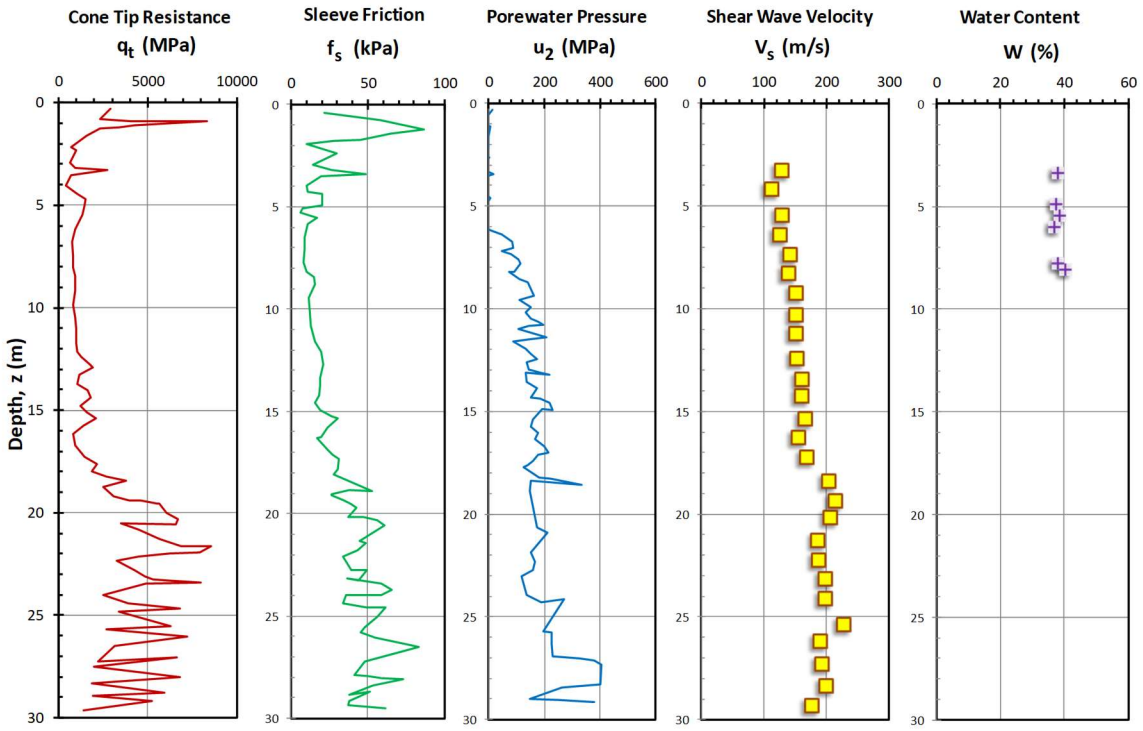

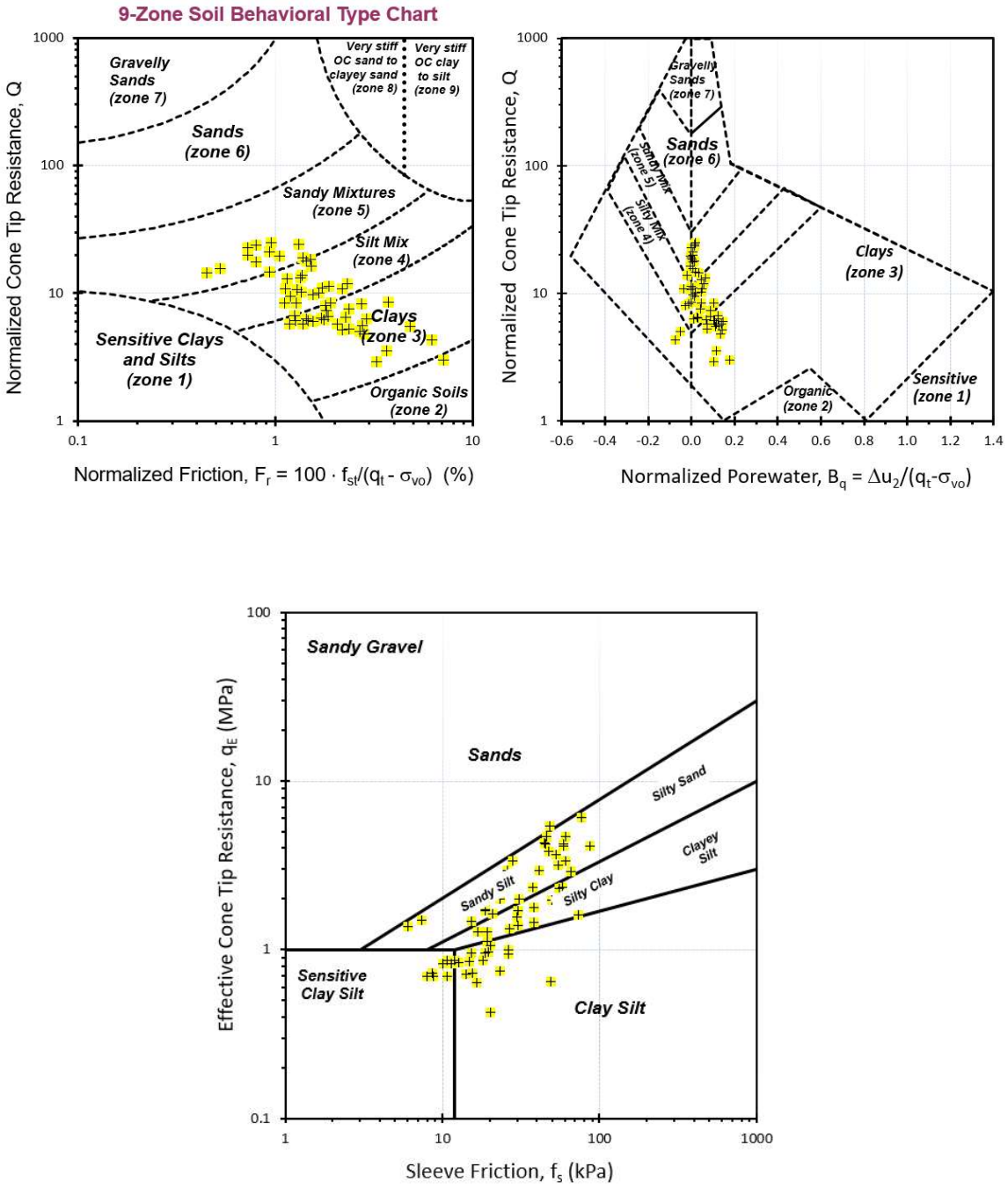


**CPT soil classification using 9-zone Robertson SBT and Fellenius and Eslami soil profiling charts for Dyke Road, Richmond, BC**

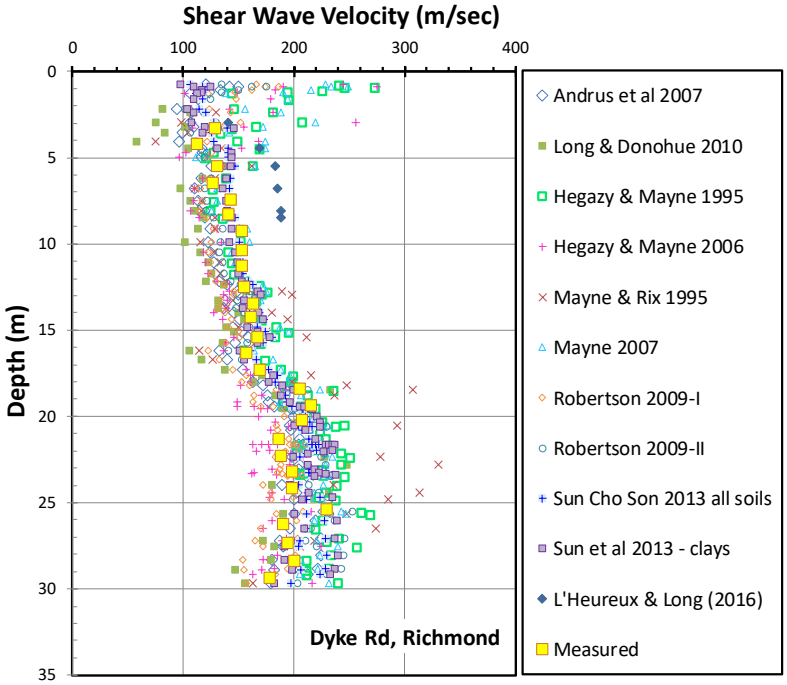


**Measured and predicted shear wave velocity profiles using different correlations for Dyke Road, Richmond, BC**

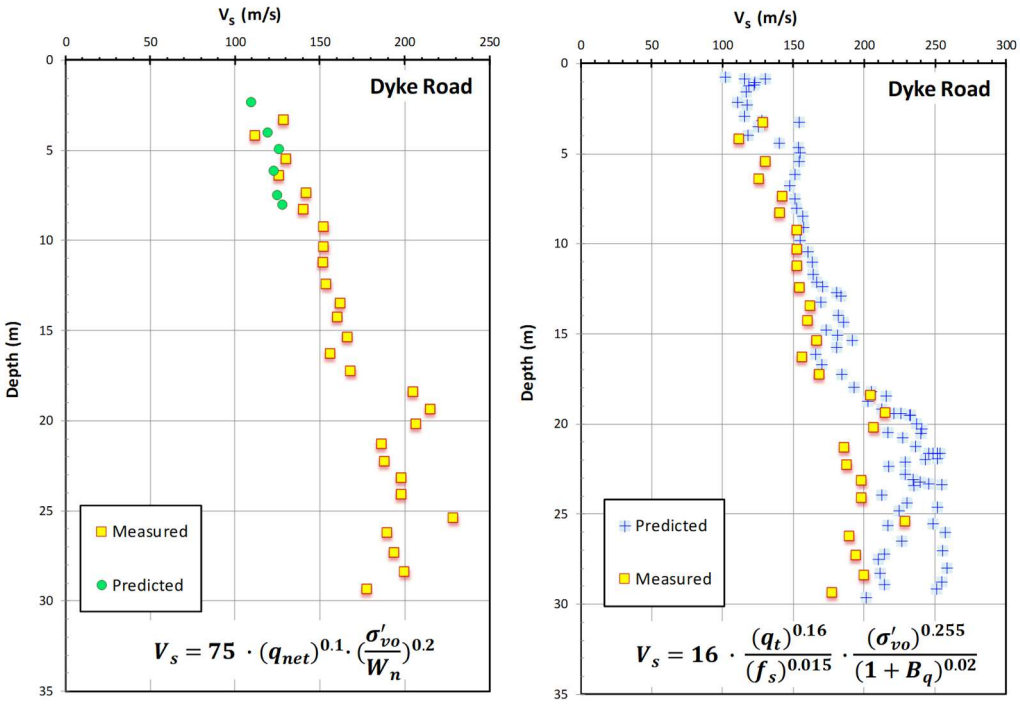


**Measured and predicted shear wave velocity profiles using the two proposed correlations for Dyke Road, Richmond, BC**

## Ford Design Center, Evanston, IL

Data after Mayne (2007 b)

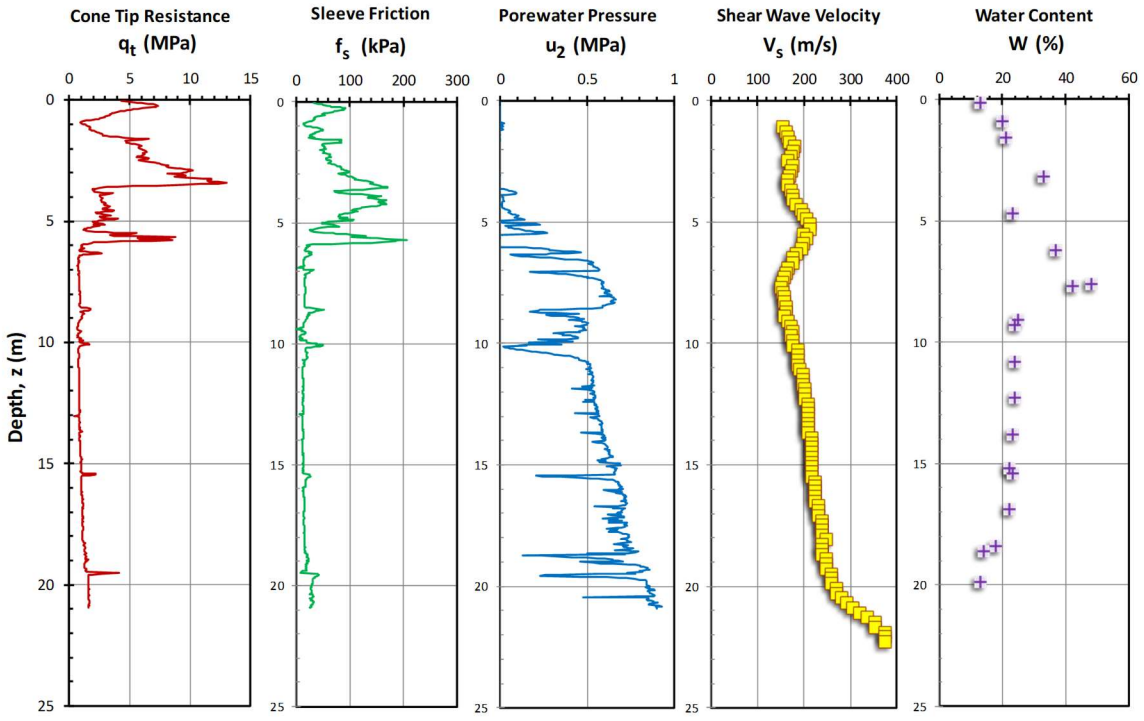

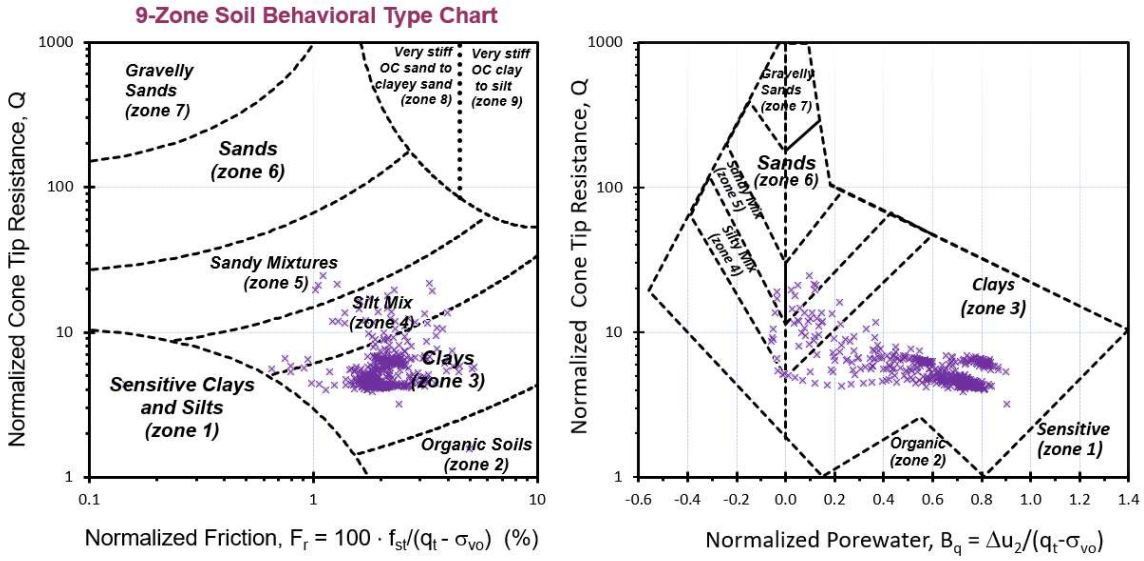


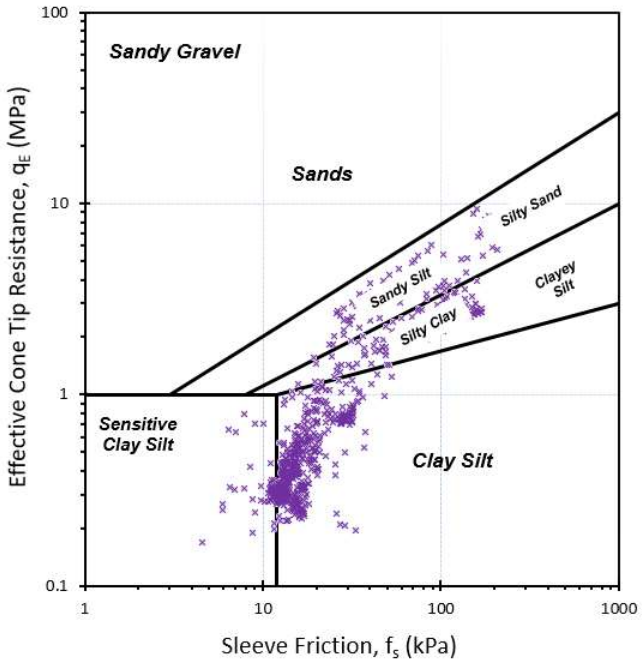


**CPT soil classification using 9-zone Robertson SBT and Fellenius and Eslami soil profiling charts for Ford Design Center, Evanston, IL**

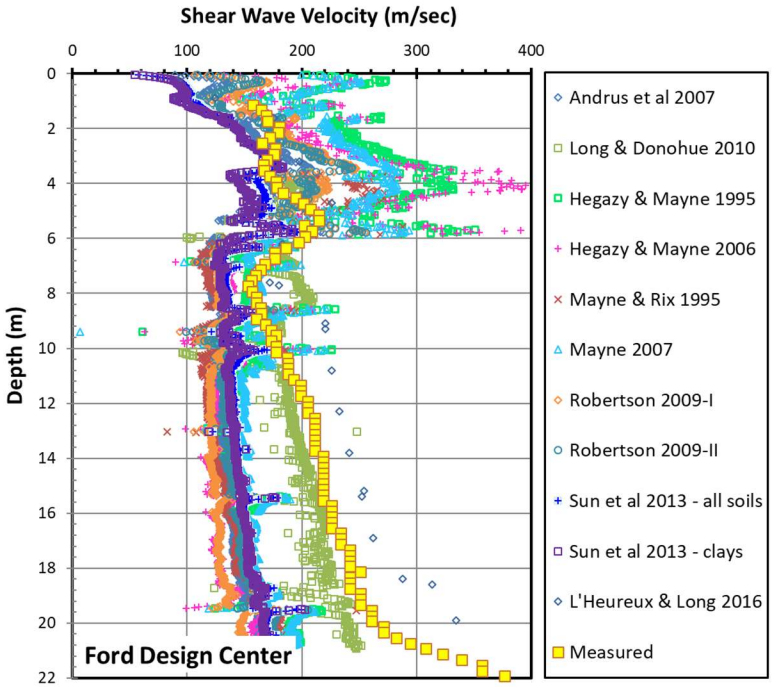


**Measured and predicted shear wave velocity profiles using different correlations for Ford Design Center, Evanston, IL**

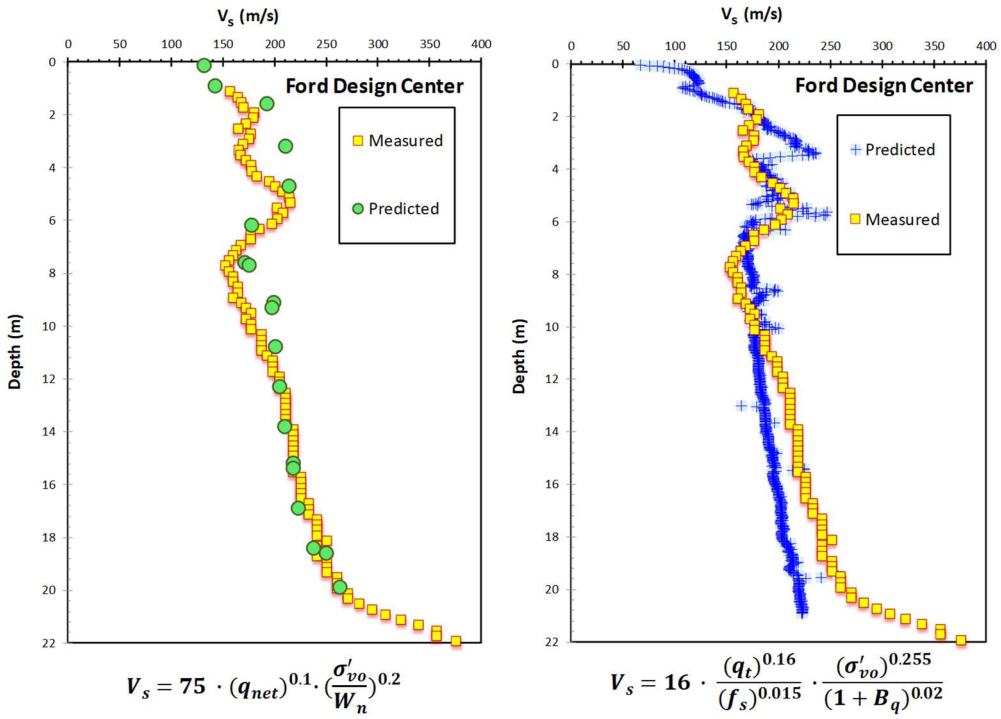


**Measured and predicted shear wave velocity profiles using the two proposed correlations for Ford Design Center, Evanston, IL**

## Gloucester, Ontario

Data after Styler & Mayne (2013)

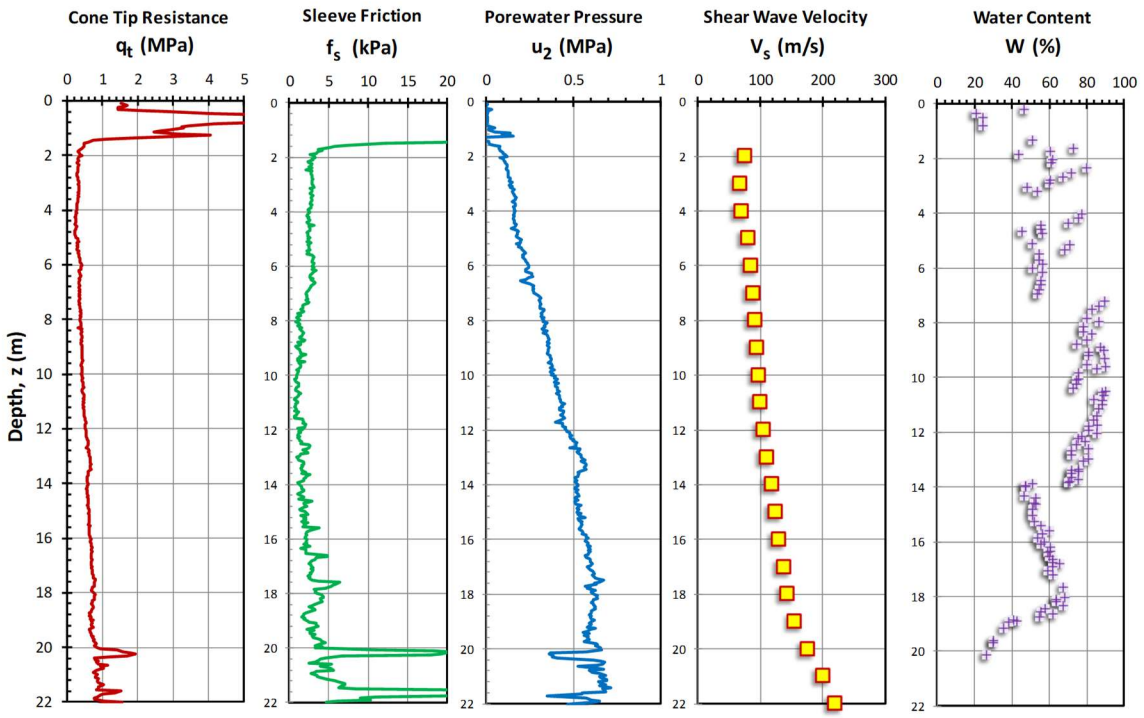

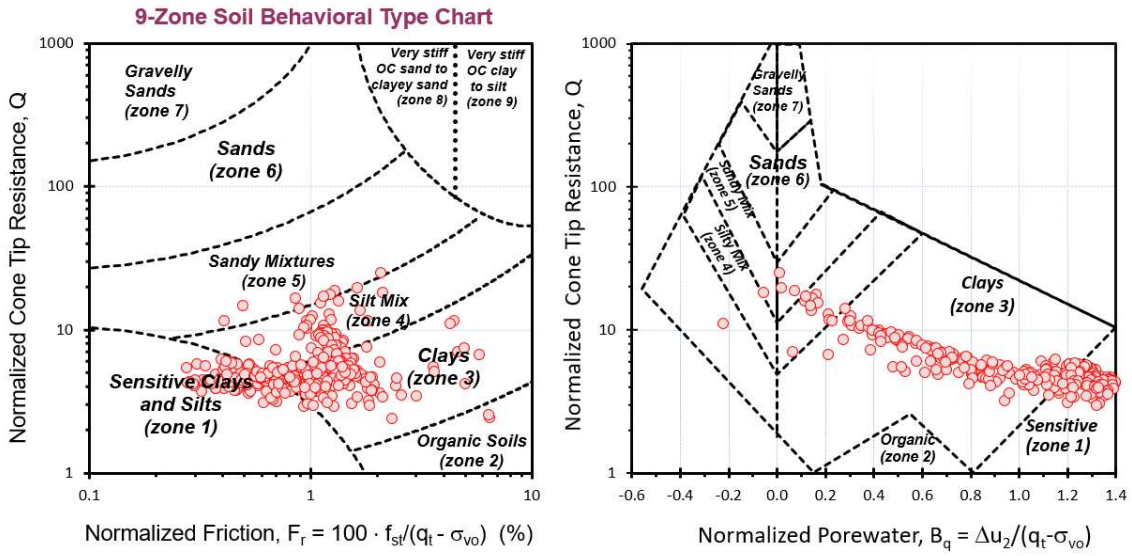


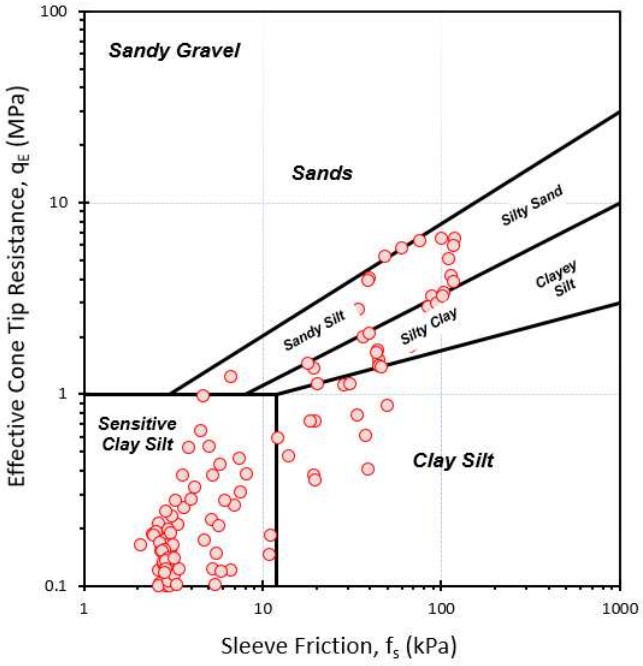


**CPT soil classification using 9-zone Robertson SBT and Fellenius and Eslami soil profiling charts for Gloucester, Ontario**

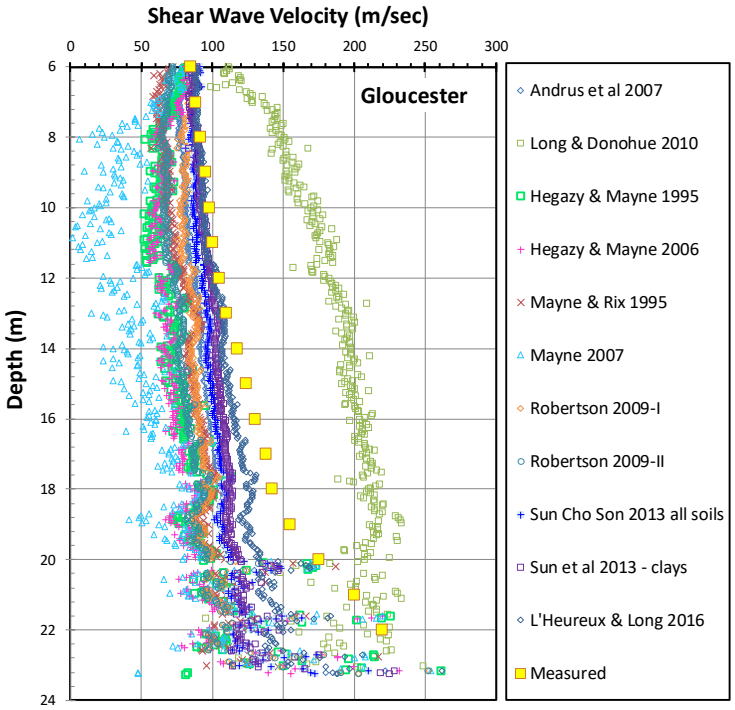


**Measured and predicted shear wave velocity profiles using different correlations for Gloucester, Ontario**

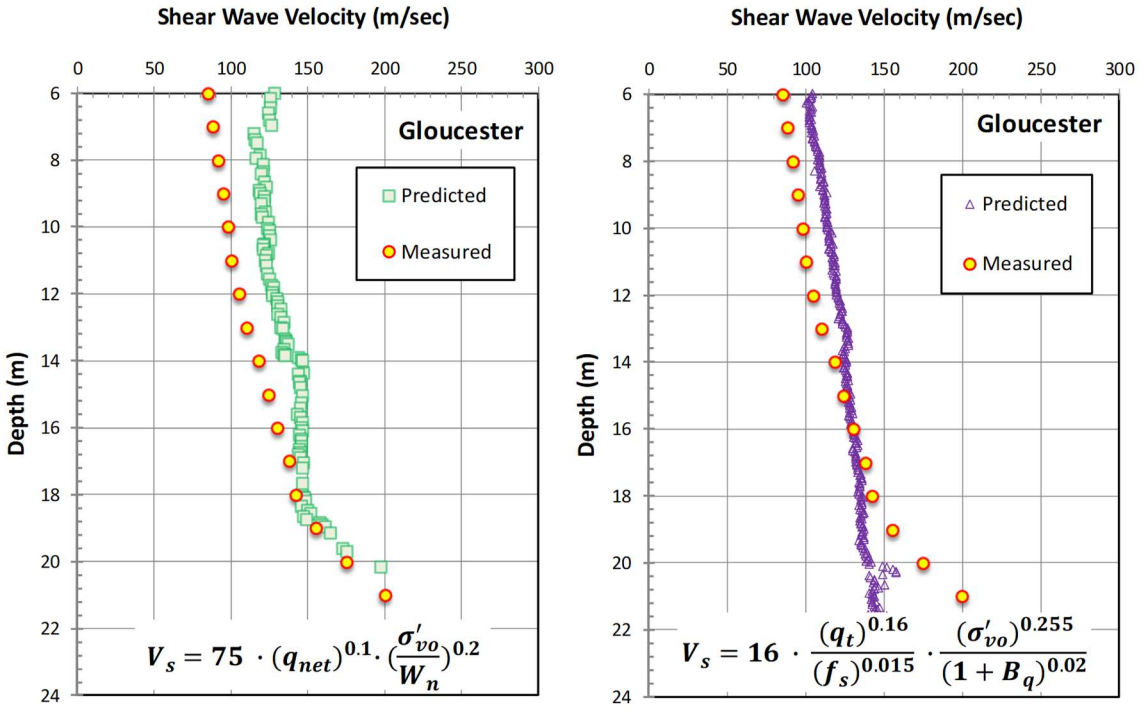


**Measured and predicted shear wave velocity profiles using the two proposed correlations for Gloucester, Ontario**

## Golden Ears Bridge, Langley, BC

Data after Niazi et al. (2010)

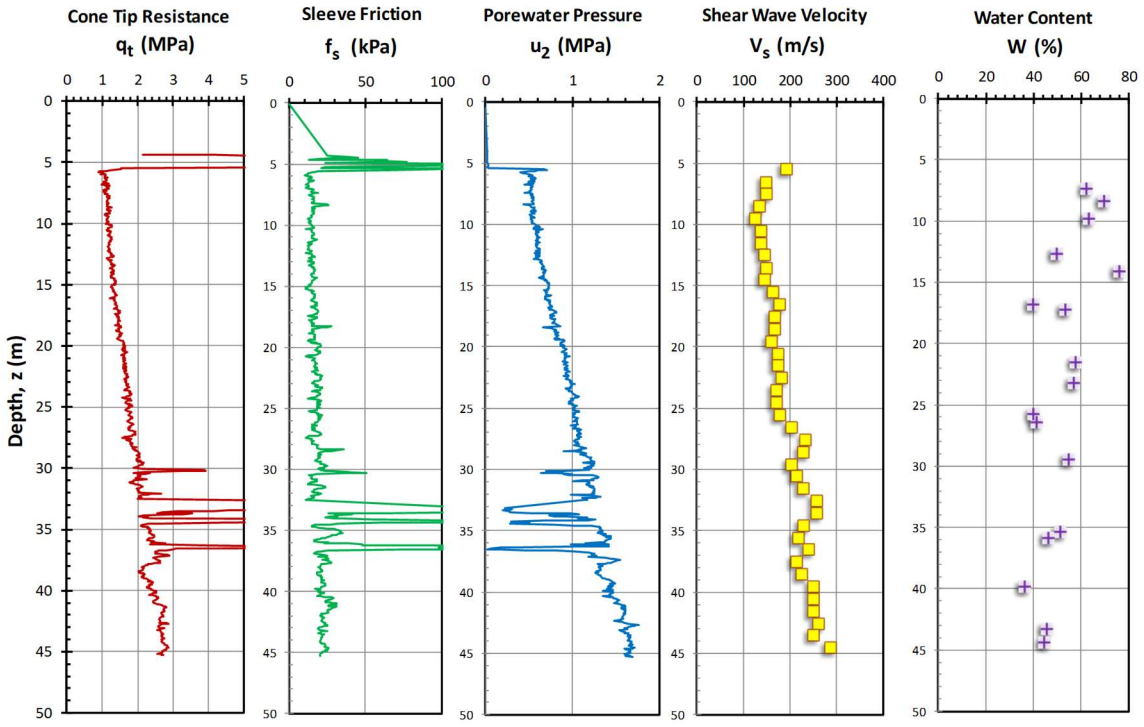

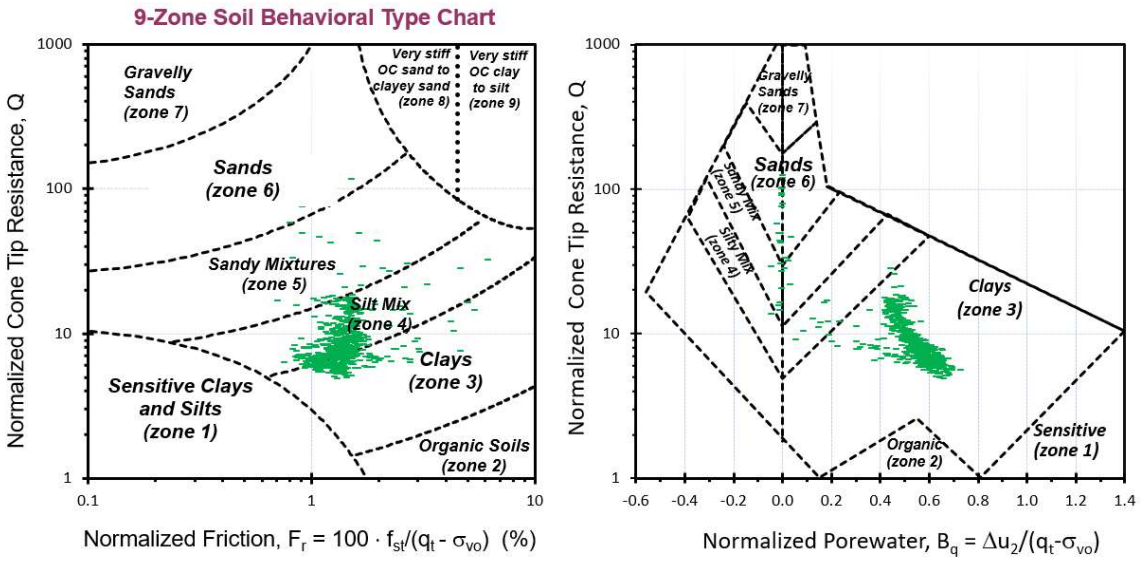


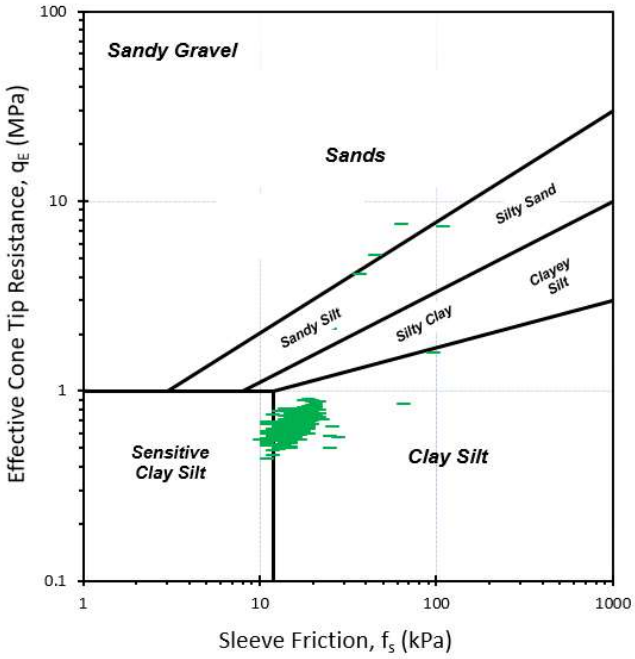


**CPT soil classification using 9-zone Robertson SBT and Fellenius and Eslami soil profiling charts for Golden Ears Bridge, Langley, BC**

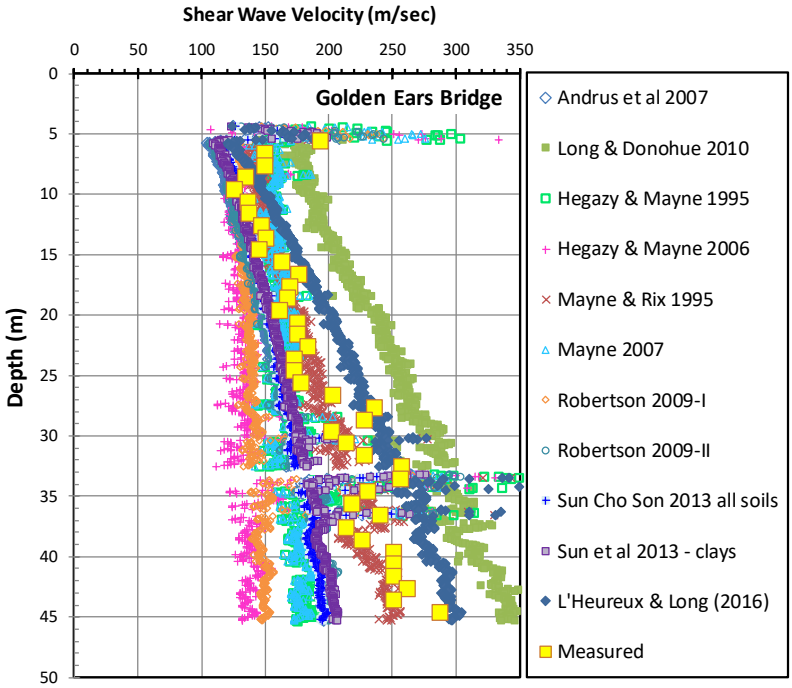


**Measured and predicted shear wave velocity profiles using different correlations for Golden Ears Bridge, Langley, BC**

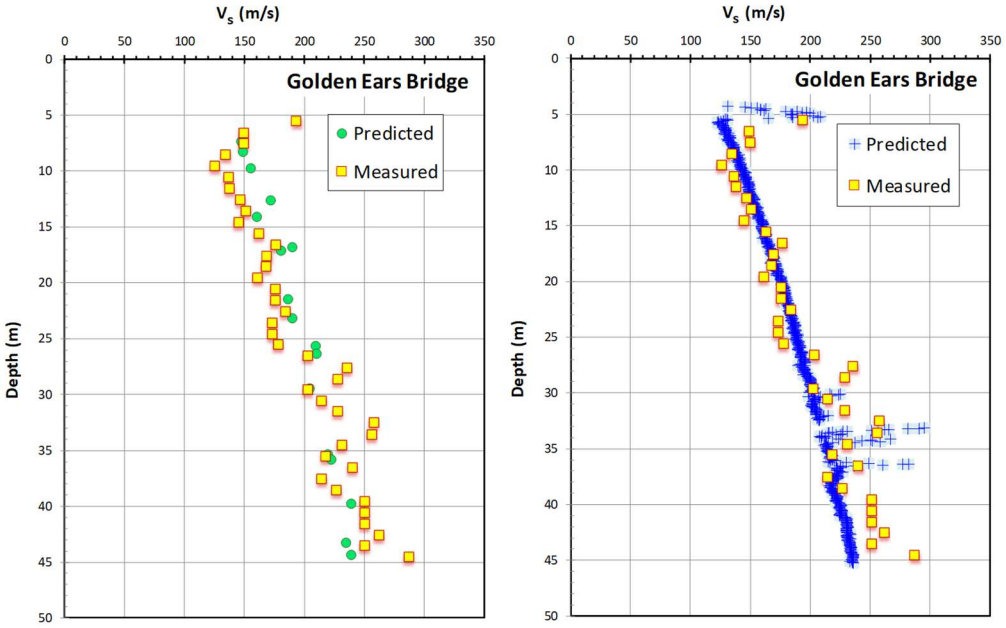


**Measured and predicted shear wave velocity profiles using the two proposed correlations for Golden Ears Bridge, Langley, BC**

## Haney clay, BC

Data after Woeller – ConeTec (2004)

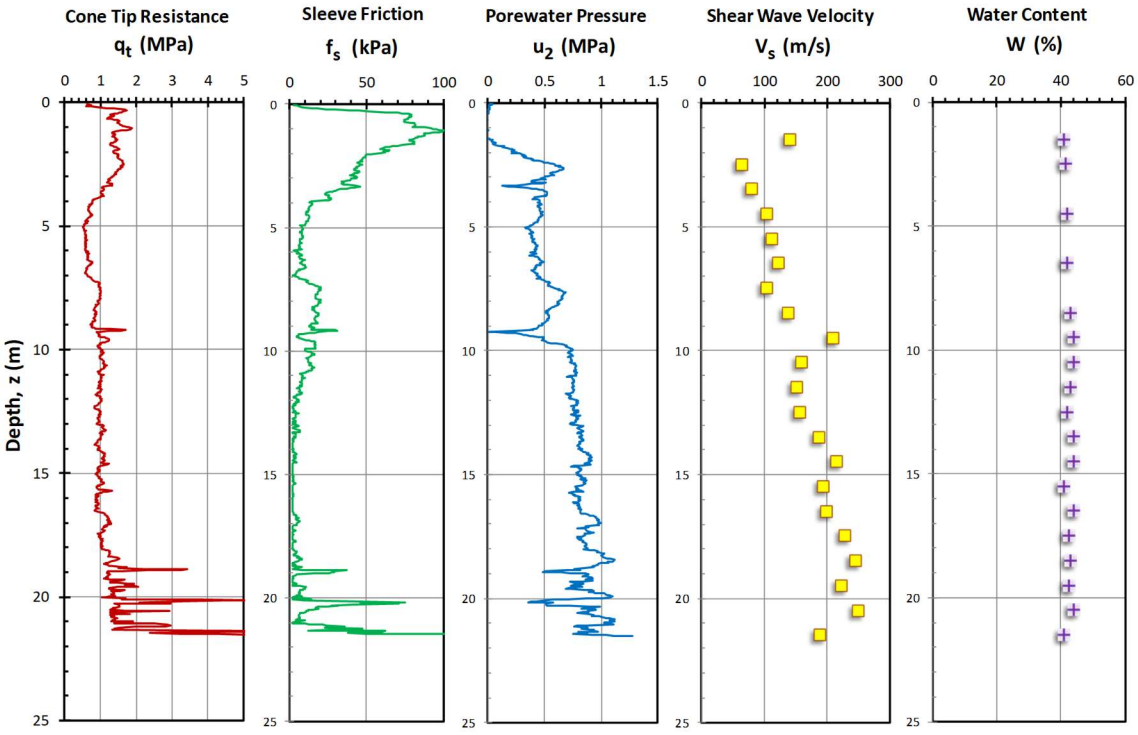

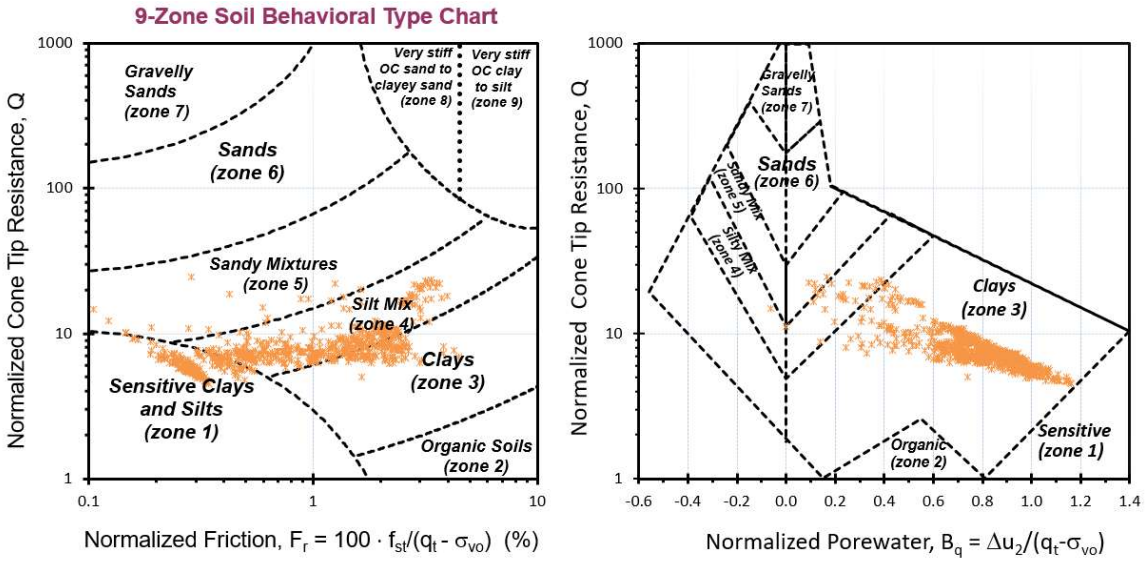


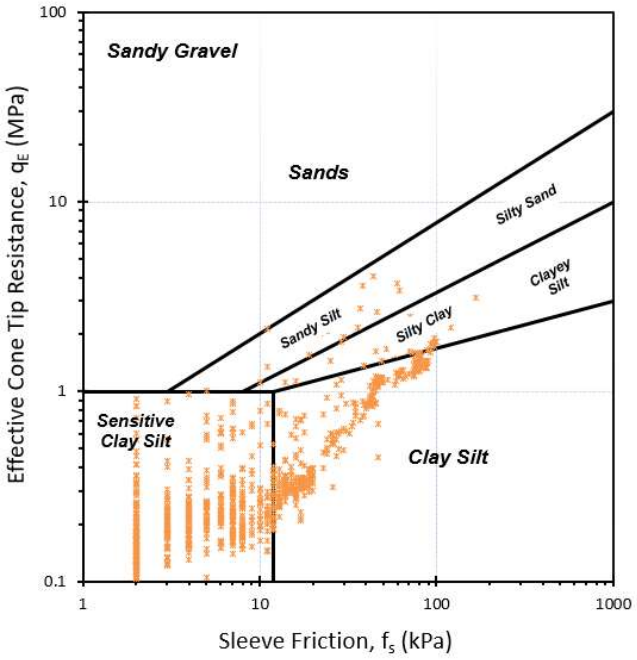


**CPT soil classification using 9-zone Robertson SBT and Fellenius and Eslami soil profiling charts for Haney clay, BC**

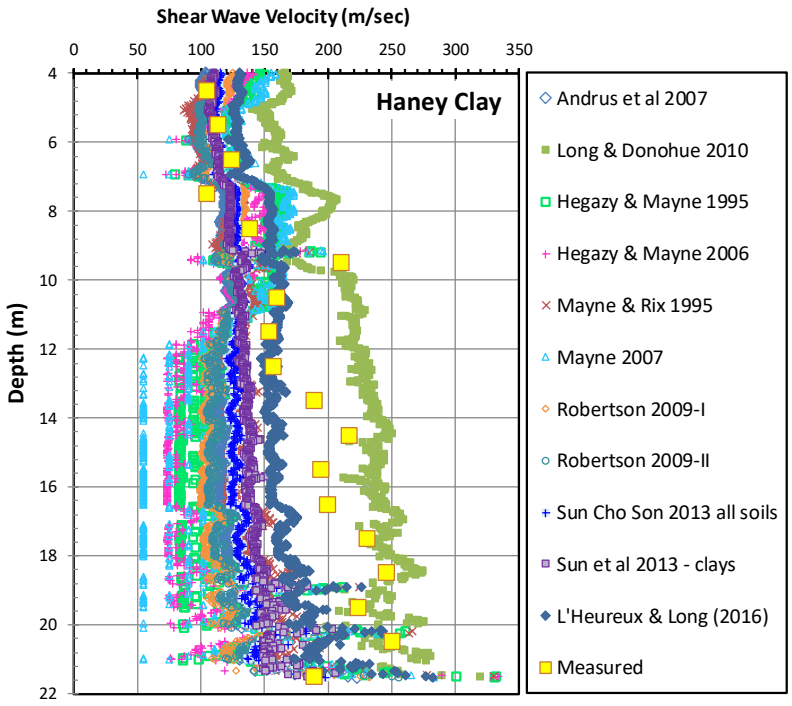


**Measured and predicted shear wave velocity profiles using different correlations for Haney clay, BC**

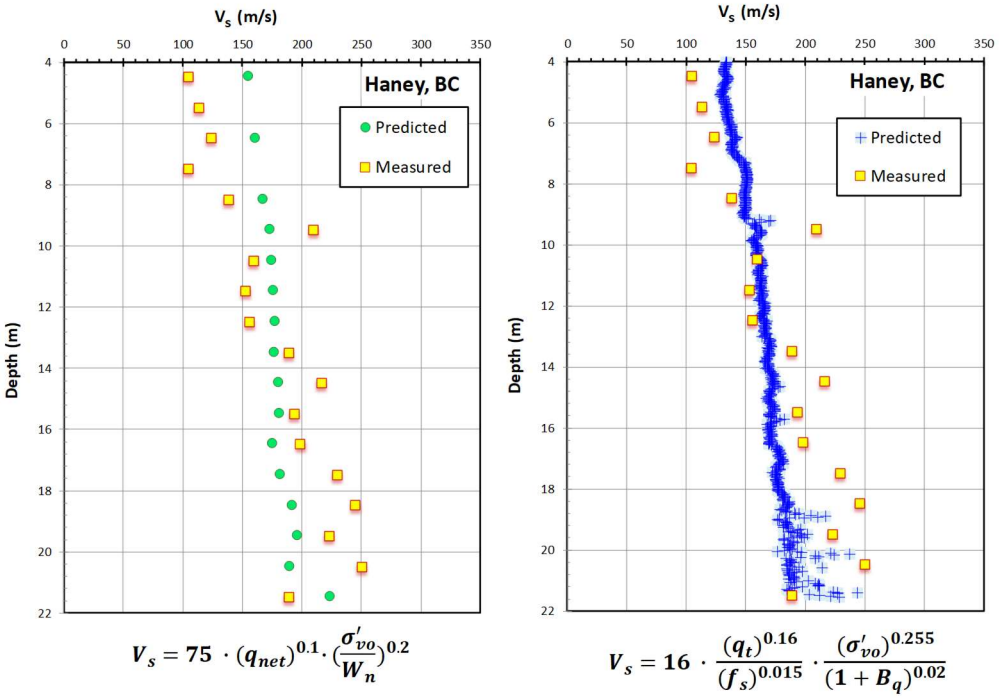


**Measured and predicted shear wave velocity profiles using the two proposed correlations for Haney clay, BC**

## Louiseville, Québec

Data after Yafrate & DeJong (2006)

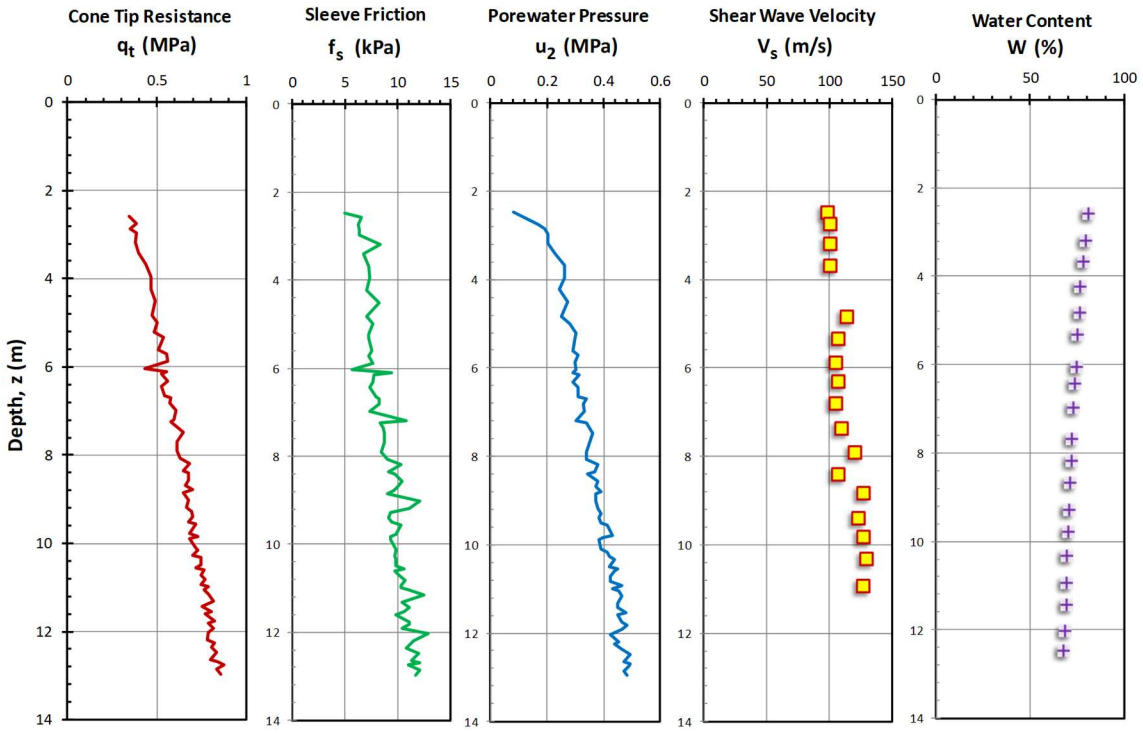

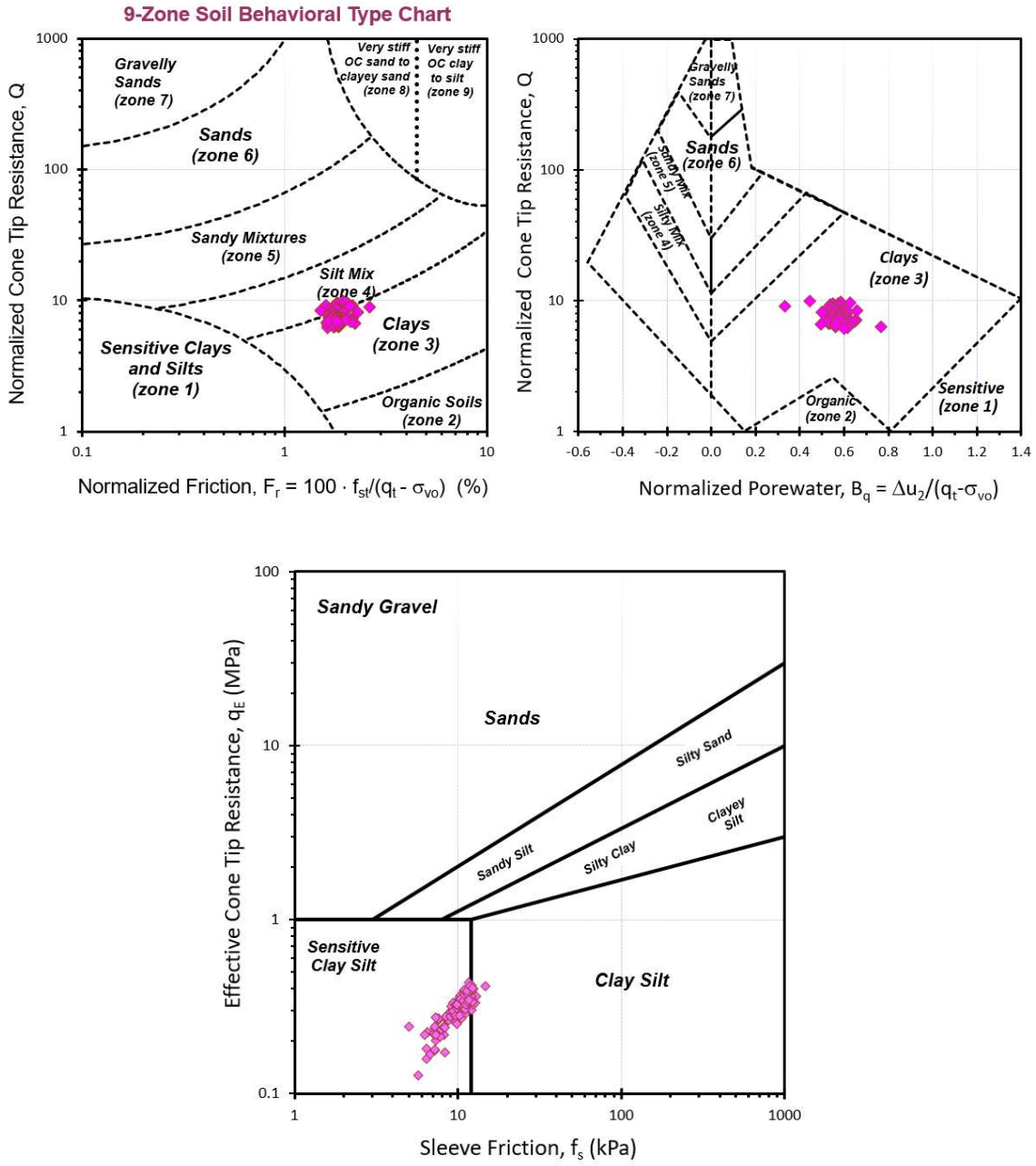


**CPT soil classification using 9-zone Robertson SBT and Fellenius and Eslami soil profiling charts for Louiseville, Québec**

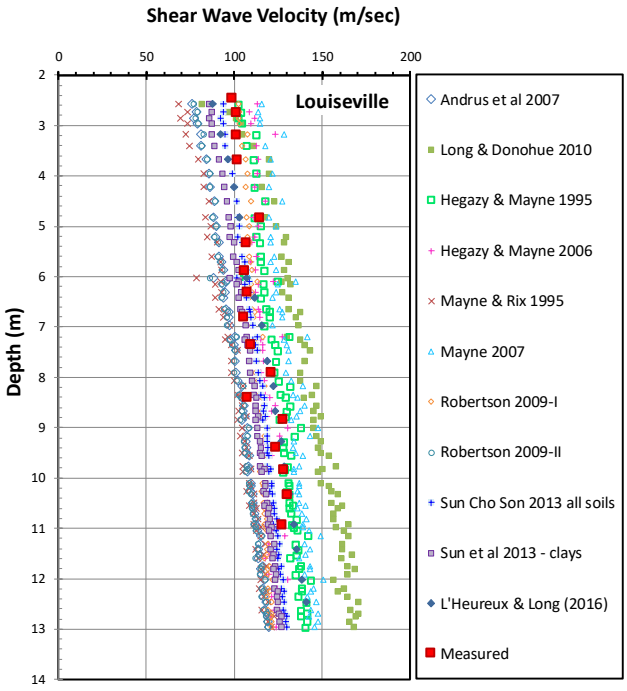


**Measured and predicted shear wave velocity profiles using different correlations for Louiseville, Québec**

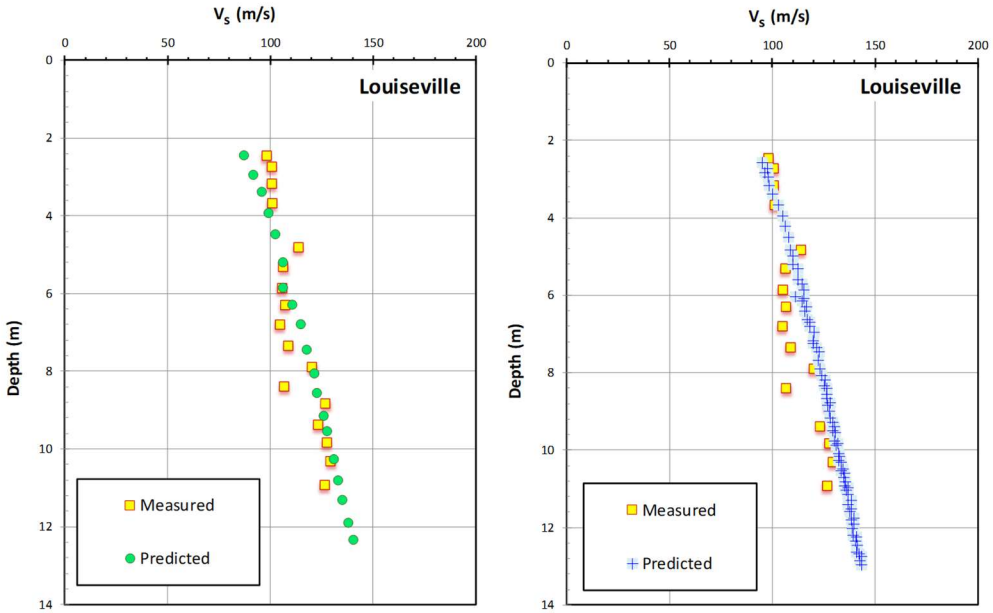


**Measured and predicted shear wave velocity profiles using the two proposed correlations for Louiseville, Québec**

## Martin's Point Bridge, Maine

Data after Hardison (2015)

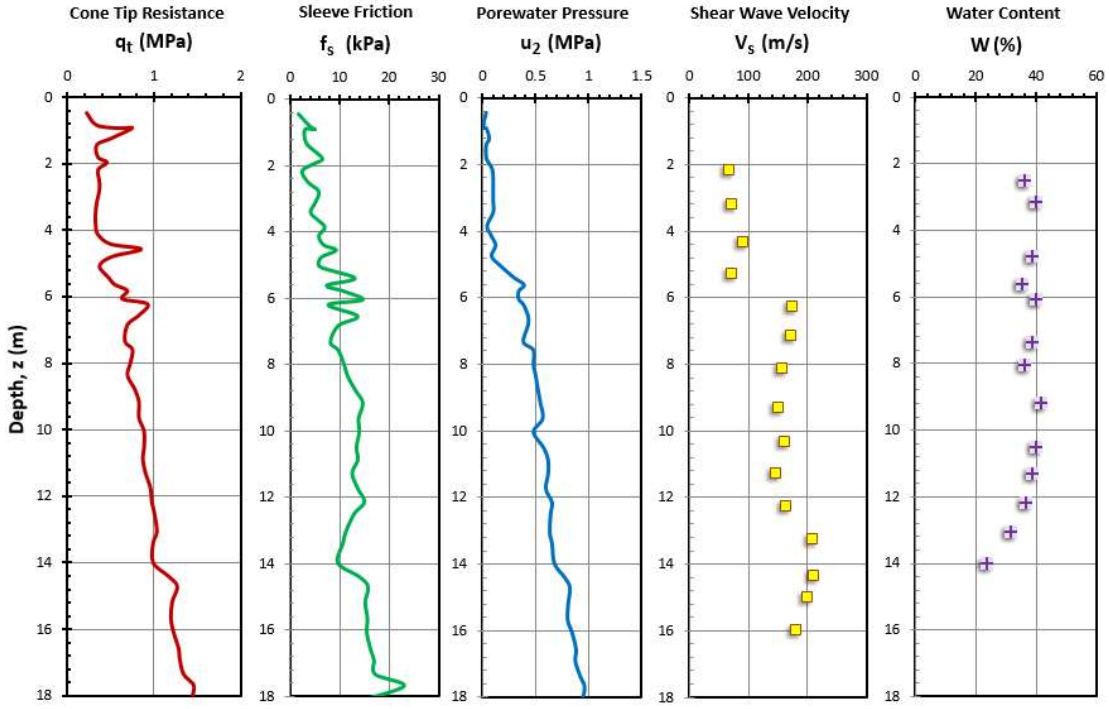

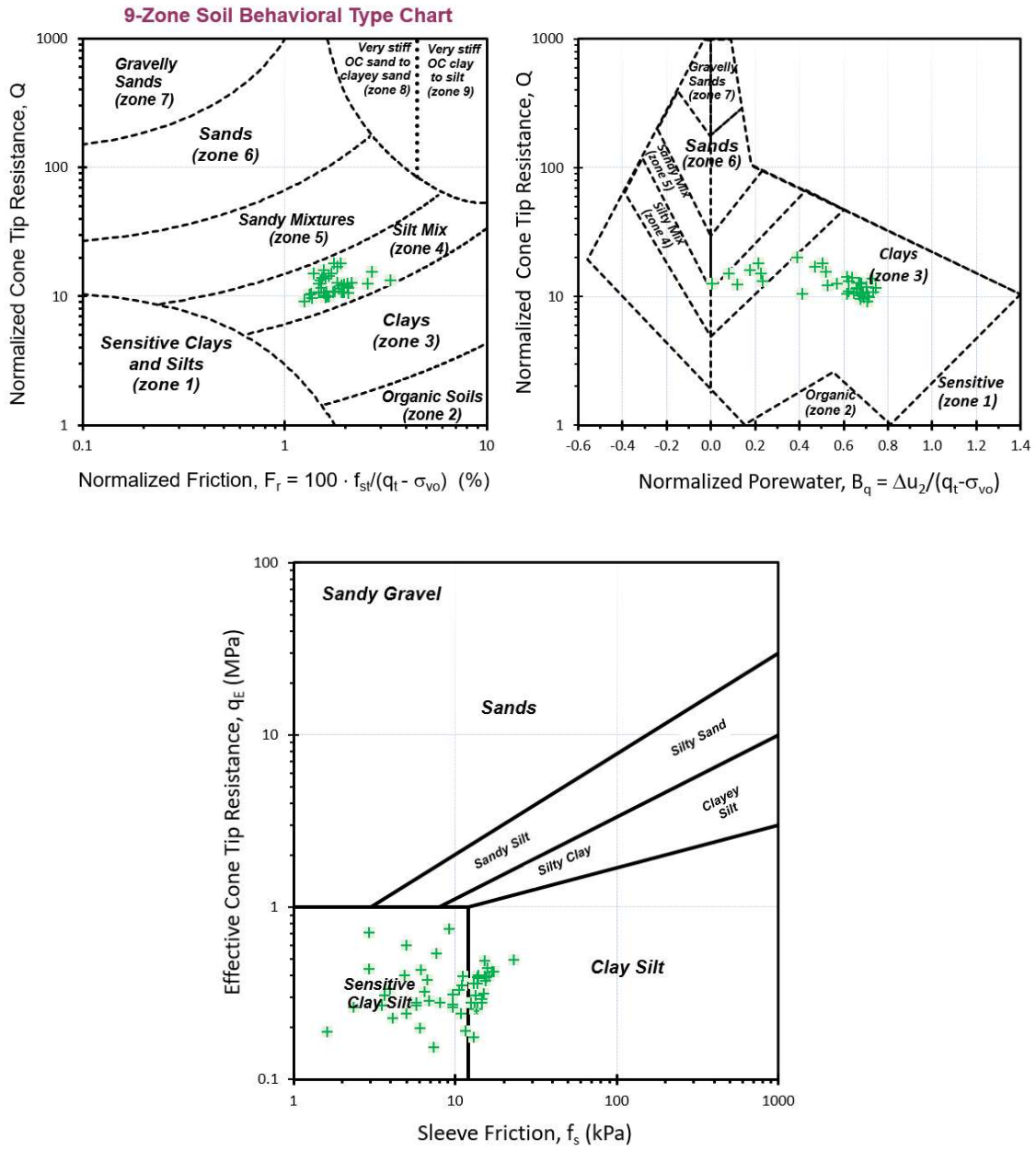


**CPT soil classification using 9-zone Robertson SBT and Fellenius and Eslami soil profiling charts for Martin's Point Bridge, Maine**

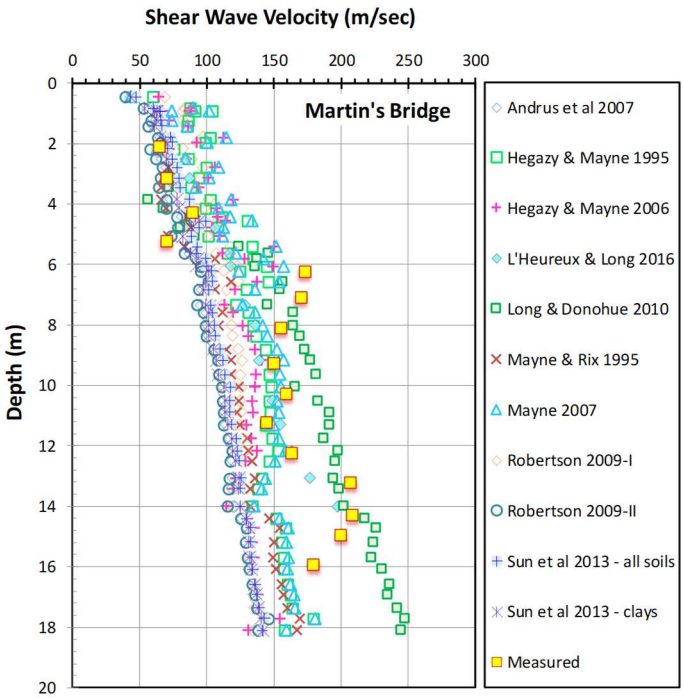


**Measured and predicted shear wave velocity profiles using different correlations for Martin's Point Bridge, Maine**

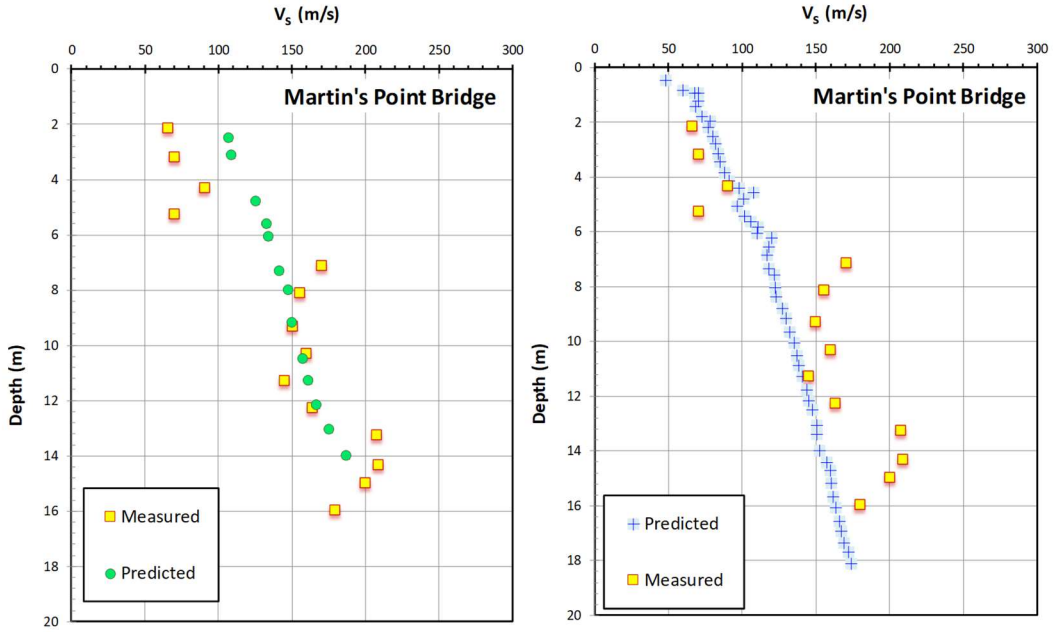


$$V_s = 75 \cdot (q_{net})^{0.1} \cdot \left(\frac{\sigma'_{vo}}{W_n}\right)^{0.2}$$

$$V_s = 16 \cdot \frac{(q_t)^{0.16}}{(f_s)^{0.015}} \cdot \frac{(\sigma'_{vo})^{0.255}}{(1+B_q)^{0.02}}$$

**Measured and predicted shear wave velocity profiles using the two proposed correlations for Martin's Point Bridge, Maine**

## Massey Tunnel, Delta, BC

Data after Kong – Golder Associates Limited (2015)

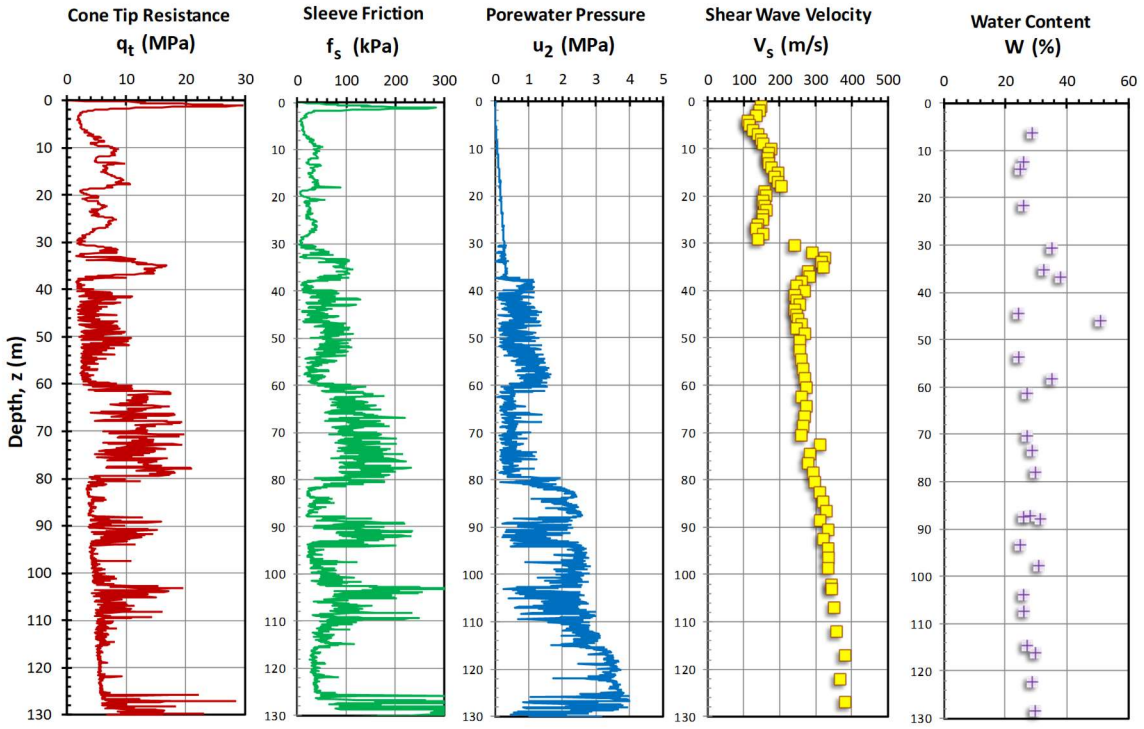


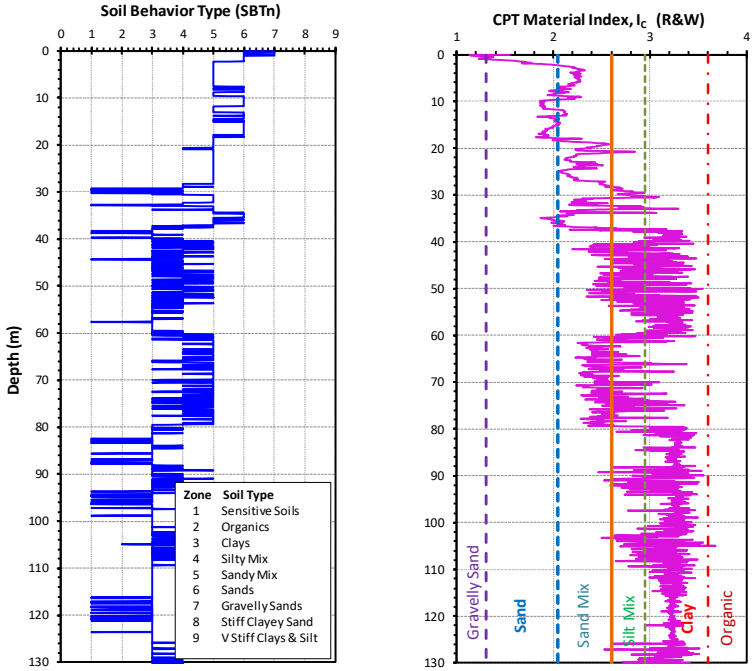

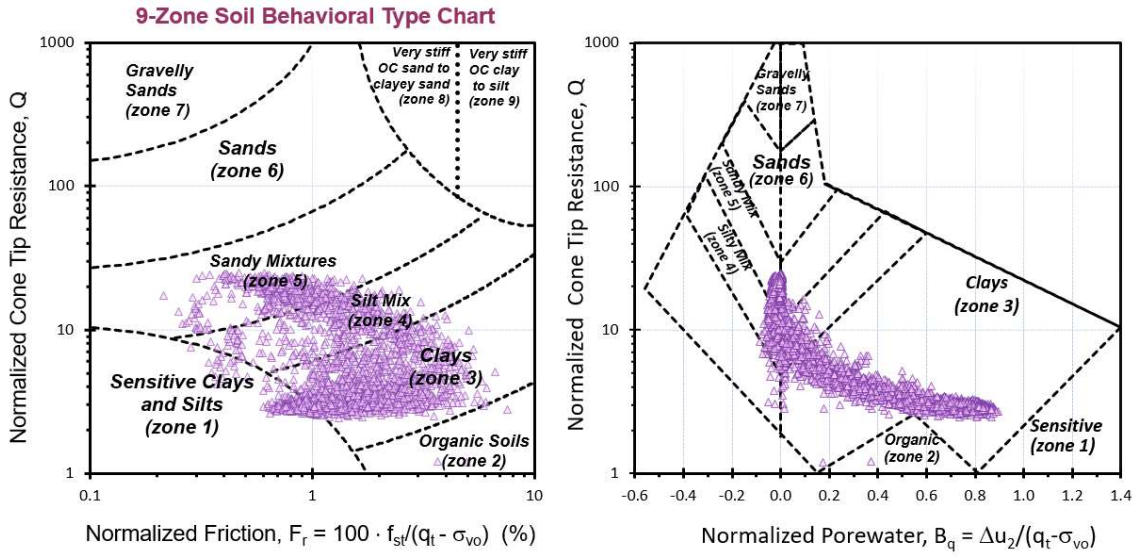


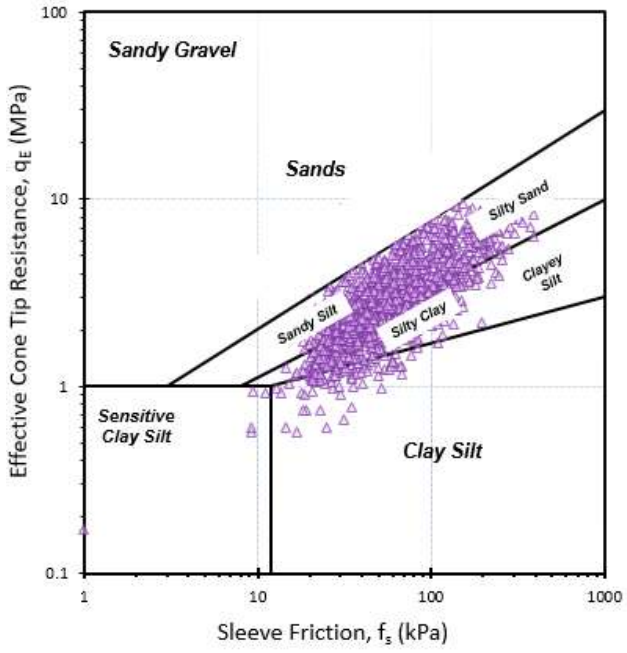


**CPT soil classification using 9-zone Robertson SBT and Fellenius and Eslami soil profiling charts for Massey Tunnel, Delta, BC**

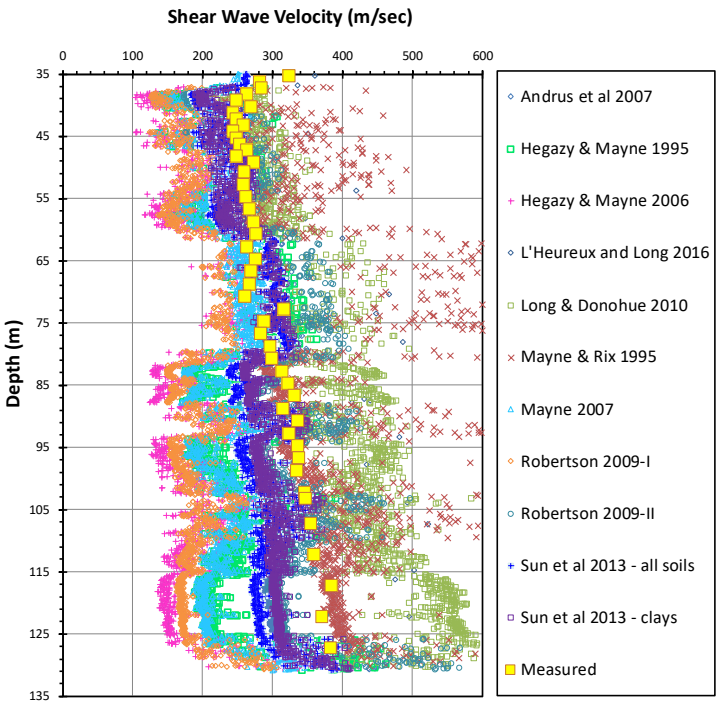


**Measured and predicted shear wave velocity profiles using different correlations for Massey Tunnel, Delta, BC**

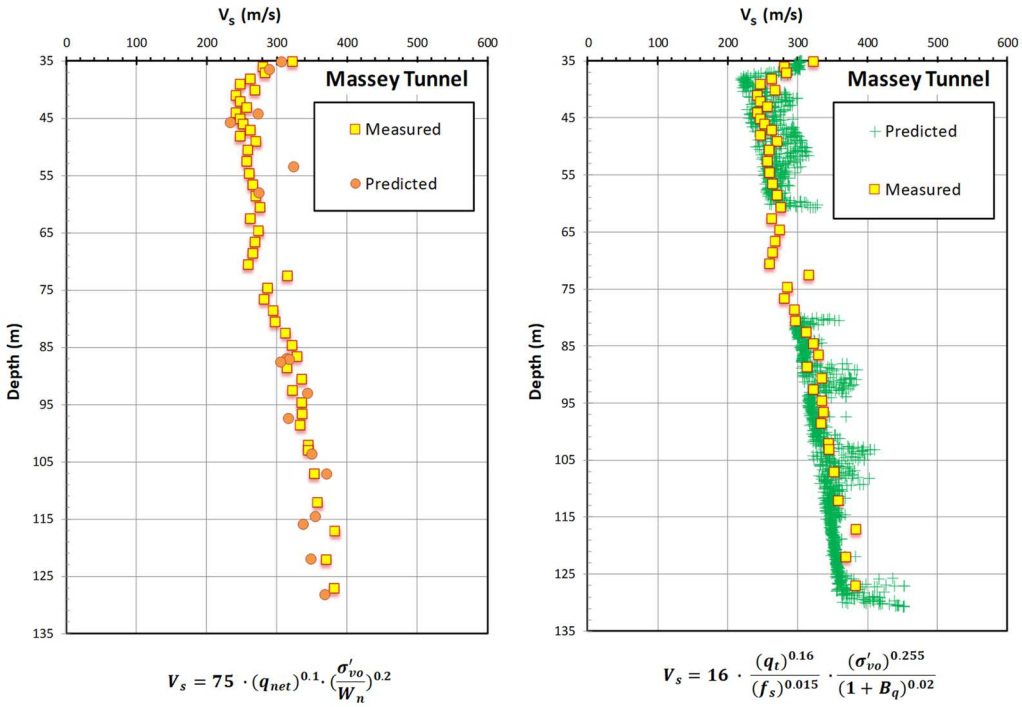


**Measured and predicted shear wave velocity profiles using the two proposed correlations for Massey Tunnel, Delta, BC**

## McDonald's Farm, Vancouver

Data after Campanella et al. (1986)

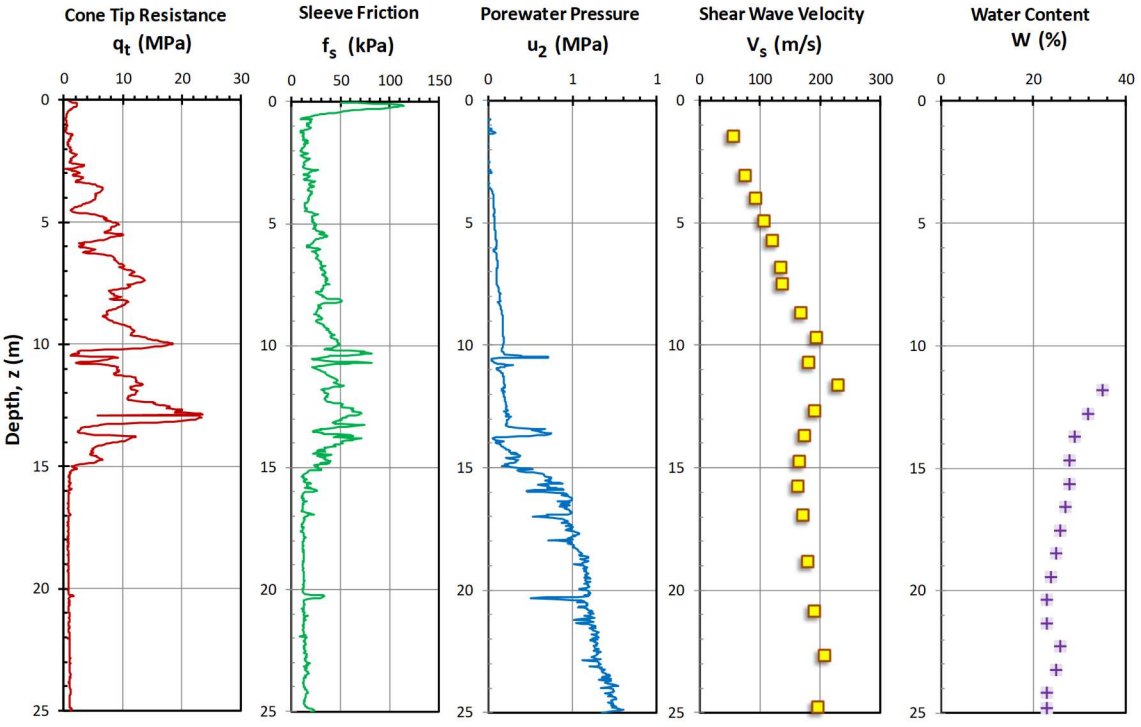

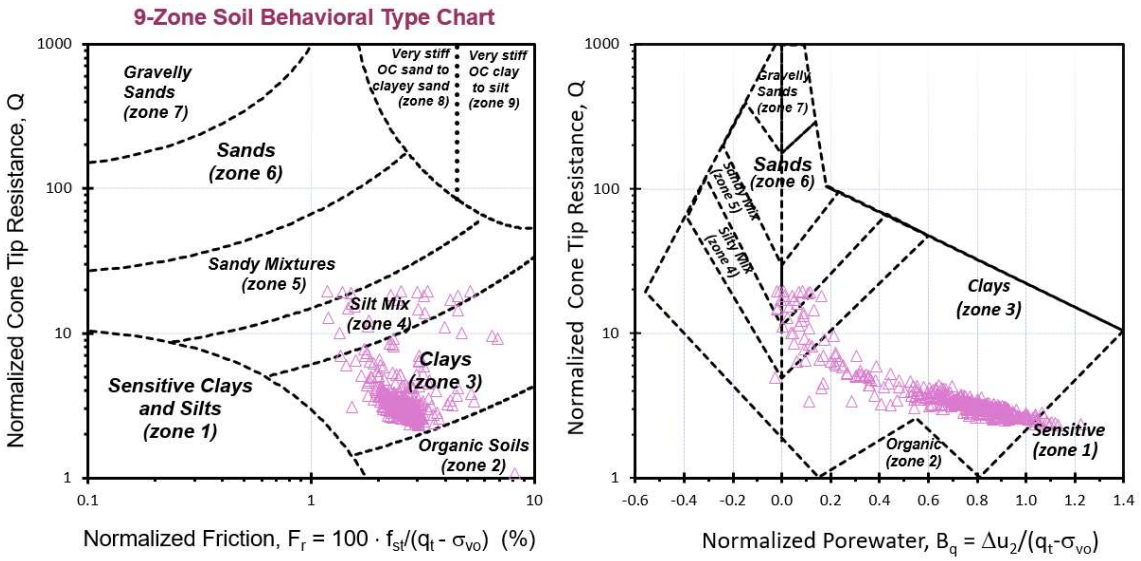


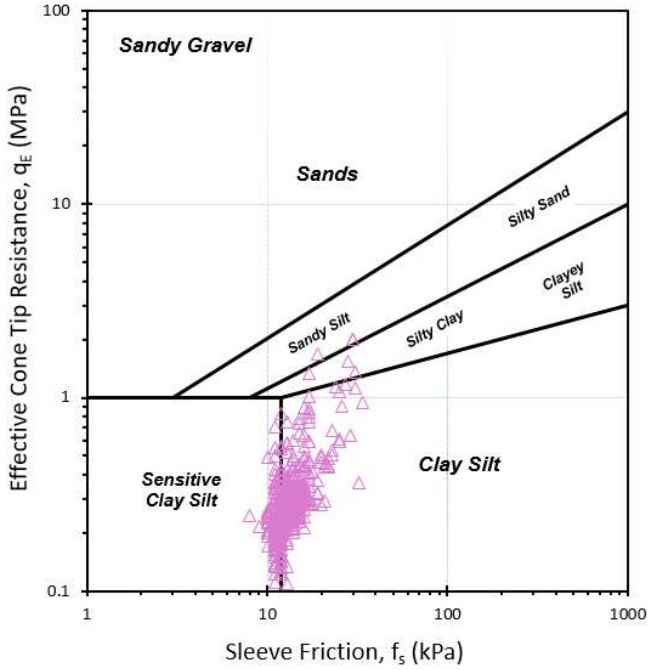


**CPT soil classification using 9-zone Robertson SBT and Fellenius and Eslami soil profiling charts for McDonald's Farm, Vancouver**

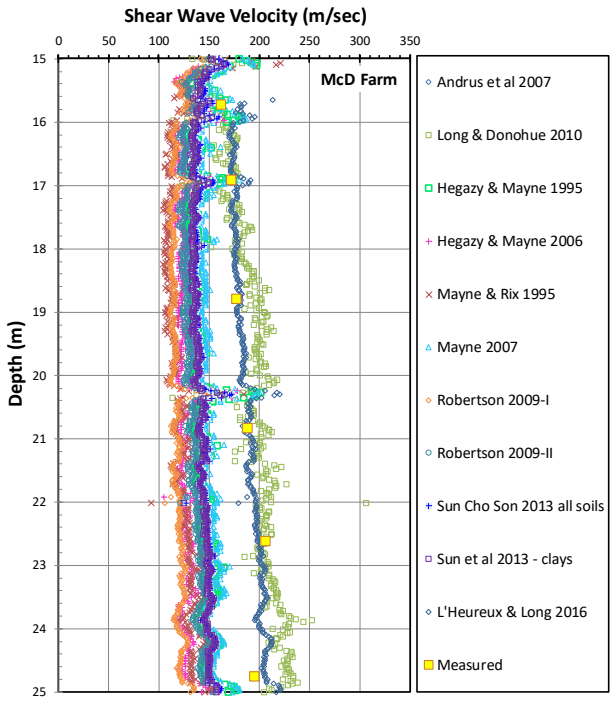


**Measured and predicted shear wave velocity profiles using different correlations for McDonald's Farm, Vancouver**

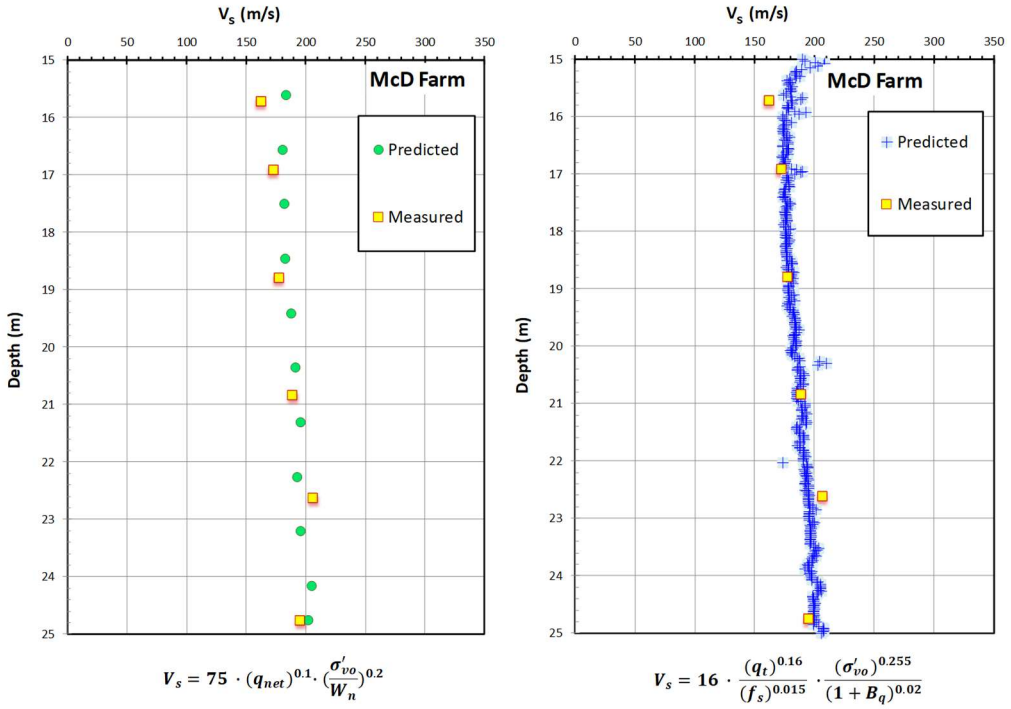


**Measured and predicted shear wave velocity profiles using the two proposed correlations for McDonald's Farm, Vancouver**

## Newbury, MA

Data after Landon (2007)

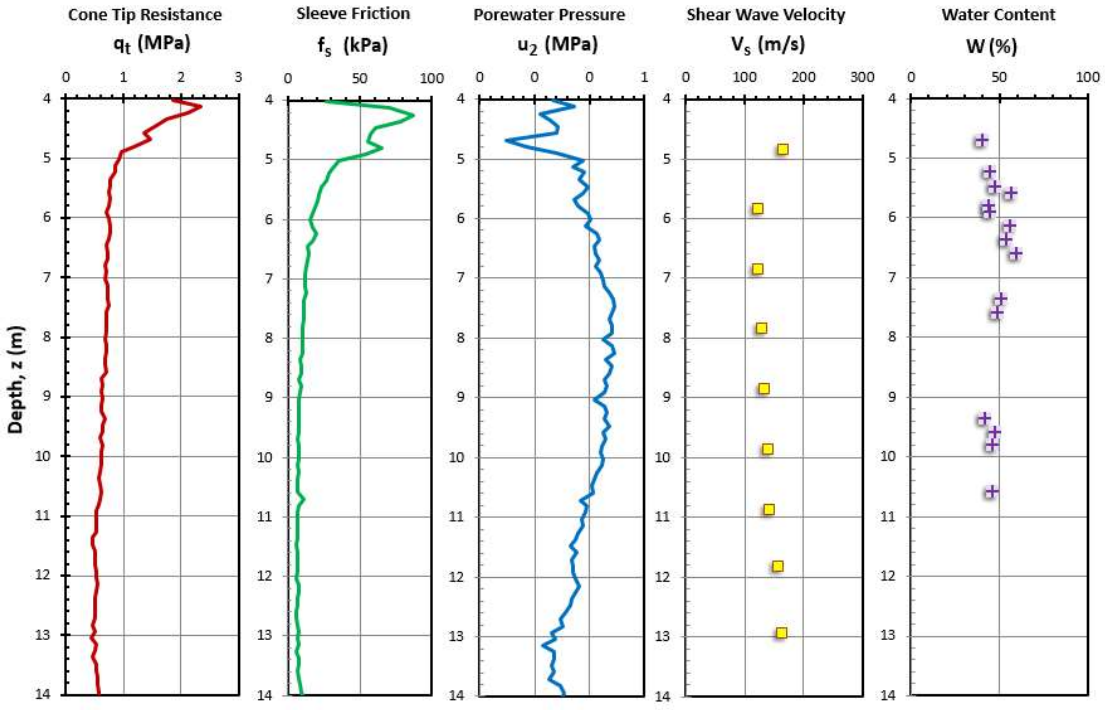

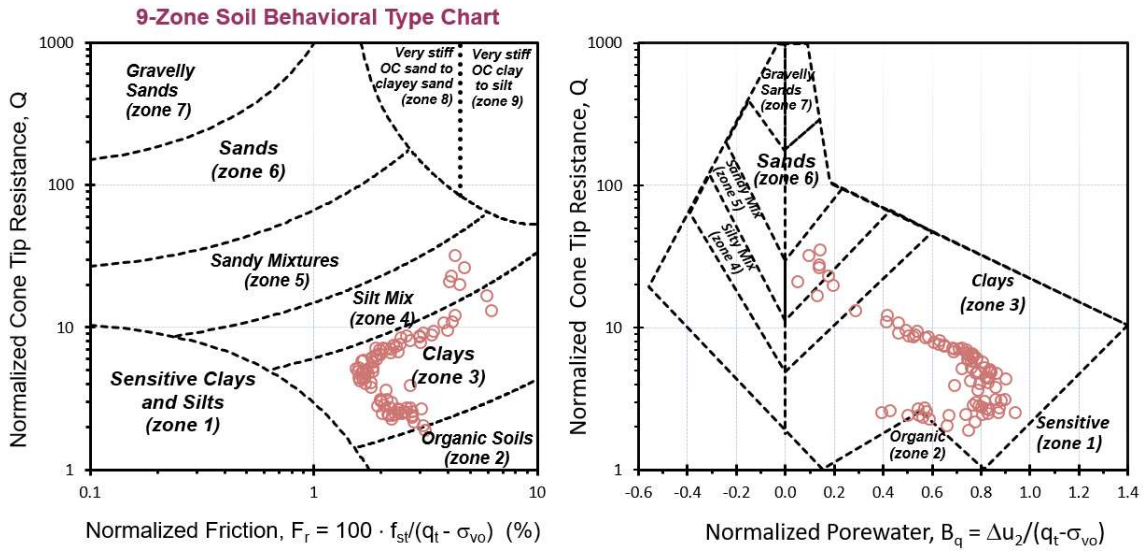


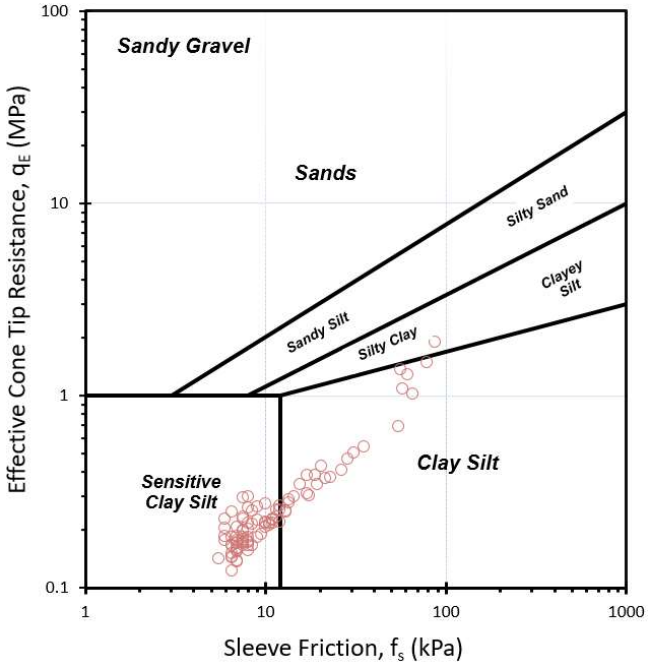


**CPT soil classification using 9-zone Robertson SBT and Fellenius and Eslami soil profiling charts for Newbury, MA**

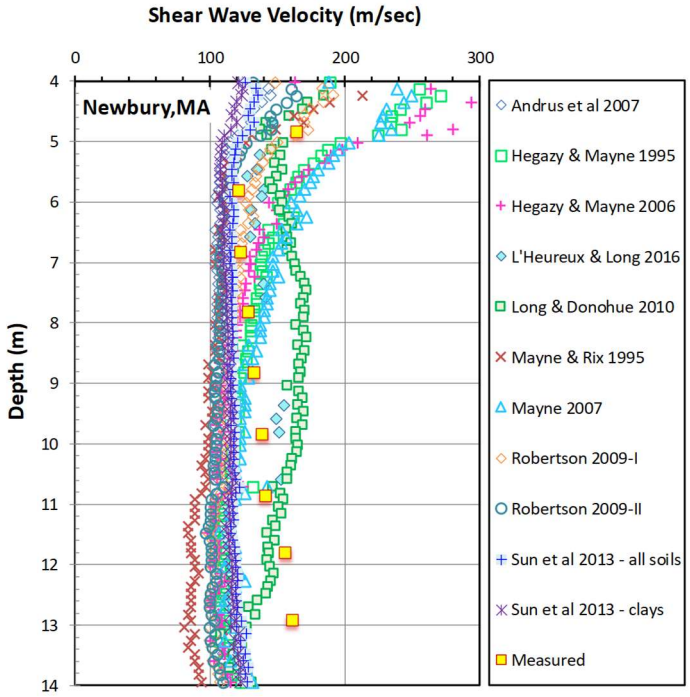


**Measured and predicted shear wave velocity profiles using different correlations for Newbury, MA**

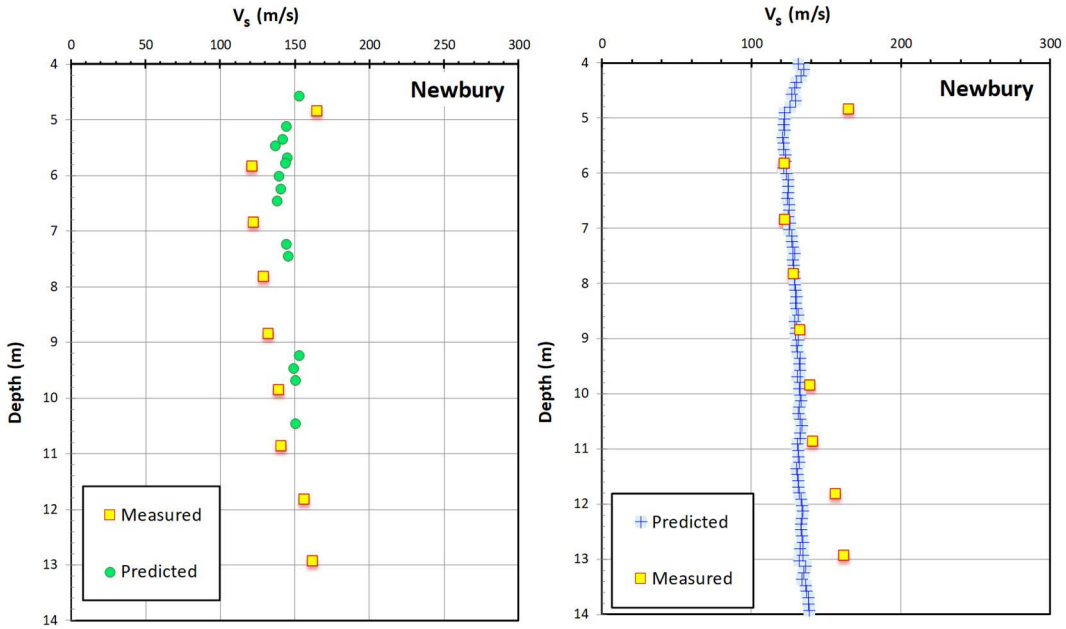


$$V_s = 75 \cdot (q_{net})^{0.1} \cdot \left(\frac{\sigma'_{vo}}{W_n}\right)^{0.2}$$

$$V_s = 16 \cdot \frac{(q_t)^{0.16}}{(f_s)^{0.015}} \cdot \frac{(\sigma'_{vo})^{0.255}}{(1+B_q)^{0.02}}$$

**Measured and predicted shear wave velocity profiles using the two proposed correlations for Newbury, MA**

## Pier Park, Richmond, BC

Data after Christian et al. (1998)

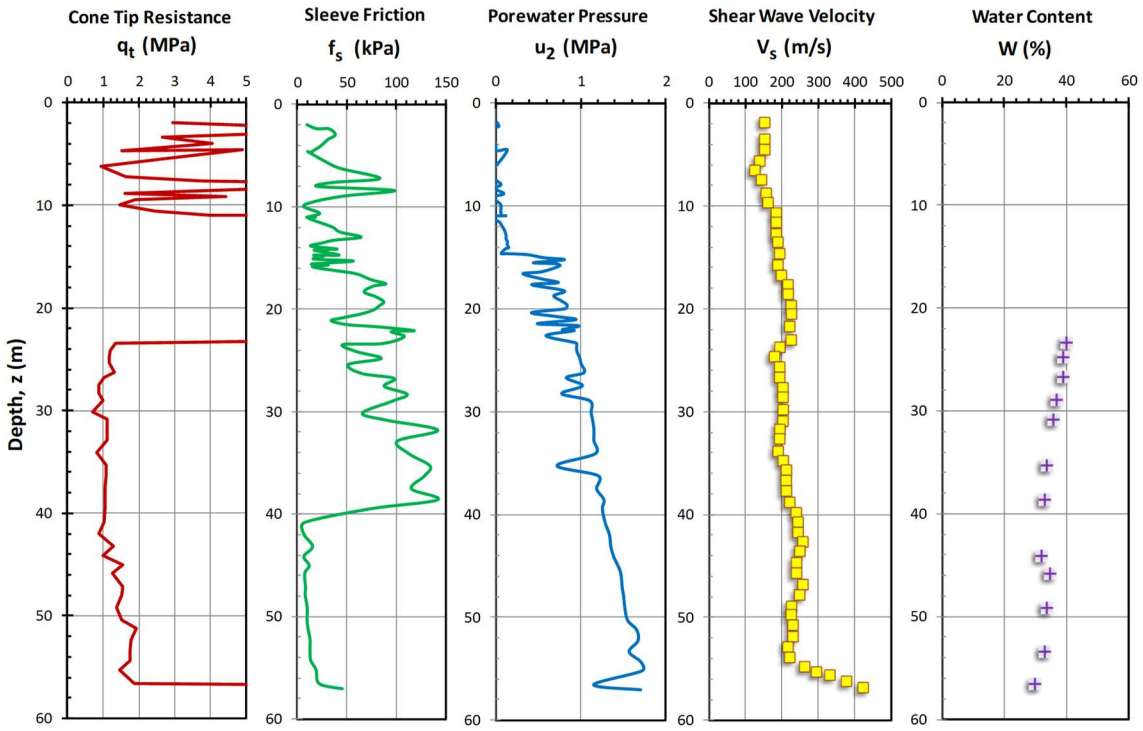

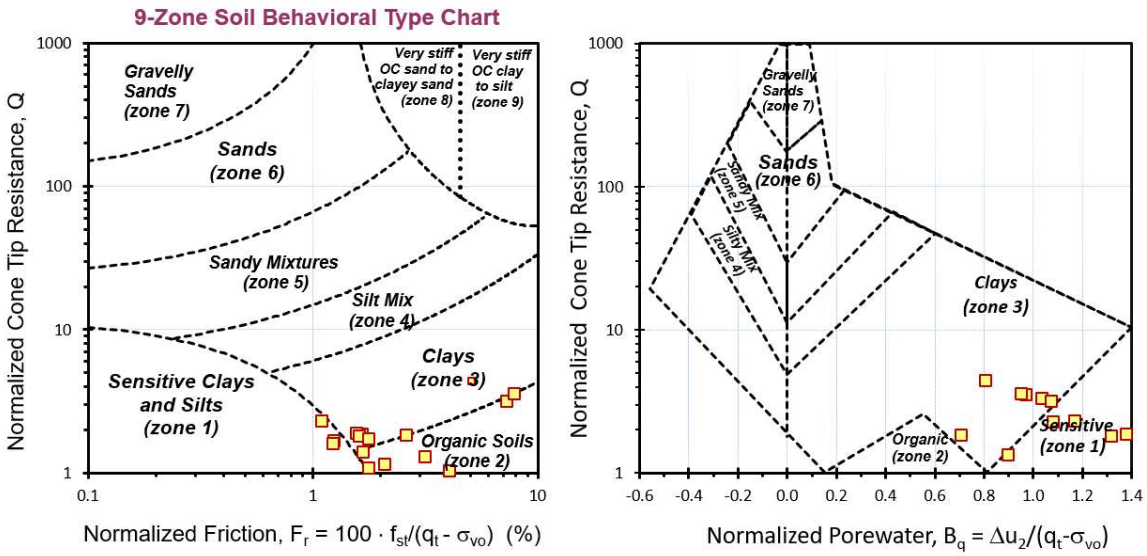


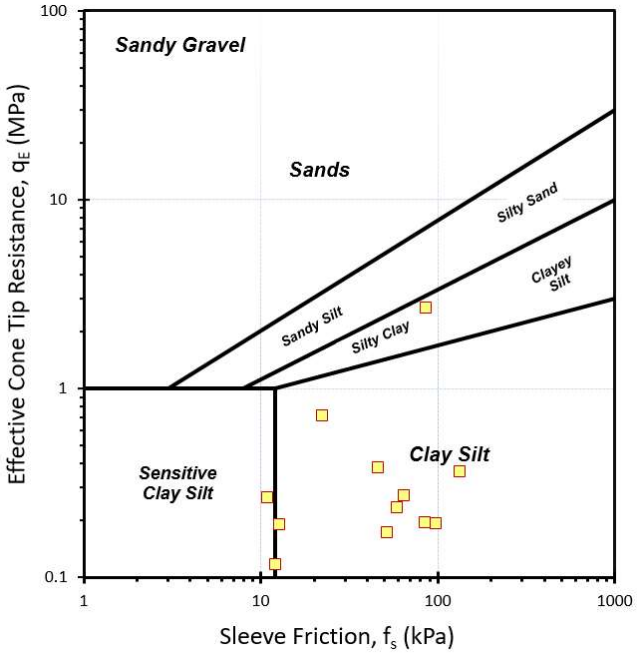


**CPT soil classification using 9-zone Robertson SBT and Fellenius and Eslami soil profiling charts for Pier Park, Richmond, BC**

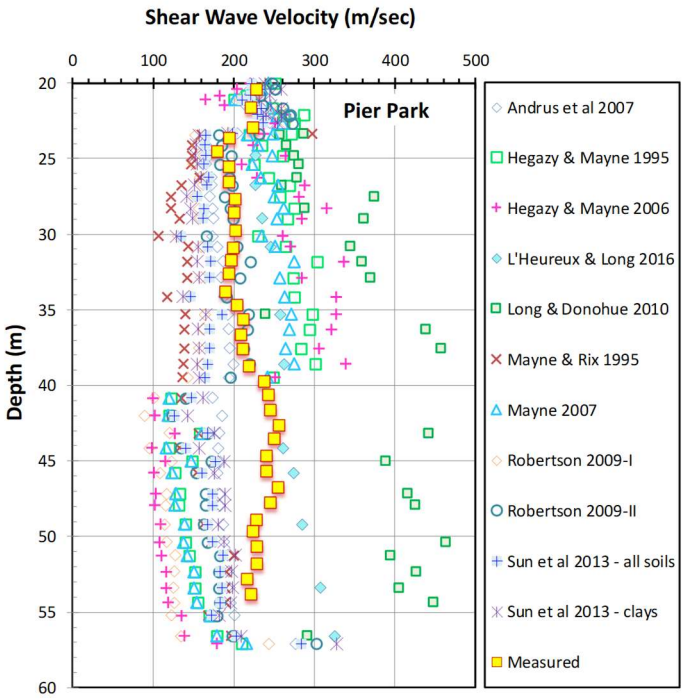


**Measured and predicted shear wave velocity profiles using different correlations for Pier Park, Richmond, BC**

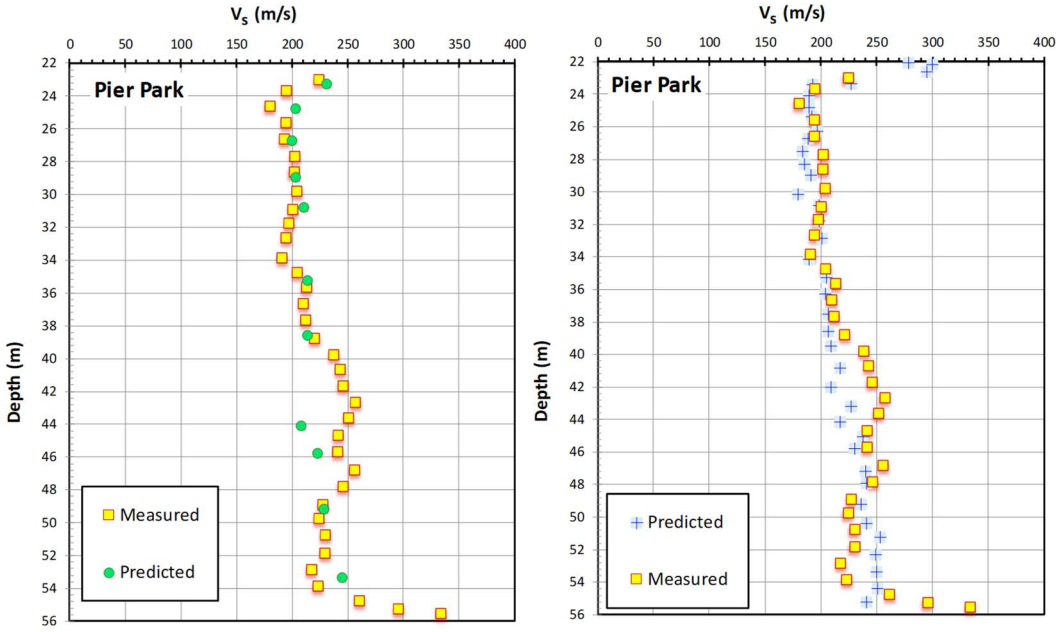


$$V_s = 75 \cdot (q_{net})^{0.1} \cdot \left(\frac{\sigma'_{vo}}{W_n}\right)^{0.2}$$

$$V_s = 16 \cdot \frac{(q_t)^{0.16}}{(f_s)^{0.015}} \cdot \frac{(\sigma'_{vo})^{0.255}}{(1 + B_q)^{0.02}}$$

**Measured and predicted shear wave velocity profiles using the two proposed correlations for Pier Park, Richmond, BC**

## Quyon, Québec

Data after Wang et al. (2015)

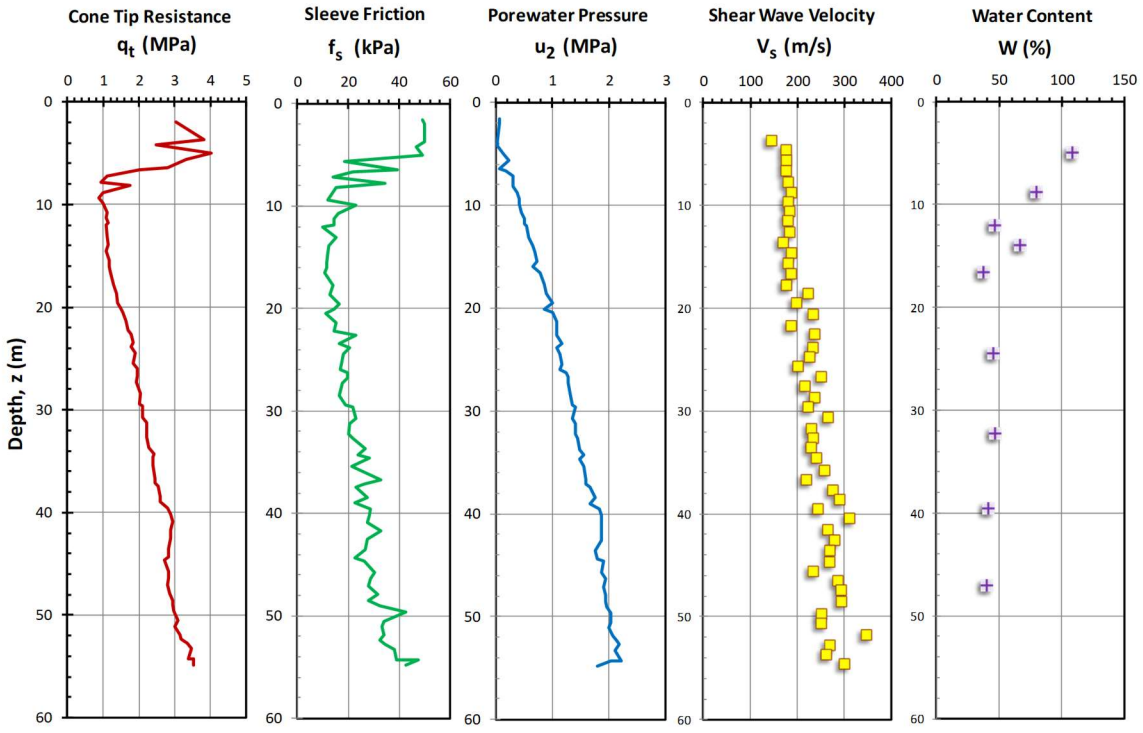

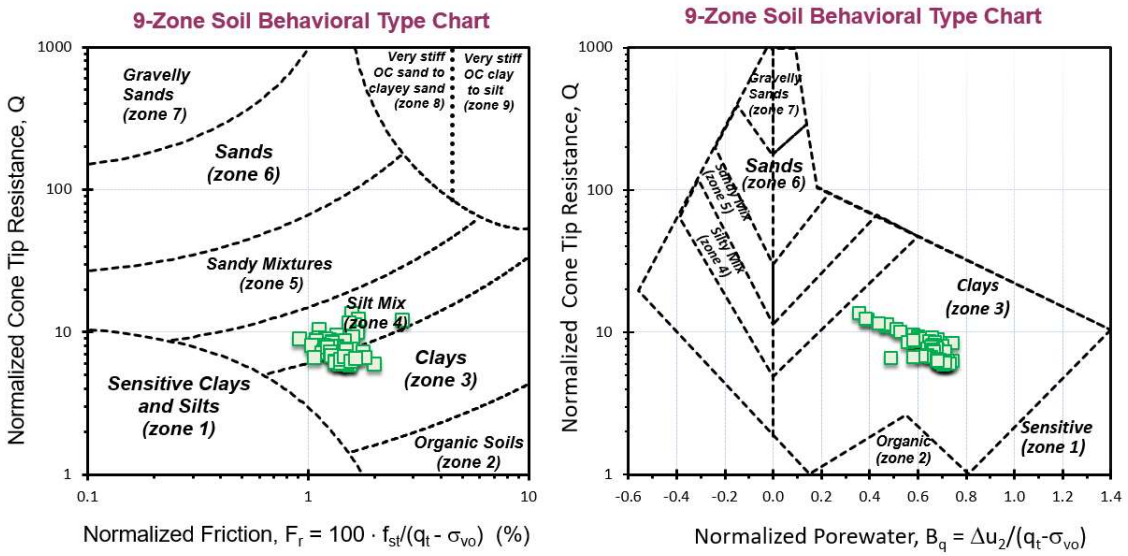


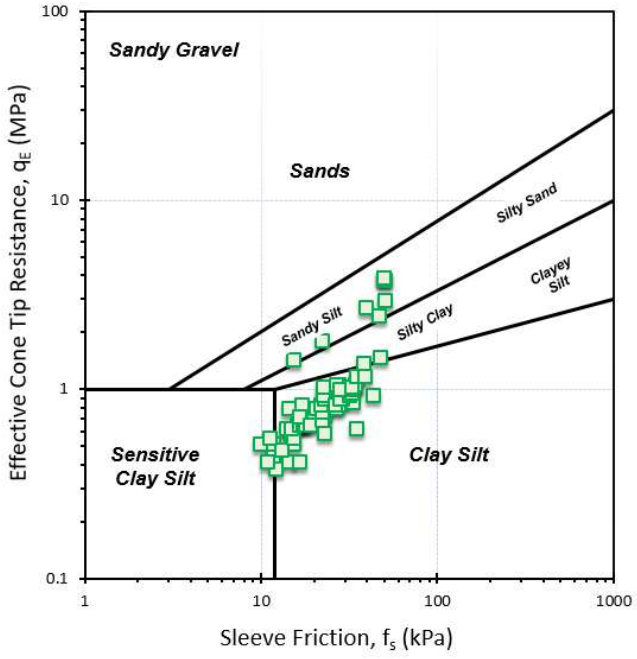


**CPT soil classification using 9-zone Robertson SBT and Fellenius and Eslami soil profiling charts for Quyon, Québec**

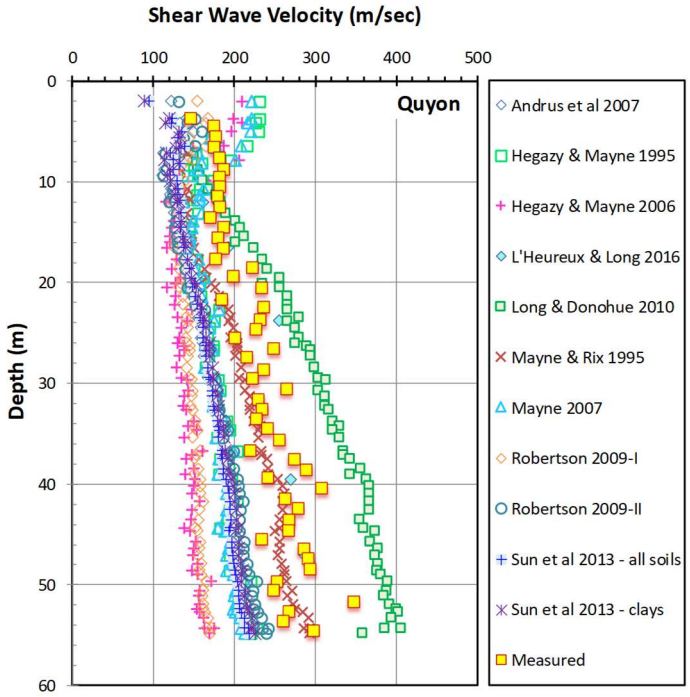


**Measured and predicted shear wave velocity profiles using different correlations for Quyon, Québec**

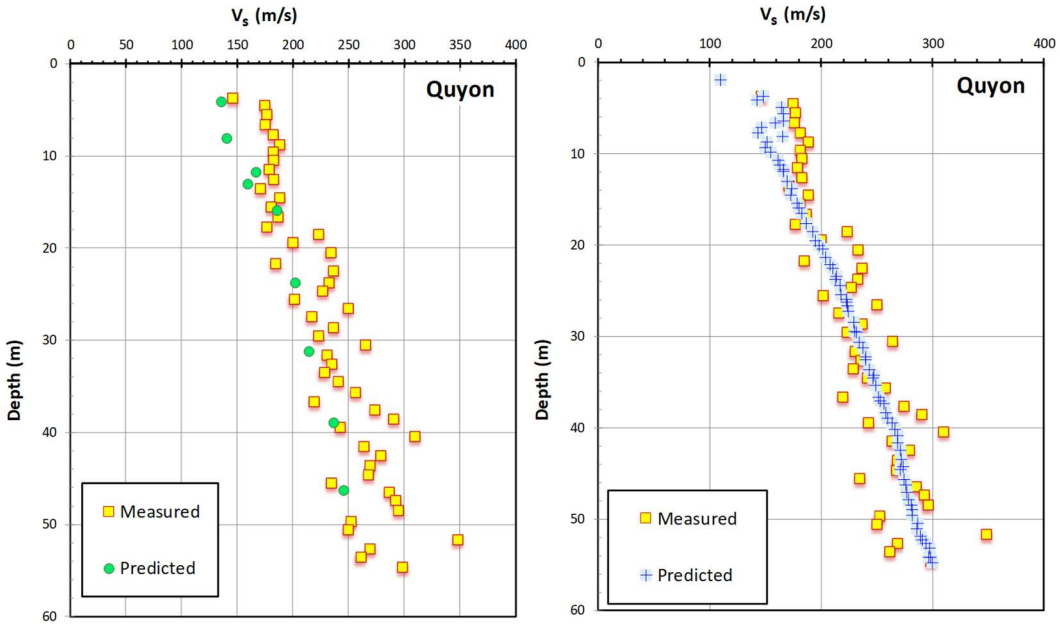


$$V_s = 75 \cdot (q_{net})^{0.1} \cdot \left(\frac{\sigma'_{vo}}{W_n}\right)^{0.2}$$

$$V_s = 16 \cdot \frac{(q_t)^{0.16}}{(f_s)^{0.015}} \cdot \frac{(\sigma'_{vo})^{0.255}}{(1+B_q)^{0.02}}$$

**Measured and predicted shear wave velocity profiles using the two proposed correlations for Quyon, Québec**

## Route 197 Bridge, Maine

Data after Hardison (2015)

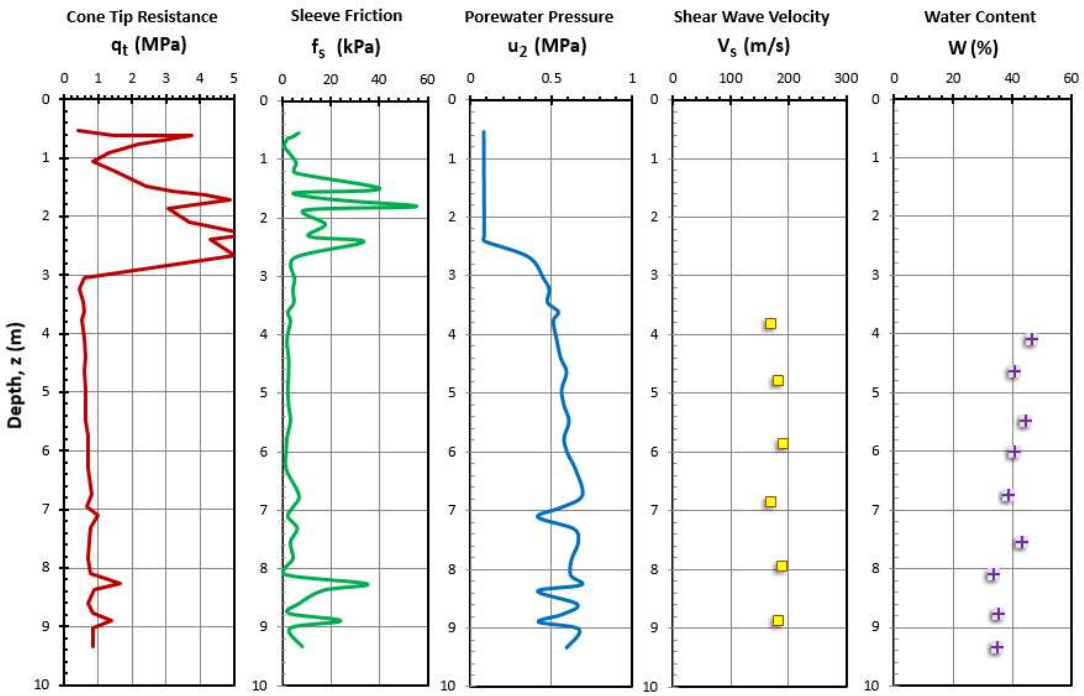

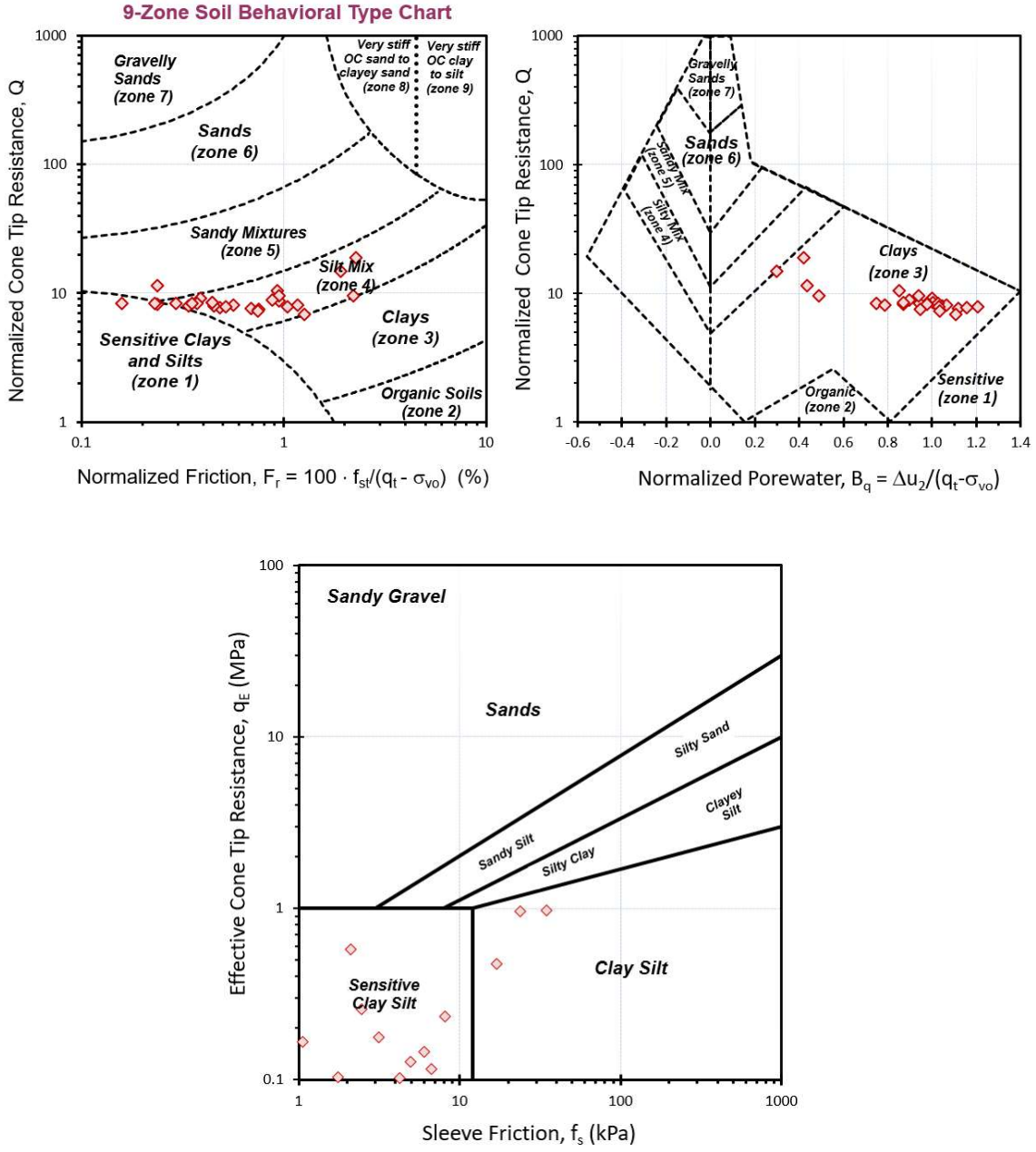


**CPT soil classification using 9-zone Robertson SBT and Fellenius and Eslami soil profiling charts for Route 197 Bridge, Maine**

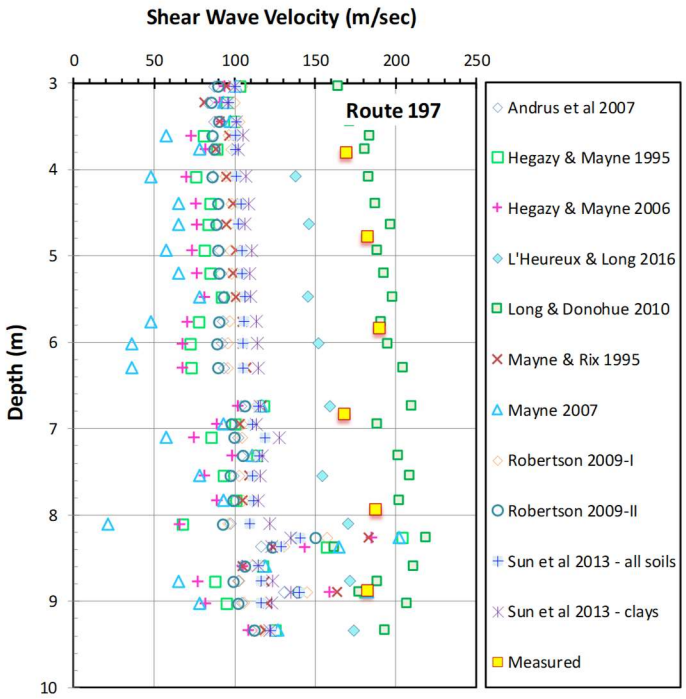


**Measured and predicted shear wave velocity profiles using different correlations for Route 197 Bridge, Maine**

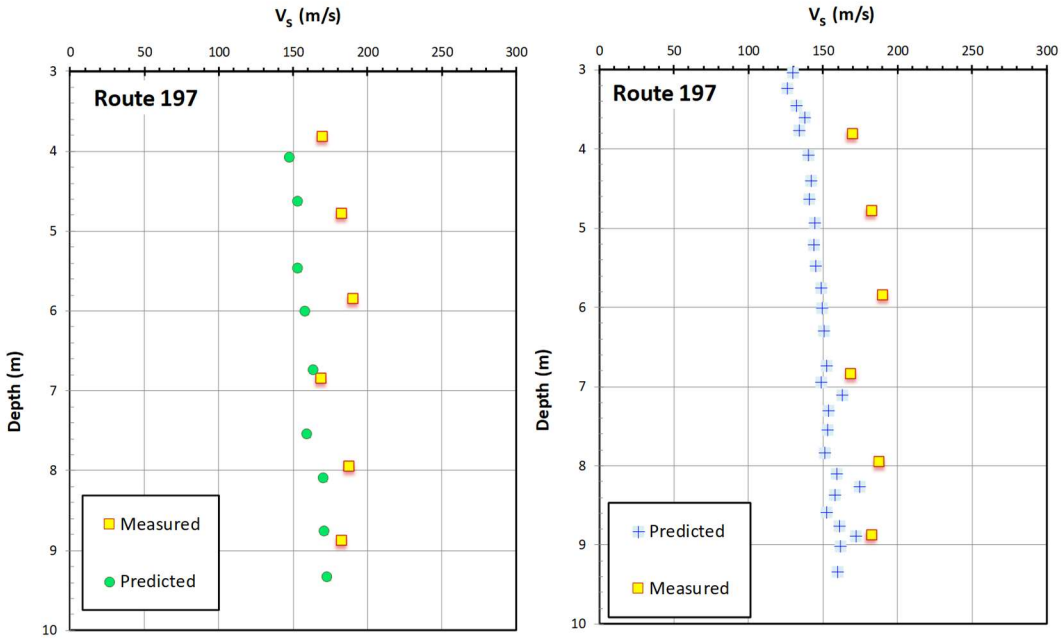


$$V_s = 75 \cdot (q_{net})^{0.1} \cdot \left(\frac{\sigma'_{vo}}{W_n}\right)^{0.2}$$

$$V_s = 16 \cdot \frac{(q_t)^{0.16}}{(f_s)^{0.015}} \cdot \frac{(\sigma'_{vo})^{0.255}}{(1 + B_q)^{0.02}}$$

**Measured and predicted shear wave velocity profiles using the two proposed correlations for Route 197 Bridge, Maine**

## Route 26 / 100, Falmouth Bridge, Maine

Data after Hardison (2015)

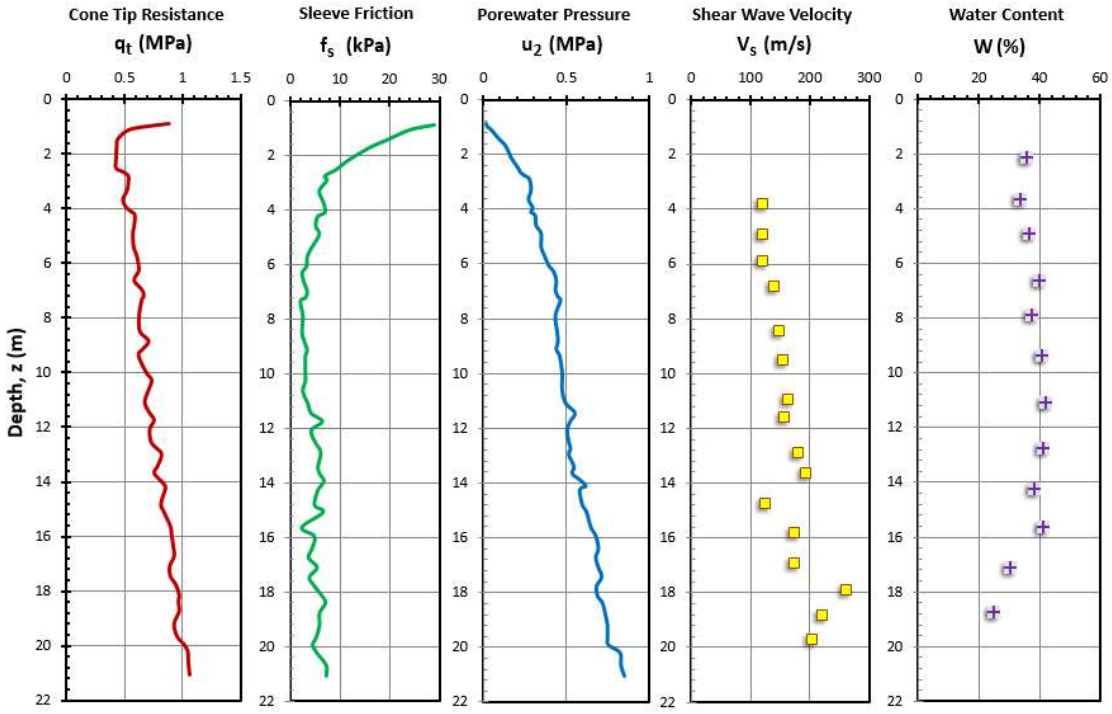

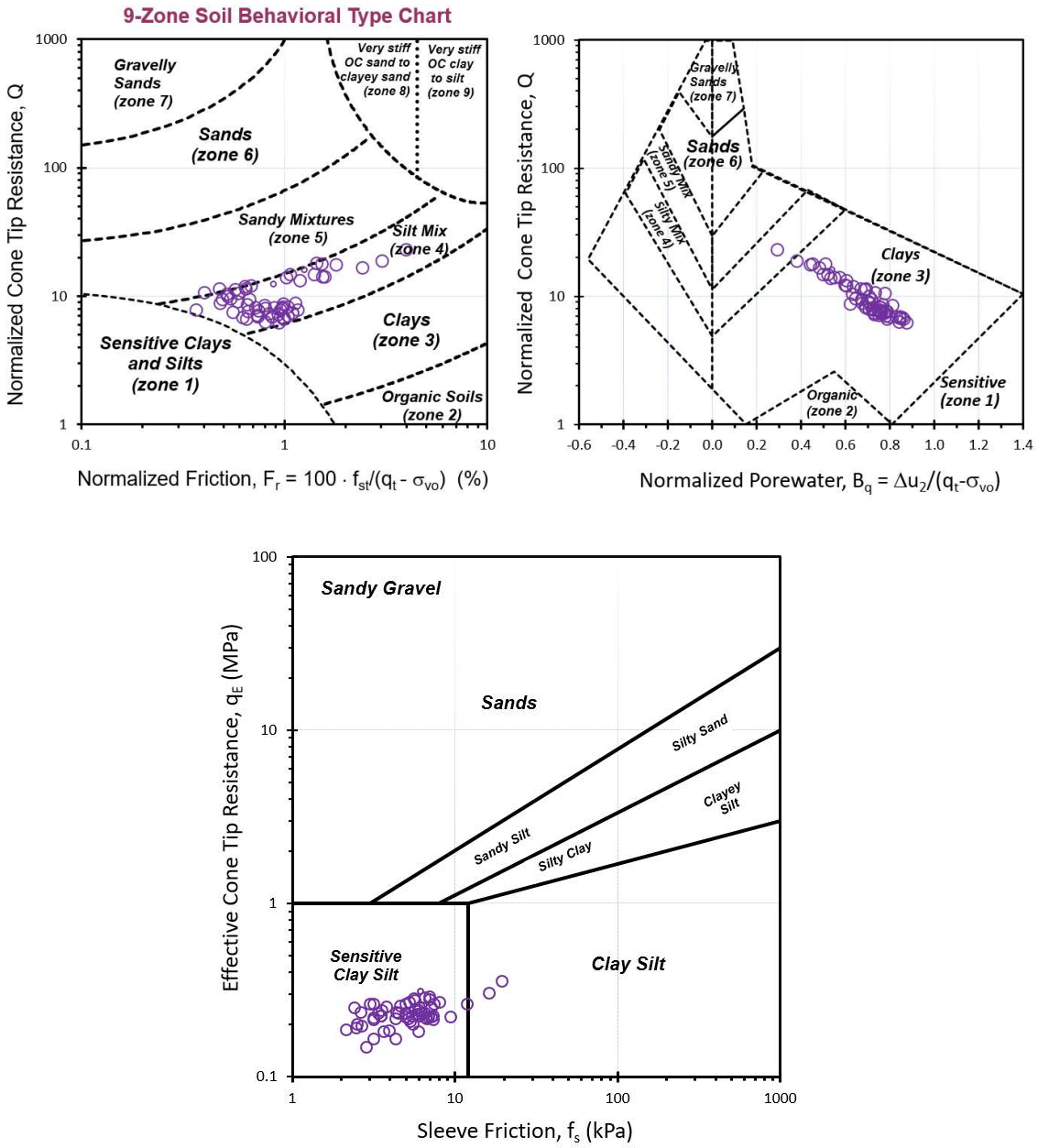


**CPT soil classification using 9-zone Robertson SBT and Fellenius and Eslami soil profiling charts for Route 26 / 100, Falmouth Bridge, Maine**

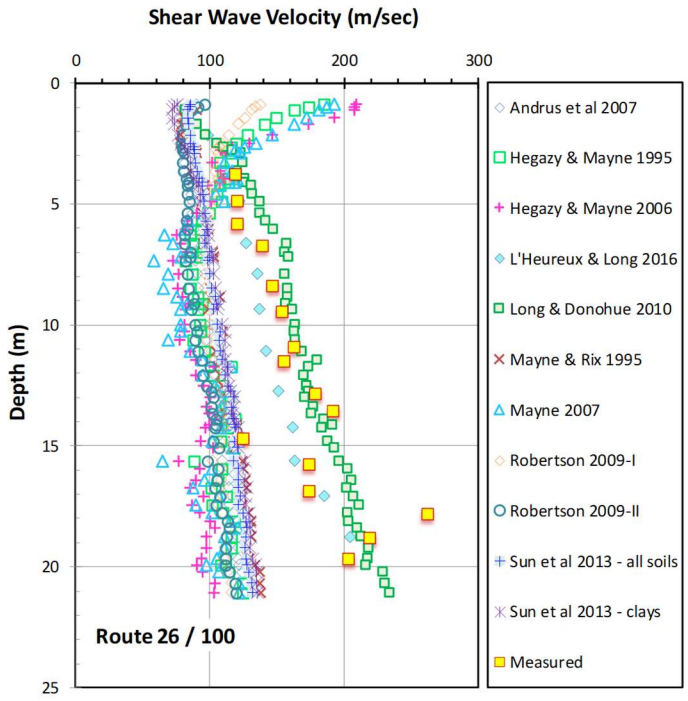


**Measured and predicted shear wave velocity profiles using different correlations for Route 26 / 100, Falmouth Bridge, Maine**

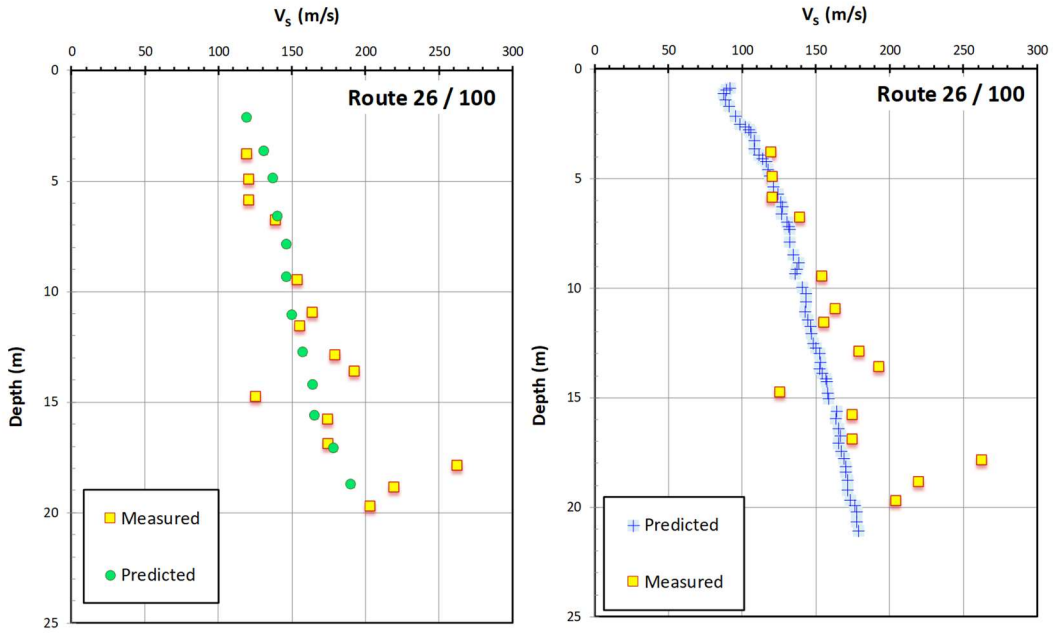


$$V_s = 75 \cdot (q_{net})^{0.1} \cdot \left(\frac{\sigma'_{vo}}{W_n}\right)^{0.2}$$

$$V_s = 16 \cdot \frac{(q_t)^{0.16}}{(f_s)^{0.015}} \cdot \frac{(\sigma'_{vo})^{0.255}}{(1+B_q)^{0.02}}$$

**Measured and predicted shear wave velocity profiles using the two proposed correlations for Route 26 / 100, Falmouth Bridge, Maine**

## Sandpoint, Idaho

Data after Altaee & Fellenius (2002); Mayne (2005)

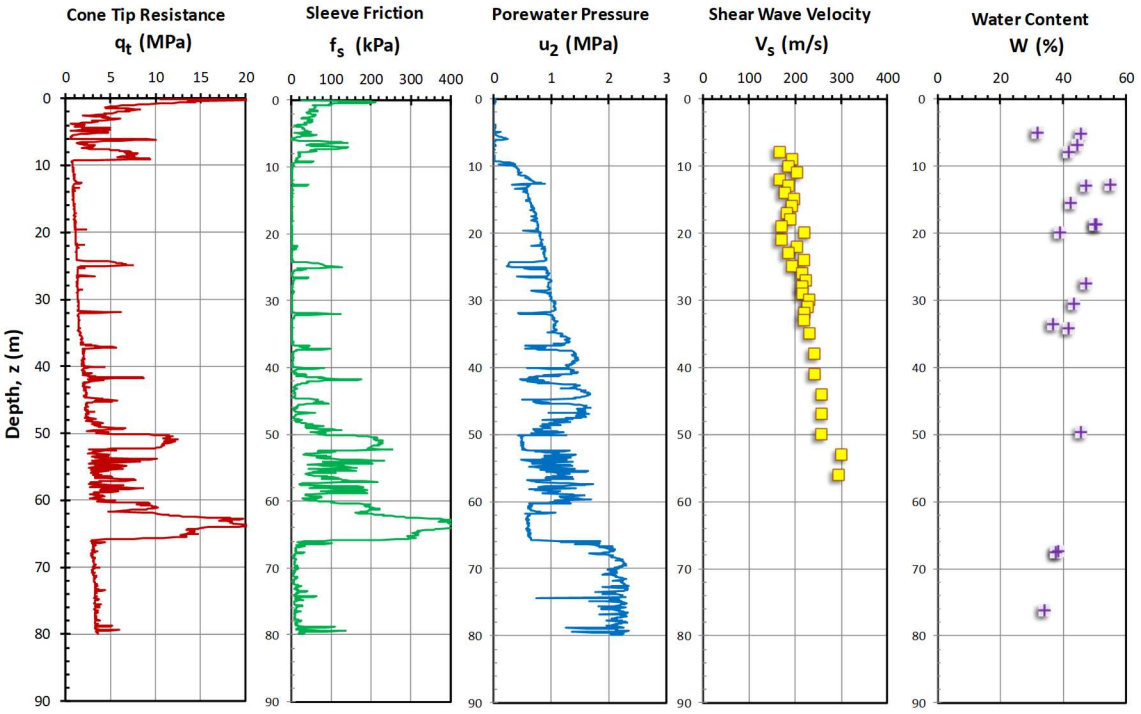

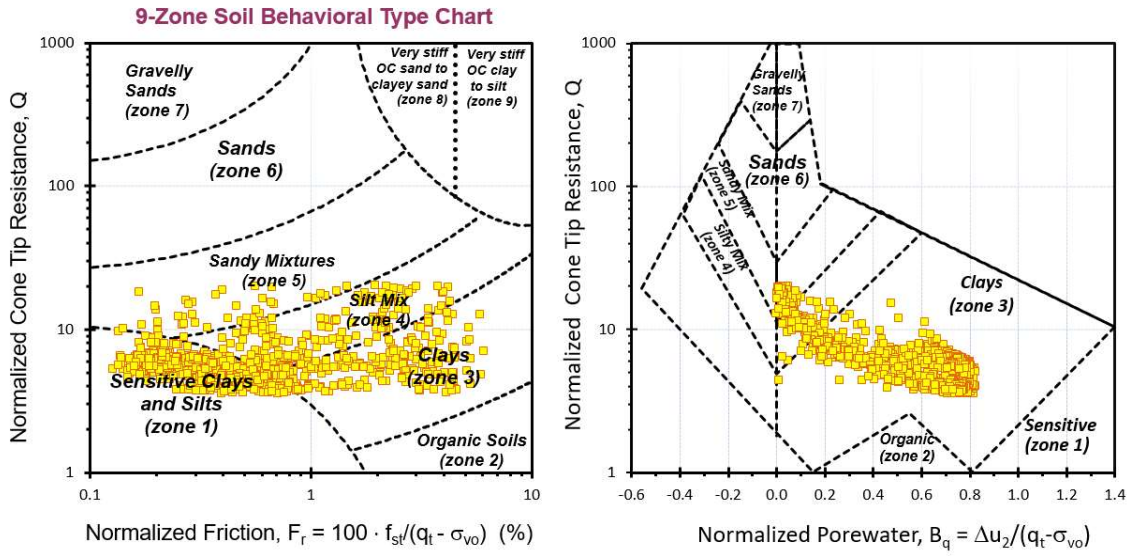


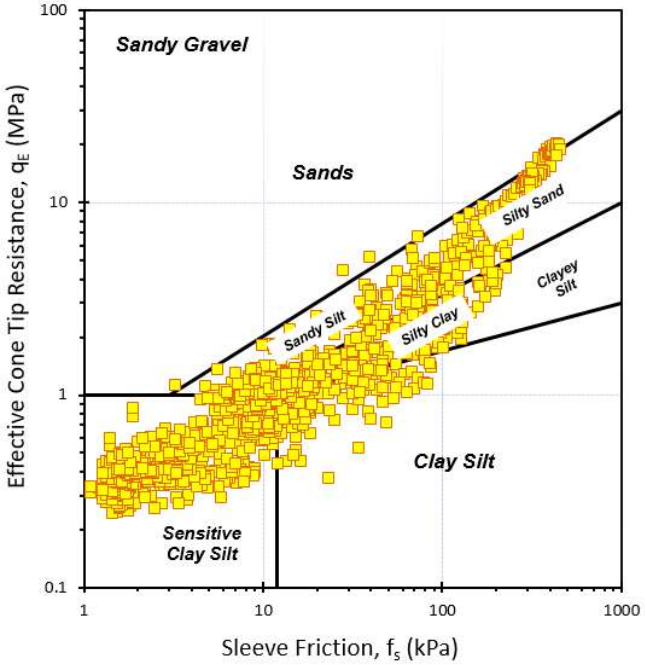


**CPT soil classification using 9-zone Robertson SBT and Fellenius and Eslami soil profiling charts for Sandpoint, Idaho**

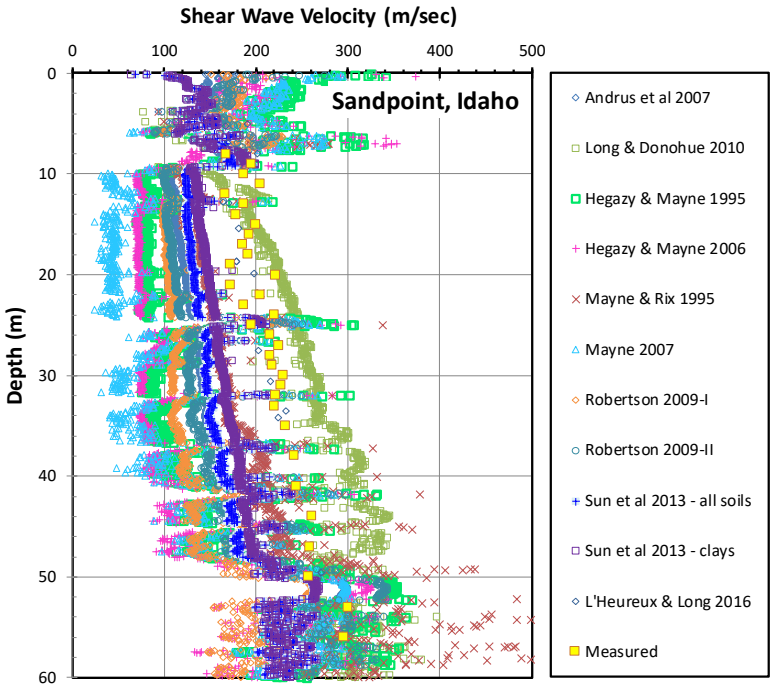


**Measured and predicted shear wave velocity profiles using different correlations for Sandpoint, Idaho**

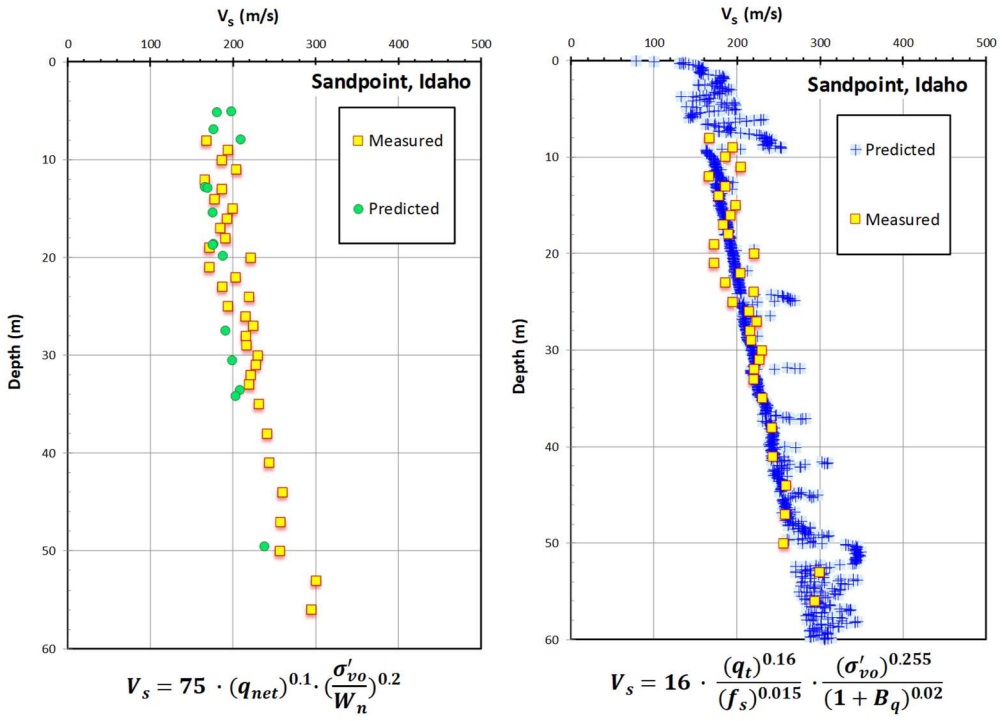


**Measured and predicted shear wave velocity profiles using the two proposed correlations for Sandpoint, Idaho**

## Saint Alban, Québec

Data after Lefebvre et al. (1994); Leroueil et al. (1995)

[1]

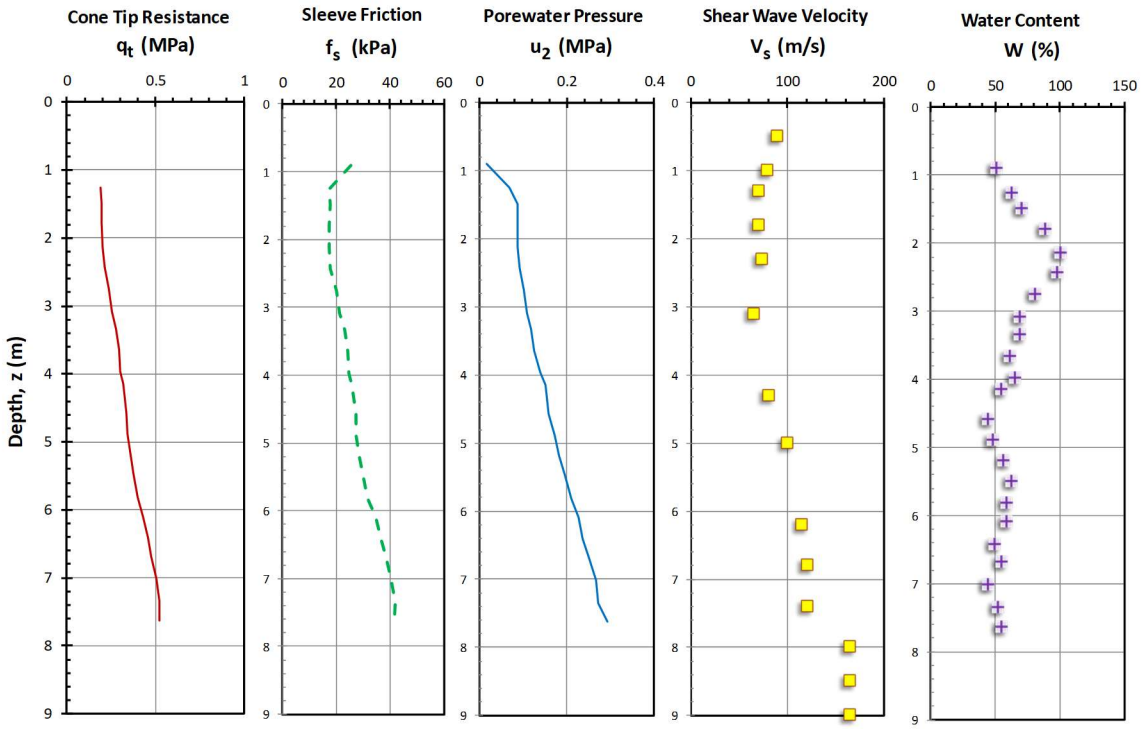


[1] Shear wave velocity is measured using spectral analyses of surface waves (SASW) and sleeve friction is measured using Laval piezocone with fs ≈ 0.1($q_t$–$\sigma_{v0}$) as per Leroueil et al. (1995).

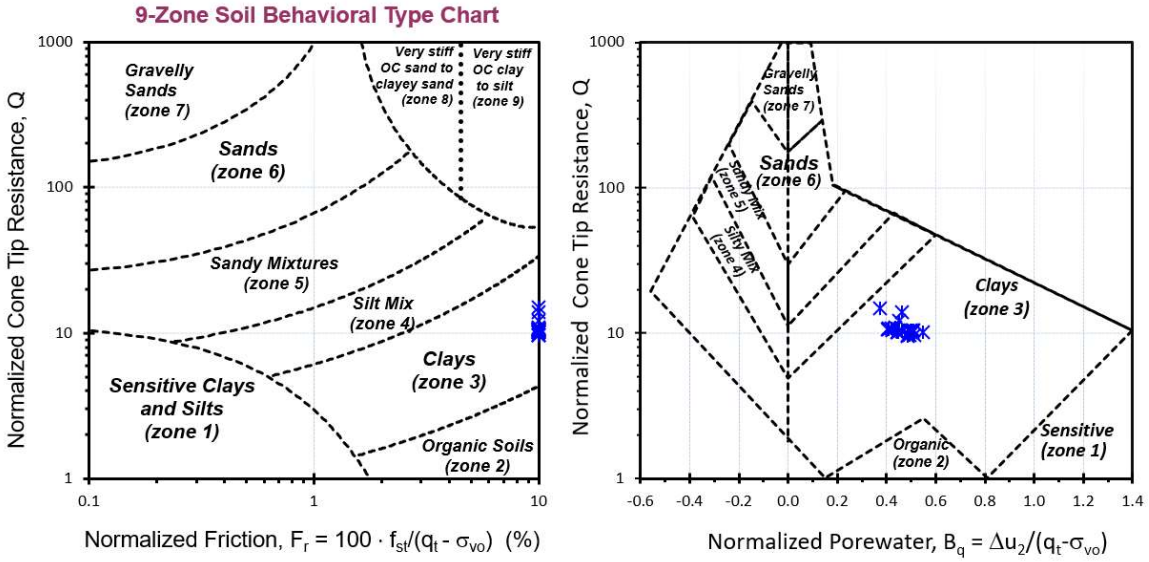


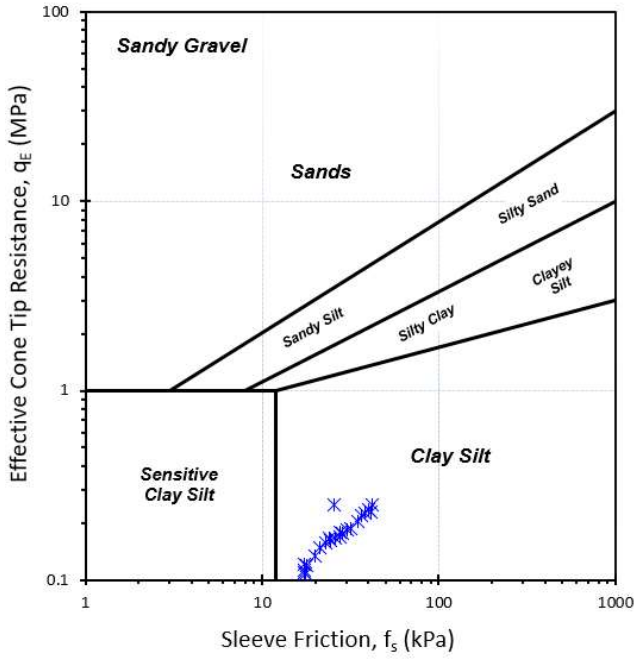


**CPT soil classification using 9-zone Robertson SBT and Fellenius and Eslami soil profiling charts for Saint Alban, Québec**

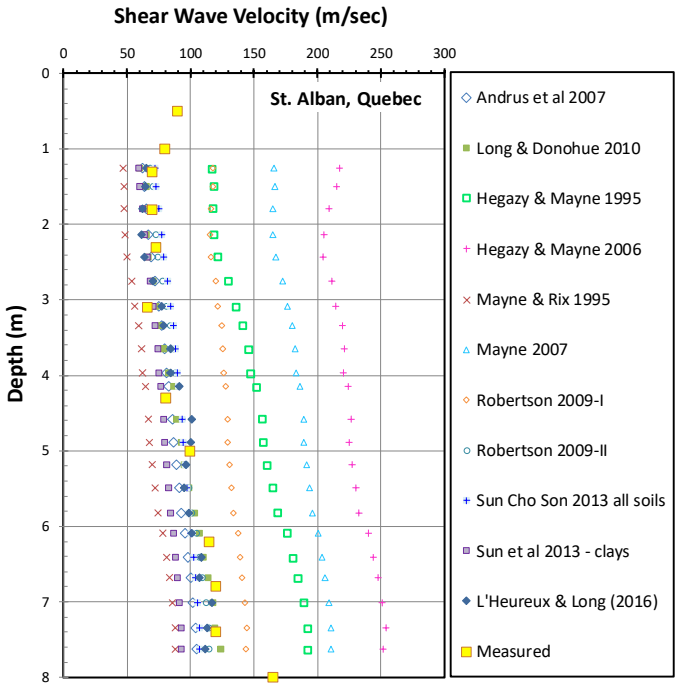


**Measured and predicted shear wave velocity profiles using different correlations for Saint Alban, Québec**

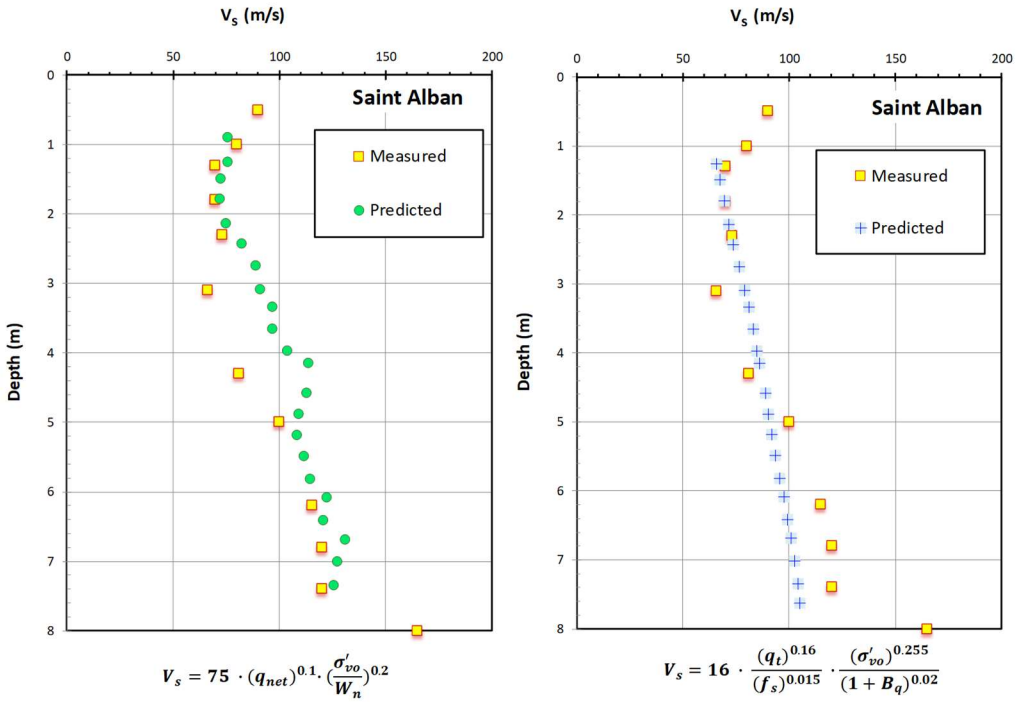


**Measured and predicted shear wave velocity profiles using the two proposed correlations for Saint Alban, Québec**

## Vancouver, BC

Data after Mayne & Woeller (2015)

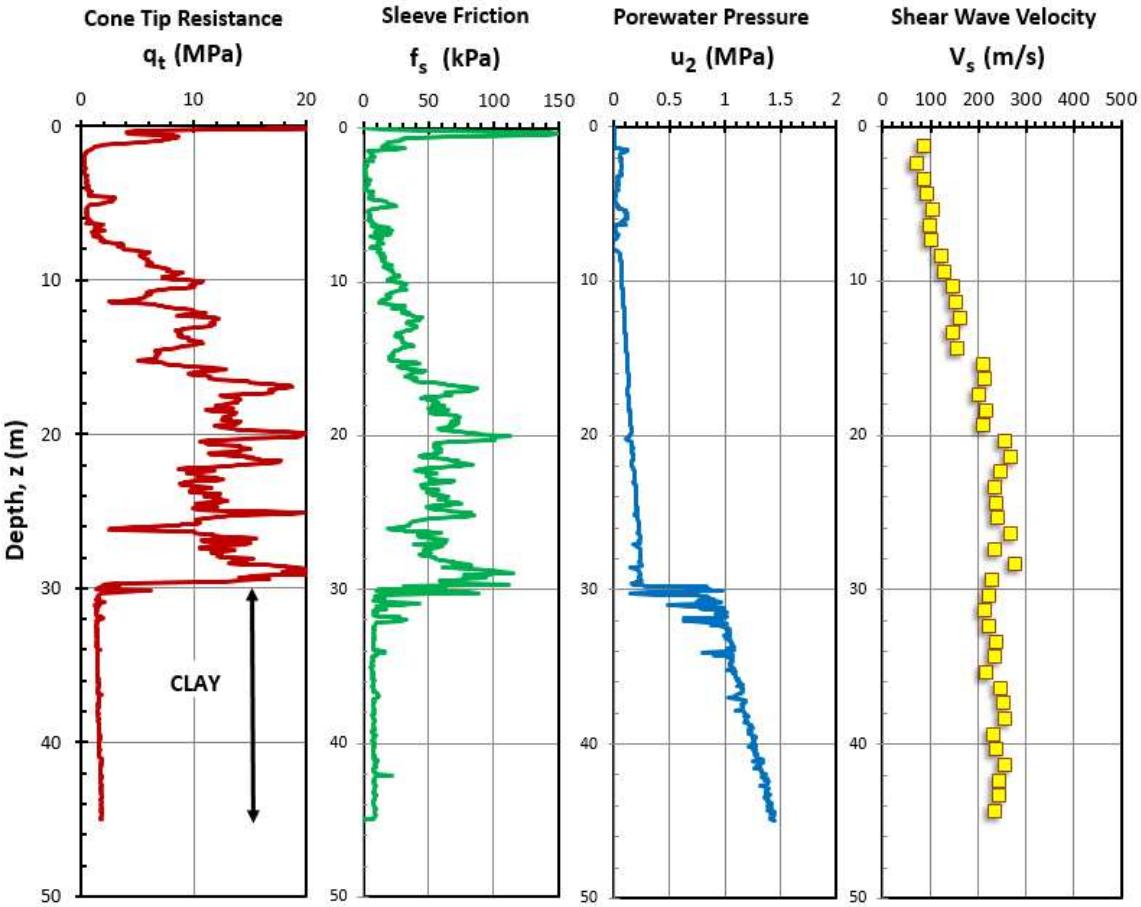

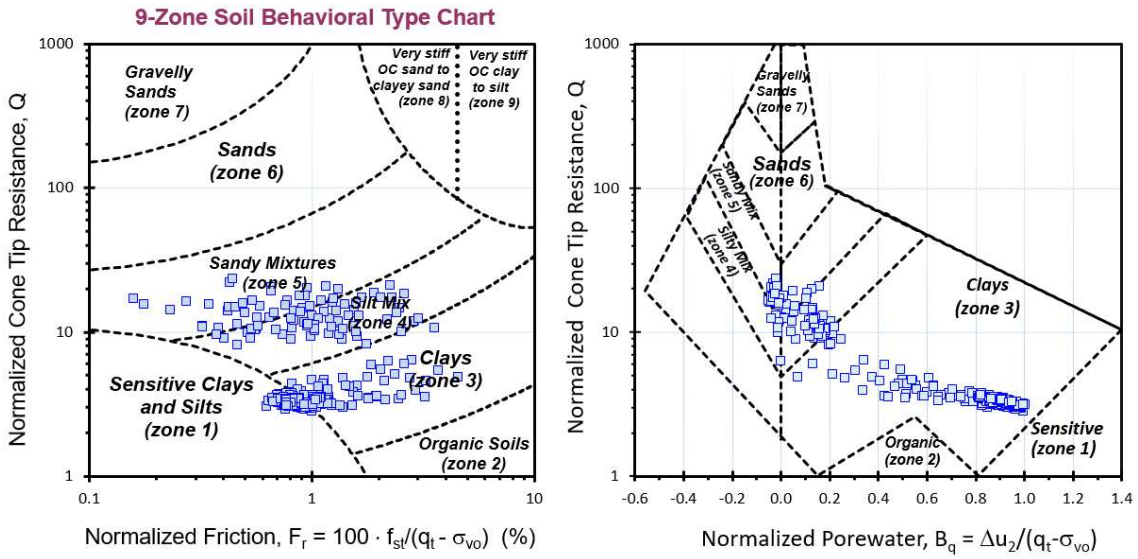


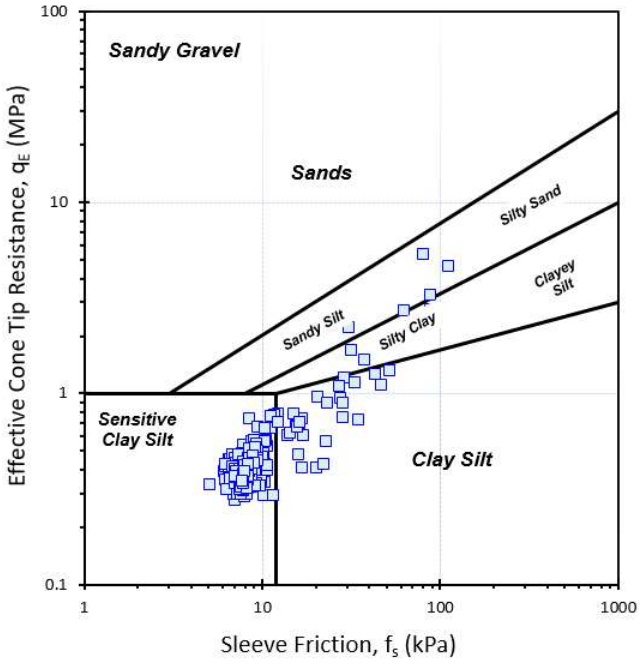


**CPT soil classification using 9-zone Robertson SBT and Fellenius and Eslami soil profiling charts for Vancouver, BC**

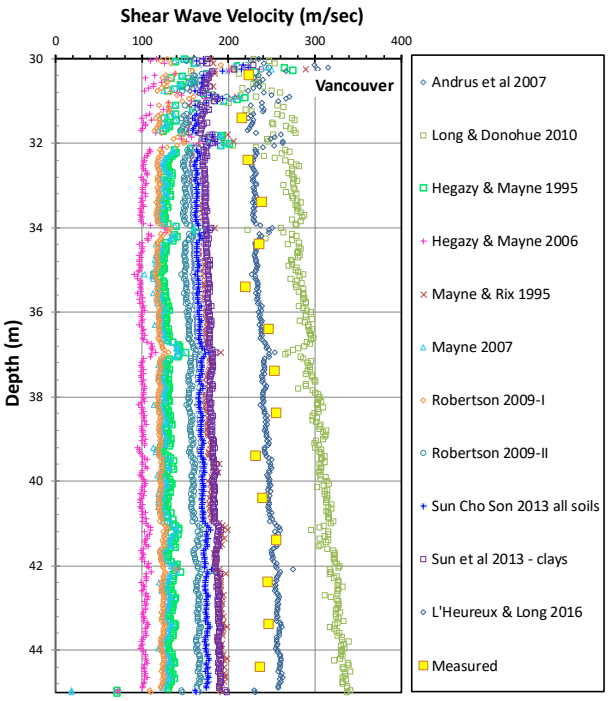


**Measured and predicted shear wave velocity profiles using different correlations for Vancouver, BC**

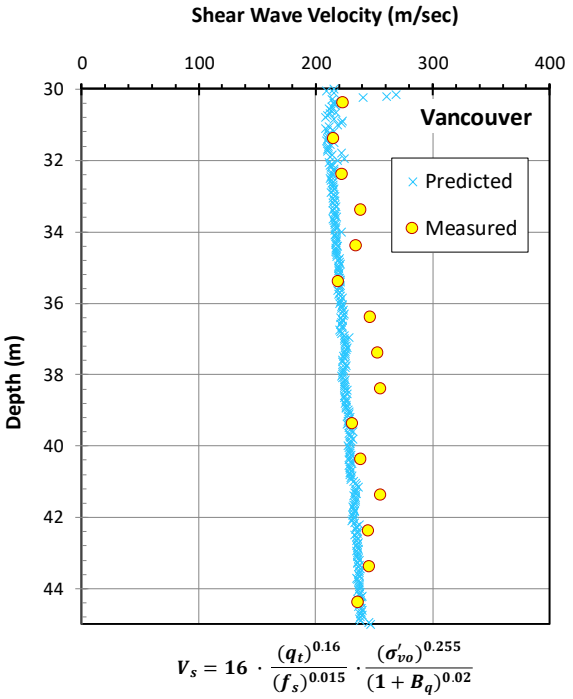


**Measured and predicted shear wave velocity profiles using the two proposed correlations for Vancouver, BC**

# APPENDIX H

# Additional Plots for Calibration of Analytical Model for Estimating Undrained Shear Strength in Clays

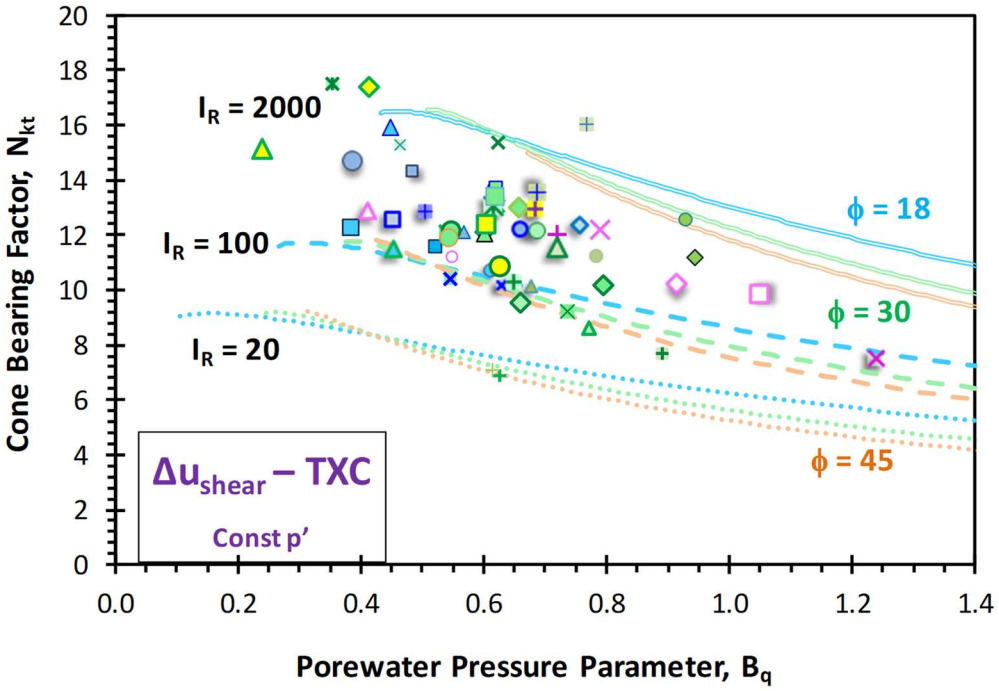


Figure H.1. Cone bearing factors ($N_{kt}$) versus $B_q$ using shear-induced excess porewater pressures from constant p' triaxial compression test and parametric ranges of effective friction angle and rigidity index

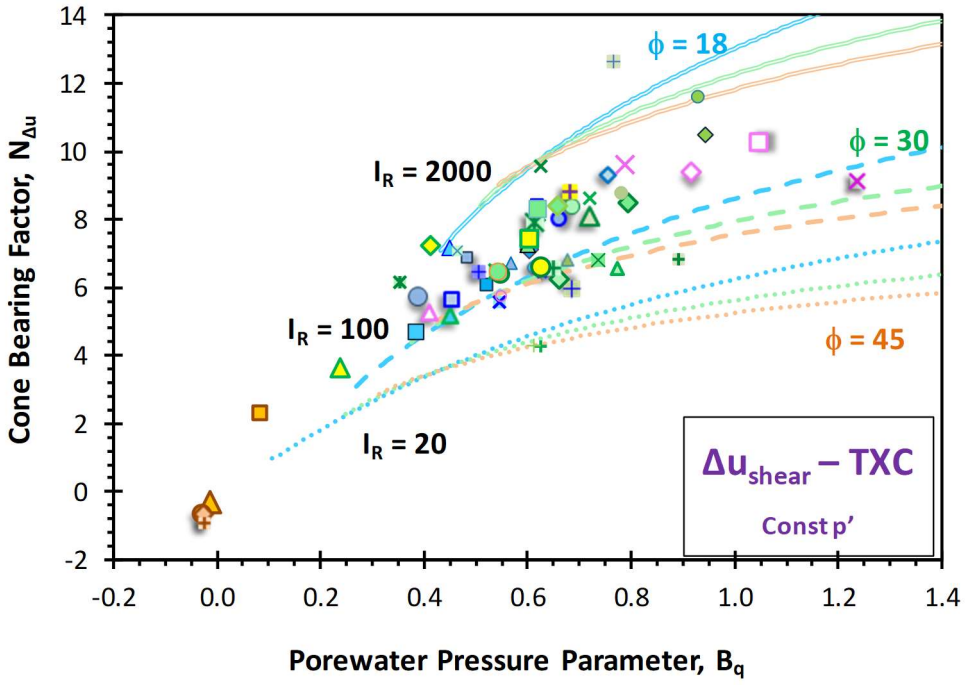


Figure H.2. Cone bearing factors ($N_{Du}$) versus $B_q$ using shear-induced excess porewater pressures from constant p' triaxial compression test and parametric ranges of effective friction angle and rigidity index

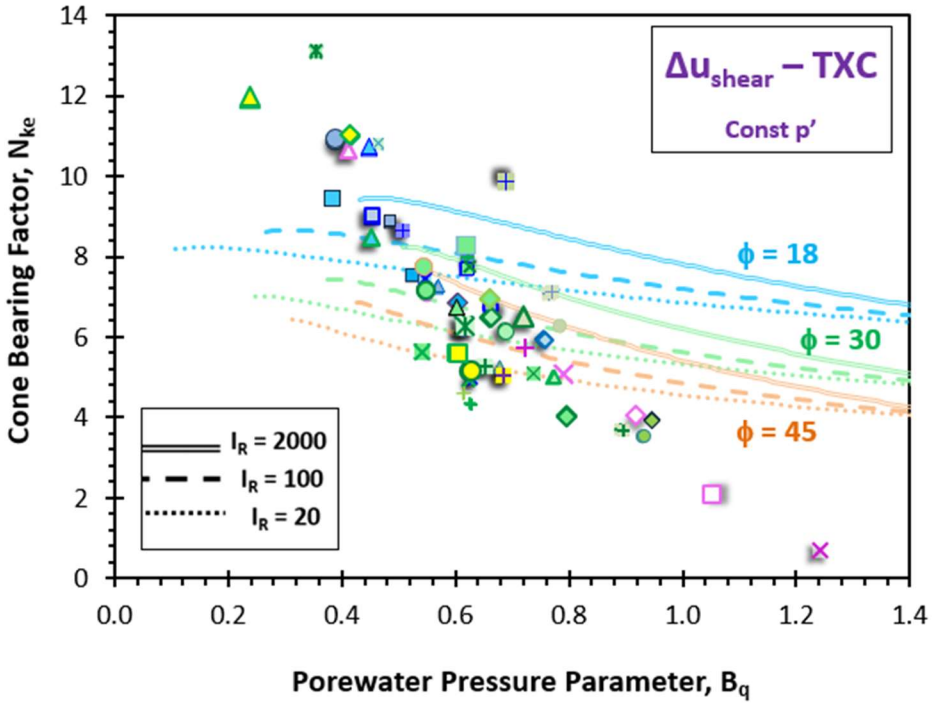


Figure H.3. Cone bearing factors ($N_{ke}$) versus $B_q$ using shear-induced excess porewater pressures from constant p' triaxial compression test and parametric ranges of effective friction angle and rigidity index

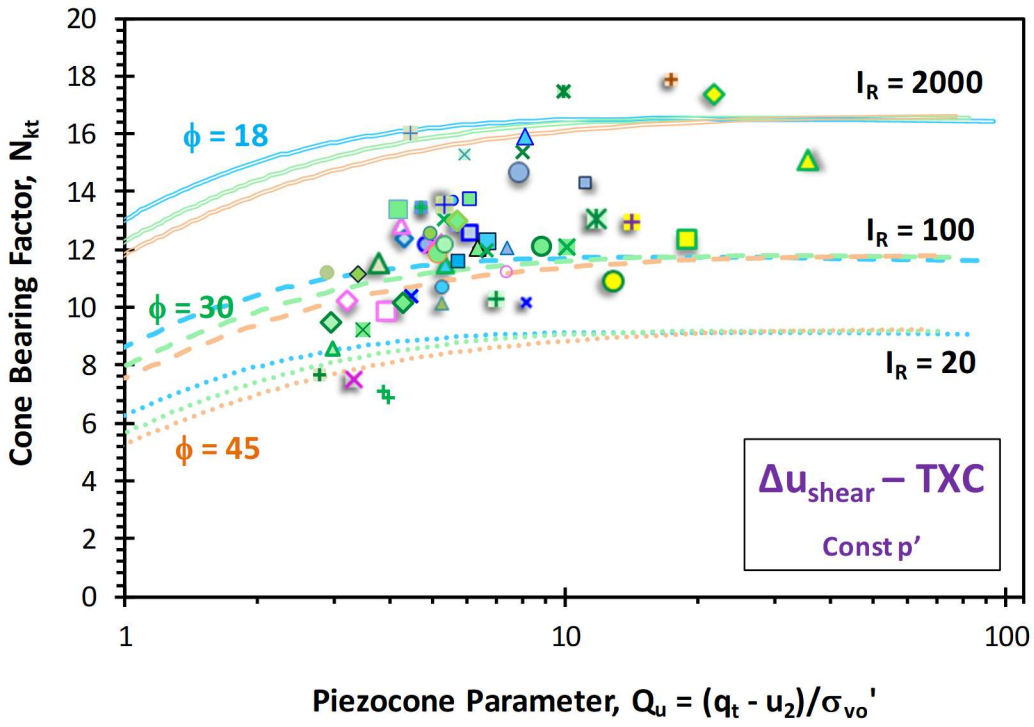


Figure H.4. Cone bearing factors ($N_{kt}$) versus $Q_u$ using shear-induced excess porewater pressures from constant p' triaxial compression test and parametric ranges of effective friction angle and rigidity index

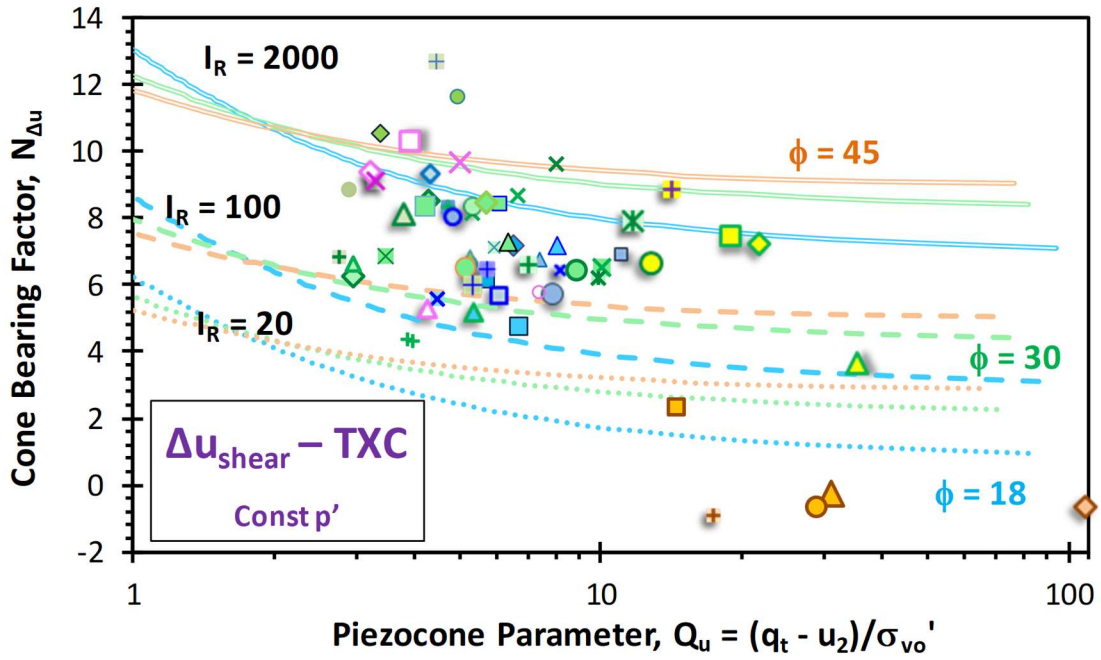


Figure H.5. Cone bearing factors ($N_{Du}$) versus $Q_u$ using shear-induced excess porewater pressures from constant p' triaxial compression test and parametric ranges of effective friction angle and rigidity index

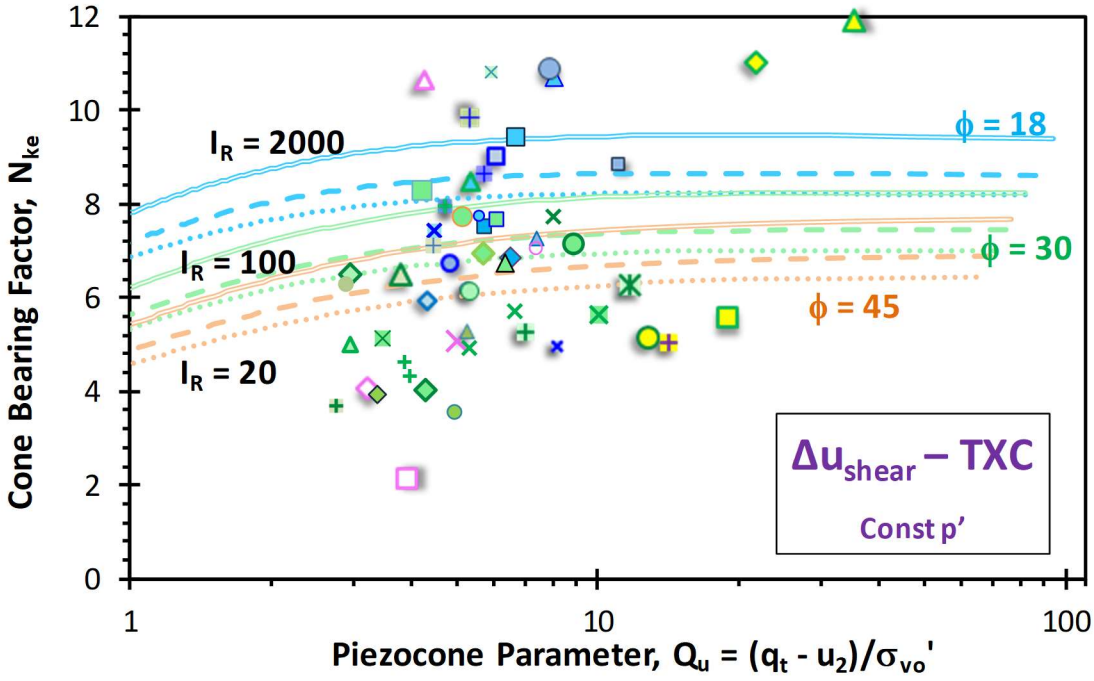


Figure H.6. Cone bearing factors ($N_{ke}$) versus $Q_u$ using shear-induced excess porewater pressures from constant p' triaxial compression test and parametric ranges of effective friction angle and rigidity index

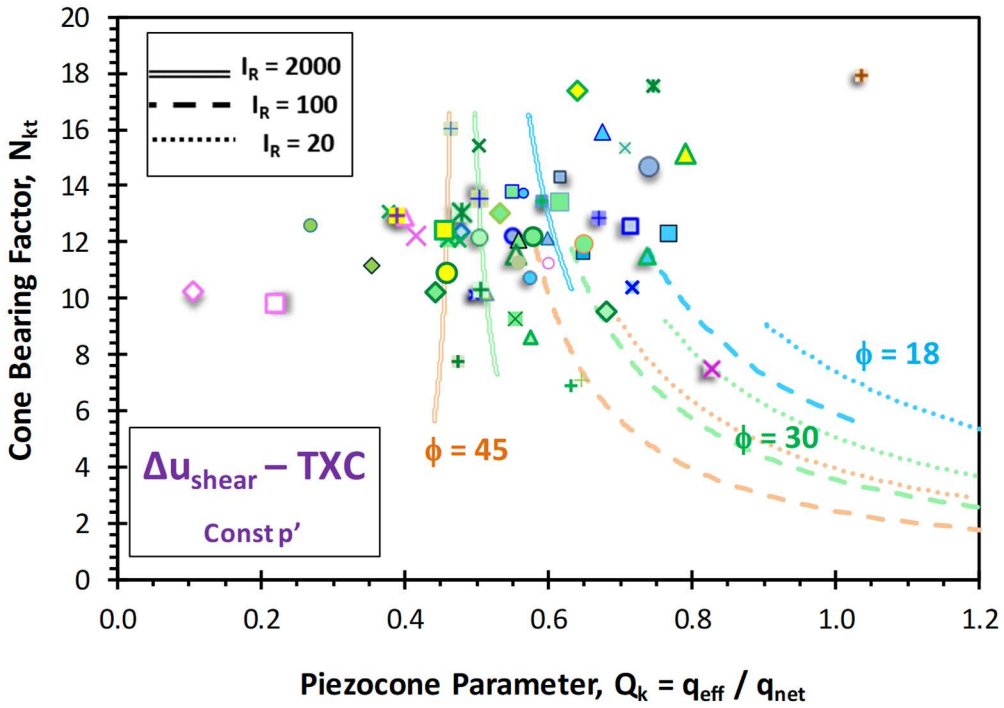

Figure H.7. Cone bearing factors ($N_{kt}$) versus $Q_k$ using shear-induced excess porewater pressures from constant p' triaxial compression test and parametric ranges of effective friction angle and rigidity index

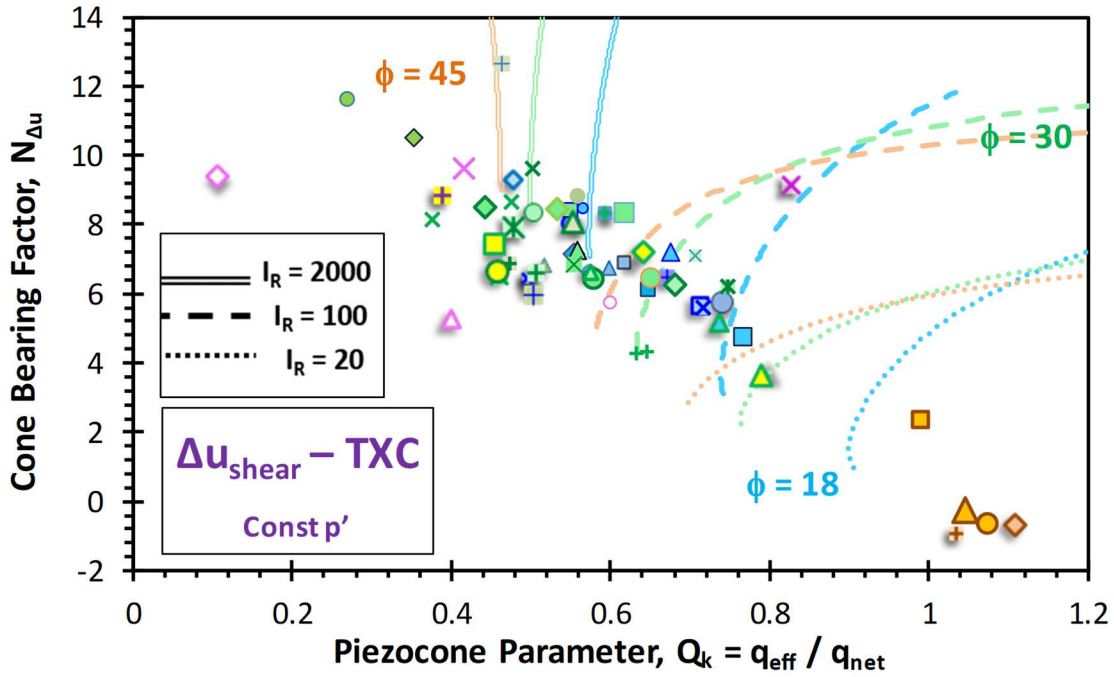


Figure H.8. Cone bearing factors ($N_{Du}$) versus $Q_k$ using shear-induced excess porewater pressures from constant p' triaxial compression test and parametric ranges of effective friction angle and rigidity index

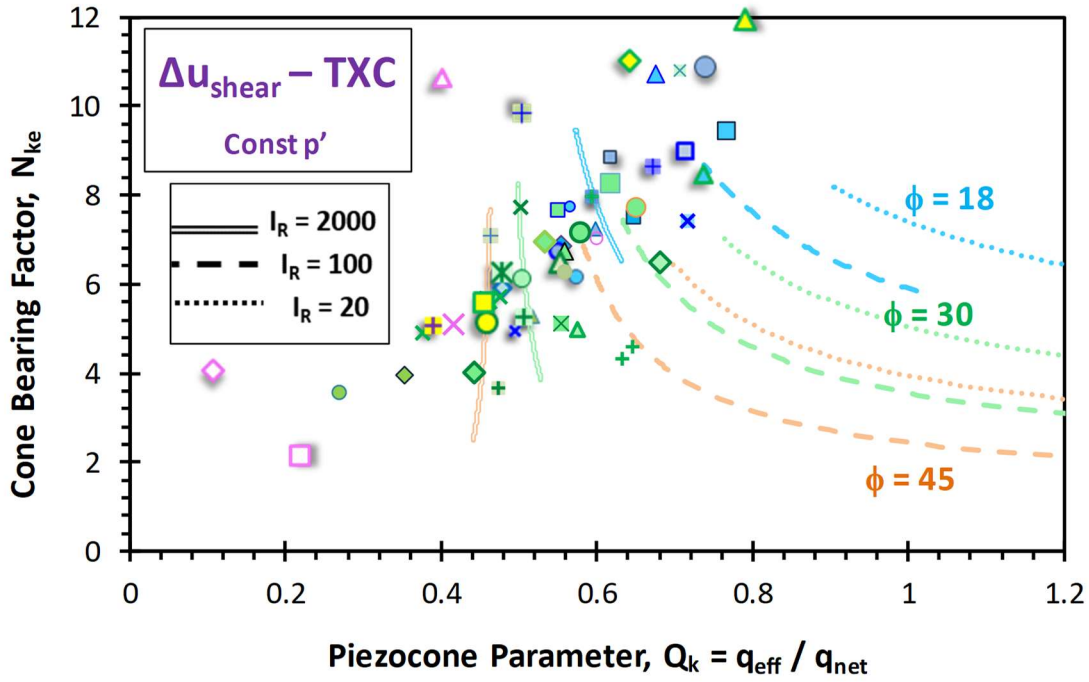

Figure H.9. Cone bearing factors ($N_{ke}$) versus $Q_k$ using shear-induced excess porewater pressures from constant p' triaxial compression test and parametric ranges of effective friction angle and rigidity index

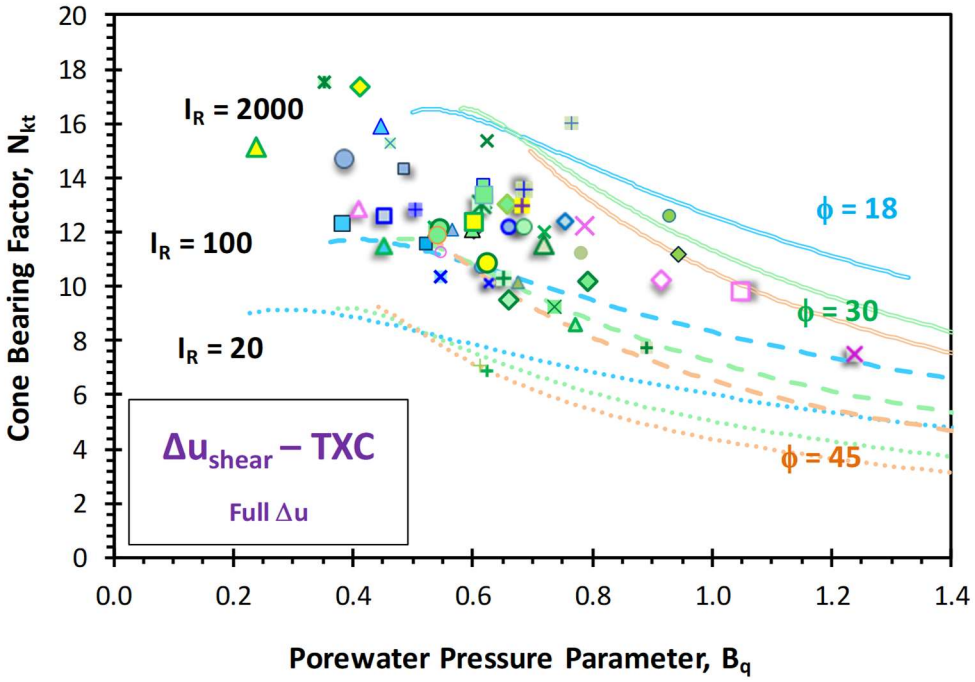


Figure H.10. Cone bearing factors ($N_{kt}$) versus $B_q$ using excess porewater pressures from conventional triaxial compression test and parametric ranges of effective friction angle and rigidity index

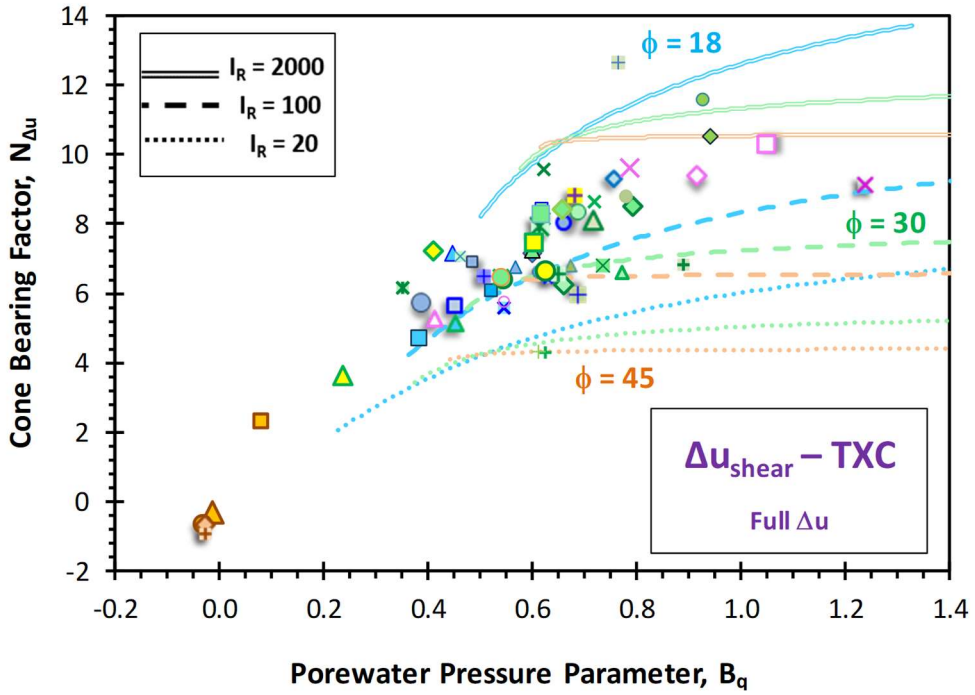


Figure H.11. Cone bearing factors ($N_{Du}$) versus $B_q$ using excess porewater pressures from conventional triaxial compression test and parametric ranges of effective friction angle and rigidity index

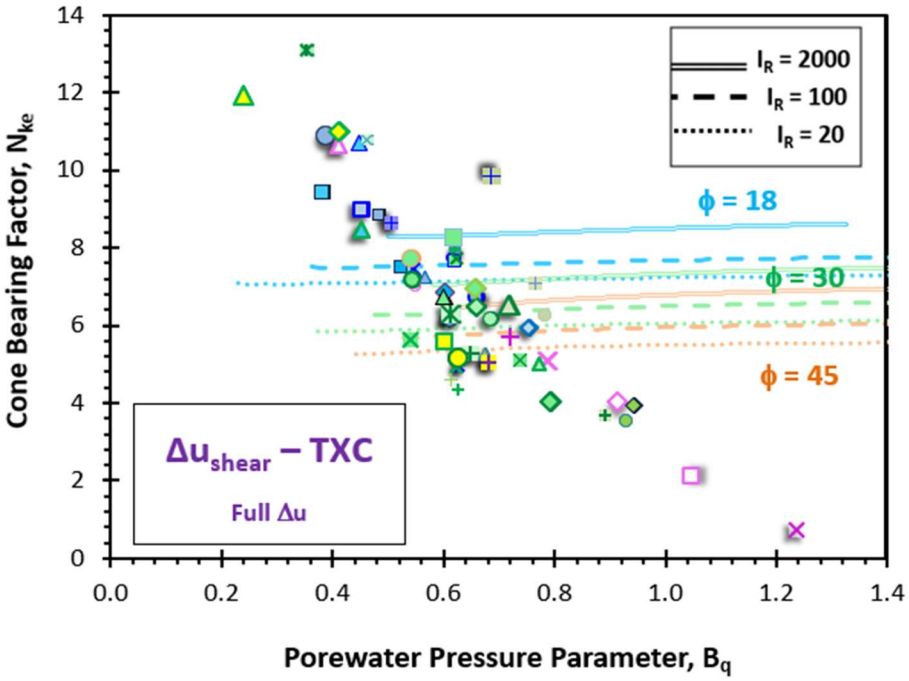


Figure H.12. Cone bearing factors ($N_{ke}$) versus $B_q$ using excess porewater pressures from conventional triaxial compression test and parametric ranges of effective friction angle and rigidity index

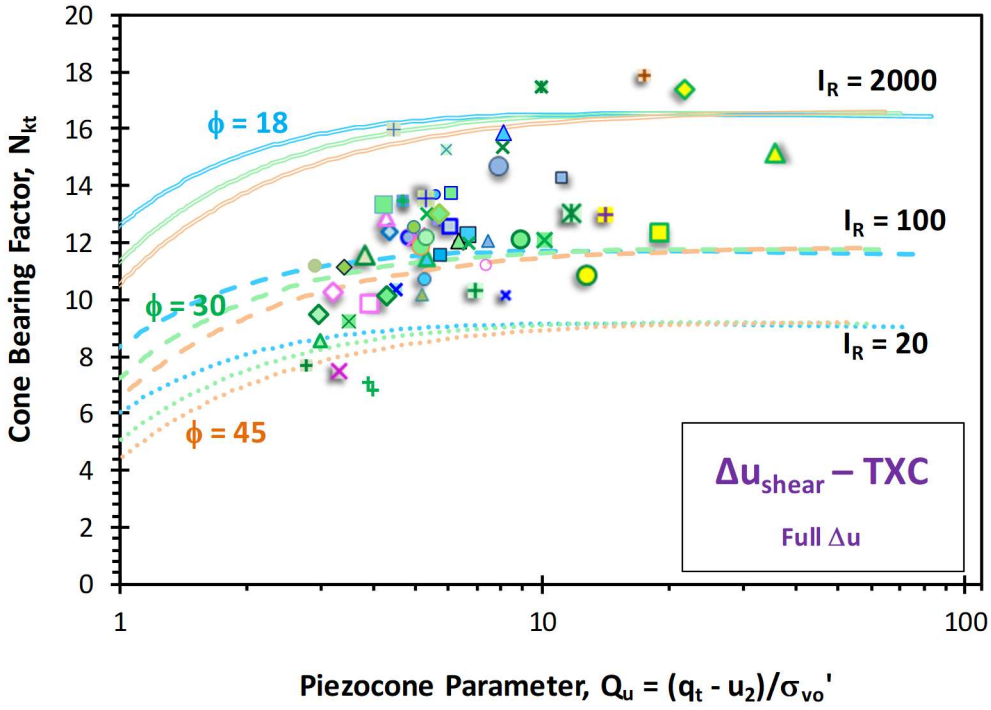


Figure H.13. Cone bearing factors ($N_{kt}$) versus $Q_u$ using excess porewater pressures from conventional triaxial compression test and parametric ranges of effective friction angle and rigidity index

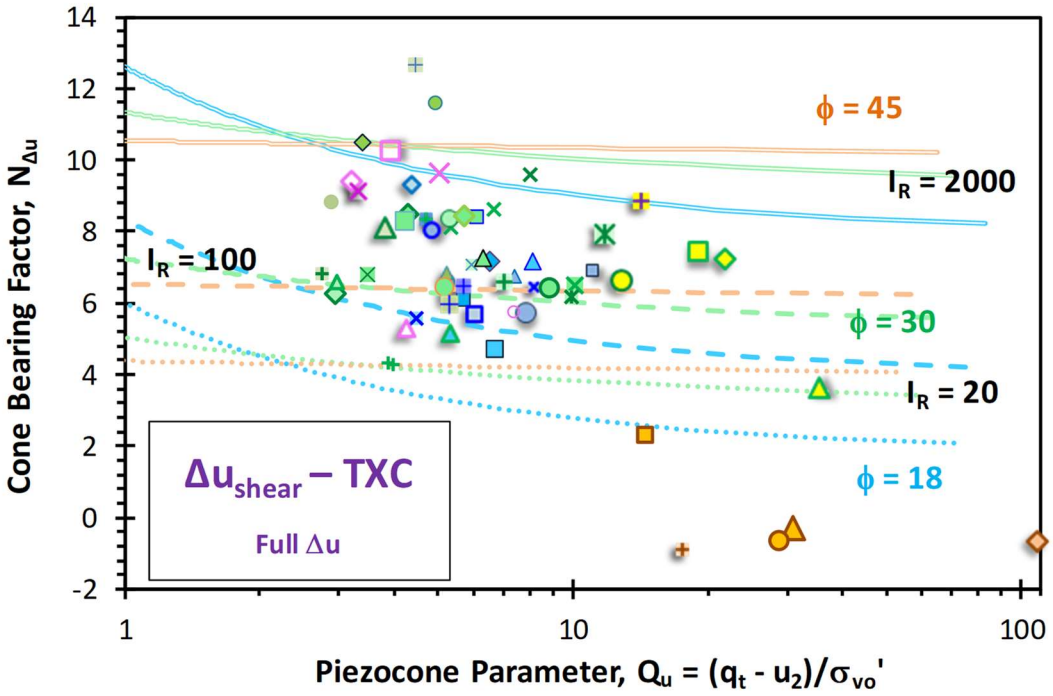


Figure H.14. Cone bearing factors ($N_{Du}$) versus $Q_u$ using excess porewater pressures from conventional triaxial compression test and parametric ranges of effective friction angle and rigidity index

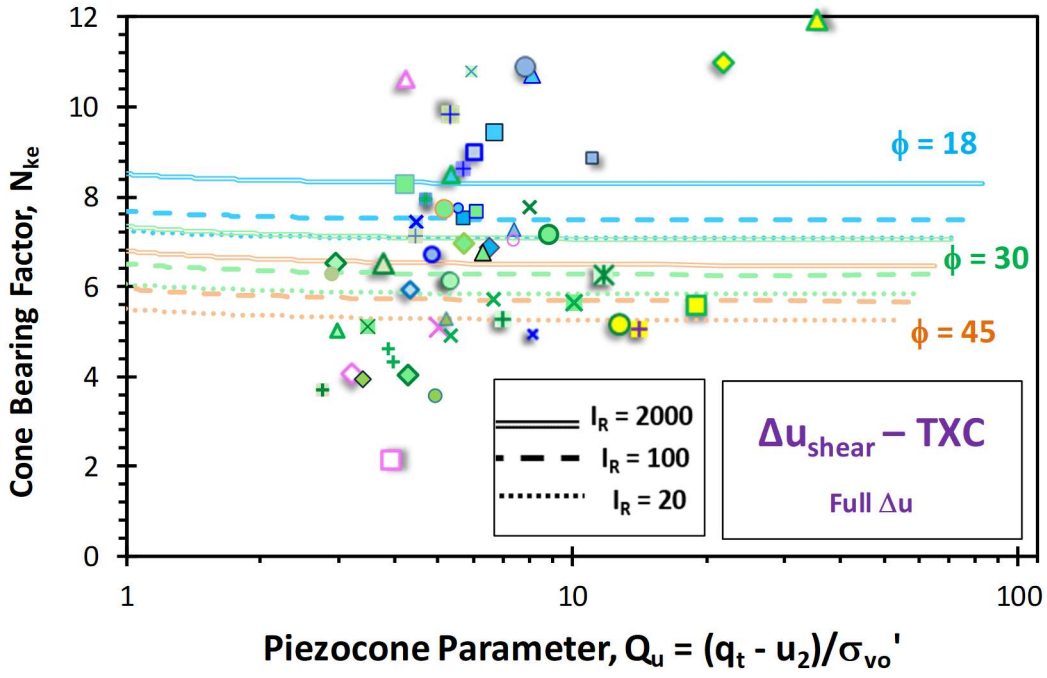


Figure H.15. Cone bearing factors ($N_{ke}$) versus $Q_u$ using excess porewater pressures from conventional triaxial compression test and parametric ranges of effective friction angle and rigidity index

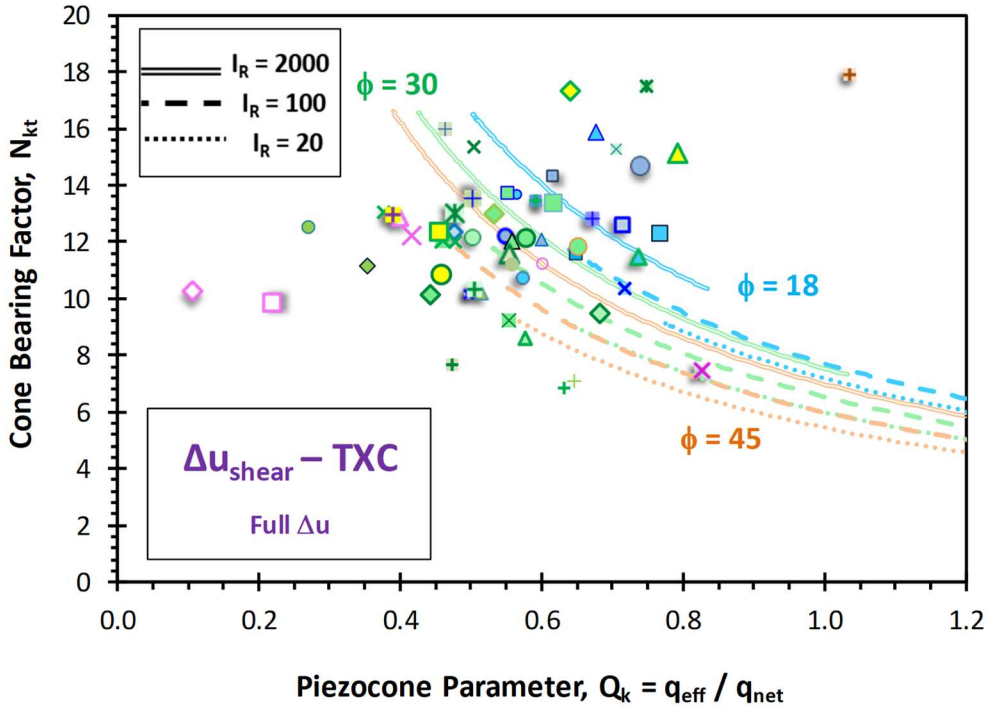


Figure H.16. Cone bearing factors ($N_{kt}$) versus $Q_k$ using excess porewater pressures from conventional triaxial compression test and parametric ranges of effective friction angle and rigidity index

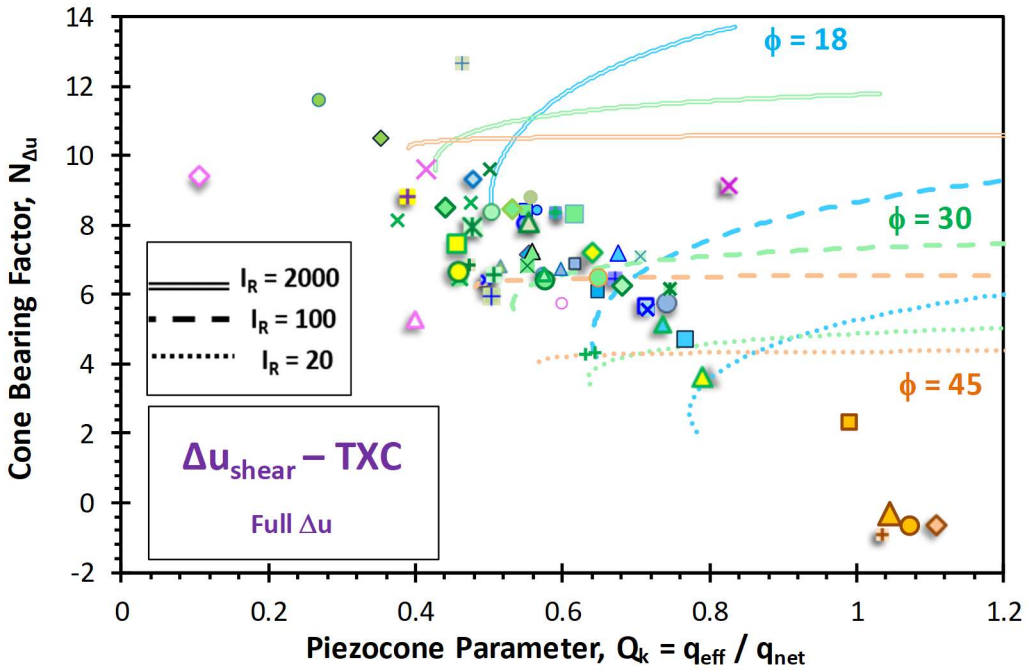


Figure H.17. Cone bearing factors ($N_{Du}$) versus $Q_k$ using excess porewater pressures from conventional triaxial compression test and parametric ranges of effective friction angle and rigidity index

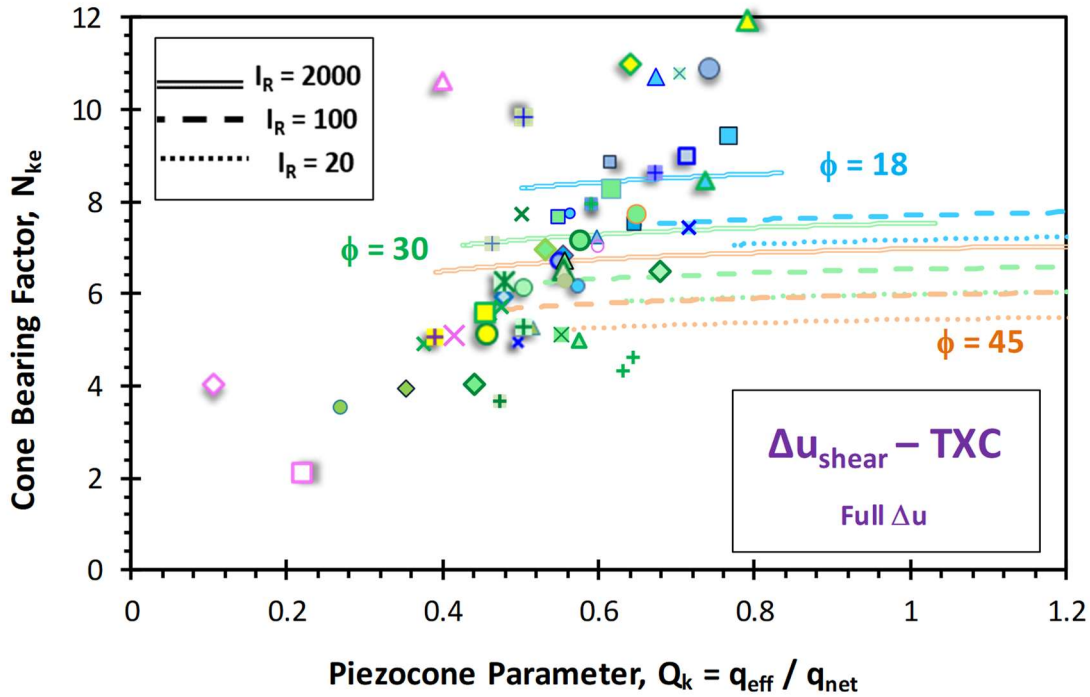


Figure H.18. Cone bearing factors ($N_{ke}$) versus $Q_k$ using excess porewater pressures from conventional triaxial compression test and parametric ranges of effective friction angle and rigidity index

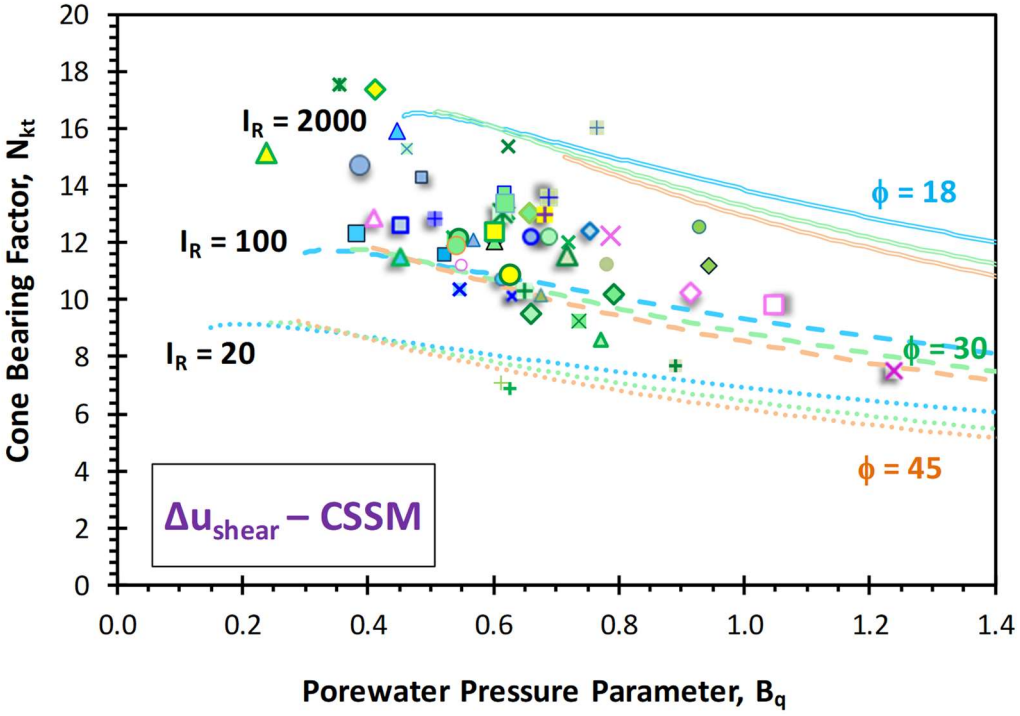


Figure H.19. Cone bearing factors ($N_{kt}$) versus $B_q$ using shear-induced porewater pressures from simplified CSSM and parametric ranges of effective friction angle and rigidity index

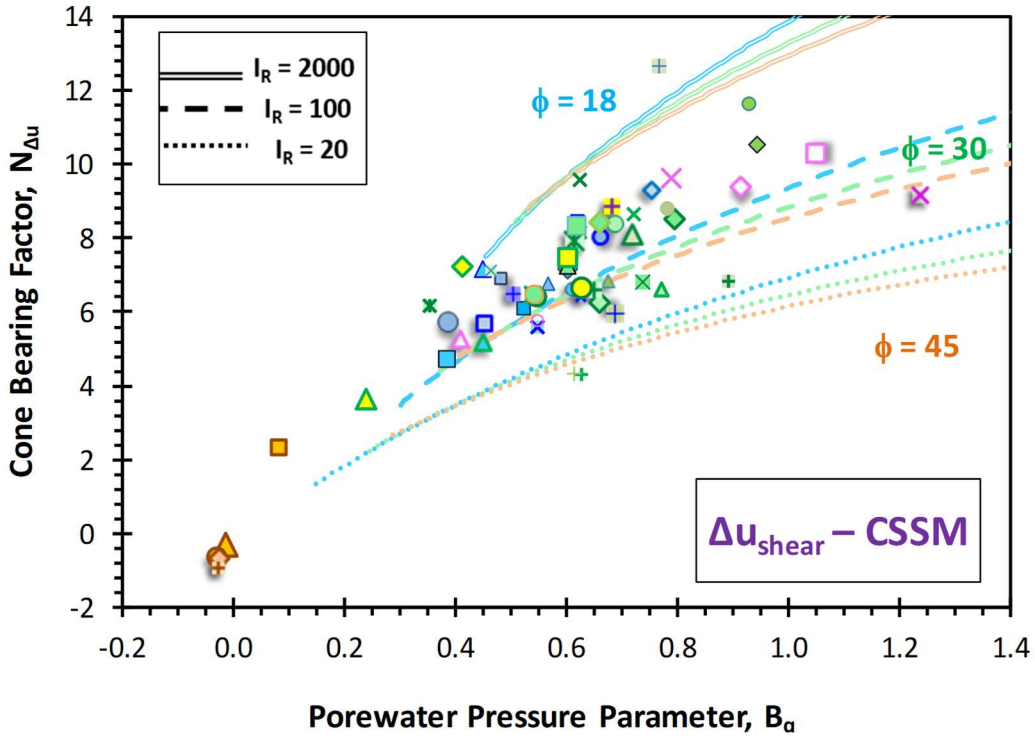


Figure H.20. Cone bearing factors ($N_{Du}$) versus $B_q$ using shear-induced porewater pressures from simplified CSSM and parametric ranges of effective friction angle and rigidity index

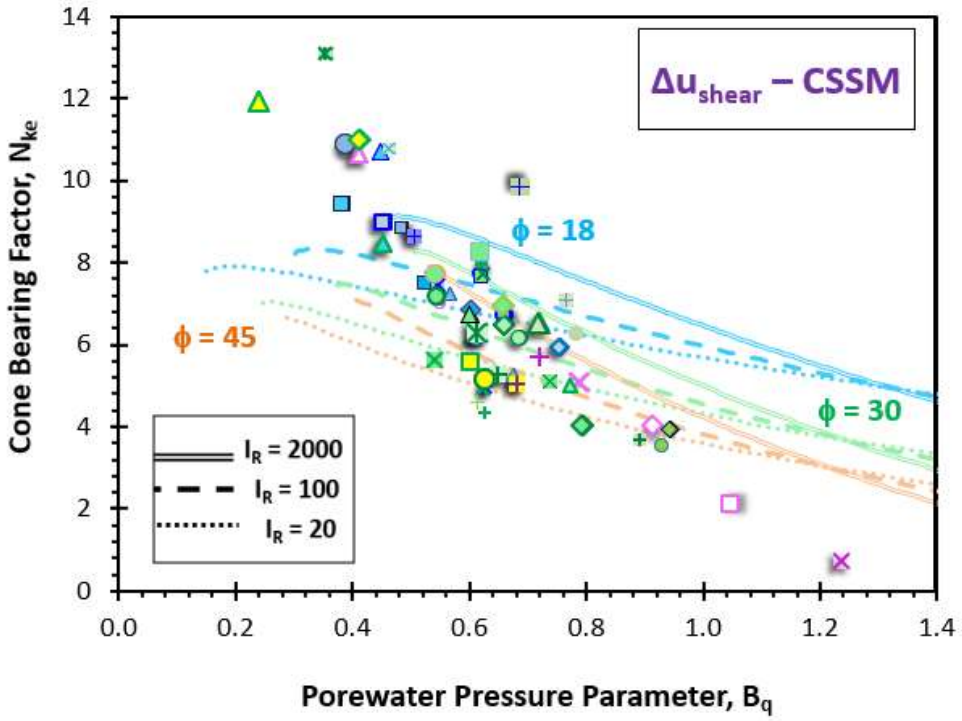


Figure H.21. Cone bearing factors ($N_{ke}$) versus $B_q$ using shear-induced porewater pressures from simplified CSSM and parametric ranges of effective friction angle and rigidity index

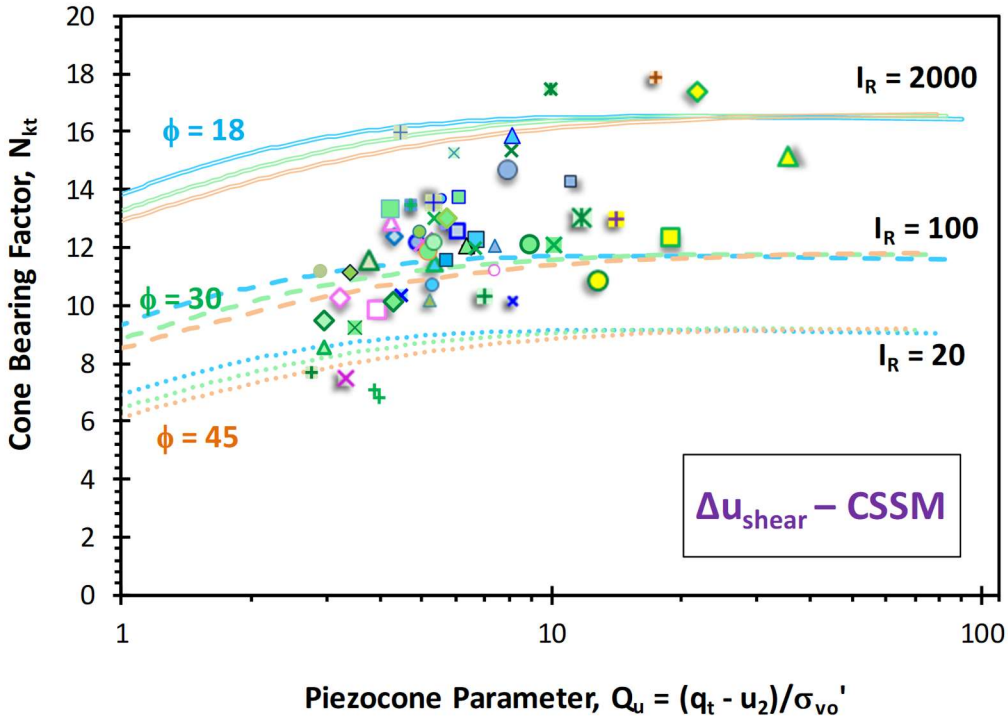


Figure H.22. Cone bearing factors ($N_{kt}$) versus $Q_u$ using shear-induced porewater pressures from simplified CSSM and parametric ranges of effective friction angle and rigidity index

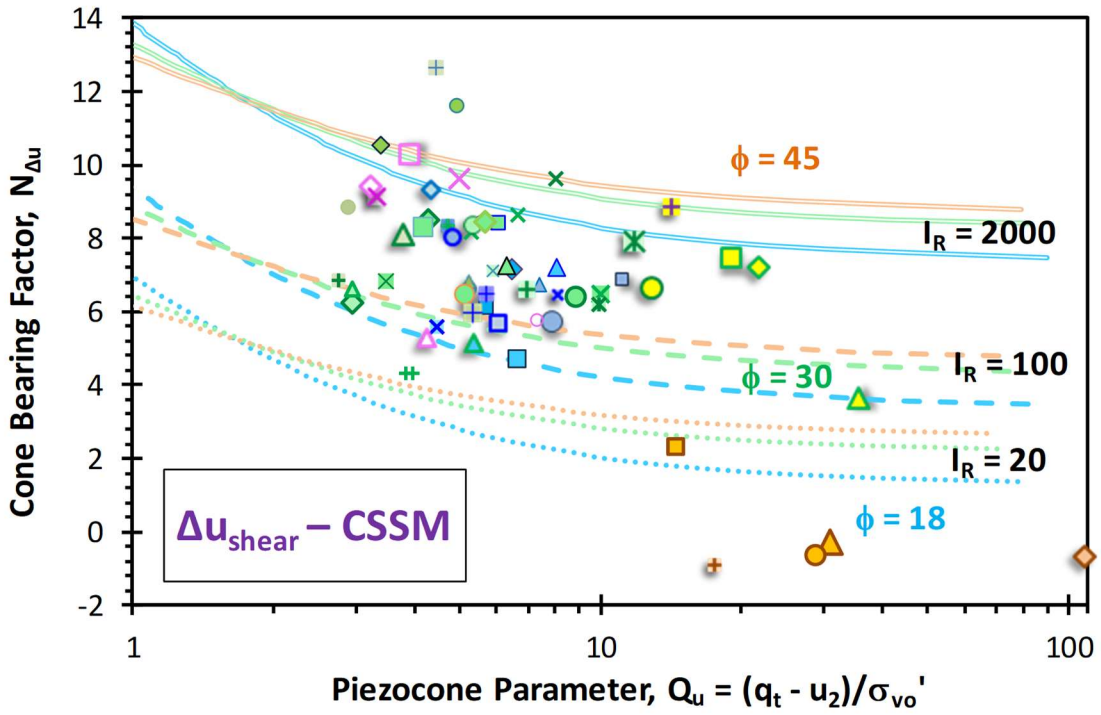


Figure H.23. Cone bearing factors ($N_{Du}$) versus $Q_u$ using shear-induced porewater pressures from simplified CSSM and parametric ranges of effective friction angle and rigidity index

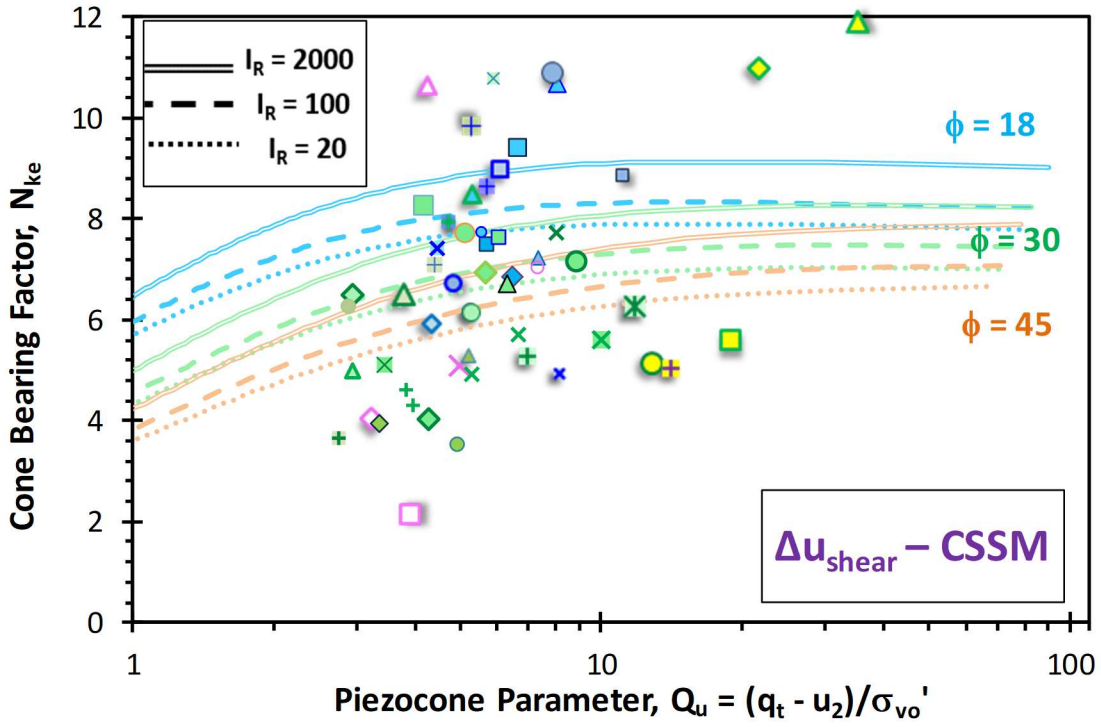


Figure H.24. Cone bearing factors ($N_{ke}$) versus $Q_u$ using shear-induced porewater pressures from simplified CSSM and parametric ranges of effective friction angle and rigidity index

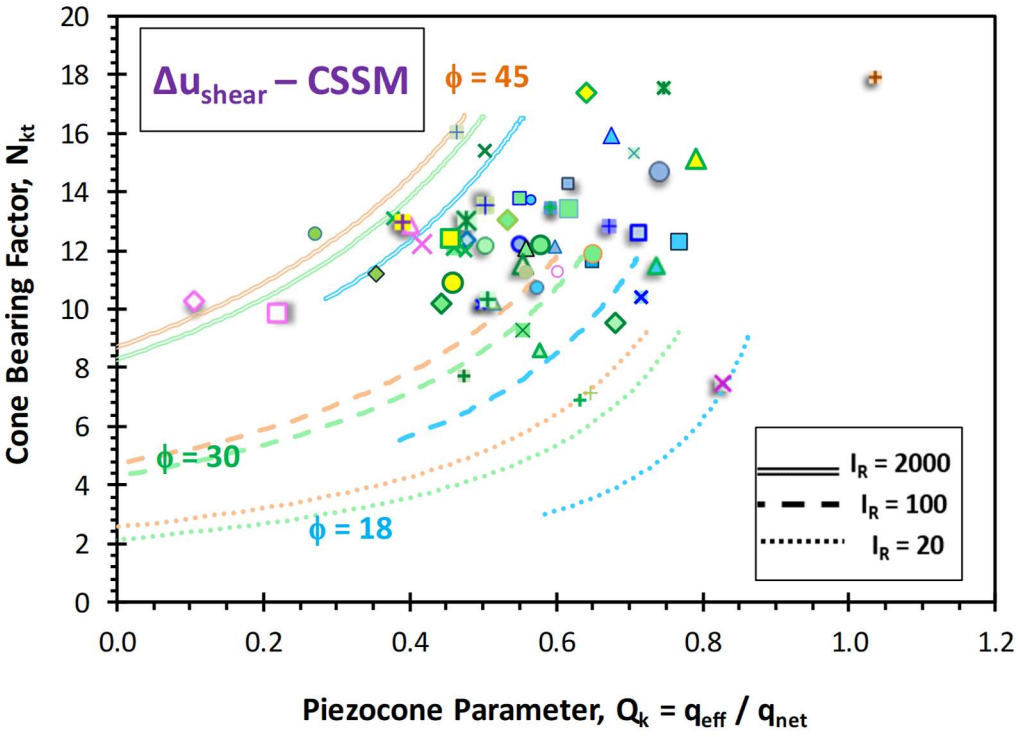


Figure H.25. Cone bearing factors ($N_{kt}$) versus $Q_k$ using shear-induced porewater pressures from simplified CSSM and parametric ranges of effective friction angle and rigidity index

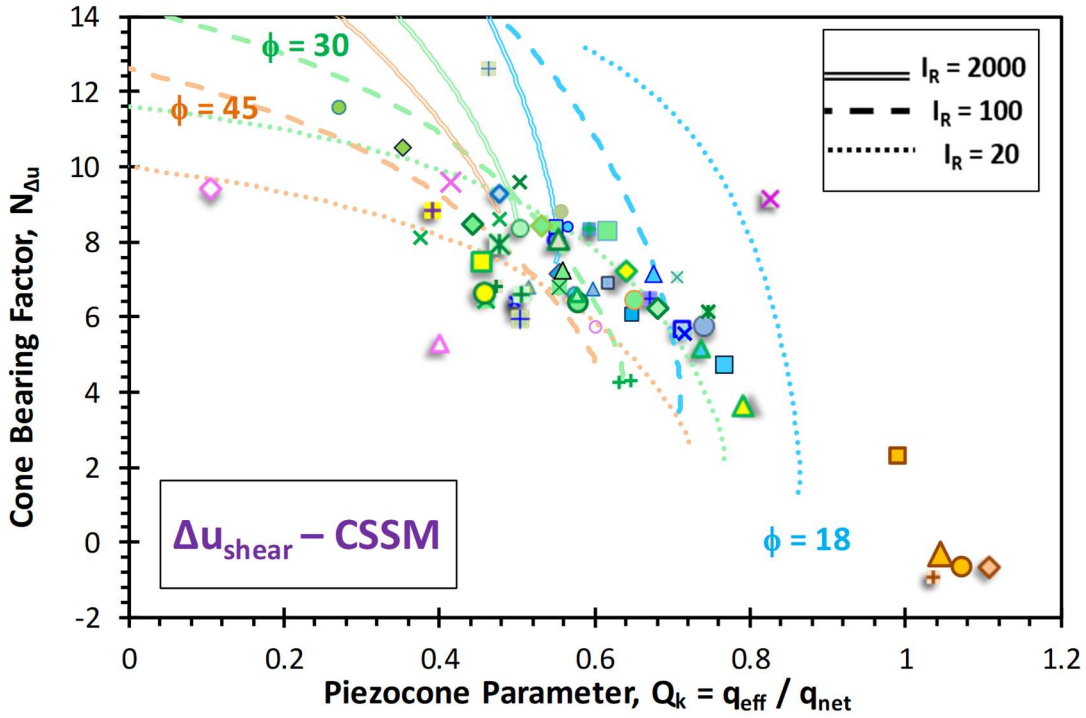


Figure H.26. Cone bearing factors ($N_{Du}$) versus $Q_k$ using shear-induced porewater pressures from simplified CSSM and parametric ranges of effective friction angle and rigidity index

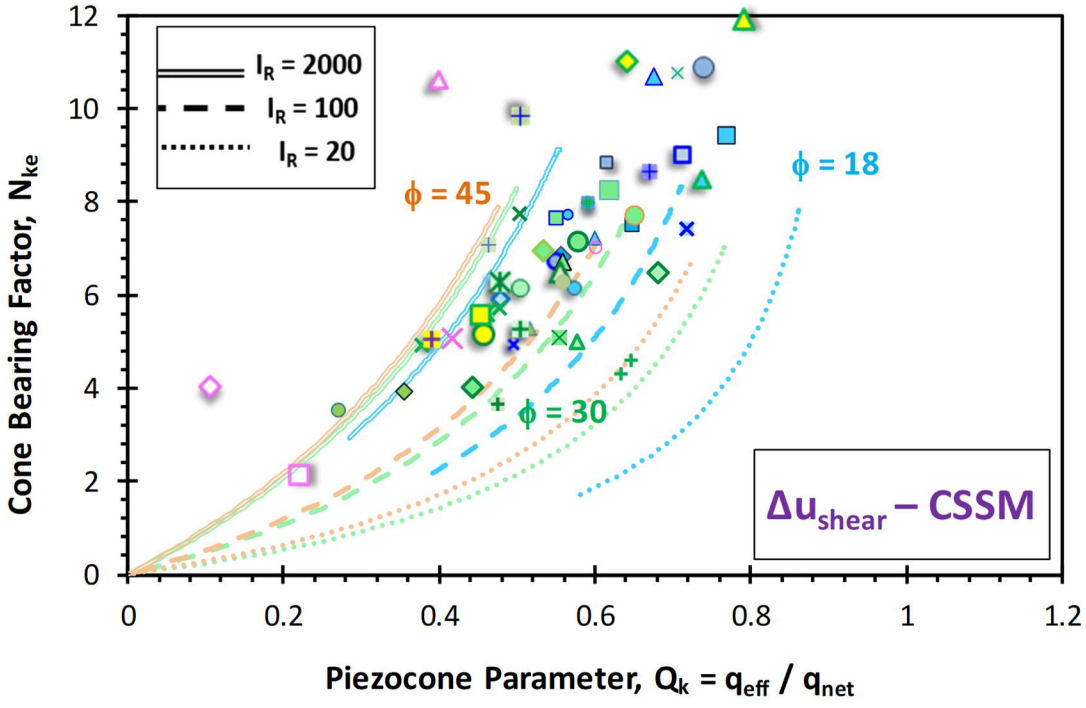


Figure H.27. Cone bearing factors ($N_{ke}$) versus $Q_k$ using shear-induced porewater pressures from simplified CSSM and parametric ranges of effective friction angle and rigidity index

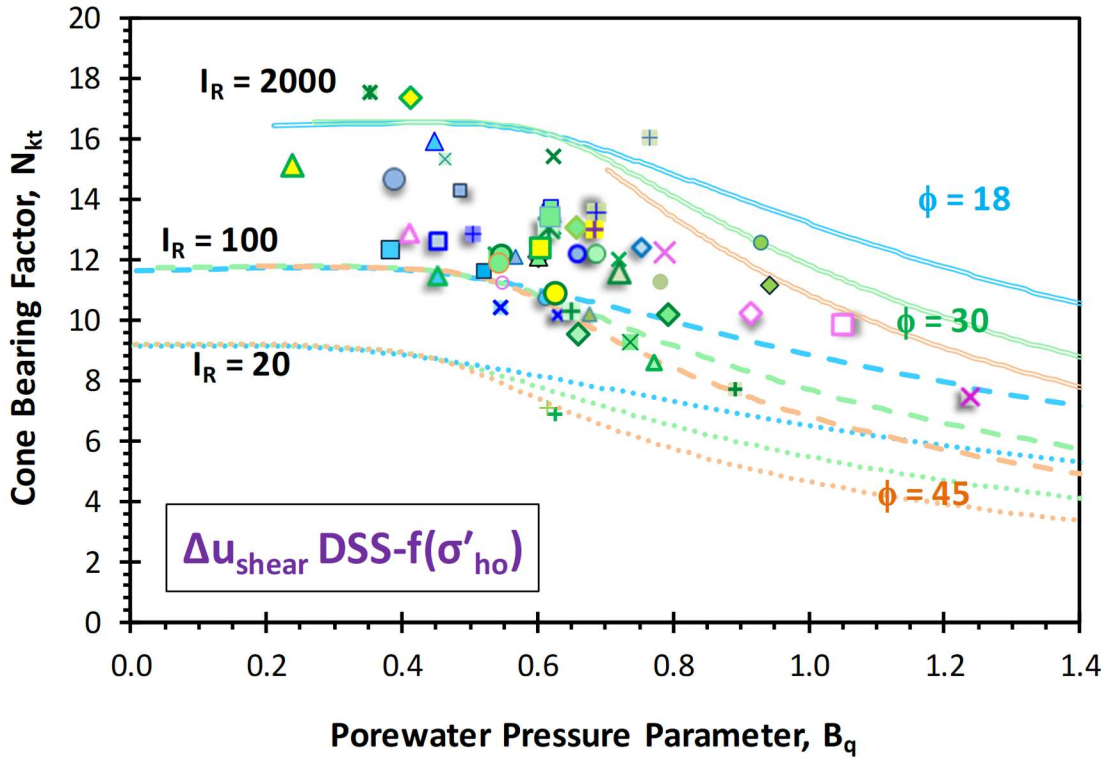


Figure H.28. Cone bearing factors ($N_{kt}$) versus $B_q$ using shear-induced porewater pressure from horizontal DSS tests and parametric ranges of effective friction angle and rigidity index

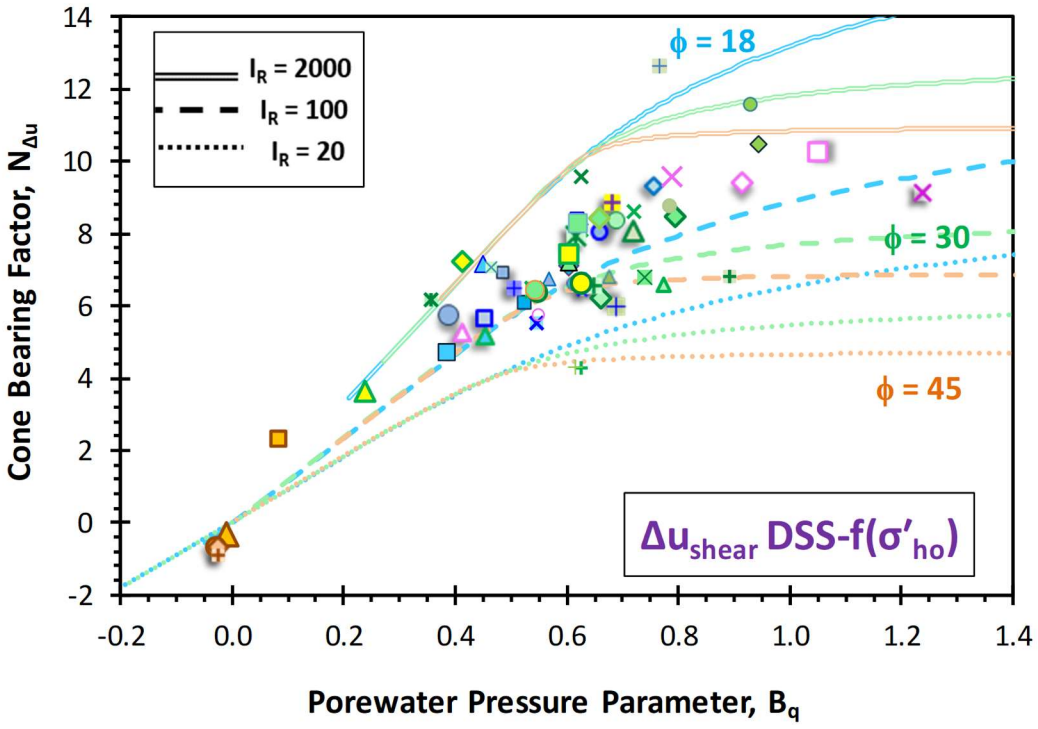


Figure H.29. Cone bearing factors ($N_{Du}$) versus $B_q$ using shear-induced porewater pressure from horizontal DSS tests and parametric ranges of effective friction angle and rigidity index

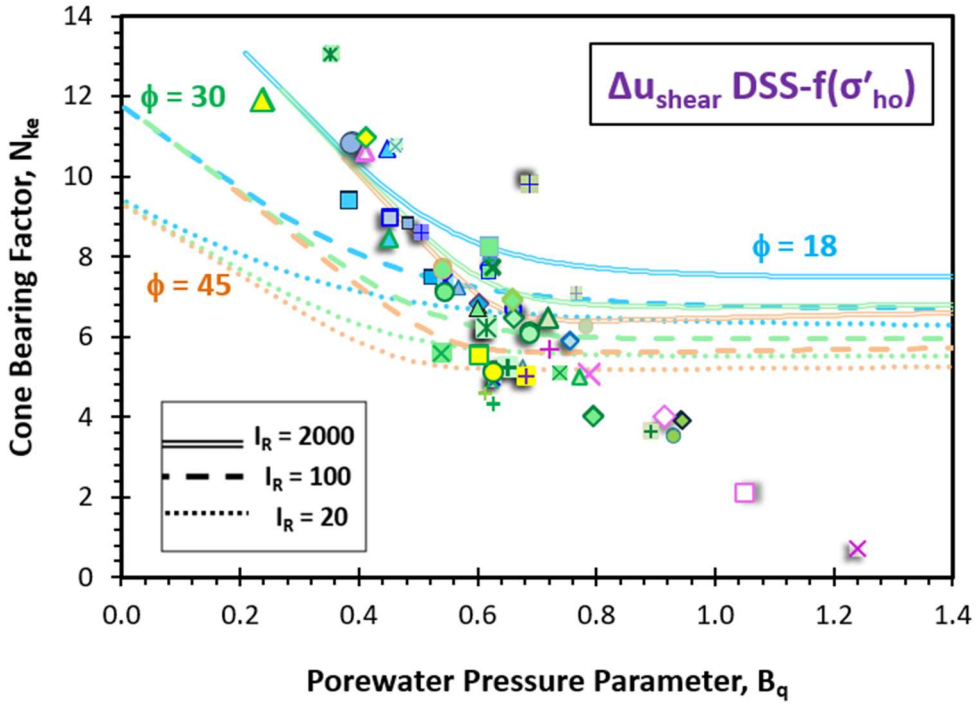


Figure H.30. Cone bearing factors ($N_{ke}$) versus $B_q$ using shear-induced porewater pressure from horizontal DSS tests and parametric ranges of effective friction angle and rigidity indeH

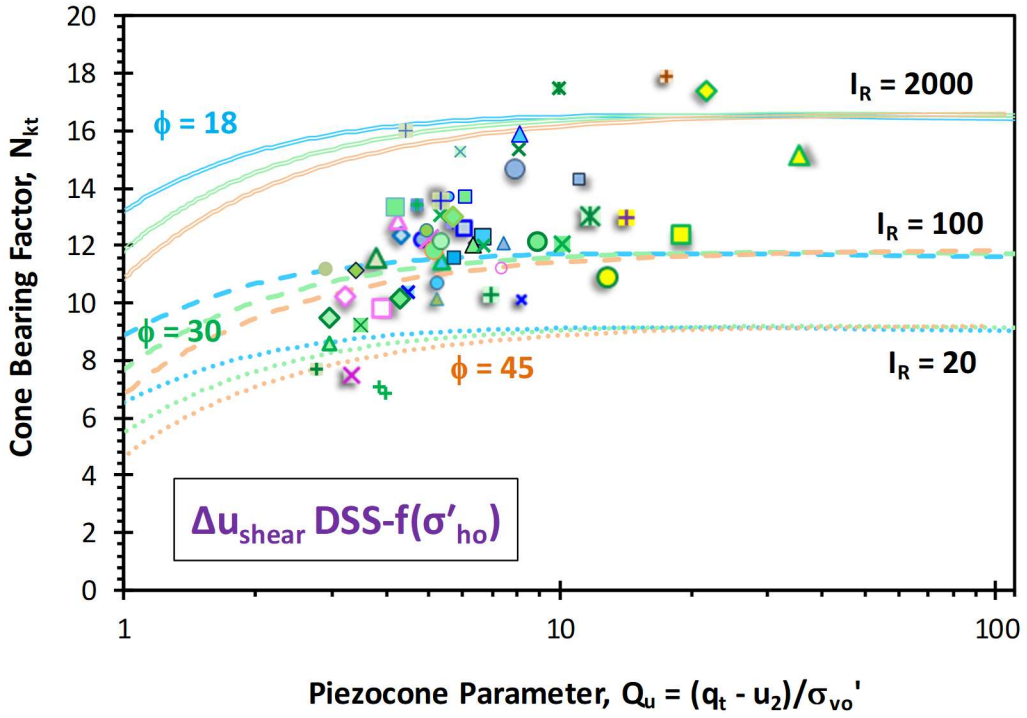


Figure H.31. Cone bearing factors ($N_{kt}$) versus $Q_u$ using shear-induced porewater pressure from horizontal DSS tests and parametric ranges of effective friction angle and rigidity index

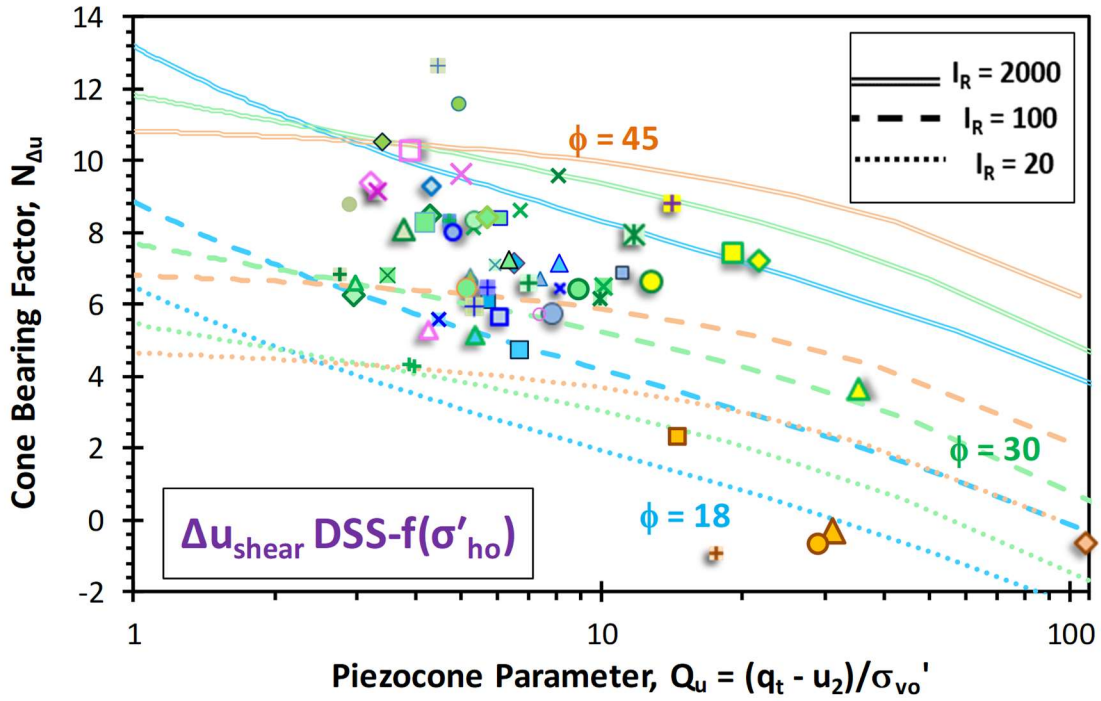


Figure H.32. Cone bearing factors ($N_{Du}$) versus $Q_u$ using shear-induced porewater pressure from horizontal DSS tests and parametric ranges of effective friction angle and rigidity index

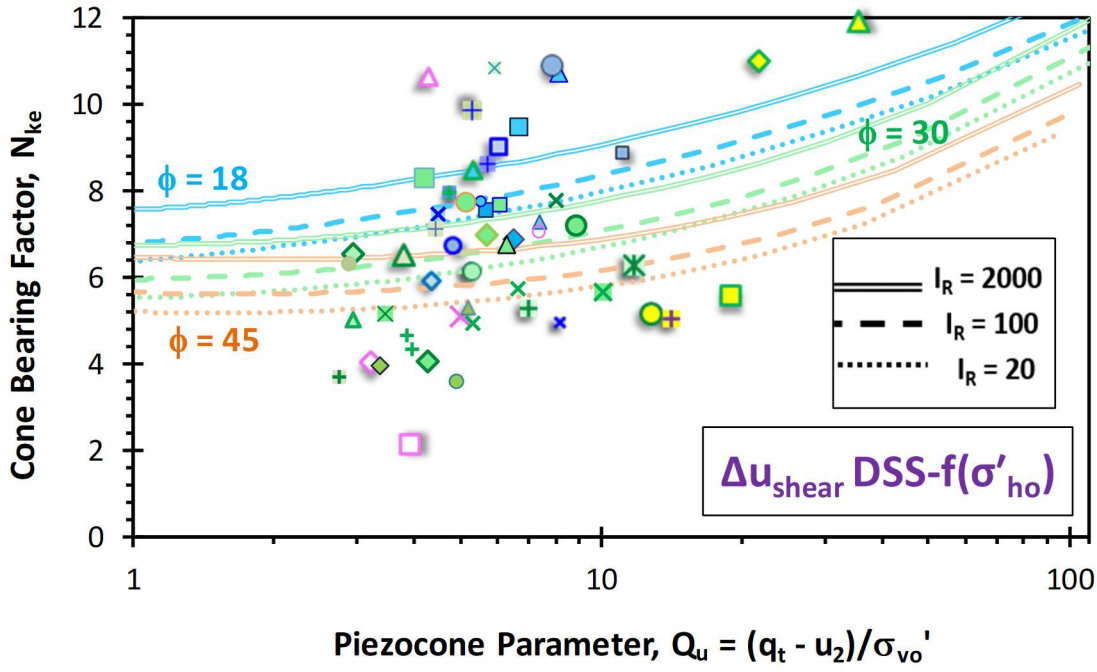


Figure H.33. Cone bearing factors ($N_{ke}$) versus $Q_u$ using shear-induced porewater pressure from horizontal DSS tests and parametric ranges of effective friction angle and rigidity index

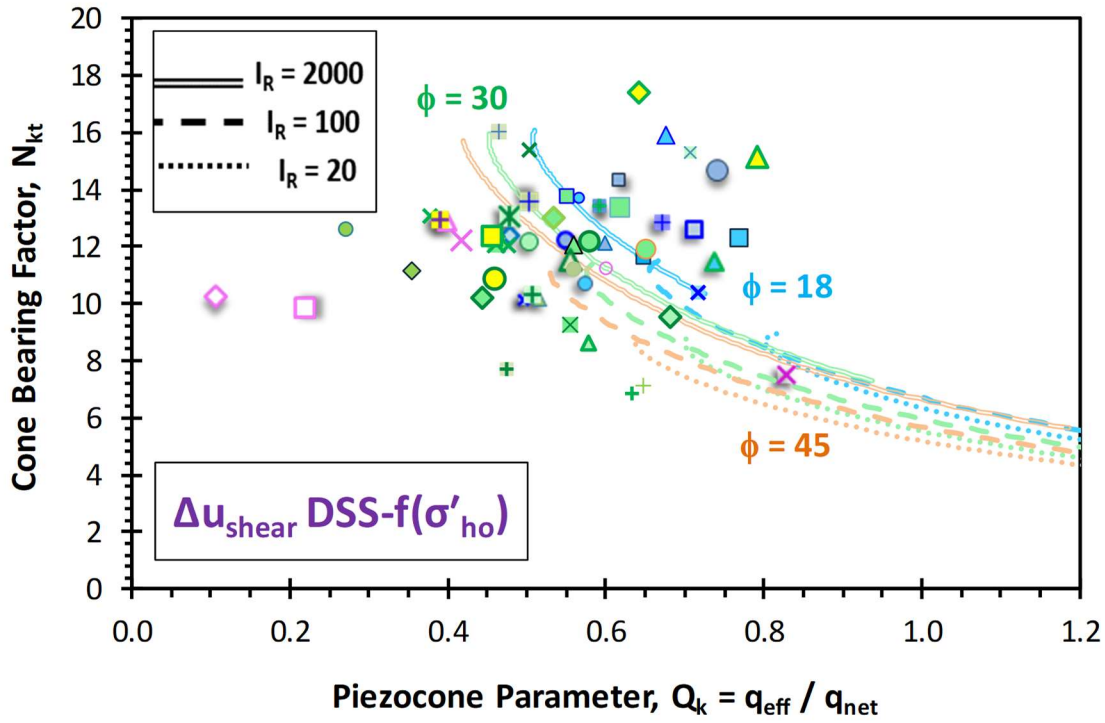


Figure H.34. Cone bearing factors ($N_{kt}$) versus $Q_k$ using shear-induced porewater pressure from horizontal DSS tests and parametric ranges of effective friction angle and rigidity index

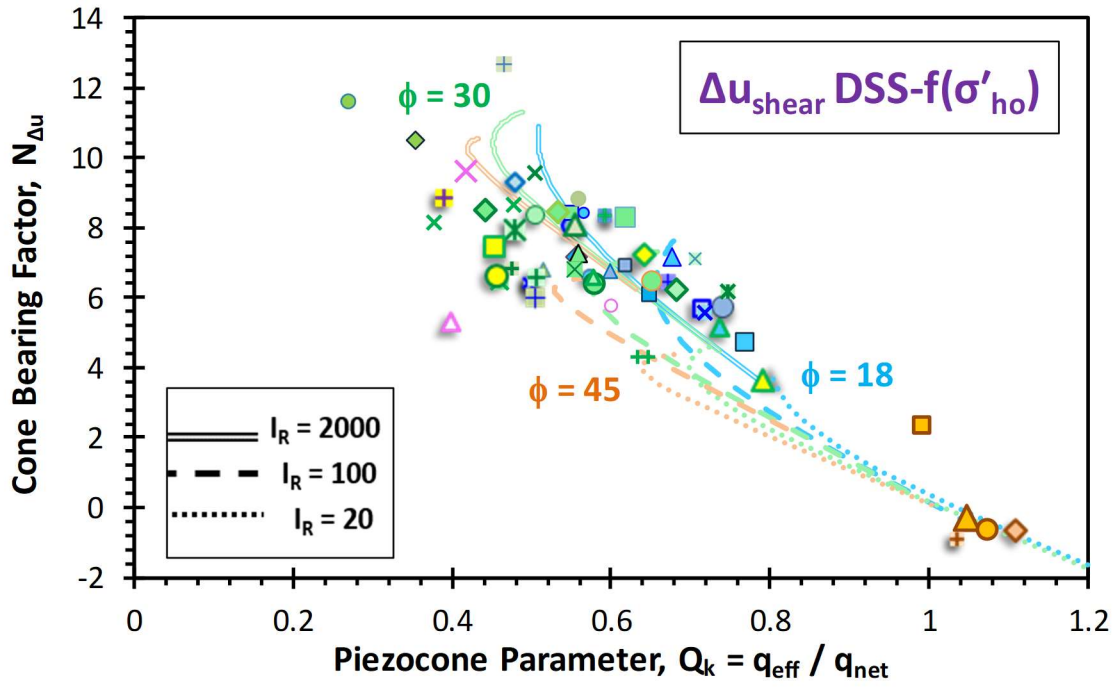


Figure H.35. Cone bearing factors ($N_{Du}$) versus $Q_k$ using shear-induced porewater pressure from horizontal DSS tests and parametric ranges of effective friction angle and rigidity index

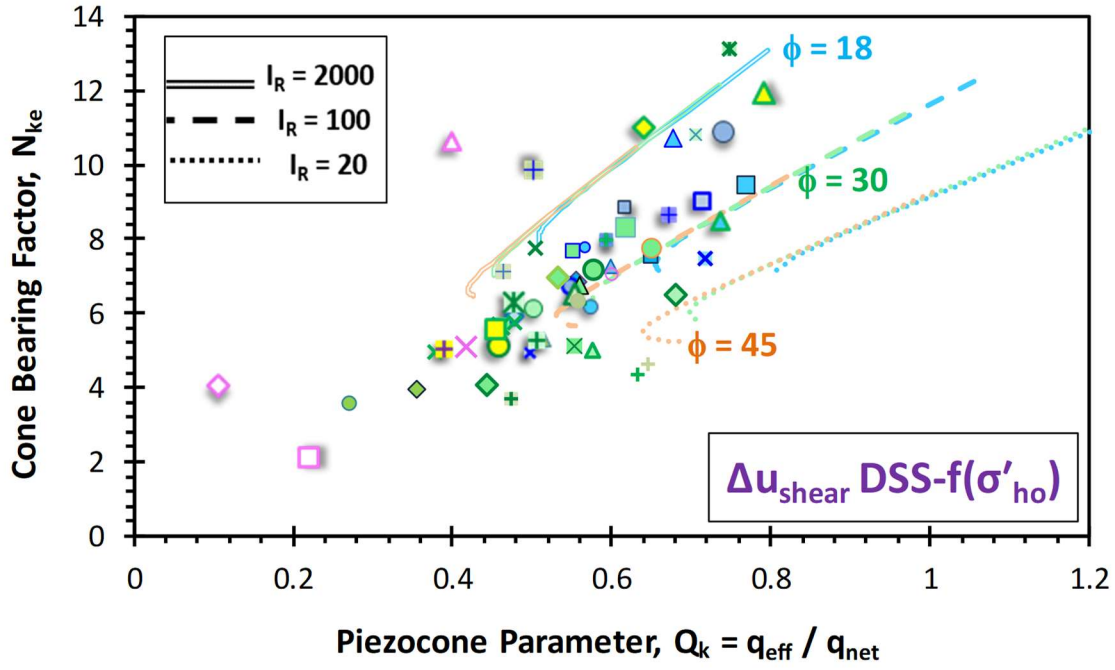


Figure H.36. Cone bearing factors ($N_{ke}$) versus $Q_k$ using shear-induced porewater pressure from horizontal DSS tests and parametric ranges of effective friction angle and rigidity index

# APPENDIX I

## Derivation of OCR Expressions for Calibration of Analytical Model for Estimating Stress History in Clays

## Constant p' Triaxial Compression Test

Derivation of OCR as a function of normalized porewater pressure (U*)

$$s_u = S^* OCR^{\Lambda} \sigma'_{vo}$$

$$\Delta u = \Delta u_{oct} + \Delta u_{sh}$$

$$\Delta u_{oct} = \frac{4}{3} \cdot \ln I_R \cdot s_u$$

$$\Delta u_{sh} = p'_o - p'_f = \frac{\sigma'_{vo}}{2} \cdot (1 + K_0) - \frac{s_u}{\sin \phi'}$$

$$\Delta u = \frac{4}{3} \cdot \ln I_R \cdot s_u + \frac{\sigma'_{vo}}{2} \cdot (1 + K_0) - \frac{s_u}{\sin \phi'}$$

$$\frac{\Delta u}{\sigma'_{vo}} = \frac{4}{3} \cdot \ln I_R \cdot \frac{s_u}{\sigma'_{vo}} + \frac{1}{2} \cdot (1 + K_0) - \frac{s_u}{\sigma'_{vo} \sin \phi'}$$

$$\frac{\Delta u}{\sigma'_{vo}} - \frac{1}{2} \cdot (1 + K_0) = \frac{s_u}{\sigma'_{vo}} [\frac{4}{3} \cdot \ln I_R - \frac{1}{\sin \phi'}]$$

$$\frac{\Delta u}{\sigma'_{vo}} - \frac{1}{2} \cdot (1 + K_0) = S^* OCR^{\Lambda} \cdot [\frac{4}{3} \cdot \ln I_R - \frac{1}{\sin \phi'}]$$

$$OCR^{\Lambda} = \frac{(\Delta u / \sigma'_{vo}) - 0.5\,(1 + K_o)}{(S^*)(1.33\ \ln\ _R - 1/sin\emptyset)}$$

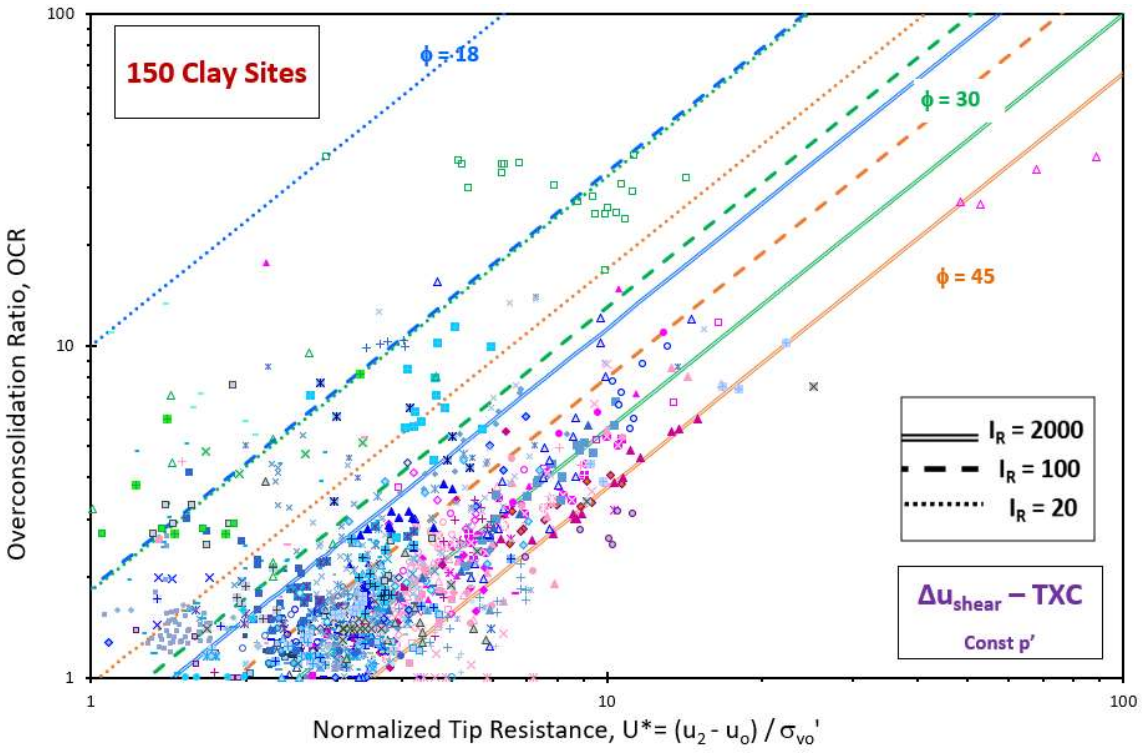


Figure I.1. Overconsolidation ratio versus normalized porewater pressure (U*) for shear-induced excess porewater pressure from triaxial compression test with constant p' for different effective friction angles and rigidity index values

## Constant p' Triaxial Compression Test

Derivation of OCR as a function of normalized effective cone resistance ($Q_u$)

$$N_{kt} = \frac{q_{net}}{s_u} = \frac{q_t - \sigma_{vo}}{s_u}$$

$$q_t = \sigma_{vo} + N_{kt} \cdot s_u$$

$$\Delta u = \frac{4}{3} \cdot \ln I_R \cdot s_u + \frac{\sigma'_{vo}}{2} \cdot (1 + K_0) - \frac{s_u}{\sin \phi'}$$

$$u_2 = u_o + \frac{4}{3} \cdot \ln I_R \cdot s_u + \frac{\sigma'_{vo}}{2} \cdot (1 + K_0) - \frac{s_u}{\sin \phi'}$$

$$q_t - u_2 = [\sigma_{vo} + N_{kt} \cdot s_u] - [\, u_o + \frac{4}{3} \cdot \ln I_R \cdot s_u + \frac{\sigma'_{vo}}{2} \cdot (1 + K_0) - \frac{s_u}{\sin \phi'}\,]$$

$$q_t - u_2 = \sigma'_{vo} + [N_{kt} \cdot s_u] - \frac{4}{3} \cdot \ln I_R \cdot s_u - \frac{\sigma'_{vo}}{2} \cdot (1 + K_0) + \frac{s_u}{\sin \phi'}$$

$$q_t - u_2 = \sigma'_{vo}\,[\,1 - \frac{1}{2} \cdot (1 + K_0)] + s_u \left[N_{kt} - \frac{4}{3} \cdot \ln I_R + \frac{1}{\sin \phi'}\right]$$

$$[q_t - u_2] - \sigma'_{vo}\,[\,1 - \frac{1}{2} \cdot (1 + K_0)] = s_u \left[N_{kt} - \frac{4}{3} \cdot \ln I_R + \frac{1}{\sin \phi'}\right]$$

$$\frac{s_u}{\sigma'_{vo}} \left[N_{kt} - \frac{4}{3} \cdot \ln I_R + \frac{1}{\sin \phi'}\right] = \frac{[q_t - u_2]}{\sigma'_{vo}} - \frac{1}{2}[\,(1 - K_0)]$$

$$S^* OCR^{\Lambda} \left[N_{kt} - \frac{4}{3} \cdot \ln I_R + \frac{1}{\sin \phi'}\right] = \frac{[q_t - u_2]}{\sigma'_{vo}} - \frac{1}{2}[\,(1 - K_0)]$$

$$OCR^{\Lambda} = \frac{(q_t - u_2/\sigma'_{vo}) - 0.5\,(1 - K_o)}{\left(N_{kt} + \frac{1}{sin\phi} - 1.33 \quad _R\right)(S^*)}$$

$$N_{kt} = 3.4 + 1.6\ \ln I_R - 1.9\Delta + 1.3\alpha_c$$

$$\Delta = \frac{\sigma'_{vo} \cdot (1-K_o)}{2s_u} = \frac{\sigma'_{vo} \cdot (1-K_o)}{2 \cdot S^* OCR^{\Lambda} \sigma'_{vo}}$$

$$OCR^{\Lambda} = \frac{(q_t - u_2/\sigma'_{vo}) - 0.5\,(1-K_o)}{\left(N_{kt} + \frac{1}{sin\emptyset} - 1.33 \ln I_R\right)(S^*)}$$

$$OCR^{\Lambda} = \frac{(q_t - u_2/\sigma'_{vo}) - 0.5\,(1-K_o)}{\left(3.4 + 0.26\,\ln I_R - \frac{1.9(1-K_o)}{2 \cdot S^* OCR^{\Lambda}} + 1.3\alpha_c + \frac{1}{sin\emptyset}\right)(S^*)}$$

$$OCR^{\Lambda} = \frac{(q_t - u_2/\sigma'_{vo}) - 0.5\,(1-K_o)}{\left(3.4 + 0.26\,\ln I_R + 1.3\alpha_c + \frac{1}{sin\emptyset}\right)(S^*) - \frac{0.95(1-K_o)}{OCR^{\Lambda}}}$$

$$OCR^{\Lambda}\left(3.4 + 0.26 \ln I_R + 1.3\alpha_c + \frac{1}{sin\emptyset}\right)(S^*) - 0.95(1-K_o) = \left(\frac{q_t - u_2}{\sigma'_{vo}}\right) - 0.5(1-K_o)$$

$$OCR^{\Lambda}\left(3.4 + 0.26 \ln I_R + 1.3\alpha_c + \frac{1}{sin\emptyset}\right)(S^*) = \left(\frac{q_t - u_2}{\sigma'_{vo}}\right) + 0.45(1-K_o)$$

$$OCR^{\Lambda} = \frac{(q_t - u_2/\sigma'_{vo}) + 0.45\,(1-K_o)}{(S^*)\left(3.4 + 0.26\,\ln I_R + 1.3\alpha_c + \frac{1}{sin\emptyset}\right)}$$

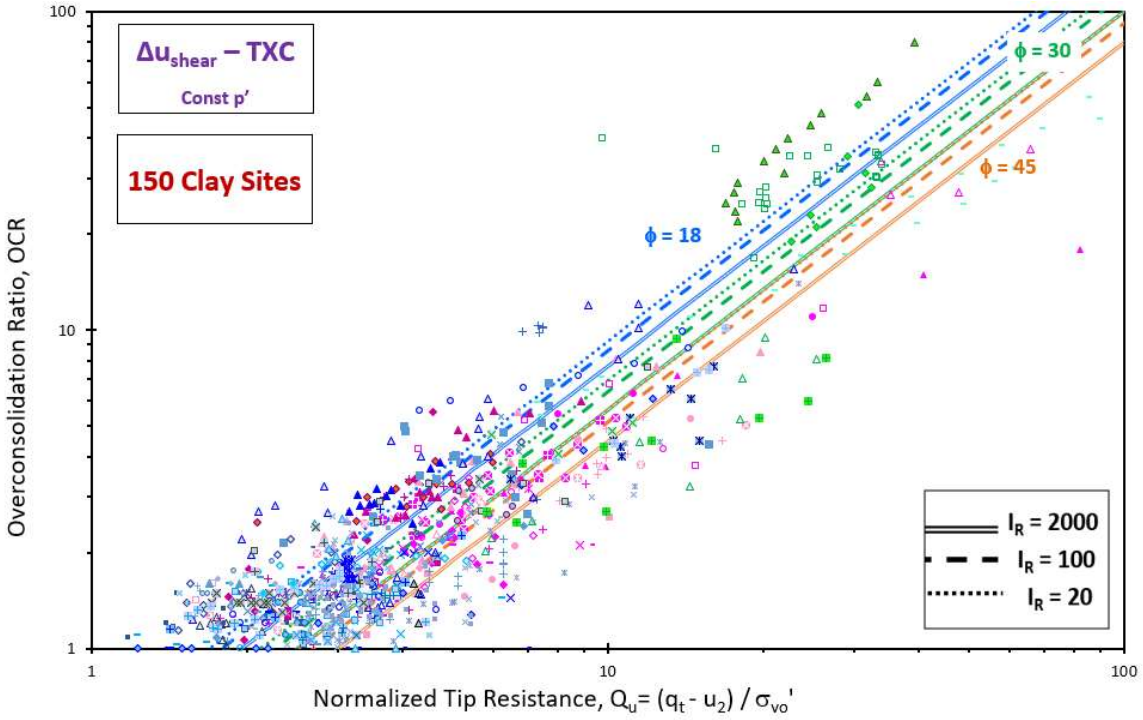


Figure I.2. Overconsolidation ratio versus normalized effective cone tip resistance ($Q_u$) using shear-induced excess porewater pressure from constant p' triaxial tests and parametric values of effective friction angle and rigidity index

## Conventional Triaxial Compression Test

Derivation of OCR as a function of normalized porewater pressure (U*)

$$s_u = S^* OCR^{\Lambda} \sigma'_{vo}$$

$$\Delta u = \Delta u_{oct} + \Delta u_{sh}$$

$$\Delta u_{oct} = \frac{4}{3} \cdot \ln I_R \cdot s_u$$

$$\Delta u_{sh} = p_{f\,Total} - p'_f = K_0 \cdot \sigma'_{vo} + s_u \cdot (1 - \frac{1}{\sin \phi'})$$

$$\Delta u = \frac{4}{3} \cdot \ln I_R \cdot s_u + K_0 \cdot \sigma'_{vo} + s_u \cdot (1 - \frac{1}{\sin \phi'})$$

$$\Delta u = s_u \cdot \left[\frac{4}{3} \cdot \ln I_R + 1 - \frac{1}{\sin \phi'}\right] + K_0 \cdot \sigma'_{vo}$$

$$\frac{\Delta u}{\sigma'_{vo}} = K_0 + \frac{s_u}{\sigma'_{vo}} [\frac{4}{3} \cdot \ln I_R + 1 - \frac{1}{\sin \phi'}]$$

$$\frac{\Delta u}{\sigma'_{vo}} - K_0 = S^* OCR^{\Lambda} \cdot [\frac{4}{3} \cdot \ln I_R + 1 - \frac{1}{\sin \phi'}]$$

$$OCR^{\Lambda} = \frac{(\Delta u / \sigma'_{vo}) - K_o}{(S^*)(1 + 1.33 \ln I_R - 1/sin\emptyset)}$$

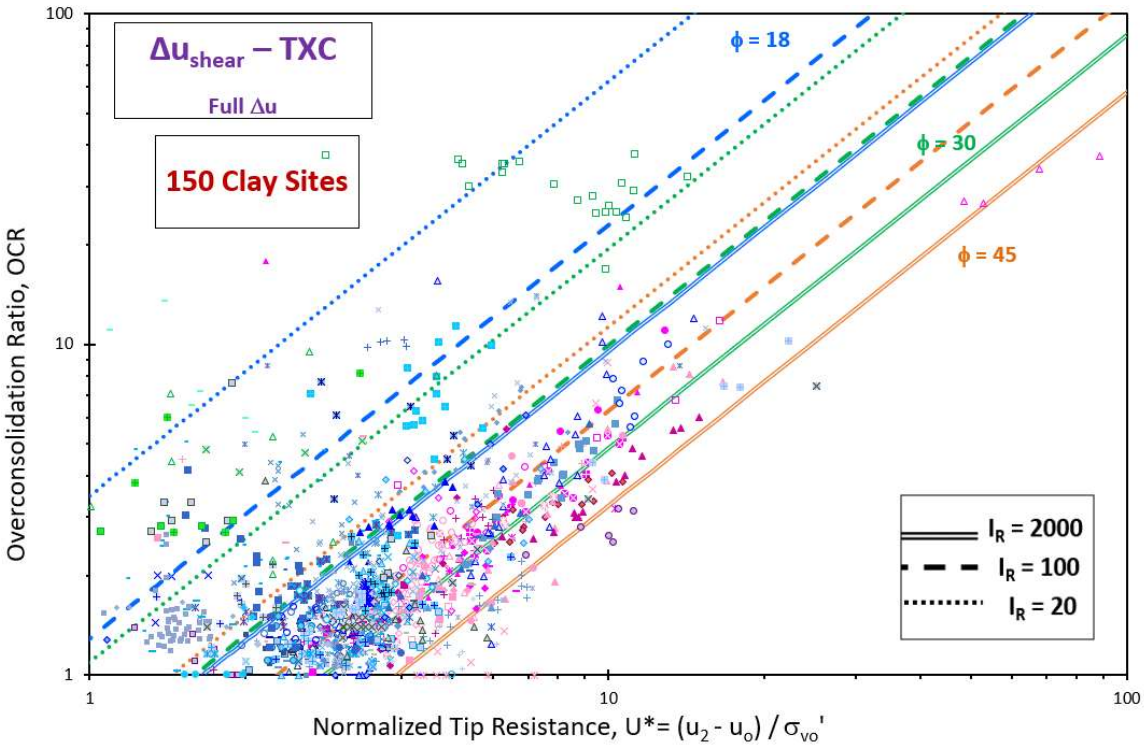


Figure I.3. Overconsolidation ratio versus normalized porewater pressure (U*) for full excess porewater pressure from conventional triaxial compression test for different effective friction angle and rigidity index values

## Conventional Triaxial Compression Test

Derivation of OCR as a function of normalized effective cone resistance ($Q_u$)

$$N_{kt} = \frac{q_{net}}{s_u} = \frac{q_t - \sigma_{vo}}{s_u}$$

$$q_t = \sigma_{vo} + N_{kt} \cdot s_u$$

$$\Delta u = \frac{4}{3} \cdot \ln I_R \cdot s_u + K_0 \cdot \sigma'_{vo} + s_u \cdot (1 - \frac{1}{\sin \phi'})$$

$$u_2 = u_o + \frac{4}{3} \cdot \ln I_R \cdot s_u + K_0 \cdot \sigma'_{vo} + s_u \cdot (1 - \frac{1}{\sin \phi'})$$

$$q_t - u_2 = [\sigma_{vo} + N_{kt} \cdot s_u] - [u_o + \frac{4}{3} \ln I_R \cdot s_u + K_0 \cdot \sigma'_{vo} + s_u \cdot (1 - \frac{1}{\sin \phi'})]$$

$$q_t - u_2 = \sigma'_{vo}(1 - K_0) + [N_{kt} \cdot s_u] - \frac{4}{3} \cdot \ln I_R \cdot s_u - s_u \cdot (1 - \frac{1}{\sin \phi'})$$

$$q_t - u_2 = \sigma'_{vo}(1 - K_0) + s_u [N_{kt} - \frac{4}{3} \cdot \ln I_R - 1 + \frac{1}{\sin \phi'})$$

$$\frac{[q_t - u_2]}{\sigma'_{vo}} = [(1 - K_0)] + \frac{s_u}{\sigma'_{vo}} \left[N_{kt} - \frac{4}{3} \cdot \ln I_R - 1 + \frac{1}{\sin \phi'}\right]$$

$$\frac{[q_t - u_2]}{\sigma'_{vo}} - [(1 - K_0)] = S^* OCR^{\Lambda} \left[N_{kt} - \frac{4}{3} \cdot \ln I_R - 1 + \frac{1}{\sin \phi'}\right]$$

$$OCR^{\Lambda} = \frac{(q_t - u_2/\sigma'_{vo}) - (1 - K_o)}{\left(N_{kt} - 1 + \frac{1}{sin}\emptyset - 1.33 \ln I_R\right)(S^*)}$$

$$N_{kt} = 3.4 + 1.6 \ln I_R - 1.9\Delta + 1.3\alpha_c$$

$$\Delta = \frac{\sigma'_{vo} \cdot (1 - K_o)}{2 s_u} = \frac{\sigma'_{vo} \cdot (1 - K_o)}{2 \cdot S^* OCR^{\Lambda} \sigma'_{vo}}$$

$$OCR^{\Lambda} = \frac{(q_t - u_2/\sigma'_{vo}) - (1 - K_o)}{\left(N_{kt} - 1 + \frac{1}{sin\emptyset} - 1.33 \ln I_R\right)(S^*)}$$

$$OCR^{\Lambda} = \frac{(q_t - u_2/\sigma'_{vo}) - (1 - K_o)}{\left(2.4 + 0.26 \ln I_R - \frac{1.9(1 - K_o)}{2 \cdot S^* OCR^{\Lambda}} + 1.3\alpha_c + \frac{1}{sin\emptyset}\right)(S^*)}$$

$$OCR^{\Lambda} = \frac{(q_t - u_2/\sigma'_{vo}) - (1 - K_o)}{\left(2.4 + 0.26 \ln I_R + 1.3\alpha_c + \frac{1}{sin\emptyset}\right)(S^*) - \frac{0.95(1 - K_o)}{OCR^{\Lambda}}}$$

$$OCR^{\Lambda}\left(2.4 + 0.26 \ln I_R + 1.3\alpha_c + \frac{1}{sin\emptyset}\right)(S^*) - 0.95(1 - K_o) = \left(\frac{q_t - u_2}{\sigma'_{vo}}\right) - (1 - K_o)$$

$$OCR^{\Lambda}\left(2.4 + 0.26 \ln I_R + 1.3\alpha_c + \frac{1}{sin\emptyset}\right)(S^*) = \left(\frac{q_t - u_2}{\sigma'_{vo}}\right) - 0.05(1 - K_o)$$

$$OCR^{\Lambda} = \frac{(q_t - u_2/\sigma'_{vo}) - 0.05\,(1 - K_o)}{(S^*)(2.4 + 0.26 \ln {}_R + 1.3\alpha_c + \frac{1}{sin\emptyset})}$$

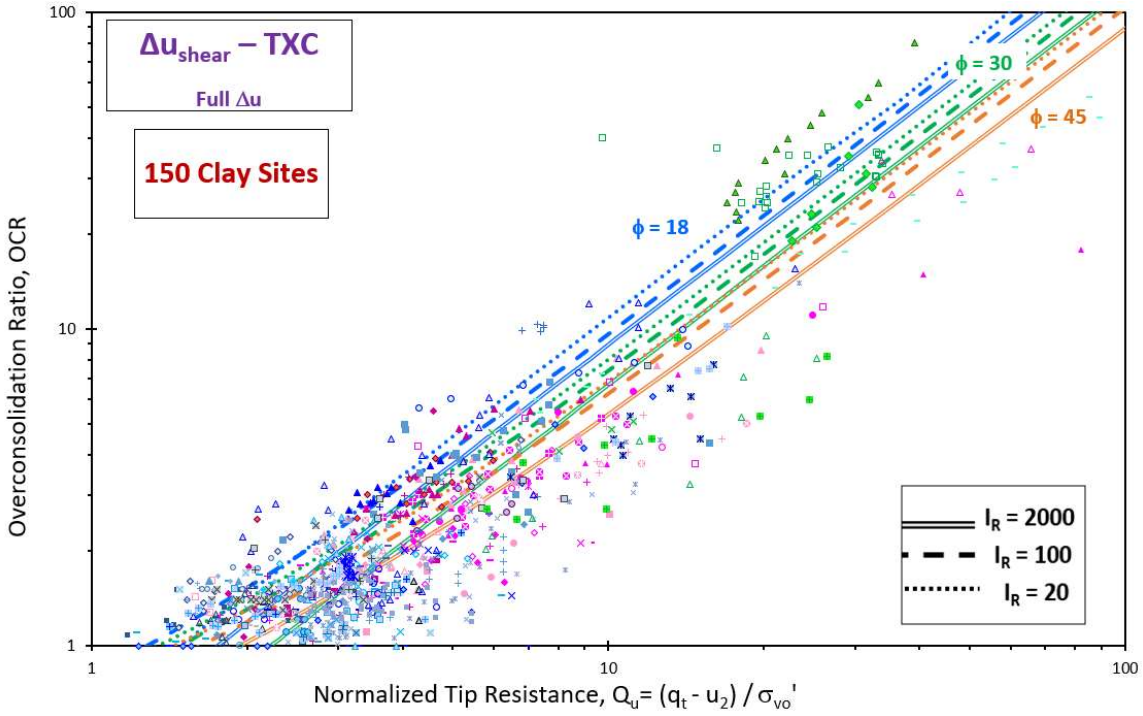


Figure I.4. Overconsolidation ratio versus normalized effective cone tip resistance ($Q_u$) for full excess porewater pressure from conventional triaxial compression test for different effective friction angle and rigidity index values

## Simplified CSSM

Derivation of OCR as a function of normalized porewater pressure (U*)

$$s_u = S^* OCR^{\Lambda} \sigma'_{vo}$$

$$\Delta u = \Delta u_{oct} + \Delta u_{sh}$$

$$\Delta u_{oct} = \frac{4}{3} \cdot \ln I_R \cdot s_u$$

$$\Delta u_{sh} = \sigma'_{vo} \cdot [1 - ({}^{OCR}/_{2})^{\Lambda}]$$

$$\Delta u = \frac{4}{3} \cdot \ln I_R \cdot s_u + \sigma'_{vo} \cdot [1 - \left({}^{OCR}/_{2}\right)^{\Lambda}]$$

$$\frac{\Delta u}{\sigma'_{vo}} = \frac{s_u}{\sigma'_{vo}} \left[\frac{4}{3} \cdot \ln I_R\right] + [1 - \left({}^{OCR}/_{2}\right)^{\Lambda}]$$

$$\frac{\Delta u}{\sigma'_{vo}} - 1 = \frac{s_u}{\sigma'_{vo}} \left[\frac{4}{3} \cdot \ln I_R\right] - \left({}^{OCR}/_{2}\right)^{\Lambda}$$

$$\frac{\Delta u}{\sigma'_{vo}} - 1 = S^* OCR^{\Lambda} \left[\frac{4}{3} \cdot \ln I_R\right] - ({}^{OCR}/_{2})^{\Lambda}$$

$$\frac{\Delta u}{\sigma'_{vo}} - 1 = OCR^{\Lambda} \cdot [S^* \cdot \frac{4}{3} \cdot \ln I_R - \left({}^{1}/_{2}\right)^{\Lambda}]$$

$$OCR^{\Lambda} = \frac{({}^{\Delta u}/_{\sigma'_{vo}}) - 1}{(S^*)(1.33 \ln {}_{R}) - 0.5^{\Lambda}}$$

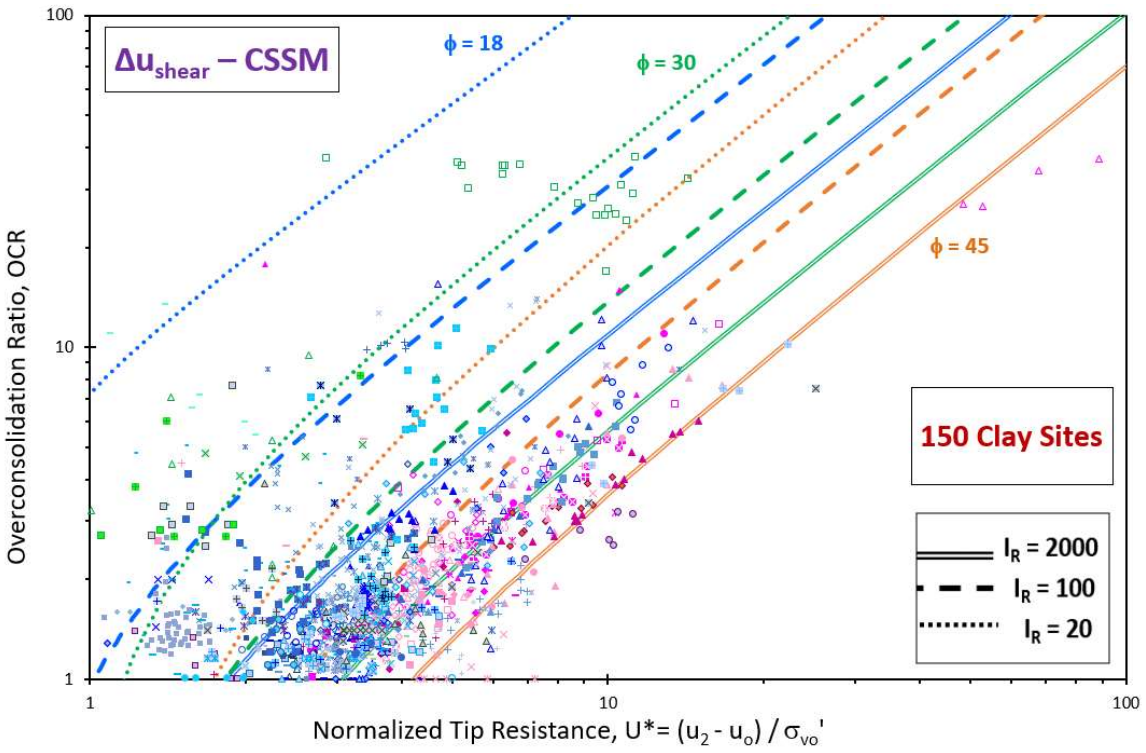


Figure I.5. Overconsolidation ratio versus normalized porewater pressure (U*) for CSSM approximate shear-induced excess porewater pressure for different effective friction angle and rigidity index values

## Simplified CSSM

Derivation of OCR as a function of normalized effective cone resistance ($Q_u$)

$$N_{kt} = \frac{q_{net}}{s_u} = \frac{q_t - \sigma_{vo}}{s_u}$$

$$q_t = \sigma_{vo} + N_{kt} \cdot s_u$$

$$\Delta u_{sh} = \sigma'_{vo} \cdot [1 - (OCR/2)^{\Lambda}]$$

$$\Delta u = \frac{4}{3} \cdot \ln I_R \cdot s_u + \sigma'_{vo} \cdot [1 - (OCR/2)^{\Lambda}]$$

$$u_2 = u_o + \frac{4}{3} \cdot \ln I_R \cdot s_u + \sigma'_{vo} \cdot [1 - (OCR/2)^{\Lambda}]$$

$$q_t - u_2 = [\sigma_{vo} + N_{kt} s_u] - u_o - [\frac{4}{3} \cdot \ln I_R \, s_u + \sigma'_{vo} [1 - (OCR/2)^{\Lambda}]$$

$$q_t - u_2 = \sigma'_{vo} \left( (OCR/2)^{\Lambda} \right) + s_u \, [N_{kt} - \frac{4}{3} \cdot \ln I_R]$$

$$\frac{[q_t - u_2]}{\sigma'_{vo}} = \left( (OCR/2)^{\Lambda} \right) + \frac{s_u}{\sigma'_{vo}} \left[ N_{kt} - \frac{4}{3} \cdot \ln I_R \right]$$

$$\frac{[q_t - u_2]}{\sigma'_{vo}} = \left( (OCR/2)^{\Lambda} \right) + S^* OCR^{\Lambda} \left[ N_{kt} - \frac{4}{3} \cdot \ln I_R \right]$$

$$\frac{[q_t - u_2]}{\sigma'_{vo}} = OCR^{\Lambda} \{ (1/2)^{\Lambda} + S^* \left[ N_{kt} - \frac{4}{3} \cdot \ln I_R \right] \}$$

$$OCR^{\Lambda} = \frac{(q_t - u_2 / \sigma'_{vo})}{(N_{kt} - 1.33 \ln I_R)(S^*) + 0.5^{\Lambda}}$$

By expanding for $N_{kt}$

$$N_{kt} = 3.4 + 1.6 \ln I_R - 1.9\Delta + 1.3\alpha_c$$

$$\Delta = \frac{\sigma'_{vo} \cdot (1-K_o)}{2s_u} = \frac{\sigma'_{vo} \cdot (1-K_o)}{2 \cdot S^* OCR^{\Lambda} \sigma'_{vo}}$$

$$OCR^{\Lambda} = \frac{\left(q_t - \frac{u_2}{\sigma'_{vo}}\right)}{(N_{kt} - 1.33 \ln I_R)(S^*) + 0.5^{\Lambda}}$$

$$OCR^{\Lambda} = \frac{\left(q_t - \frac{u_2}{\sigma'_{vo}}\right)}{\left(3.4 + 0.26 \ln I_R - \frac{1.9(1-K_o)}{2 \cdot S^* OCR^{\Lambda}} + 1.3\alpha_c\right)(S^*) + 0.5^{\Lambda}}$$

$$OCR^{\Lambda} = \frac{\left(q_t - \frac{u_2}{\sigma'_{vo}}\right)}{(3.4 + 0.26 \ln I_R + 1.3\alpha_c)(S^*) - \frac{0.95(1-K_o)}{OCR^{\Lambda}} + 0.5^{\Lambda}}$$

$$OCR^{\Lambda}\left[(3.4 + 0.26 \ln I_R + 1.3\alpha_c)(S^*) + 0.5^{\Lambda}\right] = \left(q_t - \frac{u_2}{\sigma'_{vo}}\right) + 0.95\,(1-K_o)$$

$$OCR^{\Lambda} = \frac{(q_t - u_2/\sigma'_{vo}) + 0.95\,(1-K_o)}{(S^*)(3.4 + 0.26 \ln I_R + 1.3\alpha_C) + 0.5^{\Lambda}}$$

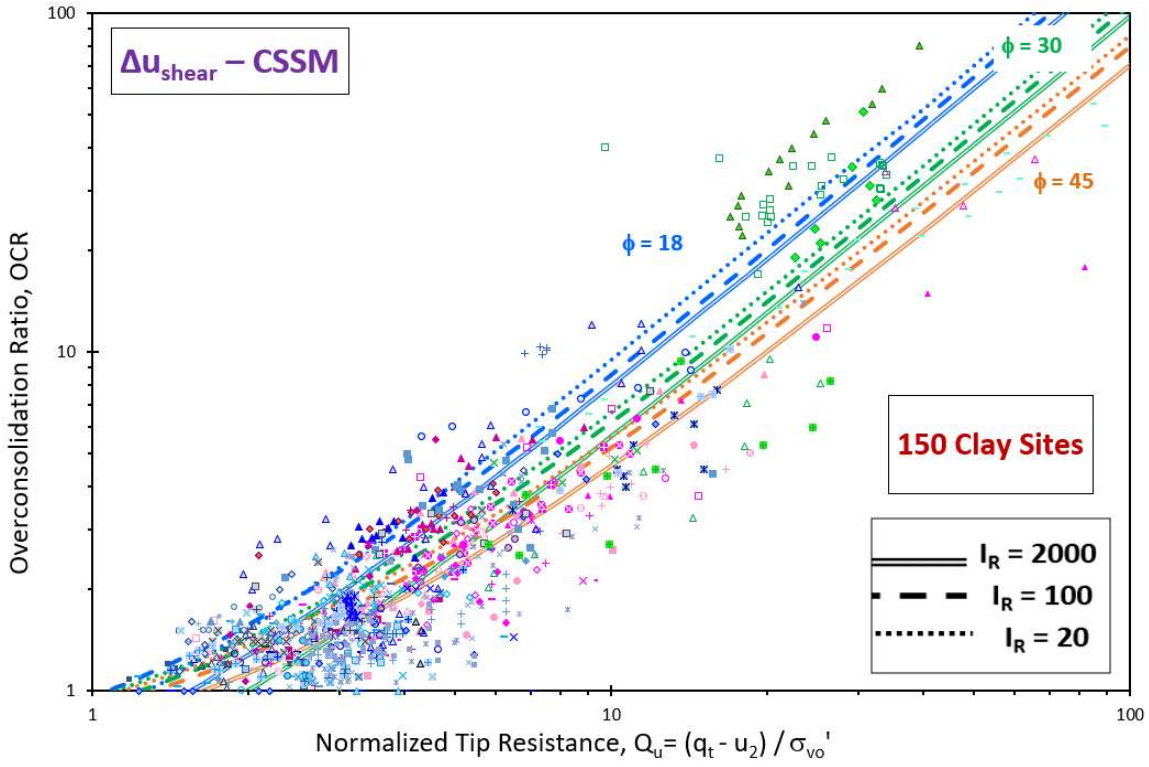


Figure I.6. Overconsolidation ratio versus normalized effective cone tip resistance ($Q_u$) for CSSM approximate shear-induced excess porewater pressure for different effective friction angle and rigidity index values

## Horizontal DSS Test

Derivation of OCR as a function of normalized porewater pressure (U*)

$$s_u = S^* OCR^{\Lambda} \sigma'_{vo}$$

$$\Delta u = \Delta u_{oct} + \Delta u_{sh}$$

$$\Delta u_{oct} = \frac{4}{3} \cdot \ln I_R \cdot s_u$$

$$\Delta u_{sh} = \sigma'_{vo} \cdot (1 - \frac{1}{2} \cos \phi' \cdot OCR^{\Lambda}) \cdot K_o$$

$$\Delta u = \frac{4}{3} \cdot \ln I_R \cdot s_u + \sigma'_{vo} \cdot (1 - \frac{1}{2} \cos \phi' \cdot OCR^{\Lambda}) \cdot K_o$$

$$\frac{\Delta u}{\sigma'_{vo}} = \frac{s_u}{\sigma'_{vo}} \left[\frac{4}{3} \cdot \ln I_R\right] + (1 - \frac{1}{2} \cos \phi' \cdot OCR^{\Lambda}) \cdot K_o$$

$$\frac{\Delta u}{\sigma'_{vo}} - K_o = \frac{s_u}{\sigma'_{vo}} \left[\frac{4}{3} \cdot \ln I_R\right] - (\frac{K_o}{2} \cos \phi' \cdot OCR^{\Lambda})$$

$$\frac{\Delta u}{\sigma'_{vo}} - K_o = S^* OCR^{\Lambda} \left[\frac{4}{3} \cdot \ln I_R\right] - (\frac{K_o}{2} \cos \phi' \cdot OCR^{\Lambda})$$

$$\frac{\Delta u}{\sigma'_{vo}} - K_o = OCR^{\Lambda} \cdot [S^* \cdot \frac{4}{3} \cdot \ln I_R - \frac{K_o}{2} \cos \phi']$$

$$OCR^{\Lambda} = \frac{(\Delta u / \sigma'_{vo}) - K_o}{(S^*)(1.33 \ln I_R) - \frac{K_o}{2} cos\emptyset}$$

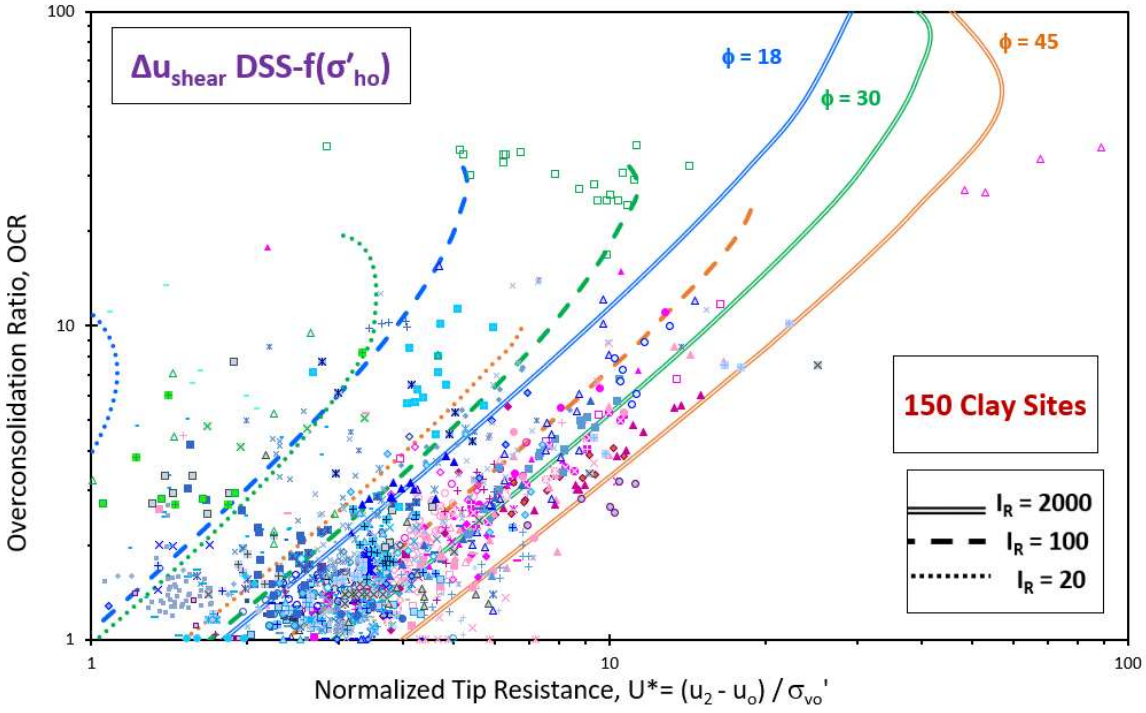


Figure I.7. Overconsolidation ratio versus normalized porewater pressure (U*) for shear-induced excess porewater pressure from DSS-f($\sigma'_{ho}$) for different effective friction angle and rigidity index values

## Horizontal DSS Test

Derivation of OCR as a function of normalized effective cone resistance ($Q_u$)

$$N_{kt} = \frac{q_{net}}{s_u} = \frac{q_t - \sigma_{vo}}{s_u}$$

$$q_t = \sigma_{vo} + N_{kt} \cdot s_u$$

$$\Delta u_{sh} = \sigma'_{vo} \cdot (1 - \frac{1}{2}\cos\phi' \cdot OCR^{\Lambda}) \cdot K_o$$

$$\Delta u = \frac{4}{3} \cdot \ln I_R \cdot s_u + \sigma'_{vo} \cdot (1 - \frac{1}{2}\cos\phi' \cdot OCR^{\Lambda}) \cdot K_o$$

$$u_2 = u_o + \frac{4}{3} \cdot \ln I_R \cdot s_u + \sigma'_{vo} \cdot (1 - \frac{1}{2}\cos\phi' \cdot OCR^{\Lambda}) \cdot K_o$$

$$q_t - u_2 = [\sigma_{vo} + N_{kt} s_u] - u_o - [\frac{4}{3} \cdot \ln I_R \, s_u + \sigma'_{vo}(1 - \frac{1}{2}\cos\phi' \cdot OCR^{\Lambda}) \cdot K_o]$$

$$q_t - u_2 = \sigma'_{vo}\left(1 - K_o + \frac{K_o}{2}\cos\phi' \cdot OCR^{\Lambda}\right) + s_u\,[N_{kt} - \frac{4}{3} \cdot \ln I_R]$$

$$\frac{[q_t - u_2]}{\sigma'_{vo}} = \left(1 - K_o + \frac{K_o}{2}\cos\phi' \cdot OCR^{\Lambda}\right) + \frac{s_u}{\sigma'_{vo}}\left[N_{kt} - \frac{4}{3} \cdot \ln I_R\right]$$

$$\frac{[q_t - u_2]}{\sigma'_{vo}} = \left(1 - K_o + \frac{K_o}{2}\cos\phi' \cdot OCR^{\Lambda}\right) + S^* OCR^{\Lambda}\left[N_{kt} - \frac{4}{3} \cdot \ln I_R\right]$$

$$\frac{[q_t - u_2]}{\sigma'_{vo}} = (1 - K_o) + OCR^{\Lambda}\{\left(\frac{K_o}{2}\cos\phi'\right) + S^*\left[N_{kt} - \frac{4}{3} \cdot \ln I_R\right]\}$$

$$OCR^{\Lambda} = \frac{\left(q_t - \frac{u_2}{\sigma'_{vo}}\right) - (1 - K_o)}{(N_{kt} - 1.33 \ln I_R)(S^*) + 0.5\, cos\emptyset\, K_o}$$

By expanding for $N_{kt}$

$$N_{kt} = 3.4 + 1.6\ \ln I_R - 1.9\Delta + 1.3\alpha_c$$

$$\Delta = \frac{\sigma'_{vo} \cdot (1-K_o)}{2s_u} = \frac{\sigma'_{vo} \cdot (1-K_o)}{2 \cdot S^* OCR^{\Lambda} \sigma'_{vo}}$$

$$OCR^{\Lambda} = \frac{\left(q_t - \frac{u_2}{\sigma'_{vo}}\right) - (1-K_o)}{(N_{kt} - 1.33 \ln I_R)(S^*) + 0.5\, cos\emptyset\, K_o}$$

$$OCR^{\Lambda} = \frac{\left(q_t - \frac{u_2}{\sigma'_{vo}}\right) - (1-K_o)}{\left(3.4 + 0.26 \ln I_R - \frac{1.9(1-K_o)}{2 \cdot S^* OCR^{\Lambda}} + 1.3\alpha_c\right)(S^*) + 0.5\, cos\emptyset\, K_o}$$

$$OCR^{\Lambda} = \frac{\left(q_t - \frac{u_2}{\sigma'_{vo}}\right) - (1-K_o)}{(3.4 + 0.26 \ln I_R + 1.3\alpha_c)(S^*) - \frac{0.95(1-K_o)}{OCR^{\Lambda}} + 0.5\, cos\emptyset\, K_o}$$

$$OCR^{\Lambda}[(3.4 + 0.26 \ln I_R + 1.3\alpha_c)(S^*) + 0.5\, cos\emptyset\, K_o] = \left(q_t - \frac{u_2}{\sigma'_{vo}}\right) - 0.05\,(1-K_o)$$

$$OCR^{\Lambda} = \frac{\left(q_t - \frac{u_2}{\sigma'_{vo}}\right) - 0.05\,(1-K_o)}{(S^*)(3.4 + 0.26 \ln I_R + 1.3\alpha_C) + 0.5\, cos\emptyset\, K_o}$$

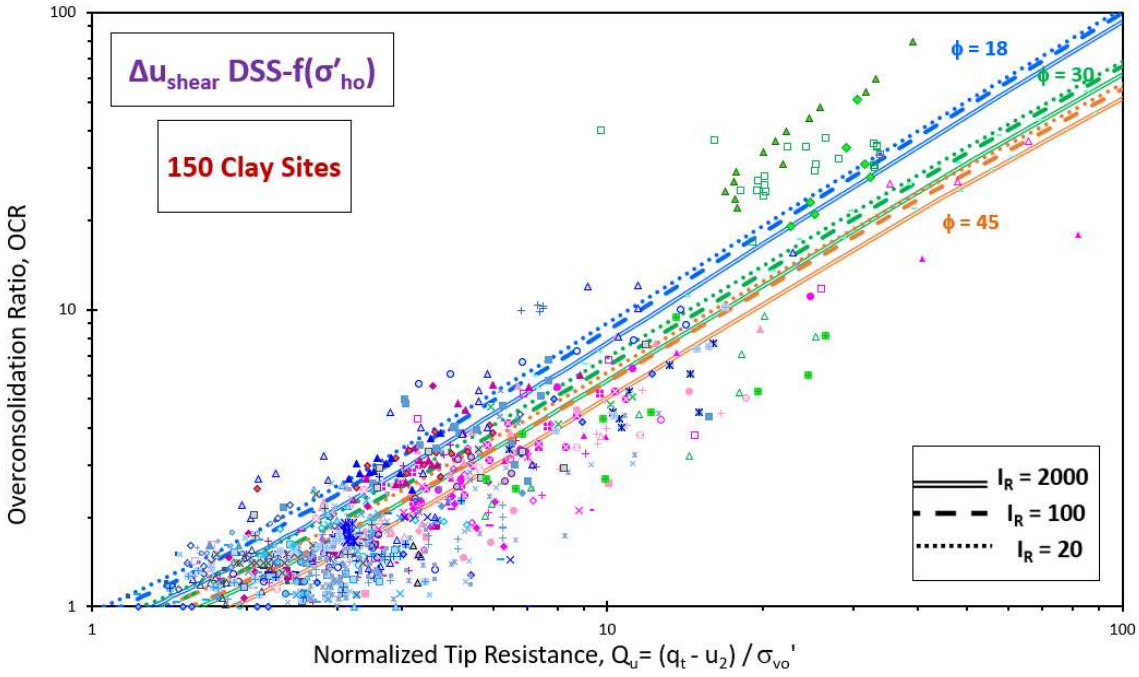


Figure I.8. Overconsolidation ratio versus normalized effective cone tip resistance ($Q_u$) for shear-induced excess porewater pressure from DSS-f($\sigma'_{ho}$) for different effective friction angle and rigidity index values

# APPENDIX J

## Relationship between
## Undrained Shear Strength
## and Shear Wave Velocity for Clays

# Relationship between Undrained Shear Strength and Shear Wave Velocity for Clays

Shehab S. AGAIBY[a,1] and Paul W. MAYNE[a]

[a] *Georgia Institute of Technology, Atlanta, United States*

**Abstract.** The interrelationship between undrained shear strength ($s_u$) and downhole shear wave velocity ($V_{sVH}$) of normally consolidated (NC) and lightly overconsolidated (LOC: OCR < 2) to overconsolidated (OC) to highly overconsolidated (HOC: OCR > 10) clays is investigated in the presented study. The main objective of this research program is to develop a worldwide database of high quality in-situ geophysical and laboratory strength data from thirty-seven well-documented geotechnical sites from locations in Australia, Brazil, Canada, China, Italy, Japan, South Korea, North Sea, Norway, Singapore, Sweden, Thailand, United Kingdom, USA, and Vietnam. The study includes undrained shear strength measurements on undisturbed samples of normally to lightly overconsolidated intact to overconsolidated and fissured clays using anisotropically-consolidated triaxial compression tests (CAUC). Shear wave velocities were measured in the field by downhole tests (DHT), in many cases via seismic piezocones (SCPTu). Analyses of the compiled database found approximate trends between undrained shear strength and shear wave velocity. Tentative correlations are explored by including other various parameters such as Atterberg limits, void ratio, overconsolidation ratio (OCR), and effective vertical stresses. The correlative trends may aid geotechnical engineers in helping to assess $s_u$ profiles in clay deposits in

[1] Corresponding Author: Geosystems Engineering Group, School of Civil and Environmental Engineering, Georgia Institute of Technology, 790 Atlantic Drive, Atlanta, Georgia, USA 30332-0355
Email: sagaiby3@gatech.edu

preliminary investigations and as an independent method in collaboration with sampling, lab testing, and other field data.

**Keywords.** Clays, Downhole Test, OCR, Shear Wave Velocity, Triaxial Tests, Undrained Shear Strength

## 1. Introduction

The profiling of in-situ shear wave velocity provides a means to evaluate several soil parameters such as stiffness, unit weight and stress history [1]. For the purpose of the current study, the focus is on the estimation of undrained shear strength ($s_u$) from shear wave velocity ($V_s$) that is measured in the field using either in-situ tests or geophysical methods. Accurate and detailed in-situ $V_s$ measurements are critical and essential for the fields of geotechnics and geophysics and can be utilized to provide an acceptable estimate of the undrained shear strength without the need to use low quality disturbed samples and/or rely on uncertain results from laboratory tests affected by sample preparation or reconsolidation procedures.

## 2. Undrained Shear Strength Measurement

Undrained shear strength ($s_u$) is considered one of the most critical parameters in geotechnical engineering practice and design. The measured undrained shear strength is affected by many variables, including: initial stress state (isotropic or $K_0$ consolidation), strength anisotropy, loading direction (compression or extension), and boundary conditions (plane strain or triaxial) defining the shearing mode in the test. Other influencing factors include: strain rate, sensitivity, ageing, inherent fabric anisotropy, strain compatibility, thixotropy, and specimen quality associated with

sampling disturbance [2]. A comparison of different testing methods in the lab: $K_o$ consolidated triaxial compression & extension tests ($CK_0UC$ & $CK_0UE$), direct simple shear test (DSS) and in the field: field vane test (FV) for measuring $s_u$ is given in Figure 1(a) that shows the significance of shearing mode for soft clay at the national geotechnical experimentation site of Bothkennar, UK [3]. At a depth of 6 m, for instance, $s_u$ varies by a factor of over 3 for these four modes.

### 3. Shear Wave Velocity Measurement

A key parameter for static and dynamic geotechnical analyses is the small-strain shear modulus ($G_{max}$) which represents the initial fundamental stiffness of soils and rocks. The shear modulus is obtained from shear wave velocity ($V_s$) and the total mass density ($\rho$), where: $G_{max} = G_0 = \rho \cdot V_s^2$. The value of $G_{max}$ can be determined using either in-situ and/or laboratory methods. Laboratory methods include testing undisturbed soil specimens using resonant column, torsional shear, bender elements, shear plates, non-resonance methods, and/or triaxial tests with local strain measurements. Lab-based techniques have several shortcomings; including sampling disturbance that may break weak inter-particle bonds, stress relief, in addition to ageing, diagenesis, and depositional process effects; that could affect small-strain stiffness measurements. Hence, $V_s$ is most reliably measured in-situ rather than in the laboratory. The shear wave has directional and polarized characteristics, multiple types of $V_s$ can be measured: $V_{sij}$ where 'i' is the direction of propagation and 'j' is the direction of polarization ($V_{sVH}$, $V_{sHV}$, and $V_{sHH}$) where subscripts 'V' is for vertical and 'H' is for horizontal. For in-situ measurements, the most common shear wave mode is obtained by downhole testing DHT (ASTM D 7400) measuring the $V_{sVH}$ mode (the focus of current study), which is carried out in either drilled-cased-grouted boreholes or by

seismic CPT or seismic DMT. By comparing different in-situ methods for $V_s$, it is obvious that the specific methods provide different resolutions for $V_s$ measurements at different depths. To illustrate, Figure 1(b) shows profiles of measured $V_{sVH}$, $V_{sHV}$, $V_{sHH}$, and $V_s$ measured using Rayleigh waves ($V_{sRW}$) in soft clay at Bothkennar, UK [3].

By examining prior correlations reported by researchers, it is evident that there is no unique relation between undrained shear strength and shear wave velocity. Hence, a global study was undertaken that includes data from well documented clays.

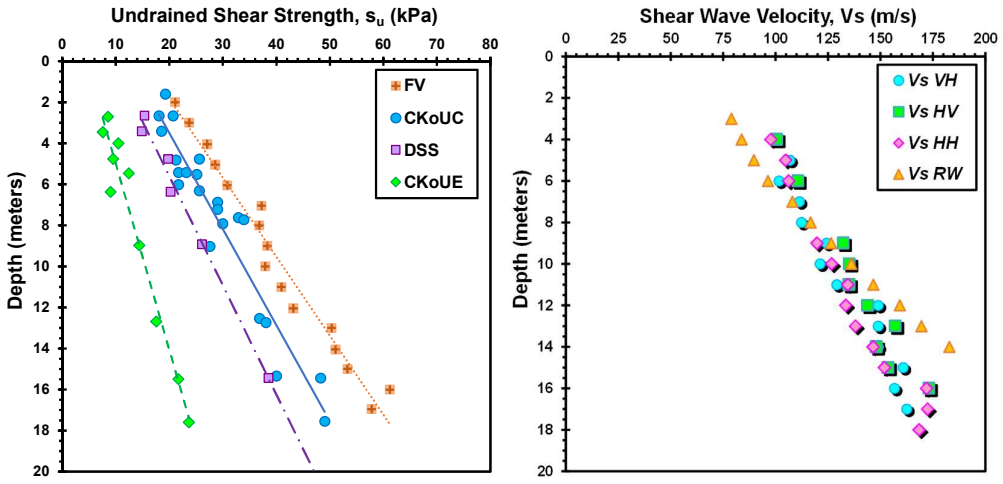


(a) (b)

**Figure 1. (a)** Profiles of four different undrained shear strength modes **(b)** Profiles of four different shear wave velocity modes in Bothkennar soft clay, UK [3]

## 4. Compiled $s_{uTC}$ and $V_{sVH}$ Database

For the current comprehensive study, a special database has been carefully collected from a total of 37 well-documented worldwide geotechnical test sites. The sites mostly include soft to firm young to aged clays, but also consider stiff to hard clays, and fissured fine-grained soils. For the undrained shear strength, only high-end laboratory

tests were included with a focus on the triaxial compression mode, designated $s_{uTC}$. Regarding the shear wave velocity, only in-situ data were compiled using downhole shear wave velocity, $V_{sVH}$ which is primarily measured using DHT, SCPT, and SDMT. At each of the studied sites, complementary data included in-situ void ratio ($e_o$) and one-dimension consolidation tests for stress history profiles that were obtained from published sources with detailed understanding of the site-specific geologic conditions. In addition, laboratory data such as water content, Atterberg limits, and unit weight were collected. The compiled database can be classified into two main categories: (1) soft to firm NC to LOC clays that have 1 < OCRs < 2.5. These are presented in Table 1 and include 31 clay sites with a total 360 CAUC or $CK_oUC$ tests with their corresponding $V_{sVH}$ measurements; (2) overconsolidated (OC) clays that have OCRs > 2.5. The latter are listed in Table 2 with 6 clay sites with a total of 60 CAUC or $CK_0UC$ tests along with their corresponding $V_{sVH}$ values at same elevations.

## 5. Relationship between Undrained Shear Strength and Shear Wave Velocity

By considering the geotechnical sites from Table 1, Figure 2 shows the mean trend plus or minus 2 standard deviations between $s_{uTC}$ (measured in kPa) and $V_{sVH}$ (measured in m/sec) for NC to LOC clays to be:

$$s_{uTC} = 0.152 \cdot V_{sVH}^{1.14} \quad (1)$$

**Table 1.** Summary of Compiled $s_{uTC}$ and $V_{sVH}$ Database for Intact Normally Consolidated (NC) to Lightly Overconsolidated (LOC) Clays

| Site + Location | Soil Type | Reference Sources + Index |
|---|---|---|
| Amherst, MA, USA | Soft Varved | DeGroot & Lutenegger (2003) [4]; Hegazy (1998) [5] |
| Ariake, Japan | Soft Clay | Tanaka, et al. (2001) [6] |
| Backebol, Sweden | Postglacial | Larsson(1980) [7]; Larsson& Mulabdic (1991) [8,9] |
| Ballina, Australia | Soft Estuarine | Pineda, et al. (2014) [10] |
| Belfast, Ireland | Soft Clay Silt | Lehane (2003) [11] |
| Bothkennar, UK | Soft Silty Clay | Hight, et al. (2003) [3] |
| Burswood, Australia | Soft Clay | Low, et al. (2011) [12] |
| Busan, Korea | Soft Clay | Chung, et al. (2011 & 2012) [13 & 14] |
| Chicago, IL, USA | Glacial Clay | Chung & Finno (1992) [15]; Finno et al (2000) [16] |
| Fiumicino, Italy | Soft Clay | Cavalera & Scarpelli (1980) [17]; Monaco (2007)[18] |
| Hai-Phong, Vietnam | Soft Alluvial | Watabe, et al. (2004) [19] |
| Islais Creek, CA, USA | Soft Bay Mud | Pestana, et al. (2002) [20] |
| Kurihama, Japan | Alluvial | Tanaka (1995) [21]; Shibuya & Tanaka (1996) [22] |
| Lake Bonneville, UT, USA | Sensitive Clay | Garner (2007) [23]& Cole (2003) [24] |
| Lianyungang, China | Soft Clay | Liu, et al. (2008) [25] |
| Lierstranda, Norway | Sensitive Clay | Lunne & Lacasse (1999) [26] |
| Lilla Mellosa, Sweden | Soft Organic | Larsson & Mulabdic (1991 a, b) [8, 9] |
| Louiseville, Quebec, Canada | Champlain Sea | Leroueil (2003)[27]; Yafrate & DeJong (2006) [28] |
| Newbury, MA, USA | Soft Silty Clay | Landon (2007) [29] |
| Nong Ngu Hao, Thailand | Soft Bangkok | Shibuya & Tamrakar (2002)[30] |
| Norrkoping, Sweden | Varved Clay | Kennet (1994) [31]; Larsson & Mulabdic (1991)[8, 9] |

| Site + Location | Soil Type | Reference Sources + Index |
|---|---|---|
| Northwestern Univ. IL, USA | Soft Clay | Finno, et al (2000) [16] |
| Onsoy, Norway | Soft Marine | Lunne, et al. (2003) [32] |
| Pentre, UK | Silt Deposit | Lambson, et al. (1993) [33] |
| Sarapui, Brazil | Very Soft Clay | Ortigao (1983) [34]; Almeida & Marques (2003) [35] |
| Saro Road 6/900, Sweden | Soft Organic | Larsson & Mulabdic (1991 a, b) [8, 9] |
| Saro Road 7/600, Sweden | Organic Clay | Larsson & Mulabdic (1991 a, b) [8, 9] |
| Singapore Clay, Singapore | Soft Marine | Tanaka, et al. (2001) [6] |
| South Gloucester, Canada | Sensitive Leda | Bozozuk (1972)[36]; Yafrate & DeJong (2006) [28] |
| Sutthisan, Thailand | Soft Bangkok | Shibuya & Tamrakar (2002) [30] |
| Troll, North Sea | Soft Clay | Lunne, et al. (2007) [37] |

**Table 2.** Summary of Compiled $s_{uTC}$ and $V_{sVH}$ Database for Fissured and Overconsolidated (OC) Clays

| Site + Location | Soil Type | Reference Sources + Index |
|---|---|---|
| Beaumont Clay, TX, USA | Stiff Fissured | O'Neill &Yoon(1995) [38]; Mahar&O'Neill (1983)[39] |
| Brent Cross, UK | Fissured-HOC | Hight, et al. (2003) [40] |
| Heathrow - T5, UK | London Clay | Hight, et al. (2003) [40] |
| Montalto di Castro, Italy | Stiff OC Clay | Jamiolkowski, et al. (1982 & 1994) [41 & 42] |
| Pisa Clay, Italy | Pancone Clay | LoPresti, et al. (2003) [43] |
| Port of Anchorage, AK, USA | Stiff Clay | Zapata-Medina(2012)[44]; Mayne & Pearce(2005)[45] |

Similarly, by investigating the additional geotechnical sites listed in Table 2, Figure 3 shows the studied relation for all the clays under study, ranging from NC to LOC

obtained from Table 1 to OC and/or fissured HOC clays, the relationship between $s_{uTC}$ (measured in kPa) and $V_{sVH}$ (measured in m/sec) can be expressed as:

$$s_{uTC} = 0.0672 \cdot V_{sVH}^{1.33} \tag{2}$$

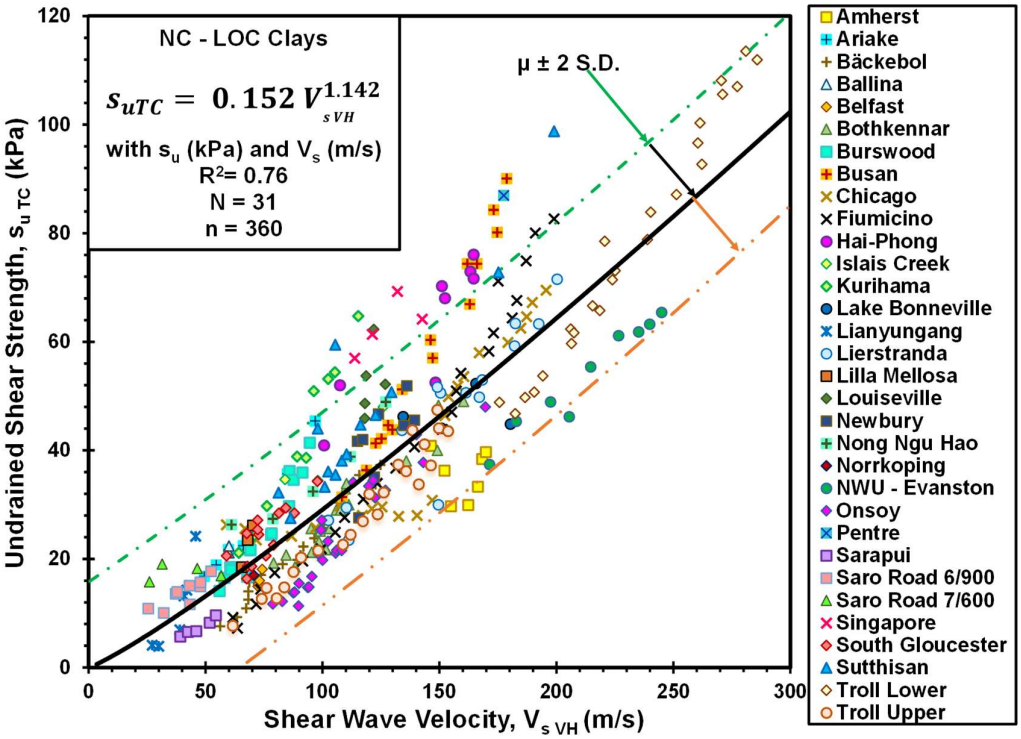


**Figure 2.** Triaxial compression undrained shear strength vs. downhole shear wave velocity for NC to LOC intact clays in arithmetic scale.

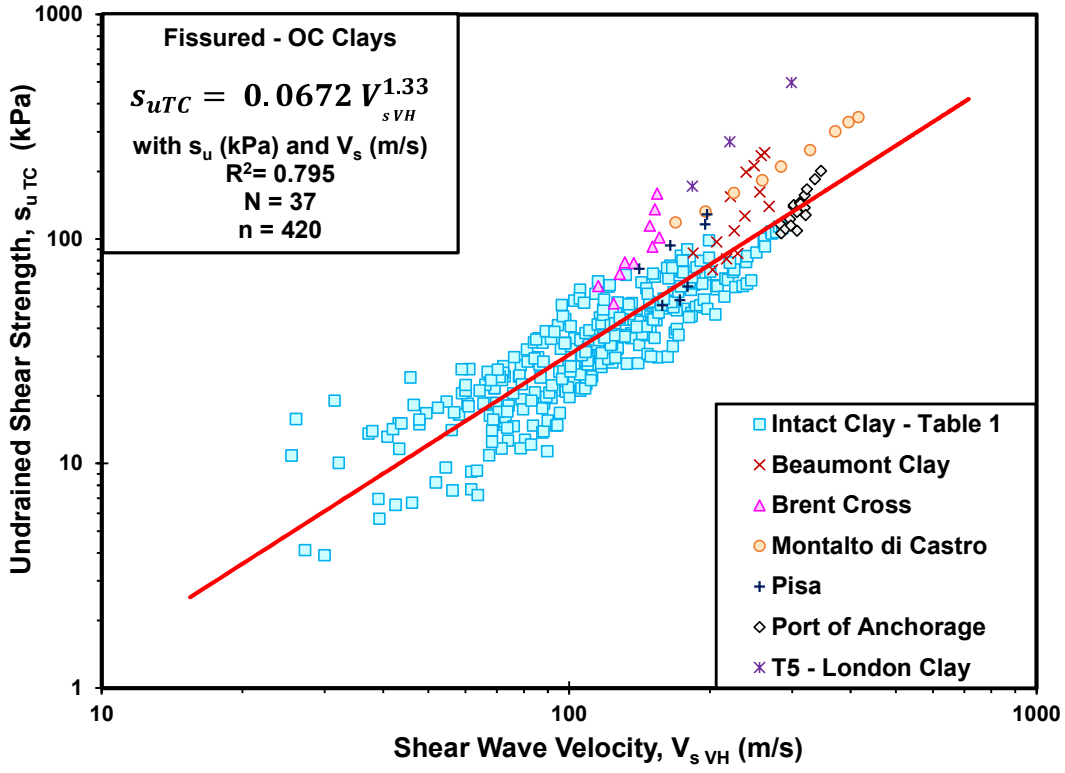


**Figure 3.** Triaxial compression undrained shear strength vs. downhole shear wave velocity for intact NC, LOC, to OC and HOC fissured clays in logarithmic scale.

### 6. Generalized Expression for $s_{uTC}$ and $V_{sVH}$

To gain a more comprehensive understanding for the studied relationship, a number of additional parameters were investigated such as stress history, void ratio, Atterberg limits, and effective vertical overburden stresses. In-situ shear wave velocity can be used as an index for the magnitude of preconsolidation stress of clays, where void ratio decreases when the clay deposit is subjected to higher pre-stressing leading to an increase in the magnitude of shear wave velocity [46]. According to basic expressions calculating the small strain shear modulus and undrained shear strength from the literature, it is evident that these parameters are both dependent on the stress history profile, expressed in the form of OCR.

Multiple regression analyses were used to combine different parameters and investigate their significance for the $s_{uTC}$ versus $V_{sVH}$ relations that produced a generalized expression. Figure 4 compares the actual measurements of $s_u$ (in kPa) to the estimated values using $V_{sVH}$ (in m/sec), $e_0$, OCR, PI (in %), and effective vertical stress (in kPa). The generalized expression obtained can be written as:

$$s_{uTC} = 0.038\left(V_{sVH}\right)^{1.083} PI^{0.14} OCR^{0.31} e_0^{\ 0.07} \left(\sigma'_{vo}\right)^{0.23} \tag{3}$$

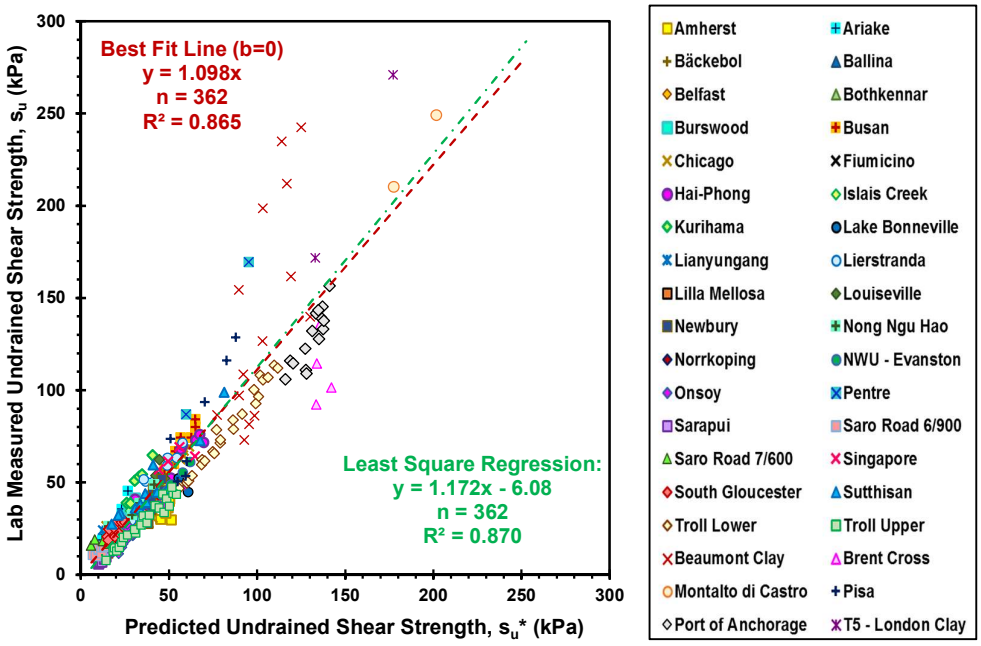


**Figure 4.** Measured $s_{uTC}$ vs. predicted value from $V_{sVH}$ for NC and OC clays using generalized expression.

By considering the results of multiple regression analyses, it can be noted that the predicted values for fissured and HOC clays from Table 2 do not agree well with the actual measurements, as in the case of intact and LOC clays. It can be also concluded that using more than three variables at a time (effective stresses, e, OCR, and PI) did not provide sufficiently good enough statistical results for correlations where low

significance level for the void ratio was observed, which is also expressed by the small exponent value. This can be attributed to the redundant effects between void ratio and OCR (or $\sigma_{vo}'$) such that a single variable dominates. When less variables (PI, effective stress and either $e_0$ or OCR) are involved, the overall correlations are improved albeit some outliers, discrepancies, and uncertainties still remain.

## 7. Conclusions

A careful compiled database study was analyzed to produce a general expression for evaluating undrained shear strength ($s_u$) from downhole shear wave velocity ($V_{sVH}$). The data were collected from 37 worldwide well-documented natural soils primarily covering NC to LOC intact soft to firm clays, but also included results from a few OC to HOC fissured clays. The study focused primarily on benchmark $s_u$ values obtained from high-level laboratory triaxial compression tests (CAUC) and in-situ downhole shear wave velocity measurements from downhole tests in cased boreholes or seismic piezocone tests.

## References


[1] P.W. Mayne, Integrated ground behavior: In-situ and lab tests, *Deformation Characteristics of Geomaterials*, **2** (Proc. Lyon, France), Taylor & Francis, (2005): 155-177.

[2] P.W. Mayne, M.R. Coop, S. Springman, A-B. Huang, and J. Zornberg, State-of-the-Art Paper (SOA-1): GeoMaterial Behavior and Testing. *Proc. 17th Intl. Conf. Soil Mechanics & Geotechnical Engineering*, **4** (ICSMGE, Alexandria, Egypt), Millpress/IOS Press Rotterdam: (2009): 2777-2872.

[3] D.W. Hight, M.A. Paul, B.F. Barras, J.J.M. Powell, D.F.T. Nash, P.R. Smith, R.J. Jardine, and D.H. Edwards. The characterisation of the Bothkennar clay. *Characterisation & Engineering Properties of Natural Soils*, ***1***, Balkema, Rotterdam, (2003): 543-597.

[4] D.J. DeGroot & A.J. Lutenegger, Geology and engineering properties of Connecticut Valley varved clay, *Characterization & Eng. Proprieties of Natural Soils* **1**, Balkema, Rotterdam, (2003): 695–724.

[5] Y.A. Hegazy, *Delineating Geostratigraphy by Cluster Analysis of Piezocone Data,* Doctoral Dissertation, School of Civil & Environmental Engineering, Georgia Institute of Technology, 1998.

[6] H. Tanaka, J. Locat, S. Shibuya, T.S. Tan, and R.S. Dinesh, Characterization of Singapore, Bangkok, and Ariake clays, *Canadian Geotechnical Journal* **38.2** (2001): 378-400.

[7] R. Larsson, Undrained shear strength in stability calculation of embankments and foundations on soft clays, *Canadian Geotechnical Journal* **17.4** (1980): 591-602.

[8] R. Larsson & M. Mulabdić, Shear moduli in Scandinavian clays: Report No.**40**, Swedish Geotechnical Institute, Linköping, (1991a): 127 p.

[9] R. Larsson & M. Mulabdić, Piezocone tests in clays: Report No.**42**, Swedish Geotechnical Institute, Linköping, (1991b): 240 p.

[10] J.A. Pineda, A. McConnell, and R.B. Kelly, Performance of an innovative direct-push piston sampler in soft clay. *Proc. CPT'14*, Las Vegas, Nevada (2014): 279 – 288.

[11] B.M. Lehane, Vertically loaded shallow foundation on soft clayey silt, *Proc. The Institution of Civil Engineers - Geotechnical Engineering 156.1* (2003): 17-26.

[12] H.E. Low, M.L. Maynard, M.F. Randolph, and D.J. DeGroot. Geotechnical characterisation and engineering properties of Burswood clay. *Géotechnique* **61.7** (2011): 575-591.

[13] S.G. Chung, Y.P. Hong, J.M. Lee, and S.C. Min, Evaluation of the undrained shear strength of Busan clay, *KSCE Journal of Civil Engineering* **16.5** (2012): 733-41.

[14] S.G. Chung, C.K. Ryu, S.C. Min, J.M. Lee, Y.P. Hong, and E. Odgerel, Geotechnical characterization of Busan clay, *KSCE Journal of Civil Engineering* **16.3** (2012): 341-50.

[15] C.K. Chung & R. Finno, Influence of depositional processes on the geotechnical parameters of Chicago glacial clays, *Engineering Geology* **32.4** (1992): 225-242.

[16] R.J. Finno, S.L. Gassman, and M. Cavello, The NGES at Northwestern Univ., National Geotechnical Experimentation Sites, *GSP* **93**, ASCE, Reston/Virginia, (2000): 130-159.

[17] L. Cavalera & G. Scarpelli, Anisotropy of the undrained strength of normally consolidated clays (in Italian), *G Riv Ital Geotec* **14, N3,** July–Sept (1980): 181-190.

[18] P. Monaco, S. Marchetti, and G. Totani, The flat dilatometer Test (DMT): design applications and recent developments, *Common Ground*, Proc. 10th Australia-New Zealand Conference on Geomechanics, Brisbane, Australia, 21-24 October, Vol. 2, (2007): 516-521.

[19] Y. Watabe, M. Tanaka, and J. Takemura, Evaluation of in-situ $K_o$ for Ariake, Bangkok and Hai-Phong clays, *Proc. The 2nd Int. Conf. on Site Characterization,* Porto, Portugal, Vol. 2 (2004): 1765-1772.

[20] J. Pestana, C. Hunt, and J. Bray, Soil deformation and excess pore pressure field around a closed-ended pile, *Journal of Geotechnical and Geoenvironmental Engineering* **128.1** (2002): 1-12.

[21] H. Tanaka, National Report-the Current State of CPT in Japan, *International Symposium on Cone Penetration Testing*: Linköping, Sweden, Sweden: Swedish Geotechnical Society, (1995): 115-124.

[22] S. Shibuya & H. Tanaka. Estimate of clastic shear modulus in Holocene soil deposits. *Soils and Foundations* **36.4** (1996): 45-55.

[23] M.P. Garner, *Loading rate effects on axial pile capacity in clays*. Doctoral Dissertation, Brigham Young Univ. Department of Civil and Environmental Engineering, Provo, Utah, 2007.

[24] R. Cole, *Full-Scale effects of passive earth pressure on the lateral resistance of pile caps*, Doctoral Dissertation, Dept. Civil and Environmental Eng, Brigham Young University, Provo, UT, 2003.

[25] S.Y. Liu, G.J. Cai, L.Y. Tong, and G.Y. Du, Approach on the engineering properties of Lianyungang marine clay from piezocone penetration tests. *Marine Georesour Geotechnol* **26 (3)**, (2008): 189-210.

[26] T. Lunne & S. Lacasse, Geotechnical characteristics of low plasticity clays, *Proc. International Symposium on Characterization of Soft Marine Clays*, Japan 26-28 February (1997): 33-56.

[27] S. Leroueil & K. Hamouche, Geotechnical characterization & properties of sensitive clay from Québec, *Characterization & Eng. Properties of Natural Soils* **2**. Lisse: Swets & Zeitlinger, (2003): 363-393.

[28] N.J. Yafrate & J.T. DeJong, Interpretation of sensitivity and remolded undrained shear strength with full flow penetrometers, *The Sixteenth International*

*Offshore and Polar Engineering Conference,* International Society of Offshore and Polar Engineers, San Francisco, CA, USA, (2006): 572-577.

[29] M.M. Landon, *Development of a non-destructive sample quality assessment method for soft clays*, Doctoral Dissertation, University of Massachusetts, Amherst, 2007.

[30] S. Shibuya & S.B. Tamrakar, Engineering properties of Bangkok clay. *Characterization and Engineering Properties of Natural Soils*. Balkema, Rotterdam, Netherlands (2002): 645-692.

[31] A. Kennet, Y. Yu, and B. Westerberg, Behavior and modelling of Swedish natural soft clays, *Proc. 13th ICSMFE,* New Delhi, India (1994): 57-60.

[32] T. Lunne, M. Long, and C. Forsberg, Characterization and engineering properties of Onsøy clay. *Characterization & Eng. Properties of Natural Soils* **1**, Lisse: Swets & Zeitlinger (2003): 395-428.

[33] M.D. Lambson, D.G. Clare, and R.M. Semple, Investigation and interpretation of Pentre and Tilbrook Grange soil conditions, Large-scale pile tests in clay: *Proc. Recent Large-scale Fully Instrumented Pile Tests in Clay*, Institution of Civil Engineers, London, 23-24 June 1992.

[34] J.A. Ramalho-Ortigao, M.L. Werneck, and A.L. Willy, Embankment failure on clay near Rio de Janeiro, *Journal of Geotechnical Engineering* **109.11** (1983): 1460-1479.

[35] M.S.S. Almeida, and M.E.S. Marques, The behavior of Sarapuí soft clay, *Characterization and Engineering Properties of Natural Soils*. Vol. 1, Lisse: Swets & Zeitlinger (2003): 477-504.

[36] M. Bozozuk, *The Gloucester test fill,* Doctoral Dissertation, Purdue University, 1972.

[37] T. Lunne, M. Long, and M. Uzielli, Characterization and engineering properties of Troll clay, *Characterization & Eng. Properties of Natural Soils*, Lisse: Swets & Zeitlinger **4** (2007):1939-1972.

[38] M.W. O'Neill & G. Yoon, Engineering properties of overconsolidated Pleistocene soils of Texas Gulf coast, *Transportation Research Record* **1479**, National Res. Council, Washington, DC (1995): 81-88.

[39] L.J. Mahar & M.W. O'Neill, Geotechnical characterization of desiccated clay, *Journal of Geotechnical Engineering* **109.1** (1983): 56 -71.

[40] D.W. Hight, F. McMillan, J.J.M. Powell, R.J. Jardine , & C.P. Allenou, Some characteristics of London clay, *Characterization & Eng. Properties of Natural Soils* **2**, Balkema, Rotterdam, (2003): 851–907.

[41] M. Jamiolkowski, R. Lancellotta, M.L. Tordella, and M. Battaglio, Undrained strength from CPT, *Proc. European Symposium on Penetration Testing*, Amsterdam (1982): 599-606.

[42] M. Jamiolkowski & D.C.F. LoPresti, Validity of in-situ tests related to real behavior, *Proc. 13th ICSMGE,* New Delhi Vol. 5 (1994): 51-55.

[43] D.C.F. LoPresti, M. Jamiolkowski, and M. Pepe, Geotechnical characterization of the subsoil of Pisa Tower, *Characterization & Eng. Properties of Natural Soils* **2**, Balkema, Rotterdam, (2003): 909-946.

[44] D.G. Zapata-Medina, *Evaluation of dynamic soil parameter change due to construction-induced stresses*, Ph.D. dissertation, Northwestern University, Civil Engineering, 260p, 2012.

[45] P.W. Mayne & R.A. Pearce, Site characterization of Bootlegger cove formation clay for Port of Anchorage, *Frontiers in Offshore Geotechnics* (Proc. ISFOG, Perth), (2005): 951-955.

[46] P.W. Mayne, P.K. Robertson, and T. Lunne, Clay stress history evaluated from seismic piezocone tests. *Geotechnical Site Characterization* **2** Balkema, Rotterdam, Netherlands, (1998): 1113-1118.

# APPENDIX K

## Use of Shear Wave Velocity to Estimate Stress History and Undrained Shear Strength of Clays

# Use of shear wave velocity to estimate stress history and undrained shear strength of clays

S.S. Agaiby & P.W. Mayne
*Geosystems Engineering, Georgia Institute of Technology, Atlanta, GA, USA*

ABSTRACT: A quality database of downhole shear wave velocity profiles ($V_{sVH}$) from 64 worldwide well-documented clay sites has been compiled to provide a first-order estimate of stress history of clays. The database primarily includes soft-to-firm normally consolidated (NC) to lightly overconsolidated where OCR < 2, as well as some stiff to hard overconsolidated (OC) and fissured clays. The stress history is expressed in terms of effective yield stress or preconsolidation stress ($\sigma_p'$) which was measured in the laboratory by oedometer and/or consolidation tests on undisturbed samples. The in-situ $V_{sVH}$ were measured by downhole tests (DHT), mostly using seismic piezocones (SCPTu) or seismic dilatometers (SDMT). The estimated stress history is applied to provide an evaluation of undrained shear strength ($s_u$) of intact clays using a SHANSEP type approach which considers different shearing modes. The approach can be used as an independent estimate of stress history and undrained shear strength of clays reliant on only the in-situ measured shear wave velocity.

## 1 INTRODUCTION

### 1.1 *Stress History*

The stress history of a soil can be used to delineate the geological processes which have occurred over many thousands of years and can be considered the focal point for soil behavior in terms of strength, flow, and compressibility. Stress history is often denoted by the preconsolidation stress ($\sigma_p'$) that can be defined as the maximum effective overburden stress experienced by the soil during its stress history. The overconsolidation ratio (OCR) is a convenient normalized and dimensionless parameter based on $\sigma_p'$ and current effective

vertical stress ($\sigma_{v0}'$) such that: OCR = $\sigma_p'/\ \sigma_{v0}'$. More recently, the terms yield stress ($\sigma_{vy}'$) and yield stress ratio (YSR = $\sigma_{vy}'/\sigma_{vo}'$) have been introduced to include the additional effects of diagenesis, bonding, and ageing.

## 1.2 *Stress History Evaluation Methods*

The most basic and conventional means to determine stress history is a laboratory one-dimensional consolidation test using a consolidometer (ASTM D2435). The specimen is subjected to constrained compression in either a mechanical oedometer, pneumatic or hydraulic consolidometer, or automated constant rate of strain (CRS) device. On the basis of the oedometer test, many methods have been proposed to evaluate $\sigma_p'$ from the compression measurements. However, the results are dependent on the plotting methods and curve-fitting procedures. Casagrande (1936) analyzed the stress history and established the first and most common method to obtain $\sigma_p'$ using a graphical method. Afterwards, others attempted to improve and develop new methods in order to determine the preconsolidation stress more definitively such as the Schmertmann (1955) reconstruction method, Janbu (1969) stress-strain and modulus-strain method, Butterfield (1979) approach with a bilogarithmic representation, and Becker et al. (1987) work-energy method. In fact, at least 28 methods are available for these purposes (Ku and Mayne 2013).

## 1.3 *Stress History Evaluation Problems*

Laboratory based techniques are associated with many issues: disturbance which can be attributed to sampling process, specimen handling, disturbance, and stress relief due to bringing the sample from depths to the ground surface with possible swelling. Other issues include: lack of information on sampling effective stress before testing, specimen trimming

method, load application duration, secondary consolidation consideration, temperature, salt concentration in pore fluid, friction between specimen ring and the soil, load increment ratio and schedule, lack of proper saturation, specimen slenderness, and capacity of loading frame (Germaine & Germaine, 2009).

To overcome issues associated with the laboratory methods, $\sigma_p'$ can be estimated using empirical correlations or analytical solutions with in-situ test measurements that avert the issues of sample disturbance and these are also faster and more economical than laboratory tests. Many relationships for stress history evaluation have been proposed for various in-situ tests such as cone penetration test (CPT), flat dilatometer test (DMT), standard penetration test (SPT), vane shear test (VST) and pressuremeter test (PMT), as discussed for instance by Mayne (1995).

Herein, a direct relationship between $\sigma_p'$ and $V_s$ was sought following the concepts and logic previously established by Mayne et al. (1998) and Mayne (2005) on smaller datasets.

## 2 SHEAR WAVE VELOCITY

Shear wave velocity ($V_s$) can be measured using either invasive and/or non-invasive geophysics, as well as obtained on small lab specimens. Shear waves can be measured in all geomaterials where it serves as an excellent reference benchmark in comparing stiffness and stress states. The measured $V_s$ profile is fundamentally applicable to both static and dynamic geotechnical analyses as it provides the small-strain shear modulus.

The magnitude of shear modulus can be measured from small specimens in the laboratory using resonant column, ultrasonics, bender elements, and/or triaxial tests with local

strain sensors, however, these methods have several issues: sampling disturbance difficulties, loss of ageing and diagenesis effects in addition to stress relief. Hence, $V_s$ is best measured in-situ rather than in the laboratory.

Field methods for $V_s$ measurement can be either invasive or non-invasive. Invasive methods include cased borehole methods such as: crosshole test (CHT), downhole test (DHT), uphole test (UHT), and P-S suspension logger, as well as direct push methods: seismic cone penetration test (SCPT) and seismic flat dilatometer test (SDMT) which are efficient versions of the DHT mode that measures a vertically-propagating horizontally-polarized shear wave velocity, or $V_{sVH}$ mode. Non-invasive methods include refraction survey, reflection survey, and surface wave methods using either active sources to measure Rayleigh waves: spectral analyses of surface waves (SASW), multi-channel analyses of surface waves (MASW), and continuous surface wave method (CSW), or passive source techniques, such as passive surface waves (PSW) or reflection microseism (ReMi).

## 3 COMPILED DATABASE

A comprehensive database was prepared from a total of 64 well-documented worldwide geotechnical test sites. The sites primarily include soft to firm normally-consolidated young to aged clays, as well as a few sites from stiff to hard overconsolidated clays and fissured fine-grained soils. Only high-end laboratory tests were included with a focus on one-dimension consolidation tests for stress history profiles measured using standard 1D consolidation tests with a constant load increment duration of 24 hr ($IL_{24}$) and successive load increments applied at end-of-primary consolidation tests ($IL_{EOP}$), and constant rate of strain (CRS) consolidation tests.

Regarding $V_s$ data, only in-situ results were compiled from downhole shear wave velocity ($V_{sVH}$) which can be measured using DHT, SCPT, and SDMT. At each of the studied sites, complementary field and lab data were also often available such as: Atterberg limits and unit weight for evaluating the effective vertical overburden pressure.

In the events where no undisturbed samples or natural water contents were available, unit weight was estimated using indirect methods such (Mayne 2005):

$$\gamma_t\,(\mathrm{kN/m^3}) = 8.63\log(V_s) - 1.18\log(z) - 0.53 \quad (1)$$

where $V_s$ (m/s) and depth z reported in meters.

The compiled database has a total pairing of 790 one-dimension consolidation tests along with their corresponding $V_{sVH}$ values which can be classified into 3 main groups: (a) normally consolidated (NC) intact to lightly overconsolidated (LOC) intact clays; (b) overconsolidated (OC) intact clays; and (c) highly overconsolidated (HOC) fissured clays.

A compilation of information from 36 different NC-LOC intact clays with a total of n = 486 preconsolidation effective stress ($\sigma_p'$) measurements were collected, as presented in Table 1. The NC-LOC group had characteristic stress histories that are low and probably due to effects of secondary compression and ageing, although some minor erosion and/or groundwater changes may have also caused a prestressing effect. The NC-LOC are represented by a range $1 < OCR < 2$.

In contrast, the OC clays generally exhibit $2 < OCRs < 5$ and include intact and lightly cemented clays from 19 test sites with a total of 204 $\sigma_p'$ measurements, as presented in Table 2. Finally, the HOC clays group includes fine-grained soils with $OCRs > 5$ and a total of 9 hard to fissured clay sites with 100 $\sigma_p'$ measurements, as listed in Table 3. The

reference sources of data and information in the presented tables are given in an abbreviated form (i.e., CEPNS = *Characterization & Engineering Properties of Natural Soils*, Taylor & Francis, London) due to the need to conserve space in allocated pages.

**Table 1.** Soft/firm clays (1<OCRs < 2) with paired $\sigma_p'$ and $V_{sVH}$

| Site | Location | Reference(s) |
|---|---|---|
| AIT | Bangkok | Watabe et al. (2004), 2nd ISC (2), Porto: 1765-1772. |
| Amherst, MA | USA | DeGroot & Lutenegger (2003), CEPNS (1): 695 - 724. |
| Ariake | Japan | Tanaka et al. (2001), Canadian Geot. J. 38 (2): 378-400. |
| Bäckebol | Sweden | Larsson & Mulabdić (1991), SGI (40) |
| Belfast | Ireland | Lehane (2003), Geot. Engrg. 156 (1) ICE, London: 17-26. |
| Bothkennar | UK | Hight et al. (1992) Géotechnique Vol. 42 (2): 303-347 |
| Burswood | Australia | Low et al (2011) Géotechnique Vol. 61(7): 575-591 |
| Busan | Korea | Chung et al. (2012), KSCE J. Civil Engrg. 16(3): 341-50 |
| Drammen | Norway | Long & Donohue (2007), Canadian Geotechnical J. 44 (5): 533 – 544. |
| Evanston, IL | USA | Finno et al. (2000), National Geot-ech Sites, ASCE GSP 93: 130-159 |
| Fucino | Italy | Burghignoli et al. (1991), 10th ECSMFE (1), Florence: 27-40. |
| Hachirougata | Japan | Tanaka (2006), CEPNS (3): 1831-1852 |
| Higashi | Japan | Shibuya et al. (1995), Earthquake Geotechnical Eng. (1): 77-82 |
| Kobe | Japan | Nakase et al. (1988), J. Geotech. Eng. 114(7): 844-858. |
| Kurihama | Japan | Shibuya & Tanaka (1996), Soils & Foundations 36(4): 45-55. |
| Lianyungang | China | Liu (2008), Marine Georesources & Geotechnology 26(3): 189-210. |

| Site | Location | Reference(s) |
|---|---|---|
| Lierstranda | Norway | Long & Donohue (2007), Canadian Geotechnical J. 44 (5): 533 – 544. |
| Lilla Mellösa | Sweden | Larsson & Mulabdić (1991), Swedish Geot. Institute Report 42. |
| Munkedal | Sweden | Larsson & Mulabdić (1991), Swedish Geot. Inst. Report 42. |
| Museumpark | Norway | Long & Donohue (2007), Canadian Geot. J. 44(5): 533-544. |
| Norrköping | Sweden | Larsson & Mulabdić (1991), Swedish Geot. Institute Report 42. |
| Onsøy | Norway | Lunne et al. (2003), CEPNS (1): 395-428 |
| Pentre | UK | Lambson et al. (1992), Large-scale Pile Tests in Clay, ICE:134-196 |
| Perniö | Finland | Lehtonen (2015), PhD Thesis, Tampere University: 213 p |
| Sarapui | Brazil | Almeida & Marques (2003), CEPN (1): 477-504. |
| Sarapui II | Brazil | Jannuzzi et al. (2015), Eng. Geology (190): 77-86. |
| Saro Rd 6-900 | Sweden | Larsson & Mulabdić (1991) Swedish Geot. Institute Report 42. |
| Saro Rd 7-600 | Sweden | Larsson & Mulabdić (1991) Swedish Geot. Institute Report 42. |
| Singapore | Singapore | Tanaka et al. (2001), Canadian Geot. J. 38(2): 378-400 |
| Skä Edeby | Sweden | Larsson & Mulabdić (1991) Swedish Geot. Institute Rpt 42. |
| S. Gloucester ON | Canada | Bozozuk (1972), PhD Thesis, Purdue Univ.: 208p. |
| Sutthisan | Bangkok | Shibuya & Tamrakar (2003), CEPNS, (2): 645-692. |
| Taipei | Taiwan | Chin et al. (2007), CEPNS (4): 1755-1803 |
| Troll Upper | North Sea | Lunne et al. (2007), CEPNS (4): 1939-1972 |
| Tuve | Sweden | Larsson & Mulabdić (1991) Swedish Geot. Institute Rpt 42. |
| Valen | Sweden | Larsson & Mulabdić (1991) Swedish Geot. Institute Rpt 42. |

**Table 2.** Overconsolidated Clays with 2.0 < OCR < 5.0

| Site | Location | Reference(s) |
|---|---|---|
| Beaumont, TX | USA | Mahar & O'Neill (1983), J. Geotech Engrg. 109(1): 56 - 71. |
| Bonneville, UT | USA | Gardner (2007) MS Thesis, Brigham Young Univ: 142p. |
| Cooper Marl, SC | USA | Camp (2004), *GeoSupport* GSP 124, ASCE Reston VA: 1-18. |
| Hai-Phong | Vietnam | Watabe et al. (2004), 2nd ISC (2), Porto. |
| Hamilton, CA | USA | Nguyen (2007) MS Thesis, MIT: 366p. |
| Hilleren | Norway | Long et al. (2009), J. Geotech. and Geoenvir. Engrg. 135(2): 185-198. |
| I-395, ME | USA | Hardison (2013) MS Thesis. Univ. Maine |
| Louiseville, Quebec | Canada | Leroueil & Hamouche (2003), CEPNS (2): 363-393. |
| Montalto di Castro | Italy | Jamiolkowski & LoPresti (1994), 13th ICSMGE, (5):51-55. |
| Newbury, MA | USA | Landon (2007), PhD Thesis, U.Mass. Amherst: 701p. |
| Newport, OR | USA | Ferguson (2015), Seismic Evaluation Big Creek Dams: 561p. |
| Oseberg | North Sea | Rutledal et al. (2000), SEG: 570-573 |
| Pisa | Italy | LoPresti et al. (2003), CEPNS (2): 909-946. |
| Port of Anchorage, AK | USA | Mayne & Pearce (2005), Frontiers Offshore Geot, Perth: 951-955. |
| Route 197 Bridge, ME | USA | Hardison (2013) MS Thesis, Univ. Maine: 394p. |
| Saint Alban, Quebec | Canada | Levesque et al. (2007), CEPNS (4): 2645-2677. |
| Troll Lower | North Sea | Lunne et al. (2007), CEPNS (4). |
| Lower 232 St., BC | Canada | Sully (1991) PhD Thesis, Univ. British Columbia: 485p. |
| 200th St., BC | Canada | Sully (1991) PhD Thesis, UBC: 485p |

**Table 3.** HOC and Fissured Clays with OCRs > 5

| Site | Country | Reference(s) |
|---|---|---|
| AGS, NJ | USA | Stoll et al. (1988), J. Acoustical Society of America 83(1): 93-102. |
| Brent Cross | UK | Hight et al.(2003),CEPNS(2):851–907 |
| Chattenden | UK | Butcher & Powell (1995), 11th ECSMFE (1), Copenhagen: 27-36 |
| Cowden | UK | Hight et al.(2003),CEPNS(2):851–907 |
| Heathrow | UK | Hight et al.(2003),CEPNS(2):851–907 |
| Madingley | UK | Butcher & Powell (1995),11th ECSMFE, Copenhagen |
| Martin's Point Bridge, ME | USA | Hardison (2013) M.Sc. Thesis Univ. Maine: 394p. |
| Oxford | UK | Bates & Phillips (2000), J. Applied Geophysics (44): 257-273 |
| Tornhill | Sweden | Larsson (1991), SGI Rept 59: 169p. |

## 4 ESTIMATING STRESS HISTORY FROM SHEAR WAVE VELOCITY

Using multiple regression analyses and investigating the compiled database from 64 clay sites given in Tables 1 to 3, a relationship between the preconsolidation stress, $\sigma_p'$ (measured in kPa), the downhole shear wave velocity, $V_{sVH}$ (measured in m/sec), and the effective vertical overburden stress, $\sigma_{v0}'$ (measured in kPa) was developed, as shown in Figure 1, andcan be expressed:

$$\sigma_P' = 0.18 \cdot (V_{sVH})^{1.14} \cdot (\sigma_{vo}')^{0.26} \quad (2)$$

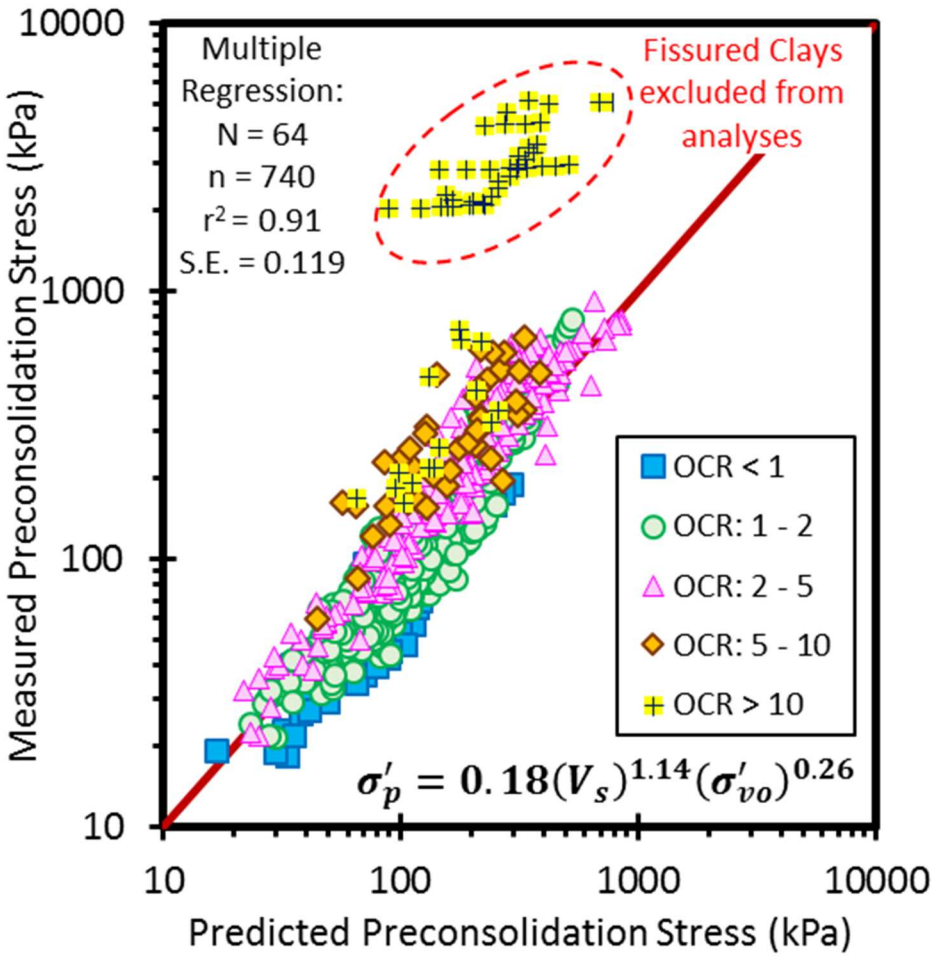


**Figure 1.** Measured versus predicted preconsolidation stress in terms of downhole shear wave velocity and effective vertical overburden stress for different OCR ranges

Notably, the highly overconsolidated and fissured clays were found to behave differently and did not fit any of the developed expressions, therefore were excluded from the regression analyses.

By considering the results plotted in Figure 1, an good agreement between the measured and the predicted $\sigma_p'$ values is achieved for intact clays. Hence, the proposed expression can be used as a first order estimate of stress history where only shear wave velocity data are available prior any other geotechnical investigations. Exception is again noted to the data from fissured overconsolidated clays that have discontinuities and joints.

By considering the complementary compiled data, it was interesting to investigate the effect of the plasticity characteristics of the studied clays expressed in terms of plasticity index (PI), as shown in Figure 2. The clays can be divided into 4 subgroups based on their plasticity ranges where the higher the plasticity the lower the preconsolidation stress. Note here that the majority of data are from low OCR clays in the NC-LOC range.

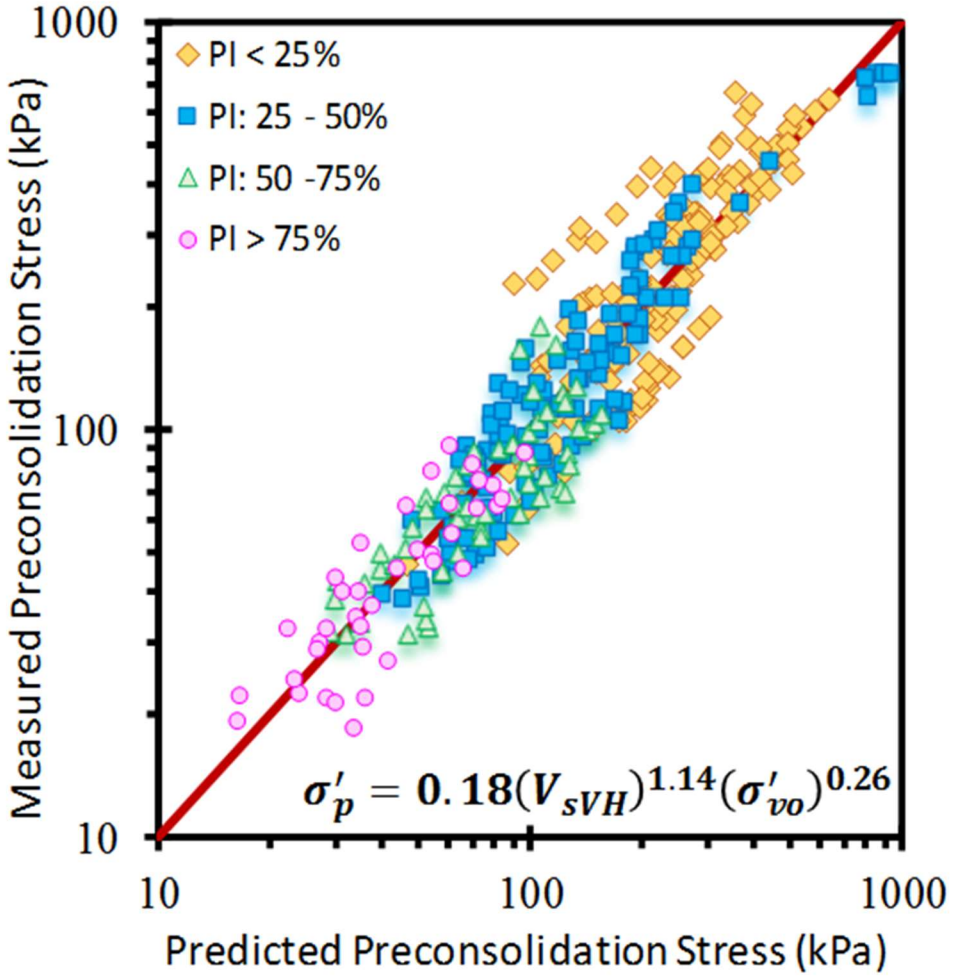


**Figure 2.** Measured versus predicted preconsolidation stress in terms of downhole shear wave velocity and effective vertical overburden stress for different PI values

## 5 UNDRAINED SHEAR STRENGTH AND CASE STUDY APPLICATIONS

Different laboratory and field testing techniques can be used to directly measure undrained shear strength and provide a reference profile of $s_u$ with depth (e.g., Ladd & DeGroot 2003;

Lunne et al. 2003). An alternate means to a direct evaluation involves the estimating of the magnitude of $s_u$ in clays through utilization of stress history (i.e., OCR) of the clay deposit to profile a family of undrained strengths for different modes using normalized strength ratios:

$$(s_u/\sigma_{vo}') = S \cdot OCR^m \quad (3)$$

where the coefficient S and exponent m can be found using SHANSEP (Stress History And Normalized Soil Engineering Parameters), as detailed by Ladd (1991) and Ladd & DeGroot (2003).

The value of $S = (s_u/\sigma_{vo}')_{NC}$ is found experimentally by extensive laboratory testing with companion series of plane strain compression (PSC), simple shear (SS), and plane strain extension (PSE) tests on the soils at varied OCRs, or by series of triaxial compression (TC), simple shear (DSS), and triaxial extension (TE) tests. Representative S values as suggested by Ladd (1991) are 0.30 for TC, 0.21 for DSS, and 0.15 for TE. The exponent *m* can be determined experimentally and has been generally found to be on the order of 0.8 ± 0.1.

### 5.1 ***Bothkennar Clay***

Bothkennar is a soft silty estuarine clay that is located on the south side of the River Forth, between Edinburgh and Glasgow in Scotland (Hight et al., 2003). The clay has the following average index parameters and soil properties: $e_0 = 1.69$, $w_n = 61\%$, LL = 72.6%, PI = 41.8%, clay fraction of 30%, $G_s = 2.65$, and bulk density ($\rho$) = 1.607 Mg/m$^3$. The behavior in one-dimensional compression was investigated by Hight et al. (1992) using three types of consolidation tests: conventional incremental load tests, continuous load tests, and restricted flow tests as presented in Figure 3b. These give an average OCR = 1.54 with depth.

Results of downhole $V_{sVH}$ profiles from SCPT were measured by Hepton (1988) and presented in Figure 3a. These data along with the profile of the effective vertical stress are used to provide an estimate for $\sigma_p'$ using Equation (2) showing a good agreement as shown in Figure 3b.

The evaluated stress history profile is used to estimate $s_{uDSS}$, $s_{uTC}$, and $s_{uTE}$ profiles for Bothkennar clay via Equation (3), with adopted S values of 0.3 for TC, 0.21 for DSS, and 0.15 for TE and an exponent of m = 0.8, as presented in Figure 3c. Laboratory $CK_0UC$, DSS, and $CK_0UE$ tests on undisturbed samples from the site are reported by Hight et al. (2003). Comparison of results show good agreement between measured and estimated profiles.

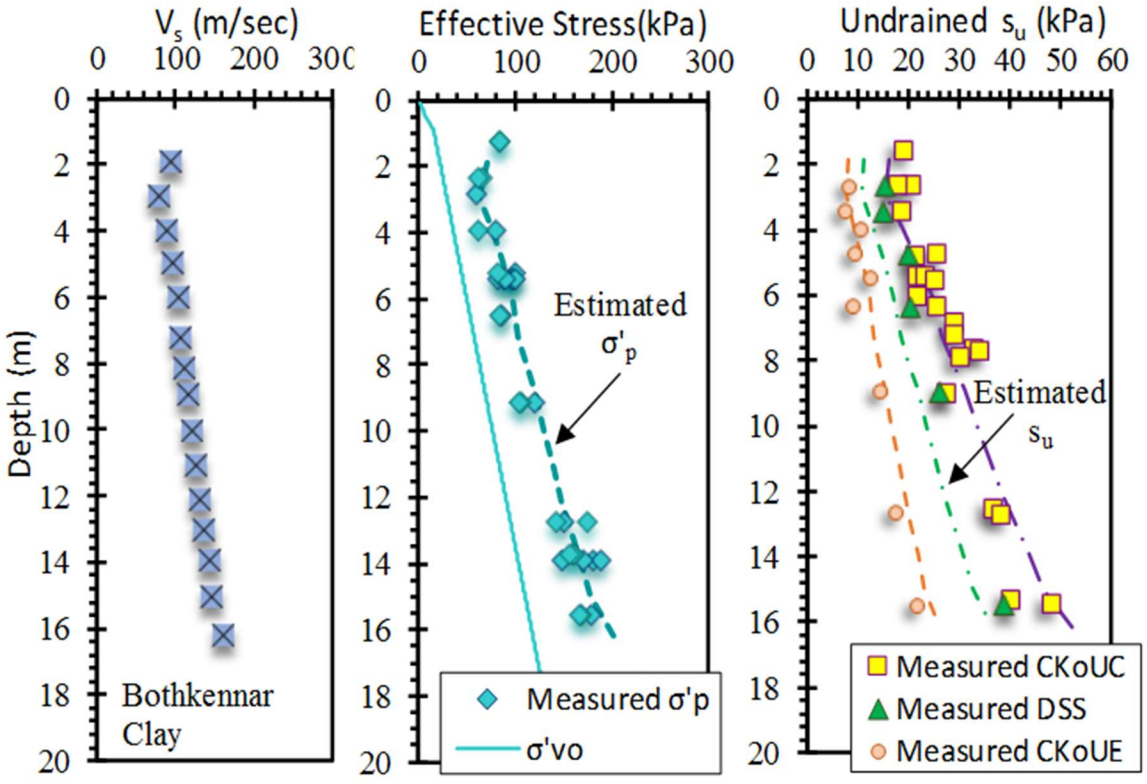


**Figure 3.** Profiles at Bothkennar soft clay: (a) Measured downhole shear wave velocity profile; (b) Estimated preconsolidation stress compared to lab-measured values; (c) Lab-measured and $V_s$-estimated TC, DSS, and TE strengths

## 5.2 *Busan Clay*

Busan (or Pusan) is a soft clay that covers the Nakdong River delta in South Korea (Locat and Tanaka 1999). The clay has the following average index parameters and soil properties: $e_0$ = 1.59, $w_n$ = 58.4%, LL = 61.5 %, PI = 27.2%, clay fraction of 27%, $G_s$ = 2.71, and bulk density ($\rho$) = 1.60 Mg/m$^3$ (Chung et al., 2011). The behavior in one-dimensional compression was investigated by Singh & Chung (2015) using three test types: standard 1D consolidation tests with a constant load increment duration of 24 h ($IL_{24}$) and a successive load increments applied after 100% primary consolidation (end-of-primary consolidation, $IL_{EOP}$); and a constant rate of strain (CRS) consolidation test.

Results of downhole $V_{sVH}$ profiles from SCPT are reported by Chung and Kweon (2013) and presented in Figure 4a. These data along with the profile of the effective vertical stress are used to provide an estimate for $\sigma_p'$ using Equation (2) showing a good agreement as shown in Figure 4b. The estimated stress history profile is used to evaluate the OCR profile to estimate $s_{uDSS}$, $s_{uTC}$, and $s_{uTE}$ with adopted S values of 0.30 for TC, 0.21 for DSS, and 0.15 for TE and an exponent m = 0.8 using Equation (3) as presented in Figure 4c. Laboratory $CK_0UC$ and $CK_0UE$ tests on undisturbed samples are reported by Chung et al. (2012). By comparing the undrained shear strength profiles, the estimated values compare well with lab data.

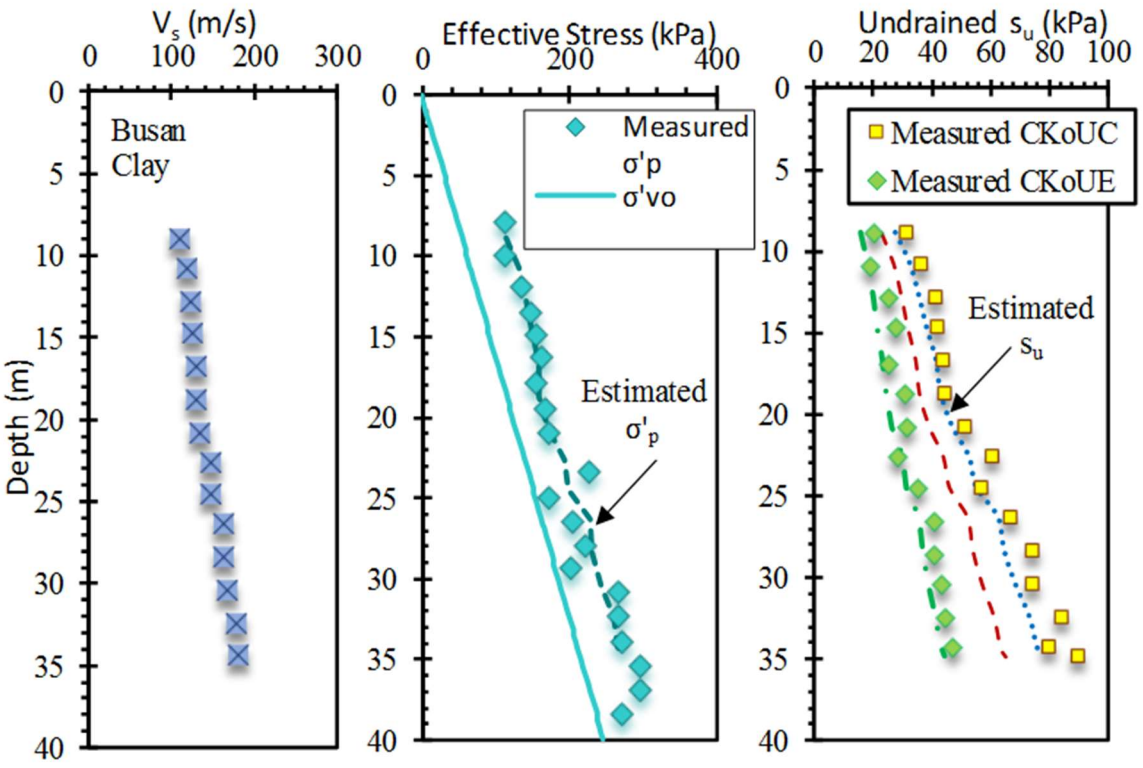


**Figure 4.** Profiles in soft Busan clay: (a) Measured downhole shear wave velocity; (b) Estimated preconsolidation stress compared to lab-measured stress history profile; (c) Lab-measured and $V_s$-estimated TC, DSS, and TE strengths

### 5.3 *Onsøy Clay*

Onsøy is a soft marine clay that is located in Norway, southeast of Oslo (Lunne et al., 2003). The soil profile at Onsøy consists of a one meter thick weathered crust followed by an 8-m thick soft clay layer underlain by a soft medium plastic clay layer over the remaining thickness of 36 m over bedrock. The clay has the following average index parameters and soil properties: clay fraction of 53 %, $e_0$ = 1.75, $w_n$= 64%, LL= 68%, PI= 35%, $G_s$= 2.71, and bulk density ($\rho$) = 1.587 Mg/m$^3$. The profile of preconsolidation stress from one-dimensional oedometer tests has been measured in several investigations (e.g. Lunne et al., 2001). These give an average OCR = 1.69.

The profile of the field measured $V_{sVH}$ from seismic cone test is presented in Figure 5a. These data along with the profile of the effective vertical stress are used to provide an estimate for $\sigma_p'$ using Equation (2) showing a good agreement as shown in Figure 5b. The estimated stress history profile is used to evaluate the OCR profile to estimate $s_{uDSS}$, $s_{uTC}$, and $s_{uTE}$ for Onsøy clay with typical S and m values as in Bothkennar and Busan clays as presented in Figure 5c. Laboratory $s_u$ from DSS, $CK_0UC$, and $CK_0UE$ tests have been obtained and reported by Lunne et al. (2006). Reasonable agreement is evident between measured and estimated values.

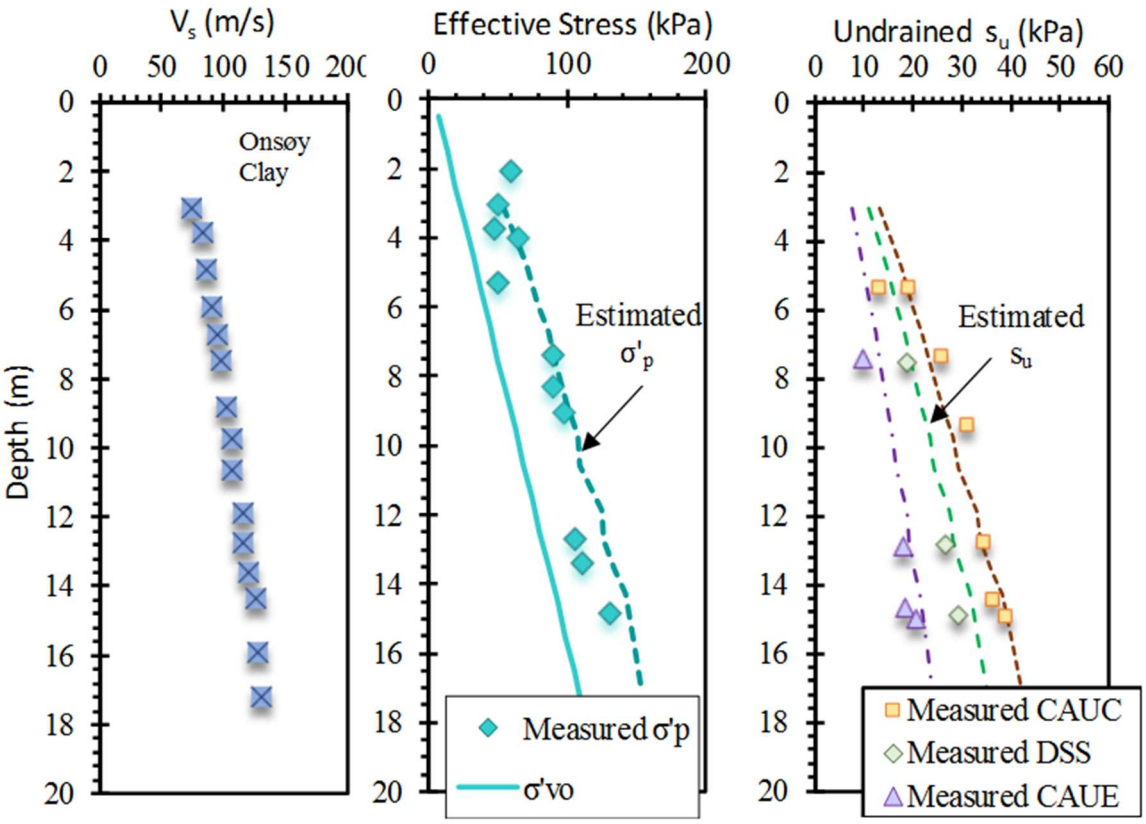


**Figure 5.** Profiles in soft clay at Onsøy, Norway: (a) Measured downhole shear wave velocity; (b) Estimated preconsolidation stress compared to lab measured stress history profile; (c) Measured and estimated DSS, TC, and TE strengths

## 6 SUMMARY AND CONCLUSIONS

A compiled database study was statistically analyzed to produce a general expression for $\sigma_p'$ from downhole shear wave velocity ($V_{sVH}$) and effective vertical overburden stress ($\sigma_{v0}'$). The data were collected from 64 worldwide well-documented natural soils primarily covering primarily NC to LOC clays, as well as some OC and HOC fissured clays. Case studies were used to verify the ability of the proposed expression in estimating stress history in comparison with reference values from consolidation tests on undisturbed samples.

The derived stress history profiles were used to estimate the undrained shear strengths under three different shearing modes: triaxial compression, direct simple shear, and triaxial extension using the SHANSEP approach.

## 7 ACKNOWLEDGMENTS

The authors appreciate the support of ConeTec Investigations of Richmond, BC and Design House Engineering Consultancy of New York, NY in support of this research effort.

## 8 REFERENCES

Becker D.E., Crooks J.H., Been K., Jefferies M.G. 1987. Work as a criterion for determining in situ and yield stresses in clays. *Canadian Geotechnical Journal* 24 (4): 549-564.

Butterfield (1979). A natural compression law for soils, *Geot-echnique*, Vol. 29 (4): 468-480.

Casagrande A. 1936. The determination of the preconsolidation load and its practical significance. *Proc. 1st Intl. Conf. Soil Mech. & Foundation Engrg.* (3), Cambridge, Mass: 60-64.

Chung, S.G., & Kweon, H.J., 2013. Oil-operated fixed-piston sampler and its applicability. *Journal of Geotechnical and Geoenvironmental Engineering*, 139 (1), 134-142.

Chung, S.G., Hong, Y.P., Lee, J.M., & Min, S.C. 2012. Evaluation of the undrained shear strength of Busan clay. *KSCE Journal of Civil Engineering*, 16 (5), 733-741.

Chung, S.G., Ryu, C.K., Min, S.C., Lee, J.M., Hong, Y.P., & Odgerel, E. 2011. Geotechnical characterization of Busan clay. *KSCE Journal of Civil Engineering*, 16 (2), 341-350.

Germaine, J.T. & Germaine, A.V. 2009. *Geotechnical Laboratory Measurements for Engineers*. Wiley & Sons: 359p

Hepton, P. 1988. Shear wave velocity measurements during penetration testing. *Penetration Testing in the UK*. Thomas Telford, London: 275–278.

Hight, D.W., Bond, A.J., & Legge, J.D. 1992. Characterization of the Bothkennar clay. *Géotechnique*, 42(2), 303-347.

Hight, D.W., Paul, M.A., Barras, B.F., Powell, J.M., Nash, D.T., Smith, P.R., Jardine, R.J., & Edwards, D.H., 2003. The characterization of the Bothkennar clay. *Characterization and Engineering Properties of Natural Soils*, Balkema, Rotterdam, Vol. 1: 543-597.

Janbu, N. (1969), The resistance concept applied to deformation of soils, *Proc. 7th ICSMFE*, Mexico, Vol. 1: 191-196.

Ku, T. and Mayne, P.W. (2013). Yield stress history evaluated from paired in-situ shear moduli of different modes. *Engineering Geology* 152, Elsevier: 122-132.

Ladd C.C. 1991. Stability evaluation during staged construction. *J. Geotechnical Engineering*. Vol. 117 (4): 540-615.

Ladd, C.C. & DeGroot, D.J. 2003. Recommended practice for soft ground site characterization. *Soils and Rock America 2003*, Vol. 1, (Proc. 12th PCSMGE, MIT), Verlag Gluckauf Publishing, Essen: 3-57.

Locat, J. & Tanaka, H. 1999. Microstructure, mineralogy and physical properties; Techniques and application to the Busan clays. *Proc. KSG'99 Dredging and Geoenvironmental Conference*, Seoul: 15-31.

Lunne, T., Berre, T., Andersen, K.H., Strandvik, S. & Sjursen, M., 2006. Effects of sample disturbance and consolidation procedures on measured shear strength of soft marine Norwegian clays. *Canadian Geotechnical J.* 43(7), 726-50.

Lunne, T., Long, M., & Forsberg, C.F., 2003. Characterization and engineering properties of Onsøy clay. *Characterization and Engineering Properties of Natural Soils*, Vol. 1, Singapore, Balkema / Swets & Zeitlinger, Lisse: 395-428.

Lunne, T., Nerland, Ø. & Solhell, E. 2001. Quality of CPTU. Factual report, field tests at Onsøy. *NGI report No. 20011099-1*, 16/7/01, Oslo.

Mayne, P.W., (1995). Profiling yield stress in clays by in-situ tests, *Transportation Research Record* 1479, National Academy Press, Washington, DC: 43-50.

Mayne, P.W. 2005. Invited keynote: Integrated ground behavior: in-situ and lab tests, *Deformation Characteristics of Geomaterials*, Vol. 2 (Proc. IS Lyon'03), Taylor & Francis Group, London: 155-177.

Mayne, P.W., Robertson, P.K., & Lunne, T. 1998. Clay stress history evaluated from seismic piezocone tests, *Geotechnical Site Characterization*, Vol. 2 (Proc. ISC-1, Atlanta), Balkema, Rotterdam: 1113-1118.

Schmertmann, J.H. 1955, The undisturbed consolidation behavior of clay, *Transactions, ASCE*, Vol. 120, p. 1201.

Singh, V.K., & Chung, S.G. 2015. Evaluation of overconsolidation ratios from laboratory and in situ tests on Busan clay. *Engineering Geology*, 199: 38-47.

# APPENDIX L

## Evaluation of undrained shear strength and stress history in intact clays using seismic piezocone tests

# Evaluation of undrained shear strength and stress history in intact clays using seismic piezocone tests

Shehab S. Agaiby & Paul W. Mayne
Georgia Institute of Technology, Atlanta, Georgia,USA, 30332-0355
David Woeller
ConeTec, Richmond, British Columbia, Canada V6V1J8

ABSTRACT

When using cone penetration tests in soft-firm clays, the effective preconsolidation stress ($\sigma_p'$) and undrained shear strength ($s_u$) are conventionally analysed using the net cone resistance ($q_{net} = q_t - \sigma_{vo}$). Where for the stress history a constant coefficient ($K_p$) is used with a mean value of 0.3 such that $\sigma_p' = K_p \cdot q_{net}$. And for the undrained shear strength a bearing factor ($N_{kt}$) is either assumed ($N_{kt} \approx 15 \pm 5$) or calibrated with other reference test values, such as the vane shear test (VST) or specific laboratory mode (CAUC, DSS, UC), such that $s_u = q_{net}/N_{kt}$. In this study, an updated database of seismic piezocone tests (SCPTu) collected from 34 worldwide well-documented clay sites has been compiled to provide a direct evaluation of effective preconsolidation stress and undrained shear strength under anisotropic triaxial compression (CAUC) using two independent readings from the seismic piezocone test: cone tip resistance ($q_t$) and downhole shear wave velocity ($V_{sVH}$). The database ranges from soft-to-firm normally consolidated (NC) and lightly overconsolidated (LOC: OCR < 2) intact clays. The two assessments provide very comparable close estimates for the stress history and undrained shear strength indicating the applicability of using each reading independently or together for crosschecking.

RÉSUMÉ

Lors de l'utilisation des tests de pénétration de cône, l'histoire des contraintes d'argile exprimée en termes de contrainte effective de préconsolidation ($\sigma_p'$) et la résistance au cisaillement ($s_u$) sont classiquement analysés en utilisant la résistance du cône net ($q_{net} = q_t - \sigma_{vo}$). Si, pour l'histoire de stress un coefficient constant ($K_p$) est utilisé avec une valeur moyenne de 0.30 telle que $\sigma_p' = K_p \cdot q_{net}$. Et pour la résistance au cisaillement

d'un facteur de palier ($N_{kt}$) est soit supposé ($N_{kt} \approx 15 \pm 5$) ou étalonné avec d'autres valeurs de test de référence, tels que le test aube de cisaillement (VST) ou en mode laboratoire (CAUC, DSS, UC), de telle sorte que $s_u = q_{net} / N_{kt}$. Dans cette étude, une base de données mise à jour des tests de piézocône sismiques (SCPTu) recueillies auprès de 34 sites d'argile dans le monde entier bien documentés a été compilé pour fournir une évaluation directe de la contrainte de préconsolidation efficace et résistance au cisaillement sous compression anisotrope triaxial (CAUC) en utilisant deux lectures indépendantes de l'essai de piézocône sismique: cône résistance de pointe ($q_t$) et de la vitesse des ondes de cisaillement de fond ($V_{sVH}$). La base de données varie de doux au cabinet normalement consolidé (NC) et légèrement surconsolidée (LOC: OCR <2) Les argiles intactes. Les deux évaluations fournissent des estimations proches très comparables pour l'histoire du stress et résistance au cisaillement indiquant l'applicabilité de l'utilisation de chaque lecture indépendamment ou ensemble pour recoupement.

## 1 INTRODUCTION

Different approaches and theoretical solutions have been investigated in the literature for evaluating the undrained shear strength and stress history of clays based on different considerations and assumptions such as bearing capacity theory (Terzaghi ,1943), cavity expansion theory (Skempton 1951; Vesić 1975), strain path method (Teh, 1987), or analytical solutions such as the combined cavity expansion - critical state soil mechanics as discussed by Chen and Mayne (1994). In addition, in-situ testing has been used to develop correlations and factors for estimating both undrained shear strength and clay stress history directly or indirectly using various field methods, such as cone penetration tests (CPT) and flat plate dilatometer tests (DMT).

## 2 UNDRAINED SHEAR STRENGTH

Undrained shear strength ($s_u$) is considered one of the most critical parameters in geotechnical engineering since it often controls the bearing capacity of footings and pile foundations in clays. Different testing techniques can be used to measure undrained shear strength and provide a reference profile of $s_u$ with depth.

Significant ranges and variations can be observed when comparing strength profiles with depth using different testing techniques from in-situ and laboratory devices. This highlights the non-uniqueness of undrained shear strength and its dependence on the specific testing method and shearing mode (Ladd 1991). Undrained shear strength is also affected by several factors such as initial stress state (isotropic vs. $K_o$ consolidation), strength anisotropy, loading direction (compression vs. extension), and boundary conditions (plane strain vs. triaxial). Other influencing effects include: strain rate, sensitivity, ageing, inherent fabric anisotropy, strain compatibility, thixotropy, and specimen quality associated with sampling disturbance (Ladd & DeGroot, 2003).

The highest quality laboratory tests require a recompression stage before the shearing phase which is applied in certain modes of laboratory testing such as: anisotropically consolidated triaxial series and direct simple shear types. Those tests intend to re-establish the geostatic stress regime prior to undrained shear. Thus, other various basic lab techniques such as: unconfined compression (UC), unconsolidated undrained (UU), pocket penetrometer, and torvane should be considered only as index tests and not true measurements of $s_u$ (Ladd, 1991). When comparing in-situ and laboratory-based values for $s_u$, the observed ranges become even more widespread where $s_u$ generally increases with depth and takes on the hierarchy of $s_u$ (compression)

> $s_u$ (simple shear) > $s_u$ (extension). An alternative approach to directly assessing undrained shear strength for a particular mode is by linking its evaluation to in-situ test measurements such as the seismic piezocone penetration test.

## 3 STRESS HISTORY

The preconsolidation stress ($\sigma_p'$) can be defined as the maximum effective overburden stress experienced by the soil during its stress history. More recently, the term yield stress ($\sigma_y'$) has been used to accommodate mechanical overconsolidation plus other effects such as diagenesis, ageing, cementation, groundwater fluctuations.

The most basic and conventional means to determine stress history is a laboratory one-dimensional consolidation test using an oedometer (ASTM D2435). The specimen is subjected to constrained compression in either a mechanical oedometer, electro-pneumatic or hydraulic consolidometer, or automated constant rate of strain (CRS) device. On the basis of the consolidation test, many methods have been proposed to delineate $\sigma_p'$ from the compression measurements. However, the results are dependent on the plotting methods and curve-fitting procedures. Different graphical methods have been introduced in the literature, starting from Casagrande (1936) to the reconstruction method by Schmertmann (1955), modulus approach (Janbu 1969), Butterfield's (1979) linear bi-logarithmic representation; to the work-energy method as introduced by Becker et al. (1987). In fact, no less than 28 different procedures have been identified (Ku & Mayne, 2013).

Laboratory based techniques are associated with many issues: disturbance which can be attributed to the sampling process, specimen handling and stress relief due to removal of the sample from depths beneath the ground surface. To overcome issues

associated with laboratory methods, $\sigma_p'$ can be determined using direct correlations with in-situ measurements from cone penetration, flat dilatometer, and vane shear tests that are faster, economical, and more productive than laboratory tests.

## 4 SEISMIC PIEZOCONE PENETRATION TESTING

The seismic piezocone test (SCPTu) is a modified hybrid in-situ test that combines the recordings of an electronic cone penetrometer (ASTM D5778) with geophysical downhole shear wave velocity measurements (ASTM D7400) into one sounding. Details on the procedures are given by Campanella et al. (1986) and Mayne & Campanella (2005).

With seismic piezocone testing, one can obtain continuous readings of cone tip resistance ($q_t$), sleeve friction ($f_s$), and porewater pressure ($u_2$) that are recorded approximately every 0.02 m, in addition to the shear wave velocity ($V_s$) obtained at 1-m depth intervals. The latter is performed via a downhole test (DHT) where the measured value is a vertically-propagated and horizontally-polarized mode of shear wave velocity ($V_{sVH}$).

## 5 COMPILED DATABASE

For the current study, a special database has been carefully collected from a total of 34 well documented worldwide geotechnical test sites having a total of 305 data points. The sites under study are soft to firm normally-consolidated (NC) young to aged lightly-overconsolidated (LOC) intact clays and silts with an average overconsolidation ratio $1.0 < OCR < 2.5$, as presented in Table 1. For each site, results from seismic piezocone soundings were collected with the profiles of the four main measurements with depth ($q_t$, $f_s$, $u_2$, and $V_{sVH}$). For the undrained shear strength, only high-end

laboratory tests were included with a focus on undrained shear strengths from the triaxial compression mode ($s_{uTC}$). For the stress history, results from one-dimension consolidation tests for stress history profiles measured using standard consolidation tests with a constant load increment duration of 24 hr., $IL_{24}$ and successive load increments applied at end-of-primary consolidation tests, $IL_{EOP}$; and constant rate of strain (CRS) consolidation tests.

Figure 1 presents the list of clay sites and corresponding colored symbols that are used herein.


**Figure 1.** List of clay sites and their symbols for the compiled database under study

## 6 ESTIMATING STRESS HISTORY

The relationship between the clay stress history expressed in terms of the effective preconsolidation stress ($\sigma_p'$) and the net cone tip resistance ($q_{net} = q_t - \sigma_{v0}$) has been extensively investigated for a variety of clay types as reported by Mayne and Holtz (1988). The general expression is in the form of $\sigma_p' = K_p \cdot (q_t - \sigma_{v0})$, where $K_p$ is a coefficient that ranges from 0.2 to 0.45 with a more commonly used value of 0.31 as reported by Chen and Mayne (1994). By investigating the same relationship on the compiled SCPTu database presented in the current study, a very close coefficient was obtained as presented in Figure 2 and can be expressed as:

$$\sigma_p' = 0.318 \cdot (q_t - \sigma_{v0}) \quad [1]$$

A similar trend was verified by Demers & Leroueil (2002).

**Table 1**. $s_{uTC} - \sigma_p'$ - SCPTu database for normally consolidated (NC) to lightly overconsolidated (LOC) clays

| Site + Location | Description | Reference(s) |
|---|---|---|
| Amherst, MA, USA | Soft Varved | DeGroot & Lutenegger (2003) |
| Ariake, Japan | Soft Clay | Tanaka et al. (2001) |
| Bäckebol, Sweden | Postglacial | Larson & Mulabdic ($1991_{a,b}$) |
| Ballina, Australia | Soft Estuarine | Pineda et al. (2014) |
| Belfast, Ireland | Soft Clay Silt | Lehane (2003) |
| Bothkennar, UK | Soft Silty Clay | Hight, et al. (2003) |
| Burswood, Australia | Soft Clay | Low et al. (2011) |
| Busan, Korea | Soft Clay | Chung et al. ($2012_{a,b}$) |
| Evanston, IL, USA | Soft Till | Finno et al. (2000) |
| Hai-Phong, Vietnam | Soft Alluvial | Watabe, et al. (2004) |
| Hilleren, Norway | Sensitive | Long et al. (2009) |

| Site + Location | Description | Reference(s) |
|---|---|---|
| I-395, ME, USA | Presumpcot | Hardison (2015) |
| Islais Creek, CA, USA | Soft Bay Mud | Pestana et al. (2002) |
| Kurihama, Japan | Alluvial | Tanaka (1995); Shib-uya & Tanaka (1996) |
| Lianyungang, China | Soft Clay | Liu et al. (2008) |
| Lierstranda, Norway | Sensitive Clay | Lunne& Lacasse(1997) |
| Lilla Mellosa, Sweden | Soft Organic | Larson & Mulabdic ($1991_{a,b}$) |
| Louiseville, Canada | Champlain Sea | Leroueil, & Hamouche (2003) |
| Newbury, MA, USA | Soft Silty Clay | Landon (2007) |
| Nong Ngu Hao, Bangkok | Soft Bangkok | Shibuya & Tamrakar (1999) |
| Onsoy, Norway | Soft Marine | Lunne et al. (2003) |
| Os, Norway | Glaciomarine Silt | Long et al. (2010) |
| Pentre, UK | Silt Deposit | Lambson et al. (1993) |
| Perniö, Finland | Soft Clay | Lehtonen (2015) |
| Sarapui, Brazil | Very Soft Clay | Almeida & Marques (2003) |
| Saro Rd 6/900, Sweden | Soft Organic | Larson & Mulabdic ($1991_{a,b}$) |
| Saro Rd 7/600, Sweden | Organic Clay | Larson & Mulabdic ($1991_{a,b}$) |
| Singapore | Soft Marine | Tanaka et al. (2001) |
| S. Gloucester, Canada | Sensitive Leda | Landon (2007) |
| Sutthisan, Bangkok | Soft Bangkok | Shibuya & Tamrakar (1999) |
| Taipei, Taiwan | Silty Clay | Chin et al. (2006) |
| Tiller, Norway | Sensitive Clay | Gylland et al. (2013) |
| Troll, North Sea | Soft Offshore | Lunne et al. (2007) |

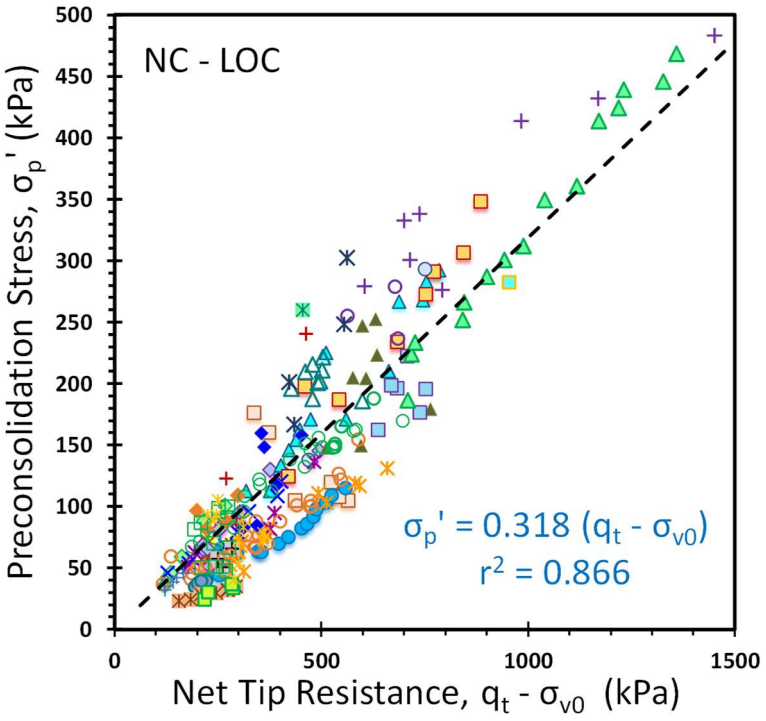


**Figure 2.** Trend of preconsolidation stress ($\sigma_p'$) with net tip resistance ($q_{net}$)

By comparing the laboratory measured values obtained using oedometer and CRS consolidation tests with the estimated values using $q_{net}$ as presented in Figure 3, a good agreement can be seen indicating the suitability of the tip resistance in estimating stress history.

Earlier efforts by Mayne et al. (1998) and Mayne (2005) related preconsolidation stress to shear wave. Referencing the larger updated database presented herein and relying on $V_{sVH}$ as a second independent variable from the SCPTu, the relationship between preconsolidation stress (kPa) and shear wave velocity ($V_{sVH}$ in m/s) was determined as presented in Figure 4, and can be expressed:

$$\sigma_p' \text{ (kPa)} = 0.14 \cdot (V_{s\,VH})^{1.4} \qquad [2]$$

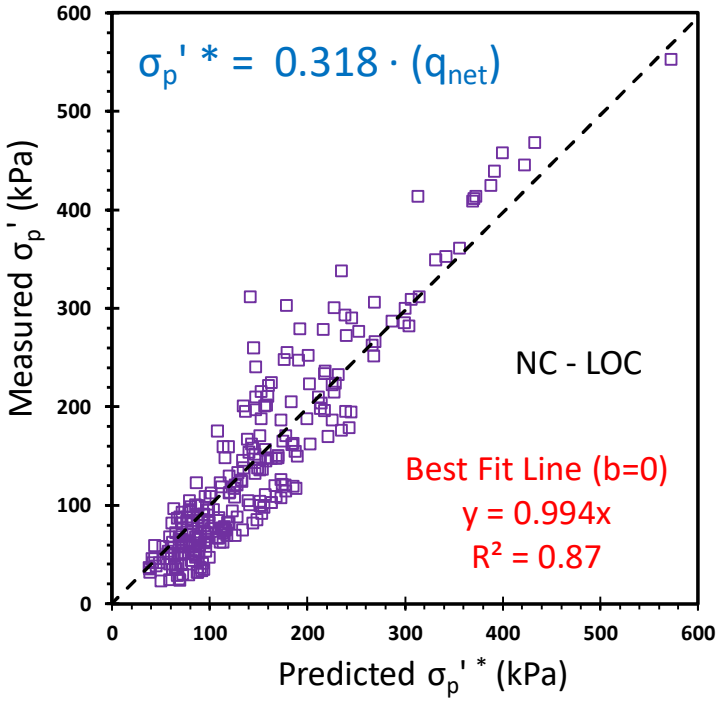


**Figure 3.** Laboratory measured versus predicted preconsolidation stress ($\sigma_p'$) using net tip resistance ($q_{net}$)

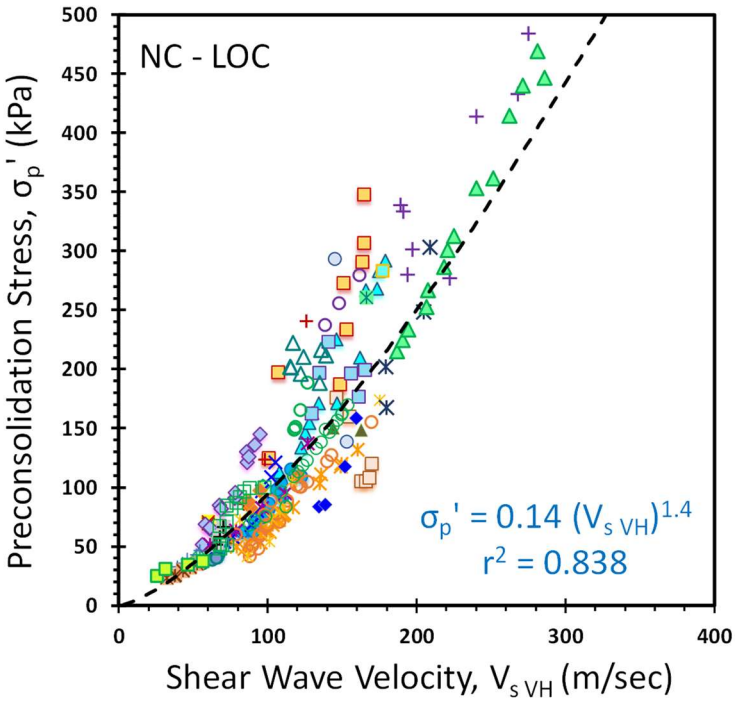


**Figure 4.** Trend of preconsolidation stress ($\sigma_p'$) with downhole shear wave velocity ($V_{sVH}$)

Figure 5 compares the laboratory measured values with the estimated values using $V_{sVH}$ indicating comparable results and good agreement.

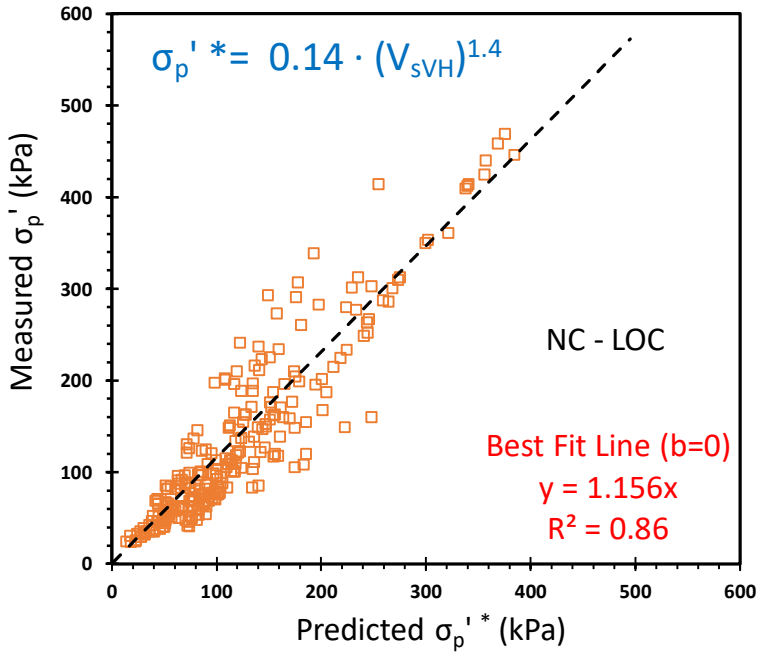


**Figure 5**. Laboratory measured versus predicted preconsolidation stress ($\sigma_p'$) using downhole shear wave velocity ($V_{sVH}$).

Table 2 shows the arithmetic statistics on the estimated effective preconsolidation stresses ($\sigma_p'$) compared to the actual measured value using two independent readings from the SCPTu: (a) $q_{net}$ and (b) $V_{sVH}$. The reported indices include: mean value of the measured-to-predicted ratio, standard deviation (SD), and coefficient of variation (COV = SD/mean). In addition, regression statistics are given between the independent variables ($q_{net}$ or $V_{sVH}$) and the dependent variable ($\sigma_p'$) to provide slope (m) of measured versus predicted, coefficient of determination ($r^2$), and standard error of the y-estimator (SEY). By comparing the two methods, they show generally comparable statistics indicating that both methods can be used for independent assessment or for crosschecking.

**Table 2**. Statistics on preconsolidation stress prediction using net tip resistance ($q_{net}$) and shear wave velocity ($V_s$)

| Stats on $\sigma_p'$ Prediction | | Using $q_{net}$ | Using $V_s$ |
|---|---|---|---|
| Measured / Predicted | Count | 300 | 300 |
| | Mean | 0.92 | 1.10 |
| | SD | 0.287 | 0.309 |
| | COV | 0.312 | 0.280 |
| | Low | 0.35 | 0.55 |
| | High | 2.21 | 2.02 |
| Regression Analysis | Slope, m | 0.992 | 1.156 |
| | $r^2$ | 0.87 | 0.86 |
| | S.E.Y. | 35.92 | 42.05 |

## 7 EVALUATING UNDRAINED SHEAR STRENGTH

The main readings from piezocone soundings can be used to evaluate the profile of peak undrained shear strength with depth using expressions based on net cone resistance ($q_t - \sigma_{vo}$), excess pore pressure ($\Delta u = u_2 - u_0$), and/or effective cone resistance ($q_{eff} = q_t - u_2$) together with their corresponding cone factors $N_{kt}$, $N_{\Delta u}$, and $N_{ke}$. The most commonly used factor is $N_{kt}$ with values reported in the literature ranging from 6 to 15 as found by Karlsrud et al. (1996). A mean value of $N_{kt} = 12$ was suggested by Low et al. (2010) for soft-firm clays. By investigating the same relationship on the compiled CAUC-SCPTu database, a similar mean value of $N_{kt} = 11.3$ was obtained as presented in Figure 6 and is expressed in Equation 3:

$$s_{u\,TC} = (q_t - \sigma_{vo}) / 11.3 \quad [3]$$

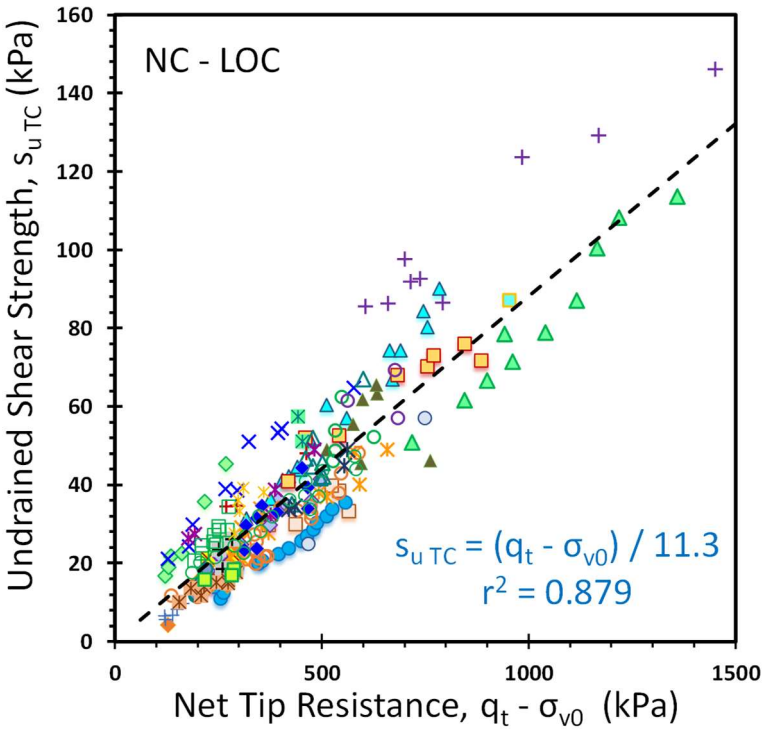


**Figure 6.** Relationship between undrained shear strength ($s_{uTC}$) in triaxial compression and net cone resistance ($q_{net}$)

Figure 7 provides a comparison between the laboratory measured values and estimated values using net cone tip resistance indicating good agreement.

The shear wave velocity from the seismic piezocone test can also be used to develop an independent assessment of undrained shear strength for the triaxial compression mode. An earlier study was conducted by Agaiby & Mayne (2015) exploring the link between undrained shear strength and shear wave velocity on a database with more variety of different clays than here, including overconsolidated and fissured clays. In consideration of the CAUC-SCPTu database under study, a comparable correlation for NC-LOC clays is found, as presented in Figure 8.

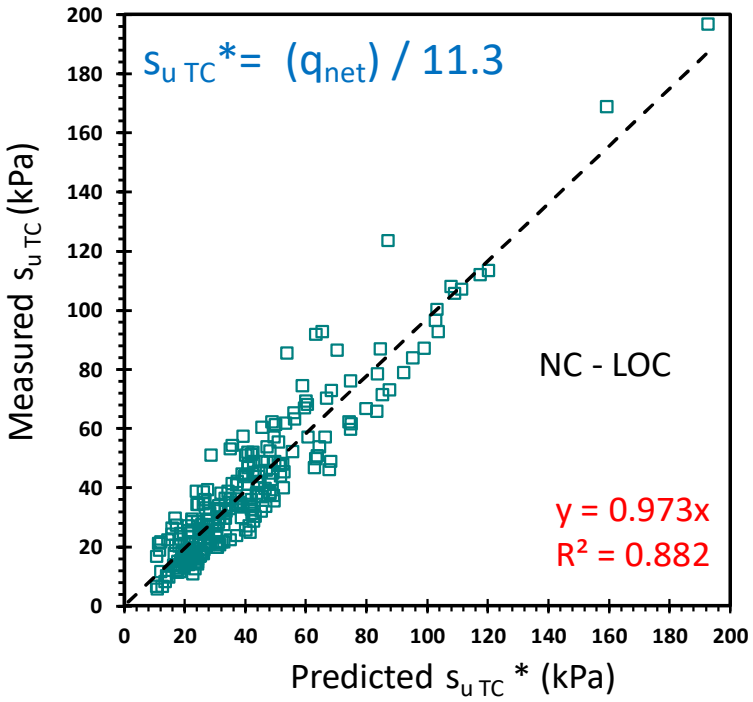


**Figure 7.** Laboratory measured versus predicted undrained shear strength ($s_{u\,TC}$) using net tip resistance ($q_{net}$)

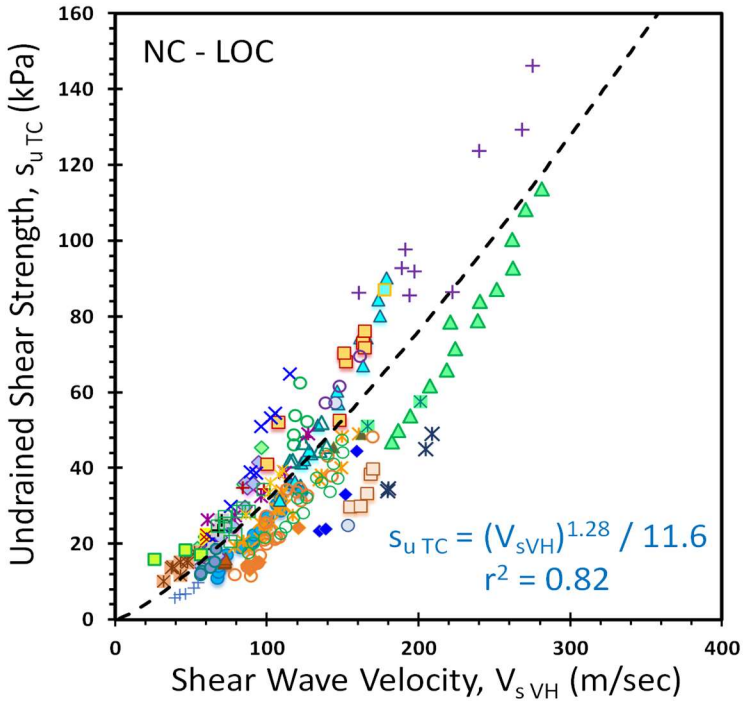


**Figure 8.** Relationship between CAUC undrained shear strength ($s_{uTC}$) and downhole shear wave velocity ($V_{sVH}$)

The relationship can be expressed according to Equation (4) which is units-dependent, specifically where $s_{uTC}$ (kPa) and $V_{sVH}$ (m/s). A comparison between the measured and predicted values is presented in Figure 9 indicating the applicability of using downhole shear wave velocity from seismic piezocone testing as an independent means to assess $s_{uTC}$.

$$s_{u\,TC} = (V_{s\,VH})^{1.28} / 11.6 \qquad [4]$$

where $s_u$ (kPa) and $V_s$ (m/sec).

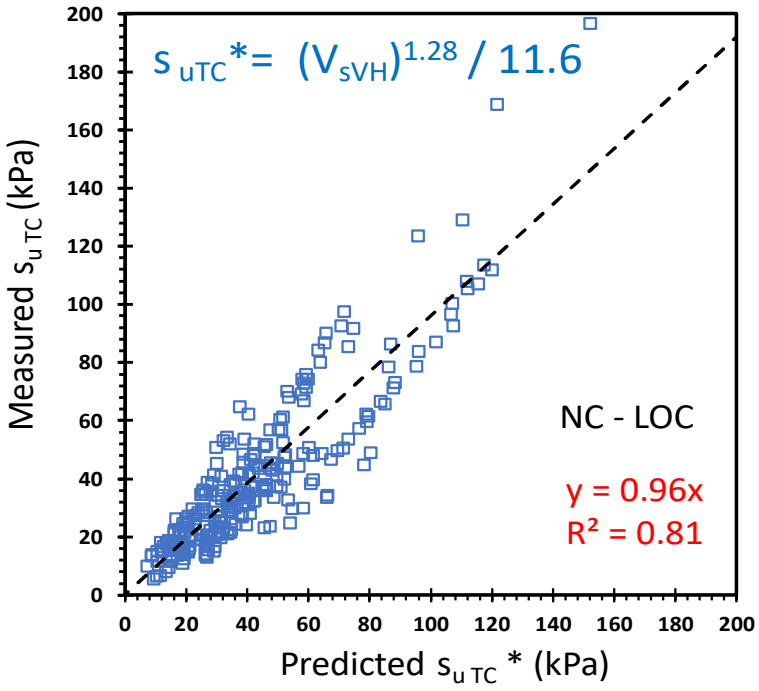


**Figure 9**. Laboratory measured versus predicted undrained shear strength ($s_{u\,TC}$) using shear wave velocity ($V_{sVH}$)

Table 3 shows the arithmetic statistics on the ratios of measured-to-predicted undrained shear strength under triaxial compression mode ($s_{uTC}$) using either $q_{net}$ or $V_{sVH}$. The reported statistics include: mean value of measured $s_u$/ predicted $s_u$, standard deviation (SD), and coefficient of variation (COV = SD/mean). In addition, regression

statistics are given between the dependent variable ($q_{net}$ or $V_{sVH}$) and the independent variable ($s_{uTC}$) to provide slope (m), coefficient of determination ($r^2$), and standard error of the y-estimator (SEY). The two methods are very comparable giving close statistics and indicating the suitability of both techniques for undrained shear strength estimation.

**Table 3**. Statistics on undrained shear strength prediction using net tip resistance ($q_{net}$) and shear wave velocity ($V_s$)

| Stats on $s_u$ Prediction | | Using $q_{net}$ | Using $V_s$ |
|---|---|---|---|
| Measured / Predicted | Count | 305 | 305 |
| | Mean | 0.97 | 0.97 |
| | SD | 0.259 | 0.276 |
| | COV | 0.267 | 0.284 |
| | Low | 0.48 | 0.46 |
| | High | 1.82 | 1.72 |
| Regression Analysis | Slope, m | 0.973 | 0.960 |
| | $r^2$ | 0.88 | 0.81 |
| | S.E.Y. | 8.07 | 10.28 |

## 8 CASE STUDIES

The aforementioned relationships are utilized in two case studies to illustrate the advantages and versatility of SCPTu for profiling undrained strength and effective preconsolidation stress in clays.

### 8.1 Golden Ears Bridge, British Columbia

The Golden Ears Bridge is a cable-stayed bridge over the Fraser River connecting Langley and Surrey in British Columbia, Canada. The soil deposits consist mainly of a thick layer of normally consolidated to lightly overconsolidated clay with sand lenses and sand layers. The clay has the following average index parameters: natural water

content, $w_n$ = 48%, liquid limit, LL = 65%, plasticity index, and PI = 37%. Undrained shear strengths were evaluated using Nilcon field vane tests (Amini et al. 2008) which can be converted to their equivalent triaxial compression values using Chandler (1987) method.

Seismic piezocone tests were performed at the site and data were input into the two strength assessment approaches. (a) using cone tip resistance as presented in Figure 10; and (b) using downhole shear wave velocity as presented in Figure 11. The estimated undrained shear strength values are compared to field vane data as plotted in Figures 10b and 11b, respectively. It is evident that both methods provide comparable values.

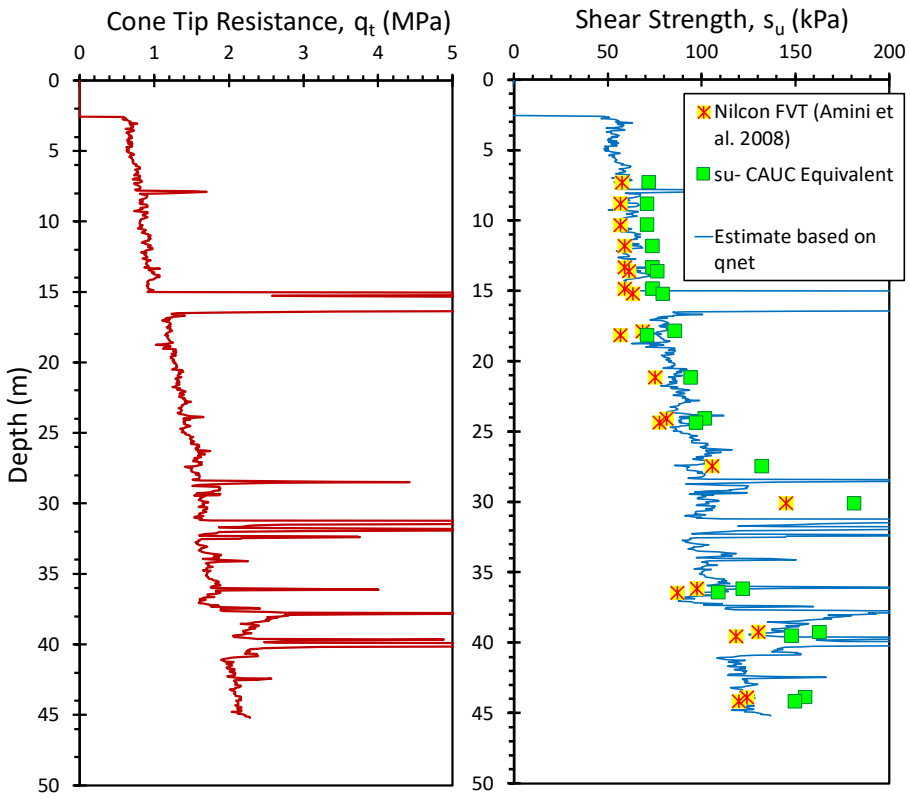


**Figure 10.** Profiles at Golden Ears: (a) Measured CPT $q_t$; (b) estimated $s_u$ using $q_{net}$ compared to field vane values

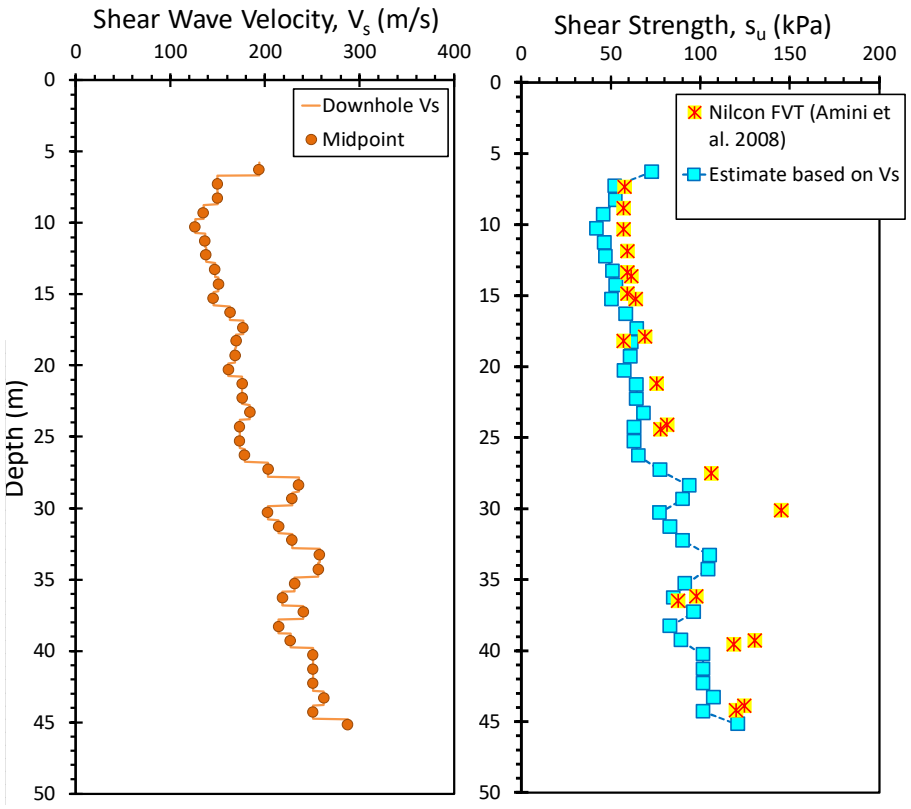


**Figure 11.** Profiles at Golden Ears: (a) Measured DHT $V_{sVH}$; (b) estimated $s_u$ using $V_{sVH}$ compared to field vane values

### 8.2 South Gloucester, Ontario

South Gloucester is a national Canadian research site that is located in Ontario and underlain by the well-known sensitive Leda - Champlain Sea clay. The clay has the following average index parameters: natural water content, $w_n$ = 64%, liquid limit, LL = 52%, plasticity index, and PI = 26% (Bozozuk and Leonards, 1972).

Downhole shear wave velocity is reported by Styler & Mayne (2013). Here, laboratory measured undrained shear strengths were obtained from $CK_0UC$ tests on undisturbed samples and preconsolidation stresses measured using conventional oedometer reported by Bozozuk (1972) and constant rate of strain consolidation tests

reported by Landon (2007). The downhole shear wave velocity is presented in Figure 12a and derived $s_u$ and $\sigma_p'$ profiles are shown in Figures 12b and 12c, respectively.

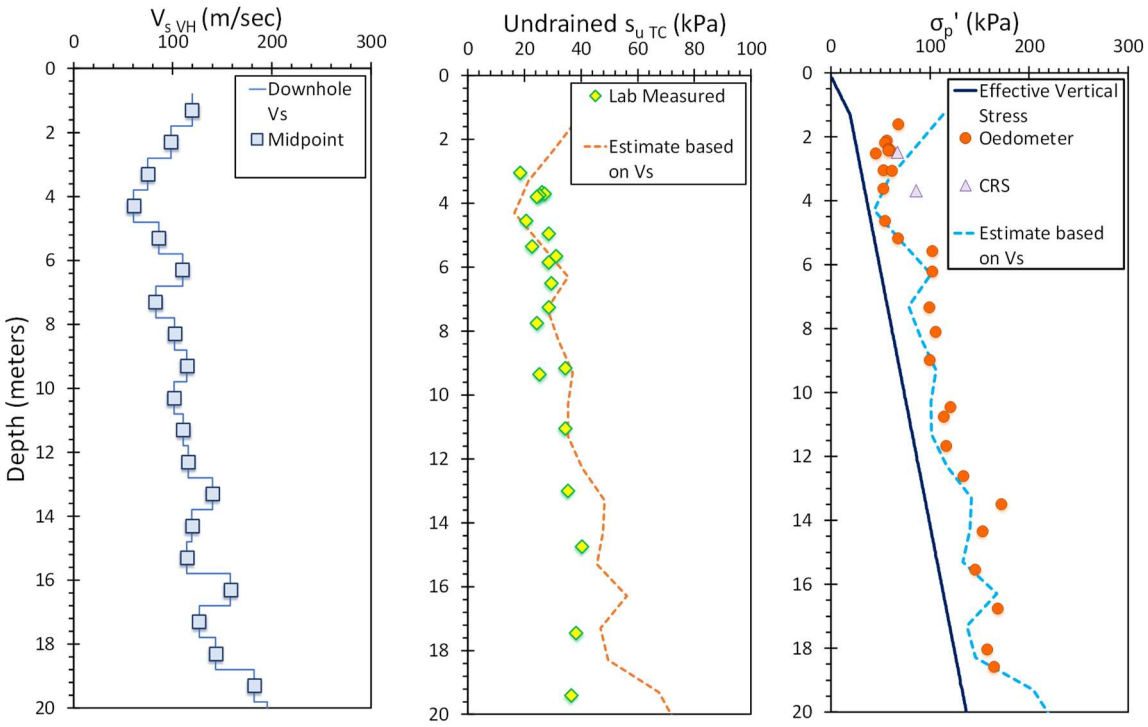


**Figure 12.** (a) Measured $V_{sVH}$ for South Gloucester; (b) Estimated $s_{uTC}$ using $V_{sVH}$ compared to lab measured values; (c) Estimated $\sigma_p'$ using $V_{sVH}$ compared to lab

A more recent piezocone sounding at Gloucester was conducted that included dissipations (McQueen et al. 2016) and these data were used in Figure 13. By comparing the $s_u$ and $\sigma_p'$ profiles, it can be seen that the SCPTu-estimated values using both $q_{net}$ and $V_s$ assessments are quite comparable to the actual laboratory measurements.

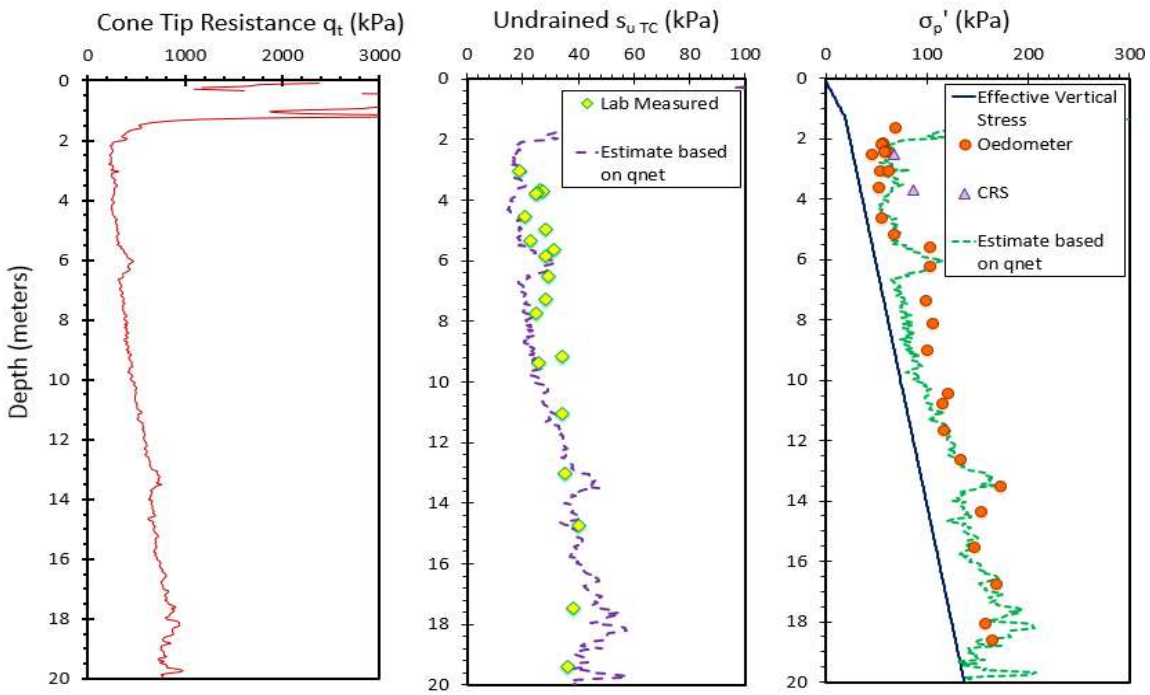


**Figure 13**. Profiles at Gloucester: (a) cone resistance, $q_t$; (b) CAUC undrained shear strengths from CAUC tests and $q_{net}$; (c) preconsolidation stresses

## 9 SUMMARY AND CONCLUSIONS

A SCPTu-compiled database was prepared and analyzed to provide assessments of the undrained shear strength under triaxial compression mode ($s_{uTC}$) and the effective preconsolidation stress ($\sigma_p'$) for soft-firm intact clays. Two independent evaluations can be made using: (a) net cone tip resistance ($q_{net}$); and/or (b) downhole shear wave velocity ($V_{sVH}$).

The data were collected from 34 worldwide well-documented natural clay soils primarily covering NC to LOC intact soft to firm clays. The obtained relationships provide similar statistical results when compared to the laboratory measured data indicating the applicability of using two independent readings from the same sounding to cross check the estimated strength and stress history.

Case study applications from the Golden Ears Bridge BC and South Gloucester ON were used to illustrate the applicability of the proposed expressions in estimating the profiles of $s_{uTC}$ and $\sigma_p'$.

The proposed expressions can be used for preliminary explorations in clay deposits taking advantage of two independent readings from the seismic piezocone testing.

## ACKNOWLEDGMENTS

The authors appreciate the continued support of ConeTec Investigations of Richmond BC and Design House Consultancy of New York NY in supporting research effort on in-situ testing.

## REFERENCES

Agaiby, S.S. and Mayne, P.W. 2015. Relationship between undrained shear strength and shear wave velocity for clays. *6th Intl. Symp. Deformation Characteristics of Geomaterials,* (IS-Buenos Aires), Vol. 6, 358-364.

Almeida, M.S.S. and Marques, M.E.S. 2003. The behavior of Sarapuí soft clay. *Characterisation and Engineering Properties of Natural Soils,* Vol.1, Swets & Zeitlinger, Lisse: 477-504.

Amini, A, Fellenius, B.H., Sabbagh, M., Naesgaard, E., and Buehler, M., 2008. Pile loading tests at Golden Ears Bridge. *61st Canadian Geotechnical Conference, Edmonton*, 8p.

Becker, D.E., Crooks J.H., Been K., Jefferies M.G. 1987. Work as a criterion for determining in situ and yield stresses in clays. *Canadian Geotechnical Journal*, Vol.24: 549-564.

Bozozuk, M. 1972. The Gloucester test fill. *PhD*. dissertation, Dept. of Civil Engineering, Purdue University: 208p.

Bozozuk, M. and Leonards, G.A. 1972. The Gloucester test fill. *Performance of Earth and Earth-Supported Structures,* Vol. 1, Part 1, ASCE, Reston, VA: 299-317.

Butterfield. 1979. A Natural Compression Law for Soils, *Geotechnique*, Vol. 29, No. 4, pp. 468-480.

Campanella, R.G., Robertson, P.K. and Gillespie, D. 1986. Seismic cone penetration test. *Use of In-Situ Tests in Geot. Engrg.* (GSP 6), ASCE, Reston/VA, 116-130.

Casagrande A. 1936. The determination of the preconsolidation load and its practical significance. *1st International Soil Mechanics and Foundation Eng. Conference*, Vol.3, Cambridge, Mass., 60-64.

Chandler, R.J. 1988. The in situ measurement of the undrained shear strength of clays using the field vane. *Int. Symp. on Vane Shear Strength Testing of Soils: Field and Laboratory Studies.* ASTM STP 1014, 13-44.

Chen, B.Y. and Mayne, P.W. 1994, *Profiling the Overconsolidation Ratio of Clays by Piezocone Tests*, *Report No. GIT-CEE/GEO-94-1* submitted to National Science Foundation by Georgia Institute of Technology, Atlanta, 280 p.

Chin, C.T., Chen, J.R., Hu, I.C., Yao, D., & Chao, H.C. 2007. Engineering characteristics of Taipei clay. *Characterization and Engineering Properties of Natural Soils,* Vol. 4, Taylor & Francis, London: 1755-1804.

Chung, S.G., Hong, Y.P., Lee, J.M., and Min, S.C. $2012_a$. Evaluation of the undrained shear strength of Busan clay, *KSCE Journal of Civil Engineering,* 16.5: 733-41.

Chung, S.G., Ryu, C.K., Min, S.C., Lee, J.M., Hong, Y.P., and Odgerel, E. $2012_b$. Geotechnical characterization of Busan clay, *KSCE Journal of Civil Engineering* 16.3: 341-50.

DeGroot, D.J. and Lutenegger, A.J. 2003. Geology and engineering properties of Connecticut Valley varved clay. *Characterization and Engineering Properties of Natural Soils*, Vol. 1, Balkema, Rotterdam: 695–724.

Demers, D. and Leroueil, S. 2002. Evaluation of preconsolidation and OCR from piezocone tests in Quebec. *Canadian Geot. J.* 39 (1): 174-192.

Finno, R.J., Gassman, S.L. and Cavello, M. 2000. The NGES at Northwestern Univ., *National Geotechnical Experimentation Sites*, *GSP 93*, ASCE, Reston, Virginia: 130-159.

Gnanendran, C.T., and Selvadurai, A.P.S. 2001. Strain measurement and interpretation of stabilizing force in geogrid reinforcement, *Geotextiles and Geomem-branes* 19: 177-194

Gylland, A., Long, M., Emdal, A. and Sandven. R. 2013. Characterisation and engineering properties of Tiller clay. *Engineering Geology,* 164: 86-100.

Hardison, M.A. 2015. Correlation of engineering parameters of the Presumpscot Formation to the seismic cone penetration test, *MSc. Thesis*, Dept Civil Engrg., University of Maine: 393 p.

Hepton, P. 1988. Shear wave velocity measurements during penetration testing. *Penetration Testing in the UK*. Thomas Telford, London: 275–278.

Hight, D.W, Paul, M.A., Barras, B.F., Powell, J.J.M., Nash, D.T, Smith, P.R., Jardine, R.J. and Edwards, D.H. 2003. The characterisation of the Bothkennar clay. *Characterisation & Engineering Properties of Natural Soils*, Balkema, Vol. 1, Rotterdam: 543-597.

Ingold, T.S. and Miller, K.S. 1983. Drained axisymmetric loading of reinforced clay, *Journal of Geotechnical Engineering*, ASCE, 109: 883-898.

Janbu, N. 1969. The Resistance Concept Applied to Deformation of Soils, *7th International Conf. on Soil mechanics & Foundation Eng*, Mexico, Vol. 1, 191-196.

Karlsrud, K., Lunne, T.& Brattlien, K. 1997. Improved CPTu interpretations based on block samples. *Publikasjon-Norges Geotekniske Institutt*, *202*, Oslo: 195-201.

Konrad, J-M. & Law, K.T. 1987. Undrained shear strength from piezocone tests. *Canadian Geotechnical J.* 24 (3): 392-405.

Ku, T. and Mayne, P.W. 2013. Yield stress history evaluated from paired in-situ shear moduli of different modes. *Engineering Geology* 152, Elsevier: 122-132.

Ladd, C.C. 1991. Stability evaluation during staged construction, *Journal of Geotechnical Engineering Division*, ASCE, 117(4), 540-615.

Ladd, C.C. and DeGroot, D.J., 2003. Recommended practice for soft ground site characterization. *Proc. 12th Panamerican Conference on Soil Mechanics and Geotechnical Engineering*, Vol. 1, Soil and Rock America, Boston, MA, 3-57.

Lambson, M.D, Clare, D.G. and Semple, R.M. 1993. Investigation and interpretation of Pentre and Tilbrook Grange soil conditions. Large-scale Pile Tests in Clay: *Recent Large-scale Fully Instrumented Pile Tests in Clay*, Thomas Telford, London: 134-196.

Landon, M.M. 2007. Development of a non-destructive sample quality assessment method for soft clays, *PhD Dissertation*, Uni.of Massachusetts, Amherst: 701p.

Larsson, R. and Mulabdić, M. 1991a. Shear moduli in Scandinavian clays: *Report No. 40*, Swedish Geotechnical Institute, Linköping, 127 p.

Larsson, R. and Mulabdić, M. 1991b. Piezocone tests in clays: *Report No. 42*, *SGI*, Linköping, 240 p.

Lehane, B.M. 2003. Vertically loaded shallow foundation on soft clayey silt, *ICE-Geotechnical Engineering*, 156.1: 17-26.

Lehtonen, V.J. 2015. Modelling undrained shear strength and pore pressure based on an effective stress soil model in limit equilibrium method. *PhD Dissertation*, Julkaisu-Tampere University of Technology: 213p.

Leroueil, S., and Hamouche, K. 2003. Geotechnical characterization and properties of a sensitive clay from Québec. *Characterisation & Engineering Properties of Natural Soils,* Vol 1, Lisse: Swets & Zeitlinger: 363-393.

Leshchinsky, D. and Perry, E.B. 1987. A design procedure for geotextile reinforced walls, *Geosynthetics '87*, IFAI, New Orleans, LA, USA, 1: 95-107.

Liu, S.Y., Cai, C.J., Tong, L.Y. and Du, G.Y. 2008. Approach on engineering properties of Lianyungang marine clay from piezocone penetration tests. *Marine Georesources & Geotechnology* 26(3): 189-210.

Long, M., El Hadj, N., & Hagberg, K. 2009. Quality of conventional fixed piston samples of Norwegian soft clay. *Journal of* G*eotechnical and Geoenvironmental Engineering*, 135.2: 185-198.

Long, M., Gudjonsson, G., Donohue, S., & Hagberg, K. 2010. Engineering characterisation of Norwegian glaciomarine silt. *Engineering Geology*, 110.3: 51-65.

Low, H.E., Lunne, T., Andersen, K.H., Sjursen, M.A., Li, X. and Randolph, M.F. 2010. Estimation of intact and re-moulded undrained shear strengths from penetration tests in soft clays. *Geotechnique* 60 (11): 843-859.

Low, H.E., Maynard, M.L., Randolph, M.F. and DeGroot, D.J. 2011. Geotechnical characterization and engineering properties of Burswood clay. *Géotechnique,* 61(7): 575-591.

Lunne, T. and Lacasse, S. 1997. Geotechnical characteristics of low plasticity clays. *International Symposium on Characterization of Soft Marine Clays*, Japan: 33-56.

Lunne, T., Long, M. and Forsberg, C. 2003. Characterization and engineering properties of Onsøy clay. *Characterization & Engrg. Properties of Natural Soils*, Vol. 1, Swets & Zeitlinger, Lisse: 395-428.

Lunne, T., Long, M., and Uzielli, M. 2007. Charac-terisation and engineering properties of Troll clay. *Characterisation and Engineering Properties of Natural Soils, Singapore*, Vol. 3, Taylor & Francis: 1939-1972.

Mayne, P.W. and Holtz, R.D. 1988. Profiling stress history from piezocone soundings, *Soils and Foundations*, Vol. 28, No. 1, pp. 16-28.

Mayne, P.W., Robertson, P.K., and Lunne, T. 1998. Clay stress history evaluated from seismic piezocone tests, *Geotechnical Site Characterization*, Vol. 2, Balkema, Rotterdam, pp. 1113-1118.

Mayne, P.W. 2005. Invited Keynote: Integrated Ground Behavior: In-Situ and Lab Tests, *Deformation Characteristics of Geomaterials*, Vol. 2 (Proc. IS Lyon'03), Taylor & Francis Group, London: 155-177.

Mayne, P.W. and Campanella, R.G. 2005. Versatile site characterization by seismic piezocone tests, *Proc.16$^{th}$ Int. Conf. on Soil Mechanics & Geotechnical Eng.*, ICSMGE, Osaka, Vol. 2, Rotterdam: 721-724.

McQueen, W., Miller, B., Mayne, P. W., & Agaiby, S. 2016. Piezocone dissipation tests at the Canadian Test Site No.1, Gloucester, Ontario. *Canadian Geotechnical Journal*, 53: 884-888.

Pestana, J., Hunt, C. & Bray, J. 2002. Soil deformation and excess pore pressure field around a closed-ended pile, Journal of G*eotechnical and Geoenvironmental Engineering,* 128(1): 1-12.

Schmertmann, J.H. 1955, The Undisturbed Consolidation Behavior of Clay, *Transaction, ASCE*, Vol. 120, p. 1201

Shibuya, S. and Tamrakar, S.B. 1999. In-situ and laboratory investigations into engineering properties of Bangkok clay. *Characterization of Soft Marine Clays*, Balkema, Rotterdam, 1: 107-132.

Shibuya, S. and Tanaka, H. 1996. Estimate of elastic shear modulus in Holocene soil deposits. *Soils and Foundations*, 36.4: 45-55.

Styler, M.A. and Mayne, P.W. 2013. Site investigation using continuous shear wave velocity measurements during cone penetration testing at Gloucester, Ontario. *GeoMontreal 2013*, 66th Canadian Geotechnical Conf., Paper 345

Tanaka, H. 1995. National Report-the Current State of CPT in Japan, *Proc. International Symposium on Cone Penetration Testing*, Vol. 1, Swedish Geotechnical Society, Linköping:115-124.

Tanaka, H., Locat, J., Shibuya, S., Soon, T., and Shiwakoti, D. 2001. Characterization of Singapore, Bangkok and Ariake clays. *Canadian Geotechnical Journal*, *38*(2): 378-400.

Teh, C.I. 1987. An analytical study of the cone penetration test*, PhD Dissertation*, University of Oxford, 254 p.

Terzaghi, K. 1943. *Theoretical Soil Mechanics*, John Wiley & Sons, Inc., Hoboken, NJ, USA.

Vesić, A. 1975. *Principles Of Pile Foundation Design*, Duke University, Durham, NC.

Watabe, Y. Tanaka, M., and Takemura, J. 2004. Evaluation of in-situ Ko for Ariake, Bangkok and Hai-Phong clays, *Geotechnical & Geophysical Site Character-ization*, Vol. 2 (Proc. ISC-2, Porto), Millpress: 1765-1772.

# APPENDIX M

# Geotechnical Load Factored Resistance Design (LFRD) Calculations of Settlement and Bearing Capacity of GDOT Shallow Bridge Foundations and Retaining Walls

**GEORGIA DOT RESEARCH PROJECT 14-26**

**FINAL REPORT**

# IMPLEMENTATION OF AASHTO LRFD SPECIFICATIONS: BEARING CAPACITY AND SETTLEMENT CALCULATIONS FOR SHALLOW FOUNDATIONS OF BRIDGES AND WALLS


OFFICE OF MATERIALS & RESEARCH
**RESEARCH & DEVELOPMENT BRANCH**

GDOT Research Project No. RP 14-26

# Geotechnical Load Factored Resistance Design (LFRD) Calculations of Settlement and Bearing Capacity of GDOT Shallow Bridge Foundations and Retaining Walls

Final Report

# IMPLEMENTATION OF AASHTO LRFD SPECIFICATIONS: BEARING CAPACITY AND SETTLEMENT CALCULATIONS FOR SHALLOW FOUNDATIONS OF BRIDGES AND WALLS

by

Shehab S. Agaiby
Research Assistant - Geosystems Engineering

and

Paul W. Mayne, PhD, P.E.
Professor - Civil & Environmental Engineering

Georgia Institute of Technology
Civil & Environmental Engineering
790 Atlantic Drive
Atlanta, Georgia 30332-0355

Contract with

Georgia Department of Transportation
Office of Materials & Research
15 Kennedy Drive
Forest Park, GA 30297-2534

9 August, 2016

TECHNICAL REPORT STANDARD TITLE PAGE

| | | |
|---|---|---|
| 1. Report No.:<br>FHWA-GA-16-1426 | 2. Government Accession No.: | 3. Recipient's Catalog No.: |

| | |
|---|---|
| 4. Title and Subtitle:<br>Geotechnical LFRD Calculations of Settlement and Bearing Capacity of GDOT Shallow Bridge Foundations and Retaining Walls | 5. Report Date:<br>9 August 2016 |
| | 6. Performing Organization Code: |
| 7. Authors:<br>Shehab S. Agaiby and Paul W. Mayne | 8. Performing Organization Report No.:<br>GDOT 14-26 (GTRC 2006Y13) |
| 9. Performing Organization Name and Address:<br>Georgia Tech Research Corporation<br>505 Tenth Street, N.W.<br>Atlanta, GA 30332-0402 | 10. Work Unit No.: |
| | 11. Contract or Grant No.:<br>RP14-26/00135290 |
| 12. Sponsoring Agency Name and Address:<br>Georgia Department of Transportation<br>Office of Materials & Research<br>15 Kennedy Drive<br>Forest Park, GA 30297-2534 | 13. Type of Report and Period Covered:<br>Final Report: April 2015 - June 2016 |
| | 14. Sponsoring Agency Code: |

15. Supplementary Notes:

Prepared in cooperation with the U.S. Department of Transportation, Federal Highway Administration

16. Abstract:

The AASHTO codes for Load Resistance Factored Design (LRFD) regarding shallow bridge foundations and walls have been implemented into a set of spreadsheet algorithms to facilitate the calculations of bearing capacity and footing settlements on natural soils in the State of Georgia. Specifically, the approach applies to soils exhibiting drained behavior during loading, including clean to silty and clayey sands and granular soils of the Atlantic Coastal Plain and residual silty sands to sandy silts of the Appalachian Piedmont and Blue Ridge geologies. The methodology permits the sizing of foundations based on site-specific data input for a given project, using in-situ field data obtained from either: (a) standard penetration tests (SPT), (b) cone penetration tests (CPT), and/or (c) flat plate dilatometer tests (DMT). This report provides the background information concerning the equations, calculation procedures, and reference sources that are used. Specifically, the technical review covers the calculations of bearing capacity from limit plasticity theory, settlement predictions using elastic continuum solutions, and geoparameter evaluations from SPT, CPT, and DMT, as well as examples for each of these tests.

| | |
|---|---|
| 17. Key Words:<br>Bridge foundations, bearing capacity, geotechnical design, footings, settlements, wall foundations | 18. Distribution Statement: |

| | | | |
|---|---|---|---|
| 19. Security Classification (of this report):<br>Unclassified | 20. Security Classification (of this page):<br>Unclassified | 21. Number of Pages:<br>158 | 22. Price: |

Form DOT 1700.7 (8-69)

# Table of Contents

# LIST OF FIGURES

# LIST OF TABLES

# 1. Introduction and Research Objectives

## 1.1 Introduction

Per the 2007 AASHTO bridge specifications, a systematic means for the calculation of bearing stresses and settlements of shallow foundations supporting bridge piers and retaining walls in light of load resistance factored design (LRFD) was identified (Paikowsky et al. 2010). As the process is iterative between bridge design team, which contains the structural engineering group, and the geotechnical engineering branch, who analyze the foundation systems, a series of design charts and spreadsheet solutions for selecting and optimizing the foundation sizes were deemed necessary for implementation.

For shallow foundation systems, the magnitude of foundation displacements increases with the applied loading and bearing stresses, thus consideration of the current factor of safety (FS) should be given. The success of the predicted foundation response depends upon a number of different factors, each of which can be quantified in terms of their reliability, uncertainty, and accuracy. Important factors can include: foundation size and shape, analysis method, input data, geologic setting, and other variables. On the geotechnical resistance side, the site exploration phase can obtain data using: (a) soil borings with SPT N-values; (b) cone penetrometer testing (CPT) with up to 3 or more continuous electronic readings with depth; and (c) flat plate dilatometer testing (DMT) that provides 2 pressure measurements at 20-cm vertical depth intervals.

Foundation settlements can be assessed using a variety of different methods, including theoretical (e.g. elasticity solutions; spring models), empirical/statistical approaches, and

numerical simulations (e.g., finite differences, finite elements). In our experience, the utilization of elastic continuum theory provides a sound and rational framework that permits the consideration of all foundation sizes, shapes, and various ground conditions, including homogeneous, finite/infinite, and layered media (e.g. Harr 1966; Poulos & Davis 1974; Mayne & Poulos 1999, 2001; Das 2011).

## 1.2 Geology of the state of Georgia

The state of Georgia is composed of four separate geologic areas, as illustrated by **Figure 1.1**: Piedmont; Blue Ridge, Coastal Plain, and Valley & Ridge/Plateau. As such, the natural soils and rocks, as well as compacted fills made from native geomaterials in these regions, can behave somewhat differently from each other. We can group the Appalachian Piedmont and Blue Ridge together due to their similarity. Here, the ground is underlain by residuum derived by the in-place weathering of metamorphic and igneous bedrock. Primary rock types include gneiss and schist, with later intrusions of granitic formations. The residual soils are often found to be silty, ranging from micaceous fine sandy silts to silty fine sands, that transition with depth to saprolites, partially-weathered rocks, and bedrock refusal.

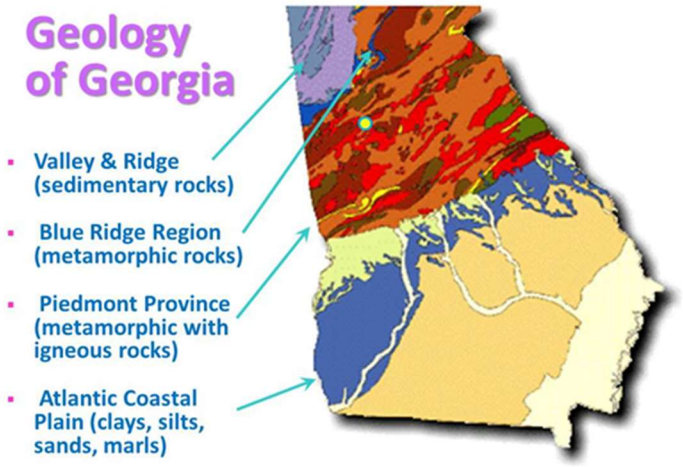


**Figure 1.1** *Geology of the State of Georgia*

In contrast, the Coastal Plain consists of various marine sediments that were deposited in various times ranging from very old Cretaceous to Miocene to recent Holocene ages, including complex interbedding of clays, silts, sands, and gravels. Finally, the Valley & Ridge/Plateau include sedimentary type bedrocks (shales, limestones, sandstones) that have also produced a clayey to sandy type residuum cover, as well as karstic terrain, sinkholes, and caves (Weary, 2005).

## 1.3 Research Objectives

The project will provide a methodology for the sizing of spread footing foundations for GDOT bridge structures and retaining walls which address AASHTO design recommentations in computing bearing stresses and settlements by changing from Allowable Stress Design (ASD) to Load Resistance Factor Design (LRFD), as discussed by Sargand & Masada (2006), Samtani et al., (2010), Paikowski et al. (2010), and others.

The main research objective was to create training documents and excel spreadsheets to allow the use of standard penetration tests (SPT), cone penetration tests (CPT), and/or dilatometer test (DMT) data, as well as specific foundation information, as input to generate the necessary bearing capacity and settlement calculations and graphs in accordance with LRFD guidelines and supporting AASHTO, NCHRP, and FHWA documentation. The focus and applicability were directed for foundations on granular soils and/or soils exhibiting drained behavior, since less than 1% of shallow foundations for highway bridges are placed on clay soils (Paikowsky et al. 2010).

The two LRFD criteria (limit state and service state) are used to develop graphs of applied foundation stress (factored bearing capacity) versus footing effective width at various adopted settlement tolerances for a given foundation length (L) or rectangular distortion (L/B ratio) of shallow footings. Three different output formats can be generated for the bearing capacity (BC) versus settlement design chart: (a) bearing capacity vs. effective footing width for different settlement values at constant length (L) value, (b) bearing capacity vs. effective footing width for different settlement values at constant rectangular distortion ratio (L/B), and (c) bearing capacity vs. settlement chart for different footing width values at constant L/B ratio. Separate spreadsheets for different site-specific input data (SPT, CPT, and DMT) were developed.

## 1.4 Prior Efforts and Recommended Procedures

Elastic theory provides the primary and accepted solutions for the calculations of stresses beneath shallow foundations and the associated displacements (e.g. Harr 1966; Gibson

1967, Fraser & Wardle 1976, Poulos & Davis 1974). In fact, the well-known Schmertmann (1970) CPT procedure for footing settlements, as well as his DMT methodology (Schmertmann 1986), both utilize elastic theory as the basis for settlement calculations. Elastic solutions also provide a common basis for evaluating pile load tests and load-displacement and axial load transfer distributions (Niazi & Mayne 2012; Niazi et al. 2014).

The use of the DMT modulus within an elastic continuum framework has shown to be quite successful in forecasting foundation settlements in the Piedmont residual soils (e.g. Brown & Mayne 2012; Mayne 2005). In the Piedmont, the DMT modulus has also been related to both the SPT $N_{60}$ value (Mayne & Frost 1988; Mayne & Brown 2003) and to measured CPT resistances (Mayne & Liao 2004). The measured shear wave velocity ($V_s$) of the ground has also been shown to provide a fundamental stiffness that is important in foundation deformation problems (Burns et al. 2008; Mayne & Poulos 1999; 2001; Elhakim & Mayne 2008).

In coastal plain deposits, the use of elasticity theory is also warranted, albeit perhaps fewer case studies of actual foundation measurements have been published and reported in Georgia, primarily because the majority of the state population is located around Atlanta that lies within the Piedmont geology.

An alternative approach to elasticity theory that has become attractive is the development of direct in-situ methods that are derived from full-scale foundation response (i.e., load-displacement-capacity) which are then statistically related to the SPT, CPT, DMT, and/or $V_s$ measurements (Mayne 2007; Viswanath & Mayne 2012, Uzielli & Mayne 2012; Mayne et al. 2012; Mayne & Woeller 2014).

Supporting materials from NHI, FHWA, and other state DOTs recommend that calculations including graphs be prepared by the geotechnical engineer that will display the varying bearing stresses, foundation sizes, and settlement criteria for each foundation element. There are many forms to display the BC-settlement-footing size design charts. **Figure 1.2** presents a schematic of bearing resistance contours as a function of effective footing width for different settlement values (1s, 2s, and 3s) combining both strength limit state and service limit state criteria. Alternatively, **Figure 1.3** presents a schematic of bearing resistance contours as a function of expected settlement value for different effective width values ($B'_{f1}$, $B'_{f2}$ , $B'_{f3}$, and $B'_{f4}$).

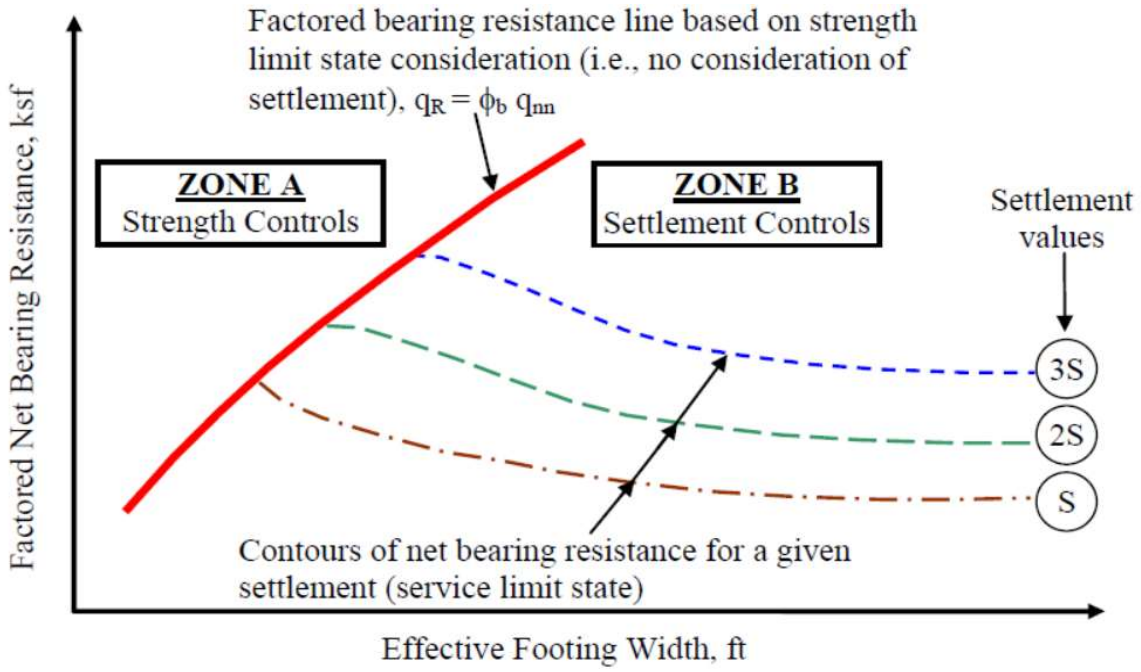


**Figure 1.2** *Schematic Bearing resistance chart showing strength limit state and service limit state criteria as a function of effective footing width (Samtani et al., 2010)*

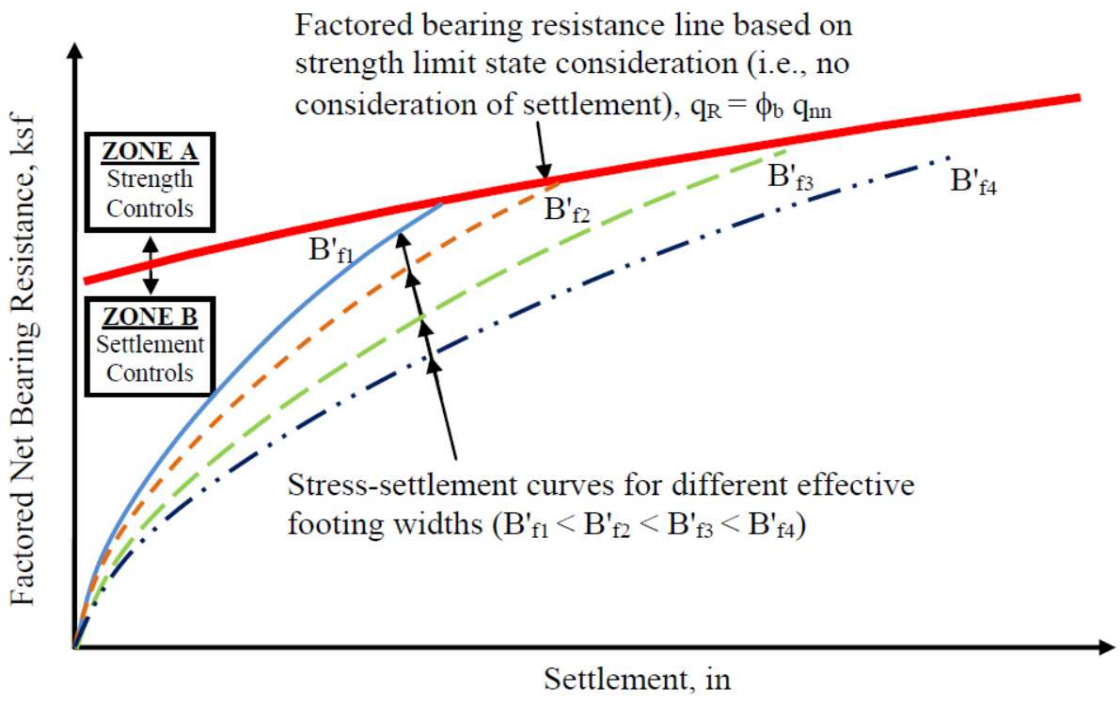


**Figure 1.3** *Schematic alternative bearing resistance chart in format of stress vs. settlement curves for range of effective footing widths and settlements (Samtani et al., 2010)*

Prior efforts by other DOTs concerning AASHTO LRFD design of shallow foundations have been reviewed, including documents prepared by AZDOT (as shown in **Figure 1.4**), and MnDOT (as shown in **Figure 1.5**), as well as DOTs from OH, WA, CA, SC, and MO. Preliminary graphs of applied bearing stress versus effective footing sizes and foundation settlement have been prepared for granular soils (sands) to address LRFD criteria.

For the case of footings bearing on clays and fine-grained soils with time-dependent behavior, a case-by-case study is recommended since the expected performance of the foundations under drained primary consolidation settlements may also be accompanied by time-rate-of-consolidation, as well as possible undrained distortion displacements and considerations of long-term creep.

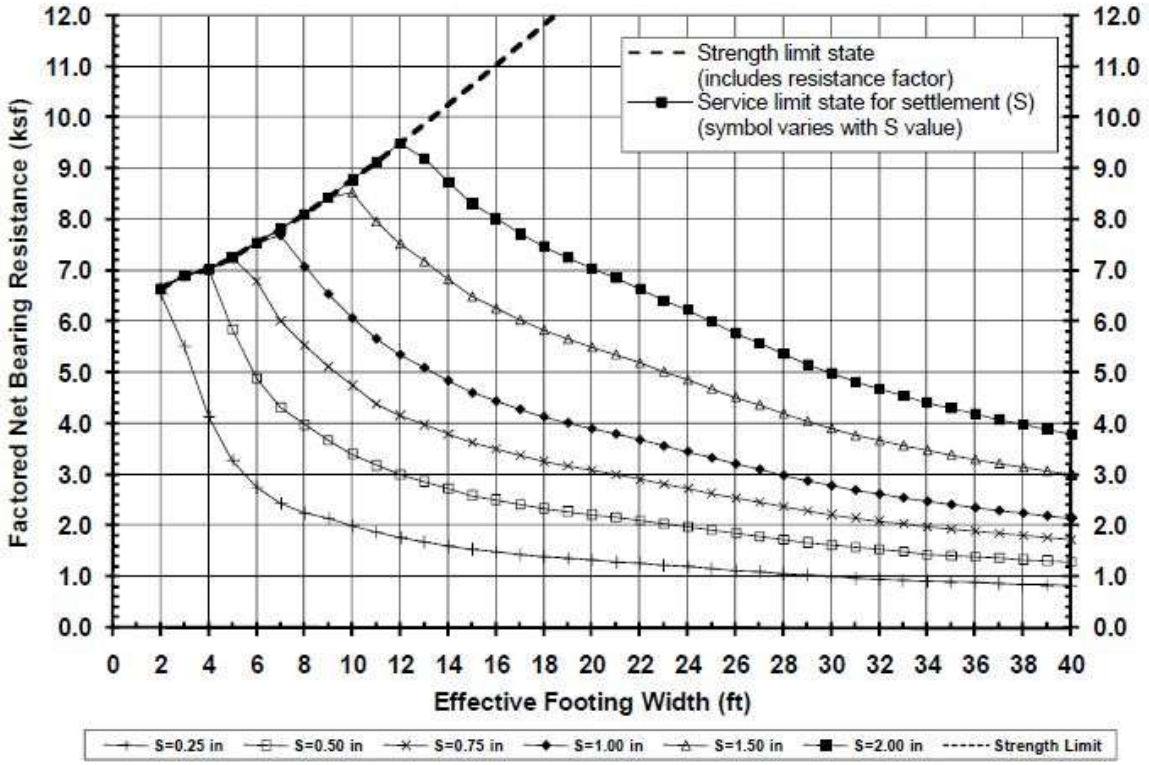


**Figure 1.4** *Excerpt from AzDOT Design Manual (ADOT SF-2, 2010)*

Exception to the above would be for the residual soils of the Piedmont and Blue Ridge geologies since these are comprised mainly of fine sandy silts (ML and MH) to silty fine sands (SM), and occasional clayey sands (SC), sometimes used with a modified type of USCS symbols, i.e. SM-ML. These residual soils behave essentially under a drained response (or partially drained response) during foundation loading because the coefficient of consolidation ($c_v$) and permeability (k) are sufficiently high such that undrained behavior is not experienced under normal rates of construction. Details on the interpretion and behavior of Piedmont soils have been documented by Mayne et al. (2000), Mayne & Brown (2003), and Brown & Mayne (2012).

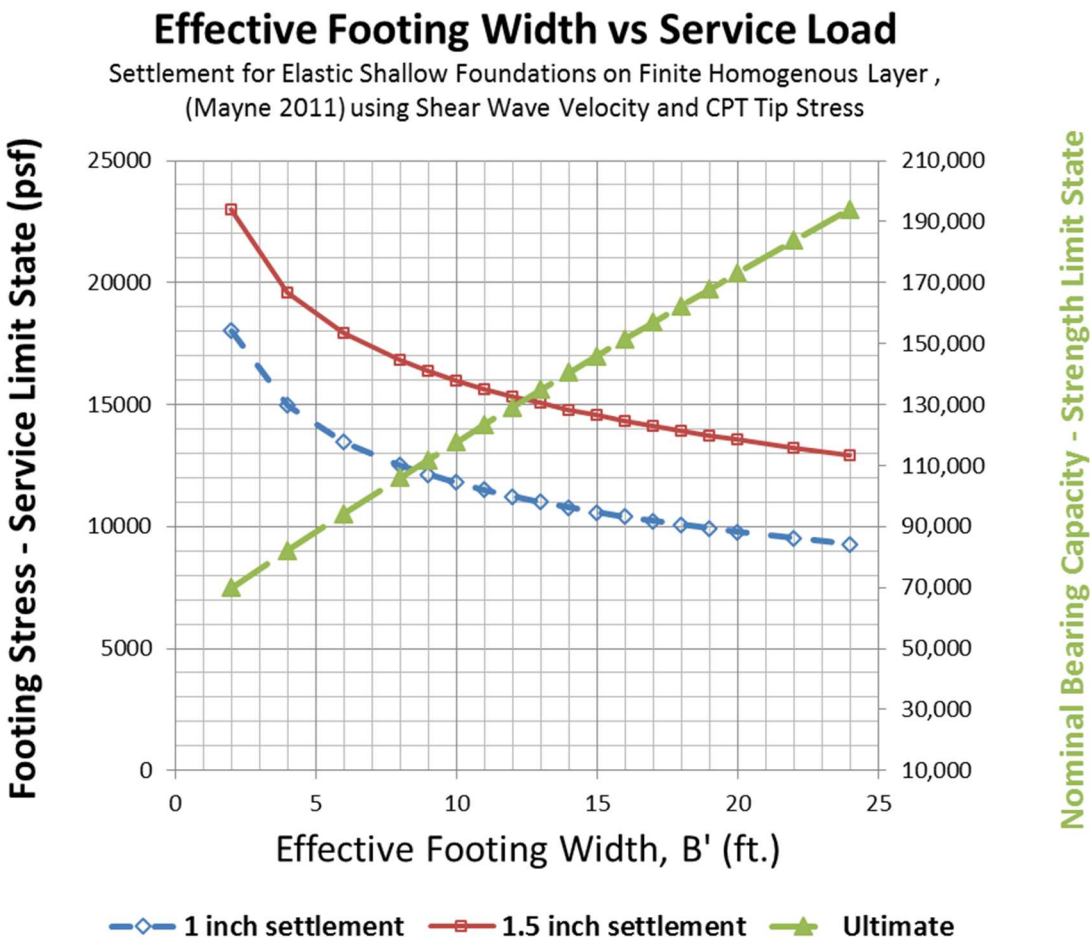


**Figure 1.5** *Excerpt from MnDOT Design Manual (courtesy Rich Lamb)*

## 2. Bearing Capacity of Shallow Foundations

Foundations must be designed to preclude ultimate collapse or failure of the soil under loading. For a vertically-loaded foundation, an ultimate stress condition exists. The maximum force is referred to as the bearing capacity which is associated with full mobilization of the shear strength of the underlying soil along a prescribed failure surface. In Load Resistance Factored Design (LRFD), this is termed as "limit state".

Theoretical solutions of the "limit state" or geotechnical bearing capacity problem have been developed using upper and lower bound plasticity theorems, limit equilibrium, and cavity expansion theory, as well as numerical modeling simulations. Depending upon the specific assumptions made regarding the soil stress-strain characteristics, drainage conditions, rate of loading, boundary conditions, initial stress state, homogeneity, uniformity, or layering, a number of different solutions have been generated and published in the geotechnical literature.

In the presented section, the general shear solution used in conventional practice is based on limit plasticity theory and set of solutions as summarized by Vesić (1975) with the following assumptions: plastic equilibrium, plane strain conditions, soil above the foundation level is surcharged, and the general failure zones can be presented as active Rankine, radial shear (Prandtl), and passive Rankine zones as presented in **Figure 2.1**.

The form of the general bearing capacity equation has three main components:

$$q_n = c \cdot N_c + \tfrac{1}{2} \cdot B \cdot \gamma \cdot N_\gamma + \sigma_{vo}' \cdot N_q \qquad [2.1]$$

**ultimate bearing stress = cohesion term + unit weight term + surcharge term**

where c is either the undrained shear strength ($s_u$) in total stress analyses (TSA) or effective cohesion intercept (c') in effective stress analyses (ESA), $\sigma_{vo}'$ = effective overburden vertical stress, B = foundation width (i.e., smaller dimension for rectangular foundation, or d = diameter of equivalent circular foundation), γ = average bulk or effective unit weight of the soil (depending upon the prevailing groundwater conditions), and the N terms are bearing factors that are functions of the foundation shape and effective stress friction angle (ϕ') of the soil. Specifically, the corresponding respective bearing capacity factor terms are those for cohesion ($N_c$) defined by Prandtl (1921), self weight ($N_\gamma$) defined by Vesić (1975), and overburden or surcharge ($N_q$) defined by Reissner (1924). The equations defining the bearing capacity (N) factors are presented in **Table 2.1** and plotted in **Figure 2.2** as a function of the effective friction angle (ϕ') of the soil.

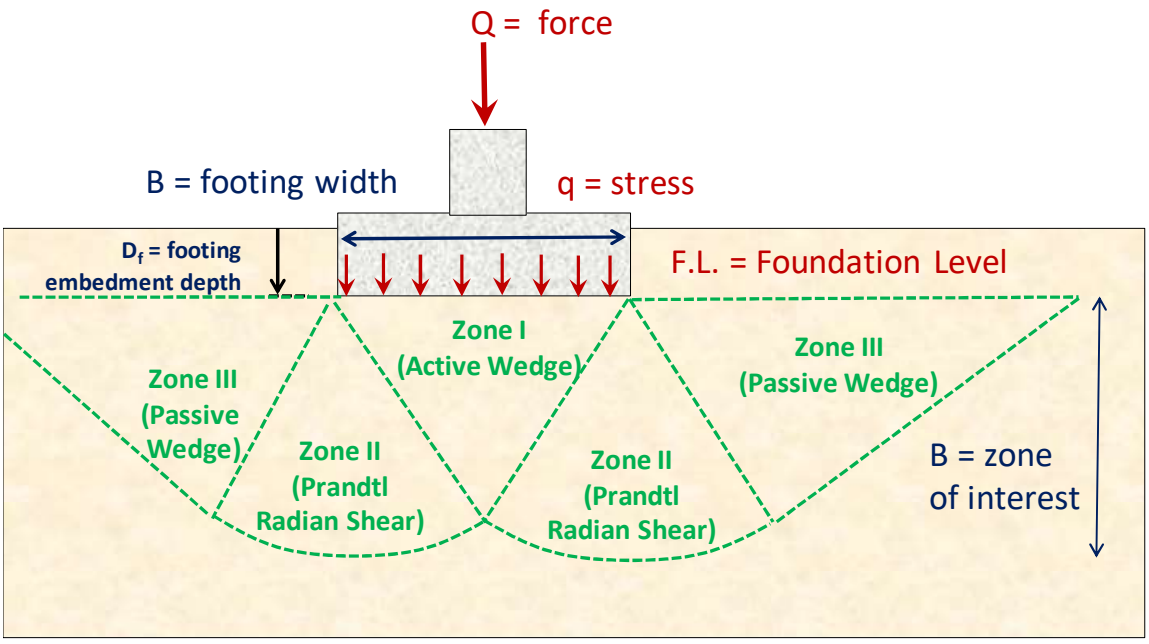


**Figure *2.1*** *Geometry of failure zones beneath foundation as per Vesić limit plasticity solution (1975)*

**Table 2.1** *Bearing Capacity Factors for strip footing: $N_c$ (Prandtl, 1921), $N_q$ (Reissner, 1924), and $N_\gamma$ (Vesic, 1975)*

| Factor | Type Analysis | Friction Angle | Cohesion Term ($N_c$) | Unit Weight Term ($N_\gamma$) | Surcharge Term ($N_q$) |
|---|---|---|---|---|---|
| Bearing Capacity Factors $N_c$, $N_\gamma$, $N_q$ | TSA | $\phi' = 0$ | $2 + \pi$ | n/a | 1.0 |
| | ESA | $\phi' > 0$ | $(N_q - 1)\cdot\cot\phi'$ | $2\cdot(N_q + 1)\cdot\tan\phi'$ | $\exp(\pi\cdot\tan\phi')\cdot\tan^2(45+\phi'/2)$ |

Notes: n/a = not applicable; TSA = total stress analysis (e.g., "undrained" loading); ESA = effective stress analysis (e.g., "drained" loading).

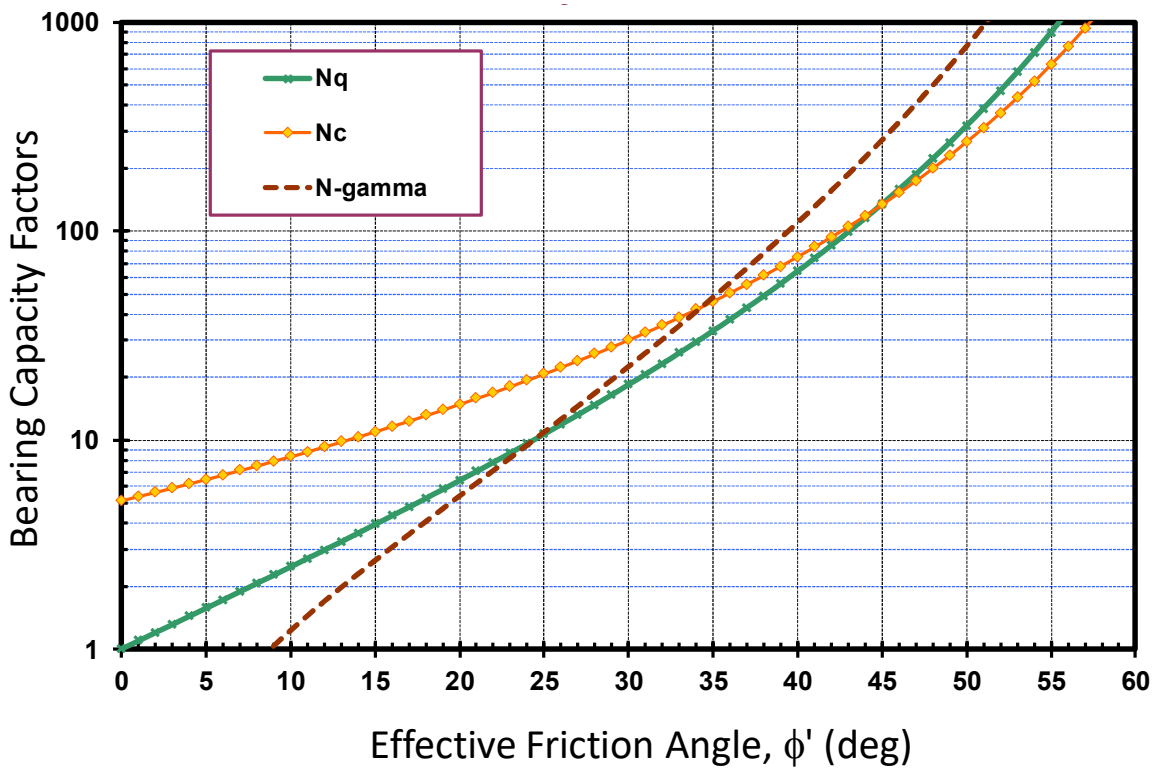


**Figure 2.2** *Bearing Capacity Factors ($N_q$, $N_c$, $N_\gamma$) for Spread Footing Foundations (plane strain case for strip footing)*

The bearing capacity terms ($N_q$, $N_c$, $N_\gamma$) must each be modified to account for a number of additional factors, as specified in AASHTO (2008), including foundation shape

(rectangular distortion ratio L/B), embedment depth ($D_f$), groundwater depth ($D_w$), and load inclination. This results in:

$$q_n = c \cdot N_{cm} + 0.5 \cdot \gamma \cdot B \cdot N_{\gamma m} \cdot C_{w\gamma} + \gamma \cdot D_f \cdot N_{qm} \cdot C_{wq} \quad [2.2]$$

where $C_{wq}$ and $C_{w\gamma}$ are correction factors to account for the buoyance effect of the groundwater and can be defined using **Table 2.2** following AASHTO (2014).

Moreover, one should also consider the possibilities of groundwater table fluctuations over the life of the structure. That is, if the footing is located near a river, lake, coastal region, or high groundwater, a raised water level or flooding may occur at some time in the future and that prospect should be analyzed as the worst case scenario.

**Table 2.2** *Coefficients $C_{wq}$ and $C_{w\gamma}$ for Various Groundwater Cases (AASHTO, 2014)*

| Depth to water table, $D_w$ | Modifier for surcharge bearing term, $C_{wq}$ | Modifier for friction bearing term, $C_{w\gamma}$ |
|---|---|---|
| $D_w \leq 0$ | 0.5 | 0.5 |
| $D_w = D_f$ | 1.0 | 0.5 |
| $D_w > 1.5\ B + D_f$ | 1.0 | 1.0 |

Notes: B = foundation width; $D_w$ = Groundwater Depth; $D_f$ = Foundation Embedment Depth

The modified bearing factor terms ($N_{cm}$, $N_{\gamma m}$, $N_{qm}$) can be defined as follows:

$$N_{cm} = N_c\, s_c\, i_c \quad [2.3]$$

$$N_{\gamma m} = N_\gamma\, s_\gamma\, i_\gamma \quad [2.4]$$

$$N_{qm} = N_q\, s_q\, i_q\, d_q \quad [2.5]$$

Each of the modified bearing factors have dual subscripts, with the first subscript: "c, $\gamma$, and q" for bonding (cohesion), unit weight, and surcharge/overburden, respectively; and the second subscript "m" for modified that accounts for the footing shape (*s*) presented in **Table 2.3**, the load inclination (*i*) illustrated in **Figure 2.3** and presented in **Table 2.4**, and the footing embedment depth (*d*) presented in **Table 2.5**.

The bearing capacity equation can also be modified to account for eccentric loading, base tilt, sloping ground surface, and soil rigidity. These effects require the use of additional modifier terms designated as zeta ($\zeta$) factors presented elsewhere (Vesić, 1975; Kulhawy et al., 1983; Paikowsky et al. 2010).

**Table 2.3** *Foundation Shape Factors $s_c$, $s_q$, and $s_\gamma$ for Bearing Capacity (AASHTO, 2014)*

| Factor | Friction Angle | Cohesion Term ($s_c$) | Unit Weight Term ($s_\gamma$) | Surcharge Term ($s_q$) |
|---|---|---|---|---|
| Shape Factors $s_c$, $s_\gamma$, $s_q$ | $\phi' = 0$ | $1 + \left(\frac{B}{5L}\right)$ | 1.0 | 1.0 |
| | $\phi' > 0$ | $1 + \left(\frac{B}{L}\right)\left(\frac{N_q}{N_c}\right)$ | $1 - 0.4\left(\frac{B}{L}\right)$ | $1 + \left(\frac{B}{L}\tan\phi'\right)$ |

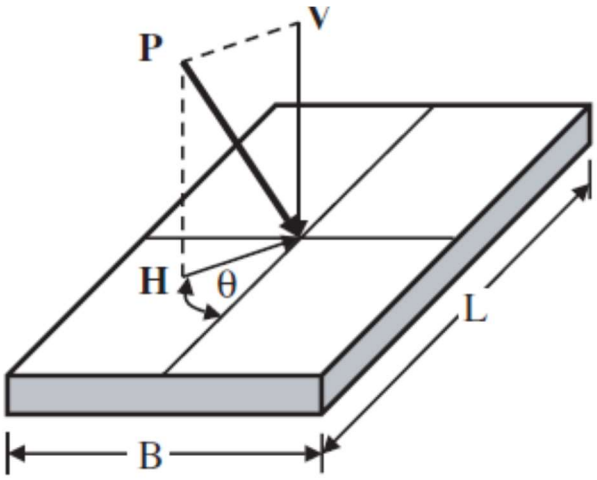


**Figure 2.3** *Inclined load without eccentricity and the projected direction, θ*

(V: vertical load, H: horizontal load, P: projected load, and θ: inclination angle)
(from Paikowsky et al., 2010)

**Table 2.4** *Load Inclination Factors $i_c$, $i_q$, and $i_\gamma$ for Bearing Capacity (AASHTO, 2014)*

| Factor | Friction Angle | Cohesion Term ($i_c$) | Unit Weight Term ($i_\gamma$) | Surcharge Term ($i_q$) |
|---|---|---|---|---|
| Load Inclination Factors $i_c$, $i_\gamma$, $i_q$ | $\phi' = 0$ | $1 - \frac{n.H}{c.B.L.N_c}$ | 1.0 | 1.0 |
| | $\phi' > 0$ | $i_q - \frac{1 - i_q}{N_q - 1}$ | $\left[1 - \frac{H}{V + c.B.L.\cot\phi_f}\right]^{(n+1)}$ | $\left[1 - \frac{H}{V + c.B.L.\cot\phi_f}\right]^{n}$ |

NOTE:

Where n = $\left[\frac{(2+ L'/B')}{(1+ L'/B')}\right] cos^2\theta + \left[\frac{(2+ B'/L')}{(1+ B'/L')}\right] sin^2\theta$

**Table 2.5** *Depth Factor $d_q$ for Bearing Capacity (AASHTO, 2014)*

| Friction Angle, $\phi'$ (Degrees) | $D_f$ /B | $d_q$ |
|---|---|---|
| 32 | 1 | 1.20 |
| | 2 | 1.30 |
| | 4 | 1.35 |
| | 8 | 1.40 |
| 37 | 1 | 1.20 |
| | 2 | 1.25 |
| | 4 | 1.30 |
| | 8 | 1.35 |
| 42 | 1 | 1.15 |
| | 2 | 1.20 |
| | 4 | 1.25 |
| | 8 | 1.30 |

Note: $\phi' = \phi_f$ = effective stress friction angle of soil

The depth correction is recommended only when the soil above the foundation level is as competent as the soil below the foundation level, otherwise it should be taken as 1.0 (AASHTO, 2014). The depth correction factor can be expressed as:

$$d_q = 1 + 2\tan\phi'\cdot(1-\sin\phi')^2 \cdot \arctan(D_f/B) \qquad \text{(Note: arctan in radians)} \qquad [2.6]$$

The three terms of the general bearing capacity equation were derived separately, thus it is appropriate to apply them using one term at a time. The equation is used directly for either shallow or deep foundations and the calculation is performed for either totally undrained ($c = c_u = s_u$ that assumes "$\phi = 0$" analysis) or else fully drained ($\phi'$ and $c' = 0$). Specifically, the term "undrained" loading refers to a condition of constant volume ($\Delta V/V = 0$) in the soil medium, while "drained" loading applies to the case of no excess porewater pressures ($\Delta u = 0$). Partially-drained and partly undrained are intermediate states.

For static loading of sands and granular soils, it is most common for a drained analysis to be conducted. The exception here would be in the case of footings on loose saturated sands in high seismicity areas where soil liquefaction potential is high and can be anticipated during a large earthquake. For foundations on clays and cohesive silts, both a short-term (undrained) analysis and a long-term (drained) analysis should be performed. Using the modified bearing factors, the general bearing capacity solution reduces to the following two cases:

***UNDRAINED:*** *assuming "$\phi = 0$" for fast loading in silts, clays, and soils with low permeability ($\Delta V/V = 0$).* In this case, $N_{qm} = 1$ and therefore:

$$q_n = c \cdot N_{cm} + 0.5 \cdot \gamma \cdot B \cdot N_{\gamma m} \cdot C_{w\gamma} \quad [2.7]$$

***DRAINED:*** *assuming c' = 0 for all loading conditions on sands and for the slow drained loading of silts and clays with $\Delta u = 0$.* In this case, the bearing capacity is:

$$q_n = \gamma \cdot D_f \cdot N_{qm} \cdot C_{wq} + 0.5 \cdot \gamma \cdot B \cdot N_{\gamma m} \cdot C_{w\gamma} \quad [2.8]$$

## 2.1 B.C. of Shallow Foundations in Practice

In the case of shallow footings bearing at or near the ground surface, the overburden term ($\sigma_{vo}'$) is small and can be neglected. The usual approach for *shallow foundations* is simplified to:

**2.1.1 Undrained Loading:** $q_n = c \cdot N_{cm} = N_{cm} \cdot s_u$ [2.9]

where $N_{cm}$ = 5.14 for strip footing; 5.65 for rectangle (A/B = 2), and 6.14 for square or circular footing. The parameter $c = c_u = s_u$ =undrained shear strength of the soil (generally applied to clays and silty soils) is taken as a representative value from the footing base to

a depth of approximately B to 1.5B beneath the base. The value of $s_u$ is best assessed from the relationship:

$s_u/\sigma_{vo}' = ½ \sin\phi' \, OCR^{\Lambda}$ [2.10]

where $\phi'$ = effective stress friction angle, OCR = overconsolidation ratio, and $\Lambda = 1 - C_s/C_c$ where $C_s$ = swelling index and $C_c$ = virgin compression index. If $\phi'$ is unknown, assume a value $\phi' = 28°$ to $30°$. The value of $\Lambda$ is generally ≈ 0.8 to 0.9.

**2.1.2 Drained Loading:** $q_n = 0.5 \cdot \gamma \cdot B \cdot N_{\gamma m} \cdot C_{w\gamma}$ [2.11]

where $N_{\gamma m}$ is the modified bearing factor for friction and expressed as a function of both effective friction angle ($\phi'$), foundation shape (A = plan dimension length and B = plan dimension width), as plotted in **Figure 2.4**. The value for water table correction factor ($C_{w\gamma}$) depends upon the bearing elevation, groundwater depth, and footing size. Values of bearing factor $N_{\gamma m}$ and $C_{w\gamma}$ are given by the aforementioned equations and γ = average bulk unit weight of the soil.

## 2.2 Load Resistance Factored Design (LRFD)

After computing the nominal bearing stress ($q_n$) of the shallow foundation under design, it is recommended per AASHTO (2008) bridge specifications to compute a factored bearing resistance ($q_R$) following the load resistance factored design (LRFD) method. In LRFD, a bearing resistance factor $\phi_b$ is used to compute the factored resistance where:

$q_R = \phi_b \cdot q_n$ [2.12]

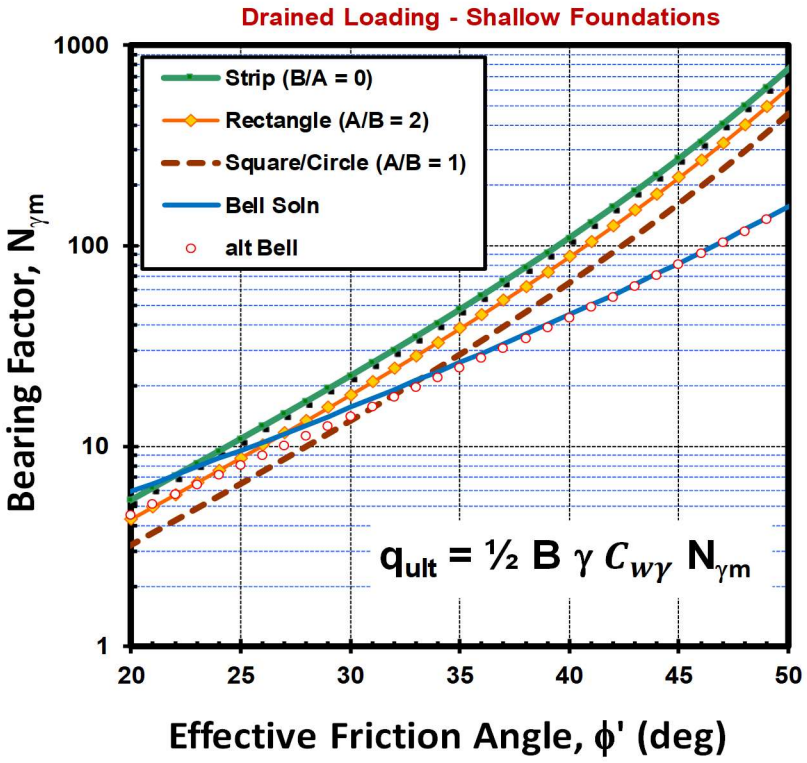


| Bearing Factor, $N_{\gamma m}$ | | |
|---|---|---|
| ϕ' (deg) | Strip Footing | Circle or Square |
| 20.0 | 5.39 | 3.23 |
| 21.0 | 6.19 | 3.72 |
| 22.0 | 7.13 | 4.28 |
| 23.0 | 8.20 | 4.92 |
| 24.0 | 9.44 | 5.66 |
| 25.0 | 10.87 | 6.52 |
| 26.0 | 12.54 | 7.52 |
| 27.0 | 14.47 | 8.68 |
| 28.0 | 16.71 | 10.03 |
| 29.0 | 19.33 | 11.60 |
| 30.0 | 22.40 | 13.44 |
| 31.0 | 25.99 | 15.59 |
| 32.0 | 30.20 | 18.12 |
| 33.0 | 35.17 | 21.10 |
| 34.0 | 41.05 | 24.63 |
| 35.0 | 48.01 | 28.81 |
| 36.0 | 56.29 | 33.77 |
| 37.0 | 66.16 | 39.70 |
| 38.0 | 77.99 | 46.79 |
| 39.0 | 92.20 | 55.32 |
| 40.0 | 109.36 | 65.61 |
| 41.0 | 130.15 | 78.09 |

**Figure 2.4** *Values of bearing factor $N_{\gamma m}$ as a function of effective friction angle ϕ'*

The values of the bearing resistance factor $\phi_b$ can be obtained from one of two sources: (a) AASHTO LRFD design manual; or (b) calibration based on statistical analyses. **Table 2.6** presents the recommended values of $\phi_b$ according to the latest AASHTO LRFD-7 design manual (2014) where the resistance factors are developed using reliability theory and calibration by fitting substantial representative statistic data to the Allowable Stress Design (ASD). In ASD, the calculated factors of safety (FS) range from 2.5 to 3.0 and correspond to bearing resistance factors ($\phi_b$) of 0.55 to 0.45, respectively. The main issue with using such a table is the applicability of the same resistance factor value for all grades of soil type regardless of the loading conditions or the particular strength characteristics;

i.e., $\phi_b$ = 0.50 for all clays irrespective of its undrained shear strength, liquidity index, plasticity characteristics, or continuity (intact versus fissured); or $\phi_b$ = 0.50 for all sands using CPT regardless of its relative density, friction angle, or mineralogy (quartz-silica versus carbonate-calcareous content).

**Table 2.6** *Recommended Resistance Factors for Geotechnical Resistance of Shallow Foundations at the Strength Limit State (after AASHTO, 2014)*

| **Method / Soil / Condition** | | | **Resistance Factor** |
|---|---|---|---|
| **Bearing Resistance** | **Resistance Factor, $\phi_b$** | Theoretical Method (Munfakh et al., 2001), for Clays | 0.50 |
| | | Theoretical Method (Munfakh et al., 2001), for Sands using CPT | 0.50 |
| | | Theoretical Method (Munfakh et al., 2001), for Sands using SPT | 0.45 |
| | | Semi-empirical methods (Meyerhof, 1957), for all soils | 0.45 |
| | | Footings on Rock | 0.45 |
| | | Plate Load Test (PLT) | 0.55 |

To overcome the wide applicability of the values recommended by the AASHTO, a second source was used to define the bearing resistance factors as presented in **Table 2.7** following the recommendations of Paikowsky et al. (2010) that focused on granular soils with friction angles ranging from $30° < \phi' < 45°$ and relative densities with $D_R > 35\%$. The soils were divided into distinct classes based on effective friction angle and different loading conditions. Corresponding LRFD reduction factors were suggested based on statistical analyses ($\lambda$ and COV) of *computed bias resistance*, defined as the ratio of measured/predicted resistance for a database of well documented case studies.

**Table 2.7** *Recommended Resistance Factors for Shallow Foundations on Natural Deposits of Granular Soil (after Paikowsky et al., 2010)*

<table>
<tr><th rowspan="3">Soil Friction Angle, ϕ'</th><th colspan="4">Loading Conditions</th></tr>
<tr><th rowspan="2">Vertical – Centric or Eccentric</th><th rowspan="2">Inclined - Centric</th><th colspan="2">Inclined - Eccentric</th></tr>
<tr><th>Positive</th><th>Negative</th></tr>
<tr><td>30° - 34°</td><td>0.40</td><td rowspan="3">0.40</td><td rowspan="2">0.35</td><td>0.65</td></tr>
<tr><td>35° - 36°</td><td>0.45</td><td rowspan="2">0.70</td></tr>
<tr><td>37° - 39°</td><td>0.50</td><td rowspan="2">0.40</td></tr>
<tr><td>40° - 44°</td><td>0.55</td><td>0.45</td><td rowspan="2">0.75</td></tr>
<tr><td>> 45°</td><td>0.65</td><td>0.50</td><td>0.45</td></tr>
</table>

Using the aforementioned limit plasticity solutions and modifier terms for shape, depth, and groundwater conditions, plus the recommended resistance factors from AASHTO LRFD specifications, the bearing capacity stresses for the limit state were determined for a variety of rectangular footings of different widths (B) and rectangular distortions (L/B). The soil input parameters for bearing capacity determinations concerning footings on granular soils includes evaluations of the unit weight ($\gamma$) and effective friction angle ($\phi'$) that were determined from in-situ test results (e.g., SPT, CPT, DMT), as detailed in later sections of this report.

Even though the Piedmont/Blue Ridge soils may classify as fine-grained soils per USCS, in reality, their behavior is primarily a drained to partially-drained response during normal rates of construction for shallow foundations and MSE walls. The methodology discussed herein would be considered applicable for these geomaterials.

# 3. Settlement Computation for Shallow Foundations

## 3.1 Foundation Displacements and Settlements

For static loading of building foundations, there can be up to three types of displacements that may occur during the construction and occupancy phases: (1) immediate or initial undrained distortion (mainly on soft clays); (2) drained settlement due to primary consolidation (all built footings experience this phase); and (3) long-term creep due to secondary compression (primarily significant in organic clays and peats). These settlements can be written together as:

$$\rho_{total} = \frac{q \cdot d \cdot I \cdot (1 - v_u^2)}{E_u} + \frac{q \cdot d \cdot I \cdot (1 - v^2)}{E'} + \frac{C_{\alpha e}}{1 + e_o} \Delta z \cdot \log t$$

**Total** = **undrained distortion** + **drained settlement** + **long-term creep**

***Displacements:*** *initial* *primary consolidation* *secondary compression*

The undrained distortion phase only occurs if the rate of loading is fast relative to the low permeability of the ground, generally involving deep thick deposits of soft saturated clays and silts. If this phase is relevant, then Poisson's ratio is $v_u$ = 0.5 corresponding to zero volume change and concerns over undrained bearing capacity may prevail. For foundations situated on clay subsoils, it is standard practice to calculate vertical deflections during undrained loading using a three-dimensional elastic solution (Skempton and Bjerrum, 1957; D'Appolonia et al., 1971; Foott and Ladd, 1981). The undrained stiffness is expressed by an undrained modulus ($E_u$) that is derived from triaxial

tests or in-situ field method such as the pressuremeter test (PMT). Vertical deflections that occur under undrained loading are properly termed as “undrained distortion”.

The most common and prevalent settlement component is that due to drained primary consolidation, normally calculated from e-log$\sigma_v'$ graphs, as obtained from one-dimensional consolidation tests on undisturbed samples. The settlement calculations rely on evaluating the effective preconsolidation stress ($\sigma_{vmax}'$), the recompression index ($C_r$), virgin compression index ($C_c$), and swelling index ($C_s$). If time-rate-of-consolidation will occur, the coefficient of consolidation ($c_v$) is also required. Full details on these calculation procedures are given elsewhere (Perloff and Baron, 1976; Lambe and Whitman, 1979; Holtz and Kovacs, 1981). In consolidation settlement, the footing loading should not exceed the preconsolidation stress in the ground. Elasticity theory is used in the aforementioned approach to calculate the vertical stress increase in the underlying sublayers of soil.

An alternate approach uses the constrained modulus (D') also evaluated from one-dimensional consolidation test data, where $D' = \Delta\sigma'_v / \Delta\varepsilon_v$ and is related to the equivalent elastic Young's modulus E’ by (Lambe & Whitman 1979):

$$D' = \frac{E\prime\cdot(1-\nu\prime)}{(1+\nu\prime)(1-2\upsilon\prime)} \qquad [3.1]$$

For strain levels associated with foundation deflections, the majority of strains in the soil mass are small strains on the order $\varepsilon < 0.1\%$ and a value of Poisson’s ratio in the range of $0.1 < \nu' < 0.2$ is appropriate. The drained moduli can be determined using laboratory tests

on undisturbed samples (e.g., oedometer tests, drained triaxial tests), or field tests (e.g., pressuremeter and/or flat dilatometer tests), provided that the tests are conducted at strain rates relevant to drained loading ($\Delta u = 0$) and appropriate stress levels and/or relevant strains comparable to the full scale situation. In sands, the material permeability is high and permits rapid drainage upon loading. In clays and silts, the rates can be very slow depending upon the permeability and degree of overconsolidation.

Settlements due to drained primary consolidation occur for every footing or foundation under working loads. That is, every foundation that has ever been built and loaded to design has experienced some movement or settlement that occurred under drained primary consolidation. Thus, this is the type of settlement deserving primary attention for the majority of bridge and wall structures. For special cases when these structures bear on soft compressible clays, a case-by-case basis of geotechnical analyses will be necessary.

Creep over time (t) continues unabated for many decades or longer. Creep settlements are therefore analogous to getting older; i.e., time marches on but cannot cease. Thus, creep is not normally a significant foundation problem, except in cases involving very soft organic soils, particularly OH clays, silts, and peats. The phenomenon of creep in soils is represented by the coefficient of secondary compression ($C_{\alpha e}$). The magnitude of $C_{\alpha e}$ has been linked to the virgin compression index ($C_c$). Thus, $C_{\alpha e}$ may be estimated from the empirical relationships (Mesri, 1973): sands ($C_{\alpha e}/C_c$) = 0.03; inorganic clays and silts: ($C_{\alpha e}/C_c$) = 0.04; organic clays ($C_{\alpha e}/C_c$) = 0.06 to 0.08.

As the GDOT bridge structures and walls will be considered for foundations situated on sands and granular geomaterials, as well as natural Piedmont soils (fine sandy silts and silty fine sands), the focus herein is for calculating drained settlements due to primary consolidation. For this, elasticity theory may be used to calculate the magnitudes of shallow foundation settlements in two ways: (a) propagating induced stresses with depth and using results from e-log$\sigma_v$' data; or (b) displacement influence factors where strains are accumulated with depth and elastic moduli (D' and/or E') are input parameters. Poulos and Davis (1974) provide a compilation of rigorous elastic solutions that are specific to the following cases: foundation shape (circular, square, rectangular), soil homogeneity (modulus either constant or varying with depth), finite layer depth, multi-layering, foundation roughness, interface roughness, Poisson effect (radial strains), foundation stiffness (footing versus mat), and drainage conditions (undrained versus drained).

Foundation settlements for sands are not commonly evaluated via one-dimensional consolidation theory because of the difficulties in sampling of undisturbed specimens for laboratory testing. Instead, drained settlements on sands are usually calculated using displacement influence factors (Gibson 1967; Harr, 1966; Poulos & Davis 1974; Harr 1977; Das 2011) and data obtained from in-situ tests (Beradi, et al., 1991; Fellenius 1996, 2009; Sargand et al. 2003; Mayne 2006).

The method of displacement influence factors is justifiably applicable to calculating both undrained distortional-type and drained consolidation-type settlements for all soil types. It can be shown that the one-dimensional e-log$\sigma_v$′ approach is merely a subset of the

more general three-dimensional elasticity solution (Fellenius, 1996; 2009), whereby the radial strains are neglected and correspond to the simple elastic case with Poisson's ratio ν = 0. In lieu of the compression indices, a constrained modulus is used to describe the stiffness of the soil matrix compressibility, where $m_v$ = coefficient of volumetric compressibility (Janbu, 1969; Schmertmann, 1986). For the recompression portion of the e-log$\sigma_v'$ curve, corresponding to overconsolidated soils, for example, it is a simple matter to show that (Stamatopoulos and Kotzias, 1978):

$$D' = 1/m_v = \ln(10)\ \sigma_{vo}'\ (1+e_o) / C_r \qquad [3.2]$$

## 3.2 Foundation Displacements

The general form for settlement calculation by displacement influence factors is:

$$s = \rho = \frac{q \cdot B \cdot I}{E_s} \qquad [3.3]$$

where s = ρ = foundation settlement, q = applied stress, B = foundation width, $E_s$ = equivalent average elastic soil modulus, and I = displacement influence factor. Rigorous solutions to obtain the displacement influence factors are fairly involved and require the establishment of equilibrium equations, continuity equations, constitutive relationships, and kinematics, as well as complex integrals (Ueshita and Meyerhof, 1967; Gibson, 1967; Stark and Booker, 1997). The solutions depend upon several parameters, including foundation shape (A and B), Poisson's ratio (ν), modulus variation with depth, soil layering, finite layer thickness (h), foundation roughness, and interface adhesion.

A great variety and number of solutions exist in the literature for different theories, initial governing assumptions, foundation geometries, and specific situations ( Poulos and Davis, 1974; Teferra and Schultz, 1988). Most of the solutions are given in normalized forms, but the graphical or chart presentations may make it appear that there are significant differences amongst the various solutions, whereas in fact, the solutions are quite similar. Mayne and Poulos (1999) provide an approximate solution for obtaining displacement influence factors using numerical integration, and illustrate compatibility with a number of well-known rigorous solutions that have been presented in differing formats.

## 3.3 Approximate Displacement Influence Factors

The displacement influence factor can be defined as summation of all vertical deflections occurring directly beneath the foundation and within the elastic medium. The maximum value is sought, as referenced to the center of the foundation base. The general derivation for the displacement influence factor is given by (Davis and Poulos, 1968):

$$I = \int_0^{h/d} \varepsilon_z \cdot dz^* \qquad [3.4]$$

where z* = z/d = normalized depth and the vertical strains ($\varepsilon_z$) are summed from the base of the footing to some particular depth of interest, for instance, from z* = 0 to z* = h/d, where h = depth to an incompressible layer such as bedrock. In the case of the flexible foundation, the unit strains may be calculated from the constitutive relationship of Hooke's Law:

$$\varepsilon_z = \frac{1}{E}\left[\Delta\sigma_z - \nu \cdot \left(\Delta\sigma_x + \Delta\sigma_y\right)\right] \qquad [3.5]$$

where $\Delta\sigma_z$ = change in vertical stress at depth z and $\Delta\sigma_{x,y}$ = change in lateral stress in x and y directions at depth z. The incremental change of vertical stress with depth ($\Delta\sigma_z$ ) is well-known and derived by integrating the Boussinesq point load over a distributed surface area (Perloff and Baron, 1976):

$$\Delta\sigma_z/q = 1 - \frac{1}{\left[1+\left(\frac{a}{z}\right)^2\right]^{\frac{3}{2}}} \qquad [3.6]$$

where a is an equivalent radius of the footing under study.

The influence factors $I_z$ for a uniform rectangular loading (q) is presented in **Figure 3.1,** specifically under the center, corner, far, and close edges (mid-center). The approximate spreadsheet solution is compared to the rigorous Giroud (1968) solution.

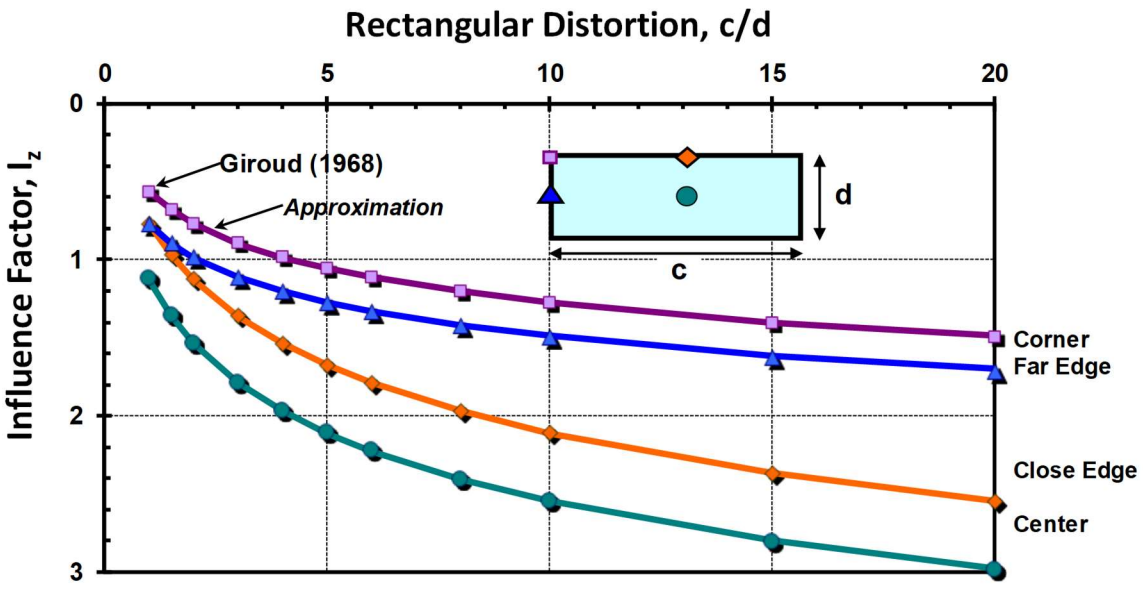


**Figure 3.1** *Displacement Influence Factors for Different Points (center, corner, edges) under a Uniform Rectangular Loading.*

The vertical stress increase ($\Delta\sigma_z$) under the center of a uniform rectangular surface loading with length (c) and width (d) can be computed using (Harr 1977):

$$Center \quad : \Delta\sigma_z / q = \frac{2}{\pi}\frac{mn}{\sqrt{1+m^2+n^2}}\frac{1+m^2+2n^2}{(1+n^2)(m^2+n^2)} + \frac{2}{\pi}\sin^{-1}\left(\frac{m}{\sqrt{m^2+n^2}\sqrt{1+n^2}}\right) \quad [3.7]$$

$$where \quad m = c/d \quad and \quad n = 2z/d$$

It is common geotechnical practice, in fact, to consider only vertical stress increases when calculating settlements of shallow foundations (Schmertmann 1986), and to use the results of one-dimensional consolidation tests to evaluate the compressibility characteristics of the various soil layers (Holtz and Kovacs 1981). In the one-dimensional uniaxial case, the lateral strains are neglected and the resulting vertical strains for the influence factor can be calculated from:

$$\varepsilon_z = \frac{\Delta\sigma_z}{D'} \quad [3.8]$$

For the special case with v = 0, the interrelationship is D′ = E′. Using the calculated vertical stress changes with depth for a circular area of unit diameter (d = 2a = 1) under unit stress (q = 1) over a homogeneous elastic material of unit modulus (D′ =1), it is an easy matter to calculate the incremental strains via a spreadsheet and numerically integrate the results over a specified depth of interest. The distributions of unit vertical strains ($\Delta I_z$) with depth are shown in **Figure 3.2**. The strains are summed over a large dimensionless depth (z* = z/d > 25) on a spreadsheet to give a practical solution to the semi-infinite elastic half-space (z* = ∞). For the case where v = 0, the integration of $\Delta I_z$ with depth gives a cumulative influence factor I = 1, corresponding to the general Boussinesq case. For the

more general case of triaxial stresses, the incremental increase in horizontal stress for axisymmetrical loading under a uniform circle is given by (Poulos and Davis, 1974):

$$\Delta\sigma_r/q = \frac{1}{2} + v' - \frac{(1+v')}{[1+(a/z)^2]^{0.5}} + \frac{1}{2\cdot[1+(a/z)^2]^{1.5}} \quad [3.9]$$

For these situations (v > 0), the vertical strains $\varepsilon_z$ can be calculated using both $\Delta\sigma_z$ (eqn 3.6) and $\Delta\sigma_r$ (eqn 3.9) with Hooke's Law (eqn 3.5), giving the other curves shown in **Figure 3.2**. These approximate the rigorous solutions for a rough or adhesive interface between the elastic compressible medium and underlying incompressible layer. In fact, these serve as the basis for the well-known footing settlement method using CPT results introduced by Schmertmann (1970) and revised method (Schmertmann et al. 1978).

Using a spreadsheet, the integral sign for calculating displacement influence factors is replaced by the summation over small layers. Thus, for a homogeneous soil, the influence factor is:

$$I_h = \sum \Delta I_z \cdot (\Delta z/d) \quad [3.10]$$

## 3.4 Poisson's Ratio

Recent research has shown that the drained value of Poisson's ratio (v′) corresponding to foundation settlements is less than earlier thought (Mayne and Poulos, 1999). The conventional external measurements of specimen strains in routine laboratory triaxial tests have been found to reflect difficulties due to end effects, stress nonuniformity, capping problems, and seating errors, resulting in the reporting of inappropriate values

of ν′ on the order of 0.30 to 0.45 and measured soil stiffnesses that are too low (Jamiolkowski, et al., 1994, LoPresti, 1995).

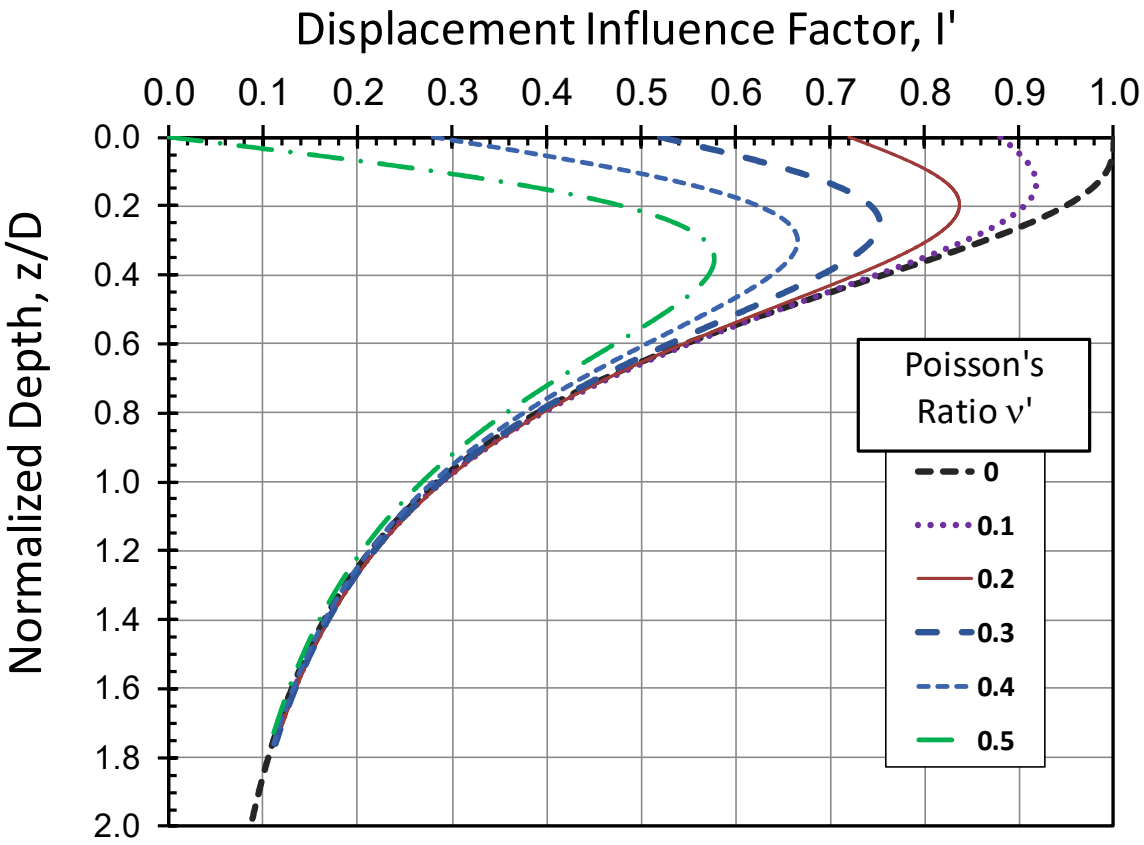


**Figure 3.2** *Strain Influence Factors from Elastic Theory for a Circular Foundation and Varying Soil Poisson's Ratio*

Accurate measurements are now possible using local strain devices mounted midlevel on soil specimens and measured internally to the triaxial cell (e.g., Tatsuoka and Shibuya, 1992). The range of strain levels relevant to foundation deformation problems is between 0.01% and 0.2% (Jardine, et al. 1985; Burland, 1989), and therefore, the appropriate value of Poisson's ratio to use in elastic continuum solutions for drained loading is $0.1 < \nu' < 0.2$ for all soil types, including sands (Tatsuoka, et al., 1994; Lehane & Cosgrove 2000) and clays (Jamiolkowski et al., 1995; LoPresti et al,. 1995).

For undrained conditions involving short-term loading of clays, it remains appropriate to use the value from elastic theory with $v_u$ = 0.5. However, this case is not considered applicable to the method and procedures discussed in this report.

## 3.5 Finite Layer Thickness

For situations where the compressible geomaterial layer is of finite thickness (h) and underlain by an incompressible stratum (bedrock), spreadsheet integration is performed over a limited depth from z = 0 to z = h (Széchy and Varga, 1978). The displacement influence factor ($I_h$) can be expressed in terms of the foundation geoemetry (expressed in the rectangular distortion ratio, c/d) and in terms od normalized layer thickness, h/d. An algorithm to fit the Harr (1966) solution can be expressed as:

$$I_h = \frac{1}{0.9 - \dfrac{1}{1.69 + 2.08/[(c/d) - 0.8]} + [0.116 \cdot \ln(c/d) + 0.654] \cdot \dfrac{1}{(h/d) + 0.001}} \quad [3.11]$$

Results for the displacement influence factor ($I_h$) are shown in **Figure 3.3** for a uniformly-loaded (flexible) rectangular foundation with different distortion ratio (c/d) ranging from c/d = 1 for a square footing to c/d > 10 for a strip footing. The soil layer is finite and represented by the ratio of thickness to width (h/d).

## 3.6 Foundation Rigidity

The foundation stiffness affects the overall distribution of stresses and corresponding displacements. Analytical solutions for a infinitely thick layer indicate that the magnitude of deflection of a rigid circular footing is 0.785 times that of the centerpoint of a flexible

foundation. Thus, it is convenient to define a foundation flexibility factor (after Brown, 1969b):

$$K_F \approx \frac{E_{FDN}}{E_{s(av)}} \cdot \left(\frac{t}{a}\right)^3 \qquad [3.12]$$

where a = foundation radius, $E_{FDN}$ = elastic modulus of foundation material (reinforced concrete), $E_{s(AV)}$ = representative elastic soil modulus beneath the foundation base (i.e., value of $E_s$ at depth z = a), and t = foundation thickness. If the percentage of concrete and reinforcing steel are known, the value of $E_{FDN}$ may be calculated. Alternatively, for many reinforced concrete foundations, an approximate value may be assumed on the order of $E_{FDN} \approx$ 30 GPa = 313,283 tsf.

The above definition of foundation flexibility is reasonable for footings and rafts, even though the nominal effects of ν' have been omitted (Horikoshi and Randolph, 1997). The variation of displacement influence factor for a circular foundation resting on an infinite elastic half-space has been previously evaluated in terms of the foundation flexibility factor, $K_F$, using finite element analysis (Brown, 1969b), as presented in **Figure 3.4**. The limiting values from analytical solutions for perfectly flexible and perfectly rigid are shown at $I_F$ = 1 and π/4, respectively. According to **Figure 3.4**, the following categories can be made: (a) perfectly rigid with $K_F > 10$; (b) intermediate flexibility with $0.01 < K_F < 10$, and (c) perfectly flexible with $K_F < 0.01$. As an approximation, the aforementioned influence factor can be expressed as a correction factor for foundation flexibility (or rigidity):

$$I_F \approx \frac{\pi}{4} + \frac{1}{4.6+10 \cdot K_F} \qquad [3.13]$$

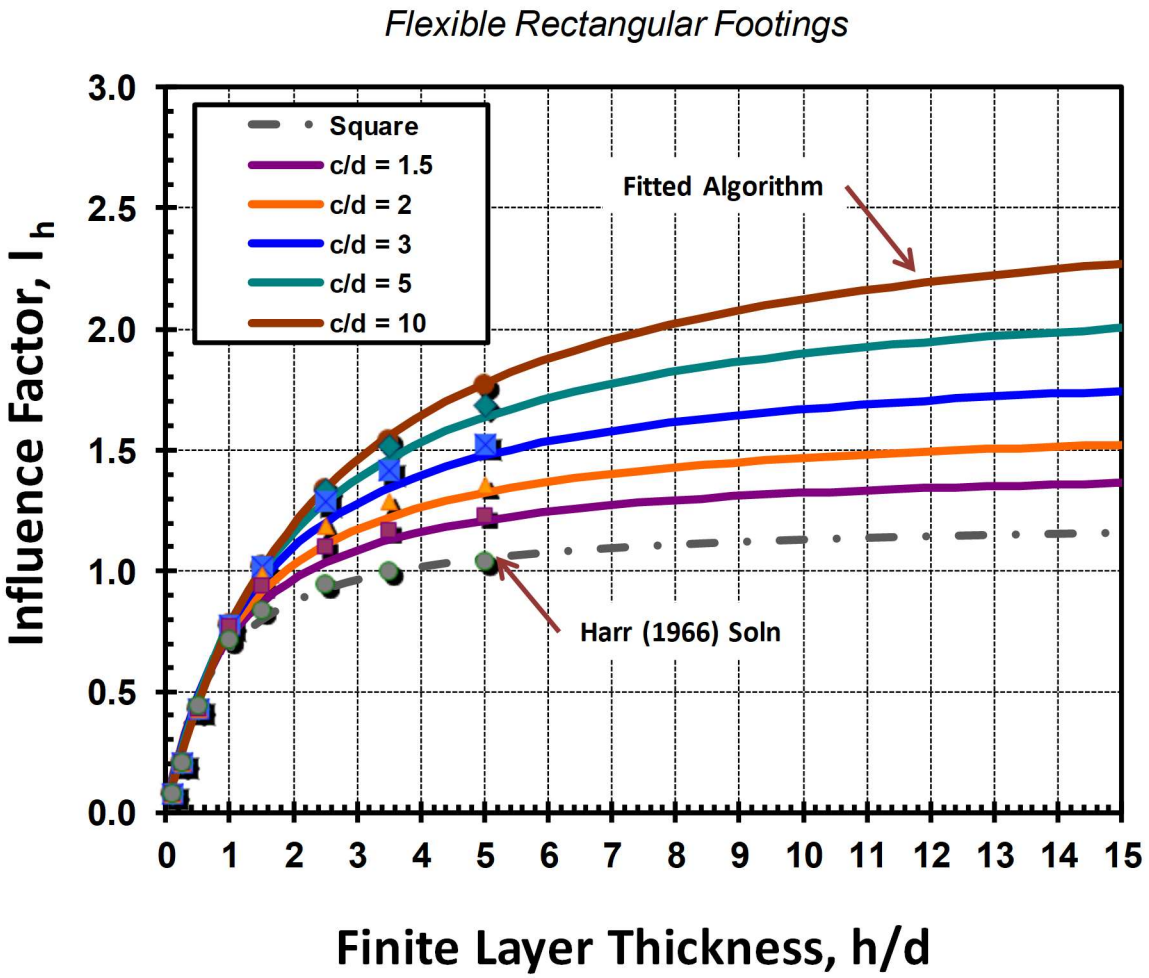


**Figure 3.3** *Displacement Influence Factors for Flexible Rectangular Footing of Different Geometries on Finite Elastic Layer.*

For a rectangular raft or structural mat or footing, Horikoshi and Randolph (1997) discuss the expressions available for foundation flexibility. In order to be compatible for the expression for the circular foundation stiffness, the most rational definition for a rectangular foundation is given by:

$$K_F = 5.57 \cdot \frac{E_{mat}}{E_{soil}} \cdot \frac{(1-\nu_s^{\,2})}{(1-\nu_{mat}^{\,2})} \cdot \left(\frac{B}{L}\right)^{0.5} \cdot \left(\frac{t}{L}\right)^{3} \qquad [3.14]$$

where B = raft (mat) width, L = raft length, t = mat thickness. Here, $E_{mat} = E_{FDN}$ as detailed earlier.

Note that for a rigid circular footing, the magnitudes of settlements are equal at the center and and edge, whereas for perfectly flexible circular mats, the edge settlements are about two-thirds the magnitude of the centerpoint settlement. Thus, the settlements at the edge of a circular foundation ($\rho_{edge}$) can be approximately given by:

$$\frac{\rho_{edge}}{\rho_{center}} \approx 1 - \frac{1.533}{4.6+10 \cdot K_F} \qquad [3.15]$$

If analyzing a square or rectangular footing, a similar approach can be established because the corner settlements of a perfectly flexible foundation are about one-half those at at the centerpoint, whereas for a rigid foundation all points are the same (Poulos and Davis, 1974). So, for square and rectangular foundations, the magnitude of corner settlements can be calculated from:

$$\frac{\rho_{corner}}{\rho_{center}} \approx 1 - \frac{2.3}{4.6+10 \cdot K_F} \qquad [3.16]$$

A rigorous solution shows some slight dependency on the finite layer thickness (Fraser and Wardle, 1976). For consistent comparisons in results, the evaluation of foundation flexibility for slender rectangular rafts should be made using the procedure of Horikoshi and Randolph (1997).

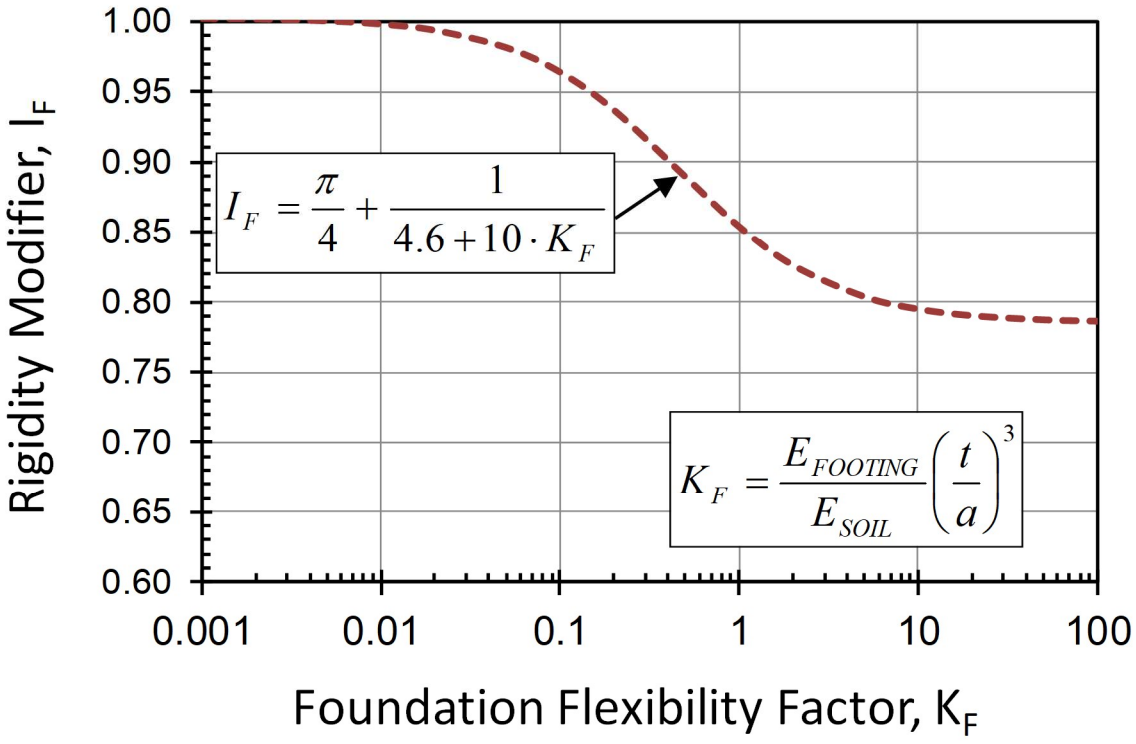


**Figure 3.4** *Effect of Foundation Rigidity on Centerpoint Settlement of Circular Foundation (after Mayne and Poulos, 1999)*

## 3.7 Foundation Embedment

Most footings are embedded below grade in order to protect against frost heave, erosion, and facilitate construction. In many textbooks, the effect of foundation embedment on the settlement response has apparently been overestimated because of the erroneous mixing of various elastic solutions. A detailed discussion of this topic is given by Christian and Carrier (1978). A numerical assessment by finite elements (Burland, 1970) provides a more realistic evaluation of the problem. The correction factor ($I_E$, or originally designated $\mu_o$) has been presented in terms of the ratio of embedment depth ($z_e$) to foundation diameter (d) and Poisson's ratio (v) of the supporting soil medium, as shown in **Figure 3.5**. The effects of embedment can be seen to be relatively modest, unless the foundation

rests quite deep. The numerical results can be roughly expressed by the empirical formula:

$$I_E \approx 1 - \frac{1}{3.5 \cdot \exp(1.22\upsilon - 0.4) \cdot (1.6 + \frac{d}{z_e})} \quad [3.17]$$

## 3.8 Final Form of Settlement Equation

The final form of the settlement equation for shallow rectangular spread footing foundations that accounts for foundation dimensions, finite layer thickness, footing flexibility, and embedment is given by:

$$s_c = \rho_c = \frac{q \cdot B \cdot I_h \cdot I_F \cdot I_E \cdot (1 - \upsilon^2)}{E'} \quad [3.18]$$

where $s_c$ = centerpoint settlement, q = uniform applied stress, B = the width (smaller dimension of rectangular footing), $I_h$ = foundation geometry influence factor, $I_F$ = foundation flexibility influence factor, $I_E$ = embedment factor, and E' = representative elastic modulus of the supporting soil medium.

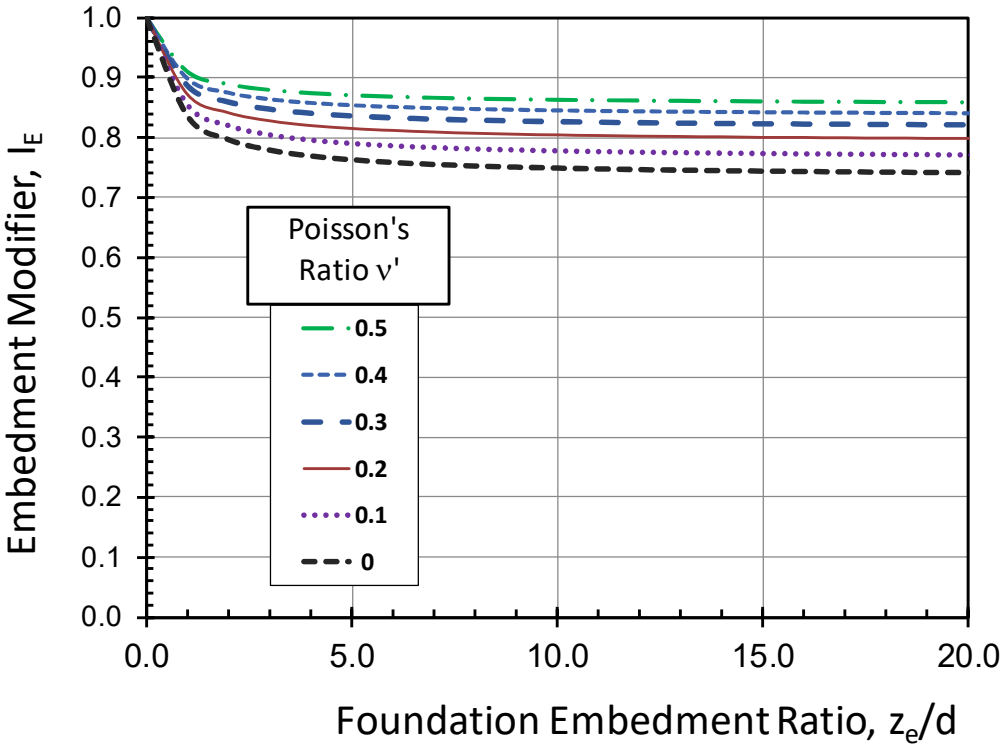


**Figure 3.5** *Embedment Modifier Term for Shallow Foundation Settlements (after Mayne and Poulos, 1999)*

# 4. Input Parameters Using Standard Penetration Tests (SPT)

## 4.1 Overview of the Standard Penetration Test (SPT)

The standard penetration test (SPT) is performed during the advancement of a soil boring to obtain an approximate measure of the dynamic soil resistance, as well as a disturbed drive sample (split barrel type). The test was introduced by the Raymond Pile Company in 1902 and remains today as one of the most common in-situ test worldwide following AASHTO T206 and ASTM D 1586 standards. The main advantages of the SPT are obtaining both a sample and a number. The test is simple, rugged, and suitable in many soil types except for soft clays and coarse gravels. The SPT is usually performed using a conventional geotechnical drill rig and can provide a rough index of the relative strength and compressibility of the soil.

The SPT is conducted at the bottom of a soil boring that has been prepared using either flight augers or rotary wash drilling methods. At depth intervals of about 1.5 m (5 ft), the drilling process is interrupted to perform the SPT which involves driving a thick hollow open pipe at the bottom of the borehole during impacts from a drop hammer.

## 4.2 Equipment

Equipment necessary for performing a standard penetration test include a rotary drill rig, drilling rods, split-barrel (or split spoon) sampler, and a drop weight system. A truck-mounted drill rig is shown in **Figure 4.1) a** and track-mounted rig in **Figure 4.1) b**. Illustrative views of the split barrel sampler are presented in **Figure 4.2**. Over the past century, different types of SPT hammer systems have been used, including: pinweight,

donut, safety, and automatic free-fall versions. The SPT resistance is highly-dependent upon the type of hammer and energy efficiency, and also influenced by the borehole size, type of rods, length of rods, operator performing the test, and other factors (Skempton 1986; Kulhawy & Mayne 1990).


***Figure 4.1*** *Drilling Rigs for Conducting SPT: (a) CME truck rig (b) GeoProbe Systems*

## 4.3 Procedures

Test procedures for the SPT consist of repeatedly dropping a 63.5-kg (140 lb) hammer from a height of 760 mm (30 in) to drive a split-barrel sampler three successive vertical increments of 150 mm (6 in) each, as illustrated in **Figure 4.3**. The number of blows required to drive the sampler each increment and recorded. The initial increment is considered a seating drive. The blows required for the second and third increments are totaled to provide number of blows/300 mm (i.e., blows/foot), referred to as the measured SPT resistance or "N-value" (Sabatini et al., 2002).

**Figure 4.2** *Split-Barrel Samplers used in SPT: (a) closed and (b) open*

Since the SPT is highly dependent upon the equipment and operator performing the test, it is often difficult to obtain repeatable results, particularly amongst different drillers and rigs at the same site. The factors affecting the SPT results include energy inefficiency, type of hammer, number of rope turns, conditions of sheaves and rotating cathead (e.g., lubricated, rusted, bent, new, old), age of rope, actual drop height, vertical plumbness, weather moisture conditions (wet, dry, freezing), inadequate cleaning of hole, careless measure of drop, inaccurate hammer weight, eccentricity of drop, and other issues (Skempton 1986; Sabatini et al. 2002).

When performing an SPT and recording information on the field log, the following items are of note: (1) N is always recorded as an integer; (2) a test is ended and noted as SPT "refusal" if driving resistance is recorded as 50 blows over a 25-mm increment or less (e.g. N > 50/1"); and (3) if the N-value is less than one, then the geoengineer or engineering geologist should record the actual penetration that occurred. For instance, in very soft clays, a value of 1 blow could drive the split barrel sampler the entire vertical distance (i.e., 1/18"), or no driving performed whatsoever, but merely the full or partial

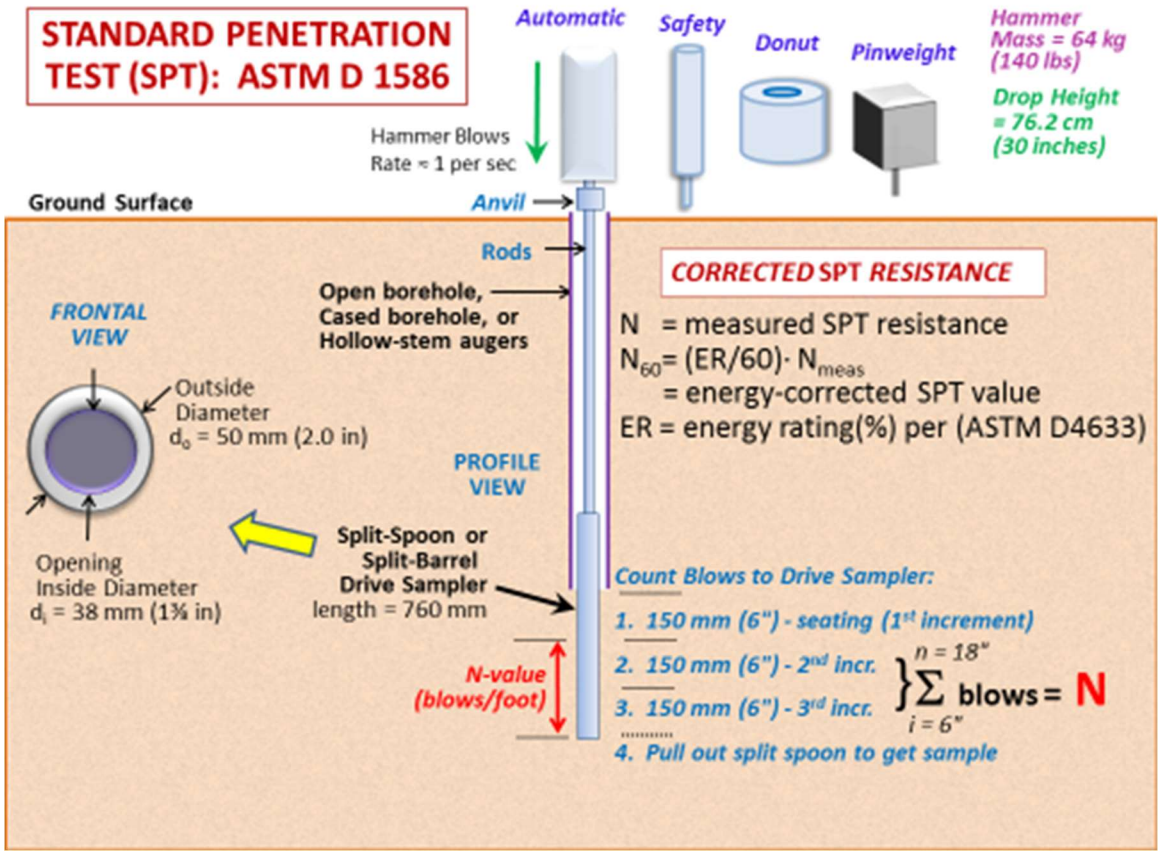


**Figure 4.3** *Illustration of Setup and Procedure for the Standard Penetration Test (SPT)*

penetration occurred due to the added weight of the hammer (WOH) or even just the weight of the rods (WOR).

In the USA, for the most part, many drilling and field testing firms have upgraded to an auto-hammer system in order to facilitate the operations and obtain more consistent results. **Figure 4.4** shows a selection of auto-hammers available for commercial SPT work.


**Figure 4.4** *Various AutoHammers from Different Manufacturers*

## 4.4 Corrections to the SPT N-value

Numerous correction factors to the measured N-value are necessary because of energy inefficiencies and procedural variation in practice. When all factors are applied to the field recorded N-value ($N_{meas}$), the corrected SPT-N value is calculated as:

$$N'_{60} = C_E . C_B . C_S . C_R . N_{measured} \quad [4.1]$$

where the approximate magnitude of corrections for energy efficiency ($C_E$), borehole diameter ($C_B$), sampling method ($C_S$), and rod length ($C_R$) as presented in **Table 4.1** are discussed elsewhere (Skempton 1986, Kulhawy & Mayne 1990, Youd et al. 2001, Boulanger & Idriss 2014). The most important factor is the energy efficiency which is

obtained by a one time calibration using the procedures outlined in ASTM D 4633. Note, in some instances, such as nuclear power plant investigations, the calibration must be checked annually.

The efficiency of the system can be obtained by comparing the kinetic energy, KE, ($KE=\frac{1}{2}mv^2$), with the potential energy, PE, of the system, (PE=mgh), where m = mass, v = impact velocity, g = 9.8 $m/s^2$ = 32.2 $ft/s^2$ = gravitational constant, and h = drop height. The energy ratio (ER) is defined as KE/PE. The theoretical energy of a free-fall system is 4200 in-lb (140 lb falling 30 inches), but is always less due to frictional losses, eccentric loading, wear, and other factors. Calibration of energy efficiency recommended by ASTM D-4633 with strain gages and accelerometer measurements (usually not done by commercial firms). Standard of practice varies from about 35% to 85% with cathead system, but averages about 60%. Newer automatic trip-hammers are available that provide consistent results, however the energy efficiencies still may range from 45% to 97% and depend upon the specific system.

When the necessity for correcting SPT values for energy inefficiently were finally acknowledged circa 1985, a mean ER $\approx$ 60 % was the average standard of practice based on the 1902 to 1985 timeframe (Skempton 1986; Kulhawy & Mayne 1990). The N-values had been primarily obtained from safety and donut hammers, with some data from older pinweight types. Unfortunately, the reference value was established for that timeset (1985) and raw SPT resistances must now always be corrected to $N_{60}$, corresponding to an energy efficiency of 60%.

**Table 4.1** *Definition of different correction factors: depth effect ($C_N$), energy efficiency ($C_E$), borehole diameter ($C_B$), sampling method ($C_S$), and rod length ($C_R$)*

| Factor | Influencing Variable | Field Case | Factor Values |
|---|---|---|---|
| $C_N$ | Depth effect due to increasing effective overburden stress ($\sigma_{vo}'$) | Note: $\sigma_{atm}$ = 1 atmosphere = 1.013 bars = 101.3 kPa = 1.058 tsf | $C_N = (\sigma_{atm}/\sigma_{vo}')^{0.5} \leq 2$ |
| $C_E$ | $C_E$ = ER/60<br>where ER = hammer energy ratio (ASTM D 4633) | Hammer Type:<br>*Automatic:*<br>*Safety:*<br>*Donut:*<br>*Pinweight:* | Range of Factor $C_E$<br>1.0 to 1.6<br>0.8 to 1.3<br>0.6 to 0.8<br>0.5 to 0.7 |
| $C_B$ | Borehole diameter, b (mm) | $65 < b \leq 115$<br>b = 150 mm<br>b = 200 mm | $C_B$ = 1.00<br>$C_B$ = 1.05<br>$C_B$ = 1.15 |
| $C_S$ | Split-barrel sampler | With liner:<br>No liner: | $C_S$ = 1.0<br>$C_S$ = 1.2 |
| $C_R$ | Drill rod length, L (meters) | L > 10 m<br>6 < L< 10 m<br>4 < L < 6 m<br>3 < L < 4 m<br>L < 3 m | $C_R$ = 1.00<br>$C_R$ = 0.95<br>$C_R$ = 0.85<br>$C_R$ = 0.80<br>$C_R$ = 0.75 |

*Note: common US practice is no liner.

**Figure 4.5** shows results from two side-by-side borings with SPTs at the same site in Vermont, as conducted for the Vermont Department of Transportation (VTRANS). This case exemplifies the need for correcting N-values to a common reference energy level. The energies were measured for each strike of the hammer and gave an average ER of 81 % for the CME auto hammer and an average ER of 48 % for the safety hammer at this site. The individual trends for the measured N-values from CMR auto and safety hammers are

quite apparent in **Figure 4.5a** whereas a consistent profile is obtained in **Figure 4.5b** once the data have been corrected to ER = 60%. The N values corresponding to 60 % efficiency are termed $N_{60}$ and are given by:

$$N_{60} = (ER/60) \cdot N_{measured} \quad [4.2]$$

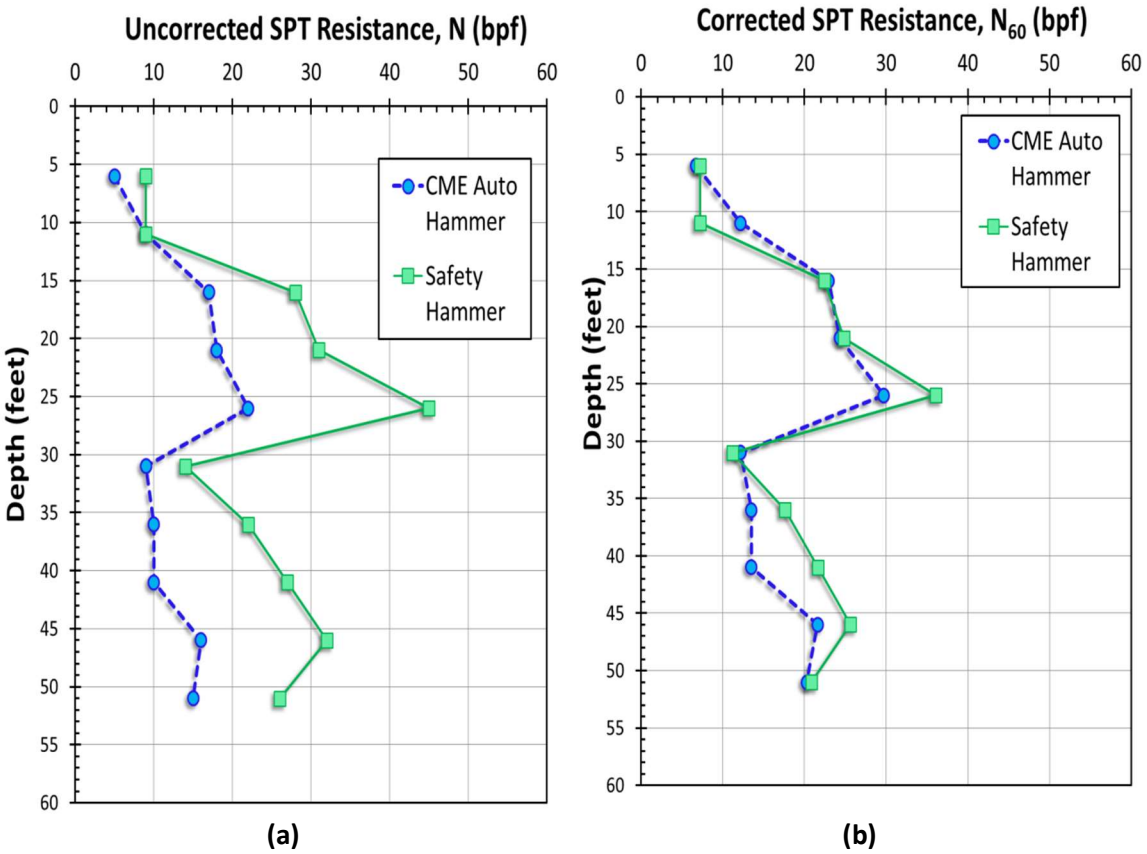


**Figure 4.5** *SPT- N values from Vermont: (a) Uncorrected data; and (b). Corrected data to 60 % efficiency. (Data from VTRANS, 2008)*

A second example of the large differences in N-values obtained from two different hammer systems in presented in **Figure 4.6.** The SPTs have been performed at the national geotechnical experimentation site (NGES) at Northwestern University, Evanston, Illinois. The results are from tests in a fine sand layer (0.15 mm < $D_{50}$ < 0.30 mm) that extends to a depth of around 6.7 m (22 ft). The two sets of N-values were obtained using a safety hammer and an auto hammer.

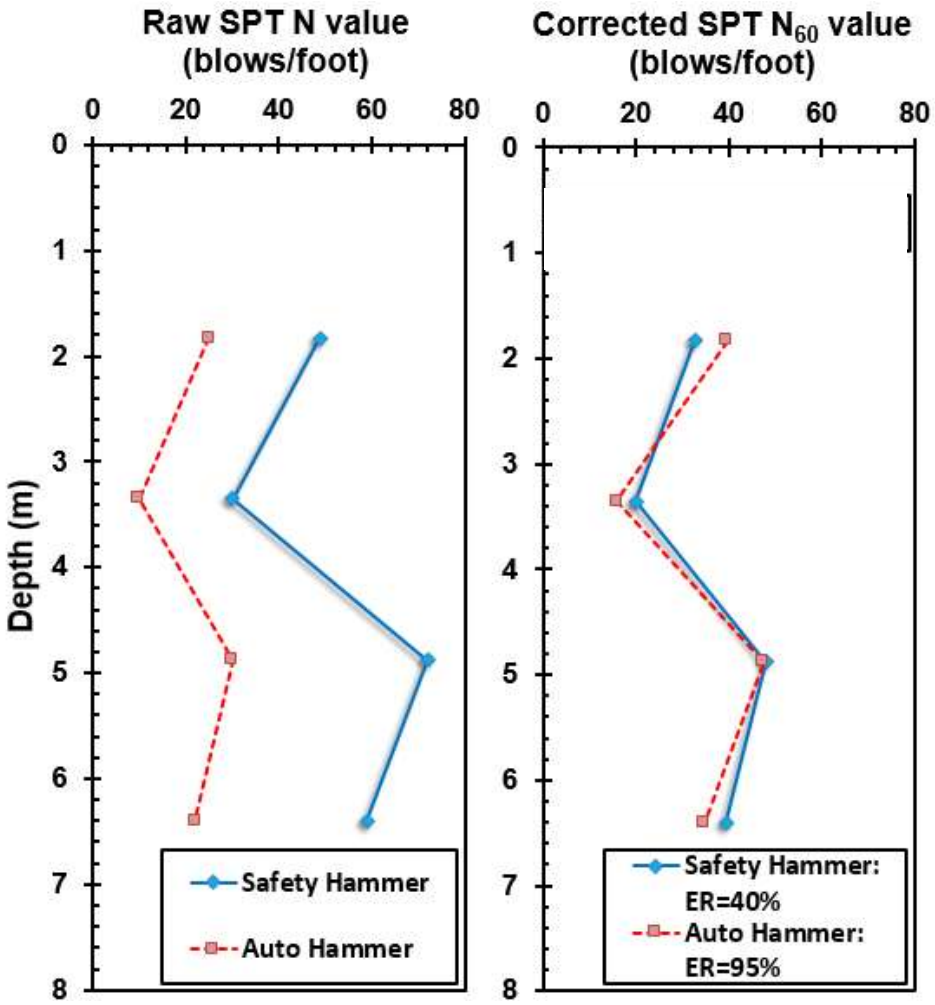


**Figure 4.6** *SPTs at Northwestern University: (a) Uncorrected N values; (b) Energy-Corrected $N_{60}$ values.*

Using the above energy corrections, it is evident that the corrected $N_{60}$ profiles are in good agreement for both hammer systems. However, without the ER correction, the SPT resistances from the auto hammer are too low ($C_E$ = 1.58), while those from the safety hammer are too high ($C_E$ = 0.67). Both require significant corrections.

**Table 4.2** *Summary of Energy Ratios (ER) Measured from AutoHammers in USA*

| AutoHammer System | Mean Energy Ratio (ER) % | Standard Deviation of ER (%) | Location or Agency |
|---|---|---|---|
| Diedrich D-120 | 46 | ± 8.7 | UDOT |
| Diedrich D-50 | 56 | ± 2 | TN |
| CME 850 | 62.7 | ± 4.0 | UDOT |
| BK-81 w/ AW-J rods | 68.6 | ± 7.5 | ASCE/WA |
| Mobile B-80 | 70.4 | ± 4.6 | UDOT |
| CME hammer w skid | 72.9 | ± 4.2 | Washington |
| Diedrich D50 | 76 | ± 5.3 | FDOT |
| CME 45c Skid | 77.4 | ± 5 | VTRANS |
| Diedrich D-120 | 78 | ± 4 | TN |
| CME 55 | 78.4 | ± 8.2 | FDOT |
| CME 850 | 79 | ± 2 | TN |
| CME 45c Track | 80.6 | ± 3.9 | VTRANS |
| CME 45 | 80.7 | ± 10.1 | FDOT |
| CME 45c Track | 81.1 | ± 5.8 | VTRANS |
| CME 85 | 81.2 | ± 3.9 | FDOT |
| CME 75 w/ AW-J rods | 81.4 | ± 4.7 | ASCE/WA |
| CME 75 | 83.1 | ± 5.1 | FDOT |
| CME 75 Track | 84 | ± 5.3 | VTRANS |
| CME 55 Track | 85 | ± 4.9 | VTRANS |
| CME 750 | 86.6 | ± 6.2 | UDOT |
| CME 55 Track | 87.4 | ± 5.4 | VTRANS |
| Mobile B-57 | 88 | ± 3 | TN |
| Mobile B-57 | 93 | ± 3 | TN |
| CME 75 rig | 94.6 | ± 2.1 | UDOT |

**NOTE: Range is factor of 2.1**

There is a general misconception by geoengineers that if the SPT is performed using an autohammer, the results do not need to be corrected for energy content. **Table 4.2** shows a compilation of energy measurements by different organizations at different sites in the USA, all using automatic hammers. These ER data represent thousands of field measurements (ASTM D 4633) for each hammer strike and indicate a documented range of ER from 45% to 95% for autohammer efficiencies. Therefore, one cannot assume a value of ER for a valid correction of energy on a particular system. Interestingly, the state-of-the-practice using autohammers has now risen to a mean value ± one standard deviation of $ER_{ave} \approx 82\% \pm 7\%$ based on some 17,825 ER measurements taken in the past five years (Honeycutt et al. 2014). Unfortunately, the correction reference value remains stuck to the value from 1985 vintage, i.e. $N_{60}$.

Since SPT N-values in the same geomaterial will increase with increasing effective overburden stress, the energy-corrected blowcount ($N_{60}$) is often stress-normalized to an equivalent effective overburden stress of 1 atmosphere (≈ 100 kPa ≈ 1 tsf), also called an overburden correction. The stress-normalized and energy-corrected blowcount is referred to as $(N_1)_{60}$, and is equal to:

$$(N_1)_{60} = C_N \cdot N_{60} \qquad [4.3]$$

where $C_N$ is the stress normalization parameter calculated as:

$$C_N = \left(P_a \Big/ \sigma'_{v0}\right)^n \qquad [4.4]$$

where $P_a$ is atmospheric pressure in the same units as $\sigma_{vo}'$ (i.e., 1 atm ≈ 1 bar ≈ 100 kPa ≈ 1 tsf), and n is a stress exponent typically equal to 0.5 in clean sands (Liao & Whitman, 1986; Kulhawy & Mayne 1990) and increases to 1 in clays (Mayne & Kemper, 1988).

## 4.5 Soil Unit Weight from SPT

The soil unit weight ($\gamma_t$) is needed in the calculation of overburden stresses. The unit weight relates to the more fundamental mass density ($\rho_t$):

$$\gamma_t = \rho_t \cdot g_a \qquad [4.5]$$

where $g_a$ = gravitational constant (= 9.8 m/s$^2$ = 32.2 ft/s$^2$).

Unit weights are best obtained by securing "undisturbed" samples (thin-walled Shelby tubes; piston samples) and weighing a known volume of soil. The ratio of weight to volume is the unit weight.

Soil identity relationships provide information about the initial state of the soil. One primary identity is:

$$G_s \cdot w_n = S \cdot e_0 \qquad [4.6]$$

where $G_s$ = specific gravity of solids (for "normal" soils: $G_s = 2.70 \pm 0.1$), $w_n$ = natural water content, S = degree of saturation (S ranges from zero in dry soil to 100% in fully saturated soils), and $e_0$ = initial void ratio.

A second identity for the general case of unit weight is:

$$\gamma_t = \frac{1+w}{1+e} \cdot G_s \cdot \gamma_w \qquad [4.7]$$

where $\gamma_t$ = unit weight of water (= 9.8 kN/m$^3$ = 62.4 pcf for freshwater). Depending upon the water content and degree of saturation, two boundary cases are commonly taken in soil mechanics: (a) dry soil (with w = 0); and (b) fully-saturated soil with S = 1 (and then: $e = G_s \cdot w$). This gives:

Dry unit weight: $$\gamma_{dry} = \frac{G_s \cdot \gamma_w}{1+e} \qquad [4.8]$$

Saturated unit weight: $\gamma_{sat} = \frac{G_s + e}{1 + e}\gamma_w$ [4.9]

For solid rock (no voids), the unit weight is simply: $\gamma_{rock} = G_s \cdot \gamma_w$ Thus, for $G_s = 2.7$: $\gamma_{rock} = 27$ kN/m$^3$ = 172 pcf). Thus for practical use, the hierarchy for assignment of unit weights would be: $\gamma_{dry} \leq \gamma_t \leq \gamma_{sat} < \gamma_{rock}$.

For soils above the groundwater table, a dry unit weight would apply for no capillarity (i.e., clean sands), while if full capillarity exists (e.g., clays), then a saturated unit weight would be appropriate. If the soil is partially saturated, the total unit weight will depend upon the ambient degree of saturation, likely a value that changes with the weather, humidity, and temperature. For soils below the water table, it is often taken that the total unit weight is equal to the saturated unit weight. In some cases, calculations involve the effective unit weight ($\gamma' = \gamma_{sat} - \gamma_w$), also referred to as the buoyant unit weight or submerged unit weight.

When undisturbed samples or natural water contents are not available, the unit weight can be estimated from the shear wave velocity ($V_s$ in m/s) and depth (z in meters):

$$\gamma_t\,(\mathrm{kN/m^3}) = 8.63\log(V_s) - 1.18\log(z) - 0.53 \quad [4.10]$$

The relationship is shown in **Figure 4.7** and applies to particulate geomaterials that are not cemented or bonded, thus would not be applicable to saprolites, rocks, cemented or structured diatomaceous or calcareous or carbonate soils.

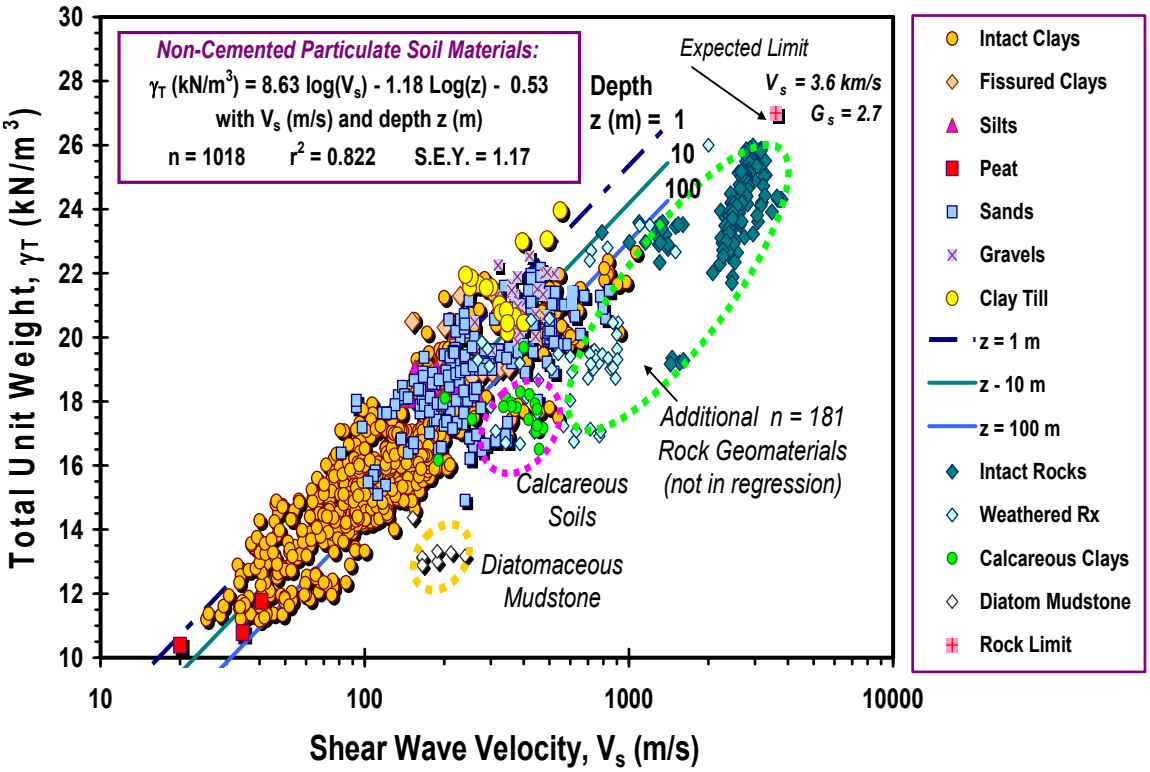


**Figure 4.7** *Relationship for unit weight in terms of shear wave velocity and depth (Mayne, 2005)*

A more fundamental trend is derived in terms of effective overburden $\sigma_{vo}'$ (in kPa) rather than depth z where $\gamma_t$ is expressed:

$$\gamma_t\,(\mathrm{kN/m^3}) = 8.64\log(V_s) - 0.74\log(\sigma'_{v0}) - 0.40 \qquad [4.11]$$

where $V_s$ (m/s) and $\sigma_{vo}' = \sigma_{vo} - u_0$ = effective vertical overburden stress (kPa), $\sigma_{vo} = \int \gamma_t\, dz$ = total overburden stress, $u_0$ = hydrostatic porewater pressure = $h_w \cdot \gamma_w$, and $h_w$ = height of the water table at that elevation.

As these estimated unit weights are in terms of saturated values, a relationship between dry and saturated unit weights can be developed from [4.8] and [4.9] to allow the evaluation of dry unit weights for those conditions (**Figure 4.8**).

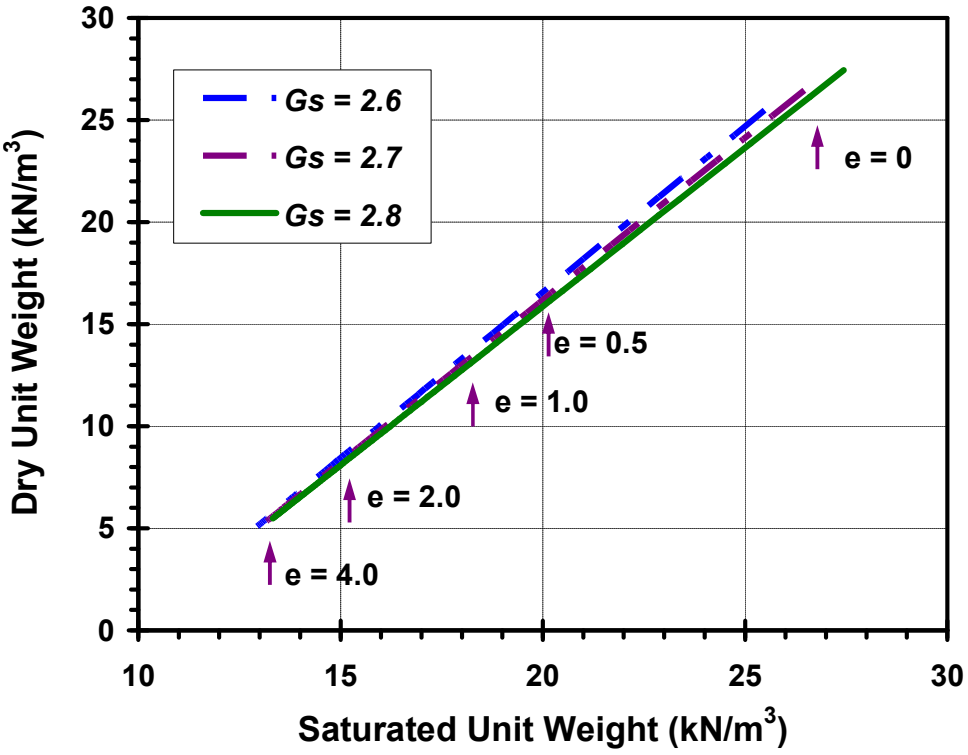


**Figure 4.8** *Interrelationship between dry unit weight and wet unit weight.*

By using the measured in-situ SPT resistance (N value), one can estimate the corresponding shear wave velocity ($V_s$) value to be used in estimating in the unit weight of the soil following Equations [4.10] and [4.11].

Imai and Tonouchi (1982) compiled a database of a variety of ground conditions through Japan where they collected data points from over 400 boreholes covering different soil types ranging from alluvial to diluvial clays, gravels, peats, and sands, in addition to special soils such as loam, fill, and sirasu. The database included 1654 measured SPT resistance N values with an average energy rating of 78 % with corresponding shear wave velocity (S-wave) measured mainly using a suspension logging method. **Figure 4.9** illustrates the

direct relationship between the measured shear wave velocity ($V_s$) and the SPT (N-value) and the relationship can be expressed as:

$$V_s\ (\frac{m}{s}) = 97.0\ N^{0.314} \qquad [4.12]$$

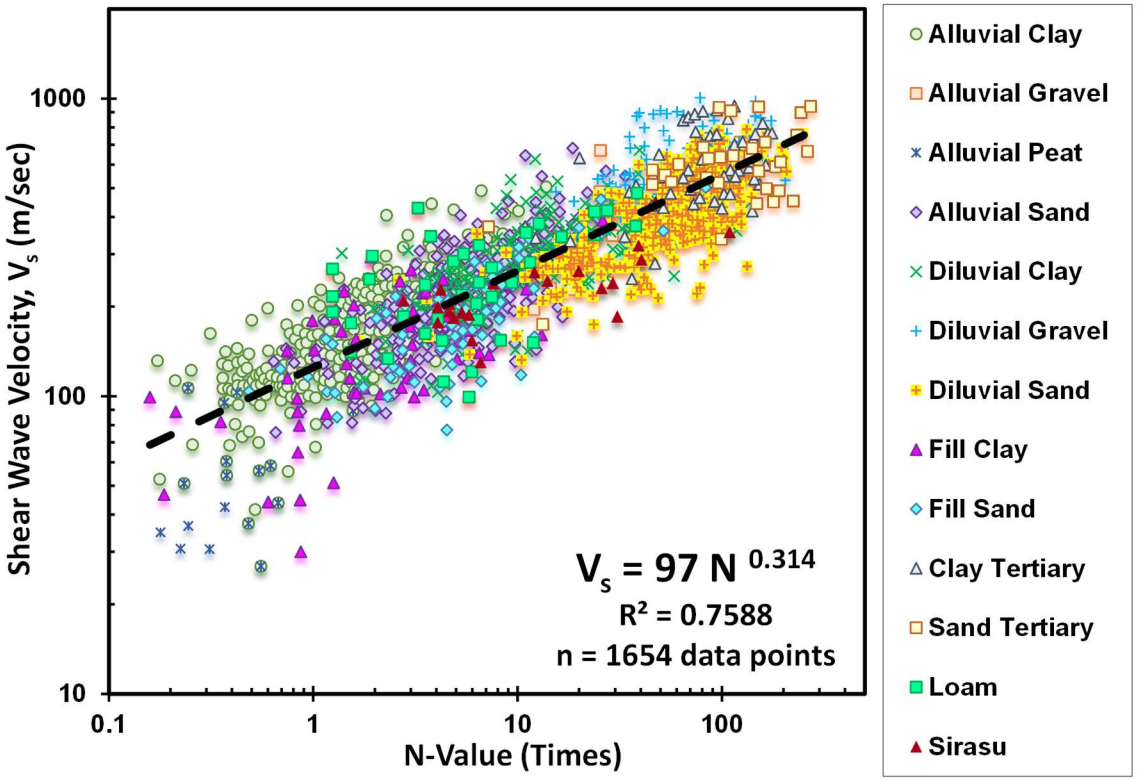


**Figure 4.9** *Relationship between shear wave velocity $V_s$ and SPT N-value (data after Imai & Tonouchi, 1982)*

## 4.6 Effective Friction Angle from SPT

In-situ penetration tests can be used to relate the effective stress friction angle ($\phi'$) of granular materials to the penetration resistance, which is $N_{60}$ value for the SPT. Meyerhof (1956) presented baseline relationships for evaluating the drained friction angle of cohesionless soils, where he considered the state of packing of the granular soil

(expressed in terms of relative density) and presented typical ranges for the standard penetration resistance, N and the corresponding friction angle, $\phi'$.

A more reliable correlation between $\phi'$ and stress-normalized SPT resistance, $(N_1)_{60}$, was derived by Hatanaka and Uchida (1996) where high quality undisturbed samples of natural sands were obtained by special freezing method. Once mounted in the triaxial cell and allowed to thaw, specimens permitted direct measurements of $\phi'$ in triaxial compression tests. Corresponding field SPT data were obtained at the same elevations as the undisturbed samples using a Japanese automatic trip hammer system where energy efficiency is reported as 78 percent. For an reference 60% efficiency in the U.S., the expression for peak $\phi'$ is presented in **Figure 4.10** and is given as:

$$\emptyset^{\circ} = \sqrt{15.4\,(N_1)_{60}} + 20^{\circ} \qquad [4.13]$$

It is important to recognize that these correlations have been developed for relatively clean sands. Some limited experience with this expression in residual silty fine sands (Mayne & Harris 1993) and fine sandy silts of the Applachian Piedmont geology (Mayne et al. 2000) have shown good agreement with laboratory triaxial tests on undisturbed samples.

The SPT should not be used to estimate the drained friction angle of gravelly soils, unless the correlations are verified and/or modified based on local experience. The size of gravel particles can be larger than the inner diameter of the split sampler used in the SPT test, thus affecting the penetration resistance in gravelly geomaterials.

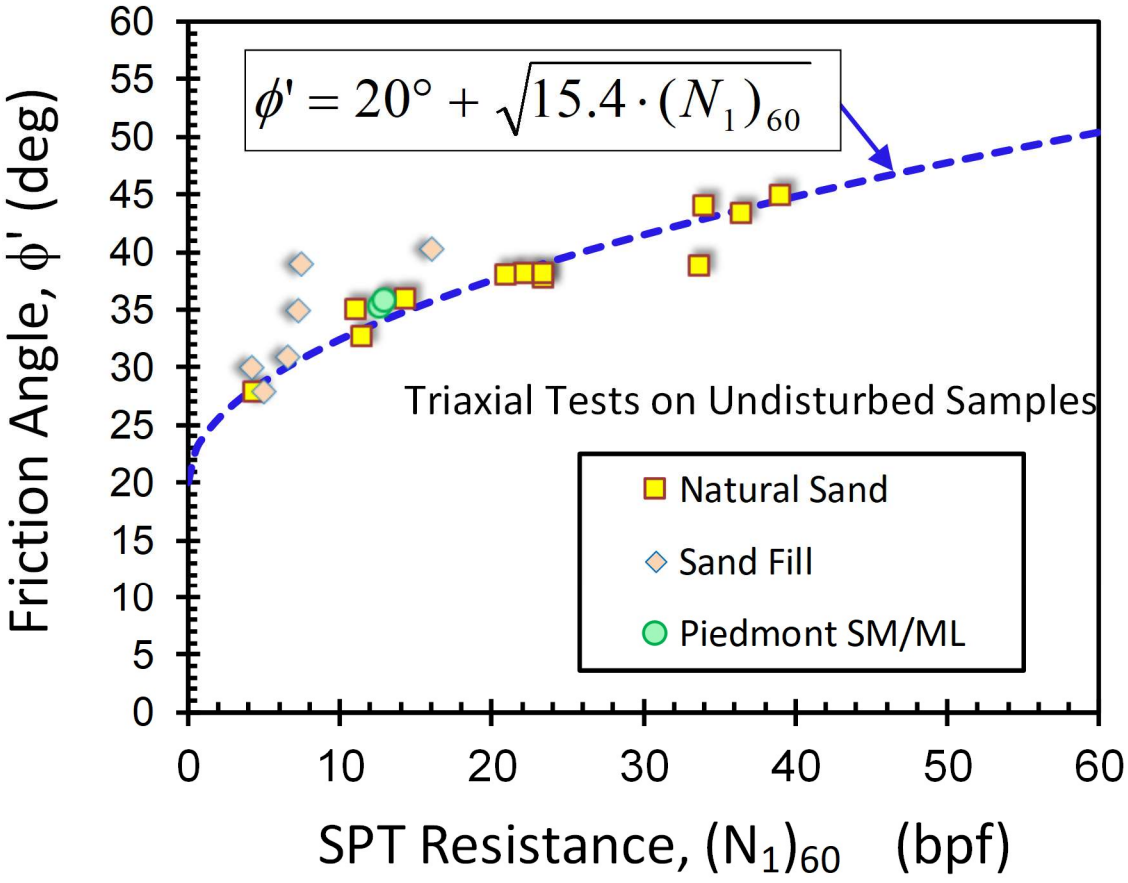


**Figure 4.10** *Peak friction angle of sands from SPT resistance (data from Hatanaka & Uchida, 1996; Mayne & Brown, 2003)*

In the case of clays, there is no direct relationship between the SPT ressitance and the effective stress friction angle. A review of compiled data for clay effective friction angle values (ϕ') from approximately 200 different clays versus their plasticity index values (n = 453 data points); as collected from Diaz-Rodriguez et al. (1992); Terzaghi, et al. (1996); Locat, Tanaka, and Lee (2003); Kulhawy and Mayne (1990); and Bhandari and Yatabe (2007); as presented in **Figure 4.11**, it can be seen that the clay friction angle exhibits a mean value of ϕ' = 28.6 degrees with a standard deviaton of about 5 degrees (Mayne 2013). Contrary to some claims, no correlation for ϕ' with PI exists for natural clays.

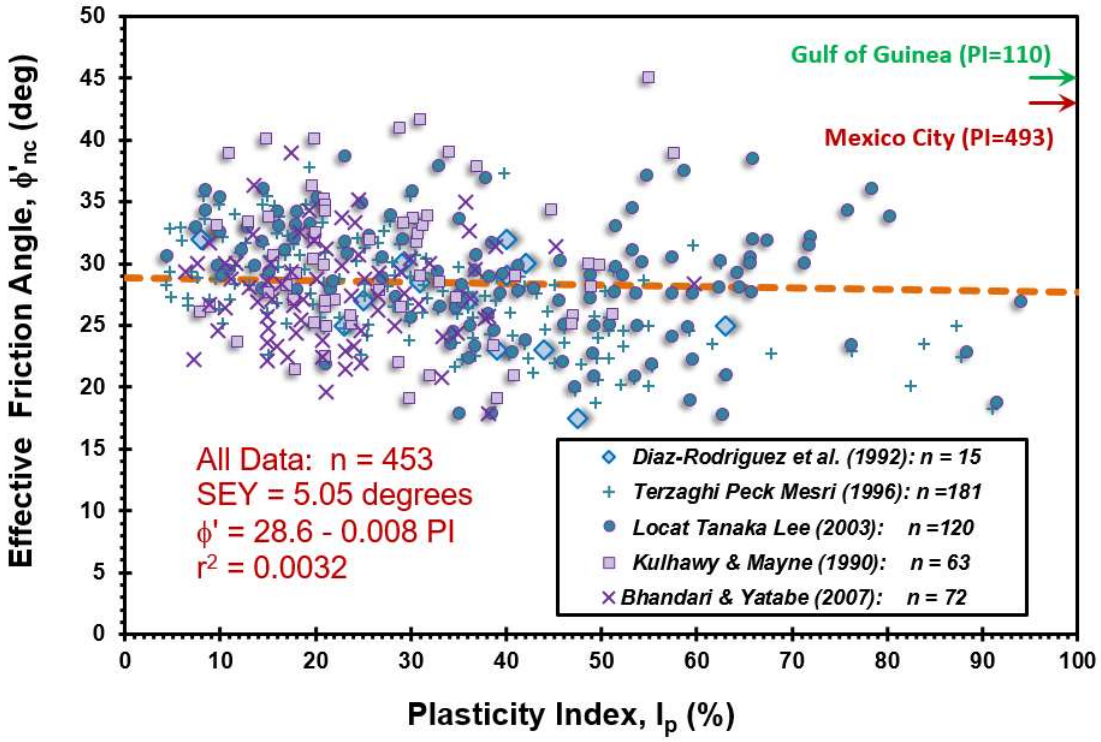


**Figure 4.11** *Effective stress friction angle of clays versus Plasticity Index*

## 4.7 Soil Modulus of Elasticity from SPT

Elasticity theory can be used to represent the stiffness of soil where it allows for interrelationships between the equivalent elastic Young's modulus (E'), shear modulus (G'), and constrained modulus (D') in terms of the Poisson's ratio (ν'). In-situ methods such as the flat dilatometer test (DMT) and pressuremeter test (PMT) can be directly used to measure an elastic modulus (E') which in turn can be related to corrected penetration resistance ($N_{60}$) measured at the same location.

For the Piedmont residual soils, Mayne & Frost (1988) compiled over 160 flat dilatometer tests with supplementary routine soil borings and cone penetrometer soundings in the vicinity of Washington DC, VA, and MD. The DMT elastic moduli were compared with

values obtained from laboratory tests and backcalculated moduli from field performance of full-scale foundation measurements. By considering the SPT penetration resistance measured at the same testing locations which had an average energy rating of 60 % in the late 1980s, a direct relationship between the derived elastic modulus (E') obtained from flat dilatometer tests (DMT) assuming v' = 0.2 and corrected SPT penetration resistance ($N_{60}$) was developed, as shown in **Figure 4.12** and expressed by:

$$E_D \text{ (bars)} = 22 \cdot \sigma_{atm} \cdot (N_{60})^{0.82} \qquad [4.14]$$

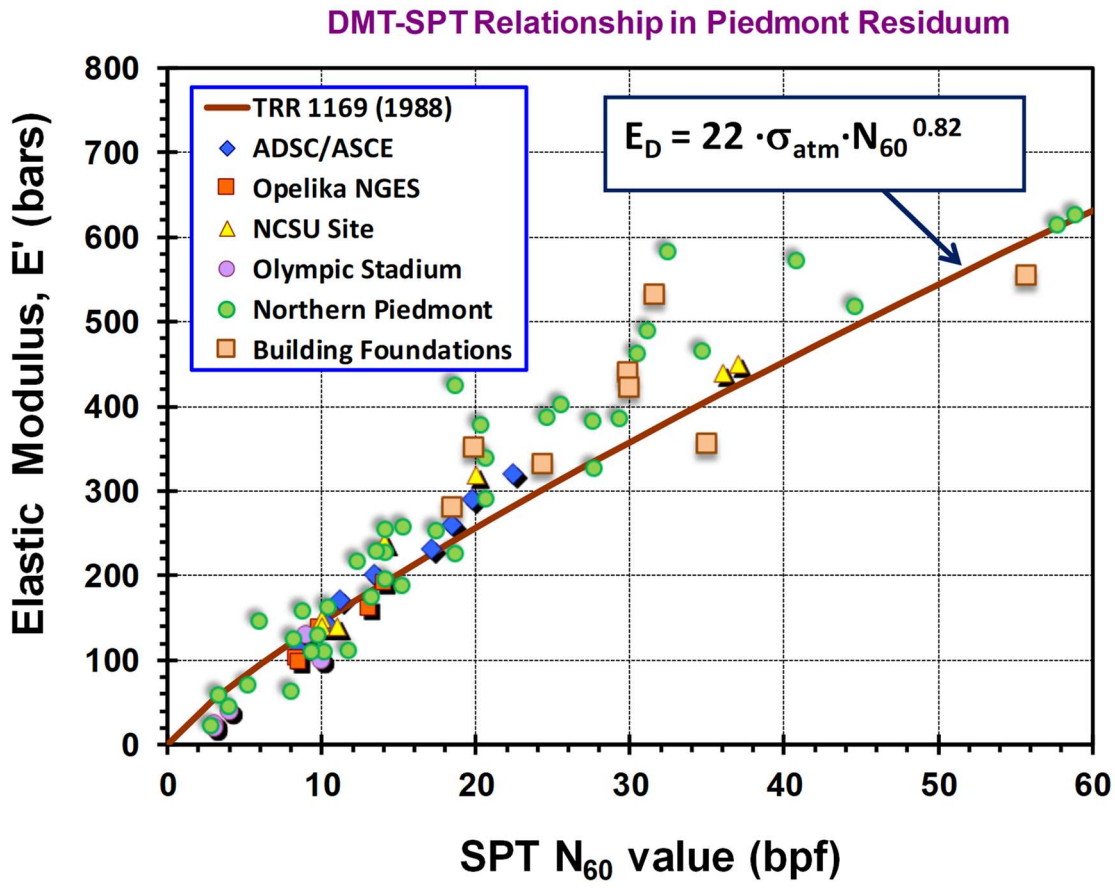


**Figure 4.12** *DMT modulus versus SPT relationship in Piedomnt Residuum (data from Mayne & Frost, 1988)*

The database was expanded to include more soil types such as silty sands and clayey sands (Atlantic Coastal Plain) and plotting them with the residual silts and sands of the Piedmont geology as presented in **Figure 4.13**. It can be seen that Equation 4.14 is still valid and applicable, yet can be considered on the conservative side for some of the sands.

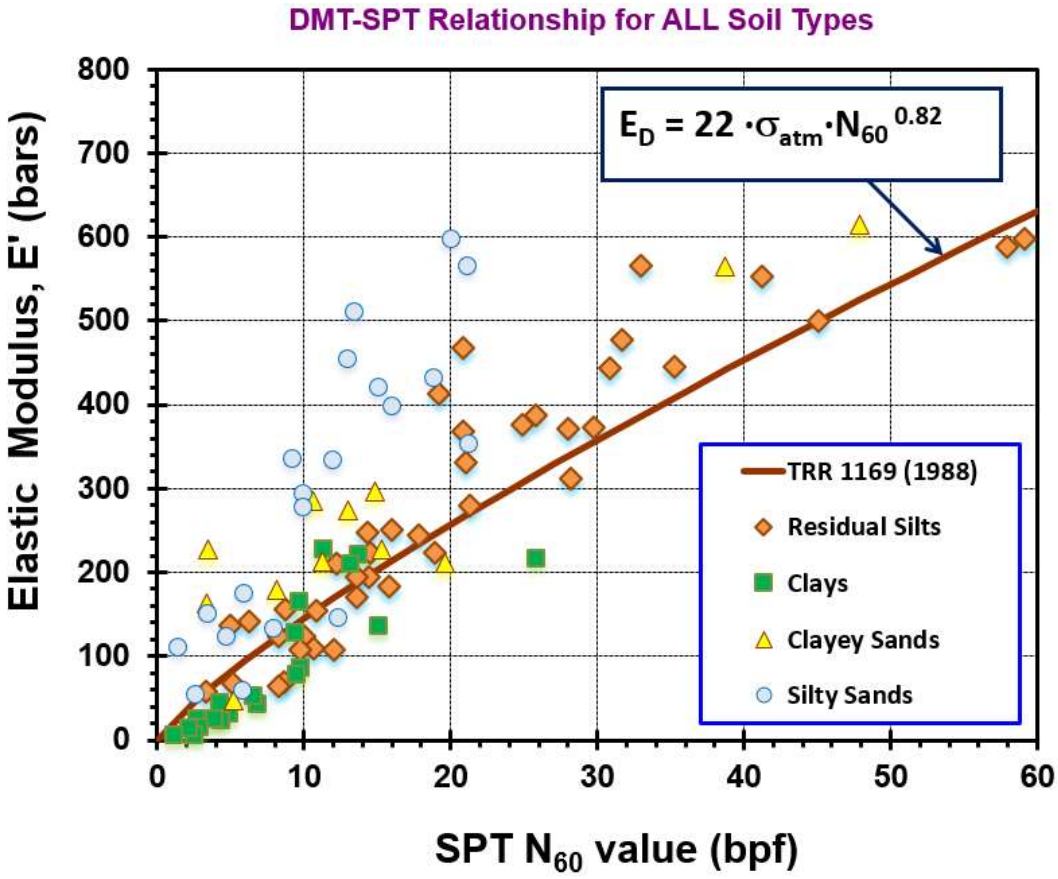


**Figure 4.13** *DMT modulus versus SPT $N_{60}$ relationship for a variety of soil types (modified after Gordon & Mayne 1986).*

## 4.8 Stress History from SPT

The stress history of a soil can be used to represent the geological conditions and evolutionary changes that the soil has undergone over the years and thus be considered as the focal point for geotechnical design applications since it relates to many

fundamental aspects of the soil behavior in terms of strength, stiffness, and compressibility. The preconsolidation stress ($\sigma_p'$) can be defined as the maximum effective overburden stress experienced by the soil during its stress history. Soils are often prestressed because of overburden removal, erosion, glaciation, and/or excavation, which are mechanical means. Also, soils can develop a pseudo-preconsolidation due to effects of ageing, desiccation, groundwater changes, exposure to wet-dry cycles, and repeated freezing-thawing. The overconsolidation ratio (OCR) is a classic normalized and dimensionless parameter based on the $\sigma_p'$ and effective vertical stress ($\sigma_{v0}'$), such that:

$$OCR = \sigma_p' / \sigma_{v0}' \qquad [4.15]$$

The most basic and conventional means to determine stress history is via laboratory one-dimensional consolidation testing per ASTM D2435. The specimens are subjected to constrained compression in either a mechanical oedometer, electro-pneumatic or hydraulic consolidometer, or automated constant rate of strain (CRS) device. On the basis of the consolidation test, many methods have been proposed to delineate $\sigma_p'$ from the compression measurements. However, the results are dependent on the plotting methods and curve-fitting procedures. Laboratory based techniques are associated with many issues, including: disturbance which can be attributed to the sampling process, specimen handling, and stress relief due to removal of the sample from depths beneath the ground surface. To overcome issues associated with laboratory methods, $\sigma_p'$ can be determined using direct correlations with in-situ test measurements such as standard

penetration, cone penetration, flat dilatometer, and/or vane shear tests that are faster, more economical, and productive than laboratory tests.

Kulhawy and Mayne (1990) investigated the relationship between the SPT resistance (N) and the effective preconsolidation stress ($\sigma_p'$) for 51 fine-grained soils. These were mainly firm to stiff to hard clays which were not sensitive nor structured, resulting in the following expression:

$$\sigma_p' \approx 0.47 \cdot \sigma_{atm} \cdot \mathrm{N} \qquad [4.16]$$

Although the reported penetration resistance values were not specifically corrected for energy effciciency, the SPT data were obtained primarily using safety hammers for which the average ER ≈ 60%. Later, a more detailed study investigated the relationship between energy-corrected standard penetration resistance ($N_{60}$) and the preconsolidation stress for different soil types as presented in **Figure 4.14** and as expressed:

$$\sigma_p' \approx 0.47 \cdot \sigma_{atm} \cdot (\mathrm{N}_{60})^{\mathrm{m}} \qquad [4.17]$$

where m is an exponent that depends on the soil type: m = 0.6 for clean quartzitic sands and gravels, m = 0.7 for silty or clayey sands, m = 0.8 for sandy silts (e.g., Piedmont), m = 0.9 for silts to clayey silts, and m = 1.0 for intact “vanilla” clays (Mayne 1992). Fissured clays may exhibit an exponent value with 1.1 or higher, depending upon the extent and frequency of the discontinuities and joints.

The OCR can then be calculated from eqn [4.15]. For clays and silts where the OCR < 1, an underconsolidated state is identified. This is a very precarious and unstable condition and should be reviewed by the chief engineer and/or senior geotechnical engineer.

Clays and silts with 1 < OCR < 2 are normally consolidated to lightly overconsolidated deposits that are prone to problems of instability, bearing capacity, and high compressibility problems, and these too should be reviewed by senior geotechnical staff. Since there is some uncertainty in the correlative trends, a value of OCR < 3 has been used to conservatively identify these soft clays and silts. Additional laboratory and/or in-situ testing may be warranted before proceeding forward with foundations in these geomaterials.

Soils exhibiting a range: 2 < OCR < 10 are moderately overconsolidated and generally do not exhibit difficulties during construction and not normally associated with issues of strength, compressibility, and stiffness.

Finally, fine-grained soils that have very high OCRs > 30 are often cracked and fissured and have discontinuities which may present issues in slopes, drainage, walls below grade, and foundations. If heavilly overconsolidated and highly plastic, these may also be prone to swelling problems and exhibit characteristics of expansive clays and other concerns.

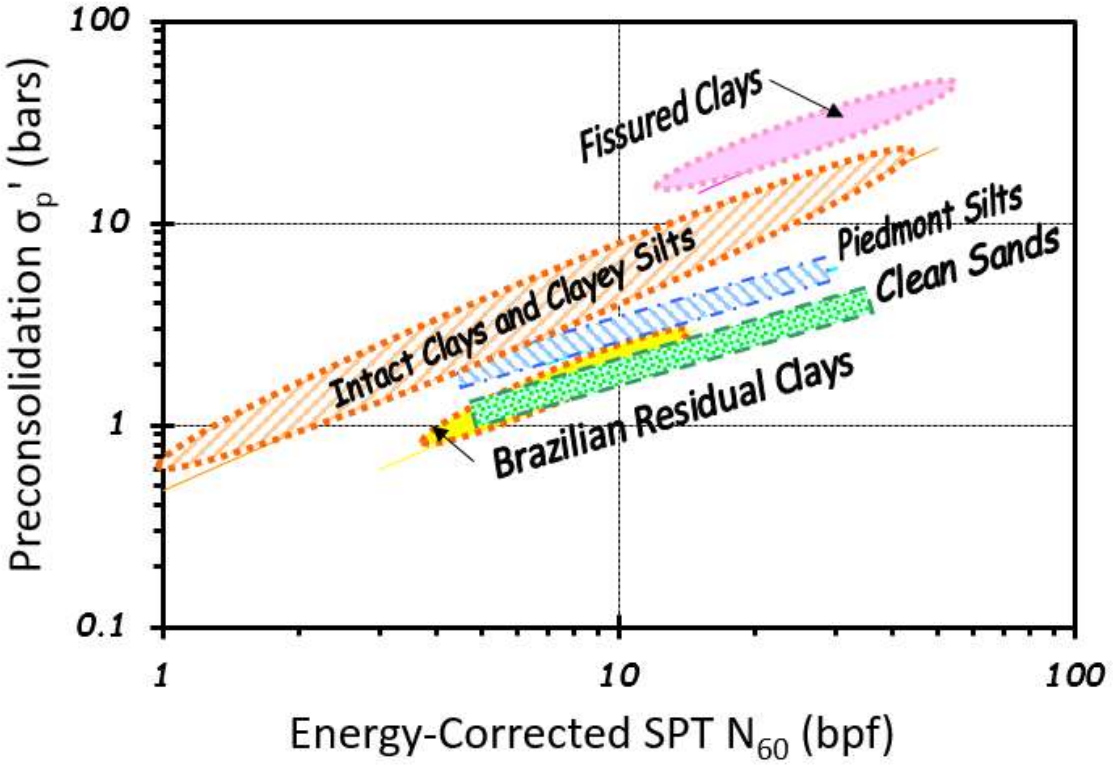


**Figure 4.14** *Effective preconsolidation stress versus $N_{60}$ for soils (after Mayne 2007b).*

# 5. Input Parameters Using Cone Penetration Tests (CPT)

## 5.1 Overview of the Cone Penetration Test (CPT)

The cone penetration test (CPT) involves the hydraulic pushing of an instrumented steel probe at a constant rate to obtain continuous vertical profiles of stress, friction, and pressure with depth. Cone penetration testing can be conducted for measurement of tip and sleeve resistances (i.e., CPT) or the additional readings of penetration porewater pressures using a piezocone (i.e., CPTu). Some equipment includes the ability to measure shear wave velocities, called a seismic piezocone test and designated SCPTu.

By recording continuous measurements vertically with depth, the CPT is an excellent tool for profiling strata changes, delineating the interfaces between soil layers, soil consistency, and detecting small lenses, inclusions, and stringers within the ground. The data presentation from a CPT sounding includes cone resistance ($q_t$), sleeve friction ($f_s$), and porewater pressures ($u_2$) plotted with depth in side-by-side graphs. The records are stored digitally and can be post-processed to interpret a number of geotechnical engineering parameters that relate to unit weight, soil strength, preconsolidation, stiffness, stress state, and permeability (Lunne, et al. 1997; Mayne, 2007).

## 5.2 Equipment

Equipment necessary for performing a cone penetration test includes a penetrometer, set of cone rods or drill rods, electrical cable, a data acquisition system, and hydraulic actuator with sufficient reaction mass to advance the penetrometer. This can be a conventional drilling rig or a CPT truck weighing 20 to 25 tons.

A standard cone penetrometer is a 35.7-mm diameter cylindrical probe with a 60$^{o}$ apex at the tip, 10-cm$^2$ cross-sectional area, and a 150-cm$^2$ sleeve surface area. More robust penetrometers are available with a 44-mm diameter body, a 15-cm$^2$ projected tip area, and 200- to 225-cm$^2$ sleeve surface area. **Figure 5.1** shows a number of different cone penetrometers and piezocones. Standard cone rod is typically 1 m in length with a 35.7 mm outer diameter and a 22 mm inner diameter opening. An electronic cable runs through the hollow rods and attaches to a data acquisition system at the ground surface. The newest data acquisition systems are digital types, yet many older systems consist of a signal conditioner, an analog to digital (A-D) converter, and computer processor. Data are typically recorded every 2 to 5 cm of vertical penetration (Sabatini et al., 2002).

For a piezocone penetration test (CPTu), the penetration porewater pressures are monitored using a transducer and porous filter element. Porewater readings can be taken at the apex or mid-face (designated $u_1$), shoulder (just above the cone tip, or $u_2$), or behind the sleeve ($u_3$). The standard required position per ASTM D 5778 is the shoulder position (type 2) because the $u_2$ value is required for the correction of tip resistance. Filter elements consist of high-density polypropylene, ceramic, or sintered metal. Fluids for saturation include: water, glycerine, or silicone.

For the seismic piezocone test, a geophone is located approximately 500 mm uphole from the cone tip. The geophone detects shear waves generated at the ground surface at depth intervals of approximately 1-meter, corresponding to successive rod additions.

**Figure 5.1** *Different cone penetrometers and piezocones used in production testing and research*

## 5.3 Procedures

Test procedures for the CPT consist of hydraulically pushing the cone at a rate of 20 mm/s in accordance with ASTM D 5778 using either a standard drill rig or specialized cone truck. The advance of the probe requires the successive addition of rods at approximately 1 m intervals. Readings of measured tip resistance ($q_c$), sleeve friction ($f_s$), inclination (i), and pore pressure ($u_2$) are taken at least every 5-cm, as illustrated in **Figure 5.2**.

Careful saturation of the porous filter and transducer ports is paramount for piezocone testing. Poor saturation will lead to a compressible measurement system, and thus the full magnitude of the penetration pore pressure response will not be recorded. If water or water mixtures are used as the saturation fluid, a fluid filled membrane should be wrapped around the element to maintain saturation until the probe enters the ground. Glycerin and silicon oil are typically viscous enough to prevent desaturation of the element before penetration into the ground. Typically a pause in penetration will occur

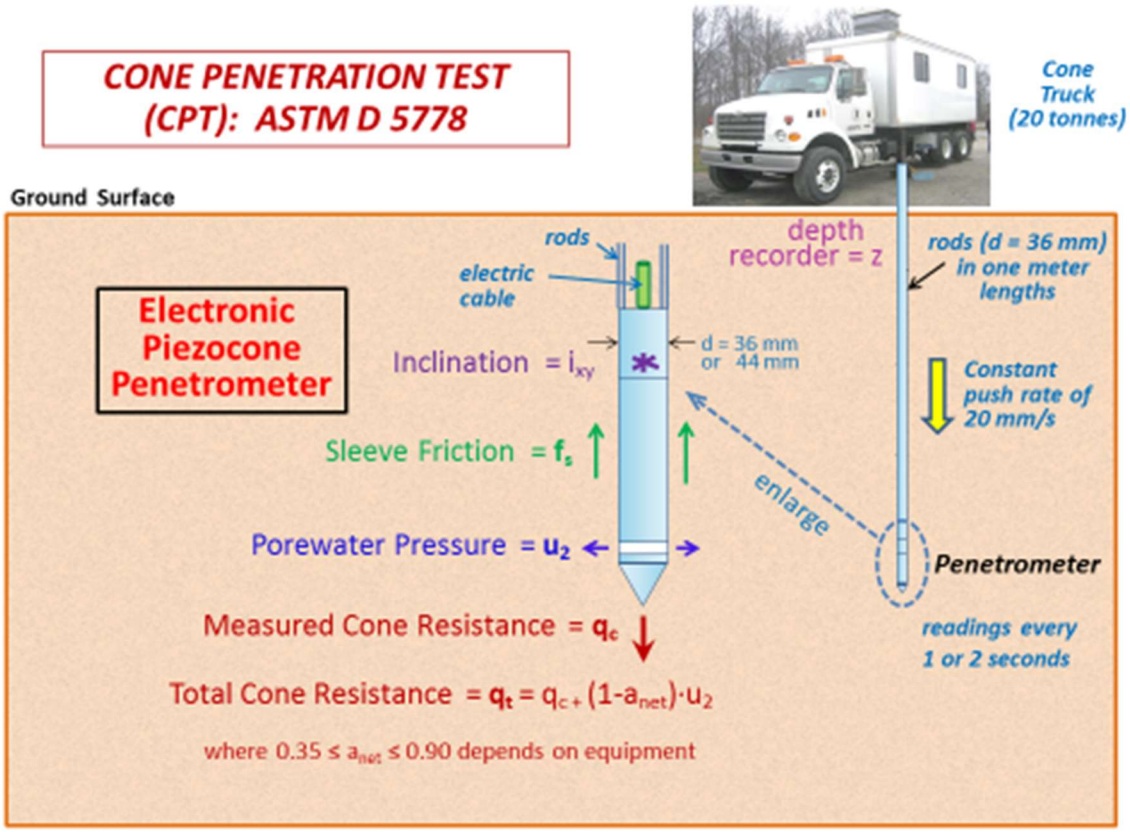


**Figure 5.2** *Depiction of Cone Penetration Testing (CPT) Setup and Procedures*

to add new rods. This is referenced as the rod break. The depth at each rod break should be recorded and compared to the expected depth.

For the seismic piezocone (SCPTu), downhole shear wave velocity tests are performed at each 1-m rod break. A special instrumented hammer is used to trigger a surface source rich in shear waves (typically a horizontal steel beam). The steel beam is coupled to the ground under a hydraulic outrigger of the cone truck or drill rig, or under the tire of a support vehicle. The horizontal distance between the source beam and cone rod should be minimized (typically < 1 m) to ensure a relatively vertically-propagating shear wave. A

horizontal geophone located within the penetrometer serves as a receiver for the signal, which is displayed on the screen of an oscilloscope. First arrival times for shear waves are recorded with respect to depth, to provide interpretations of shear wave velocity of the overlying soil material (Sabatini et al., 2002).

## 5.4 Parameters Measured

Electric and electronic penetrometers have standard readings of measured cone tip resistance ($q_c$) and sleeve friction ($f_s$), as shown in **Figure 5.3 (a)**. Piezocone penetrometers obtain penetration porewater pressures using filters located at the shoulder ($u_2$; **Figure 5.3 (b)**) or the midface ($u_1$; **Figure 5.3 (c)**). A horizontal geophone in the seismic piezocone (**Figure 5.3 (d)**) can be used to record mechanically induced shear waves from the surface, leading to determination of shear wave arrival time ($t_s$) and shear wave velocity ($V_s$).

The cone tip resistance ($q_c$) is the measured axial force over the projected tip area. It is a point stress related to the bearing capacity of the soil. In sands, the tip resistance is primarily controlled by the effective stress friction angle, relative density, and effective horizontal stress-state. For intact clays, the tip resistance is primarily controlled by the undrained shear strength and preconsolidation stress. Particularly in clays and silts, the measured $q_c$ must be corrected for porewater pressures acting on the cone tip geometry, thus obtaining the corrected or total cone tip resistance, $q_t$ (Lunne et al., 1997):

$$q_t = q_c + (1 - a_n) \cdot u_2 \qquad [5.1]$$

where $a_n$ is the net area ratio determined from laboratory calibration and $u_2$ is the shoulder penetration porewater pressure. The net area ratio is approximated as the ratio

of the unequal end areas of the cone (**see Figure 5.4**). The net area ratio ($a_n$) is penetrometer-specific and is obtained by isotropic pressurization of the cone in a triaxial cell. It is best to use penetrometers with a value of net area ratio $a_n \geq 0.80$ to minimize the necessary correction. Contract specifications should always request the actual calibration curves and clear indication that $q_c$ readings have been adjusted to provide the proper $q_t$ values. Notedly, the correction is paramount for intact clays and silts where excess porewater pressures will occur ($q_t > q_c$), while in clean sands, the correction is negligible and thus $q_t \approx q_c$.

Because soil samples are not normally taken during CPT, soil types must be deduced or inferred from the measured readings. As a general rule of thumb, measured cone tip resistances in sands are rather high ($q_t > 5$ MPa or 50 tsf), reflecting the prevailing drained strength conditions, whereas measured values in clays are low ($q_t < 5$ MPa or 50 tsf) and indicative of undrained soil response owing to low permeability.

The sleeve friction ($f_s$) is a shear stress determined as the axial side load acting along the cylindrical surface area of a smooth sleeve. This value is often expressed as the Friction Ratio (FR) which is defined as the ratio of the sleeve friction to cone tip resistance, designated $FR = R_f = 100 \cdot f_s/q_t$, thus reported in percent. The friction ratio is generally indicative of soil type (Lunne et al., 1997). In clean quartz sands to siliceous sands, it is observed that friction ratios are low: $R_f < 1\%$, whereas in clays and clayey silts of low sensitivity, $R_f > 4\%$. However, in soft sensitive to quick clays, the friction ratio can be quite low, approaching zero in many instances.

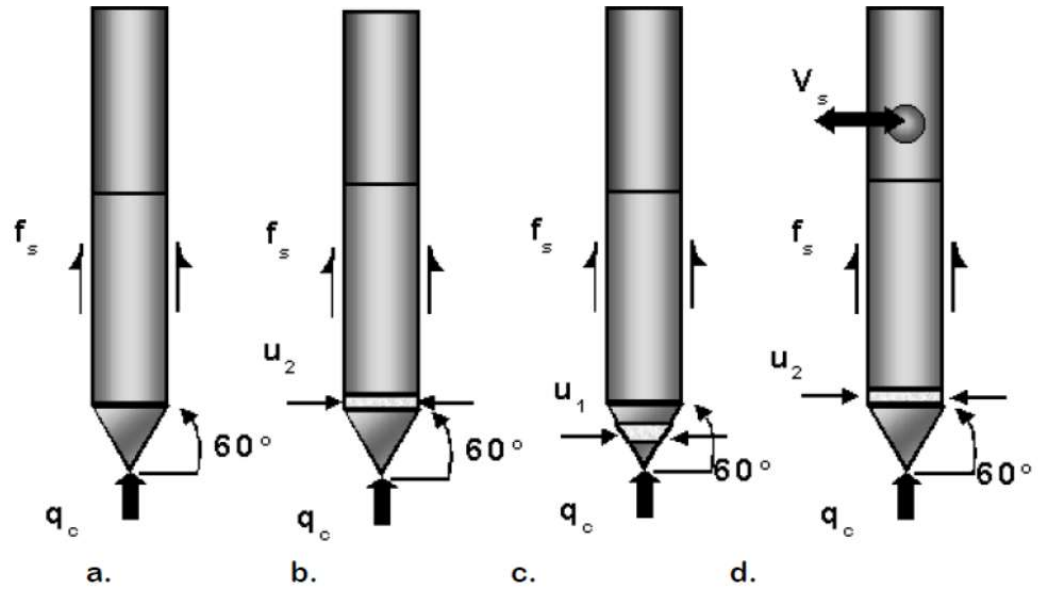


**Figure 5.3** *Measurement locations on cone penetrometers: a. Electric Cone Penetrometer, CPT; b. Piezocone Penetrometer with filter behind tip, CPTu$_2$; c. Piezocone with mid-face filter, CPTu$_1$; d. Seismic Piezocone, SCPTu$_2$*

The penetration porewater pressures are monitored using a pressure transducer and porous filter element. These readings represent the fluid pressures between the soil particles during penetration. At the shoulder position, the pressures are near hydrostatic in sands ($u_2 \approx u_0$) whilst considerably higher than hydrostatic ($u_2 > u_0$) in soft to firm to stiff intact clays. Using values for total stress, $\sigma_{vo}$, and hydrostatic pore pressure, $u_0$, the pore pressure parameter, $B_q = (u_2 - u_0) / (q_t - \sigma_{vo})$, is used as a means to normalize CPTu data for the purpose of soil classification and undrained shear strength estimation. At the mid-face location ($u_1$), penetration porewater pressures are always positive, while at the $u_2$ location measurements range from positive in intact (i.e., nonfissured) geomaterials to as low as negative one atmosphere (-100 kPa) in fissured clays and dense silts. The data

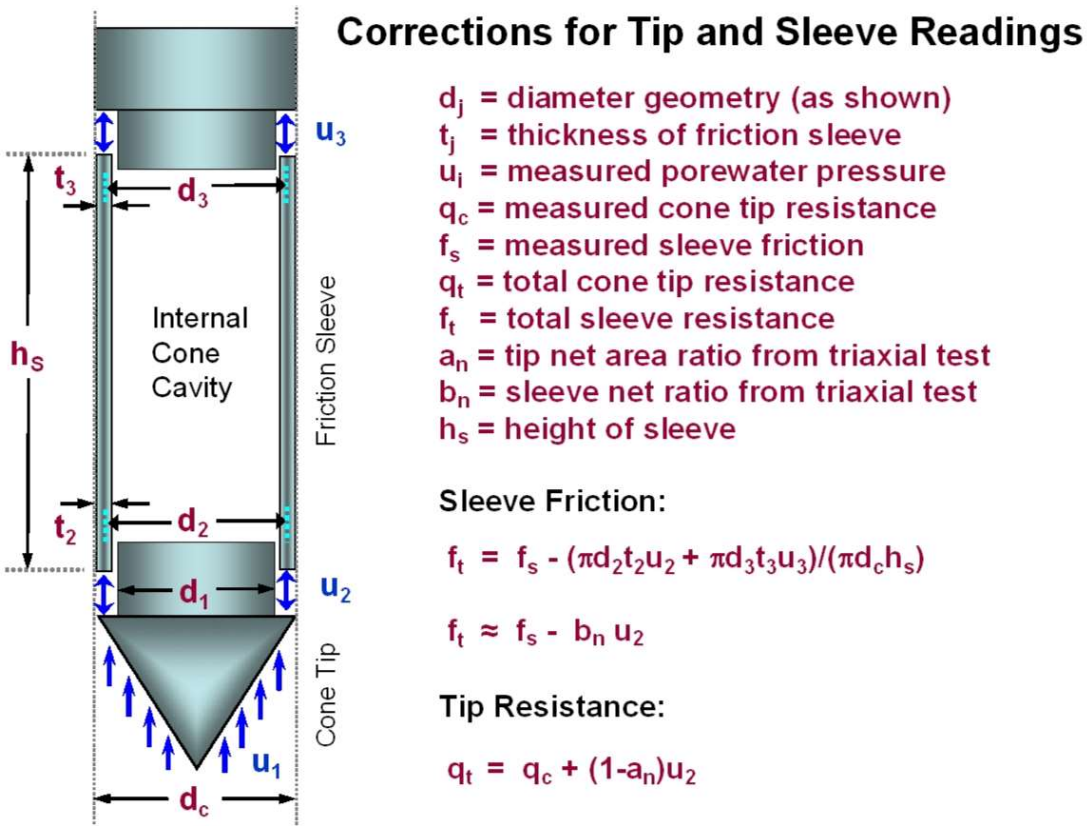


**Figure 5.4** *Illustration of unequal end areas of CPT (after Jamiolkowski et al. 1985)*

resulting from a CPT, CPTu, or SCPTu are combined to provide several useful index and performance parameters.

## 5.5 Soil Identification and Classification from CPT

Since soil samples are not normally taken during cone penetration testing, then indirect methods must be utilized in evaluating various soil types of the strata encountered. Different approaches can be used: (a) correlation with adjacent boreholes and recovered samples; (b) rules-of-thumb; (c) empirical soil behavioral type (SBT) charts; (d) probabilistic methods.

The simple rules of thumb rely on one or more of the cone readings, where a reference cone tip value $q_t$ = 5 MPa (50 tsf) should be identified, whereby measured $q_t$ > 5 MPa imply clean "hourglass" sands and $q_t$ < 5 MPa suggest "vanilla" clays. For the friction sleeve, it is convenient to plot this in terms of friction ratio, FR = $f_s/q_t$ (%). As such, clean sands are identified by FR < 1%, whereas fine-grained soils (silts and clays) exhibit FR > 1%. Lastly, using the porewater pressure channel, it is advantageous to plot the hydrostatic porewater pressure line as a reference:

$$u_0 = h_w \gamma_w \qquad [5.2]$$

where $h_w$ = height of the water (depth less groundwater table) and $\gamma_w$ = unit weight of water (freshwater: $\gamma_w$ = 9.81 KN/m$^3$ = 62.4 pcf).

Above the groundwater table, the ambient hydrostatic $u_0$ is taken equal to zero in clean sands; however, in clays and fine-grained materials, $u_0$ can be negative to account for capillarity effects depending upon the degree of saturation, recent rainfall, and other site features. In clean "hourglass" sands, the measured porewater pressures are often close to hydrostatic ($u_2 \approx u_0$). However, if the sands are very dense, dilatancy may result in $u_2$ readings below $u_0$. Below the groundwater table, intact clays can be found by examining where $u_2 >> u_0$.

To facilitate the identification of soil types by computer software, a number of empirical soil behavioral type (SBT) charts have been proposed. Robertson, et al. (1986) presented a 12-zone SBT system that uses a three-axes plot of cone tip resistance ($q_t$), friction ratio (FR), and normalized porewater pressure ($B_q$). Due to the inconvenience of working with 3-d graphs directly, the system is usually presented in two matched graphs: (a) $q_t$ vs. FR

(%); and (b) $q_t$ vs $B_q$. Other system are also in use for particular geologies (Kulhawy & Mayne 1990)

In order to account for depth effects on the readings, stress-normalized CPT parameters have been defined by Lunne, et al. (1997) as follows:

$Q = (q_t-\sigma_{vo})/\sigma_{vo}'$ [5.3]

$F = 100 \cdot f_s/(q_t-\sigma_{vo})$ [5.4]

For automation in a spreadsheet or software, it is convenient to use the CPT material index, $I_c$ which is defined (Robertson & Wride, 1998):

$$I_c = \sqrt{\{3.47 - \log(Q)\}^2 + \{1.22 + \log(F)\}^2} \quad [5.5]$$

The aforementioned stress normalization for tip resistance directly with effective overburden stress works well in soft clays and silts, however in sands the stress normalization is proportional to the square root of effective stress, probably due to particle grain crushing effects. In this case, a modified normalized cone tip resistance has been defined as (Robertson, 2004; 2009):

$$Q_{tn} = \frac{(q_t - \sigma_{vo})}{\sigma_{atm}} \cdot \left( \frac{\sigma_{atm}}{\sigma_{vo}'} \right)^n \quad [5.6]$$

where $\sigma_{atm}$ = 1 atmosphere ≈ 1 bar = 100 kPa and the exponent n is varies with soil type, with typical values of 1.0 in the general case of clays ($I_c$ > 2.95), n = 0.75 for silty soils, and n = 0.5 for clean sands ($I_c$ < 2.05). Since the exponent *n* is a function in the material index $I_c$ which is a function in the modified normalized cone tip reistance $Q_{tn}$ which is also a

function in the same exponent *n* then an iterative approach is needed to find the appropriate exponent *n* to identify the SBT zone number for mixed soil types.

$$n = 0.381 \cdot (I_c) + 0.05 \cdot (\frac{\sigma_{vo}'}{\sigma_{atm}}) - 0.15 \quad [5.7]$$

By plotting the data in terms of $Q_{tn}$ versus *F*, a modified 9-zone SBT system has been developed (Robertson, 2009), as presented in **Figure 5.5**. In this system, basic "vanilla" clay is found in zone 3 while "hourglass" sands form zone 6. The SBT classifications can be identified as per Robertson (2009) following **Table 5.1** and as plotted in **Figure 5.6**.

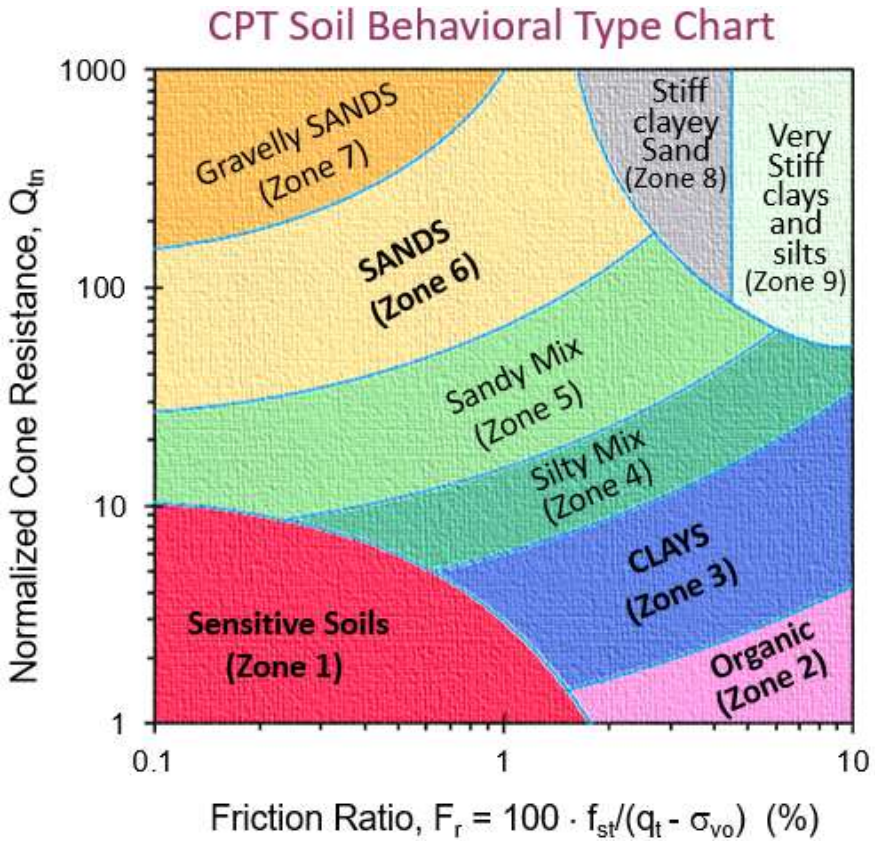


***Figure 5.5*** *Colorized Soil Behavioral Type (SBTn) Chart for normalized CPT readings (after Robertson 2009)*

**Table 5.1** *Soil Behavioral Type and Zone Number as defined by CPTu Material Index, $I_c$*

| Soil Classification | SBT Zone | Range CPT Material Index $I_c$ |
|---|---|---|
| Stiff sands and clays | 8 and 9 | (see note 1) |
| Sands with gravels | 7 | $I_{cRW} < 1.31$ |
| Sands: clean to silty | 6 | $1.31 < I_{cRW} < 2.05$ |
| Sandy mixtures | 5 | $2.05 < I_{cRW} < 2.60$ |
| Silty mixtures | 4 | $2.60 < I_{cRW} < 2.95$ |
| Clays | 3 | $2.95 < I_{cRW} < 3.60$ |
| Organic soils | 2 | $I_{cRW} > 3.60$ |
| Sensitive soils | 1 | (see note 2) |

Notes: 1. Zone 8 (1.4 < F < 4.5 %) and Zone 9 (F > 4.5 %) and following criterion:

$$Q_{tn} \geq \frac{1}{0.006 \cdot (F - 0.9) - 0.0004 \cdot (F - 0.9)^2 - 0.002}$$

2. Sensitive soils of zone 1 identified when Q < 12 exp (-1.4 F)

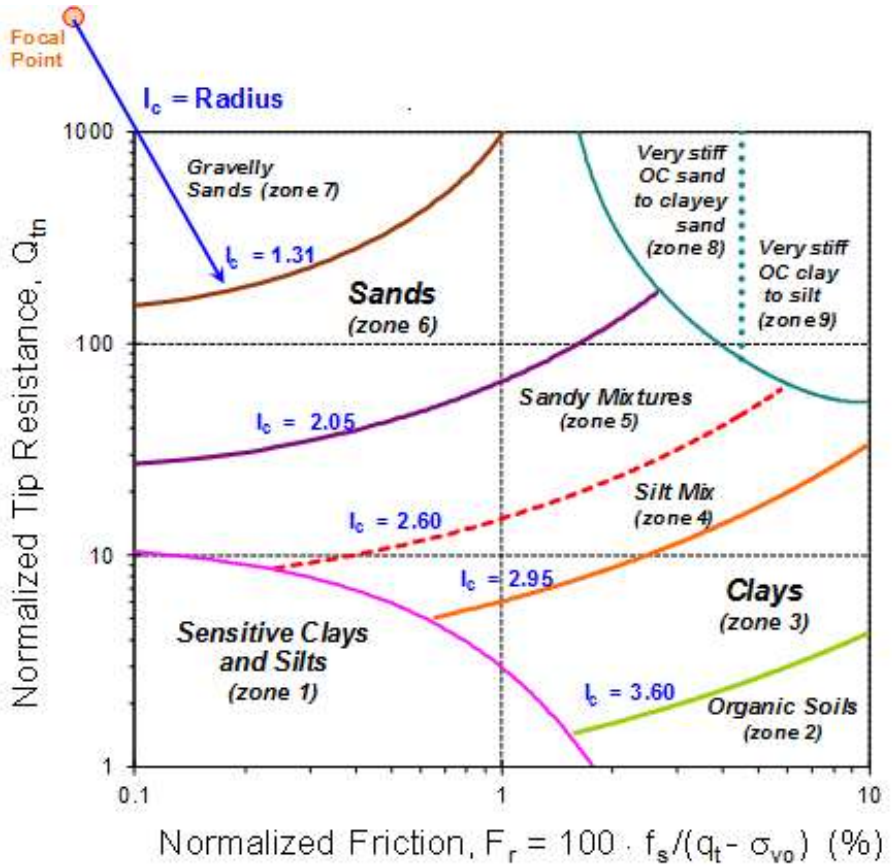


***Figure 5.6*** *CPT Soil Classification Zones Using Nine-Part Soil Behavioral Type (after Robertson 2009)*

## 5.6 Soil Unit Weight from CPT

A direct relationship for unit weight from CPT resistances has been sought (Mayne, et al. 2010). The findings are given in **Figure 5.7** and indicate that the sleeve friction provides a reasonable first-order estimate on $\gamma_t$. An initial value is assumed in order to process the first results using $\sigma_{vo}'$ and then later adjusted based on the derived profile of $\gamma_t$ from the CPT readings. The expression for total unit weight in terms of sleeve friction is:

$$\gamma_t = 1.95\, \gamma_w\, (\sigma'_{v0}/\sigma_{atm})^{0.06}\, (f_s/\sigma_{atm})^{0.06} \qquad [5.8]$$

where $\sigma_{atm}$ = 1 atmosphere = 1 bar = 100 kPa ≈ 1 tsf. The expression works well in normal "vanilla-flavoured" clays and "hourglass quartz" sands, but is not applicable to highly plastic and diatomaceous soils, such as Japanese mudstone or infamous Mexico City clays.

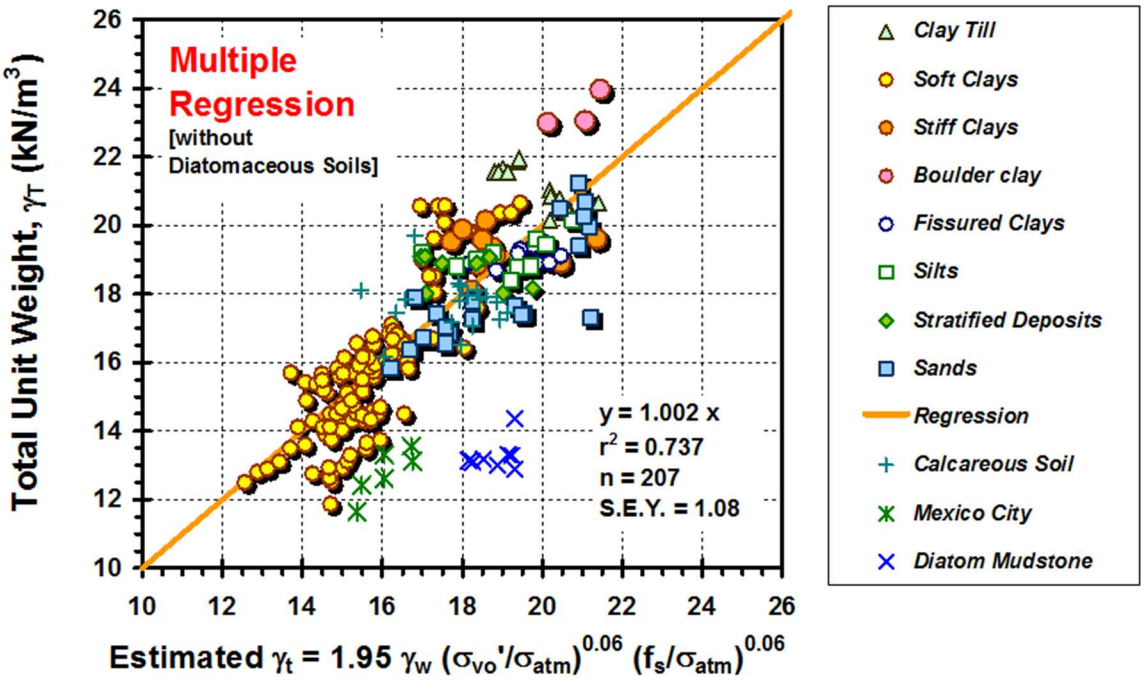


**Figure 5.7** *Unit weight directly estimated from CPT sleeve resistance and effective stress (Mayne et al., 2010).*

A direct unit weight relationship with the sleeve friction is also observed, as presented in **Figure 5.8:**

$$\gamma_t = 26 - \frac{14}{1+[\,0.5 \cdot \log\,(f_s+1)]^2} \qquad [5.9\ a]$$

where the specific units include: $\gamma_t$ (kN/m$^3$) and fs (kPa). Alternatively, a simpler expression for the majority of sleeve reading ranges is given by:

$$\gamma_t = 12 + 1.5\ln(f_s + 0.1\,) \qquad [5.9\ b]$$

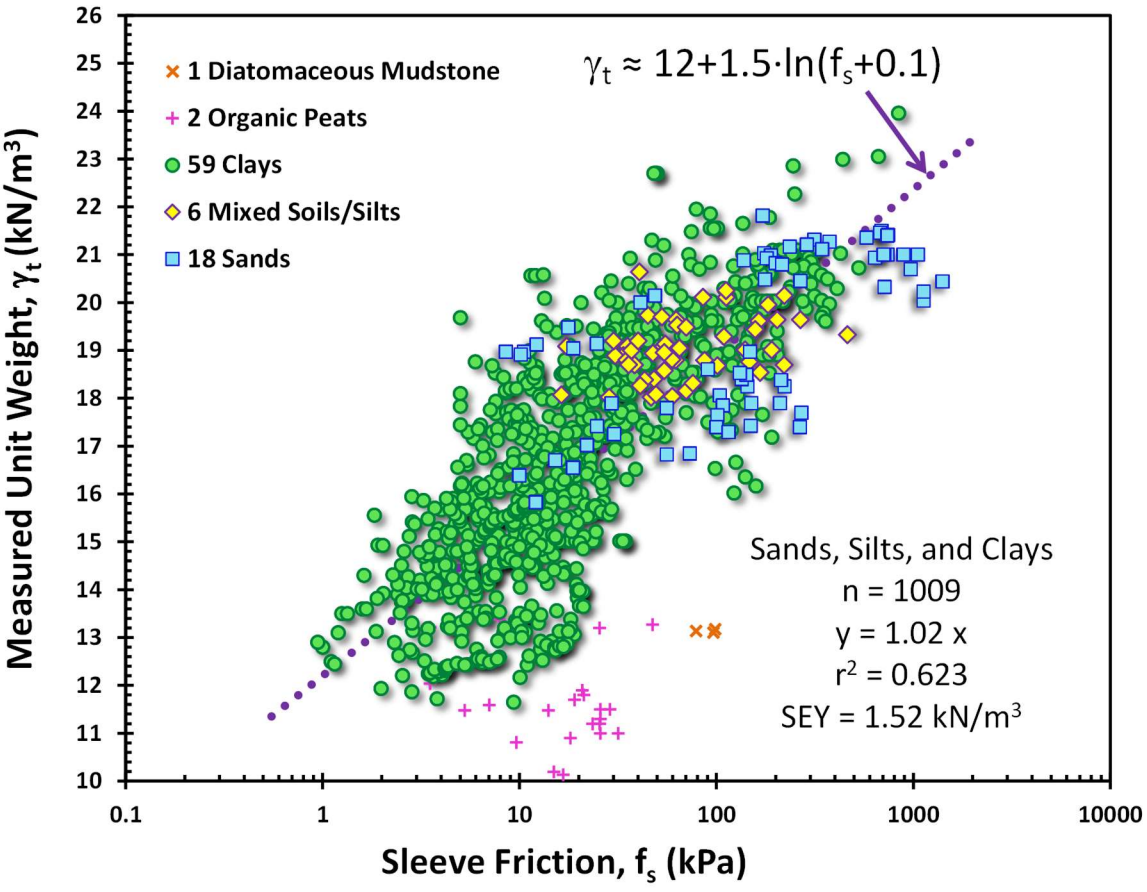


**Figure 5.8** Unit weight directly estimated from CPT sleeve resistance (Mayne, 2014)

## 5.7 Effective Friction Angle from CPT

The drained (effective stress) friction angle ($\phi'$) of soils is a fundamental property that controls the strength, behavioral response to loading, and initial stress state. The effective friction angle of sands (also termed angle of internal friction) represents the strength of the material in stability analyses and is often required for assessing the coefficient of lateral stress ($K_0$), footing bearing capacity, pile end-bearing resistance, and side resistance in deep foundations. In terms of the commonly-adopted Mohr-Coulomb strength criterion, the shear strength ($\tau_{max}$) is expressed:

$$\tau = c' + \sigma'_n \tan\phi' \qquad [5.10]$$

where c' = effective cohesion intercept (generally: c' = 0 for unbonded geomaterials). In most cases, the normal stress can be taken equal to the effective vertical overburden stress: $\sigma_n' = \sigma_{vo}'$.

For granular soils, the peak friction angle ($\phi_p'$) of sands is composed of two components: (1) a basic frictional value (designated $\phi_{cs}'$ for critical state) that is due to particle grain shape, compressibility characteristics and mineralogy; and (2) a dilatancy term (quantified by $\psi$, the dilatancy angle) which reflects the relative packing of particles ($e_0$ or $D_R$) and ambient stress level ($\sigma_{vo}'$ or p'). Together, the two components combine to produce a peak friction angle:

$$\phi'_p \approx \phi'_{cs} + \psi' \qquad [5.11]$$

Characteristic values of $\phi_{cs}'$ are on the order of 32º for quartz sands, 33º for silty quartz sands with up to 20% fines content, 34º for siliceous sands (approx. half quartz-half

feldspar), 39º for calcareous sands, and 40º for feldspathic sands (Bolton 1986; Salgado et al. 2000; Jamiolkowski et al. 2001). The friction angle also depends upon mode of testing (i.e., plane strain vs. triaxial) and direction of loading (compression vs. extension). For the assessment of $\phi_p'$ of sands from CPT, there are several approaches: (a) use of a dilatancy framework where $q_c$ provides the input value of $D_R$ (Bolton, 1986); (b) inverse bearing capacity, such as from cavity expansion or limit plasticity theories (Yu & Mitchell, 1998; Schnaid 2009); (c) numerical simulation by finite elements, finite differences, and/or discrete elements (e.g., Salgado et al. 1998); or (d) direct CPT methods (Lunne et al. 1997). Because of the difficulties in procuring intact samples of natural sands, many early approaches were either benchmarked to or based on reconstituted samples where small triaxial specimens were prepared at similar relative densities and confining stress levels to those of larger calibration chamber tests subjected to CPTs. The methods of reconstitution, however, were not standardized (pluviation, compaction, vibration, sedimentation, moist tamping, slurry). Furthermore, the CPT data were not corrected for boundary conditions from limited size chambers.

Towards an improved solution, an elite database was compiled from special and expensive undisturbed samples of clean sands (Mayne 2006). Primarily, these sands were initially frozen in-place using one-dimensional thermal technologies. After careful mounting of specimens in triaxial apparatuses with membranes and confinement, they were allowed to thaw, and then sheared to failure to derive $\phi_p'$ corresponding to undisturbed intact sands. The sites for these sands were subjected to SPT, CPT, and $V_s$ measurements, as well as other lab and field testing.

The triaxial data from undisturbed sands can be seen to fit nicely with the expression derived by Kulhawy & Mayne (1990) that was developed on the basis of CPT calibration chamber data that have been corrected for boundary effects and stress-normalized:

$$\phi^\circ = 17.6^\circ + 11.\ \log\left(\frac{(q_t/\sigma_{atm})}{\sqrt{(\sigma'_{vo}/\sigma_{atm})}}\right) \qquad [5.12]$$

The relationship in **Figure 5.9** primarily applied to clean quartz to siliceous sands, yet there is some evidence it has applicability in natural sands with up to 30 percent silt content.

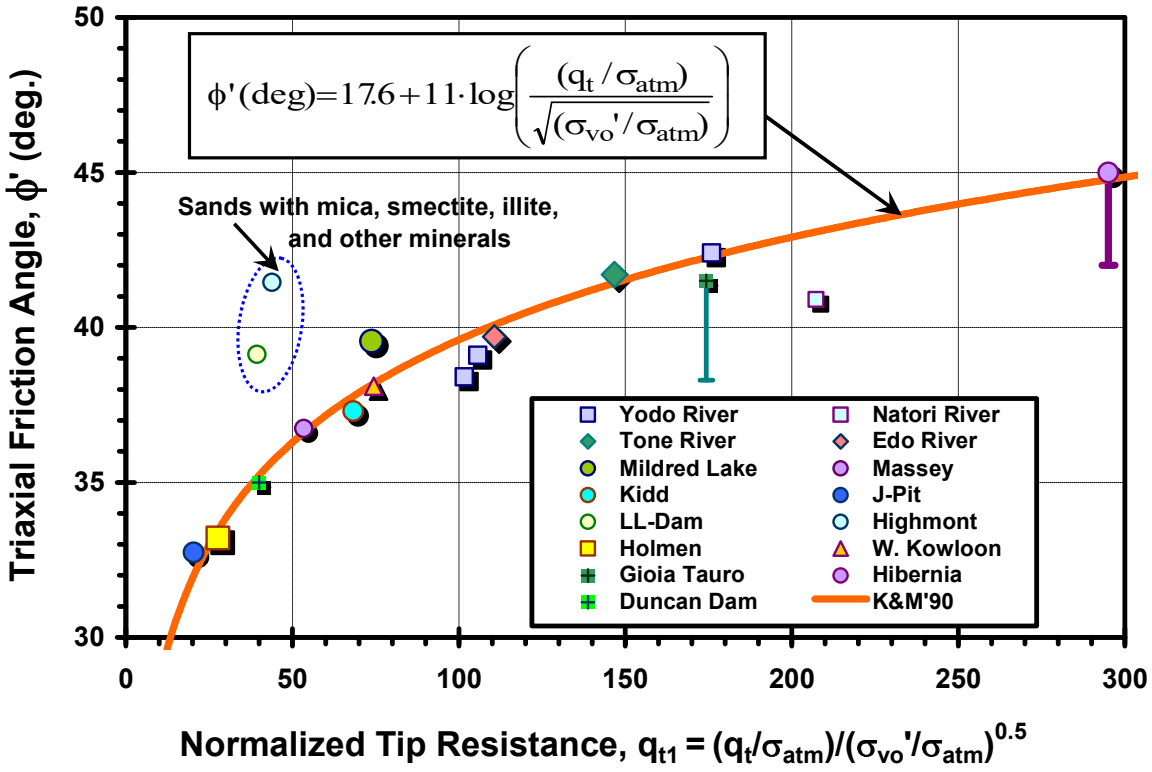


**Figure 5.9** *Direct CPT approach for evaluating ϕ' in clean sands (Mayne, 2006)*

As for clays an average approximate friction angle value of 28 degrees is assigned following **Figure 4.11.**

## 5.8 Modulus of Elasticity from CPT

Deformation of the ground is an important facet that must be addressed during analysis and design of the proposed construction. Many office type buildings are built towards tolerable settlements of less than 25 mm (1 inch), while open structures such as parking garages are able to withstand up to 50 mm (2 inches) of vertical movement. Large bridge structures can sustain up to 75 mm (3 inches) displacements, yet earthen embankments may undergo deflections of 100 to 1000 mm during initial loading, primary consolidation, and long-term secondary compression (creep). For the latter, the full consideration of deformations can be expressed:

$$s_{total} = s_{initial} + s_{consolidation} + s_{creep} \quad [5.13]$$

as detailed earlier in Section 3.1.

Elastic theory allows for interrelationships between the equivalent elastic Young's modulus (E), shear modulus (G), and constrained modulus (D) in terms of the Poisson's ratio, such that:

$$E = 2 \cdot G \cdot (1 + \upsilon) \quad [5.14]$$

$$D' = E' \cdot \frac{(1 - \nu')}{(1 + \nu')(1 - 2\nu')} \quad [5.15]$$

Note that the constrained modulus (designated by the symbol D', but also by the nomenclature M') takes on only a drained value as it is measured directly in a one-

dimensional consolidation test (oedometer), while the moduli E and G can have drained (E' and G') as well as undrained values ($E_u$ and $G_u$). At the value of $\nu' \approx 0$, elastic theory states that the constrained modulus equals the Young's modulus, thus D'/E' = 1. At a value $\nu' \approx 0.2$ that is characteristic of sands and granular soils (Jamiolkowski et al. 1994; Lehane & Cosgrove 2000), the ratio D'/E' = 1.1 and therefore the constrained modulus and drained Young's modulus are often used somewhat interchangeably. In terms of the compressibility parameters from consolidation testing, the constrained modulus can be expressed:

OC Soils: $$D' = \frac{1+e_0}{C_s} \cdot \ln(10) \cdot \sigma_v' \quad [5.16]$$

NC Soils: $$D' = \frac{1+e_0}{C_c} \cdot \ln(10) \cdot \sigma_v' \quad [5.17]$$

where D' corresponds to the current effective stress state ($\sigma_{vo}'$). For an approximate evaluation of the constrained modulus (and drained Young's modulus) from CPT results, the common approach is expressed in the form:

$$D' \approx \alpha_D \cdot (q_T - \sigma_{V0}) \quad [5.18]$$

where $\alpha_D$ is an empirical scaling factor that has been shown to depend upon soil type, confining stress level, overconsolidation, and other factors (Kulhawy & Mayne, 1990).

**Figure 5.10** shows that for wide range of soil types: $\alpha_D \approx 5$ is an approximate starting place, excepting soft plastic organic clays and cemented geomaterials. The original database for this compilation was based on laboratory consolidometer data to provide the corresponding D' for clays and silts, while the consolidation phase of calibration chamber tests were used to obtain D' for clean quartz sands (Mayne 2007b).

For Piedmont residual soils, Mayne & Liao (2004) showed a direct relationship between the elastic modulus (E') obtained from flat dilatometer tests (DMT) and cone resistance ($q_t$) from CPT. This is quite compatible with the aforementioned study for sediments reported in terms of constrained modulus (D'). Revisiting those data, the net cone resistance can be used to show the relationship in **Figure 5.11**.

$$E' \text{ (DMT)} = 5\ (q_t - \sigma_{vo}) \qquad [5.19]$$

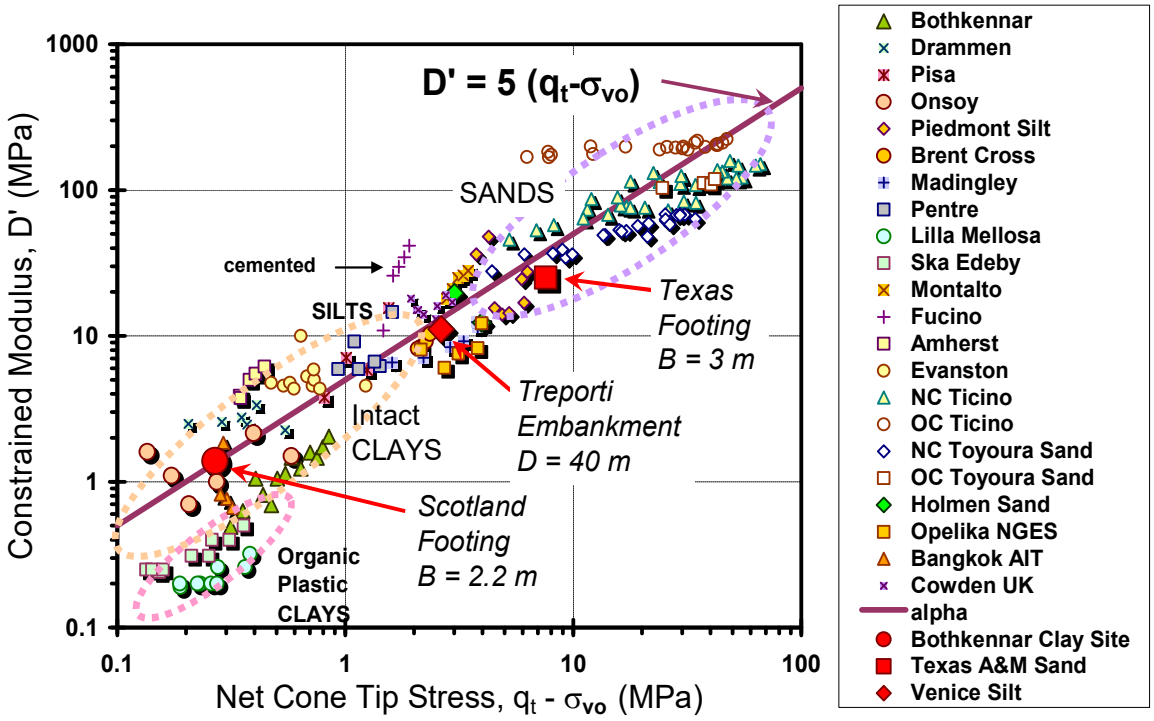


**Figure 5.10** *Overall trend between drained constrained modulus and net cone tip resistance in various soils, including three case studies with backfigured moduli*

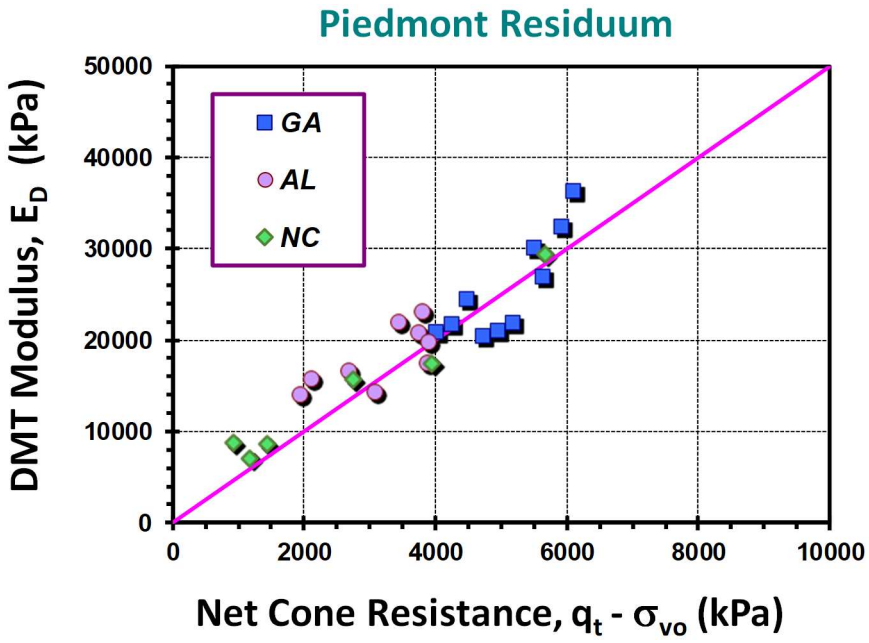


**Figure 5.11** *Relationship between the DMT elastic modulus and the net cone tip resistance in Piedmont soils (modified after Mayne and Liao, 2004)*

## 5.9 Stress History from CPT

For estimating the effective preconsolidation stress using the cone penetrometer readings, a general equation for all types of natural soils, including sands, silts, clays, and mixed soil types has been introduced by Mayne et al. (2009) as presented in **Figure 5.12.** The generalized expression is expressed as:

$$\sigma_p{}' = 0.33 \cdot (q_t - \sigma_{vo})^{m'} \cdot (\sigma_{atm}/100)^{1-m'} \qquad [5.20]$$

where the *exponent m'* is a parameter that increases with fines content and decreases with mean grain size. The approximate value of parameter m' ≈ 0.72 in clean quartz sands, 0.8 in silty sands, up to m' = 1.0 in intact clays of low sensitivity, and may even take greater values in fissured geomaterials. Using the CPT material index $I_c$ one can identify the magnitude of the parameter m' for general profiling of $\sigma_p$' in homogeneous or

heterogeneous deposits, as well as mixed soils. **Figure 5.13** shows the concluded trends, based on a review of the investigated data. For basic uncemented and non-structured soils, the exponent m' can be estimated as follows:

$$m' = 1 - \frac{0.3}{1 + (I_c / 2.65)^{20}} \qquad [5.21]$$

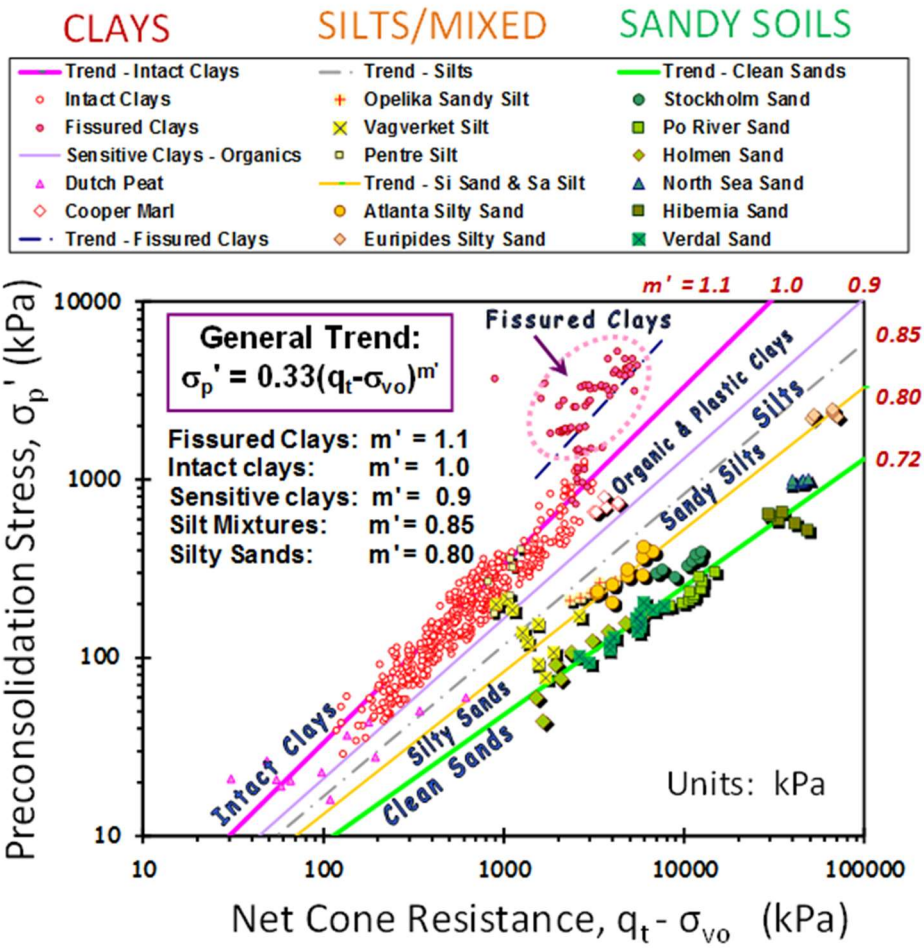


**Figure 5.12** *General Approach to $\sigma_p'$ interpretation of soils by CPT net cone resistance. (Mayne, et al. 2009)*

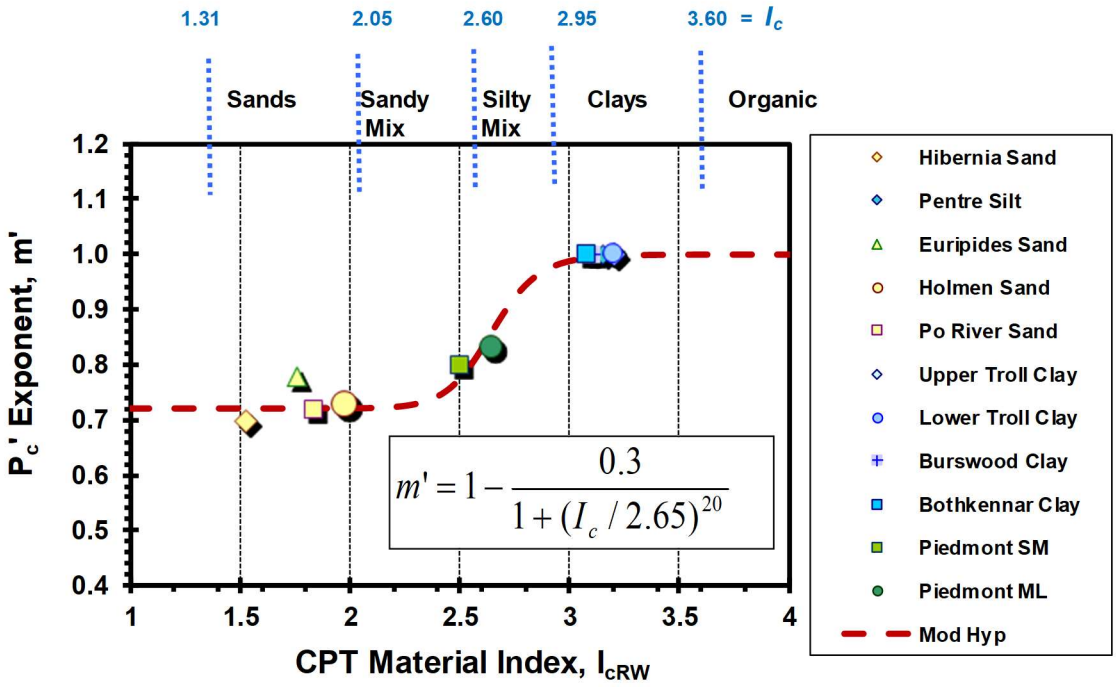


**Figure 5.13** *Preconsolidation exponent parameter m' versus CPT material index, $I_c$*

# 6. Input Parameters Using the Flat Dilatometer Tests (DMT)

## 6.1 Overview of the Flat Dilatometer Test (DMT)

The flat plate dilatometer test (DMT) is an in-situ method that involves pushing an instrumented flat steel blade into soils and recording two horizontal pressures at each test depth. The specific pressure measurements are utilized to obtain stratigraphy and estimates of geoparameters, including: unit weight, at-rest lateral stresses, elastic modulus, stress history, and shear strength. The flat dilatometer test (DMT) was developed in Italy and then introduced in North America and Europe (Marchetti, 1980).

The flat dilatometer test is simple, robust, repeatable, quick, economic, and operator-independent. The field of application of the DMT is very wide, ranging from extremely soft soils to dense sands. However, the DMT is difficult to push in very dense and hard materials and not applicable to gravels. The DMT analyses primarily relies on correlative relationships and requires calculations for local geologies. No borehole cuttings or spoil are generally produced by this test, although it is possible to advance a conventional soil boring and then perform the DMT downhole within the borehole.

## 6.2 DMT Equipment

The device consists of a tapered stainless steel blade with 18° wedge tip that is vertically advanced into the ground at 20-cm or 30-cm intervals per ASTM D 6635. The blade has a cutting edge to penetrate the soil. The steel blade has nominal dimensions of 240 mm length, 95 mm width, and 15 mm thickness and is connected to a readout pressure gauge.

The steel blade is connected to a control unit on the ground surface by a pneumatic-electrical tube (transmitting gas pressure and electrical continuity) running through the insertion rods. A nitrogen gas tank, connected to the control unit by a pneumatic cable, supplies the gas pressure required to expand the membrane. The control unit is equipped with a pressure regulator, pressure gauges, audio-visual signal, and vent valves. A circular 60-mm diameter flexible steel membrane that is located on one side of the blade is inflated pneumatically to give the pressure readings (Sabatini et al., 2002) . **Figure 6.1** shows a flat plate dilatometer blade and the associated control unit.

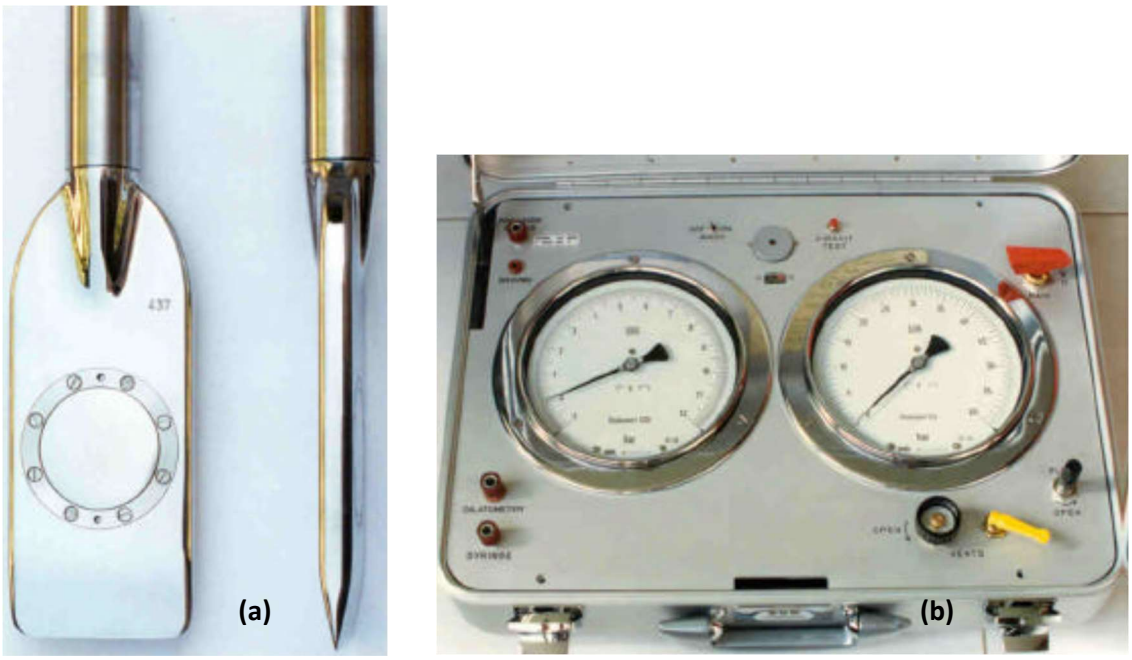


**Figure 6.1** *Main Components of the Flat Dilatometer Test: a. Steel DMT blade with inflatable membrane; and b. Pressure Control Unit*

## 6.3 Procedures for the DMT

Procedures for the test are given by ASTM D 6635 and Schmertmann (1986). **Figure 6.2** provides an overview of the DMT test and its setup. Two calibrations ($\Delta$A and $\Delta$B) are taken before the sounding to obtain corrections for the membrane stiffness in air. The test starts by advancing the steel blade into the ground at 20 mm/s using common field equipment such as drill rigs, cone trucks, or hydraulic ram systems. Discrete tests are performed typically at 200-mm (8-in) depth intervals, or in US practice at 300-mm (1 foot) intervals.

After blade penetration, the membrane is inflated using nitrogen pressure to obtain two readings: (a) A-pressure reading, required to make the membrane flush with the flat blade, and (b) B-pressure reading, required to move the center of the membrane 1.1 mm into the soil. The membrane is deflated just after the B-reading. The blade is then advanced to the next test depth and the procedure repeated to obtain another A and B at each depth. Each depth is accomplished in about 1 minute.

Two calibration readings are taken for membrane stiffness: $\Delta$A = pressure required in air to move the flexible membrane inward a distance 0.05 mm; $\Delta$B = pressure required in air to move membrane outward a distance 1.1 mm. Each of the pressure readings A and B are then converted into $p_0$ (contact pressure) and $p_1$ (expansion pressure), respectively per Figure 6.2. Additional details on the operations and mechanics of the DMT are given elsewhere (Marchetti and Crapps, 1981; Marchetti 1999; and Marchetti et al. 2001).

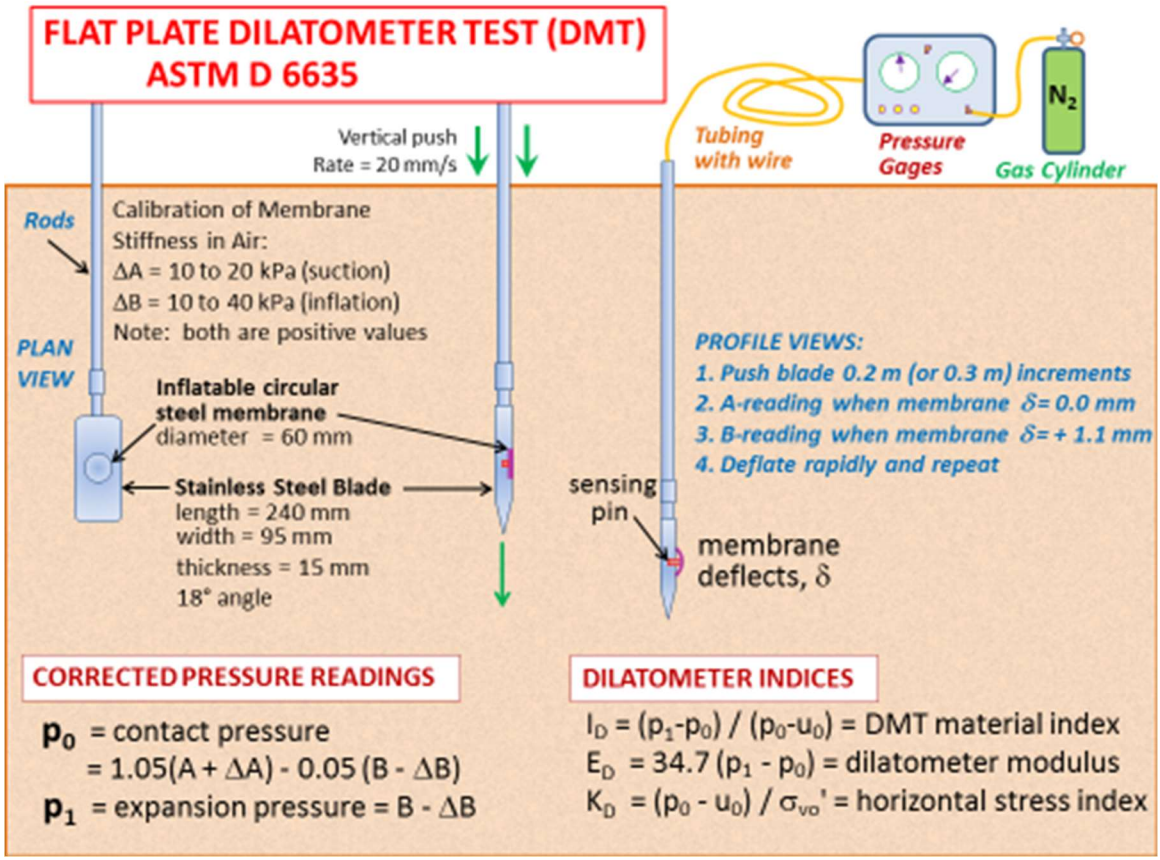


**Figure 6.2** *Illustration of Setup and Procedure for the Flat Dilatometer Test (DMT)*

## 6.4 DMT Index Parameters

The field A- and B- readings need to be corrected for membrane stiffness effects to obtain the liftoff pressure, $p_o$, and expansion pressure, $p_1$. Correction of the readings has been presented by Schmertmann (1986):

$$p_0 = 1.05\,(A + \Delta A - z_m) - 0.05\,(B - \Delta B - z_m) \qquad [6.1]$$

$$p_1 = B - \Delta B - z_m \qquad [6.2]$$

where ΔA and ΔB reported as positive absolute values are the calibration factors for applied suction and expansion of the membrane in air, respectively, and $z_m$ is the gage

offset zero reading when vented to atmospheric pressure and it is typically set to zero for a new gage.

The two dilatometer pressures, $p_0$ and $p_1$, are combined with the hydrostatic water pressure, $u_o$, to provide three index parameters: (a) material index $I_D$, (b) horizontal stress index $K_D$, and (c) dilatometer modulus $E_D$. These were developed by Marchetti (1980) to provide information on the stratigraphy, soil types, and the evaluation of soil parameters. Hydrostatic water pressure ($u_0$) can be evaluated based on available groundwater table information. If not available, then a special "C" reading can be made in clean sands to evaluate the $u_0$ value at that elevation and determine the groundwater table.

The material index, $I_D$, is related to the soil classification and is presented as:

$$I_D = (p_1 - p_0)/(p_0 - u_0) \quad [6.3]$$

The above definition of $I_D$ was introduced having observed that the $p_0$ and $p_1$ profiles are systematically "close" to each other in clay and "distant" in sand. According to Marchetti (1980), the soil type can be identified: clay: $0.1 < I_D < 0.6$, silt: $0.6 < I_D < 1.8$, and sand: $1.8 < I_D < 10$. In general, $I_D$ provides an expressive profile of soil type, and for normal soils, a reasonable soil description.

The horizontal stress index, $K_D$, is related to the in-situ horizontal stress-state of the soil. The index $K_D$ will always be greater than $K_0$ due to disturbance caused during insertion of the blade. This parameter is presented as:

$$K_D = (p_0 - u_0)/\sigma'_{v0} \quad [6.4]$$

$K_D$ provides the basis for several soil parameter correlations and is a key result of the dilatometer test. The horizontal stress index $K_D$ can be regarded as $K_0$ amplified by the

penetration (Marchetti et al., 2001). In NC clays; with no aging, structure, cementation; the value of $K_D \approx 2$. The $K_D$ profile is similar in shape to the OCR profile with depth, hence can be used to better understand the soil deposit and its stress history (Marchetti 1980, Jamiolkowski et al. 1988).

## 6.5 Soil Unit Weight from DMT

The total soil unit weight ($\gamma_t$) can be evaluated from the material index and dilatometer modulus as presented in **Figure 6.3**. For spreadsheet use, the approximate expression is:

$$\gamma_t = 1.12\,\gamma_w(E_D/\sigma_{atm})^{0.1}(I_D)^{-0.05} \qquad [6.5]$$

where $\gamma_w$ = unit weight of water and $\sigma_{atm}$ = atmospheric pressure. For each successive layer, the cumulative total overburden stress ($\sigma_{vo}$) can be calculated, as this is needed for the determination of the effective vertical overburden stress ($\sigma_{vo}' = \sigma_{vo} - u_o$) and the evaluation of the $K_D$ parameter (Mayne et al., 2002).

## 6.6 Effective Friction Angle from DMT

The peak friction angle in sands can be assessed using the flat plate dilatometer test. A wedge plasticity solution for the CPT was presented by Marchetti (1985) that was later cross-correlated for CPT-DMT relationships by Campanella & Robertson (1991). The wedge solutions relate the DMT lateral stress index ($K_D$) as a function of $\phi'$ and lateral stress state including active, at-rest (NC), and passive conditions. The passive case provides a generally conservative evaluation of peak friction angle and gives a good

agreement with field data from different sand sites (Mayne, 2001). The expression for the passive case as presented in **Figure 6.4** can be approximated by a hyperbola in the form:

$$\phi' = 20° + \frac{1}{0.04 + 0.06/K_D} \quad [6.6]$$

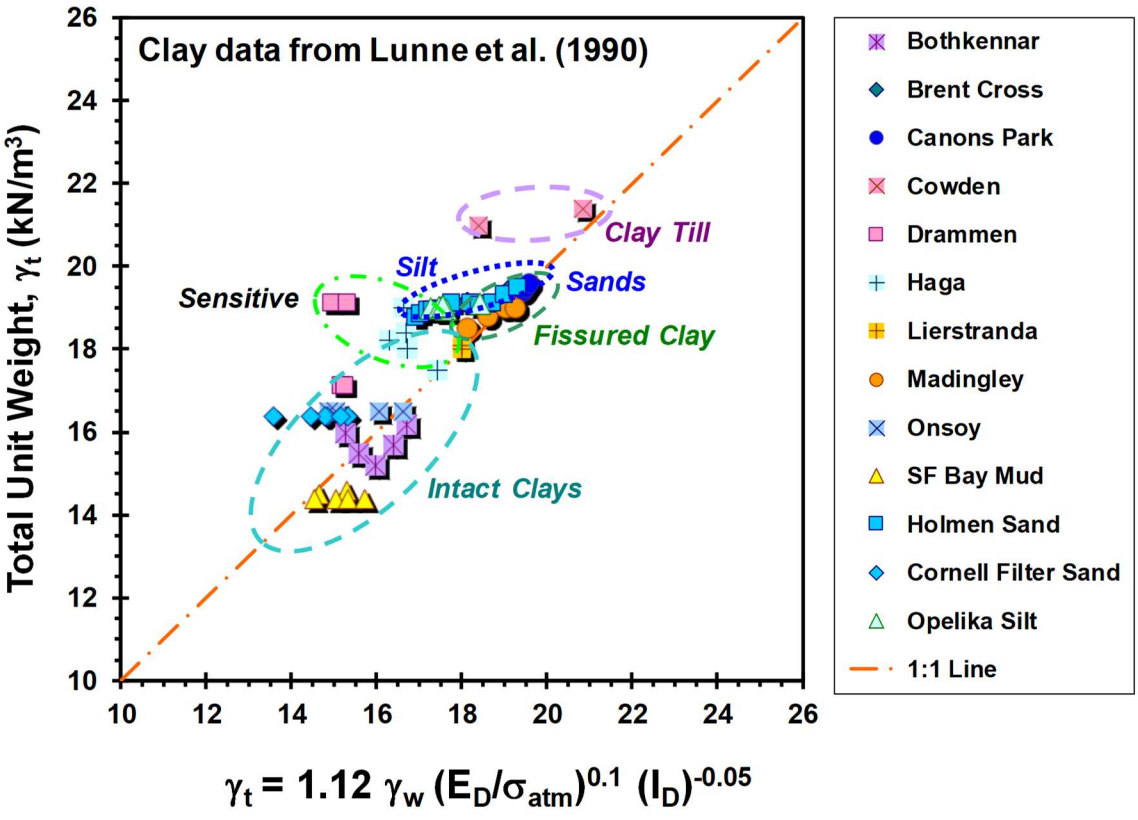


**Figure 6.3** *Total Unit Weight in terms of DMT Index Parameters (Mayne et al., 2002)*

## 6.7 Modulus of Elasticity from DMT

The dilatometer modulus $E_D$ is obtained from $p_0$ and $p_1$ from the theory of elasticity (Gravesen 1960). For the 60 mm membrane diameter and required 1.1 mm displacement, it is found (Marchetti 1980):

$$E_D = 34.7\ (p_1 - p_0) \quad [6.7]$$

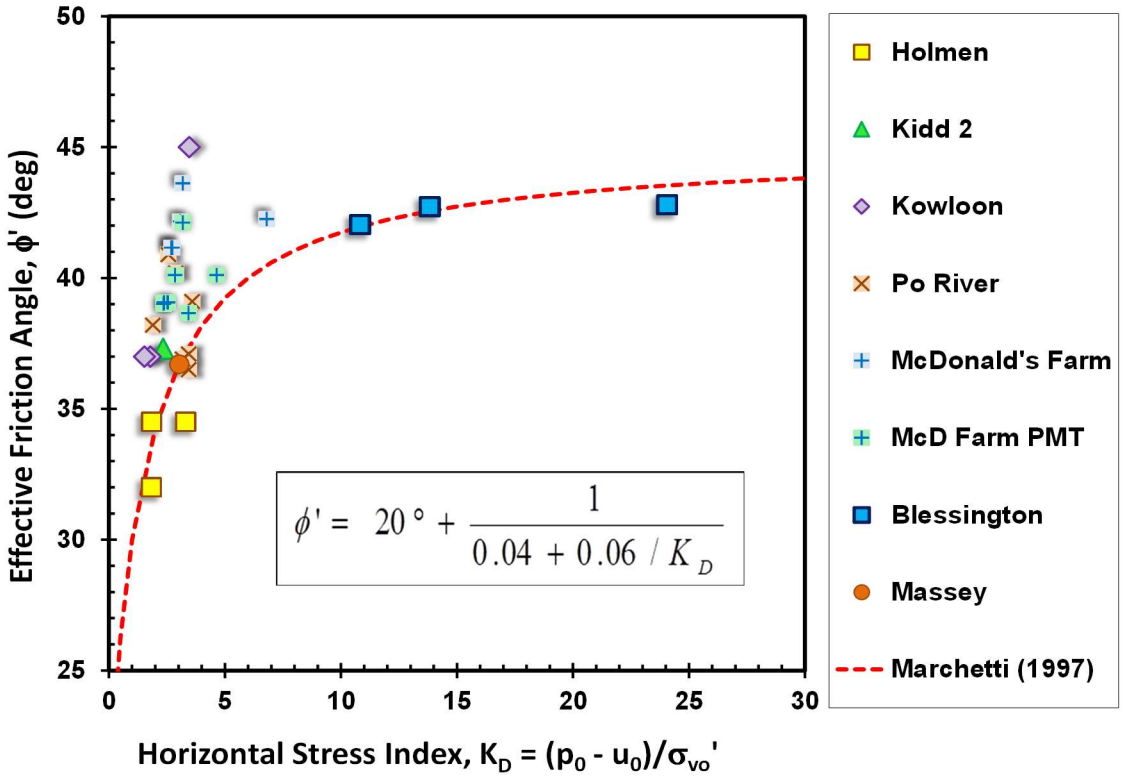


**Figure 6.4** *Effective Friction Angle of Sands in terms of DMT Horizontal Stress Index (modified after Mayne 2015)*

An example illustrating the evaluation of the dilatometer material index and modulus from the $p_0$ and $p_1$ readings is illustrated in **Figure 6.5** for a local test site in Cherokee County, GA. The constrained modulus M determined from the flat dilatometer test (designated as $M_{DMT}$) is the drained tangent modulus at $\sigma'_{v0}$ and is conceptually equivalent to the oedometer modulus obtained in the laboratory ($E_{oed} = 1/m_v$). $M_{DMT}$ can be evaluated using a correction factor $R_M$ to the dilatometer modulus $E_D$ using an adjustment factor $R_M$ :

$$M_{DMT} = R_M . E_D \qquad [6.8]$$

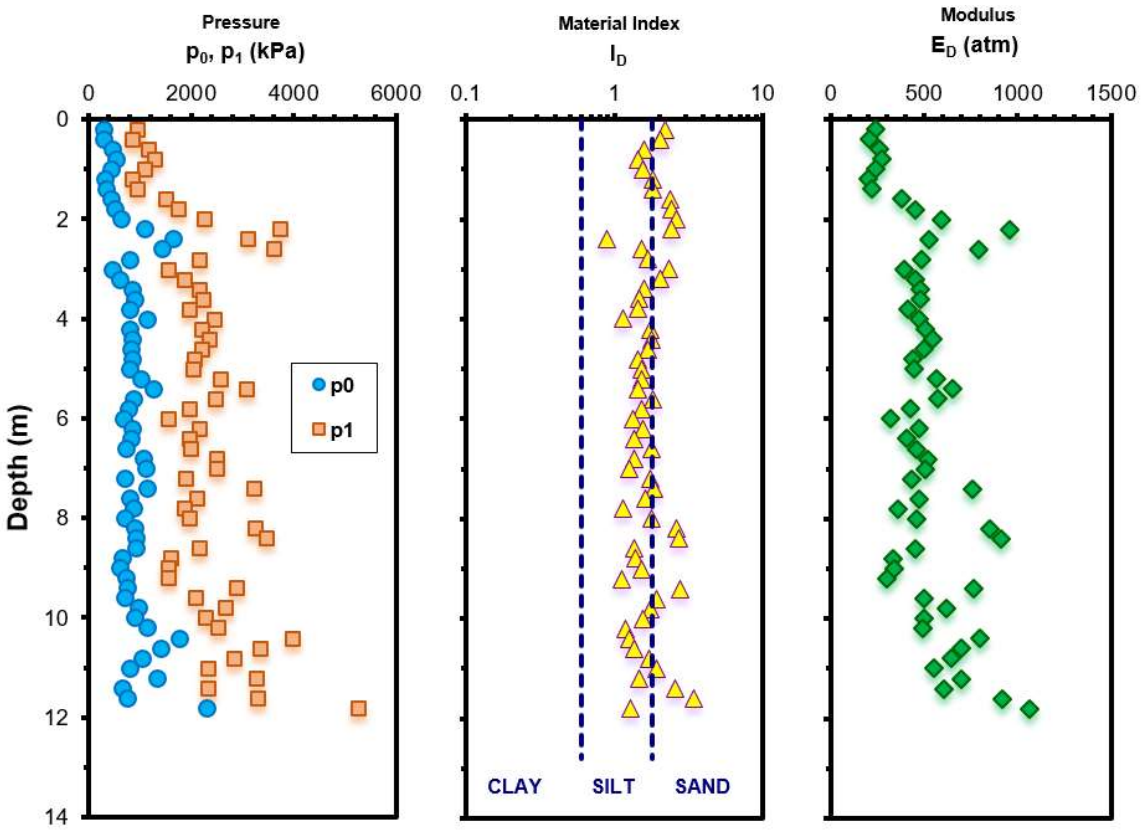


**Figure 6.5** *Illustration of direct evaluation of $E_D$ from DMT readings ($P_0$ and $P_1$) at site in Cherokee County, GA within the Blue Ridge-Piedmont geology*

The equations defining $R_M$ as a function of both $I_D$ and $K_D$ are described by (Marchetti 1980) and are given in **Table 6.1**.

**Table 6.1** *Equations defining correction factor $R_M = M_{DMT}/E_D$*

| | |
|---|---|
| For $I_D < 0.6$ | $R_M = 0.14 + 2.36 \log K_D$ |
| For $I_D > 3$ | $R_M = 0.5 + 2 \log K_D$ |
| For $0.6 < I_D < 3$ | $R_M = R_{M,0} + (2.5 - R_{M,0}) \log K_D$<br>with $R_{M,0} = 0.14 + 0.15 (I_D - 0.6)$ |
| For $K_D > 10$ | $R_M = 0.32 + 2.18 \log K_D$ |
| If $R_M < 0.85$ | Set $R_M = 0.85$ |

The Young's modulus E' of the soil skeleton can be derived from $M_{DMT}$ using the theory of elasticity equation:

$$E' = \frac{(1+\upsilon')(1-2\upsilon')}{(1-\upsilon')} M_{DMT} \quad [6.9]$$

In sands, using a typical value for Poisson's ratio $\nu' = 0.2$, then $E' = 0.9\ M_{DMT}$.

## 6.8 Stress History from DMT

Initial studies by Marchetti (1980) investigated the relationship between the overconsolidation ratio (OCR) and the DMT horizontal stress index, $K_D$. The correlation was based on the results of database from only five clays that was later investigated by Mayne (1995) to include data from 24 clays ranging from intact to calcareous to fissured clays as presented in **Figure 6.6**. The correlation is expressed in terms of net contact pressure ($p_0 - u_0$):

$$\sigma_p' \approx 0.5 \cdot (p_0 - u_0) \quad [6.10]$$

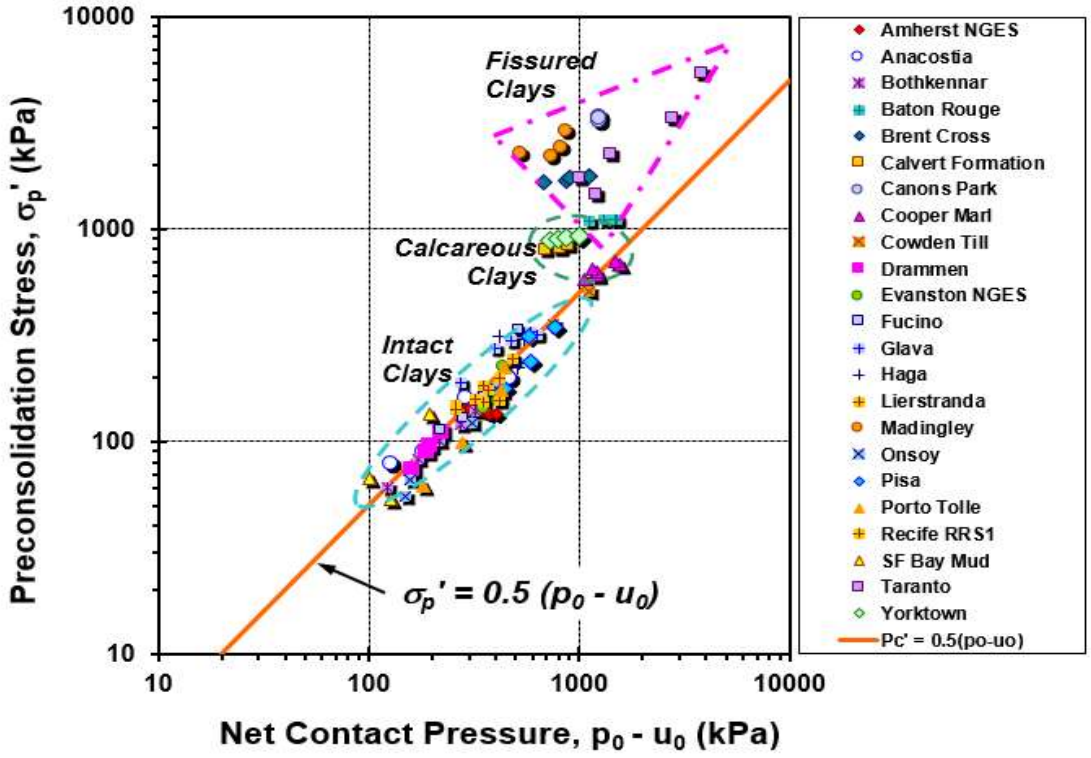


**Figure 6.6** *Relationship between effective preconsolidation stress and dilatometer net contact pressure ($p_0 - u_0$) for clays*

The database was expanded to include other soil types such as sands and silts (including Appalachian Piedmont silts and sands) as shown in **Figure 6.7.** It can be seen that **Equation 6.10** is generally applicable for all soil types and can be used to provide an estimate for effective preconsolidation stress.

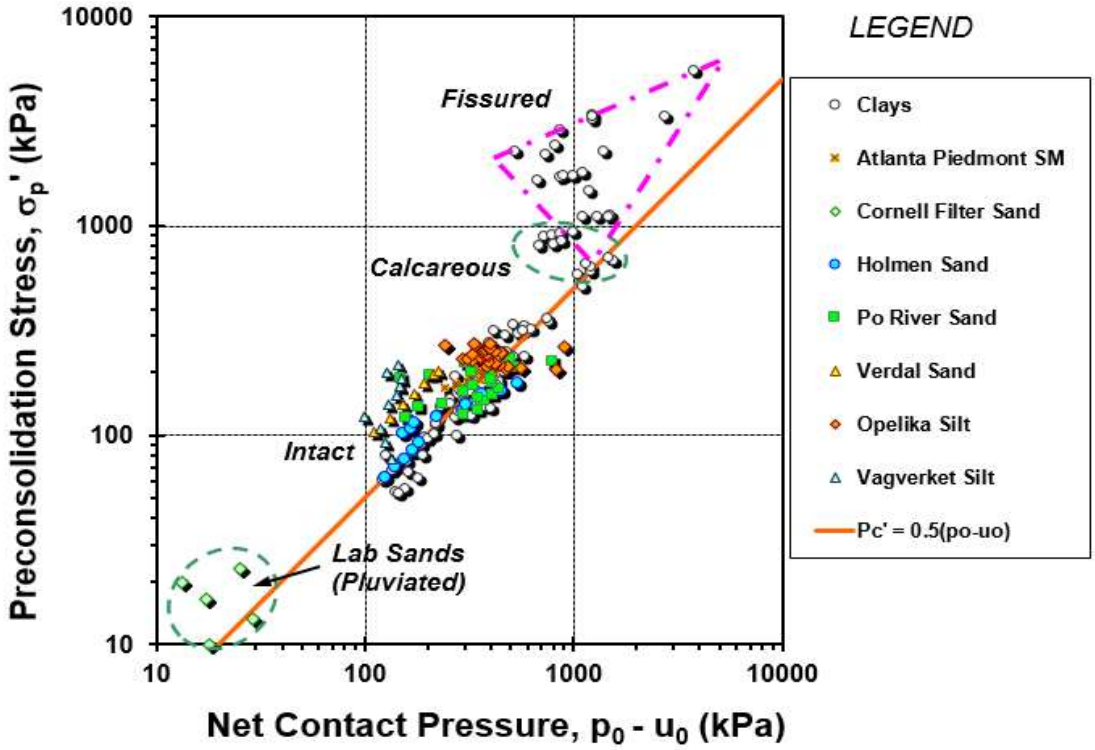


**Figure 6.7** *Relationship between effective preconsolidation stress and dilatometer net contact pressure ($p_0 - u_0$) for all soil types*

# 7. References


AASHTO (2008). Interim Revisions to *AASHTO LRFD Bridge Design Specifications,* 4th Edition, 2007. American Association of State Highway and Transportation Officials, Washington, DC.

AASHTO (2014). AASHTO LRFD Bridge Design Specifications, 7th Edition, with 2015 and 2016 Interim Revisions, LRFDUS-7-M. American Association of State Highway and Transportation Officials, Washington, DC. www.transportation.org

ADOT SF-2 (2010). Limiting Eccentricity Criteria for Spread Footings based on Load and Resistance Factor Design (LRFD) Methodology. *Memorandum* from N.H. Wetz, J.D. Wilson, A. Islam and N. Viboolmate to J. Lawson and J. Nehme, Dated December 1, 2010, Arizona Department of Transportation. Phoenix, AZ. Download document from: www.azdot.gov/Highways/Materials/Geotech_Design/Policy.asp

Beradi, R., Jamiolkowski, M., and Lancellotta, R. (1991). "Settlement of shallow foundations in sands: Selection of stiffness on the basis of penetration resistance". *Geotechnical Engineering Congress 1991*, Vol. 1 (GSP No. 27), ASCE, Reston, Virginia: 185-200.

Bhandary, N. P., & Yatabe, R. (2007). "Ring shear tests on clays of fracture zone landslides and clay mineralogical aspects". *Landslide risk and sustainable disaster management. Proceedings of first general assembly of Internal Consortium on Landslides.* Springer, Germany, 183-192.

Bolton, M.D. (1986). The strength and dilatancy of sands. *Geotechnique* 36 (1): 65-78.

Boswell, L.F. and Scott, C.R. (1975), "A flexible circular plate on a heterogeneous elastic half-space: influence coefficients for contact stress and settlement". *Geotechnique* 25 (3), 604-610.

Boulanger, R.W. and I.M. Idriss, *CPT and SPT Based Liquefaction Triggering Procedures*, Report No. UCD/CGM-14/01, Center for Geotechnical Modeling, Univ. California-Davis, 138 pages; 2014.

Brown, D.A. and Mayne, P.W. (2012). Piedmont residual soils and rocks. *GeoStrata* Vol. 16 (issue 6), ASCE, Reston, Virginia: 18-22.

Brown, P.T. (1969a). "Numerical analyses of uniformly loaded circular rafts on elastic layers of finite depth". *Geotechnique* 19 (2), 301-306.

Brown, P.T. (1969b). "Numerical analyses of uniformly loaded circular rafts on deep elastic foundations". *Geotechnique* 19 (3), 399-404.

Burland, J.B. (1970). Discussion of Session A, *Proceedings, Conference on In-Situ Investigations in Soils and Rocks*, British Geotechnical Society, London, 61-62.

Burland, J.B. (1989). Ninth Bjerrum Memorial Lecture: "Small is beautiful: the stiffness of soils at small strains". *Canadian Geotechnical Journal* 26 (4), 499-516.

Burns, S.E., Mayne, P.W., and Santamarina, J.C., editors (2008). *Deformational Characteristics of Geomaterials*, Vol. 2 (Proceedings 4th International Symposium on Deformation Characteristics of Geomaterials, Atlanta), Millpress/IOS Press, Amsterdam: Vols. 1 and 2: total 953 pages.

Campanella, R.G. and Robertson, P.K. (1991). "Use and interpretation of a research dilatometer." *Canadian Geotechnical Journal* 28 (1), 113-126.

Carrier, W.D., III, and Christian, J.T. (1973). "Rigid circular plate resting on a non-homogeneous elastic half-space". *Geotechnique* 23 (1), 67-84.

Christian, J.T. and Carrier, W.D., III (1978). "Janbu, Bjerrum, and Kjaernsli's chart reinterpreted". *Canadian Geotechnical Journal* 15 (1), 123-128.

D'Appolonia, D.J., Poulos, H.G., and Ladd, C.C. (1971), "Initial settlement of structures on clay". ASCE *Journal of the Soil Mechanics and Foundations Division* 97 (SM10), 1359-1377.

Das, B. (2011). *Principles of Foundation Engineering, Seventh Edition*, Cengage Learning, Stamford, Conn., 794 pages.

Davis, E.H. and Poulos, H.G. (1968). "The use of elastic theory for settlement prediction under three-dimensional conditions". *Geotechnique* Vol. 18 (1), 67-91.

Diaz-Rodriguez, A., Leroueil, S. and Aleman, J. (1992). "Yielding of Mexico City clay and other natural clays". *Journal of Geotechnical Engineering* 118 (7): 981–995.

Elhakim, A.F. and Mayne, P.W. (2008). Footing stress-displacement response using small-strain modulus. *Deformational Characteristics of Geomaterials*, Vol. 2 (Proc. 4th Intl. Symposium DCG, Atlanta), Millpress/IOS Press, Amsterdam: 937-944.

Fellenius, B.H. (1996; 2009). *Basics of Foundation Design: A geotechnical textbook and a background to the UniSoft programs.* BiTech Publishers, Richmond, British Columbia, 134 pages: www.fellenius.net

Foott, R. and Ladd, C.C. (1981), "Undrained settlement of plastic and organic clays". ASCE *Journal of Geotechnical Engineering Division (ASCE),* Vol. 107 (GT8), 1079-1094.

Fraser, R.A. and Wardle, L.J. (1976). "Numerical analysis of rectangular rafts on layered foundations". *Geotechnique* Vol. 26 (4), 613-630.

Gibson, R.E. (1967), "Some results concerning displacements and stresses in a nonhomogeneous elastic half-space". *Geotechnique* Vol. 17 (1), 58-67.

Gordon, D. and Mayne, P.W. (1986). Geotechnical report at Surry Power Station, Virginia, submitted to Virginia Power, Richmond VA by Law Engineering Associates, McLean, VA.

Gravesen, S. (1960). "Elastic Semi-Infinite Medium Bounded by a Rigid Wall with a Circular Hole". Laboratoriet for Bygninsteknik, Danmarks Tekniske Højskole, *Meddelelse No. 10*, Copenhagen.

Harr, M.E. (1966), *Foundations of Theoretical Soil Mechanics* , McGraw-Hill, New York, 81-100.

Harr, M.E. (1977), *Mechanics of Particulate Media* , McGraw-Hill, New York, 330-342.

Hatanaka, M. and Uchida, A. (1996). "Empirical correlation between penetraion resistance and effective friction of sandy soil.", *Soils & Foundations*, Vol. 36 (4), Japanese Geotechnical Society, 1-9.

Hegazy, Y.A. and Mayne, P.W. (1995). Statistical correlations between $V_s$ and CPT data for different soil types. *Proceedings, Intl. Symp. on Cone Penetration Testing*, Vol. 2, Swedish Geotechnical Society, Linköping: 173-178. Download from: www.usucger.org

Holtz, R.D. and Kovacs, W.D. (1981). *An Introduction to Geotechnical Engineering*, Prentice-Hall, Englewood Cliffs, NJ, 733 p.

Honeycutt, J.N., Kiser, S.E. and Anderson, J.B. (2014). "Database Evaluation of Energy Transfer for CME Automatic Hammer SPT", *Journal of Geotechnical & Geoenvironmental Engineering* Vol. 140 (1): 194-200.

Horikoshi, K. and Randolph, M.F. (1997). "On the definition of raft-soil stiffness ratio for rectangular rafts". *Geotechnique* Vol. 47 (5), 1055-1061.

Imai, T., and Tonouchi, K. (1982). "Correlation of N-value with S-wave velocity and shear modulus." *Proceedings of the 2nd European Symposium on Penetration Testing,* Vol. 1, Amsterdam: pp. 67 – 72.

Jamiolkowski, M., Ghionna, V., Lancellotta, R. and Pasqualini, E. (1988). "New Correlations of Penetration Tests for Design Practice". *Penetration Testing 1988* (Proc. ISOPT-1, Orlando), Vol. 1, Balkema Publishers, Rotterdam: 263-296.

Jamiolkowski, M., Ladd, C.C., Germaine, J.T., and Lancellotta, R. (1985). "New Developments in Field and Lab Testing of Soils." *Proceedings 11th International Conference on Soil Mechanics and Foundation Engineering*, Vol. 1, San Francisco, Calif. pp. 57–154.

Jamiolkowski, M., Lancellotta, R., and LoPresti, D.C.F. (1995). "Remarks on the stiffness at small strains of six Italian clays". *Pre-Failure Deformation of Geomaterials*, Vol. 2 (Proc. Sapporo), Balkema, Rotterdam, 817-836.

Jamiolkowski, M., Lancellotta, R., LoPresti, D.C.F., and Pallara, O. (1994), "Stiffness of Toyoura sand at small and intermediate strain". *Proceedings, 13th Intl. Conf. on Soil Mechanics and Foundation Engineering* (3), New Delhi, India, 169-173.

Jamiolkowski, M., LoPresti, D.C.F., and Manaserro, M. (2001). Evaluation of relative density and shear strength of sands from CPT and DMT. *Soil Behavior and Soft Ground Construction*, GSP 119, ASCE, Reston, Virginia: 201-238.

Janbu, N. (1969). "The resistance concept applied to deformations of soils.", *Proceedings, 7th International Conference on Soil Mechanics and Foundation Engineering* (1), Mexico City, 191-196.

Jardine, R.J., Fourie, A., Maswoswe, J., and Burland, J.B. (1985). "Field and lab measurements of soil stiffness." *Proceedings , 11th International Conference on Soil Mechanics and Foundation Engineering* (2), San Francisco, 511-514.

Kulhawy, F. H., O'Rourke, T. D., Stewart, J. P., and Beech, J. F. (1983). *Transmission Line Structure Foundations for Uplift-Compression Loading, EPRI Final Report EL-2870*. Electric Power Research Institute, Palo Alto: www.epri.com.

Kulhawy, F.H. and Mayne, P.W. (1990). "Manual on Estimating Soil Properties for Foundation Design.", *Report EL-6800*, Electric Power Research Institute, Palo Alto, 306 p. www.epri.com

Lambe, T.W. and Whitman, R.V. (1979). *Soil Mechanics*, *SI Version*, John Wiley & Sons, New York, 153-158.

Larsson, R. and Mulabdić, M. (1991). Piezocone Tests in Clays. *Report No. 42*, Swedish Geotechnical Institute, Linköping, 240 p.

Lehane, B.M. and Cosgrove, E. (2000). Applying triaxial compression stiffness data to settlement prediction of shallow foundations on cohesionless soil. *Proc. Institution of Civil Engineers, Geotechnical Engineering*, Vol. 143 (4), London: 191-200.

Liao, S.S., and Whitman, R.V. (1986). "Overburden Correction Factors for SPT in Sand." *Journal of Geotechnical Engineering*, ASCE, Vol. 112, No. 3, pp. 373-377.

Locat, J., Tanaka, H., Tan, T.S., Dasari, G.R. and Lee, H. (2003). "Natural soils: geotechnical behavior and geological knowledge". *Characterisation & Engineering Properties of Natural Soils*, Vol. 1 (Proc. Singapore Workshop), Swets & Zeitlinger, Lisse: 3–28.

LoPresti, D.C.F. (1995). "General report: measurement of shear deformation of geomaterials". *Pre-Failure Deformation of Geomaterials*, Vol. 2 (Proc. Sapporo), Balkema, Rotterdam, 1067-1088.

LoPresti, D.C.F., Pallara, O., and Puci, I. (1995). "A modified commercial triaxial testing system for small strain measurements". ASTM *Geotechnical Testing Journal* 18 (1), 15-31.

Lunne, T., Powell, J.J.M., Hauge, E.A., Mokkelbost, K.H., and Uglow, I.M. (1990). "Correlation for dilatometer readings with lateral stress in clays." *Transportation Research Record* 1278, National Academy Press, Washington, D.C., 183-193.

Lunne, T., Robertson, P.K. and Powell, J.J.M. (1997). *Cone Penetration Testing in Geotechnical Practice*. EF Spon/Blackie Academic, Routledge Publishers, London, 312 p.

Marchetti, S. (1980). "In-situ tests by flat dilatometer." *Journal of the Geotechnical Engineering Division (ASCE)*, Vol. 106 (3), 299-321.

Marchetti, S. (1985). "On the field determination of $K_0$ in sand." *Proceedings, 11th International Conference on Soil Mechanics & Foundation Engineering* (ICSMFE, San Francisco), Vol 5, Balkema, Rotterdam: 2667-2672.

Marchetti, S. (1997). "The flat dilatometer: design applications." *Proceedings of the* 3rd *Geotechnical Engineering Conference*, Cairo University, 1-25.

Marchetti, S. (1999). "On the calibration of the DMT membrane." L'Aquila Univ., *Unpublished report*, March. http://marchetti-dmt.it/

Marchetti, S. and Crapps, D.K. (1981). "Flat Dilatometer Manual." *Internal Report* of G.P.E. Inc., Gainesville, Florida. www.gpe.org

Marchetti, S., Monaco, P., Totani, G., and Calabrese, M. (2001). "The flat dilatometer test (DMT) in soil investigations–A report by the ISSMGE committee TC16." *Proceedings of the 2nd International Flat Dilatometer Conference,* Arlington, VA: pp. 7-48. www.usucger.org

Massarsch, K.R. (1994). "Settlement Analysis of Compacted Granular Fill". *Proc. XIII Intl. Conf. Soil Mechanics & Foundation Engineering,* New Delhi, Vol. 1, 325- 328.

Mayne, P.W. (1992). "In-situ characterization of Piedmont residuum in Eastern US". *Proc. National Science Foundation (NSF) US-Brazil Geo-Workshop: Application of Classical Soil Mechanics to Structured Soils*, Belo Horizonte: 89–93.

Mayne, P.W. (2001). Invited Keynote: ""Stress-Strain-Strength-Flow Parameters from Enhanced In-Situ Tests".", *Proceedings, International Conference on In-Situ Measurement of Soil Properties & Case Histories* (In-Situ 2001), Bali, Indonesia, 27-47.

Mayne, P.W. (2005). ""Unforeseen large settlements of mat foundation on Piedmont residuum".", *International Journal of Geoengineering Case Histories:* Vol. 1 (1): 5-17. Online GeoEngineer journal at: *http://casehistories.geoengineer.org/contents.html*

Mayne, P.W. (2005). Invited Keynote: "Integrated Ground Behavior: In-Situ and Lab Tests.", *Deformation Characteristics of Geomaterials*, Vol. 2 (Proc. IS Lyon'03), Taylor & Francis Group, London: 155-177.

Mayne, P.W. (2006). "In-situ test calibrations for evaluating soil parameters." *Characterisation and Engineering Properties of Natural Soils*", Vol. 3, (Proc. Singapore), Taylor & Francis Group, London: 1602-1652.

Mayne, P.W. (2006). "The 2006 James K. Mitchell Lecture: Undisturbed sand strength from seismic cone tests." *Geomechanics & Geoengineering:* Vol. 1 (4): 239-257.

Mayne, P.W. (2007). *NCHRP Synthesis 368 on Cone Penetration Test.* Transportation Research Board, National Academies Press, Washington, D.C., 118 pages. Download from: www.trb.org

Mayne, P.W. (2007b). Invited Overview Paper: In-situ test calibrations for evaluating soil parameters, *Characterization & Engineering Properties of Natural Soils*, Vol. 3 (Proc. Singapore 2006), Taylor & Francis Group, London: 1602-1652.

Mayne, P.W. (2013). Updating our geotechnical curricula via a balanced approach of in-situ, laboratory, and geophysical testing of soil. *Proceedings, 61st Annual Geotechnical Conference*, Minnesota Geotechnical Society, University of Minnesota, St. Paul: 65-86.

Mayne, P.W. (2014) "Interpretation of geotechnical parameters from seismic piezocone tests." In *Proceedings 3rd International Symposium on Cone Penetration Testing, (CPT'14*, Las Vegas): 47-73. Download from: www.cpt14.com

Mayne, P.W. (2015). Peak friction angle of undisturbed sands using DMT. *Proceedings, Third International Conference on Flat Dilatometer*, (DMT'15, Rome), paper ID 20: pp. 237-

242: www.dmt15.com

Mayne, P.W. and Brown, D.A. (2003). ""Site characterization of Piedmont residuum of North America"." *Characterization and Engineering Properties of Natural Soils*, Vol. 2, Swets & Zeitlinger, Lisse, 1323-1339.

Mayne, P.W. and Frost, D.D. (1988). "Dilatometer Experience in Washington, DC and Vicinity", *Transportation Research Record 1169*, National Academy Press, Washington, DC, pp. 16-23

Mayne, P.W. and Harris, D.E. (1993). *Axial Load-Displacement Behavior of Drilled Shaft Foundations in Piedmont Residuum*. FHWA Reference No. 41-30-2175 Report to ADSC/ASCE by Georgia Tech, School of Civil & Environmental Engineering, Atlanta, GA: 172 p. Download: http://geosystems.ce.gatech.edu/Faculty/Mayne/papers/index.html

Mayne, P.W. and Kemper, J.B. (1988). "Profiling OCR in Stiff Clays by CPT and SPT." ASTM *Geotechnical Testing Journal*, Vol. 11, No. 2, pp. 139-147.

Mayne, P.W. and Liao, T. (2004). ""CPT-DMT interrelationships in Piedmont residuum".", *Geotechnical & Geophysical Site Characterization*, Vol. 1, (Proc. ISC-2, Porto), Millpress, Rotterdam, 345-350.

Mayne, P.W. and Poulos, H.G. (1999). "Approximate Displacement Influence Factors for Elastic Shallow Foundation Systems", ASCE *Journal of Geotechnical & Geoenvironmental Engineering*, Vol. 125, No. 6: 453-460.

Mayne, P.W. and Woeller, D.J. (2014). Direct CPT method for footings on sands, silts, and clays. *Geocharacterization for Modeling and Sustainability* (GSP 235: Proc. GeoCongress 2014, Atlanta), ASCE, Reston, Virginia: 1983-1997.

Mayne, P.W., Brown, D., Vinson, J., Schneider, J.A., and Finke, K.A. (2000). "Site characterization of Piedmont residual soils at the NGES, Opelika, Alabama", *National Geotechnical Experimentation Sites,* (GSP No. 93), American Society of Civil Engineers, Reston/VA: 160-185.

Mayne, P.W., Christopher, B., Berg, R., and DeJong, J. (2002). "*Subsurface Investigations - Geotechnical Site Characterization*." Publication No.FHWA-NHI-01-031, National Highway Institute, Federal Highway Administration, Washington, D.C., 301 pages

Mayne, P.W., Coop, M.R., Springman, S., Huang, A-B., and Zornberg, J. (2009). State-of-the-Art Paper (SOA-1): Geomaterial Behavior and Testing. *Proc. 17th Intl. Conf. Soil Mechanics & Geotech. Engrg.*, (ICSMGE, Alexandria, Egypt), Vol. 4, Millpress/IOS Press Rotterdam: 2777-2872.

Mayne, P.W., Peuchen, J., and Bouwmeester, D. (2010). Estimation of soil unit weight from piezocone readings in onshore soils. *Proc. 2nd Intl. Symposium on Cone Penetration Testing*, Vol. 2, Huntington Beach, CA: 169-176. www.cpt10.com

Mayne, P.W., Uzielli, M. and Illingworth, F. (2012). Shallow footing response on sands using a direct method based on cone penetration tests. *Full Scale Testing and Foundation Design* (Proceedings GSP 227 honoring Bengt Fellenius), ASCE, Reston, Virginia: 664-679.

Mesri, G. (1973). "Coefficient of Secondary Compression". *Journal of the Soil Mechanics and Foundations Division, Proc. ASCE*, Vol. 99, No. SM1, pp. 123-137.

Meyerhof, G. G. (1957). "The Ultimate Bearing Capacity of Foundations on Slopes." In *Proc., 4th International Conference on Soil Mechanics and Foundation Engineering,* Vol. 1, London, UK: 384-386.

Meyerhof, G.G. (1956). "Penetration tests and bearing capacity of cohesionless soils." *Journal of the Soil Mechanics and Foundations Division* ASCE Vol. 82 (SM1): 1-19.

Munfakh, G., Arman, A., Gollin, J. G., Hung, J. C. J., and Brouillette, R. P. (2001). *Shallow Foundations Reference Manual, FHWA-NHI-01—023.* Federal Highway Administration, U.S. Department of Transportation, Washington, DC.

Niazi, F.S. and Mayne, P.W. (2012). Field stiffness reduction evaluations from back-analysis of pile load tests. *Proceedings GeoCongress 2012* (GSP 225, Oakland), ASCE, Reston, Virginia: 155-160.

Niazi, F.S., Mayne, P.W. and Woeller, D.J. (2014). Pile axial load-displacement response from geophysical component of seismic CPT. *Proceedings, 3rd Intl. Symposium on Cone Penetration Testing*, Las Vegas, Omnipress: 1103-1112. www.cpt14.com

Paikowsky, S.G., Canniff, M.C., Lesny, K., Kisse, A., Amatya, S., and Muganga, R. (2010). *LRFD Design and Construction of Shallow Foundations for Highway Bridge Structures*. NCHRP Report 651, National Cooperative Highway Research Program, Transportation Research Board, Washington, DC: 149 pages. www.trb.org

Perloff, W.H. and Baron, W. (1976). *Soil Mechanics: Principles and Applications*, John Wiley & Sons, New York, 745.

Plewes, H.D., Pillai, V.S., Morgan, M.R. and Kilpatrick, B.L. (1994). "In-situ sampling, density measurements, and testing of foundation soils at Duncan Dam." *Canadian Geotechnical Journal* 31 (6): 927-938.

Poulos, H.G. (1968). "The behaviour of a rigid circular plate resting on a finite elastic layer". *Civil Engineering Transactions* , Vol. CE 10, Institution of Engineers, Australia, 213-219.

Poulos, H.G. and Davis, E.H. (1974). *Elastic Solutions for Soil and Rock Mechanics*. John Wiley & Sons, New York: 411 pages. Downloadable from: www.usucger.org

Prandtl, L. (1921). Ueber die Eindringfestigkeit (Haerte) plastischer Baustoffe und die Festigkeit von Schneiden. Zeitschrift für angewandte Mathematik und Mechanik 1, Band 1, 15–20.

Reissner, H. (1924). “"Zum Erddruckproblem."” *Proc., 1st International Congress of Applied Mechanics,* Delft, 295–311.

Robertson, P.K. (2004). "Evaluating soil liquefaction and post-earthquake deformations using the CPT". *Geotechnical & Geophysical Site Characterization*, Vol. 1 (Proc. ISC-2, Porto), Millpress, Rotterdam: 233-249.

Robertson, P.K. (2009). "Interpretation of cone penetration tests: a unified approach". *Canadian Geotechnical Journal*, Vol. 46, No. 11, pp. 1337-1355.

Robertson, P.K. and Wride, C.E. (1998). "Evaluating cyclic liquefaction potential using the cone penetration test." *Canadian Geotechnical Journal*, Vol. 35, No. 3, pp. 442-459.

Robertson, P.K., Campanella, R.G., Gillespie, D. and Greig, J. (1986). "Use of piezometer cone data". *Use of In-Situ Tests in Geotechnical Engineering* (GSP 6), ASCE, Reston/VA: 1263-1280.

Sabatini, P.J., Bachus, R.C., Mayne, P.W., Schneider, J.A. and Zettler, T.E. (2002). *Manual on Evaluating Soil & Rock Properties*, *Geotechnical Engineering Circular No. 5*, Report No. FHWA-IF-02-034, Federal Highway Administration, Washington, D.C., 385 pages.

Salgado, R., Bandini, P., and Karim, A. (2000) "Shear strength and stiffness of silty sand." *Journal of Geotechnical and Geoenvironmental Engineering* 126, no. 5: 451-462.

Salgado, R., Mitchell, J. K., and Jamiolkowski, M. (1998). "Calibration chamber size effects on penetration resistance in sand." *Journal of Geotechnical and Geoenvironmental Engineering* 124, no. 9: 878-888.

Samtani, N.C., Nowatzki, E.A., and Mertz, D.R. (2010). *Selection of Spread Footings on Soils to Support Highway Bridge Structures* (No. FHWA-RC/TD-10-001). Federal Highway Administration, U.S. Department of Transportation, Washington, DC: 98 pages.

Sargand, S.M., Masada, T., and Abdalla, B. (2003). "Evaluation of cone penetration test based settlement prediction methods for shallow foundations on cohesionless soils at highway bridge construction sites. *Journal of Geotechnical & Geoenvironmental Engineering*, Vol. 129 (10): 900-908.

Sargand, S.M. and Masada, T. (2006). Further Use of Spread Footing Foundations for Highway Bridges. *Final Rept. FHWA-OH-2006/8*, Ohio University and Ohio Research Institute for Transportation and the Environment (ORITE), Athens, OH: 332 pages.

Schmertmann, J.H. (1970). "Static cone to compute static settlement over sand", *Journal of the Soil Mechanics and Foundations Division* (ASCE) 96 (SM3), 1011-1043.

Schmertmann, J.H. (1986). "Dilatometer to compute Foundation Settlement". *Use of In-Situ Tests in Geotechnical Engineering*, (Proc. In-Situ'86, Virginia Tech, Blacksburg, VA), GSP 6, ASCE, Reston, Virginia: 303-321.

Schmertmann, J.H., Hartman, J.P., and Brown, P.R. (1978). "Improved strain influence factor diagrams". *Journal of Geotechnical Engineering Division (ASCE)* Vol. 104, 1131-1135.

Schnaid, F. (2009). *In-Situ Testing in Geomechanics: the Main Tests*. CRC Press / Taylor & Francis Group, London: 352 p.

Skempton, A.W. (1986). "SPT procedures and the effects in sands of overburden pressure, relative density, particle size, aging, and overconsolidation." *Geotechnique*, Vol. 36, No. 3, 425-447.

Skempton, A.W. and Bjerrum, L. (1957), "A contribution to the settlement analysis of foundations on clay", *Geotechnique,* Vol. 7 (4), 168-178.

Small, J.C. (1995). "FLEA5 - finite layer elastic analysis: users manual for PC version for Windows". *Report FLEA5*, Geotechnical Research Centre, University of Sydney, Australia.

Stamatopoulos, A.C. and Kotzias, P.C. (1978). "Soil compressibility as measured in the oedometer". *Geotechnique* 28 (4), 363-375.

Sully, J.P. and Eschesuria, H.J. (1988). In-situ density measurement with the nuclear cone penetrometer. *Penetration Testing 1988*, Vol. 2 (Proc. ISOPT, Orlando), Balkema, Rotterdam: 1001-1006.

Széchy, K. and Varga, L. (1978). *Foundation Engineering: Soil Exploration and Spread Foundations* . Technical University of Budapest, Akadémiai Kiadó, Hungary, 351-353.

Tatsuoka, F. and Shibuya, S. (1992). "Deformation characteristics of soils and rocks from field and laboratory tests". *Report of the Institute of Industrial Science*, Vol. 37, No. 1, Serial No. 235, The University of Tokyo, 138 p.

Tatsuoka, F., Teachavorasinsku, S., Dong, J., Kohata, Y. and Sato, T. (1994). "Importance of measuring local strains in cyclic triaxial tests on granular materials". *Dynamic Geotechnical Testing II* (STP 1213), ASTM, Philadelphia, 288-302.

Taylor, B.B., Lewis, J.F. and Ingersoll, R.W. (1993) "Comparison of interpreted seismic profiles to geotechnical borehole data at Hibernia." *Proceedings of the 4th Canadian Conference on Marine Geotechnical Engineering*, St. John's, Newfoundland: 685-708.

Terzaghi, K., Peck, R. B., & Mesri, G. (1996). *Soil Mechanics in Engineering Practice*. John Wiley & Sons: 565p.

Thompson, G.R. and Long, L.G. (1989) "Hibernia geotechnical investigation and site characterization." *Canadian Geotechnical Journal* 26 (4): 653-678.

Ueshita, K. and Meyerhof, G.G. (1967). "Deflection of multilayer soil systems". *Journal of the Soil Mechanics and Foundations Division* (ASCE) 93 (SM5), 257-282.

Ueshita, K. and Meyerhof, G.G. (1968). "Surface displacement of an elastic layer under uniformly-distributed loads". *Highway Research Record 228*, National Research Council, Washington, D.C., 1-10.

Uzielli, M. and Mayne, P.W. (2012). Load-displacement uncertainty of vertically-loaded shallow footings on sands and effects on probabilistic settlement estimation. *Georisk: Assessment and Management of Risk for Engineered Systems and GeoHazards*. Vol. 6 (1): Taylor & Francis: 50-69.

Vesić, A. (1975). "Bearing Capacity of Shallow Foundations." *Foundation Engineering Handbook,* H. F. Winterkorn and H. Y. Fang, eds., Van Nostrand Reinhold, New York: 121–147.

Viswanath, M. and Mayne, P.W. (2012). Direct SPT method for footing response in sands using a database approach. *Geotechnical and Geophysical Site Characterization 4,* Vol. 2 (Proc. ISC-4, Pernambuco), CRC Press, London: 1131-1137.

Weary, D.J. (2005). An Appalachian regional karst map and progress towards a new national karst map. *US Geological Survey Report 5160* part A: 93-101: www.usgs.gov

Youd, T.L., et al., (2001) "Liquefaction Resistance of Soils: Summary Report from the 1996 NCEER and 1998 NCEER/NSF Workshops on Evaluation of Liquefaction Resistance of Soils". *Journal of Geotechnical and Geoenvironmental Engrg.* 127 (10): 817-833.

Yu, H.S. and Mitchell, J.K. (1998). "Analysis of cone resistance: review of methods" *Journal of Geotechnical and Geoenvironmental Engineering* 124, (2): 140-149.

# Appendix A: Guidelines on how to use the Excel spreadsheets

**Guidelines on Using the BC-Settlement Design Spreadsheet using SPT input data**

1. Open the input data tab and enter the project relevant information in the data entry cells that include: GDOT project ID, project name, project location, boring number, and the testing date.
2. Under the input tab, fill the footing input parameters: embedment depth (feet), footing thickness (feet), layer thickness (feet), modulus of elasticity of foundation material (ksf), ground water table (feet), and the energy rating (%) of the conducted SPT.
3. Under the input tab, check the foundation shape and geometry, if the footing length (L) is known then fill it in the relevant cell in feet, otherwise determine if your footing is square (using L/B ratio of 1), rectangular (using 1 < L/B ratio < 10) or strip (using L/B ratio of 10 or more). If the footing width (B) is known or a specific value needs to be investigated then fill the relevant cell in feet.
4. Fill in the specific settlement values that need to be evaluated in inches.
5. In the input tab fill in the SPT raw readings: fill in the depth (feet) and the SPT readings, either: (a) individual blows for 6-inch increments #1, #2, and #3; or (b) the summed up $N_{measured}$ value in blows per foot. Corrected depth values will be automatically generated to account for the correct readings depth which is at the bottom of the boring minus one-half foot ($z = d_b$ - 0.5 ft where $d_b$ = depth of borehole). Also fill in each of the soil type cells following the USCS classification system.
6. After providing the soil type cell according to USCS, a number of unfavorable problematic soil types will be highlighted, flagged and colored: silts, clays, organics, and peat.
7. Next to the soil type column check if there are any messages of “CONTACT SENIOR GEOTECH ENGINEER” which will appear in the case of organics with low plasticity (OL), or organics with high plasticity (OH), or peat (PT), indicating the insuitability of the studied location.
8. Also check if there are any messages of “CONTACT GEOTECH ENGINEER – CHECK OCR PROFILE” which will appear in case of soft normally consolidated to lightly over consolidated clays or silts with low overconsolidation ratio values < 3. A guideline on acceptable and unacceptable OCRs is provided in Section 4.8 of this report.
9. Check the percentage of clay readings relative to the total number of readings which should be acceptable if the value is below 10% and provided that OCRs > 3.
10. After filling the data in the input tab, the averaged geoparameters (soil unit weight, angle of internal friction, and soil modulus of elasticity) will be automatically calculated and averaged in the SPT-CALCS tab.

11. Under the Geoparameter Plots tab there will be summary plots of $N_{measured}$, $N_{60}$, unit weight (γ), soil modulus of elasticity (E), angle of internal friction (ϕ), and overconsolidation ratio (OCR) versus depth in both metric and English units.
12. Under the summary tab, there will be plots of all LRFD solutions for shallow foundations bearing capacity and settlement design charts for square, rectangular, and strip footings on granual soils.
13. Based on the type of analyses required, choose the corresponding tab for more details. In the analyses tabs, a default value of 0.2 is assigned for the Poisson's ratio of the soil (drained behavior) and of the foundation material. And since the spreadsheet is evaluating bearing capacity and settlement for granular soils then a default effective cohesion intercept (c') value of zero is assigned. All other values are automatically populated based on previously entered information.
14. For factored bearing resistance versus footing width for different settlement values use the tabs: Constant L, Square, Rectangle, or Strip. If the footing width (B) is known or a specific value is needed for investigation and filled in the input data tab, then this value will be calculated and highlighted in green in all the analyses tables.
15. The constant L tab will be used if the footing length (L) is known and filled in the input data tab. Use the square tab in case of square footings with L/B ratio = 1. For rectangular footings use the rectangle tab with the intermediate value of 1 < L/B ratio < 10. For strip footings use the strip tab that uses L/B ratio of 10 or more.
16. For a different representation of the results, there are plots in terms of factored bearing resistance versus settlement for different footing width values. Using this representation there are two options; either a footing with a constant length L for which you will use the stress-settlement for constant L tab or a square footing with L / B ratio = 1 for which you will use the stress-settlement-square tab.

**Guidelines on Using the BC-Settlement Design Spreadsheet using CPT input data**

1. Open the input tab and enter the project relevant information in the data entry cells that include: GDOT project ID, project name, project location, boring number, and the testing date.
2. Under the input tab, complete the footing input parameters: embedment depth (feet), footing thickness (feet), layer thickness (feet), modulus of elasticity of foundation material (ksf), and the ground water table (feet).
3. Under the input tab, check the foundation shape and geometry, if the footing length is known then fill it in the relevant cell in feet, otherwise determine if your footing is square (using L/B ratio of 1), rectangular (using 1 < L/B ratio < 10) or strip (using L/B ratio of 10 or more). If the footing width (B) is known or a specific value needs to be investigated then fill the relevant cell in feet.
4. Fill in the specific settlement values that need to be evaluated in inches.
5. In the input tab, fill in the CPT readings: put the depth (feet) and the corresponding CPT readings: cone tip resistance ($q_t$ in ksf), sleeve friction ($f_s$ in ksf), and porewater pressure ($u_2$ in ksf). Hint: The input of CPT data is probably best accomplished by preparing the CPT data with depth, $q_t$, $f_s$, and $u_2$ in a matrix of four columns wide by many rows of the full length of the sounding and cutting & pasting the data over the input page at the proper columns.
6. The soil type cell with depth will be automatically evaluated indicating the type of the soil formation encountered. For the unfavorable problematic soil types (i.e., silts, clays, and organics) the cells will be highlighted, flagged and colored.
7. Check if there are any messages of “CONTACT GEOTECH ENGINEER – CHECK OCR PROFILE” which will appear in case of normally consolidated to lightly over consolidated clays or silts or sensitive clays with low overconsolidation ratio values < 3. See Section 4.8 on a discussion of acceptable and unacceptable OCRs in clays.
8. Next to the soil type column check if there are any messages of “CONTACT SENIOR GEOTECHNICAL ENGINEER” which will appear in the case of organic clays indicating the insuitability of the studied location.
9. Check the percentage of clay readings relative to the total number of readings which should be acceptable if the value is below 10% provided that OCRs > 3.
10. After completing the data input, the values of the geoparameters (soil unit weight, effective friction angle, and soil modulus of elasticity) will be automatically calculated and averaged in the CPT-CALCS tab.
11. Under the Geoparameter Plots tab there will be summary plots of cone tip resistance ($q_t$), sleeve friction ($f_s$), and porewater pressure ($u_2$), unit weight, soil modulus of elasticity, angle of internal friction, and overconsolidation ratio versus depth, reported in both metric and English units.

12. Under the summary tab, there will be plots of all LRFD solutions for shallow foundations bearing capacity and settlement design charts for square, rectangular, and strip footings on granual soils.
13. In the analyses tabs, a default value of 0.2 is assigned for the Poisson's ratio of the soil (drained behavior) and of the foundation material. A default effective cohesion intercept (c') value of zero is assigned. All other values are automatically populated based on previously entered information.
14. For factored bearing resistance versus footing width for different settlement values use the tabs: Constant L, Square, Rectangle, or Strip. If the footing width (B) is known or a specific value is needed for investigation and filled in the input data tab, then this value will be calculated and highlighted in green in all the analyses tables.
15. The constant L tab will be used if the footing length (L) is known and filled in the input data tab. Use the square tab in case of square footings with L/B ratio = 1. For rectangular footings use the rectangle tab with the intermediate value of 1<L/B ratio < 10. For strip footings use the strip tab that uses L/B ratio of 10 or more.
16. For a different representation of the results, there are plots in terms of factored bearing resistance versus settlement for different footing width values. Using this representation there are two options; either a footing with a constant length L for which you will use the stress-settlement for constant L tab or a square footing with L / B ratio = 1 for which you will use the stress-settlement-square tab.

**Guidelines on Using the BC-Settlement Design Spreadsheet using DMT input data**

1. Open the input tab and enter the project relevant information in the data entry cells that include: GDOT project ID, project name, project location, boring number, and the testing date.
2. Under the input tab, fill the footing input parameters: embedment depth (feet), footing thickness (feet), layer thickness (feet), modulus of elasticity of foundation material (in ksf), calibration factor ΔA (in bars), calibration factor ΔB (in bars), and the ground water table (feet). Additional details on the calibration factors ($\Delta$A and $\Delta$B) are provided in Sections 6.3 and 6.4 of this report. In usual practice, values of these calibration factors are around 0.1 to 0.3 bars.
3. Under the input tab, check the foundation shape and geometry, if the footing length is known then fill it in the relevant cell in feet, otherwise determine if your footing is square (using L/B ratio of 1), rectangular (using 1 < L/B ratio < 10) or strip (using L/B ratio of 10 or more). If the footing width (B) is known or a specific value needs to be investigated then fill the relevant cell in feet.
4. Fill in the specific settlement values that need to be evaluated in inches.
5. In the input tab fill in the DMT raw readings: input the depth (feet) and the DMT readings: A and B in bars. Hint: it may prove easier to set up a three column data set with the readings: depth, A, B; and then cut & paste these into the Input Cells.
6. The soil type cell with depth will be automatically evaluated indicating the type of the soil formation encountered. For the unfavorable problematic soil types (silts or clays) the cells will be highlighted and colored.
7. Check if there are any messages of "CONTACT GEOTECH ENGINEER – CHECK OCR PROFILE" which will appear in case of normally-consolidated to lightly overconsolidated clays or silts with low overconsolidation ratio values < 3. Guidance as to acceptable and unacceptable OCRs are discussed in Section 4.8 of this report.
8. Check the percentage of clay readings relative to the total number of readings which should be acceptable if the value is below 10%, provided that OCRs > 3.
9. After completing the data in the input tab, the averaged geoparameters (soil unit weight, effective friction angle, and soil modulus of elasticity) will be automatically calculated and averaged in the DMT-CALCS tab.
10. Under the Geoparameter Plots tab there will be summary plots of the DMT $p_0$ and $p_1$, unit weight, soil modulus of elasticity, angle of internal friction, and overconsolidation ratio versus depth in both metric and English units.
11. Under the summary tab, there will be plots of all LRFD solutions for shallow foundations bearing capacity and settlement design charts for square, rectangular, and strip footings on granual soils.

12. In the analyses tabs, a default value of 0.2 is assigned for the Poisson's ratio of the soil and of the foundation material. A default effective cohesion intercept (c') value of zero is assigned. All other values are automatically populated based on previously entered information.
13. For factored bearing resistance versus footing width for different settlement values use the tabs: Constant L, Square, Rectangle, or Strip. If the footing width (B) is known or a specific value is needed for investigation and filled in the input data tab, then this value will be calculated and highlighted in green in all the analyses tables.
14. The constant L tab will be used if the footing length (L) is known and completed in the input data tab. Use the square tab in case of square footings with L/B ratio = 1. For rectangular footings use the rectangle tab with the intermediate value of 1<L/B ratio<10. For strip footings use the strip tab that uses L/B ratio of 10 or more.
15. For a different representation of the results, there are plots in terms of factored bearing resistance versus settlement for different footing width values. Using this representation there are two options; either a footing with a constant length L for which you will use the stress-settlement tab for constant L or a square footing with L / B ratio = 1 for which you will use the stress-settlement-square tab.

# Appendix B: Illustrated Example using SPT data

| Standard Penetration Test Data | | |
|---|---|---|
| GDOT Project ID: | Test Data Number 2 | ← data entry |
| Project Name: | Georgia LRFD Site | ← data entry |
| Location: | Newnan | ← data entry |
| Boring Number: | SPT-X552 | ← data entry |
| Date: | 18 March 2016 | ← data entry |

SPT procedures per ASTM D 1586

**Figure B.1** *Raw SPT Input Data*

**Footing Input Parameters:**

| | | |
|---|---|---|
| Embedment Depth, $D_f$ (ft) = | 3 | ← data entry |
| Footing Thickness, t (ft) = | 3 | ← data entry |
| Layer Thickness, h (ft) = | 66 | ← data entry |
| Modulus of Foundation, $E_{FDTN}$ (ksf) = | 600000 | ← data entry |

| | | | |
|---|---|---|---|
| Ground Water Table | 28 | feet | ← data entry |
| Energy Rating | 61 | % | ← data entry |

**Figure B.2** *Footing Input Parameters and Energy Rating*

**FOUNDATION SHAPES and GEOMETRY**

| | | |
|---|---|---|
| Footing Length L (ft) = | 100 | ← data entry if known |
| Square - L/B = | 1 | |
| Rectangular - L/B = | 5 | |
| Strip - L/B = | 10 | |
| Footing Width B (ft) = | 10 | ← data entry if known |

**Figure B.3** *Foundation Shape and Geometry*

| | |
|---|---|
| Total Number of Readings | 25 |
| Number of Clay Readings | 3 |
| % Clay Readings | 12.00 |

**Figure B.4** *Percentage of Clay Readings*

| SPECIFIC SETTLEMENT VALUE (in) | |
|---|---|
| 0.5 | ← data entry |
| 1 | ← data entry |
| 1.5 | ← data entry |
| 2 | ← data entry |
| 2.5 | ← data entry |
| 3 | ← data entry |
| 4 | ← data entry |

**Figure B.5** *Specific Settlement Values Input*

| | SPT Readings | | | | | | |
|---|---|---|---|---|---|---|---|
| | Depth (ft) | #1 | #2 | #3 | Corrected Depth (ft) | N_measured | Soil Type | |
| | 0.00 | | | | | | | |
| data entry → | 2.50 | 6 | 9 | 11 | 3.50 | 20.00 | OL | CONTACT CHIEF ENGINEER |
| data entry → | 5.00 | 5 | 8 | 10 | 6.00 | 18.00 | SP | |
| data entry → | 7.50 | 6 | 9 | 11 | 8.50 | 20.00 | SP | |
| data entry → | 10.00 | 5 | 7 | 13 | 11.00 | 20.00 | SP | |
| data entry → | 12.50 | 5 | 8 | 22 | 13.50 | 30.00 | PT | CONTACT CHIEF ENGINEER |
| data entry → | 15.00 | 6 | 8 | 10 | 16.00 | 18.00 | SP | |
| data entry → | 20.50 | 8 | 9 | 9 | 21.50 | 18.00 | SP | |

**Figure B.6** *Raw SPT Input Data*

| | GEOPARAMETER | SI Units | | English Units | |
|---|---|---|---|---|---|
| Average | Unit Weight | 18.68 | $kN/m^3$ | 0.1189 | kcf |
| | Friction Angle ϕ | 38.496 | degrees | 38.496 | degrees |
| | Modulus of Elasticity | 347.20 | bar | 725.15 | ksf |

**Figure B.7** *Average Unit Weight, Friction Angle, and Soil Modulus of Elasticity using SPT Input Data*

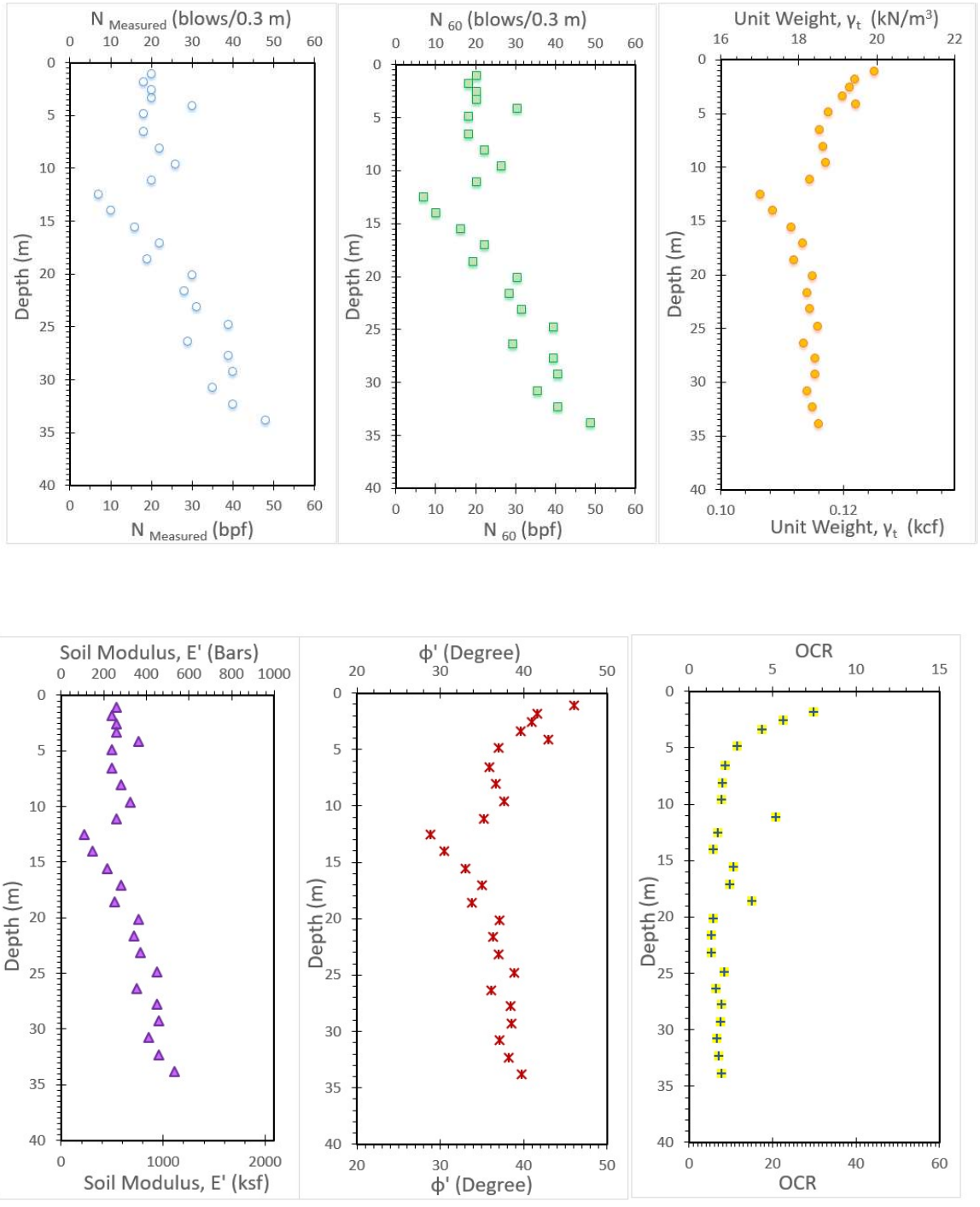


**Figure B.8** *Profiles of SPT Input and Output Data*

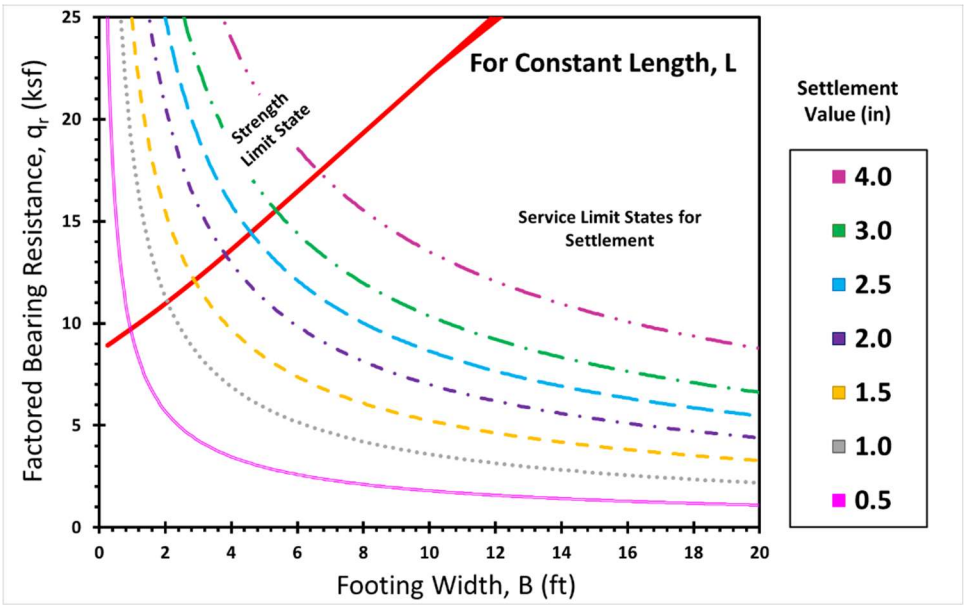


**Figure B.9** *Factored BC-Footing Width Design Chart with different settlement contours for Constant L value*

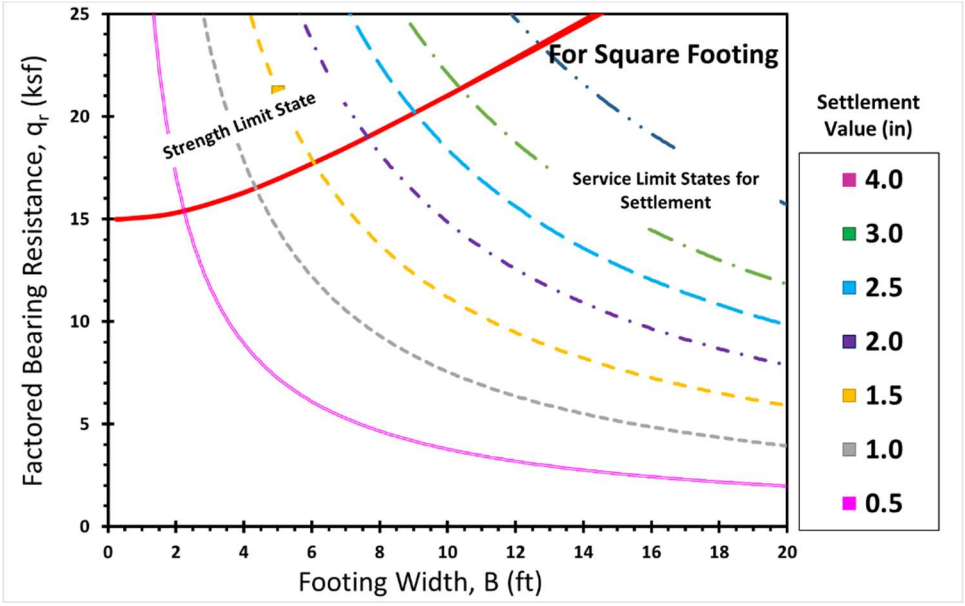


**Figure B.10** *Factored BC-Footing Width Design Chart with different settlement contours for Square Footing (Constant L/B ratio = 1)*

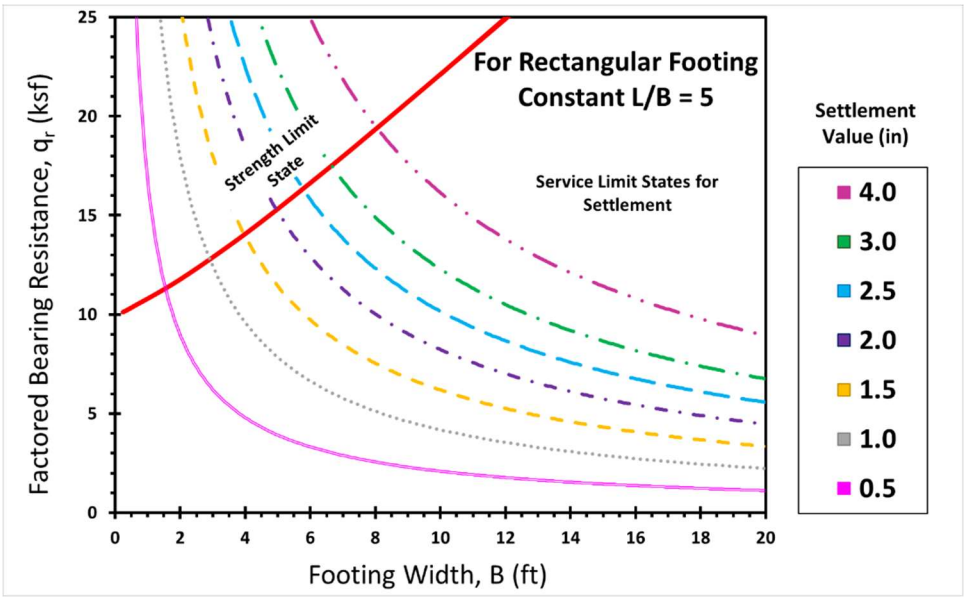


**Figure B.11** *Factored BC-Footing Width Design Chart with different settlement contours for Rectangular Footing (L/B = 5)*

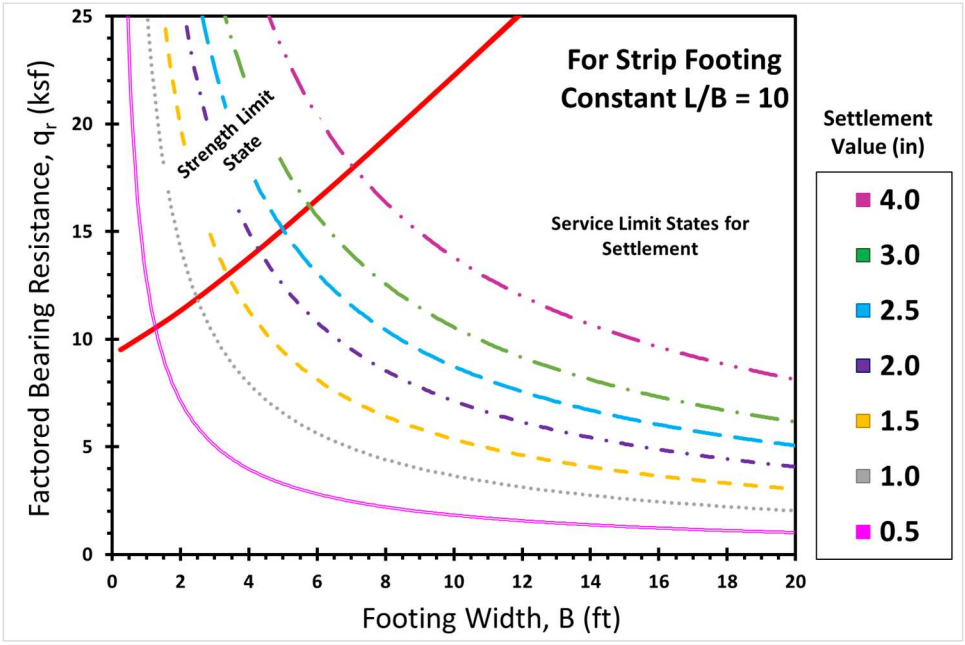


**Figure B.12** *Factored BC-Footing Width Design Chart with different settlement contours for Strip Footing (L/B = 10)*

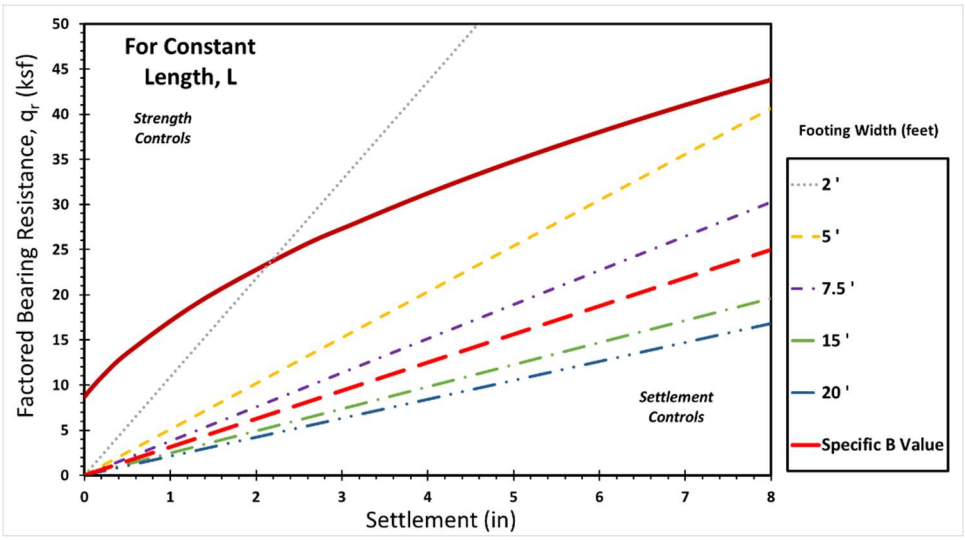


**Figure B.13** *Factored BC-Settlement Design Chart with different footing width contours for footings with Constant Length*

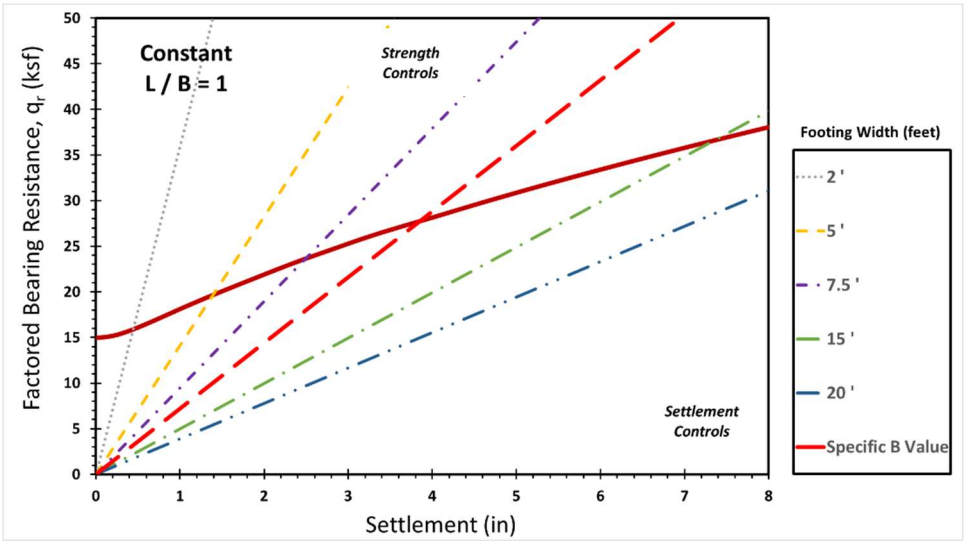


**Figure B.14** *Factored BC-Settlement Design Chart with different footing width contours for Square Footing (L/B = 1)*

# Appendix C: Illustrated Example using CPT data

| Cone Penetration Test Data | | |
|---|---|---|
| GDOT Project ID: | Test Data Number 1 | ← data entry |
| Project Name: | xxxxx | ← data entry |
| Location: | xxxxx | ← data entry |
| Boring Number: | CPT-01 | ← data entry |
| Date: | 18 March 2016 | ← data entry |

CPT procedures per ASTM D 5778

**Figure C.1** *Raw CPT Input Data*

**Footing Input Parameters:**

| | | |
|---|---|---|
| Embedment Depth, $D_f$ (ft) = | 3 | ← data entry |
| Footing Thickness, t (ft) = | 3 | ← data entry |
| Layer Thickness, h (ft) = | 66 | ← data entry |
| Modulus of Foundation, $E_{FDTN}$ (ksf) = | 600000 | ← data entry |

Ground Water Table | 3.28 | feet ← data entry

**Figure C.2** *Footing Input Parameters*

FOUNDATION SHAPES and GEOMETRY

| | | |
|---|---|---|
| Footing Length L (ft) = | 100 | ← data entry if known |
| Square – L/B = | 1 | |
| Rectangular – L/B = | 5 | |
| Strip – L/B = | 10 | |
| Footing Width B (ft) = | 10 | ← data entry if known |

**Figure C.3** *Foundation Shape and Geometry*

| | |
|---|---|
| Total Number of Readings | 755 |
| Number of Clay Readings | 5 |
| % Clay Readings | 0.662 |

**Figure C.4** *Percentage of Clay Readings*

| | | CPT Readings | | |
|---|---|---|---|---|
| | Depth (ft) | $q_t$ (ksf) | $f_s$ (ksf) | $u_2$ (ksf) |
| | 0.00 | | | |
| data entry → | 0.46 | 12.90 | 0.01 | 0.00 |
| data entry → | 0.52 | 19.66 | 0.04 | 0.00 |
| data entry → | 0.59 | 27.24 | 0.05 | 0.00 |
| data entry → | 0.66 | 36.87 | 0.08 | 0.00 |
| data entry → | 0.72 | 45.88 | 0.14 | 0.00 |
| data entry → | 0.79 | 52.64 | 0.16 | 0.00 |
| data entry → | 0.85 | 55.71 | 0.20 | 0.00 |
| data entry → | 0.92 | 57.96 | 0.22 | 0.00 |
| data entry → | 0.98 | 60.83 | 0.28 | 0.00 |
| data entry → | 1.05 | 64.51 | 0.32 | 0.00 |
| data entry → | 1.12 | 67.38 | 0.38 | 0.00 |
| data entry → | 1.18 | 70.87 | 0.39 | 0.00 |
| data entry → | 1.25 | 74.35 | 0.42 | 0.00 |
| data entry → | 1.31 | 77.22 | 0.46 | 0.00 |
| data entry → | 1.38 | 77.21 | 0.49 | 0.00 |
| data entry → | 1.44 | 76.80 | 0.50 | 0.00 |

**Figure C.5** *Raw CPT Input Data*

| Depth (ft) | Soil Type |
|---|---|
| 0.00 | |
| 0.46 | gravelly SAND |
| 0.52 | gravelly SAND |
| 0.59 | gravelly SAND |
| 0.66 | gravelly SAND |
| 0.72 | gravelly SAND |
| 0.79 | gravelly SAND |
| 0.85 | gravelly SAND |
| 0.92 | gravelly SAND |
| 0.98 | gravelly SAND |
| 1.05 | gravelly SAND |
| 1.12 | gravelly SAND |
| 1.18 | gravelly SAND |
| 1.25 | gravelly SAND |
| 1.31 | gravelly SAND |
| 1.38 | SAND |

**Figure C.6** *Soil Type based on CPTu Input Data*

| | GEOPARAMETER | SI Units | | English Units | |
|---|---|---|---|---|---|
| Average | Unit Weight | 19.09 | $kN/m^3$ | 0.1215 | kcf |
| | Friction Angle ϕ | 39.498 | degrees | 39.498 | degrees |
| | Modulus of Elasticity | 39925.55 | kPa | 833.86 | ksf |

**Figure C.7** *Average Unit Weight, Friction Angle, and Soil Modulus of Elasticity from CPT Input Data*

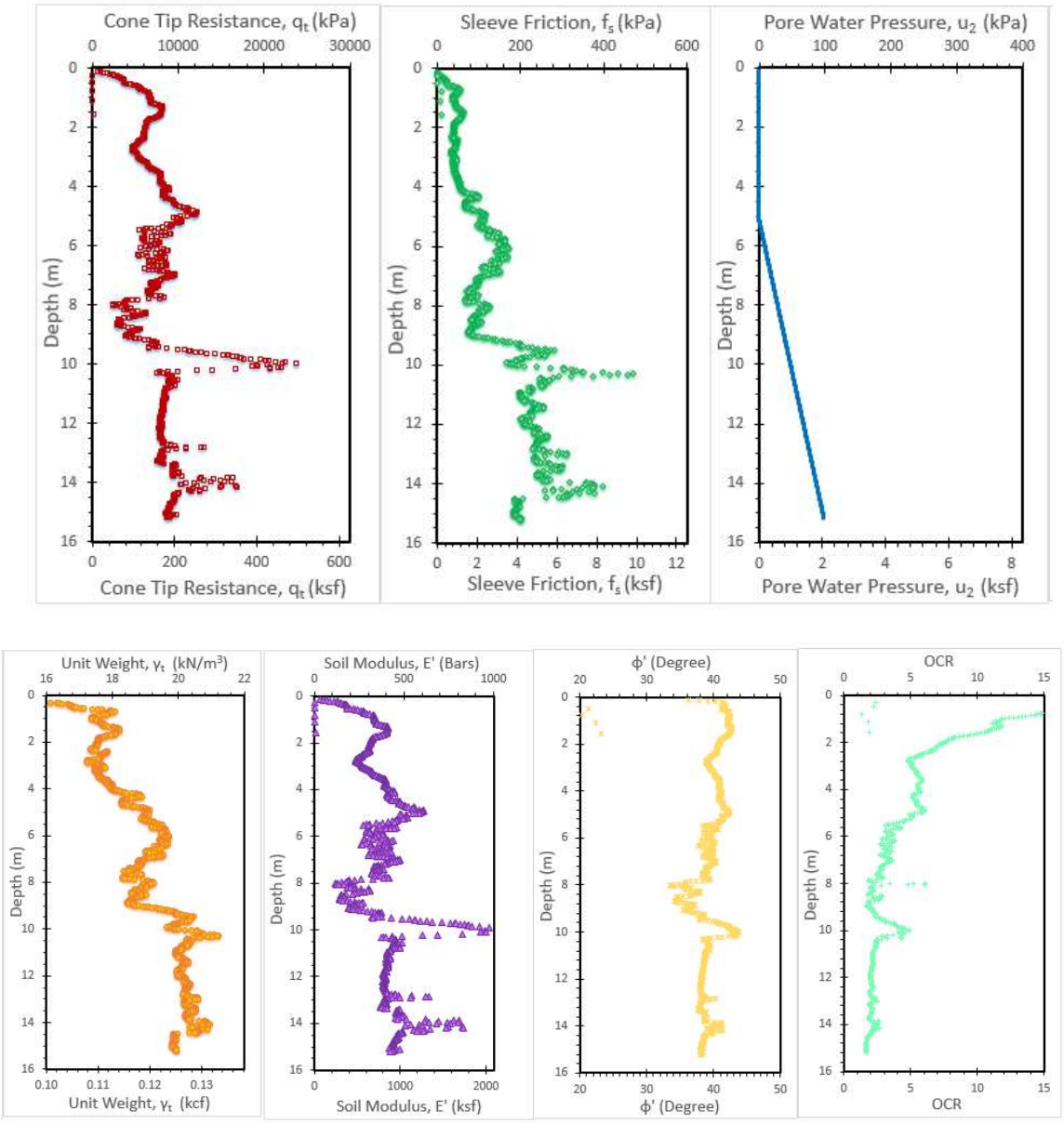


**Figure C.8** *CPT Profiles of Input and Output Data*

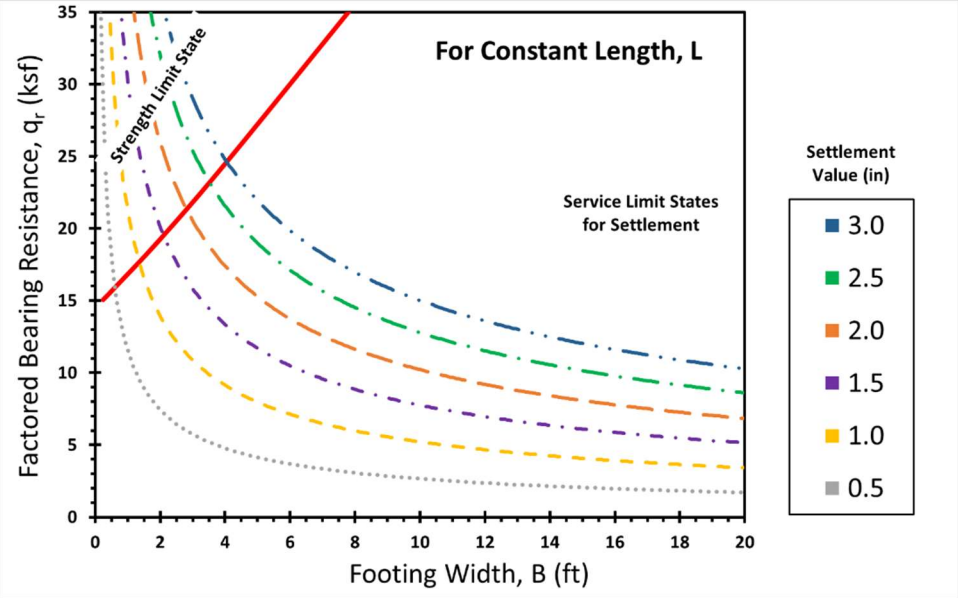


**Figure C.9** *Factored BC-Footing Width Design Chart with different settlement contours for Constant L value*

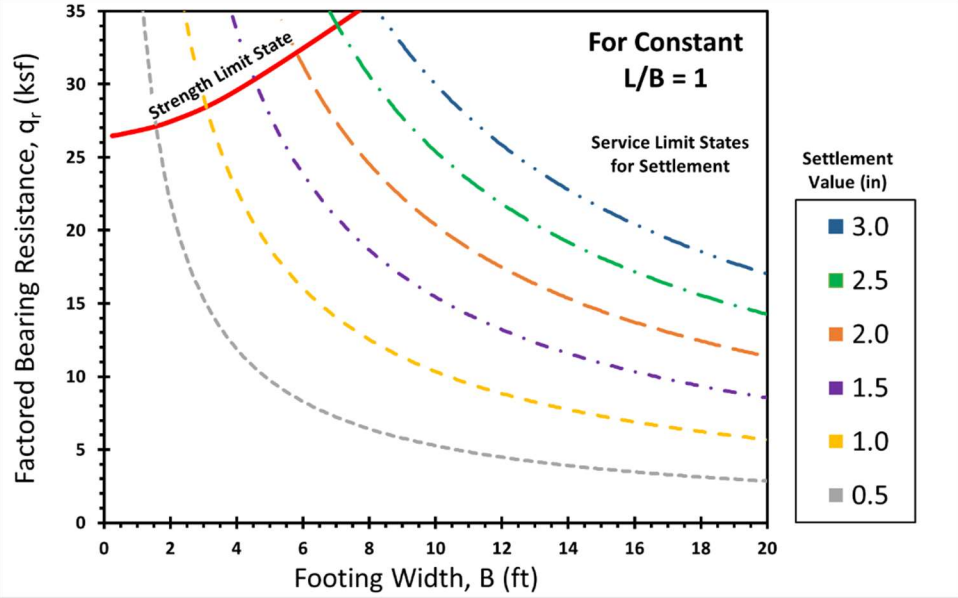


**Figure C.10** *Factored BC-Footing Width Design Chart with different settlement contours for Square Footing (Constant L/B ratio = 1)*

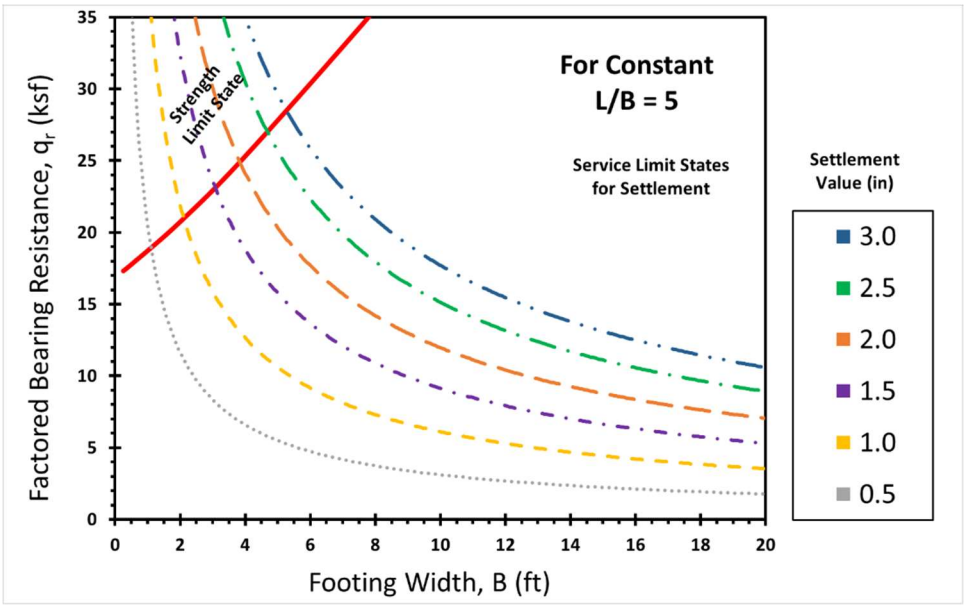


**Figure C.11** *Factored BC-Footing Width Design Chart with different settlement contours for Rectangular Footing (L/B = 5)*

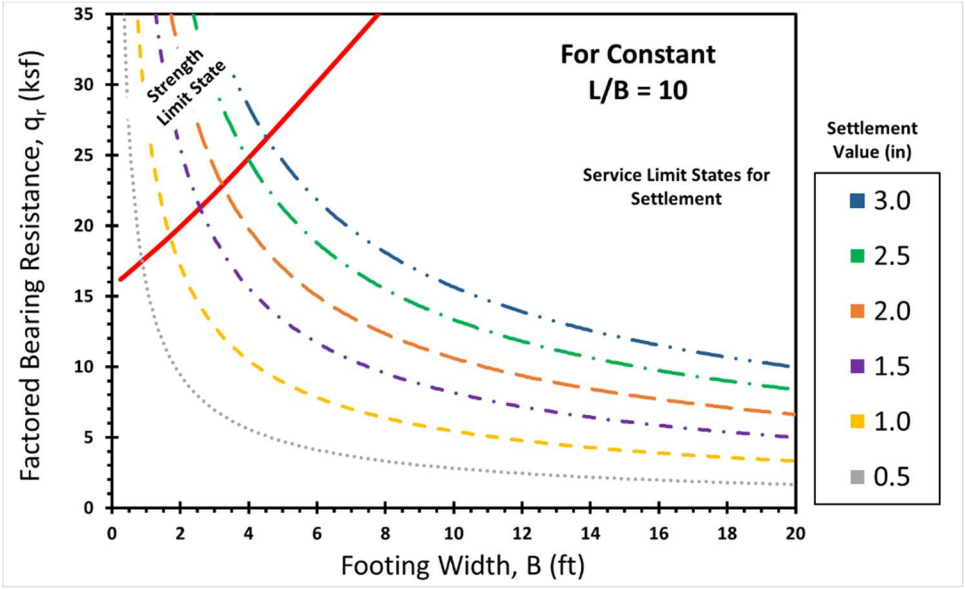


**Figure C.12** *Factored BC-Footing Width Design Chart with different settlement contours for Strip Footing (L/B = 10)*

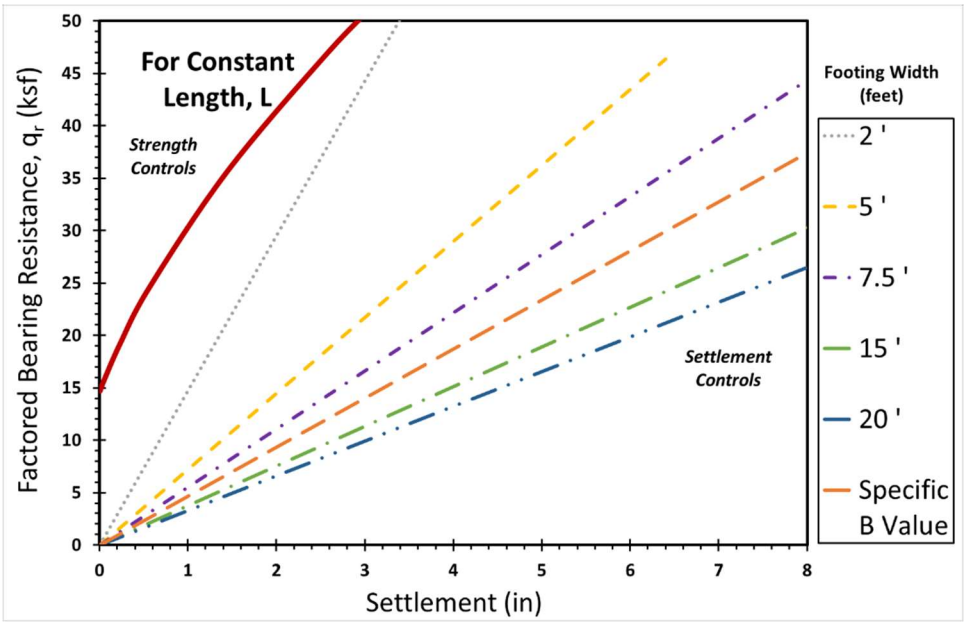


**Figure C.13** *Factored BC-Settlement Design Chart with different footing width contours for footings with Constant Length*

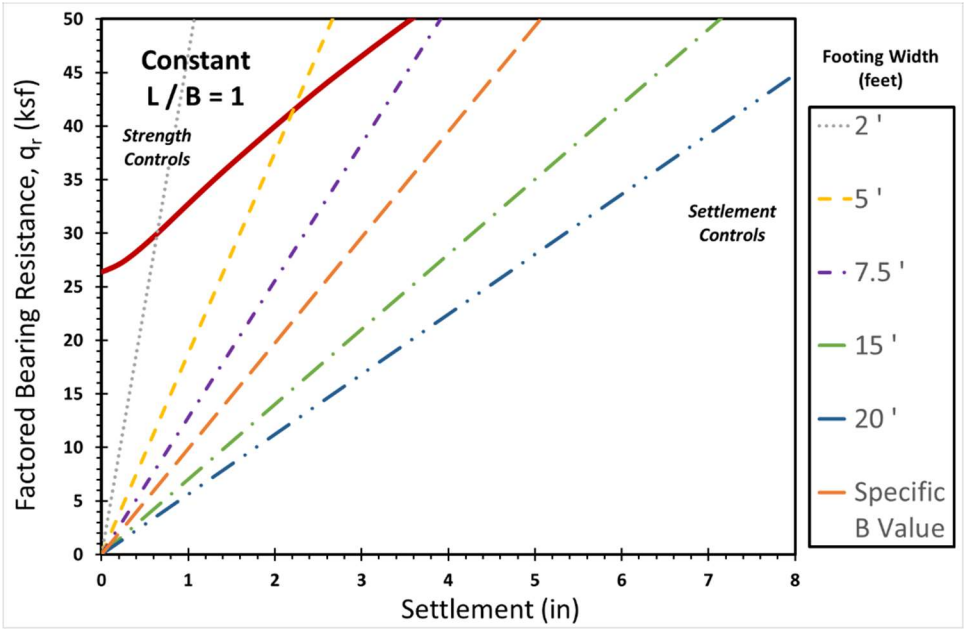


**Figure C.14** *Factored BC-Settlement Design Chart with different footing width contours for Square Footing (L/B = 1)*

# Appendix D: Illustrated Example using DMT data

| Flat Plate Dilatometer Test Data | | |
|---|---|---|
| GDOT Project ID: | Test Data Number 1 | ← data entry |
| Project Name: | xxxxx | ← data entry |
| Location: | xxxxx | ← data entry |
| Boring Number: | DMT-01 | ← data entry |
| Date: | 18 March 2016 | ← data entry |

DMT procedures per ASTM D 6635

**Figure D.1** *Raw Input DMT Data*

**Footing Input Parameters:**

| | | |
|---|---|---|
| Embedment Depth, $D_f$ (ft) = | 3 | ← data entry |
| Footing Thickness, t (ft) = | 3 | ← data entry |
| Layer Thickness, h (ft) = | 66 | ← data entry |
| Modulus of Foundation, $E_{FDTN}$ (ksf) = | 600000 | ← data entry |

| | | | |
|---|---|---|---|
| Calibration Factor ΔA | 0 | bar | ← data entry |
| Calibration Factor ΔB | 0 | bar | ← data entry |
| Ground Water Table | 3.28 | feet | ← data entry |

**Figure D.2** *Footing Input Parameters and DMT Calibration Factors*

FOUNDATION SHAPES and GEOMETRY

| | | |
|---|---|---|
| Footing Length L (ft) = | 100 | ← data entry if known |
| Square - L/B = | 1 | |
| Rectangular - L/B = | 5 | |
| Strip - L/B = | 10 | |
| Footing Width B (ft) = | 10 | ← data entry if known |

**Figure D.3** *Foundation Shape and Geometry*

| | |
|---|---|
| Total Number of Readings | 51 |
| Number of Clay Readings | 1 |
| % Clay Readings | 1.96 |

**Figure D.4** *Percentage of Clay Readings*

| | | DMT Readings | |
|---|---|---|---|
| | Depth (ft) | A (bar) | B (bar) |
| | 0.00 | | |
| data entry → | 0.66 | 2.40 | 8.30 |
| data entry → | 1.31 | 2.10 | 6.90 |
| data entry → | 1.97 | 1.80 | 9.20 |
| data entry → | 2.62 | 1.30 | 7.80 |
| data entry → | 3.28 | 1.70 | 8.70 |
| data entry → | 3.94 | 3.00 | 12.20 |
| data entry → | 4.59 | 1.90 | 12.00 |
| data entry → | 5.25 | 2.60 | 12.70 |
| data entry → | 5.91 | 3.80 | 13.60 |
| data entry → | 6.56 | 1.50 | 9.00 |
| data entry → | 7.22 | 1.90 | 8.40 |
| data entry → | 7.87 | 1.40 | 7.70 |
| data entry → | 8.53 | 1.90 | 8.30 |
| data entry → | 9.19 | 2.00 | 10.00 |
| data entry → | 9.84 | 2.10 | 10.40 |
| data entry → | 10.50 | 2.00 | 10.50 |

**Figure D.5** *Raw DMT Input Data*

| Depth (ft) | Soil Type |
|---|---|
| 0.00 | |
| 0.66 | Silty Sand |
| 1.31 | Silty Sand |
| 1.97 | Sand |
| 2.62 | Sand |
| 3.28 | Sand |
| 3.94 | Sand |
| 4.59 | Sand |
| 5.25 | Sand |
| 5.91 | Silty Sand |
| 6.56 | Sand |
| 7.22 | Sand |
| 7.87 | Sand |
| 8.53 | Sand |
| 9.19 | Sand |
| 9.84 | Sand |
| 10.50 | Sand |

**Figure D.6** *Soil Type based on DMT Input Data*

| | GEOPARAMETER | SI Units | | English Units | |
|---|---|---|---|---|---|
| Average | Unit Weight | 18.53 | $kN/m^3$ | 0.1179 | kcf |
| | Friction Angle ϕ | 39.412 | degrees | 39.412 | degrees |
| | Modulus of Elasticity | 43148.34 | kPa | 901.17 | ksf |

**Figure D.7** *Average Unit Weight, Friction Angle, and Soil Modulus of Elasticity using DMT Input Data*

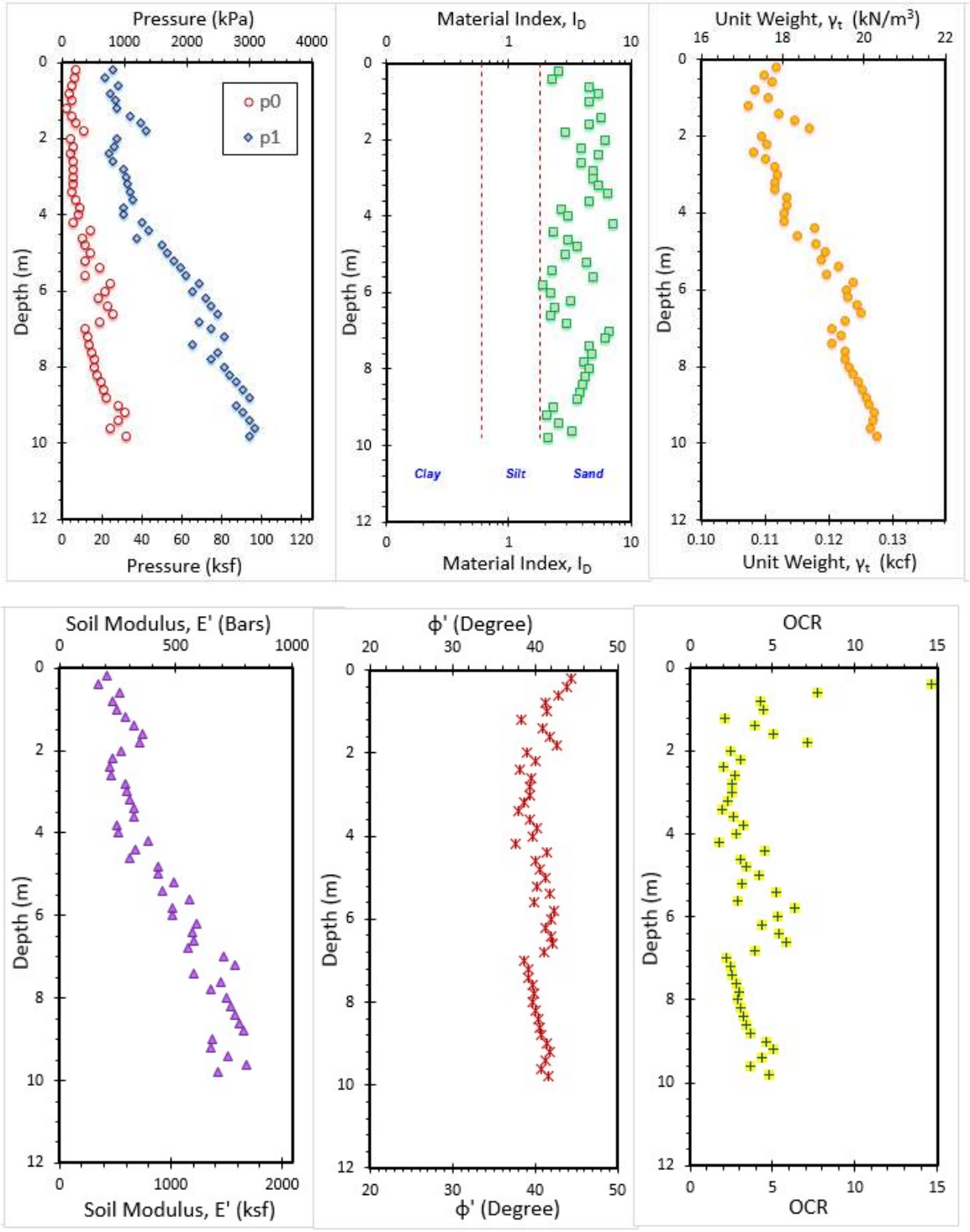


**Figure D.8** *Profiles of DMT Input and Output Data*

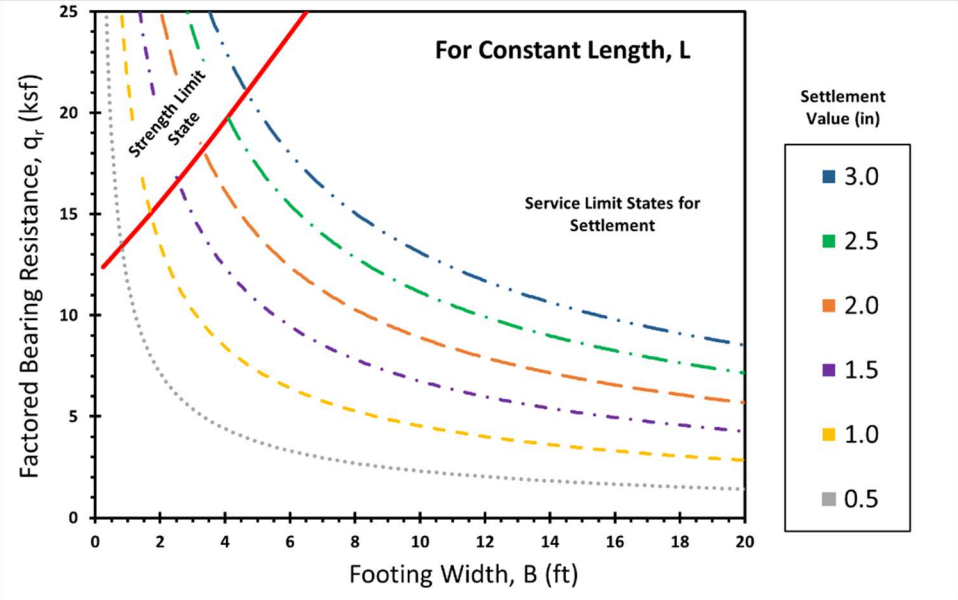


**Figure D.9** *Factored BC-Footing Width Design Chart with different settlement contours for Constant L value*

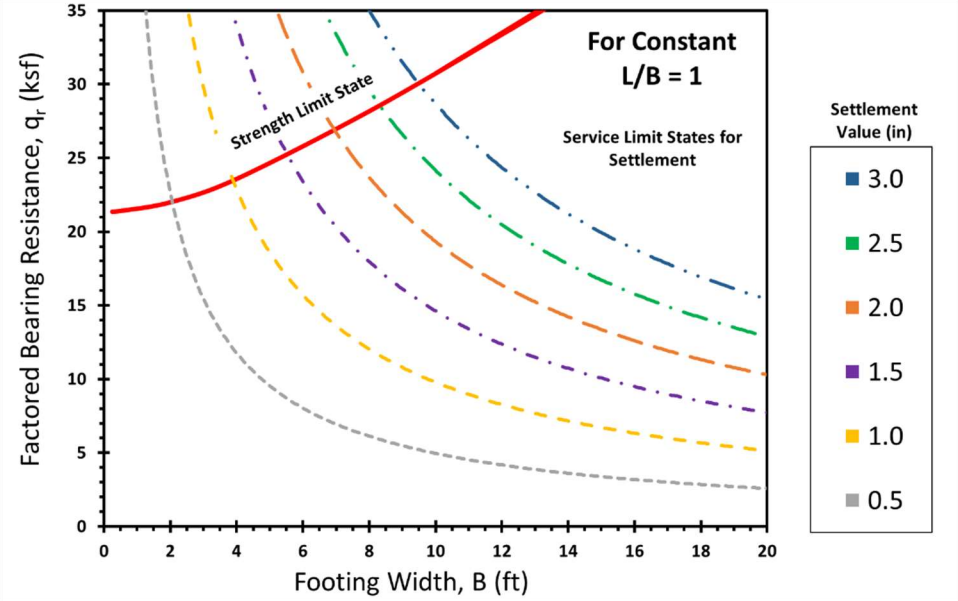


**Figure D.10** *Factored BC-Footing Width Design Chart with different settlement contours for Square Footing (Constant L/B ratio = 1)*

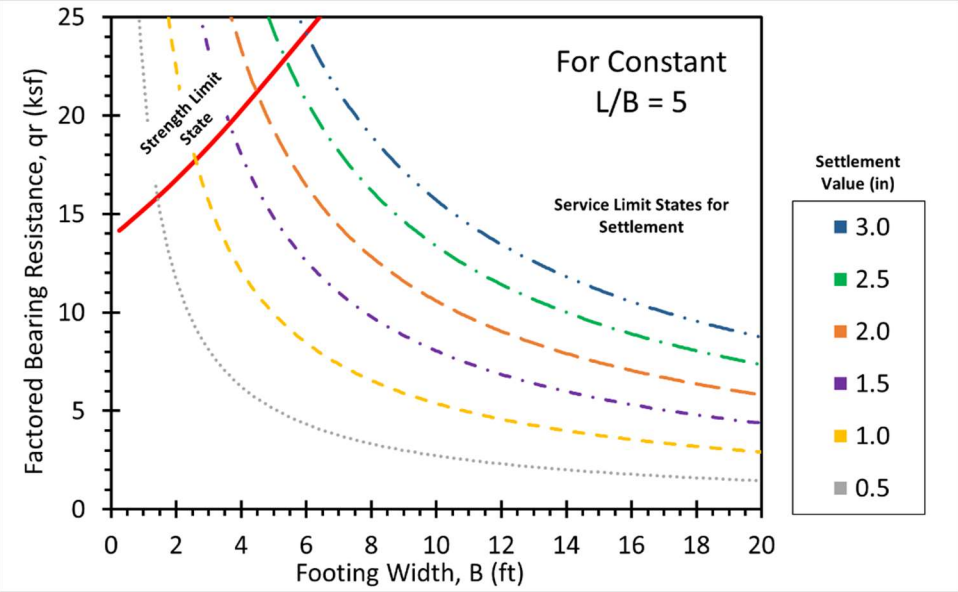


**Figure D.11** *Factored BC-Footing Width Design Chart with different settlement contours for Rectangular Footing (L/B = 5)*

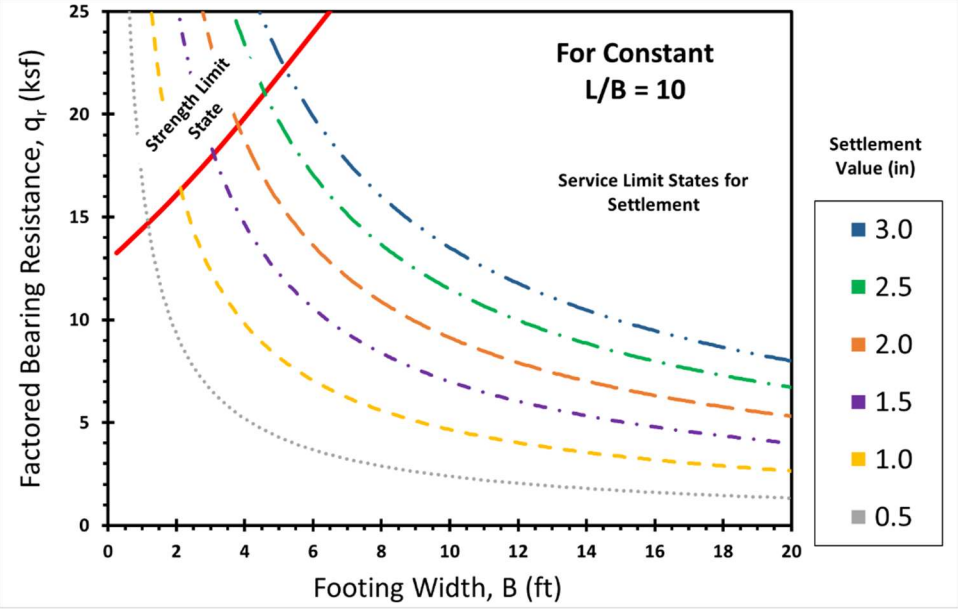


**Figure D.12** *Factored BC-Footing Width Design Chart with different settlement contours for Strip Footing (L/B = 10)*

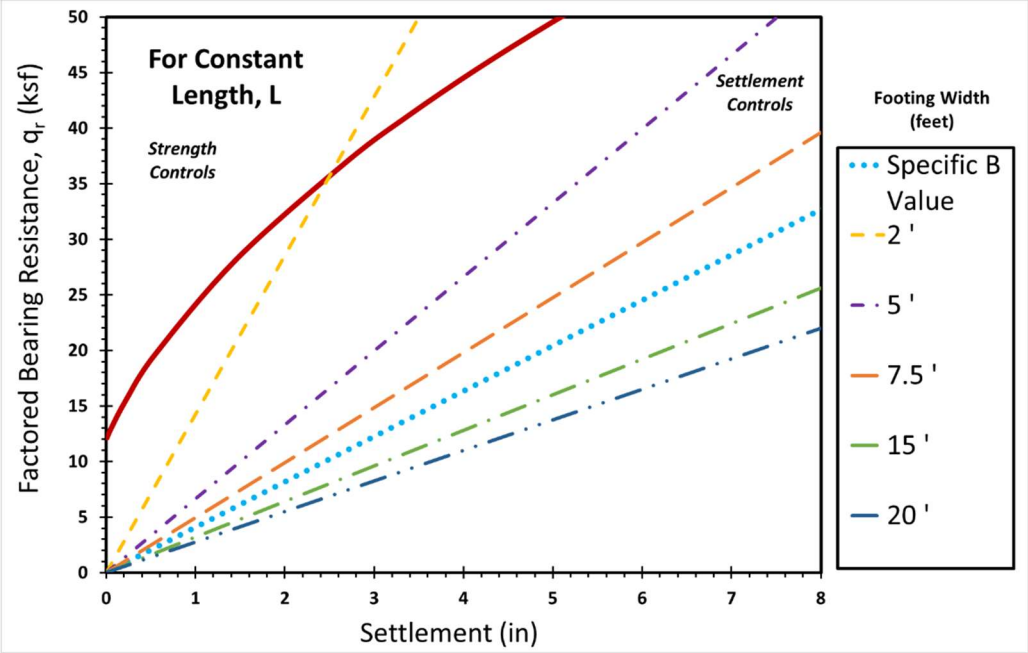


**Figure D.13** *Factored BC-Settlement Design Chart with different footing width contours for footings with Constant Length*

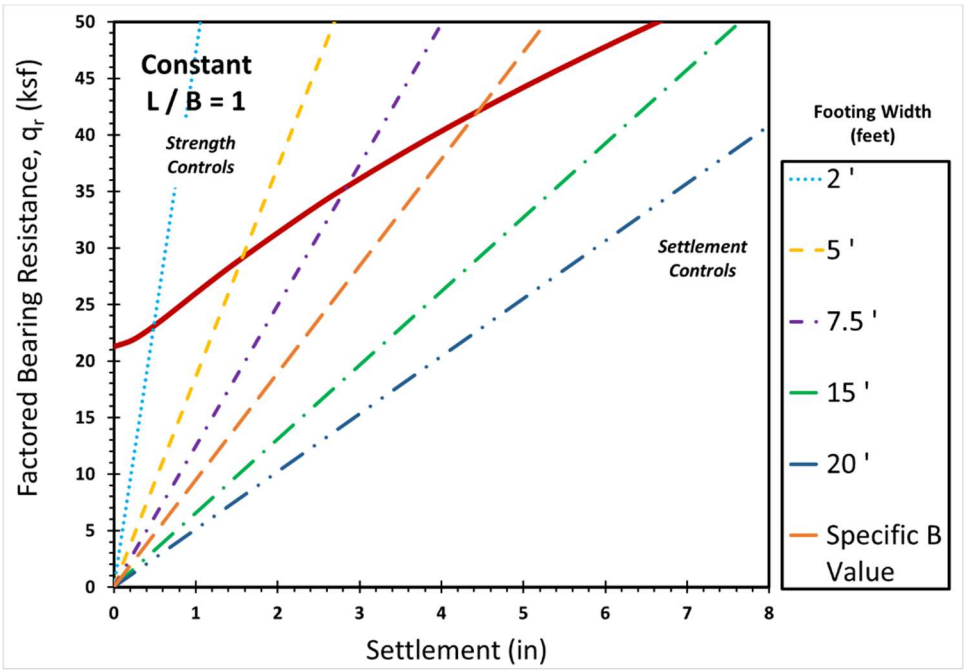


**Figure D.14** *Factored BC-Settlement Design Chart with different footing width contours for Square Footing (L/B = 1)*

## REFERENCES


Aas G, Lacasse S, Lunne T, Hoeg K. (1986). Use of in situ tests for foundation design on clay, *Use of In-Situ Tests in Geotechnical Engineering* (GSP 6, Virginia Tech, Blacksburg), ASCE, Reston, VA: 1–30.

Abu-Farsakh M, Tumay M, Voyiadjis G. (2003). Numerical parametric study of piezocone penetration test in clays. *International Journal Geomechanics*, ASCE; 3(2):170–81.

Abuhajar, O., El Naggar, M.H., and Newson, T. (2010) Review of Available Methods for Evaluation of Soil Sensitivity for Seismic Design. *International Conference on Recent Advances in Geotechnical Earthquake Engineering and Soil Dynamics*. San Diego, California, paper No. 1.32b: 1- 8.

Agaiby, S. and Mayne, P.W. (2016). *Geotechnical LRFD Calculations of Settlement and Bearing Capacity of GDOT Shallow Bridge Foundations and Retaining Walls.* Report No. FHWA-GA-16-1426 prepared by Georgia Tech Research Corp. for Georgia Dept. of Transportation, Forest Park, GA: 160 p.

Agaiby, S. and Mayne, P.W. (2017). Interpretation of geotechnical parameters using in-situ data for Bolivian Experimental Site for Testing (B.E.S.T.), *Proceedings, 3rd Bolivian Conference on Deep Foundations*, Vol. 2, Univ. Privada de Santa Cruz de la Sierra, Omnipress.

Agaiby, S., Mayne, P.W. and Woeller, D.J. (2016). Evaluation of undrained shear strength and stress history in intact clays using seismic piezocone tests. *Proceedings of 69th Canadian Geotechnical Conference: GeoVancouver 2016,* Vancouver Canada*:* www.cgs.ca

Agaiby, S., Ouyang, Z., and Mayne, P.W. (2017). Helical Probe Tests in Residual Soils of the Appalachian Piedmont. *Geomechanics and Geoengineering: An international Journal*. Submitted and approved for publication.

Agaiby, S.S., and Mayne, P.W. (2018). Modified cavity expansion - critical state solution for evaluating stress history and piezodissipation from CPTU in sensitive or structured clays (Tentatively accepted, *Canadian Geotechnical Journal*, pending changes)

Agaiby, S.S., and Mayne, P.W. (2015). Relationship between undrained shear strength and shear wave velocity for clays.*, Proceedings of the 6th International Symposium*

*on Deformation Characteristics of Geomaterials*, Vol. 6 (Buenos Aires, Argentina), IOS Press, Rotterdam: 358-364.

Agaiby, S.S., and Mayne, P.W. (2016). Use of shear wave velocity to estimate stress history and undrained shear strength of clays. *Proc. 5th Intl. Conf. on Geotechnical & Geophysical Site Characterization* (ISC-5, Jupiters Gold Coast Australia), Vol. 1: Australian Geomechanics Society: 461 – 467.

Agaiby, S.S., Cargill, E.P., Ku, T., and Mayne, P.W. (2016). Continuous-interval seismic piezocone testing in Piedmont residuum. *In Pursuit of Best Practices - Proceedings 5th Intl. Conf. on Geotechnical & Geophysical Site Characterization* (ISC-5), Jupiters Gold Coast Australia. Vol. 2: Australian Geomechanics Society: 1065 – 1070.

Almeida, M. and Parry, R.H.G. (1985). Small cone penetrometer/and piezocone tests in laboratory consolidated clay. *Geotechnical Testing Journal*, 8(1): 14-24.

Almeida, M.S.S, and Marques, M.E.S. (2003). The behaviour of Sarapuí soft clay. *Characterization and Engineering Properties of Natural Soils*. Vol. 2, Swets & Zeitlinger, Lisse, The Netherlands: 477-504.

Almeida, M.S.S., Marques, M.E.S., & Baroni, M. (2010) Geotechnical parameters of very soft clays from CPTu. *Proc.2nd Intl. Symposium on Cone Penetration Testing*, Vol. 2 (CPT10, Huntington Beach, California), Omnipress, 8p.

Al-Raziqi, A.A., Huat, B.B. and Munzir, H.A. (2003) Potential usage of hyperbolic method for prediction of organic soil settlement. *Proc. 2nd International Conference on Advances in Soft Soil Engineering and Technology*, Putrajaya, Malaysia, pp. 439–45.

Altaee, A., and Fellenius, B.H. (2002). *Evaluation and Analysis of Results of Static Loading Test US95 Sandpoint North and South, Sandpoint, Idaho*. Report No. 0005CS193, prepared for CH2M Hill, Boise, ID by Urkkada, Ottawa, ON: 69p.

Amini, A., Fellenius, B.H., Sabbagh, M., Naesgaard, E. and Buehler, M. (2008). Pile loading tests at Golden Ears Bridge. *Proc. GeoEdmonton: 61st Canadian Geotechnical Conference*, Edmonton, AB, September 21-24, 2008, 8p.

Amundsen, T., Lunne, T., Christophersen, H. P., Bayne, J. M., & Barnwell, C. L. (1985). Advanced deep-water soil investigation at the Troll East Field. *Advances in*

*Underwater Technology and Offshore Engineering,* Springer Netherlands, Vol. 3: 165-186.

Andersen, K.H., and Stenhamar, P. (1982). Static plate loading tests on overconsolidated clay. *Journal of the Geotechnical Engineering Division*, *108*(7), 918-934.

Andrejko, M.J., Fiene, F., and Cohen, A.D. (1983) Comparison of ashing techniques for determination of the inorganic content of peats. *Testing of Peats and Organic Soils*, ASTM STP 820, pp. 5–20.

Andrus, R.D., Mohanan, N.P., Piratheepan, P., Ellis, B.S. and Holzer, T.L. (2007). Predicting shear-wave velocity from cone penetration resistance. *Proceedings, 4th International Conference on Earthquake Engineering*, Thessaloniki, Greece, Paper No. 1454.

Arman A. (1969). A definition of organic soils (an engineering identification). *Engineering Research Bulletin No. 101*, Louisiana State University, Division of Engineering Research, submitted to Louisiana Department of Highways.

Athir, N., Hache, R. and Fall, M. (2013). Cone and ball penetration tests in Ottawa's sensitive marine clays. *Proc. GeoMontreal 2013*, 66th Canadian Geotechnical Conference, Paper 519, Canadian Geotechnical Society: www.cgs.ca

Azzouz, A. and Lutz, D. (1986). Shaft behavior of pile in plastic Empire Clay. *Journal of Geotechnical Engineering*, ASCE, 112(4): 389-406.

Azzouz, A.S., Baligh, M.M., & Ladd, C.C. (1983). Cone penetration and engineering properties of the soft Orinoco Clay. *Behavior of Offshore Structures.* (BOSS) Vol. 1: 161-180.

Baaijens, A. and Kolk, H.J. (2004). Axial pile capacity design method for offshore driven piles in sand. *Report No. P1003*, Issue 3, American Petroleum Institute, Contract No. 2003-100825, Fugro, Leidschendam, The Netherlands: 122 p.

Baldi, G, Bellotti, R, Ghionna, V, Jamiolkowski, M and Lo Presti, DCF. (1989). Modulus of sands from CPTs and DMTs. *Proc. 12th International Conference on Soil Mechanics and Foundation Engineering,* Vol. 1, Rio de Janeiro, Balkema, Rotterdam, 165-170.

Baligh, M.M. (1975). Theory of deep site static cone penetration resistance. Massachusetts Institute of Technology, Department of Civil Engineering, Cambridge, Mass. Publication No. R75-56.

Baligh, M.M. (1984). The simple-pile approach to pile installation in clay. *Proceedings*, *Analysis and Design of Pile Foundations*, San Francisco, ASCE, Reston: 310-330.

Baligh, M.M. (1985). Strain path method, *J. Geotech. Eng., ASCE*, **111**, (9), 1108–1136.

Baligh, M.M. (1986). Undrained deep penetration, II: pore pressures. *Geotechnique*, Vol. 36, No. 4, 486-501.

Baligh, M.M., Vivatrat, V., and Ladd, C.C. (1980). Cone penetration in soil profiling. *Journal of the Geotechnical Engineering*, ASCE, 106(4): 447-461.

Battaglio, M., Bruzzi, D., Jamiolkowski, M., and Lancellotta, R. (1987). Interpretation of CPT's and CPTU's. *Proceedings, 4th International Geotechnical Seminar: Field Instrumentation and In-Situ Measurements,* Singapore, 129-143.

Bechai, M., Law, K.T., Craig, C.B.H., and Konrad, J.M. (1986). In-situ testing of marine clay for towerline foundations. *Proc. 39th Canadian Geotechnical Conference*, Ottawa: 115-122.

Becker D.E., Crooks J.H., Been K., Jefferies M.G. (1987). Work as a criterion for determining in situ and yield stresses in clays. *Canadian Geotechnical Journal*, Vol. 24: 549-564.

Begemann, H.K.S., (1965). The friction jacket cone as an aid in determining the soil profile. *Proceedings of the 6th International Conference on Soil Mechanics and Foundation Engineering*, ICSMFE, Montreal, Vol. 2: 17 - 20.

Bensaid, M.A. (1985). *Mesures In-Situ Des Pressions Interstitielles - Application a la Reconnaissance Des Sols*. Ph.D. Thesis, Ecole Nationale Des Ponts et Chaussees, Paris, 371 p. (in French)

Bergenstahl, L. (1991). Preloading of an embankment on deep soft clay. *Proceedings, l0th European Conf. on Soil Mechanics and Foundation Engrg*., Firenze, Vol. 2, 307-310.

Berre, T. (2014). Test fill on soft plastic marine clay at Onsøy, Norway. *Canadian Geotechnical Journal* 51 (1): 30-50.

Bihs, A., Long, M., Marchetti, D., & Ward, D. (2010). Interpretation of CPTU and SDMT in organic Irish soils. *Proceedings 2nd Intl. Symposium on Cone Penetration Testing*, Vol. 2 (CPT10, Huntington Beach, California), Omnipress: 257-264.

Bjerrum, L. (1954). Geotechnical properties of Norwegian marine clay. *Geotechnique*, *4* (2), 49-69.

Bouchard, R. and Tavenas, F., (1981). *Étude du tassement de remblais par Conmul. Remblai autoroute 40, Batiscan.* Rapport GCS-81-05, Département de génie civil. Université Laval, Québec. 104 p.

Bouclin, G. (1990). *Perméabilité de l ´argile de Saint-Esprit et anisotropie de perméabilité.* Mémoire de maîtrise, département de génie civil. Université Laval, Québec, 197 p.

Bozozuk, M. (1972). The Gloucester test fill. *Ph.D. Dissertation*, Purdue University, Dept. of Civil Engineering, West Lafayette, IN: 208 p.

Bozozuk, M. and Leonards, G.A. (1972). The Gloucester test fill. *Performance of Earth and Earth-Supported Structures,* Vol. 1, Part 1 (Proc. Spec. Conf. Purdue Univ.), ASCE, Reston, VA: 299-317.

Broussard, N.S. (2012). *Estimating rigidity index based on cone penetrometer measurements.* M.Sc. Thesis, University of California, Davis, 86p.

Brown, D. (2002). Effect of construction on axial capacity of drilled foundations in piedmont soils. *Journal of Geotechnical and Geoenvironmental Engineering*, (128) 12: 967 – 973

Bruzzi, D., and Battaglio, M. (1987). Pore pressure measurements during cone penetration tests. I quadermi dell'ISMES (Experimental Institute for Models and Structures), Milan, Italy.

Burghignoli A., Cavalera L., Chieppa V., Jamiolkowski M., Mancuso C., Marchetti S., Pane V., Paoliani P., Silvestri F., Vinale F., Vittori E. & A.G. (1991). Geotechnical characterization of Fucino clay. *Proceedings of the X European Conference on Soil Mechanics and Foundation Engineering*, Florence, Vol. 1: 27-40.

Burns, S.E. and Mayne, P.W. (1998a). Monotonic and dilatory porewater pressures during piezocone dissipation tests in clay, *Canadian Geotechnical Journal*, Vol. 35 (6): 1063-1073.

Burns, S.E. and Mayne, P.W. (1998b). *Penetrometers for Soil Permeability and Chemical Detection.* Report GIT-CEEGEO-98-1 to National Science Foundation (NSF), Washington, D.C. and Army Research Office (ARO), Raleigh, NC, submitted by Georgia Tech Research Corp, Atlanta, GA: 198 p.

Burns, S.E. and Mayne, P.W. (2002). Analytical cavity expansion-critical state model for piezo-cone dissipation in fine-grained soils. *Soils & Foundations*, Vol. 42 (2): 131-137.

Butterfield (1979). A natural compression law for soils, *Geotechnique*, Vol. 29, No. 4, pp. 468-480.

Cai, G., Liu, S., & Puppala, A.J. (2016). Evaluation of geotechnical parameters of a lagoonal clay deposit in Jiangsu Lixia River area of China by seismic piezocone tests. *KSCE Journal of Civil Engineering*, *20*(5), 1769-1782.

Cai, G., Puppala, A.J. and Liu, S. (2014). Characterization on the correlation between shear wave velocity and piezocone tip resistance of Jiangsu clays. *Engineering Geology*, *171*, 96-103.

Camp, W.M. (2004). Drilled and driven foundation behavior in a calcareous clay. *GeoSupport 2004: Drilled Shafts, Micropiling, Deep Mixing, Remedial Methods, and Specialty Foundation Systems* (pp. 1-18). GSP 124, ASCE, Reston/VA

Camp, W.M., (2004). Site characterization and subsurface conditions for the Cooper River Bridge. *Geo-Trans Conference*, Los Angeles Vol. 1, ASCE, Reston/VA: 347-360.

Campanella, R.G., and Robertson, P.K. (1991). Use and interpretation of a research dilatometer. *Canadian Geotechnical Journal* 28 (1): 113-126.

Campanella, R.G., and Robertson, P.K., (1988). Current status of the piezocone test. Proceedings of First International Symposium on Penetration Testing, ISOPT-1, Orlando, March 22 - 24, Vol. 1, pp. 93 - 116.

Campanella, R.G., Baziw, E.J., and Sully, J.P., (1989). Interpretation of seismic cone data using digital filtering techniques. *Proceedings, 12th International Conference on Soil Mechanics and Foundation Engineering*, Vol. 1 Rio de Janeiro, Balkema, Rotterdam, 195-198.

Campanella, R.G., Robertson, P.K. and Gillespie, D. (1986). Seismic cone penetration test. *Use of In-Situ Tests in Geotechnical Engineering* (GSP 6), ASCE, Reston, VA: 116-130.

Campanella, R.G., Sully, J.P., and Robertson, P.K. (1988). Interpretation of piezocone soundings in clay. *Penetration Testing in the UK*, Thomas Telford, London, 203-208.

Campanella, RG., Gillespie, D., and Robertson, P.K., (1982). Pore pressures during cone penetration testing, *Proceedings of the 2nd European Symposium on Penetration Testing*, ESOPT-2, Amsterdam, Vol. 2: 507 - 512.

Caquot, A. and Kerisel, J. (1956). *Traite de mecanique des sols.* Paris: Gauthier-Vaillars.

Casagrande, A. (1936). The determination of the preconsolidation load and its practical significance. *Proceedings 1st Intl. Conf. on Soil Mechanics & Foundation Engineering*, Vol. 3, Harvard Univ., Cambridge, MA: 60-64.

Ceccato, F., & Simonini, P. (2017). Numerical study of partially drained penetration and pore pressure dissipation in piezocone test. *Acta Geotechnica*, *12*(1), 195-209.

Ceccato, F., Beuth, L., & Simonini, P. (2017). Adhesive contact algorithm for MPM and its application to the simulation of cone penetration in clay. *Procedia Engineering*, *175*, 182-188.

Chai, J.C., Sheng, D., Carter, J.P., and Zhu, H. (2012). Coefficient of consolidation from non-standard piezocone dissipation curves. *Computers and Geotechnics* 41 (1): 13-22.

Chameau, J.L., Reyna, F., and Frost, J.D. (1991). Ground motion analyses at several sites in San Francisco after the Loma Prieta Earthquake. *Geotechnical Report* 9119, Purdue University, West Lafayette, 285 p.

Chandler, R.J. (1988). The in-situ measurement of the undrained shear strength of clays using the field vane. *Int. Symp. on Vane Shear Strength Testing of Soils: Field and Laboratory Studies*. ASTM STP 1014, 13-44.

Chen, B.Y. and Mayne, P.W. (1994). *Profiling the Overconsolidation Ratio of Clays by Piezocone Tests*, Report No. GIT-CEE/GEO-94-1 submitted to National Science Foundation by Georgia Institute of Technology, Atlanta, 280 p.

Chen, B.Y. and Mayne, P.W. (1996). Statistical relationships between piezocone measurements and stress history of clays. *Canadian Geotechnical Journal* 33 (3): 488-498.

Chern, J.C. (1992). Geotechnical Investigation of the Keelung River Site. *Draft Internal Report*, Sinotech Engineering Consultants, Inc., Taiwan.

Chew, V.C. (1993). Underfoot: a geologic guide to the Appalachian Trail. second edition, *Proc. Appalachian Trail Conference*, Harpers Ferry, West Virginia, 237 p.

Chiasson, P., Lafleur, J., Soulié, M., & Law, K. T. (1995). Characterizing spatial variability of a clay by geostatistics. *Canadian Geotechnical Journal*, *32*(1), 1-10.

Chin, C.T., Chen, J.R., Hu, I.C., Yao, D., and Chao, H.C. (2007). Engineering characteristics of Taipei clay. *Characterization and Engineering Properties of Natural Soils,* Vol. 4 (Singapore). Taylor & Francis, London: 1755-1805.

Cho, G.C. & Santamarina, J.C. (2001). Unsaturated particulate materials-particle-level studies. *Journal of Geotechnical and GeoEnvironmental Engineering*, 127(1): 84-96.

Christian, H.A., Howie, J.A., Hunter, J.A., and Weemees, I. (1998). Sensitivity of leached marine silts and clays at the base of the Fraser River delta. *Proceedings of the 12th Annual One-Day Symposium: Site Characterization, Vancouver Geotechnical Society, Vancouver: 1-18.*

Chung, C.K., and Finno, R.J. (1992). Influence of depositional processes on the geotechnical parameters of Chicago glacial clays. *Engineering Geology*, *32*(4), 225-242.

Chung, S G., Hong, Y.P., Lee, J.M., and Min, S.C. (2011). Evaluation of the undrained shear strength of Busan clay. *KSCE Journal of Civil Engineering*, *16*(5), 733-741.

Chung, S.F. (2005). Characterization of soft soils for deepwater developments. *Ph.D. Dissertation*, School of Civil & Resource Engineering, University of Western Australia.

Chung, S.G., & Kweon, H.J., (2013). Oil-operated fixed-piston sampler and its applicability. *Journal of Geotechnical and Geoenvironmental Engineering*, 139(1), 134-142.

Chung, S.G., Ryu, C.K., Min, S.C., Lee, J.M., Hong, Y.P., and Odgerel, E. (2012). Geotechnical characterization of Busan clay. *KSCE Journal of Civil Engineering*, *16*(3), 341-350.

Cole, R. (2003), *Full-scale effects of passive earth pressure on the lateral resistance of pile caps*, Doctoral Dissertation, Dept. Civil and Environmental Engineering, Brigham Young University, Provo, Utah, 345p.

Colreavy, C., O'loughlin, C.D., & Randolph, M.F. (2015). Estimating consolidation parameters from field piezoball tests. *Géotechnique*, *66*(4), 333-343.

Coutinho, R.Q. (2007). Characterization and engineering properties of Recife soft clays-Brazil. *Characterization and Engineering Properties of Natural Soils.* Vol. 4 (Singapore). Taylor & Francis, London: 2049-2099.

Coutinho, R.Q., and Bello, M.I. (2014). Geotechnical characterization of Suape soft clays, Brazil. *Soils and Rocks*, 37(3), Sao Paulo: 257-276.

Crawford, C.B., and Campanella, R.G. (1991). Comparison of field consolidation with laboratory and in situ tests. *Canadian Geotechnical Journal*, 28(1): 103-112.

Crooks, J.H.A. (1981). A qualitative stress-strain (time) model for soft clays. *Proc. ASTM Symp. Laboratory Shear Strength of Soil*, STP 740, 685- 699.

Crooks, J.H.A., Been, K., Becker, D.E., and Jefferies, M.G. (1988). CPT interpretation in clays. *Penetration Testing 1988* (Proc. ISOPT-1, Orlando), Balkema, Rotterdam, Vol. 2, 715-722.

Cruz, I.R. (2009). *An evaluation of seismic flat dilatometer and lateral stress seismic piezocone*, M.Sc. thesis, Dept. of Civil Engineering, Univ. of British Columbia, Vancouver, BC, Canada, 200p.

Cruz, I.R., and Mayne, P.W. (2006). Interpretation of CPTU Tests carried out in lacustrine Mexico City Clay, *Site & Geomaterial Characterization* (GSP 149), Proc. GeoShanghai, ASCE, Reston, VA: 24-31.

D'Ignazio, M., Länsivaara, T. T., & Jostad, H. P. (2017). Failure in anisotropic sensitive clays: finite element study of Perniö failure test. *Canadian Geotechnical Journal*, (999), 1-21.

Dafalias, Y. F., Manzari, M. T., & Akaishi, M. (2002). A simple anisotropic clay plasticity model. *Mechanics Research Communications*, *29*(4), 241-245.

Dafalias, Y. F., Manzari, M. T., & Papadimitriou, A. G. (2006). SANICLAY: simple anisotropic clay plasticity model. *International Journal for Numerical and Analytical Methods in Geomechanics*, *30*(12), 1231-1257.

de Beer, E.E., (1977). Static cone penetration testing in clay and loam. *Sondeer Symposium,* Utrecht.

DeGroot, D.J., and Lutenegger, A.J. (2003). Geology and engineering properties of Connecticut Valley varved clay. *Characterization and Engineering Properties of Natural Soils*, Vol. 1, Swets & Zeitlinger, Lisse: 695-724.

DeGroot, D.J., Lunne, T., Sheahan, T.C., and Ryan, R.M. (2003). Experience with downhole block sampling in clays using conventional drilling equipment. *Proc. 12th Pan American Conf. Soil Mechanics & Geotechnical Engineering*, Vol. 1 (SARA = Soil and Rock America, MIT, Cambridge, MA), Verlag Glückauf, Essen: 521-526.

Dehler, W., & Labuz, J. (2007). Cone Penetration Testing in Pavement Design. *Report No. MN/RC 2007-36*, Department of Civil Engineering, University of Minnesota, Published by Minnesota Department of Transportation, St. Paul: 116p.

DeJong, J. T., & Randolph, M. (2012). Influence of partial consolidation during cone penetration on estimated soil behavior type and pore pressure dissipation measurements. *Journal of Geotechnical and Geoenvironmental Engineering*, 138(7), 777-788.

DeJong, J.T., Yafrate, N.J., and DeGroot, D.J. (2011). Evaluation of undrained shear strength using full-flow penetrometers. *Journal of Geotechnical & Geoenvironmental Engineering* 2011(1): 1-14.

Delisle, M.C. and Leroueil, S., (2000). *Détection, à l'aide du piézocône, de zones ramollies dans les pentes argileuses et évaluation de leur comportement mécanique.* Rapport GCT-2000-07 présenté au Ministère des Transports du Québec, département de génie civil. Université Laval. Québec, 205 p.

Demers, D. (2001). *Contribution au developpement de l'usage du piezocone dans les sols argileux*. Philosophiae Doctor (Ph.D.) Thèse, Université Laval, Québec, Département de génie civil, faculté des sciences et de génie, 485p. (French text)

Demers, D., and Leroueil, S. (2002). Evaluation of preconsolidation pressure and the overconsolidation ratio from piezocone tests of clay deposits in Quebec. *Canadian Geotechnical Journal* 39 (1): 174-192.

Di Buò, B., D'Ignazio, M., Selänpää, J., and Länsivaara, T. (2016). Preliminary results from a study aiming to improve ground investigation data. *Proceedings of the 17th Nordic Geotechnical Meeting (NGM 2016)*, Challenges in Nordic Geotechnic Reykjavik, Vol. 1: 25-28.

Diaz-Rodriguez, J. A., Leroueil, S., & Aleman, J. D. (1992). Yielding of Mexico City clay and other natural clays. *Journal of geotechnical engineering*, *118*(7), 981-995.

Doherty, P., Kirwan, L., Gavin, K. and Igoe, D. (2012). Soil properties at the UCD geotechnical research site at Blessington. *Proc. Bridge and Concrete Research in Ireland*, Dublin Institute of Technology and Trinity College Dublin: 499-504.

Douglas, B.J., and Olsen, R.S., (1981). Soil classification using electric cone penetrometer. American Society of Civil Engineers, ASCE, Proceedings of Conference on Cone Penetration Testing and Experience, St. Louis, October 26 - 30, pp. 209 - 227.

Duncan, M.J., and Buchignani, A.L., (1976). *An engineering manual for settlement studies*. Department of Civil Engineering, University of California, Berkeley, June 1976, 94 p.

Duraisamy, Y., Huat, B. B. K. and Muniandy, R. (2009) Compressibility behavior of fibrous peat reinforced with cement columns. *Geotechnology and Geological Engineering*, 27(5), 619–29.

East, D.R. and Ulrich, B.F. (1989). The electric piezocone for profiling of mine tailings deposits. *Engineering Geology and Geotechnical Engineering*, Balkema, Rotterdam, 35-38.

Eden, W.J. and Law, K.T. (1980). Undrained shear strength results obtained by different test methods in soft clays. *Canadian Geotechnical J.* 17 (2): 369-381.

Edil, T. B., and Wang, X. (2000) Shear strength and $K_0$ of peats and organic soils. *Geotechnics of High Water Content Materials,* ASTM STP 1374, American Society for Testing and Materials, West Conshohocken, PA, pp. 209–25.

Edil, T.B. (2001). Site characterization in peat and organic soils. *Proc. Intl. Conf. on In-Situ Measurement of Soil Properties and Case Histories*, Bali, Indonesia: 49-59.

Edil, T.B. (2003). Recent advances in geotechnical characterization and construction over peats and organic soils. *Proceedings of the 2nd International Conferences in Soft Soil Engineering and Technology*, Putrajaya (Malaysia), pp. 3-26.

Eslami, A., (1996). Bearing capacity of piles from cone penetrometer test data. Ph.D. Thesis, University of Ottawa, Department of Civil Engineering, 516 p.

Eslami, A., Alimirzaei, M., Aflaki, E., and Molaabasi, H. (2017). Deltaic soil behavior classification using CPTu records—Proposed approach and applied to fifty-four case histories. *Marine Georesources & Geotechnology*, *35*(1), 62-79.

Eslami, A., and Fellenius, B.H., (1997). Pile capacity by direct CPT and CPTu methods applied to 102 case histories. Canadian Geotechnical Journal, Vol. 34, No. 6, pp. 880 - 898.

Farrag, K., Vetter, D., Hill, B. and Esposito, R., (2005). *Soil compaction measuring device study.* Report GRI-04/0067, Gas Research Institute, Des Plaines, IL: 132 pages.

Farrell, E. R. (1997). Some experience in the design and performances of roads and road embankment on organic soils and peats. *Proc. Conference on Recent Advances in Soft Soil Engineering*, Kuching, Sarawak, pp 66–84.

Fellenius, B.H., and Eslami, A., (2000). *Soil profile interpreted from CPTu data*. "Year 2000 Geotechnics" Geotechnical Engineering Conference, Asian Institute of Technology, Bangkok, Thailand, November 27 - 30, 2000,18 p.

Finno, R.J. and Chung, C.K. (1992). Stress-strain strength responses of compressible Chicago glacial clays, *Journal of Geotechnical Engineering*, ASCE, Vol. 119, No. 10, 1607-1625.

Finno, R.J., Gassman, S.L., and Calvello, M. (2000). The NGES at Northwestern University. *National Geotechnical Experimentation Sites* (GSP 93), ASCE, Reston, VA: 130 - 159.

Garner, M.P. (2007). *Loading rate effects on axial pile capacity in clays*. M.Sc. Thesis, Department of Civil and Environmental Engineering, Brigham Young University, Utah: 142p

Germaine, J.T. & Germaine, A.V. (2009). *Geotechnical Laboratory Measurements for Engineers*. Wiley & Sons: 359p

Gerscovich, D. M., (1983). Properties of the desiccated crust of the Sarapuí soft clay deposit (in Portuguese). M. Sc. Thesis. PUC-RIO, Rio de Janeiro, Brazil.

Gibson, R.E. (1950). Discussion of "The bearing capacity of screw piles and concrete cylinder" by G. Wilson. *J. of the Institution of Civil Engineers,* 34: 382p.

Gnanendran, C.T., and Selvadurai, A.P.S. (2001). Strain measurement and interpretation of stabilizing force in geogrid reinforcement, *Geotextiles and Geomembranes,* 19: 177-194

Gravesen, S. (1960). Elastic Semi-Infinite Medium Bounded by a Rigid Wall with a Circular Hole. Laboratoriet for Bygninsteknik, Danmarks Tekniske Højskole, *Meddelelse No. 10*, Copenhagen.

Grondin, G, Tanguay, L., Leroueil, S. and Bouclin, G, (1991). *Efficiency of vertical drains in a sensitive clay deposit.* Compte-rendus de la 44erac conference canadienne de géotechnique. Calgary, vol. l, Paper no 2. p. 21-28.

Gylland, A. S., Jostad, H. P., and Nordal, S. (2014). Experimental study of strain localization in sensitive clays. *Acta Geotechnica*, 9(2): 227-240.

Gylland, A., Long, M., Emdal, A., and Sandven, R. (2013). Characterization and engineering properties of Tiller clay. *Engineering Geology*, *164*, 86-100.

Habtegiorghis, B.L. (2012). *Interpretation of CPTu results in silty clay and assessment of strength parameters: geotechnical investigation of silty clay at Gunnestad, Sande municipality, Norway.* Master's thesis, 119p.

Hamza, M.M, Shahien, M.M, and Ibrahim, M.H. (2005). Characterization and undrained shear strength of Nile delta soft deposits using piezocone. *Proceedings 16th International Conference on Soil Mechanics and Geotechnical Engineering*, Osaka, Vol. 16(2) Rotterdam: Millpress: 687-692.

Hansbo S. (1957). A new approach to the determination of the strength of clay by the Fall Cone test. *Proceedings, No. 14, Royal Swedish Geotechnical Institute,* Stockholm.

Hanzawa H, Kishida T, Fukusawa, T, Asada H (1994). A case study of the application of direct shear and cone penetration tests to soil investigation, design and quality control for peaty soils. *Soils and Foundations*, 4 (1): 13-22.

Hardison, M. (2015). *Correlation of engineering parameters of the Presumpscot Formation to the seismic cone penetration test (SCPTu)*. M.Sc., University of Maine, Orono: 394p.

Harris, D.E. and Mayne, P.W., (1994). Axial Load Behavior of Drilled Shaft Foundations in Piedmont Residuum, *Proceedings*, *International Conference on Design and Construction of Deep Foundations*, Vol. II (Orlando), Federal Highway Administration, Washington, DC: 352-368.

Hatanaka, M. and Uchida, A. (1996). Empirical correlation between penetration resistance and effective friction of sandy soil, *Soils & Foundations*, Vol. 36 (4): 1-9.

Hebib S., and Farrell, E.R. (2003). Some experiences on the stabilizations of Irish peats. *Canadian Geotechnical Journal* 40 (1): 107-120.

Hegazy, Y.A. (1998). *Delineating geostratigraphy by cluster analysis of piezocone data.* Doctoral dissertation, School of Civil & Environmental Engineering, Georgia Institute of Technology, 494p.

Hegazy, Y.A., and Mayne, P.W. (1995), Statistical Correlations Between $V_s$ and CPT Data for Different Soil Types, *Proceedings, Cone Penetration Testing (CPT'95),* Vol. 2, Linköping, Swedish Geotechnical Society, pp. 173-178.

Hegazy, Y.A., and Mayne, P.W. (2006). A global statistical correlation between shear wave velocity and cone penetration data, *Site & Geomaterial Characterization* (GSP 149), [Proc. GeoShanghai], ASCE, Reston/VA: 243-248.

Hepton, P. (1988). *Shear wave velocity measurements during penetration testing. Penetration Testing in the UK*. London: Thomas Telford: 275–278.

Hight, D.W., F. McMillan, J.J.M. Powell, R.J. Jardine, and C.P. Allenou. (2003). Some Characteristics of London Clay. *Characterization and Engineering Properties of Natural Soils*. Vol. 2, Swets & Zeitlinger, Lisse: 851-908.

Hight, D.W., Paul, M.A., Barras, B.F., Powell, J.J.M., Nash, D.F.T., Smith, P.R., Jardine, R.J., and Edwards, D.H. (2003). The characterization of the Bothkennar clay. *Characterization and Engineering Properties of Natural Soils,* Vol. 1, Swets & Zeitlinger, Lisse: 543-597.

Hinchberger, S.D. and Rowe, R.K. (1998). Modelling the rate-sensitive characteristics of the Gloucester foundation soil. *Canadian Geotechnical J.* 35 (5): 769-789.

Holtz, R.D., Kovacs, W. and Sheahan, T. (2011). *An Introduction to Geotechnical Engineering*, Second Edition, Pearson: 864 pages.

Hong, S.J., Lee, M.J., Kim, J.J. and Lee, W.J. (2010). Evaluation of undrained shear strength of Busan clay using CPT. *Proc. 2nd International Symposium on Cone Penetration Testing,* (CPT'10, Huntingdon Beach, CA). Omnipress, Paper No. 2-23.

Houlihan, M.F. and Blodgett, A.B. (1989). Landfill geotechnical evaluation- Charles City County Landfill. *Draft Report No. P1123, Geosyntec Consultants*, Inc., Atlanta, Georgia.

Houlsby, G. T. (1988). Piezocone penetration test. *Penetration Testing in the UK*, Thomas Telford, London: 141-146.

Houlsby, G.T., and Teh, C.I. (1988). Analysis of the piezocone in clay. *Penetration Testing 1988*, Vol. 2, (Proc. ISOPT, Orlando), Balkema, Rotterdam: 777-783.

Hryciw, R.D., Ghalib, A M., & Raschke, S.A. (1998). In-situ soil characterization using Vision Cone Penetrometer (VisCPT). *Geotechnical Site Characterization,* Vol. 2 (Proc. ISC-1, Atlanta), Balkema, Rotterdam: 1081-1086.

Hryciw, R.D., Zheng, J., Ohm, H.S., & Li, J. (2014). Innovations in optical geocharacterization. *Geo-Congress 2014: Geo-Characterization and Modeling for Sustainability* (Atlanta), ASCE, Reston, VA: 97-116.

Huang, P.T., Patel, M., Santagata, M.C. & Bobet, A. (2009). Classification of organic soils. Final Report, *FHWA/IN/JTRP-2008/2,* Project No. C- 36-36TT, Joint Transportation Research Program, Indiana Department of Transportation and Purdue University, 195p.

Huat, B.B., Prasad, A., Asadi, A., and Kazemian, S. (2014). *Geotechnics of Organic Soils and Peat*. CRC Press/ Balkema, Taylor & Francis Group, London, UK, ISBN: 978-0-415-65941-3.

Huat, B.B.K. (2004). *Organic and Peat Soils Engineering*. University Putra Malaysia Press, Serdang, Malaysia, pp. 20-80.

Hughes, J.M.O., Jefferies, M.G., and Morris, D.L. (1984). Self-bored pressuremeter testing in the Arctic offshore. *Proceedings, 16th Offshore Technology Conference*, Houston, Vol. 1, 255-264.

Idriss, I.M., and Boulanger, R.W. (2006). Semi-empirical procedures for evaluating liquefaction potential during earthquakes. *Soil Dynamics & Earthquake Engineering* 26: 115-130.

Imai, T., and Tonouchi, K. (1982). Correlation of N-value with S-wave velocity and shear modulus. *Proc. 2nd European Symp. on Penetration Testing*, Vol. 1, Amsterdam: 67 – 72.

Ingold, T.S. and Miller, K.S. (1983). Drained axisymmetric loading of reinforced clay, *Journal of Geotechnical Engineering*, ASCE, 109: 883-898.

Jaime, A. and Romo, M.P. (1988). The Mexico earthquake of September 19, 1985 – correlations between dynamic and static properties of Mexico City clay. Earthquake Spectra, 4: 787 – 804.

Jamiolkowski, M. and LoPresti, D.C.F. (1994). Validity of in situ tests related to real behavior. *Proceedings 13th ICSMGE*, Vol. 5, New Delhi, 51-55.

Jamiolkowski, M., Ghionna, V., Lancellotta, R. and Pasqualini, E. (1988). New Correlations of Penetration Tests for Design Practice. *Penetration Testing 1988* (Proc. ISOPT-1, Orlando), Vol. 1, Balkema Publishers, Rotterdam: 263-296.

Jamiolkowski, M., Ghionna, V.N., Lancellota, R., and Pasqualini, E. (1988). New correlations of penetration tests for design practice. *Penetration Testing 1988* (Proc. ISOPT-1, Orlando), Vol. 2, Balkema, Rotterdam: 263-296.

Jamiolkowski, M., Ladd, C.C., Germaine, J., and Lancellotta, R. (1985). New developments in field and lab testing of soils. *Proceedings, 11th International Conference on Soil Mechanics and Foundations Engineering*, Vol. 1, San Francisco, Balkema, Rotterdam: 57-154.

Jamiolkowski, M., Lancellotta, R., Tordella, M.L., and Battaglio, M. (1982). Undrained Strength from CPT. *Proc European Symposium on Penetration Testing*, Vol. 2, 599-606, Balkema, Amsterdam.

Janbu, N. (1969). The Resistance Concept Applied to Deformation of Soils, *Proc. 7th International Conf. on Soil mechanics & Foundation Engineering*, Mexico, Vol. 1, 191-196.

Jannuzzi, G.M.F., Danziger, F.A.B., & Martins, I. S. M. (2015). Geological–geotechnical characterization of Sarapuí II clay. *Engineering Geology*, *190*, 77-86.

Jardine, R. J., Brosse, A., Coop, M. R., and Hosseini, K. R. (2015). Shear strength and stiffness anisotropy of geologically aged stiff clays. *Deformation Characteristics of Geomaterials.* IOS Press, Amsterdam, 156-191.

Jardine, R.J., Gens, A., Hight, D.W., and Coop, M.R. (2004). Developments in understanding soil behavior. *Advances in Geotechnical Engineering* (Proc. Skempton Conference, London), Thomas Telford, London: 103-240.

Jefferies, M. and Been, K. (2006). *Soil Liquefaction – A Critical State Approach*. Taylor and Francis, New York, NY, pp. 580.

Jefferies, M.G., and Davies, M.P. (1991). Soil classification by the cone penetration test: Discussion. *Canadian Geotechnical Journal*, *28*(1), 173-176.

Jefferies, M.G., and Davies, M.P., (1993). Use of CPTU to estimate equivalent SPT N60. *Geotechnical Testing Journal*, ASTM, 16(4): 458-468.

Jefferies, M.G., Been, K., (2016). *Soil Liquefaction — A Critical State Approach*. 2nd Edition. CRC Press, London: 676 p.

Jefferies, M.G., Crooks, J.H.A., Becker, D.E., and Hill, P.R. (1987) Independence of geostatic stress from overconsolidation in some Beaufort Sea clays. *Canadian Geotechnical Journal*, Vol. 24, No. 3, 342-356.

Jefferies, M.G., Ruffell, J.P., Crooks, J.H.A., and Hughes, J.M.O. (1985) Some aspects of the behavior of Beaufort Sea Clays. *Strength Testing of Marine Sediments, Laboratory and In-Situ Measurements, ASTM STP 883,* American Society of Testing and Materials, West Conshohocken, PA: 487-514.

Jones, G.A. and Rust, E. (1982). Piezometer penetration testing. *Proceedings, 2nd European Symposium on Penetration Testing*, Amsterdam, Vol. 2, 607-613.

Jones, G.A. and Van Zyl, D.J.A. (1981). The piezometric probe- a useful investigation tool. *Proceedings, l0th International Conference on Soil Mechanics and Foundation Engineering*, San Francisco, Vol. 2, Balkema, Rotterdam: 489-496.

Juran, I. (1983). Application of the piezocone penetrometer to in-situ soil investigations. *Proceedings, International Symposium on In-Situ Testing*, Paris, Vol. 2, 309-315.

Juran, I. and Tumay, M.T. (1989). Soil stratification using dual pore pressure piezocone test. *Transportation Research Record 1235*, Washington, D.C., 68-78.

Karlsrud, K., Lunne, T.& Brattlien, K. (1996). Improved CPTu interpretations based on block samples. *Publikasjon-Norges Geotekniske Institutt*, *202*, Oslo: 195-201.

Karlsrud, K., Lunne, T., Kort, D.A. and Strandvik, S. (2005). CPTU correlations for clays. *Proc. 16th ICSMGE*, Vol. 2 (Osaka), Millpress, Rotterdam: 693-702.

Kazemian, S., and Huat, B.B. (2009). Compressibility characteristics of fibrous tropical peat reinforced with cement column. *Electronic Journal of Geotechnical Engineering*, *14*, 1-13.

Kazemian, S., Asadi, A, and Huat BBK (2009). Laboratory study on geotechnical properties of tropical peat soils. *International J. Geotechnical. Environ*., 1: 69-79

Keaveny, J., (1985). *In-situ determination of drained and undrained soil strength using the cone penetration test*, Ph.D. Dissertation, University of California, Berkeley, 371p.

Keaveny, J.M. and Mitchell, J.K. (1986). Strength of fine-grained soils using the piezocone. *Use of In-Situ Tests in Geotechnical Engineering* (GSP 6), ASCE, Reston, VA: 668-699.

Kees, G., (2005). *Hand-held electronic cone penetrometers for measuring soil strength*. Technical Report 0524–2837–MTDC. Missoula, MT: U.S. Department of Agriculture Forest Service, Missoula Technology and Development Center, Montana: 12 pages.

Kelly, B.C. (2006). Compression and consolidation anisotropy of some soft soils. *Geotechnical & Geological Engineering* 24: 1715-1728.

Kennet, A., Yu, Y. and Westerberg, B. (1994). Behavior and modeling of Swedish natural soft clays, *Proc. 13th ICSMFE,* New Delhi, India: Vol. 1: 57-60.

Kong, S.P. (2015), *Geotechnical Data Report, Highway 99 and Interchanges: George Massey Tunnel Replacement Project Report*, British Columbia. Ministry of Transportation and Infrastructure, Golder Associates Limited,143 p.

Konrad, J. M., Bozozuk, M., & Law, K. T. (1985). Study of in-situ tests methods in deltaic silt. *Proceedings of 11th International Conference on Soil Mechanics and Foundation Engineering,* Vol. 2, San Francisco, Balkema, Rotterdam: 879-886.

Konrad, J.M. (1987). Piezo-friction-cone penetrometer testing in soft clays. *Canadian Geotechnical Journal*, Vol. 24, No. 4, 645-652.

Konrad, J.M., and Law, K. (1987a). Undrained shear strength from piezocone. *Canadian Geotechnical Journal* 24: 392-405.

Konrad, J.M., and Law, K. (1987b). Preconsolidation pressure from piezocone tests in marine clays. *Geotechnique*, 37(2): 177-190.

Koutsoftas, D. (1989). Factual report: site investigation for completion of preliminary design, Phase I, Muni Metro Turnaround Facility. *Report No. 185-215-03,* Dames & Moore, Inc., San Francisco, 3 volumes.

Koutsoftas, D. and Foott, R. (1982). Replacement Airport at Chek Lap Kok. *Civil Engineering Design Studies Report*. Dames & Moore, Inc., Hong Kong, 5 volumes.

Koutsoftas, D.C. and Ladd, C.C. (1985). Design strengths for an offshore clay. *Journal of Geotechnical Engineering* 111(3): 337-355.

Kowalczyk, S., Zawrzykraj, P., Maślakowski, M. (2017). Application of the electrical resistivity method in assessing soil for the foundation of bridge structures: a case study from the Warsaw environs, Poland. *Acta Geodyn. Geomater*. 14, No. 2 (186), 221–234.

Krage, C. P., Broussard, N. S., & DeJong, J. T. (2014). Estimating rigidity index ($I_R$) based on CPT measurements. *Proceedings of the 3rd International Symposium on Cone Penetration Testing,* (CPT'14, Las Vegas): 727-735. www.cpt14.com

Ku, T. & Mayne, P.W. (2012). Frequent-interval SDMT and continuous SCPTu for detailed shear wave velocity profiling in soils. *Geotechnical Engineering Journal*, 43(4), South East Asian Geotechnical Society: 34-40.

Ku, T. and Mayne, P.W. (2013). Yield stress history evaluated from paired in-situ shear moduli of different modes. *Engineering Geology* 152 (1), Elsevier: 122-132.

Ku, T., Mayne, P.W & Cargill, E. (2013a). Continuous-interval shear wave velocity profiling by auto-source and seismic piezocone tests. *Canadian Geotechnical J.* 50(1): 382–390.

Ku, T., Weemees, I., Cargill, E., Mayne, P.W. & Woeller, D. (2013b). Post-processing continuous shear wave signals taken during cone penetrometer testing. ASTM *Geotechnical Testing J*. 36(4): 543-553.

Kulhawy, F.H. and Mayne, P.W. (1990). *Manual on Estimating Soil Properties for Foundation Design, Report No. EL-6800,* Electric Power Research Institute, Palo Alto, CA, August 1990, 306 pages. Download from: www.epri.com

Kullingsjö, A. (2007). *Effects of deep excavations in soft clay on the immediate surroundings-Analysis of the possibility to predict deformations and reactions against the retaining system*. Chalmers University of Technology, Göteborg, Sweden, 334p.

L'Heureux, J. S. and Long, M. (2016). Correlations between shear wave velocity and geotechnical parameters in Norwegian clays. *Proc.17th Nordic Geotechnical Meeting (NGM 2016)*, Reykjavik, Iceland; 299-308.

L'Heureux, J.S., Locat, A., Leroueil, S., Demers, D. and Locat, J. (2014). *Landslides in Sensitive Clays: From Geosciences to Risk Management*, Advances in Natural and Technological Hazards Research 36, Springer, New York: DOI 10.1007/978-94-007-7079-9

La Rochelle, P., Trak, B., Tavenas, F., and Roy, M. (1974). Failure of a test embankment on a sensitive Champlain clay deposit. *Canadian Geotechnical Journal*, 11(1), 142-164.

La Rochelle, P., Zebdi, M., Leroueil, S., Tavenas, F., and Virely, D. (1988). Piezocone tests in sensitive clays of Eastern Canada. *Penetration Testing 1988* (Proc. ISOPT-1, Orlando), Balkema, Rotterdam, Vol. 1, 831-841.

Lacasse, S., and D'orazio, T.B. (1990). Interpretation of self-boring and push-in pressuremeter tests. *Pressuremeters: Proceedings of 3rd International Symposium on Pressuremeters* (Oxford), Thomas Telford, London: 273 - 285.

Ladanyi, B. (1967). Deep punching of sensitive clays. *Proceedings of 3rd Pan American Conference on Soil Mechanics and Foundation Engineering,* Caracas, Vol. 1: 533-546.

Ladanyi, B., and Johnston, G.H. (1974). Behavior of circular footings and plate anchors in permafrost. *Canadian Geotechnical Journal*, *11*(4), 531-553.

Ladd, C.C. (1991). Stability evaluation during staged construction, *Journal of Geotechnical Engineering Division*, ASCE, 117(4), 540-615.

Ladd, C.C. and DeGroot, D.J., (2003). Recommended practice for soft ground site characterization. *12th Panamerican Conference on Soil Mechanics and Geotechnical Engineering*, Soil and Rock America, Vol. 1, Boston, MA, 3-57.

Ladd, C.C., Foott, R., Ishihara, K., Schlosser, F., and Poulos, H.G. (1977). Stress-Deformation and Strength Characteristics. *Proc. 9th International Conference on Soil Mechanics and Foundation Engineering*, Vol. 2, Tokyo: 421-494.

Laflamme, J.F. and Leroueil, S., (1999). *Analyse des pressions interstitielles mesurées aux sites d ́excavation de Saint-Hilaire et de Rivière-Vachon, Québec.* Rapport GCT-99-10 présenté au Ministère des Transports du Québec, département de Génie civil. Université Laval.

Lafleur, J., Silvestri, V., Asselin, R., and Soulie, M. (1988). Behavior of a test excavation in soft Champlain Sea clay. *Canadian Geotechnical Journal*, Vol. 25, No. 4, 705-715.

Lambson, M.D, Clare, D.G., and Semple, R.M. (1993) Investigation and Interpretation of Pentre and Tilbrook Grange Soil Conditions. *Large-scale Pile Tests in Clay:* Thomas Telford, London: 134-196.

Landon, M.E., DeGroot, D.J. and Jakubowski, J. (2004). Comparison of shear wave velocity measurements in-situ and on block samples of a marine clay. *Proceedings of the 57th Canadian Geotechnical Conference* (GeoQuebec 2004): Session 4E: 22-28.

Landon, M.M. (2007). Development of a non-destructive sample quality assessment method for soft clays. *Ph.D. Dissertation*, Department of Civil Engineering University of Massachusetts, Amherst: 701 p.

Landon, M.M., DeGroot, D.J. and Jakubowski, J. (2004). Comparison of shear wave velocity measurements in-situ and on block samples of a marine clay. *Proceedings of the 57th Canadian Geotechnical Conference* (GeoQuebec 2004): Session 4E: 22-28.

LaRochelle, P., Zebdi, M., Leroueil, S., Tavenas, F., and Virely, D. (1988). Piezocone tests in sensitive clays of Eastern Canada. *Penetration Testing 1988* (Proc. ISOPT-1, Orlando), Balkema, Rotterdam, Vol. 1, 831-841.

Larsson, R. (1997). *Investigations and Load Tests in Silty Soils*. SGI Report R-54, Swedish Geotechnical Institute, Linköping: 260 p.

Larsson, R. (2001). *Investigations and Load Tests in Clay Till*. SGI Report R-59, Swedish Geotechnical Institute, Linköping: 169p.

Larsson, R. and Åhnberg, H. (2005). On the evaluation of undrained shear strength and preconsolidation pressure from common field tests in clay. *Canadian Geotechnical J.* 42 (4): 1221-1231.

Larsson, R. and Mulabdić, M. (1991). Piezocone tests in clays: *Report No. 42*, Swedish Geotechnical Institute, Linköping, 240 p.

Larsson, R. and Mulabdić, M. (1991). Shear moduli in Scandinavian clays: *Report No. 40*, Swedish Geotechnical Institute, Linköping, 127 p.

Larsson, R., and Åhnberg, H. (2003). Long-term effects of excavations at crests of slopes. *SGI Report No. 61,* Swedish Geotechnical Institute, Linköping: 372 p.

Larsson, R., Westerberg, B., Albing, D., Knutsson, S., and Carlsson, E. (2007). *Sulfidjord: geoteknisk klassificering och odränerad skjuvhållfasthet*. Luleå tekniska Universitet. SGI Report R-69, Swedish Geotechnical Institute, Linköping: 169p.

Law, K. T. (1975). Analysis of embankments on sensitive clays. *Ph.D. Dissertation*, Civil Engineering, The University of Western Ontario, 521p.

Law, K.T., and Eden, W.J. (1980). Influence of cutting shoe size in self-boring pressuremeter tests in sensitive clays. *Canadian Geotechnical Journal* 17 (1): 165-173.

Lefebvre, G., Leboeuf, D., Rahhal, M.E., Lacroix, A., Warde, J., and Stokoe II, K.H. (1994). Laboratory and field determinations of small-strain shear modulus for a structured Champlain clay. *Canadian Geotechnical Journal,* 31(1), 61-70.

Lehane, B.M. (2003). Vertically loaded shallow foundation on soft clayey silt. *Proceedings of the Institution of Civil Engineers-Geotechnical Engineering*, *156*(1), 17-26.

Lehtonen, V. (2015). Modelling undrained shear strength and pore pressure based on an effective stress soil model in Limit Equilibrium Method. *Tampereen teknillinen yliopisto. Julkaisu-Tampere University of Technology. Publication; 1337*; 213p.

Lehtonen, V. J., Meehan, C. L., Länsivaara, T., & Mansikkamäki, J. (2015). Full-scale embankment failure test under simulated train loading. *Géotechnique*, *65*(12), 961-974.

Leonards, G.A., and Girault, P. (1961). A study of the one-dimensional consolidation test. Proc. 5th ICSMGE, Vol. 1 (Paris): 213-218. www.issmge.org

Leroueil, S. and Hight, D. (2003). Behavior and properties of natural soils and soft rocks. C*haracterization and Engineering Properties of Natural Soils*, Vol. 1, Swets and Zeitlinger, Lisse: 29-254.

Leroueil, S. and Jamiolkowski, M. (1991). Exploration of soft soil and determination of design parameters. *Proceedings, GeoCoast*, Vol. 2, Port & Harbor Res. Institute, Yokohama: 969-998.

Leroueil, S., and Hamouche, K. (2003). Geotechnical characterization and properties of a sensitive clay from Québec. *Characterisation and Engineering Properties of Natural Soils*. Vol. 1., Swets & Zeitlinger, Lisse: 363-393.

Leroueil, S., Bouclin, G., Tavenas, F., Beregeron, L., and LaRochelle, P. (1990). Permeability anisotropy of natural clays as a function of strain. *Canadian Geotechnical J,* 27 (5): 568-579.

Leroueil, S., Demers, D., La Rochelle, P., Martel, G., and Virely, D. (1995). Practical use of the piezocone in eastern Canada clays. In *CPT'95, Proceedings of the International Symposium on Cone Penetration Testing,* Vol. 2*,* Swedish Geotechnical Society, Linköping, Sweden: 515-521.

Leroueil, S., Hamouche, K., Ravenasi, F., Boudali, M., Locat, J., & Virely, D. (2003). Geotechnical characterization and properties of a sensitive clay from Quebec. *Characterization and Engineering Properties of Natural Soils*, Vol. 1, Swets & Zeitlinger, Lisse: 363-394.

Leroueil, S., Samson, L., and Bozozuk, M. (1983). Laboratory and field determination of preconsolidation pressures at Gloucester. *Canadian Geotechnical Journal*, 1983, 20(3): 477-490.

Leshchinsky, D. and Perry, E.B. (1987). A design procedure for geotextile reinforced walls, *Geosynthetics '87, IFAI*, New Orleans, LA, USA, 1: 95-107.

Levesque, C.L., Locat, J. and Leroueil, S. (2007). Characterization of postglacial sediments of the Saguenay Fjord, Quebec, *Characterization and Engineering Properties of Natural Soils,* Vol. 4 (IS-Singapore), Taylor & Francis Group, London, 2645-2677.

Liao, S.S., and Whitman, R.V. (1986). Overburden Correction Factors for SPT in Sand. *Journal of Geotechnical Engineering*, ASCE, Vol. 112 (3): 373-377.

Liao, T. & Mayne, P.W. (2006). Automated post-processing of shear wave signals, *Proc. 8th US National Conference on Earthquake Engineering*, San Francisco, pp. 460.1-460.10

Lishtvan II, Bazin ET, Kosov BI (1985). Physical properties of peat and peat deposits (in Russia). Nauka I Technika Press, Miñsk. 134-145.

Liu, S.Y., Cai, G.J., Tong, L.Y., and Du, G.Y. (2008). Approach on the engineering properties of Lianyungang marine clay from piezocone penetration tests. *Marine Georesources and Geotechnology*, *26*(3), 189-210.

Liyanapathirana, D. S. (2009). Arbitrary Lagrangian Eulerian based finite element analysis of cone penetration in soft clay. *Computers and Geotechnics*, *36*(5), 851-860.

Liyanapathirana, D.S. (2016) Numerical simulation of deep penetration of a piezocone in a strain-softening clay, *International Journal of Geotechnical Engineering*, 10:2, 174-182.

Lo Presti, D.C.F., Jamiolkowski, M., and Pepe, M. (2003). Geotechnical characterization of the subsoil of Pisa Tower. *Characterization and Engineering Properties of Natural Soils,* Vol. 2, Singapore, Balkema / Swets & Zeitlinger, Lisse: 909-946.

Lo, K.Y., Bozozuk, M. and Law, K.T. (1976). Settlement analysis of the Gloucester test fill. *Canadian Geotechnical J.* 13 (4): 339-354.

Locat, A. (2012). Rupture progressive et étalements dans les argiles sensibles, *PhD Dissertation,* Université Laval, 216p.

Locat, J. and Tanaka, H. (1999). Microstructure, mineralogy, and physical properties; Techniques and application to the Busan clays. *Proc. KSG'99 Dredging and Geoenvironmental Conference*, Seoul: 15-31.

Locat, J., Tanaka, H., Tan, T.S., Dasari, G.R., and Lee, H. (2003). Natural soils: geotechnical behavior and geological knowledge. Characterization and Engineering Properties of Natural Soils, Vol. 1, Swets & Zeitlinger, Lisse: 3-28.

Long, M. (2008). Design parameters from in-situ tests in soft ground - recent developments. *Geotechnical & Geophysical Site Characterization*, Vol. 1 (Proc. ISC-3, Taipei), Taylor & Francis, London: 89-116.

Long, M., & Donohue, S. (2007). In situ shear wave velocity from multichannel analysis of surface waves (MASW) tests at eight Norwegian research sites. *Canadian Geotechnical Journal*, *44*(5), 533-544.

Long, M., and Menkiti, C.O (2007). Characterization and engineering properties of Dublin Boulder clay. *Characterization and Engineering Properties of Natural Soils– Natural Soils,* Vol. 3, Taylor & Francis Group, London: 2003-2045.

Long, M., Donohue, S., O'Connor, P., and Quigley, P. (2009). Relationship between shear wave velocity and undrained shear strength of Irish glacial till. *Proceedings Near Surface 15th European Meeting of Environmental and Engineering Geophysics*. Dublin. Paper A13: 5p.

Long, M., El Hadj, N., and Hagberg, K. (2009). Quality of conventional fixed piston samples of Norwegian soft clay. *Journal of Geotechnical and Geoenvironmental Engineering*, *135*(2), 185-198.

Long, M., Gudjonsson, G., Donohue, S., & Hagberg, K. (2010). Engineering characterization of Norwegian glaciomarine silt. *Engineering Geology*, *110*(3), 51-65.

Long, M.M., and O'Riordan, N.J. (1988). The use of piezocone in the sign of a deep basement in London clay. *Penetration Testing in the U.K.,* Thomas Telford, London, U.K.,173- 176.

Low, H. E., Landon Maynard, M., Randolph, M. F., & DeGroot, D. J. (2011). Geotechnical characterization and engineering properties of Burswood clay. *Géotechnique*, *61*(7), 575-591.

Low, H.E. (2009). Performance of penetrometers in deepwater soft soil characterization. *Ph.D. Thesis*. Centre for Offshore Foundation Systems, School of Civil & Resource Engrg., Univ. Western Australia: 300 p.

Low, H.E., Lunne, T., Andersen, K.H., Sjursen, M.A., Li, X. and Randolph, M.F. (2010). Estimation of intact and re-moulded undrained shear strengths from penetration tests in soft clays. *Geotechnique,* 60 (11): 843-859.

Low, H.E., Randolph, M.F. and Kelleher, P. (2007). Comparison of pore pressure generation and dissipation rates from cone and ball penetrometers. *Proc. 6th Intl. Offshore Site Investigation and Geotechnics Conf.*, Society of Underwater Technology, London: 547-556.

Lu, Q., Randolph, M.F., Hu, Y., Bugarski, L.C. (2004). A numerical study of cone penetration in clay. *Geotechnique*; 54(4):257–267.

Lundstrom, K. Larsson.R, and Dahlin.T. (2009). *Mapping of quick clay formations using geotechnical and geophysical methods: Landslides*, Springer-Verlag, Vol. 6, p. 1-15.

Lunne, T. (2010). The CPT in offshore soil investigations – a historic perspective. *Proceedings, 2nd Intl. Symp. on Cone Penetration Testing*, Vol. 1, Huntington Beach, CA; Omnipress: 71-113.

Lunne, T. and Lacasse, S., (1999). Geotechnical characteristics of low plasticity clays. *Proceedings of the International Symposium on Characterization of Soft Marine Clays - Bothkennar, Drammen, Quebec, and Ariake Clays*, Yokosuka, Japan, 33-56.

Lunne, T., Berre, T., Andersen, K.H., Strandvik, S. and Sjursen, M. (2006). Effects of Sample Disturbance and Consolidation Procedures on Measured Shear Strength of Soft Marine Norwegian Clays. *Canadian Geotechnical Journal* 43 (7): 726-750.

Lunne, T., Christoffersen, H.P. and Tjelta, T.I. (1985). Engineering Use of Piezocone Data in North Sea Clays. *Proc., 11th International Conference on Soil Mechanics and Foundation Engineering*, San Francisco, Vol. 2, Balkema, Rotterdam: 907-912.

Lunne, T., Eidsmoen, T., Gillespie, D., and Howland, J. (1986). Laboratory and field evaluation of cone penetrometers. *Use of In-Situ Tests in Geotechnical Engineering (GSP 6),* American Society of Civil Engineers, Reston, VA: 714-729.

Lunne, T., Eidsmoen, T.E., Powell, J.J.M., and Quarterman, R.S.T. (1986). Piezocone testing in overconsolidated clays. *Proc. of the 39th Canadian Geotechnical Conference, Ottawa;* 209-218.

Lunne, T., Long, M., and Uzielli, M. (2007). Characterization and Engineering Properties of Troll Clay. *Characterization and Engineering Properties of Natural Soils.* Vol. 4, Taylor & Francis, London: 1939-1972.

Lunne, T., Long, M., and Forsberg, C. F. (2003). Characterization and engineering properties of Onsøy clay. *Characterization and Engineering Properties of Natural Soils*, Vol. 1, Swets & Zeitlinger, Lisse: 395-427.

Lunne, T., Long, M., and Forsberg, C.F. (2003). Characterization and engineering properties of Holmen, Drammen sand. *Characterization and engineering properties of natural soils*, *2*, 1121-1148.

Lunne, T., Nerland, O. & Solhell, E. (2001). Quality of CPTU. Factual report, field tests at Onsøy. *NGI report No. 20011099-1*, 16/7/01, Oslo.

Lunne, T., Randolph, M., Sjursen, M.A., Low, H.E. and Gue, C.S. (2006). *Shear strength parameters determined by in-situ tests for deep water soft soils*. NGI-COFS Report 20041618-1. Joint Industry Project by the Norwegian Geotechnical Institute, Oslo and Centre for Offshore Foundation Systems, Perth: 558 pages.

Lunne, T., Robertson, P.K. and Powell, J.J.M. (1997). *Cone Penetration Testing in Geotechnical Practice*, EF Spon/Blackie Academic - Routledge Publishing, New York: 312 p.

Lutenegger, A.J. (2000). NGES at the Univ. of Massachusetts. *National Geotechnical Experimentation Sites* (Proc. Amherst, GSP 93), ASCE, Reston, VA: 102-129.

Lutenegger, A.J. (2015). Dilatometer Tests in Sensitive Champlain Sea Clay: Stress History and Shear Strength. *Proceedings of the 3rd International Conference on the Dilatometer, Rome, Italy.*

Lutenegger, A.J. and Kabir, M.G. (1987). Pore pressures generated by two penetrometers in clays. *Report No. 87-2*, Department of Civil and Environmental Engineering, Clarkson University, Potsdam, New York, 44 p.

Lutenegger, A.J. and Kabir, M.G. (1988). Interpretation of piezocone results in over-consolidated clays. *Penetration Testing in the UK*, Thomas Telford, London, 43-46.

Lutenegger, A.J. and Timian, D.A. (1986). Flat plate penetrometer tests in marine clays. *Proc. 39th Canadian Geotechnical Conference*, Ottawa: 301-309.

Ma, H., Zhou, M., Hu, Y., & Hossain, M. S. (2017). Interpretation of layer boundaries and shear strengths for stiff-soft-stiff clays using cone penetration test: LDFE Analyses. *International Journal of Geomechanics*, *17*(9), 06017011: 1-11.

Ma, H., Zhou, M., Hu, Y., & Hossain, M.S. (2016). Interpretation of layer boundaries and shear strengths for soft-stiff-soft clays using CPT data: LDFE analyses. *Journal of Geotechnical and Geoenvironmental Engineering*, *142*(1), 04015055: 1-12.

Magnan, J. P. (1994) Construction on peat. State of the art in France. *Advances in Understanding and Modelling the Mechanical Behaviour of Peat* (eds. E. J. den Haan et al.), Balkema, Rotterdam, pp. 369–80.

Mahar, L.J., & O'Neill, M.W. (1983). Geotechnical characterization of desiccated clay. *Journal of Geotechnical Engineering*, *109*(1), 56-71.

Marchetti, S. (1980). In-situ tests by flat dilatometer. *Journal of the Geotechnical Engineering Division (ASCE)*, Vol. 106 (3): 299-321.

Marchetti, S. (1980). In-situ tests by flat dilatometer. *Journal of the Geotechnical Engineering Division (ASCE)*, Vol. 106 (3), 299-321.

Marchetti, S. (1985). On the field determination of $K_0$ in sand. *Proc.11th International Conf. on Soil Mechanics & Foundation Engrg.* (San Francisco), Vol 5, Balkema, Rotterdam: 2667-2672.

Marchetti, S., (1980). In-situ tests by flat dilatometer. *Journal of the Geotechnical Engineering Division (ASCE)*, 106 (3), 299-321.

Marchetti, S., Monaco, P., Totani, G., and Calabrese, M. (2001). The flat dilatometer test (DMT) in soil investigations–A report by the ISSMGE committee TC16. *Proceedings of the 2nd International Flat Dilatometer Conference,* Arlington, VA: pp. 7-48. www.usucger.org

Masood, T. and Mitchell, J.K. (1993). Estimation of in-situ lateral stresses in soils by cone penetration test. *Journal of Geotechnical Engineering*, 119(10): 1624-1639.

Mayne, P. W., (2008). Piezocone profiling of clays for maritime site investigations. *Proceedings of the 11th Baltic Sea Geotechnical Conference*, Gdansk, Poland, Vol. 1, 151-178.

Mayne, P.W. & McGillivray, A.V. (2008). Improved shear wave measurements using autoseis sources. *Deformational Characteristics of Geomaterials*, Vol. 2 (Proc. 4th ISDCG, Atlanta), Millpress/IOS Press, Amsterdam: 853-860.

Mayne, P.W. (1987). Determining preconsolidation stress and penetration pore pressures from DMT contact pressures, *Geotechnical Testing Journal*, ASTM, Vol. 10, No. 3: 146-150.

Mayne, P.W. (1989). Site characterization of Yorktown formation for new accelerator. *Foundation Engineering: Current Principles (GSP 22)*, ASCE, Reston, Virginia, Vol. 1, 1-15.

Mayne, P.W. (1991). Determination of OCR in Clays by Piezocone Tests Using Cavity Expansion and Critical State Concepts, *Soils and Foundations*, Vol. 31 (2): 65-76.

Mayne, P.W. (1992). In-situ characterization of Piedmont residuum in Eastern US. *Proc. National Science Foundation (NSF) US-Brazil Geo-Workshop*: Application of Classical Soil Mechanics to Structured Soils, Belo Horizonte: 89–93.

Mayne, P.W. (1995). Profiling yield stress in clays by in-situ tests, *Transportation Research Record* 1479, National Academy Press, Washington, DC: 43-50.

Mayne, P.W. (2001). Stress-strain-strength-flow parameters from enhanced in-situ tests. *Proceedings International Conference on In-Situ Measurement of Soil Properties & Case Histories* (In-Situ 200), Bali, Indonesia, 47-69.

Mayne, P.W. (2005). Integrated ground behavior: In-situ and lab tests. *Deformation Characteristics of Geomaterials*, Vol. 2 (Proc. Lyon, France), Taylor & Francis, London, United Kingdom, pp. 155-177.

Mayne, P.W. (2006). The 2006 James K. Mitchell Lecture: Undisturbed sand strength from seismic cone tests. *Geomechanics & Geoengineering*: Vol. 1 (4): 239-257.

Mayne, P.W. (2007a). Invited Overview Paper: In-situ test calibrations for evaluating soil parameters, *Characterization & Engineering Properties of Natural Soils*, Vol. 3 (Proc. Singapore 2006), Taylor & Francis Group, London: 1602-1652.

Mayne, P.W. (2007b). *NCHRP Synthesis 368 on Cone Penetration Test*. Transportation Research Board, National Academies Press, Washington, D.C., 118 pages. Download from: www.trb.org

Mayne, P.W. (2008). Keynote paper: Piezocone profiling of clays for maritime site investigations. *Geotechnics in Maritime Engineering*, Vol. 1, Proc., 11th Baltic Sea Geotechnical Conference, Gdansk, Polish Committee on Geotechnics: 333-350.

Mayne, P.W. (2013). Evaluating yield stress of soils from laboratory consolidation and in-situ cone penetration tests. *Sound Geotechnical Research to Practice*, (GSP 230 in honor of R.D. Holtz), ASCE, Reston/VA: 406-420.

Mayne, P.W. (2013). Updating our geotechnical curricula via a balanced approach of in-situ, laboratory, and geophysical testing of soil. *Proceedings, 61st Annual Geotechnical Conference*, Minnesota Geotechnical Society, University of Minnesota, St. Paul: 65-86.

Mayne, P.W. (2014). Interpretation of geotechnical parameters from seismic piezocone tests. *Proceedings, 3rd Intl. Symp. Cone Penetration Testing*, (CPT'14, Las Vegas); edited by P.K. Robertson and K.L. Cabal): 47-73. www.cpt14.com

Mayne, P.W. (2014). Development of an automated methodology for evaluation of undrained shear strength of offshore clays from piezocone penetration tests. *Report 122931* submitted by Georgia Tech Research Corp. (Project: 2006U94) to Fugro Engineers, Leidschendam, The Netherlands, 192 p.

Mayne, P.W. (2014). Generalized CPT method for evaluating yield stress in soils. *Geo-Congress 2014: Geo-Characterization and Modeling for Sustainability* (Atlanta), ASCE, Reston, VA: 1336-1346).

Mayne, P.W. (2015). Peak friction angle of undisturbed sands using DMT. *Proceedings, Third International Conference on Flat Dilatometer*, (DMT'15, Rome), paper ID 20: 237-242: www.marchetti-dmt.it

Mayne, P.W. (2016). Evaluating effective stress parameters and undrained shear strengths of soft-firm clays from CPT and DMT. *Australian Geomechanics Journal* 51 (4): 27-55.

Mayne, P.W. (2016). Invited keynote: Evaluating effective stress parameters and undrained shear strengths of soft-firm clays from CPT and DMT. *In Pursuit of Best Practices - Proc. 5th Intl. Conf. on Geotechnical & Geophysical Site Characterization* (ISC-5, Jupiters Resort, Gold Coast), Australian Geomechanics Society, Vol. 1: 19-40

Mayne, P.W. (2017). Stress history of soils from cone penetration tests. *Soils & Rocks*, Såo Paulo, 40(3): September-December, 14p.

Mayne, P.W., and Brown, D.A. (2003). Site characterization of Piedmont residuum of North America. *Characterization and Engineering Properties of Natural Soils*, Vol. 2, Swets & Zeitlinger, Lisse, 1323-1339.

Mayne, P.W., and Campanella, R.G. (2005). Versatile site characterization by seismic piezocone tests, *Proc.16th Int. Conf. on Soil Mechanics & Geotechnical Eng*., ICSMGE, Osaka, Vol. 2, Rotterdam: 721-724.

Mayne, P.W., and Frost, D.D. (1988). Dilatometer Experience in Washington, DC and Vicinity, *Transportation Research Record 1169*, National Academy Press, Washington, DC: 16-23.

Mayne, P.W., and Gordon, D. (1987). Geotechnical Exploration - North Anna Radwaste Facility. *Report No. W7-5768*, Law Engineering, McLean, Virginia, submitted to Virginia Power Corp, Richmond, VA: 230 p.

Mayne, P.W., and Holtz, R.D. (1988). Profiling stress history from piezocone soundings, *Soils and Foundations*, Vol. 28, No. 1, pp. 16-28.

Mayne, P.W., and Kemper, J.B. (1988). Profiling OCR in Stiff Clays by CPT and SPT. *ASTM Geotechnical Testing Journal*, Vol. 11 (2): 139-147.

Mayne, P.W., and Kulhawy, F.H. (1982). $K_0$-OCR Relationships in Soil, *Journal of the Geotechnical Engineering Division*, ASCE, Vol. 108, GT6, pp. 851-872.

Mayne, P.W., and Kulhawy, F.H. (1990). Direct and indirect measurements of in-situ $K_o$ in clays, *Transportation Research Record 1278*, Washington, DC: 141-149.

Mayne, P.W., and Liao, T., (2004). CPT-DMT interrelationships in Piedmont residuum, *Geotechnical & Geophysical Site Characterization*, Vol. 1, (Proc. ISC-2, Porto), Millpress, Rotterdam, 345-350.

Mayne, P.W., and Pearce, R.A., (2005). Site characterization of Bootlegger Cove Formation clay for Port of Anchorage, *Frontiers in Offshore Geotechnics* (Proc. ISFOG, Perth*),* Taylor & Francis Group, London: 951-955.

Mayne, P.W., and Rix, G.J. (1995). Correlations Between Shear Wave Velocity and Cone Tip Resistance in Clays, *Soils and Foundations* 35 (2), pp. 107-110.

Mayne, P.W., and Woeller, D.J. (2015). Advances in seismic piezocone testing. Geotechnical Engineering for Infrastructure & Development (Proc. XVI ECSMGE, Edinburgh), Vol. 6, ICE Publishing, London: 3005-3009.

Mayne, P.W., Christopher, B., Berg, R., and DeJong, J. (2002). *Subsurface Investigations -Geotechnical Site Characterization*. Publication No. FHWA-NHI-01-031, National Highway Institute, Federal Highway Administration, Washington, D.C., 301 pages.

Mayne, P.W., Coop, M.R., Springman, S., Huang, A-B., Zornberg, J., (2009). State-of-the-art paper (SOA-1): Geomaterial Behavior and Testing, *Proceedings of the 17th Intl. Conf. Soil Mechanics & Geotechnical Engineering*, Vol. 4 (ICSMGE, Alexandria, Egypt), Millpress/IOS Press Rotterdam, 2777-2872.

Mayne, P.W., Peuchen, J., and Baltoukas, D. (2015). Piezocone evaluation of undrained strength in soft to firm offshore clays. *Frontiers in Offshore Geotechnics III*, Vol. 2 (Proc. ISFOG, Oslo), Taylor & Francis Group, London: 1091-1096.

Mayne, P.W., Robertson, P.K., and Lunne, T. (1998). Clay stress history evaluated from seismic piezocone tests, *Geotechnical Site Characterization*, Vol. 2, Balkema, Rotterdam, pp. 1113-1118.

Mayne, P.W., Styler, M., Woeller, D., and Sharp, J. (2017). Identifying contractive soils by CPT material index for flow liquefaction concerns. *Proceedings of the 70th Canadian Geotechnical Conference: GeoOttawa 2017,* Ottawa, Canada: www.cgs.ca

McGillivray, A. V. (2007). *Enhanced integration of shear wave velocity profiling in direct-push site characterization systems*. Ph.D. Dissertation. Civil & Environmental Engineering, Georgia Institute of Technology, 393p.

McGillivray, A.V. & Mayne, P.W. (2008). An automated seismic source for continuous shear wave profiling. *Geotechnical & Geophysical Site Characterization,* (Proc. ISC-3, Taipei), Taylor & Francis Group, London: 1347-1352.

McQueen, W., Miller, B., Mayne, P. W., & Agaiby, S. (2016). Piezocone dissipation tests at the Canadian Test Site No.1, Gloucester, Ontario. *Canadian Geotechnical Journal*, 53: 884-888.

McRostie, G.C. and Crawford, C.B. (2001). Canadian Geotechnical Research Site No. 1 at Gloucester. *Canadian Geotechnical J.* 38 (5): 1134-1141.

Merani, J. M., Hunt, C. E., Donahue, J. L., & Bray, J. D. (2016). CPT Interpretation in Highly Organic Soils and Soft Clay Soils. *Geo-Chicago 2016,* GSP 236, ASCE, Reston, VA: 412-421.

Mesri G., Ajlouni M (2007). Engineering properties of fibrous peats. *J. Geotechnical & Geoenvironmental Engineering* 133(7): 851-866.

Mesri G., Stark, T.D., Ajlouni, M.A., Chen, C.S. (1997). Secondary compression of peat with or without surcharging. *J. Geotech. Geoeviron. Eng.,* 123(5): 411-421.

Mesri G., Stark, T.D., Chen, C.S. (1994). $C_c/C_\alpha$ concept applied to compression of peat. discussion. *J. Geotech. Geoenv. Eng*., 120:764-766.

Mesri, G., Rokhsar, A. and Bohor, B.F. (1975). Composition and compressibility of typical samples of Mexico City clay. *Geotechnique* 25 (3): 527-554.

Meyerhof, G.G. (1951). The ultimate bearing capacity of foundations. *Geotechnique,* 2(4): 301 – 332.

Mimura, M. (2003). Characteristics of some Japanese natural sands-data from undisturbed frozen samples. *Characterization and Engineering Properties of Natural Soils.* Vol. 2, Swets and Zetlinger, Lisse, Netherlands: 1149-1168.

Mitchell, J.K., and Lunne, T. (1978). Cone resistance as measure of sand strength. *Journal of the Geotechnical Engineering Division*, 104 (GT 7): 995-1012 (ASCE 13901).

Mitchell, J.K., and Soga, K. (2005). *Fundamentals of Soil Behavior*. 3rd edition, Wiley press, ISBN: 978-0-471-46302-3, 592 p.

Młynarek Z., Wierzbicki J., Gogolik, S., and Bogucki, M. (2014) Shear strength and deformation parameters of peat and gyttja from CPTu, SDMT and VT tests. CPTu and DMT in soft clays and organic soils. *Proc. of the 5th International Workshop,* Polish Committee on Geotechnics, Vol. 1: 193 – 209.

Montafia, A. (2013). Influence of physical properties of marine clays on electric resistivity and basic geotechnical parameters. *Master's thesis*, Department of Civil and Transport Engineering, Norwegian University of Science and Technology NTNU; 119p.

Moss, R.E.S., Seed, R.B., and Olsen, R.S. (2006). Normalizing the CPT for overburden stress. *Journal of Geotechnical & Geoenvironmental Engineering* 132 (3): 378-387,

Nader, A., Fall, M., and Hache, R. (2015). Characterization of sensitive marine clays by using cone and ball penetrometers: example of clays in Eastern Canada. *Geotechnical and Geological Engineering*, 33(4): 841-864.

Nakase, A., Kamei, T., & Kusakabe, O. (1988). Constitutive parameters estimated by plasticity index. *Journal of Geotechnical Engineering*, *114*(7), 844-858.

Nash, D.F.T., Sills, G.C., & Davison, L.R. (1992). One-dimensional consolidation testing of soft clay from Bothkennar. *Geotechnique*, *42*(2), 241-256.

Newcomb, D.E. and Birgisson, B., (1999). *Measuring in-situ mechanical properties of pavement subgrade soils.* NCHRP Synthesis of Highway Practice 278, Transportation Research Board, Washington, DC: 84 pages.

Nguyen, H. Q. (2007). *Reanalysis of the settlement of a levee on soft bay mud.* M.Sc. Thesis, Department of Civil and Environmental Engineering, Massachusetts Institute of Technology, 366 p.

Niazi, F., Mayne, P.W., and Woeller, D. (2010). Evaluating drilled shaft O-cell response at Golden Ears Bridge from in-situ seismic cone tests. *The Art of Foundation Engineering Practice.* Proceedings Volume in honor of Clyde Baker (GSP 198), ASCE, Reston, Virginia: 452-469.

Niazi, F.S., Mayne, P.W., and Woeller, D.J. (2011). Calibration of hybrid SCE-CSSM analytical model for piezocone penetration in clays. *Proc. 14th Pan-Am Conference and 64th Canadian Geotechnical Conference*, Toronto. http://panam-cgc2011.ca

NIFS (2015). *Detection of brittle materials. Summary report with recommendations*. Final report. NIFS Report no. 126/2015 (www.naturfare.no)

Norconsult AB (2016), Detaljplan Gillet 1 m. fl, Torshälla, Eskilstuna Kommun Markteknisk undersökningsrapport, Geoteknik MUR/Geo, 104P.

O'Loughlin, C.D., and Lehane, B.M. (2003) A study of the link between composition and compressibility of peat and organic soils. *Proc., 2nd International Conference on Advances in Soft Soil Engineering and Technology*. Putrajaya, Malaysia: 135-152.

Ohta, H., Nishihara, A., and Morita, Y. (1985). Undrained Stability of Consolidated Clays. *Proceedings, 11th International Conference on Soil Mechanics and Foundation Engineering*, San Francisco, Vol. 2, Balkema, Rotterdam: 613-616.

Olsen, R.S. and Malone, P.G. (1988). Soil classification and site characterization using the CPT. *Penetration Testing 1988*, Vol. 2 (Proc. ISOPT-1, Orlando), Balkema, Rotterdam: 887-893.

Olsen, R.S. and Mitchell, J.K. (1995). CPT stress normalization and prediction of soil classification. Proc. CPT'95, Vol. 2, Swedish Geotechnical Society, Linkoping: 257-262.

Ortigao, R.J.A., Werneck, M.L., and Lacerda, W.A. (1983). Embankment failure on clay near Rio de Janeiro. *Journal of Geotechnical Engineering*, *109*(11), 1460-1479.

Ouyang, Z. and Mayne, P.W. (2016). Effective friction angle of soft-firm clays from flat dilatometer. Geotechnical Engineering, *Intl. Journal of the Institution of Civil Engineers*, London: Paper 1600073. pub. online 29 Nov 2016.

Ozkul, Z.H., Bik, M. and Remmes, B. (2013). Piezocone profiling of a deepwater clay site in the Gulf of Guinea. *Proc. Offshore Technology Conference*, Houston, TX: OTC Paper 24136.

Pane, V., Brignoli, E., Manassero, M., and Soccodato, C. (1995). Cone penetration testing in Italy. *Proceedings of the International Symposium on Cone Penetration Testing* (CPT'95), Swedish Geotechnical Society, Linkoping, Sweden, Vol. 1: 101-114.

Paré, J.J., Bozozuk, M., Brzezinski, L.S., Dascal, O., Eide, O., Ladd, C.C., Law, K.T., Lavallée, J.G., Lefebvre, G., Mesri, G., Rosenberg, P., Tavenas, F., (1983) *Comité de spécialistes sur les argiles sensibles du complexes NBR. Rapport final.* Rapport interne présenté au Service Géologie et Mécanique des sols de la Société d'énergie de la Baie James (SEBJ), 158 p.

Pestana, J.M., Hunt, C.E. and Bray, J.D. (2002). Soil Deformation and Excess Pore Pressure Field around a Closed-Ended Pile. *Journal of Geotechnical and Geoenvironmental Engineering* 128 (1): 1-12.

Pineda, J.A., McConnell, A. & Kelly, R.B. (2014). Performance of an innovative direct-push piston sampler in soft clay. *In Proceedings of the 3rd symposium on cone penetration testing* (eds P.K. Robertson, K.L. Cabal, and R.E.S. Moss), pp 279–288. Las Vegas, NV, USA: CPT14 Press.

Pineda, J.A., Suwal, L.P., Kelly, R.B., Bates, L., and Sloan, S.W. (2016). Characterization of Ballina clay. *Géotechnique*, *66*(7), 556-577.

Piratheepan, P., (2002), *Estimating shear-wave velocity from SPT and CPT data*. Master of Science Thesis, Clemson University, SC.

Potyondy, J. G. (1961). Skin friction between various soils and construction materials. *Geotechnique*, *11*(4), 339-353.

Powell, J.J.M., and Quarterman, R.S.T. (1988). The interpretation of cone penetration tests in clays with particular reference to rate effects. *Penetration Testing 1988*, Vol. 2 (Proc. ISOPT-1, Orlando), Balkema, Rotterdam: 903-909.

Powell, J.J.M., and Lunne, T. (2005). A comparison of different sized piezocones in UK clay. *Proceedings of the 16th International Conference on Soil Mechanics and Geotechnical Engineering*, Osaka, Japan, 729-734.

Powell, J.J.M., Quarterman, R.S.T. and Lunne, T. (1988). Interpretation and Use of the Piezocone Test in UK. *Penetration Testing in the UK*, Thomas Telford, London, 47-52.

Qiu, G. (2014). Numerical analysis of penetration tests in soils. *Ports Contain. Ships Futur. Gener, Hamburg, Germany*, 183-196.

Quigley, R.M. (1980). Geology, mineralogy, and geochemistry of Canadian soft soils: a geotechnical perspective. *Canadian Geotechnical J.* 17 (2): 261-285.

Rad, N.S. and Lunne, T. (1989). Direct correlation between piezocone test results and undrained shear strength of clay. *Penetration Testing 1988* (Proc. ISOPT-1, Orlando), Balkema, Rotterdam, Vol. 2: 911-917.

Radharkrishna, H.S., Cragg, C.B.H., Tsang, R. and Bozozuk, M. (1986). Uplift and compression behavior of drilled piers in Leda clay. *Proc. 39th Canadian Geotechnical Conference*, Ottawa: 123-130.

Ramalho-Ortigao, J. A., Werneck, M. L., & Lacerda, W. A. (1983). Embankment failure on clay near Rio de Janeiro. *Journal of Geotechnical Engineering*, *109*(11), 1460-1479.

Randolph, M.F. (2004). Characterization of soft sediments for offshore applications. *Geotechnical and Geophysical Site Characterization*, Vol. 1 (Proc. ISC-2, Porto), Millpress, Rotterdam: 209-232.

Rathje, E., Wright, S.G., Stokoe, K.H., Adams, A., Tobin, R. and Salem, M., (2006). *Evaluation of non-nuclear methods for compaction control.* Report FHWA/TX-06/0-4835-1. Center for Transportation Research, Univ. Texas at Austin: 143 pages.

Robertson, P. K., Campanella, R. G., Gillespie, D., and Grieg, J. (1986). Use of piezometer cone data. *Use of In-Situ Tests in Geotechnical Engineering* (GSP No. 6), ASCE, Reston, VA: 1263 - 1280.

Robertson, P.K. (1990). Soil classification using the cone penetration test. *Canadian Geotechnical J.* 277 (1): 151-158.

Robertson, P.K. (2004). Evaluating soil liquefaction and post-earthquake deformations using the CPT. *Geotechnical & Geophysical Site Characterization*, Vol. 1 (Proc. ISC-2, Porto), Millpress, Rotterdam: 233-249.

Robertson, P.K. (2009). Interpretation of cone penetration tests – a unified approach. *Canadian Geotechnical Journal*, Vol. 46 (11): 1337 - 1355.

Robertson, P.K. (2010). Soil behavior type from the CPT: an update. In *2nd International Symposium on Cone Penetration Testing, USA* (pp. 9-11).

Robertson, P.K. (2016). Cone penetration test (CPT)-based soil behavior type (SBT) classification system—an update. *Canadian Geotechnical Journal*, *53*(12), 1910-1927.

Robertson, P.K., and Cabal, K.L. (2016). Guide to cone penetration testing for geotechnical engineering. 6th Edition, *Gregg Drilling and Testing Inc., USA*,143p.

Robertson, P.K., and Wride, C.E. (1998). Evaluating cyclic liquefaction potential using the cone penetration test. *Canadian Geotechnical Journal*, 35(3): 442–459.

Robertson, P.K., Campanella, R.G., Gillespie, D., and Greig, J. (1986). Use of piezometer cone data. *Use of In-Situ Tests in Geotechnical Engineering (GSP 6)*, ASCE, Reston/VA: 1263-1280.

Robertson, P.K., Sully, J.P., Woeller, D.J., Lunne, T., Powell, J.J.M. and Gillespie, D. (1992). Estimating coefficient of consolidation from piezocone tests. *Canadian Geotechnical Journal* 39 (4): 539-550.

Robinson, K.E., and Taylor, H., (1969). Selection and performance of anchors for guyed transmission towers. *Canadian Geotechnical Journal,* 6 (1), 119-137.

Robitaille, D., Demers, D., Potvin, J., and Pellerin, F. (2002). Mapping of landslide-prone areas in the Saguenay region, Quebec, Canada. *Proceedings of the international conference on instability–planning and management, Ventnor, Isle of Wight* (161-168).

Rocha Filho, P. and Alencar, J. (1985). Piezocone Tests in Rio de Janeiro Soft Clay. *Proceedings, 11th International Conference on Soil Mechanics and Foundation Engineering*, San Francisco, Vol. 2, Balkema, Rotterdam: 859-862.

Roy, S., (1990). *Etude du comportement en chambre triaxiale d'un pieu à frottement foncé dans une argile sensible.* Mémoire de maîtrise, département de Génie civil. Université Laval, Québec, 220p.

Rutledal, H., Ertresvåg, E. T., & Berge, O. E. (2000). Interpretation and analysis of the 1997 3D multicomponent seismic survey covering a part of the Oseberg field in the North Sea. In *SEG Technical Program Expanded Abstracts 2000,* Society of Exploration Geophysicists: 570-573.

Sabbagh, M.E, and Koutsoftas, D. (2011). Staged construction on soft clay: A design case history. *Proceedings of the 17th International Conference on Soil Mechanics and Geotechnical Engineering: The Academia and Practice of Geotechnical Engineering*. M. Hamza et al., 3491-3494.

Sambhandharaksa, S. (1977). *Stress-strain-strength anisotropy of varved clays.* Doctoral dissertation, Massachusetts Institute of Technology, 529p.

Sandven et al. (2015). Detection of brittle materials. Summary report with recommendations. Final report. NIFS Report no. 126/2015, prepared for multiconsilt; 149p (www.naturfare.no)

Sandven, R. (1990). *Strength and Deformation Properties of Fine-Grained Soils Obtained from Piezocone Tests*. Ph.D. Thesis, Norwegian Institute of Technology, Trondheim, 337 p.

Santamarina, J.C. & Fratta, D. (1998). *Introduction to Discrete Signals and Inverse Problems in Civil Engineering*, ASCE, Reston, VA.

Saye, S.R., Lutenegger, A.J., Santos, J., and Kumm, B.P. (2013). Assessing overconsolidation ratios in soil with piezocone: referencing soil index properties. *Journal of Geotechnical and Geoenvironmental Engineering*, *139*(7), 1075-1085.

Saye, S.R., Santos, J., Olson, S.M., and Leigh, R.D. (2017). Linear trendlines to assess soil classification from cone penetration test data. *Journal of Geotechnical and Geoenvironmental Engineering*, *143*(9), 04017060.

Schmertmann, J.H. (1955), The undisturbed consolidation behavior of clay, *Transactions, ASCE*, Vol. 120, p. 1201

Schmertmann, J.H. (1986). Dilatometer to compute Foundation Settlement. *Use of In- Situ Tests in Geotechnical Engineering*, (Proc. In-Situ'86, Virginia Tech, Blacksburg, VA), GSP 6, ASCE, Reston, Virginia: 303-321.

Schmertmann, J.H., (1978). Guidelines for cone test, performance, and design. *Federal Highway Administration, Report FHWA-TS-78209*, United States Department of Transportation, Washington, DC, 145 p.

Schnaid, F., Sills, G.C., Soares, J. M., and Nyirenda, Z., (1997). Predictions of the coefficient of consolidation from piezocone tests. *Canadian Geotechnical Journal* 34, 315-327.

Schneider, J.A., Hotstream, J.N., Mayne, P.W. and Randolph, M.F. (2012). Comparing CPTu Q-F and Q-$\Delta u_2/s_{vo}'$ soil classification charts. *Geotechnique Letters*, Vol. 2 (4): 209-215.

Schneider, J.A., Randolph, M.F., Mayne, P.W., and Ramsey, N.R. (2008). Analysis of factors influencing soil classification using normalized piezocone tip resistance and pore pressure parameters. *Journal of Geotechnical & Geoenvironmental Engrg.* 134 (11): 1569-1586.

Senneset, K., Sandven, R. and Janbu, N. (1989). Evaluation of soil parameters from piezocone tests. *Transportation Research Record* 1235, National Research Council, Washington, DC: pp. 24-37.

Serratrice, J.F. (2013). Soils sensibility classification method from piezocone data. *Proc. 18th International Conf. Soil Mechanics & Geotechnical Engineering* (ICSMGE, Paris), Presses de Ponts: 611-614, In French.

Shahri, A.A., and Naderi, S. (2016). Modified correlations to predict the shear wave velocity using piezocone penetration test data and geotechnical parameters: a case study in the southwest of Sweden. *Innovative Infrastructure Solutions*, *1*(1), 1-9.

Shahri, A.A., Malehmir, A. and Juhlin, C. (2015). Soil classification analysis based on piezocone penetration test data: A case study from a quick clay landslide site in southwestern Sweden. *Engineering Geology* 189: 32-47l.

Shibuya, S. and Tamrakar, S.B. (1999). In-situ and laboratory investigations into engineering properties of Bangkok clay. *Characterization of Soft Marine Clays*, Balkema, Rotterdam, 1: 107-132.

Shibuya, S. and Tanaka, H. (1996). Estimate of elastic shear modulus in Holocene soil deposits. *Soils and Foundations*, 36.4: 45-55.

Shibuya, S., and Tamrakar, S.B. (2003). Engineering properties of Bangkok clay. *Characterization and Engineering Properties of Natural Soils*. Vol. 1, Swets & Zeitlinger, Lisse, the Netherlands, 645-692.

Shibuya, S., Mitachi, T., Yamashita, S., & Tanaka, H. (1995). Effects of sample disturbance on $G_{max}$ of soils: A case study. *Proceedings of the First International Conference on Earthquake Geotechnical Engineering*, Vol. 1, 77–82.

Sills, G.C., May, R.E., Henderson, T., and Nyirenda, Z. (1988). Piezocone measurements with four pore pressure positions. *Penetration Testing in the UK*, Thomas Telford, London, 247-250.

Simonini, P. (2004). Characterization of the Venice lagoon silts from in-situ tests and the performance of a test embankment, *Geotechnical and Geophysical Site Characterization,* Vol. 1 (ISC-2, Porto), Millpress, Rotterdam: 187-207.

Singh, V.K., & Chung, S.G. (2015). Evaluation of overconsolidation ratios from laboratory and in situ tests on Busan clay. *Engineering Geology*, 199: 38-47.

Singha, S. (1998). Presentation of in-situ testing program results, US 17 over the Cooper River Charleston, SC, prepared for Parsons Brinckerhoff Quade & Douglas.

Skempton, A. W. and Petley, D. J. (1970) Ignition loss and other properties of peats and clays from Avonmouth, King's Lynn and Cranberry Moss. *Géotechnique*, 20(4), 343–56.

Skempton, A.W. (1951). The bearing capacity of clays, *Building Research Congress*, National Research Council, 180–189.

Skempton, A.W. (1986). Standard penetration test procedures and effects in sands. *Geotechnique* 36 (3): 425-447.

Skomedal, E. and Bayne, J.M. (1988). Interpretation of pore pressure measurements from advanced cone penetration testing. *Penetration Testing in the UK*, Thomas Telford, London, 279-283.

Sowers, G.F., and Hedges, C.S., (1966). Dynamic cone for shallow in-situ penetration testing, vane shear and cone penetration resistance testing of in-situ soils. *American Society of Testing Materials (ASTM)* Special Technical Publication No. 399, Philadelphia, PA.

Stuedlein, A. W. (2008). *Bearing capacity and displacement of spread footings on aggregate pier reinforced clay*. Ph.D. Dissertation. University of Washington, 585p.

Styler, M.A., and Mayne, P.W. (2013). Site investigation using continuous shear wave velocity measurements during cone penetration testing at Gloucester, Ontario. *Proceedings, GeoMontreal 2013*, 66th Canadian Geotechnical Conference, Paper 345.

Su, S.F. and Liao, H.J. (2002). Influence of strength anisotropy on piezocone resistance in clay. *J. of Geotechnical and Geoenvironmental Engineering,* 128 (2): 166-173.

Sugawara, N. (1988). On the possibility of estimating in-situ OCR using piezocone. *Penetration Testing 1988* (Proc. ISOPT-1, Orlando), Balkema, Rotterdam, Vol. 2, 985-991.

Sully, J.P. (1991). *Measurement of in-situ lateral stress during full-displacement penetration tests.* Ph.D. Thesis, Civil Engineering, University of British Columbia, Vancouver: 485 p.

Sun, C.G., Cho, C.S., Son, M., and Shin, J.S. (2013). Correlations between shear wave velocity and in-situ penetration test results for Korean soil deposits. *Pure and Applied Geophysics*, *170*(3), 271-281.

Talme, O.A., Wenner, C.G., and Pajuste, M. (1966). *Secondary changes in the strength of clay layers and the origin of sensitive clays*. National Swedish Institute for Building Research.

Tanaka, H. (1995). National Report-the Current State of CPT in Japan. *International Symposium on Cone Penetration Testing: CPT '95,* Vol. 1, Linköping, Sweden: Swedish Geotechnical Society, 115-24.

Tanaka, H. (2006). Geotechnical Properties of Hachirogata Clay. *Characterization and Engineering Properties of Natural Soils, Vol. 3*. Taylor & Francis, London: 1831-1852.

Tanaka, H., Locat, J., Shibuya, S., Soon, T. T., and Shiwakoti, D.R. (2001). Characterization of Singapore, Bangkok, and Ariake Clays. *Canadian Geotechnical Journal* 38(2), 378-400.

Tanaka, H., Masanori, T., Shinya, S., and Toshihiko, S. (2003). Development of a new cone penetrometer and its application to great depths of Pleistocene clays. *Soils and Foundations* 43.6: 51-61.

Tavenas, F. and Tremblay, M. (1981) *Essais au piézocône sur les sites B-2 et B-6.* Rapport GCS-81-09, Département de génie civil, Université Laval. Quéébec, 47 p.

Tavenas, F., and Leroueil, S. (1990). Laboratory and in situ stress-strain-time behavior of soft clays. *International Symp Geotech Eng Soft Soils Mexico City,* Vol. 2: 1-46.

Tavenas, F., Leroueil, S. and Roy, M. (1982). The piezocone test in clays: Use and limitations. *Proceedings 2nd European Symposium on Penetration Testing*, Vol. 2, Amsterdam, Balkema Publishing: 889-894.

Teh, C.I. (1987). An analytical study of the cone penetration test*, Ph.D. Dissertation*, University of Oxford, 254 p

Teh, C.I., and Houlsby, G.T. (1991). An analytical study of the cone penetration test in clay. *Geotechnique* Vol. 41 (1): 17-31.

Terzaghi, K. (1943). *Theory of Consolidation, in Theoretical Soil Mechanics*, John Wiley & Sons, Inc., Hoboken, NJ, USA.

Terzaghi, K., Peck, R.B., and Mesri, G. (1996). *Soil Mechanics in Engineering Practice*. John Wiley & Sons: 565 p.

Thompson, G.R., and Long, L.G. (1989). Hibernia geotechnical investigation and site characterization. *Canadian Geotechnical Journal*, *26*(4), 653-678.

Tilahun, T.K. (2013). *The identification of quick clay layers from various sounding methods* (Master's thesis, Institutt for bygg, anlegg og transport). Norwegian University of Science and Technology, Department of Civil and Transport Engineering, Trondheim: 134 p.

Trauth, M.H. (2010). *MATLAB Recipes for Earth Sciences*, 3rd ed., Springer, New York.

Tumay, M.T., and Acar, Y.B. (1985). Piezocone penetration testing in soft cohesive soils. *Strength Testing of Marine Sediments (STP 883)*, ASTM, Philadelphia, 72-82.

Tumay, M.T., Abu-Farsakh, M.Y., and Zhang, Z. (2008). From theory to implementation of a CPT-based probabilistic and fuzzy soil classification. *From Research to Practice in Geotechnical Engineering*, GSP 180, ASCE, Reston, Virginia: 259-276.

Tümay, M.T., Hatipkarasulu, Y., Marx, E.R. and Cotton, B. (2013). CPT/PCPT-based organic material profiling. *Proc. 18th ICSMGE*, Paris: 633-636.

Tümay, M.T., HatipKarasulu, Y., Młynarek, Z., and Wierzbicki, J. (2011). Effectiveness of CPT-based classification methods for identification of subsoil stratigraphy. *Proc. 15th European Conf. on Soil Mechanics & Geot. Engineering*, Athens, Greece, Vol. 1, IOS/Millpress, Rotterdam: 91-98.

Uzielli, M., Mayne, P.W. and Cassidy, M.J. (2013). Probabilistic assessment of design strengths for sands from in-situ testing data. *Modern Geotechnical Design Codes of Practice, Advances in Soil Mechanics & Geotechnical Engineering*, Vol. 1, IOS-Millpress, Amsterdam: 214-227.

Vaid, Y.P. (1971). *Comparative behavior of an undisturbed clay under triaxial and plane strain conditions*, Doctoral dissertation, University of British Columbia, 252p.

Valsson, S.M. (2016). Detecting Quick Clay with CPTu. *Proceedings of the 17th Nordic Geotechnical Meeting*. Challenges in Nordic Geotechnic, Iceland. Reykjavik Proceedings, 143–152.

van den Berg, P. (1994). Analysis of soil penetration, *Ph.D. thesis*, TU Delft, The Netherlands, 182p.

van den Berg, P., Borst, R. D., and Huetink, H. (1996). An Eulerean finite element model for penetration in layered soil. *Intl. J. Numerical &. Analytical Methods Geomech*anics, 20(12), 865–886.

Vardanega, P.J. and Bolton, M.D. (2013). The stiffness of clays and silts: normalizing shear modulus and shear strain. *Journal of Geotechnical & Geoenvironmental Engineering,* doi:10.1061/(ASCE)GT.1943.5606.0000887.

Vesić, A. (1975). *Principles of Pile Foundation Design*, Duke University, Dept. of Civil Engineering, Durham, NC.

Vesić, A.S. (1972). Expansion of cavities in infinite soil mass. *Journal of the Soil Mechanics and Foundations,* ASCE, Vol. 98, No. 3, 265-290.

Vesić, A.S. (1977). Design of Pile Foundations. *Synthesis of Highway Practice 42*. Transportation Res. Board, National Research Council, Washington, DC: 68 p.

Villet, W.C.B., and Darragh, R.D. (1985). Interpretation of piezometric cone tests in highly overconsolidated offshore silts. *Proceedings, 17th Offshore Technology Conference*, Houston, Vol. 2, 187-200.

Wair, B.R., DeJong, J.T., and Shantz, T. (2012). *Guidelines for estimation of shear wave velocity profiles*. Pacific Earthquake Engineering Research Center, University of California, 95p.

Walker, J. and Yu, H. S. (2006). Adaptive finite element analysis of cone penetration in clay, *Acta Geotecnica*, **1**, 43–57.

Wang, B., Brooks, G.R., and Hunter, J.A. M. (2015a). Geotechnical data from a large landslide site at Quyon, Report 7904, Quebec Geological Survey of Canada: 54 p.

Wang, B., Brooks, G.R., and Hunter, J.A. M. (2015b). Geotechnical investigations of a large landslide site at Quyon, Québec. Proc. GeoQuébec 2015, Paper ID 355, 68th Canadian Geotechnical Conference.

Watabe, Y. (1999). Mechanical properties of $K_0$-consolidation and shearing behavior observed in triaxial tests for five worldwide clays - Drammen, Louiseville, Singapore, Kansai, and Ariake clay. *Proceedings of the International Symposium on Characterization of Soft Marine Clays*, (IS Yokosuka, Japan), Balkema, Rotterdam: 241-254.

Watabe, Y., Shiraishi, Y., Murakami, T., and Tanaka, M. (2007). Variability of physical and consolidation test results for relatively uniform clay samples retrieved from Osaka Bay. *Soils and Foundations*, *47*(4), 701-716.

Watabe, Y., Tsuchida, T., and Adachi, K. (2002). Undrained shear strength of Pleistocene clay in Osaka Bay. *Journal of Geotechnical and Geoenvironmental Engineering*, *128*(3), 216-226.

Weary, D.J. (2005). An Appalachian regional karst map and progress towards a new national karst map. *US Geological Survey Report 5160* part A: 93-101: www.usgs.gov

Weech, C. (2002). Installation and load testing of helical piles in a sensitive fine-grained soil. *M.Sc. Thesis*, Department of Civil Engineering, University of British Columbia, Vancouver, BC, Canada.

Westerberg, B., Müller, R., & Larsson, S. (2015). Evaluation of undrained shear strength of Swedish fine-grained sulphide soils. *Engineering Geology*, *188*, 77-87.

Whittle, A.J. (1992). Constitutive modeling for deep penetration problems in clay. in *Proceedings of 3rd International Conference on Computational Plasticity: fundamentals and applications*, Barcelona, Vol. 2, 883–894.

Whittle, A.J., Sutabutr, T., Germaine, J.T., and Varney, A. (2001). Prediction and interpretation of pore pressure dissipation for a tapered piezo-probe. *Geotechnique*, *51*(7), 601-617.

Wightman, W., Jalinoos, F., Sirles, P., & Hanna, K., (2003). Application of geophysical methods to highway-related problems, *Report No. FHWA-IF-04-021*, Federal Highway Admin., Washington, DC: 742 pp.

Woeller, D. 2004. Personal Communication.

Wroth, C. P. (1984). The interpretation of in situ soil tests. *Geotechnique*, *34*(4), 449-489.

Yafrate, N.J. and DeJong, J.T. (2006). Interpretation of sensitivity and remolded undrained shear strength with full-flow penetrometers. *Proc. Intl. Society for Offshore and Polar Engineering* (ISOPE-06, San Francisco): 572-577.

Yamaguchi, H., Ohira, Y., Kogure, K. and Mori, S. (1985) Deformation and strength properties of peat. *Proc. 11th International Conference on Soil Mechanics and Foundation Engineering*, San Francisco, 4, pp. 2461–4.

Yamashita, S., Hori, T., & Suzuki, T. (2003). Effects of fabric anisotropy and stress condition on small strain stiffness of sands. *Deformation Characteristics of Geomaterials*, Swets & Zeitlinger, Lisse, vol. 1: 187-194.

Yokel, F. Y. and Mayne, P.W., (1986). *Helical Probe Tests for Shallow Soil Exploration*, Report NDSIR 86-3351, National Institute of Standards & Technology, Gaithersburg, MD: 51 pages.

Yokel, F. Y. and Mayne, P.W., (1988). Helical Probe Tests: Initial Test Calibration, *ASTM Geotechnical Testing Journal*, 11 (3), 179-186.

Yoon, Gil, and O'neill, M. (1995). Engineering properties of overconsolidated Pleistocene soils of Texas Gulf. *Transportation Research Record* 1479, National Academies Press, Washington DC: 81-88.

Yu, H.S. (1993). Singular plastic fields in steady penetration of a rigid cone, *J. Applied Mechanics*, 60, 1061–2000.

Yu, H.S., and Mitchell, J.K. (1998). Analysis of cone resistance: review of methods. *Journal of Geotechnical and Geoenvironmental Engineering*, *124*(2), 140-149.

Yu, H.S., Herrmann, L.R., and Boulanger, R.W. (2000). Analysis of steady cone penetration in clay. *Journal of Geotechnical and Geoenvironmental Engineering*, *126*(7), 594-605.

Zapata-Medina, D. G. (2012). *Evaluation of dynamic soil parameter changes due to construction-induced stresses* Ph.D. dissertation, Northwestern University, Civil Engineering, 260p.

Zebdi, M., (1987) *Contribution à l'étude de l'essai au piézocône dans les argiles sensibles.* Thèse de maîtrise, département de Génie civil. Université Laval, 316 p. (French text)

Zein, A. K. M. (2017). Estimation of undrained shear strength of fine grained soils from cone penetration resistance. *International Journal of Geo-Engineering*, *8*(1), 9p. online version.

Zhang, Z. and Tumay, M.T. (1999). Statistical to fuzzy approach toward CPT soil classification. *Journal of Geotechnical & Geoenvironmental Engineering* 125 (3): 179-186.

Zuidberg, H., Schaap, L., and Beringer, F. (1982). A Penetrometer for Cone Resistance and Dynamic Pore Pressure. *Proceedings, 2nd European Symposium on Penetration Testing*, Amsterdam, Vol. 2, 963-970.

Zwanenburg, C., & Jardine, R. J. (2015). Laboratory, in situ and full-scale load tests to assess flood embankment stability on peat. *Géotechnique*, *65*(4), 309-326.